

Geothermal Power Plants

Geothermal Power Plants

Principles, Applications, Case Studies and Environmental Impact

Fourth Edition

Ronald DiPippo, Ph.D.

Chancellor Professor Emeritus
University of Massachusetts Dartmouth
North Dartmouth, MA, USA



AMSTERDAM • BOSTON • HEIDELBERG • LONDON
NEW YORK • OXFORD • PARIS • SAN DIEGO
SAN FRANCISCO • SINGAPORE • SYDNEY • TOKYO
Butterworth-Heinemann is an imprint of Elsevier



Butterworth-Heinemann is an imprint of Elsevier
225 Wyman Street, Waltham, MA 02451, USA
The Boulevard, Langford Lane, Kidlington, Oxford OX5 1GB, UK

First edition 2005; Second edition 2008; Third edition 2012; Fourth edition 2016

Copyright © 2016 Elsevier Ltd. All rights reserved.

Previous editions copyright: © 2005, 2008, 2012 Elsevier Ltd. All rights reserved.

No part of this publication may be reproduced or transmitted in any form or by any means, electronic or mechanical, including photocopying, recording, or any information storage and retrieval system, without permission in writing from the publisher. Details on how to seek permission, further information about the Publisher's permissions policies and our arrangements with organizations such as the Copyright Clearance Center and the Copyright Licensing Agency, can be found at our website: www.elsevier.com/permissions.

This book and the individual contributions contained in it are protected under copyright by the Publisher (other than as may be noted herein).

Notices

Knowledge and best practice in this field are constantly changing. As new research and experience broaden our understanding, changes in research methods, professional practices, or medical treatment may become necessary.

Practitioners and researchers must always rely on their own experience and knowledge in evaluating and using any information, methods, compounds, or experiments described herein. In using such information or methods they should be mindful of their own safety and the safety of others, including parties for whom they have a professional responsibility.

To the fullest extent of the law, neither the Publisher nor the authors, contributors, or editors, assume any liability for any injury and/or damage to persons or property as a matter of products liability, negligence or otherwise, or from any use or operation of any methods, products, instructions, or ideas contained in the material herein.

ISBN: 978-0-08-100879-9

British Library Cataloguing-in-Publication Data

A catalogue record for this book is available from the British Library

Library of Congress Cataloguing-in-Publication Data

A catalog record for this book is available from the Library of Congress

For information on all Butterworth-Heinemann publications
visit our website at <http://store.elsevier.com/>

Typeset by MPS Limited, Chennai, India
www.adi-mps.com

Printed and bound in the United States of America



Working together
to grow libraries in
developing countries

www.elsevier.com • www.bookaid.org

Publisher: Joe Hayton

Acquisitions Editor: Lisa Reading

Editorial Project Manager: Natasha Welford

Production Project Manager: Lisa Jones

Designer: Victoria Pearson

Cover photo of Ngatamariki power plant, New Zealand, courtesy of Ormat Technologies, Inc.;
cover diagram of Las Pailas power plant, Costa Rica, by author.

Dedication

In memory of these educators who by their inspiration and belief in me had a profound, positive, and lasting impact on the arc of my life.

Angela McElroy
Providence Regent Avenue School

John L. Lafferty
Providence Classical High School

Joseph Kestin
Brown University

Gordon F. Anderson
Southeastern Massachusetts University

Foreword to the Fourth Edition

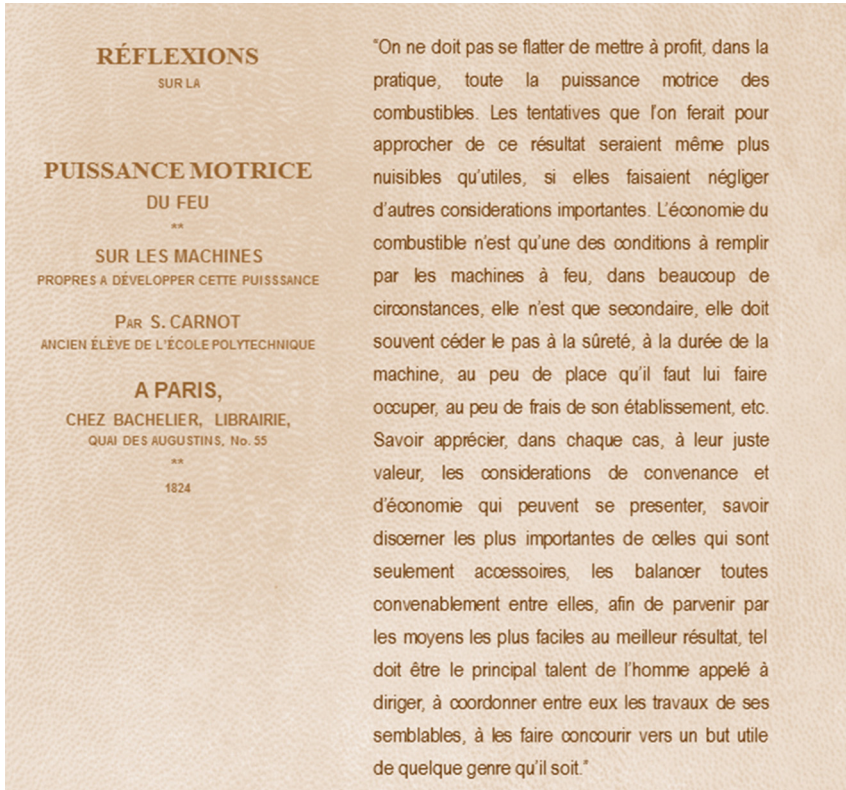
Design of a successful geothermal power plant is the result of a sound theoretical analysis combined with a series of practical compromises based as much as possible on past experience. The fourth and expanded edition of Ron DiPippo's *Geothermal Power Plants* combines effectively these two elements. As already recognized by Sadi Carnot, the analysis cannot be limited to the thermal efficiency (called by Carnot "The economy of the combustible") of the power plant. The concluding paragraph of his famous treatise makes this so clear and so relevant today, in particular for geothermal projects, that it deserves quotation in full:

The economy of the combustible is only one of the conditions to be fulfilled in heat engines. In many cases it is only secondary. It should often give precedence to safety, to strength, to the durability of the engine, to the small space which it must occupy, to small cost of installation, etc. To know how to appreciate in each case, at their true value, the consideration of convenience and economy which may present themselves; to know how to discern the more important of those which are only accessories to balance them properly against each other, in order to attain the best results by the simplest means: such should be the leading characteristics of the man called to direct, to co-operate towards one useful end, of whatsoever sort it may be.

Sadi Carnot, *Reflections on the Motive Power of Fire*, Paris, 1824

In geothermal energy development, a multidisciplinary approach is a must. The disciplines involved range from geology, hydrology, geophysics, drilling, well design, and power plant engineering.

Since the last edition of DiPippo's book, many power plants have been added in the United States, Africa, Turkey, Central America, the Caribbean, New Zealand, and Europe. This edition fulfills the constant need for updated information and insight. Just like previous editions, it provides a most complete picture of the geothermal disciplines. It draws from both the theory and the practice of operating power plants. It covers the complete life cycle of their development, from resource exploration, through the construction of the power plant, to sustaining the hydrothermal reservoir. It emphasizes the concept of exergy-based utilization efficiency, which is crucial for geothermal power plants. Thus, as with previous editions, it will further promote geothermal energy development, since it includes elements



and information not previously covered. This book provides information and insight that are crucial if we want to move forward, and to come up with innovations that will further unlock the potential of geothermal energy. The constant improvement of geothermal energy effectiveness is a must, considering the new challenges from competing renewables such as solar and wind, and therefore the publication of this new edition of DiPippo's book is extremely timely.

During my time at Ormat, we have also used, and greatly benefited, from the previous editions of this book for the development of different configurations of geothermal power plants to maximize the effectiveness of each resource, and to manage specific reservoirs to produce the most energy possible without compromising the sustainability of the geothermal field. I strongly recommend the fourth edition to all practitioners and students in all facets of this fascinating industry.

Lucien Y. Bronicki

Founder and past CTO of Ormat Technologies, Inc.

Reno, Nevada

February 23, 2015

Preface and Acknowledgements to the Fourth Edition

What's New in the Fourth Edition?

It has been ten years since the publication of the first edition of this book. Over that time, growth in geothermal power has been steady, but not spectacular. Several countries including Turkey, Indonesia, and New Zealand have seen rapid expansion of their geothermal portfolios. Others with long histories of geothermal exploitation such as the United States, Italy, and Iceland continue to advance by updating existing plants with more modern and efficient equipment and exploring for and discovering new sites which then become home to new power plants.

This edition represents a major revision from the third edition. Several case study chapters from the first edition that had appeared in the second and third editions have been replaced with new ones that focus on plants and places of great current interest.

The new chapters are on developments in New Zealand (Chapter 13), Indonesia (Chapter 14), Latin America and the Caribbean (Chapter 15), in the state of Nevada in the United States (Chapter 16). Nevada has seen extensive development of geothermal resources, mainly so-called “blind systems” scattered across the generally barren landscape and presents several cases worthy of study.

Significant additions have been made to several other chapters. Low-temperature resources are discussed in Chapter 1 along with the more conventional ones. The subject of reinjection is tackled as part of the chapter on Reservoir Engineering (Chapter 4). Chapter 5 now includes a presentation on triple-flash systems that have become more in use recently. Chapter 8 on binary plants starts with a correction from the third edition about the little-known geothermal plant at Kiabukwa in the Democratic Republic of the Congo. It is important to set the record straight about this small but pioneering plant. Also a new section has been added to Chapter 8 dealing with pumps, both downhole and surface types, owing to the critical role they play in all kinds of geothermal energy conversion systems. A small section emphasizing the difference between thermal and exergy efficiencies has been added to Chapter 10.

The case study chapter on Larderello has been revised and expanded based on new research by the author that resulted in a recent publication; see Ref. [2] in

Chapter 13. The EGS power plants section in Chapter 22 has been extensively revised and updated with added details on the pilot plant at the Habanero site in the Cooper Basin of Australia and several new plants in Germany. Generally throughout the book, updates were made where needed as projects have progressed since the last edition. The worldwide data tables (Appendix A) have been updated based on the presentations at the *World Geothermal Congress 2015* in Melbourne, Australia.

The practice problems have grown in scope over each edition and have been further expanded with new problems and are now conveniently collected in groups at the end of appropriate chapters. Many problems have been revised and all of them are now in metric units, except for those dealing with wells and drilling where the United States Customary System of Units persists as the worldwide standard of usage. Furthermore, all problems have been re-solved and numerical examples in the text reworked using the NIST REFPROP software package for consistency throughout the book. Answers to selected problems have been revised as well.

A Few Observations

In carrying out the research for this edition, it became clear that certain truths are now evident about geothermal power generation. First and perhaps most important, geothermal power plants are long-lived. Fields such as Larderello, The Geysers, Wairakei, Cerro Prieto, Krafla, and Kamojang continue to deliver geothermal fluids to fuel their power stations after decades of operation. This underscores the renewable nature of geothermal energy. We as an industry have learned how to develop and sustain geothermal resources.

Some power plants have outlived their technical lifetimes and been replaced with more modern units, while others have been demolished to make way for more efficient steam gathering systems. Some units that were sited at the margins of highly productive fields have fallen by the wayside, victims of an overly optimistic outlook for a particular field. A few relatively new plants have suffered similar fates. This reminds us of the admonition stated so clearly by my mentor, Dr. Joseph Kestin, in the Preface to my first book *Geothermal Energy as a Source of Electricity*: In 1979 he wrote “*Geothermal electricity, unlike fossil or nuclear, cannot be ordered: it must be developed, for there is nothing more hazardous than a premature order for conversion equipment.*” A corollary to his warning is that it is just as bad to oversize and overbuild a plant for more power than a field can support. The consequences of this error are usually disastrous for the project owner and its investors and, if this happens enough, can heighten the wariness of the investment community, making it more difficult to finance future

projects, irrespective of the quality of the project. The irony is that a properly sized, but smaller, plant has a much better chance of being seen as a success.

The impact of public policy including regulations and financial incentives cannot be overstated. The case of Indonesia is a good illustration. A whole new chapter is devoted to Indonesian geothermal developments. There is no country with more potential for geothermal power than Indonesia. The evidence is plain to see. A nearly unbroken chain of volcanoes meets the eye. Many are still active. Enough sites have now been developed and explored to establish an expectation of as much as 29,000 MW of geothermal electric generation, or the equivalent of 29 large nuclear power plants. But only about 1340 MW is online so far. The potential was recognized as long ago as the 1920s, not long after the very first geothermal power plants began operating in Italy. But without a clear mandate to develop the resources, nothing happened until the 1970s when the two Oil Crises awakened the world to the need for alternative and indigenous energy sources. It was then that Indonesia, an oil-exporting country, recognized that their oil could be exported for foreign exchange and that its vast geothermal potential—that could not be exported—could and should be used domestically. But the path of development so eagerly embarked upon was blocked by the financial crisis that enveloped Asian nations in 1997–98, none more so than Indonesia. This left power plants that were under construction in half-finished conditions, and delayed others indefinitely. Now at last there appears to be a coherent plan in place for smooth development of the enormous geothermal potential of this highly populous and growing nation.

Similar stories could be told about other countries. It is easy but often painful to learn from one's own mistakes; far wiser to learn from the mistakes of others. The geothermal industry has always been open about its activities, candidly sharing experiences good and bad. The case studies in this book provide the reader with the opportunity to learn how to avoid problems and how to adopt best practices in project development and execution.

A Newcomer's Introduction to Geothermal Power Conversion

As with all previous editions, this book focuses on the energy conversion systems needed to make electricity from geothermal energy. Ten years ago this book was essentially alone in covering this topic. Now there are several books with similar titles and that is good. There are more books on thermodynamics, or calculus, than arguably might be needed, but in the diversity of presentations a richer picture of the subject is drawn. So it will be with geothermal power plants, as more and more authors share their experience and understanding with their readers.

Having taught this subject at the University of Massachusetts Dartmouth for 25 years and later after retirement at the School for Renewable Energy Science at Akureyri in Iceland, at the National Geothermal Academy at the University of Nevada, Reno, and at short courses of the Geothermal Resources Council, I see the next generation of the geothermal community coming into its own. Like me 40 years ago, these people need the best education they can get. I was fortunate to have worked with and learned from some of the giants in our industry, and I hope that this book in some way advances the knowledge of young people starting their careers.

I remind myself that many readers may not have the background or experience in electric power generation to dive into some of the chapters of this book without some prior information gathering. Of course nowadays the internet makes that less of a challenge than it was 40 years ago. Nevertheless, as we all have come to appreciate, the internet is not infallible. Thus, I offer the next few paragraphs to geothermal newcomers as a kind of orientation.

To understand better how geothermal energy can be a source of electricity, it is instructive to start with a brief review of how fossil fuels are used in conventional electric generating stations. Then we will be able to see similarities and differences between conventional and geothermal power plants.

Fossil fuels—oil, gas, coal—are created by nature. We discover them usually deep underground after they have been put into a very energy-intensive form. We bring them to the surface by drilling or mining the fuels. Once at the surface they can be transported to sites where their energy content is released by igniting them. The fossil fuels can be stored for later use, an important distinction between them and geothermal “fuels.”

The combustion of fossil fuels releases the chemical energy that nature stored in the molecular bonds that hold the fuel together. The energy is released as thermal energy in the form of high temperature combustion gases. As the gases cool while passing through the combustion chamber, heat is transferred to a working fluid, usually water, in a power cycle. Electricity flows from the cycle in which the water is recycled through the power system receiving a continuous supply of heat from the combustion chamber. The efficiency of such plants is normally expressed as the “thermal efficiency”—the ratio of the electricity generated to the heat needed to drive the cycle. For typical cycles, values range from 35% to 60%, depending on the fuel and the design of the plant.

An alternative measure of performance is the so-called Second Law or exergy efficiency. This accounts for the thermodynamic potential of the fuel before it is burned. The exergy is the maximum theoretical electrical output that could be obtained from the fuel if the energy transformations take place ideally with no losses. A fuel has thermodynamic value because its stored energy means that it is not in complete equilibrium with the surroundings: the greater the disequilibrium, the greater the potential to generate useful power. In other words, the larger the

difference between the fuel's energy level relative to the surroundings, the more power that can theoretically be extracted for useful purposes. The exergy efficiency is the ratio of the electricity generated to the exergy of the fuel prior to combustion. In the case of fossil fuels, for technical reasons, there is very little difference numerically between the thermal efficiency and the exergy efficiency.

Now, in the case of geothermal "fuels," nature is once again the agent for creating the fuel. Geologic forces deep in the earth over long periods of time create reservoirs of hot fluid containing high exergy. The movement of gigantic tectonic plates that form the crust of the earth, volcanoes fed by extremely hot molten rock, coupled with rainfall create the geothermal fuel. We can discover these reservoirs using scientific methods and tap into them by drilling wells. Once the geofluids are brought to the surface, we can put them to use to drive power plants. But unlike fossil fuels that can be put into storage tanks or piled up in coal yards, geothermal "fuels" cannot be stored. They must be used as soon as they reach the surface or their inherent thermodynamic value will be lost. The only possibility for storage is to keep the wells closed and retain the geofluid in the reservoir for later use. However, once a reservoir is tapped, there are economic and practical reasons that militate against such a strategy.

There are fundamentally two ways to use the geothermal fuel to make electricity. The first is by using a plant that is very similar to ones used with fossil fuels, but minus the combustion. The hot geofluid, which is far lower in temperature than the combustion gases released by burning fossil fuels, is simply cooled to a temperature allowed by the surroundings while the heat released is transferred to a working fluid in a cycle using a heat exchanger. That fluid, however, is usually not water as in a fossil plant, but a low-boiling-point fluid such as a hydrocarbon or refrigerant. Because two different fluids are in use—geothermal fluid and a working fluid—such plants are called "binary" plants.

The working fluid in a binary plant operates in a closed cycle generating electricity while receiving a continuous supply of heat from the geothermal "fuel" as it cools. Once it has cooled down, the geofluid is discarded, usually returned to the reservoir via injection wells. Thus in principle, this operation is thermodynamically identical to what happens in fossil-powered plants, and therefore the thermal efficiency may be used to assess the performance. Typical values for geothermal binary plants are 5–18%, depending on the temperature of the geofluid and the design of the plant.

As with the fossil plants, binary plants may also be assessed using the exergy efficiency. In this case we compare the electricity generated to the exergy of the geothermal fluid as it arrives at the plant (or as it exists in the reservoir). Again, the exergy is the ideal amount of electricity that could be generated from the geofluid if all processes are ideal with no losses. In this case there is a significant numerical difference between the thermal efficiency and exergy efficiency.

Typical exergy efficiencies for binary plants are 20–50%, again depending on the temperature of the geofluid and the design of the plant.

The other way to use the geothermal “fuel” is to pass it directly to a turbine (or other machine) and make electricity without the need for a heat exchanger. This can be done if the geofluid has sufficiently high temperature and pressure, giving it a high exergy. If the geofluid comes out of the well having liquid mixed with steam, the liquid must first be removed. Once the geosteam has been used to drive the turbine-generator, its temperature and pressure are lower, and it could be disposed of to the surroundings, although this might not be desirable or permitted environmentally. But in principle, that is all that needs to be done to use many geofluids. Geothermal plants of this kind are called dry (or direct) steam, single-flash, double-flash, etc.

It is important to recognize that there is no heat transfer needed to drive geothermal steam plants since all the energy needed to produce the electricity is contained within the geothermal fuel in the form of exergy. Their performance is measured thermodynamically by the exergy efficiency, namely, the ratio of the electricity produced to the exergy of the geothermal fuel. Note that the thermal efficiency obviously cannot be used in this case since no heat is transferred to drive the plant. In fact, the power plant will work best when everything is well insulated to avoid any heat transfer from the hot geofluid. Typical exergy efficiencies for dry-steam and flash-steam plants are 45–75%, again depending on the condition and temperature of the geofluid and the design of the plant. Note that these are comparable to or even greater than thermal or exergy efficiencies for fossil-fueled or nuclear plants.

The understanding of geothermal power plants may be further enhanced by drawing a comparison between geothermal and hydroelectric plants. Hydro plants operate by using water that exists at an elevation higher than other nearby sites. Nature made the high ground and produced rain or melting snow to fill lakes and rivers there. Waterfalls occur naturally where the terrain changes from high to low elevation. We take advantage of the potential of the water at high elevation, i.e., high potential energy or high exergy, by passing it through a turbine on its way down to capture some of that potential and convert it to electricity. Once it passes through the turbine, it is discarded. Eventually the water from the high ground will end up in the ocean at normal sea level, having lost all of its potential for power generation.

Because there is no heat transfer needed to run a hydroelectric plant, its performance cannot be evaluated using a thermal efficiency. The efficiency is measured as the ratio of the electricity generated to the potential energy of the water at the high elevation relative to the lower level downstream of the plant, or in other words, to the exergy of the high-elevation water. The similarity of this to the geothermal steam plants is obvious. Throughout this book, these basic notions will be elaborated upon, but it is helpful to keep the broad picture in mind.

Acknowledgments

I wish to thank the following people for their help during the writing of the Fourth Edition. I extend, first of all, my deepest appreciation to Lucien Bronicki, founder and retired CTO of Ormat Technologies, Inc., for writing the Foreword. Lucien wrote the Foreword to the last edition and this time has written a very compelling essay that harkens back to the famous little book by Sadi Carnot, *Reflections on the Motive Power of Fire*. He shows how the thoughts of Carnot, expressed in 1824 before anyone had figured out the basics of what we now call *Thermodynamics*, have important relevance in today's world of geothermal power.

Johannes Hopmans, Chemical and Power Plant Facilities Consultant, Batangas City, Philippines, brought it to my attention an error in the example in Section 9.4. This prompted me to revisit all numerical work and the practice problems throughout the book in an effort to eliminate inconsistencies. Liz Johnson, California Division of Oil, Gas & Geothermal, provided me with the latest production and reinjection data for The Geysers power plants. Lauren Rosa and Arisa Sato, Fuji Electric Co., Ltd., sent me data on Fuji's geothermal turbine installations. Zvi Krieger, Hilel Legmann, and Josh Nordquist, Ormat Technologies, Inc., shared with me information, photos, and technical details on Ormat's plants in Nevada and New Zealand. Hank Leibowitz, Waste Heat Solutions LLC, shared the heat and mass balance diagram for the Beowawe bottoming binary cycle. Alexander Richter, ThinkGeoEnergy, and Fridrik Ómarsson, Mannvit, procured and granted permission to use the photo of the Berlin, El Salvador, binary plant in Section 15.3.2. Ben Humphreys, Geodynamics, Ltd., answered many questions about the pilot plant at the Innamincka EGS site in Australia. Lisa Shevenell, Nevada Bureau of Mines and Geology, helped me find my way through the extensive online databases of the NBMG. Fabrizio Bizzarri, ENEL Green Power, kindly shared information on the world's first commercial hybrid concentrating solar power and geothermal hybrid plant at Stillwater, Nevada. Kevin Kitz, US Geothermal Inc., supplied operating data and information on the San Emidio plant in Nevada.

Lisa Reading and Natasha Welford, my editors at Elsevier, encouraged me to tackle this new edition and steered it through the proposal, approval, and implementation process in a professional and efficient manner. The Elsevier production team, particularly Lisa Jones, kept the book as on time and as free of errors as is humanly possible. I finally thank all those who have helped me grasp the nuances and subtleties of geothermal power plants in various ways through planned and random conversations; any errors of commission or omission are solely mine.

The color figures are designated with *[WWW]* at the end of the caption. All of the figures used in this book may be viewed at booksite.elsevier.com/9780081008799.

Ronald DiPippo

Dartmouth, Massachusetts

January 2015

Preface and Acknowledgements to the Third Edition

This edition represents a major revision and extension of the original edition published in 2005. In the roughly six years since the First Edition appeared, the inexorable movement toward cleaner and more sustainable energy resources has continued. Despite growing evidence of global changes to our environment that will have huge consequences for future generations, the world has not moved as rapidly toward less polluting and more sustainable sources of primary energy as might be expected in the face of the coming crisis.

Nevertheless geothermal energy can become a significant source of renewable, sustainable, and clean energy to the world, both for direct heat and electric power generation. In the latter case—the subject of this book—it is worthwhile to repeat the words of my mentor Professor Joseph Kestin, who back in 1979, wrote: *“Geothermal electricity, unlike fossil or nuclear, cannot be ordered: it must be developed, for there is nothing more hazardous than a premature order for conversion equipment.”* Apparently this simple lesson needs to be relearned by each generation and especially by those who aim to develop new sites, new resources, or new technologies.

It was in fact this unique aspect of geothermal energy that intrigued me when I first became involved with it back in the 1970s. As an academic and a researcher, I looked for the basic principles that would guide the exploitation of geothermal energy. Beyond the fundamental geology, chemistry, and physics, much of what was needed turned out to be highly site-specific. Back then there were few geothermal plants in operation and nearly all of them were dry-steam plants. Even so there were significant differences among the resources that necessitated specific engineering designs to cope with the variations.

Now that a very wide spectrum of resources is being tapped to generate power, the need to study and thoroughly characterize each site and then craft the power plant to match the resource is even more important. We may understand the basic science that governs the processes, but the applications will require innovative solutions to problems encountered all the way from exploration through drilling and plant design, construction, operation, and maintenance. Therefore, this edition includes more case studies in Part Three.

Chapter 19 focuses on two new and growing power plants in Iceland, the Nesjavellir and Hellisheidi plants. Iceland has experienced a spectacular increase in geothermal power generation since 2007, growing its installed capacity from 422.4 MW to 715.4 MW, a 69% increase over four years. And this has been accomplished without retiring any of its older plants. Iceland now has 31 operating units compared to 24 in 2007.

Chapter 20 tells the story of Raft River in Idaho, one of the first fields to be developed for geothermal power back in the 1970s and early 1980s. The original pilot plant was soon dismantled after a short demonstration run but after 20 years of inactivity, the site has been brought back to life. The lessons learned from the original plant and the new one are presented in this chapter.

Chapter 21 highlights another country making great strides in geothermal development, thanks in large measure to legislative reforms that opened geothermal energy to private companies. Turkey now is host to eight geothermal units, three of them modern gleaming examples of highly efficient units. Turkey went from having two units with an installed capacity of 27.8 MW in 2007 to eight units at 95 MW in mid-2011, more than tripling its geothermal generating capacity in four years. And more plants are expected to be built in the near future.

Chapter 22 deals with the future hope for geothermal power, Enhanced Geothermal Systems or EGS. In the Second Edition, EGS was covered as part of the presentation of advanced energy conversion systems (Chapter 9) but so much has happened in the last four years that even a chapter devoted solely to EGS is not adequate to address the subject. It is a tale full of hope yet disappointments. It is not yet certain what role EGS will play in the development of geothermal power, but it remains a most important technology that must be further refined before it can be truly considered commercial. The new chapter details many research and development efforts and the lessons that should be learned from them.

The other new addition is an appendix that explains how a convenient new software program, REFPROP, developed by and available from the U.S. National Institute of Standards and Technology (NIST), can be used to implement spreadsheet systems simulators. Appendix H includes a tutorial on the use of the program and worked examples showing how to use it in conjunction with Excel to model a geothermal binary plant.

All the data tables on power plants around the world have been completely updated to mid-2011 (Appendix A). Updates and revisions have been made to several chapters from the Second Edition, with a new section on solar-geothermal hybrid plants (Chapter 9) and an extension of exergy analysis to pumps and to production well performance (Chapter 10). A couple of typos from the Second Edition have been corrected and hopefully not too many new ones have crept into this one.

I wish to thank the following people for various forms of assistance during the writing of the Third Edition. First of all, I extend my deepest appreciation to Lucien Bronicki, the Chairman and CTO of Ormat, for writing the Foreword. The previous editions lacked a Foreword and to have one of the most successful geothermal entrepreneurs write one for this edition is very special and meaningful to me. Several people provided valuable information on the plants in Turkey: Umran Serpen (Istanbul Technical University); Marshall Ralph and Bill Harvey (Power Engineers); Henry Veizades (Veizades & Associates); and Riza Kaderli (Guris). Lucien Bronicki and Zvi Kreiger (Ormat) generously provided me with flow diagrams and performance data for several of their recent binary installations, and Lucien reviewed some new sections for accuracy. Einar Gunnlaugsson (Orkuveita Reykjavíkur) clarified the historical timeline of development for the Nesjavellir and Hellisheidi plants. Ernst Huenges and Stephanie Frick (Deutsches GeoForschungsZentrum-GFZ) were kind enough to send me a copy of their excellent book, *Geothermal Energy Systems*, that was edited by Ernst and which has extensive research material related to EGS. Tiffany Gasbarrini, my editor at Elsevier, encouraged me to tackle this new edition and steered it through the proposal, approval, and implementation process in a professional and efficient manner. The Elsevier production team, particularly Lisa Lamenzo and Charles Roumeliotis, did an outstanding job of keeping the book on time and as free of errors as is humanly possible. I finally thank all those who have helped me grasp the nuances and subtleties of geothermal power plants in various ways through planned and random conversations; any errors of commission or omission are solely mine.

The color figures are designated with [WWW] at the end of the caption. All of the figures used in this book may be viewed at elsevierdirect.com/companions/9780080982069.

Ronald DiPippo
Dartmouth, Massachusetts
August 2011

Preface and Acknowledgements to the Second Edition

In the roughly three years since the First Edition of this book appeared, the world has become increasingly alarmed about the consequences of global climate change. The debate over the causes of the documented warming of the planet has essentially come to an end. Attention is focused on collective actions that must be taken now to slow, or reverse, the rising temperatures and to stabilize the situation as soon as possible.

So-called “greenhouse gases” such as carbon dioxide have been identified as the main contributors to global warming. Since the dawn of the Industrial Age some two hundred years ago, humans have been mining and converting carbon, in the form of hydrocarbons stored for millions of years underground, into carbon dioxide. The combustion of fossil fuels is largely responsible for the quality of life that many have come to take for granted and which appears threatened.

Given the diversity of economies and cultures among the world’s countries, it may be futile to hope for a coherent, comprehensive, and effective global energy policy. Such a policy must begin by acknowledging the critical role of energy, particularly electricity, in improving the standard of living for all peoples. It must then find ways to minimize the environmental impact of converting energy resources to serve a myriad of applications. As fossil fuels, especially petroleum, become scarcer, it is likely that the world will rely more heavily on electricity for many daily needs, including vehicular transportation. Thus, the use of renewable, non-polluting sources of electric power will be in great demand.

Geothermal energy has been just such an environmentally-friendly supplier of electricity for over 100 years. The First Edition of this book had several sections devoted to the environmental effects of geothermal power generation, but lacked a thorough, self-contained treatment of the subject. Chapter 19 of this edition answers that deficiency. The presentation is objective, and covers the environmental strengths and weaknesses of geothermal power technology. The strengths, relative to other means of generating power, stem from the inherent nature of geothermal energy and how it is used to generate electricity. The potentially detrimental aspects are site-specific, vary in severity depending on the characteristics of a given resource, and present challenges to the developers of geothermal plants. Fortunately these potential problems have been and continue to be

addressed with effective mitigation techniques. The result is that geothermal energy has an excellent reputation as one of the most environmentally benign sources of electricity.

Despite its advantages in a world increasingly looking for clean sources of energy, geothermal power has experienced only slow, albeit steady growth over the last 10–15 years (see Appendix A, Figure A.1). The strong growth experienced in the aftermath of the oil shocks of the 1970s has not been sustained. The availability and price of oil continues to be an important influence on the growth of geothermal power. Also the lack of new discoveries of sizeable hydrothermal resources has certainly been a contributing factor in this slowdown.

The next major growth period may result from the perfection of techniques being developed to create Enhanced or Engineered Geothermal Systems or EGS (see Sect. 9.8). With research starting in 1973 in the United States and continuing in several countries, EGS holds out the promise of affording any region the opportunity to generate power from the hot rocks that lie beneath the surface at great depths. Encouraging work is being done in Europe and Australia in areas lacking typical hydrothermal systems that could provide a template for other regions. A 2006 MIT study by a panel of experts from a variety of disciplines concluded that, with appropriate funding for research, development, and demonstration, as much as 100,000 MW could be competitively on-line by the year 2050 in the United States alone (see Ref. [1] in Chap. 19).

This edition includes updated statistics on the state of geothermal power plants around the world (Appendix A), as well as 43 new practice problems, along with the answers to many of them, augmenting the ones in the First Edition (Appendices F and G).

One of the objectives of the new edition was to produce a less expensive volume. To achieve this we eliminated color illustrations. However, over 70 color photographs and illustrations are available to readers via the Internet. Considering that there were only 15 color illustrations in the First Edition, this constitutes a significant enhancement for the reader.

I owe a debt of thanks to Jonathan Simpson (Elsevier) for all his help in making this new edition a reality, and to the reviewers of the prospectus who convinced him that this was a worthwhile venture. José Antonio Rodríguez (LaGeo S.A. de C.V.) generously gave permission for the use of the Berlín power plant photograph that graces the cover, and for the aerial photograph of the Ahuachapán plant (Figure 19.12); both plants are in El Salvador. Curt Robinson (Geothermal Resources Council) likewise granted permission to reproduce the photograph of the Zunil landslide (Figure 19.9). I am grateful to Ian Thain (Geothermal & Energy Technical Services Ltd.) who shared some of his historical recollections from Wairakei, and to Richard Glover (Glover Geothermal Geochemistry) for clarifications regarding the Wairakei Geyser Valley and his

review of Sect. 19.5.1. Dan Schochet (Ormat) and Larry Green (Geothermal Development Associates) provided the latest information on their companies' installations. Lastly, I thank my wife, Joan, for her meticulous proofreading of the new material. Her pages of corrections reminded me that somewhere in my life I could have benefited from a course in typing.

Ronald DiPippo

Dartmouth, Massachusetts

May 2007

Preface and Acknowledgements to the First Edition

It was the Fourth of July in the year 2004. Brilliant fireworks streamed across the evening sky. Had this been any of a thousand cities and towns in the United States, the event would not be unusual. But why would a tiny village in the Tuscany region of Italy be celebrating on America's Independence Day?

One hundred years ago on that very day in the village of Larderello, geothermal energy was born as a source of electric power generation. Over the following century, geothermal energy has grown to be the most reliable, efficient, and environmentally-benign renewable source of electric power. Indeed, more than twenty countries across the world where geothermal energy is now used for power production could have been celebrating this historic event.

Geothermal energy is the residual thermal energy in the earth left over from the planet's origins. The temperature of the core of the earth is estimated to be 6650°C (12,000°F). The molten rock that flows inexorably beneath the relatively thin surface crust attains temperatures of about 2200°C (4000°F). The fact that living creatures can walk on the surface of the earth without feeling the effect of this terribly hot fluid testifies to the insulating nature of the solid rock that separates the surface from the molten rock.

If one were to drill a very deep well from the surface into the earth and were to measure the temperature as a function of depth, one would find a fairly constant increase of about 3°C for each 100 m of depth (1.6°F per 100 ft). This rate is typical in normal areas, but there are anomalous regions associated with volcanic or tectonic activity where the temperature gradients far exceed these normal values. For example, at Larderello, Italy where the first engine driven by geothermal steam was built, the gradient is 10–30 times higher than normal. This means that temperatures over 300°C (575°F) can be found at a depth of 1 km (3300 ft), easily reachable with today's drilling technology. If fluids exist in reservoirs at such elevated temperatures and can be brought to the surface through wells, they can serve as the working fluids for electric generating stations. Such fluids are complex mixtures of high-pressure, mineral-laden water, with gases dissolved into solution as a result of the contact of the very hot water with various types of rocks in the reservoir.

It is the challenge of geothermal scientists and engineers to locate these reservoirs of hot fluids, design means to bring them to the surface in an economical and reliable fashion, process them in a suitable power plant to generate electricity, and then to dispose of the spent fluid in an environmentally acceptable manner, usually by returning the fluid to the reservoir through injection wells. The system must be so designed to perform satisfactorily for at least 25–30 years to be deemed economically viable.

The engineering challenge is further heightened by the variable nature of geothermal reservoirs and fluids. While it is possible to categorize reservoirs and fluids into several general types, the detailed characteristics of each reservoir vary to the extent that each site must be studied and well understood before the resource can be properly developed. The development process includes the determination of the location, depth, orientation, number, and type of wells that are needed; the type and size of power plant to be built; the method of disposal of the spent geothermal fluid; and the type of abatement systems that may be needed to conform to local environmental regulations. All of these must be addressed in order to perform a preliminary economic analysis to decide on the project's feasibility.

It is not uncommon for the preliminary work to take several years, and in the case of particularly difficult fluids, a decade or more, before a power plant can be put into operation. The geothermal field near the Miravalles volcano in Costa Rica was discovered in 1976 but the first power unit did not come on-line until 1994. The time devoted to geoscientific studies is necessary to avoid unwise investment in risky ventures. Once a field is properly understood, however, developers can often proceed with additional units in short order. At Miravalles, Unit 1 (55 MW) was followed by a small wellhead unit (5 MW) in 1995, Unit 2 (55 MW) in 1998, Unit 3 (27.5 MW) in 2000, and Unit 5 (15.5 MW) in 2004. A geothermal reservoir adjacent to the Salton Sea in southern California was discovered accidentally in the 1950s, but the extremely aggressive geothermal brines resisted commercial use until the 1980s. It took a massive research and development effort to come up with technological methods to tame these very hot, highly corrosive and scaling fluids. These technical advances led to the construction of six power plants with a total installed capacity of over 650 MW as of 2004.

The uses to which geothermal energy can be put cover a wide spectrum from low-temperature applications, such as greenhouse heating and aquaculture, to high-temperature applications, including absorption chillers for refrigeration and air conditioning and power generation. Normal earth conditions can be exploited by earth-coupled heat pumps for year-round climate control in buildings, so-called Geoexchange® systems. The spectrum of applications is given by the well-known Lindal diagram shown in [Figure I.1](#).

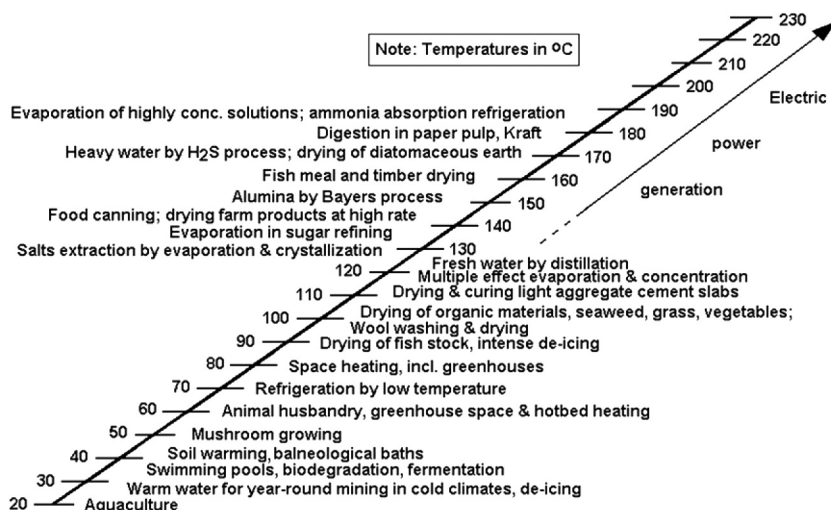


FIGURE I.1 Modified Lindal diagram showing applications for geothermal fluids.

This book focuses on the higher-temperature end of the spectrum where geothermal energy can provide for the generation of electricity—generally regarded as the highest grade and most useful form of energy known to humankind.

The first part of this book deals with the geological nature and origins of geothermal energy, as well as the exploration efforts that are needed in the early stages of the development process. The means of acquiring the geothermal fluids via production wells conclude the first part.

The designer of geothermal power plants nowadays has available a wide assortment of plant designs to cope with the wide diversity of geothermal resources. This was not always the case, as was mentioned earlier for example with the Salton Sea resource. Through research and painful trial and error, there is now no resource that cannot be exploited by means of a suitably designed system.

In the second part, we describe the many types of energy conversion systems that are being used to generate electricity from geothermal energy. Both basic principles and practical applications will be covered. Included are some advanced systems that may one day reach the commercial stage.

The third and last part of the book presents several case studies of power plants selected from six different countries around the world. Examples include plants of different types and sizes, using fluids with various characteristics, in areas having widely differing environments. Each case typically includes a description of the geology, the resource, the environment, the wells and piping system, the energy conversion system(s), the plant performance, and operating

experience. Since geothermal resources are dynamic, it is more than likely that some of the power plants or the geofluid gathering systems will be different as of the reading of this book relative to the writing of it (mid 2004). Geothermal engineers and scientists must be prepared to cope with changes in the properties of the reservoir and the wells, and to modify the energy conversion systems accordingly, over the life of the plant.

In most chapters, I have included quotations, some from long ago and some recent, some from famous people and some from folks who are known to relatively few. These words provide insight into the nature of scientific and geothermal phenomena, and remind us of the challenges we face in turning Nature's bounty to the benefit of humankind.

I published my first book on geothermal energy in 1980: *Geothermal Energy as a Source of Electricity*. That effort was funded by the U.S. Department of Energy. I owe a debt of thanks to the late Joseph Kestin, the project leader at Brown University, for giving me the opportunity to work on his exciting project that also led to the publication of the reference book, *Sourcebook on the Production of Electricity from Geothermal Energy*. I am also indebted to Clifton B. McFarland, the DOE program manager, for his far-sighted leadership and encouragement. During the 1970s and 1980s when I was a research professor at Brown University, I benefited greatly from discussions and collaborations with H. Ezzat Khalifa, now an engineering professor at Syracuse University, with whom I published several papers on hybrid fossil-geothermal power plant systems. I also wish to thank Gustavo Calderon, now retired from the Interamerican Development Bank, for giving me the opportunity, starting in the early 1980s, to broaden my geothermal experience internationally through service on geothermal advisory panels in Costa Rica, Guatemala, El Salvador and Kenya.

I acknowledge with deep appreciation Gordon Bloomquist (Washington State U.) and John Lund (Oregon Institute of Technology) for their reviews of the prospectus for this book and for their thoughtful comments and suggestions. Ted Clutter (Executive Director of the Geothermal Resources Council) was always ready to help me locate or identify a photo or reference. He also provided me with his photograph of the geothermal power plants at Mammoth, California, which graces the cover of the book.

My editor at Elsevier Advanced Technology, Geoff Smaldon, has been supportive and encouraging throughout the writing and publication process. Thanks to the power of electronic communication, he and I have remained in close contact even though he is in Oxford, England, and I in Dartmouth, Massachusetts. I compliment Geoff and the publication staff at Elsevier for their efficiency in producing this volume in a remarkably short time.

During the writing of this book I received the cooperation of many other individuals in the geothermal community and elsewhere who generously granted

permission for me to use their previously published works, to reprint their photographs, who helped track down elusive references, and who offered suggestions that I believe improved the content and presentation of the material.

At the risk of inadvertently offending an overlooked colleague, I am indebted to the following individuals: Stefano Bellani and Marnell Dickson (IGG/CNR), Guido Cappetti, Adolfo Fiordelisi and Iris Perticone (Enel GreenPower), Jamie Claire and Tsuyoshi Yamada (Toshiba), Julie Gonzalez and Christine Hopf-Lovette (EPRI), Steve Cole (Memphis, TN), Paige Gibbs (UMass Dartmouth), Luis Gutiérrez-Negrín (CFE), Shaun Hardy (Carnegie Inst.), Tom Haynes (Hughes Christensen), Susan Hodgson (CA DOGG, ret.), Roland Horne (Stanford U.), Donald Hudson (Reno, Nevada), Eduardo Iglesias (IGA), John Jacobson (Kuster), Marcelo Lippmann (LBNL), Kenneth McCombs (McGraw-Hill), Ed McCrae, Shunji Nakamura and Ricky Takada (MHIA), Dick Meeuwig (Nevada BMG), David Michetti (Calpine), Paul Moya (ICE), Oleg Povarov (Assn. Geothermal Energy Soc.), Andrea Rossetto (Torreglia, Italy), Paolo Santini (GE-Florence), Subir Sanyal (GeothermEx), Dan Schochet and Graciela Sapiro-Goldman (Ormat), Marlene Vogelsang (PG&E), and François-D. Vuataz (U. Neuchâtel).

Lastly, I thank my wife, Joan, for her patience, understanding, and support throughout the many months of my self-imposed exile as this work took shape. She was always eager to read drafts and could be counted on to offer valuable suggestions for a clearer exposition of the subject matter.

Ronald DiPippo

Dartmouth, Massachusetts

March 2005

Part 1



RESOURCE IDENTIFICATION AND DEVELOPMENT

- Geology of Geothermal Regions
- Exploration Strategies and Techniques
- Geothermal Well Drilling
- Reservoir Engineering

A man must stand in fear of just those things that truly have the power to do us harm, of nothing else, for nothing else is fearsome.

Dante Alighieri, *The Divine Comedy: The Inferno*—1306–1321

The first part of the book deals with the geological aspects of geothermal resources—how the forces of nature shaped the earth in a way to create reservoirs capable of supplying energy for geothermal power plants. We discuss the means to identify and characterize geothermal prospects, and the techniques for drilling wells into geothermal formations to extract the hot fluids for use in power stations. The last part of this section of the book examines the physical principles of fluid flow through the porous rocks that constitute the reservoir, and the modern computer simulation methods that are used to model the behavior of the reservoirs.

2 Geothermal Power Plants



Volcan Rincon de la Vieja, Guanacaste province, Costa Rica.

Location: 10.8N, 85.3W

Elevation: 6,286 feet (1,916 m)

Photo by Federico Chavarria Kopper, published by Smithsonian Inst. Global Volcanism Program website: <http://www.volcano.si.edu/world/volcano.cfm?vnum=1405-02> [WWW].



Volcan Pacaya, Guatemala (foreground)

Location: 14.38N, 90.60W

Elevation: 8,371 feet (2,552 m),
and Volcan Agua (background)

Location: 14.5N, 90.7W

Elevation: 12,333 feet (3,760 m)

Ref: Volcano World, U. of N. Dakota.

http://volcano.und.nodak.edu/vwdocs/volcimages/south_america/guat/pacaya.html [WWW].



Chapter 1

Geology of Geothermal Regions

Chapter Outline

1.1 Introduction	3
1.2 The Earth and its Atmosphere	4
1.3 Active Geothermal Regions	7
1.4 Model of a Hydrothermal Geothermal Resource	10
1.5 Other Types of Geothermal Resources	12
1.5.1 Hot Dry Rock	12
1.5.2 Geopressure	14
1.5.3 Magma Energy	15
1.5.4 Deep Hydrothermal	17
1.5.5 Low Temperature	18
References	19
Problems	21

Birth and death. Like us, geothermal features begin and end, moving through cycles of their own. We draw towards them, lured by change, beauty, and an unusual cast of the familiar—water, rocks, and heat. We search them for answers to mysteries in our own lives, like birth and death.

Susan F. Hodgson—1995

1.1 Introduction

Geothermal energy—Earth's heat—can be found anywhere in the world. But the high-temperature energy that is needed to drive electric generation stations is found in relatively few places. The purpose of this opening chapter is to provide the geologic framework within which high-temperature geothermal resources can be understood, both with regard to their occurrence and their nature.

Readers who are unfamiliar with the rudiments of Earth science may wish to consult any of the standard texts on the subject, for example, Refs. [1–4]. Those interested in the history of geologic thought, dramatic geological events, and

ancient geothermal energy usage will find fascinating reading in Refs. [5–8]. W.A. Duffield provides an excellent, brief introduction to modern geologic theory of volcanoes in a beautifully illustrated book [9]. In selecting general texts on geology, one must be aware that any book written before 1970 will not include the most recent thinking on the structure of the Earth and the dynamic mechanisms that give it its life. We refer to the theory of plate tectonics, now universally accepted, which provides us with the basic tools to understand the origins of high-temperature geothermal resources.

1.2 The Earth and its Atmosphere

In 1915 A.L. Wegener (1880–1930) put forth a highly controversial theory of continental drift in the first edition of his book, *The Origin of Continents and Oceans* [10]. Although he elaborated on it in later editions of his book in 1920, 1922, and 1929, the controversy persisted. His theory was motivated by the observation that the continents, particularly South America and Africa, seemed to be pieces of a global jigsaw puzzle that had somehow been pulled apart. He reasoned that all land masses were once connected in a gigantic supercontinent he named “Pangaea.” He posited that the now separated continents floated and drifted through a highly viscous sea floor. This part of his theory was later proved incorrect but the basic notion of drifting continents was right. Wegener’s problem was in identifying correctly the forces that ripped apart the pieces and in fact keeps them moving.

Studies that began in the 1950s and continued into the 1960s matched the ages of rocks found along the northeastern coast of South America and the northwestern coast of Africa [11]. The correlation of rock ages ran from Recife in Brazil to Trinidad off the coast of Venezuela on the South American side and from Luanda to Sierra Leone on the African side. Oceanic research also showed that new land was being created on either side of the mid-Atlantic Ridge, the so-called “sea-floor spreading” phenomenon [12]. By dating these deposits, Earth scientists were able to confirm the movement of the vast plates that constitute the crust of the Earth. Continents are part of the crust and have been in constant motion since the beginning of the Earth some 4.5 billion years ago.

An excellent animation of this motion starting about 740 million years ago can be viewed at the web site of the University of California at Berkeley’s Museum of Paleontology [13]. From this animation it is clear that Pangaea existed as a supercontinent for only a blink of geological time, around 200 million years ago, having itself been formed from the collision of several land masses beginning in the Precambrian era.

While there is no controversy today over the theory of plate tectonics, there remains much uncertainty about the detailed structure of the inner Earth. A great deal of research has gone into exploring and characterizing the Earth's atmosphere but only one or two projects have aimed at probing the depths of the Earth. One of them, Project Moho, intended to drill through the thinnest part of the oceanic crust (about 5 km thickness) to enter the mantle. In 1909 Croatian scientist A. Mohorovičić (1857–1936) had observed, at a certain depth, a discontinuity in the velocity of seismic waves caused by earthquakes. He deduced that this represented a boundary between the generally solid crust and the generally molten mantle. This interface has become known as the Mohorovičić Discontinuity (or simply the Moho) in his honor [1]. However, Project Moho was halted in 1966 apparently for lack of funds and produced no results.

Another deep drilling effort, the Salton Sea Deep Drilling Program, ran from 1984 to 1988 with funding from the U.S. Department of Energy (DOE) but failed to achieve much [14,15]. One well was drilled to a total depth of 10,564 ft but suffered a collapsed liner at 6380 ft. Although this was later repaired, the deepest measurements were taken at 5822 ft and indicated a temperature of roughly 290°C. Neither the depth nor the temperature was particularly remarkable given the state of geothermal drilling at the time. At the conclusion of this effort, the following problems were cited as serious barriers to any future deep drilling program (to say, 50,000 ft): extremely high temperatures in the well, loss of control of the orientation of the well, lost circulation of drilling fluids, and fishing for equipment lost downhole.

Currently there is an international consortium of 11 countries called the International Continental Scientific Drilling Program (ICDP) [16] that funds projects to give insight into Earth processes and to test geologic models. The Drilling Project of Cretaceous Songliao Basin (DPCSB) was started on April 13, 2014 using a drill rig with a depth capability of 10,000 m. The objective is to recover a sedimentary record from the Cretaceous that will shed light on the earth's response to geological events and improve our understanding of the mechanism of climate change [17].

Thus our knowledge of the planet Earth beyond a depth of a few kilometers is based on indirect evidence. What we accept as the model for the Earth's inner structure is burdened with uncertainty, particularly the temperature as a function of depth. Table 1.1 summarizes the model of the Earth and its atmosphere; shown are the distances from the surface of the Earth to each significant layer, the temperature thought to exist there, and the density. The crustal thickness is for continental areas; oceanic crusts are much thinner, about 7–10 km on average. The wide spread in the temperatures at the deepest levels reflects the speculative nature of these estimates.

TABLE 1.1 Data on the earth and its atmosphere from various sources.

Region	Distance from surface km	Temperature °C	Density g/cm ³
Thermosphere	300	1125	3.6×10^{-14}
Mesosphere	85	-95	2×10^{-8}
Stratosphere	50	0	1×10^{-6}
Troposphere	12	-60	3×10^{-4}
Surface	0	10	2.7 continental
Crust	35	1100	3.0 oceanic
Mantle	2900	3700 to 4500	3.3
Liquid (iron) core	5100	4300 to 6000	5.7 to 10.2
Solid inner (iron) core	6350	4500 to 6600	11.5
(center)			11.5

Distances are not shown to scale.

These layers are usually depicted as concentric spheres, much like the inside of a golf ball, in ultra-simplified schematics. However, the interfaces are likely so irregular and the boundaries so fuzzy that such a representation is misleading.

Sometimes the analogy is drawn between the Earth and a chicken's egg, with the Earth's crust compared to the shell of an egg. Relating the thickness of the Earth's crust, 35 km for continental regions, to its diameter, roughly 12,700 km, we get a ratio of 35/12,700 or 0.00276. If we apply the same ratio to an egg with a diameter of say, 50 mm, we would find a shell thickness of 0.138 mm or 0.0054 in. In fact the shell of an egg is about 1/64 in or about 0.016 in. Thus an egg's shell is about three times thicker proportionally than the crust of the Earth. Put in other words, if the Earth's crust was in proportion to the shell of an egg, it would be about 100 km thick instead of 35 km.

Since the temperature at the base of the crust is about 1100°C, the temperature gradient between the surface (assuming a surface at 10°C) and the bottom of the crust is 31.1°C/km or about 3.1°C/100 m. This is usually taken as the normal conductive temperature gradient. Good geothermal prospects occur where the thermal gradient is several times greater than normal. The rate of natural heat flow per unit area is called the normal heat flux; it is roughly 1.2×10^{-6} cal/cm²·s, in nonthermal areas of the Earth.

The Earth's crust is composed of various types of rocks which contain some radioactive isotopes, in particular, uranium (U-235, U-238), thorium (Th-232), and potassium (K-40). The heat released by these nuclear reactions is thought to be responsible for the natural heat that reaches the surface. Table 1.2 lists three rock types and their radioactive constituents.

TABLE 1.2 Radioactive elements in common rocks in the Earth's crust.

Rock	Concentration			Heat generation, 10^{-6} cal/g · year		
	U, ppm	Th, ppm	K, %	U	Th	K
Granite	4.7	20	3.4	3.4	4.0	0.9
Basalt	0.6	2.7	0.8	0.44	0.54	0.23
Peridotite	0.016	0.004	0.0012	0.012	0.001	0.0003

These basic ideas are enough for us to move on to explore how the motion of the tectonic plates creates the conditions favorable for the exploitation of geothermal energy.

1.3 Active Geothermal Regions

The relative motion of plates, of any size, gives rise to several possible interactions. These are shown in Figure 1.1.

When a plate comes under compression, it can relieve the stress by folding, by cracking and thrusting one piece upon the next, by cracking and trenching beneath the next, and by thickening. Trenching or subduction is one of the most important mechanisms that give rise to high-temperature geothermal regions. When a plate is subjected to tension, it can relieve the stress by cracking open and rifting, by cracking in several places leading to down-dropping, and by thinning. All of these responses to tension lead to anomalous geothermal regions that may be conducive to exploitation.

Two plates may also slide past each other along what is called a transform fault, perhaps the most famous of which is the San Andreas Fault running along much of the length of California in the United States [18]. While this fault, and others related to it, have caused immeasurable harm and financial loss from numerous earthquakes, it also has given rise to several commercial geothermal resources that have been beneficial.

The coincidence of earthquake zones and geothermal regions has been depicted in a National Oceanic and Atmospheric Administration (NOAA) map (see Figure 1.2) showing the collocation of these two phenomena [19]. The loci of earthquakes correspond very closely with the boundaries of the massive crustal plates that comprise the tectonic model of the Earth's surface structure.

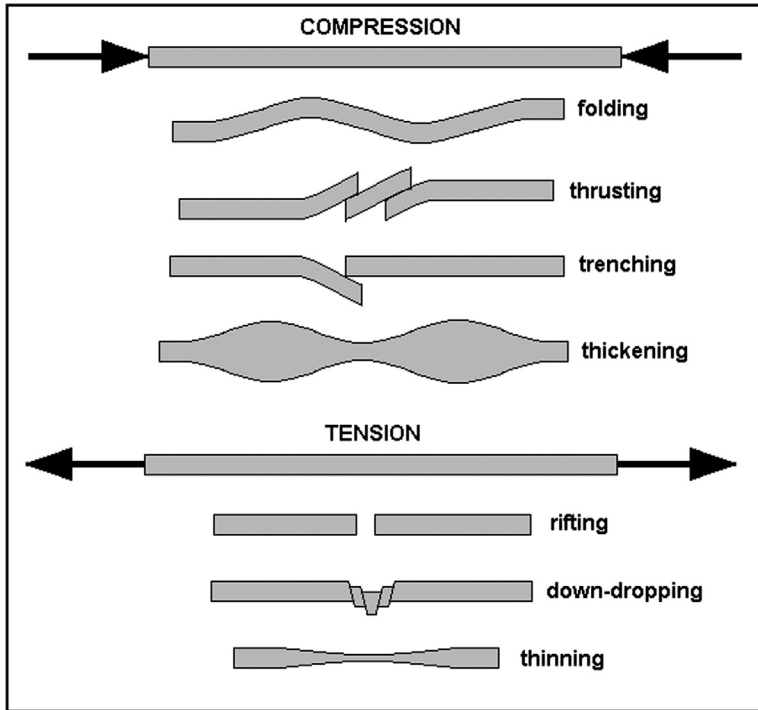


Figure 1.1 Response of plates to compression and tension.

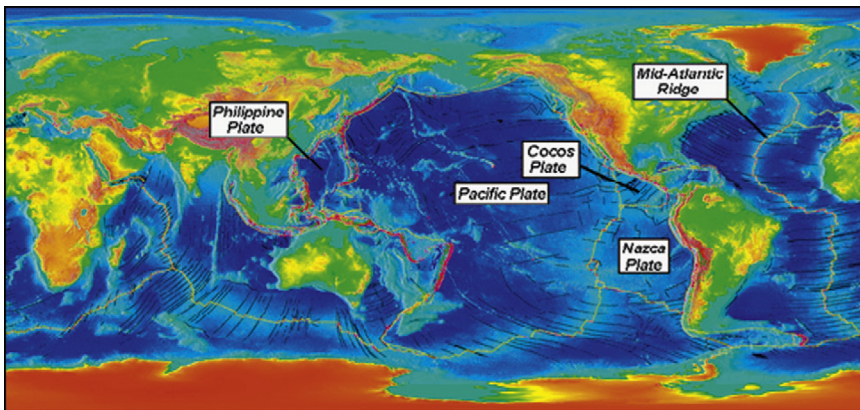


Figure 1.2 Collocation of earthquakes, tectonic plate boundaries, and geothermal regions. After Ref. [19] [WWW].

The plate boundaries experience various kinds of interactions as depicted in Figure 1.1. From the viewpoint of geothermal exploitation, the most important of these occur along the edges of the gigantic Pacific Plate, the so-called “Pacific Ring of Fire.” If we include the two adjacent eastern plates, the Cocos and the Nazca plates, as well as the western one, the Philippine Plate, then the following countries (in clockwise order) are affected: United States, Mexico, Guatemala, El Salvador, Honduras, Nicaragua, Costa Rica, Panama, Colombia, Ecuador, Peru, Bolivia, Chile, New Zealand, Micronesia, Papua New Guinea, Indonesia, Philippines, China, Japan, and Russia. All 21 of these countries have exploitable geothermal resources and 13 of them have geothermal power plants in operation as of December 2014. Generally speaking, subduction zones exist beneath all land masses in contact with the Pacific, Cocos, and Nazca plates, except the contiguous United States and Mexico where transform boundaries exist. The Alaskan Aleutian Islands lie in a subduction zone and Hawaii lies over a localized hot spot in the middle of the Pacific Plate.

The mid-Atlantic Ridge, a rift zone, is home to Iceland and the Azores, two volcanic islands that have put their geothermal resources to practical use for many years. Other regions such as the Mediterranean and Himalayan belts and the East African Rift zone also are being exploited for geothermal power.

Figure 1.3 shows a conceptual diagram of a subduction zone typical of what is found along the Central and South American coasts [20]. Oceanic crust is sliding from left to right and diving beneath the continental land mass. The shaded slab labeled lithosphere is the very upper layer of the mantle which moves as a nearly

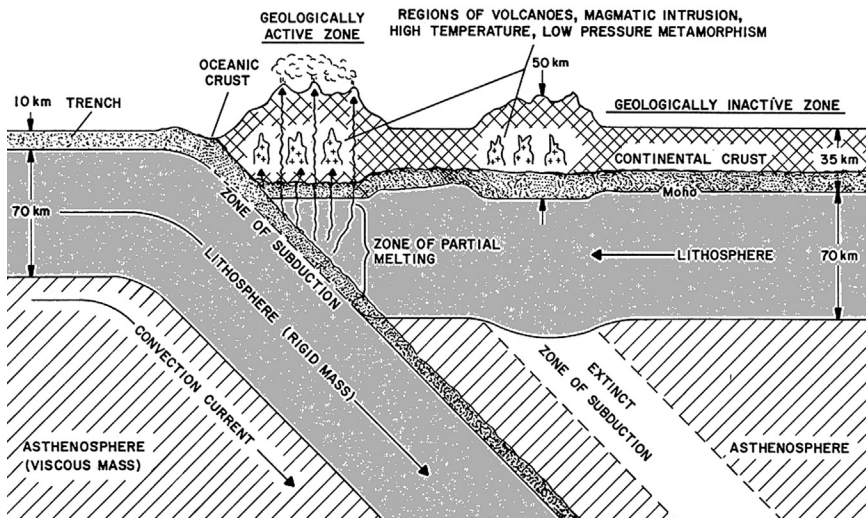


Figure 1.3 Schematic model of a trench or subduction zone. After Ref. [20].

rigid body. Below it lies the asthenosphere which is the molten but highly viscous part of the mantle. The trenching crust carries with it sea-floor sediments as it rubs against the edge of the continent. This relative motion is not smooth but marked by abrupt jolts whenever the stress built up in the interface exceeds the frictional resistance. This creates very deep-seated earthquakes that can have devastating effects. Nearly all the major cities of Central America, for example, have felt the power of such earthquakes. Partial melting of the lithosphere at the interface is believed to give rise to plutons of molten rock that tend to move upward owing to their lower density and higher temperature than the native rock. It is the emergence of these magma bodies, sometimes violently, that account for the nearly unbroken string of active volcanoes from Guatemala to the southern tip of Chile. These magmatic zones offer ample heat sources to accompany high precipitation that occurs over the region to create many potential hydrothermal geothermal systems.

An example of a nonmagmatic hydrothermal system is the geothermal province known as the Basin and Range in Nevada, United States. This geologic region was created by extensional forces that have given rise to alternating ranges of mountains separated by valleys (basins). Steep faults associated with the edges of the mountain ranges are targets for geothermal development and currently support 51 geothermal power units, totaling 336 MW, as of December 2014.

1.4 Model of a Hydrothermal Geothermal Resource

There appear to be five features that are essential to making a hydrothermal (i.e., hot water) geothermal resource commercially viable. They are:

- A large heat source
- A permeable reservoir
- A supply of water
- An overlying layer of impervious rock
- A reliable recharge mechanism.

A highly schematic depiction of such a system is shown in [Figure 1.4](#), first presented by D.E. White [21].

Cold recharge water is seen arriving as rain (point A) and percolating through faults and fractures deep into the formation where it comes in contact with heated rocks. The permeable layer offers a path of lower resistance (point B) and as the liquid heats it becomes less dense and tends to rise within the formation. If it encounters a major fault (point C) it will ascend toward the surface, losing pressure as it rises until it reaches the boiling point for its temperature (point D). There it flashes into steam which emerges as a fumarole, a hot spring, a mud pot,

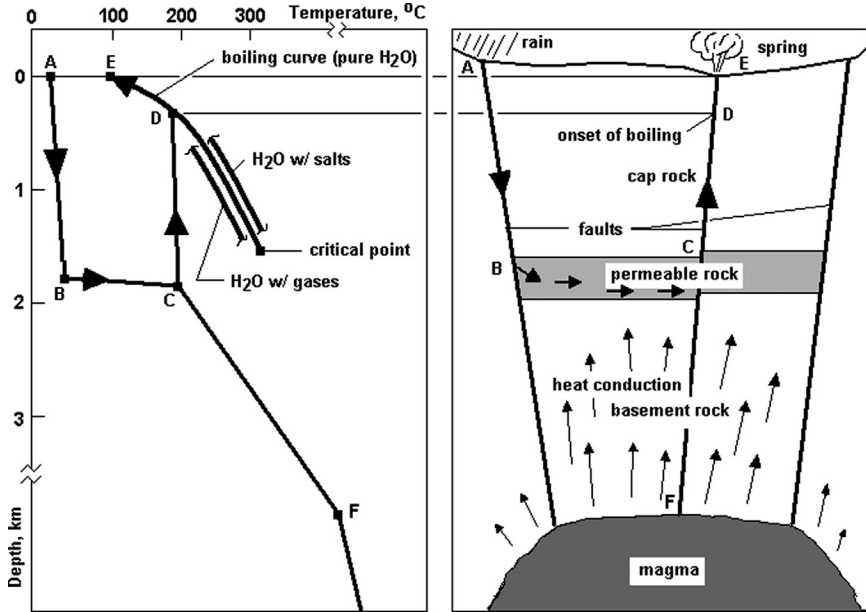


Figure 1.4 Schematic model of a hydrothermal geothermal system. *After Ref. [21].*

or a steam-heated pool (point E). The boiling curve is the locus of saturation temperatures that correspond to the local fluid hydrostatic pressure. We will have more to say about this in Chapter 4.

The intent of a geothermal development project is to locate such systems and produce them by means of strategically drilled wells. As might be presumed, most (but not all) hydrothermal systems give away their general location through surface thermal manifestations such as the ones described earlier.

If any one of the five features listed as needed for a viable hydrothermal resource is lacking, the field generally will not be worth exploiting. For example, without a large heat source geofluid temperatures will be relatively low, that is, the thermal energy of the system will be insufficient to support exploitation long enough to make it economic. Without sufficient permeability in the formation, the fluid will not be able to move readily through it, that is, it will not be able to remove much of the stored thermal energy in the rock. Furthermore, low permeability will cause poor well flow or, even worse, may prevent any production from the reservoir. Without fluid in the system there is no heat transfer medium and the thermal energy of the formation will remain in the reservoir. Without an impermeable cap rock, the geofluids will easily escape to the surface appearing as numerous thermal manifestations and the pressure in the formation will quickly dissipate. And lastly, without a reliable and ample recharge to the reservoir, the geofluid will eventually become depleted when it supplies a power plant.

With the exception of requirements (A) and (D), deficiencies in the others have been addressed through research and field practice. Insufficient permeability can sometimes be remedied by artificial means such as hydraulic fracturing (called “hydrofracking”) in which high-pressure liquid is injected from the surface through wells to open fractures by means of stress cracking. However, unless the newly created widened fractures are held open with “proppants” they will reclose when the injection ceases. If little water is present in the formation or recharge is meager, all unused geofluid from the plant can be reinjected. Furthermore, external fluids can be brought to the site by some means and injected into the formation. In Chapter 12 we will discuss such a process at The Geysers field in Northern California in the United States in which treated municipal waste water from nearby communities is sent to the field via pipeline to assist in the maintenance of an inventory of fluid in the reservoir.

1.5 Other Types of Geothermal Resources

As of 2014, hydrothermal resources are the predominant geothermal systems that have been developed commercially for electric power generation. However, there are five other forms of geothermal energy that someday may reach the large-scale commercial stage. They are: hot dry rock (HDR or enhanced geothermal systems, EGS), geopressure, magma energy, deep hydrothermal, and low-temperature systems. We will briefly describe each of these.

1.5.1 HOT DRY ROCK

There are many geothermal prospects that have high temperature but are lacking fluid in the formation or the permeability is too low to support commercial development. These systems can be “enhanced” by engineering the reservoirs through hydraulic fracturing. An injection well is drilled into the hot formation to a depth corresponding to the promising zone. Cold water is injected under high pressure to open existing fractures or create new ones. Once the formation reaches a state of sufficient volume and permeability, another well (or wells) is (are) drilled to intercept the newly formed “reservoir.” Ideally, a closed loop is thus created whereby cold water is pumped down the injection well and returned to the surface through the production well after passing through the hot, artificially fractured formation [22]. The ideal HDR concept is illustrated in [Figure 1.5](#).

Considerable research has gone into development of the HDR concept and a good deal continues today. [Table 1.3](#) summarizes some of these projects [23]. These and many other HDR (EGS) projects will be described in detail later in the book in Chapter 23, devoted entirely to this subject.

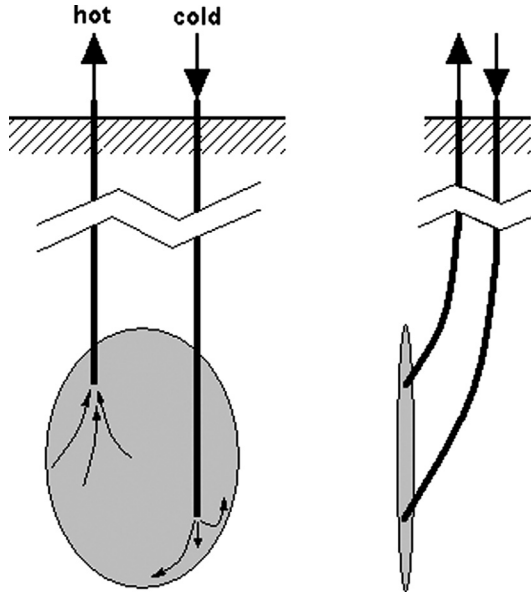


Figure 1.5 Ideal HDR production scheme.

TABLE 1.3 HDR projects worldwide [23].

Country	Location	Dates
United States	Fenton Hill, New Mexico	1973–1996
	Newberry Volcano, Oregon	2010–present
United Kingdom	Rosemanowes	1977–1991
Germany	Bad Urach	1977–1990
Japan	Hijiori	1985–2002
	Ogachi	1986–2007
France	Soultz	1987–present
Switzerland	Basel	1996–2009
Australia	Hunter Valley	2001–2015
	Cooper Basin	2002–present

There are many practical problems in developing a HDR system. It is difficult to control very deep, directional, geothermal wells. Drilling techniques in the oil industry now permit wells to be turned 90° while being drilled, allowing the well to drain several vertical pockets of petroleum. However, oil wells tend to be shallower than the ones envisioned for HDR, the temperatures encountered

are far lower, and the rocks are not as hard as those found in geothermal regions. Furthermore, the HDR wells must be precisely aimed to hit the deep target in order to form a closed fluid circuit. Lastly, if some of the engineered fractures are not connected to the production well, injected fluid may be lost to the formation. This would require continuous makeup water to maintain the power plant in operation. Some of these difficulties appear to have been at least partially solved in the ongoing research, particularly at the Japanese sites; see Chapter 23.

1.5.2 GEOPRESSURE

Along the western and northern coastline of the Gulf of Mexico, there is a potent energy resource called “geopressure.” During the drilling for oil and gas in the sedimentary coastal areas of Texas and Louisiana, fluids have been encountered with pressures greater than hydrostatic and approaching lithostatic. Hydrostatic pressure increases with depth in proportion to the weight of water, that is, at about $0.465 \text{ lbf/in}^2/\text{ft}$. However, in formations where the fluid plays a supportive role in maintaining the structure of the reservoir, the weight of the solid overburden roughly doubles the gradient to approach the lithostatic value of $1.0 \text{ lbf/in}^2/\text{ft}$.

Geopressured reservoirs were formed along the Gulf Coast through the steady deposition of sediments that created an overburden on the underlying strata. Figure 1.6 is a simplified cross-section through a geopressured reservoir.

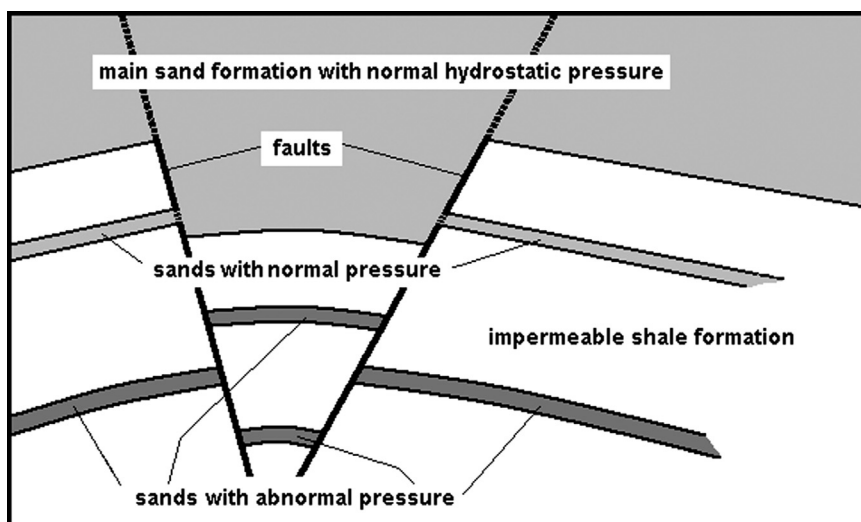


Figure 1.6 Cross-section schematic of geopressured reservoir.

Periodically, subsidence occurred causing compaction of the rock layers. Subsidence also resulted in steeply dipping faults that can isolate elements of the formation. With the heavy overburden and no way to dissipate the load, the pressure within these lenses of sand grows to levels in excess of hydrostatic.

In the geopressured reservoirs of the Gulf Coast, the pressures were sufficiently high to prevent drilling for oil and gas. With improved understanding of these zones and better drilling techniques, these reservoirs can now be safely drilled.

Geopressured reservoirs are characterized by three important properties that make them potentially attractive for geothermal exploitation: (1) very high pressure, (2) high temperature, and (3) dissolved methane.

The first property allows the use of a hydraulic turbine to extract the mechanical energy stored in the form of high pressure; the second property allows the use of a heat engine of some kind to extract the thermal energy; and the last property allows for either the combustion of the gas on site for power generation or for sale to enhance the economics of a development project.

However, there are six criteria that must be satisfied before geopressured reservoirs can be commercially developed; these are:

- Is the fluid hot enough, say $>150^{\circ}\text{C}$?
- Is there sufficient methane dissolved in the fluid?
- Is the high-pressure sand sufficiently permeable?
- Is the high-pressure sand sufficiently thick?
- Is the sand formation fault-bounded but not too fractured?
- Can we guarantee that no subsidence will occur?

The economic viability of a geopressured geothermal project requires a “yes” answer to all of these questions. In Section 9.6.3 we discuss a pilot plant that attempted to prove the concept of a geopressured geothermal plant, but this resource has yet to achieve commercial status.

1.5.3 MAGMA ENERGY

The next geothermal resource is the one that goes directly to the source of the heat, namely, a magma body relatively close to the surface of the Earth. The concept is to drill a well into the magma, insert an injection pipe, and pump cold water down the well under great pressure. The cold fluid will solidify the molten magma into a glassy substance that should crack under the thermal stress imposed on it. If the water can be made to return to the surface by passing upward through the cracked, extremely hot glassy material, it would reach the surface hot and ready for use in a Rankine-type power plant.

As simple as it is to describe the concept, it is not as easy to carry out such a plan. The U.S. DOE conducted two research projects aimed at understanding the magma environment in the 1970s and 1980s. The first one was carried out at the lava lake within the crater of Kilauea Iki on the island of Hawaii [24]. This effort succeeded in drilling through the solidified crust of the lake into the still-molten lava that had a temperature of about 1000°C (1830°F). In fact 105 m of core were obtained from the melt zone and several experiments were run to understand the mechanism of energy extraction from a lava body.

The second research program, the Magma Energy Program, was directed at obtaining a better scientific understanding of the existence and behavior of large magma bodies within calderas. The one selected for study in the mid-1980s was the Long Valley caldera in central California and the research was performed by the Sandia National Laboratory of Albuquerque, New Mexico [25]. The caldera is an oval-shaped region about 18×32 km with a prominent resurgent dome. At the time, the dome had risen some 235 mm over the period from 1980 to 1985, making it both scientifically interesting and practically important to gain a clearer understanding of the phenomenon.

The original goals of the program were to:

- Demonstrate the existence of crustal magma bodies at depths less than 25,000 ft
- Develop and test new drilling technology for hostile environments
- Better understand the creation and evolution of the Long Valley caldera
- Better define the hydrothermal system related to the caldera.

An ambitious exploration well was planned, targeted for a final depth of 20,000 ft (6000 m) [26]. The conceptual design of the well is shown in Figure 1.7 (to scale in vertical direction). Since an existing 40-in diameter mud riser was in place to a depth of 39 ft from an earlier aborted well, this was used instead of the planned 40-in surface casing. The well was to be drilled in four phases: Phase I—to 2500 ft, Phase II—to 7500 ft, Phase III—to 14,000 ft or 300°C (600°F), whichever came first, and Phase IV—to a total depth of 20,000 ft and 500°C (900°F). In 1989, Phase I was successful in reaching 2568 ft with the 20-in casing, after encountering massive lost circulation at the shallowest depths. Phase II was completed to 7588 ft in November 1991 [27]. Core samples were taken at the 2568 ft and the 7588 ft points by drilling ahead some 100–200 ft. The well was not continued beyond Phase II owing to a shift in DOE policy away from fundamental research and more toward applied research. In 1996 the well was handed over to the U.S. Geological Survey for use as a monitoring well [28].

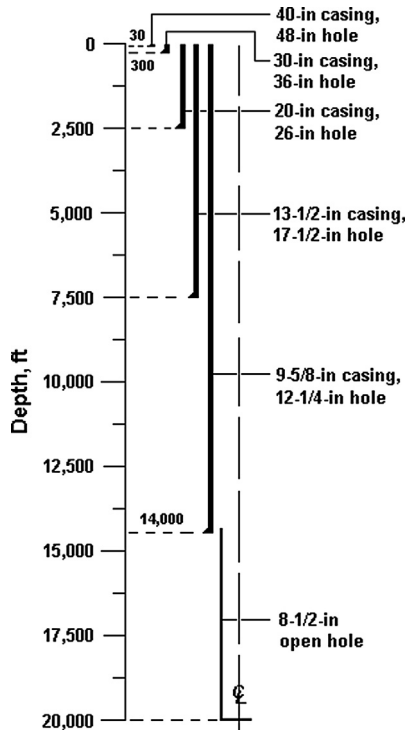


Figure 1.7 Conceptual design of Long Valley magma energy exploratory well. Vertical dimensions are shown to scale. After Ref. [26].

Since the well only reached depths that were routinely achieved at other geothermal fields, it failed to produce much new drilling technology. For example, it had been planned to develop insulated drill pipe to maintain the drilling muds at reasonable temperatures in extremely high-temperature formations; this was not done. It did produce some scientific information that led to a better understanding of the nature of the Long Valley caldera, but no further projects have appeared to try to tap the vast amount of thermal energy contained in near-surface magma bodies.

1.5.4 DEEP HYDROTHERMAL

The next of the geothermal resources is one that has only recently been accessed and developed. Deep hydrothermal resources are those that lie at depths of 2500–4000 m and deeper. They may lie in areas marked by normal geothermal temperature gradients, and as such may yield fluids at only low to moderate temperatures. For example, in a place where the gradient is say 30°C/km, fluids found at 4000 m might be in the range of 120–140°C.

Deep drilling in Europe and Australia as a part of HDR (EGS) efforts has discovered that reservoirs of fluid exist at these depths and that the formations possess some permeability. In fact, deep sedimentary layers can be exploited even without hydrofracturing the formation, although stimulation can be used to improve reservoir performance. These wells produce geofluids that can be used in energy conversion systems specifically designed for lower temperature fluids. The waste discharge fluid from the power plant may often be further utilized for direct heating of buildings and homes before being reinjected. The cost of such deep wells is significantly higher than the usual shallower geothermal wells, but with sufficient financial incentives offered by governments, private developers are able to successfully exploit what were previously thought to be uneconomic geothermal resources. Chapter 22 covers this subject in more detail.

1.5.5 LOW TEMPERATURE

A histogram of geothermal resources in the United States reveals, not surprisingly, that the vast majority are low-temperature systems; see [Figure 1.8 \[29\]](#). Roughly 59% of all known resources have temperatures less than 130°C. The worldwide distribution is probably similar. These resources are often associated with small hot springs and have been dismissed by power plant developers.

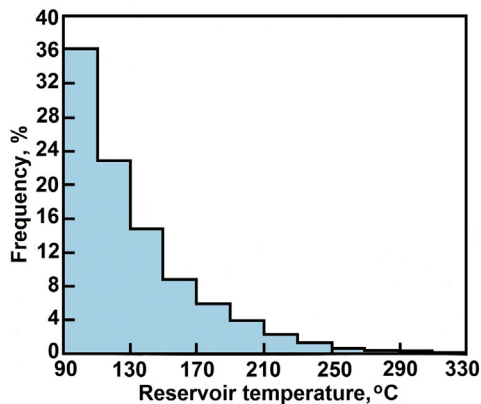


Figure 1.8 Histogram of known geothermal resources in the United States. The distribution uses 20°C intervals and is based on the best fit to the cumulative frequency. The number of resources increases exponentially as the temperature gets lower. After Ref. [29] [WWW].

A few decades ago, it was thought that geofluids needed to be about 150°C in order to be economically exploited for electric power. Of course such geofluids could be used in any number of direct heat applications; see Figure I.1, Preface to First Edition. Engineering development of binary plants, including Kalina types, together with financial incentives offered by governments have changed the picture, and in many cases allow these resources to be feasibly used for geothermal power plants. On the one hand, because they are low in temperature, these geofluids are generally less burdened with dissolved solids and are less aggressive from a corrosion and scaling standpoint. But on the other hand, having a small temperature difference between the resource and the surroundings means that the energy conversion efficiency will be very low. Consequently, large mass flow rates will be needed to generate meaningful amounts of power, leading to relatively large pieces of equipment and high specific cost, that is, high capital cost per kilowatt.

A few examples of small power plants with low-temperature geofluids include Chena Hot Springs (Alaska) with 74°C geofluid, Husavik (Iceland) with 121°C geofluid, Paisley (Oregon) with 113°C geofluid, and Oregon Institute of Technology with 91°C geofluid.

Furthermore, the use of coproduced waters from oil and gas wells can be included in this category, such as at the demonstration unit at the Rocky Mountain Oilfield Testing Center (RMOTC) that generated an average of 171 kW from 47 kg/s of 91°C water [30]. Although the thermal conversion efficiency is extremely low, 1–2%, the resource is a waste stream that would otherwise be put to no good use. The cumulative amount of similar coproduced fluids in the United States alone is staggering and represents from 4600 to 22,000 MW of electricity, depending on the waste water temperature.

References

- [1] Leet LD, Judson S, Kauffman ME. *Physical geology. 5th ed.* Englewood Cliffs, NJ: Prentice-Hall; 1978.
- [2] Plummer CC, McGeary D, Carlson DH. *Physical geology. 8th ed.* New York, NY: McGraw-Hill Comp. Inc.; 2001.
- [3] Press F, Siever R. *Earth. 2nd ed.* San Francisco, CA: W.H. Freeman and Company; 1978.
- [4] Tarbuck EJ, Lutgens FK. *Earth science. 8th ed.* Englewood Cliffs, NJ: Prentice-Hall; 1997.
- [5] Cataldi R, Hodgson SF, Lund JW, editors. *Stories from a heated earth: our geothermal heritage.* Sacramento, CA: Geothermal Resources Council and International Geothermal Association; 1999.
- [6] Sigurdsson H. *Melting the earth: the history of ideas on volcanic eruptions.* New York, NY: Oxford University Press; 1999.
- [7] Krafft M. *Volcanoes: fire from the earth.* Discoveries, Harry N. Abrams, Inc., Publishers; 1993.

- [8] Winchester S. *Krakatoa: the day the world exploded: August 27, 1883*. New York, NY: HarperCollins; 2003.
- [9] Duffield WA. *Volcanoes of Northern Arizona: sleeping giants of the Grand Canyon region*. Grand Canyon, AZ: Grand Canyon Association; 1997.
- [10] Waggoner BM. Alfred Wegener (1880–1930). University of California Berkeley Museum of Paleontology, <<http://www.ucmp.berkeley.edu/history/wegener.html>>; 1996.
- [11] Hurley PM, Rand JR. Review of age data in West Africa and South America. In: Phinney RA, editor. *The history of the earth's crust*. Princeton, NJ: Princeton University Press; 1968.
- [12] Wilson JT. "Continental Drift", Offprint No. 868. *Scientific American*. San Francisco, CA: W.H. Freeman and Company; April, 1963.
- [13] University of California Berkeley Museum of Paleontology, <<http://www.ucmp.berkeley.edu/geology/anim1.html>>; 1999.
- [14] Anon. Salton sea scientific drilling program monitor. U.S. Department of Energy, Issues 1–5, October 1995–April 1996.
- [15] Anon. Salton sea scientific drilling program quarterly reports No. 1–11, October 1984–January 1988.
- [16] <http://www.ICDP-Online.org>.
- [17] Songliao Basin Drilling Project, International Continental Scientific Drilling Program, <<http://www.icdp-online.org/projects/world/asia/songliao-basin/>>.
- [18] Anderson DL. "The San Andreas Fault", Offprint No. 896 5. *Scientific American*, vol. 225. San Francisco, CA: W.H. Freeman and Company; November 1971. p. 52–66.
- [19] Reprinted and modified from National Oceanic and Atmospheric Administration, National Geophysical Data Center, Boulder, CO, <<http://www.ngdc.noaa.gov/mgg/global/relief/SLIDES/JPEGfull/Slide18.jpg>>; May 10, 2004.
- [20] DiPippo R. *Geothermal Energy as a Source of Electricity: A Worldwide Survey of the Design and Operation of Geothermal Power Plants*, U.S. Dept. of Energy, DOE/RA/28320-1. Washington, DC: U.S. Gov. Printing Office; 1980.
- [21] White DE. Characteristics of geothermal resources. In: Kruger P, Otte C, editors. *Geothermal energy: resources, production, stimulation*. Stanford, CA: Stanford University Press; 1973.
- [22] Smith MC. The hot dry rock program. *Los Alamos science*. Winter/Spring; 1983. p. 86–87.
- [23] Development of a Hot Dry Rock Power Generation System. New Energy and Industrial Technology Development Organization, Kanagawa, Japan, <<http://www.nedo.go.jp/chinetsu/iea/ann3e.htm>>; 2004.
- [24] Hardee HC, Dunn JC, Hills RG, Ward RW. Probing the melt zone of Kilauea Iki lava lake, Kilauea volcano, Hawaii. *Geophys Res Lett* 1981;8(12):1211–14.
- [25] Chu TY, Dunn JC, Finger JT, Rundle JB, Westrich HR. The magma energy program. *Geothermal Resour Coun Bull* 1990;19(2):42–52.
- [26] Finger JT, Eichelberger JC. "The magma energy exploration well". *Geothermal Resour Coun Bull* 1990;19(2):36–41.
- [27] Anon. Phase II drilling at Long Valley Exploratory well completed, *Geothermal Progress Monitor*, Report No. 14, DOE/CE-0394, U.S. Dept. of Energy; 1992. p. 6.
- [28] Anon. Transfer of Long Valley well on schedule, *Geothermal Progress Monitor*, Report No. 18, DOE/EE-0121, U.S. Dept. of Energy; 1996. p. 8.
- [29] Muffler LJP, editor. *Assessment of geothermal resources of the United States—1978*. *Geol. Survey Circ*. 790, U.S. Geological Survey; 1979.
- [30] Williams T, et al. Operational results for co-production of electricity from oilfield operations. Presentation at AAPG 2012 Convention, NREL/PR-2000-57088; April 24, 2012.

Problems

- 1.1. It has been suggested that the radioactive decay of certain elements in the earth's crust can account for the observed normal heat flux at the surface. Assume the crust is made only of granite containing certain amounts of uranium, thorium, and potassium. The average heat flux at the surface of the earth is about $1.5 \times 10^{-6} \text{ cal/cm}^2 \cdot \text{s}$. Calculate the thickness of crust needed to give this heat flux using data given in [Table 1.2](#). Compare your calculated thickness with the actual thickness, and discuss the reasonableness of this theory.
- 1.2. In Problem 1.1, we discussed the possibility that the normal heat flux through the earth's crust is caused by radioactive decay of certain elements. Let us consider a different possibility, namely, that heat conduction from the hot molten mantle through the crust might give rise to the normal (not anomalous) heat flux. Use Fourier's law of one-dimensional heat conduction (i.e., that the heat flux is proportional to the temperature gradient times the thermal conductivity), choose a reasonable value for the thermal conductivity of the rock comprising the crust, and calculate the required temperature difference to produce the observed normal heat flux. What temperature do you find, therefore, at the bottom of the crust? Interpret your finding.
- 1.3. In continental areas, the average geothermal heat flux is about $1.2 \times 10^{-6} \text{ cal/cm}^2 \cdot \text{s}$. Assume that three-fourths of this is attributed to the crust. Using an average thermal conductivity for rock, calculate the temperature (above the average surface temperature) at the Moho.
- 1.4. In the center of the East Mesa geothermal field in southern California, there is a high heat flux anomaly, reaching about seven times higher than normal. Perhaps this is caused by a magma intrusion inside the crust. Assuming the magma has a temperature of about 1000°C , estimate the depth of the magma intrusion. The surface temperature is about 35°C on average.
- 1.5. It is often said that geothermal fluids must exceed 150°C in order to be practical for generating electricity. Allowing a surface temperature of 25°C , how deep must one drill to hit this temperature at a location having a normal temperature gradient.
- 1.6. Write a short essay describing a typical hydrothermal geothermal system. Consider a liquid-dominated reservoir; include a geological cross-section through the reservoir. Show a typical temperature-depth curve and explain its features. List the requirements for the site to be viable for long-term electric power production.

22 Geothermal Power Plants

- 1.7. Write a short essay on the origins and nature of geothermal energy from a global perspective. Give a thorough discussion of the theory of plate tectonics. Discuss the source of the normal geothermal temperature gradient and normal heat flux received at the surface of the earth. List and describe as many surface thermal manifestations of anomalous geothermal behavior as you can.
- 1.8. Using the Internet, research the origins and nature of the magma-type of geothermal energy. Write a short essay on the geologic environment, typical characteristics of the resource, status of commercial development and prospects for continued development, impediments to widespread use, potential environmental impacts, etc. Include sketches and schematic diagrams wherever appropriate to illustrate your essay.
- 1.9. Using the Internet, research the origins and nature of the HDR (or EGS)-type of geothermal energy. Write a short essay on the geologic environment, typical characteristics of the resource, status of commercial development and prospects for continued development, impediments to widespread use, potential environmental impacts, etc. Include sketches and schematic diagrams wherever appropriate to illustrate your essay.
- 1.10. A heat-flow map of the Northeast United States shows a localized anomaly near the town of Conway, New Hampshire. Research this area using the Internet and describe the source for the anomaly. Using an inferred temperature gradient of $2.36^{\circ}\text{C}/100\text{ m}$ beginning at a depth of 15 m below the surface where the year-round temperature is about 8°C , calculate the depth needed to reach the following temperatures commonly associated with standard types of geothermal power plants: (a) 120°C (very low-temperature binary plants); (b) 150°C (typical binary plants); (c) 200°C (low-temperature flash plants); (d) 250°C (typical flash plants). Finally, discuss the practicality of using this resource for power generation.
- 1.11. Using the Internet, research the origins and nature of the geopressed-type of geothermal energy. Write a short essay on the geologic environment, typical characteristics of the resource, status of commercial development and prospects for continued development, impediments to widespread use, potential environmental impacts, etc. Include sketches and schematic diagrams wherever appropriate to illustrate your essay.
- 1.12.
 - a. Describe the three major types of interactions between adjacent crustal plates according to the theory of plate tectonics. Include simple sketches to illustrate your answer.
 - b. Describe how each of these interactions may give rise to geothermal anomalies.
 - c. Name at least one currently exploited geothermal area (i.e., generating electrical power) associated with each of the three types.



Chapter 2

Exploration Strategies and Techniques

Chapter Outline

2.1 Introduction	23
2.2 Objectives of an Exploration Program	24
2.3 Phases of an Exploration Program	25
2.3.1 Literature Survey	25
2.3.2 Airborne Survey	26
2.3.3 Geologic Survey	27
2.3.4 Hydrologic Survey	30
2.3.5 Geochemical Survey	30
2.3.6 Geophysical Survey	35
2.4 Synthesis and Interpretation	40
2.5 The Next Step: Drilling	41
References	41
Problems	43

For a successful technology, reality must take precedence over public relations, for Nature cannot be fooled.

Richard P. Feynman—1988

2.1 Introduction

It has been said that there are no commercial geothermal fields that could not have been discovered by an intelligent layperson. If this were true, then the strategies and sophisticated techniques we will discuss in this chapter would be unnecessary.

While it is certainly true that nearly all successful geothermal projects are at sites where thermal manifestations existed, it is nevertheless a fact that many false steps have been taken in developing these fields—before the introduction of systematic exploration programs. In the early days of the geothermal industry, it

was common to drill wells close to thermal manifestations such as fumaroles, hot springs, mud pots, and even geysers. The result was usually the extermination of the manifestations, perhaps some short-term production from the well, but often the true source of the geothermal energy was missed.

The scientific tools that are now available and routinely used at geothermal prospects allow for better characterization of the resource before the costly phase of deep well drilling. By defining the subsurface nature of the field, a more reliable determination of drilling sites can be made, increasing the probability of a successful discovery well and of a successful field development campaign.

2.2 Objectives of an Exploration Program

There are five things a geothermal exploration program should accomplish:

- Locate areas underlain by hot rock.
- Estimate the volume of the reservoir, the temperature of the fluid in it, and the permeability of the formation.
- Predict whether the produced fluid will be dry steam, liquid, or a two-phase mixture.
- Define the chemical nature of the geofluid.
- Forecast the electric power potential for a minimum of 20 years.

As mentioned most geothermal fields are marked by thermal features that give away the fact that there is a heat source somewhere in the vicinity. Even without gushing outlets of hot fluids, the ground itself may be hotter than normal. Without the heat supply there will be no geothermal resource.

Unless a significant volume of permeable rock exists, any production from the reservoir will be small and short-lived, and unless a reasonable minimum fluid temperature can be assured, the energy production will be too small to make the project commercially viable.

The physical and chemical properties of the geofluid under production conditions are important in deciding on the feasibility of a power project. It may be difficult to obtain this information without drilling wells, but a good exploration program should give a reasonable estimate for these properties. The ultimate exploration tool is the drilling of deep wells based on the findings of the scientific surveys.

The last bulleted item is the main outcome of the exploration phase, namely, can the field be expected to support a geothermal power plant of a certain capacity for a sufficient period of time to convince investors that the project will be worthwhile.

2.3 Phases of an Exploration Program

In this section we describe the usual steps in a full exploration program. As mentioned, the site may be fairly promising based on prior observations, but these steps are necessary to fully characterize the resource. In typical chronological order, the phases are:

1. Literature survey
2. Airborne survey
3. Geologic survey
4. Hydrologic survey
5. Geochemical survey
6. Geophysical survey.

We could have included drilling as the final phase of the exploration program, but we include here only the geoscientific studies that lead up to the drilling phase. Some of the scientific phases may be combined to save time and to create synergy among the various investigations. It is clear from the wide range of disciplines cited in the listing, that a team of individuals from one or more companies with appropriate expertise is needed to carry out the exploration of a geothermal prospect. Let us examine each of these phases in some detail.

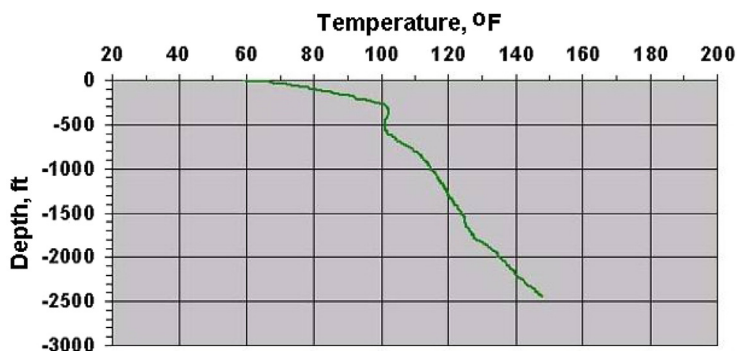
2.3.1 LITERATURE SURVEY

It is likely that someone at some time has taken a look at whatever site is now under consideration. With the use of the Internet, it is an easy matter to search the existing literature for prior studies. There are now extensive databases online for most geothermal prospects. For example, Ref. [1] provides information on hot springs in the United States and several other countries. Ref. [2] contains data on all wells and springs with temperatures greater than 20°C for the following states in the United States: Alaska, Arizona, California, Colorado, Idaho, Montana, Nebraska, Nevada, New Mexico, North Dakota, Oregon, South Dakota, Texas, Utah, Washington, and Wyoming. A total of 11,775 sites are included. There is also a compilation of chemical information for the fluids at each of these springs and wells.

The United States Geological Survey (USGS) maintains an excellent database for wells drilled in the United States [3]. For example, one can find well log data for many wells drilled in Nevada [4]; Table 2.1 and Figure 2.1 illustrate the type of information that is available there [5]. A large body of data can also be found at the USGS web site [6]. For sites that may not have made their way onto the Worldwide Web, a trip to a local library or town hall will often turn up interesting reports on regional sites. With this type of information in hand, the remaining phases can be planned more effectively.

TABLE 2.1 Well data for Fish Lake Valley well FPL-1 [5].

<i>Well ID:</i>	FLP-1	<i>Log Date:</i>	12/4/92	<i>County, State:</i>	Esmeralda, NV
<i>Latitude:</i>	37°55.3'	<i>Longitude:</i>	117°59.4'	<i>Elevation (ft):</i>	5300
<i>Company:</i>	Magma Power	<i>Prospect:</i>	Fish Lake Valley		

**Figure 2.1** Temperature profile for Fish Lake Valley well FPL-1 [5] [WWW].

2.3.2 AIRBORNE SURVEY

Aerial photography of the prospective site can yield the following information:

- Structural nature of the field
- Locations of thermal anomalies and manifestations (via infrared imaging, IR)
- Aeromagnetic data
- Geographic benchmarks to guide later ground surveys
- Geologic mapping (in conjunction with geologic survey).

The use of stereographic images can reveal the surface expression of faults that are very important in defining the possible avenues of fluid flow through the formation. Warm ground will show up in IR photographs; if the area receives snowfall, the same information is clearly visible from patterns of snow melt. IR surveys can consist of color photographs in the 1–2 μm wavelength range, false-color photographs, or IR scanning using either 3–5 μm or 8–14 μm wavelengths [7]. To be useful, an IR survey ought to be able to detect very small temperature anomalies, of the order of 0.05–0.5°C over areas of up to hundreds of square kilometers. A rise of 0.5°C over the normal background would be the result of a heat flux about 50 times greater than the normal heat flux. Also a reliable IR survey must be able to distinguish a true geothermal effect from one caused by weather, hydrology, terrain, or topography [8,9].

Aeromagnetic measurements are thought to reveal areas of hydrothermally altered rock because the process changes magnetic rock to nonmagnetic rock. Thus a magnetic low is interpreted as evidence of possible hot geothermal fluids. However, there are enough cases where this method has not been definitive in outlining a hydrothermal area that a magnetic low by itself is not considered sufficient; it should be integrated with the results of other methods. Reliable aeromagnetic data may be used to help validate and constrain numerical models of the reservoir at a later stage of development; see Chapter 4.

2.3.3 GEOLOGIC SURVEY

A geologic survey is usually the first work to be conducted “on the ground” and aims at detecting and characterizing the following:

- Tectonic and stratigraphic setting
- Recent faulting
- Distribution and age of young volcanic rocks
- Location and nature of thermal manifestations
- Hydrothermally altered ground and rocks.

This phase is typically conducted by a geovolcanologist, a geologist with special training and experience in volcanic systems. The history of the creation and evolution of the site over geologic time is of more than scientific interest; it can offer insights into the present, unseen state of the deep formation. Many geothermal fields owe their existence to past volcanism, sometimes fairly recent. The eruption history, including the timing of events, the nature and volume of the material ejected, and the extent of the debris field, all contribute to the full picture. In a sense, the geologist is in the odd position of having to foretell the past to explain the present.

Two products of the geologist’s work are a geologic map of the area and the first draft of conceptual model for the hydrothermal system. The geologic map is a large-scale, multicolor rendering of the types of rocks that appear at the surface. An example of a geologic map is given in [Figure 2.2](#). This is an excerpt from the full map for the Long Valley caldera in California, provided by the USGS [\[10\]](#); the reader may wish to explore the full map in more legible detail by accessing the USGS web site at Ref. [\[10\]](#).

[Figure 2.3](#) is such a detailed view for the northwest section of the caldera. Note that Interstate Highway Rt. 395 runs across the middle of the map in a NW–SE direction. Each colored area represents a different kind of rock unit (type and age) at the surface, lines are drawn to show the type and location of contacts and faults, and strike and dip symbols show, respectively, the planar

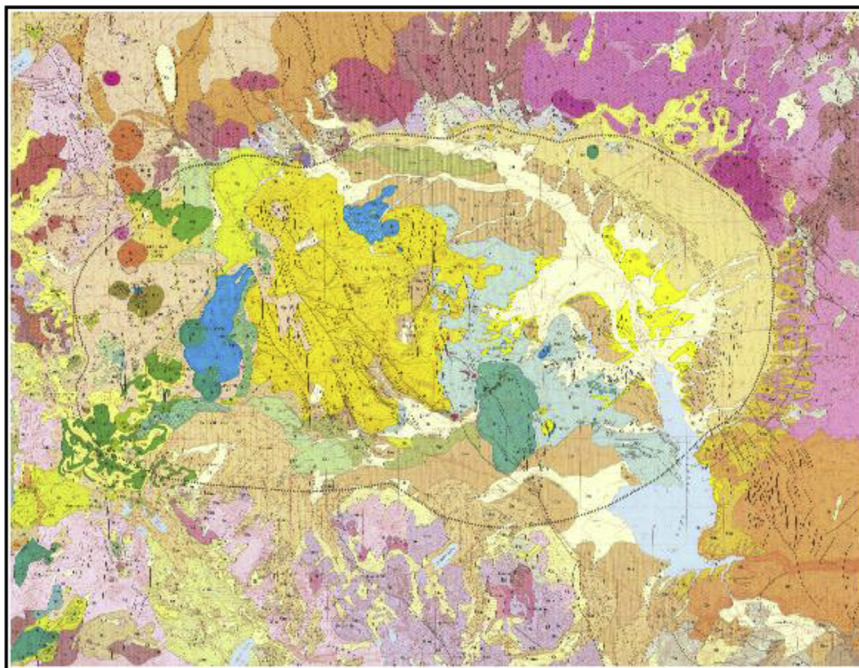


Figure 2.2 Excerpt of geologic map of the Long Valley caldera, California [10] [WWW].

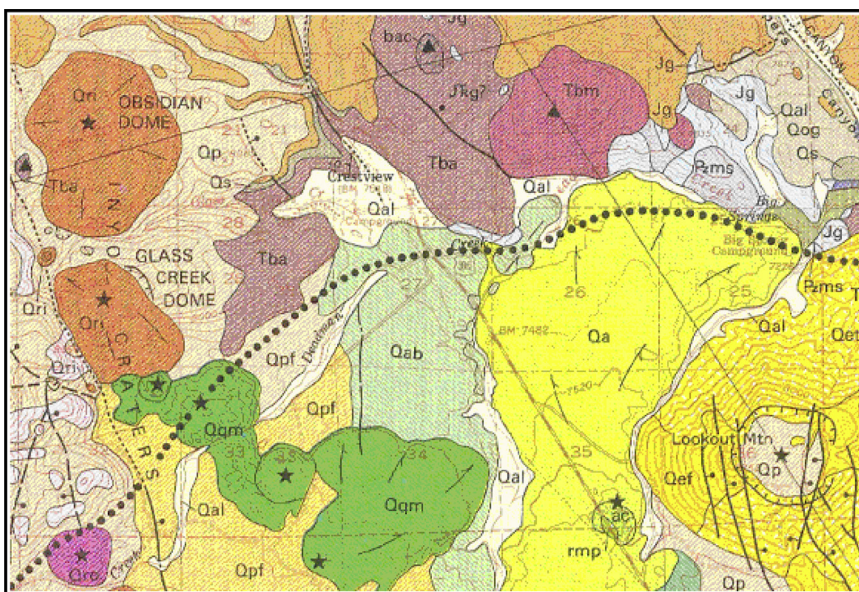


Figure 2.3 Detail of Long Valley geologic map: northwest section of the caldera (dotted line) [10] [WWW].

orientation of the faults and their angle of steepness [11]. Geologists name the various units based on the location where that particular unit was first discovered or best displayed. For example, the unit designated “Qqm” (dark green) in Figure 2.3 is called “quartz latite of Mammoth Mountain.” Other more common units are simply given their geologic names and described in detail regarding their existence at this particular site. For example, the unit “Qp” (tan) in Figure 2.3 is named “pyroclastic fall deposits” from the Holocene and Pleistocene periods, and identified as coming from eruptions of the Mono-Inyo Craters chain [10].

The conceptual model of the geothermal system depicts graphically the major subsurface features of the system, including the locations of rock units, faults, and fluid flow paths. The job of creating this map begins with the geologic survey and continues as more data comes in from the other surveys. It is not uncommon for the conceptual model to evolve even after the field goes into production, as reservoir information from production and injection wells becomes available. A sample conceptual model of the Long Valley caldera, adapted from Ref. [12], is shown in Figure 2.4. This is a cross-section through the same field shown in the geologic map of Figure 2.2. As the focus of the exploration program narrows to the region of highest geothermal potential, the conceptual model also becomes more limited in areal extent but finer in detail. The development of the conceptual model usually involves reconciling conflicting opinions of geoscientists who may interpret the survey data differently.

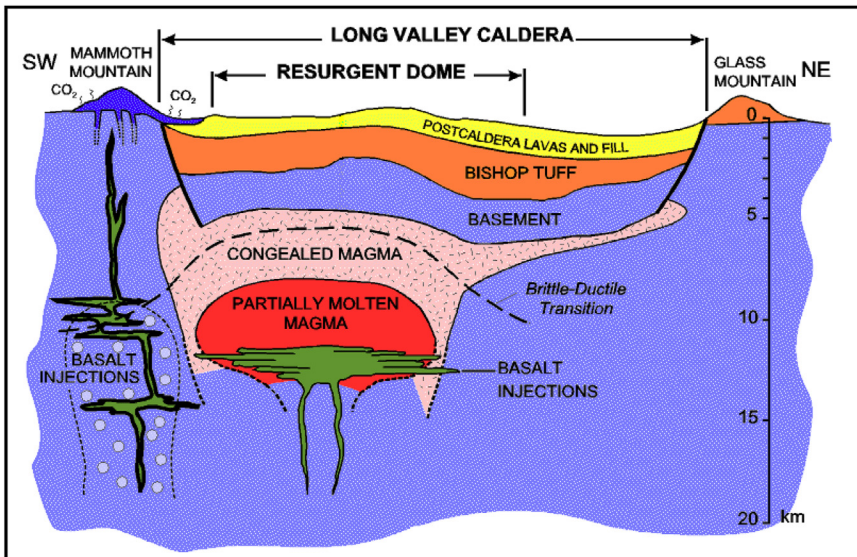


Figure 2.4 Conceptual model of Long Valley caldera showing main structural features. After Ref. [12] [WWW].

2.3.4 HYDROLOGIC SURVEY

Since one of the vital prerequisites for a commercial geothermal field is the presence of water in the formation in ample quantities, the hydrologic survey is an important part of the exploration program. It is conducted by a hydrologist, usually a civil engineer with expertise in groundwater behavior. Sometimes the person or group conducting the geologic survey also performs the hydrologic survey. The objective is to learn as much as possible about the fluids in the system, including their age, chemical and physical properties, abundance, flow paths, and recharge modes.

The hydrologic survey will typically involve study of the following:

- Meteorological data
- Temperature and flow rates of both hot and cold springs
- Chemical analysis of springs
- Water table in existing water wells
- Water movements both on the surface and in the reservoir.

By performing a mass balance on all the observed streams, the hydrologist can make an estimate of the volume of fluid in the formation and the rates of throughput, critical information for estimating the production capacity of the reservoir. In the area of chemical analysis of the springs, there is a natural overlap with the next phase of the program, the geochemical survey.

2.3.5 GEOCHEMICAL SURVEY

The geochemist has several important responsibilities, namely:

- Identify whether the resource is vapor- or liquid-dominated
- Estimate the minimum temperature of the geofluid
- Determine the chemical properties of the fluid both in the reservoir and in the produced state
- Characterize the recharge water, including its nature and sources.

There are several well-established methods for carrying out this task. The difficulty often comes in the interpretation of the results of the various diagnostic tests. The quest for clear and accurate answers to vital questions such as geofluid temperature is often frustrated by complicating factors that are only vaguely understood at the early stages of exploration. Let us focus on the determination of the geofluid temperature in the reservoir to illustrate this point.

High-temperature liquids moving through porous rock quickly reach equilibrium with various elements found in the rocks. The most important of these for estimating the fluid temperature are quartz (silica, SiO_2), sodium (Na), potassium (K), and calcium (Ca).

The concentration of silica in the geofluid produced from a reservoir can be correlated with the geofluid temperature using the solubility of quartz as a function of temperature, $Q = Q(t)$. This function has been determined by laboratory tests in pure water and in solutions with compositions typical of fluids in a geothermal environment. The solubility of quartz depends not only on the fluid temperature but also on its salinity and pH. At the high temperatures found in a hydrothermal reservoir, the solubility of silica is controlled by quartz, a crystalline form of silica, but at the lower temperatures encountered in the waste fluids after their use in a power plant, the solubility is controlled by the amorphous form of silica.

The functional relationship between the quartz concentration and the fluid temperature for pure water is given by the Eqs. (2.1) and (2.2):

$$t(Q) = a_0 + a_1Q + a_2Q^2 + a_3Q^3 + a_4\log_{10}Q \quad (2.1)$$

where the coefficients are:

$$\begin{aligned} a_0 &= -42.198 \\ a_1 &= 0.28831 \\ a_2 &= -3.6686 \text{ E-04} \\ a_3 &= 3.1665 \text{ E-07} \\ a_4 &= 77.034. \end{aligned}$$

The units of the concentration, Q , are mg/kg or ppm, the units of the temperature, t , are $^{\circ}\text{C}$, and the limits of the validity of the correlation are $t = 20\text{--}330^{\circ}\text{C}$ [13].

It is sometimes necessary to calculate the quartz concentration for a known temperature; then the following correlation may be used:

$$Q(t) = b_0 + b_1t + b_2t^2 + b_3t^3 + b_4t^4 + b_5t^5 + b_6t^6 + b_7t^7 \quad (2.2)$$

where the coefficients are:

$$\begin{aligned} b_0 &= 7.0281 \\ b_1 &= -0.228748 \\ b_2 &= 1.20057 \text{ E-02} \\ b_3 &= -1.50598 \text{ E-04} \\ b_4 &= 1.42552 \text{ E-06} \\ b_5 &= -6.0991 \text{ E-09} \\ b_6 &= 1.34828 \text{ E-11} \\ b_7 &= -1.29355 \text{ E-14}. \end{aligned}$$

The units of Q and t are the same as in Eq. (2.1), and the limits of the validity of the correlation are $t = 20\text{--}340^\circ\text{C}$.

The corresponding relationship for amorphous silica is given in Eq. (2.3):

$$\log_{10}S(t) = c_0 + c_1t + c_2t^2 + c_3t^3 \quad (2.3)$$

where the coefficients are:

$$c_0 = -1.34959$$

$$c_1 = 1.625 \text{ E-}02$$

$$c_2 = -1.758 \text{ E-}05$$

$$c_3 = 5.257 \text{ E-}09.$$

The units of the amorphous concentration, S , are mg/kg or ppm, the units of the temperature, t , are $^\circ\text{C}$, and the limits of the validity of the correlation are $t = 90\text{--}340^\circ\text{C}$ [14].

When a geofluid reaches the surface through a hot spring, a fluid sample can be taken and the amount of silica can be measured. If, on the one hand, the fluid remained in a liquid state from the reservoir to the sample with no flashing of steam, then the silica concentration will be the same in the reservoir as in the sample. This case leads to what is called the “no steam loss” silica geothermometer: the thermometric function for this case is [15]:

$$t(S) = \frac{1309}{5.19 - \log_{10}S} - 273.15 \quad (2.4)$$

Alternatively, one could calculate the temperature using Eq. (2.1), inserting the measured silica concentration for Q .

If, on the other hand, the liquid partially flashed to steam (which is quite likely given that the spring is at atmospheric pressure), then the silica concentration in the reservoir fluid will be less than what is observed in the sample owing to the concentrating effect of having all the silica in a smaller amount of liquid. The two concentration values are related as follows:

$$Q(t_{res}) = S(t_{atm}) \times (1 - x_{atm}) \quad (2.5)$$

where x_{atm} is the quality (or dryness fraction) of the liquid–vapor mixture at atmospheric conditions. It is a function of the reservoir fluid enthalpy (which depends on the fluid temperature) and the fluid enthalpy at atmospheric conditions:

$$x_{atm} = \frac{h_f(t_{res}) - h_f(t_{atm})}{h_{fg}(t_{atm})} \quad (2.6)$$

where the numerator is the difference between the enthalpy of a saturated liquid at the reservoir temperature and one at atmospheric conditions, and the

denominator is the latent heat of evaporation at atmospheric conditions. For standard atmospheric pressure, we can use *Steam Tables* [16] to find $h_f(100^\circ\text{C}) = 419.04 \text{ kJ/kg}$ and $h_{fg}(100^\circ\text{C}) = 2257.0 \text{ kJ/kg}$.

The problem then is to find a reservoir temperature such that Eqs. (2.1) or (2.2), (2.5), and (2.6) give a consistent set of results for the measured value of $S(t_{\text{atm}})$. When this is worked out, the result is called the “maximum steam loss” silica geothermometer: the thermometric correlation function for this case is:

$$t(S) = 75.272 + 0.72077S - 1.5807 \times 10^{-3}S^2 + 1.9924 \times 10^{-6}S^3 - 9.6957 \times 10^{-10}S^4 \quad (2.7)$$

Both of these geothermometers assume the geofluid is pure water at neutral pH. Figure 2.5 gives the inferred geofluid temperature for these two cases.

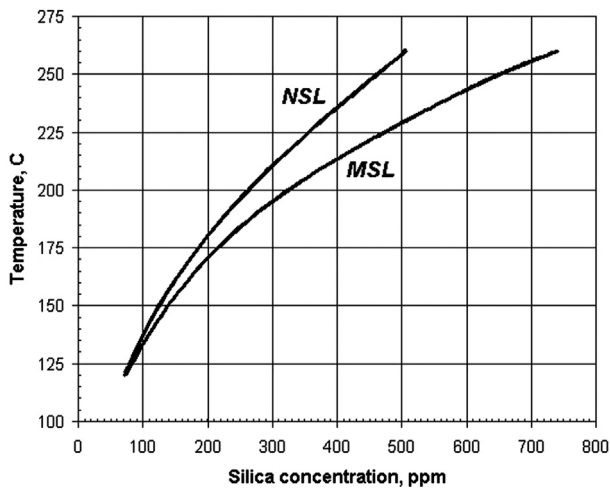


Figure 2.5 Silica geothermometers: NSL = no steam loss; MSL = maximum steam loss.

Thus we see that a decision must be made regarding the process followed by the geofluid from the reservoir to the surface before selecting which silica geothermometer to use to estimate the reservoir temperature. For example, a measurement of 500 ppm silica could mean either a reservoir temperature of 260°C (NSL) or 230°C (MSL), a significant difference. Also if any silica precipitates from the geofluid before the sample is taken, the results will be invalid, and the geothermometer will underestimate the reservoir temperature. Another possibility is that the reservoir silica equilibrium might be controlled by a form of silica other than quartz, such as chalcedony or cristobalite, thereby rendering the

analysis developed above inapplicable. The molality and pH of the reservoir fluid will also influence the accuracy of silica geothermometry. All of these issues require an intelligent judgment on the part of the geochemist.

Besides using silica equilibrium, one can apply the sodium/potassium, Na/K, ratio as a measure of reservoir temperature. The thermometric function is:

$$t = \frac{1217}{\log_{10} \frac{\{Na\}}{\{K\}} + 1.483} - 273.15 \quad (2.8)$$

where {Na} and {K} are the concentrations of sodium and potassium in the geofluid. The equation applies for temperatures greater than 150°C [15]. This formula is a correlation of field data with considerable scatter, particularly below 150°C. It seems to be reliable in the 180–200°C range, and where the ground-water that could dilute the geofluid is low in Na and K [15].

The last geothermometer based on dissolved minerals in liquid geofluid we will mention is the Na/K/Ca-geothermometer. The following thermometric equation is useful for calcium-rich geofluids:

$$t = \frac{1647}{\log_{10} \frac{\{Na\}}{\{K\}} + \beta \left[\log_{10} \frac{\sqrt{\{Ca\}}}{\{Na\}} + 2.06 \right] + 2.47} - 273.15 \quad (2.9)$$

Use $\beta = 4/3$: if $t < 100^\circ\text{C}$, you are done; if $t > 100^\circ\text{C}$, recalculate using $\beta = 1/3$ [15].

There is an entirely different suite of geothermometers based on gas geochemistry. These involve equilibrium reactions among carbon dioxide (CO₂), carbon monoxide (CO), hydrogen (H₂), hydrogen sulfide (H₂S), and methane (CH₄) in the presence of water vapor (H₂O). For example, the following three thermometric functions are correlations to worldwide field data that relate the concentrations (in mols/kg) of three gases to the reservoir temperature [17]; note these temperatures, denoted by T , are in kelvins:

$$\log_{10}\{CO_2\} = -1.09 - \frac{3894.55}{T} + 2.532 \log_{10}T \quad (2.10)$$

$$\log_{10}\{H_2S\} = -11.80 - 0.06035T - \frac{17,691.09}{T} + 27.163 \log_{10}T \quad (2.11)$$

$$\log_{10}\{H_2\} = -3.04 - \frac{10,763.54}{T} + 7.003 \log_{10}T \quad (2.12)$$

Each of these formulas may be solved numerically for temperature for a given gas concentration. By and large, the method of gas geochemistry leads to

sets of simultaneous reaction equations that must be solved iteratively or graphically to find the temperature that satisfies all the governing gas equations [18,19].

Lastly, geochemical studies may be able to identify the general patterns of fluid movement through the formation. A search for radon emissions can often identify active faults and fractures that may be conduits for fluid flow.

2.3.6 GEOPHYSICAL SURVEY

Geophysics is the application of principles of mechanics, thermal science, and electrical science to the delineation and characterization of geothermal systems. The geophysical phase of exploration typically provides the final piece of the puzzle and should lead directly to the identification of the best locations to drill the first deep wells. The geophysicist usually has the available data from the previously described surveys and uses this information to decide which tests to perform. Some of the most useful techniques include:

- Heat flux measurements
- Temperature gradient surveys
- Electrical resistivity surveys
- Seismic methods, both active and passive
- Gravity surveys.

The properties that are measured during the geophysical phase include:

- Temperature
- Electrical conductivity or resistivity
- Density
- Velocity of propagating waves in solid material
- Magnetic susceptibility
- Local gravitational acceleration.

The geophysicist is aided in determining heat flux and thermal gradients by having data from shallow wells (about 100–200 m deep). Recall from Chapter 1 that in nonthermal areas the normal temperature gradient is about $3.1^{\circ}\text{C}/100\text{ m}$, and the normal heat flux is roughly $1.2 \times 10^{-6} \text{ cal}/\text{cm}^2 \cdot \text{s}$. By convention, $1 \times 10^{-6} \text{ cal}/\text{cm}^2 \cdot \text{s}$ or $1 \mu\text{cal}/\text{cm}^2 \cdot \text{s}$ is called 1 heat flow unit or 1 HFU. When the mode of heat transfer is pure conduction, the phenomenon conforms to Fourier's Law which, in one-dimensional form, is:

$$\dot{Q} = -kA \frac{dT}{dx} \quad (2.13)$$

or

$$q = -k \frac{dT}{dx} \quad (2.14)$$

where \dot{Q} is the thermal power or heat flow per unit time (in J/s), k is the thermal conductivity of the material (in $\text{J/m} \cdot \text{s} \cdot ^\circ\text{C}$ or $\text{W/m} \cdot ^\circ\text{C}$), A is the area through which the heat flows (in m^2), and dT/dx is the temperature gradient driving the heat flow (in $^\circ\text{C/m}$). When Eq. (2.13) is divided by A , one obtains the equation for the heat flux, q , Eq. (2.14). The negative sign indicates that the heat flows in the direction of decreasing temperature, in accordance with the Second Law of Thermodynamics; see Appendix D. Approximate values of thermal conductivity for typical rocks are:

- Granite 1.73–3.98 $\text{W/m} \cdot ^\circ\text{C}$
- Limestone 1.26–1.33 $\text{W/m} \cdot ^\circ\text{C}$
- Marble 2.07–2.94 $\text{W/m} \cdot ^\circ\text{C}$
- Sandstone 1.60–2.10 $\text{W/m} \cdot ^\circ\text{C}$.

Considering the near-surface formation, conduction will be the predominant means of heat transfer, absent fluid circulation. The thermal conductivity will tend to increase with depth as the formation compacts under the increasing weight of the overburden. The heat flux will be more or less constant in steady-state conditions. Therefore, from Eq. (2.14) we expect that the temperature gradient will decrease with depth in a conductive environment. This is important in the interpretation of shallow gradients because extrapolation to deeper depths will generally lead to erroneously high values, as can be seen in Figure 2.6.

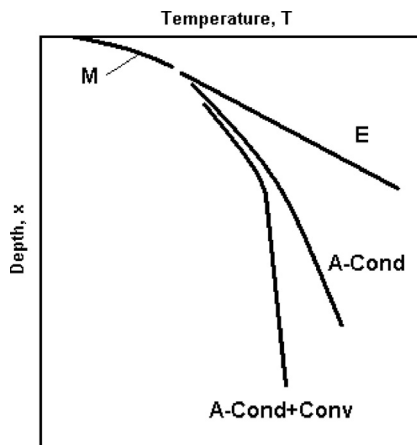


Figure 2.6 Temperature gradients. M = measured; E = linear extrapolation; A-Cond = actual with pure conduction; A-Cond + Conv = actual with a deep convective zone.

Where convection plays a role, as one would hope in a permeable geothermal formation, this tends to create a more or less isothermal zone: the lower end of the A-Cond + Conv curve in [Figure 2.6](#).

High heat flow is a good indicator of a geothermal system. High temperatures close to the surface will result in high heat flux but can be misleading as to the hottest subsurface zone. There are several possible causes of a high heat flow:

- Presence of hot water close to the surface
- Exothermic reactions in the formation
- High radioactive content of the country rocks
- Friction along faults.

Geophysical surveys are geared to detect the first of these as the primary indicator of the thermal anomaly. But because hot fluids can move laterally as well as vertically in a porous medium, the surface expression of the highest heat flux may not coincide with the hottest reservoir region and may divert attention away from the source of the geofluid. An example is shown in [Figure 2.7](#), drawn roughly from the case of the Dunes field in the Imperial Valley, California.

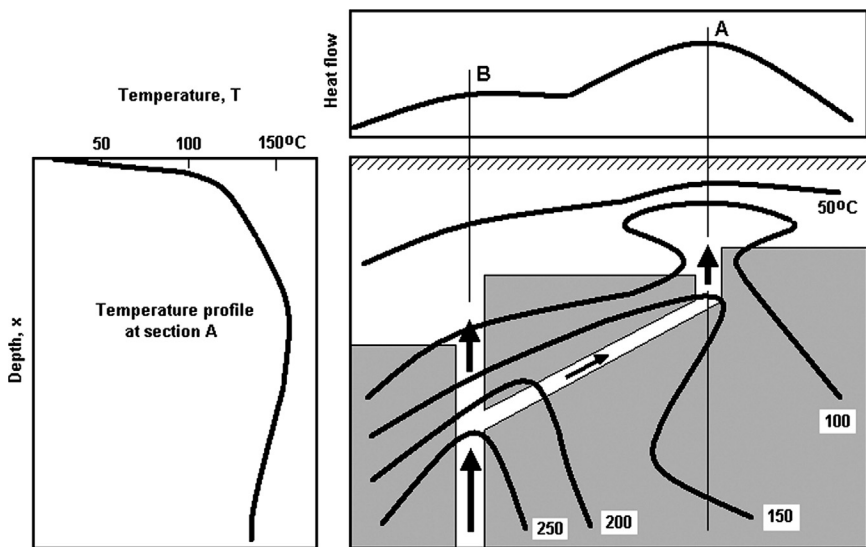


Figure 2.7 Heat flow and temperature gradient with lateral flow in reservoir.

In this case, the impressive heat flow anomaly at point A is associated with a side-flow, laterally displaced from the main source of the geofluid beneath point

B. The temperature reversal at a relatively shallow depth is the key indicator of this effect. This phenomenon has been seen in many geothermal fields and is a warning to incorporate several types of measurements into the conceptual model of a field. Any single indicator can often be misleading.

Electrical measurements are another important element in the geophysical exploration phase. The electrical resistivity, ρ , is one of the most commonly measured quantities; it is measured in units of $\text{ohm} \cdot \text{m}$. Low resistivity can be caused by the presence of hot water with dissolved minerals in a porous medium. Generally rocks are poor conductors of electricity and exhibit high resistivity, but when an electrolyte fills the pore spaces, the average resistivity will be reduced. Also rocks that have been hydrothermally altered to clayey material are better conductors than the native country rock. Therefore whenever low resistivities are found, a high-temperature hydrothermal reservoir may be present.

Dakhnov's Law gives the relation between resistivity and temperature [20]:

$$\rho_0 = \frac{\rho_{18}}{1 + 0.025(t - 18)} \quad (2.15)$$

where ρ_0 is the resistivity of a rock with its pore space filled with a fluid having a resistivity ρ_{18} at 18°C . Archie's Law expresses the formation resistivity ρ_0 relative to that of the fluid filling the pores ρ_w [21]:

$$\rho_0 = \frac{\rho_w}{\phi^m} \quad (2.16)$$

where ϕ is the porosity of the rock (expressed as a fraction) and m is the so-called cementation factor. For loosely consolidated sediments, $m \approx 1.2-1.5$; for well-cemented or crystalline rock, $m \approx 1.9-2.2$ [21]. Meidav [21] presents graphs and nomograms that facilitate the use of these equations.

Because the resistivity depends on the salinity of the pore water as well as its temperature, care must be taken in interpreting resistivity measurements. For example, sea water having about 32,000 ppm of NaCl at 18°C has the same resistivity as chloride water with 10,000 ppm NaCl at 100°C . Also since gases are poor electrical conductors, a dry steam reservoir will appear as a resistivity high in the midst of a relative low. Resistivities of $5-10 \text{ ohm} \cdot \text{m}$ or lower are usually taken as a good indicator of a hot hydrothermal resource when confirmed by other indicators, such as a high temperature gradient.

Areas of active faults and fissures can be detected by monitoring the field for seismic activity. Swarms of microearthquakes indicate possible fluid conduits and can lead to good sites for well drilling.

Measurements of the variation in the local gravitational acceleration across the field can reveal different masses beneath the surface. Sensitive instrumentation is needed, capable of detecting changes of the order of 0.01 mGal, where $1 \text{ Gal} = 1 \text{ cm/s}^2$. The standard gravitational acceleration at the surface of the earth is 981 Gal or 981,000 mGal. So a gravimeter with a sensitivity of 1 part in 98 million is needed. The reading essentially gives the density or the specific gravity of the formation. Since the reading is affected by the presence of hills or valleys in the neighborhood of the instrument, and since the data must be referenced to a standard elevation (typically sea level), the raw data must be corrected. To do this accurately, high-precision topographic information must be available for the field. Once the corrected value is found, it is compared to what the normal gravity should be for the location of the instrument; any difference is called the Bouguer gravity anomaly, BA , given by:

$$BA = g_0 - (\delta_0 - 0.3086h + 2\pi\rho Gh - \tau) \quad (2.17)$$

where g_0 is the standard gravity at the location of the instrument, δ_0 is the theoretical gravity at the latitude of the instrument but at sea level, $0.3086h$ gives the change in gravity as a function of elevation h above sea level, $2\pi\rho Gh$ is the infinite-slab correction to account for the attraction of a slab of material with a density ρ extending in all horizontal directions and lying between the instrument and sea level, and τ is the terrain correction to account for elevation changes near the instrument [22].

Low-density volcanic rocks or partially molten magmatic plutons will create gravity lows. Very sensitive measurements may be able to track the movement of liquids through porous rock and thus be useful for monitoring the effects of production and injection of geofluids during the operation of a power plant. As with all geoscientific surveys, gravity data should be viewed in light of other indicators before drawing conclusions.

Although it is impossible to set down hard and fast interpretations of any geothermal exploration results, rough inferences may be drawn from Figure 2.8 where electrical resistivity is cross-plotted against the temperature gradient. The shaded region is clearly the most desirable. These inferences should be seen as tentative unless confirmed by other studies. This type of diagram in which more than one indicator is used will provide a segue to the last section on exploration.

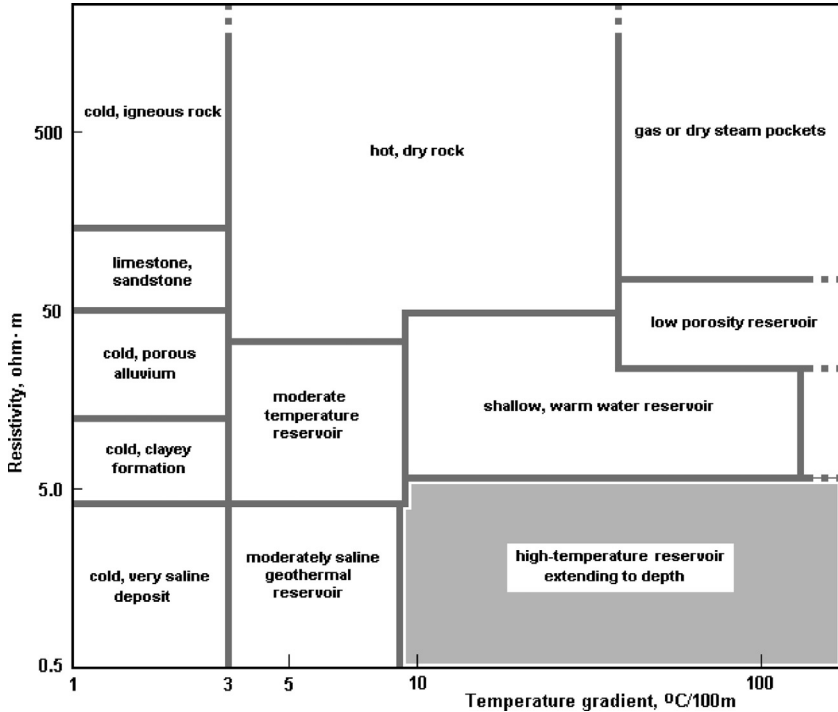


Figure 2.8 Map of resistivity versus temperature gradient with possible interpretations.

2.4 Synthesis and Interpretation

When the geoscientific surveys have been completed, it is necessary to synthesize all the acquired data and to draw conclusions based on the totality of the evidence. As we have seen, any one survey can give a misleading indication. The best way to visualize the comprehensive picture of the geothermal prospect is to construct, on a workable scale, a composite map, or synthesis map, of the site. The main purpose of the synthesis map is to identify the best targets for the first few deep wells.

The base map should be a simplified geologic map with at least 50-m topographic contours, and it should contain, at minimum, the following information:

- Roadways, buildings, and dwellings
- Major geologic structures such as caldera borders, principal faults both observed and inferred, recent lava flows, basement outcrops, and outlines of suspected buried units of low permeability
- All thermal manifestations, identified by type, temperature, and chemical nature

- Radon concentration contours (if performed)
- Seismic activity
- Gravity contours
- Electrical resistivity contours.

Besides this map, there should be several elevation cross-sections taken through the field, preferably orthogonal, showing the extent of various geologic units down to and including the upper basement, faults, and resistivity layers. These elevation sections usually correspond to the lines along which the resistivity surveys were performed.

With the availability of modern three-dimensional computer graphics, the synthesis can be presented in a convenient, user-friendly, visually appealing format.

As the field is developed, and more wells are drilled, this vital set of drawings or computer representation must be periodically updated to serve as an ongoing guide to the next steps. Lithologic logs from deep wells will allow a better definition of the subsurface and should improve the probabilities for successful wells. Lastly, additional geoscientific work may be required during field development to refine the understanding of the field and to guide step-out drilling.

2.5 The Next Step: Drilling

After all the scientific exploration has been done, the results synthesized and interpreted, a decision will be made regarding the next phase, namely the drilling of several, typically three, deep exploratory wells. If the synthesis map and its cross-sections accurately represent the geothermal system, the task of siting the wells will be straightforward. The drilling phase will be more costly by far than the exploration phase and should be undertaken only after a rigorous program of geoscientific studies has been carried out, with positive indications. The next chapter will deal with geothermal drilling.

References

- [1] Hot springs enthusiast, <<http://www.hotspringsenthusiast.com/USsprings.asp>>.
- [2] Western states geothermal databases CD, Geo-Heat Center, Oregon Institute of Technology, Klamath Falls, OR, <<http://geoheat.oit.edu/database.htm>>.
- [3] National geologic map database, U.S. Geologic Survey, Menlo Park, CA, <<http://ngmdb.usgs.gov/>>.
- [4] Great Basin Borehole Temperature Logs, U.S. Geologic Survey, Menlo Park, CA, <<http://geopubs.wr.usgs.gov/open-file/of99-425/webmaps/GB%20map.html>>.
- [5] Well log for Fish Lake Valley, Nevada, Well FLP-1, U.S. Geologic Survey, Menlo Park, CA, <http://geopubs.wr.usgs.gov/open-file/of99-425/frameset_FLP-1_ENG.html>.

- [6] USGS Fact Sheets, U.S. Geologic Survey, Menlo Park, CA, <<http://water.usgs.gov/wid/index-state.html#CA>>.
- [7] Duprat A, Omnes G. The costs of geophysical programs in geothermal exploration. Proc. Second U.N. Symposium on the development and use of geothermal resources, V.2. San Francisco, CA: Lawrence Berkeley Laboratory; 1975. p. 963–70.
- [8] Del Grande NK. An advanced airborne infrared method for evaluating geothermal resources. Proc. Second U.N. Symposium on the development and use of geothermal resources, V.2. San Francisco, CA: Lawrence Berkeley Laboratory; 1975. p. 947–53.
- [9] Dickinson DJ. An airborne infrared survey of the Tauhara geothermal field, New Zealand. Proc. Second U.N. Symposium on the development and use of geothermal resources, V.2. San Francisco, CA: Lawrence Berkeley Laboratory; 1975. p. 955–61.
- [10] Geologic Map of Long Valley Caldera, Mono-Inyo Craters Volcanic Chain, and Vicinity, Eastern California, R.A. Bailey, U.S. Geological Survey, Menlo Park, CA, <<http://geopubs.wr.usgs.gov/dds/dds-81/GeologicalMaps/ScannedMap/sheet1.pdf>>; 1989.
- [11] Geologic maps, U.S. Geological Survey, National Park Service, Menlo Park, CA, <<http://www2.nature.nps.gov/geology/usgsnps/gmap/gmap1.html>>; 2000.
- [12] Long valley coring project, International Continental Scientific Drilling Program, Potsdam, Germany, <<http://www.icdp-online.org/sites/longvalley/wellsite/well.html>>; 2003.
- [13] Fournier RO, Potter II RW. A revised and expanded silica (Quartz) geothermometer. *Geoth Res Council Bull* 1982;11(10):3–12.
- [14] Fournier RO, Marshall WL. Calculations of amorphous silica solubilities at 25 and 300°C and apparent cation hydration numbers in aqueous salt solutions using the concept of effective density of water. *Geochim Cosmochim Acta* 1983;47:587–96.
- [15] Fournier RO. Application of water geochemistry to geothermal exploration and reservoir engineering. In: Rybach L, Muffler LJP, editors. Chapter 4 in *Geothermal systems: principles and case histories*. New York, NY: John Wiley & Sons; 1981.
- [16] Keenan JH, Keyes FG, Hill PG, Moore JG. *Steam tables: thermodynamic properties of water including vapor, liquid, and solid phases (International Edition—Metric Units)*. New York, NY: John Wiley & Sons, Inc.; 1969.
- [17] Arnorsson S, Gunnlaugsson E. New gas geothermometers for geothermal exploration—calibration and application. *Geochim Cosmochim Acta* 1985;49:1307–25.
- [18] D’Amore F, Truesdell AH. Calculation of geothermal reservoir temperatures and steam fractions from gas compositions, V. 9—Pt. I. *Geothermal Resources Council Trans*; 1985. pp. 305–310.
- [19] D’Amore F, Mussi M, Grassi S, Alaimo R. Pantelleria Island (Sicily, Italy): a gas geochemical survey. Proc. World geothermal congress, V.2. Auckland, NZ: International Geothermal Association; 1995. pp. 1007–12.
- [20] Dakhnov VN. Geophysical well logging. *Quart Colo Sch Mines* 1962;57(2):443 [Keller GV, Trans.]
- [21] Meidav T, Application of electrical resistivity and gravimetry in deep geothermal exploration, *Geothermics—Special Issue 2*, U.N. Symposium on the Development and Utilization of Geothermal Resources, Pisa, V.2, Pt. 1, 1970; p. 303–10.
- [22] Diment WH, Resource characteristics: exploration, evaluation, and development. In: Kestin J, editor-in-Chief, DiPippo R, Khalifa HE, Ryley DJ, editors. *Sourcebook on the production of electricity from geothermal energy*. U.S. Dept. of Energy, DOE/RA/4051-1, U.S. Gov. Printing Office, Washington, DC; 1980 [chapter 2].
- [23] DiPippo R. Geothermal energy as a source of electricity: a worldwide survey of the design and operation of geothermal power plants. U.S. Dept. of Energy, DOE/RA/28320-1, U.S. Gov. Printing Office, Washington, DC; 1980.

Problems

- 2.1.** With reference to [Figure 2.1](#), calculate the (a) shallow and (b) deep temperature gradients, in °F/100 ft and °C/100 m. Compare these to the normal temperature gradient. Discuss possible reasons for the relatively isothermal section between the shallow and deep portions.
- 2.2.** For each of the geofluid samples listed in the table below, apply the following geothermometers to obtain estimates of the reservoir fluid temperature: a. SiO₂ (maximum steam loss), b. SiO₂ (no steam loss), c. Na/K, and d. Na/K/Ca. AH wells are from Ahuachapán, H wells from Hatchobaru, and CP wells from Cerro Prieto; All data are in units of ppm and are taken from Ref. [\[23\]](#).

Substance	Well number					
	AH-1	AH-5	AH-26	H-4	H-6	CP-avg
Chloride, Cl	10,600	9,110	10,130	3,850	5,150	14,370
Sodium, Na	5,800	5,000	5,600	2,200	2,860	7,760
Potassium, K	1,000	680	900	243	300	1,660
Silica, SiO ₂	577	470	500	922	620	850
Calcium, Ca	425	440	430	34	108	545

- 2.3.** Suppose a sample from a well has a Na/K = 6.97.
- Estimate the reservoir temperature using the Na/K geothermometer equation.
 - Suppose further that the sample has a Ca^{1/2}/Na = 1.5. Estimate the temperature using the Na/K/Ca geothermometer.
- 2.4.** An alternative formulation for the Na/K geothermometer has been offered [\[15\]](#):

$$t = \frac{855.6}{\log_{10} \frac{\{Na\}}{\{K\}} + 0.8573} - 273.15$$

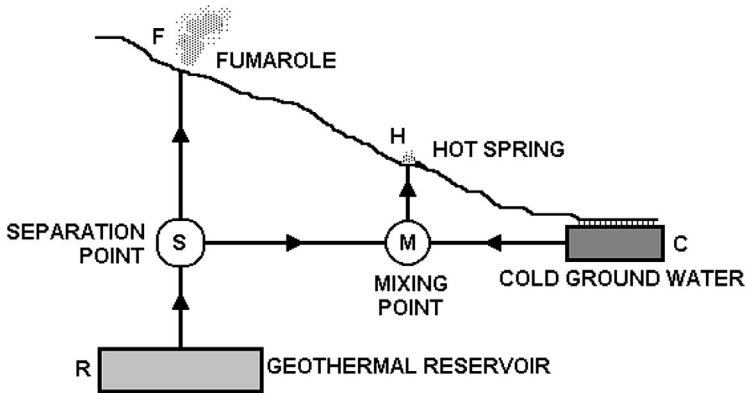
Compare this formulation to the one given in [Eq. \(2.8\)](#). Calculate and plot the results from 150°C to 350°C. On one graph, plot t (°C) on the ordinate and $\{Na\}/\{K\}$ on the abscissa showing the curves for both formulations. Discuss the disagreement between these curves, the limits of applicability, and the relative reliability.

- 2.5.** Use the silica geothermometer to estimate the reservoir fluid temperature if the two-phase fluid from a test well is separated at the surface into its liquid and vapor phases at 100°C and the concentration of silica in the liquid is: a. 300, b. 400, c. 500, d. 600, e. 700 ppm.

- 2.6. Compare the results of using Eqs. (2.1) and (2.4) to determine the geofluid temperature for the “no steam loss” case over a range of silica concentrations from 200 to 700 ppm. Discuss the possible causes of any differences you find.
- 2.7. Write a short essay on the methods of prospecting for geothermal systems. Are certain methods more useful for high- or low-temperature systems? Include sketches and schematic diagrams wherever appropriate to illustrate your essay.
- 2.8. Three potential geothermal sites have been studied using temperature gradient surveys (typically to depths of about 500 m) and electrical resistivity surveys (typically down to about 1000 m). The results are summarized in the table below.

Site name	Temperature gradient, °C/100 m	Electrical resistivity, ohm · m
Diablo Springs	75	3 (minimum)
Caliente	100	300 (minimum)
Evergreen	5	2 (minimum)

- Which site(s) appear to have reasonable potential as a hydrothermal resource?
 - Which site(s) appear to be a possible candidate for a hot-dry-rock resource?
 - Which site(s) appear to be a possible candidate for a dry steam resource?
 - Which site appears to be the worst candidate for a practical geothermal resource?
- In all cases, fully explain the reasoning behind your answers.
- 2.9. A 150-m deep temperature gradient hole shows a gradient that is six times greater than the normal temperature gradient. Based on this information, calculate the expected temperature in the reservoir at depths of (A) 500 m and (B) 2000 m. Discuss the reliability of these two answers and the factors that affect the reliability.
- 2.10. An ultra-simplified mixing model for a hydrothermal system is shown in the figure shown below. The system is shown in an unexploited state in which geofluid from the reservoir rises through the formation. At some point underground, steam separates from the geofluid and continues to rise to the surface, emerging as a fumarole. The hot geothermal liquid flows laterally from the separation point until it mixes with cold ground water. The mixed fluid then rises to the surface and emerges as a hot spring.



Physical quantities that are easily measured are:

T_C , temperature of the ground water

T_H , temperature of the hot spring

T_F , temperature of the fumarole

P_A , atmospheric pressure (assumed = 100 kPa).

Your task is to develop the analytical model for this hypothetical situation. Your objective is to determine the temperature of the fluid in the reservoir, T_R . Include all assumptions you make and justify them. For example, it might be reasonable to take all underground processes as adiabatic (no heat loss). Hint: The amount of silica present in the geofluid and groundwater is conserved as the fluids move through the formation, but the silica in the geofluid is partitioned into the liquid phase when the steam separates out.

Using your analytical model, estimate T_R for the following sets of conditions:

- a. $T_C = 20^\circ\text{C}$; $T_H = 65^\circ\text{C}$; $T_F = 105^\circ\text{C}$
 - b. $T_C = 25^\circ\text{C}$; $T_H = 75^\circ\text{C}$; $T_F = 110^\circ\text{C}$
 - c. $T_C = 30^\circ\text{C}$; $T_H = 85^\circ\text{C}$; $T_F = 115^\circ\text{C}$
- 2.11.** As explained in [Section 2.3.5](#), the amount of silica in the liquid separated from a two-phase geofluid mixture at the surface can be used to estimate the temperature of the liquid in the reservoir. [Equation \(2.7\)](#) applies to separation at one standard atmosphere of pressure. Do not use [Eq. \(2.7\)](#) in solving this problem; use instead [Eqs. \(2.1\), \(2.2\), \(2.3\), \(2.5\), and \(2.6\)](#).

For a local atmospheric pressure of 91 kPa (corresponding to an elevation of roughly 850 m above sea level), calculate the estimated reservoir temperature if the observed silica concentration in the separated liquid is: (A) 300 ppm; (B) 500 ppm; (C) 700 ppm; (D) 900 ppm.

- 2.12.** This problem will illustrate the correspondence (or lack thereof) between various geothermometers. Consider the following set of geochemical data obtained from the Ahuachapán field in El Salvador.

Component	Concentration, ppm
Chloride	10,430
Sodium	5,690
Potassium	950
Calcium	443
Silica, SiO ₂	537

- a. Calculate the estimated reservoir temperature from: (a) the Na/K geothermometer, Eq. (2.8) and (b) the Na/K/Ca geothermometer, Eq. (2.9).
 - b. Assuming that the result obtained for the Na/K/Ca geothermometer is correct, calculate the expected concentration of silica that you would find in the liquid separated from the two-phase well flow if the separation temperature is 100°C.
 - C. Compare the answer for Part (B) with the value given in the data set, and discuss any difference between these values.
- 2.13.** In the absence of other data, which of the following, each taken by itself, would be more encouraging for the existence of a high-temperature, liquid-dominated geothermal reservoir:
- a. High or low temperature gradient?
 - b. High or low heat flux?
 - c. High or low gravity anomaly?
 - d. High or low magnetic anomaly?
 - e. High or low silica concentration in springs?
 - f. High or low mercury concentration in soils?

Explain the level of confidence you have in each case.

- 2.14.** Consider the following set of geochemical data obtained from the Pauzhetka field in the Kamchatka geothermal region of Russia:

Component	Concentration, ppm
Chloride	1,633
Sodium	986
Potassium	105
Calcium	52

- a. Calculate the estimated reservoir temperature from: (a) the Na/K geothermometer, Eq. (2.8) and (b) the Na/K/Ca geothermometer, Eq. (2.9).

- b. Assuming that the result obtained for the Na/K geothermometer is correct, calculate the expected concentration of silica that you would find in the liquid separated from the two-phase well flow if the separation temperature is 100°C .
- 2.15. Geophysical measurements have been performed on five geothermal prospective sites. The data are shown in the table below where the gradients were obtained from shallow wells and the resistivity values are the minimum observed.

Site designation	Temperature gradient, $^{\circ}\text{C}/100\text{ m}$	Electrical resistivity, $\text{ohm} \cdot \text{m}$
A	25	1
B	100	500
C	5	10
D	10	200
E	2	2

Bearing in mind that either indicator can be misleading by itself, match the descriptions listed below (only five will be relevant) to the sites in the table.

Option	Description
1	Moderate-temperature reservoir
2	Deep, high-temperature reservoir
3	Gas or dry steam pockets or cap
4	Cold, igneous rocks
5	Hot dry rocks
6	Cold, high-salinity reservoir



Chapter 3

Geothermal Well Drilling

Chapter Outline

3.1 Introduction	49
3.2 Site Preparation and Drilling Equipment	50
3.3 Drilling Operations	51
3.4 Safety Precautions	56
References	58
Problems	58

The well blew up like a volcano, everything came flying up—mud, tools, rocks, and steam. After things settled down, there was just clean steam. But the noise was loud enough to hear all over the valley.

Glen Truitt, on the drilling of well No. 1 at The Geysers—1922

3.1 Introduction

The confirmation of the optimistic outcome of the exploration phase comes with the successful drilling of the first exploratory well. [Figures 3.1 and 3.2](#) show wells that have struck productive formations [\[1\]](#).

Generally three wells are drilled as the first step in the field confirmation stage. The wells are sited at the most promising locations as determined by the synthesis of all the exploration studies. If possible they should form a triangle in the hope of defining a productive area of the field. Since these wells must be viewed as part of the exploration program, as much information as possible should be collected during their drilling. This includes the taking of core samples from at least some portions of the well to help understand the lithology of the formation. This data must be incorporated into the conceptual model of the field prior to undertaking the next step—the drilling of the developmental wells.

In this chapter we will briefly describe the drilling process; for a more detailed and quantitative presentation, the reader is advised to consult Edwards et al. [\[2\]](#) who devote several chapters of their book to drilling.



Figure 3.1 Discharge from a well at the Ahuachapán field, El Salvador [1] [WWW].

3.2 Site Preparation and Drilling Equipment

Geothermal fields are often remote, far from developed areas, and require significant site preparation before drilling can begin. During the scientific exploration phase, access to the site had to be sufficient only to allow a few people to reach and sample thermal springs and other manifestations, to drive small vehicles, run electrical equipment across the terrain, etc. But for this stage, roads will need to be constructed that can carry heavy equipment to the designated drilling targets. In volcanic environments, this can be challenging owing to rugged terrain. To minimize the number of drill pads, several wells can be drilled from a single pad,



Figure 3.2 Initial blowing of an Indonesian well at the Dieng geothermal field [1] [WWW].

the wellheads being only tens of meters apart. Directional drilling, however, allows the productive sections of the wells to be widely separated, perhaps by as much as 500–1000 m, to avoid interference. Generally, the first or “discovery” well is a deep vertical well (say 2500 m) to allow as much information as possible to be gathered about the formation.

A typical well pad with all equipment to support a 3000 m drill rig is shown in Figure 3.3. An area of roughly 90×45 m (300×150 ft) is required, including buffer space around the equipment and structures.

Figure 3.4 shows the major pieces of equipment used at the drill rig. Note the relative thicknesses of the drill pipe and the drill collar which holds the bit.

3.3 Drilling Operations

The creation of the hole relies on the compressive forces exerted on the rock by the multitoothed drill bit. Rotary drilling is the standard method in geothermal drilling whereby a string of drill pipe is hung from a derrick and turned by an engine, typically a diesel. The top section of the pipe, called the “Kelly,” is square in cross-section to allow it to be rotated by the action of a rotary table through which it passes. The bit is a tri-cone roller bit, based on the 1909

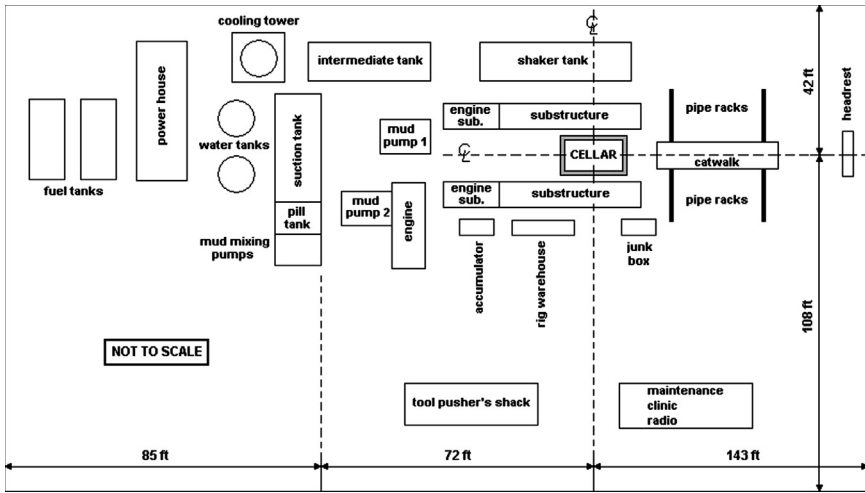


Figure 3.3 Drill pad to support a 3000 m rig. After Ref. [3].

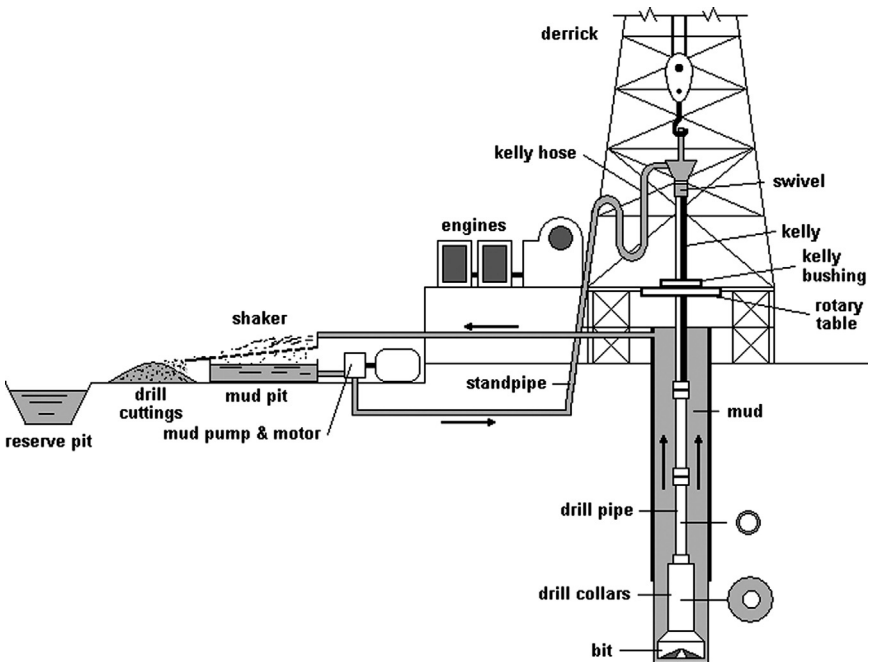


Figure 3.4 Typical drill rig setup; not to scale.

invention of Howard R. Hughes, Sr. (1870–1924), that applies very concentrated loads on the rock face causing it to crack and spall; see [Figure 3.5](#). The rock fragments or chips must be removed for the bit to proceed.

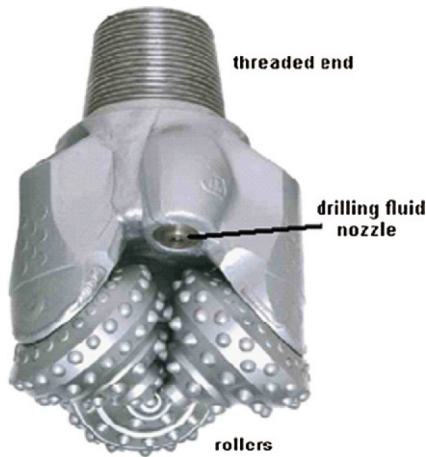


Figure 3.5 A tri-cone roller bit designed for hard rock formations, manufactured by Hughes Christensen [4].

The drilling fluid, or “mud,” is a critical element in the operation; it serves four vital functions:

- Removes the rock chips
- Cools the drill bit and drill string
- Lubricates the drill string
- Prevents the collapse of the well wall during drilling.

The mud is pumped down the center of the drill pipe to the bit where it passes through nozzles that accelerate and direct it onto the rock beneath the bit. It sweeps up the chips as it flows under the bit and carries them with it as it returns to the surface through the annulus between the well wall and the drill string. When it gets to the surface it flows over a screen and shaker to dislodge the chips which are preserved and examined by the geologist. The mud then is returned to the bottom by the mud pump. When the formation is hot, it is necessary to cool the mud before returning it to the well. A cooling tower is shown in the plan layout in [Figure 3.3](#), but has been omitted from [Figure 3.4](#). Owing to unplanned deviations of the bit during drilling, the drill pipe may come in contact with the wall over some length; the mud lubricates the contact surface helping to reduce the friction. Finally, by exerting pressure against the wall, the mud can keep the formation intact until a permanent casing can be put in place.

The drilling mud is an engineered fluid, designed to perform its specific tasks [5]. It is basically water with numerous additives that can alter the viscosity and density. The density can range from 62.4 lbm/ft³ (pure water) to 150 lbm/ft³. Clays are blended into solution to achieve desired properties. A severe disadvantage to using mud as the drilling fluid arises when the formation is tight, with little permeability except for a few narrow fractures bearing the geofluid. The mud can clog the fractures and destroy what little permeability was there. In such cases, mud can be used until the productive zone is approached, but beyond that point, the drilling fluid is changed to air or aerated mud. Whereas the ability of air to lift rock chips from a large diameter hole is poor, at the lower end of the well in the production zone, the well diameter is smaller and air can do the job effectively.

If the bit encounters a highly permeable zone, the drilling mud may be absorbed by the formation and the return upflow will be less than the downflow. This is called a “lost circulation” problem. Sometimes the loss is great enough to prevent any returns at all—a “total lost circulation.” This is a highly desirable outcome when the well is in the production zone because it signals excellent permeability and a potential big producer. But if this happens in the low-temperature shallow zone, it is very troublesome because drilling cannot continue without drilling mud. Much effort has gone into finding special materials to close these “thief zones” [6].

It is always a judgment call by the drilling engineer, in consultation with the geoscientists, as to whether a lost circulation zone within the upper part of the reservoir should be cemented. This is a permanent solution to the lost circulation problem, but the permeable zone will be lost for any possible production should the rest of the well turn out to be unproductive. This dilemma tends to occur in the early stages of field development before a clear picture of the reservoir has emerged.

The running and cementing of the casings is a critical task [7]. A standard way to perform this operation is depicted in Figure 3.6. When a hole has been dug to the desired depth, the casing is lowered into the hole (Figure 3.6A). The cement is mixed and a volume somewhat greater than the annular volume between the inside of the hole and the outside of the casing is forced down the inside of the casing with a plug (Figure 3.6B), using drilling mud as the pusher. Direct displacement of the cement should lead to the complete filling of the annulus with cement by the time the plug comes to rest on the float collar (Figure 3.6C). The return of the excess cement to the surface signals a successful job.

One of the main problems encountered involves the loss of cement to the formation through permeable zones, the same lost circulation zones mentioned earlier. Geothermal formations are notorious for having large porous zones that can be caused by any number of reasons. For example, interfaces between different rock layers can be highly permeable, or a particularly porous volcanic deposit may be encountered. In fact, cavern-like openings have been found in many fields that cause the drill string to drop precipitously for several meters. If such a zone

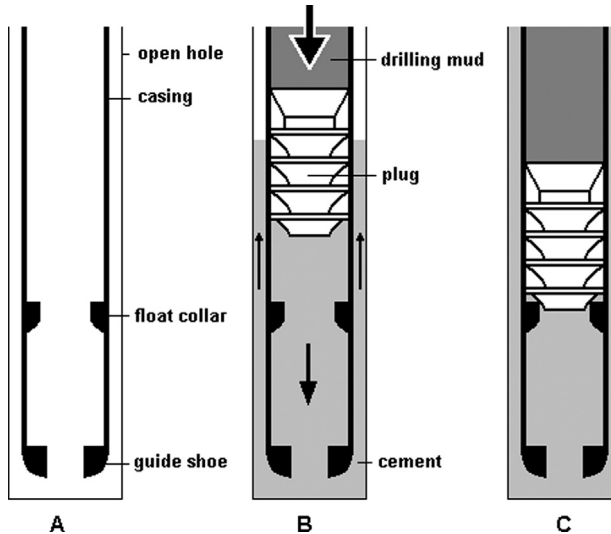


Figure 3.6 Cementing a casing in three steps.

exists, it provides an easy outlet for the cement and the cement may not return to the surface by the time the plug is on the bottom. This leaves an uncemented length of casing that can no longer be cemented by the displacement method. The casing cannot be left in this unsecured condition. The uncemented annulus is probably filled with liquid. If this section becomes heated during later operation of the well, the trapped liquid will heat up, try to expand, and its pressure will rise dramatically, most likely leading to the collapse of the casing. This certainly would mean the loss of the well and could even cause a blowout if the weak section is fairly close to the surface.

The only way to repair this is to perform a so-called “squeeze job” whereby cement is forced directly into the annulus from the surface. This, however, is fraught with risk because some drilling mud could still remain in the annulus as the cement falls into place via rivulets, not as a contiguous volume. One way to mitigate this is first to heat the casing by sending steam or hot water down a central pipe, until all the liquid has evaporated. While this will eliminate the possibility of liquid getting trapped in the annulus, there is still a chance that air pockets could exist when the job is done. But air is compressible, unlike a liquid, so that if it is heated, its pressure will not increase as greatly as with a liquid and is therefore less likely to cause a collapse of the casing. Another approach is to add perlite or gels with a bridging agent such as gilsonite to the cement during the displacement method in the hope that these will enter the permeable zones, swell up, and fill in the voids [6].

As is customary with any kind of deep well, the drilling is done in stages. A shallow anchor casing is cemented into a large hole, followed by the surface casing. The production casing is the longest one and terminates just short of the main production zone; see Figure 3.7. The well may be drilled deeper and left as an open hole or fitted with a slotted liner, set so that the slots align with the production zone. In some wells, the production casing is carried all the way to the surface, but in others it may be hung from the surface casing.

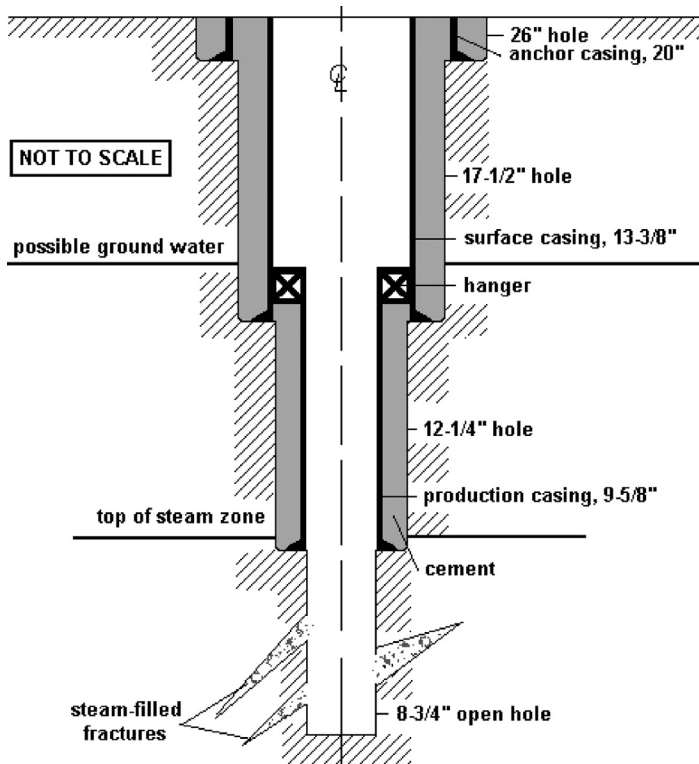


Figure 3.7 Typical well completion for a dry steam reservoir.

3.4 Safety Precautions

There is always the risk of a blowout when drilling a geothermal well. This occurs when an unexpected, high-pressure permeable zone is encountered. Enough of these dramatic and dangerous events have happened so that there are now strict regulations in most countries on the proper safety precautions to be followed during drilling [8].

The use of blowout preventers is standard practice nowadays; see [Figure 3.8](#). These are a set of fast-acting ram-type valves attached to the surface casing, and through which the drill pipe rotates. In the event of a “kick” from the well, these valves are slammed tight around the drill string, effectively closing off the well. Another valve attached to the wellhead just above the casing allows for controlled venting of the well to a silencer until the well is brought under control, usually by quenching the well with cold water.

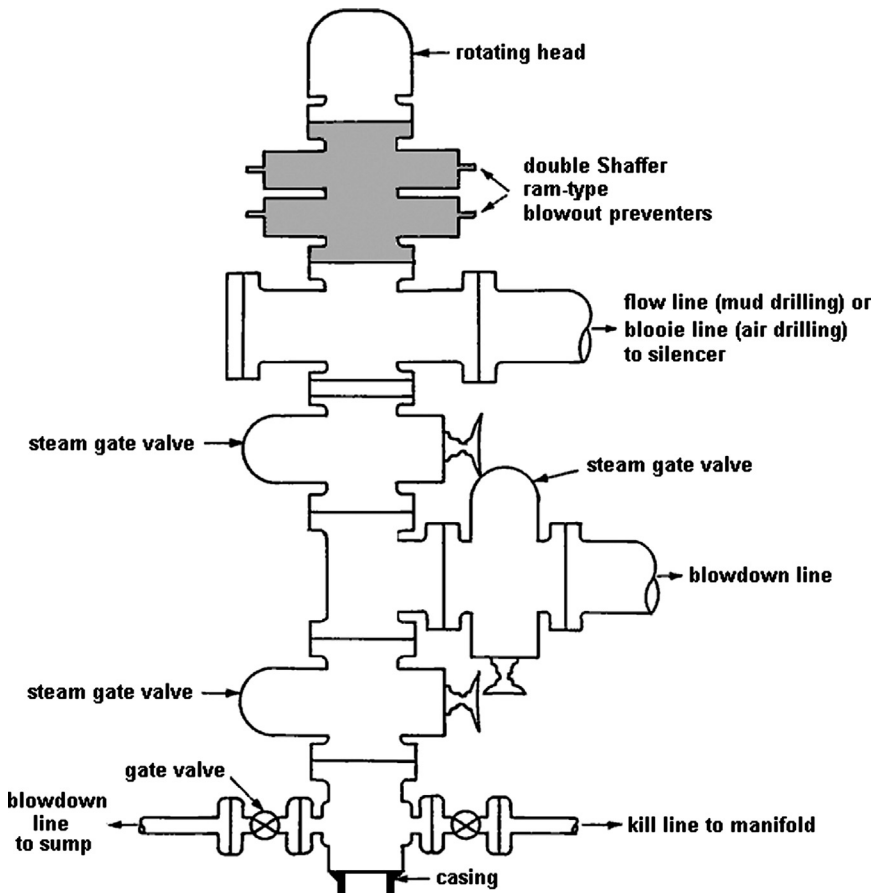


Figure 3.8 Typical blowout preventer system at The Geysers, California.

The presence of toxic gases such as hydrogen sulfide, H_2S , can lead to severe injuries and even fatalities unless proper procedures are followed [9]. The cellar of a well is a particularly dangerous place since both H_2S and carbon dioxide, CO_2 , are heavier than air. If there are any leaks from the well or casing, these gases can accumulate in the cellar. Inexpensive H_2S and CO_2 sensors should be installed wherever there is the possibility of high concentrations of these gases.

These gases and others can be extremely corrosive and can lead to casing failures unless the proper materials are used. In a new field before the fluids are thoroughly analyzed and the corrosion potential is assessed, this can lead to blowouts even after the well has been completed. If a break occurs in the casing string the pressurized geofluids can escape outside the wellbore and cause severe damage to surface equipment and injuries to personnel who may be nearby. Blowout preventers cannot stop such failures should they occur during drilling, and of course once a well is completed the blowout preventers are no longer in place and the well is controlled by the set of wellhead valves.

References

- [1] Foramines: the geothermal drilling contractor. Brochure 606.88.26, Paris, France, undated.
- [2] Edwards LM, Chilingar GV, Rieke III HH, Fertl WH, editors. *Handbook of geothermal energy*. Houston, TX: Gulf Publishing Company; 1982 (Chapters 5–8).
- [3] PNOG Energy Drilling, Inc., PNOG Rig No. 4, National 610, Metro Manila, Philippines, undated.
- [4] Hughes Christensen Drill Bit Catalog. Hughes Christensen Company, The Woodlands, TX, <<http://www.bakerhughes.com/hcc/literature/products/catalog.pdf>>; 2001.
- [5] Hutchison SO, Anderson GW. What to consider when selecting drilling fluids. World Oil, October 1974, reprint.
- [6] Shyrook SH. Geothermal cementing. In: Edwards LM, Chilingar GV, Rieke III HH, Fertl WH, editors. *Handbook of geothermal energy*. Houston, TX: Gulf Publishing Company; 1982 (Chapter 7).
- [7] Shyrook SH, Smith DK. Geothermal cementing—the state of the art. Report No. C-1274, Halliburton Services, Duncan, OK, undated.
- [8] Anon., Drilling and operating geothermal wells in California, 4th ed., Pub. No. PR7S, California Dept. of Conservation, Div. of Oil and Gas, Sacramento, CA; 1986.
- [9] Dosch MW, Hodgson SF. Drilling and operating oil, gas, and geothermal wells in an H₂S environment, Pub. No. M10, California Dept. of Conservation, Div. of Oil and Gas, Sacramento, CA; 1986.

Problems

Note: These exercises use the US Customary System of Units because they are the universally accepted units in the drilling industry.

- 3.1. An intermediate casing is about to be cemented in place in a vertical well using the displacement method (see [Figure 3.6](#)). The previous casing has a 22-in outside diameter (OD) with a 0.5-in wall thickness, and extends from the surface down to a depth of 250 ft. The new casing has a 16-in OD and a 0.438-in wall thickness and weighs 75 lbf/ft. It will be suspended and centralized in the hole a distance of 15 ft above the bottom of the 20-in diameter hole which was drilled to a total of 1450 ft. If the float collar is

10 ft above the bottom of the casing and a 5% margin of safety is allowed for the return of cement, calculate the required volume of cement (in units of cubic yards) to secure the new casing to the formation.

3.2. Using the same conditions given in Problem 3.1, calculate:

- a.** The net force on the rig hoist when the drill bit is at the bottom of the hole, if a 4-in OD drill pipe is used that weighs 12.93 lbf/ft. The bit assembly weighs approximately 800 lbf. The drilling fluid has a density of 80 lbm/ft³ and is assumed to be circulating and completely filling the annulus between the drill string and the formation.
- b.** The required holding strength of the hoist when the casing is being positioned for cementing in the well.



Chapter 4

Reservoir Engineering

Chapter Outline

4.1 Introduction	62
4.2 Reservoir and Well Flow	62
4.2.1 Darcy's Law	63
4.2.2 Reservoir-Well Model: Ideal Case	63
4.2.3 Reservoir-Well Model: Basic Principles	64
4.2.4 Liquid-Only Flow	66
4.2.5 Location of the Flash Horizon	67
4.2.6 Two-Phase Flow in the Well	70
4.2.7 Complete Model: Reservoir to Wellhead with Wellbore Flashing	71
4.3 Well Testing	75
4.3.1 Desired Information	75
4.3.2 Pressure and Temperature Instrumentation	75
4.3.3 Direct Mass Flow Rate Measurements	76
4.3.4 Indirect Mass Flow Rate Measurements	78
4.3.5 Transient Pressure Measurements and Analysis	80
4.4 Calcite Scaling in Well Casings	82
4.5 Reservoir Modeling and Simulation	83
4.5.1 Input	85
4.5.2 Architecture	85
4.5.3 Calibration and Validation	86
4.5.4 History Matching	87
4.5.5 Use of the Model	87
4.5.6 Examples of Reservoir Simulators	88
4.6 Reinjection	88
4.6.1 Motivation	88
4.6.2 Strategies	90
4.6.3 Examples	91
References	96
Problems	98

I venture to predict that great engineering work will be done in the future in conducting water to Plutonic regions, for the more abundant abstraction and upbringing of their heat energy.

Frank A. Perret—November 12, 1925

4.1 Introduction

Reservoir engineering is the art of describing quantitatively the behavior of fluids in a porous or fractured rock formation and using that description to effectively manage the production and injection of those fluids. This task is complicated by the fact that no one can be sure of the underground patterns of fractures or porosity that give rise to the permeable channels through which the fluids may move. Furthermore, even if that were possible for one moment, the fracture patterns very likely will change over time since the geothermal environment is a geologically dynamic one.

The product of the reservoir engineer is the reservoir working model, built on the conceptual model produced from the earlier scientific studies and the results of exploratory drilling, but incorporating a computer simulation of the reservoir fluid properties. Such a model can be used to forecast the evolution of the field under different scenarios of production and injection. This is an extremely important tool in the development of a geothermal resource because it tells us the long-range anticipated capability of the field to support a given amount of electrical generation.

The flow of fluids in a porous medium and in wells has been thoroughly studied from both a theoretical and an experimental viewpoint [1–9]. Most of the literature pertains to oil and gas applications. However, the vast amount of accumulated data from tests at numerous geothermal fields constitutes a wealth of information to serve the needs of reservoir researchers.

In the rest of this chapter, we will present some of the theoretical findings for specific, idealized conditions, describe some of the tests that are performed on wells, and show how this information is used to generate the reservoir working model.

4.2 Reservoir and Well Flow

The flow in a geothermal well cannot be viewed in isolation; it must be coupled to the flow of fluid in the reservoir. The only exception to this rule would be when the reservoir offers no resistance to fluid flow, a physical impossibility. While it is not easy to describe the flow of a geofluid passing through a more or less vertical well owing to possible changes in phase and flow pattern, at least the geometry of the conduit is known. In the reservoir, it is far more difficult, if not

impossible, to describe the flow analytically because the path of the fluid is unknowable. As such, the analytical approach relies on a “lumped parameter” method in which the details are smoothed out and averaged values of important properties are used instead.

4.2.1 DARCY’S LAW

One analytical approach that can be solved exactly involves flow through an idealized porous medium consisting of a bed of packed granules, the so-called “Darcy flow” problem, the solution to which is known as Darcy’s Law, after H.P.G. Darcy (1803–1858) [10]. Here the medium is seen as one of homogeneous permeability, K , the fluid is characterized by an absolute viscosity, μ , and moves very slowly (“slug flow”), in one direction, horizontally, under a pressure gradient, dP/dx . Darcy’s Law for this case yields the following equation for the fluid velocity, \mathcal{V} :

$$\mathcal{V} = -\frac{K}{\mu} \frac{dP}{dx} \quad (4.1)$$

where the negative sign indicates that the fluid moves in the direction of decreasing pressure.

In honor of Darcy, the unit of permeability is called the darcy, and is defined as follows: 1 darcy corresponds to the slow flow of a single-phase fluid having a viscosity of 1 centipoise (cP) and a volumetric flow rate of $1 \text{ cm}^3/\text{s}$ through an area with a cross-section of 1 cm^2 under the driving force of a pressure gradient of 1 atm/cm . For geothermal reservoirs, permeabilities are much smaller than a darcy and a more appropriate unit is $1/1000$ of a darcy, the millidarcy, mD. A typical permeability for a geothermal reservoir would be 10–70 mD.

4.2.2 RESERVOIR-WELL MODEL: IDEAL CASE

The simplest model of the reservoir-well system is depicted in [Figure 4.1](#).

By continuity of mass, the flow through the well must equal the flow through the reservoir under steady conditions. If the fluid in the system is liquid (i.e., essentially incompressible), then the volumetric flows must also be equal. Using Darcy’s Law and continuity, it can be shown that the pressure distribution in the reservoir as a function of the radial distance from the centerline of the well is given as:

$$P(r) = \frac{\mu \dot{V}_w}{2\pi K L_R} \ln r \quad (4.2)$$

where \dot{V}_w is the volumetric flow rate into the well through the interface between the well and the reservoir, and L_R is the reservoir thickness. The pressure

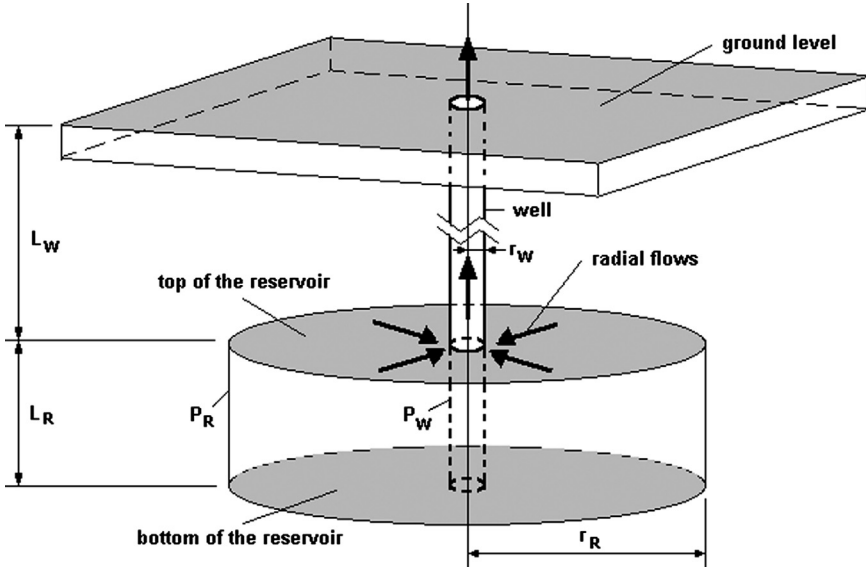


Figure 4.1 Schematic of simplified reservoir-well system.

increases with increasing distance from the well, approaching the undisturbed reservoir pressure logarithmically. The difference between the far-field reservoir pressure and the pressure at the well face is known as the drawdown, ΔP :

$$\Delta P \equiv P(r = r_R) - P(r = r_w) = \frac{\mu \dot{V}_w}{2\pi K L_R} \ln \frac{r_R}{r_w} \quad (4.3)$$

Thus, for this highly idealized case, the volumetric flow rate entering the well is given by:

$$\dot{V}_w = \frac{2\pi K L_R}{\mu \ln \frac{r_R}{r_w}} \Delta P \quad (4.4)$$

If the fluid flowing up the well undergoes a phase change (e.g., flashes into vapor), then the volumetric flow rate at the surface will be different from Eq. (4.4) owing to compressibility effects. The mass flow rates however will be the same. This case will be studied in Section 4.2.6.

4.2.3 RESERVOIR-WELL MODEL: BASIC PRINCIPLES

The approach described here is based on a model by Ryley [4,11] which uses the fundamental equations of fluid mechanics but replaces the problematic parameters with averaged empirical quantities. This leads to working equations that produce reasonable results when compared to field measurements.

The reservoir pressure may be assumed to be caused by a column of cold water distant from the well, as shown in Figure 4.2. The density of the cold water exceeds that of the hot geofluid in the reservoir-well system, thereby creating a natural siphon that will cause the well in the figure to spontaneously begin flowing as soon as the wellhead valve is opened. The exact mechanism responsible for the far-field reservoir pressure is unimportant to the argument we make here.

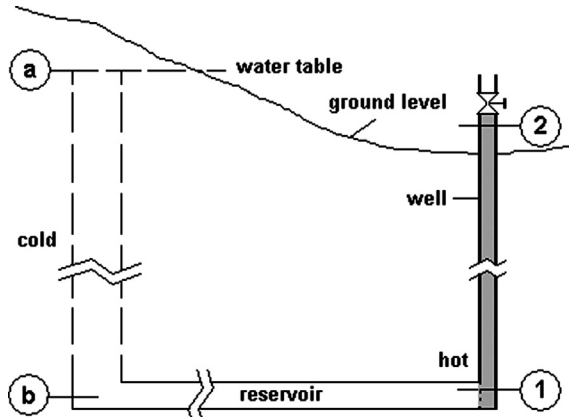


Figure 4.2 Possible pressurizing mechanism for geothermal well.

Considering first only the well between states 1 and 2, the First Law of Thermodynamics for an open system in steady flow may be written as:

$$\dot{Q} - \dot{W} = \dot{m} \left[(h_2 - h_1) + \frac{1}{2} (\mathcal{V}_2^2 - \mathcal{V}_1^2) + g(z_2 - z_1) \right] \quad (4.5)$$

where the left-hand terms are the heat and work flow rates between the well and its surroundings, and the right-hand terms are, in order, the enthalpy, kinetic and potential energy differences from the top of the well to the bottom. Unless there is a pump in the well, the work term will vanish. Given the low thermal conductivity of rock and cement (used to secure the well casings) and the rapidity with which the geofluid moves up the well, we can ignore the heat term to a first approximation. When one takes into account the units of the right-hand terms and the realistic values for these terms, it will turn out that the kinetic energy difference is relatively small. Thus we find:

$$h_2 \approx h_1 - gL_w \quad (4.6)$$

Unless the well is very deep and low in temperature, the term “ gL_w ” will be negligible compared to the geofluid enthalpy and may be ignored. In this way we find that the well flow can be approximated fairly accurately as isenthalpic, that is, one of constant enthalpy.

Now we will apply the momentum equation of fluid mechanics to the well flow. This is essentially an application of Newton's Second Law of Motion written per unit of well area, namely:

$$-dP - \frac{dF}{A} - \rho g dz = \rho \mathcal{V} d\mathcal{V} \quad (4.7)$$

where the terms on the left-hand side represent all the forces (per unit area) acting on an elemental fluid body of length dz passing up the well, and the right-hand side is the mass times acceleration (per unit area). The forces are, in order, the pressure forces acting on the ends of the fluid column, the friction forces caused by contact with the well casing, and the hydrostatic body force due to weight of the fluid above the elemental volume. Note that all the force terms are negative and oppose the motion of the fluid up the well, and that consequently the acceleration will also be negative.

We are interested in knowing the pressure as a function of height in the well, $P = P(z)$, and eventually in knowing the relationship between the mass flow rate and the wellhead pressure, $\dot{m} = \dot{m}(P_2)$. This requires us to integrate the momentum equation from the bottom of the well to the top. Before we attempt this, we can express the elemental friction force in terms of the friction factor, f , as follows:

$$dF = \frac{1}{2} \rho \mathcal{V}^2 \times f \times C dz \quad (4.8)$$

where $C = 2\pi r_w = \pi D$ is the circumference of the well interior. Now we can express the difference between the downhole pressure and that at the wellhead as follows:

$$P_1 - P_2 = \int_{\mathcal{V}_1}^{\mathcal{V}_2} \rho(z) \mathcal{V}(z) d\mathcal{V} + \frac{2}{D} \int_{z_1}^{z_2} f \rho(z) \mathcal{V}^2(z) dz + g \int_{z_1}^{z_2} \rho(z) dz \quad (4.9)$$

The formal integration of the three right-hand terms cannot be carried out unless the friction factor is known, along with the dependency of the density and velocity on the distance along the well. When flashing occurs in the well, these terms are not obvious.

4.2.4 LIQUID-ONLY FLOW

A particularly simple special case involves only the flow of liquid in the system. Here there is no acceleration term, and the velocity and density can be taken as constants. Thus the pressure difference along the well is given by:

$$P_1 - P_2 = \frac{2f\rho\mathcal{V}^2 L_w}{D} + g\rho L_w \quad (4.10)$$

where the friction factor may be found from the Swamee–Jain equation [12],

$$f = \frac{0.25}{\left\{ \log_{10} \left[\frac{\varepsilon/D}{3.7} + \frac{5.74}{\text{Re}^{0.9}} \right] \right\}^2} \quad (4.11)$$

with ε being the absolute roughness of the well casing and Re being the Reynolds number:

$$\text{Re} = \frac{\rho \mathcal{V} D}{\mu} = \frac{\dot{m} D}{\mu A} = \frac{4 \dot{m}}{\mu \pi D} \quad (4.12)$$

4.2.5 LOCATION OF THE FLASH HORIZON

Another case that can be handled easily involves the determination of the location of the flash horizon in the well, that is, the elevation where the liquid flashes into vapor. Here we will couple the reservoir to the well and follow the flow of liquid through the system.

With reference to Eq. (4.4), if we recognize that the volumetric flow rate is equal to the mass flow rate divided by the density, that is,

$$\dot{V} = \dot{m} / \rho \quad (4.13)$$

we can arrive at the following expression for the drawdown pressure difference:

$$\Delta P = P_R - P_1 = \frac{\mu \ln(r_R/r_W)}{2\pi K L_R \rho_R} \dot{m} \equiv C_D \dot{m} \quad (4.14)$$

where we have introduced C_D , the drawdown coefficient. Thus the pressure at the bottom of the well under flowing conditions can be found from the reservoir pressure, the mass flow rate, and the drawdown coefficient:

$$P_1 = P_R - C_D \dot{m} \quad (4.15)$$

The drawdown coefficient may be found as follows. The reservoir pressure, P_R , can be found by measuring the pressure in the well opposite the inflow zone under static conditions, that is, when $\dot{m} = 0$. If the pressure is measured at the same location under flowing conditions, along with the mass flow rate using surface equipment, then the drawdown coefficient can be calculated using Eq. (4.15). Note that the inverse of C_D is called the productivity index, J_I .

To locate the flash horizon, we need to consider the flow from the reservoir into the well and up the well to the place where the geofluid pressure falls to the saturation pressure corresponding to the geofluid temperature. That is, at the flash point:

$$P_F = P_{sat}(T_R) \quad (4.16)$$

If we combine Eqs. (4.10) and (4.14) and eliminate the velocity using the continuity equation, we end up with:

$$P_2 = P_R - \left[\frac{\mu}{\rho_R} \right] \left[\frac{1}{KL_R} \right] \left[\frac{\ln(r_R/r_W)}{2\pi} \right] \dot{m} - \left[\frac{1}{\rho} \right] \left[\frac{32}{\pi^2} \right] \left[\frac{fL_W}{D^5} \right] \dot{m}^2 - \rho g L_W \quad (4.17)$$

This equation is written from the reservoir to the top of the well, but we only want to apply it to the flash point. Therefore, the working equation to solve for the flash horizon is:

$$P_{sat}(T_R) = P_R - \left[\frac{\mu}{\rho_R} \right] \left[\frac{1}{KL_R} \right] \left[\frac{\ln(r_R/r_W)}{2\pi} \right] \dot{m} - \left[\frac{1}{\rho} \right] \left[\frac{32}{\pi^2} \right] \left[\frac{fL_F}{D^5} \right] \dot{m}^2 - \rho g L_F \quad (4.18)$$

where L_F is the distance up the well from the feed zone up to the flash horizon. The depth from the surface to the feed zone is L_W , so that the depth to the flash horizon is simply $L_W - L_F$. We can simplify Eq. (4.18) using the drawdown coefficient and solve for the flash horizon:

$$L_F = \frac{P_R - P_{sat}(T_R) - C_D \dot{m}}{\rho g + C_2 \dot{m}^2} \quad (4.19)$$

where a new term C_2 has been defined as:

$$C_2 \equiv \left[\frac{1}{\rho} \right] \left[\frac{32}{\pi^2} \right] \left[\frac{f}{D^5} \right] \quad (4.20)$$

The observant reader will detect that the friction factor f in Eq. (4.20) is itself a function of the mass flow rate through the Reynolds number; see Eqs. (4.11) and (4.12). This dependency is weak for fully developed, high Reynolds number, turbulent flow, but is not negligible for many geothermal applications.

From Eq. (4.19), one can see that the flash horizon moves down the well (i.e., L_F gets smaller) as the mass flow rate increases. The flash point will reach the feed zone of the well for sufficiently high flow rates and eventually will move into the reservoir. Once two-phase flow occurs in the formation, our linear drawdown equation, Eq. (4.15) will no longer be valid, and the process becomes highly complex.

The velocities of the liquid and vapor phases will differ as they flow through the formation since the resistance offered by the porous rock to the vapor will be less than for the liquid. This will cause the vapor to be produced at a higher rate than the liquid, and the enthalpy of the two-phase mixture to exceed the value expected for isenthalpic flow. Thus, the appearance of “excess enthalpy” at the wellhead is an indication of flashing in the formation. Likewise, the wellhead dryness fraction will be greater than for isenthalpic flow.

Numerical example: Flash horizon—Before moving on to the two-phase flow region above the flash point, it is instructive to consider a numerical example of Eq. (4.19). This will also provide a feeling for the order of magnitude of the terms in the equation.

Given data:

$$P_R = 20 \text{ MPa}, \quad \dot{m} = 75 \text{ kg/s}, \quad L_W = 2000 \text{ m}, \quad T_R = 250^\circ\text{C}, \\ D = 0.244 \text{ m (or 9-5/8 in)}, \quad g = 9.81 \text{ m/s}^2, \quad P_1 = 17 \text{ MPa @ } \dot{m} = 75 \text{ kg/s}$$

From *Steam Tables* [13], we can find the appropriate properties for the geofluid (assumed to be pure water): $P_{sat} = 3.973 \text{ MPa}$, $\rho = 799.2 \text{ kg/m}^3$, and $\mu = 0.000107 \text{ kg/m} \cdot \text{s}$.

The drawdown is found from the given data:

$$C_D = \frac{P_R - P_1}{\dot{m}} = \frac{20 - 17}{75} = 0.040 \frac{\text{MPa}}{\text{kg/s}}$$

The Reynolds number and the friction factor are found from Eqs. (4.12) and (4.11):

$$\text{Re} = \frac{4\dot{m}}{\mu\pi D} = \frac{4 \times 75}{0.000107 \times \pi \times 0.244} = 3,657,613 \\ f = \frac{0.25}{\left\{ \log_{10} \left[\frac{\varepsilon/D}{3.7} + \frac{5.74}{\text{Re}^{0.9}} \right] \right\}^2} = \frac{0.25}{\left\{ \log_{10} \left[\frac{0.0457/244}{3.7} + \frac{5.74}{3,657,613^{0.9}} \right] \right\}^2} = 0.01392$$

We have used a surface roughness of 0.0457 mm, assuming commercial steel casing.

The factor C_2 may now be calculated as:

$$C_2 = \left[\frac{1}{\rho} \right] \left[\frac{32}{\pi^2} \right] \left[\frac{f}{D^5} \right] = \left[\frac{1}{799.2} \right] \left[\frac{32}{\pi^2} \right] \left[\frac{0.01392}{0.244^5} \right] = 0.06528 \text{ kg}^{-1} \text{ m}^{-2}$$

And finally we can calculate the height of the flash horizon above the feed zone (assumed to be at the bottom of the well):

$$L_F = \frac{P_R - P_{sat}(T_R) - C_D \dot{m}}{\rho g + C_2 \dot{m}^2} = \frac{20 - 3.973 - 0.040 \times 75}{799.2 \times 9.81 + 0.06528 \times 75^2} \\ = \frac{13.027}{7840.15 + 367.2} = 1587 \text{ m}$$

Thus, the fluid flashes from liquid to a two-phase mixture starting at a depth of 413 m below the wellhead.

Without going into the numbers, if this well could flow at 150 kg/s, then the flash depth would be 921 m below the wellhead, still within the wellbore but some 508 m deeper. Theoretically, a mass flow rate of 400.67 kg/s would place the flash point at the entrance to the well since the drawdown ($0.040 \times 400.67 = 16.027$ MPa) results in the saturation pressure being reached as the fluid arrives at the well ($20 - 16.027 = 3.973$ MPa). Since this is a very high flow rate for a single well, for the conditions considered in this example, it is likely that flashing would always occur in the wellbore. Over time however, should the reservoir pressure fall, as can be expected during exploitation, the drawdown may cause the fluid to flash in the formation. For example, in this case, if the reservoir pressure were to drop to 10 MPa, then a mass flow greater than 151 kg/s will lead to flashing in the formation.

4.2.6 TWO-PHASE FLOW IN THE WELL

We now return to the more difficult task of modeling the two-phase flow that takes place from the flash horizon upward to the wellhead. We may begin with Eq. (4.9) rewritten to apply from the flash point, state F , to the wellhead, state 2:

$$P_F - P_2 = \int_{\mathcal{V}_F}^{\mathcal{V}_2} \rho_{LV}(z) \mathcal{V}_{LV}(z) d\mathcal{V} + \frac{2}{D} \int_{z_F}^{z_2} f_{LV} \rho_{LV}(z) \mathcal{V}_{LV}^2(z) dz + g \int_{z_F}^{z_2} \rho_{LV}(z) dz \quad (4.21)$$

In order to integrate Eq. (4.21), we are at once confronted with the problem of deciding what to use for the various two-phase properties denoted by the subscript LV . These include the density, velocity, and friction factor. This general problem has been the subject of many research efforts and continues to this day. In addition to the Refs. [1–9], the reader may wish to consult Refs. [14–17] for more details.

We will adopt the lumped-parameter approach presented by Ryley [11] in which mean effective values are used for these two-phase terms. These may then be viewed as constants and the equation readily integrates to:

$$P_F - P_2 = \frac{\bar{\rho}_{LV}}{2} (\mathcal{V}_2^2 - \mathcal{V}_1^2) + \frac{2}{D} \bar{f}_{LV} \bar{\rho}_{LV} \bar{\mathcal{V}}_{LV}^2 (z_2 - z_F) + g \bar{\rho}_{LV} (z_2 - z_F) \quad (4.22)$$

Note that the velocity at the flash point is taken as equal to that at the well feed zone since the liquid is incompressible up to that point. We now must give quantitative meaning to each of the mean effective terms.

- \mathcal{V}_2 : The exit velocity is that velocity which will generate the same kinetic energy carried by the two-phase mixture. That is,

$$\frac{\mathcal{V}_2^2}{2} = x_2 \frac{\mathcal{V}_{g2}^2}{2} + (1 - x_2) \frac{\mathcal{V}_{f2}^2}{2} \quad (4.23)$$

where x_2 is the mass fraction of vapor (called the quality) of the exiting two-phase mixture, defined as [18]:

$$x_2 = \frac{\rho_{g2} A_{g2} \mathcal{V}_{g2}}{\rho_{f2} A_{f2} \mathcal{V}_{f2} + \rho_{g2} A_{g2} \mathcal{V}_{g2}} \quad (4.24)$$

The area terms account for the portions of the exit area occupied by the two phases. The slip ratio, k_2 , relates to the velocity of the two phases:

$$k_2 \equiv \frac{\mathcal{V}_{g2}}{\mathcal{V}_{f2}} \quad (4.25)$$

Thus the exit velocity can be expressed as:

$$\mathcal{V}_2 = \mathcal{V}_{g2} \left[x_2 + \frac{1 - x_2}{k_2^2} \right]^{1/2} \quad (4.26)$$

- $\bar{\rho}_{LV}$: The average density over the two-phase region is taken simply as the average of the values at the flash horizon and at the exit:

$$\bar{\rho}_{LV} = \frac{1}{2} \left[\rho_R + x_2 \rho_{g2} + (1 - x_2) \rho_{f2} \right] \quad (4.27)$$

- $\bar{\mathcal{V}}_{LV}$: Recognizing that the mass flow rate is equal to the product of the density, the cross-sectional area and the velocity, we apply this notion to get an expression for the mean effective two-phase velocity:

$$\bar{\mathcal{V}}_{LV} = \frac{\dot{m}}{\bar{\rho}_{LV} A} \quad (4.28)$$

- f_{LV} : The two-phase friction factor cannot be expressed in terms of any other property as we have done for the other mean effective quantities. The only thing we can do is to recognize that it will be larger than the liquid friction factor, f , but how much larger, we cannot say. Multipliers in the range of 2–3 are probably acceptable.

4.2.7 COMPLETE MODEL: RESERVOIR TO WELLHEAD WITH WELLBORE FLASHING

We may now assemble the pieces of the model to obtain the governing equation for the pressure behavior from the undisturbed reservoir to the wellhead including

flashing within the well. The pressure drop from the far reservoir to the well entrance point is given by Eq. (4.15); from the entry point to the flash horizon by Eq. (4.10); and from the flash horizon to the wellhead by Eq. (4.22). Thus we obtain:

$$P_2 = P_R - C_D \dot{m} - g(\rho_R L_F + \bar{\rho}_{LV} d_F) - \frac{2}{D} \bar{f}_{LV} \bar{\rho}_{LV} \bar{V}_{LV}^2 d_F - \frac{32 f L_F}{\pi^2 D^5 \rho_R} \dot{m}^2 - \frac{\bar{\rho}_{LV}}{2} \left[C_3^2 \left(x_2 + \frac{1 - x_2}{k_2} \right) - \frac{16}{\pi^2 D^4 \rho_R^2} \right] \dot{m}^2 \quad (4.29)$$

where d_F is the depth to the flash horizon from the wellhead, and the factor C_3 is defined as:

$$C_3 = \frac{x_2 \rho_{f2} + (1 - x_2) \rho_{g2} k_2}{\rho_{f2} \rho_{g2} A} \quad (4.30)$$

The wellhead dryness fraction, x_2 , can be computed from the following equation using an isenthalpic process from the reservoir to the surface:

$$x_2 = \frac{h_R - h_{f2}}{h_{g2} - h_{f2}} \quad (4.31)$$

with h_R evaluated for a saturated liquid at the reservoir temperature.

By the time the fluid has made its way from the far reaches of the reservoir to the wellhead, the pressure has been reduced from P_R to P_2 by the following effects, starting with the second term on the right-hand side of Eq. (4.29):

- Drawdown in the reservoir
- Hydrostatic pressure drop in the well, liquid section and two-phase section
- Frictional pressure drop in the two-phase section
- Frictional pressure drop in the liquid section
- Accelerational pressure drop in the two-phase section.

Our objective of finding the dependency of the mass flow rate on the wellhead pressure, $\dot{m} = \dot{m}(P_2)$, is implicit in Eq. (4.29). All properties of the liquid may be found from *Steam Tables* at the reservoir temperature, using saturated liquid values. The properties of the two phases at the wellhead, saturated liquid and saturated vapor, can also be taken from the *Steam Tables* once the wellhead pressure is specified. The drawdown coefficient may be assumed from earlier measurements. The two-phase friction factor may either be treated as a variable parameter or set equal to some multiple, say 2 or 3, of the liquid friction factor. Ryley [11] showed that a wellhead slip ratio of about 5 gave the correct behavior.

The algorithm for the calculation of the mass flow rate as a function of the wellhead pressure begins by positing a mass flow rate and then determining the flash horizon as described in Section 4.2.5 for a well of known diameter. All values that depend on the mass flow rate in Eq. (4.29) are then found. Then one assumes a value for P_2 and evaluates all the terms that depend on it. If Eq. (4.29) is satisfied when all these values are inserted in the equation, then that wellhead pressure corresponds to the selected mass flow rate. If not, then an iterative procedure is followed until the equation is satisfied. By choosing a suite of values for mass flow rate and carrying out the procedure just described, the so-called productivity curve can be determined, that is, the mass flow rate \dot{m} versus the wellhead pressure P_2 .

Several numerical examples are presented in Ref. [11] which demonstrate that the method is capable of giving both qualitative and quantitative results that compare very favorably with actual well behavior. Typical productivity curves are shown schematically in Figure 4.3. The general shape of the curves is not affected by the values of the friction factors—liquid and two-phase—but as the friction factors increase, the flow rate decreases for a given wellhead pressure.

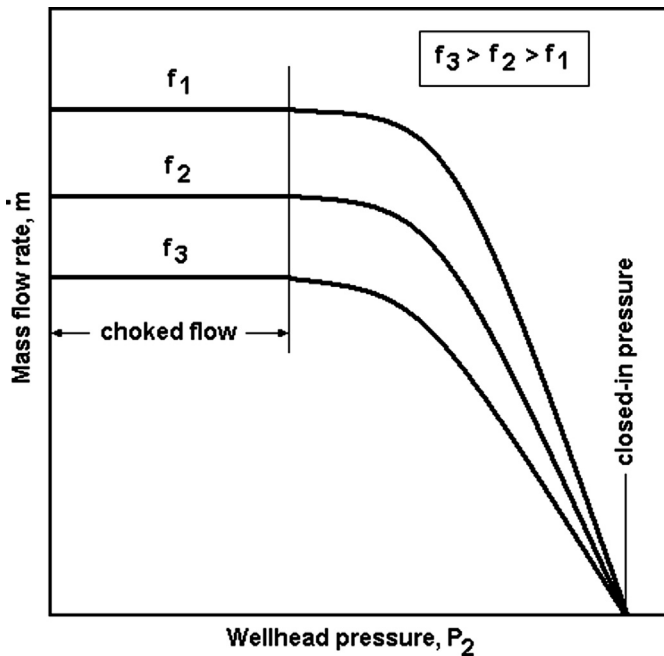


Figure 4.3 Typical productivity curves from Eq. (4.29).

Practically, at a certain wellhead pressure, further lowering of the pressure does not result in an increase in the flow rate, and we say the flow is choked. Note that the numerical solution of Eq. (4.29) shows that the mass flow rate reaches a maximum as the wellhead pressure is reduced, and tends to decrease as P_2 is further reduced. Thus, one simply cuts off the calculation at the maximum point and keeps the flow rate constant for lower pressures.

We may sum up the phenomenon of reservoir-well flow with reference to Figure 4.4 where the mass flow rate is plotted against the pressure. The productivity curve is the heavy line at the left. The line labeled P_1 is the pressure at the inlet to the well from the feed zone. The reservoir pressure is P_R and the pressure corresponding to the lowest stable mass flow rate is the maximum discharge pressure, P_{MD} . The shaded region at bottom left is unstable and is not modeled by the method developed in this section. Also shown is the saturation pressure P_{sat} corresponding to the reservoir temperature.

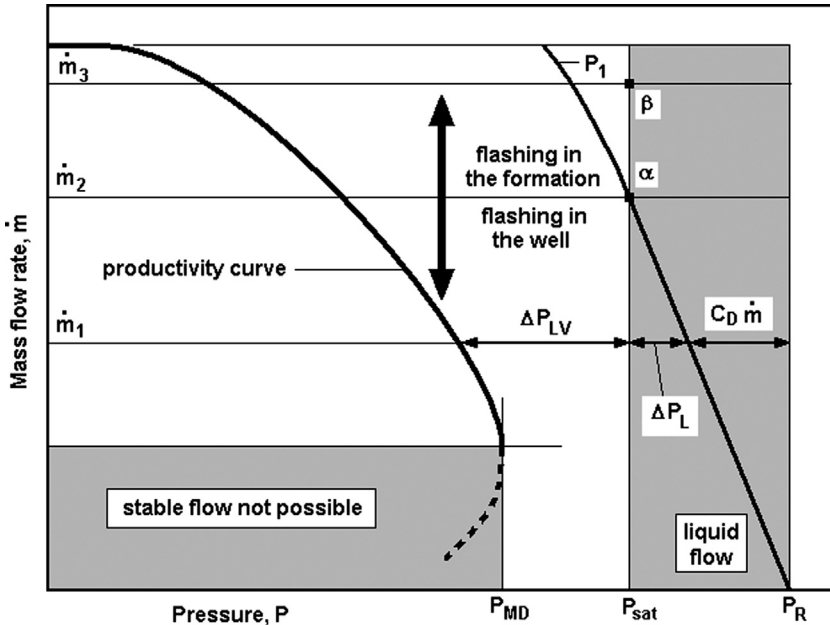


Figure 4.4 Flow domains from reservoir to wellhead.

Three mass flows are highlighted. For \dot{m}_1 , starting at the right and moving to the left, we first see the drawdown within the reservoir, followed by the frictional and hydrostatic pressure drop in the liquid, and finally the two-phase pressure drop. The flashing begins within the well. For \dot{m}_2 , the flashing begins just at the point where the fluid enters the well, state α . For \dot{m}_3 , the flashing begins somewhere in the formation, state β , and the pressure drop from there to the wellhead is caused solely by two-phase flow effects.

4.3 Well Testing

The testing methods for geothermal wells have been adapted from the oil and gas industry [3,5]. The objective of a well-testing program is to determine as much as possible about the reservoir and the geofluid, and in particular the ability of the reservoir-well combination to produce an acceptable flow rate under thermodynamic conditions suitable to generate electricity. It would be very useful to be able also to forecast the lifetime over which the well can maintain this level of production, but this is more difficult, if not impossible, at the early well-testing stage.

4.3.1 DESIRED INFORMATION

Here is what we want to know at the outset of the testing program:

- Pressure in the well as a function of depth, including at feed zones
- Temperature in the well as a function of depth, including at feed zones
- Pressure in the reservoir, under static and flowing conditions
- Reservoir permeability or permeability-thickness product
- Mass flow rates of both liquid and vapor phases
- Chemical composition of both liquid and vapor phases, downhole and at the surface
- Condition of the well.

The last item refers to possible damage to the permeable zones in the formation, for example, by drilling mud, caking, or cement invasion. The condition of the casings is also important.

4.3.2 PRESSURE AND TEMPERATURE INSTRUMENTATION

Pressures measured on the surface can be made using any standard means such as Bourdon gauges, a Fortin barometer, differential manometers, etc. Pressure gauges attached to pipes or vessels give readings of pressure relative to atmospheric pressure (so-called “gauge” pressure). The atmospheric pressure at the site must be added to the gauge pressure to obtain absolute pressure; property tables require absolute pressure. The atmospheric pressure varies with altitude, a , as will the boiling temperature of water. The following two equations may be used to estimate these two effects up to an altitude, a , of 2600 m above sea level:

$$P_{atm}(a) = 101.3 - 0.0120a \quad (4.32)$$

where the pressure is measured in kPa and altitude is in m;

$$T_{sat}(P_{atm}) = 27.14 \ln P_{atm} - 25.397 \quad (4.33)$$

where the temperature is measured in °C.

Pressures in the geothermal well can be accurately measured with piezoelectric pressure transducers. One device that is commercially available can measure pressures up to 34,000 kPa with an accuracy of 8 kPa. The same device also incorporates a resistance thermometer with an accuracy of 0.15% (full scale). The whole package can operate in a hot geothermal well at up to 300°C (570°F) for as long as 9 hours [19]. The data are recorded with the aid of a USB port on a computer running Windows 98 or higher. As can be seen in Figure 4.5, the assembly is about 5 ft long and has a diameter of less than 2 in and weighs about 21 lbs (9.5 kg). It is lowered on a wireline through a gland seal and set at any depth to measure the pressure and temperature simultaneously.

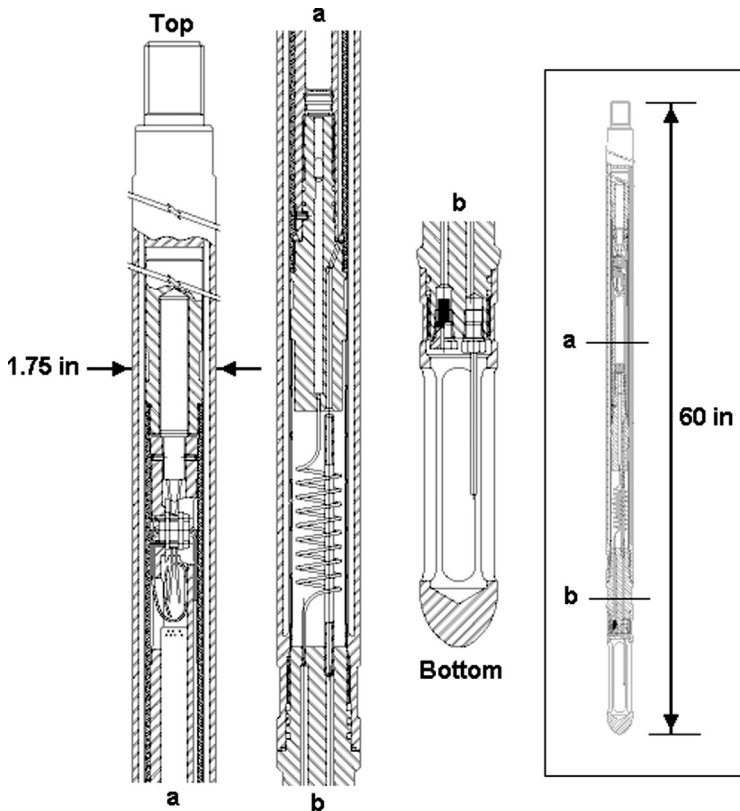


Figure 4.5 Kuster K10 geothermal tool for pressure and temperature measurements [19].

4.3.3 DIRECT MASS FLOW RATE MEASUREMENTS

Mass flow rates of two-phase geofluids are best measured directly by first separating the two phases, and measuring the flow rates of the liquid and vapor

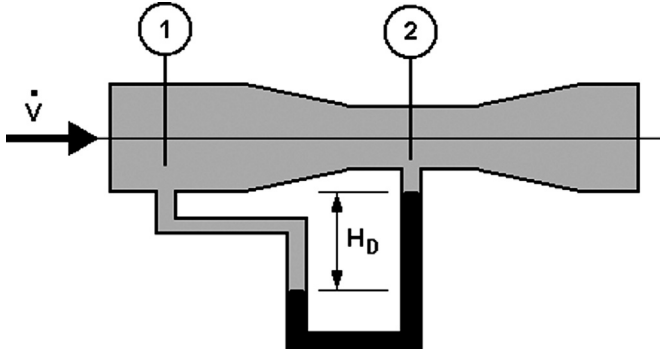


Figure 4.6 Venturi flow meter.

individually by means of venturi meters or calibrated orifices. Venturis are very accurate for determining volumetric flow rates; see [Figure 4.6](#). If the fluid density is known, then the mass flow rate can easily be calculated. The volumetric flow rate can be found from:

$$\dot{V} = C_V A_2 \sqrt{\frac{2g(P_1 - P_2)/\gamma}{1 - (A_2/A_1)^2}} \quad (4.34)$$

where C_V is the venturi calibration constant, γ is the specific gravity of the fluid in the U-tube manometer, and the pressure difference is related to the reading of the manometer:

$$\frac{P_1 - P_2}{\gamma} = \gamma H_D - H_D = H_D(\gamma - 1), \quad [\text{liquid flow}] \quad (4.35)$$

where the units of both sides of [Eq. \(4.35\)](#) are equivalent head of water. For steam flow, the density of steam above the manometer is negligible and [Eq. \(4.35\)](#) becomes simply

$$\frac{P_1 - P_2}{\gamma} = \gamma H_D, \quad [\text{steam flow}] \quad (4.36)$$

Care must be taken to ensure that the liquid from the separator is cooled some 20–30°C below saturation and is free of entrained steam. Even a small amount on the order of 0.5% can introduce unacceptably large errors in the liquid flow measurements [\[20\]](#).

A sharp-edged orifice plate (see [Figure 4.7](#)) may also be used for these measurements. They are much less expensive than venturi meters and are more suitable for field measurements. Venturi meters are more appropriate when accurate measurements are needed for steam flow rates being delivered to a power station.

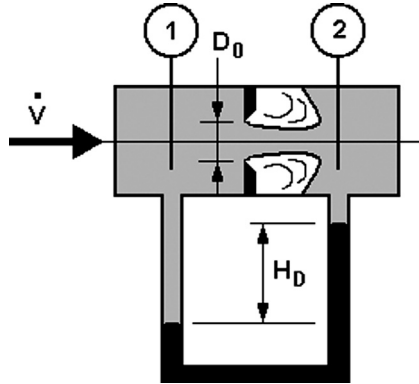


Figure 4.7 Sharp-edged orifice flow meter.

The theoretical advantage of a sharp-edged orifice meter (compared with a rounded-edged one) is that the reading is not sensitive to the fluid viscosity and therefore should not be sensitive to the fluid temperature. However, it is difficult to make a true sharp-edged orifice, and abrasive fluids will soon wear down the knife-edge anyway, so that orifices need to be calibrated. The volumetric flow rate is found from:

$$\dot{V} = C_0 A_0 \sqrt{2g(P_1 - P_2)/\gamma} \left[1 + \frac{1}{2} C_0^2 \left(\frac{D_0}{D_1} \right)^4 \right] \quad (4.37)$$

where C_0 , the orifice coefficient, is determined by calibration.

The mass flow rate is calculated from the volumetric flow rate using:

$$\dot{m} = \rho \dot{V} = \dot{V}/v \quad (4.38)$$

where ρ is the fluid density and v is the specific volume.

4.3.4 INDIRECT MASS FLOW RATE MEASUREMENTS

One means to determine the mass flow rates of the liquid and vapor phases involves the somewhat cumbersome procedure of feeding the total well flow (or a known fraction thereof) into a large insulated vessel partially filled with a known amount of cold water. This technique requires fast-acting valves to allow an accurate timing of the flow into the vessel; see [Figure 4.8](#).

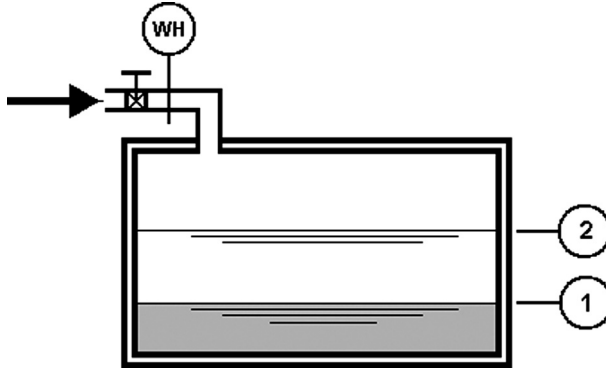


Figure 4.8 Calorimeter method for wellhead flow measurement.

At time t_1 the liquid in the vessel resides at state 1; during a period of time Δt , the vessel is filled to state 2, receiving two-phase fluid at state WH . The First Law of Thermodynamics applied to the vessel over the time interval Δt (open, unsteady system) yields the working equation for the enthalpy of the two-phase mixture:

$$h_{WH} = \frac{m_2 u_2 - m_1 u_1}{m_2 - m_1} \quad (4.39)$$

where u stands for the internal energy of the geofluid. If the wellhead pressure, P_{WH} , is known, this allows one to calculate the quality at the wellhead and the flow rates of the two phases.

Another more commonly used method is the James' lip pressure method [20]. James conducted experiments using discharge pipes of 3, 6, and 8 in diameter and arrived at an empirical correlation that can be used to determine the total, two-phase well flow:

$$\dot{m} = 8,953.5 \frac{DP^{0.96}}{h^{1.102}} \quad (4.40)$$

where \dot{m} is the total mass flow rate (in t/h or 10^3 kg/h), D is the internal diameter of the pipe (in mm), h is the two-phase enthalpy (in kcal/kg), and P is the pressure (in kg/cm², abs) measured by a pressure gauge located on 1/4-in tap, 1/4-in back from the lip of the pipe discharging freely into the atmosphere under choked conditions. The enthalpy cannot be measured directly and must be found using a silencer in which the liquid and vapor are separated at atmospheric pressure. A 90°-notched weir measures the flow of liquid, and the enthalpy can be found by solving the equation:

$$h^{1.102} + C_w h = C_w h_g \quad (4.41)$$

in which h_g is the enthalpy of saturated vapor at atmospheric pressure (from *Steam Tables*) and the weir factor C_W is given by:

$$C_W = \frac{1.052 P^{0.96} D^2}{\dot{m}_f h_{fg}} \quad (4.42)$$

with h_{fg} being the enthalpy of evaporation at atmospheric pressure. The liquid mass flow rate can be found from the standard weir formula:

$$\dot{m}_f \approx 2.6 L_W^{2.5} \quad (4.43)$$

where L_W is the height of the water passing over the weir measured from the bottom of the notch ($L_W > 1$ ft).

4.3.5 TRANSIENT PRESSURE MEASUREMENTS AND ANALYSIS

A series of time-dependent pressure measurements made after changes in the mass flow rate from a well can be used to determine several properties of the reservoir [5]. A common test is the *pressure buildup test*. The procedure is to conduct a steady flow test at a certain volumetric flow rate \dot{V}_1 for a period of time, t_1 , during which the downhole pressure opposite the feed zone is monitored. The well is then closed in and the pressure is monitored for an additional time duration, Δt . This procedure is shown schematically in Figure 4.9.

The governing equation for the shut-in, downhole pressure behavior is [5]:

$$P_{dh,s} = P_i - \frac{\dot{V}_1 \mu}{4\pi K L_R} \ln \left[\frac{t_1 + \Delta t}{\Delta t} \right] \quad (4.44)$$

where P_i is the static reservoir pressure. Since the pressure difference depends on the log of the time, a plot of pressure versus log of the dimensionless time should yield a straight line. This behavior is shown in Figure 4.10, a semilog graph known as a Horner plot, for some hypothetical data.

The data may be extrapolated to infinite time, that is, $\Delta t \rightarrow \infty$ or $(t_1 + \Delta t)/\Delta t \rightarrow 1$, to obtain the initial static pressure, P_i . From Eq. (4.44) it can be seen that the magnitude of the slope of the line, m , is given by:

$$m = 2.3026 \frac{\dot{V}_1 \mu}{4\pi K L_R} \quad (4.45)$$

or

$$K L_R = 2.3026 \frac{\dot{V}_1 \mu}{4\pi m} \quad (4.46)$$

Thus the product of the formation permeability and the reservoir thickness can be deduced from a pressure buildup test.

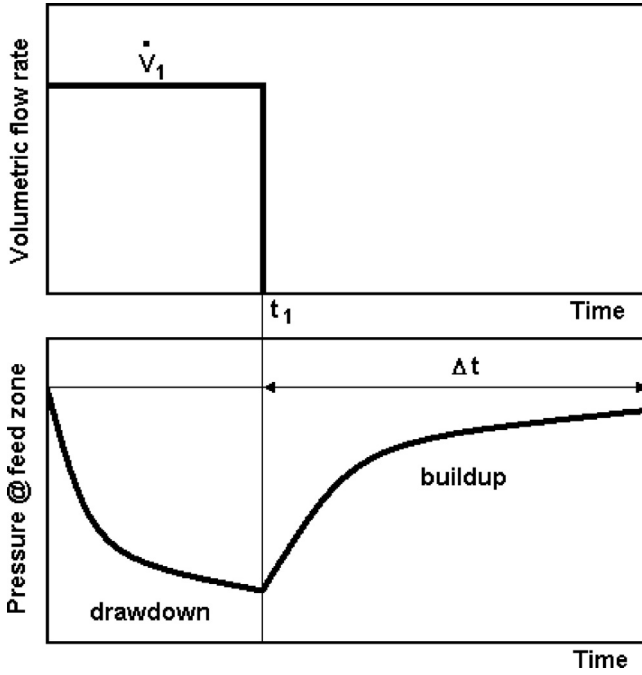


Figure 4.9 Pressure buildup test.

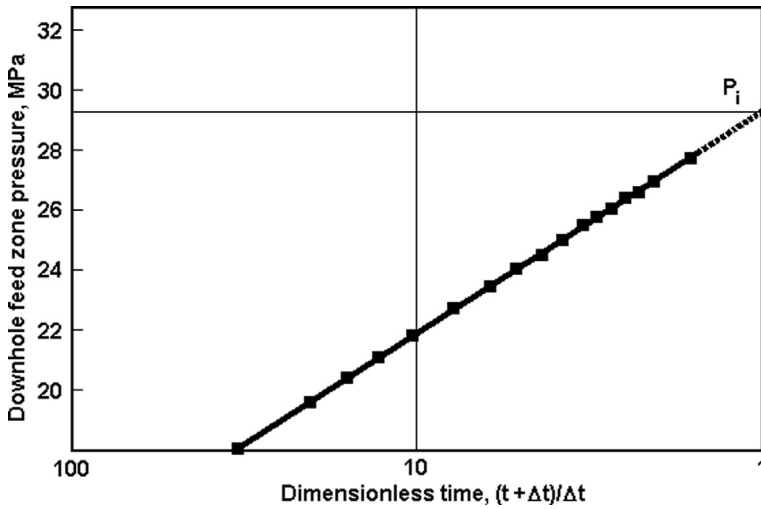


Figure 4.10 Horner plot for pressure buildup test.

It is also possible to infer whether or not there is a “skin effect,” that is, an added resistance to flow caused by well damage. In such a case, a “skin factor” s is defined as shown below to account for an additional pressure drop between the far reservoir and the interior of the well:

$$\Delta P_{skin} \equiv s \frac{\dot{V} \mu}{2\pi K L_R} \quad (4.47)$$

Many other kinds of transient flow tests may be carried out. These include drawdown tests with multiple steps and interference tests among several wells. In the latter, a chemical tracer is injected into one well while other wells are producing. The producers are monitored for the return of the tracer, thereby revealing the connectivity among the various wells. The reader is referred to Refs. [2,9] for more details.

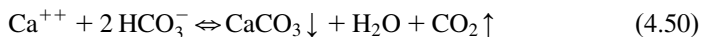
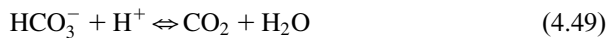
4.4 Calcite Scaling in Well Casings

One of the common problems seen in geothermal wells is the deposition of calcium carbonate or calcite, CaCO_3 , in the well casing, starting just above the flash horizon. It is not uncommon for high-temperature geofluids to be close to saturation with respect to calcite as they flow through the formation. The solubility of calcite, however, varies inversely with temperature, so that it cannot precipitate from the geofluid merely because of a decrease in temperature, other factors being constant. The other properties of the geofluid that influence the solubility are:

- Partial pressure of carbon dioxide, CO_2
- pH
- Salinity
- Calcium ion concentration.

The first two factors are interrelated; when the geofluid flashes in the well, the steam that is released carries with it most of the CO_2 . This in turn causes the pH of the liquid to rise dramatically, and results in the geofluid becoming supersaturated with respect to calcite. Precipitation occurs immediately and can lead to severe narrowing of the wellbore for several meters just above the flash horizon.

The chemical equilibrium reactions that control the process are [21]:



The loss of carbon dioxide ($\text{CO}_2 \uparrow$) upon flashing can be seen to cause the precipitation of calcite ($\text{CaCO}_3 \downarrow$) from Eq. (4.50). The fraction of CO_2 , relative to the original amount dissolved in the brine, that leaves the brine with the flashed steam can be found from [22]:

$$X_{\text{CO}_2} = \frac{1/A}{[(1/x) - 1] + (1/A)} \quad (4.51)$$

where A is a separation coefficient [23] and x is the dryness fraction of the two-phase, steam–liquid mixture. The separation coefficient is a function of temperature and the salinity of the brine, as shown in Figures 4.11 and 4.12. The dryness fraction can be calculated from Eq. (4.31). For example, if 1 M brine at 200°C undergoes a 12% flash, then 98.5% of the CO_2 will end up in the vapor phase.

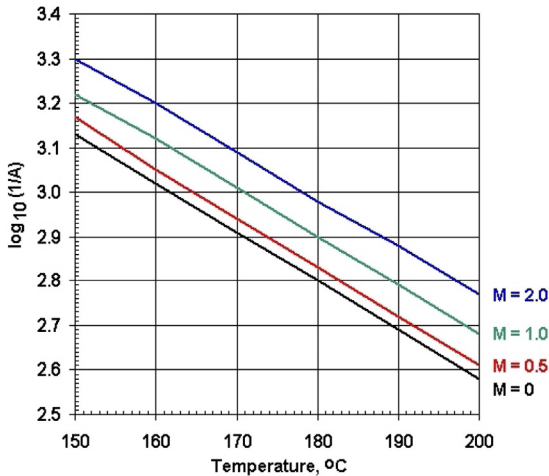


Figure 4.11 $\log_{10}(1/A)$ as a function of temperature for various molalities [WWW].

4.5 Reservoir Modeling and Simulation

A reservoir simulator is a computer code that embodies all of the essential properties of the formation, the geofluid, and the environment together with the physical and chemical laws controlling their interactions to allow the extrapolation of the performance of the reservoir from the present time to a future time, usually several decades away.

The information derived from such a code is valuable to those interested in developing and financing a power plant. Often a reservoir model is the only

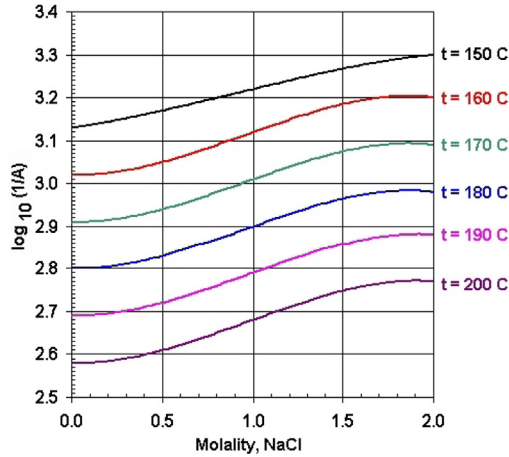


Figure 4.12 $\log_{10}(1/A)$ as a function of molality for various temperatures [WWW].

predictive tool available at the early stages of development to assure potential investors that their money will be wisely spent. It is also a requirement for most feasibility studies when considering a new project or the expansion of an existing one.

Nowadays, with the widespread use of personal computers with powerful capabilities once reserved for mainframe or minicomputers, it is far easier to conduct reservoir modeling studies. However, the relative ease with which such studies can be performed does not mean that the results can be viewed as any more reliable. Reservoir simulations require a solid understanding of the geothermal system, based on the geoscientific exploration results including the results of the first few deep wells. Unless this information has been crafted into a model truly representative of the geothermal system, one that may extend for tens of square kilometers on the surface and several thousand meters below the surface, and unless suitable methods of solution for complex equations have been devised, then the results of the simulation will have little predictive value.

Reservoir modeling and simulation is the subject of annual symposia and numerous technical articles. The reader is referred to the following sources for detailed presentations: Refs. [1,2,24–38]. Several universities, companies, and governmental laboratories have developed their own versions of reservoir simulators, usually identified by unique acronyms. The private ones are usually proprietary and all computer programs periodically evolve to newer versions. In Section 4.5.6, we list some of the more commonly used geothermal reservoir simulators, briefly highlight their features, and include references for details on each one.

4.5.1 INPUT

A reservoir model must be built on a proper conceptual model of the field. If the conceptual model has flaws, as often happens in the early stages of field development, the reservoir model will reflect these errors. For this reason, it is recognized that the reservoir model must be updated as the conceptual model improves.

The input includes as much of the following information as possible:

- Geology: rock types and ages, outcrops, surface topology, faults, calderas, craters, eruptive centers, discontinuities
- Hydrology: rainfall patterns, surface water flows
- Geophysics: surveys of electrical resistivity, gravity, magnetics, temperature gradients, heat flux
- Geochemistry: hot and cold spring compositions, flow rates and temperatures, estimated reservoir temperatures
- Well data: type of well (production or reinjection), locations, depths, casing design, pressure and temperature profiles both static and flowing, and productivity curves.

All of this data permit the construction of the conceptual model which should indicate the areal extent of the reservoir, the areas of natural fluid discharge and recharge, the natural heat flow from the reservoir by conduction through rock and by convection through thermal manifestations, and an estimate of the vertical extent of the geothermal system.

4.5.2 ARCHITECTURE

Since it is virtually impossible to write down analytical equations to describe all the physical and chemical processes going on in a geothermal reservoir and to solve them analytically in a closed form, all reservoir models rely on some type of finite difference or finite element numerical technique. The field is divided into discrete cells, both horizontally and vertically, and the governing equations of mass and energy conservation are written in finite difference form for each element of the matrix. The conditions on the boundaries of each cell provide the connections among the cells and permit the solution to extend over the entire reservoir.

The choices of the cell boundaries are arbitrary and may be selected for computational convenience, but usually they coincide with major structural features such as faults or permeability barriers. The size of the cells is also arbitrary and the grid usually is made finer in the neighborhood of well-defined features, such as wells, where data are plentiful and reliable. Outlying areas can be

represented by large blocks having average properties without greatly influencing the results of the model. The geometric shape of the cells is also arbitrary, ranging from simple squares or rectangles to circles or irregular polygons. It is often convenient to situate each well within its own element.

The vertical extent of the reservoir is modeled by layering the matrix into several distinct horizons. For young fields with little production history, it is not uncommon to have six or more layers covering, for example, the surface and the atmosphere, the impermeable cap rock, a liquid-dominated zone, a particular rock formation, a deep permeable zone, and the basement rock. In more developed fields with a long production history, models are much finer in structure and can have dozens of layers [39].

4.5.3 CALIBRATION AND VALIDATION

Once the governing spatial- and time-dependent physical and chemical equations have been written, and the code created along with the method of solution, it is then necessary to calibrate and validate the model. This crucial step is needed to guarantee that the model (and its solution technique) is reliable, stable, and correctly represents the state of the reservoir going back in time perhaps as much as 250,000 years—from the unexploited, natural state of the reservoir to the present. In this way, the model can be relied upon to accurately model the ancient natural state of the system, as well as the present, unexploited state of the system, and to offer the modeler confidence in making predictions about the future state of the system.

This is a very tedious computational process. Imagine a mathematical model involving strongly coupled, nonlinear, partial differential equations represented by a computer code with hundreds of input parameters, many of them ill-defined owing to insufficient data. The set of equations is said to be mathematically under-constrained, having many more parameters than can be determined or inferred from field measurements. A solution in such a case will not be unique, there being many possible conditions that will satisfy this set of equations. Judgment is needed by the user of the code to make good choices for the adjustable parameters to arrive at reasonable results.

In what is called the “manual” method, the parameters first are adjusted by the reservoir engineer to give the best fit possible to the current state of the system. The two parameters most often used are the permeabilities of the various rock formations and the boundary conditions [40]. Then the code is run from the natural state forward in time and the physical characteristics of reservoir are

computed at large time steps. The evolution of the field is thus depicted. Stability of the code requires that eventually the system should reach a steady state that conforms to the observed present state. If the results of this computation are unsatisfactory for any reason, then the modeler must adjust the parameters and rerun the simulation until satisfactory results are obtained.

This process can be partly automated in a sense by having the reservoir properties adjusted by a programmed subroutine within the code to minimize the difference between the code output and selected observed data. The automatic method is called “inverse” modeling, but still requires the intervention of the modeler in choosing the properties that will serve as criteria of the goodness of the fit and the magnitude of the errors that are acceptable. Inverse modeling is more demanding on computer speed and memory than manual modeling, and may require parallel processing using several personal computers.

4.5.4 HISTORY MATCHING

The first use of the model is to match the data obtained from the early wells. The model should be able to reproduce the observed changes in the reservoir over the period of production and injection. When this is done during the feasibility stage of a new field, such data may be scanty, but the model still must be able to match it. This usually means another adjustment of the parameters in the model, and a recalculation of the natural state model, followed by more iterations to bring the model into agreement with all the data. As more production and injection data become available, the model should be revised accordingly.

Here again, this process of history matching can be done either manually or automatically. This cycle of periodically updating the reservoir simulator is tedious, time-consuming, and expensive, but absolutely essential if one is to have any confidence in projecting the behavior of the field over many years of operation.

4.5.5 USE OF THE MODEL

A validated reservoir model may be used to forecast the behavior of the system when it is subjected to various exploitation scenarios. This involves running the model for future times after having placed projected future production and injection wells at specific locations in the field, that is, mathematically inserting fluid sinks (production wells) and sources (injection wells) into the reservoir. The desired outputs from the model include the evolution of pressure and temperature, the formation of vapor zones, the movement of chemical and thermal fronts

through the reservoir, the onset of chemical and thermal breakthroughs from injection wells to production wells, the level of electrical generation that can be supported for a specified number of years, typically 20–30 years, and the number of replacement wells that must be drilled over the years to maintain the electrical output.

Given the complexity of the rock–fluid interaction in an imprecisely known geometric structure, it is easy to see how such a modeling process is subject to considerable uncertainty. Furthermore, since geothermal regions are dynamic and subject to geologic forces that can change the structure of the formation, opening new fissures or closing old ones, moving fault blocks laterally as well as vertically, the assumed constant geometric structure may be altered by natural forces. This could play a role when the simulator is used over the millennia of the natural state computation, during which the reservoir is assumed to have a fixed configuration. Indeed, the field may be altered by geologic forces during the anticipated life of the power plant, as has been the case at some geothermal power plants around the world.

Notwithstanding these difficulties, reservoir models, after they have been validated and calibrated against whatever data are available and periodically updated, have proved to be reasonably reliable tools for simulating the state of geothermal systems. An excellent review of over 125 field simulations based on questionnaires filled out by companies and individuals can be found in Ref. [40].

4.5.6 EXAMPLES OF RESERVOIR SIMULATORS

Table 4.1 lists some of the reservoir models in use today. The models fall into one of three categories: finite difference (FDM), finite element (FEM), or integral finite difference (IFDM). Some of the features are cited but the reader should consult the references for the particulars on each model.

4.6 ReInjection

4.6.1 MOTIVATION

Without a properly designed reinjection plan, a geothermal reservoir may become depleted before achieving the anticipated economic return. This is a lesson learned over more than a century of geothermal exploitation. Indeed it was not until 1968 when the first reinjection took place at a geothermal field, The Geysers dry steam field in northern California. Prior to that, all waste geofluid from the plants at Larderello in Italy's Tuscany Region and at Wairakei in New Zealand

TABLE 4.1 Selected geothermal reservoir simulators.

Code	Type	Features	Reference
TETRAD	FDM	Simulates 3D multiphase groundwater flow and heat transport; uses regular rectangular mesh.	[28]
HYDROTHERM	FDM	Simulates 3D multiphase groundwater flow and heat transport, handles temperatures from 0–1200°C; uses pressure and enthalpy as independent variables.	[29]
NIGHTS	FDM	Handles natural state calibration for liquid-dominated reservoirs.	[30]
STAR	FDM	Fifth generation code for multiphase, multicomponent heat and mass transfer in 3D geometric structures.	[31]
AQUA 3D	FEM	3D groundwater flow and contamination transport.	[32]
FEHMN	FEM	Handles nonisothermal multiphase multicomponent flow in porous media; permeability and porosity of the medium depend on pressure and temperature.	[33]
SHAFT	IFDM	Uses integral FDM; original LBL reservoir.	[34]
MULKOM	IFDM	Multidimensional model, simulates coupled transport of water, vapor, noncondensable gas, and heat in porous and fractured media.	[34]
TOUGH	IFDM	Handles transport of unsaturated groundwater and heat.	[34]
TOUGH2	IFDM	Able to handle different fluid mixtures: water + water with tracer; water + CO ₂ ; water + air; water + air, with vapor pressure lowering; and water + H ₂ .	[35]
iTOUGH2	IFDM	Inverse modeling; automatic calibration, history matching, and error analysis.	[36,37]

had been disposed via surface discharge to streams and rivers. Both Wairakei and Larderello were so productive that little thought was given to replenishing the fluid removed from the reservoir.

Furthermore, at dry steam fields, there is only a small fraction of the mass of steam produced that ends up being converted into liquid condensate that could be reinjected, roughly 10–15%. Thus little would be gained from returning this to the reservoir, even assuming it could be returned in an optimum location. With liquid-dominated reservoirs, a much higher fraction of the produced fluid is available for reinjection, up to as much as 80–85% for flash plants and 100% for binary plants. This is both an opportunity and a potential problem. Clearly by returning this fluid to the reservoir system, it might be possible to extend the life-time of the project and even attain stable, long-term sustainability. However, unless some part of the field can be found having sufficient permeability while not in direct communication with the producing areas, there may not be enough injection capacity to allow full operation of the power plant. In reality once reinjection became more common, often failed wells that had been drilled for

production were put to use as injection wells regardless of where they happened to be, as long as they had sufficient permeability. Once reservoir modeling with sophisticated computer tools came into being, it was then possible better to site injection wells so as to minimize adverse effects on production wells.

4.6.2 STRATEGIES

There are two objectives regarding reinjection strategies. The first one is disposal of waste geofluid; the second is reservoir replenishment and/or pressure support. In either case prerequisite knowledge to permit a successful implementation involves an understanding of the fluid conduits throughout the reservoir formation. The undisturbed pressure distribution and the changes induced by production should be known before siting and drilling injection wells, but often this is learned only after the field is put into operation.

Generally, disposal wells are sited in the outflow regions of the reservoir. It might be possible to inject at depths different from the producing depths provided there are horizontal barriers to prevent “short-circuiting” of the injectate into the production zones. There is some advantage to injecting deeper than the production layer since the formation temperature will usually be higher and reheating of the injectate will happen quickly preventing any possible precipitation of silica. Of course deeper wells are more expensive to drill. Using a disposal strategy implies that there is little expectation that the injectate will someday return to be reproduced. The intent is merely to avoid possible environmental impacts on ground and surface waters since nowadays national or local regulations often prohibit surface disposal of geothermal fluids. Depending on how close these wells are to the production area, there may be some effect on pressure maintenance.

Using reinjection to support the longevity of the reservoir is a more challenging objective. Wells for this purpose tend to be located within or close to the productive zones of the field, perhaps in lower temperature areas. Noncommercial production wells are sometimes used as injectors in this case. There is the risk of thermal or chemical breakthrough that could be problematic especially in smaller fields where production is obtained along a single fault system, such as the Basin and Range province in the United States. Conversely, in large fields it is sometimes necessary to forgo production by “sacrificing” good producing wells and using them for reinjection, as at the Miravalles field in Costa Rica. Even when carried out successfully initially, a reinjection scheme may have to be revised later due to unanticipated interference with production wells.

Since geothermal reservoirs are in geologically active areas, even minor seismic events can cause new fractures to open or existing ones to close, altering the flow

patterns in the formation. The effect of injecting fluid under pressure can by itself cause such changes, especially if the area of formation around the injection well has low permeability necessitating relatively high injection pressures. Induced seismicity has been observed in several fields as a result of such operation.

Thus, while reinjection is now recognized as one essential element to creating a long-lived power generation project, achieving a successful operation is fraught with serious challenges that must be faced throughout the lifetime of the project. Monitoring wells and tracer tests will give early warning of impending trouble and allow time to adjust to and mitigate the problem. It is not uncommon for field operators to change the gathering system, converting injectors to producers and vice versa during the years of operation to maintain an optimal situation.

4.6.3 EXAMPLES

Discussions of reinjection may be found later in this book in the Case Studies section. Here only a few examples will be presented to illustrate how the reinjection situation can be handled. An exhaustive survey of geothermal reinjection experience may be found in Ref. [41].

Ahuachapán, El Salvador—From 1975 to 1981, three units totaling 95 MW were installed at this field in western El Salvador. All wells were drilled vertically within an area of about 1.05 km²; see Figures 4.13 and 5.5. Being a

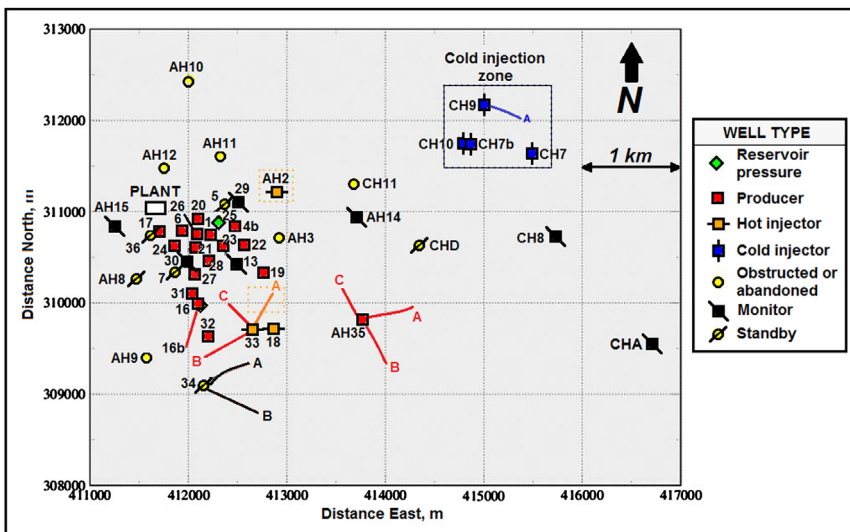


Figure 4.13 Ahuachapán well field as of 2012. After Ref. [43] [WWW].

liquid-dominated reservoir, Ahuachapán had significant volumes of waste brine to deal with. A few wells were designated for injection, AH2, AH8, and AH17 are shown in [Figure 4.13](#), but interference with producers was soon observed. Only about 63% of the waste brine could be reinjected [\[42\]](#). Additionally, the 37% of waste brine at atmospheric conditions was supersaturated with silica prompting the construction of a concrete labyrinth structure through which the waste brine was passed prior to disposal. The holdup time of roughly one hour was sufficient to allow most of the silica to polymerize and precipitate on the walls of the labyrinth. Given that the reinjection capability of the field could not cope with the amount of geofluids generated, together with the fact that land use in the plant area is agricultural, mainly coffee growing, it was decided to dispose of the waste to the Pacific Ocean, some 75 km to the west. A canal of 1 m² cross-section with some 68 km made of concrete and 7 km of steel pipe used for siphons traversed the countryside and ended just north of a beach on the Pacific shore.

Following the end of the Salvadoran civil war in the early 1990s, a new development program was undertaken to expand the useful area of the field and to locate suitable reinjection sites. The canal was taken out of commission, destroyed, and the land reclaimed. By 2004 all waste brine was being reinjected. Today the cold waste geofluid is transported via pipeline to the adjacent Chipilapa field for injection; see [Figure 4.13](#) [\[43\]](#). At present it is necessary to provide booster pumps near the Chipilapa wells to assure adequate reinjection to handle the waste brine at full power plant load.

Salavatlı, Turkey—The Salavatlı field lies in the western section of the Menderes Graben in Turkey. As a medium-temperature resource, it is exploited with binary power plants. As such, a high volume of geofluid is processed to provide heat to drive the plants. The plant site is in a busy area filled with industry, agriculture and residences, close to a major highway. There is no option but to reinject all of the produced geofluid in an environmentally benign manner. Since the first unit came online in 2006, a great deal of monitoring and research has been carried out continuously to locate low-pressure and low-temperature zones in the reservoir that would be suitable hosts for reinjection wells [\[44\]](#). [Figure 4.14](#) shows the locations of all wells at the site which supports four power units with a total capacity of 52.45 MW; roughly 1110 kg/s must be produced and reinjected continuously. With the injection wells located at the periphery of the field, there has been no significant interference between producers and injectors while the pressure in the production zone has been maintained [\[44\]](#).

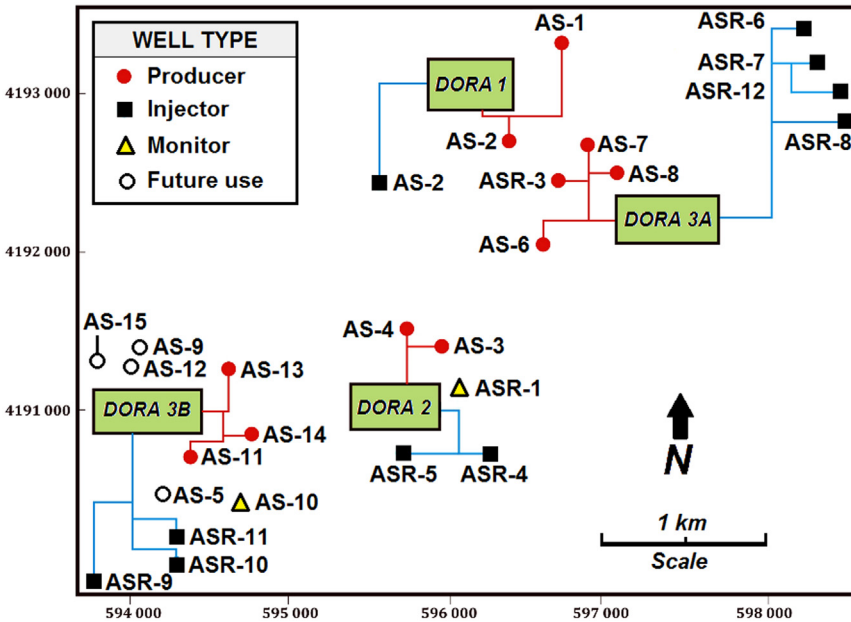


Figure 4.14 Well field for Salavatl power units Dora 1, 2, 3A, and 3B. After Ref. [44] [WWW].

Cerro Prieto, Baja California, Mexico—The vast Cerro Prieto liquid-dominated geothermal field, encompassing an area of roughly 33 km², lies 31 km south of the U.S.–Mexico border in the southern extension of the Imperial Valley. The field is extremely flat lying between 12 and 15 masl. It first began generating power in 1973, and by 2000 there were a total of 720 MW installed in 13 units spread over four power plants; see Figure 4.15. Reinjection of waste brine began in 1989 at a time when 620 MW was being generated. Prior to that time, all waste brine was piped to a large evaporation pond at the west side of the field, a geothermally altered area marked by numerous thermal manifestations such as fumaroles and mud pots. Since it was unsuitable for agriculture, industry, or residential use, it seemed an appropriate way to dispose of the waste brine. Over the years the pond grew in size; today it covers about 14.9 km². From the air, it forms a striking blue lagoon within an otherwise brown and arid landscape; see Figures 4.15 and 4.16.

As huge and productive as the field was, it nevertheless suffered from partial depletion. This motivated the search for a means to curtail the drop in

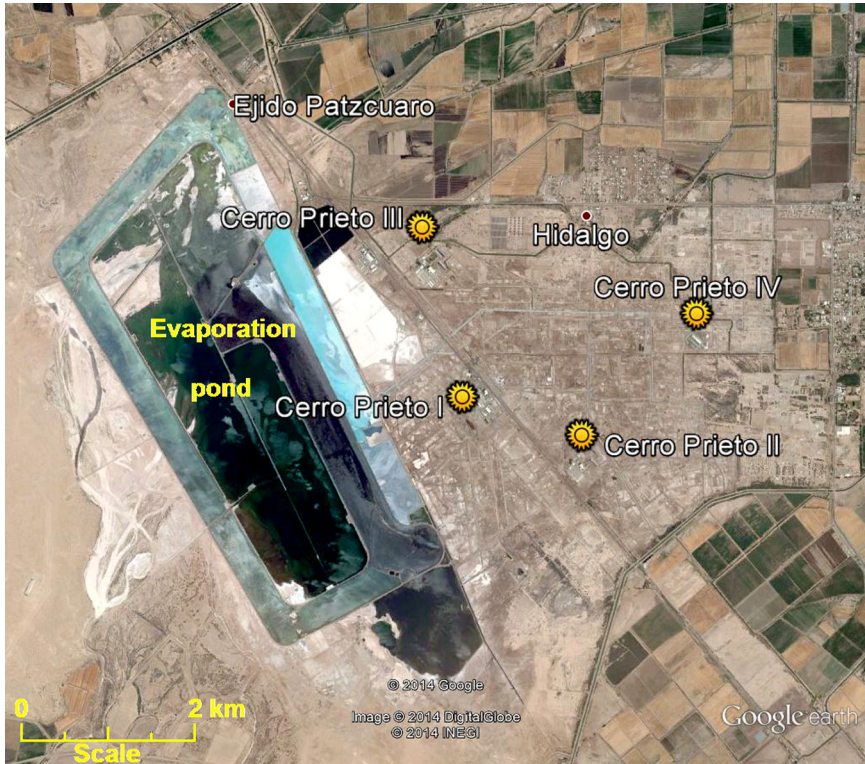


Figure 4.15 Aerial view of Cerro Prieto geothermal field, Baja California, Mexico showing the four power stations and the evaporation pond. *Image from Google Earth, June 15, 2014 [WWW].*

productivity via appropriately sited injection wells. At first, wells of opportunity were converted into injectors—old, exploration, or abandoned wells—but since these were not properly sited for reinjection they proved inadequate [45]. Some were close to production wells in the heart of the productive area of the field. Later purpose-drilled injection wells were located next to and even within the evaporation pond on dikes that separated sections of the pond. Owing to evaporation, the concentration of dissolved solids and heavy isotopes such as deuterium in the pond fluids is higher than in the produced fluid. For example, the chloride in the pond brine is about five times greater than in the produced fluid. This turns out to be an excellent means of tracing the movement of the injectate through the reservoir. It was observed that injection in well E6 had a positive effect on steam production in well E55 roughly 1.5 years after the start of injection; E55 is about 890 m northeast of E6 in the southernmost area of the field [45]; see Figure 4.17.

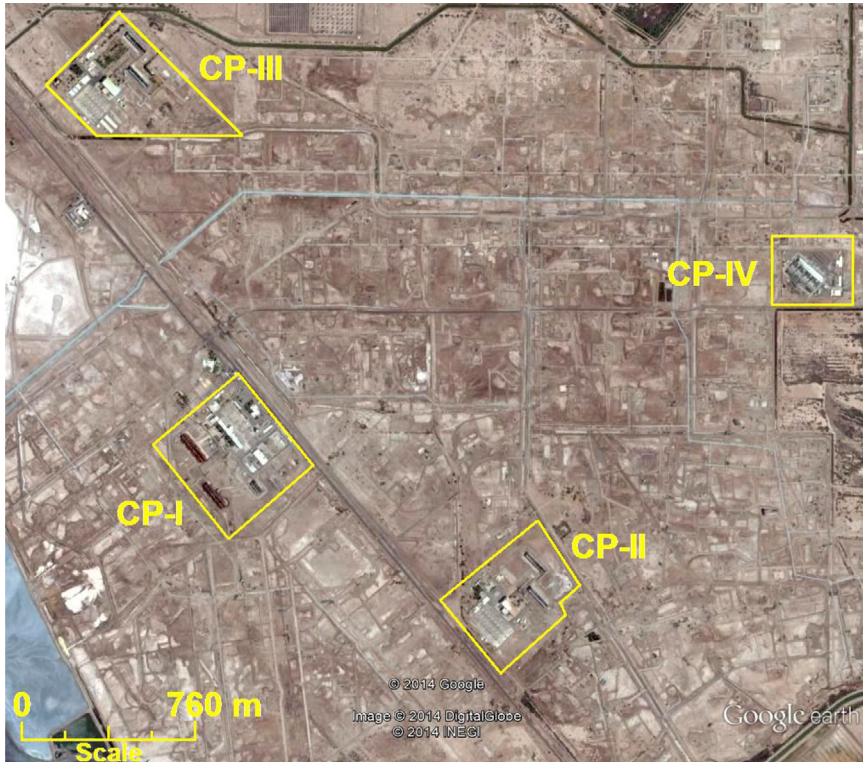


Figure 4.16 Cerro Prieto power plants *Image from Google Earth, June 15, 2014 [WWW].*

Prior to the effect of injection, well E55 exhibited a decline in steam production of 2.8 kg/s per year. Once the impact was felt, steam production jumped 35% or 3.9 kg/s over one month.

Thereafter, for the next two years, the steam decline rate fell to 0.8 kg/s per year, and then roughly to 2 kg/s per year for the next three years. So in this case there was a step increase in production followed in the short term by a much smaller decline rate but then by a somewhat higher decline rate but still less than prior to injection.

It is noteworthy that the four oldest units, 4×37.5 MW generators, in Cerro Prieto I were shut down in 2011–2012 from lack of steam at the field; only Unit 5, a 30 MW bottoming double-flash plant remains in service [46]. The injection wells are close to these units (Figure 4.17). Since these units are also not as efficient as newer ones, it was decided to better utilize the available steam in the more modern units.

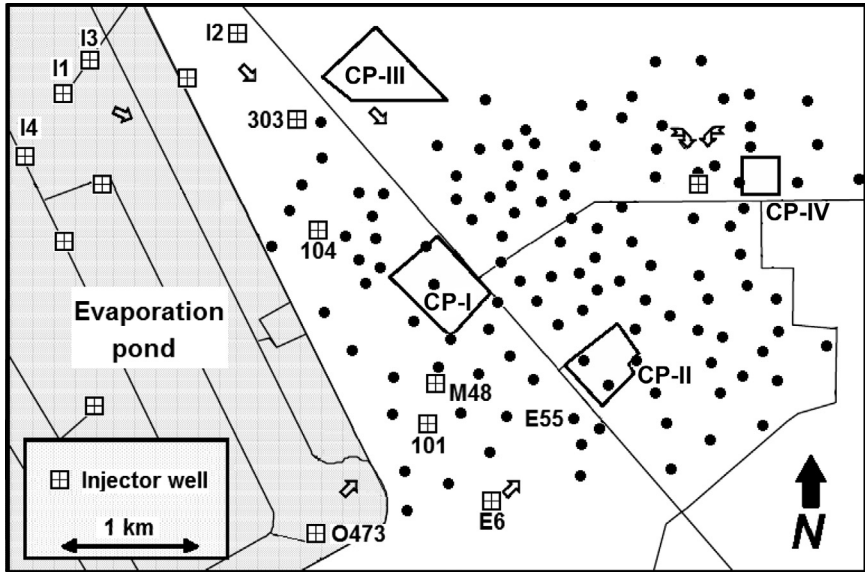


Figure 4.17 Cerro Prieto power stations, production and injection wells, and evaporation pond. Modified from Ref. [45].

References

- [1] Proceedings of the Stanford Workshops on Geothermal Reservoir Engineering, vols. 1–40. Stanford University, Stanford, CA; 1975–2015.
- [2] Samaniego VF, Cinco-Ley H. Reservoir engineering concepts [chapter 9]. In: Edwards LM, Chilingar GV, Rieke III HH, Fertl WH, editors. Handbook of geothermal energy. Houston, TX: Gulf Publishing Company; 1982.
- [3] Golan M, Whitson CH. Well performance. 2nd ed. Englewood Cliffs, NJ: Prentice-Hall; 1991.
- [4] Ryley DJ. Analysis of the flow in the reservoir-well system. In: Kestin J, editor-in-chief, DiPippo R, Khalifa HE, Ryley DJ, editors. Sourcebook on the production of electricity from geothermal energy. U.S. Dept. of Energy, DOE/RA/4051-1, U.S. Gov. Printing Office, Washington, DC; 1980 [section 2.6].
- [5] Matthews CS, Russell DG. Pressure buildup and flow tests in wells. New York, NY: Society of Petroleum Engineers, American Institute of Mining, Metallurgical, and Petroleum Engineers; 1967.
- [6] Cheremisinoff NP, editor. Encyclopedia of fluid mechanics, V. 3, gas-liquid flows. Houston, TX: Gulf Publishing Company; 1986.
- [7] Dake LP. Fundamentals of reservoir engineering. Elsevier Scientific; 2001.
- [8] Ahmed T. Reservoir engineering handbook. 2nd ed. Butterworth-Heinemann; 2002.
- [9] Smith C, Tracy GW, Farrar RL. Applied reservoir engineering, vols. 1 and 2. Tulsa, OK: Oil & Gas Consulting International; 1999.
- [10] Darcy H. The public fountains of the City of Dijon: experience and application, principles to follow and formulas to be used in the question of the distribution of water [Brown G, Catani B, Trans. 1999]. Original published in 1856.

- [11] Ryley DJ. The mass discharge of a geofluid from a geothermal reservoir-well system with flashing flow in the bore. *Geothermics* 1980;9:221–35.
- [12] Swamee PK, Jain AK. Explicit equations for pipe flow problems. *J Hydraul Eng* 1976;102:657 ASCE.
- [13] Keenan JH, Keyes FG, Hill PG, Moore JG. Steam tables: thermodynamic properties of water including vapor, liquid, and solid phases (International Edition—Metric Units). New York, NY: John Wiley & Sons, Inc.; 1969.
- [14] Delhaye JM, Giot M, Riethmuller ML, editors. Thermohydraulics of two-phase systems for industrial design and nuclear engineering. New York, NY: Hemisphere Publishing Corp, McGraw-Hill; 1981.
- [15] Ginoux JJ, editor. Two-phase flows and heat transfer with application to nuclear reactor design problems. New York, NY: Hemisphere Publishing Corp, McGraw-Hill; 1978.
- [16] Hsu Y-Y, Graham RW. Transport processes in boiling and two-phase systems including near-critical fluids. New York, NY: Hemisphere Publishing Corp, McGraw-Hill; 1976.
- [17] Wallis GB. One-dimensional two-phase flow. New York, NY: McGraw-Hill; 1969.
- [18] Ryley DJ. Property definition in equilibrium wet steam. *Int J Mech Sci* 1964;6:445–54.
- [19] Kuster Company, Long Beach, CA, <<http://www.kusterco.com/manuals.htm>>; 2003.
- [20] James R. Factors controlling borehole performance. *Geothermics—Special Issue 2*, U.N. symposium on the development and utilization of geothermal resources, Pisa 1970;2(Pt. 2):1502–15.
- [21] Ellis AJ, Mahon WAJ. Chemistry and geothermal systems. New York, NY: Academic Press; 1977.
- [22] Eskesen JH, Whitehead A, Brunot AW. Cycle thermodynamics. In: Kestin J, editor-in-chief, DiPippo R, Khalifa HE, Ryley DJ, editors. Sourcebook on the production of electricity from geothermal energy. U.S. Dept. of Energy, DOE/RA/4051-1, U.S. Gov. Printing Office, Washington, DC; 1980 [section 4.1.2].
- [23] Ellis AJ, Golding RM. Solubility of carbon dioxide above 100°C in water and sodium chloride solutions. *Amer J Sci* 1963;261:47.
- [24] Lippmann MJ. Numerical modeling of injection. A course on injection technology. Pisa, Italy: J. Rivera, Convenor, Int'l. School of Geothermics; 1995. p. 113–45 [chapter 3].
- [25] Bullivant, DP, O'Sullivan MJ, Blakeley MR. A graphical interface for a geothermal reservoir simulator. In: Proc. world geothermal congress 4, Florence, Italy, 1995, p. 2971–6.
- [26] White SP, Kissling WM, McGuinness MJ. Models of the Kawareu geothermal reservoir. *Geotherm Resour Coun Trans* 1997;21:33–9.
- [27] Williamson KH. Development of a reservoir model for the geysers geothermal field Special Report No. 17 Monograph on the geysers geothermal field. Davis, CA: Geothermal Resources Council; 1991. p. 179–87.
- [28] Vinsome PKW, Shook GM. Multipurpose simulation. *J Pet Sci Eng* 1993;9:29–38.
- [29] Hayba DO, Ingebritsen SE. Rep. 94-4045 The computer model HYDROTHERM, a three-dimensional finite-difference model to simulate ground-water flow and heat transfer in the temperature range of 0 to 1,200°C. Menlo Park, CA: U.S. Geological Survey Water Resources Investigations; 1994.
- [30] Pritchett JW. NIGHTS: a single-phase geothermal reservoir simulator. In: Proc. world geothermal congress 4, Florence, Italy, 1995, p. 2955–8.
- [31] Pritchett JW. STAR: a geothermal reservoir simulation system. In: Proc. world geothermal congress 4, Florence, Italy, 1995, p. 2959–63.
- [32] Vatnaskil Consulting Engineers. AQUA lecture notes and user's manual, Reykjavik, Iceland; 1993.
- [33] Zyvoloski GA, Dash Z, Kelkar K. Rep. LANL-12062 FEHMN 1.0: finite element heat and mass transfer code. Los Alamos, NM: Los Alamos National Laboratory; 1991.

- [34] Pruess K. SHAFT, MULKOM, TOUGH: a set of numerical simulators for multiphase fluid and heat flow. *Geothermia, Revista Mexicana de Geoenergía* 1988;4(1):185–202.
- [35] Pruess K. Rep. LBL-29400 TOUGH2—A general-purpose numerical simulator for multiphase fluid and heat flow. Berkeley, CA: Lawrence Berkeley Laboratory; 1991.
- [36] Finsterle S. Multiphase inverse modeling: review and iTOUGH2 applications. *Vadose Zone J* 2004;3:747–62.
- [37] Finsterle S. Multiphase inverse modeling lecture notes. Berkeley, CA: Lawrence Berkeley National Laboratory; 2000. <<http://esd.lbl.gov/iTOUGH2>>.
- [38] O’Sullivan MJ, Pruess K, Lippmann MJ. Geothermal reservoir simulation: the state-of-practice and emerging trends. In: *Proc. world geothermal congress 2000, Kyushu-Tohoku, Japan, 2000*, p. 4065–70.
- [39] Mannington W, O’Sullivan M, Bullivant D. Computer modelling of the Wairakei-Tauhara Geothermal System, New Zealand. *Geothermics* 2004;33:401–19.
- [40] O’Sullivan MJ, Pruess K, Lippmann MJ. State of the art of geothermal reservoir simulation. *Geothermics* 2001;30:395–429.
- [41] Rivera Diaz A, Kaya E, Zarrouk SJ. Reinjection in geothermal fields: a worldwide review update. In: *Proc. world geothermal congress 2015, Melbourne, Australia, April 19–25, 2015*.
- [42] DiPippo R. U.S. Dept. of Energy, DOE/RA/28320-1 *Geothermal energy as a source of electricity: a worldwide survey of the design and operation of geothermal power plants*. Washington, DC: U.S. Gov. Printing Office; 1980.
- [43] Mayorga H. Geothermal reinjection systems in El Salvador. In: *Presented at short course on geothermal development and geothermal wells, UNU-GTP and LaGeo, Santa Tecla, El Salvador, March 11–17, 2012*.
- [44] Serpen U, Aksoy N, Öngür T. Reinjection update of Salavatlı geothermal field in Turkey. In: *Proc. world geothermal congress 2015, Melbourne, Australia, April 19–25, 2015*.
- [45] Gutierrez HP, Helio MR. 28 years of production at Cerro Prieto geothermal field. In: *Proc. world geothermal congress 2000, Kyushu-Tohoku, Japan, May 28–June 10, 2000*.
- [46] Peralta O, Castro T, et al. H₂S emissions from Cerro Prieto geothermal power plant, Mexico, and air pollutants measurements in the area. *Geothermics* 2013;46:55–65.

Problems

- 4.1.** Consider a deep well filled with pure water from the surface to its total depth. Calculate the so-called “boiling point curve,” that is, calculate the temperature required to just begin to boil the water at any given depth. Your answer will be a table and a graph showing the boiling temperature versus depth. Do the calculation in two ways:
- a. Assume that the water has a uniform constant standard density throughout the entire column, and
 - b. Account for the variability of density with depth (or equivalently with temperature) by dividing the column into a series of finite steps over which an average density may be used for each step.

When you have completed the calculations, discuss any difference between these two approaches and compare the results with the simple

formula given by James, namely, $t/^\circ\text{C} = 69.56 (z/\text{m})^{0.2085}$. At what depth is the critical point reached for both of your calculations and for James' formulation?

- 4.2. A hot water reservoir is discovered at a depth of 915 m. Downhole instrumentation indicates a pressure of 10.3 MPa and a temperature of 260°C . A control valve at the surface maintains a constant mass flow rate up the well and keeps the fluid pressure at the wellhead equal to 828 kPa. Assume adiabatic conditions along the well and neglect the effects of friction. Calculate the state of the geofluid at the wellhead under these conditions. Sketch the process from the well bottom to the wellhead on a temperature-entropy diagram. If flashing occurs in the wellbore, estimate the depth below the surface at which it takes place.
- 4.3. A production well exists in a hypothetical hydrothermal reservoir with a permeability $K = 100$ mD and a thickness (in the production zone) $L_R = 100$ m. The reservoir fluid has a viscosity $\mu = 1$ cp, and the well has a diameter of 9-5/8 in.
 - a. Assuming a volumetric well flow rate $\dot{V} = 100$ L/s, calculate the drawdown pressure difference ΔP in kPa as a function of the size of the reservoir (i.e., as a function of the reservoir radius r_r). Express r_r in m, and plot your results out to $r_r = 1000$ m.
 - b. Assuming a reservoir radius $r_r = 200$ m, find the drawdown as a function of flow rate \dot{V} , and plot your results up to $\dot{V} = 200$ L/s.
- 4.4. A vertical geothermal well is 1400 m deep and has a 9-5/8" OD (8.921" ID) commercial steel casing from top to bottom. During flow tests, it is observed that the bottom-hole pressure is 13.75 MPa when the flow rate is 50 kg/s, and that it is 12.5 MPa when the flow rate is 100 kg/s. The reservoir temperature is 240°C .
 - a. Calculate and plot the depth from the surface to the flash horizon as a function of well flow rate for the range 0–150 kg/s, assuming the geofluid is pure water.
 - b. Write a computer program or spreadsheet to analyze the well flow problem described in Part (a). The program input variables should be: reservoir temperature, well depth and casing diameter, and two pairs of data on flow rate versus bottom-hole pressure. The output should include the depth to the flash horizon plus anything else you think is important.
- 4.5. Consider a vertical, constant diameter, geothermal well. The well has a total depth L_T , a diameter $D = 7\text{-}5/8"$, and a wall friction factor f , and carries a flow rate \dot{m} . The reservoir is characterized by a pressure P_R , a temperature T_R , and a drawdown coefficient C_D . The flash horizon is at an elevation L_F above the reservoir (or above the well bottom).

- a. Determine the flash horizon as a function of wall friction factor (over a range of 0–0.020) for the following conditions:

$$T_R = 260^\circ\text{C}, P_R = 5520 \text{ kPa}, \dot{m} = 13 \text{ kg/s}, C_D = 75 \text{ kPa/(kg/s)}.$$

- b. Determine the flash horizon as a function of mass flow rate (over a range of 5–65 kg/s) for the following conditions:

$$T_R = 235^\circ\text{C}, P_R = 5800 \text{ kPa}, f = 0.008, C_D = 75 \text{ kPa/(kg/s)}.$$

- c. Determine the flash horizon as a function of drawdown coefficient (over a range of 45–120 kPa/(kg/s) for the following conditions:

$$T_R = 205^\circ\text{C}, P_R = 16,550 \text{ kPa}, f = 0.008, \dot{m} = 13 \text{ kg/s}.$$

- d. Determine the flash horizon as a function of reservoir temperature (over a range of 150–315°C) for the following conditions:

$$P_R = P_{sat}(T_R) + 3500 \text{ kPa}, \dot{m} = 13 \text{ kg/s}, f = 0.008, C_D = 75 \text{ kPa/(kg/s)}.$$

- e. Suppose, for each part, the total well depth is $L_T = 1800 \text{ m}$. Discuss the ramifications of the flash horizon calculations. In particular, focus on the feasibility of placing a downhole pump in the well to increase the flow rate, that is, the productivity of the well, and/or to prevent flashing anywhere in the well. When you consider a pumped well, you may assume that a pump will produce a flow rate 2.5 times greater than the self-flowing rate. Assuming that the pump requires a net positive suction head of 15 m of water to avoid cavitation at the pump inlet, identify an example from the above calculations where it is possible to locate a pump in a well at a depth (from the surface) of less than 300 m.

- 4.6. A liquid-dominated reservoir has a geofluid temperature of 230°C , a static reservoir pressure of 100 bar, and a linear drawdown coefficient of 0.50 bar/(kg/s) . A 1200 m well having an inside diameter of 9.625 in is drilled into the reservoir. The Moody friction factor may be taken as constant and equal to 0.015. The local gravitational acceleration is the standard value of 9.81 m/s^2 . Determine the depth from the wellhead to the flash point if the total mass flow rate in the well is 50 kg/s, assuming the feed zone is at the bottom of the well.

- 4.7. A well is drilled into a liquid-dominated reservoir where the fluid temperature is 250°C , the static reservoir pressure is 65 bar, and a linear drawdown coefficient is 0.35 bar/(kg/s) .

- a. Determine the mass flow rate of geofluid that will cause the fluid to flash just as it enters the well.
- b. Describe in some detail qualitatively what will happen if the mass flow rate is (i) less than this value and (ii) greater than this value.

- 4.8.** It is possible to find the static reservoir pressure and the assumed linear drawdown coefficient from measurements taken during flow tests. Pressure readings are taken downhole next to the feed zone and the total flow is measured on the surface using a separator. Data from tests at two different flow rates are given in the table below.

Test no.	Mass flow rate, kg/s	Feed zone pressure, bar
1	45	140
2	58	133

- a. Calculate the linear drawdown coefficient.
 - b. The static reservoir pressure.
- 4.9.** The first successful geothermal well to be drilled in Honduras was at the Platanares field. PLTG-1 was a slim exploration well but was capable of producing geofluid. Some data pertaining to the well are given in the following table.

Item	Value
Depth	625 m
Inside diameter	3.0 in
Well roughness	0.00006 m
Reservoir pressure	6000 kPa
Reservoir fluid temperature	160°C
Drawdown coefficient	50 kPa/(kg/s)
Mass flow rate	5.152 kg/s

- a. Calculate the depth of the flash horizon from the surface.
 - b. Estimate the quality (or dryness fraction) of the geofluid at the wellhead.
 - c. Assuming thermodynamic equilibrium between the liquid and vapor phases at the wellhead, calculate the average pressure gradient over the two-phase section of the well.
- 4.10.** A geothermal well is constructed with two casings of different diameter, thereby having an abrupt step increase in cross-sectional area at a certain point along the well. The lower casing has an inside diameter of 5.921 in; the upper one has an ID of 8.921 in. The lower casing runs from the bottom of the well where the feed zone is located to a height of 1065 m; the upper casing runs from top of the lower casing to the surface and is 457 m long. The casing material is commercial steel and has a roughness factor of 0.046 mm.

The reservoir fluid is a pressurized liquid at a temperature of 260°C. During flow tests the following data were obtained:


Test no.	Mass flow rate, kg/s	Feed zone pressure, kPa
1	43	14,180
2	57	13,510

- a. Determine the linear drawdown coefficient (units = kPa/(kg/s)).
 - b. If the well were flowed at 45 kg/s, what drawdown coefficient would be needed for the fluid to just be on the verge of flashing in the formation?
 - c. For the actual drawdown coefficient, find the level of the flash horizon if the mass flow rate is 68 kg/s. In doing this calculation, you may ignore the effect of the Reynolds number on the Moody friction factor in the Swamee–Jain equation, Eq. (4.11).
 - d. Find the minimum mass flow rate for the flash point to be located in the lower casing.
 - e. Find the location of the flash horizon if the flow rate is 23 kg/s. You may ignore the pressure drop associated with the abrupt enlargement.
 - f. Find the liquid level below the surface when the well is closed in, that is, when there is no flow.
- 4.11.** A geothermal well is completed into a liquid-dominated reservoir. The casing has an inside diameter of 9.626 in; the friction factor is 0.005; and the total length of the well is 760 m, with the feed zone at the bottom. The static reservoir pressure is 7930 kPa and the reservoir has a linear drawdown coefficient of 22.8 kPa/(kg/s). The geofluid temperature in the reservoir and up to the flash point is 205°C.
- a. Calculate the depth of the flash horizon from the surface if the wellhead valve is adjusted to give a mass flow rate of 68 kg/s.
 - b. Assuming this flow rate is achieved with a wellhead pressure of 828 kPa, calculate the wellhead quality (or dryness fraction).
- 4.12.** A geothermal well is completed into a liquid-dominated reservoir. The well is of the stepped type having an abrupt step from a 7-5/8-in slotted liner to a 9-5/8-in production casing. During long-term flow testing at a constant wellhead valve setting, a very gradual decline in flow rate is observed. At some moment, a much more rapid decrease in flow occurs eventually causing the well to die. It is known that the geofluid contains about 1% of carbon dioxide (by weight of steam flow).
- a. Discuss possible reasons for the loss of the well.
 - b. Suggest some ways to restore the well to production and to assure that future wells do not suffer the same fate.

- 4.13.** During the early stages of development at the Ahuachapán field in El Salvador, flow tests were conducted on several wells in October 1976; the results are summarized in the table below. Estimate the reservoir temperature for each of the wells and for the field average. Other methods indicated that the reservoir temperature was about 230°C. Discuss the results and the validity of the approximations used in the analysis.

Well	P_{sep} kPa	\dot{m}_v kg/s	\dot{m}_{tot} kg/s
AH1	665.3	13.20	94.90
AH4	699.4	23.66	126.63
AH6	670.5	17.65	62.62
AH20	626.3	10.74	55.46
AH21	650.9	12.51	93.80
AH26	640.9	12.37	70.71
10-well avg.	653.4	13.55	72.55

Part 2



GEOHERMAL POWER GENERATING SYSTEMS

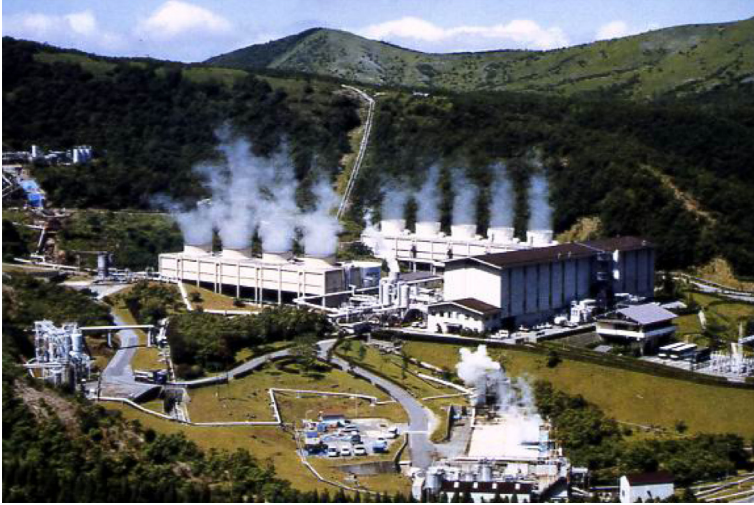
- Single-Flash Steam Power Plants
- Double- and Triple-Flash Steam Power Plants
- Dry-Steam Power Plants
- Binary Cycle Power Plants
- Advanced Geothermal Energy Conversion Systems
- Exergy Analysis Applied to Geothermal Power Systems

The First Law of thermodynamics says you can't get something for nothing; the Second Law says you can't even break even.

Anonymous

The second part of the book covers the energy conversion systems that take the geothermal fluids from the production wells, process them for use, produce electricity in a power plant, and finally dispose of the fluids in an effective and environmentally benign manner. We present the thermodynamic principles governing the design and operation of the power plants and illustrate them with several practical examples. The traditional types of plant

include flash-steam and direct dry-steam plants, as well as binary plants. Advanced systems are covered, some of which are already at the commercial stage while others require more development. We conclude this section with a general presentation of the use of the Second Law of thermodynamics for power plant analysis. This so-called exergy analysis is an effective tool for the design of efficient power plants.



Hatchobaru 110 MW power station, Units 1 and 2, Kyushu, Japan.

Photo: Kyushu Electric Power Co., Inc., Fukuoka, Japan [WWW].



Chapter 5

Single-Flash Steam Power Plants

Chapter Outline

5.1 Introduction	108
5.2 Gathering System Design Considerations	108
5.2.1 Piping Layouts	108
5.2.2 Pressure Losses	110
5.3 Energy Conversion System	114
5.4 Thermodynamics of the Conversion Process	119
5.4.1 Temperature-Entropy Process Diagram	120
5.4.2 Flashing Process	120
5.4.3 Separation Process	121
5.4.4 Turbine Expansion Process	121
5.4.5 Condensing Process	123
5.4.6 Cooling Tower Process	123
5.4.7 Utilization Efficiency	126
5.5 Example: Single-Flash Optimization	127
5.5.1 Choked Well Flow	127
5.5.2 Non-Choked Well Flow	129
5.6 Optimum Separator Temperature: An Approximate Formulation	130
5.7 Environmental Aspects for Single-Flash Plants	132
5.7.1 General Considerations	132
5.7.2 Considerations Pertaining to Single-Flash Plants	133
5.8 Equipment List for Single-Flash Plants	136
5.8.1 Wellhead, Brine, and Steam Supply System	136
5.8.2 Turbine-Generator and Controls	137
5.8.3 Condenser, Gas Ejection, and Pollution Control (Where Needed)	137
5.8.4 Heat Rejection System	138
5.8.5 Backup Systems	138
5.8.6 Noise Abatement System (Where Required)	138
5.8.7 Geofluid Disposal System	138
References	139
Nomenclature for Figures in Chapter 5	140
Problems	140

In theory, there is no difference between theory and practice. In practice, there is.
Yogi Berra

5.1 Introduction

The single-flash steam plant is the mainstay of the geothermal power industry. It is often the first power plant installed at a newly developed liquid-dominated geothermal field. As of December 2014, there are 185 units of this kind in operation in 17 countries around the world. Single-flash plants account for 32% of all geothermal plants. They constitute about 43% of the total installed geothermal power capacity in the world, and the average unit power rating is slightly less than 28 MW per unit. Full details can be found in Appendix A, Tables A.1–A.5.

5.2 Gathering System Design Considerations

When the geothermal wells produce a mixture of steam and liquid, the single-flash plant is a relatively simple way to convert the geothermal energy into electricity. First the mixture is separated into distinct steam and liquid phases with a minimum loss of pressure. This is done in a cylindrical cyclonic pressure vessel, usually oriented with its axis vertical, where the two phases disengage owing to their inherently large density difference. The siting of the separators is part of the general design of the plant and there are several possible arrangements.

A typical 30 MW single-flash power plant needs 5–6 production wells and 2–3 injection wells. These may be drilled at sites distributed across the field or several may be drilled from a single pad using directional drilling to intercept a wide zone of the reservoir. In either case, a piping system is needed to gather the geofluids from the production wells and transport them to the powerhouse and to the points of disposal. Often the initial piping system is modified if new power units are added later on.

5.2.1 PIPING LAYOUTS

The separators can be located (1) at the powerhouse, (2) at satellite stations in the field, or (3) at the wellheads.

Figure 5.1 shows five production wells feeding two-phase fluid to a large cyclone separator at the powerhouse. The separated steam enters the turbine via short pipelines and the separated liquid is sent to two injection wells.

Figure 5.2 depicts an arrangement in which the production wells are connected to two satellite separator stations located in the field. Steam from the separators

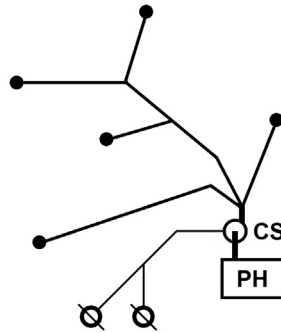


Figure 5.1 Two-phase gathering system: cyclone separator (CS) at the powerhouse (PH). Filled circles = production wells; open circles = injection wells.

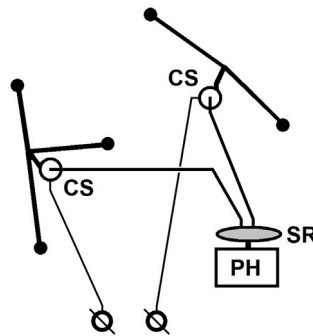


Figure 5.2 Gathering system with satellite separator stations: steam pipelines to a steam receiver (SR) at the powerhouse.

flows to the powerhouse in two pipelines and meets at the steam collector. The separated liquid streams from the satellites flow to the two injection wells. An arrangement of this type is used at the Miravalles power station in Costa Rica; where seven satellites are used. [Figure 5.3](#) is a photograph of the sole separator station at the Las Pailas plant in Costa Rica [1].

[Figure 5.4](#) shows wellhead separators at each production well. This design requires individual steam lines from each separator to the steam collector at the powerhouse. Water lines run from the separators to the injection wells and may be combined. This system was installed, for example, at the Ahuachapán power station in El Salvador; the Ahuachapán layout for the first two units is shown in [Figure 5.5](#) [2].



Figure 5.3 Las Pailas separator station [1]; separators right foreground and vent/silencers left rear. *Photo courtesy of Paul Moya [WWW].*

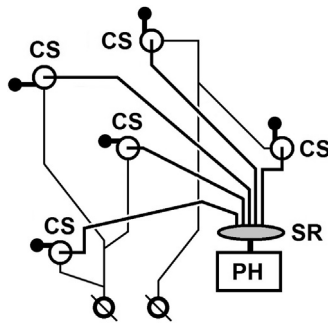


Figure 5.4 Gathering system with individual wellhead separators.

5.2.2 PRESSURE LOSSES

One of the main concerns in the design of the gathering system is the pressure loss in the steam lines from the wellhead to the powerhouse. The steam pressure drop is a function of the diameter, length, and configuration of the steam piping,

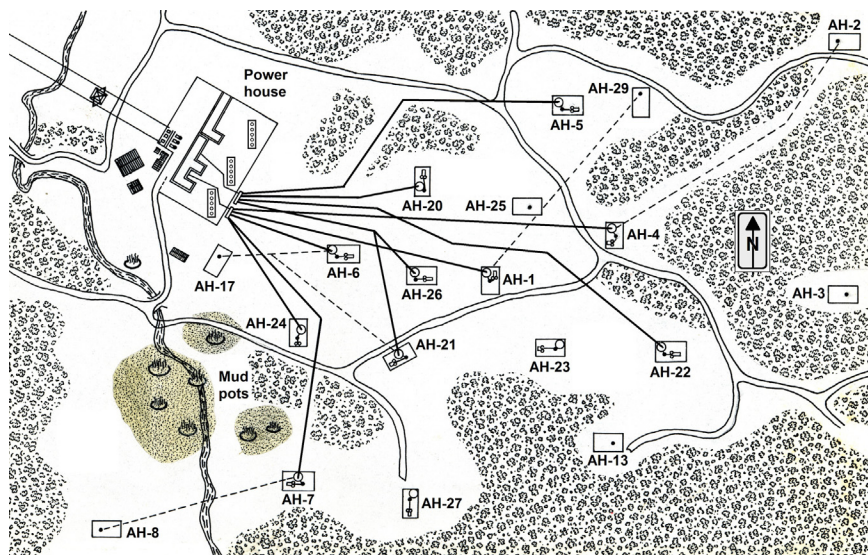


Figure 5.5 Ahuachapán pipelines for Units 1 and 2. This was modified when Unit 3 was added and when new wells were completed. After Ref. [2].

as well as the density and mass flow rate of the steam. Of these the most critical variable is the pipe diameter. Equation (5.1) is a correlation for steam pressure drop caused by friction:

$$\Delta P_f = 0.8 \frac{L \dot{m}^{1.85}}{\rho D^{4.97}} \quad (5.1)$$

where L is the length of the pipe (ft), \dot{m} is the mass flow rate (lbm/h), ρ is the density (lbm/ft³), and D is the inside diameter of the pipe (in). The pressure drop is given in lbf/in². Note that Eq. (5.1) is not dimensionally homogeneous; the 0.8 factor accounts for the particular units chosen.

Since the density of steam is relatively low, the change in pressure due to changes in pipe elevation is much smaller than the friction term given by Eq. (5.1). The diameter plays a huge role in the pressure drop since it is inversely proportional to the diameter raised to essentially the fifth power. By installing pipes of a larger diameter, the pressure loss can be drastically reduced but the extra cost of the larger pipes may be unacceptable economically. A thermodynamic-economic optimization study will lead to the optimum pipe size.

The pressure drop in the liquid lines is less of a concern since the liquid is going to be disposed of by injection, but unnecessarily high pressure losses might require pumps to maintain sufficient reinjection pressure. The frictional pressure drop in the liquid pipes depends on the same variables as in steam pipes plus the

friction factor which in turn is a function of the pipe diameter, internal roughness, and the viscosity of the liquid. Equation 5.2 gives the pressure loss (lbf/in²) in a horizontal liquid pipeline:

$$\Delta P_f = 1.75 \times 10^{-4} \frac{f L \dot{m}^2}{\rho D^5} \quad (5.2)$$

where f is the friction factor given by the Swamee–Jain equation:

$$f = \frac{0.25}{\left\{ \log_{10} \left[\frac{\varepsilon/D}{3.7} + \frac{5.74}{\text{Re}^{0.9}} \right] \right\}^2} \quad (5.3)$$

where ε is the pipe internal roughness (e.g., 1.48×10^{-4} ft for commercial steel pipe) and Re is the Reynolds number:

$$\text{Re} = \frac{4}{\pi} \frac{\dot{m}}{\mu D} \quad (5.4)$$

where μ is the absolute viscosity (e.g., 1.223×10^{-4} lbfm/ft · s for water at 145 lbf/in², abs and 300°F). If there is a change in the elevation of the pipe, the gravity head contribution must be included:

$$\Delta P_g = \rho g \Delta H \quad (5.5)$$

where g is the local gravitational acceleration (e.g., $g = 32.2$ ft/s² at sea level) and ΔH is the change in elevation (ft). The term “gravity head” is positive for down-comers and negative for risers.

The pressure loss in a two-phase, steam–liquid pipeline is far more complex and less reliably predicted analytically [3]. Correlations may be used to estimate the pressure drop but often field tests are conducted to determine the losses experimentally. The situation is complicated by the fact that the two phases may flow in any of the several different patterns depending on the pipe orientation and the relative amounts of the phases present.

For upward flow in a vertical pipe, starting from all liquid flow at the bottom, the following flow patterns are encountered in sequence as the fluid moves up the pipe:

- Bubbly flow (bottom of pipe)
- Bubbly-slug flow
- Slug flow
- Slug-annular flow
- Annular flow
- Annular-mist flow
- Mist flow
- All vapor flow, eventually for a sufficiently long pipe.

For flow in a horizontal pipe, the following flow patterns are encountered under certain circumstances:

- Bubbly flow
- Stratified flow
- Wavy flow
- Plug flow
- Slug flow
- Annular flow.

For each flow pattern, the mechanism for the pressure loss is different and requires the use of empirical correlations. Many of these have been developed and the subject is still being researched.

In general, the pressure loss in a two-phase pipeline consists of three terms: (1) the frictional pressure drop (viscous effects), (2) the gravitational pressure drop (body force effects), and (3) the accelerational pressure drop (inertial effects). The viscous term may be found, for example, from a correlation by Lockhart and Martinelli [4] that gives the ratio of the two-phase pressure drop to the single-phase, steam-only pressure drop. The gravity term enters when the pipeline changes its elevation and requires knowledge of the average density of the two-phase fluid over a length of pipe, and the variation of the density along the pipeline. This is usually expressed in terms of the void fraction, i.e., the fraction occupied by the vapor of the cross-section of a short length of the pipe. Lockhart and Martinelli also provided correlations for void fraction [4]. The acceleration term results from the application of the momentum equation and plays a significant role at and just beyond the point where the liquid initially flashes from a liquid to a vapor when the pressure falls to the saturation pressure corresponding to the local fluid temperature. This is important in a production well, for example, if the flash point is encountered between the fluid entry point and the wellhead, as we saw in Section 4.2. This term is often small for horizontal or gentle-sloped two-phase pipelines and may be neglected for these cases.

James [5] has offered a very simple formulation for the two-phase pressure drop as simply the steam-phase pressure drop divided by the square root of the local dryness fraction. His formula reduces to the steam pressure drop if the dryness fraction is equal to 1, but it fails to give the correct result at the other extreme for all liquid flow, that is, when the dryness fraction becomes 0. Thus, the simple James rule should be viewed as a rough approximation that should only be used when the dryness fraction exceeds 0.5. In any case, its use for a long two-phase pipeline requires a step-by-step, iterative calculation with adjustments being made to the dryness fraction as the pressure falls and the dryness fraction increases.

The important conclusion from these considerations is that two-phase pipelines can be designed as elements of a geothermal gathering system but proper account must be taken of the pressure drop since it can be larger than that in single-phase steam lines. The presence of unsteady flow patterns such as slug flow can cause excessive vibrations and should be avoided by proper selection of pipe diameters. The so-called flow pattern “maps” [4] can guide the designer to safe regimes.

Another important aspect concerns the flow of liquid that is removed from the cyclone separators. That fluid is in a saturated state and any loss in pressure can cause it to flash into vapor. For example, if the liquid is conveyed upward immediately after leaving the separator, the reduction in the gravity head will lower the pressure and one can expect flashing and vibrations that could damage the equipment. Furthermore, if the fluid is conveyed horizontally over a significant distance, the frictional pressure drop may lead to flashing in the pipeline before the fluid reaches the injection well. This will create a vapor barrier and inhibit the flow of the fluid down the well. In such a case, it may be necessary to bleed the vapor from the wellhead or to install a booster pump upstream of the vapor breakout point. It is preferable to have the injection piping run downhill. Any drop in temperature of the liquid will mitigate the problem of flashing but will exacerbate the potential problem of chemical precipitation; see Section 6.6.

5.3 Energy Conversion System

The terminology “single-flash system” indicates that the geofluid has undergone a single flashing process, i.e., a process of transitioning from a pressurized liquid to a mixture of liquid and vapor as a result of lowering the geofluid pressure below the saturation pressure corresponding to the fluid temperature.

The flash process may occur in a number of places: (1) in the reservoir as the fluid flows through the permeable formation with an accompanying pressure drop; (2) in the production well anywhere from the entry point to the wellhead as a result of the loss of pressure due to friction and the gravity head; or (3) in the inlet to the cyclone separator as a result of a throttling process induced by a control valve or an orifice plate. It is often the case in a newly developed field that the flashing occurs in the wellbore initially, but with time as the field undergoes exploitation and the reservoir pressure declines, the flash point may move down the well and even enter the formation. Sometimes, the term “separated steam” is used for this type of plant owing to the manner in which the steam is obtained for use in the turbine.

While the actual location of the flash point can be important in the operation of a power plant, from the point of view of understanding the thermodynamics of the energy conversion process, it is irrelevant. We will assume that the geofluid

starts off as a compressed liquid somewhere in the reservoir, that it experiences a flashing process somewhere, that the two-phases are separated, and that the steam is then used to drive a turbine which in turn drives the electric generator. A simple schematic of this operation is given in Figure 5.6 [6], where the main components of a single-flash plant are shown.

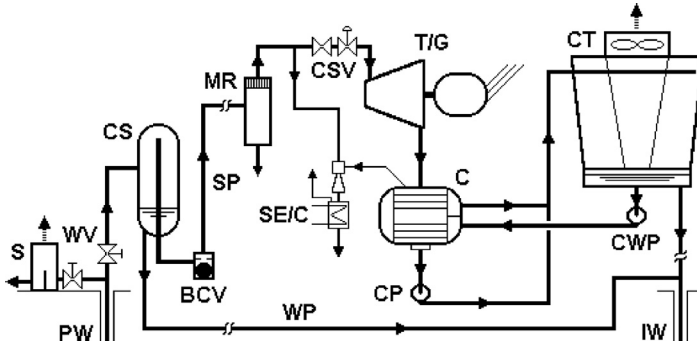


Figure 5.6 Simplified single-flash power plant schematic [6].

At each production well, PW, there is an assemblage of equipment to control and monitor the flow of the geofluid from the well to the plant. This equipment includes: several valves, WV, a silencer, S (simple cyclone separator for emergency venting), piping, and instrumentation (pressure and temperature gauges). If wellhead separators are used, the cyclone separator, CS, will be located close to the wellhead on the same pad.

A classic example of a wellhead arrangement showing the separator and other equipment is given in Figure 5.7 [2]. Wellhead valves are seen above the cellar at right. Two-phase flow passes through the long-radius bend and enters the cyclone separator tangentially. Steam is collected from the center of the vessel by a stand-pipe, seen emerging from the bottom. The steam then passes through a ball check valve, BCV, at the left, emerges from the top, and flows to the powerhouse. The separated liquid flows into a holding tank (small vertical vessel to the right of the bottom of the separator), from which it can go either to the silencer seen to right rear or to injection wells.

It is important to separate the two phases efficiently prior to the steam being admitted to the turbine. Liquid entrained in the steam can cause scaling and/or erosion of piping and turbine components. Generally, the quality of the steam entering the turbine should be at least 99.995% dry. Although there are a few designs in use for the cyclone separators, the industry has generally settled on the simple Webre-type separator, which is depicted in Figure 5.7. Lazalde–Crabtree [7]



Figure 5.7 Wellhead separator system at Ahuachapán, El Salvador. *Photo by author [2].*

published an approach to designing such vessels. He presented two variations: one for a primary two-phase separator and one for a moisture remover. The designs were based on a combination of theory and empirical correlations. His recommended geometry of the two vessels is given in [Figure 5.8](#).

To achieve a very high level of steam quality, Lazalde–Crabtree recommends the guidelines given in [Table 5.1](#).

A variation on these designs is used at several plants in Iceland. Originally, vertical separators were deployed but since about 1995 these have been replaced with horizontal ones of the design shown in [Figure 5.9](#). The main principle of separation here is gravity, augmented by a set of vane baffle plates fitted to the bottom of the vessel and a horizontal perforated droplet removal plate at the entrance to the steam exit chamber.

There are advantages and disadvantages to each type of separator [\[8\]](#). The advantages for the vertical design include: cleaner steam, a sharper cut-off, wider pressure range, and easier maintenance; the disadvantages include: size limitations and the height of construction. For the horizontal design the advantages include: no size constraints and greater throughput per vessel; the disadvantages include: horizontal mist eliminators are needed for high quality steam and greater maintenance. Of the two separators, generally horizontal ones are less expensive to build and install.

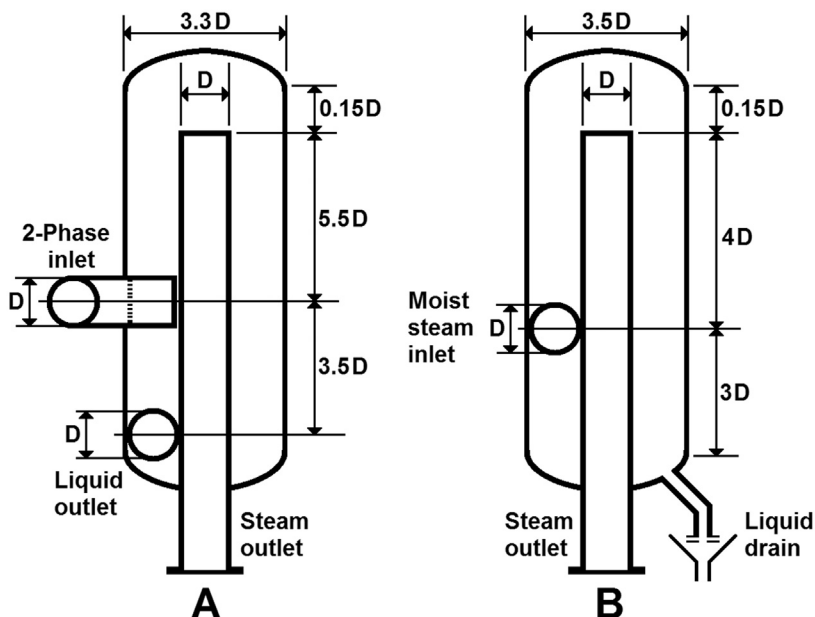


Figure 5.8 General design specifications for cyclone separator (A) and cyclone moisture remover (B) [7].

TABLE 5.1 Separator and moisture remover design guidelines [7].

Parameter	Separator	Moisture remover
Maximum steam velocity at the two-phase inlet pipe	45 m/s (150 ft/s)	60 m/s (195 ft/s)
Recommended range of steam velocity at the two-phase inlet pipe	25–40 m/s (80–130 ft/s)	35–50 m/s (115–160 ft/s)
Maximum upward annular steam velocity inside cyclone	4.5 m/s (14.5 ft/s)	6.0 m/s (20 ft/s)
Recommended range of upward annular steam velocity inside cyclone	2.5–4.0 m/s (8–13 ft/s)	1.2–4.0 m/s (4–13 ft/s)

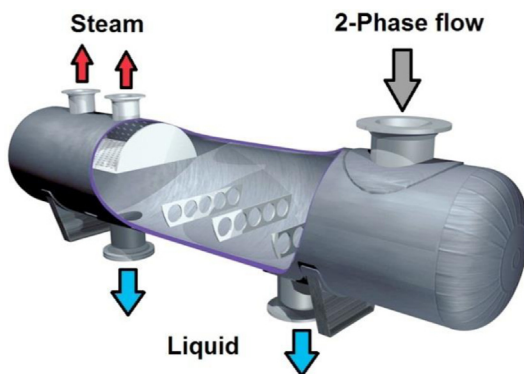


Figure 5.9 Sectioned view of a horizontal separator as used at Icelandic plants [WWW].

Where the separators are situated at a distance from the powerhouse, the steam transmission pipelines are fitted with traps to capture and remove moisture that may form from condensation within the pipes. Prior to being admitted to the turbine, the steam may be scrubbed to remove any fine moisture droplets that may have formed in the transmission pipelines and escaped the steam traps. The moisture remover, MR in [Figure 5.6](#), is usually located directly outside the powerhouse.

The turbines used in geothermal applications must be made of corrosion-resistant materials owing to the presence of gases such as hydrogen sulfide that can attack ordinary steel. Various alloys have been successfully used for turbine steam-path elements, for example, nozzles, blades, diaphragms, etc. Generally, 12% chromium steel is used for steam-path components: AISI Type 403/410 or AISI Type 405 alloy steels [9].

The design of the steam path through the blades is similar to that for a nuclear generating station because the steam enters the turbine essentially as a saturated vapor at a moderate to low pressure. This is markedly different from the steam conditions normally found at a coal, oil, or gas-fired power plant where highly superheated steam is used. Typical geothermal turbine inlet steam conditions are saturated with pressures that range from 5 to 10 bar (80–140 lbf/in²). As a result, significant amounts of moisture appear in the steam path of geothermal turbines, particularly in the lowest pressure stages. These relatively slow moving droplets strike the back of the leading edge of the blades causing erosion unless this area is reinforced. Cobalt-rich alloy strips, such as Stellite[®], are inlaid at these critical areas to protect them from damage.

Since the corrosive effects of geothermal fluids depend on the chemical composition of the geofluids, it is often considered wise to conduct *in situ* materials testing before deciding on the selection of materials for the plant. In these field tests, various samples (coupons) of alternative materials are subjected to long-term exposure to the geothermal liquids and vapors under conditions closely matching those expected during plant operation. The following properties are observed: corrosion, corrosion fatigue, stress corrosion cracking, erosion, and tensile strength [9,10]. [Table 5.2](#) shows typical materials used for critical turbine elements [11].

Turbines for single-flash units are typically rated at 25–55 MW and consist of 4–5 stages of impulse-reaction blades. Both single-flow and double-flow designs are in use. Overall isentropic efficiencies in the upper 80% range have been obtained.

The steam from the turbine is condensed by means of either a surface-type condenser, C, as shown in [Figure 5.6](#) or in a direct-contact condenser of either the

TABLE 5.2 Typical turbine element materials [11].

Component	Material
Piping	ASTM A106, Gr B; ASTM A335, Gr P11, or P22
H.P. casings	ASTM A356, Gr 1, 6, 9, or 10
L.P. casings	ASTM A285 or A515
Valve bodies	ASTM A216 or A217
Fasteners	ASTM A193 and A194
Rotors	ASTM A470
Blades	AISI 403
Nozzle blades	AISI 403
Bands	AISI 405

barometric or low-level type. Most plants now employ surface condensers in which the geothermal steam passes through the shell side and cooling water passes through the tube side. This maintains physical and chemical separation between the geothermal steam and the cooling water, and allows more effective removal and treatment of noncondensable gases. Gases such as carbon dioxide and hydrogen sulfide co-exist with the natural steam and do not condense at the temperatures in the condenser. Therefore, unless they are removed they will increase the overall pressure in the condenser and lower the turbine power output. Steam jet ejectors with aftercondensers, SE/C (in Figure 5.6), and/or vacuum pumps are used for this purpose.

The cooling water is usually obtained from a cooling tower that recirculates a portion of the condensed steam after it has been cooled by partial evaporation in the presence of a moving air stream (items CT and CWP in Figure 5.6). This means that geothermal flash-steam plants do not need a significant supply of cooling water, a major advantage in areas that are arid. A small amount of freshwater is needed, however, to provide for replacement of tower blowdown.

5.4 Thermodynamics of the Conversion Process

The analysis presented here is based on fundamental thermodynamic principles, namely the principle of energy conservation (i.e., the First Law of thermodynamics) and the principle of mass conservation. An exposition of the subject may be found in any standard text such as those by Moran and Shapiro [12] and Çengel and Boles [13], to mention only two. The general equation of the First Law is given in Section 10.2.

5.4.1 TEMPERATURE-ENTROPY PROCESS DIAGRAM

The processes undergone by the geofluid are best viewed in a thermodynamic state diagram in which the fluid temperature is plotted on the ordinate and the fluid specific entropy is plotted on the abscissa. A temperature-entropy diagram for the single-flash plant is shown in Figure 5.10.

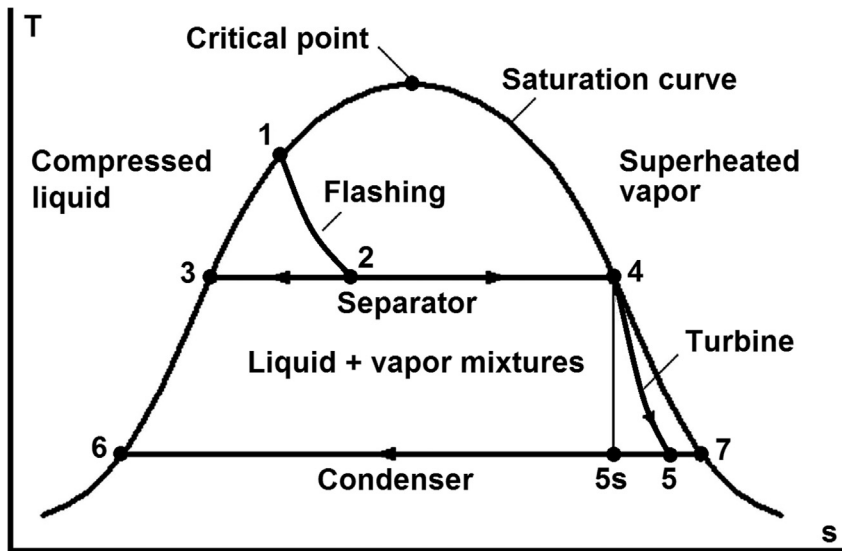


Figure 5.10 Temperature-entropy state diagram for single-flash plants.

5.4.2 FLASHING PROCESS

The sequence of processes begins with geofluid under pressure at state 1, close to the saturation curve. The flashing process is modeled as one at constant enthalpy, i.e., an isenthalpic process, because it occurs steadily, spontaneously, essentially adiabatically, and with no work involvement. We also neglect any change in the kinetic or potential energy of the fluid as it undergoes the flash. Thus we may write:

$$h_1 = h_2 \quad (5.6)$$

This was discussed in Section 4.2.3 when we examined the flow of a geofluid from the reservoir to the wellhead.

5.4.3 SEPARATION PROCESS

The separation process is modeled as one at constant pressure, that is, an isobaric process, once the flash has taken place. The quality or dryness fraction, x , of the mixture that forms after the flash, state 2, can be found from:

$$x_2 = \frac{h_2 - h_3}{h_4 - h_3} \quad (5.7)$$

by using the so-called lever rule from thermodynamics. This gives the steam mass fraction of the mixture and is the amount of steam that goes to the turbine per unit total mass flow into the separator.

5.4.4 TURBINE EXPANSION PROCESS

The work produced by the turbine per unit mass of steam flowing through it is given by:

$$w_t = h_4 - h_5 \quad (5.8)$$

assuming no heat loss from the turbine and neglecting the changes in kinetic and potential energy of the fluid entering and leaving the turbine. The maximum possible work would be generated if the turbine operated adiabatically and reversibly, i.e., at constant entropy or isentropically. The process shown in [Figure 5.10](#) from 4 to 5s is the ideal process. We define the isentropic turbine efficiency, η_t , as the ratio of the actual work to the isentropic work, namely,

$$\eta_t = \frac{h_4 - h_5}{h_4 - h_{5s}} \quad (5.9)$$

The power developed by the turbine is given by:

$$\dot{W}_t = \dot{m}_s w_t = x_2 \dot{m}_{total} w_t \quad (5.10)$$

This represents the gross mechanical power developed by the turbine. The gross electrical power will be equal to the turbine power times the generator efficiency:

$$\dot{W}_e = \eta_g \dot{W}_t \quad (5.11)$$

All auxiliary power requirements for the plant must be subtracted from this to obtain the net, salable power. These so-called parasitic loads include all pumping power, cooling tower fan power, and station lighting.

Before [Eq. \(5.9\)](#) can be used computationally, it must be recognized that the isentropic efficiency of a turbine is affected by the amount of moisture that is present during the expansion process; the higher the moisture, the lower the

efficiency. This effect can be quantified by using the so-called Baumann rule [14] which says that a 1% average moisture causes roughly a 1% drop in turbine efficiency. Since geothermal turbines generally operate in the wet region, we must account for the degradation in performance. Adopting the Baumann rule, we find the isentropic efficiency for a turbine operating with wet steam to be given by:

$$\eta_{rw} = \eta_{td} \times \left[\frac{x_4 + x_5}{2} \right] \quad (5.12)$$

where the dry turbine efficiency, η_{td} , may be conservatively assumed to be constant at, say, 85%:

$$\eta_{td} = 0.850 \quad (5.13)$$

From Figure 5.10, it is clear that the quality at the turbine outlet, state 5, depends on the turbine efficiency. State 5 is determined by solving Eq. (5.9) using the turbine efficiency and the fluid properties at state 5s, the ideal turbine outlet state, which are easily calculated from the known pressure and entropy values at state 5s. The ideal outlet enthalpy is found from:

$$h_{5s} = h_6 + [h_7 - h_6] \times \left[\frac{s_4 - s_6}{s_7 - s_6} \right] \quad (5.14)$$

where the entropy term, by itself, gives the fluid outlet dryness fraction for an ideal turbine. When the Baumann rule is incorporated into the calculation, the following working equation emerges for the enthalpy at the actual turbine outlet state:

$$h_5 = \frac{h_4 - A \left[1 - \frac{h_6}{h_7 - h_6} \right]}{1 + \frac{A}{h_7 - h_6}} \quad (5.15)$$

where the factor A is defined as:

$$A \equiv 0.425(h_4 - h_{5s}) \quad (5.16)$$

These equations are based on the assumption that the quality at the turbine inlet, x_4 , is equal to one, i.e., the entering steam is a saturated vapor. If the inlet is wet (as will be the case for the double-flash system to be discussed in the next chapter), then Eq. (5.15) must be modified as follows:

$$h_5 = \frac{h_4 - A \left[x_4 - \frac{h_6}{h_7 - h_6} \right]}{1 + \frac{A}{h_7 - h_6}} \quad (\text{for } x_4 < 1) \quad (5.17)$$

5.4.5 CONDENSING PROCESS

Turning next to the surface-type condenser shown in Figure 5.6, the First Law of thermodynamics leads to the following equation that relates the required flow rate of cooling water, \dot{m}_{cw} , to the steam flow rate, $x_2\dot{m}_{total}$:

$$\dot{m}_{cw} = x_2\dot{m}_{total} \left[\frac{h_5 - h_6}{\bar{c} \Delta T} \right] \quad (5.18)$$

where \bar{c} is the assumed constant specific heat of the cooling water ($\approx 1 \text{ Btu/lbm} \cdot ^\circ\text{F}$ or $4.2 \text{ kJ/kg} \cdot \text{K}$) and ΔT is the rise in cooling water temperature as it passes through the condenser.

For a direct-contact condenser (see Figure 5.11), the appropriate equation is:

$$\dot{m}_{cw} = x_2\dot{m}_{total} \left[\frac{h_5 - h_6}{\bar{c}(T_6 - T_{cw})} \right] \quad (5.19)$$

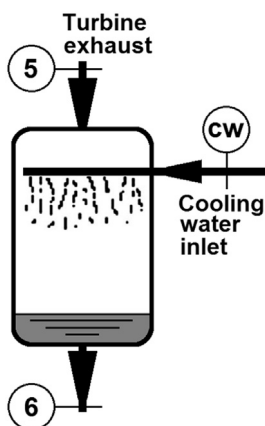


Figure 5.11 Direct-contact condenser. Vessel is assumed to be perfectly insulated.

5.4.6 COOLING TOWER PROCESS

The cooling tower must be designed to accommodate the heat load from the condensing steam. With reference to Figure 5.12, the steam condensate that has been pumped from the condenser hotwell is sprayed into the tower where it falls through an air stream drawn into the tower by a motor-driven fan at the top of the tower. The ambient air enters with a certain amount of water vapor, determined

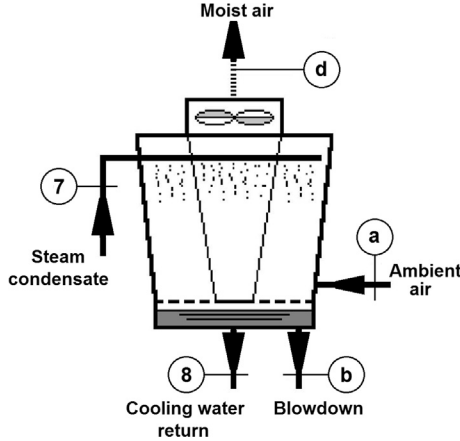


Figure 5.12 Cooling tower schematic. This type is called a mechanical, induced-draft cooling tower.

by its relative humidity, and picks up more water vapor as the condensate partially evaporates. The evaporation process requires heat that comes from the water itself, thereby dropping its temperature.

The internal process involves the exchange of both heat and mass between the air and the water. The following First Law equation describes the overall operation of the tower, excluding the fan and assuming steady flow and overall adiabatic conditions:

$$\dot{m}_7 h_7 - \dot{m}_8 h_8 = \dot{m}_d h_d - \dot{m}_a h_a + \dot{m}_b h_b \quad (5.20)$$

There are two other equations needed to analyze the process: mass conservation of water and mass conservation of air. Recall that both the entering and leaving air streams contain water in the vapor phase (in different percentages). The conservation equations are:

$$\dot{m}_7 + \dot{m}_{wa} = \dot{m}_8 + \dot{m}_b + \dot{m}_{wd} \quad (\text{Conservation of water}) \quad (5.21)$$

$$\dot{m}_{ad} = \dot{m}_{aa} \quad (\text{Conservation of dry air}) \quad (5.22)$$

where the terms \dot{m}_{wa} and \dot{m}_{wd} represent the water content of the incoming and leaving air streams, respectively. These can be found from the specific humidity, ω , of the air streams:

$$\dot{m}_{wa} = \omega_a \dot{m}_a \quad (5.23)$$

and

$$\dot{m}_{wd} = \omega_d \dot{m}_d \quad (5.24)$$

These five governing equations are used with the properties of steam, water, and moist air, either in tabular, graphic (psychrometric chart), or electronic form to determine the various flow rates needed for given design conditions.

Cooling towers are also characterized by two other parameters: the *range* and the *approach*. The range is the change in water temperature as it flows through the tower, namely, $T_7 - T_8$, with reference to Figure 5.12; the approach is the difference between the water outlet temperature and the wet-bulb temperature of the incoming air, namely, $T_8 - T_{wb,a}$. Since the ideal outlet water temperature is the wet-bulb temperature of the incoming air, the approach is a measure of how closely the tower approaches ideal performance, i.e., zero approach or $T_8 = T_{wb,a}$.

Cooling towers for geothermal power plants are much larger in cooling capacity than for conventional fossil or nuclear power plants of the same power rating. Since the cooling tower must be sized to reject the heat of condensation of the geothermal steam, we can examine the ratio of that heat, \dot{Q}_o , to the power output of the plant, \dot{W}_e .

Let us consider first a power plant that operates on a cycle. In Chapter 8 we will cover such geothermal plants in detail. Here, it is necessary only to understand that for any cyclic power plant, the First Law of thermodynamics says that the net heat added to the cycle must equal the net work delivered by the cycle, or in terms of thermal and mechanical power,

$$\dot{Q}_{in} - \dot{Q}_o = \dot{W}_e \quad (5.25)$$

Also for a cyclic plant, we can define the thermal efficiency, η_{th} , as follows:

$$\eta_{th} = \frac{\dot{W}_e}{\dot{Q}_{in}} \quad (5.26)$$

Binary geothermal plants (see Chapter 8) generally have thermal efficiencies in the range of 10–13%.

It is easy to show [15] that

$$\frac{\dot{Q}_o}{\dot{W}_e} = \frac{1}{\eta_{th}} - 1 \quad (5.27)$$

Fossil-fired, combined steam-and-gas-turbine plants typically have thermal efficiencies of 50–55%, coal-fired plants are about 35–40% efficient, and nuclear plants about 33–35% efficient. Thus, the rate of heat discharged per unit power generated for these three types of plant are, on average, 0.9, 1.7, and 1.9, respectively, whereas a typical geothermal binary plant discharges 7.7 units of waste heat for each unit of useful output. Thus, a 50 MWe geothermal binary plant must have a cooling tower 8.5 times larger in cooling capacity than that for a 50 MWe combined cycle plant.

Although flash-steam plants are not cyclic in operation and the thermal efficiency given in Eq. (5.26) is not applicable, the waste heat can nevertheless be calculated using

$$\dot{Q}_o = x_2 \dot{m}_{total} (h_5 - h_6) \quad (5.28)$$

for the single-flash plant described above. This can then be compared to the net power using the equations in Section 5.4.4. The general qualitative conclusion regarding the relative size of the cooling systems for flash-steam plants in comparison to conventional plants is the same as for a binary plant, namely, they are larger than cooling systems at conventional plants of the same power rating. One often sees a 5-cell cooling tower used for a 30 MW geothermal flash plant, whereas that same tower could easily accommodate a 250 MW state-of-the-art combined cycle plant.

5.4.7 UTILIZATION EFFICIENCY

Lastly, the performance of the entire plant may be assessed using the Second Law of thermodynamics by comparing the actual power output to the maximum theoretical power that could be produced from the given geothermal fluid. This involves determining the rate of exergy carried into the plant with the incoming geofluid. An in-depth presentation of Second Law analysis of geothermal plants is given in Chapter 10.

The specific exergy, e , of a fluid that has a pressure, P , and a temperature, T , in the presence of an ambient pressure, P_0 , and an ambient temperature, T_0 , is given by:

$$e = h(T, P) - h(T_0, P_0) - T_0[s(T, P) - s(T_0, P_0)] \quad (5.29)$$

When this is multiplied by the total incoming geofluid mass flow rate, we obtain the maximum theoretical thermodynamic power or the exergetic power:

$$\dot{E} = \dot{m}_{total} e \quad (5.30)$$

The ratio of the actual net power to the exergetic power is defined as the utilization efficiency or the Second Law (exergetic) efficiency of the plant:

$$\eta_u \equiv \frac{\dot{W}_{net}}{\dot{E}} \quad (5.31)$$

All types of power plant can be compared on the basis of the utilization efficiency, no matter the source of the primary energy—be it coal, oil, nuclear,

biomass, hydro, solar, wind, or geothermal. Plants can also be designed to maximize η_u when the value of the primary energy (or exergy) is a significant factor in the economics of the operation.

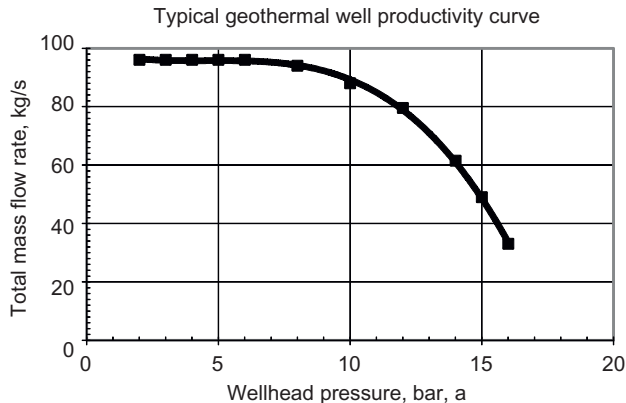
5.5 Example: Single-Flash Optimization

In this section, we will examine the problem of selecting the separator conditions that will yield the best overall plant performance in terms of the power generation. Two hypothetical cases will be studied.

5.5.1 CHOKED WELL FLOW

Let us consider a geothermal resource of the liquid-dominated type having a known reservoir temperature of 240°C. A single geothermal well is drilled having the following productivity data, i.e., the total geofluid mass flow rate (liquid and vapor) measured in kg/s as a function of the wellhead pressure measured in bar,a:

P-wh	m-dot total
2	96.0
3	96.0
4	96.0
5	96.0
6	96.0
8	94.0
10	88.0
12	79.5
14	61.5
15	49.0
16	33.0
bar,a	kg/s



The data are plotted in the figure where it can be seen that the flow increases rapidly as the well is opened and the pressure is lowered. However, once the pressure reaches about 7–8 bar, the flow rate stabilizes and no further lowering of the pressure can raise the total mass flow rate. Such a well is called “choked.”

The question now is posed: What wellhead pressure should be chosen to maximize the power output from a single-flash plant connected to this well?

In solving this problem, we will assume that the well is connected directly to a wellhead separator, allowing us to neglect any pressure loss between the wellhead and the separator. Furthermore, we will neglect any other pressure losses associated with transmitting the separated steam from the separator to the turbine.

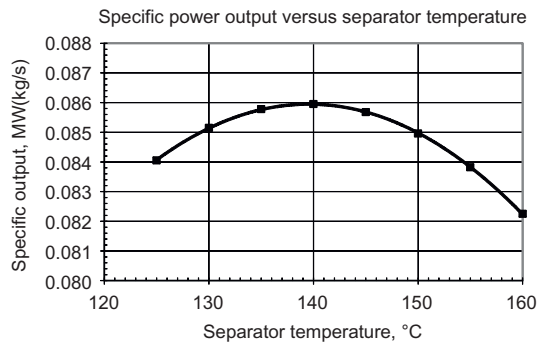
It is not difficult to accommodate these losses, but the methodology of optimization is more clearly demonstrated by ignoring them here. We will also assume that it is possible to operate the condenser at a pressure of 0.123 bar or a condensing steam temperature of 50°C.

The Eqs. (5.6)–(5.17) are used to analyze the flashing, separation, and turbine expansion processes. The calculations will proceed in two phases: in phase 1 we will determine the specific power output for a range of separator pressures (or equivalently, temperatures), and in phase 2 we will find the total power by factoring in the variation of the total flow rate as a function of the separator pressure. Phase 1 calculations are independent of the well productivity and yield the result in units of MW/(kg/s).

The calculations rely on accurate properties of the geothermal fluid, here assumed to be pure water. Thus, normal *Steam Tables* [16,17] are used to find all thermodynamic properties for the liquid and the vapor.

The results of the phase 1 calculations are given in the table and figure below.

T-sep	P-sep	w (MW/kg/s)
125	2.321	0.08405
130	2.701	0.08515
135	3.120	0.08578
140	3.613	0.08595
145	4.154	0.08568
150	4.758	0.08496
155	5.431	0.08382
160	6.178	0.08225



It can be seen that the maximum specific power occurs at a separator temperature of about 140°C or a separator pressure of 3.6 bar,a. The optimum specific power is about 86 kW for each kg/s of total flow from the well. Notice that the optimum separator temperature is close to the average temperature between the reservoir and the condenser, namely, 145°C [(240°C + 50°C)/2 = 145°C]. This simple relationship can be used as a first approximation to determine the best separator temperature. In the following section, we will derive this “rule of thumb.”

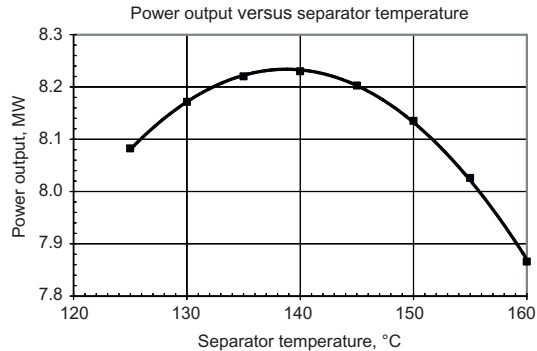
Next, the actual well flow rate is found from the productivity curve at each assumed wellhead pressure and multiplied by the corresponding specific power to obtain the actual power in MW. For this purpose it is convenient to correlate the productivity curve with the best least-squares fit. An excellent fit is obtained using a cubic equation:

$$\dot{m}_{total} = 99.663 - 2.6287 P_2 + 0.5802 P_2^2 - 0.04212 P_2^3 \quad (5.32)$$

where the pressure is in bar,a and the mass flow rate is in kg/s.

The results of the phase 2 calculations are shown below. The maximum gross power is 8.23 MW, indicative of a very good well. In this case, the optimum power occurs at essentially the same separator conditions as does the optimum specific power. This happens because the well flow curve is choked and the flow rate is nearly constant in the range of pressures around the optimum point. We will next consider an example where the well is not choked.

T-sep	P-sep	m-dot total	W-dot (MW)
125	2.321	96.16	8.082
130	2.701	95.97	8.171
135	3.120	95.83	8.220
140	3.613	95.75	8.230
145	4.154	95.74	8.203
150	4.758	95.75	8.135
155	5.431	95.75	8.026
160	6.178	95.64	7.866

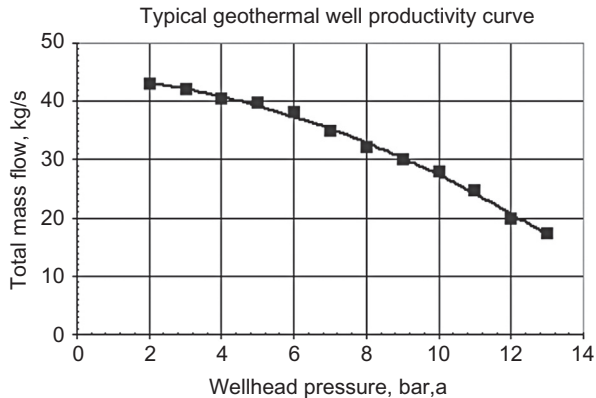


5.5.2 NON-CHOKED WELL FLOW

Many wells do not reach their maximum flow rate except at very low wellhead pressures. These very low pressures are not usually appropriate as turbine inlet conditions. This type of productivity curve is often the result of low reservoir permeability or too small a diameter for the well casing. Such wells are not very productive and will lead to a different outcome in the optimization procedure.

Let us now assume the well is characterized by the following production data:

P-wh	m-dot total
2	43.0
3	42.1
4	40.6
5	39.7
6	38.1
7	35.0
8	32.2
9	30.0
10	28.0
11	24.7
12	20.0
13	17.3
bar,a	kg/s

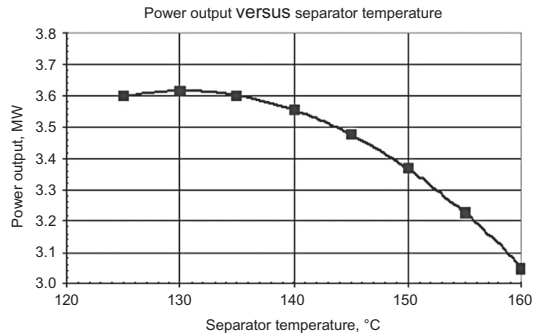


The data can be correlated very well with the second-order equation:

$$\dot{m}_{total} = 44.333 - 0.3363 P_2 - 0.1357 P_2^2 \quad (5.33)$$

The results of the phase 1 calculations are the same as for the first case and are not repeated here. The results of the phase 2 calculations are shown below. The optimum power output is about 3.61 MW and occurs at a separator temperature of 130°C and a pressure of 2.7 bar,a. Here we see that the two optima, namely, the best specific power and the best total power do not occur at the same values of separator pressure and temperature.

T-sep	P-sep	m-dot total	W-dot (MW)
125	2.321	42.82	3.599
130	2.701	42.43	3.613
135	3.120	41.96	3.600
140	3.613	41.35	3.554
145	4.154	40.59	3.478
150	4.758	39.66	3.370
155	5.431	38.50	3.227
160	6.178	37.07	3.049



The utilization efficiency, Eq. (5.31), can be seen to be equal to the ratio of the specific power output to the specific exergetic power (since the total mass flow rate appears in both the numerator and the denominator, and so cancels out). Thus the maximum utilization efficiency will not be influenced by the total mass flow rate and will coincide with the conditions for the optimum specific power. If we take the dead-state temperature to be 25°C, then the specific exergy for the 240°C liquid-dominated reservoir fluid is 236.52 kJ/kg. Thus, for the two examples shown in this section, the optimum value of the utilization efficiency is the same, namely, 36.3% (= 85.95/236.52). For the latter case, the designer must decide on whether it is more economical to design for the highest utilization of the reservoir fluid or for the highest power output.

5.6 Optimum Separator Temperature: An Approximate Formulation

This derivation is based on the process diagram as shown in Figure 5.10. The goal is to find the separator temperature, T_2 ($=T_3 = T_4$), that maximizes the specific work output, w , from the plant. We will consider only the turbine work and neglect any pumping or other parasitic workloads.

The specific work per unit mass of geofluid is:

$$w = x_2(h_4 - h_5) \quad (5.34)$$

To a first approximation,

$$h_1 - h_6 \approx c(T_1 - T_6) \quad (5.35)$$

and

$$h_3 - h_6 \approx c(T_3 - T_6) \quad (5.36)$$

assuming that c , the average specific heat for saturated liquid, is constant between states 1 and 6. It is convenient for this derivation to arbitrarily set the enthalpy to zero at state 6:

$$h_6 \equiv 0 \text{ (reference datum)} \quad (5.37)$$

Thus,

$$h_1 = c(T_1 - T_6) = h_2 \quad (5.38)$$

and

$$h_3 = c(T_3 - T_6) \quad (5.39)$$

From the definition of the latent heat of evaporation, it follows that

$$h_4 - h_3 = h_{fg} \quad (5.40)$$

where we adopt the *Steam Table* “ fg ” subscript notation for the latent heat. Thus,

$$h_4 = h_3 + h_{fg} = c(T_3 - T_6) + h_{fg} \quad (5.41)$$

Now we invoke a little-known approximation, namely,

$$h_4 - h_3 \approx h_5 - h_6 \quad (5.42)$$

For the range of temperatures typical of geothermal systems, this approximation is good to about 1.5%. Note that the actual turbine outlet state 5 is used in [Eq. \(5.42\)](#), not the ideal isentropic state 5s. Then, it follows that

$$h_{fg} \approx h_5 - h_6 \approx h_5 \quad (5.43)$$

Now we can express the separator quality, x_2 , as follows:

$$x_2 = \frac{h_2 - h_3}{h_{fg}} = \frac{c(T_1 - T_6) - c(T_3 - T_6)}{h_{fg}} = \frac{c(T_1 - T_3)}{h_{fg}} \quad (5.44)$$

The specific work can now be expressed as the following function:

$$w = \frac{c}{h_{fg}}(T_1 - T_3)(h_4 - h_5) = \frac{c^2}{h_{fg}}(T_1 - T_3)(T_3 - T_6) \quad (5.45)$$

It is necessary only to differentiate this expression with respect to T_3 , set the result equal to zero, and solve for T_3 , a typical application of the calculus of variations [18]. In carrying out the differentiation, we simplify the task by assuming that the multiplier, c^2/h_{fg} , is a constant. This approximation is weaker than the one used in Eq. (5.42) but for this purpose is acceptable. The differentiation goes as follows:

$$\frac{dw}{dT_3} = (T_1 - T_3)(1) + (T_3 - T_6)(-1) = T_1 - T_3 - T_3 + T_6 = 0 \quad (5.46)$$

Solving for T_3 , we find the optimum value of the separator temperature is given approximately as:

$$T_{3,opt} = \frac{T_1 + T_6}{2} \quad (5.47)$$

Since this rule indicates that the temperature range between the reservoir and the condenser is divided into two equal segments, this rule is sometimes called the “equal-temperature-split” rule. This approximate rule applies to all flash plants regardless of the number of flashes [11]. For a double-flash plant (see Chapter 6), the rule says: (1) the temperature difference between the reservoir and the first flash is equal to (2) the temperature difference between the first flash and the second flash, and is also equal to (3) the temperature difference between the second flash and the condenser.

5.7 Environmental Aspects for Single-Flash Plants

5.7.1 GENERAL CONSIDERATIONS

There are several potential environmental impacts from geothermal plants [11,19,20]; Table 5.3 shows a listing that may be applied to all kinds of geothermal power plants.

TABLE 5.3 Geothermal power plant environmental concerns.

Possible impact	Details	Abatement techniques
Air pollution	H ₂ S emissions	Several effective commercial systems in use
Water pollution	Surface discharge of waste brine; groundwater contamination	Reinjection
Noise pollution	Drilling; well testing	Rock mufflers; silencers
Visual pollution	Unsightly pipes and buildings in pristine areas	Use low-level structures; paint equipment in blending colors
Land usage	Well pads; pipe routes, powerhouse, and substation	Much lower impact than conventional plants
Water usage	Cooling tower makeup (for binary plants only)	Use air-cooled condensers
Land subsidence	Liquid removal from subsurface can lead to surface depressions	Rare, most dramatic at Wairakei, New Zealand
Greenhouse gases	CO ₂ emissions	Very low emissions relative to conventional fossil plants
Loss of natural wonders	Thermal manifestations may disappear; for example, the geysers at Beowawe and Steamboat Springs, Nevada	Do not develop resources in or adjacent to national parks

5.7.2 CONSIDERATIONS PERTAINING TO SINGLE-FLASH PLANTS

There are specific places at a single-flash plant where emissions can occur during normal operation. These include:

- Wellhead and station silencers and mufflers
- Steam traps and drains from pipelines
- Vents from the noncondensable gas ejectors
- Water vapor plume from a wet cooling tower
- Cooling tower blowdown.

Geothermal steam contains noncondensable gases such as hydrogen sulfide, H₂S, carbon dioxide, CO₂, methane, CH₄, and others in very small amounts. Uncontrolled venting of steam releases all these gases to the atmosphere. Under normal conditions, these gases are isolated in the condenser, drawn into the ejectors, and if necessary, treated before release to the atmosphere. There are many reliable, cost-effective means for removing H₂S if the amount that would be vented exceeds regulated limits [11]. The CO₂ that is released from flash

plants is not abated but constitutes a relatively minor source of greenhouse gases: flash plants emit about 0.06 kg/kWh compared with 0.59 kg/kWh for a natural-gas-fired gas turbine and 1.13 kg/kWh for a coal-fired plant [19].

The separated brine contains practically all the dissolved minerals that existed in the geofluid in the reservoir but in higher concentrations. Some of the elements typically found in brines would adversely affect surface or groundwaters if allowed to mix with them. These elements include:

Arsenic, As	Lithium, Li
Boron, B	Magnesium, Mg
Calcium, Ca	Potassium, K
Chloride, Cl	Silicon, Si
Fluoride, F	Sodium, Na.

The main way to prevent water contamination is to reinject the waste brine back into the reservoir. This is now the accepted means of disposing of geothermal waste fluids at plants around the world. Reinjection has the added benefit of restoring some of the fluid that was extracted during production and in providing pressure support in the reservoir. Poor siting of the injection wells, however, can cause premature cooling of the production wells; reservoir simulators can be used to avoid this problem (see Chapter 4).

The noise associated with well drilling and the testing of wells occurs mainly during the early phases of field development and later sporadically as makeup wells are needed during normal operation. There are several effective methods to abate the noise coming from movement of geothermal steam, including cyclone silencers and rock mufflers that reduce the velocity of the steam being vented. An unabated, wide-open geothermal well discharging vertically into the atmosphere produces a noise level of 71–83 dB(A) at a distance of 900 m; by comparison, a noisy urban area has a level of 80–90 dB(A) [19]. Unabated venting is a rare occurrence nowadays but was very much in fashion in the early days of geothermal development to demonstrate the raw power of the natural steam.

A single-flash plant is relatively economical in terms of land required to support the operation compared to other means of generating electricity. A flash plant needs roughly 1200 m²/MW, including well pads, pipe routes, power plant, and substation. By comparison, a nuclear plant needs about 10,000 m²/MW (power station only), a coal-fired plant needs 40,000 m²/MW (power station plus area to be strip-mined for 30 years), and a solar photovoltaic plant needs 66,000 m²/MW (power station only) [20].

Whenever large quantities of subsurface water are removed, there is the possibility that the overburden may sink into the space previously occupied by the water. Most geothermal reservoirs, however, reside in competent rock and the

geofluid does not materially contribute to the structural strength of the formation. The one exception is Wairakei, New Zealand, where significant subsidence has occurred over the 57 years of exploitation [2]. With the general adoption of reinjection at flash-steam plants, the problem of subsidence has all but disappeared.

There is no question that commercial development of liquid-dominated geothermal reservoirs has destroyed some natural thermal manifestations, in particular, geysers [21]. The hydrothermal and geological conditions that are necessary to produce a geyser are extremely delicate and fragile. Nature itself routinely disrupts these mechanisms through earthquakes, as is evidenced by the ever-changing thermal features at Yellowstone National Park in the United States.

Two other sites in the United States used to have natural geysers, Beowawe and Steamboat Springs, both in Nevada, but they have been extinguished. Each is the site of geothermal power plants. Other kinds of thermal manifestations, such as fumaroles and hot ground, still exist at both sites. A photo of a geyser erupting at Steamboat in 1986 is shown in Figure 5.13 [22], and one of the same area taken in 1998 is shown in Figure 5.14 where only steam is seen rising from a deep boiling water table within a narrow fracture. The first power plant opened at Steamboat in 1986 and the site now is home to 11 units having a total installed capacity of 112 MW.



Figure 5.13 Geyser at Steamboat Springs in 1986. Photo by D. Hudson [22] [WWW].



Figure 5.14 Steam rising from fractures at Steamboat Springs in 1998. *Photo by author [WWW].*

5.8 Equipment List for Single-Flash Plants

The outline below gives the major equipment for a single-flash power plant [6].

5.8.1 WELLHEAD, BRINE, AND STEAM SUPPLY SYSTEM

- Wellhead valves and controls
 - Blowout preventer (while drilling)
 - Master valves
 - Bleed lines
- Separator vessels
 - Vertical cyclone type
 - Bottom-outlet steam discharge
 - External or integral water collecting tank
- Ball check valves
- Steam piping, insulation, and supports
 - Condensate traps
 - Expansion loops or spools

- Steam header
- Final moisture remover
 - Vertical demister
- Atmospheric discharge silencers
 - Rock mufflers or cyclone silencers with weir flow control
- Brine piping, insulation, and supports

5.8.2 TURBINE-GENERATOR AND CONTROLS

- Steam turbine-generator with accessories
 - Multistage, impulse-reaction turbine
 - Interstage moisture removal (optional)
 - Single-cylinder, single-flow or double-flow
 - Tandem-compound, four-flow
 - Rotor material: stainless steel (typ. 12% Cr, 6% Ni, 1.5% Mo)
 - Blade material: stainless steel (typ. 403, 13% Cr)
 - Stator material: carbon steel
 - Direct coupled, hydrogen or air cooled, two- or four-pole synchronous
 - Generator with static excitation
 - Lubricating oil system
- Control system
 - Digital-computer-based distributed control system
 - Continuous data acquisition system
 - Programmable component controller
 - Full automation and remote control (optional)
- Air compressor
 - One- or two-stage, motor-driven units for plant and/or instrument air

5.8.3 CONDENSER, GAS EJECTION, AND POLLUTION CONTROL (WHERE NEEDED)

- Condenser
 - Direct-contact or surface-type
 - Barometric or low-level jet type
 - Integral gas cooler
 - Material for wetted surfaces: stainless steel (typ. 316 or 316L)
- Condensate pumps and motors
 - Vertical, centrifugal can pumps
 - Stainless-steel wetted surfaces
 - Low-head, high volume design
 - Two 100% capacity units
 - Electric-motor driven

- Gas removal system
 - Steam jet ejectors with inter- and after-coolers
 - Turbocompressors
 - Hybrid ejector/compressor
- NCG treatment system
 - H₂S removal via commercially available methods

5.8.4 HEAT REJECTION SYSTEM

- Water cooling tower
 - Multi-cell, mechanically induced-draft, counter-flow or cross-flow type
 - Natural-draft type (rarely used)
 - Drift eliminator
 - Fire-retardant materials of construction
- Cooling water pumps and motors
 - Vertical, centrifugal, wet-pit type
 - Stainless-steel wetted surfaces
 - Low-head, high-volume flow type
 - Four 25% or two 50% capacity units
 - Electric-motor driven
- Cooling water treatment system
 - Chemical additives to control pH to 6.5–8.0

5.8.5 BACKUP SYSTEMS

- Standby power supply
 - Back-feed from grid
 - Diesel generator

5.8.6 NOISE ABATEMENT SYSTEM (WHERE REQUIRED)

- Rock mufflers for stacked steam
- Acoustic insulation for noisy fluid handling components

5.8.7 GEOFLUID DISPOSAL SYSTEM

- Injection wells for excess condensate and cooling tower blowdown
- Emergency holding ponds for wells and separators
 - Impermeable lagoons for temporary disposal of waste brine

References

- [1] DiPippo R, Moya P. Las Pailas geothermal binary power plant, Rincón de la Vieja, Costa Rica: Performance assessment of plant and alternatives. *Geothermics* 2013;48:1–15.
- [2] DiPippo R. U.S. Dept. of Energy, DOE/RA/28320-1. *Geothermal energy as a source of electricity: a worldwide survey of the design and operation of geothermal power plants*. Washington, DC: U.S. Gov. Printing Office; 1980.
- [3] Cheremisinoff NP, editor. *Encyclopedia of fluid mechanics*, vol. 3, gas-liquid flows. Houston, TX: Gulf Publishing Company; 1986.
- [4] Wallis GB. *One-dimensional two-phase flow*. New York, NY: McGraw-Hill, Inc.; 1969.
- [5] James R. Pipeline transmission of steam-water mixtures for geothermal power. *N Z Eng* 1968;23:55–61.
- [6] DiPippo R. Geothermal Power Systems Section 8.2 In: Elliott TC, Chen K, Swanekamp RC, editors. *Standard handbook of powerplant engineering*. 2nd ed. New York, NY: McGraw-Hill, Inc.; 1998. p. 8.27–60.
- [7] Lazalde-Crabtree H. Design approach of steam-water separators and steam dryers for geothermal applications. *Geothermal Resour Coun Bull* September 1984;11–20.
- [8] Eliasson ET. Power generation from high-enthalpy geothermal resources. *Geo-Heat Center Bull* June 2001;26–34.
- [9] Kozaki K. Geothermal power plant. *Fuji Electric Rev* 1980;26(4):110–19.
- [10] Anon. KSI-EI057-1 Basic planning of geothermal steam turbine plant. Tokyo, Japan: Toshiba Corp.; 1983.
- [11] Kestin J, Editor-in-chief, DiPippo R, Khalifa HE, Ryley DJ, editors. *Sourcebook on the production of electricity from geothermal energy*, U.S. Dept. of Energy, DOE/RA/4051-1, U.S. Gov. Printing Office, Washington, DC; 1980.
- [12] Moran MJ, Shapiro HN. *Fundamentals of engineering thermodynamics*. 5th ed. Hoboken, NJ: John Wiley & Sons; 2004.
- [13] Çengel YA, Boles MA. *Thermodynamics: an engineering approach*. 4th ed. New York, NY: McGraw-Hill; 2002.
- [14] Baumann K. Some recent developments in large steam turbine practice. *J Inst Elect Eng* 1921;59:565.
- [15] DiPippo R. Geothermal power technology. In: Meyers RA, editor. *Handbook of energy technology & economics*. New York, NY: Wiley-Interscience; 1983 [chapter 18].
- [16] CATT2: Computer-aided thermodynamic tables 2 (Ver. 1.0a). Intellipro, Inc., Wiley College Software; 2001.
- [17] Keenan JH, Keyes FG, Hill PG, Moore JG. *Steam tables: thermodynamic properties of water including vapor, liquid, and solid phases (international edition—metric units)*. New York, NY: John Wiley & Sons, Inc.; 1969.
- [18] Sokolnikoff IS, Redheffer RM. *Mathematics of physics and modern engineering*. 2nd ed. New York, NY: McGraw-Hill; 1966.
- [19] Pasqualetti MJ. Geothermal energy and the environment: the global experience. *Energy* 1980;5:111–65.
- [20] DiPippo R. Geothermal energy: electricity generation and environmental impact. In: Jackson T, editor. *Renewable energy: prospects for implementation*. Sweden: Stockholm Environment Institute; 1993. p. 113–22.
- [21] Jones GL. Geysers/Hot springs damaged or destroyed by man. Wyo-Jones Geysers Page, <<http://www.wyojones.com/destroye.htm>>; 2002.
- [22] Nevada Bureau of Mines and Geology. University of Nevada, Reno, <<http://www.nbmng.unr.edu/geothermal/pix.php?id=geyser-MainTer1986>>; 2004.

Nomenclature for Figures in Chapter 5

BCV	Ball check valve
C	Condenser
CP	Condensate pump
CS	Cyclone separator
CSV	Control and stop valves
CT	Cooling tower
CW	Cooling water
CWP	Cooling water pump
IW	Injection well
MR	Moisture remover
PH	Powerhouse
PW	Production well
S	Silencer
SE/C	Steam ejector/condenser
SP	Steam piping
SR	Steam receiver
T/G	Turbine/generator
WP	Water (brine) piping
WV	Wellhead valve

Problems

- 5.1. Many geothermal power plants use a flash process to generate steam. Using software for the properties of pure water substance, calculate and plot the percentage of steam that can be obtained by flashing (i.e., at constant enthalpy) a saturated liquid from a given initial pressure to various final pressures. Show the calculated results both in tabular and graphical form. Initial pressure should be on the abscissa and range from 5 to 50 bar. Do the calculations for initial pressures of 5, 15, 20, 25, and 50 bar. Values of steam percent should appear on the ordinate of the graph and be read from your curves for any final pressure down to 1 bar.
- 5.2. Consider two alternative steam turbine designs for a single-flash geothermal plant. Turbine A has four stages with moisture removal between stages. The moisture is simply extracted after each row of moving blades and throttled to the condenser. Thus, each stage sees saturated vapor at the leading edge. Turbine B has no moisture removal and can be characterized by an overall wet-turbine efficiency found from the Baumann rule assuming 85% dry expansion efficiency. *Note:* Unless otherwise stated, use this assumption when employing the Baumann rule for all problems in this book.

Inlet conditions to both machines are: 182°C, saturated vapor; condenser temperature is 48°C. The four-stage turbine A has its stages designed such that the temperature differences between successive stages are the same.

Each stage is described by its own wet-turbine efficiency. If the mass flow rate at turbine inlet is 125 kg/s, compare the power developed by the two designs. Discuss the implications of the results.

- 5.3.** A single-flash geothermal steam plant receives geofluid from a reservoir having a temperature of 240°C. The condenser temperature is 50°C. Neglect pressure losses in surface pipelines. Use the Baumann rule for the turbine efficiency.
- Determine the specific work output (in kJ/kg of geofluid) if the separator operates at 170°C.
 - Write a computer program or spreadsheet to investigate the effect of separator temperature on the specific work output. From your program, find the optimum value of the separator temperature and pressure, as well as the maximum specific work output. Compare your finding to the prediction of the “equal-temperature-split” rule. *Note:* Some software packages include a function that can optimize one variable of a complex solution. This may be used here to determine the optimum point, but the variation of the work output as a function of the separator temperature is also important.
- 5.4.** Your task is to analyze a single-flash plant. You must set it up for approximately optimum utilization efficiency by using the “rule of thumb” given in this chapter to find the optimum separator temperature. The turbine efficiency may be found using the Baumann rule. The geofluid exists in the reservoir as a pressurized liquid at a temperature of $T_1 = 270^\circ\text{C}$ and $h_1 = 1185 \text{ kJ/kg}$. The turbine exhaust temperature is $T_5 = 50^\circ\text{C}$. The productivity curve for an average well is given by:

$$\dot{m} = 100.23 - 2.339 \times 10^{-2}P + 4.028 \times 10^{-5}P^2 - 1.02 \times 10^{-7}P^3$$

where P is the absolute wellhead pressure in kPa and \dot{m} is the total well flow in kg/s.

- Calculate the power output of the turbine in kW.
 - Calculate the ratio of the heat rejected from the geofluid in the condenser to the power output of the turbine.
 - Assuming a dead state at $T_0 = 25^\circ\text{C}$, calculate the Second Law utilization efficiency based on: (i) wellhead conditions; (ii) reservoir conditions.
- 5.5.** A single-flash plant is to be designed to operate at a liquid-dominated reservoir having a temperature of 245°C. The plant condensing temperature will be 40°C and the dead-state temperature is 25°C. The separator temperature may be found from the “equal-temperature-split” rule of thumb. The turbine efficiency should be found using the Baumann rule. The wells at the field may be characterized by the following average productivity curve:

$$\dot{m} = 100.23 - 0.02339P + 2.06 \times 10^{-5}P^2$$

where \dot{m} is the total mass flow rate in kg/s and P is the wellhead pressure in kPa.

- a. Calculate the power output from one of the wells.
 - b. Calculate the utilization efficiency of the plant based on (i) wellhead conditions and (ii) reservoir conditions.
 - c. From the results of Part (a), calculate the so-called “pseudo thermal efficiency,” defined as the ratio of the power output to the imagined “heat added” as if the plant operated on a cycle (which it does not). Compare this to the results from Part (b) and discuss.
- 5.6.** The results in Problem 5.5 were obtained by ignoring any pressure loss between the wellhead and the turbine inlet. Clearly this is a simplification. This exercise will explore the effect of this assumption.
- a. Keep the same turbine inlet pressure as before, but find the required wellhead pressure if a 0.457-m diameter steam pipe from the wellhead separator to the turbine runs for an equivalent length of 800 m.
 - b. Recalculate the total mass flow rate from the well, the steam flow to the turbine, and the (reduced) power output.
 - c. Discuss the power loss and how it could be mitigated. Include economic considerations.



Chapter 6

Double- and Triple-Flash Steam Power Plants

Chapter Outline

6.1 Introduction	144
6.2 Gathering System Design Considerations	144
6.3 Energy Conversion Systems	147
6.4 Thermodynamics of the Conversion Processes	148
6.4.1 Temperature-Entropy Process Diagrams	148
6.4.2 Flash and Separation Processes	149
6.4.3 HP- and LP-Turbine Expansion Processes	150
6.4.4 Condensing and Cooling Tower Processes; Utilization Efficiency	152
6.4.5 Optimization Methodology	152
6.5 Example: Double-Flash Optimization	153
6.6 Scale Potential in Waste Brine	156
6.6.1 Silica Chemistry	156
6.6.2 Silica Scaling Potential in Flash Plants	158
6.7 Environmental Aspects for Double- and Triple-Flash Plants	161
6.8 Equipment List for Double- and Triple-Flash Plants	161
6.8.1 Wellhead, Brine, and Steam Supply System	161
6.8.2 Turbine Generator and Controls	161
6.8.3 Condenser, Gas Ejection, and Pollution Control (Where Needed)	162
6.8.4 Heat Rejection System	162
6.8.5 Backup Systems	162
6.8.6 Noise Abatement System (Where Required)	162
6.8.7 Geofluid Disposal System	162
References	162
Problems	163

6.1 Introduction

The double-flash steam plant is an improvement on the single-flash design that can produce 15–20% more power output for the same geothermal fluid conditions. The plant is more complex, more costly, and requires more maintenance, but the extra power output often justifies the installation of such plants. Double-flash plants are fairly numerous and are in operation in 10 countries. As of December 2014, there are 54 units of this kind in operation, about 9.4% of all geothermal plants, and the average unit power is 35 MW per unit. See Appendix A, Tables A.1–A.5, for more details.

Triple-flash plants add another stage of flashing, thereby further raising the efficiency of exergy utilization but at the expense of increased complexity, more equipment, and higher capital costs. In some cases of high-temperature resources, these systems can be justified. One of the challenges is to avoid precipitation of silica, either in the plant equipment or in the piping/well system. As of December 2014, there are only four units of this kind in operation, about 0.7% of all geothermal plants, but the average unit power is nearly 75 MW per unit, the largest size of any type of geothermal power system. See Appendix A, Tables A.1–A.5, for more details.

Since many aspects of double- and triple-flash plants are similar to a single-flash plant, we will generally follow the same format as in Chapter 5, but focus on the differences between the concepts. The fundamental new feature is one or two additional flash processes imposed on the separated liquid leaving the primary separator in order to generate additional steam, albeit at lower pressures than the primary steam.

6.2 Gathering System Design Considerations

For double-flash plants, the addition of the second flash process increases the number of possible arrangements beyond the ones discussed in Section 5.2.1. Practically, the alternatives are as follows:

- Separators and flashers at each wellhead, with high- and low-pressure steam lines to the powerhouse, and hot water pipelines from each production well to the injection wells (Figure 6.1).

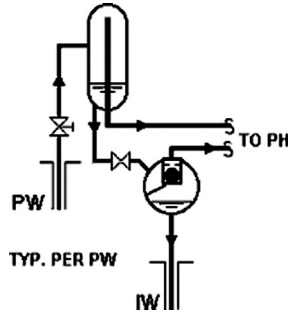


Figure 6.1 Wellhead separators and flashers.

- Two-phase pipelines from each well to the powerhouse, with separator(s) and flasher(s) at the powerhouse, and short high- and low-pressure steam lines to turbine(s), and hot water pipelines from powerhouse to injection wells (Figure 6.2).

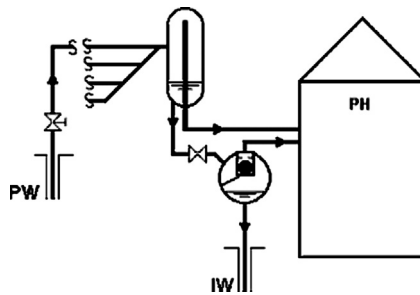


Figure 6.2 Separators and flashers at powerhouse.

- Two-phase pipelines from several wells to satellite separator/flasher stations in the field, with high- and low-pressure steam lines from satellites to powerhouse, and hot water pipelines from satellites to injection wells (Figure 6.3).

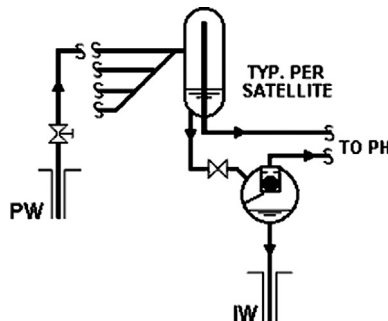


Figure 6.3 Satellite separator-flasher stations.

- Two-phase pipelines from several wells to satellite separators in the field, with high-pressure steam lines and hot water pipelines to powerhouse, with flasher(s) at the powerhouse, and short low-pressure steam lines to turbine, and hot water pipelines from the powerhouse to injection wells (Figure 6.4).

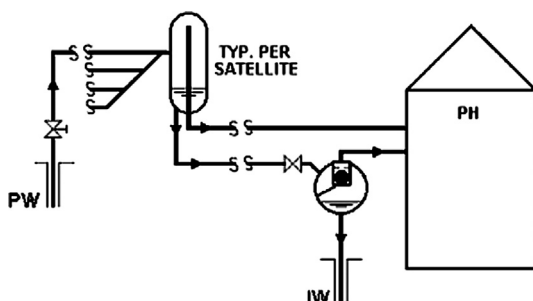


Figure 6.4 Satellite separator stations and flasher at powerhouse.

This listing is not exhaustive. For example, there may be a set of conditions that favor wellhead separators with satellite flashers, or some combination of the above arrangements. The best choice will be determined by the economics, taking into account site-specific conditions including the temperature, pressure, and chemical nature of the geofluid, well distribution (both production and injection) relative to the powerhouse location, topography of the site, and method of fluid disposal, including any required scale-control techniques. The latter are now routinely used at many plants and involve both downwell treatment to prevent calcite scaling in the production wells and/or post-plant treatment to prevent silica deposition in the injection piping and wells. These potential problems are common to both single- and double-flash plants and will be discussed in [Section 6.6](#).

An example of the type of system shown in [Figure 6.2](#) is presented in [Figure 6.5](#).

Clearly there are a great many possible arrangements for gathering systems when a triple-flash plant is used, but the emerging technology seems to favor two-phase geofluid flow from production wells to a central separation and flashing station where the three steam flows are produced. The station is close to the powerhouse. [Section 13.3.2](#) discusses one of the newest of this type of plant, the Nga Awa Purua power plant in New Zealand.

The formulations presented in [Section 5.2.2](#) for pressure drops apply here and need not be repeated.

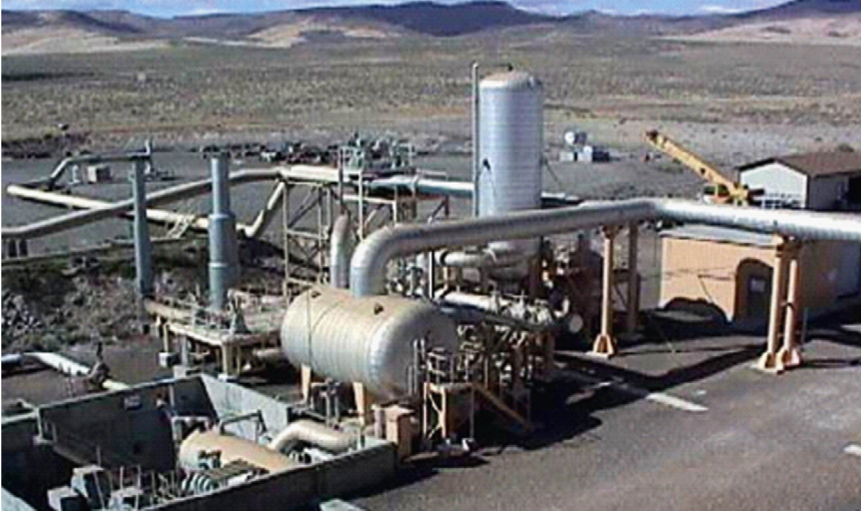


Figure 6.5 Separator-flasher arrangement at the 17 MW Beowawe double-flash plant, Nevada, USA. Two-phase flow pipelines enter from left rear; vertical vessel is the cyclone separator and the large horizontal vessel is the flasher. The smaller horizontal vessel in the cellar is the water holding tank from which the waste fluid is pumped to the injection wells. *Photo by author [WWW].*

6.3 Energy Conversion Systems

The schematic diagram for a double-flash plant is shown in [Figure 6.6 \[1\]](#). The design differs from the single-flash plant in [Figure 5.6](#) in that a flasher has been added and there is a low-pressure steam line from it to the turbine in addition to the high-pressure one from the separator. The cooling tower is not shown in [Figure 6.6](#).

The turbine is shown as a dual-admission, single-flow machine where the low-pressure steam is admitted to the steam path at an appropriate stage so as to merge smoothly with the partially expanded high-pressure steam. Other designs are possible. Two separate turbines could be used, one for the high-pressure steam and one for the low-pressure steam. In this case, the turbines could exhaust to a common condenser or to two separate condensers operating at different levels of vacuum ([Figure 6.7](#)). For larger power ratings, say, 55 MW or higher, double-flow turbines would be a good choice in order to minimize the height of the last-stage blades. Usually, geothermal turbines have at most 25–27 in (635–686 mm) high last-stage blades, but at least one plant, Darajat Unit 2 in Indonesia, uses 30 in (762 mm) high blades [\[1\]](#).

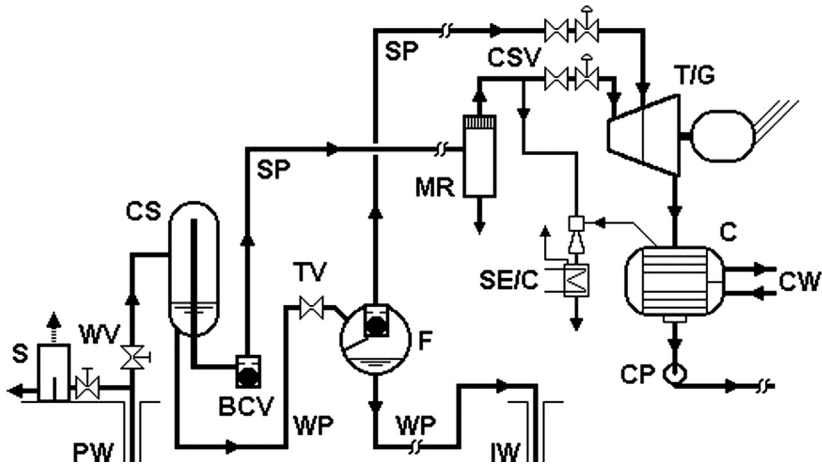


Figure 6.6 Simplified double-flash power plant schematic.

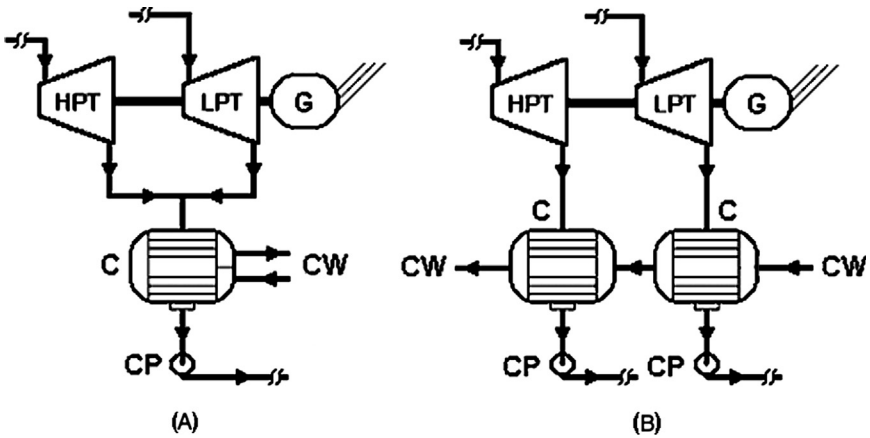


Figure 6.7 Double-flash plant with separate high- and low-pressure turbines.

6.4 Thermodynamics of the Conversion Processes

6.4.1 TEMPERATURE-ENTROPY PROCESS DIAGRAMS

The processes for the double-flash plant are shown in the temperature-entropy diagram in Figure 6.8. The extension of this to a triple-flash system is straightforward but tedious. The reader is referred to Figure 13.19 for a specific example.

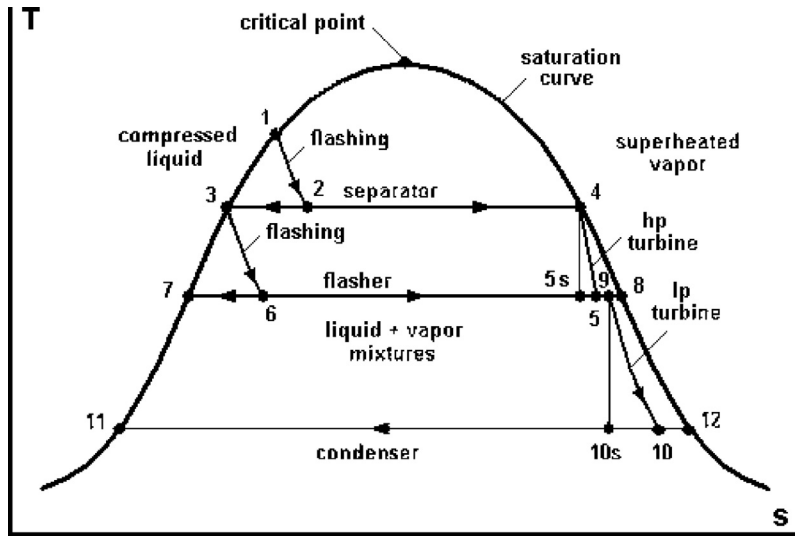


Figure 6.8 Temperature-entropy process diagram for double-flash plant with a dual-admission turbine.

Likewise, the equations set forth in the following sections for double-flash plants can readily be extended to the triple-flash case and this is left as an exercise for the reader (see Problem 6.7).

6.4.2 FLASH AND SEPARATION PROCESSES

With reference to Figure 6.8, the two flash processes, 1–2 and 3–6, are analyzed in the same way as the flash process for the single-flash plant in Section 5.4.2. Each process generates a fractional amount of steam given by the quality, x , of the two-phase mixture. Each flash is followed by a separation process. The governing equations are as follows:

$$h_1 = h_2 \quad (6.1)$$

$$x_2 = \frac{h_2 - h_3}{h_4 - h_3} \quad (6.2)$$

$$h_3 = h_6 \quad (6.3)$$

$$x_6 = \frac{h_3 - h_7}{h_8 - h_7} \quad (6.4)$$

The masses of the steam and liquid (brine) are needed at each stage and these are found from:

$$\dot{m}_{hps} = x_2 \dot{m}_{total} = \dot{m}_4 = \dot{m}_5 \quad (6.5)$$

$$\dot{m}_{hpb} = (1 - x_2) \dot{m}_{total} = \dot{m}_3 = \dot{m}_6 \quad (6.6)$$

$$\dot{m}_{lps} = (1 - x_2) x_6 \dot{m}_{total} = \dot{m}_8 \quad (6.7)$$

$$\dot{m}_{lpb} = (1 - x_6)(1 - x_2) \dot{m}_{total} = \dot{m}_7 \quad (6.8)$$

These mass flows will be used to calculate the power generated from the two stages of turbine expansion, the amount of waste liquid to be disposed of, as well as the heat that must be rejected through the condenser.

6.4.3 HP- AND LP-TURBINE EXPANSION PROCESSES

Using the same assumptions employed in Section 5.4.4, we can determine the power generated from each of the turbines. We will further assume that a dual-admission turbine is used. If two individual turbines are employed, the analysis follows closely the one used to describe the turbine for the single-flash plant (Section 5.4.4). Figure 6.9 shows a cross-section of a dual-admission turbine.

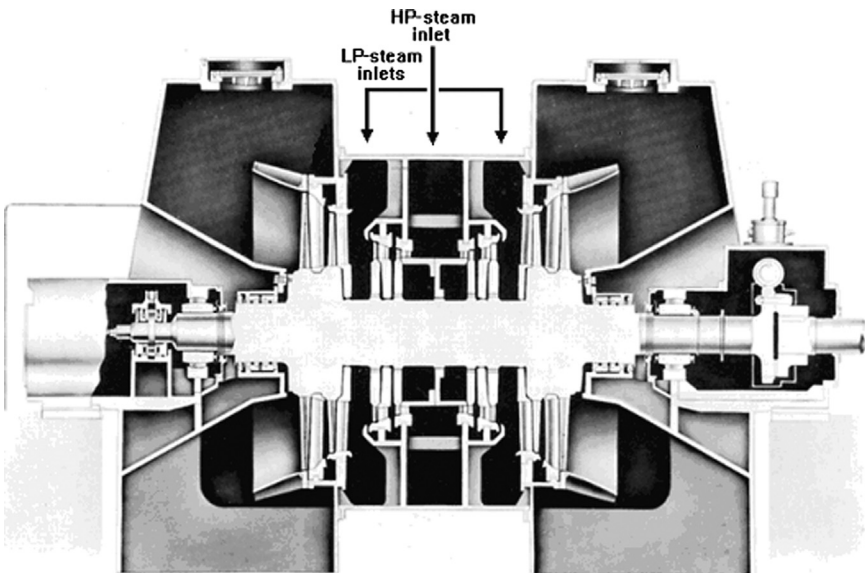


Figure 6.9 Cross-section of a dual-admission steam turbine. Modified from Ref. [2].

The HP turbine may be analyzed according to the methodology used for the single-flash turbine, namely:

$$w_{hpt} = h_4 - h_5 \quad (6.9)$$

$$\eta_{hpt} = \frac{h_4 - h_5}{h_4 - h_{5s}} \quad (6.10)$$

$$\dot{W}_{hpt} = \dot{m}_{hps} w_{hpt} = x_2 \dot{m}_{total} w_{hpt} \quad (6.11)$$

The actual outlet state from the high-pressure stage of the turbine must be found using the Baumann rule, exactly as in Section 5.4.4:

$$h_5 = \frac{h_4 - A \left[1 - \frac{h_7}{h_8 - h_7} \right]}{1 + \frac{A}{h_8 - h_7}} \quad (6.12)$$

where the factor A is defined as:

$$A = 0.425(h_4 - h_{5s}) \quad (6.13)$$

At this point in the analysis, we must augment the mass flow through the turbine because the low-pressure steam from the flasher is admitted to the steam path, and joins the partially expanded high-pressure steam. With reference to [Figure 6.8](#), the partially expanded steam is at state 5, the low-pressure steam is at state 8 (saturated vapor), and the mixed steam, ready to enter the low-pressure turbine stages, is at state 9. The First Law of thermodynamics and conservation of mass allow us to find the properties of the mixed state:

$$\dot{m}_5 h_5 + \dot{m}_8 h_8 = (\dot{m}_5 + \dot{m}_8) h_9 \quad (6.14)$$

or

$$h_9 = \frac{x_2 h_5 + (1 - x_2) x_6 h_8}{x_2 + (1 - x_2) x_6} \quad (6.15)$$

The low-pressure turbine may now be analyzed as follows:

$$w_{lpt} = h_9 - h_{10} \quad (6.16)$$

$$\dot{W}_{lpt} = \dot{m}_9 (h_9 - h_{10}) = (\dot{m}_5 + \dot{m}_8) (h_9 - h_{10}) \quad (6.17)$$

$$h_{10} = \frac{h_9 - A \left[x_9 - \frac{h_{11}}{h_{12} - h_{11}} \right]}{1 + \frac{A}{h_{12} - h_{11}}} \quad (6.18)$$

$$A = 0.425(h_9 - h_{10s}) \quad (6.19)$$

$$h_{10s} = h_{11} + [h_{12} - h_{11}] \times \left[\frac{s_9 - s_{11}}{s_{12} - s_{11}} \right] \quad (6.20)$$

$$\eta_{lpt} = \frac{h_9 - h_{10}}{h_9 - h_{10s}} \quad (6.21)$$

The total power generated is the sum of the power from each turbine:

$$\dot{W}_{total} = \dot{W}_{hpt} + \dot{W}_{lpt} \quad (6.22)$$

Finally, the gross electrical power is found from:

$$\dot{W}_{e,gross} = \eta_g \dot{W}_{total} \quad (6.23)$$

6.4.4 CONDENSING AND COOLING TOWER PROCESSES; UTILIZATION EFFICIENCY

The analysis presented in Sections 5.4.5, 5.4.6, and 5.4.7 may be used here, provided the mass flow rate is changed to be the sum of the HP- and LP-steam flows. The exergy of the incoming geofluid is the same as before.

6.4.5 OPTIMIZATION METHODOLOGY

The optimization process for a double-flash plant is more complicated than for a single-flash plant because of the extra degree of freedom in the choice of operating parameters. For each choice of separator pressure (or temperature), there will be a range of possible flasher pressures (or temperatures), one of which will yield the highest power output. For the spectrum of separator pressures, one will find corresponding flasher pressures that yield the best output. Among this array of results there will be a single overall best optimum point. We can display this concept in a simple diagram (Figure 6.10).

In the upper portion, P_2 is the separator pressure and T_6/T_2 is the ratio of the flash temperature to the separator temperature. For each point a on the upper curve, there will be some best power output \dot{W} (point b) that sits atop a curve (shown by the thin line) that comes from varying the flash pressure P_6 . The lower heavy curve represents the locus of all such “best” points that come from allowing P_2 to vary over its practical range of values. Point d is the best of the best and defines the optimum plant choices for both separator and flash conditions. Point c shows the optimum ratio of temperatures for the separator and flasher.

The numerical computation of all states needed to accomplish this optimization can be easily programmed and the results plotted for any combination of reservoir and condenser conditions. As shown in Section 5.5, this two-parameter

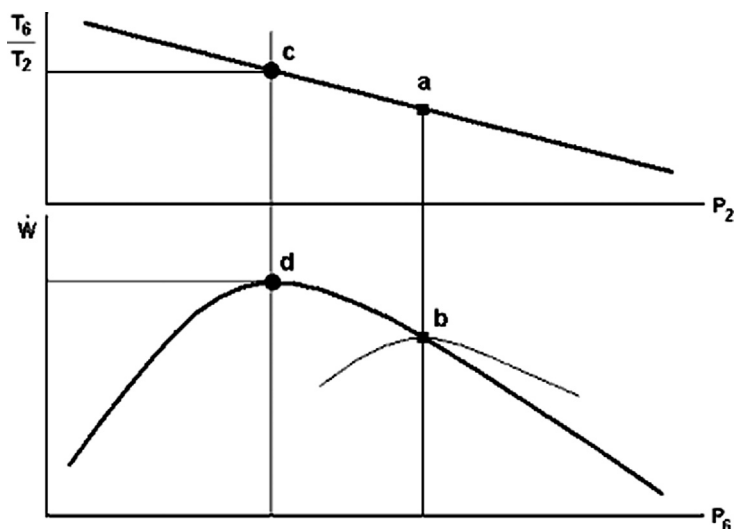


Figure 6.10 Double-flash optimization process.

search can begin by using the “equal-temperature-split” rule to get first approximations to the optimum separator and flash temperatures, and then the computer can explore combinations of values on either side of these first guesses.

Similarly, for a triple-flash optimization, the “equal-temperature-split” rule will provide a very good starting point for a computer search for the highest specific output or highest utilization efficiency. Nowadays, spreadsheets may be used in a “solver” mode to optimize a particular objective with regard to another variable. Here, the process must be repeated owing to the extra degree of freedom, that is, there are three independent variables to be chosen such that the utilization efficiency is maximized, subject to site-specific constraints. Owing to the near certainty of chemical precipitation potential, some form of mitigation or inhibition will be needed. But this aspect goes beyond the thermodynamic optimization.

6.5 Example: Double-Flash Optimization

The following example is based on a report written by the author for the Electric Power Research Institute [3]. The reservoir fluid temperature is 245°C and the well productivity curve is defined as the following second-order function:

$$\dot{m}_{total} = 93.239 + 16.625P_2 - 32.584P_2^2 \quad (6.24)$$

where P_2 is the wellhead pressure in MPa (all pressures are absolute, unless otherwise noted) and \dot{m}_{total} is the total two-phase mass flow rate in kg/s. The condenser operates at a pressure of $P_{10} = 13.793$ kPa. This gives a condensing temperature of 52.24°C.

The optimization considers the two cases: (1) seeking the best power output for the given productivity curve, and (2) seeking the best specific output per unit mass of total well flow. The results are not the same. REFPROP was incorporated into a spreadsheet for the calculations; see Appendix F. Table 6.1 shows the results of the two-parameter search; only the best values for the outputs are shown as functions of the separator temperature.

TABLE 6.1 Double-flash optimum conditions for $T_1 = 245^\circ\text{C}$ and $T_{10} = 52.24^\circ\text{C}$.

T_2 °C	P_2 MPa	T_6 °C	P_6 MPa	w kJ/kg	\dot{m}_{total} kg/s	\dot{W}_{total} MWe
200	1.555	121.5	0.2083	109.18	40.31	4.401
190	1.255	117.0	0.1805	111.21	62.77	6.980
180	1.003	112.5	0.1558	112.22	77.14	8.657
170	0.7922	108.0	0.1340	112.16	85.96	9.641
160	0.6182	103.0	0.1128	110.97	91.06	10.105
150	0.4762	98.5	0.09611	108.59	93.77	10.182
140	0.3615	94.0	0.08154	104.95	94.99	9.969

As can be easily seen the specific and total power outputs reach their respective maxima at different points. The variation in these terms can be seen in Figures 6.11 and 6.12. If one desires the best total power, then the separator temperature should be $\sim 152^\circ\text{C}$ and the flash temperature should be $\sim 100^\circ\text{C}$; this will yield a power of ~ 10.2 MW. Alternatively, if one desires the best specific power (i.e., the highest utilization efficiency), then the separator should be at $\sim 175^\circ\text{C}$ and the flash temperature should be $\sim 110^\circ\text{C}$; this will yield a specific power of ~ 112.4 kJ/kg. For a dead-state temperature of 20°C , this set of conditions yields a utilization efficiency of 43.4%. This may be compared to a utilization efficiency of 41.9% at the best power point. This is roughly an advantage of 3.6%.

If one were to perform the optimization of a single-flash plant for the same given conditions as specified here, the optimum power output would be 8.37 MW, thereby demonstrating that the optimized double-flash plant is capable of generating 22% more gross power than an optimized single-flash plant, all other assumptions being the same.

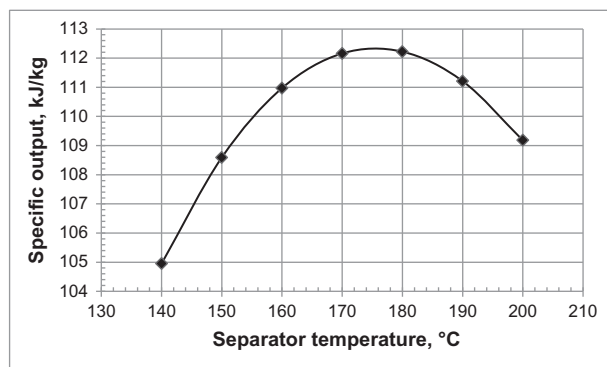


Figure 6.11 Best specific output as a function of separator temperature.

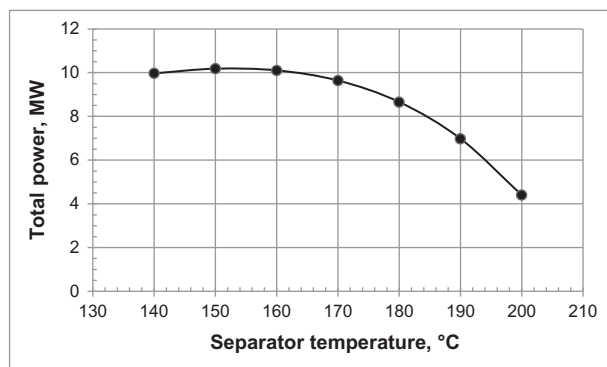


Figure 6.12 Best total power output as a function of separator temperature.

In carrying out these calculations, no attention has been paid to any practical limitations that may exist which would restrict the range of separator and flasher operating conditions. For example, it is not practical to operate the flasher at a pressure below atmospheric pressure because the waste brine would have to be pumped out, thereby increasing the parasitic power load and adding complexity to the overall operation. Another consideration that is particularly important for double-flash plants is the potential of chemical scaling in the waste liquid in and leaving the flash vessel. This will be addressed in the next section.

6.6 Scale Potential in Waste Brine

Nearly all minerals exhibit higher solubility in water as the temperature of the water increases. One notable exception is calcium carbonate which we have seen in Chapter 4 can become a problem in geothermal production wells.

6.6.1 SILICA CHEMISTRY

One of the minerals that is always found in geofluids is silica, SiO_2 . Silica can exist in several structural forms, from amorphous to highly crystalline, that is, quartz. Each form has its own solubility characteristic but all show increasing solubility with increasing temperature in the range of temperatures encountered in geothermal reservoirs; see [Figures 6.13 and 6.14](#). This means that as the temperature of the geofluid decreases as it undergoes the processes in the power plant, the silica that was dissolved into the brine when it was hot and flowing through the fractured rocks of the reservoir will eventually begin to precipitate from the solution as solid silica.

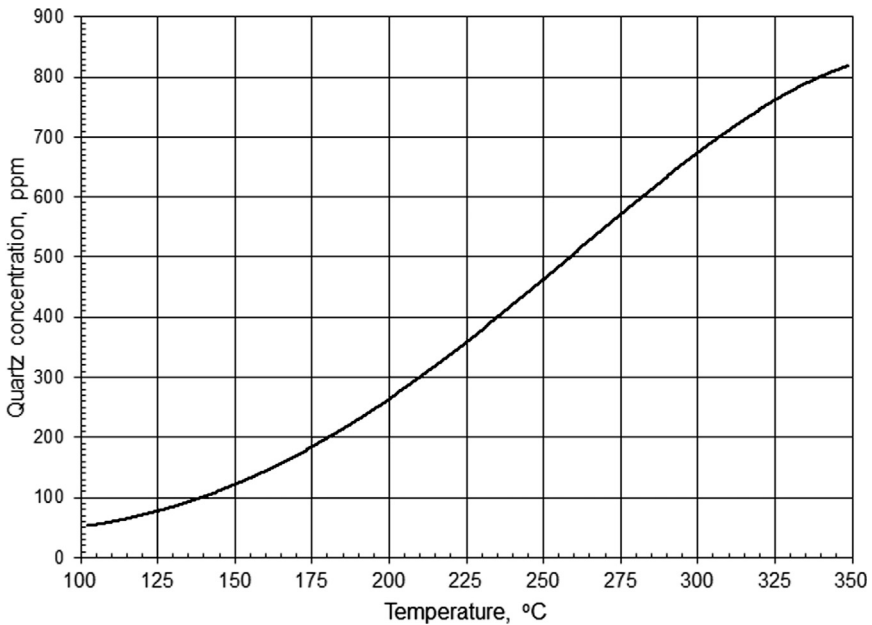


Figure 6.13 Solubility of quartz as a function of temperature in pure water.

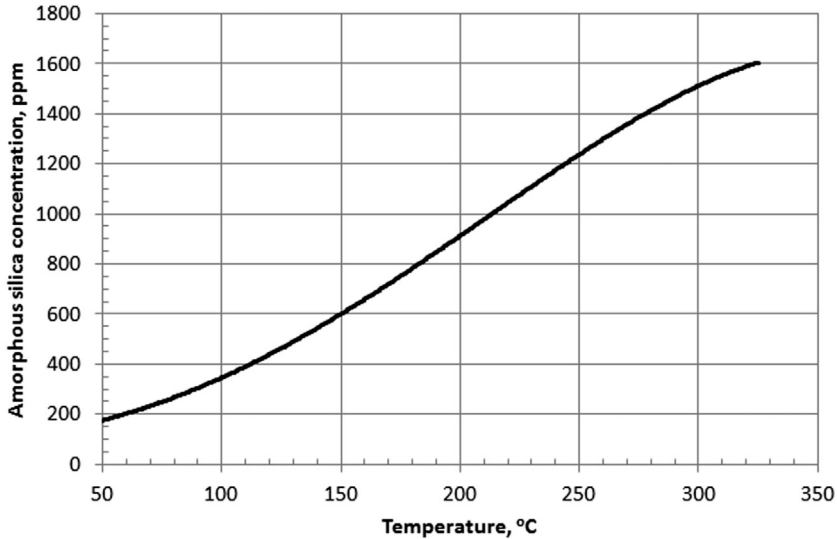


Figure 6.14 Solubility of amorphous silica as a function of temperature in pure water.

The interesting feature is that the solubility in the reservoir fluid is controlled by quartz whereas at the low temperatures typical of waste brines it is controlled by amorphous silica [4]. Fortunately, the latter form has a much higher solubility than the former. By the time a brine has cooled to, say 125°C, it is typically supersaturated with respect to quartz but undersaturated with respect to amorphous silica. Thus with proper design of the processes, it is possible to avoid the precipitation of the amorphous silica while the fluid is traveling through the plant components. It is always possible for precipitation to occur in the injection wells or in the reservoir once the waste fluid returns to the formation. Of course, any reheating of the waste brine in the formation will reduce the potential for precipitation in the reservoir that could adversely affect the permeability of the formation and reduce the injectability of the waste fluid.

The solubility of silica is a function not only of the fluid temperature but also its salinity and pH. The figures shown above are for pure water. Qualitatively, for a given temperature and pH, the higher the salinity (i.e., higher molality), the lower the solubility of both quartz and amorphous silica in aqueous solutions. For a given temperature and salinity, the solubility of amorphous silica is essentially independent of the pH for low values but rises dramatically as pH climbs above neutral, that is, $\text{pH} > 7$. The effect is more pronounced for fluids with high salinity [5].

The kinetics of the precipitation reaction plays a crucial role in the potential for scaling in geothermal plant components. If precipitation can be slowed it may be possible to process the fluid and dispose of it before scaling can occur. Alternatively, if the precipitation can be accelerated, it may be possible to force the fluid to give up its scale-causing minerals in a rapid and controlled manner, thereby allowing the purged fluid to be used without fear of further precipitation. Both of these effects have been used at geothermal plants in the Imperial Valley of the United States where highly saline, corrosive brines are encountered. There are five parameters that influence the kinetics of the silica precipitation (essentially a polymerization process) [6]:

1. The initial degree of supersaturation (i.e., actual SiO_2 concentration – equilibrium concentration)
2. Temperature
3. Salinity or molality of the solution
4. pH of the solution
5. Presence (or absence) of colloidal or particulate siliceous material.

The first and second factors can be controlled by proper selection of separator and flash conditions for a given geofluid. The third factor is a fluid characteristic that cannot be controlled. The fourth and fifth factors can be adjusted as the fluid moves through the plant from production wells, through pipes and other components, and eventually into injection wells. When the pH is made low (i.e., acidic), the rate of precipitation is very slow and the fluid can be viewed as temporarily stabilized. When the pH is made higher, the rate increases dramatically, reaching its maximum at near-neutral pH = 6.0–7.5, and then slowing as pH approaches 9.0–9.5. In fact, the rates for pH = 5.3 and pH = 9.0 are about the same [4].

The last factor in the list has been exploited successfully for the Imperial Valley plants. The geofluid is “seeded” with silica particles in large flash-crystallizers allowing favorable precipitation sites for the supersaturated solution. After two stages of such a process, the silica is removed, dried, compacted, and disposed of. The steam that is generated is ready for use in turbines and the waste liquid is clean enough to be reinjected without fear of clogging the reservoir [7].

6.6.2 SILICA SCALING POTENTIAL IN FLASH PLANTS

Since double-flash plants are often built on the hotter resources, the dissolved silica is typically higher than for single-flash plants. Furthermore, because of

the additional flash process, the waste brine becomes more highly concentrated in silica than in a single-flash plant. The situation is worse for triple-flash plants.

The derivation of the working equations to describe the silica scaling problem is based on Figure 6.8, the temperature-entropy diagram presented earlier; the reader should review this figure before proceeding further.

Let us begin at state 1 where the geofluid exists at the reservoir temperature, T_1 . It will carry a load of silica determined by the solubility function for quartz. If we assume the water is pure, then we can represent this function with the polynomial:

$$Q(T) = 41.598 + 0.23932t_1 - 0.011172t_1^2 + 1.1713 \times 10^{-4}t_1^3 - 1.9708 \times 10^{-7}t_1^4 \quad (6.25)$$

where the temperature is in units of degrees Celsius and the quartz concentration is in mg/kg or in parts per million (ppm). As the fluid undergoes various flashing and separation processes, we will assume that the silica remains in the liquid phase. Thus the concentration of the silica will increase according to the following analysis:

$$S(t_3) = \frac{Q(t_1)}{1 - x_2} \quad (6.26)$$

and

$$S(t_7) = \frac{Q(t_1)}{(1 - x_2)(1 - x_4)} \quad (6.27)$$

where $S(t_3)$ and $S(t_7)$ represent the silica concentrations in the liquid at states 3 and 7, respectively. The symbol S is used to remind us that the controlling silica equilibrium is that of amorphous silica, not quartz. Since the quality after each flash is about 0.12–0.15, the concentration will increase by roughly 15.5% after the first flash (well to separator) and overall by 33.5% (well to waste brine from flash vessel).

Figure 6.15 shows the results of calculations for a single-flash plant at a 225°C resource and a double-flash plant at a 250°C resource. The curve labeled Q is the equilibrium solubility for quartz; the one labeled S is for amorphous silica. The line a–b shows the increase in concentration of silica in the brine as it undergoes a two-stage flash process from 250°C to 117°C. The latter temperature is the flash temperature found by applying the “equal-temperature-split” rule for an optimum double-flash plant. The vertical distance from point f to point b above the

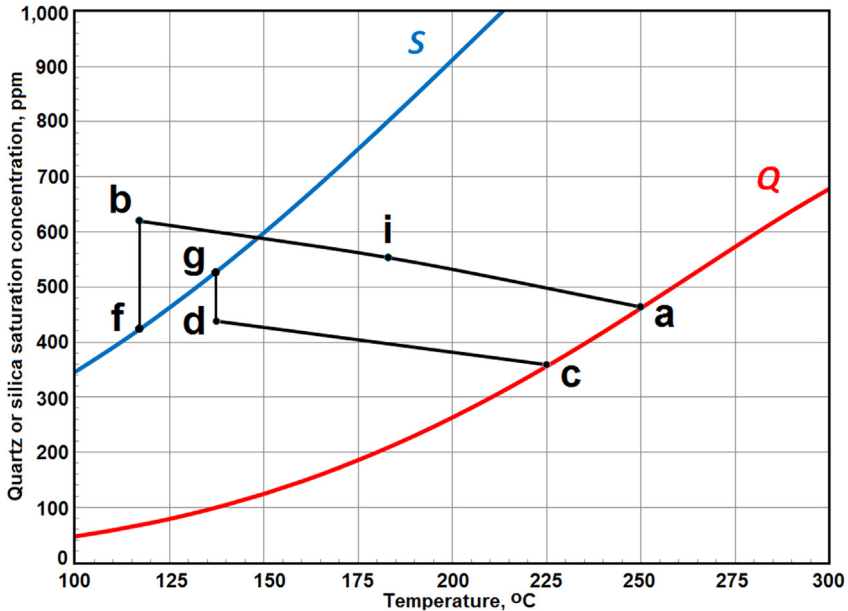


Figure 6.15 Silica condition after flash processes [8] [WWW].

equilibrium curve indicates that the solution is supersaturated with respect to amorphous silica, the amount of supersaturation being 214 ppm. Thus the fluid is prepared to lose that amount of silica as soon as precipitation commences.

The line c–d shows the increase in concentration of silica in the brine as it undergoes a one-stage flash process from 225°C to 137.5°C. The latter temperature is the separation temperature found by applying the “equal-temperature-split” rule for an optimum single-flash plant. Since point d lies below point g, the solution is in equilibrium with respect to amorphous silica, and no precipitation would be expected.

In general, the hotter the resource, the higher the silica concentration in the incoming geofluid, the greater the supersaturation in the waste brine, from either type of flash plant, and the greater the likelihood of precipitation in the flash vessel, the piping leading to the injection wells, or in the injection wells or in the formation. A more thorough treatment of this subject can be found in Ref. [8].

One last comment on this phenomenon—the silica precipitation problem is less likely to occur in binary plants (See Chapter 8) because the geofluid is not flashed, but only cooled. Thus, there is no increase in the concentration of the silica as the fluid passes through the plant. With reference to Figure 6.15, the fluid follows a horizontal line from right to left in a binary plant which tends to keep the fluid in the safe region below the amorphous silica equilibrium curve.

6.7 Environmental Aspects for Double- and Triple-Flash Plants

Double- and triple-flash plants have the same potential environmental impacts as single-flash plants that were described in Section 5.7. In the matter of water pollution, the waste brine from double- and triple-flash plants will in general carry more highly concentrated contaminants than single-flash plants. Thus the need for reinjection in this case is even more urgent.

6.8 Equipment List for Double- and Triple-Flash Plants

Since the equipment used at double- and triple-flash plants is very similar to that found at single-flash plants, we will present here a non-annotated list and include annotations only for items unique to double- and triple-flash plants.

6.8.1 WELLHEAD, BRINE, AND STEAM SUPPLY SYSTEM

- Wellhead valves and controls
- Separator vessels
- Flash vessels
 - Vertical or horizontal low-pressure tanks
 - Inlet valves or orifice plates to control pressure drop
 - Operating pressure greater than atmospheric
- Chemical scaling mitigation system, especially for triple-flash plants
- Steam scrubbers, especially for triple-flash plants
- Final moisture remover for all pressure level steam lines
- Ball check valves (optional)
- Steam piping, insulation, and supports
- Steam header for all level-pressure steam flows
- Final moisture remover (strainer)
- Atmospheric discharge silencers
- Brine piping, insulation, and supports

6.8.2 TURBINE GENERATOR AND CONTROLS

- Dual- or triple-pressure steam turbine generator with accessories
 - Single cylinder with dual-admission or two single-admission cylinders (double-flash plants)
 - Single cylinder, double-flow with triple admission (triple-flash plants)
- Control system
- Air compressor

6.8.3 CONDENSER, GAS EJECTION, AND POLLUTION CONTROL (WHERE NEEDED)

- Condenser
- Condensate pumps and motors
- Gas removal system
- Noncondensable gases treatment system

6.8.4 HEAT REJECTION SYSTEM

- Water cooling tower
- Cooling water pumps and motors
- Cooling water treatment system

6.8.5 BACKUP SYSTEMS

- Standby power supply

6.8.6 NOISE ABATEMENT SYSTEM (WHERE REQUIRED)

- Rock mufflers for stacked steam
- Acoustic insulation for noisy fluid-handling components

6.8.7 GEOFLUID DISPOSAL SYSTEM

- Injection wells for excess condensate and cooling tower blowdown
- Emergency holding ponds for wells and separators
- Scale inhibitor injection system, if needed.

References

- [1] Anon. Darajat geothermal power plant: largest geothermal turbine with single casing construction. Tokyo, Japan: Mitsubishi Heavy Industries, Ltd; 1997.
- [2] Anon. Geothermal power generation by Mitsubishi, JA-243. Tokyo, Japan: Mitsubishi Heavy Industries, Ltd.; 1976.
- [3] DiPippo R. Geothermal power cycle selection guidelines. Part 2 of Geothermal Information Series, DCN 90-213-142-02-02, Electric Power Research Institute, Palo Alto, CA; 1990.
- [4] Kitahara S. The polymerization of silicic acid obtained by the hydrothermal treatment of quartz and the solubility of amorphous silica. Rev Phys Chem Japan 1960;30:131–7.

- [5] Kindle CH, Mercer BW, Elmore RP, Blair SC, Myers DA. Geothermal injection treatment: process chemistry, field experiences, and design options. DE-AC06-76RLO 1830, PNL-4767, Pacific Northwest Laboratory; September 1984.
- [6] Ellis AJ, Mahon WAJ. *Chemistry and geothermal systems*. New York, NY: Academic Press; 1977.
- [7] Newell DG, Whitescarver OD, Messer PH. Salton Sea Unit 3 47.5 MWE geothermal power plant. *Geothermal Resour Coun Bull* 1989;18(5):3–5.
- [8] DiPippo R. A simplified method for estimating the silica scaling potential in geothermal power plants. *Geothermal Resour Coun Bull* 1985;14(5):3–9.

To the engineer, all matter in the universe can be placed into one of two categories: (1) things that need to be fixed, and (2) things that will need to be fixed after you've had a few minutes to play with them. Engineers like to solve problems. If there are no problems handily available, they will create their own problems. Normal people don't understand this concept; they believe that if it ain't broke, don't fix it. Engineers believe that if it ain't broke, it doesn't have enough features yet.

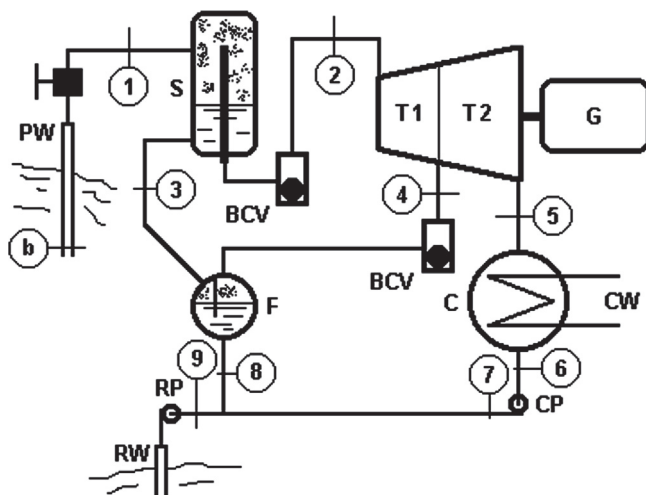
Scott Adams, *The Dilbert Principle*—2004

Problems

- 6.1. A double-flash geothermal steam power plant operates from a reservoir at 300°C . The condenser temperature is 50°C . Secondary steam from the flash vessel is mixed with the primary steam at the plenum between the high- and low-pressure sections of the turbine. Neglect pressure losses in surface piping and use the Baumann rule for the turbine efficiencies, assuming a dry turbine expansion efficiency of 85%.
 - a. Determine the specific work output (in kJ/kg of geofluid) if the separator and flash vessels operate at 230°C and 140°C , respectively.
 - b. Write a computer program or spreadsheet to determine the optimum combination of separator and flash vessel temperatures, that is, that combination which yields the maximum specific work output. Compare your findings to the prediction of the “equal-temperature-split” rule.
- 6.2. The flow diagram shown below is for the fictitious El Diablo geothermal power plant at the imaginary Big Mist Hot Springs, Nevada, which is being built by the nonexistent Terra Electric Power Company (TEPCO). The wells produce a mixture of liquid and vapor at state 1. An ideal separator (i.e., no pressure loss) produces saturated vapor (primary steam) at 2 and saturated liquid at 8. The secondary steam is mixed with the primary steam at the pass-in section of the turbine, between the 1st and 2nd sections of the

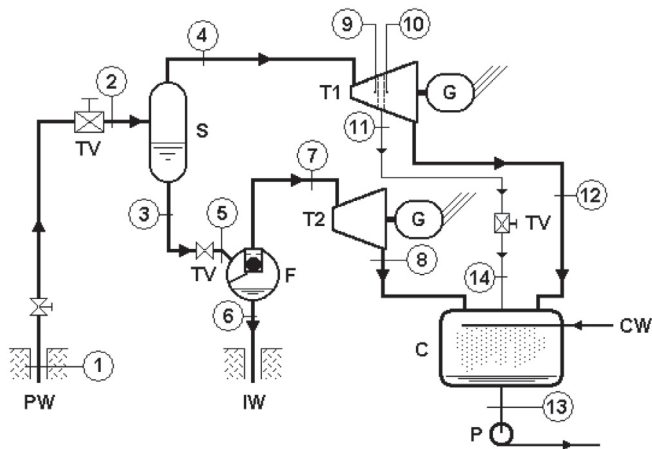
turbine. A closed-type, shell-and-tube heat exchanger is used in conjunction with a supply of cooling water. The condensed geothermal steam is pumped and mixed with the liquid coming from the flasher, and is returned to the formation through reinjection wells by means of reinjection pumps. You may use the following assumptions:

1. Assume flow from state b to 1 follows a throttling process.
2. Assume turbines operate isentropically.
3. Neglect pump work, i.e., for computational purposes, state 7 is identical to 6 and that states 6, 7, 8, and 9 all lie on the saturated liquid line.
4. Assume a wet cooling tower is used at the plant, and that the ambient wet-bulb temperature is 27°C .
5. Apply the “equal-temperature-split” rule for flash-point selection.
6. Assume the geofluid is pure water substance.
7. Wellhead temperature, $T_1 = 171^{\circ}\text{C}$.
8. Wellhead geofluid dryness fraction, $x_1 = 0.133$.
9. Condenser temperature, $T_5 = 51^{\circ}\text{C}$.



Legend: PW = Production Well (typical); S = Separator; F = Flasher;
 BCV = Ball Check Valve; T1, T2 = 1st and 2nd Sections of the Turbine;
 G = Generator; CW = Cooling Water; C = Condenser;
 CP = Condensate Pump; RP = Reinjection Pump, RW = Reinjection Well.

- a. Determine the bottom-hole temperature, T_b , if flashing takes place just at the bottom of the well.
 - b. Sketch the processes involved in the operation of the plant in a temperature-entropy diagram. Label all states in agreement with the given plant schematic. Additional states may be defined as needed.
 - c. Make a table giving the specific enthalpy at all 10 labeled state points (including state b), and at any other points that you think are important.
 - d. For each kilogram that flows from the wells, calculate the mass flow through each section of the turbine.
 - e. Calculate the work output of the plant per unit mass flowing from the wells.
 - f. Calculate the geothermal energy resource utilization efficiency, η_u .
 - g. Assume a *typical* flow rate for a single well, and calculate roughly how many production wells would be needed for a 50 MW unit.
- 6.3.** Consider the double-flash power plant shown in the figure. The geofluid is produced from a liquid-dominated reservoir (state 1). The separator (S) and the flasher (F) generate high- and low-pressure steam (saturated) for the two turbines T1 and T2. Turbine T1 is equipped with a moisture removal section where moisture that is formed during the expansion from state 4 to state 9 is drained away at state 11, and flashed to the condenser. This drain is located at the point where the steam temperature is exactly 50°C below that of the inlet steam.



Plant Data: $T_1 = 280^\circ\text{C}$; $T_9 = T_{10} = T_4 = 50^\circ\text{C}$; $T_{13} = 40^\circ\text{C}$; dead state $T_0 = 25^\circ\text{C}$.

Your task is to design and analyze this plant. You may employ the “equal-temperature-split” rule for setting the separator and flasher conditions.

- a. Begin by making a careful sketch of the plant processes in a $T-s$ diagram. Label all states in accordance with the state points shown in the schematic. You may use the Baumann rule in determining the actual efficiency of each turbine, that is, the two sections of T1 and the whole of T2, taking the dry expansion efficiency as 85%.
- b. The analysis will be facilitated if you first find the specific enthalpy h at the following state points: 1, 2, 3, 4, 5, 6, 7, 8, 9, 10, 11, and 12.
- c. Assuming that the total mass flow rate from the well is 1 kg/s, calculate the power output (in kW) of: (i) the high-pressure section of T1; (ii) the low-pressure section of T1; and (iii) turbine T2.
- d. If the actual total well flow is 1000 kg/s, what is the total gross power of the plant (in MW)?
- e. Calculate the Second Law utilization efficiency, η_u , for the plant, based on the condition of the geofluid in the reservoir.
- f. If the original geofluid in the reservoir has a concentration of 595 ppm of silica (as quartz), calculate the concentration of silica in the separated liquid at states 3 and 6.
- g. Using the Fournier and Marshall correlation for amorphous silica solubility, namely,

$$\log_{10}s = -6.116 + 0.01625T - 1.758 \times 10^{-5}T^2 + 5.257 \times 10^{-9}T^3$$

where T is in kelvins and s must be multiplied by 58,400 to obtain ppm, determine whether or not the separated liquid at states 3 and 6 is super-saturated with respect to amorphous silica. What are the implications of your findings?

- 6.4. Your task is to assess the potential for a silica scaling problem associated with the operation of flash plants at a 225°C, liquid-dominated resource. You may assume that the condenser will run at 50°C, and that the “equal-temperature-split” rule of thumb will be used to determine the separator (and flash) temperature for a single- (and double-) flash plant. There is a quartz concentration in the reservoir geofluid of 360 ppm. Assess the silica scaling potential for:
 - a. a single-flash plant.
 - b. a double-flash plant. In case you expect a problem, suggest some ways of averting trouble (without abandoning the site).

- 6.5.** A double-flash plant is being considered for a high-temperature geothermal field. Your task is to assess the power potential and the likelihood of a silica scaling problem. The resource is liquid-dominated at 300°C. The condenser will run at 60°C. A dual-admission turbine will be employed (see Figure 6.6). The “equal-temperature-split” rule of thumb will be used to determine the separator and flash temperatures.
- Calculate the specific work output of the turbine (i.e., in kJ/kg of total well flow), using the Baumann rule with an 85% dry expansion efficiency.
 - Assuming a typical well produces a total flow of 75 kg/s, calculate the power output per well.
 - Assuming the reservoir fluid is saturated with respect to quartz, calculate the supersaturation of the residual brine with respect to amorphous silica.
 - If the brine is supersaturated and the plant will be designed to generate 55 MW, calculate the potential amount of silica that could precipitate in kg/day. Discuss the ramifications of this, for example, where will the precipitation occur and how to alleviate the problem.
- 6.6.** Two variants of a double-flash plant are being considered for a geothermal field. The resource is liquid-dominated at 204°C. The condenser will run at 38°C. The “equal-temperature-split” rule of thumb will be used to determine the separator and flash temperatures. One variant will use a dual-admission turbine (see Figure 6.6) and the other will use two separate high- and low-pressure turbines (see Figure 6.7A). The efficiency of each turbine should be found using the Baumann rule and a dry isentropic turbine efficiency of 85%. Determine for each plant:
- The specific work output (i.e., in kJ/kg of total well flow).
 - The utilization efficiency if the dead state is at 27°C.
 - Assuming a typical well produces a total flow of 95 kg/s, calculate the number of wells needed for each plant to generate 50 MW. Discuss the findings.
- 6.7.** This exercise is modeled after the Nga Awa Purua (Taonga) triple-flash plant in New Zealand, but the specifications are simplified and drawn to suit this question. One double-flow turbine with two pass-in points per flow receives saturated steam from each of three separators. There are mixing plenums between each section of the turbine. The following data are known:
- Reservoir temperature, $T_R = 335^\circ\text{C}$ (saturated liquid), wellhead temperature, $T_1 = 230^\circ\text{C}$, HP separator temperature, $T_2 = 220^\circ\text{C}$, IP separator temperature, $T_5 = 172^\circ\text{C}$, LP separator temperature, $T_{10} = 125^\circ\text{C}$, condenser temperature, $T_{15} = 43^\circ\text{C}$.

A spreadsheet solution is recommended. Use the Baumann rule with a dry expansion efficiency of 85% in your analysis.

Calculate:

- a.** The specific work output (i.e., in kJ/kg of total well flow) for each of the three turbine sections.
- b.** The actual isentropic efficiency for each turbine section taken as a whole.
- c.** The gross power output, in MW, if the geofluid mass flow rate to the plant is 520 kg/s.
- d.** The gross utilization efficiency if the dead state is at 30°C.
- e.** Compare the three flash temperatures to what the “equal-temperature-split” rule would give. Modify your spreadsheet solution by substituting the temperatures from the rule. Compare and discuss the power output values.



Chapter 7

Dry-Steam Power Plants

Chapter Outline

7.1 Introduction	170
7.2 Origins and Nature of Dry-Steam Resources	171
7.3 Steam Gathering System	177
7.4 Energy Conversion System	179
7.4.1 Turbine Expansion Process	180
7.4.2 Condensing and Cooling Tower Processes; Utilization Efficiency	183
7.5 Example: Optimum Wellhead Pressure	183
7.6 Environmental Aspects of Dry-Steam Plants	185
7.7 Equipment List for Dry-Steam Plants	187
7.7.1 Steam Supply System	187
7.7.2 Turbine Generator and Controls	187
7.7.3 Condenser, Gas Ejection, and Pollution Control (Where Needed)	187
7.7.4 Heat Rejection System	187
7.7.5 Backup Systems	188
7.7.6 Noise Abatement System (Where Required)	188
7.7.7 Condensate Disposal System	188
References	188
Nomenclature for Figures in Chapter 7	189
Problems	190

A few yards further brought us into the midst of puffing geysers, or steam-jets, for I knew not by what other name to call them. Fumes of sulphur here met our nostrils at every step, while the rustling steam, as it spouted from a hundred cavities, completely enveloped us . . . The whole of this violent commotion was accompanied by a tremendous noise beneath the Earth's surface . . .

John Russell Bartlett, describing *The Geysers in California*—1854

7.1 Introduction

Dry-steam plants were the first type of geothermal power plant to achieve commercial status. Their history goes back more than 110 years to 1904 when Prince Piero Ginori Conti built and operated a tiny steam engine using the natural steam jets that issued from the ground at Larderello in the Tuscany region of Italy (Figure 7.1). Since the geofluid consisted solely of steam, it was fairly easy to hook up a mechanical device to take advantage of the available energy. Although the Prince's engine only generated enough electrical power to illuminate five light bulbs in his factory, it was the springboard for larger plants.

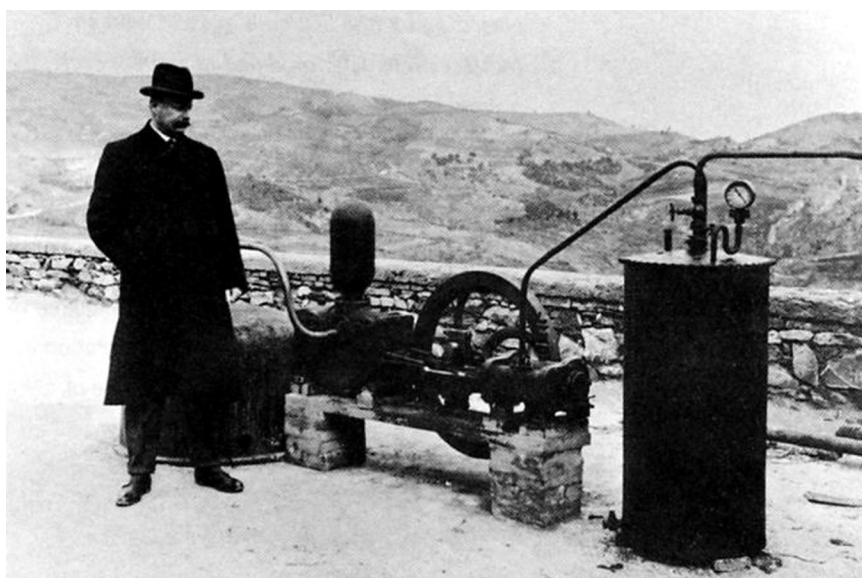


Figure 7.1 Prince Piero Ginori Conti and his 15 kW geothermal steam engine. *Enel S.p.A.—Museo della Geotermia Larderello—Archivio Fotografico [1].*

Dry-steam plants tend to be simpler and less expensive than their flash-steam cousins in that there is no geothermal brine to contend with. As we will see, this is a mixed blessing when it comes to maintaining reservoir performance. Although there are only two major dry-steam fields in the world—Larderello and The Geysers, in Northern California, United States—there are 68 units of this type in operation as of December 2014, about 12% of all geothermal plants. Dry steam plants account for 2865 MW installed or about 24% of the total geothermal worldwide capacity. The average dry-steam unit has a rating of 42.1 MW. Some fields in Indonesia exhibit dry-steam characteristics but may arise from the formation of steam caps; see Chapter 14. See Appendix A for more plant statistics.

7.2 Origins and Nature of Dry-Steam Resources

Large dry-steam reservoirs have been discovered only in two areas of the world: Larderello and The Geysers. There are limited dry-steam areas in Japan (Matsukawa), Indonesia, and New Zealand (Poihipi Road section of Wairakei). White [2] estimated that only about 5% of all hydrothermal systems with temperatures greater than 200°C are of the dry-steam type. The rare occurrence of geothermal reservoirs producing dry or superheated steam rather than liquid-dominated reservoirs producing liquid–vapor mixtures begs the questions: “Why are these so unique?” and “What gives rise to them?”

The general characteristic of a dry-steam reservoir is that it comprises porous rock featuring fissures or fractures, either occluded or interconnected, that are filled with steam. Whereas the steam also contains gases such as carbon dioxide, hydrogen sulfide, methane, and others in trace amounts, there is little or no liquid present. The steam appears to have either magmatic or meteoric origins. The first possibility involves the slow evolution of vapor from magma chambers located at great depth and at very high temperatures close to that of molten rock [3]. The second one involves the percolation of rainwater through faults and fractures to great depth where it encounters high temperature rock [2].

Measurements of the relative amounts of various isotopes of water, H_2^{16}O , H_2^{18}O , H_2^{17}O , and HDO , in geothermal fluid samples, compared to the natural amounts of the same isotopes, indicate that the most likely source of the fluids in geothermal reservoirs is meteoric waters [4]. This simple conclusion must be tempered by the uncertainty arising from the possible mixing of meteoric fluids that have percolated to great depths with magmatic vapors, making it difficult, if not impossible, to distinguish one from the other once the fluids have reached the surface.

The mechanism of fluid behavior in a dry-steam reservoir is complex and several models have been proposed [2–9]. The emerging consensus is that there are three sources for the steam that is seen in the production wells. The first contribution comes from steam residing in fissures and fractures in competent rock. The second comes from the vaporization of liquid that formed as condensate from steam that has come in contact with the cooler lateral and upper boundaries of the reservoir. The last one arises from evaporation off the top of a deep brine reservoir over a prolonged period of steam production which causes a decrease in reservoir pressure [8,9].

These mechanisms are depicted schematically in Figure 7.2. Note that the lateral boundaries of the vapor-dominated reservoir are seen as being highly impermeable. If this were not true, liquid would flood the steam zone from the sides, collapsing the steam in the formation. The only liquid in the steam zone comes from the condensate and water trapped in fissures that have only limited

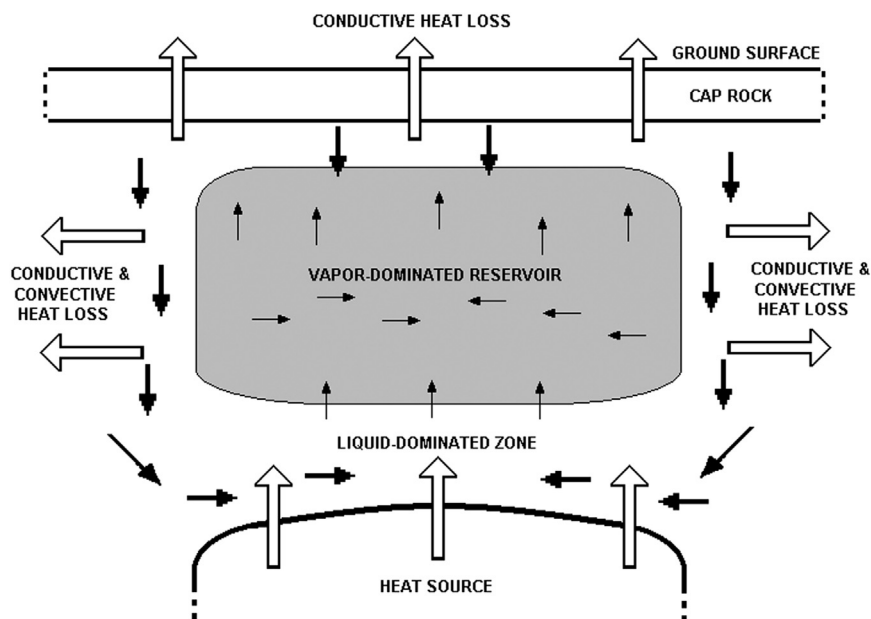


Figure 7.2 Proposed model for creation and operation of a dry-steam reservoir. Open arrows represent heat flow; filled arrows show movement of liquid; small arrows show steam movement. After Ref. [7].

vertical extent. A production well provides a preferential flow path allowing the removal of steam and causing a cone of depression in the pressure in the surrounding formation. This pressure reduction leads to further steam generation by causing the trapped liquid to evaporate. In this way the formation may eventually completely dry out, leaving only the condensate and the deep liquid as the sole means to provide additional steam.

The natural recharge enters the system primarily through the lateral boundaries that may be demarcated by major faults with significant offsets. Surface water then can reach the depth of the liquid-dominated zone. If the rate of recharge is less than the rate of production, the deep liquid zone will retreat to even greater depth as the reduced pressure causes more and more evaporation to occur. The initial presence of the steam zone is thought to be attributable to such an imbalance between the natural steam loss through the upper layers of the formation relative to the natural recharge. In their natural states, prior to exploitation, both the Larderello and The Geysers fields were marked by extensive surface thermal manifestations such as fumaroles, mud volcanos, steam-heated pools, and steaming, acid-altered ground and rocks [10–12]. Over time, the permeability of the near-surface formation decreases as minerals precipitate from the geofluid and seal the fissures and fractures that had originally served as fluid conduits.

Many authors have cited the close correlation between the observed temperatures in dry-steam reservoirs and the temperature that corresponds to the maximum enthalpy for saturated steam [3–8]. Saturated steam exhibits a maximum enthalpy of $h = 2804.2 \text{ kJ/kg}$ at roughly $T = 235^\circ\text{C}$ and $P = 30.6 \text{ bar}$ [13]. The enthalpy-entropy (or Mollier) diagram for water is shown schematically in Figure 7.3 (to scale, but with an arbitrary numerical entropy scale).

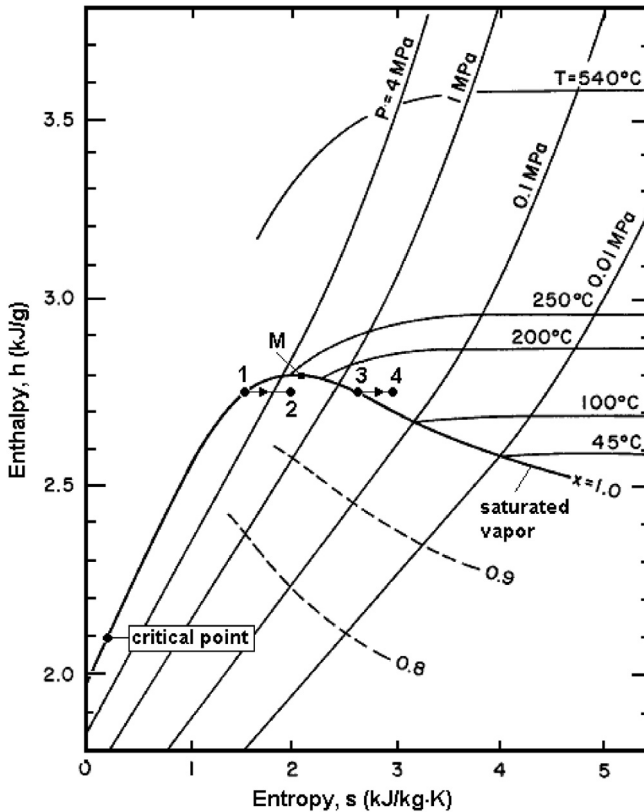


Figure 7.3 Mollier diagram for water; M = maximum enthalpy point on the saturation line.

Since the First Law of thermodynamics dictates that steam undergoing an expansion process without heat or work transfer must do so at constant enthalpy, saturated steam at a temperature lower than 235°C experiencing an isenthalpic pressure loss will become superheated (process $3 \rightarrow 4$), whereas one at a temperature higher than 235°C will first form a liquid–vapor mixture (process $1 \rightarrow 2$). It is reasonable to assume that the geofluid in the deepest part of the reservoir will

be hottest. It will tend to rise because of its lower density and will undergo a pressure drop as it passes through the restrictive passages in the formation. At each step then, a fraction of liquid will separate out of the steam and tend to flow downward due to its higher density, leaving the now dry steam to continue upward. This brings the steam into a yet lower pressure domain and the process repeats itself [5]. In fact, in whatever direction the steam travels, the pressure will continue to fall due to frictional effects.

This reasoning explains well how the rising steam can reach the maximum enthalpy point but does not explain how the steam stabilizes there as a saturated vapor at 235°C. Further pressure reduction, for instance, would mean the steam would become superheated. James [5] points out that during production, the steam would flow at essentially constant temperature through the hot rock and would tend to follow an isothermal process. He estimated that this could result in as much as 35°C superheat.

McNitt [6] offers a thermodynamic argument to explain this phenomenon based on the amount of heat needed to evaporate a unit of liquid relative to the amount of heat available when a steam bubble condenses.

Referring to Figure 7.4, when a hypothetical bubble forms at level *j* and begins to move upward, there are two possibilities: either it will shrink and eventually collapse or it will continue to rise. If it collapses, it would release its heat of condensation to the surrounding liquid. If that amount of heat is sufficient to create another bubble at the higher level, then a continuous steam phase will be created. If not, then the liquid will form the continuous phase. Since this hypothesis calls for the internal exchange of heat between the vapor and liquid phases, the overall process may be viewed as adiabatic, and the process followed by the bubble may be modeled as isenthalpic. The lines in the temperature-entropy diagram labeled *j*–*i* represent lines of constant enthalpy.

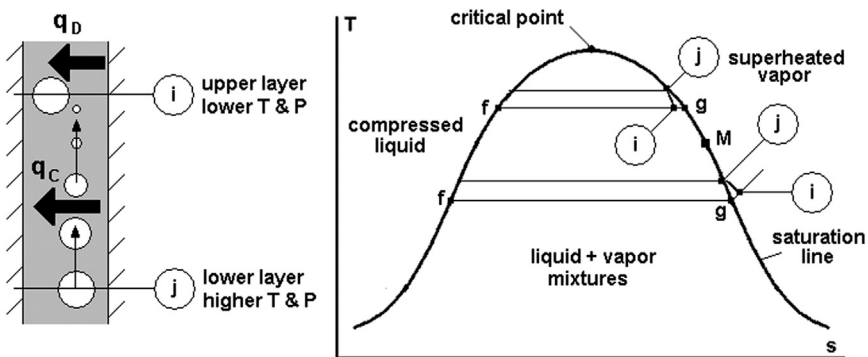


Figure 7.4 Hypothesis for creation of stable steam zone at 235°C. After Ref. [6].

The argument turns on the relative sizes of the following two terms:

$$q_C \equiv h_g(P_j) - h_f(P_i) \quad (7.1)$$

and

$$q_D \equiv h_g(P_i) - h_f(P_i) \quad (7.2)$$

The term defined as q_C is the heat per unit mass delivered by the rising bubble as it condenses in going from state j to state i . The term defined as q_D is the heat per unit mass required to form a bubble at the upper level, at state i . If $q_C > q_D$, then the steam phase will be continuous; if $q_C < q_D$, then the liquid phase will be continuous. But it is obvious that this difference is simply $h_g(P_j) - h_g(P_i)$, which is always negative for initial states with temperatures greater than T_M , the temperature corresponding to the maximum enthalpy point on the saturated vapor line (shown as point M), and which is always positive for initial states with temperatures lower than T_M .

Thus, we see that the steam phase should begin where the reservoir temperature approximates the maximum-enthalpy temperature of 235°C. At depths below this temperature level, we would expect the pressure to vary with depth hydrostatically, but above this level, that is, throughout the dry-steam reservoir, we would expect roughly constant temperature and pressure. The pressure and temperature gradients through the shallow levels of cap rock including the zone of condensation would be close to the boiling point curve, that is, a column of water that has a temperature at each point along the column that is equal to the saturation temperature corresponding to its hydrostatic pressure. See [Figure 7.5](#).

It is clear from [Figure 7.5](#) that the dry-steam reservoir is characterized by a pressure far below the hydrostatic pressure at the same depth. This pressure deficiency can only be maintained if the permeability of the surrounding formation is very low, effectively isolating the steam field from the influx of liquid from the lateral portions of the greater field. This phenomenon will play a key role when fluid is injected into the formation to prolong the life and productivity of the field. Clearly, the fluid will be readily accepted, in effect, sucked into the reservoir, but the liquid could have the unwanted result of flooding the steam field unless the injection wells are carefully sited and the injection rate is balanced against the rate of steam extraction.

In the first major attempt to restore fluid to a dry-steam field during exploitation, a program of injection was begun in 1989 in the southeast area of The Geysers [14]. The site was selected with the objective of counteracting the observed drying out of the reservoir in a region still marked by high temperature. Significant amounts of superheat, up to 80°F (44°C), had been seen in the output of wells in the southeast area of the field but the reservoir temperature had remained constant at about 450°F (232°C). The experiment showed

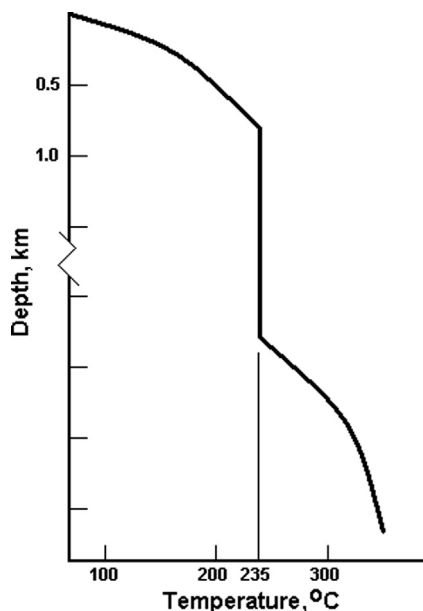


Figure 7.5 Temperature versus depth schematic for a dry-steam system. *After Ref. [4].*

that the injection resulted in an increase in steam flow from the production wells, equivalent to about 20 MW of additional power, and set the stage for larger programs of injection involving waste water from neighboring communities in Lake County [15] and Santa Rosa [16]. This will be discussed further in Section 12.6.

In summary, a dry-steam reservoir owes its existence to a combination of highly fortuitous circumstances. First there must be heat source relatively close to the surface (~ 5 km depth) to raise the temperature of connate water to the boiling point. There must be sufficient permeability above the reservoir to allow steam to escape to the surface over geologically long periods of time, thereby lowering the liquid level dramatically. There must be sufficient interconnectedness of fissures and fractures within the reservoir to allow the fluid to circulate inside the reservoir. There must be sufficient lateral impermeability between the reservoir and the surrounding rock to prevent flooding of the steam reservoir by cooler groundwater. And finally, the uppermost levels of the formation need to become largely impermeable via the mechanism of self-sealing caused by mineral precipitation. The difference between the huge dry-steam reservoirs at Larderello and The Geysers and other dry-steam “caps” lies in the extent to which these conditions are present and how long the processes have been in progress.

7.3 Steam Gathering System

The connection between the wells and the powerhouse for a dry-steam plant is relatively simple compared to a flash-steam plant. At the well, there are the usual valves plus a steam purifier. The latter is merely an in-line, axial centrifugal separator designed to remove particulate matter from the steam before it enters the piping system. The steam pipes are covered with insulation and mounted on stanchions, and include expansion loops to accommodate pipe movement from a cold to a hot condition. Steam traps are sited strategically along the pipes to remove condensate which is then conveyed by separate lines to holding ponds and eventual reinjection. See [Figures 7.6 and 7.7](#).

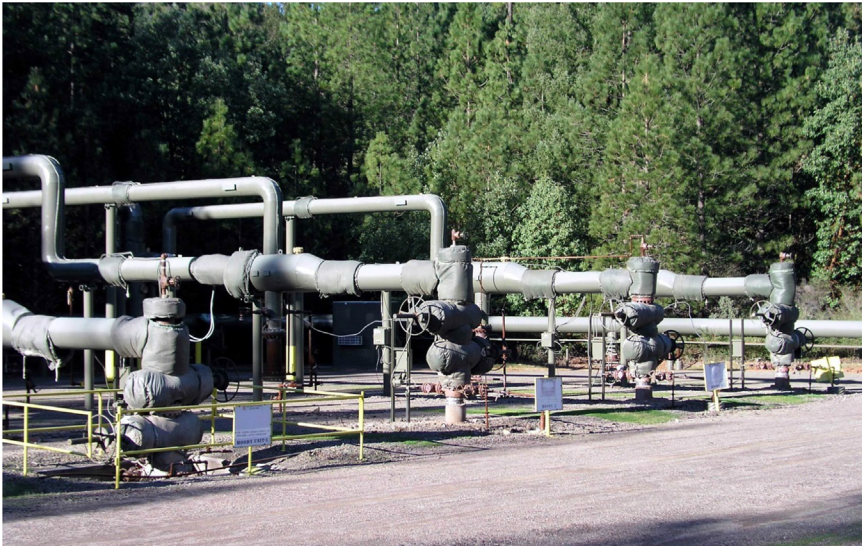


Figure 7.6 Wellhead pipelines at The Geysers. Note axial separators to remove particulate matter. Several wells are sited on a single drilling pad to reduce the amount of land needed for well pads. The wells are drilled directionally to intercept a large reservoir volume. *Photo courtesy of Calpine Corporation [17] [WWW].*

As the steam line approaches the powerhouse, there is an emergency pressure relief station. This allows for the temporary release of steam in the event of a turbine trip. The steam generally passes through a silencer before entering the atmosphere. It has been found preferable to maintain the wells in a steady open mode rather than cycling the wells through open and closed positions. At the powerhouse one finds a steam header, a final moisture remover, typically a vertical cyclone separator or a baffled demister, and a venturi meter for accurate measurement of the steam flow rate. See [Figures 7.8 and 7.9](#).



Figure 7.7 Steam pipeline and steam trap with condensate drain line at The Geysers. *Photo by author [WWW].*



Figure 7.8 Emergency steam relief valves at The Geysers. *Photo by author [WWW].*



Figure 7.9 Rock mufflers for emergency steam stacking at The Geysers. *Photo by author [WWW].*

7.4 Energy Conversion System

Once the steam reaches the powerhouse, a dry-steam plant is essentially the same as a single-flash steam plant. The turbines are single-pressure units with impulse-reaction blading, either single-flow for smaller units or double-flow for larger units (say, 60 MW or greater). The condensers can be either direct-contact (barometric or low-level) or surface-type (shell-and-tube). For small units, it is often advantageous to arrange the turbine and condenser side by side, rather than the more usual condenser-below-turbine arrangement seen in most power plants.

With the exception of the particulate remover (PR) in place of the cyclone separator (CS), the flow diagram shown in [Figure 7.10](#) is identical to [Figure 5.6](#) for a single-flash plant [\[18\]](#).

The processes undergone by the steam are shown in [Figure 7.11](#). Since the wells produce saturated steam (or slightly superheated steam), the starting point (state 1) is located on the saturated vapor curve. If the steam is superheated, point 1 merely moves slightly to the right. The turbine expansion process 1–2 generates somewhat less power output than the ideal, isentropic process 1–2s. Heat is rejected to the surroundings in the condenser via the cooling water in process 2–3. Although the analysis of the operation is the same as for the single-flash plant, we repeat the equations here for ease of reference.

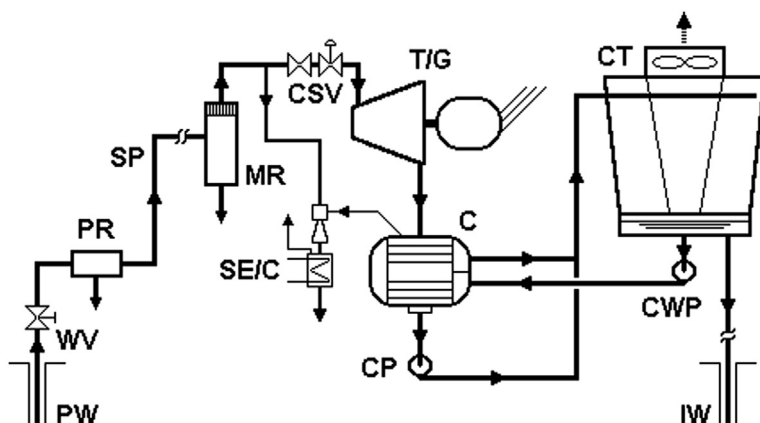


Figure 7.10 Simplified schematic flow diagram for a dry-steam plant [18].

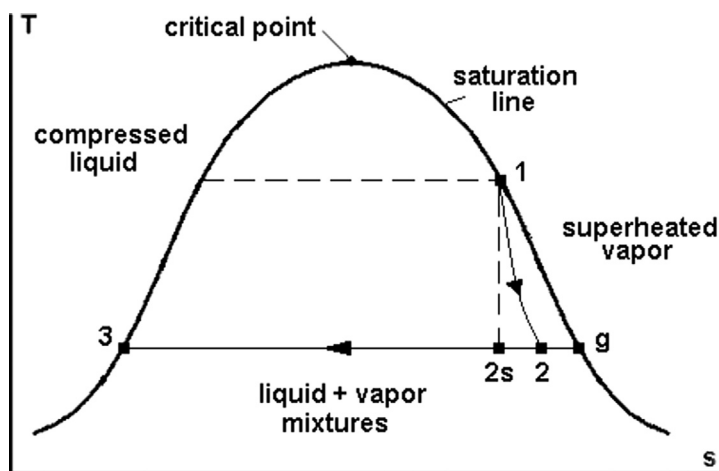


Figure 7.11 Temperature-entropy diagram for a dry-steam plant with saturated steam at the turbine inlet.

7.4.1 TURBINE EXPANSION PROCESS

The work produced by the turbine per unit mass of steam flowing through it is given by:

$$w_t = h_1 - h_2 \quad (7.3)$$

assuming an adiabatic turbine and neglecting the changes in kinetic and potential energy of the fluid entering and leaving the turbine. The maximum possible work would be generated if the turbine operated adiabatically and reversibly, i.e., at constant entropy or isentropically.

The isentropic turbine efficiency, η_t , is the ratio of the actual work to the isentropic work, namely,

$$\eta_t = \frac{h_1 - h_2}{h_1 - h_{2s}} \quad (7.4)$$

The power developed by the turbine is given by:

$$\dot{W}_t = \dot{m}_s w_t = \dot{m}_s (h_1 - h_2) = \dot{m}_s \eta_t (h_1 - h_{2s}) \quad (7.5)$$

The gross electrical power will be equal to the turbine power times the generator efficiency:

$$\dot{W}_e = \eta_g \dot{W}_t \quad (7.6)$$

The net power is this amount reduced by all parasitic loads including condensate pumping power, cooling tower fan power, and station lighting.

Adopting the Baumann rule to account for the degradation in performance of a wet-steam turbine, we find:

$$\eta_{rw} = \eta_{td} \times \left[\frac{1 + x_2}{2} \right] \quad (7.7)$$

where the dry turbine efficiency, η_{td} , may conservatively be taken to be constant at 85%:

$$\eta_{td} = 0.850 \quad (7.8)$$

The thermodynamics properties at state 2 are determined by solving Eq. (7.4) using the turbine efficiency and the fluid properties at state 2s, the ideal turbine outlet state, which are easily calculated from the known pressure and entropy values at state 2s. The ideal enthalpy is found from:

$$h_{2s} = h_3 + [h_g - h_3] \times \left[\frac{s_1 - s_3}{s_g - s_3} \right] \quad (7.9)$$

where the entropy term gives the fluid outlet dryness fraction for an ideal turbine. When the Baumann rule is incorporated into the calculation, the following working equation emerges for the enthalpy at the actual turbine outlet state:

$$h_2 = \frac{h_1 - A \left[1 - \frac{h_3}{h_g - h_3} \right]}{1 + \frac{A}{h_g - h_3}} \quad (7.10)$$

where the factor A is defined as

$$A \equiv 0.425(h_1 - h_{2s}) \quad (7.11)$$

These equations assume that the turbine-inlet steam is saturated. If the inlet is superheated (as often happens after a period of operation), then a more complex algorithm must be followed. First, the portion of the expansion process that occurs in the superheated region is analyzed using the dry turbine expansion efficiency of 85%. Then when the steam enters the wet region, the remaining expansion is analyzed using the same equations given above.

The location of the state point where the expansion passes through the saturated vapor curve is found by trial and error. The method for doing the calculation is outlined below with the aid of Figure 7.12. Three isobars are shown: P_1 is the inlet steam pressure, P_2 is the condenser pressure, and P_4 is the pressure at which the expansion enters the wet region (unknown). Since we assume that the dry turbine efficiency is known and constant for the process from 1–4, we may write:

$$\eta_d = \frac{h_1 - h_4}{h_1 - h_{4s}} \quad (7.12)$$

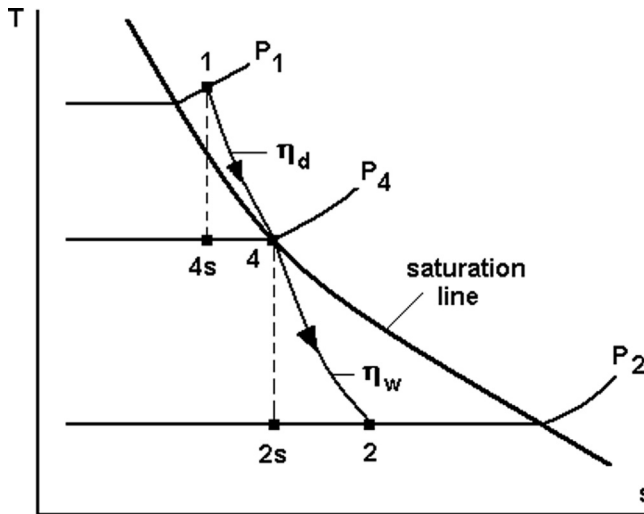


Figure 7.12 Dry and wet turbine expansion processes for superheated inlet steam.

Both h_4 and h_{4s} depend on P_4 which is what we are trying to determine. The first step is to guess a value for P_4 . Then h_4 is found directly from *Steam Tables*, and h_{4s} may be calculated from:

$$h_{4s} = h_f + x_{4s}h_{fg} = h_f + \left[\frac{s_1 - s_f}{s_{fg}} \right] h_{fg} \quad (7.13)$$

where the enthalpy of saturated liquid and the enthalpy of evaporation at P_4 are given by h_f and h_{fg} , respectively. With h_4 and h_{4s} now both determined for the

assumed value of P_4 , the turbine efficiency is calculated from Eq. (7.12) and compared to 0.85. Unless the calculated efficiency is equal to 0.85, it is necessary to try another pressure and repeat the calculations until agreement is reached. Then the specific power output from the dry expansion is:

$$w_{td} = h_1 - h_4 \quad (7.14)$$

and the specific power output from the wet expansion is:

$$w_{tw} = h_4 - h_2 \quad (7.15)$$

where a process similar to that outlined earlier will lead to the value of h_2 .

As with all thermodynamic modeling of complex processes, this must be viewed as an approximation. It is known that steam can enter the wet region and remain in the vapor phase, out of thermodynamic equilibrium, for a portion of the full process. The locus of states where the first liquid droplets appear is called the Wilson line. It is generally accepted that the line of 95% dryness fraction is the limit for steam to persist in a state of metastable equilibrium [19]. Given this uncertainty together with the fact that the dry expansion in a dry-steam turbine is a small part of the total expansion, it is often acceptable to treat the entire process as taking place in the wet region and to use the analysis given at the beginning of this section, that is, Eqs. (7.3)–(7.11).

7.4.2 CONDENSING AND COOLING TOWER PROCESSES; UTILIZATION EFFICIENCY

The working equations for the condenser, cooling tower, and the utilization efficiency are the same as for the flash-steam plants already considered and will not be repeated. The reader is referred to Sections 5.4.5–5.4.7.

7.5 Example: Optimum Wellhead Pressure

This example will treat the problem of deciding on the optimum wellhead pressure for a dry-steam plant receiving saturated vapor at the wellhead. As with the previous examples, we will ignore pressure losses in pipelines. We will assume that we can control the pressure at the wellhead by means of a throttle valve. The well productivity curve can be approximated as an elliptical equation in terms of the mass flow rate of steam as a function of the wellhead pressure:

$$\left[\frac{\dot{m}}{\dot{m}_{max}} \right]^2 + \left[\frac{P}{P_{ci}} \right]^2 = 1 \quad (7.16)$$

where \dot{m}_{max} is the maximum observed mass flow rate and P_{ci} is the closed-in wellhead pressure. This function is shown schematically in [Figure 7.13](#). Assuming that values for these two parameters are available from well tests, the mass flow rate at any pressure can be calculated from:

$$\dot{m} = \dot{m}_{max} \sqrt{1 - (P/P_{ci})^2} \quad (7.17)$$

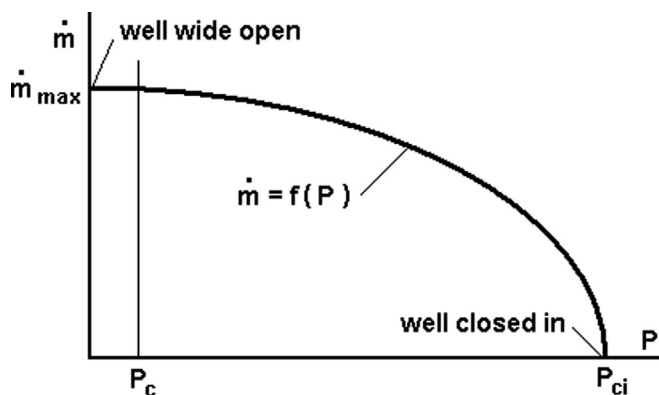


Figure 7.13 Dry-steam productivity curve.

Opening the wellhead valve will result in lower pressures and higher flow rates, but the enthalpy of the steam will remain the same since it is a throttling process.

The effect of this operation can be seen in [Figure 7.14](#), a Mollier diagram for steam.

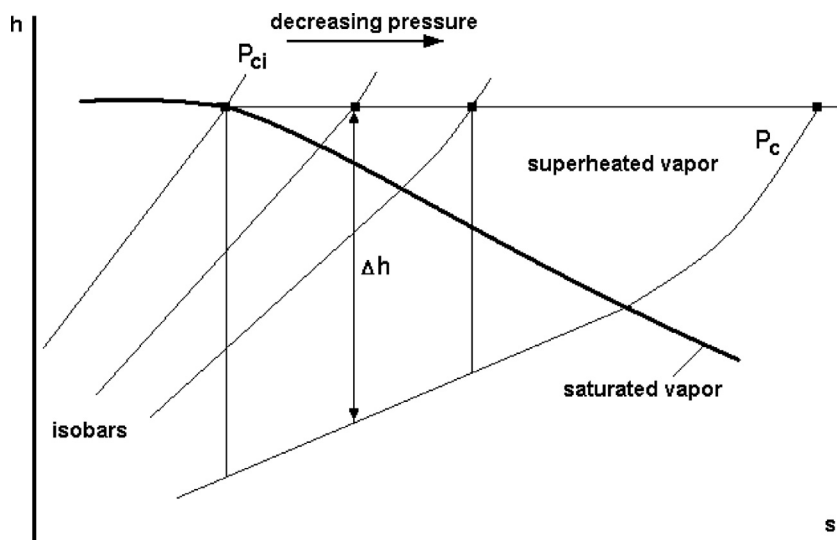


Figure 7.14 Ideal turbine expansion processes for various wellhead pressures.

The turbine power is proportional to the product of the steam mass flow rate and the enthalpy drop Δh (shown for an ideal isentropic process for simplicity). There are two limits to the wellhead pressure: the closed-in pressure, P_{ci} , for which there is no steam flow, and the condenser pressure, P_c , for which there is no enthalpy drop. Thus the power vanishes at the two extreme positions for the wellhead pressure, indicating there is some wellhead pressure for which the power will be a maximum.

It is convenient computationally to solve for the power output per maximum steam flow rate:

$$\frac{\dot{W}}{\dot{m}_{max}} = \frac{\dot{W}}{\dot{m}} \times \frac{\dot{m}}{\dot{m}_{max}} = (h_1 - h_2) \times \sqrt{1 - (P/P_{ci})^2} \quad (7.18)$$

where $(h_1 - h_2)$ is the isentropic enthalpy drop across the turbine (shown as Δh in Figure 7.14). It is not hard to solve this problem for a nonisentropic turbine; see Problem 7.1.

For this illustration, we have selected the following parameters to define the problem: (Note—all pressures are absolute.)

closed-in pressure, $P_{ci} = 2.10$ MPa; $P_2 = P_c = 14.0$ kPa; $h_1 = 2800$ kJ/kg.

The results of the calculations are shown in Table 7.1. These were obtained using an Excel spreadsheet with REFPROP to obtain steam properties.

A graph of the power output per maximum steam flow is shown in Figure 7.15. It can be seen that the optimum operating point occurs at a wellhead pressure of 0.9 MPa. At that setting, the plant can produce a gross power of 581.9 kW/(kg/s). Thus, if a steam well can produce a maximum flow rate of 25 kg/s, that would be equivalent to a gross output of 14.66 MW. Recall however that the turbine is assumed to be ideal; for a realistic turbine, this would drop to about 11.7 MW.

It is also noteworthy that the curve is relatively flat near the optimum point. Over the range of wellhead pressures from 0.8 to 1.0 MPa, the power output is within 0.4% of the optimum value. This offers the designer wide latitude in selecting the operating pressure without sacrificing much in the way of power generation.

7.6 Environmental Aspects of Dry-Steam Plants

Dry-steam geothermal plants have very low potential impact on the environment. The geofluid consists of only steam—no liquid—so there is no mineral-laden brine to dispose of. The noncondensable gases in the steam are isolated in the condenser and removed by means of vacuum pumps or steam-jet ejectors, and they can be treated to remove hydrogen sulfide, if it is present in objectionable levels. The sulfur from certain types of abatement systems is in pure form and may be sold commercially or disposed of in an appropriate landfill [20]. The excess condensate from the cooling tower is reinjected as is any liquid trapped from the steam transmission pipelines.

TABLE 7.1 Results of optimization calculations.

P_{wh}	h_1	s_1	x_2	h_2	$h_1 - h_2$	P/P_{ci}	\dot{W}/\dot{m}_{max}
MPa	kJ/kg	kJ/kg · K	—	kJ/kg	kJ/kg	—	kW/(kg/s)
0.4	2800	7.0394	0.8641	2272.8	527.2	0.190	517.6
0.5	2800	6.9397	0.8504	2240.3	559.7	0.238	543.6
0.6	2800	6.8587	0.8393	2213.9	586.1	0.286	561.6
0.7	2800	6.7906	0.8299	2191.8	608.2	0.333	573.4
0.8	2800	6.7321	0.8219	2172.7	627.3	0.381	580.0
0.9	2800	6.6807	0.8149	2156.0	644.0	0.429	581.9
1.0	2800	6.6351	0.8086	2141.1	658.9	0.476	579.4
1.1	2800	6.5940	0.8030	2127.7	672.3	0.524	572.7
1.2	2800	6.5567	0.7979	2115.6	684.4	0.571	561.7
1.3	2800	6.5226	0.7932	2104.5	695.5	0.619	546.2
1.4	2800	6.4912	0.7889	2094.2	705.8	0.667	526.0
1.5	2800	6.4621	0.7849	2084.8	715.2	0.714	500.6
1.6	2800	6.4350	0.7812	2075.9	724.1	0.762	469.0
1.7	2800	6.4097	0.7777	2067.7	732.3	0.810	429.9
1.8	2800	6.3860	0.7745	2060.0	740.0	0.857	381.2
1.9	2800	6.3636	0.7714	2052.7	747.3	0.905	318.3
2.0	2800	6.3425	0.7685	2045.8	754.2	0.952	230.0
2.1	2800	6.3225	0.7658	2039.3	760.7	1.000	0.0

Bold-face row = optimum.

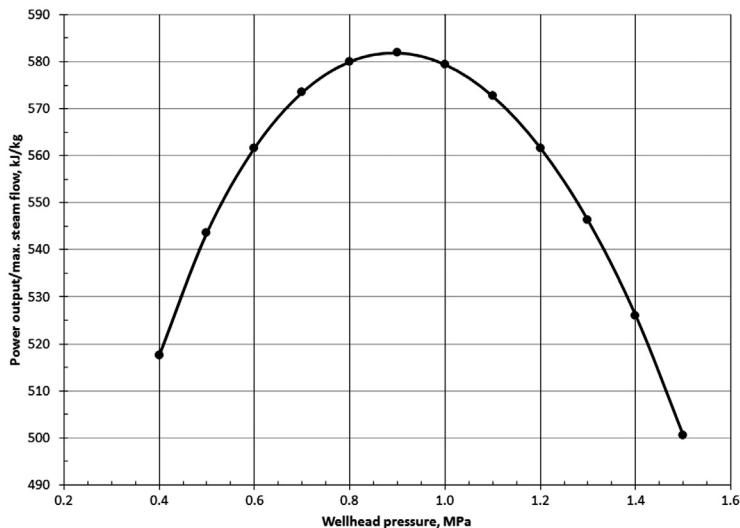


Figure 7.15 Power output per maximum steam flow rate as a function of wellhead pressure.

7.7 Equipment List for Dry-Steam Plants

The major equipment items found at dry-steam plants are quite similar to those used at a single-flash plant. The list below is drawn for dry-steam plants with annotations applied only for items that differ from those at single-flash plants [18].

7.7.1 STEAM SUPPLY SYSTEM

- Wellhead valves and controls
- Steam purifier
Wellhead, axial particulate remover
- Steam piping, insulation, and supports
- Steam header
- Final moisture remover

7.7.2 TURBINE GENERATOR AND CONTROLS

- Steam turbine generator with accessories
- Control system
- Air compressor

7.7.3 CONDENSER, GAS EJECTION, AND POLLUTION CONTROL (WHERE NEEDED)

- Condenser
- Condensate pumps and motors
- Gas removal system
Steam jet ejectors with inter- and after-coolers
Turbocompressors
Hybrid ejector/compressor
- Noncondensable gas treatment system

7.7.4 HEAT REJECTION SYSTEM

- Water cooling tower
- Cooling water pumps and motors
- Cooling water treatment system

7.7.5 BACKUP SYSTEMS

- Standby power supply

7.7.6 NOISE ABATEMENT SYSTEM (WHERE REQUIRED)

- Rock mufflers for stacked steam
- Acoustic insulation for noisy fluid handling components

7.7.7 CONDENSATE DISPOSAL SYSTEM

- Injection wells for excess condensate, and cooling tower blowdown

References

- [1] Photograph courtesy of Enel S.p.A.—Museo della Geotermia Larderello—Archivio Fotografico, November 2004.
- [2] White DE. Characteristics of geothermal resources. In: Kruger P, Otte C, editors. *Geothermal energy: resources, production, stimulation*. Stanford, CA: Stanford University Press; 1973. p. 69–94 [chapter 4].
- [3] Chierici A. Planning of a geothermoelectric power plant: technical and economic principles. Proceedings U.N. conference on new sources of energy, vol. 3, geothermal energy: II; 1964. p. 299–311.
- [4] Ellis AJ, Mahon WAJ. *Chemistry and geothermal systems*. New York, NY: Academic Press; 1977.
- [5] James R. Wairakei and Larderello: geothermal power systems compared. *N Z J Sci* 1968; 11:706–19.
- [6] McNitt JR. Origin of steam in geothermal reservoirs. Proceedings annual fall technical conference and exhibition of the society petroleum engineers, AIME, 1977, Paper SPE 6764.
- [7] D'Amore F, Truesdell AH. Models for steam chemistry at Larderello and The Geysers. Proceedings of the fifth workshop geothermal reservoir engineering, Stanford University, Stanford, CA; 1979. p. 262–76.
- [8] Truesdell AH, Box Jr. WT, Haizlip JR, D'Amore F. A geochemical overview of the geysers geothermal reservoir Spec. Rep. 17 In: Stone C, editor. *Monograph on the geysers geothermal field*. Davis, CA: Geothermal Resources Council; 1992. p. 121–32.
- [9] White DE, Muffler LJP, Truesdell AH. Vapor-dominated hydrothermal systems compared with hot-water systems. *Econ Geol* 1971;66:75–97.
- [10] Allen ET, Day AL. Steam wells and other thermal activity at the geysers. California, Publ. No. 378, Carnegie Institution of Washington, DC; 1927.
- [11] Hodgson SF. A geysers album Spec. Rep. 17 In: Stone C, editor. *Monograph on the geysers geothermal field*. Davis, CA: Geothermal Resources Council; 1992. p. 19–40.

- [12] Burgassi PD. Historical outline of geothermal technology in the Larderello region to the middle of the 20th century [chapter 13] In: Cataldi R, Hodgson SF, Lund JW, editors. *Stories from a heated earth: our geothermal heritage*. Sacramento, CA: Geothermal Resources Council and International Geothermal Association; 1999. p. 195–219
- [13] Keenan JH, Keyes FG, Hill PG, Moore JG. *Steam tables: thermodynamic properties of water including vapor, liquid, and solid phases (international edition—metric units)*. New York, NY: John Wiley & Sons, Inc.; 1969.
- [14] Enezy SL, Enezy KL, Maney J. Reservoir response to injection in the southeast geysers Spec. Rep. 17 In: Stone C, editor. *Monograph on the geysers geothermal field*. Davis, CA: Geothermal Resources Council; 1992. p. 211–9.
- [15] Dellinger M. Lake county success: generating environmental gains with geothermal power. *Geothermal Resour Coun Bull* 2004;33(3):115–19.
- [16] Anon. Recharging The Geysers: Calpine Corp. and Santa Rosa celebrate completion of the world's largest wastewater-to-energy project. *Geothermal Resour Coun Bull* 2003;32(6):242.
- [17] Michetti D. P.R. communications specialist, Calpine Corporation, San Jose, CA; December 27, 2004.
- [18] DiPippo R. Geothermal power systems [section 8.2] In: Elliott TC, Chen K, Swanekamp RC, editors. *Standard handbook of powerplant engineering*. 2nd ed. New York, NY: McGraw-Hill, Inc.; 1998. p. 8.27–60.
- [19] IAPWS, Guideline on the Tabular Taylor Series Expansion (TTSE) Method for Calculation of Thermodynamic Properties of Water and Steam Applied to IAPWS-95 as an Example, International Association for the Properties of Water and Steam, Vejle, Denmark, August 2003.
- [20] DiPippo R. U.S. Dept. of Energy, DOE/RA/28320-1 *Geothermal energy as a source of electricity: a worldwide survey of the design and operation of geothermal power plants*. Washington, DC: U.S. Gov. Printing Office; 1980.

Nomenclature for Figures in Chapter 7

C	Condenser
CP	Condensate pump
CSV	Control and stop valves
CT	Cooling tower
CWP	Cooling water pump
f	Saturated liquid
g	Saturated vapor
IW	Injection well
M	Point of maximum enthalpy for saturated steam
MR	Moisture remover
PR	Particulate remover
PW	Production well
q_c	Heat of condensation from a steam bubble
q_D	Heat of evaporation to form a steam bubble
SE/C	Steam ejector/condenser
SP	Steam piping
T/G	Turbine/generator
WV	Wellhead valve

Problems

- 7.1.** Consider the dry-steam field at The Geysers in California. The following data are available: closed-in pressure = 1.55 MPa; closed-in enthalpy = 2790 kJ/kg; enthalpy = constant for all settings of the wellhead valve; turbine is not isentropic, but is characterized by a wet-turbine efficiency, η_{tw} , given by the Baumann rule (assuming 85% dry expansion efficiency); condenser pressure = 13.8 kPa.
- Find the optimum wellhead pressure for a typical well, if the maximum well flow rate is 25 kg/s.
 - Assuming all the wells behave alike, determine the number of wells needed to power a 110 MW unit if the wells are set at: (i) the optimum wellhead pressure, or (ii) at a pressure 30% greater than the optimum pressure.
- 7.2.** Unit No. 6 at The Geysers produces 52 MW of power at the generator from a steam flow of 417,000 kg/h at a pressure of 6.9 bar and a temperature of 182°C. The reservoir conditions are known to be 32.3 bar and 238°C. The turbine exhaust pressure (condenser pressure) is 0.13 bar.
- Sketch the location of the reservoir and turbine-inlet state points on a scale Mollier chart ($h-s$). What do you observe about the enthalpy of these two states? What do you notice about these values relative to the maximum enthalpy along the saturated vapor line?
 - On the same diagram, locate the turbine exhaust state. Calculate the turbine isentropic expansion efficiency, η_t . Calculate the overall geothermal energy utilization efficiency, η_u , based on (i) reservoir and (ii) turbine-inlet conditions. A sink temperature of 48°C is appropriate for Unit No. 6.
- 7.3.** A dry-steam geothermal plant receives saturated steam at a temperature of 180°C. The condenser operates at 50°C and the local dead-state temperature is 20°C. The turbine obeys the Baumann rule; assume 85% for the dry expansion efficiency. Calculate the following:
- The actual turbine isentropic efficiency.
 - The specific work output of the turbine in kJ/kg.
 - The net utilization efficiency if 5% of the turbine output is needed for all parasitic loads.
- 7.4.** A dry-steam reservoir produces saturated vapor at the maximum enthalpy point. By adjustment of the wellhead valve, the steam is throttled to lower pressures. A pressure $P_1 = 0.800$ MPa is chosen as the wellhead and turbine-inlet pressure (ignore pressure losses in steam piping). At this point the well produces 15 kg/s. The turbine exhausts to a condenser at a pressure $P_2 = 10$ kPa.

- a. Find the turbine-inlet temperature in $^{\circ}\text{C}$.
 - b. Calculate the specific work output of the turbine in kJ/kg .
 - c. Calculate the actual turbine isentropic efficiency.
 - d. Calculate the gross power output for the turbine in MW.
- 7.5.** A dry-steam well is characterized by a closed-in pressure of $P_1 = 2.5 \text{ MPa}$ and saturated vapor. The wellhead valve is set at $P_2 = 1.03 \text{ MPa}$ at which condition the well flows 25 kg/s . You may assume the turbine is adiabatic and has a constant isentropic efficiency of 75%.
- a. Calculate the power in MW that the turbine will generate under the following two cases: (i) there is no condenser and the turbine exhausts to the atmosphere at 100 kPa , and (ii) there is a condenser that has a pressure of 13.8 kPa .
 - b. Calculate the utilization efficiency in both cases, based on the closed-in condition of the geofluid, if the dead-state temperature is 20°C .
- 7.6.** During a performance test at The Geysers Unit 6 (now one unit at McCabe plant), the following data were taken: gross power output = 55 MW , net power = 52 MW , steam flow to the turbine = 105.2 kg/s , turbine-inlet pressure = 689.7 kPa , turbine-inlet temperature = 182.2°C , condensing temperature = 51.1°C , wet-bulb temperature = 18.9°C . The resource is a saturated vapor at 238°C .
- a. Find the specific enthalpy of the (i) turbine-inlet steam and (ii) the reservoir steam. Compare the values and discuss.
 - b. Calculate the turbine isentropic efficiency.
 - c. Calculate the overall net utilization efficiency of the unit based on the reservoir condition.
- 7.7.** The heat balance diagram for the historic Unit 1 at The Geysers in 1961 shows that the plant received a total steam flow of 31.6 kg/s from several wells, of which 30.2 kg/s was admitted to the turbine, the rest being used mainly in the noncondensable gas ejectors. The generator produced $12,500 \text{ kW}$ of electrical power, of which 402 kW was used for plant auxiliaries. The inlet steam pressure was 647.6 kPa and its temperature was 175.6°C . The plant had a barometric condenser that operated at a pressure of 13.8 kPa . The wet-bulb temperature was 18.9°C .
- a. Calculate the plant utilization efficiency, (i) gross and (ii) net, based on the inlet steam condition.
 - b. Calculate the turbine isentropic efficiency, assuming the generator is 95% efficient.
 - c. Calculate the plant net utilization efficiency, based on the difference between steam inlet condition and the steam condition at the turbine exhaust.

- 7.8.** Consider a dry-steam field characterized by a closed-in wellhead pressure of 3.035 MPa and a maximum steam flow rate of 189 kg/s when the wells are wide open, i.e., the wellhead pressure is 96.6 kPa. You may assume the productivity curve is a section of an ellipse given in the form

$$\left(\frac{\dot{m}}{\dot{m}_{max}}\right)^2 + \left(\frac{P}{P_{ci}}\right)^2 = 1$$

The steam may be taken as dry, saturated at closed-in conditions and that it is simply throttled as the wellhead valve is gradually opened. The turbine may be assumed isentropic to simplify the calculations.

- a.** Determine the wellhead pressure and the steam flow rate to yield the maximum power from the resource for (i) a turbine exhausting to the atmosphere at 96.6 kPa and (ii) condensing at 13.8 kPa.
- b.** Find the maximum power for both cases.
- c.** Discuss the results, including the penalty in loss of power for off-optimum operation.



Chapter 8

Binary Cycle Power Plants

Chapter Outline

8.1 Introduction	194
8.2 Basic Binary Systems	196
8.2.1 Turbine Analysis	197
8.2.2 Condenser Analysis	198
8.2.3 Feed Pump Analysis	199
8.2.4 Heat Exchanger Analysis: Preheater and Evaporator	199
8.2.5 Overall Cycle Analysis	202
8.3 Working Fluid Selection	203
8.3.1 Thermodynamic Properties	204
8.3.2 Sonic Velocity and Turbine Size	205
8.3.3 Health, Safety, and Environmental Considerations	207
8.4 Advanced Binary Cycles	208
8.4.1 Ideal Binary Cycle	208
8.4.2 Dual-Pressure Binary Cycle	209
8.4.3 Dual-Fluid Binary Cycle	212
8.4.4 Kalina Binary Cycles	216
8.5 Example of Binary Cycle Analysis	218
8.6 Environmental Impact of Binary Cycles	223
8.7 Equipment List for Basic Binary Plants	223
8.7.1 Downwell Pumps and Motors	223
8.7.2 Brine Supply System	223
8.7.3 Brine/Working Fluid Heat Exchangers	224
8.7.4 Turbine-Generator and Controls	224
8.7.5 Working Fluid Condenser, Accumulator, and Storage System	224
8.7.6 Working Fluid Feed Pump System	224
8.7.7 Heat Rejection System	224
8.7.8 Backup Systems	224
8.7.9 Brine Disposal System	225
8.7.10 Fire Protection System (if Working Fluid is Flammable)	225

8.8 Pumps	225
8.8.1 Introduction	225
8.8.2 Downhole Pumps	225
8.8.3 Surface Pumps	229
References	231
Nomenclature for Figures in Chapter 8	233
Problems	234

A colossal column of cloud towered to a great height in the air immediately above the crater, and the outer swell of every one of its vast folds was dyed with a rich crimson luster, which was subdued to a pale rose tint in the depressions between. It glowed like a muffled torch...

Mark Twain, describing an eruption of Kilauea—1872

8.1 Introduction

Binary cycle geothermal power plants are the closest in thermodynamic principle to conventional fossil or nuclear plants in that the working fluid undergoes an actual closed cycle. The working fluid, chosen for its appropriate thermodynamic properties, receives heat from the geofluid, evaporates, expands through a prime mover, condenses, and is returned to the evaporator by means of a feed pump.

Although it is generally believed that the first geothermal binary power plant was put into operation at Paratunka near the city of Petropavlovsk on Russia's Kamchatka peninsula in 1967 [1], there is evidence that an earlier binary plant existed on the Italian island of Ischia in 1940 [1a,1b]. The plant was designed in 1939, installed in 1940, and ran until 1943. Since this all happened during World War II, very little mention of this plant is found in the literature. It was sited on the beach at Citara (today a popular resort) and was supplied with a geofluid mixture comprised of about 27.8 kg/s saturated steam and about 18 kg/s hot water at a temperature of 130°C from a single well. Ethyl chloride, C_2H_5Cl , was the working fluid, and the unit had an installed capacity of 300 kW, with an effective rating of 250 kW. Using several plausible but unconfirmed assumptions, it is estimated that the binary plant had a thermal efficiency of about 12.4% [1a].

The previous edition of this book cited a small 200 kW power plant that ran in 1952 at Kiabukwa, Democratic Republic of the Congo, about 18 km west of the city of Kamina in southern Katanga province as the first binary plant. Although Kiabukwa was certainly a novel, pioneering plant, it was not a binary plant. Further research revealed that it was a vacuum-flash plant [1a,1c]; see

8.2 Basic Binary Systems

If one were to plot a histogram of geothermal resources worldwide arranged by temperature, it would be heavily skewed toward low-temperature resources. If the geofluid temperature is 150°C (300°F) or less, it becomes difficult, although not impossible, to build a flash-steam plant that can efficiently and economically put such a resource to use. The lower the resource temperature the worse the problem becomes for flash technology. Indeed at such low temperatures it is unlikely that the wells will flow spontaneously, and if they do, there is a strong likelihood of calcium carbonate scaling in the wells.

One way to prevent the scaling problem is to produce the geofluid as a pressurized liquid by means of downwell pumps. When geofluids are produced this way, it is generally not thermodynamically wise to then flash the fluid in surface vessels and use a flash-steam plant. However, there is one plant that does so, the GEM plant at East Mesa in the Imperial Valley of California in the United States [3]. It is simpler to pass the geofluid as a compressed liquid through heat exchangers and dispose of it in injection wells still in the liquid phase. The thermodynamic irreversibilities associated with the flash process are replaced with irreversibilities from heat transfer across a finite temperature difference. With imaginative design of the heat exchangers, these losses can be minimized, as we will see later.

In its simplest form, a binary plant follows the schematic flow diagram given in Figure 8.2. The production wells PW are fitted with pumps P that are set below the flash depth determined by the reservoir properties and the desired flow rate. Sand removers SR may be needed to prevent scouring and erosion of the piping and heat exchanger tubes. Typically there are two steps in the heating–boiling process, conducted in the preheater PH where the working fluid is brought to its boiling point and in the evaporator E from which it emerges as a saturated vapor. The geofluid is everywhere kept at a pressure above its flash point for the fluid

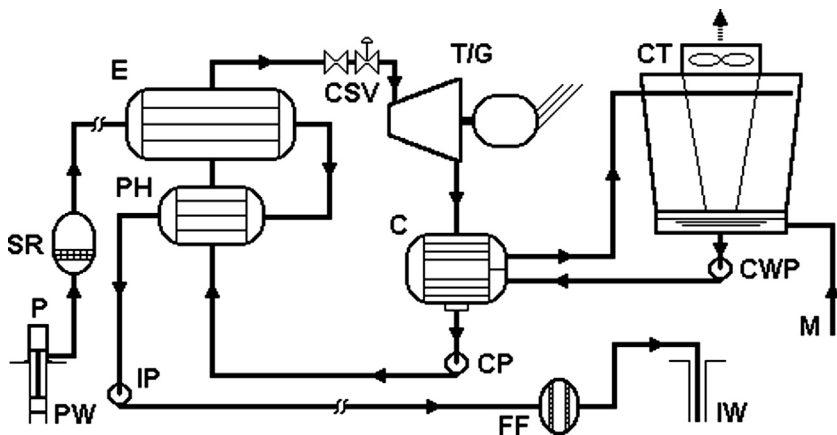


Figure 8.2 Simplified schematic of a basic binary geothermal power plant [4].

temperature to prevent the breakout of steam and noncondensable gases that could lead to calcite scaling in the piping. Furthermore, the fluid temperature is not allowed to drop to the point where silica scaling could become an issue in the preheater and in the piping and injection wells downstream of it. Thus the chemical problems described in Chapters 4 and 6 can be eliminated in principle.

The thermodynamic processes undergone by the working fluid are shown in Figure 8.3, a pressure-enthalpy, P - h diagram. This type of diagram is most often used for refrigeration and air conditioning cycles, but lends itself very well to geothermal binary cycles.

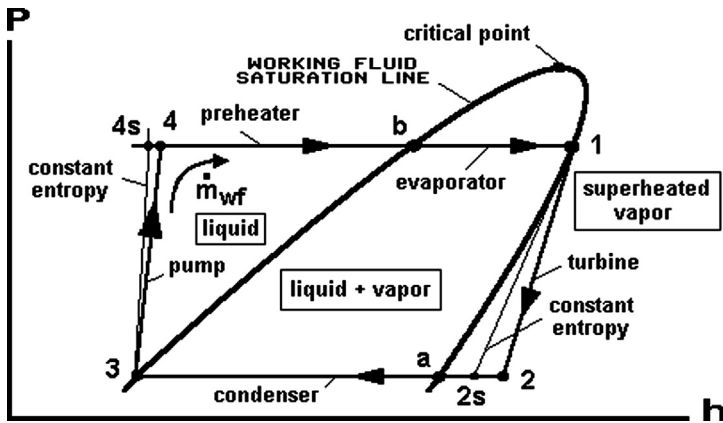


Figure 8.3 Pressure-enthalpy diagram for a basic binary plant.

8.2.1 TURBINE ANALYSIS

The thermodynamic analysis of the cycle is fairly straightforward. Beginning with the binary turbine, we find that the analysis is the same as for steam turbines. It will be useful to select the components from the system flow diagram for easy reference as we present the analysis; see Figure 8.4.

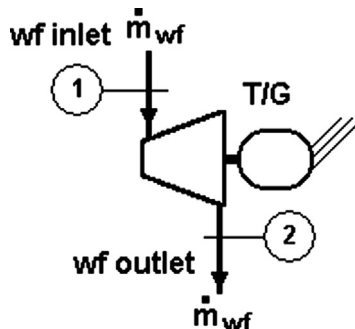


Figure 8.4 Turbine-generator for binary cycle.

With the usual assumptions of negligible potential and kinetic energy terms together with steady, adiabatic operation, the power is found from:

$$\dot{W}_t = \dot{m}_{wf}(h_1 - h_2) = \dot{m}_{wf}\eta_t(h_1 - h_{2s}) \quad (8.1)$$

where η_t is the isentropic turbine efficiency, which is a known quantity. For a given working fluid, the thermodynamic properties can easily be found from tables or correlations for whatever design parameters are chosen. The desired turbine power output will then determine the required working fluid mass flow rate.

8.2.2 CONDENSER ANALYSIS

Again the basic working equation is the same as for condensers in flash or dry-steam plants; see Figure 8.5.

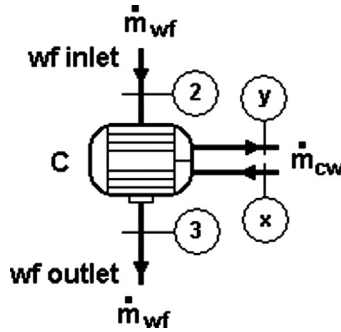


Figure 8.5 Condenser with cooling water.

The heat that must be rejected from the working fluid to the cooling medium, be it water (shown here) or air, is given by:

$$\dot{Q}_c = \dot{m}_{wf}(h_2 - h_3) \quad (8.2)$$

The relationship between the flow rates of the working fluid and the cooling water is:

$$\dot{m}_{cw}(h_y - h_x) = \dot{m}_{wf}(h_2 - h_3) \quad (8.3)$$

or

$$\dot{m}_{cw}\bar{c}(T_y - T_x) = \dot{m}_{wf}(h_2 - h_3) \quad (8.4)$$

if the cooling water may be taken as having a constant specific heat \bar{c} for the small temperature range from inlet to outlet. To dissipate the required amount of waste heat, a cooling tower with a specified range, $T_y - T_x$, will need a mass flow rate determined by Eq. (8.4).

8.2.3 FEED PUMP ANALYSIS

Using the same kind of assumptions as for the other components, the power imparted to the working fluid from the feed pump (see Figure 8.6) is:

$$\dot{W}_p = \dot{m}_{wf}(h_4 - h_3) = \dot{m}_{wf}(h_{4s} - h_3)/\eta_p \quad (8.5)$$

where η_p is the isentropic pump efficiency.

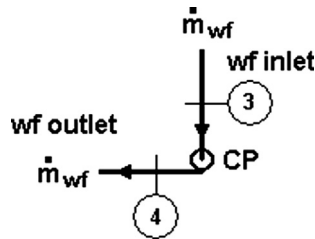


Figure 8.6 Feed pump for condensate.

8.2.4 HEAT EXCHANGER ANALYSIS: PREHEATER AND EVAPORATOR

The analysis of the heat exchanger where the geothermal brine transfers some of its thermal energy to the working fluid is another straightforward application of the principles of thermodynamics and mass conservation; see Figure 8.7.

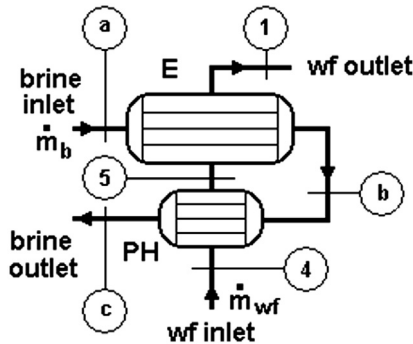


Figure 8.7 Preheater and evaporator.

We assume that the heat exchangers are well-insulated so that all the heat transfer is between the brine and the working fluid. In keeping with our overall assumptions, we also assume that the flow is steady, and that the differences in entering and leaving potential energy and kinetic energy are negligible. Considering the entire package as the thermodynamic system, the governing equation is:

$$\dot{m}_b(h_a - h_c) = \dot{m}_{wf}(h_1 - h_4) \quad (8.6)$$

If the brine has low dissolved gases and solids, the left-hand side of the equation may be approximated by the average specific heat of the brine \bar{c}_b times the temperature drop:

$$\dot{m}_b \bar{c}_b (T_a - T_c) = \dot{m}_{wf}(h_1 - h_4) \quad (8.7)$$

The following equation may be used to find the required brine flow rate for a given set of cycle design parameters:

$$\dot{m}_b = \dot{m}_{wf} \frac{h_1 - h_4}{\bar{c}_b (T_a - T_c)} \quad (8.8)$$

The design of the individual heat exchangers requires us to examine another thermodynamic diagram: the temperature-heat transfer or T - q diagram; see [Figure 8.8](#). The abscissa represents the total amount of heat that is passed from the brine to the working fluid. It can be shown either in percent or in heat units (say, kJ/kg wf).

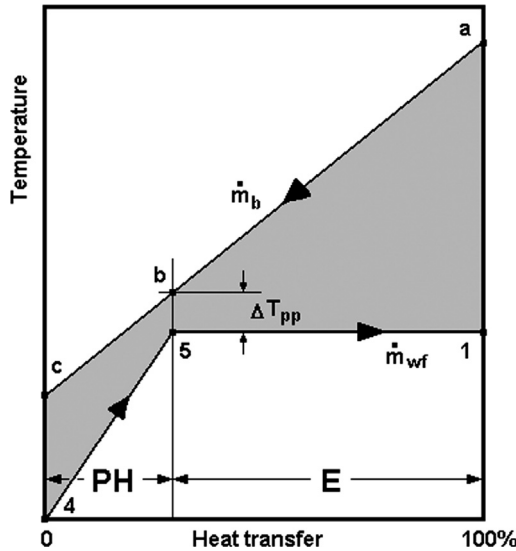


Figure 8.8 Temperature-heat transfer diagram for preheater and evaporator.

The preheater PH provides sensible heat to raise the working fluid to its boiling point, state 5. The evaporation occurs from 5 to 1 along an isotherm for a pure working fluid. The place in the heat exchanger where the brine and the working fluid experience the minimum temperature difference is called the pinch-point, and the value of that difference is designated the pinch-point temperature difference, ΔT_{pp} .

State points 4, 5, and 1 should be known from the cycle specifications: state 4 is a compressed liquid, the outlet from the feed pump; state 5 is a saturated liquid at the boiler pressure; and state 1 is a saturated vapor, the same as the turbine inlet condition. Thus, the two heat exchangers may be analyzed separately as follows:

$$\text{Preheater: } \dot{m}_b \bar{c}_b (T_b - T_c) = \dot{m}_{wf} (h_5 - h_4) \quad (8.9)$$

$$\text{Evaporator: } \dot{m}_b \bar{c}_b (T_a - T_b) = \dot{m}_{wf} (h_1 - h_5) \quad (8.10)$$

The brine inlet temperature T_a is always known. The pinch-point temperature difference is generally known from manufacturer's specifications; this allows T_b to be found from the known value for T_5 . While it is theoretically possible for the pinch-point to occur at the cold end of the preheater (for a very steep brine cooling line), this practically never happens.

The evaporator heat transfer surface area between the two fluids, A_E , can be determined from the basic heat transfer relationship:

$$\dot{Q}_E = \bar{U} A_E \text{LMTD}|_E \quad (8.11)$$

where \bar{U} is the overall heat transfer coefficient, LMTD is the log-mean-temperature difference, which for the evaporator is found from:

$$\text{LMTD}|_E = \frac{(T_a - T_1) - (T_b - T_5)}{\ln \left[\frac{T_a - T_1}{T_b - T_5} \right]} \quad (8.12)$$

and the evaporation heat transfer rate is given by:

$$\dot{Q}_E = \dot{m}_b \bar{c}_b (T_a - T_b) = \dot{m}_{wf} (h_1 - h_5) \quad (8.13)$$

The corresponding equations for the preheater are:

$$\dot{Q}_{PH} = \bar{U} A_{PH} \text{LMTD}|_{PH} \quad (8.14)$$

$$\text{LMTD}|_{PH} = \frac{(T_b - T_5) - (T_c - T_4)}{\ln \left[\frac{T_b - T_5}{T_c - T_4} \right]} \quad (8.15)$$

$$\dot{Q}_{PH} = \dot{m}_b \bar{c}_b (T_b - T_c) = \dot{m}_{wf} (h_5 - h_4) \quad (8.16)$$

The overall heat transfer coefficient \bar{U} should be determined by experiment with the appropriate fluids to be used in the plant. As a first approximation for preliminary calculations, the values shown in Table 8.1 may be used [4–7]. The uncertainty is large so caution is advised in the use of these values.

TABLE 8.1 Approximate values for \bar{U} for several situations [5–8].

Fluids	Overall heat transfer coefficient \bar{U}	
	Btu/h · ft ² · °F	W/m ² · K
Ammonia (condensing)—Water	150–250	850–1400
Propane or Butane (condensing)—Water	125–135	700–765
Refrigerant (condensing)—Water	80–150	450–850
Refrigerant (evaporating)—Brine	30–150	170–850
Refrigerant (evaporating)—Water	30–150	170–850
Steam—Gases	5–50	30–285
Steam—Water	175–600	1000–3400
Steam (condensing)—Water	175–1050	1000–6000
Water—Air	5–10	25–50
Water—Brine	100–200	570–1135
Water—Water	180–200	1020–1140

Since heat exchangers can be built in a variety of geometrical arrangements (e.g., shell-and-tube, plate, parallel flow, pure counterflow, multiple-pass counterflow or crossflow), there are correction factors that must be used with the equations given above depending on the configuration, and the reader is referred to any heat transfer book, such as Ref. [8], for more details.

8.2.5 OVERALL CYCLE ANALYSIS

Having analyzed each of the components of the basic binary plant, we can now sum up by looking at the cycle as a whole. The cycle performance can be assessed by the First Law using the thermal efficiency:

$$\eta_{th} \equiv \frac{\dot{W}_{net}}{\dot{Q}_{PH/E}} \quad (8.17)$$

Since the net power of the cycle is the difference between the thermal power input and the thermal power rejected, this formula may be rewritten as:

$$\eta_{th} = 1 - \frac{\dot{Q}_c}{\dot{Q}_{PH/E}} = 1 - \frac{h_2 - h_3}{h_1 - h_4} \quad (8.18)$$

The heat rejection ratio was derived as Eq. (5.27) in Section 5.4.6 and is repeated here:

$$\frac{\dot{Q}_c}{\dot{W}_{net}} = \frac{1}{\eta_{th}} - 1 \quad (8.19)$$

These formulas apply to the cycle, not the plant. If the net cycle power is used to supply plant auxiliary power needs, such as well pumps, cooling tower fans, station lighting, etc., then all these parasitic loads must be subtracted from the net cycle power to obtain the net plant power. Since binary cycles tend to have thermal efficiencies in the 10–13% range, any further reduction in net power can have a serious impact on plant performance.

Another measure of cycle and plant performance can be obtained using the Second Law in the form of the utilization efficiency, η_u , which is defined as the ratio of the actual net plant power to the maximum theoretical power obtainable from the geofluid in the reservoir state:

$$\eta_u \equiv \frac{\dot{W}_{net}}{\dot{E}_{res}} = \frac{\dot{W}_{net}}{\dot{m}_b[(h_{res} - h_0) - T_0(s_{res} - s_0)]} \quad (8.20)$$

where T_0 is the dead-state temperature (e.g., the local wet-bulb temperature if a water cooling tower is used), and h_0 and s_0 are the enthalpy and entropy values for the geofluid evaluated at the dead-state pressure and temperature (usually approximated as the saturated liquid values at T_0). The subjects of utilization efficiency and Second Law analysis are covered in depth in Chapter 10.

8.3 Working Fluid Selection

Before we move on to study more complex binary cycles, let us here consider the important matter of the selection of the working fluid. This design decision has great implications for the performance of a binary plant. While there are many choices available for working fluids, there are also many constraints on that selection that relate to the thermodynamic properties of the fluids as well as considerations of health, safety, and environmental impact.

8.3.1 THERMODYNAMIC PROPERTIES

Table 8.2 lists some candidate fluids and their relevant thermodynamic properties; pure water is included for comparison [9]. Clearly all of the candidate fluids have critical temperatures and pressures far lower than water. Furthermore, since the critical pressures are reasonably low, it is feasible to consider supercritical cycles for the hydrocarbons. As we will see shortly, this allows a better match between the brine cooling curve and the working fluid heating–boiling line, reducing the thermodynamic losses in the heat exchangers.

TABLE 8.2 Thermodynamic properties of some candidate working fluids for binary plants.

Fluid	Formula	T_c °C	T_c °F	P_c MPa	P_c lbf/in ²	P_s @ 300 K MPa	P_s @ 400 K MPa
Propane	C ₃ H ₈	96.95	206.5	4.236	614.4	0.9935	NA
<i>i</i> -Butane	<i>i</i> -C ₄ H ₁₀	135.92	276.7	3.685	534.4	0.3727	3.204
<i>n</i> -Butane	C ₄ H ₁₀	150.8	303.4	3.718	539.2	0.2559	2.488
<i>i</i> -Pentane	<i>i</i> -C ₅ H ₁₂	187.8	370.1	3.409	494.4	0.09759	1.238
<i>n</i> -Pentane	C ₅ H ₁₂	193.9	380.9	3.240	469.9	0.07376	1.036
Ammonia	NH ₃	133.65	272.57	11.627	1686.3	1.061	10.3
Water	H ₂ O	374.14	705.45	22.089	3203.6	0.003536	0.24559

Binary mixtures of these fluids have also been studied for use in geothermal binary plants. In particular, the thermodynamic properties of 90% *i*-C₄H₁₀ and 10% *i*-C₅H₁₂ were determined by the National Bureau of Standards (predecessor of the National Institute of Standards and Technology, NIST) in Washington Gaithersburg, MD [10] when it was chosen as the working fluid for the Heber Binary Demonstration plant in the 1980s; see Chapter 18. Mixtures evaporate and condense at variable temperature, unlike pure fluids that change phase at constant temperature. This means that subcritical-pressure boilers for mixed fluids can be better matched to the brine curves, in a manner similar to, but not exactly like, supercritical pure fluids.

Another important characteristic of binary candidate fluids is the shape of the saturated vapor curve as viewed in temperature–entropy coordinates; see Figure 8.9. This curve for water (shown as the thin line) has a negative slope everywhere, but certain hydrocarbons and refrigerants show a positive slope for portions of the saturation line. That is, there exists a local minimum in the

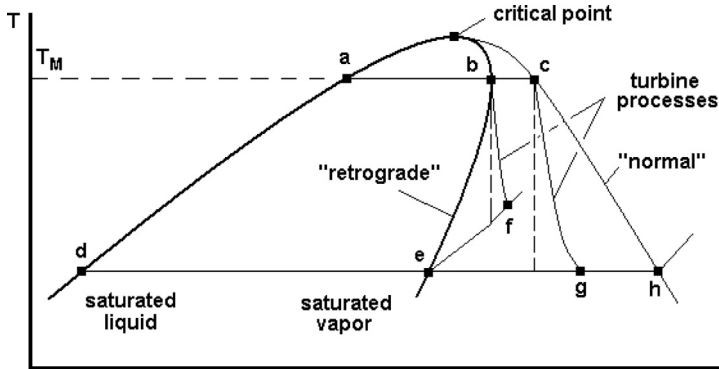


Figure 8.9 Temperature-entropy diagram contrasting normal and retrograde saturated vapor curves.

entropy at some low temperature, T_m , and a local maximum in entropy at a higher temperature, T_M . Retrograde fluids include normal- and iso-butane and normal- and iso-pentane. These fluids exhibit retrograde behavior over the following temperature ranges, $T_m \rightarrow T_M$: C_4H_{10} , $-3^\circ\text{C} \rightarrow 127^\circ\text{C}$; $i\text{-}C_4H_{10}$, $-3^\circ\text{C} \rightarrow 117^\circ\text{C}$; C_5H_{12} , $-3^\circ\text{C} \rightarrow 177^\circ\text{C}$; $i\text{-}C_5H_{12}$, $-13^\circ\text{C} \rightarrow 177^\circ\text{C}$. Since T_m is lower than any temperatures encountered in geothermal binary plants, for practical purposes these fluids can be taken as having saturated vapor lines similar to that shown in Figure 8.9. This has major implications for Rankine cycles.

On the one hand, normal fluids such as water require considerable superheat, extending the isobar a-b-c upwards, to avoid excessive moisture at the turbine exhaust, state g. On the other hand, retrograde fluids allow expansion from the saturated vapor line into the superheated region, process b-f, avoiding any moisture during the turbine expansion process. It has been shown [11] that it is possible to run a supercritical cycle in which the turbine inlet state lies above the critical point and the expansion line lies inside the wet region for a portion of the process, emerging into the superheated region, without suffering any wetness penalty in efficiency. Apparently, the fluid remains in a metastable vapor state while passing through the wet region by staying on the dry side of the Wilson line [12].

8.3.2 SONIC VELOCITY AND TURBINE SIZE

To a first approximation, the size of the turbine determines its cost, and its size can be estimated from its exit area. The mass flow rate through the turbine exit can be expressed as the product of the working fluid density, the cross-sectional area and the flow velocity:

$$\dot{m} = \rho A V \quad (8.21)$$

Since the mass flow rate is also given by:

$$\dot{m} = \dot{W}_t / w_t = \dot{W} / (h_1 - h_2) \quad (8.22)$$

the exit area can be found from:

$$A = \frac{\dot{W}_t}{h_1 - h_2} \frac{v_2}{Ka_2} \quad (8.23)$$

where we have replaced the density by its reciprocal, the specific volume v , and the fluid velocity by Ka_2 where K is a fraction and a_2 is the speed of sound in the fluid at the turbine exit. By definition, the speed of sound in a compressible medium is given by:

$$a = \left[\frac{dP}{d\rho} \right]_{s=\text{const}}^{1/2} \quad (8.24)$$

The sonic speed can be approximated from property tables and charts using finite differences:

$$a \approx \left[\frac{\Delta P}{\Delta \rho} \right]_{s=\text{const}}^{1/2} = \left[\frac{\Delta P}{\Delta(1/v)} \right]_{s=\text{const}}^{1/2} \quad (8.25)$$

We may now compare working fluids using the same power outputs and the same fraction of sonic speed at the turbine exhaust to examine their relative cross-sectional areas, and thus the relative sizes of their turbines. It turns out that ammonia has the smallest size turbine for the chosen comparison, and it is convenient to present the results as multiples of the area required for an ammonia turbine.

Table 8.3 gives the results using the approach outlined above. A similar analysis was carried out by Milora and Tester [13] using a different methodology

TABLE 8.3 Turbine size comparisons for several working fluids.^a

Fluid	Formula	Molar mass	Relative exit area ^b
Ammonia	NH ₃	17.03	1.0 (1.0)
Propane	C ₃ H ₈	44.09	2.3 (1.9)
<i>i</i> -Butane	<i>i</i> -C ₄ H ₁₀	58.12	4.1 (4.9)
<i>n</i> -Butane	C ₄ H ₁₀	58.12	5.5 (6.3)
<i>i</i> -Pentane	<i>i</i> -C ₅ H ₁₂	72.15	12.2 (NA)
<i>n</i> -Pentane	C ₅ H ₁₂	72.15	14.6 (NA)

^aTurbine inlet temperature = 400 K, saturated, except superheated for NH₃ and C₃H₈; condensing temperature = 320 K.

^bNumbers in parentheses are from Ref. [13].

involving the law of corresponding states, and their results are included in the table for comparison purposes. The analysis involves estimates and approximations, exhibited in the differences between the two approaches. However, the main result is the ranking of the working fluids by relative sizes of the turbines, and in this respect, the two approaches are in agreement. By way of comparison, steam would have a relative exit area of about 120.

8.3.3 HEALTH, SAFETY, AND ENVIRONMENTAL CONSIDERATIONS

Lastly, the environmental, safety, and health properties of potential working fluids must be considered. These include flammability, toxicity, ozone depletion potential (ODP) and global warming potential (GWP). Table 8.4 summarizes these properties for the fluids in Table 8.1, plus two chlorofluorocarbons that used to be considered candidate working fluids.

TABLE 8.4 Environmental and health properties of some candidate working fluids [14].

Fluid	Formula	Toxicity	Flammability	ODP	GWP
R-12	CCl_2F_2	Nontoxic	Nonflammable	1.0	4500
R-114	$\text{C}_2\text{Cl}_2\text{F}_4$	Nontoxic	Nonflammable	0.7	5850
Propane	C_3H_8	Low	Very high	0	3
<i>i</i> -Butane	$i\text{-C}_4\text{H}_{10}$	Low	Very high	0	3
<i>n</i> -Butane	C_4H_{10}	Low	Very high	0	3
<i>i</i> -Pentane	$i\text{-C}_5\text{H}_{12}$	Low	Very high	0	3
<i>n</i> -Pentane	C_5H_{12}	Low	Very high	0	3
R-32	CH_2F_2	Low	Low flammable	0	675
R-134a	$\text{C}_2\text{H}_2\text{F}_4$	Very low	Nonflammable	0	1300
R-245fa	$\text{C}_3\text{H}_3\text{F}_5$	Very low	Nonflammable	0	1020
Carbon dioxide	CO_2	Nontoxic	Nonflammable	0	1.0
Ammonia	NH_3	Toxic	Lower	0	0
Water	H_2O	Nontoxic	Nonflammable	0	—

The ODP is normalized at 1.0 for refrigerants R-11 and R-12 which are the worst in this regard. The GWP is normalized at 1.0 for carbon dioxide. Owing to their very high ODP and GWP, both R-12 and R-114 have been banned from use by the Copenhagen Amendment (effective as of 1994) to the Montreal Protocol (signed in 1987, effective as of 1989). The original binary plant at Paratunka in Russia that was installed in 1967 used R-12 as its working fluid.

The contribution of the hydrocarbons to global warming comes about mainly through the carbon dioxide that is a by-product of their decomposition. All of the hydrocarbon candidate fluids obviously are flammable and necessitate appropriate fire protection equipment on site, over and above the usual requirements for any power plant.

8.4 Advanced Binary Cycles

In this section we will discuss innovative and complex binary cycles, but before we tackle this subject, let us consider the theoretical optimum binary cycle for use with a geothermal hot water resource. This will give us a basis of comparison for all other types of binary plant.

8.4.1 IDEAL BINARY CYCLE

Basic binary plants have low thermal efficiencies mainly due to the small temperature difference between the heat source and the heat sink. The thermodynamic ideal cycle operating between a heat source at a temperature T_H and a heat sink at a temperature T_L is a Carnot cycle consisting of an isothermal heat addition process at T_H , followed by an isentropic expansion process, an isothermal heat rejection process at T_L , and an isentropic compression process to return the working fluid to its initial state [15].

The Carnot efficiency is the highest possible efficiency for any cycle operating between these two temperatures and is given by:

$$\eta_{CC} = \eta_{max} = 1 - \frac{T_L}{T_H} \quad (8.26)$$

where the temperatures must be in kelvins or degrees Rankine. For a geothermal binary plant using a brine at 150°C (423.15 K) and a heat sink at 40°C (313.15 K), the maximum ideal Carnot efficiency is 26%.

However, the brine is not an isothermal heat source, but in fact cools as it transfers heat to the working fluid. Thus, a more realistic ideal cycle for a geothermal binary plant is a triangular cycle consisting of an isobaric (constant pressure) heat addition process up to the brine inlet temperature T_H , followed by an isentropic expansion, and an isothermal heat rejection process at T_L to complete the cycle. It is easy to show [16] that the efficiency for the triangular cycle is given by:

$$\eta_{TRI} = \frac{T_H - T_L}{T_H + T_L} \quad (8.27)$$

For the same temperatures used in the above example, the triangular cycle yields an efficiency of 15%.

These two ideal cycles are shown in temperature-entropy coordinates in Figure 8.10.

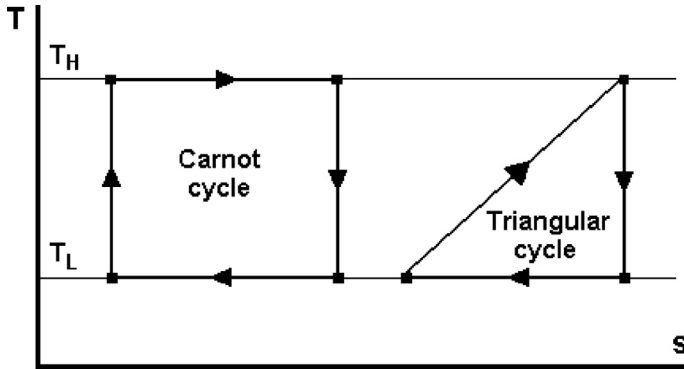


Figure 8.10 Two ideal thermodynamic cycles.

In recognition of the inherently low thermal efficiency of basic binary plants, there are several variations on the basic cycle aimed at achieving higher efficiencies. When a cycle has an efficiency of say 10%, an improvement of only one percentage point represents a 10% improvement, and this may make the difference between an economically viable project and one that is not. In the next sections we will discuss some of these innovative systems.

8.4.2 DUAL-PRESSURE BINARY CYCLE

A dual-pressure cycle is designed to reduce the thermodynamic losses incurred in the brine heat exchangers of the basic cycle. These losses arise through the process of transferring heat across a large temperature difference between the hotter brine and the cooler working fluid; see Figure 8.8, for example. By maintaining a closer match between the brine cooling curve and the working fluid heating–boiling curve these losses can be reduced.

The dual-pressure cycle has a two-stage heating–boiling process that allows the two fluids to achieve a smaller average temperature difference than the one-stage process used in a basic cycle. A schematic of a dual-pressure plant is given in Figure 8.11 and the corresponding process diagram is shown in Figure 8.12.

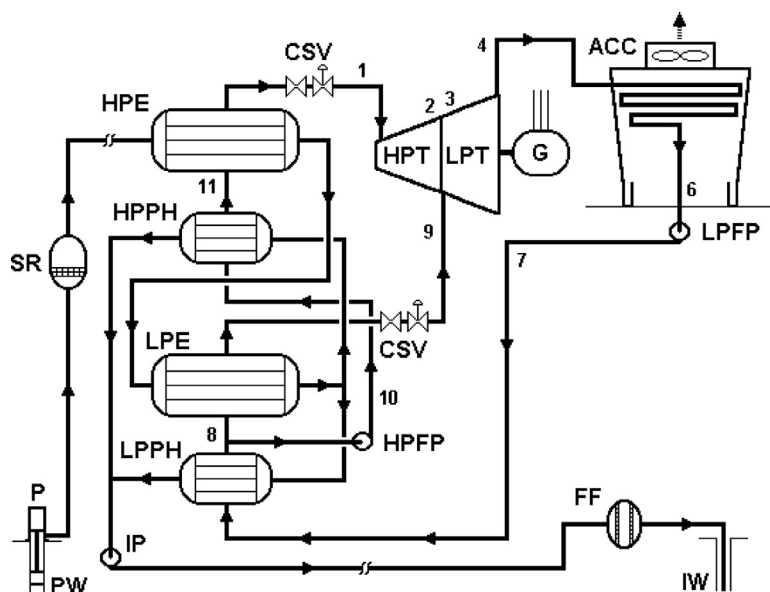


Figure 8.11 Dual-pressure binary plant: Simplified schematic flow diagram.

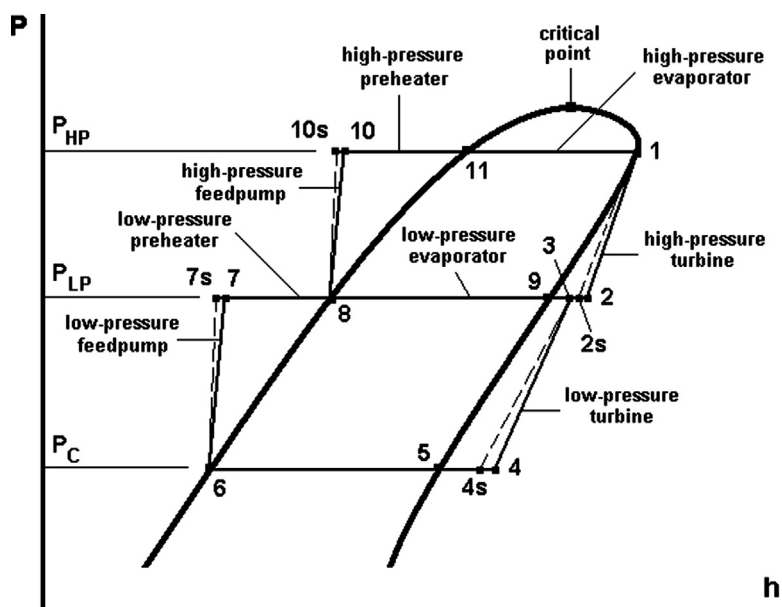


Figure 8.12 Dual-pressure binary plant: pressure-enthalpy process diagram.

A dual-admission turbine is shown in Figure 8.11 in which the low-pressure saturated vapor (state 9) is admitted to the turbine to mix with the partially expanded high-pressure vapor (state 2) to form a slightly superheated vapor (state 3). Given the small size of turbines using organic working fluids, practical considerations may lead to an alternative design using two separate turbines; see Figure 8.13.

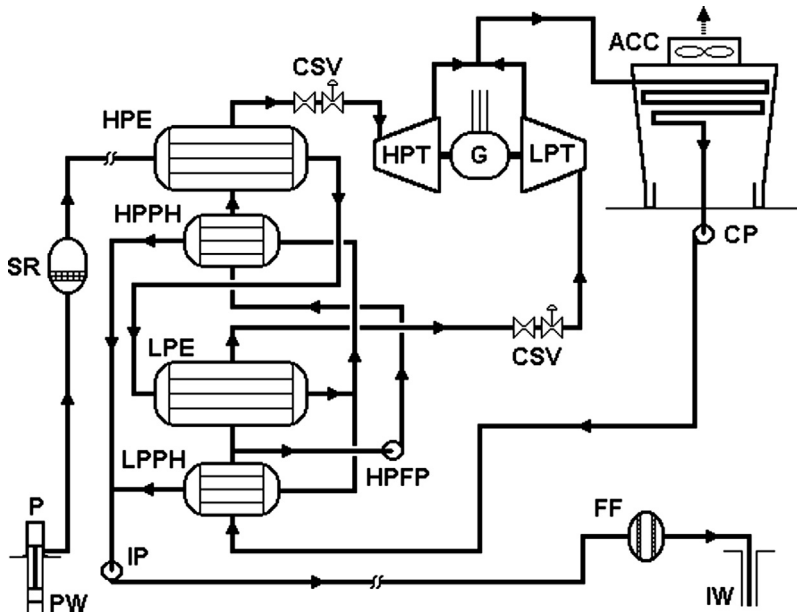


Figure 8.13 Dual-pressure binary plant: Separate high- and low-pressure turbines.

Unlike dry-steam and flash-steam plants, binary plants do not have steam condensate to serve as makeup for a water cooling tower. Thus binary plants need a separate cooling medium, either fresh water or air. An air-cooled condenser ACC is depicted here since makeup water for cooling towers is scarce at many geothermal sites.

The analysis of a dual-pressure cycle follows the same methodology as for a basic cycle but is merely longer. A detailed comparison of basic cycles (single-pressure) and the dual-pressure cycles has been conducted by Khalifa and Rhodes [17] for two different working fluids; their results are summarized in Table 8.4. The results are quite interesting. In all cases, the thermal efficiency for a dual-pressure cycle is actually lower than for a basic cycle, but the utilization efficiency for a dual-pressure cycle is significantly higher than for a basic cycle, ranging from a 6% advantage at the highest brine temperature to 24% at the lowest (Table 8.5).

TABLE 8.5 Comparison of efficiencies of single- and dual-pressure binary cycles [17].

Working fluid	Brine temperature	Thermal efficiency, %		Utilization efficiency, %	
		Basic	Dual pressure	Basic	Dual pressure
<i>i</i> -C ₄ H ₁₀	93°C (200°F)	5.5	4.6	31.9	39.7
<i>i</i> -C ₅ H ₁₂	93°C (200°F)	5.2	4.2	30.5	37.0
<i>i</i> -C ₄ H ₁₀	149°C (300°F)	10.3	9.8	48.8	56.9
<i>i</i> -C ₅ H ₁₂	149°C (300°F)	9.8	8.8	44.6	51.5
<i>i</i> -C ₅ H ₁₂	204°C (400°F)	13.7	13.1	57.7	61.2

Note: The condensing and dead-state temperatures were both taken as 38°C (100°F).

The thermal efficiency depends on the amount of heat added to the cycle but makes no distinction between high-exergy heat and low-exergy heat, and ignores the temperature difference between the fluids. Thermodynamics requires that the higher the average temperature of the heat added to a cycle, the higher will be the thermal efficiency, for the same heat sink temperature. Since a significant amount of heat is needed to evaporate the fluid from 8 to 9 (see Figure 8.12) at a relatively low temperature, this adversely affects the thermal efficiency of the dual-pressure cycle. However, the utilization efficiency depends on how effectively the exergy of the brine is used. By more closely matching the brine cooling curve with the heating and boiling curves, the average temperature difference between the two fluids is made smaller and the irreversibilities are reduced. This allows more exergy from the brine to enter the cycle and leads to a higher overall utilization efficiency.

The 5 MW Raft River Dual-Boiling plant in Idaho, United States, was the first to make use of the dual-pressure concept [18]. It was operated as a demonstration plant from 1981 to 1982 by the Idaho National Engineering Laboratory for the US Department of Energy; see Section 20.3.

8.4.3 DUAL-FLUID BINARY CYCLE

It may sound odd but the first commercial binary plant in the United States was a remarkably advanced design, the Magmamax plant at East Mesa in California's Imperial Valley. It was a 12.5 MW plant that began operations in 1979 using a dual-fluid cycle in which two different hydrocarbons were used in interlocking Rankine cycles, one a subcritical cycle and one a supercritical cycle [19,20]. We will present a detailed case study of this plant in Chapter 18; here we will describe the thermodynamic principles that underlie the design of such a system.

The dual-fluid binary cycle shown in Figure 8.14 features a heat recuperator E2 that links the upper cycle having fluid 1 and the lower cycle having fluid 2.

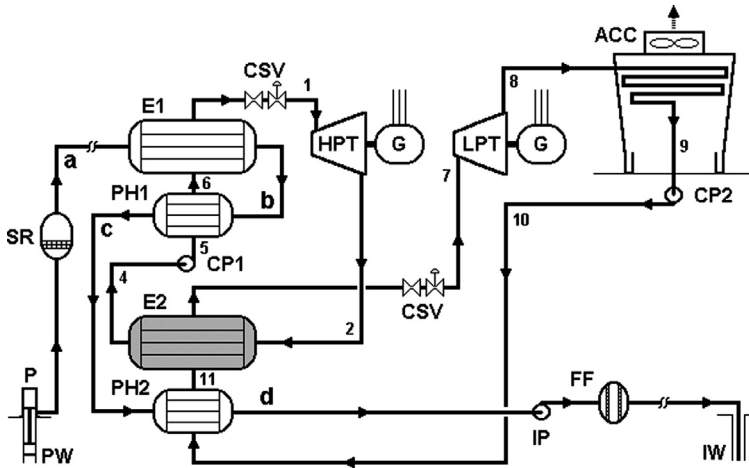


Figure 8.14 Dual-fluid cascaded binary cycle featuring a heat recuperator.

The process diagram is given in [Figure 8.15](#) in temperature-entropy coordinates. Note that there are two entropy axes, one for each working fluid; the saturation curves are drawn in a convenient location to illustrate the relationship between the two cycles. If the fluids are selected judiciously according to their thermodynamic properties, they will complement one another to create synergy in the overall dual cycle.

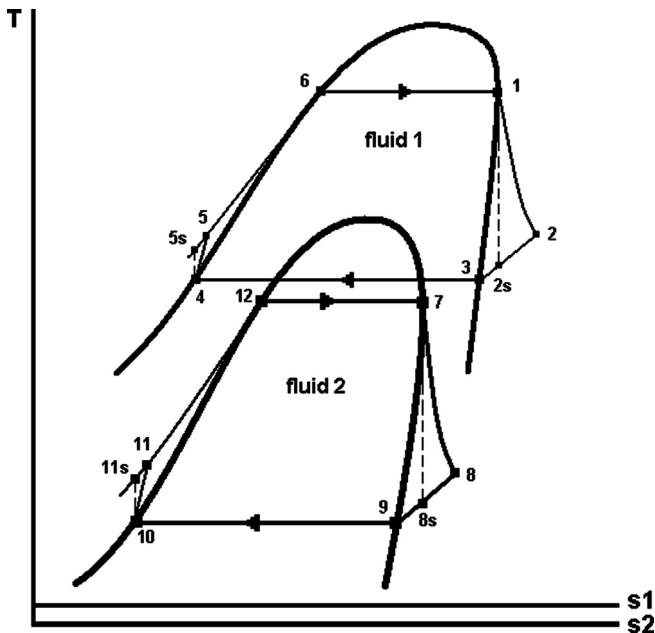


Figure 8.15 Dual-fluid process diagram in temperature-entropy coordinates.

As with the dual-pressure cycle, the motivation here is to create a good match between the brine and the working fluid heating—boiling curves. The temperature-heat transfer diagram, [Figure 8.16](#), shows this relationship. The discontinuity between state points 5 and 11 arises from the internal heat transfer between the working fluids and does not involve the brine. From the diagram it can be seen that the pinch-point occurs between state b on the brine cooling curve and state 6, the bubble point for fluid 1. The near-parallelism between the brine and the working fluids in the preheaters means that the thermodynamic irreversibilities will be low, as will the loss of exergy during the heat transfer process in those components. Since the average temperature difference in the fluid 1 evaporator is relatively large, there will be a higher loss of exergy there.

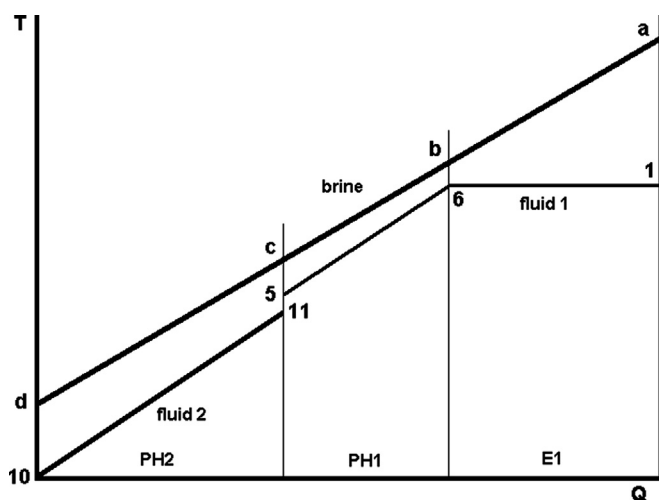


Figure 8.16 Dual-fluid binary plant: Temperature-heat transfer diagram for brine heat exchangers with subcritical working fluid pressures.

Note that all cycles considered so far in this chapter have been subcritical cycles, that is, the pressure of the working fluids in the brine heat exchangers is less than the critical pressure. If fluid 1 is raised to a supercritical pressure before entering its preheater, the temperature-heat transfer diagram would change dramatically; see [Figure 8.17](#). The sharp corner at state 6 denoting the bubble point for fluid 1 has vanished. Fluid 1 now has a smooth heating curve that takes the fluid from a cool compressed liquid to a hot supercritical vapor. There will still be a point of closest approach between the two curves, but it will be far

less pronounced. This now allows a very good match between the brine and the working fluids that will result in lower exergy losses and a higher utilization efficiency for the cycle.

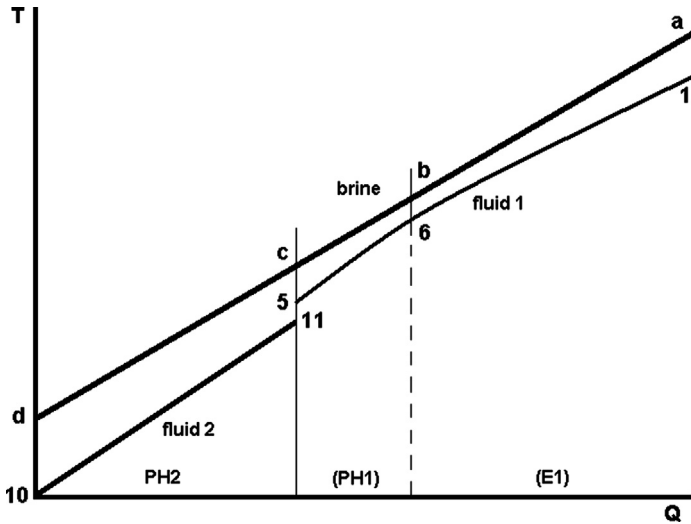


Figure 8.17 Dual-fluid binary plant: Temperature-heat transfer diagram for brine heat exchangers with supercritical pressure for working fluid 1.

The cycle thermal efficiency (net power/heat input) for a supercritical vapor generator will exceed that for a subcritical cycle. Using isobutane as the working fluid with a turbine inlet temperature of 420 K and a condensing temperature of 320 K, a turbine isentropic efficiency of 85% and a feed pump isentropic efficiency of 80%, the following results are obtained for two different vapor generator pressures:

4.0 MPa (supercritical): $\eta_{th} = 12.3\%$, $w_p = 16\%$ of $w_{net,cycle}$;

3.0 MPa (subcritical): $\eta_{th} = 11.0\%$, $w_p = 11\%$ of $w_{net,cycle}$.

The supercritical cycle has a 12% higher thermal efficiency. Notice, however, that in the supercritical cycle, the pump work is a greater fraction than of the net cycle work and is 45% higher than for the subcritical cycle.

There are practical difficulties, however, with a supercritical cycle. The higher pressures may require thicker, more costly tubing in the heat exchangers unless the fluid pressures on each side are made nearly equal. Thicker tubes offer more

resistance to heat transfer and require longer, more expensive heat exchangers. There is no distinction between the preheater and the evaporator since there is no conventional phase transition. Rather, a continuous process of increasing temperature occurs as the working fluid receives heat from the brine. In a traditional fossil-fueled power plant using supercritical water/steam, this transition occurs in a long series of tubes within the furnace, in what is called a “once-through” steam generator. In geothermal binary plants, shell-and-tube heat exchangers having the brine in the tubes and the working fluid within the shell are appropriate for sub-critical operation, but are ill-suited for supercritical operation. This was a main reason that the original Magmamax plant [19] placed the supercritical isobutane inside the tubes and the brine on the shell side of the heat exchangers.

8.4.4 KALINA BINARY CYCLES

Water-ammonia mixtures have long been used in absorption refrigeration cycles, but it was not until A. Kalina patented his Kalina cycle that this working fluid was used for power generation cycles. A typical Kalina cycle, KCS-12, is shown schematically in Figure 8.18. The features that distinguish the Kalina cycles (there are several versions) from other binary cycles are as follows:

- The working fluid is a binary mixture of H_2O and NH_3 .
- Evaporation and condensation occur at variable temperature.
- Cycle incorporates heat recuperation from turbine exhaust.
- Composition of the mixture may be varied during cycle in some versions.

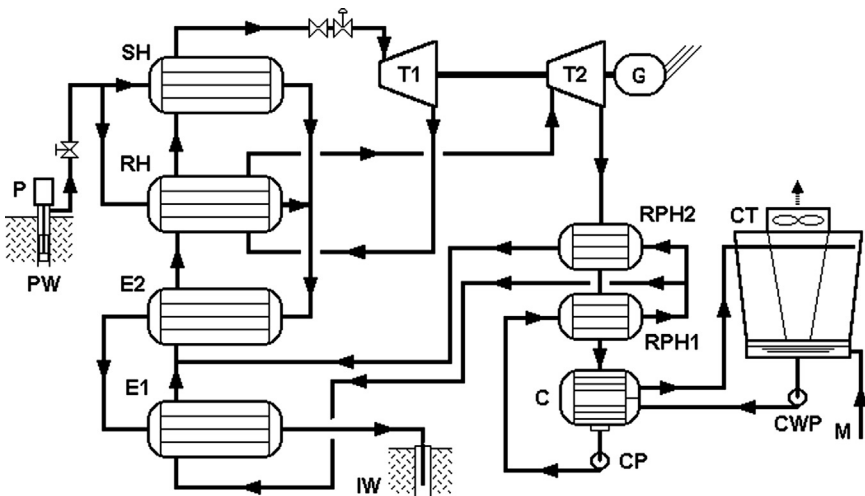


Figure 8.18 Typical Kalina cycle employing a reheater and two recuperative preheaters.

As a consequence, Kalina cycles show improved thermodynamic performance of heat exchangers by reducing the irreversibilities associated with heat transfer across a finite temperature difference. The heaters are so arranged that a better match is maintained between the brine and the mixture at the cold end of the heat transfer process where improvements in exergy preservation are most valuable.

A reheater RH is needed because the water-ammonia mixture has a normal saturated vapor line, that is, $dT/ds < 0$, leading to wet mixtures in the turbine. The plant relies on good heat exchangers because more heat is transferred than in a supercritical binary plant of the same power output. Bliem and Mines [21] showed that the Kalina cycle of Figure 8.18 requires about 25% more heat transfer. A possible advantage to using the recuperative preheaters is that they reduce the heat load on the condenser and cooling tower. The lower capital cost for a smaller condenser and cooling tower must be compared to the extra cost for the recuperators; over the long haul, the resulting higher efficiency should mean lower operating costs.

The physical plant is more complex than a basic binary plant, particularly when a distillation column is used to vary the mixture composition. The simplest configuration of Kalina cycle with variable working fluid composition is shown in Figure 8.19. The separator S allows a saturated vapor that is rich in ammonia to flow to the turbine, thus permitting a smaller and less costly turbine than for a hydrocarbon working fluid. The weak solution, a liquid rich in water, is used in the preheater and then throttled down to the turbine exhaust pressure before mixing with the strong solution to restore the primary composition. The mixture is then used in a recuperative preheater RPH prior to being fully condensed.

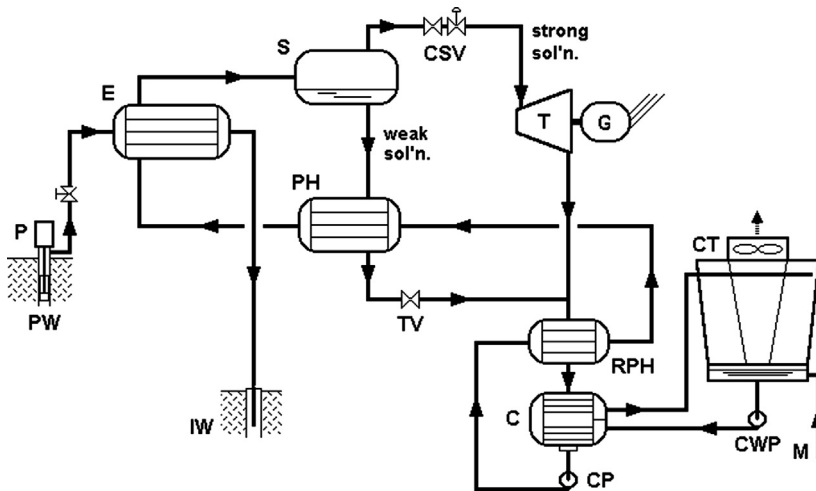


Figure 8.19 Kalina cycle with variable composition of the water-ammonia working fluid.

A possible difficulty for the Kalina cycle, one that is common to all cycles that strive for high efficiency, is maintaining very tight pinch-point temperature differences in the heat exchangers. Also, the advantage of variable temperature condensation is lessened because the condensing isobars of the ammonia-rich $\text{NH}_3\text{-H}_2\text{O}$ mixtures used in power cycles are concave upward, leading to a pinch-point. Thus, there are relatively large temperature differences at the start of and at the end of the condensing process. The same upward curvature at the hot end of the cycle produces large temperature differences in the middle of the evaporator.

8.5 Example of Binary Cycle Analysis

We will illustrate the analysis of a binary cycle using the simple case shown in Figure 8.20. We will assume the working fluid is isopentane, $i\text{-C}_5\text{H}_{12}$, and that the cycle has a subcritical boiler pressure. The net cycle power is 1200 kW, a typical value for this type of plant. Pressure losses in all heat exchangers and piping will be assumed negligible.

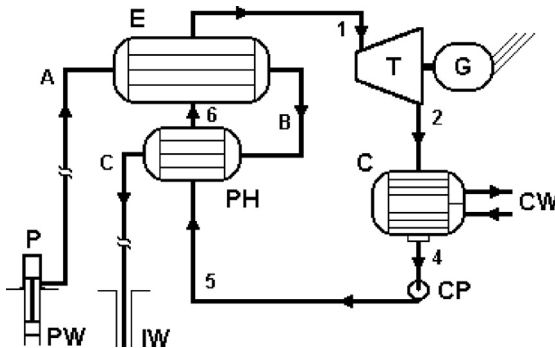


Figure 8.20 Basic binary plant with state-point notations.

The cycle specifications are as follows:

- Brine inlet temperature, $T_A = 440 \text{ K}$
- Brine specific heat, $c_b = 4.19 \text{ kJ/kg} \cdot \text{K} = \text{constant}$
- Brine density $= 897.2 \text{ kg/m}^3$ or 56 lbm/ft^3
- Pinch-point temperature difference $= 5 \text{ K}$
- Preheater-evaporator pressure, $P_5 = P_6 = P_1 = 2.0 \text{ MPa}$
- Condensing temperature, $T_4 = 320 \text{ K}$
- Turbine isentropic efficiency $= 85\%$
- Feed pump isentropic efficiency $= 75\%$.

Our objectives in this example will be to determine the following quantities:

1. Specific work of the turbine, w_t , in kJ/kg $i\text{-C}_5\text{H}_{12}$
2. Heat rejected to the cooling water, q_c , in kJ/kg $i\text{-C}_5\text{H}_{12}$
3. Specific work of the feed pump, w_p , in kJ/kg $i\text{-C}_5\text{H}_{12}$
4. Heat transferred to the working fluid, q_{IN} , in kJ/kg $i\text{-C}_5\text{H}_{12}$
5. Cycle thermal efficiency, η_{th} in %
6. Mass flow rate of $i\text{-C}_5\text{H}_{12}$, $\dot{m}_{i\text{-C}_5}$, in kg/s
7. Mass flow rate of brine, \dot{m}_b , in kg/s
8. Brine outlet temperature, T_c , in K
9. Number of wells needed if a typical well can produce 800–900 GPM.
10. Utilization efficiency for the dead-state temperature of 25°C.

While this may appear a tall order, it will be seen that a systematic approach will yield results without much difficulty.

We begin by translating the description of the plant into two thermodynamic process diagrams: a pressure–enthalpy diagram and a temperature–entropy diagram. The former will be very useful because there exist scale-drawn property charts for isopentane in P – h coordinates, and both are helpful in visualizing the cycle (Figure 8.21).

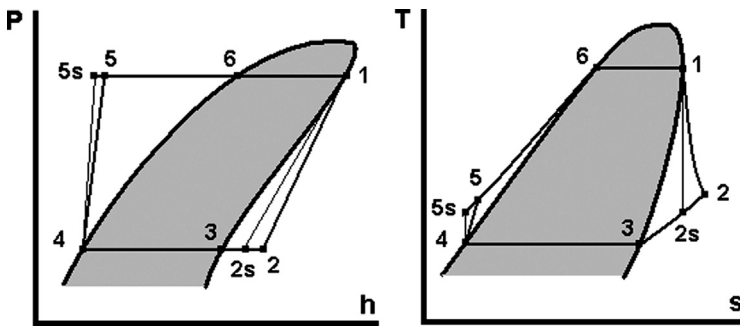


Figure 8.21 Pressure–enthalpy and temperature–entropy diagrams.

From the analysis presented in Section 8.2, it is clear that we must determine the enthalpy values for the isopentane at the six state points in the cycle. This is facilitated by using a table to keep track of the calculations. The numbers in

bold face are given or obvious. The other numbers have been found using the procedure described below.

State	P , MPa	T , K	v , m ³ /kg	s , kJ/kg · K	h , kJ/kg	Comments for h
1	2.0	427.1		2.2022	741.08	Direct from table
2	0.1866				663.38	From η_t
2s	0.1866			2.2022	649.66	Interpolation
3	0.1866	320		1.9887	578.16	Direct from table
4	0.1866	320	0.001686		249.50	Direct from table
5	2.0				253.58	From η_p
5s	2.0				252.56	From $v \times \Delta P$
6	2.0				545.73	Direct from table

The properties of isopentane were obtained from Reynolds' data book [9] which includes a scale-drawn P - h diagram.

- State 1: Saturated vapor at 2 MPa: $s_1 = 2.2022$ kJ/kg · K, $h_1 = 741.08$ kJ/kg.
- State 2: Actual turbine outlet state; must find isentropic outlet state first.
- State 2s: Isentropic turbine outlet state; $s_{2s} = s_1$, $P_2 = P_{sat}$ for $T_3 = 320$ K. By interpolation, $h_{2s} = 649.66$ kJ/kg.
- State 2: Using the definition of the turbine efficiency, Eq. (5.9), we can find h_2 : $h_2 = h_1 - \eta_t(h_1 - h_{2s}) = 663.38$ kJ/kg
- State 3: Saturated vapor at $T_3 = 320$ K: $s_3 = 1.9887$ kJ/kg · K, $h_3 = 578.16$ kJ/kg.
- State 4: Saturated liquid at $T_3 = 320$ K: $v_4 = 0.001686$ m³/kg, $h_4 = 249.50$ kJ/kg. We record the specific volume v_4 because we can use a very good approximation to find the enthalpy at state 5s.
- State 5: Actual pump outlet state; must find isentropic outlet state first.
- State 5s: Isentropic pump outlet state; $P_{5s} = 2$ MPa. Because the liquid is very nearly incompressible (i.e., constant density), to a high degree of accuracy, the value of h_{5s} can be found from: $h_{5s} \approx h_4 + v_4(P_{5s} - P_4) = 252.56$ kJ/kg.
- State 5: The definition of the pump efficiency is similar to that for the turbine but the numerator is the isentropic work and the denominator is the actual work; thus, we can find h_5 : $h_5 = h_4 + (h_{5s} - h_4)/\eta_p = 253.58$ kJ/kg.
- State 6: Saturated liquid at 2 MPa: $h_6 = 545.73$ kJ/kg.

With all the enthalpy values in hand, we can easily find the first six of our objectives:

1. Specific work of the turbine: $w_t = h_1 - h_2 = 77.70$ kJ/kg i -C₅H₁₂
2. Heat rejected to the cooling water: $q_c = h_2 - h_4 = 413.88$ kJ/kg i -C₅H₁₂

At this point we must check our assumption about the location of the pinch-point. Since the feed pump outlet temperature T_5 is not much higher than the pump inlet temperature T_4 (320 K), it is clear that the pinch-point in fact does occur at the bubble point. Indeed we notice that the brine temperature does not drop very much as it passes through the plant, losing only about 20°C.

9. Number of wells needed if a typical well can produce 800–900 GPM: The number of wells, N_W , is easily found from the previously obtained results: $N_W = \dot{m}_b / \dot{m}_{per\ well}$. The calculation involves merely attending to units conversions; let us convert the brine flow rate from kg/s to GPM:

$$96.2 \frac{\text{kg}}{\text{s}} \times \frac{2.204 \text{ lbm}}{1 \text{ kg}} \times \frac{1 \text{ ft}^3}{56 \text{ lbm}} \times \frac{1 \text{ gal}}{0.1337 \text{ ft}^3} \times \frac{60 \text{ s}}{1 \text{ min}} = 1700 \text{ GPM}$$

Therefore, $N_W = 1700/850 = 2$ wells.

10. Utilization efficiency for a dead-state temperature of 25°C: Finally the utilization efficiency can be found:

$$\eta_u = \frac{\dot{W}_{net}}{\dot{m}_b [h_A - h_0 - T_0(s_A - s_0)]}.$$

Assuming the brine behaves as pure water we can find the brine enthalpy and entropy values from Reynolds' data book [9]:

$$h_A = 705.0 \text{ kJ/kg}, s_A = 2.0096 \text{ kJ/kg} \cdot \text{K}, h_0 = 103.93 \text{ kJ/kg}, s_0 = 0.36384 \text{ kJ/kg} \cdot \text{K}.$$

Thus the result is:

$$\eta_u = \frac{1200}{96.2 \times 110.39} = \frac{1200}{10,619.2} = 0.113 \text{ or } 11.3\%$$

Discussion: The reader will observe that the thermal efficiency is fairly high for a simple binary plant (15% versus typ. 10–13%), but that the utilization efficiency is very poor, even lower than the thermal efficiency. Why? With the pinch-point located at the bubble point and with so much heat required to preheat the isopentane, the irreversibilities in the preheater are very large due to the very large average temperature difference. If the boiler pressure were lowered, the evaporating line 6-1 in Figure 8.19 would drop and point 6 would move down and to the left, providing a more balanced heat load between the evaporator and the preheater. This would also lower the brine outlet temperature, and result in a lower brine flow rate. Thus the brine exergy rate would be less for the same net power output and the utilization efficiency would rise. Can you imagine the effect this would have on the cycle thermal efficiency? Problem 8.9 at the end of the chapter will allow you to explore this problem further.

8.6 Environmental Impact of Binary Cycles

Geothermal binary plants are among the most benign of all power plants regarding environmental impact. A review of the binary plant flow diagrams in this chapter will reveal that the only impact on the environment takes place at the heat rejection side of the plant. Since the geofluid is pumped from the reservoir and returns entirely to the reservoir after passing through heat exchangers, the potentially harmful geofluid never sees the light of day. Furthermore, the cycle working fluid is contained completely within pipes, heat exchangers, and the turbine, so that it too never comes in chemical or physical contact with the environment.

The only possible form of pollution from a binary plant might be called thermal pollution, that is, the amount of heat that must be rejected from the cycle in accordance with the laws of thermodynamics. As was mentioned in Section 5.4.6, geothermal plants of all types discharge more waste heat per unit of power output than other thermal power plants. In the case of a basic binary plant, the amount of thermal power that needs to be absorbed by the surroundings is about nine times the useful power delivered by the plant [22]. Even this effect can be minimized if there is a beneficial use for the waste heat such as soil or greenhouse heating. It is interesting to note that the first binary plant at Paratunka on the cold Russian Kamchatka peninsula used the waste heat to assist farmers in extending their growing season [23].

8.7 Equipment List for Basic Binary Plants

Binary plants differ considerably in their equipment requirements from flash- or dry-steam plants. Where they do not differ, the item is simply shown as a bullet item; otherwise it carries an annotation.

8.7.1 DOWNWELL PUMPS AND MOTORS

- Multistage centrifugal pumps, lineshaft-driven from surface-mounted electric motors or submersible electric pumps

8.7.2 BRINE SUPPLY SYSTEM

- Sand removal system
Solids knock-out drum

8.7.3 BRINE/WORKING FLUID HEAT EXCHANGERS

- Preheater
Horizontal cylinder, liquid—liquid, shell-and-tube type with brine on tube side and working fluid on shell side, or vertical, corrugated plate type
- Evaporator/superheater
Horizontal cylinder or kettle-type boiler
Superheater section (optional)
Brine on tube side, working fluid on shell side

8.7.4 TURBINE-GENERATOR AND CONTROLS

- Working-fluid turbine (axial or radial flow), generator, and accessories

8.7.5 WORKING FLUID CONDENSER, ACCUMULATOR, AND STORAGE SYSTEM

- Condenser
- Dump tank and accumulator
Holding tank large enough to store full capacity of working fluid charge
- Evacuation pumps to remove working fluid to storage during maintenance

8.7.6 WORKING FLUID FEED PUMP SYSTEM

- Condensate pumps
- Booster pumps (as needed)

8.7.7 HEAT REJECTION SYSTEM

- Wet cooling system
Water cooling tower with external source of makeup water
Cooling water pumps and motors
Cooling water treatment system (as needed)
- Dry cooling system (if a source of makeup water is not available)
Air-cooled condensers with manifolds and accumulator
Induced draft fans and motors

8.7.8 BACKUP SYSTEMS

- Standby power supply

8.7.9 BRINE DISPOSAL SYSTEM

- Brine return pumps and piping
Horizontal, variable-speed, motor-driven units
High-head, high-volume flow design

8.7.10 FIRE PROTECTION SYSTEM (IF WORKING FLUID IS FLAMMABLE)

- High-pressure sprinkler system
- Flare stack

8.8 Pumps

8.8.1 INTRODUCTION

Reliable and efficient pumps are paramount for the successful operation of geothermal power plants, especially so for binary plants. Geothermal pumps may be categorized as either subsurface (or downhole) or surface pumps. The former are used almost exclusively with binary plants whereas the latter are deployed at all types of plants. Surface pumps may be used to transport or reinject brine, convey cooling water, repressurize organic working fluids, lift condensate to cooling towers, and evacuate noncondensable gases from condensers. In certain cases, where it is necessary to inject chemical inhibitors downhole to prevent scaling in the wellbore, positive displacement metering pumps are deployed at each well needing treatment.

8.8.2 DOWNHOLE PUMPS

The development of reliable downhole pumps began in the 1970s when the first binary plants were introduced commercially. Since binary plants generally exploit lower temperature geofluids that normally cannot be produced without pumping, plants could not be effectively operated until pumps could be depended upon to provide long service times. In other cases where wells were capable of self-flowing but were prone to wellbore clogging due to calcite precipitation induced by flashing in the well, pumps provided the pressure boost to maintain the noncondensable gases in solution and prevented calcite scaling. Unlike surface pumps which may be deployed in redundant sets such as three 50% capacity circulating water pumps, downhole pumps must work reliably as there can be no back up.

There are two basic types of downhole pumps: Lineshaft mechanical pumps driven by an electric motor from the wellhead and electric submersible pumps where the motor resides deep in the well below the pump impellers and is driven by electricity conducted down the well by a cable; see [Figures 8.23 and 8.24](#). Both types employ multi-stage centrifugal impellers. Each type has its advantages and disadvantages shown in [Table 8.6 \[24\]](#).

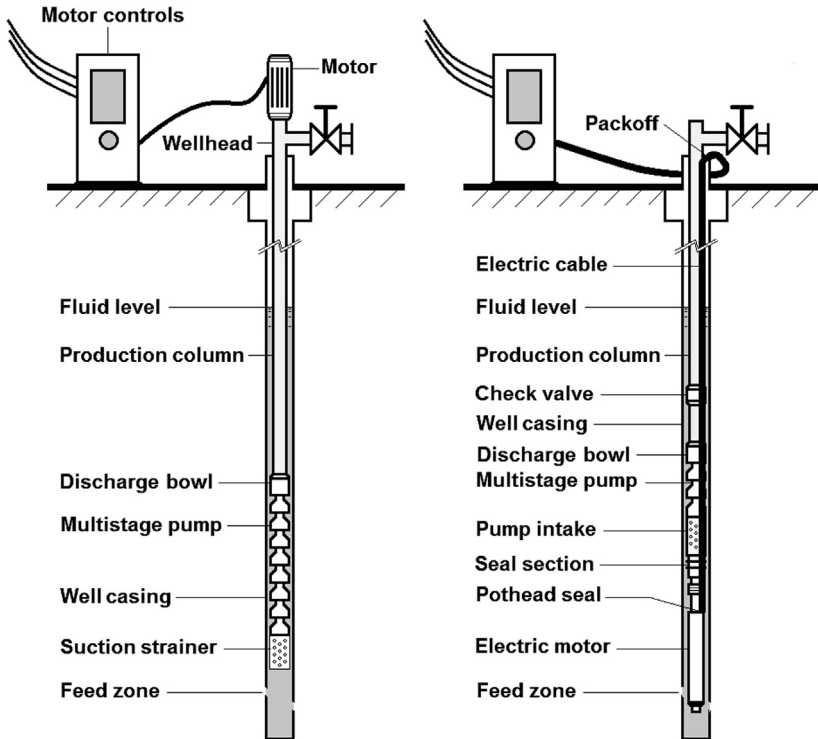


Figure 8.23 Schematic arrangement of (A) lineshaft and (B) electric submersible downhole pumps (not to scale).

There are several other possible types of downhole pumps such as gas-lift, hydraulic, and steam and gas turbine pumps, but none of these have gained commercial acceptance in the geothermal field.

The purpose of a downhole pump is to increase the flow rate over natural flow, if the well is so capable, or to produce from a well that is not capable of

self-flow. The pump must maintain the geofluid pressure high enough to prevent steam flashing or breakout of noncondensable gases. The pump must have an inlet pressure sufficiently high to avoid cavitation within the impeller. Owing to internal pressure losses on the suction side of the impeller, the brine pressure may

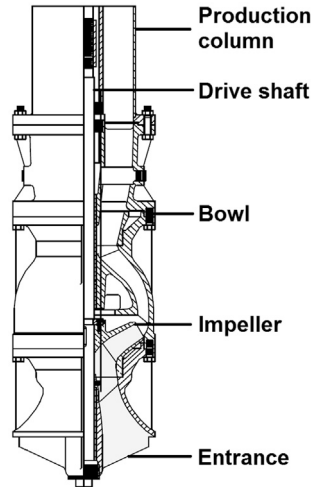


Figure 8.24 Detail of impeller-bowl assembly for an electric submersible pump.

TABLE 8.6 Typical characteristics of geothermal lineshaft and submersible downhole pumps.

Mechanical lineshaft pumps	Electric submersible pumps
Limited setting depths, ~ 350 m	Very deep settings possible, ~ 1000 m
Wells must be practically vertical	Wells need not be vertical
Time-consuming installation	Relatively quick installation
Motor, thrust bearing and seal accessible at surface	Motor, thrust bearing, seal and power cable immersed in brine
Higher temperature capability, $\sim 200^{\circ}\text{C}$	Limited upper temperature, $\sim 160^{\circ}\text{C}$
Motor sizes up to 750 kW	Motor sizes to 1500 kW
Higher pump and motor efficiency	Lower pump and motor efficiency
Less wear due to lower speeds	More wear due to higher speeds
Generally less expensive	Generally more expensive
Extensive of field experience	Limited field experience
Predictable maintenance schedule	Routine inspection maintenance
Lower likelihood of repairs	Higher likelihood of repairs
Flow rates ~ 500 m ³ /h	Flow rates ~ 900 m ³ /h
Delivery pressures up to 7 MPa	Delivery pressures up to 7.5 MPa

fall to its vapor pressure before reaching the discharge side of the pump; see Figure 8.25. From a to b to c the pressure falls due to friction and the entrance loss; friction causes the loss from c to d; from d to e the velocity increases causing additional pressure loss; the drop from f to g occurs upon entering the impeller vane tips; then the pressure increases from centrifugal force from g to h.

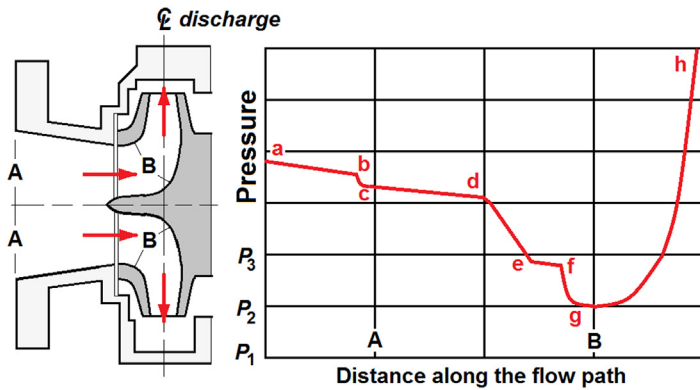


Figure 8.25 Liquid pressure behavior through a centrifugal pump [WWW].

If the vapor pressure of the liquid equals P_1 , this pump is safe from cavitation. If it is P_2 , there will likely be some cavitation. It might start at or just upstream of point g where the brine may begin to vaporize or cavitate. Small steam bubbles so formed will be carried with the liquid into a region of increasing pressure where they will collapse and exert tremendous localized pressure on the surface of the impeller vanes. This can cause pitting and erosion of the material, thus weakening the impeller. Continued or repeated cavitation can lead to fracture and pump failure, often by catastrophic means. If the vapor pressure is P_3 , there will be severe cavitation leading to premature failure of the pump; such a design must be avoided.

To avoid this problem, pump manufacturers specify a minimum net positive suction head (*NPSH*) that must be maintained at all times during pump operation [25]. This is called the *required NPSH* and is denoted as $NPSH_R$. It is the job of the engineer to so design the pumping system that a system head available to the pump is greater than the $NPSH_R$. This is called the *available NPSH*, or $NPSH_A$. The $NPSH_A$ is calculated as follows:

$$NPSH_A = H_A \pm H_Z - H_F + H_V - H_{VP} \quad (8.28)$$

where each head term is defined below. Note that each term is measured in units of length (or height) of the liquid being pumped, for example, feet of water, meters of isobutane (for surface pumps), etc.

- H_A is the absolute pressure on the free surface of the liquid being pumped.
- H_Z is the vertical distance between the free surface of the liquid and the pump centerline, positive when above and negative when below the centerline.
- H_F represents the friction losses in the suction piping, including fittings and abrupt changes in flow area that impede the liquid flowing to the pump inlet.
- H_V is the velocity head at the pump suction port; this is relatively small and often is ignored in the calculation.
- H_{VP} is the absolute vapor pressure of the liquid at the pumping temperature. Since this is the pressure that must be avoided, it is a negative term in the equation.

The $NPSH_R$ must be accounted for in all pumps, both surface and downhole. However, since failure of a downhole pump leads to very costly and time-consuming repairs while the plant is forced to operate at partial load, if at all, it is most crucial that these pumps be well designed and placed. The setting depth should maintain the $NPSH_A > NPSH_R$. In determining the appropriate setting depth, it must be recognized that the free surface of the liquid in the well will be drawn down from its static position once the pump goes into operation. Also since the vapor pressure rises as the geofluid temperature rises, consideration must be given to the case where hotter fluid may reach the well after a period of time. Thus, the drawdown and possible geofluid temperature increase must be factored in to locate the dynamic free surface of the liquid (see Section 4.2).

8.8.3 SURFACE PUMPS

Whereas downhole pumps must be designed to cope with unique geofluid conditions, surface pumps are fairly standard as they are commonly found in many industrial applications. The following sections briefly describe the major pumps needed for various types of geothermal power plants.

8.8.3.1 Flash Plants

Brine transfer and reinjection pumps. Typically these are electric motor-driven, horizontal-axis, axially-split casing, single or multistage centrifugal type. They are designed to allow high head and high volume flow. Reinjection pumps may be subject to silica scaling. Some plants may not need these if the separated brine can be reinjected at the separator pressure.

Condensate pumps. These motor-driven water pumps take suction from the hot well of the condenser and deliver it to the top of the cooling tower. Typically they are vertical-axis, multistage centrifugal, can-type units.

Cooling water circulating pumps. These motor-driven pumps collect the cooled water from the cold well of the cooling tower and deliver it to the condenser. They are similar in design to the condensate pumps but for low-head and high volume. Sometimes the cooling tower can be built at a higher elevation than the condenser allowing gravity feed thereby eliminating the need for circulating pumps.

Liquid-ring vacuum pumps. Liquid-ring vacuum pumps (LRVP) are often the choice for evacuating noncondensable gases from condensers usually in series with a steam-jet ejector. LRVP are essentially positive-displacement machines that draw the gas into the compression space by creating an increasing volume and then compressing the gas as the volume available to the gas decreases. Figure 8.26 shows a LRVP in simplified schematic form; an animated video is available from Nash Corporation: <http://www.youtube.com/watch?v=wIbIzCS1jHU>.

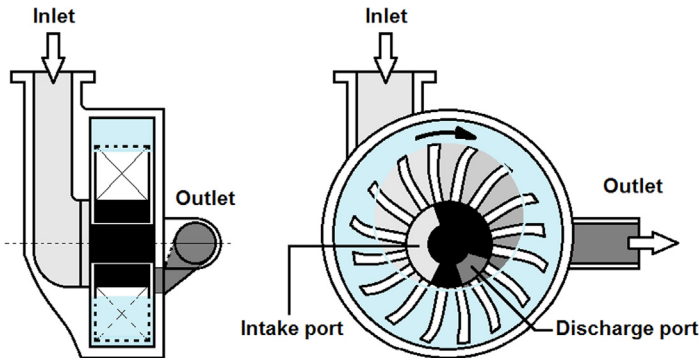


Figure 8.26 Simplified cut-away of an LRVP [WWW].

The rotating blades, driven by an electric motor, operate within a chamber partially filled with a liquid, usually water. The liquid is thrown and held against the chamber wall by centrifugal force. The blades rotate eccentrically within the chamber creating varying volumes between the inner hub and outer wall. The diagram shows a smooth liquid surface but it is actually highly turbulent. The intake and discharge ports pass through the two end plates on opposite sides. The machine operates steadily with no pulsations in the gas flow, and there is no metal-to-metal contact except with shaft bearings outside the chamber.

One problem is that some of the liquid leaves the chamber with the gas, requiring makeup. An inlet port for makeup is provided in one of the end plates (not shown in Figure 8.26). If the liquid is water, geothermal flash plants have excess steam condensate that can be used. Partial or full recovery and

recirculation of the escaping liquid can be designed into the system if the liquid cannot be economically or environmentally discharged to drain. One- or two-stage systems are available.

To determine the size and specifications of an LRVP requires the following information [26]:

- Pressure and temperature of the inlet gas
- Composition of the gas
- Gas mass flow rate and molar mass (molecular weight)
- Vapor pressure of gas components
- Gas discharge pressure
- Temperature of seal liquid, usually water
- Thermal and fluid properties of the seal liquid.

In the geothermal case, the gas involved is mainly carbon dioxide with various amounts of hydrogen sulfide and other gases in very small concentrations.

8.8.3.2 Binary Plants with Water Cooling Towers

Brine transfer and reinjection pumps. Pumps may be needed to boost the brine pressure to prevent flashing in the gathering system between the well and the heat exchangers. High-head, high-volume reinjection pumps are normally employed to return the brine to the formation under pressure. The pumps are usually motor-driven but can be powered by a dedicated turbine.

Condensate pumps. Same as for flash plants, except that the fluid being pumped is the binary cycle working fluid, typically an organic liquid or a mixture of compounds. Often the fluid is flammable or has harmful environmental effects that require special attention to seals.

Cooling water circulating pumps. Same as for flash plants.

8.8.3.3 Binary Plants with Air Cooling

Brine transfer and reinjection pumps. Same as above.

Condensate pumps. Same as above.

References

- [1] DiPippo R. U.S. Dept. of Energy, DOE/RA/28320-1 Geothermal energy as a source of electricity: a worldwide survey of the design and operation of geothermal power plants. Washington, DC: U. S. Gov. Printing Office; 1980.
- [1a] DiPippo R. Geothermal power plants: Evolution and performance assessments. *Geothermics* 2015;53:291–307.

- [1b] Sommaruga C. *Primati Italiani nello Sfruttamento di Risorse Geotermiche di Media e Bassa Temperatura: In Particolare, Pompe di Calore, Cicli Binari, Impianti a Vapore di Flash* ("Italian Records in the Exploitation of Geothermal Resources of Medium and Low Temperature: In Particular, Heat Pumps, Binary Cycles, Flash Steam Plant")—(1930–1960). Presented at Symposium La Geotermia in Italia Dal 1940 ad Oggi (Geothermal Energy in Italy from 1940 to today), University of Pisa, 2010 (in Italian).
- [1c] Rollet A. Centrale géothermique de Kiabukwa: Leçons tirées de quatre années d'exploitation ("Kiabukwa geothermal power plant: Lessons learned from four years of operation"), *Bulletin des Séances III* (6), p. 1246–62, Académie Royale des Sciences Coloniales (Nouvelle série), Rue de Livourne, 80A, Brussels, 1957. <http://www.kaowarsom.be/documents/BULLETINS_MEDEDELINGEN/1957-6.pdf>.
- [2] ENEL. Larderello field trip: electrical power generation. Florence, Italy: World Geothermal Congress; May 18–31, 1995. p. 1.
- [3] Anon. East Mesa 18.5 MW \times 2 double flash cycle geothermal power plant. Mitsubishi Heavy Industries, Ltd., Tokyo, Japan (undated).
- [4] DiPippo R. Geothermal power systems. In: Elliott TC, Chen K, Swanekamp RC, editors. *Standard handbook of powerplant engineering. 2nd ed.* New York, NY: McGraw-Hill, Inc.; 1998. p. 8.27–60 [Section 8.2].
- [5] Pitts DR, Sissom LE. *1000 Solved problems in heat transfer.* New York, NY: Schaum's Outline Series, McGraw-Hill; 1991.
- [6] Hicks TG, editor. *Standard handbook of engineering calculations.* New York, NY: McGraw-Hill; 1972.
- [7] Anon. *Engineering data book.* Tulsa, OK: Gas Processors Suppliers Association; 1972.
- [8] Incropera FP, DeWitt DP. *Fundamentals of heat and mass transfer. 4th ed.* New York, NY: John Wiley & Sons; 1996.
- [9] Reynolds WC. *Thermodynamic properties in SI: Graphs, tables and computational equations for 40 substances.* Stanford, CA: Dept. of Mechanical Engineering, Stanford University; 1979.
- [10] Gallagher JS, Linsky D, Morrison G, Levelt Sengers JMH. NBS Tech. Note 1234. *Thermodynamic properties of a geothermal working fluid; 90% isobutane-10% isopentane.* Washington, DC: National Bureau of Standards, U.S. Gov. Printing Office; 1987.
- [11] Demuth OJ, Bliem CJ, Mines GL, Swank WD. Supercritical binary geothermal cycle experiments with mixed-hydrocarbon working fluids and a vertical, in-tube, counterflow condenser. EGG-EP-7076, Idaho National Engineering Laboratory; 1975.
- [12] IAPWS. Guideline on the Tabular Taylor Series Expansion (TTSE) method for calculation of thermodynamic properties of water and steam applied to IAPWS-95 as an example, International Association for the Properties of Water and Steam, Vejle, Denmark, August 2003.
- [13] Milora SL, Tester JW. *Geothermal energy as a source of electric power: thermodynamic and economic criteria.* Cambridge, MA: MIT Press; 1976.
- [14] Anon. 1997 ASHRAE handbook fundamentals. Atlanta, GA: American Society of Heating, Refrigeration and Air-Conditioning Engineers, Inc.; 1997 [Chapter 18].
- [15] Moran MJ, Shapiro HN. *Fundamentals of engineering thermodynamics. 5th ed.* New York, NY: John Wiley & Sons; 2004.
- [16] DiPippo R. High-efficiency geothermal plant designs. *Geothermal Resour Counc Trans* 1997;21:393–8.
- [17] Khalifa HE, Rhodes BW. EPRI AP-4070 Analysis of power cycles for geothermal wellhead conversion systems. Palo Alto, CA: Electric Power Research Institute; 1985.
- [18] Bliem CJ, Walrath LF. EGG-2208 Raft river binary-cycle geothermal pilot power plant final report. Idaho Falls, ID: Idaho National Engineering Laboratory; 1983.

- [19] Hinrichs TC, Dambly BW. East Mesa Magmamax power process geothermal generating plant: a preliminary analysis. EPRI TC-80-907, Proceedings Fourth Annual Geothermal Conference and Workshop. Palo Alto, CA: Electric Power Research Institute; 1980. p. 5-1–5-14.
- [20] Hinrichs TC. Magmamax power plant—success at East Mesa. EPRI AP-3686, Proceedings Eighth Annual Geothermal Conference and Workshop. Palo Alto, CA: Electric Power Research Institute; 1984. p. 6-21–6-30.
- [21] Bliem CJ, Mines GL. EGG-EP-9207 Advanced Binary Performance Power Plants: Limits of Performance. Idaho Falls, ID: Idaho National Engineering Laboratory; 1991.
- [22] DiPippo R. Geothermal energy: electricity generation and environmental impact. In: Jackson T, editor. Renewable energy: prospects for implementation. Sweden: Stockholm Environment Institute; 1993. p. 113–22.
- [23] Moskvicheva VN, Popov AE. Geothermal power plant on the Paratunka river. Geothermics—Special Issue 2, U.N. Symposium on the Development and Utilization of Geothermal Resources, Pisa, 1970;2(Pt. 2):1567–71.
- [24] Frost J. Introduction to geothermal lineshaft production pumps. Los Angeles, CA: Course on Pumping of Geothermal Brine, Geothermal Resources Council; March 1984.
- [25] NPSH—Net positive suction head. The engineering toolbox, <http://www.engineeringtoolbox.com/npsH-net-positive-suction-head-d_634.html>; 2014 [accessed 01.07.14].
- [26] Aliasso J. How to size liquid ring vacuum pumps. Pumps and systems magazine, <<http://www.graham-mfg.com/usr/pdf/TechLibVacuum/212.PDF>>; 2014 [accessed 15.09.14].

Nomenclature for Figures in Chapter 8

ACC	Air-cooled condenser
BP	Barometric pit
C	Condenser
CP	Condensate pump
CSV	Control and stop valves
CT	Cooling tower
CWP	Cooling water pump
D	Deaerator
E	Evaporator
FE	Flash evaporator
FF	Final filter
f	Saturated liquid
g	Saturated vapor
HPE	High-pressure evaporator
HPFP	High-pressure feed pump
HPPH	High-pressure preheater
HPT	High-pressure turbine
HS	Hot spring
IP	Injection pump
IW	Injection well
LPE	Low-pressure evaporator
LPFP	Low-pressure feed pump
LPPH	Low-pressure preheater
LPT	Low-pressure turbine
M	Makeup water

P	Pump
PH	Preheater
PW	Production well
RH	Reheater
RHP	Recuperative preheater
S	Separator
SH	Superheater
SJE	Steam jet ejector
SR	Sand remover
T/G	Turbine/generator
TV	Throttle valve
V	Vent

Problems

- 8.1.** A counterflow, double-pipe heat exchanger is used in a geothermal binary plant to heat isobutane, $i\text{-C}_4\text{H}_{10}$, from 20°C to 70°C . The $i\text{-C}_4\text{H}_{10}$ flows at 100 kg/s ; the brine enters at 100°C and leaves at 45°C . The overall heat transfer coefficient is $U = 568\text{ W/m}^2 \cdot ^\circ\text{C}$.

Calculate:

- Required brine mass flow rate in kg/s .
 - Required heat transfer surface area in m^2 .
 - Second Law efficiency in %, if $T_0 = 15^\circ\text{C}$.
- 8.2.** A hydrocarbon turbine in a binary plant receives isobutane, $i\text{-C}_4\text{H}_{10}$, at 4.0 MPa and 145°C . The turbine exhausts at 275 kPa . The isentropic efficiency is 88% . Calculate:
- Specific work output of the turbine in kJ/kg .
 - Temperature of the $i\text{-C}_4\text{H}_{10}$ at turbine exhaust.
 - Ratio of exhaust-to-inlet volume.
 - Heat (in kJ/kg) that must be removed from the $i\text{-C}_4\text{H}_{10}$ (at $P = \text{constant}$) after expansion before condensation begins, that is, the desuperheat from the turbine exhaust.
- 8.3.** Consider a simple Rankine cycle using R-12 (no longer available) as the working fluid. Hot geothermal liquid is used to heat the R-12. The turbine inlet conditions are saturated vapor at 82°C ; the turbine has an isentropic efficiency of 82% ; the feed pump is isentropic; the condensing temperature is 38°C ; and the heat exchanger pinch-point temperature difference is 5.5°C .
- Calculate the Rankine cycle thermal efficiency, η_{th} .
 - If the geofluid is available at 99°C , calculate the required mass flow rate of geofluid to generate 500 kW of *net* power from the cycle.

- c. Determine the location of the pinch-point in the heat exchanger.
 - d. Calculate the geothermal resource utilization efficiency η_u if $T_0 = 15^\circ\text{C}$, and compare it with η_{th} .
- 8.4.** Consider the brine/R-12 heat exchanger in Problem 8.3.
- a. Calculate the log-mean-temperature-difference, LMTD, separately:
 - (i) for the liquid R-12 heater and (ii) for the evaporator.
 - b. Estimate the required total heat exchanger surface area in m^2 if the overall heat transfer coefficient is $U = 568 \text{ W/m}^2 \cdot ^\circ\text{C}$.
 - c. Calculate the utilization efficiency of the preheater, evaporator, and overall heat exchanger based on the transfer of exergy.
- 8.5.** Consider a simple geothermal binary plant consisting of a heat exchanger to vaporize the working fluid (R-12), a turbine ($\eta_t = 85\%$), a condenser, and a simple feed pump ($\eta_p = 75\%$). The turbine inlet conditions are: $P_1 = 2.75 \text{ MPa}$ and $T_1 = 150^\circ\text{C}$; the turbine exhaust pressure is $P_2 = 690 \text{ kPa}$. The condenser outlet condition is $P_3 = 690 \text{ kPa}$, saturated liquid. The pump outlet and heat exchanger inlet pressure is $P_4 = 3.1 \text{ MPa}$.

Calculate the following with the aid of R-12 property tables:

- a. Specific work of the turbine, w_t , kJ/kg.
 - b. Specific work of the pump, w_p , kJ/kg.
 - c. Specific heat added, q_a , kJ/kg.
 - d. Specific heat rejected, q_c , kJ/kg.
 - e. Cycle thermal efficiency (First Law), η_t , %.
- 8.6.** The plant described in Problem 8.5 is supplied with brine at $T_A = 165^\circ\text{C}$. The heat exchanger pinch-point temperature difference is 11°C .

Calculate the following with the aid of a scale P - h diagram for R-12:

- a. Ratio of the brine mass flow rate to the R-12 mass flow rate.
- b. Brine exit temperature, T_B , $^\circ\text{C}$.
- c. Second Law utilization efficiency of the overall heat exchanger based on the exergy given up the brine and the exergy received by the R-12. Use a dead-state temperature $T_0 = 15^\circ\text{C}$.

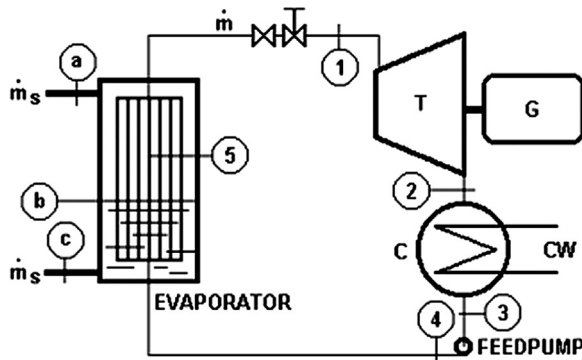
If the plant produces a *net cycle* power output of 10,000 kW, calculate:

- d. Mass flow rate of brine, in kg/s.
- e. Mass flow rate of R-12, in kg/s.
- f. Plant Second Law efficiency for the above-stated net cycle power.

The plant parasitic power requirements include: (i) well pumping power and (ii) cooling system pumps and fans. If the brine pumps require 9.8 kJ/kg brine, and the total cooling system takes 500 kW, calculate:

- g. Bottom-line, net power, and the overall plant Second Law efficiency.

- 8.7. One of the earliest power plants at Larderello employed binary-like units in which geothermal steam (saturated vapor) was used to heat and evaporate pure water which circulated in a close, simple Rankine cycle shown in the sketch. The following data are hypothetical.



Consider the following data:

$$P_a = P_b = P_c = 1.0 \text{ MPa} \quad T_c = 130^\circ\text{C} \text{ (subcooled liquid)}$$

$$\text{Turbine wet efficiency} = 0.77 \quad T_1 = 160^\circ\text{C} \text{ (saturated vapor)}$$

$$\text{Feed pump efficiency} = 1.00 \quad T_3 = 50^\circ\text{C} \text{ (saturated liquid)}$$

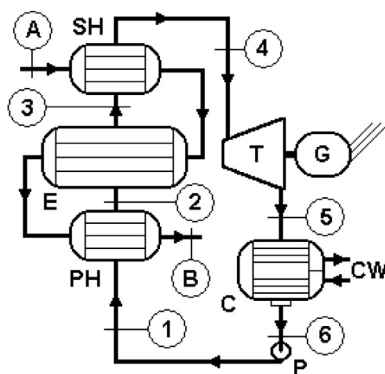
- Sketch the plant processes in a T - s diagram. Label all states using the notation given in the schematic.
 - Calculate (in kJ/kg for pure water):
 - Turbine work, w_t .
 - Feed pump work, w_p .
 - Net cycle work, w_{net} .
 - Calculate the net cycle thermal efficiency, η_{th} (in %).
 - If the plant is to produce 10,000 kW of net power, calculate:
 - Mass flow rate of pure water, in kg/s.
 - Mass flow rate of geothermal steam, in kg/s.
 - For a dead-state temperature of 25°C , find the Second Law resource utilization efficiency, η_u (in %).
- 8.8. A modular binary power plant uses propane, C_3H_8 , as the cycle working fluid. The geothermal brine is pumped from the reservoir and reaches the plant at a temperature $T_A = 420 \text{ K}$. The cycle employs a supercritical pressure in the main heat exchanger, where the pinch-point temperature difference is 5°C . The inlet conditions at the propane turbine are: $T_1 = 400 \text{ K}$ and $P_1 = 5.0 \text{ MPa}$; the turbine exhausts at $P_2 = 1.0 \text{ MPa}$. The turbine has

an isentropic efficiency of 85% and the feed pump has an isentropic efficiency of 80%. The gross turbine output is 1500 kW. You may ignore pressure losses in heat exchangers and piping.

- Prepare a system schematic and the corresponding temperature-entropy process diagram.
- Sketch the temperature-heat transfer diagram for the supercritical heat exchanger showing the brine cooling line and the propane heating curve.
- Determine the brine outlet temperature from the heat exchanger.
- Calculate the mass flow rates in kg/s for: (i) propane and (ii) brine.
- Calculate the net cycle thermal efficiency in %.
- Calculate the net plant utilization efficiency for a dead-state at 20°C in %.

Hints: Using REFPROP for the properties of propane, determine the propane heating curve on a scale T - q diagram. Knowing the brine inlet temperature, adjust the slope of the brine cooling line to obtain the correct pinch-point temperature difference. The brine outlet temperature may either be read from the diagram or calculated by similar triangles.

- Repeat the example worked in Section 8.5 with the following change to the given data: Instead of a boiler pressure of 2 MPa, use 0.8 MPa, otherwise use all the other data as given. Compare your results to those found in the example and discuss your findings.
- A binary plant uses isopentane ($i\text{-C}_5\text{H}_{12}$) as the cycle working fluid. The working fluid is superheated before entering the turbine (see figure below).



The following data are specified:

Brine inlet temperature at superheater = 425 K

$i\text{-C}_5\text{H}_{12}$ temperature in evaporator = 400 K

Turbine inlet temperature = 420 K

Turbine isentropic efficiency = 90%

Condensing temperature = 320 K

Feed pump isentropic efficiency = 100% (ideal)

Pinch-point temperature difference in heat exchanger train = 5 K

Cycle net output = 10 MW

Dead-state temperature = 298 K.

With a pressure-enthalpy process flow diagram as a visual aid, calculate:

- a. Mass flow rate of $i\text{-C}_5\text{H}_{12}$.
- b. Mass flow rate of the brine.
- c. Brine temperature leaving the preheater.
- c. Utilization efficiency of the binary plant based on the exergy of the brine entering the evaporator.

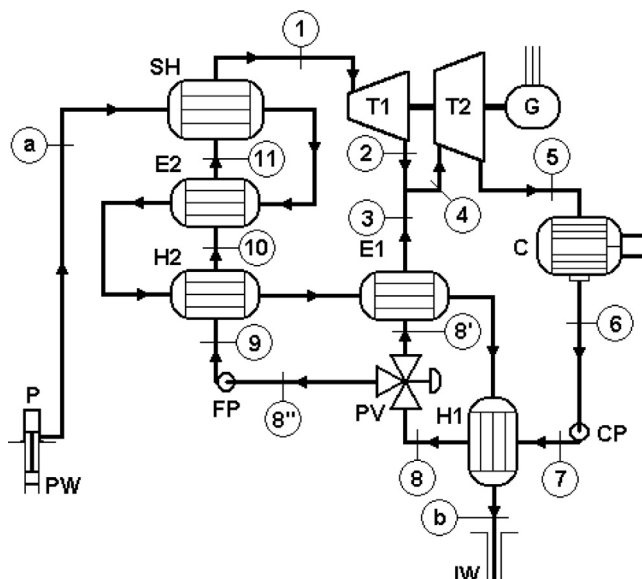
8.11. A binary plant uses isobutane ($i\text{-C}_4\text{H}_{10}$) as the cycle working fluid. The working fluid is superheated before entering the turbine. A throttle valve is located between the outlet of the superheater and the turbine inlet. Normally it operates wide open (no pressure drop). The pressure leaving the superheater is kept constant at all times at a value P_{SH} . The design turbine inlet temperature is $T_1 = 460$ K. The turbine is assumed isentropic and the turbine exhaust pressure is 0.4 MPa.

- a. Find the highest value of P_{SH} such that the turbine expansion line remains entirely in the vapor region. A scale pressure-enthalpy process flow diagram will be very useful in solving this question.
- b. Using the fixed value for P_{SH} found above, if the temperature of the $i\text{-C}_4\text{H}_{10}$ leaving the superheater drops to $T_2 = 455$ K, then the throttle valve will be activated to adjust the turbine inlet condition so that the full expansion line remains just dry. Determine the minimum pressure drop across the throttle to assure dry expansion.
- c. Calculate and compare the turbine output under design and off-design conditions, indicating the percentage loss in output.

8.12. A dual-pressure binary plant depicted in the figure below uses isobutane ($i\text{-C}_4\text{H}_{10}$) as the cycle working fluid. Saturated liquid $i\text{-C}_4\text{H}_{10}$ is pumped from the condenser C through a heater H1 from which it emerges as a saturated liquid. A proportioning valve PV allows 30% of the working fluid to flow to the evaporator E1 and 70% to flow to a feed pump FP. From there this stream is heated (H2), evaporated (E2), and superheated (SH) before entering the turbine T1. The exhaust from T1 is mixed isobarically with the saturated vapor (state 3) coming from evaporator E1 before passing into the second turbine T2. The geothermal brine passes through five heat exchangers in series before being reinjected (state b).

Data: $P_1 = P_9 = P_{10} = P_{11} = 3362 \text{ kPa}$; $T_1 = 180^\circ\text{C}$; $T_6 = 30^\circ\text{C}$; $T_0 = 25^\circ\text{C}$;
 $\eta_{T1} = \eta_{T2} = 85\%$; $\eta_{CP} = \eta_{FP} = 100\%$; $T_a = 200^\circ\text{C}$; $T_b = 100^\circ\text{C}$.

Also, the temperature in E1 is chosen as the average of the condenser temperature and the temperature in E2.



- Construct the pressure-enthalpy process flow diagram (schematically, not to scale).
- Determine the specific enthalpy of $i\text{-C}_4\text{H}_{10}$ at each state point in the cycle.
- Calculate the specific work output of the turbines in units of kJ/kg of $i\text{-C}_4\text{H}_{10}$ flowing at state 6.
- Calculate the thermal efficiency of the cycle.
- Calculate the required mass flow rate of brine (assumed pure water) per unit flow rate of $i\text{-C}_4\text{H}_{10}$.
- Calculate the utilization efficiency of the plant based on the exergy of the incoming brine.
- If a typical well can produce $90,000 \text{ kg/h}$, how many wells will be needed to generate a net power output of 10 MW ?
- Is it safe to assume that the plant as described in this problem (i.e., for the given temperatures, pressures, etc.) is actually feasible thermodynamically? To be sure of its feasibility, what should be checked?



Chapter 9

Advanced Geothermal Energy Conversion Systems

Chapter Outline

9.1 Introduction	242
9.2 Hybrid Single-Flash and Double-Flash Systems	243
9.2.1 Integrated Single- and Double-Flash Plants	244
9.2.2 Combined Single- and Double-Flash Plants	246
9.3 Hybrid Flash-Binary Systems	247
9.3.1 Combined Flash-Binary Plants	247
9.3.2 Integrated Flash-Binary Plants	249
9.4 Example: Integrated Flash-Binary Hybrid System	252
9.5 Total-Flow Systems	256
9.5.1 Axial-Flow Impulse Turbine	256
9.5.2 Rotary Separator Turbine	260
9.5.3 Helical Screw Expander	261
9.5.4 Conclusions	263
9.6 Hybrid Fossil-Geothermal Systems	263
9.6.1 Fossil-Superheat Systems	263
9.6.2 Geothermal-Preheat System	265
9.6.3 Geopressure-Geothermal Hybrid Systems	265
9.7 Combined Heat and Power Plants	267
9.8 Power Plants for Hypersaline Brines	269
9.8.1 FCRC Systems	271
9.8.2 pH Modification (pH-Mod) Systems	272
9.9 Solar-Geothermal Hybrid Plants	274
9.9.1 Basic Concept	274
9.9.2 Geothermal-Augmented Solar Thermal Plants	275
9.9.3 Solar-Augmented Binary Plants	275
9.9.4 Solar-Augmented Flash Plants	276
References	278
Nomenclature for Figures in Chapter 9	280
Problems	281

Why should we expect nature to be interested either positively or negatively in the purposes of human beings, particularly purposes of such unblushingly economic tinge?

Percy W. Bridgman, on the thermodynamic prohibition against perpetual motion machines—1941

9.1 Introduction

Geothermal resources are like human fingerprints: no two are exactly alike. Therefore, energy conversion systems must be chosen and often adapted to suit the particular resource. We have seen how single-, double-, and triple-flash systems are used for moderate- and high-temperature liquid-dominated resources, how dry-steam plants can be used at the unique dry-steam resources, and how binary plants utilize the lower-temperature liquid-dominated resources.

By way of review, the basic types of geothermal energy conversion systems that were covered in Chapters 5–8 are summarized in [Figures 9.1 and 9.2](#) and in [Table 9.1](#).

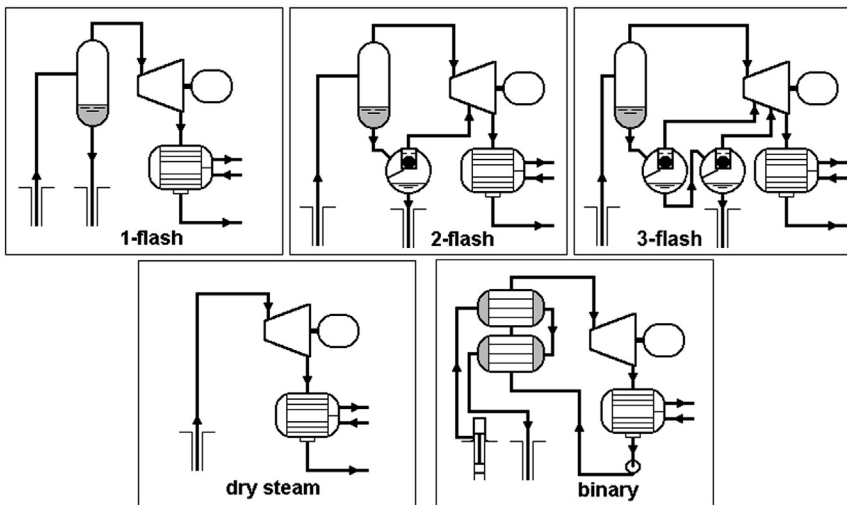


Figure 9.1 Basic geothermal energy conversion systems: simplified plant layouts.

There are some geothermal resources that demand more sophisticated energy conversion systems than the basic ones we have considered so far. Furthermore, energy conversion systems have evolved to fit the needs of specific developing fields by integrating different types of power plants into a unified, complex enterprise.

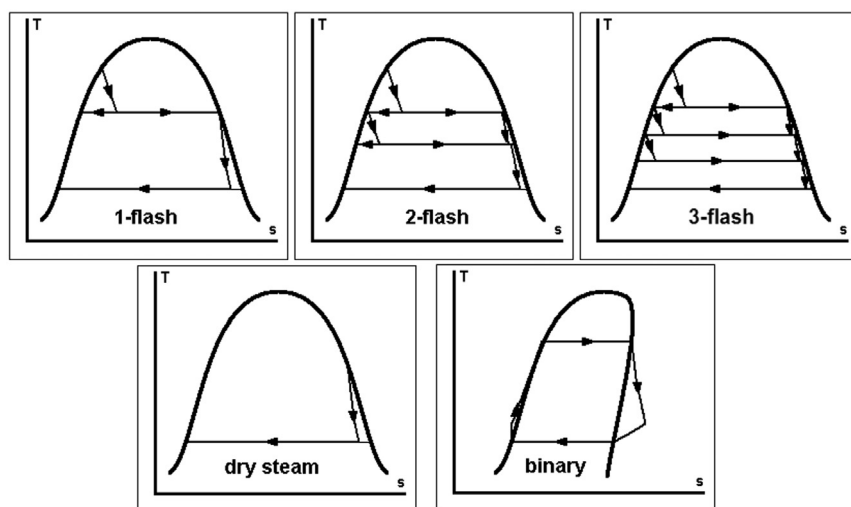


Figure 9.2 Basic geothermal energy conversion systems: simplified process diagrams.

TABLE 9.1 Comparison of basic geothermal energy conversion systems.

Type of plant	Reservoir temperatures, °C	Utilization efficiency, %	Plant cost and complexity	Current usage
Single-flash	200–260	30–35	Moderate	Widespread
Double-flash	240–320	35–45	Moderate → high	Widespread
Triple-flash	260–320	40–50	High	Selected sites
Dry-steam	180–300+	50–65	Low → moderate	Special sites
Basic binary	125–165	25–45	Moderate → high	Widespread

In this chapter we will look at some of the advanced systems for geothermal power generation. Many of these have already achieved commercial status by improving the efficiency of resource utilization. Others are in various stages of development but hold promise to meet future geothermal power needs.

9.2 Hybrid Single-Flash and Double-Flash Systems

Let us begin by considering how two of the systems we have already studied can be combined to form a hybrid type of power plant. Given the relative simplicity and reliability of single-flash plants, they are often the first type of plants installed at a newly developed field. However, their utilization efficiency is lower than that

of a double-flash plant, and there usually comes a time in the life of a field when expansion of the generating capacity becomes possible. When this happens, say because step-out wells have been successful or the electricity demand rises, it is logical to add another power unit.

Since single-flash plants have a significant amount of waste liquid from their separators that is still fairly hot, typically 150–170°C, the question arises as to whether this could be used to generate more power instead of being directly reinjected. At several fields around the world, the answer has been “Yes,” and combined single- and double-flash plants have been built. Here we will deal with the thermodynamics of such arrangements, leaving discussion of actual plants to the third part of the book.

9.2.1 INTEGRATED SINGLE- AND DOUBLE-FLASH PLANTS

When the geofluid reservoir temperature is about 220–240°C and single-flash units have been built and have been operating for some time, the addition of one more flash using the separated brine allows for a lower pressure unit. The arrangement shown in [Figure 9.3](#) consists of two single-flash units, Units 1 and 2,

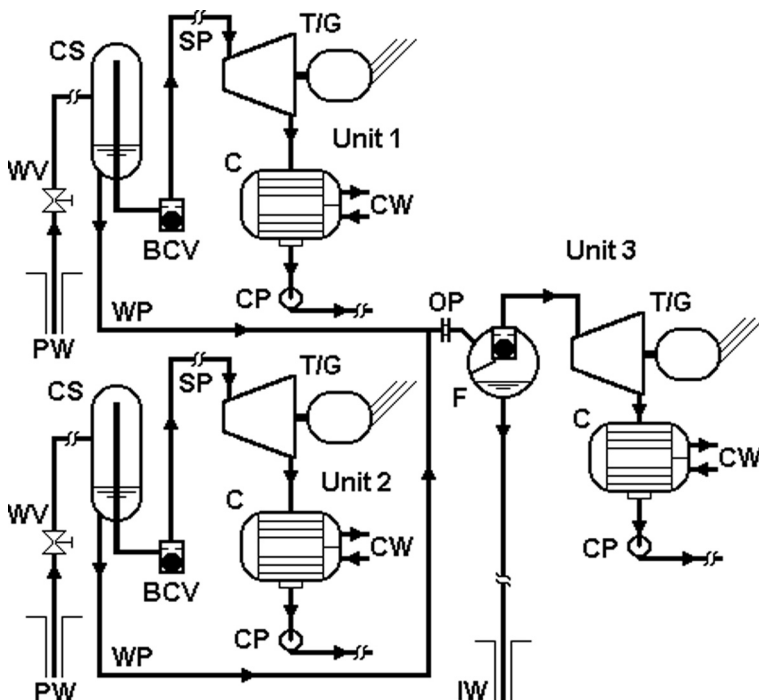


Figure 9.3 Integrated single- and double-flash facility [1].

and a third unit, Unit 3. Taken by itself, Unit 3 appears to be simply another single-flash unit, but the power plant as a whole is an integrated single- and double-flash facility since the original geofluid experiences two stages of flashing.

The advantage to this arrangement is that no new wells need to be drilled to supply the third unit. Unit 3 serves as a bottoming unit to recover some of the wasted potential from the still-hot brine. The thermodynamic process diagram is given in [Figure 9.4](#) in temperature-entropy coordinates.

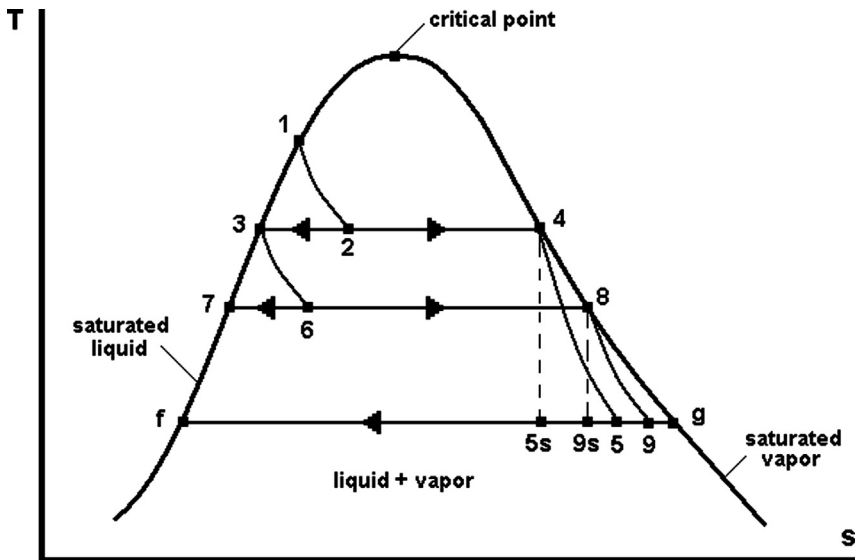


Figure 9.4 Thermodynamic temperature-entropy process diagram for integrated single- and double-flash plant as shown in [Figure 9.3](#).

One possible thermodynamic drawback to this arrangement lies in the selection of the pressure (or equivalently, the temperature) for the second flash process 3–6 in [Figure 9.4](#). Recall that we found the optimum flash conditions for a true double-flash plant were such that the temperature differences between the reservoir, the first and second flashes, and the condenser were all roughly equal. If the flash temperatures for the first two units (assumed identical) had been optimized according to this rule, then they will be too low when the third unit is added. Furthermore, it may not be feasible to redesign Units 1 and 2 owing to the changes that would have to be made to the existing equipment. Nevertheless, the flash temperature for Unit 3 can still be selected to optimize the new combination, given the existing brine condition at state 3.

9.2.2 COMBINED SINGLE- AND DOUBLE-FLASH PLANTS

When the resource temperature is equal to or greater than say 240°C , it may be possible to augment the single-flash units with a true double-flash bottoming cycle, as seen in the schematic flow diagram (Figure 9.5) and in the process diagram (Figure 9.6). For this case, the waste brine from the first units is subjected to two more flashes, resulting in two additional low-pressure steam flows. It could be argued that this constitutes a triple-flash if one simply counts the number of flashes experienced by the geofluid, but given the sequential timing of the construction of the units, the use of the term “combined single- and double-flash” seems appropriate.

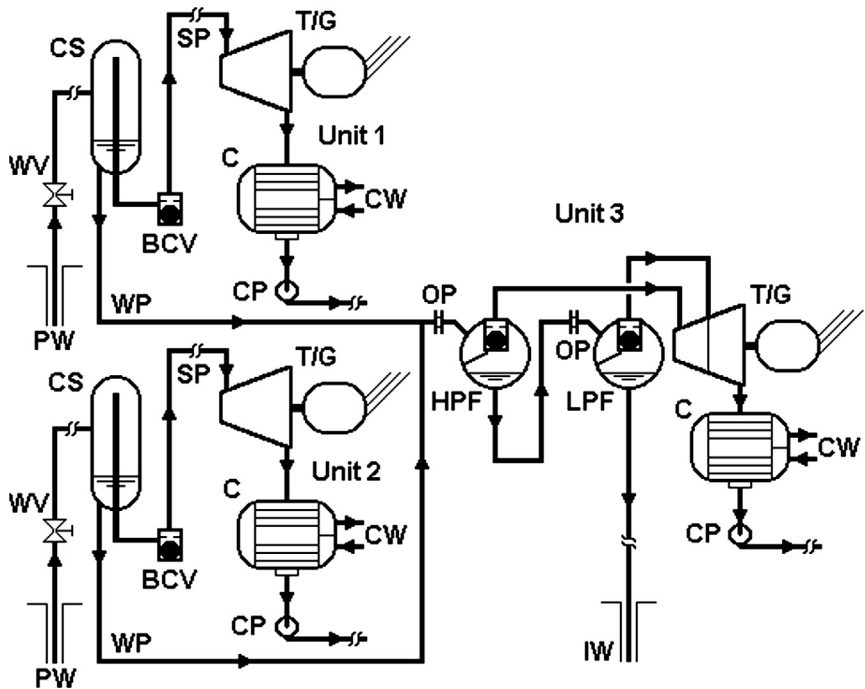


Figure 9.5 Combined single- and double-flash plant [1].

Although the thermodynamics of this arrangement are favorable, that is, a higher resource utilization efficiency than for the original single-flash plant, there may be problems with chemical scaling due to silica precipitation at the low temperatures associated with the last flash. This was discussed in Section 6.6. This arrangement would not be a good choice unless there is no possibility of silica precipitation or the plant owner is willing to invest in chemical treatment of the low-temperature brine to prevent or control scale formation.

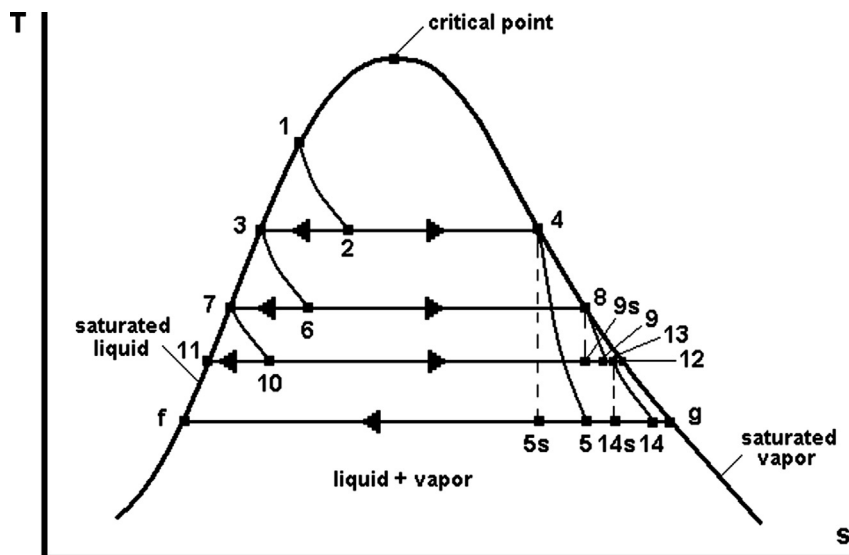


Figure 9.6 Process diagram for combined single- and double-flash plant.

9.3 Hybrid Flash-Binary Systems

An attractive alternative to the use of bottoming flash plants at existing single-flash plants is to add a binary cycle. Combined flash-binary plants are in operation at several plant sites around the world (see Appendix A).

A different approach is to design a plant, from scratch, as an integrated flash-binary plant, thereby taking advantage of the best features of both units. We will examine these two strategic alternatives in the sections that follow.

9.3.1 COMBINED FLASH-BINARY PLANTS

For this case, we assume that a single-flash plant has been running for some time, usually a few years, and the reservoir has shown itself capable of sustaining operations for many more years. The power output can be raised by adding a binary unit between the separators and the reinjection wells. A simplified schematic of such an arrangement is given in Figure 9.7.

Initially the single-flash plant operated by itself and the waste liquid from the cyclone separators, CS, was sent directly to the injection wells, IW. The binary cycle is inserted as shown to tap into the reinjection pipeline where it extracts some heat and thereby lowers the temperature of the waste brine prior to injection. The additional power generated by the binary cycle is gained without any new production wells.

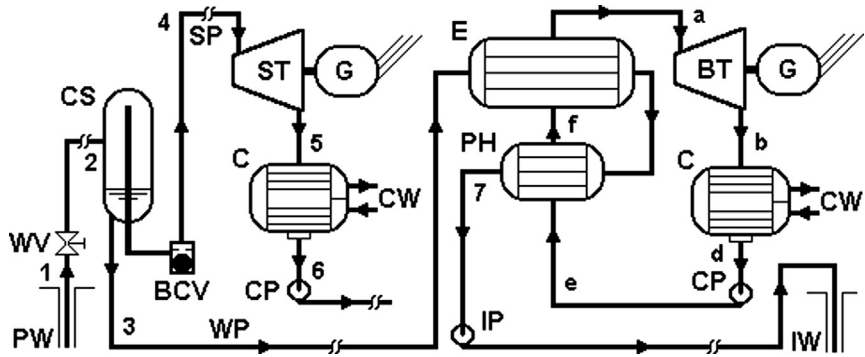


Figure 9.7 Combined single-flash and basic binary plant. After Ref. [1].

The thermodynamic process diagram is presented in Figure 9.8 in temperature-entropy coordinates to facilitate comparison with the cycles in the previous sections. The power units are coupled thermodynamically through the preheater, PH, and the evaporator, E. The First Law gives the relationship between the brine flow rate \dot{m}_b from the wells (state 1) and that of the binary cycle working fluid, \dot{m}_{wf} :

$$\dot{m}_b(1 - x_2)c_b(T_3 - T_7) = \dot{m}_{wf}(h_a - h_e) \quad (9.1)$$

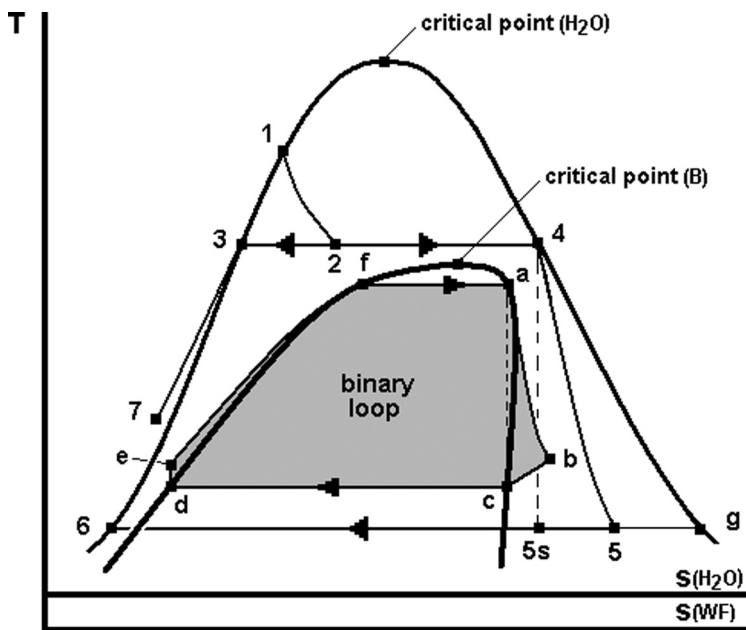


Figure 9.8 Combined single-flash/binary plant: temperature-entropy process diagram.

This equation expresses the fact that the heat extracted from the waste brine is equal to the heat absorbed by the binary cycle working fluid, assuming perfect insulation on the heat exchangers. Solving for the working fluid flow rate, we find:

$$\dot{m}_{wf} = \dot{m}_b(1 - x_2) \left[\frac{c(T_3 - T_7)}{h_a - h_e} \right] \quad (9.2)$$

Since the state points 1, 2, and 3 for the flash unit are fixed and the new state point 7 is subject to the constraint imposed by silica precipitation, only the binary cycle parameters are open for assignment. These, in turn, are subject to the constraint imposed by the pinch-point temperature difference in the heat exchangers. The analysis presented in Section 8.2 can be applied to this situation.

The fact that the waste brine is simply cooled rather than flashed to supply the bottoming cycle tends to avoid the silica scaling problem. With reference to Figure 6.15, let us assume that the brine temperature is 240°C in the reservoir. The corresponding silica concentration is about 425 ppm. If the separator operates at 150°C, the silica concentration in the waste brine rises to 526 ppm owing to the removal of 19% (mass) of the geofluid in the form of steam. As can be seen from Figure 6.15, the brine is safely undersaturated with respect to amorphous silica.

When the brine is cooled, its silica concentration remains the same and it becomes saturated when it cools to roughly 133°C. This temperature then is the safe lower limit at state 7; any further cooling places the brine in the supersaturated region and invites silica precipitation in the cool end of the heat exchanger, the reinjection piping, or wells. Therefore, the available temperature drop is about 17°C. If 1000 kg/s of waste brine is available, then the bottoming binary cycle should be able to generate about 7.3 MW assuming a conservative 10% cycle thermal efficiency.

9.3.2 INTEGRATED FLASH-BINARY PLANTS

When a binary cycle is integrated with a flash plant, the result is a plant with practically zero emissions. Where environmental concerns are significant, such plants have great appeal. An integrated single-flash/binary plant is shown schematically in Figure 9.9; the process diagram is given in two parts: Figure 9.10 for the main, upper portion and Figure 9.11 for the bottoming binary portion [2].

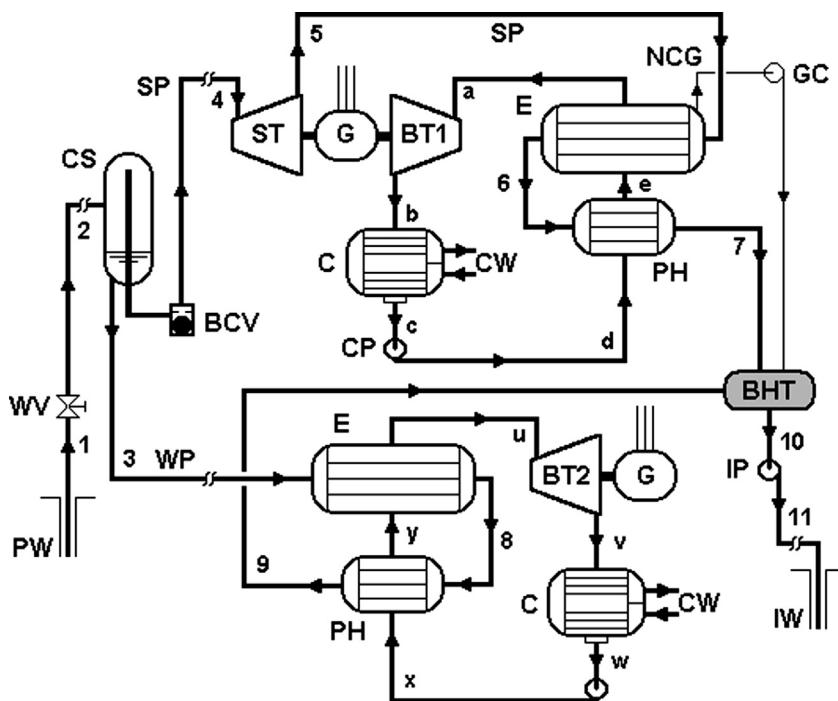


Figure 9.9 Integrated single-flash/binary plant.

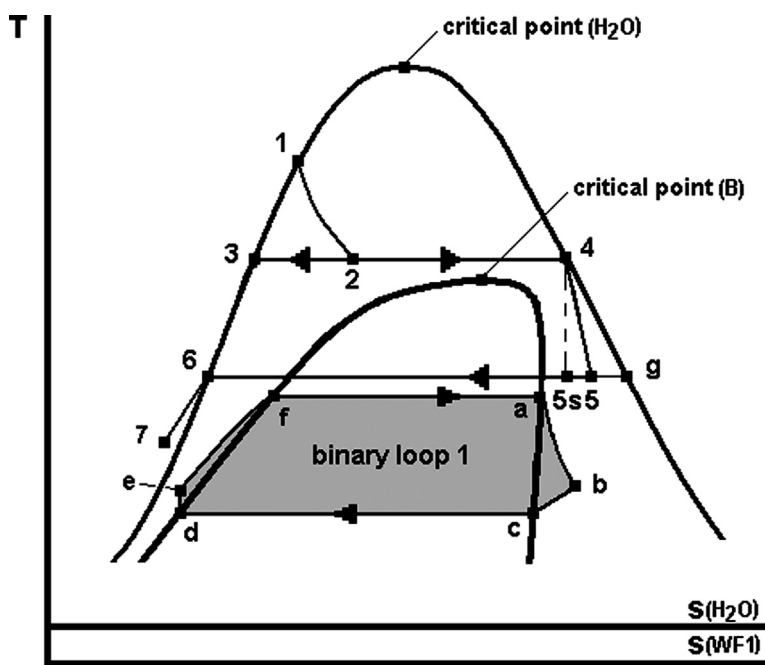


Figure 9.10 Process diagram for an integrated single-flash/binary plant: upper plant.

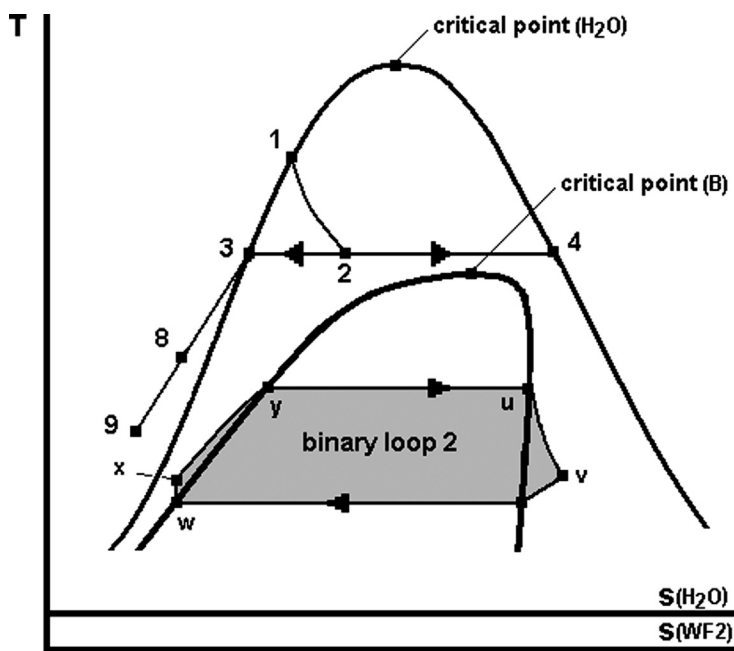


Figure 9.11 Process diagram for the bottoming binary portion of an integrated single-flash/binary plant: main portion omitted for clarity; see [Figure 9.10](#).

The geothermal steam first drives the back-pressure steam turbine and then is condensed in the upper binary cycle's evaporator E. The two turbines in the upper part of the plant may be connected to a common generator, as shown. The separated brine (state 3) is used to preheat and evaporate the working fluid in the lower binary cycle. The noncondensable gases flow with the steam through the steam turbine, ST, and into the evaporator where they are isolated, removed, and compressed for recombination with the waste brine just before being reinjected. The brine holding tank, BHT, collects all the steam condensate, waste brine, and compressed gases that go back into solution.

In principle, this plant has no emissions to the surroundings. The only environmental impact is the heat rejected to the atmosphere from the binary cycle condensers. The schematic shows water-cooled condensers but air-cooling is an option.

There is a trade-off involved in this arrangement in that the steam expansion process is cut short relative to the combined flash-binary plant. The turbine is called a back-pressure turbine because its exhaust pressure is much higher than

would be the case if it exhausted to a water-cooled condenser. The work that would be obtained from the lower-pressure stages of the turbine is forfeited in favor of using the heat of condensation (from process 5–6) to vaporize the working fluid in the binary loop. The bottoming binary cycle is a means of capturing some of the potential of the hot, separated brine, and raises the plant total output without the need for additional wells.

In the following section we will present a numerical example to illustrate the analysis of this relatively complex system.

9.4 Example: Integrated Flash-Binary Hybrid System

This example is drawn on the case just studied and will use [Figures 9.9–9.11](#). Although we will select arbitrary values for the geofluid conditions and the cycle parameters, the results will be fairly realistic. Here are the assumed conditions:

- Reservoir temperature, $T_1 = 250^\circ\text{C}$
- Brine main flow rate, $\dot{m}_b = 500 \text{ kg/s}$
- Dead-state temperature, $T_0 = 25^\circ\text{C} = 298.15 \text{ K}$
- Flash separator temperature, $T_2 = 185^\circ\text{C}$
- Steam turbine exhaust pressure, $P_5 = 1.5 \text{ bar}$
- Steam condensate outlet temperature, $T_7 = 65^\circ\text{C}$
- Brine outlet temperature, $T_9 = 165^\circ\text{C}$
- Binary cycle working fluid (both loops): n-pentane, C_5H_{12}
- Loop 1 turbine inlet temperature, $T_a = 380 \text{ K}$ (saturated)
- Loop 2 turbine inlet temperature, $T_u = 420 \text{ K}$ (saturated)
- Loops 1 and 2 condensing temperature, $T_d = T_w = 310 \text{ K}$
- Steam turbine isentropic efficiency, $\eta_{st} = 0.80$
- C_5 turbine isentropic efficiency, $\eta_{bT1} = \eta_{bT2} = 0.85$
- C_5 feed pump isentropic efficiency, $\eta_{CP1} = \eta_{CP2} = 0.75$

Our objectives are to find:

1. Power output of the steam turbine, \dot{W}_{ST}
2. Net power output of the upper binary cycle (loop 1), $\dot{W}_{B1,net}$
3. Net power output of the lower binary cycle (loop 2), $\dot{W}_{B2,net}$
4. Cycle thermal efficiency for both loops, $\eta_{b1,th}$ and $\eta_{b2,th}$
5. Overall plant utilization efficiency, η_u .

The thermodynamic properties for the brine, steam, and n-pentane are found from REFPROP [3]. The table below summarizes the important properties at all the state points in the plant.

State	P , MPa	T , °C	x	s , kJ/kg · K	h , kJ/kg	Comments
<i>Steam processes</i>						
1	3.973	250	0	2.7935	1085.77	Saturated liquid
2	1.123	185	0.1506		1085.77	$h_2 = h_1$
3	1.123	185	0		785.19	Saturated liquid
4	1.123	185	1	6.5447	2781.4	Saturated vapor
5s	0.15		0.8828	6.5447	2433.34	$s_{5s} = s_4$
5	0.15	111.3	0.9142		2502.12	From η_{ST}
6	0.15	111.3	0		467.13	Saturated liquid
7	0.15	65	NA		272.22	Comp. liquid
8	1.123	158.15	NA			From T - q diagram
9	1.123	165	NA		697.48	Comp. liquid
<i>Binary loop 1—n-pentane processes</i>						
a	0.6869	106.85	1	1.2838	470.15	Saturated vapor
bs	0.1047		NA	1.2838	399.39	$s_{bs} = s_a$
b	0.1047		NA		410.01	From η_{BT1}
c	0.1047	36.85	1		358.81	Saturated vapor
d	0.1047	36.85	0	0.006011	1.87	Saturated liquid
es	0.6869		NA	0.006011	2.83	$s_{es} = s_d$
e	0.6869		NA		3.15	From η_{CP1}
f	0.6869	106.85	0		181.94	Saturated liquid
<i>Binary loop 2—n-pentane processes</i>						
u	1.505	146.85	1	1.363	529.66	Saturated vapor
vs	0.1041		NA	1.363	426.38	$s_{vs} = s_u$
v	0.1041		NA		441.87	From η_{BT2}
w	0.1041	36.85	0	0.006011	1.87	Saturated liquid
xs	1.505			0.006011	4.16	$s_{xs} = s_w$
x	1.505	37.67	NA		4.93	From η_{CP2}
y	1.505	146.85	1		300.97	Saturated liquid

Note: Numbers in boldface are given in the specifications or are obvious from them.

The methodology used in the example of Section 8.5 has been applied here. The n-pentane mass flow rate in loop 1 can be found from the coupling equation on the preheater-evaporator combination:

$$\dot{m}_{C_5} = \dot{m}_b x_2 \left[\frac{h_5 - h_7}{h_a - h_e} \right] \quad (9.3)$$

where we will use the actual enthalpy values for the brine instead of the constant-specific-heat approximation shown in Eq. (9.2). The mass flow rate of brine from

the separator is 75.29 kg/s and from this we find $\dot{m}_{C_5} = 359.49 \text{ kg/s}$. It is now possible to calculate our first objective:

1. Power output of the steam turbine:

$$\dot{W}_{ST} = \dot{m}_4(h_4 - h_5) = 21,027 \text{ kW} \quad (9.4)$$

Next we can assess the upper binary cycle, loop 1. The turbine power is found from:

$$\dot{W}_{BT1} = \dot{m}_{C_5}(h_a - h_b) = 21,622 \text{ kW} \quad (9.5)$$

and the feed pump power is found from:

$$\dot{W}_{CP1} = \dot{m}_{C_5}(h_e - h_d) = 460.3 \text{ kW} \quad (9.6)$$

Thus the second objective may be determined:

2. Net power output of the upper binary cycle (loop 1):

$$\dot{W}_{B1,net} = \dot{W}_{BT1} - \dot{W}_{CP1} = 21,161 \text{ kW} \quad (9.7)$$

Next we assess the lower binary cycle, loop 2, in the same fashion:

$$\dot{m}_{C_5} = \dot{m}_b(1 - x_2) \left[\frac{h_3 - h_9}{h_u - h_x} \right] \quad (9.8)$$

Since the separated brine flow rate is 424.71 kg/s (i.e., $500 - 75.29$), we find the n-pentane flow for the lower cycle is $\dot{m}_{C_5} = 70.99 \text{ kg/s}$. Then the turbine and pump power follow directly:

$$\dot{W}_{BT2} = \dot{m}_{C_5}(h_u - h_v) = 6,232.8 \text{ kW} \quad (9.9)$$

and

$$\dot{W}_{CP2} = \dot{m}_{C_5}(h_x - h_w) = 217.5 \text{ kW} \quad (9.10)$$

Thus the third objective can be found:

3. Net power output of the lower binary cycle (loop 2):

$$\dot{W}_{B2,net} = \dot{W}_{BT2} - \dot{W}_{CP2} = 6,015.3 \text{ kW} \quad (9.11)$$

The cycle thermal efficiencies are the ratio of the net power output to the thermal power input for each loop. The two heat transfer terms are found from:

$$\dot{Q}_{IN1} = \dot{m}_{C_5}(h_a - h_e) = 167,882 \text{ kW} \quad (9.12)$$

and

$$\dot{Q}_{IN2} = \dot{m}_{C_5}(h_u - h_x) = 37,253 \text{ kW} \quad (9.13)$$

We can now find our fourth objective:

4. Cycle thermal efficiency for both loops:

$$\eta_{B1,th} = \frac{\dot{W}_{B1}}{\dot{Q}_{IN1}} = \mathbf{0.126} \text{ or } \mathbf{12.6\%} \quad (9.14)$$

and

$$\eta_{B2,th} = \frac{\dot{W}_{B2}}{\dot{Q}_{IN2}} = \mathbf{0.161} \text{ or } \mathbf{16.1\%} \quad (9.15)$$

The last objective requires us to find the exergy of the original reservoir fluid, taken to be a saturated liquid at the reservoir temperature. The specific exergy is:

$$e_1 = h_1 - h_0 - T_0(s_1 - s_0) = 257.54 \text{ kJ/kg} \quad (9.16)$$

and the rate at which exergy is produced from the reservoir is:

$$\dot{E}_1 = \dot{m}_1 e_1 = 128,769 \text{ kW} \quad (9.17)$$

The gross power of the whole plant (ignoring parasitic loads such as cooling tower fans and pumps) is:

$$\dot{W}_{plant} = \dot{W}_{ST} + \dot{W}_{B1,net} + \dot{W}_{B2,net} = 48,204 \text{ kW} \quad (9.18)$$

Thus, we find our last objective:

5. Overall plant utilization efficiency:

$$\eta_u = \frac{\dot{W}_{plant}}{\dot{E}_1} = \mathbf{0.374} \text{ or } \mathbf{37.4\%} \quad (9.19)$$

Discussion: Given the magnitude of the power output for the upper binary cycle, it is likely that several smaller units would be deployed rather than one large turbine-generator. Four units of nominally 5.5 MW capacity would work out well. The lower loop could use one turbine-generator set. Smaller units can be modular, largely factory assembled and tested, and ready for rapid installation.

The pinch-points in the two loops both occur at the bubble point of the n-pentane: 4.45°C in loop 1 and 11.3°C in loop 2.

The cycle thermal efficiencies are somewhat on the high side but remember that we did not account for the power needed to run the fans for air-cooled condensers or for the cooling towers, depending on which are used. For a plant of this size it is likely that several hundred kilowatts would be needed in either case.

The utilization efficiency of 37.4% is very respectable and compares closely with what one might obtain from a double-flash plant.

A plant similar to this design is operating on Leyte in The Philippines [4]. The photograph in Figure 9.12 shows that air-cooled condensers occupy much



Figure 9.12 Upper Mahiao integrated flash-binary 125 MW power plant. *Photo courtesy of Ormat [4] [WWW].*

more area than would water cooling towers, but they have the advantage of not requiring an external water supply to satisfy the make-up water needs of wet cooling towers.

9.5 Total-Flow Systems

The notion of a total-flow system arises from a desire to avoid the irreversibilities associated with the flashing processes needed for either a single- or double-flash plant. Also the separation process, while not inherently lossy, requires large pressure vessels and separate outlet pipelines for steam and water, all of which adds to the capital cost of the plant. If a way could be devised to use the geofluid directly as it emerges from the well in the prime mover, be it a turbine or some other specially designed device, significant savings would be achieved.

There have been three major development efforts aimed at producing such a system. One involved a single-stage pure impulse turbine [5], another used a positive-displacement expander (PDE) (a helical screw expander) [6,7], and the third was a novel concept of a rotary separator turbine (RST) [8]. The first one was a project of the US Department of Energy in the late 1970s and the other two were private projects that each received funding support from government and industrial organizations.

9.5.1 AXIAL-FLOW IMPULSE TURBINE

The fundamental simplicity of a total-flow machine can best be visualized using a temperature-entropy process diagram; see Figure 9.13.

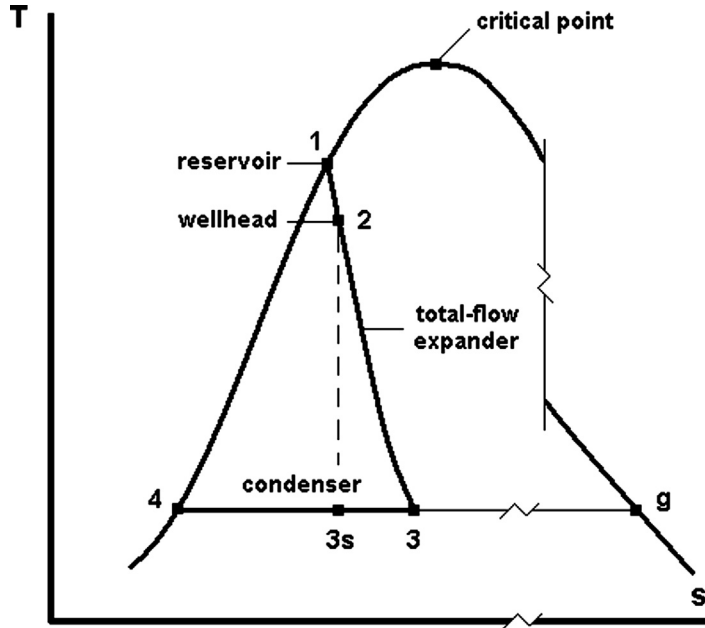


Figure 9.13 Total-flow expander concept in temperature-entropy coordinates.

If machinery could be designed and built to follow the processes in [Figure 9.13](#), the power plant would consist of only a turbine (2–3) and its generator, a condenser (3–4), and a cooling tower. An artist's conception of such a plant is given in [Figure 9.14](#) [9].

The analysis of this plant is simple; the turbine power output is given as:

$$\dot{W}_{TF} = \dot{m}_2(h_2 - h_3) = \dot{m}_2\eta_{TF}(h_2 - h_{3s}) \quad (9.20)$$

The crucial factor is the isentropic total-flow turbine efficiency:

$$\eta_{TF} = \frac{h_2 - h_3}{h_2 - h_{3s}} \quad (9.21)$$

A typical steam turbine has an efficiency of at least 80%. For the total-flow system to compete with a conventional flash plant, the efficiency of the new machine must be roughly 40–50%. This can be seen from the following argument; see [Figure 9.15](#). It is not possible to make an absolute comparison owing to the wide variation in geothermal fluid conditions and condensing temperatures, so a set of typical conditions were chosen for this comparison and are shown in the figure. For the two turbines to be equivalent, they must produce the same power output:

$$\begin{aligned} \dot{W}_{TF} &= \dot{m}_1(h_1 - h_5) = \dot{m}_1\eta_{TF}(h_1 - h_{5s}) = \dot{W}_{1F} \\ &= \dot{m}_1x_1(h_3 - h_4) = \dot{m}_1x_1\eta_{1F}(h_3 - h_{4s}) \end{aligned} \quad (9.22)$$

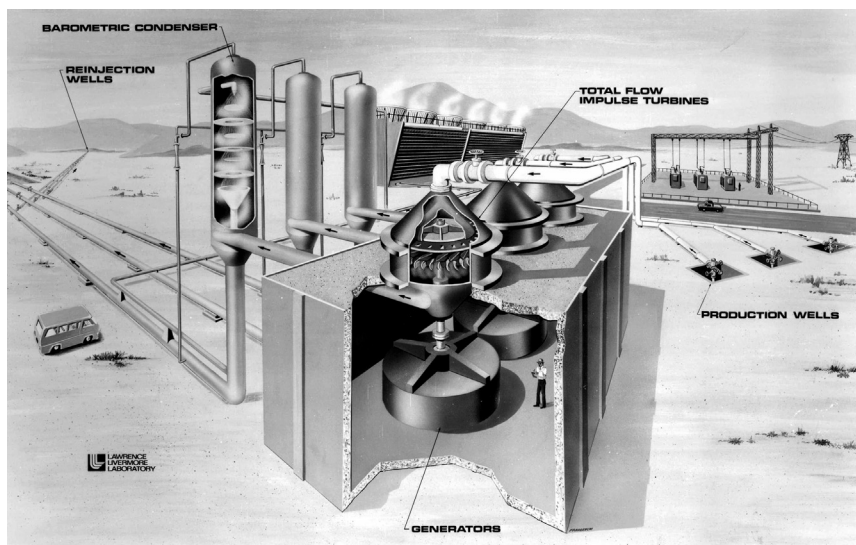


Figure 9.14 Artist's concept of a total-flow geothermal power plant [9].

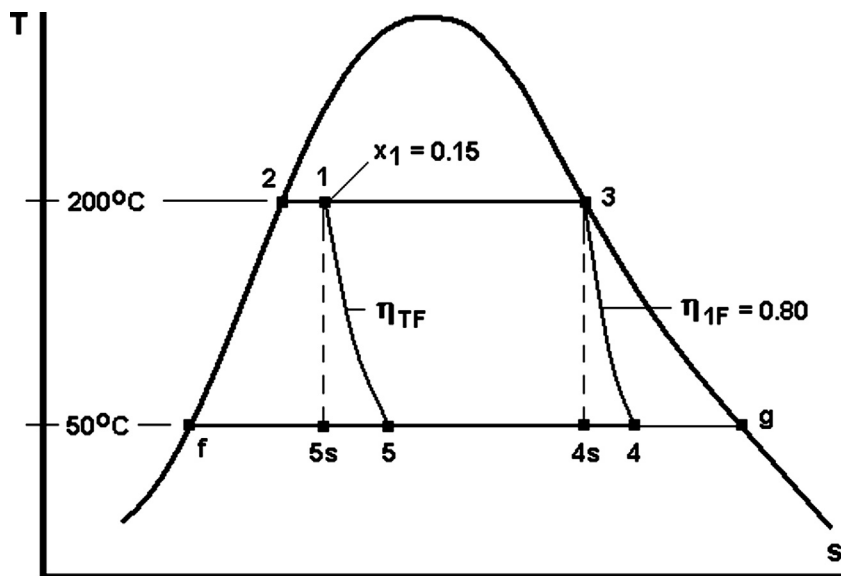


Figure 9.15 Comparison between total-flow and single-flash turbines.

Solving for the total-flow efficiency, we obtain:

$$\eta_{TF} = \eta_{1F} x_1 \left[\frac{h_3 - h_{4s}}{h_1 - h_{5s}} \right] \quad (9.23)$$

where the two isentropic turbine outlet enthalpies are found from:

$$h_{5s} = h_f + \left[\frac{s_1 - s_f}{s_{fg}} \right] h_{fg} \quad (9.24)$$

and

$$h_{4s} = h_f + \left[\frac{s_3 - s_f}{s_{fg}} \right] h_{fg} \quad (9.25)$$

For the selected conditions, the total-flow machine needs an efficiency of 42% to equal the output of the 80% efficient single-flash steam turbine. If the wellhead quality is 0.10, then the break-even efficiency becomes 49.2%. These two cases would correspond roughly to reservoir temperatures of 262°C and 242°C, respectively. The best value obtained on a prototype, single-nozzle, total-flow impulse turbine (see Figure 9.16) was 23% in laboratory tests, although it was estimated that a full-admission turbine would operate at about 45% efficiency [5]. The prototype was never installed at a geothermal site nor developed further.

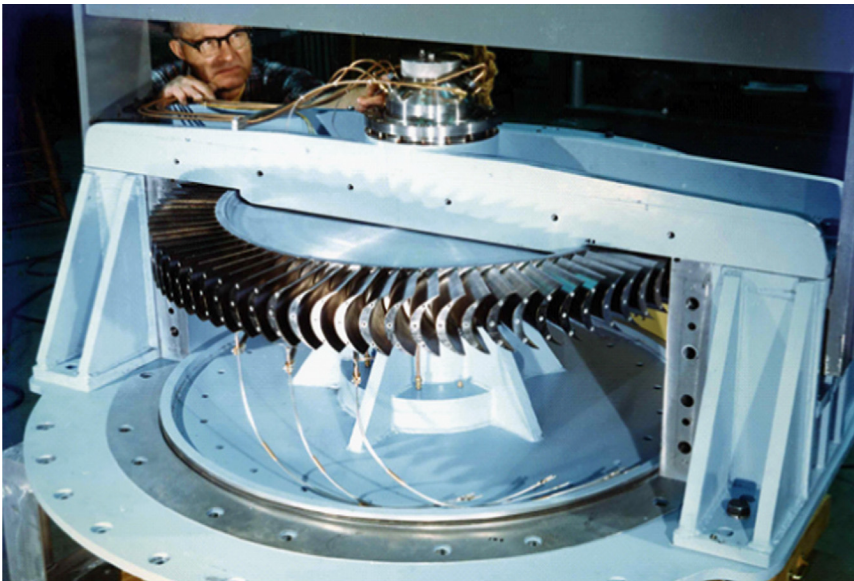


Figure 9.16 Lawrence Livermore Laboratory prototype impulse total-flow turbine [9] [WWW].

9.5.2 ROTARY SEPARATOR TURBINE

At about the same time that the total-flow turbine was being developed at the Lawrence Livermore Laboratory, a novel prime mover was also being designed and tested, a rotary separator turbine (RST) or the Biphase Turbine, after the company that invented it [8]. The features of the RST that distinguished it from other geothermal turbines included the ability to generate power using a two-phase, liquid–vapor stream, while simultaneously separating and pressurizing the liquid in preparation for reinjection. It did all this by means of five principal components:

- Two-phase nozzle
- Rotary separator
- Liquid turbine
- Liquid-transfer rotor
- Stationary diffuser.

A cross-section of the RST is shown in Figure 9.17. In a sense, the RST generates power from the kinetic energy of the moving two-phase flow by capturing the liquid energy while allowing the phases to separate by centrifugal force. One could imagine a vertical cyclone separator mounted on a turntable connected to a generator; as the two-phase fluid swirled around the inner surface, the liquid drag would cause the vessel and the generator to turn. Of course that idea is impractical, whereas the RST is compact and has performed reasonably well in several field tests.

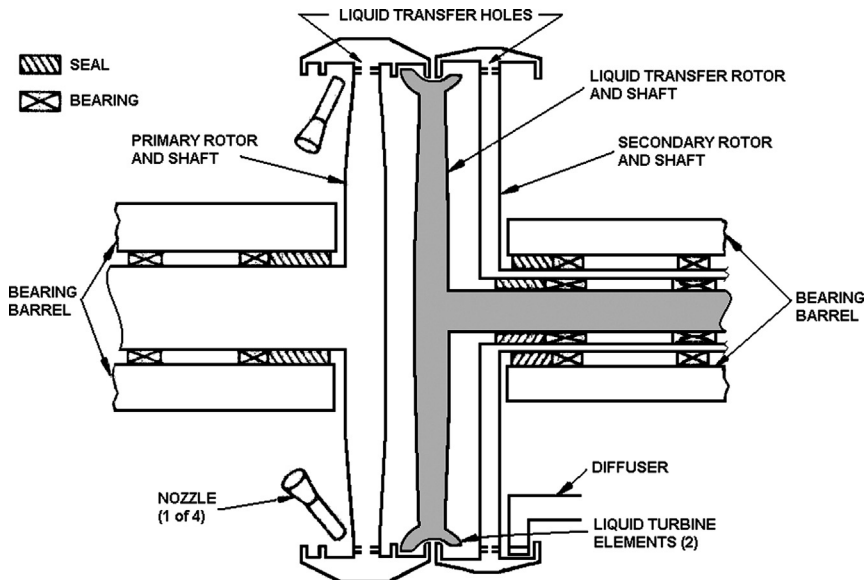


Figure 9.17 Cross-section of the RST from Biphase Turbines [10].

In its later field tests the unit was operated in conjunction with an upstream cyclone separator. The RST was packaged on a skid with a conventional steam turbine and a common generator. The liquid from the cyclone separator was sent to the RST while the steam went directly to the steam turbine. The quality of the fluid entering the two-phase nozzle is a critical parameter and this was controlled by feeding a small amount of separated steam into the nozzles. To assure equal flow to each of the four nozzles, the quality-adjusted geofluid flow was passed through a mixer-splitter unit before being admitted to the nozzles. The nozzles accelerate the flow to a high velocity and direct it onto the inner rim of the primary rotor. The liquid moves by centrifugal action and passes through the rim (liquid-transfer holes) and impinges on the liquid-transfer rotor where it gives up most of its kinetic energy. The shaft of this rotor is connected to the steam turbine shaft through a speed-increasing gearbox and so contributes to the power output of the packaged power plant. The spent liquid is transferred to the secondary rotor (again by passing through transfer holes in the web of the turbine rotor) where it is picked up by a stationary diffuser. This imparts a pressure boost to the liquid which may be sufficient to carry it to the injection wells without the need for booster pumps. The steam that is separated within the RST is removed through the RST casing and delivered to the steam turbine where it is admitted at a stage appropriate for its lowered pressure.

Extensive tests were conducted in 1981–82 at Roosevelt Hot Springs, Utah, US; the results are reported in Ref. [8]. The bottom-line machine efficiency was quoted as 27% at part load versus a 35% expected design value at full load.

Total-flow machines may also find application in vapor-compression refrigerators in place of the throttling control device where the power generated both offsets to some degree the compressor power requirements and increases the cooling effect in the evaporator [11].

9.5.3 HELICAL SCREW EXPANDER

The helical screw expander was invented by A. Lysholm [12] of Sweden who intended it for use as a compressor. It is a positive-displacement machine in which a trapped volume of fluid is conveyed between two meshing, helical, counter-rotating elements. It is easier to visualize as a compressor in which the rotors are driven by an external motor and in which the volume decreases in the axial direction, thereby compressing the fluid to a higher pressure. However, if high-pressure fluid is admitted to the device at the small-volume side, it will expand through the rotors causing them to rotate and will produce work. A cross-section of the machine is shown in Figure 9.18 [13].

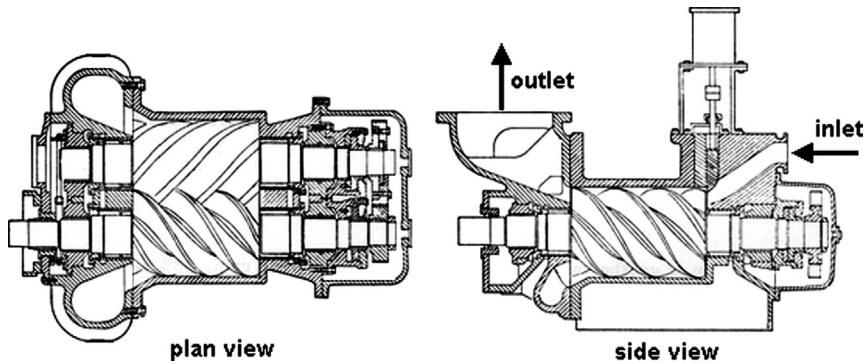


Figure 9.18 Helical screw expander for geothermal applications [13].

In 1973, Sprankle won a patent for the use of a Lysholm expander with geothermal liquid-dominated resources [14]. Sprankle's company, Hydrothermal Power Company, built and tested helical screw expanders at several geothermal fields. These machines are rugged and handle difficult fluids, that is, those that tend to deposit scale, quite well. The scrubbing action of the rotors against the inner surface of the casing tends to remove excess scale buildup; the scale that remains actually serves a useful purpose, namely, isolating the chambers to prevent fluid leakage in the axial direction.

The main obstacle that PDEs, of any design, must overcome is that of a limited volume ratio, that is, the ratio of the exit volume to the inlet volume. The engine tested in Ref. [13] could handle a maximum volume ratio of 5.3. When saturated liquid water is admitted to a PDE, it enters with a very low specific volume (high density), but as soon as it begins to expand it flashes into steam forming a two-phase mixture with a much greater specific volume. A study of this limitation [15] concluded that PDEs could not be competitive thermodynamically with double-flash plants unless PDEs could accommodate volume ratios of 10 or more. For example, at a resource with wellhead conditions of 200°C and 10% quality, a PDE with a volume ratio of 5 would need to demonstrate a machine efficiency of 81.5% to be equivalent to a double-flash steam plant under the same conditions. However, if the PDE can handle a volume ratio of 10, then it only needs to show an efficiency of 43.2% to match the double-flash plant.

A way to mitigate this limitation is to introduce a small amount of steam to the inlet of the PDE. This will raise the inlet specific volume and for the same volume ratio permit the expansion to go "deeper" into the two-phase region, producing a greater enthalpy drop and more work [15,16]. Two ways to accomplish this are (1) to preflash the liquid through a small pressure drop or (2) mix in some steam from a wellhead separator. In both cases, the PDE

would be used to supplement the output of a standard flash-steam plant, most probably a double-flash plant. This is the same approach described earlier for the RST.

Tests conducted in 1986 in New Zealand on the Model 76-1 of the Hydrothermal Power Company showed a maximum efficiency of 43% at an effective volume ratio of about 18. The machine suffered from leakage because the geofluid was nonscaling [17]; it appears that helical screw expanders thrive on scaling fluids but have more trouble maintaining tight clearances with pure fluids. Sprankle indicated that machine efficiencies of 75% should be achievable under specific power ratings and inlet geofluid quality; the higher the inlet quality, the more power that can be generated, and the easier it is to achieve an efficiency of 75% [17].

9.5.4 CONCLUSIONS

No total-flow device has achieved commercial status as a stand-alone power unit. Those that have been tested have not reached levels of machine efficiency that are sufficient to warrant their use even as supplements to standard geothermal plants. Each one examined in this section has advantages—simplicity, elegance, ingenuity, or scale-resistance—and with further development may eventually become commercially successful.

9.6 Hybrid Fossil-Geothermal Systems

Currently, the world is striving to develop as much renewable energy as is feasible to cope with growing demand and to meet environmental standards. One way to gain support for renewables is to combine them with conventional energy sources so as both to extend the life of the depletable resources and to create new applications for renewables in the existing marketplace.

Hybrid power plants combine two different sources of energy in a single plant so as to achieve higher overall utilization efficiencies than separate plants. One way to do this is to combine fossil and geothermal energy inputs in such a way as to yield a plant that outperforms two individual state-of-the-art plants, one using the fossil fuel and one a pure geothermal plant. In this section, we will examine several hybrid designs of this general type.

9.6.1 FOSSIL-SUPERHEAT SYSTEMS

The idea of using fossil fuels to enhance geothermal resources is not a new idea. It was reported in 1924 that a Frenchman P. Caufourier had proposed a hybrid

power system in which hot water from a geothermal spring would be flashed successively to generate steam and a fossil-fired superheater would raise the steam temperature prior to its admission to a multipressure turbine [18]. His system today would be called a four-stage flash-steam plant with fossil superheating; a schematic of the system is shown in Figure 9.19. Note that the waste brine was put to use in therapeutic baths, making this plant not only hybrid but multiuse as well.

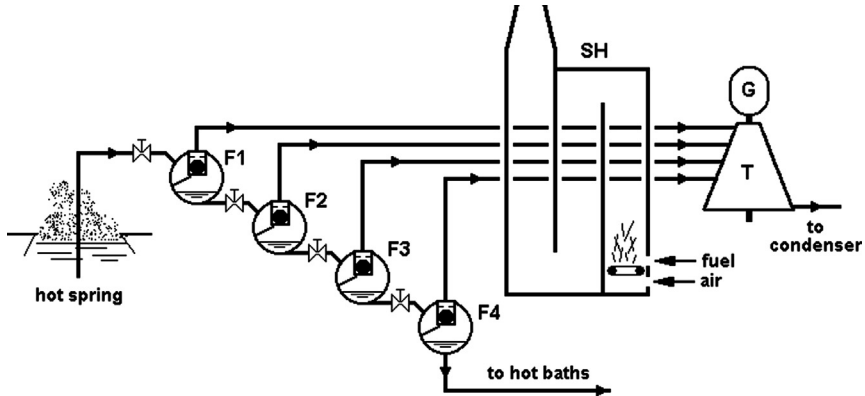


Figure 9.19 Caufourier's four-stage flash plant with fossil superheating. After Ref. [19].

Using reasonable assumptions, a thermodynamic analysis was carried out [19] that showed the hybrid plant was capable of a very high resource utilization efficiency, 65.3%, but the bulk of the output came from the geothermal contribution. A fossil-fuel effective efficiency can be defined as:

$$\eta_{ff} = \frac{\dot{W}_{hyb} - \dot{W}_{geo}}{\dot{Q}_{ff}} \quad (9.26)$$

where the numerator is the total plant output minus the output that could be obtained by using the geofluid by itself, in this case, in a four-stage flash-steam plant. The denominator is the thermal input from burning the fossil fuel. For the proposed plant $\eta_{ff} = 0.20$, a slightly low figure for its time, and certainly very low by today's fossil plant standards. For a hybrid plant to make thermodynamic sense, it must be synergistic, that is, capable of producing more than two separate, state-of-the-art plants using the same input from the two energy sources. Thus, this proposal from 1924 failed that test with regard to the fossil fuel usage. The analysis ignored the benefits of the hot water used in the spa.

A new proposal was put forth in the early 1980s for a hybrid fossil-geothermal plant at The Geysers in Northern California. A detailed analysis of the thermodynamics and economics of two schemes was carried out by the

California Energy Commission [20]. One used a simple superheater fired by natural gas to add superheat to the saturated steam produced by wells at The Geysers. The other used a natural gas-fired gas turbine with an exhaust heat recovery superheater to accomplish the same objective. Clearly the latter alternative produced much more power than the first, and in fact did so in a synergistic fashion. The fossil fuel used at The Geysers in this plan would have the highest utilization of any fossil fuel then being burned for power generation in California [20]. The simple superheating by direct firing of natural gas was found to be uneconomic even though it produced 57% more power than the basic dry-steam plant.

General studies of fossil superheating in geothermal plants were conducted at Brown University and the interested reader may consult Refs. [21–22] for more information.

9.6.2 GEOTHERMAL-PREHEAT SYSTEM

In the previous section we considered how fossil fuels might be used to enhance the performance of geothermal plants. It is also possible to use geothermal fluids to enhance the performance of fossil-fueled power plants. The geothermal-preheat systems do just that.

One of the earliest suggestions for this type of system is found in a 1961 paper by Hansen [23]. The idea is to use hot geothermal liquid as the heating medium in the feedwater heaters of a conventional fossil-fired power plant, thereby supplanting some of the extraction steam in a regenerative Rankine cycle. This would allow more power to be generated in the plant since the previously extracted steam would now be available to flow through the turbines. If the geofluid by itself was of low potential for use in a flash-steam plant, this would allow it to be used effectively in the hybrid system.

It is evident that the geothermal resource must be located close to the site of the fossil plant for this hybrid scheme to be practical. The City of Burbank, California, conducted a survey of possible sites for such a plant and concluded that Roosevelt Hot Springs, Utah, would be an economically viable site. There are nearby coal fields that could support a mine-mouth plant at which geothermal hot water could relieve the feedwater heating load. An engineering design verification study confirmed the plant's synergistic advantages [24]. The plant design was based on theoretical studies of geothermal-preheat systems at Brown University and reported in Ref. [25].

9.6.3 GEOPRESSURE-GEOTHERMAL HYBRID SYSTEMS

Along the northern shore of the Gulf of Mexico, there is a potent energy resource called "geopressure." Oil and gas drilling in the coastal areas of Louisiana and

Texas has encountered fluids with pressures greater than hydrostatic and approaching lithostatic. Hydrostatic pressure increases with depth in proportion to the weight of water, that is, at about 10.5 kPa per m (0.465 lbf/in² per ft). However, in formations where the fluid plays a supportive role in maintaining the structure of the reservoir, the weight of the solid overburden increases the gradient to the lithostatic value of 22.6 kPa per m (1.0 lbf/in² per ft).

In the geopressed reservoirs of the Gulf, sufficiently high pressure had been experienced to cause cessation of drilling for oil and gas. With improved drilling techniques, these zones can now be safely drilled.

Besides having very high pressure, these fluids are also hot and contain dissolved methane and other gases. A cleverly designed geothermal power plant can use each of these energy sources to advantage. A drastically simplified schematic flow diagram of such a plant is shown in Figure 9.20.

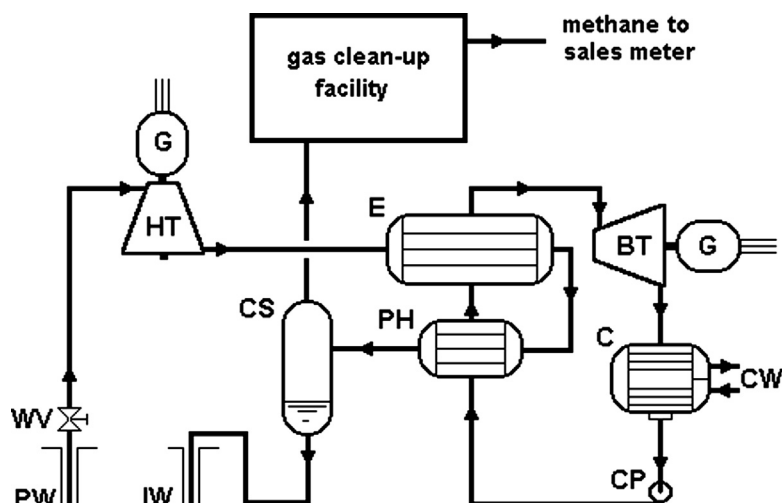


Figure 9.20 Conceptual hybrid plant utilizing a geopressed geothermal resource.

First the high-pressure fluid drives a back-pressure, hydraulic turbine, HT, generating electricity. Next it flows through the heat exchangers of a binary cycle, generating more electricity. Finally it enters a separator where the dissolved gases are liberated. The gases continue to a clean-up facility that would include scrubbers and contactors to purify the methane gas for sale. The waste brine from the separator is reinjected to help prevent subsidence which would be potentially much more serious for this type of system than a conventional hydrothermal plant.

The US DOE built and operated a small demonstration plant near Pleasant Bayou, Texas. The plant was rated at 1 MW and ran for 1 year in 1989–90.

Instead of selling the methane gas, the plant burned it on-site to drive a small gas turbine. The plant incorporated a binary cycle power generator, but no hydraulic turbine could be obtained to fit the brine conditions. A suitable hydraulic turbine might have increased the output by about 7–8%.

The feasibility of geopressured geothermal plants turns strongly on the resource characteristics: the pressure must be high enough, the fluid hot enough, and most importantly from an economic viewpoint, there must be sufficient dissolved methane. The solubility of methane in water solutions depends on pressure, temperature, and salinity. The solubility obviously increases with pressure, but at the pressures expected in geopressured reservoirs, the solubility dependency on temperature exhibits a minimum between 71 and 93°C (160 and 200°F). Furthermore, if the fluid is heavily mineralized, as is expected for these brines, the solubility decreases with increasing salinity. For example, at 121°C (250°F), the solubility of methane decreases 3–4% for each 10,000 ppm of total dissolved solids [26]. Lastly, the presence of other noncondensable gases reduces the solubility of methane.

Thus, the conditions need to be especially favorable for a geopressured resource to be commercially viable, and so far these conditions have not been found. Nevertheless, there are geopressured resources in several countries and researchers continue to explore them [27,28]. Finally, a recent study by Griggs at Louisiana State University [29] concluded that geopressured geothermal resources could be economically viable with the right set of natural gas and electricity prices, but that in the near-term it is unlikely that these conditions would occur. Meanwhile, there needs to be more work done in characterizing the resources, in optimizing the power facility including finding more efficient binary cycles, in conducting detailed economic analyses, and in clarifying legal and political issues including ownership of subsurface mineral rights [29].

9.7 Combined Heat and Power Plants

In many places it is common to combine both power generation and direct heat usage in a single geothermal plant. By capturing some of the waste heat in the leftover brine before it is reinjected, the overall utilization efficiency of the resource is enhanced. Furthermore, when that heat is provided to the community adjacent to the plant, it demonstrates to the community that the plant is indeed a “good neighbor.” There are two countries where this is widely practiced: Iceland and Japan. We will cover specific case histories in Part 3, but here we will present the basic principles of combined geothermal power and heating applications, using a single-flash steam plant as the basis for the analysis.

Figure 9.21 illustrates a single-flash power plant in which a side-stream of the separated brine is sent to a water-heating facility to supply the needs of various end users. The bank of primary heat exchangers would be located close to the power plant to avoid excessive heat loss from the brine and to allow it to be reinjected into the reservoir. A supply of freshwater is shown being delivered to the primary heat exchangers from well pumps. Secondary heat exchangers would be located close to the end users to permit the water from the mains to be heated for domestic consumption or heating purposes.

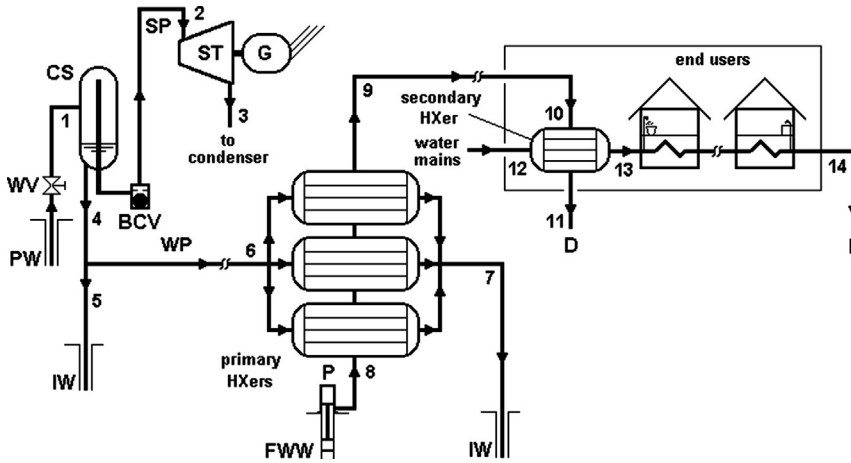


Figure 9.21 Combined geothermal heat and power plant. After Ref. [30].

The overall utilization efficiency of the plant including power generation and heating is the ratio of the sum of all beneficial output and effects to the exergy of the geothermal fluid under reservoir conditions. In terms of the states identified in Figure 9.21, this leads to the following equation:

$$\eta_u = \frac{\dot{W}_{ST} + \Delta \dot{E}_{13,14}}{\dot{E}_R} \quad (9.27)$$

where the useful heating effect, in exergy terms, is given by the difference in exergy across the end users,

$$\Delta \dot{E}_{13,14} = \dot{E}_{13} - \dot{E}_{14} = \dot{m}_{13}[h_{13} - h_{14} - T_0(s_{13} - s_{14})] \quad (9.28)$$

Since the fluid passing through the end users' facilities is a liquid, we can simplify Eq. (9.28):

$$\Delta \dot{E}_{13,14} = \dot{m}_{13} c \left[T_{13} - T_{14} - T_0 \ln \frac{T_{13}}{T_{14}} \right] \quad (9.29)$$

The reservoir fluid exergy is given by:

$$\dot{E}_R = \dot{m}_1(h_1 - T_0s_1 - e_0) \quad (9.30)$$

where

$$e_0 = h_0 - T_0s_0 \quad (9.31)$$

is the exergy of the fluid at the dead state.

For a 240°C reservoir, a 160°C separator temperature, a 50°C condensing temperature, a 125°C inlet to the secondary heat exchangers, and other reasonable assumptions, it was shown in Ref. [30] that the plant had a 33.4% utilization efficiency. Without the direct heat benefit, the single-flash plant would have a 31.2% utilization efficiency. Thus the combined plant has a 7% higher utilization plus the intangible benefits from good relations with the plant's neighbors.

To optimize such a plant, one would try to maximize the sum of the power output from the steam turbine \dot{W}_{ST} and the exergy of the fluid sent to the primary heat exchangers \dot{E}_6 . Both terms depend on the choice of separator temperature and the latter depends on the fraction of brine sent to the primary heat exchangers. Usually, there is a requirement for a certain amount of reinjection at state 5 to help maintain reservoir pressure and temperature, so that degree of freedom can be eliminated in favor of fixed amounts to reinjection and to the primary heat exchangers. Although the problem now is a simple one-dimensional optimization on thermodynamic grounds, there is one other parameter of importance in the economic sense: the monetary value of a unit of heat relative to a unit of work output. Several cases were examined in Ref. [30] and it was seen that the optimum flash temperature depends strongly on the ratio of the heat-to-work monetary values. As this ratio increases, so does the optimum flash temperature because this lowers the power output in favor of sending more exergy to the heat exchangers. Clearly, the local prices for alternative fuels and electricity will play a critical role in deciding whether or not to build a combined geothermal heat and power plant, and in the selection of the system operating parameters.

9.8 Power Plants for Hypersaline Brines

Since geothermal fluids are products of nature, it is sometimes difficult to use them as working fluids in a power plant. In fact some fluids are so challenging that it is nearly impossible to produce them from their reservoir. Geothermal brines have been found that are more acidic than battery acid, and that can clog a production well casing in a matter of a few days, or so contaminate surface vessels as to render them useless.

One of the most notorious geothermal resources is located in the Imperial Valley of Southern California, near the southeastern shore of the Salton Sea. The resource was recognized in the 1850s when explorers moving west came upon hot pools and mud volcanoes in an otherwise barren desert [31]. The latter persist to this day, driven by carbon dioxide gas emissions; see Figure 9.22.



Figure 9.22 The author at mud volcano site near the Salton Sea in California's Imperial Valley [WWW].

In 1905 the Colorado River broke through its banks and flooded the Salton Sink, creating what we know today as the Salton Sea and partially inundating the thermal manifestations. In 1925 interest was renewed in this area as a possible geothermal resource, and plans were even drawn up for a 25,000 kW power plant [32]. However, the area remained undeveloped as a source of electric power for nearly another 50 years, but was for a period of time a source of carbon dioxide for a thriving dry ice industry.

Drilling for power production began in the 1960s but the early wells were all plugged and abandoned. Some wells drilled in the 1970s are still in operation today, but the fluids that were produced resisted exploitation for power generation because of severe scaling and corrosion problems. The temperatures were high, up to 360°C (680°F), and the total dissolved solids reached as much as 300,000 ppm, placing these fluids in the hypersaline category. The chemical analysis of the fluid produced from the Magmamax No. 1 well that was drilled in 1972 about 1.5 mi from the southeast shore of the Salton Sea is given in Table 9.2 [33].

TABLE 9.2 Geothermal fluid composition for Magmamax No. 1 well, Salton Sea [33].

Element	Values
<i>Brine:</i>	<i>mg/l</i>
Chlorides	128,500
Sodium	40,600
Calcium	21,400
Potassium	11,000
Manganese	681
Strontium	440
Ammonia	360
Iron	315
Silicon	246
Zinc	244
Lithium	180
Barium	142
Magnesium	105
Lead	52
Copper	3
Total dissolved solids	219,000
pH	5.3
Oxidation reduction potential	+ 25
<i>Gases:</i>	<i>% by volume</i>
Carbon dioxide	98.14
Methane	0.68
Hydrogen sulfide	0.18
Nitrogen	0.02

As the result of an extensive research effort carried out starting in the 1970s that was funded by the US DOE, the Electric Power Research Institute, and several private companies, techniques were devised that now permit these fluids to be used for the generation of electricity in a reliable and cost-effective manner [34]. Two approaches for dealing with these aggressive brines have been used with reasonable success: (1) flash-crystallizer/reactor-clarifier (FCRC) and (2) pH modification (pH-Mod) systems. We will sketch the principles underlying these two methods.

9.8.1 FCRC SYSTEMS

In the FCRC approach, clean steam is generated in a train of separators and flash vessels, similar to what we have seen for standard flash-steam plants, but in

which the separated brine is seeded with material that induces precipitation. A simplified schematic of an FCRC power plant is shown in Figure 9.23 [34]. The seed material is obtained from the waste stream of highly concentrated brine. In this way, the unstable, supersaturated solids precipitate on the seed particles, rather than on the surfaces of the vessels and piping. The particulate matter is eventually allowed to settle in a reactor-clarifier vessel. The slurry from the reactor-clarifier is thickened and a portion of it is recirculated as seed material. The clarified liquid is pumped to a secondary clarifier and then sent to reinjection wells.

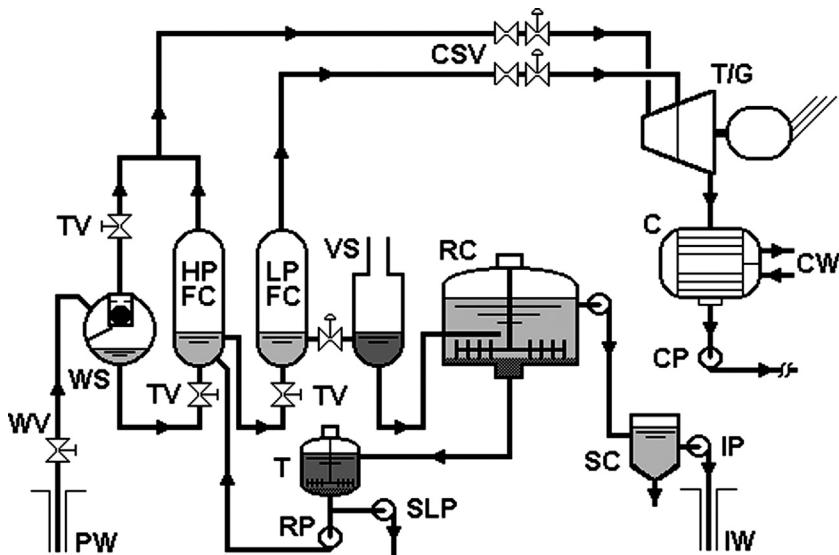


Figure 9.23 Simplified schematic flow diagram for an FCRC power plant. After Refs. [1, 34].

The most recent power plant to use this approach, Salton Sea Unit 5, has a triple-pressure turbine that receives the high-pressure steam separated at the well-head separators and expands it through the first four stages of the turbine [35]. This eliminates the throttling loss from the pressure-letdown throttle valve, TV, shown in Figure 9.23.

9.8.2 pH MODIFICATION (pH-Mod) SYSTEMS

In Section 6.6 we discussed the problem of silica scaling and how it might be controlled. One approach is to modify the pH of the brine to alter the kinetics of

the precipitation process. The technique of acidifying the brine has been used in some Salton Sea plants as an alternative to the FCRC approach. By reducing the pH of the geofluid the solubility of silica is increased, the kinetics of the reaction are slowed, and it is possible to avert precipitation, at least until the separated liquid has been processed to generate the flash steam needed for the turbine. A highly simplified flow diagram for a pH-Mod plant is shown in [Figure 9.24](#).

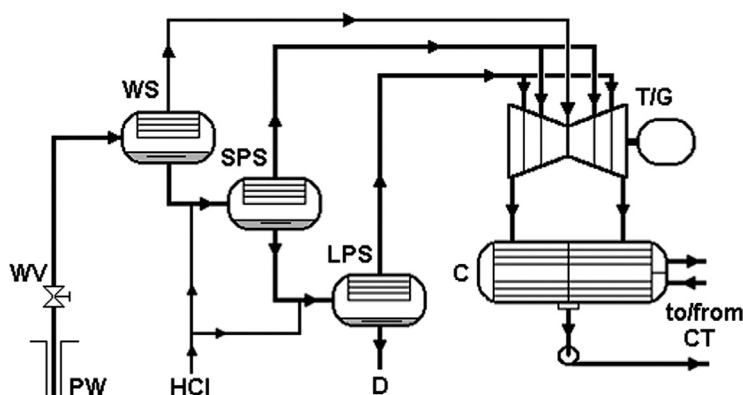


Figure 9.24 Flow diagram for pH-Mod power plant.

The addition of hydrochloric acid to the brine requires appropriate corrosion-resistant materials. However, pH-Mod plants are much simpler than FCRC plants in terms of the number of vessels needed and the operating procedures to be followed. Omitted from [Figure 9.24](#) is the processing of the discharge waste brine D. If the injection of the treated brine could lead to problems in the pipelines or the injection wells, then the brine pH could be raised. A reactor-clarifier might then be used to remove the silica to assure that the waste brine can be safely reinjected.

With the use of the FCRC and pH-Mod methods for coping with the Salton Sea brines, it has been possible to construct 10 power plants with a total capacity of 312 MW. A new 185 MW triple-flash plant was scheduled to be built. This plant would have represented the largest single geothermal power unit ever constructed, surpassing the 133 MW Unit 13 at The Geysers (now renamed Big Geysers and derated to 78 MW). However, this project has been modified; the Hudson Ranch facility, a planned staged development of three 50 MW (nom.) plants, resulted in only one 49.9 MW unit which came on-line in 2012; the other

units were canceled. This power plant was later renamed in honor of John L. Featherstone whose research led to methods of taming the aggressive Salton Sea brines. With a significant portion of the geothermal field lying offshore beneath the Salton Sea itself, it is believed that the ultimate potential of this resource is far from being fully exploited. The technologies described in this section should allow this valuable resource to eventually reach its full potential.

9.9 Solar-Geothermal Hybrid Plants

9.9.1 BASIC CONCEPT

As with any hybrid power plant, the basic idea is to achieve a synergistic outcome wherein the hybrid plant can outperform two individual state-of-the-art plants using the solar and geothermal energy sources separately; see [Figure 9.25](#). That is, the hybrid plant (H) must be so designed that the separate energy sources are used to augment each other, that is, the hybrid plant H-power must exceed the sum of the S-power and the G-power, for the same energy inputs. In [Section 9.6](#) it was shown how this could be achieved with geothermal and fossil energy sources. Since both of those sources are available on a continuous basis, it is relatively simple to devise means to achieve synergy.

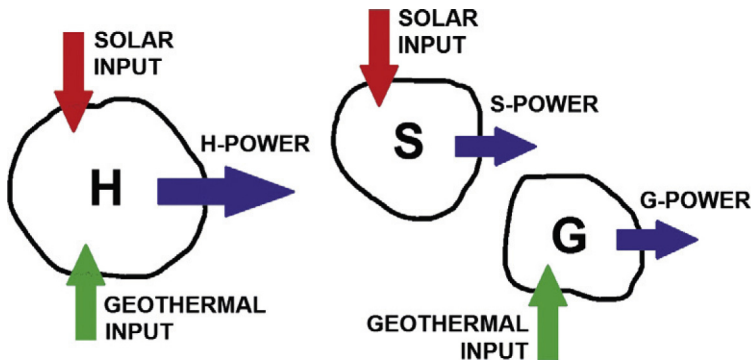


Figure 9.25 Comparison between a hybrid solar-geothermal plant and two separate solar and geothermal plants [WWW].

For the hybrid systems being considered in this section, one of the two energy sources is not available all the time; the geothermal may be assumed on hand continuously, but the solar input disappears at night and during cloudy conditions. This places serious practical constraints on possible hybrid designs.

On the economic side, solar and geothermal plants have dramatically different unit costs, with solar electricity being considerably more expensive than electricity from conventional geothermal plants. Thus, when taking into account both thermodynamic and economic performance, it is hard to avoid reaching an optimum configuration that favors all geothermal and no solar.

Nevertheless, since economics depend on local circumstances (i.e., labor costs, cost of money, material costs, financial incentives, government subsidies, etc.) and these can vary over time, it is useful to consider some possible solar-geothermal hybrid configurations that may become both thermodynamically and economically viable in the future, even if not at the present time.

9.9.2 GEOTHERMAL-AUGMENTED SOLAR THERMAL PLANTS

As mentioned in [Section 9.6.2](#), the two energy sources must be collocated or at least within easy access. In the case of a solar-assisted geothermal plant, this constraint is not so important since the solar input is available anywhere and can be used at any geothermal site, albeit with varying levels of solar insolation. However, if it is desired to augment a solar plant with geothermal energy, then collocation can be a problem. In this section we consider just such a design.

Solar thermal power plants typically use concentrating parabolic trough collectors to focus the incoming solar rays onto tubes carrying a heat transfer fluid (HTF), which in turn is used to heat and boil a secondary working fluid, usually water, to drive a Rankine cycle, usually one designed for high efficiency. Such plants resemble conventional fossil-fueled plants and have at least one feedwater heater.

If low-to-moderate temperature geothermal fluid can be found near the solar thermal plant, a synergistic design is possible wherein the geofluid is pumped through one of the feedwater heaters, eliminating a steam extraction point from the turbine, thus increasing steam flow through the last stages of the turbine and raising the power output. The system described in [Section 9.6.2](#) is an illustration of this approach for a fossil-geothermal hybrid plant. The utilization efficiency of the geothermal energy is very high in this application. In the Southwest sector of the United States there is excellent insolation and many hot springs that would allow this approach to be considered.

9.9.3 SOLAR-AUGMENTED BINARY PLANTS

If solar energy is used to augment a basic geothermal plant of the binary type, the intermittent nature of the solar input must be factored into the design.

The obvious way to alleviate this limitation is to incorporate thermal storage for the solar HTF, as shown schematically in the flow diagram in Figure 9.26. The effect of the solar energy in this design is to superheat the binary cycle working fluid while the sun is shining, thereby improving the exergy of the working fluid as it enters the turbine [36]. If the binary working fluid is one with normal condensing properties (see Figure 8.8), adding superheat can assure a fully dry expansion process and a higher turbine efficiency. After the storage system has been depleted, say 5–7 hours after sunset, bypass valves are activated and the system operates as a simple geothermal binary plant, albeit at a lower efficiency.

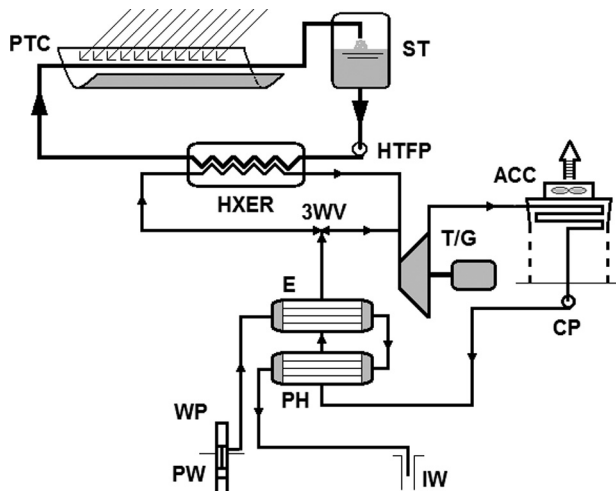


Figure 9.26 Solar-geothermal binary plant with superheating of the binary working fluid.

Whether or not the added expense of the solar system is justified by the increased output during the day will depend on local conditions, as mentioned earlier.

9.9.4 SOLAR-AUGMENTED FLASH PLANTS

The notion of using solar energy to assist geothermal flash plants is not new. Hiriart and Gutiérrez [37] describe a combination flash-steam system in which the steam line is passed through a parabolic solar collector to impart about 100°C of superheat before entering the turbine. This is enough to produce 4 MW of additional power above the base case of 20 MW for a pure geothermal flash plant. Besides offering thermodynamic advantages, the proposal appeared to have economic merit as well.

There are several ways to add solar energy to a geothermal flash plant. Figure 9.27 illustrates the possibilities for a base double-flash plant, but the ideas can be easily applied to single-flash plants. The parabolic trough collector (PTC) field and storage system has a circulating HTF that can be routed to any of several heat exchangers (HXER) to augment the flash plant. The one shown is used to superheat the low-pressure steam from the flash vessel. The HXER could also be located at sites A1, A2, and/or A3. At A1, the separated brine from the cyclone separator is heated prior to being admitted to the flash vessel, which will generate a higher fraction of low-pressure steam. At A2, the high-pressure steam is superheated prior to turbine entry. And at A3, a portion of the steam condensate is recirculated through a solar HXER for reheating and boiling, much like a conventional Rankine cycle, and returned to the low-pressure steam line [38].

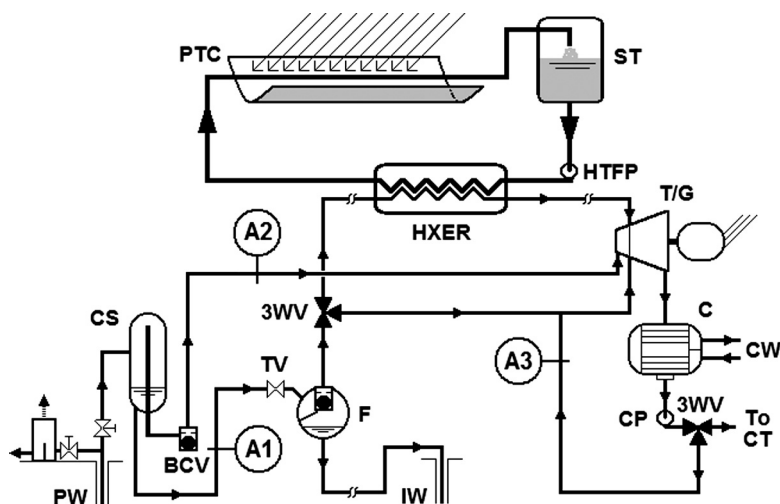


Figure 9.27 Solar-geothermal double-flash plant.

Various solar-geothermal hybrid schemes can be imagined. For example, a combined cycle (flash-binary) is amenable to hybridization [36]. Field testing of several schemes has been carried out at the Ahuachapán geothermal flash plant in El Salvador [39,40]. The main difficulty in implementing any of these arrangements lies in the intermittent nature of the solar energy. On the geothermal side, any arrangement that requires periodic shutting down of wells or electromechanical equipment would be unacceptable. Thus, without significant thermal storage, it may not be feasible to deploy such ingenious schemes.

References

- [1] DiPippo R. Geothermal power systems [section 8.2]. In: Elliott TC, Chen K, Swanekamp RC, editors. *Standard handbook of powerplant engineering*. 2nd ed. New York, NY: McGraw-Hill, Inc.; 1998. p. 8.27–60.
- [2] DiPippo R. Geothermal power cycle selection guidelines. Part 2 of Geothermal Information Series, DCN 90-213-142-02-02, Electric Power Research Institute, Palo Alto, CA; 1990.
- [3] National Institute of Standards and Technology (NIST), US Department of Commerce, <<http://www.nist.gov/srd/nist23.cfm>>.
- [4] Forte N. The 125 MW upper Mahiao geothermal power plant. *Geothermal Resour Counc Bull* 1996;25(8):299–304.
- [5] Austin AL, Lundberg AW. The LLL geothermal energy program: a status report on the development of the total-flow concept. UCRL-500-77, Lawrence Livermore Laboratory, Livermore, CA; 1978.
- [6] McKay R. Helical screw expander evaluation project: final report. DOE/ET-28329_1, JPL Pub. 2_5, Jet Propulsion Laboratory, Pasadena, CA; 1982.
- [7] Carey B. Total flow power generation from geothermal resources using a helical screw expander. *Proc. 5th New Zealand geothermal workshop*; 1983, p. 127–32.
- [8] Cerini DJ, Record J. Rotary separator turbine performance and endurance test results. *Proc. seventh annual geothermal conference and workshop*, EPRI AP-3271, Electric Power Research Institute, Palo Alto, CA; 1983, p. 5-75–5-86.
- [9] Austin AL. Status of the development of the total flow system for electric power production from geothermal energy. In: Kestin J, editor-in-chief, DiPippo R, Khalifa HE, Ryley DJ, Eds., *Sourcebook on the production of electricity from geothermal energy*, US Dept. of Energy, DOE/RA/051_1, US Gov. Printing Office, Washington, DC; 1980 [section 4.4].
- [10] Hughes EE. *Final Report, EPRI AP-4718. Summary report: rotary separator turbine*. Palo Alto, CA: Electric Power Research Institute; 1986.
- [11] Stoecker WF, Jones JW. *Refrigeration and air conditioning*. 2nd Ed. New York, NY: McGraw-Hill; 1982.
- [12] Lysholm A. Rotary compressor, US Patent No. 2,243,874; June 3, 1941.
- [13] Weiss H, Steidel R, Lundberg A. Performance test of a Lysholm Engine. Rep. No. UCRL—1861, Lawrence Livermore Laboratory, Livermore, CA; July 1975.
- [14] Sprinkle RS. Electric power generating system, US Patent No. 3,751,673; August 7, 1973.
- [15] DiPippo R. The effect of expansion-ratio limitations on positive-displacement, total-flow geothermal power systems. *Geothermal Resour Counc Trans* 1982;6:343–6.
- [16] DiPippo R. The effect of expansion-ratio limitations on positive-displacement, total-flow geothermal power systems. LA-UR-82-596, Rep. No. GEOFLO/15, Div. of Engineering, Brown University, Providence, RI; 1982.
- [17] Sprinkle R. Helical screw expander power plant model 76-1 test result analysis. *Hydrothermal Power Co*; 1986.
- [18] Anon. Recent developments in the utilization of the earth's heat. *Mech Eng* 1924;46(8):448–9.
- [19] DiPippo R. An analysis of an early hybrid fossil-geothermal power plant proposal. *Geothermal Energy Mag* 1978;6(3):31–6.
- [20] Janes J. Evaluation of a superheater enhanced geothermal steam power plant in The Geysers area. Rep. 700-84-003, California Energy Commission, Siting and Environmental Div.; 1984.
- [21] Kestin J, DiPippo R, Khalifa HE. Hybrid geothermal-fossil power plants. *Mech Eng* 1978;100:28–35.

- [22] DiPippo R, Khalifa HE, Correia RJ, Kestin J. Fossil superheating in geothermal steam power plants. *Geothermal Energy Mag* 1979;7(1):17–23.
- [23] Hansen A. Thermal cycles for geothermal sites and turbine installation at the geysers power plant, California. Paper G/41, Proc. conf. on new sources of energy, Rome, United Nations, vol. 3; 1961, p. 365–79.
- [24] Anon. System design verification of a hybrid geothermal/coal fired power plant, The Ralph M. Parsons company, Project 5905; 1978.
- [25] Khalifa HE, DiPippo R, Kestin J. Geothermal preheating in fossil-fired steam power plants. Proc. 13th intersociety energy conversion engineering conference, vol. 2; 1978, p. 1068–73.
- [26] Swanson RK. *Final Report, EPRI AP-1457. Geopressured energy availability*. Palo Alto, CA: Electric Power Research Institute; 1980.
- [27] Árpási M, Lorberer Á, Pap S. High pressure and temperature (geopressured) geothermal reservoirs in Hungary. Proc. world geothermal congress 2000, International Geothermal Association; 2000, p. 2511–4.
- [28] He L, Xiong L. Extensional model for the formation of geopressured geothermal resources in He Yinggehai Basin, South China Sea. Proc. world geothermal congress 2000, International Geothermal Association; 2000, p. 1211–6.
- [29] Griggs J. A re-evaluation of geopressured-geothermal aquifers as an energy resource. Master's thesis, Louisiana State University, Craft and Hawkins Dept. of Petroleum Engineering; August 2004.
- [30] DiPippo R. Exergy analysis of combined electricity and direct-heat geothermal flash-steam plants. *Geothermal Resour Counc Trans* 1987;11:411–16.
- [31] LeConte JL. Account of some volcanic springs in the desert of the Colorado, in Southern California. *Am J Sci Arts*, Second Ser May 1855;XIX:1–6.
- [32] Siegfried HN. Further possibilities for development in hot areas adjacent to the transmission lines of the southern Sierras Power Company Spec. Report No. 3. In: Anderson N, Hall BA, editors. *Geothermal exploration in the first quarter century*. Davis, CA: Geothermal Resources Council; 1973. p. 145–71.
- [33] Lombard GL. Operational experience at the San Diego Gas & Electric ERDA Niland geothermal loop experimental facility. Proc. EPRI annual geothermal program project review and workshops, PRI ER-660-SR, Electric Power Research Institute, Palo Alto, CA; 1978, p. 3-11–3-16.
- [34] Featherstone J, Butler S, Bonham E. Comparison of crystallizer reactor clarifier and pH mod technologies at the Salton Sea geothermal field. Proc. world geothermal congress 1995, V. 4, International Geothermal Association; 1995, p. 2391–6.
- [35] Anon. Brochure GEC 82_14. CalEnergy Company, Inc., USA Salton Sea Unit 5 geothermal power plant 1358.32 MW. Tokyo, Japan: Fuji Electric Co., Ltd.; 2001.
- [36] Greenhut AD, Tester JW, DiPippo R, Field R, Love C, Nichols K, et al., Solar-geothermal hybrid cycle analysis for low enthalpy solar and geothermal resources. Proc. world geothermal congress 2010, Paper 2615, Bali, Indonesia; 2010.
- [37] Hiriart LBG, Gutiérrez LCAN. Calor del Subsuelo Para Generar Electricidad: Combinacion Solar-Geotermia. *Ingenieria Civil*, vol. 313, May 1995, p. 13–22 (in Spanish).
- [38] Lentz A, Almanza R. Parabolic troughs to increase the geothermal wells flow enthalpy. *Solar Energy* 2006;80:1290–5.
- [39] Handal S, Alvarenga Y, Recinos M. Geothermal steam production by solar energy. *Geothermal Resour Counc Trans* 2007;31:503–10.
- [40] Alvarenga Y, Handal S, Recinos M. Solar steam booster in the Ahuachapán geothermal field. *Geothermal Resour Counc Trans* 2008;32:395–9.

Nomenclature for Figures in Chapter 9

ACC	Air-cooled condenser
BCV	Ball check valve
BHT	Brine holding tank
BT	Binary turbine
C	Condenser
CP	Condensate pump
CS	Cyclone separator
CT	Cooling tower
CW	Cooling water
D	Drain
E	Evaporator
F	Flash vessel
FWW	Freshwater well
f	Saturated liquid
G	Generator
GC	Gas compressor
g	Saturated vapor
HPF	High-pressure flash vessel
HPFC	High-pressure flash crystallizer
HT	Hydraulic turbine
HTFP	Heat transfer fluid pump
HXER	Heat exchanger
IP	Injection pump
IW	Injection well
LPF	Low-pressure flash vessel
LPFC	Low-pressure flash crystallizer
LPS	Low-pressure separator
NCG	Noncondensable gases
OP	Orifice plate
P	Pump
PH	Preheater
PTC	Parabolic trough collector
PW	Production well
RC	Reactor-clarifier
RP	Recirculating pump
SH	Superheater
S	Separator
SC	Secondary clarifier
SLP	Sludge pump
SP	Steam piping
SPS	Standard-pressure separator
ST	Steam turbine
T	Thickener
T/G	Turbine/generator
TV	Throttle valve

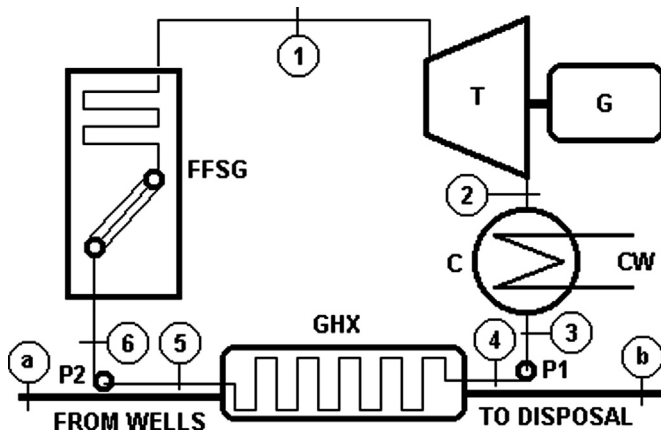
VS	Vent silencer
WP	Water piping; Well pump
WS	Wellhead separator
WV	Wellhead valve

Problems

9.1. Consider a hybrid fossil-geothermal power plant of the geothermal-preheat type shown in the schematic below. The following are given:

$$P_1 = 15 \text{ MPa}, T_1 = 538^\circ\text{C}, \eta_t = 0.80, \eta_{pumps} = 1.0,$$

$$P_2 = P_3 = 6.3 \text{ kPa}, T_a = 150^\circ\text{C}$$

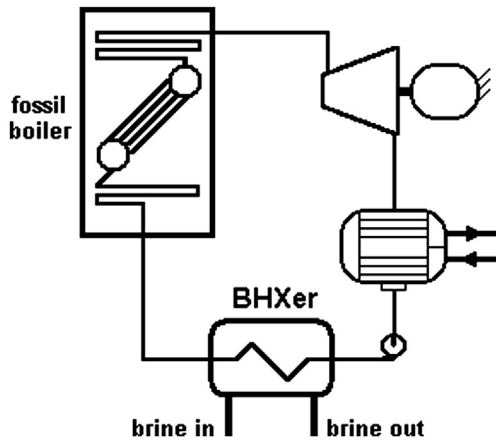


State 5 is saturated liquid, there are no pressure losses in heat exchangers or pipelines, and the temperature difference along the geothermal heat exchanger is constant. The pressure of the pure water in the GHX is equal to the square root of the product of the condenser and boiler pressures; that is, the two feed pumps have the same pressure ratio. With reference to a base fossil-fueled power plant consisting of the same elements as the hybrid plant minus the geothermal heat exchanger and the second pump (i.e., the base plant has its condensate pumped to P_6 in one pump and more sensible heating is required in the fossil-fueled boiler), determine the following:

- Net work of base fossil plant, w_f , in kJ/kg steam.
- Cycle thermal efficiency of base fossil plant, η_{THf} .
- Net work of hybrid plant, w_h , in kJ/kg steam.
- Effective fossil-fuel cycle thermal efficiency of hybrid plant, $\eta_{THf-eff}$.

- e. Hybrid plant figure of merit, *FOM*, that is, the ratio of the hybrid net output to that of the sum of a geothermal binary plant using the heat input from the geofluid with a 10% thermal efficiency and a fossil plant using the heat from the fossil fuel needed in the hybrid plant with the same efficiency as in the base plant.
 - f. For a net hybrid plant output of 250 MW, estimate the number of geothermal wells needed to supply the plant if each well can produce 65 kg/s.
 - g. Discuss the feasibility of the plant.
- 9.2.** A “total-flow” turbine is proposed that will use a geothermal liquid at 200°C (saturated liquid). What isentropic turbine efficiency must the total-flow machine have in order for it to match the thermodynamic performance of:
- a. a one-stage flash plant.
 - b. a two-stage flash plant?
- Assume the “equal-temperature-split” rule for flash points and a condenser temperature of 50°C. Use a steam turbine efficiency of 75% for the flash plants and use separate cylinders (no mixing) for the two-stage flash plant.
- 9.3.** A single-stage total-flow machine is capable of handling a two-phase mixture of geothermal fluid as it comes from the well. The geofluid temperature is 195°C and the wellhead quality is 25%. The condenser operates at 50°C. Determine the required isentropic efficiency of the total-flow machine for it to be thermodynamically equivalent to a single-flash plant having a steam turbine with an efficiency of 77% and operating with the same wellhead and condenser conditions.
- 9.4.** With reference to [Figure 9.7](#), the following conditions are given:
- Reservoir fluid = saturated liquid at 200°C;
 - Geofluid mass flow rate at wellhead = 100 kg/s;
 - $T_2 = 140^\circ\text{C}$, $T_6 = T_d = 40^\circ\text{C}$, $P_a = P_e = P_f = 3.0\text{ MPa}$;
 - Binary cycle working fluid = isobutane, $i\text{-C}_4\text{H}_{10}$;
 - Pinch-point ΔT in brine-isobutane heat exchanger = 5°C;
 - State 4 and state a are saturated vapors;
 - Dry turbine efficiency = 85%; wet turbine efficiency from Baumann rule;
 - Isobutane feed pump is isentropic.
- Calculate the following quantities:
- a. Mass flow rate of isobutane, in kg/s.
 - b. Power output of (i) steam turbine and (ii) isobutane turbine, in kW.
 - c. Power to run the isobutane feed pump, in kW.
 - d. Overall plant utilization efficiency based on the exergy of the reservoir geofluid; dead-state temperature is 25°C.

- 9.5. A very simple geothermal-preheat type of fossil-geothermal hybrid plant is shown in the schematic below.



The following data are given:

- Boiler pressure = 18.5 MPa;
- Turbine inlet temperature = 595°C;
- Condenser pressure = 14 kPa;
- Steam flow rate = 75 kg/s;
- Brine inlet temperature = 190°C;
- Terminal temperature difference at hot end of BHXer = 12°C;
- Brine outlet temperature = 70°C;
- Turbine efficiency = 0.80;
- Feed pump efficiency = 0.75.

Calculate the following quantities:

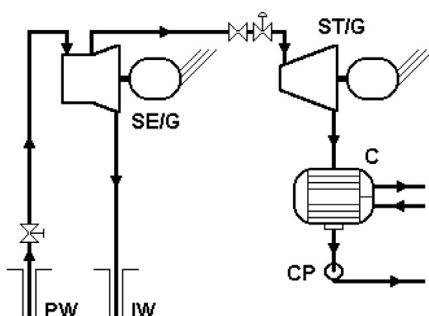
- a. Brine flow rate, in kg/s.
- b. Thermal efficiency of the hybrid plant.

Assuming that the state-of-the-art thermal efficiency of a fossil steam plant is 35% and that for a geothermal binary plant is 15%, determine the following quantities:

- c. Overall figure of merit for the hybrid plant.
- d. Fossil-fuel figure of merit.
- e. Geothermal figure of merit.

The respective figures of merit are defined as: Part (c)—the ratio of the actual hybrid plant output to the best that could be obtained using two separate state-of-the-art plants, Part (d)—the ratio of the portion of the hybrid output attributable to the fossil fuel to the output from a state-of-the-art fossil plant, and Part (e)—the ratio of the portion of the hybrid output attributable to the geothermal heat to the output from a state-of-the-art geothermal binary plant.

- 9.6. A simple fossil-superheat type of fossil-geothermal hybrid plant is being proposed. Geothermal steam from a separator is available as a saturated vapor at 195°C . A gas-fired superheater would raise the steam temperature to 535°C . The condenser operates at an absolute pressure of 13.5 kPa . You may assume that the turbines are isentropic. Calculate the following quantities:
- Work output of the hybrid plant, in kJ/kg geosteam.
 - Work output of a geothermal single-flash plant, in kJ/kg geosteam.
 - Fossil-fuel figure of merit if the fossil heat could be used in a state-of-the-art fossil plant with a thermal efficiency of 35% .
- 9.7. Use the geothermometers described in Section 2.3.5 to analyze the data given in Table 9.2 to estimate the geofluid reservoir temperature for the Magmamax No. 1 well at the Salton Sea. You may assume that the data has been corrected for reservoir conditions. Discuss the results and any differences among the values found from the various formulations.
- 9.8. A separating-expander incorporates a total-flow machine and a steam turbine in an integrated package as shown in the figure below. The two-phase flow is admitted to the SE where the steam is separated and sent to the ST while the liquid generates power as it is separated centrifugally in the SE. The liquid is sent directly to the injection wells from the SE.

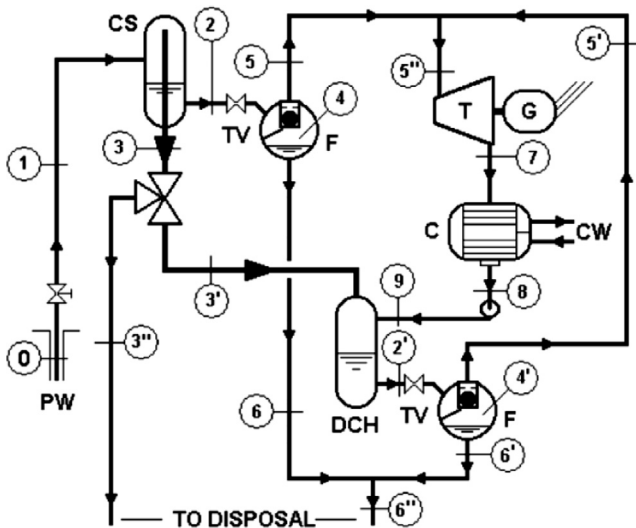


The geofluid temperature is 200°C , the steam turbine efficiency is 75% , the separating-expander efficiency is 50% , and the condenser temperature is 50°C . Calculate the dependence of the utilization factor on the intermediate temperature T_1 , that is, the temperature at which the steam is sent to the ST. At what temperature does the optimum performance occur? How does this compare with the “equal-temperature-split” rule for a simple one-stage flash plant? Use 25°C as the sink temperature.

- 9.9. The flash-steam power plant shown in the accompanying schematic is designed to utilize highly contaminated brine. The brine is produced from

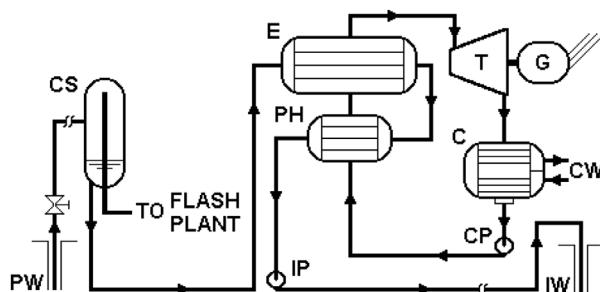
the reservoir (state 0) at a temperature of 250°C. The temperature at the cyclone separator (CS) is 205°C. The brine carries 100,000 ppm total dissolved solids plus an amount of noncondensable gases (NCG). Clean steam (state 5) is generated in the primary flasher. Since the steam from the separator is too contaminated for direct use in the turbine, a fraction of it is sent to a direct-contact heater (DCH) where it reheats the essentially pure condensate from the turbine. Then a secondary flasher generates more clean steam (state 5') which merges with the primary steam before entering the turbine. The fraction of the separated steam (state 3') used in the DCH is chosen such that a saturated liquid is produced at the outlet of the DCH (state 2'). Additional specifications are: $T_4 = 162^\circ\text{C}$; $T_7 = T_8 = 60^\circ\text{C}$; dead-state temperature = 27°C ; condensate pump is isentropic.

The plant is not optimized and is not very efficient, but does allow the use of a challenging geofluid. Waste occurs at two places: vent steam and NCG at state 3'' and concentrated brine at state 6''. Note that states with the same numerical label have identical thermodynamic properties, but differ in mass flow rates, as denoted by the primes. Throughout the analysis of the plant, assume that the geofluid flow from the reservoir is unity, that is, $\dot{m}_1 = 1 \text{ kg/s}$.



- Construct the temperature-entropy process flow diagram (not to scale, schematically).
- Calculate the following: mass flows: (i) vent steam, (ii) waste brine, (iii) steam flow to the turbine.

- c. Calculate: (i) specific power output of the turbine, using the Baumann rule and a dry efficiency of 85%, (ii) specific power to run the condensate pump, and (iii) the net power, all expressed in kW/(kg/s) of geofluid.
- d. Calculate the exergy of the following flows: (i) geofluid from the reservoir, (ii) fluid entering the separator, (iii) steam entering the turbine, (iv) vent steam, (v) waste brine. In each case, express the result in units of kJ/kg of geofluid at state 0. Note that the exergy of brine containing $N\%$ of dissolved solids is less than for pure water at the same conditions by a factor $(1 - 0.0085 N)$, that is, the fluid loses 0.85% of its exergy for each 1% of TDS in the brine. Note that the TDS concentration in the brine increases after each flash, whereas the steam may be considered pure.
- e. Calculate the utilization efficiency of the power plant based on the reservoir conditions.
- 9.10.** Your task is to design a bottoming binary plant to be used in conjunction with an existing single-flash plant. The binary plant will capture some of the waste energy (and exergy) leaving the flash plant with the residual brine. The plant schematic is shown below.



The following data are specified:

Brine inlet temperature at evaporator = 425 K;

Cycle working fluid = isopentane ($i\text{-C}_5\text{H}_{12}$);

Turbine inlet temperature = 390 K (saturated vapor);

Turbine isentropic efficiency = 85%;

Condensing temperature = 310 K;

Feed pump isentropic efficiency = 100% (ideal);

Pinch-point temperature difference in preheater-evaporator = 4 K;

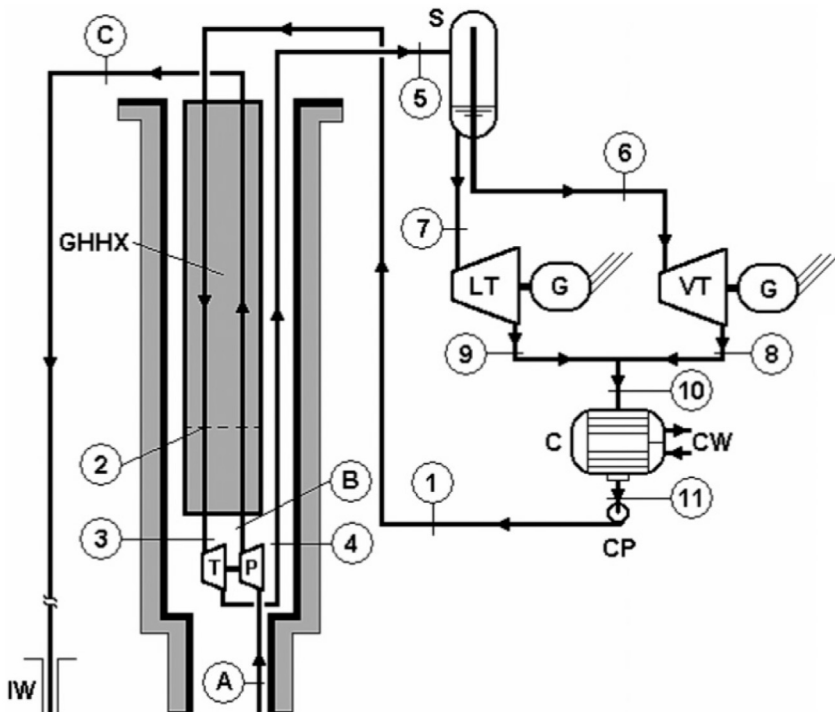
Cycle net output = 6000 kW;

Dead-state temperature = 25°C.

Using the pressure-enthalpy process flow diagram as a visual aid, calculate the following:

- Specific work output of the turbine (i.e., in kJ/kg of $i\text{-C}_5\text{H}_{12}$).
- Specific work to run the feed pump.

- 9.11.** A schematic diagram of the so-called Gravity-Head Binary Power Plant is shown in the figure below. This was proposed by Matthews Geothermal, Inc. in the 1980s as a more efficient method of generating power from geothermal fluids. Brine is pumped at 182°C from the reservoir (state A) by a downhole turbo-pump unit, TPU. The TPU is powered by the binary cycle working fluid, R-114 (no longer available), which is heated in a downhole, gravity-head heat exchanger (GHHX). The brine temperature may be taken as 182°C at state B; the pump in the TPU increases the brine pressure by 1.4 MPa. You may assume that the outer shell of the GHHX is perfectly insulated.



The R-114 enters the GHX (state 1) as a saturated liquid at 38°C. The internals of the GHX are so designed that the heating line of the R-114 coincides with the saturated liquid line from state 1 to 2. From state 2 to 3 it follows a path of constant density, $\rho = 801 \text{ kg/m}^3$, until it reaches $P_3 = 6.207 \text{ MPa}$. The pinch-point in the GHX is 5.5°C. The turbine in the TPU has an efficiency of 75%; the pump in the TPU is 70% efficient. From state 4 to the surface, the R-114 may be assumed to flow at constant enthalpy. At the separator, the R-114 has a temperature of 127°C. The vapor stream is used in an 85% efficient turbine, VT, while the liquid fraction is used in a 35% efficient liquid expander, LT. The exhaust streams from the two machines are combined and sent to a common condenser before being returned to the GHX. The condensate pump, CP, has negligible work input. REFPROP will be needed to solve this problem.

- a. Sketch the processes schematically in a pressure-enthalpy diagram for R-114.
 - b. Construct the temperature-heat transfer ($T-Q$) diagram for the GHX, making use of REFPROP for the properties of R-114.
 - c. With the aid of your construction, find the brine outlet temperature, T_C .
 - d. Calculate the ratio of the flow rates, $\dot{m}_{R-114}/\dot{m}_{\text{brine}}$.
 - e. Calculate the actual specific work of the pump in the TPU in units of kJ/kg of brine.
 - f. Calculate the actual change in specific enthalpy of the R-114 as it passes through the turbine in the TPU.
 - g. Calculate the quality (or dryness fraction) at state 5.
 - h. Calculate the specific work of: (i) the vapor turbine and (ii) the liquid expander, in units of kJ/kg of R-114.
 - i. Calculate the gross power output of the plant if the brine flow rate is 63 kg/s.
 - j. Assuming that all auxiliary power requirements amount to 20% of the gross power found above, calculate the net utilization efficiency for a dead state at 27°C.
- 9.12.** This problem investigates the efficiency of multiple-flash plants. Multiple-flash steam plants have been employed on certain resources as a means of coping with challenging conditions such as high concentrations of dissolved solids and noncondensable gases. However, they could be used at normal geothermal resources. Consider a hydrothermal resource having a saturated liquid in a reservoir at 260°C. The condensing temperature in the power plant is 49°C. The dead-state temperature is 27°C.

Calculate the following for (i) single-flash, (ii) double-flash, (iii) triple-flash, and (iv) quadruple-flash plants:

- a. Specific power output of the turbine(s) in units of kW/(kg/s) of incoming geofluid;
- b. Gross utilization efficiency.

In each case, use the “equal-temperature-split” rule to find the separator and flash temperatures. Use the Baumann rule for wet turbine efficiency where the dry efficiency is 85%. Deploy individual turbines (each with a generator) operating between their inlet condition and the condenser (i.e., do not employ pass-in turbines). Plot the results and draw conclusions about the use of multiple-flash steam plants.

- 9.13.** A basic binary plant is augmented with a parabolic solar collector to raise the temperature of the cycle working fluid prior to turbine entry. The cycle uses isopentane as the working fluid. The following conditions are known:

Evaporator pressure = 3 MPa; condenser pressure = 0.3 MPa;

Turbine inlet temperature = 225°C; turbine isentropic efficiency = 0.85;

Feed pump isentropic efficiency = 0.80.

Calculate:

- a. Specific power output of the cycle in units of kW/(kg/s) of isopentane.
- b. Net cycle thermal efficiency for (i) hybrid solar-geothermal cycle and (ii) basic binary cycle with saturated vapor at turbine inlet.
- c. Discuss the results of Part (B) in terms of the incremental thermal efficiency of the superheat added in the solar collector.
- d. Discuss the feasibility of such a hybrid system including pros and cons.



Chapter 10

Exergy Analysis Applied to Geothermal Power Systems

Chapter Outline

10.1 Introduction	292
10.2 First Law for Open, Steady Systems	292
10.3 Second Law for Open, Steady Systems	293
10.4 Exergy	294
10.4.1 General Concept	294
10.4.2 Exergy of Fluid Streams	294
10.4.3 Exergy for Heat Transfer	297
10.4.4 Exergy for Work Transfer	297
10.5 Exergy Accounting for Open, Steady Systems	298
10.6 Exergy Efficiencies and Applications to Geothermal Plants	299
10.6.1 Definitions of Exergy Efficiencies	299
10.6.2 Exergy Efficiencies for Turbines	299
10.6.3 Exergy Efficiencies for Heat Exchangers	302
10.6.4 Exergy Efficiencies for Flash Vessels	306
10.6.5 Exergy Efficiencies for Compressors	308
10.6.6 Exergy Efficiencies for Pumps	311
10.6.7 Exergy Analysis for Production Wells	313
10.7 Thermal Versus Utilization Efficiency for Geothermal Plants	315
References	316
Problems	317

The Second Law of thermodynamics holds the supreme position among the laws of Nature. If someone points out to you that your pet theory of the universe is in disagreement with Maxwell's equations—then so much the worse for Maxwell's equations. If it is . . . contradicted by observation—well, these experimentalists do bungle things sometimes. But if your theory is found to be against the Second Law of thermodynamics, I can give you no hope; there is nothing for it but to collapse in deepest humiliation.

Sir Arthur S. Eddington, *Gifford Lectures*—1927

10.1 Introduction

This chapter offers an introduction to the fundamental principles of exergy analysis which is based on the Second Law of thermodynamics. The presentation is restricted to open systems operating in steady state. These are the applications encountered in all types of power plants, including geothermal power plants, once they reach their design operating conditions. These principles also may be used to assess refrigeration plants, air-conditioning systems, and many other common engineering process plants.

After the basic working equations are derived, we will examine some of the components usually found in geothermal plants to illustrate the use of these principles. We will find that exergy analysis is the best tool for finding those elements within a plant that are most in need of redesign from an efficiency point of view.

10.2 First Law for Open, Steady Systems

Although exergy analysis relies strongly on the Second Law of thermodynamics, it also is grounded in the First Law, namely, that energy is conserved during any process while it is transformed from one form to another. We begin with the basic First Law equation for open systems operating in steady state. Briefly, an open system is one in which matter crosses the boundary of the system during the process, and in steady operation, the values of all thermodynamic properties at any point in the system remain constant with time. We adopt the macroscopic viewpoint in which properties are measured by instruments which by design average out microscopic fluctuations.

The general First Law working equation is:

$$\dot{Q} - \dot{W}_s = - \sum_{i=1}^n \dot{m}_i (h_i + 0.5V_i^2 + gz_i) \quad (10.1)$$

where each term is defined as follows:

- \dot{Q} = rate of heat transfer (thermal power) between the system and its surroundings (+ when heat enters the system)
- \dot{W}_s = rate of work transfer (mechanical power) between the system and the surroundings (+ when work is delivered to the surroundings by the system)
- i = an index that accounts for all inlets and outlets of the system
- n = total number of inlets and outlets
- \dot{m}_i = mass flow rate crossing each inlet or outlet
- h_i = specific enthalpy of the fluid at each inlet or outlet

\mathcal{V}_i = velocity of the fluid at each inlet or outlet

z_i = elevation of each inlet or outlet relative to an arbitrary datum

g = local gravitational acceleration.

The principle of conservation of mass in steady state requires that

$$\sum_{i=1}^n \dot{m}_i = 0 \quad (10.2)$$

Note that when using Eqs. (10.1) and (10.2) mass flows are taken as positive when entering the system and negative when leaving. This sign convention allows us to write the equations in summation form and must be scrupulously applied.

10.3 Second Law for Open, Steady Systems

It is instructive to write down the general Second Law formulation for open systems before specializing it to steady systems.

$$\dot{\theta}_p = \frac{dS}{d\tau} - \sum_{i=1}^n \dot{m}_i s_i - \int_{\tau_1}^{\tau_2} \frac{1}{T} \frac{dQ}{d\tau} \quad (10.3)$$

where each new term is defined as follows:

$\dot{\theta}_p$ = rate of entropy production for the system caused by irreversibilities

S = entropy of the system

τ = time

s_i = specific entropy of the fluid at each inlet or outlet

T = absolute temperature (in K or °R) associated with the heat transfer Q .

The physical meaning of the integral in the last term in Eq. (10.3) is that it represents a summation taken over the whole surface area of the open system, for the duration of the process, of all the incremental heat transfer rates divided by their corresponding absolute temperatures. In general, there may be several heat reservoirs interacting with the open system, but, as we will see shortly, this term can be drastically simplified for the present study.

Since we will be dealing only with steady systems, time derivatives of thermodynamic properties will all vanish, and the working equation reduces to:

$$\dot{\theta}_p = - \sum_{i=1}^n \dot{m}_i s_i - \int_{\tau_1}^{\tau_2} \frac{1}{T} \frac{dQ}{d\tau} \quad (10.4)$$

because the entropy S is a system property and the heat Q is not.

10.4 Exergy

10.4.1 GENERAL CONCEPT

The basic concept of exergy is that it is the maximum work (or power) output that could theoretically be obtained from a substance at specified thermodynamic conditions relative to its surroundings. While this definition is comprehensive, here we are only interested in open, steady systems. A system may receive (or discharge) fluids from (or to) the surroundings, and exchange heat and work with the surroundings.

We will seek the maximum power output from the operation of the system. To achieve this ideal outcome, there are two thermodynamic conditions that must be met:

1. All processes taking place within the system must be perfectly reversible;
2. The state of all fluids being discharged from the system must be in thermodynamic equilibrium with the surroundings.

The first condition means that no losses occur because of friction, turbulence, or any other source of irreversibility. The second condition means that the leaving fluids have no more potential to do work relative to the surroundings. For this reason, we refer to the state of the surroundings as the “dead state” because when a fluid is in equilibrium with the surroundings it may be considered “dead.”

A consequence of condition 1 is that $\dot{\theta}_p$ in Eq. (10.4) vanishes, that is,

$$-\sum_{i=1}^n \dot{m}_i s_i - \int_{\tau_1}^{\tau_2} \frac{1}{T} \frac{dQ}{d\tau} = 0 \quad (10.5)$$

In general for any system of the type we are considering, all heat transfer can be viewed ultimately as an interaction solely with the surroundings. A generalized schematic of the system and its interactions with the surroundings is given in Figure 10.1.

10.4.2 EXERGY OF FLUID STREAMS

Next we use the two conditions given above to specialize the First and Second Law equations and arrive at an exergy working equation. As a simplification, let us first consider the simplest system that can undergo a steady, open process, namely, one with only two channels, an inlet and an outlet. Also, let us, for the moment, ignore the effects of kinetic and potential energy; thus Eq. (10.1) becomes:

$$\dot{Q} - \dot{W} = \dot{m} (h_2 - h_1) \quad (10.6)$$

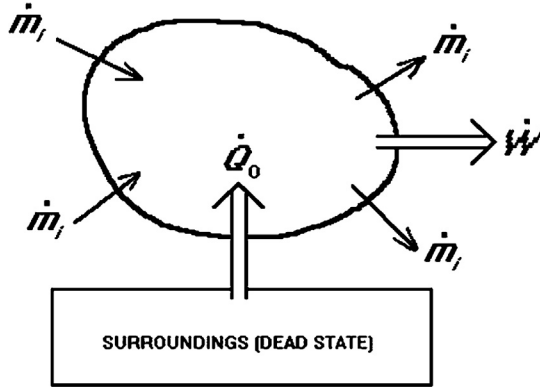


Figure 10.1 Generalized system–surroundings interactions.

where the subscript “s” on the power has been dropped for simplicity. Since the only heat transfer is between the system and the dead state, Eqs. (10.6) and (10.5) can be rewritten, respectively, as:

$$\dot{Q}_0 - \dot{W} = \dot{m} (h_2 - h_1) \quad (10.7)$$

$$-\dot{m} (s_1 - s_2) - \frac{\dot{Q}_0}{T_0} = 0 \quad (10.8)$$

Solving Eq. (10.8) for \dot{Q}_0 and substituting into Eq. (10.7), one obtains:

$$\dot{W} = \dot{m} [h_1 - h_2 - T_0(s_1 - s_2)] \quad (10.9)$$

Finally, we use the condition 2 to stipulate that the exit state 2 be identical to the dead state, and so obtain the maximum power output:

$$\dot{W}_{max} = \dot{m} [h_1 - h_0 - T_0(s_1 - s_0)] \quad (10.10)$$

This maximum output is given a special name, exergy, \dot{E} . The expression in brackets is the specific exergy, e :

$$e_1 \equiv h_1 - h_0 - T_0(s_1 - s_0) \quad (10.11)$$

This equation may be used to find the specific exergy of any fluid stream at a temperature T_1 and pressure P_1 , relative to a given set of ambient conditions T_0 and P_0 . If kinetic or potential energy effects are important, the enthalpy h_1 should be augmented by $0.5V_1^2$ or gz_1 , as appropriate. Since state 1 is really arbitrary, we can drop the subscript and obtain a general expression for the specific exergy:

$$e = h - h_0 - T_0(s - s_0) \quad (10.12)$$

where the properties at the dead state are evaluated at T_0 and P_0 . When the fluid would be a liquid at the dead-state condition, it is sufficiently accurate to take the enthalpy and entropy values for a saturated liquid at T_0 . When calculating e , T_0 must be in absolute units, either kelvins or degrees Rankine.

It is sometimes convenient to introduce a new quantity, b , called the availability function, defined as:

$$b \equiv h - T_0 s \quad (10.13)$$

The usefulness of the availability function is evident when considering a process between two given states, neither of which is the dead state. Then the maximum possible specific work output for such a process is simply:

$$e_{1,2} = h_1 - h_2 - T_0(s_1 - s_2) = b_1 - b_2 \quad (10.14)$$

Kestin [1] called this the available work, w^o , since it involves the best one can do for two specified states.

A few more words of explanation are needed regarding exergy. First, exergy is not a thermodynamic property. For a quantity to be a thermodynamic property it must be a state-function, that is, its value must be a function strictly of the state of the system. It can only depend on other system properties [2]. It is clear from the definition of exergy, Eq. (10.12), that the value of the exergy of a system depends on the dead state. A different dead state for the same system condition will yield a different value of the exergy. For this reason there are no “exergy tables”; property tables such as *Steam Tables* or *Gas Tables* [3] only include actual properties. Once the dead state is defined, however, it is an easy task to calculate exergy values for any set of system conditions.

The second point is also important; the dead state is not arbitrary [4]. It represents the local surroundings in which the system finds itself. The designation of the dead state is fundamentally different from setting the reference level for energy, enthalpy, or any other thermodynamic potential. In those cases, when we take differences between, say the energy at one state and that at another state, the reference value cancels out. This does not happen with exergy, as can be seen from Eq. (10.14) since the dead-state temperature remains in the equation. The practical way to treat the dead state is to take into account the nature of the processes under study and the environment in which the processes take place, and to choose the dead state accordingly. For example, if the system is a geothermal power plant equipped with a water cooling tower, an appropriate choice would be the design wet-bulb temperature for the cooling tower. This temperature is the ideal lower limit on the water leaving the tower. If the plant uses an air-cooled condenser, then the design dry-bulb temperature would be appropriate.

Lastly, the dead state as we have defined it here is sometimes called a restricted dead state [5]. Thermodynamic equilibrium requires that the system be

in mechanical equilibrium (i.e., equal pressure), thermal equilibrium (i.e., equal temperature), and chemical equilibrium (i.e., equal reaction potential) with its surroundings. Since chemical equilibrium does not play a role in a practical sense in most geothermal plants, we will disregard it and only require mechanical and thermal equilibrium at the dead state in calculating the exergy.

10.4.3 EXERGY FOR HEAT TRANSFER

Whenever heat is transferred from one system to another, a certain amount of exergy is also transferred. The important point in such a case is this:

The absolute amount of exergy given up by the hotter system is, in reality, always greater than the exergy received by the cooler system; only in the ideal case of reversible heat transfer are the two exergy amounts equal.

The magnitude of the exergy involved with the heat transfer process can be found from the basic concept of exergy, namely, what is the maximum work that could be produced on a continuous basis from the given amount of heat. The answer is:

The work that could be obtained using a reversible Carnot cycle operating between the temperature from which the heat is derived and the lowest practical available temperature, i.e., the ambient or dead-state temperature.

If a quantity of heat Q is transferred from a system at a temperature T to another system at some lower temperature within an environment having a dead-state temperature T_0 , then the exergy E_Q associated with the heat Q is given by:

$$E_Q = \left[1 - \frac{T_0}{T} \right] Q \quad (10.15)$$

where the factor in brackets is the familiar Carnot efficiency for an ideal cycle operating between T and T_0 . When applying Eq. (10.15), it is customary to use the magnitude of the exergy, that is, to use the magnitude of the heat transfer term Q irrespective of whether the heat is entering or leaving the system since the direction of the exergy flow will be obvious from the context.

10.4.4 EXERGY FOR WORK TRANSFER

Whenever a system experiences a work transfer process with its surroundings, exergy is also transferred. The relationship between the work and the exergy associated with it is simple:

The maximum work that can be delivered in the absence of any dissipative phenomena is exactly the amount of work itself.

Thus the exergy E_W associated with the transfer of an amount of work W is given by:

$$E_W = W \quad (10.16)$$

It should be noted that both Eqs. (10.15) and (10.16) may be written as rate equations involving the thermal power or mechanical power, respectively. Then the exergy calculated from a rate equation will be the rate of exergy transfer or exergetic power.

10.5 Exergy Accounting for Open, Steady Systems

In this section we will come up with equations that express how closely a system comes to meeting thermodynamic ideality. The technique involves isolating the system (as a “free-body” in the language of mechanics) and performing an exergy accounting analysis. The system is assumed to operate in steady state with several mass flows into and out of the system; it receives a flow of thermal power from a heat reservoir at a temperature T and delivers power to an end user residing in the surroundings, characterized by a dead-state temperature T_0 .

The exergy accounting for the open system will involve the exergy associated with each flow stream and each exergy transfer term. Unlike an energy accounting which by the First Law must always balance, an exergy accounting will in reality always show that less exergy leaves the system than enters it. In other words, some exergy will always be destroyed. If all dissipative phenomena could be eliminated and all processes carried out reversibly, then no exergy would be lost, but this could only occur in an ideal world. In our accounting we will denote the lost exergy as Δe (per unit mass).

The exergetic power input to the system is given by:

$$\dot{E}_{IN} = \dot{E}_Q + \sum_{i=1}^n \dot{m}_i e_i \quad (10.17)$$

where the summation is taken over all *incoming* streams, $i = 1, 2, \dots, n$.

The exergetic power output from the system is given by:

$$\dot{E}_{OUT} = \dot{E}_W + \sum_{j=1}^k \dot{m}_j e_j \quad (10.18)$$

where the summation is taken over all *outgoing* streams, $j = 1, 2, \dots, k$.

Thus the exergy accounting equation is simply:

$$\Delta \dot{E} = \dot{E}_{IN} - \dot{E}_{OUT} = \dot{E}_Q + \sum_{i=1}^n \dot{m}_i e_i - \dot{E}_W - \sum_{j=1}^k \dot{m}_j e_j \quad (10.19)$$

The exergy loss term $\Delta \dot{E}$ must always be numerically positive. Note that the terms associated with heat and work can be either positive or negative depending on their direction in accordance with our sign conventions.

10.6 Exergy Efficiencies and Applications to Geothermal Plants

10.6.1 DEFINITIONS OF EXERGY EFFICIENCIES

It is useful to define efficiencies based on exergy, sometimes called Second Law efficiencies or utilization efficiencies. There is no standard set of definitions in the literature, but we will describe two different approaches: “brute-force” and “functional.”

1. A “brute-force” exergy efficiency for any particular system is defined as the ratio of the sum of all output exergy terms to the sum of all input exergy terms.
2. A “functional” exergy efficiency for any particular system is defined as the ratio of the exergy associated with the desired energy output to the exergy associated with the energy expended to achieve the desired output.

The brute-force definition can be applied in a straightforward manner, irrespective of the nature of the system, once all exergy flows have been determined. The functional definition, however, requires judgment and an understanding of the purpose of the system before the working form of the efficiency equation can be formulated. In the remaining sections of this chapter we will examine the components usually found in geothermal plants and apply both exergy definitions to each of them. We will also include numerical examples to illustrate their use.

10.6.2 EXERGY EFFICIENCIES FOR TURBINES

Figure 10.2 shows a simple turbine. Incoming fluid drives a set of blades to rotate a shaft, thereby producing work output. There is exergy associated with the work

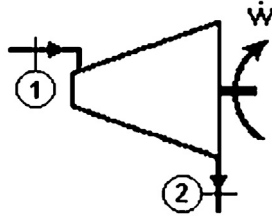


Figure 10.2 Simple turbine.

and with both streams. It is reasonable to neglect any heat transfer between the turbine and the surroundings. This analysis is general and applies to any kind of turbine.

The exergy accounting equation for the turbine is:

$$\Delta \dot{E}_t = \dot{m}_1 e_1 - \dot{m}_2 e_2 - \dot{W} \quad (10.20)$$

where the two mass flow rates must be equal by conservation of mass and the steady flow assumption. Thus, we obtain:

$$\Delta \dot{E}_t = \dot{m}(e_1 - e_2) - \dot{W} \quad (10.21)$$

or

$$\Delta e_t = e_1 - e_2 - w \quad (10.22)$$

written per unit mass flow through the turbine.

The Second Law or exergy efficiencies may be expressed as:

$$\eta_{t,BF}^{II} = \frac{e_w + e_2}{e_1} = \frac{w + e_2}{e_1} \quad (\text{brute-force}) \quad (10.23)$$

$$\eta_{t,FUN}^{II} = \frac{e_w}{e_1 - e_2} = \frac{w}{e_1 - e_2} \quad (\text{functional}) \quad (10.24)$$

The isentropic turbine efficiency is the ratio of the actual work to the work obtainable from an isentropic (reversible and adiabatic) expansion process:

$$\eta_t = \frac{w}{w_{s=const}} = \frac{h_1 - h_2}{h_1 - h_{2s}} = \frac{h_1 - h_2}{h_1 - h_2 + (h_2 - h_{2s})} \quad (10.25)$$

If we expand Eq. (10.24) we can compare the functional exergy efficiency with the isentropic efficiency, Eq. (10.25):

$$\eta_{t,FUN}^{II} = \frac{h_1 - h_2}{h_1 - h_2 + T_0(s_2 - s_1)} \quad (10.26)$$

From the temperature-entropy diagram, Figure 10.3, it is clear that

$$h_2 - h_{2s} > T_0(s_2 - s_1) \quad (10.27)$$

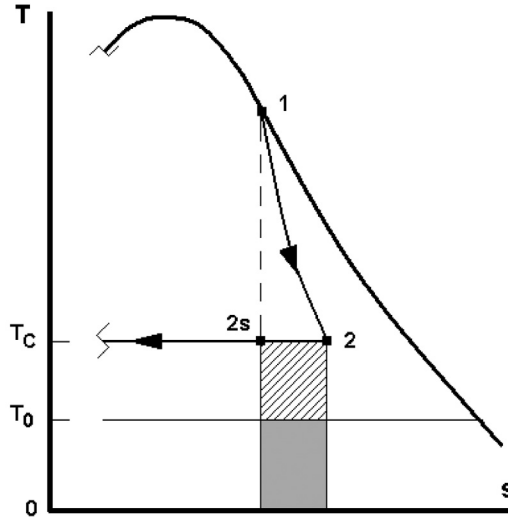


Figure 10.3 Irreversibility in temperature-entropy coordinates.

since the right-hand side is the shaded area and the left-hand side is the shaded area plus the cross-hatched area. Thus, we conclude that

$$\eta_{t,FUN}^{II} > \eta_t \quad (10.28)$$

Since the shaded area represents the difference between the ideal work output ($e_1 - e_2$) and the actual work output ($h_1 - h_2$), it is called the irreversibility, I :

$$I \equiv T_0(s_2 - s_1) \quad (10.29)$$

Numerical example: Suppose a turbine receives geothermal steam at $P_1 = 0.80$ MPa as a saturated vapor; the steam leaves at $T_2 = 50^\circ\text{C}$. The isentropic efficiency is 80%. Determine the exergy loss and both exergy efficiencies. The dead-state temperature is $T_0 = 20^\circ\text{C}$.

From *Steam Tables* [6], $h_1 = 2769.12$ kJ/kg and $s_1 = 6.6628$ kJ/kg · K. The ideal isentropic outlet state $2s$ has $s_{2s} = s_1$ and thus $h_{2s} = 2135.20$ kJ/kg. Using the definition of the turbine isentropic efficiency, Eq. (10.25), we find that $h_2 = 2261.99$ kJ/kg. The entropy at the turbine outlet is $s_2 = 7.0551$ kJ/kg · K. The specific work $w = 507.13$ kJ/kg.

We need to find the specific exergy of the steam entering and leaving; to find these we also need h_0 and s_0 . These are taken from the *Steam Tables* under saturated liquid at the temperature T_0 , namely: $h_0 = 83.96$ kJ/kg and $s_0 = 0.2966$ kJ/kg · K. Now we can find e_1 and e_2 , using Eq. (10.11): $e_1 = 818.91$ kJ/kg and $e_2 = 196.77$ kJ/kg. Next we can determine the exergy loss and the exergetic efficiencies:

$$\Delta e = e_1 - e_2 - e_w = e_1 - e_2 - w \quad (10.30)$$

which yields $\Delta e = 115.00$ kJ/kg. Lastly, using Eqs. (10.23) and (10.24), the two efficiencies are: $\eta_{t,BF}^H = 0.860$ or 86.0%, and $\eta_{t,FUN}^H = 0.815$ or 81.5%.

Notice that the loss of exergy in the turbine amounts to about 14% of the incoming exergy in the geothermal steam (i.e., $115.00/818.89 = 0.140$). Also note that the functional efficiency turned out to be somewhat larger than the isentropic efficiency, as expected.

10.6.3 EXERGY EFFICIENCIES FOR HEAT EXCHANGERS

Figure 10.4 shows a shell-and-tube heat exchanger in which a hotter fluid (stream a–b) transfers heat to a cooler fluid (stream 1–2). The fluids may be gases, liquids, or mixtures of these two phases. We will assume that the shell of the heat exchanger is perfectly insulated, i.e., adiabatic. This type of system occurs in binary geothermal plants as preheaters, evaporators, superheaters, and condensers, and in flash- and dry-steam plants as condensers.

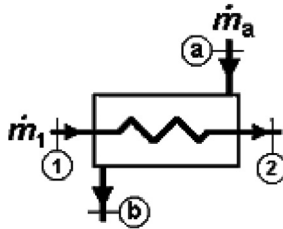


Figure 10.4 Heat exchanger.

The exergy accounting for the entire heat exchanger is:

$$\begin{aligned} \Delta \dot{E}_{HXer} &= \sum_{IN} \dot{E}_{HXer} - \sum_{OUT} \dot{E}_{HXer} = \dot{m}_a e_a + \dot{m}_1 e_1 - (\dot{m}_a e_b + \dot{m}_1 e_2) \\ &= \dot{m}_a (e_a - e_b) - \dot{m}_1 (e_2 - e_1) \end{aligned} \quad (10.31)$$

where we have incorporated the obvious fact that the mass flow rates of each fluid are the same entering and leaving the heat exchanger. Notice that in general \dot{m}_a and \dot{m}_1 will not be equal. Also, Eq. (10.31) can be read as saying the exergy destroyed in the heat exchanger is the difference between the exergy given up by the hotter fluid and the exergy acquired by the cooler one during the heat transfer process.

The ratio of the two flow rates is found from the First Law as follows:

$$\dot{m}_1(h_2 - h_1) = \dot{m}_a(h_a - h_b) \quad (10.32)$$

where we have noted that there is no work transfer and that all of the heat transfer takes place within the heat exchanger and does not cross the system boundary.

The brute-force exergy efficiency is given by:

$$\eta_{HXer,BF}^H = \frac{\dot{m}_1 e_2 + \dot{m}_a e_b}{\dot{m}_1 e_1 + \dot{m}_a e_a} \quad (10.33)$$

The functional exergy efficiency is not as obvious. Functional exergy efficiencies for heat exchangers will vary depending on the nature and purpose of the unit. Suppose, for example, it is used to preheat a stream of isobutane prior to entering an evaporator and that the heat comes from a stream of hot geothermal brine. Then we might take the ratio of the exergy gained by the isobutane to the exergy given up by the brine stream as a measure of the functional efficiency of the exchanger:

$$\eta_{HXer,FUN1}^H = \frac{\dot{m}_1(e_2 - e_1)}{\dot{m}_a(e_a - e_b)} \quad (10.34)$$

Alternatively, we might observe that the brine at state b is simply disposed of by means of reinjection back into the formation with no further use made of it, in which case we might use the following definition:

$$\eta_{HXer,FUN2}^H = \frac{\dot{m}_1(e_2 - e_1)}{\dot{m}_a e_a} \quad (10.35)$$

Numerical example—preheater-evaporator: Suppose a stream of geothermal brine is used to heat a stream of isobutane from a liquid to a saturated vapor. With reference to Figure 10.4, let \dot{m}_a be the brine flow rate and \dot{m}_1 be that for the isobutane. The heat exchanger consists of two sections: the preheater PH which raises the liquid to its boiling point and the evaporator E which changes the saturated liquid to a saturated vapor. We will assume that both the brine and the isobutane pass through the heat exchanger at constant pressure. The following data are given:

$$T_2 = 370 \text{ K}, \quad T_a = 400 \text{ K}, \quad \Delta T_{pp} = 5 \text{ K}, \quad T_0 = 293.15 \text{ K}, \quad \dot{m}_a = 85 \text{ kg/s}$$

The pinch-point, where the brine and the isobutane will come closest in temperature, $\Delta T_{pp} = 5 \text{ K}$, will most likely occur at the isobutane bubble point. We will assume this to be true and verify it as we proceed. Let us use the state point z for the brine at the pinch-point, and y for the isobutane at the pinch-point. Furthermore, we will assume that the following isobutane properties are known:

$$T_1 = 320 \text{ K}, \quad h_1 = 275.58 \text{ kJ/kg}, \quad s_1 = 1.0600 \text{ kJ/kg} \cdot \text{K}$$

Property values for both brine (pure water) and isobutane will be taken from Reynolds' property book [3].

Using Eq. (10.32) applied to the evaporator section only, we find the isobutane flow rate as:

$$\dot{m}_1 = \dot{m}_a \frac{h_a - h_z}{h_1 - h_y} = 85 \times \frac{532.7 - 427.3}{640.09 - 418.58} = 40.45 \text{ kg/s} \quad (10.36)$$

The brine outlet temperature may now be found assuming linearity of the brine cooling curve: $T_b = 358.9 \text{ K}$. So the cold-end temperature difference is 38.9 K and the pinch-point does indeed occur at the bubble point.

We now have everything needed to find the rate of exergy loss using Eq. (10.31):

$$\Delta \dot{E} = 11,997.5 - 11,355.0 = 642.5 \text{ kW} \quad (10.37)$$

Note that this amounts to only 5.4% of the total exergy given up by the brine.

The exergy efficiencies may now be found for the heat exchanger as a whole and for the evaporator and preheater sections separately. The results are shown in the table below.

Efficiency	Formula	Value
$\eta_{HXer,BF}^{II}$	$(\dot{m}_1 e_2 + \dot{m}_a e_b) / (\dot{m}_1 e_1 + \dot{m}_a e_a)$	0.9221
$\eta_{HXer,FUN1}^{II}$	$\dot{m}_1 (e_2 - e_1) / \dot{m}_a (e_a - e_b)$	0.8216
$\eta_{HXer,FUN2}^{II}$	$\dot{m}_1 (e_2 - e_1) / \dot{m}_a e_a$	0.4793
$\eta_{PH,BF}^{II}$	$(\dot{m}_1 e_y + \dot{m}_a e_b) / (\dot{m}_1 e_1 + \dot{m}_a e_z)$	0.9509
$\eta_{PH,FUN1}^{II}$	$\dot{m}_1 (e_y - e_1) / \dot{m}_a (e_z - e_b)$	0.7674
$\eta_{PH,FUN2}^{II}$	$\dot{m}_1 (e_y - e_1) / \dot{m}_a e_z$	0.1693
$\eta_{E,BF}^{II}$	$(\dot{m}_1 e_2 + \dot{m}_a e_z) / (\dot{m}_1 e_y + \dot{m}_a e_a)$	0.9616
$\eta_{E,FUN1}^{II}$	$\dot{m}_1 (e_2 - e_y) / \dot{m}_a (e_a - e_z)$	0.8500

The brute-force and the first functional efficiency indicate a reasonable performance; the second functional efficiency is very poor because we do not attribute any exergetic value to the brine as it leaves the unit. This is probably not a good basis for judgment since the brine does return to the reservoir and may eventually return to the plant after reheating in the formation. In the case of the evaporator, the second functional efficiency does not apply since the brine immediately passes to the preheater.

We can calculate the log-mean-temperature-differences ($LMTDs$) for the heat exchanger as a whole and for each section using Eq. (8.12). The results are as follows:

$$LMTD_{HXer} = 34.3^\circ\text{C}, \quad LMTD_{PH} = 16.5^\circ\text{C}, \quad LMTD_E = 14.0^\circ\text{C}$$

It will be noted that the brute-force exergy efficiencies vary inversely with the *LMTD* values, that is, the smaller the *LMTD*, the closer the match between the heating and cooling curves, the lower the thermodynamic irreversibility, and the higher the efficiency of exergy transfer.

Numerical example—mixed working fluid condenser: One of the advantages of using a mixture as the working fluid in a binary plant is the fact that the mixture changes phase at variable temperature instead of isothermally as does a pure fluid. Consider the case of a 10% isopentane–90% isobutane mixture condensing against cooling water. The properties of the mixture are available courtesy of the National Institute of Standards and Technology (NIST), the successor to the National Bureau of Standards (NBS) in Ref. [7].

In this example we will assume the working fluid mixture enters the condenser at its dew point (i.e., the first drop of liquid is about to form) and leaves at its bubble point (i.e., the last bubble of vapor has just condensed). We will take the mixture pressure to be 0.50 MPa and assume the mass flow rate is 1 kg/s (i.e., we will solve the problem per unit mass flow rate of working fluid). The cooling water enters the condenser at 25°C and leaves at 40°C. Water properties will be taken from Ref. [6]. The dead state is assumed to be 20°C = 293.15 K.

From Ref. [7] we find the following property values for the mixture:

- Dew point: $T_1 = 317.84$ K, $h_1 = -18.1$ kJ/kg, $s_1 = 0.1270$ kJ/kg · K
- Bubble point: $T_2 = 313.91$ K, $h_2 = -337.8$ kJ/kg, $s_2 = -0.8865$ kJ/kg · K.

From Ref. [6] we find the following property values for the cooling water:

- Inlet: $h_a = 104.89$ kJ/kg, $s_a = 0.3674$ kJ/kg · K
- Outlet: $h_b = 167.57$ kJ/kg, $s_b = 0.5725$ kJ/kg · K.

The mass flow rate of cooling water comes from Eq. (10.32):

$$\dot{m}_{CW} = \dot{m}_{WF} \frac{h_1 - h_2}{h_b - h_a} = 1 \times \frac{-18.1 + 337.8}{167.57 - 104.89} = 5.10 \text{ kg/s}$$

The exergy destroyed during the heat transfer process is the difference between the exergy given up by the mixture and that acquired by the cooling water:

$$\Delta \dot{E}_{COND} = \dot{m}_{WF}[h_1 - h_2 - T_0(s_1 - s_2)] - \dot{m}_{CW}[h_b - h_a - T_0(s_b - s_a)] = 9.562 \text{ kW}$$

It is interesting to compare this loss of exergy to that for the case of a pure fluid condensing under similar conditions. Let us say that 1 kg/s of pure isobutane enters the condenser at the same temperature as the mixture in the example. We will keep the cooling water temperatures the same. Of course, the isobutane would leave the condenser at the same temperature as it entered.

The new cooling water flow rate is 4.93 kg/s, and the loss of exergy is 11.258 kW. This is 17.7% higher (i.e., worse) than for the mixture, again because of the better match between the mixed working fluid and cooling water. The *LMTD* in this case is 10.4°C versus 9.1°C; it is remarkable that a mere 1.3°C increase in the *LMTD* leads to 17.7% greater loss of exergy, underscoring the need to design heat exchangers with care to achieve the greatest thermodynamic performance.

10.6.4 EXERGY EFFICIENCIES FOR FLASH VESSELS

All geothermal flash-steam plants generate vapor from a stream of compressed or saturated liquid. Figure 10.5 shows a typical flash tank and the temperature-entropy diagram for the processes.

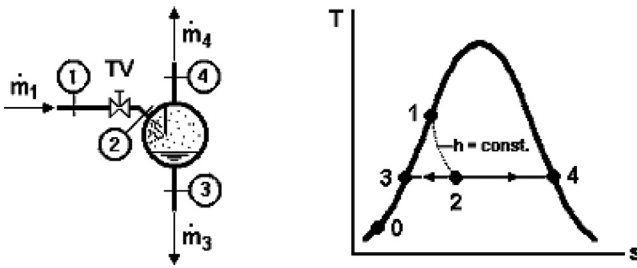


Figure 10.5 Flash vessel and process diagram.

The throttle valve (TV) creates a flow restriction which maintains a pressure drop from state 1 to state 2. State 2 is an intermediate state consisting of a two-phase mixture of saturated liquid and saturated vapor. The vessel is constructed so that the two phases are separated by centrifugal and gravity effects, producing a stream of saturated liquid at state 3 and one of saturated vapor at state 4. We assume the vessel is perfectly insulated and that the throttle operates isenthalpically.

Using the so-called “lever rule” of thermodynamics for two-phase mixtures, it is easy to find the quality at state 2:

$$x_2 = \frac{h_2 - h_3}{h_4 - h_3} = \frac{h_1 - h_3}{h_4 - h_3} \quad (10.38)$$

The specific entropy at state 2 is then found from:

$$s_2 = s_3 + x_2(s_4 - s_3) \quad (10.39)$$

We may define Second Law efficiencies for this system using the brute-force and functional forms:

$$\eta_{FV,BF}^{II} = \frac{\dot{m}_3 e_3 + \dot{m}_4 e_4}{\dot{m}_1 e_1} \quad (10.40)$$

and

$$\eta_{FV,FUN}^{II} = \frac{\dot{m}_4 e_4}{\dot{m}_1 e_1} \quad (10.41)$$

Whereas the form of Eq. (10.40) follows directly from the brute-force definition, that of Eq. (10.41) expresses the ratio of the flow rate of exergy of the steam generated to that of the incoming liquid. The reason for the latter is that the purpose of the flasher is to produce a steam flow for use in some process, in this case, a geothermal steam turbine, and therefore the exergy of the steam produced is the desired output.

The exergy loss is found from the exergy accounting equation:

$$\Delta \dot{E}_{FV} = \dot{m}_1 e_1 - \dot{m}_3 e_3 - \dot{m}_4 e_4 \quad (10.42)$$

There are no exergy terms for work or heat transfer since only flows are involved. The mass flows can be related to the incoming mass flow using the quality as follows:

$$\dot{m}_3 = (1 - x_2) \dot{m}_1 \quad (10.43)$$

and

$$\dot{m}_4 = x_2 \dot{m}_1 \quad (10.44)$$

Numerical example: Suppose an incoming liquid is a saturated liquid at 2.5 MPa and flows steadily at 100 kg/s. The TV creates a pressure drop leading to $P_2 = 0.70$ MPa. Let us assume that the pressure loss within the flash vessel is negligible, that is, $P_2 = P_3 = P_4$. The dead state is at 20°C, 1 atm. With the aid of *Steam Tables* [6], the following state-point data may be obtained; all entries except the bold ones are found directly:

State	P (MPa)	T (°C)	x	s (kJ/kg · K)	h (kJ/kg)	e (kJ/kg)
1	2.5	223.99	0	2.5547	962.11	216.19
2	0.7	164.97	0.1282	2.5967	962.11	203.88
3	0.7	164.97	0	1.9922	697.22	116.19
4	0.7	164.97	1	6.7080	2763.3	799.84
0	0.1	20	0 (assumed)	0.2966	83.96	0

Using Eqs. (10.38) and (10.39), the quality and entropy at state 2 can be calculated as: $x_2 = 0.1282$ and $s_2 = 2.5967 \text{ kJ/kg} \cdot \text{K}$. Then the specific exergy values can be found.

The mass flow rates are:

$$\dot{m}_1 = 100 \text{ kg/s}, \quad \dot{m}_3 = 87.18 \text{ kg/s}, \quad \text{and} \quad \dot{m}_4 = 12.82 \text{ kg/s}$$

Thus, the Second Law efficiencies and the exergy loss may be calculated:

$$\eta_{FV,BF}^{\text{II}} = 0.943, \text{ or } 94.3\%$$

$$\eta_{FV,FUN}^{\text{II}} = 0.474, \text{ or } 47.4\%$$

$$\Delta \dot{E}_{FV} = 1235.6 \text{ kW}$$

Since the brute-force efficiency is 94.3%, the exergy loss is 5.7% of the exergy carried by the incoming stream. Notice also that only 47.4% of the incoming exergy is preserved in the steam flow (i.e., $12.82 \times 799.84/21,619$), and that 52.6% of the exergy leaves with the separated liquid. If no further use is made of this liquid, then the exergetic performance of the flash-steam plant will suffer.

Lastly, the reader may wish to verify that the separation process that occurs after the flash preserves all the exergy in the postflash two-phase fluid (within numerical round-off error).

10.6.5 EXERGY EFFICIENCIES FOR COMPRESSORS

In the next illustration, consider a gas or vapor compressor. Geothermal plants routinely have air compressors to operate pneumatic devices and some condensing plants have compressors to remove noncondensable gases. The purpose of a compressor is to increase the pressure of the fluid, be it a gas such as air (i.e., a perfect gas) or a vapor (not a perfect gas). In both cases, the Second Law's theoretical analysis is the same; the implementation of the analysis differs.

Figure 10.6 is a schematic of a compressor. It is assumed to operate adiabatically, but irreversibly, being characterized by an isentropic efficiency, η_c . This

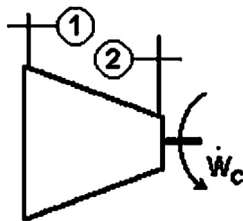


Figure 10.6 Gas compressor.

efficiency is defined in a manner similar to that for a turbine, but so as to give a value less than one, that is, it is the ratio of the ideal, isentropic work to the actual work.

In terms of the state points shown in the figure, the compressor's isentropic efficiency is given by:

$$\eta_c = \frac{h_{2s} - h_1}{h_2 - h_1} \quad (10.45)$$

where the state $2s$ refers to the ideal outlet state that would follow an isentropic process from state 1.

The specific loss of exergy during the process is given by:

$$\Delta e_c = e_1 + |w_c| - e_2 \quad (10.46)$$

where we show the absolute magnitude of the work to emphasize that it is an exergy *input*. The reader will recall that the exergy associated with work is the work itself.

The Second Law efficiencies are defined as follows:

$$\eta_{c,BF}^H = \frac{e_2}{e_1 + |e_{w_c}|} = \frac{e_2}{e_1 + |w_c|} \quad (10.47)$$

and

$$\eta_{c,FUN}^H = \frac{e_2 - e_1}{|e_{w_c}|} = \frac{e_2 - e_1}{|w_c|} \quad (10.48)$$

The functional definition is based on the view (from the standpoint of the Second Law) that the role of a compressor is to increase the exergy of the fluid and that it does so at the expense of the exergy associated with the work of compression.

Note that we have been able to ignore the mass flow rate of the fluid since it is the same at the outlet as at the inlet. Had this not been the case (say, if there was an extraction point between the inlet and the outlet), we would have to multiply each specific exergy by its appropriate flow rate. Also we would then need to use the power to run the compressor, instead of the specific work.

Numerical example: We will consider an air compressor with the following given conditions: air is compressed from state 1 where the pressure is 0.110 MPa and the temperature is 275 K to state 2 where the pressure is 1.40 MPa, the compressor having $\eta_c = 0.725$ or 72.5%. The dead state is at 20°C, 1 atm.

In solving this example, we will use the air data tables in Reynolds' data book [3], implying the air obeys the perfect gas equation of state, and that the air has specific heats, c_p and c_v , that depend on temperature. The process diagram is given in Figure 10.7.

Note that the dead state 0 is at 20°C (293.15 K) which is higher than the inlet temperature of 275 K. State $2s$ is the state that would have been reached if the

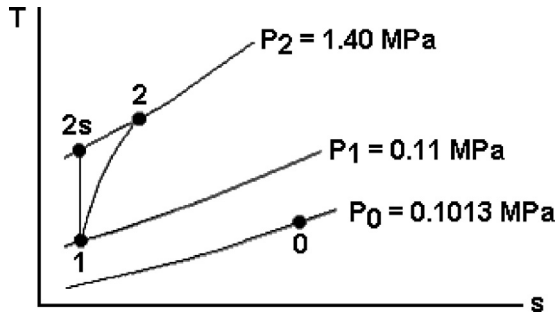


Figure 10.7 Gas compressor process diagram.

compressor was ideally isentropic. The properties at state $2s$ can be found using the relative pressure, p_r , defined as follows for isentropic processes only:

$$\frac{p_{r2s}}{p_{r1}} = \frac{P_{2s}}{P_1} \quad (10.49)$$

The values for the relative pressure are tabulated in the air tables as a function of temperature.

The air tables also include an entropy function, ϕ , that is related to the entropy change by the equation:

$$s_j - s_i = \phi_j - \phi_i - R \ln \left[\frac{P_j}{P_i} \right] \quad (10.50)$$

If the pressure is constant during a process, then the change in the entropy s is the same as the change in the entropy function ϕ . However, for a compressor this is clearly not the case and the pressure ratio term in Eq. (10.50) must be retained. From the given data together with the above equations, the results in the table below can be obtained:

State	P (MPa)	T (K)	p_r	ϕ (kJ/kg · K)	h (kJ/kg)	e (kJ/kg)
1	0.110	275	54.14	7.7559	435.0	7.504
2s	1.40		689.05	8.48606	729.567	302.04
2	1.40			8.66734	841.30	360.63
0	0.1013	293.15		7.81997	453.21	0

This is the sequence of calculations: (i) p_{r2s} from Eq. (10.49), (ii) ϕ_{2s} and h_{2s} from interpolation in air tables, (iii) h_2 from Eq. (10.45), and (iv) e_1 and e_2 from Eqs. (10.12) and (10.50). Thus, the working equations for the exergy terms are:

$$e_i = h_i - h_0 - T_0 \left[\phi_i - \phi_0 - R \ln \left(\frac{P_i}{P_0} \right) \right], \quad i = 1, 2 \quad (10.51)$$

where the gas constant for air is $R = 0.287$ kJ/kg · K.

The work to run the compressor, $h_2 - h_1$, comes to 406.3 kJ/kg. Then, the brute-force Second Law efficiency is 0.872 or 87.2%, the functional Second Law efficiency is 0.869 or 86.9%, and the exergy loss is 53.17 kJ/kg.

The same type of analysis can be carried out for a mixture of noncondensable gases provided the composition is known. It is acceptable to treat the mixture as a mixture of ideal gases as long as the pressure is not very high, that is, Dalton's law of additive partial pressures and Amagat's law of additive partial volumes may be applied to a good approximation [8]. Where more accurate results are demanded, one may turn to Kay's rule [9] using pseudo-critical properties or more elaborate equations of state such as the Benedict–Webb–Rubin equation or others like it [2].

10.6.6 EXERGY EFFICIENCIES FOR PUMPS

Pumps play a vital role in geothermal plants; see Section 8.8. They move cooling water from the basins of cooling towers to condensers, they lift geofluid from reservoirs to the surface, they force waste brine back into the reservoir, they repressurize working fluids in binary cycles, and they boost steam or working fluid condensate from the condenser hot well to the top of cooling towers. The power required to run pumps is a major parasitic load for geothermal plants and their efficient operation can help improve overall plant performance. Figure 10.8 is a schematic of a pump receiving low-pressure liquid at state 1 and discharging it at a higher pressure at state 2. From a thermodynamic analysis perspective, the internal details of the pump are unimportant, and only the properties at the inlet and outlet matter.

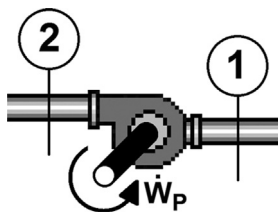


Figure 10.8 Liquid pump.

As with a compressor, the role of the pump is to increase the pressure of the fluid passing through it, in this case a liquid. From the point of view of the Second Law, its role is to raise the liquid's exergy to a desired level by expending as little work (exergy) as possible. In terms of the state points shown in the figure, the pump isentropic efficiency is given by:

$$\eta_p = \frac{h_{2s} - h_1}{h_2 - h_1} \quad (10.52)$$

where the state 2s refers to the ideal outlet state that would follow an isentropic process from state 1.

The specific loss of exergy during the process is given by:

$$\Delta e_p = e_1 + |w_p| - e_2 \quad (10.53)$$

where the absolute magnitude of the work is used to emphasize that it is an exergy *input*. The reader will recall that the exergy associated with work is the work itself.

The Second Law efficiencies are defined as follows:

$$\eta_{p,BF}^H = \frac{e_2}{e_1 + |e_{w_p}|} = \frac{e_2}{e_1 + |w_p|} \quad (10.54)$$

and

$$\eta_{p,FUN}^H = \frac{e_2 - e_1}{|e_{w_p}|} = \frac{e_2 - e_1}{|w_p|} \quad (10.55)$$

The functional definition is based on the job of a pump to increase the exergy of the fluid and that it does so at the expense of the exergy associated with the work of pressurization.

Numerical example: We will consider a condensate pump in a supercritical isopentane binary cycle with the following given conditions: state 1 is a saturated liquid at a temperature of 65°C, state 2 has a pressure of 3.5 MPa, and the pump's isentropic efficiency is 81.5%. The dead state is at 20°C, 1 atm.

The properties of isopentane will be taken from REFPROP. The process diagram is given in Figure 10.9, to scale for isopentane.

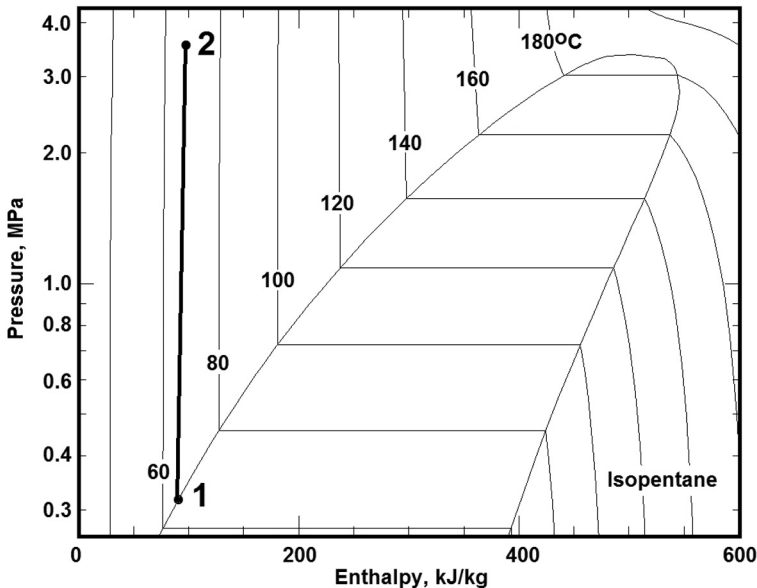


Figure 10.9 Supercritical pump process diagram.

From the given data, the results in the table below can be obtained:

State	P (MPa)	T ($^{\circ}\text{C}$)	s (kJ/kg \cdot K)	h (kJ/kg)	e (kJ/kg)
1	0.31267	65	0.27768	89.070	7.904
2s	3.5	66.492	0.27768	94.618	
2	3.5	66.999	0.28138	95.877	13.626
0	0.1	20.0	-0.059756	-17.753	0

The work to run the pump, $h_2 - h_1$, comes to 6.807 kJ/kg. Then, the brute-force Second Law efficiency is 0.926 or 92.6%, the functional Second Law efficiency is 0.841 or 84.1%, and the exergy loss is 1.085 kJ/kg.

10.6.7 EXERGY ANALYSIS FOR PRODUCTION WELLS

The last illustration of exergy principles will be a production well. Two cases will be examined: (A) artesian flow and (B) pumped flow (Figure 10.10).

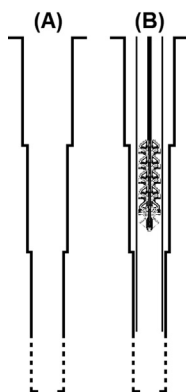


Figure 10.10 Production wells: (A) artesian flow and (B) pumped flow.

The geofluid enters the well at the bottom (state 1) and exits at the surface (state 2). When a pump is used, the fluid is kept in a liquid state under pressure all the way to the surface, but under artesian flow the fluid is assumed to flash into a two-phase mixture at some point along the well. Thermodynamically, the well should deliver the highest exergy geofluid with the least loss of exergy during the process. A pump will enhance the well mass flow rate but at the expense of the power to run the pump.

The specific loss of exergy during the well flow process is given by:

$$\Delta e_w = e_1 - e_2 \quad (10.56)$$

if the well flow is artesian, and

$$\Delta e_w = e_1 + |w_p| - e_2 \quad (10.57)$$

if the well is pumped. Since the flow rates will generally not be the same for these two cases, the total exergy flow rate will be obtained by multiplying the specific exergy terms by the appropriate mass flow rate.

The Second Law efficiencies are defined as follows:

Case A:

$$\eta_{w,BF}^{II} = \eta_{w,FUN}^{II} = \frac{e_2}{e_1} \quad (10.58)$$

Case B:

$$\eta_{w,BF}^{II} = \frac{e_2}{e_1 + |e_{w_p}|} = \frac{e_2}{e_1 + |w_p|} \quad (10.59)$$

and

$$\eta_{w,FUN}^{II} = \frac{e_2 - e_1}{|e_{w_p}|} = \frac{e_2 - e_1}{|w_p|} \quad (10.60)$$

For Case A, both definitions are the same and yield 100% efficiency if the produced exergy is equal to the exergy that entered the well from the reservoir. For Case B, the focus is on how much additional exergy is being produced with respect to the amount of exergy expended in running the pump.

Numerical example—Case A: Consider a reservoir at 180°C and 1.10 MPa, and a well capable of flowing at 50 kg/s under artesian conditions. The wellhead pressure is maintained at 0.250 MPa. The dead state is at 20°C, 1 atm.

Using REFPROP and the given conditions, the results in the table below are obtained.

State	<i>P</i> (MPa)	<i>T</i> (°C)	<i>s</i> (kJ/kg · K)	<i>h</i> (kJ/kg)	<i>x</i>	<i>e</i> (kJ/kg)
1	1.1	180	2.1391	763.10	CL	138.92
2	0.25	127.41	2.1758	763.10	0.1044	128.17
0	0.1	20.0	0.29646	84.006	CL	0

Thus, the brute-force and functional Second Law efficiencies are 0.923 or 92.3%, and the exergy loss is 10.75 kJ/kg. The total rate of exergy production is 6.41 MW.

Numerical example—Case B: Consider the same reservoir at 180°C and 1.1 MPa, but now fitted with a downhole pump capable of producing 75 kg/s at a wellhead pressure of 1.25 MPa and temperature of 182°C. The dead state is at 20°C, 1 atm.

Using REFPROP and the given conditions, the results are obtained as given in the below-mentioned table.

State	P (MPa)	T (°C)	s (kJ/kg · K)	h (kJ/kg)	x	e (kJ/kg)
1	1.1	180	2.1391	763.10	CL	138.87
2	1.25	182	2.1583	771.99	CL	142.13
0	0.1	20.0	0.29646	84.006	CL	0

Thus, the specific work to run the pump, $h_2 - h_1$, comes to 8.89 kJ/kg and the power required is 666.8 kW. The brute-force efficiency is 0.962 or 96.2% and functional efficiency is 0.367 or 36.7%. The total rate of exergy production is 10.66 MW (gross) and, after subtracting the pump power, 9.99 MW (net).

Discussion of numerical examples: The pumped well yields 3.58 MW more exergy production than allowing the well to self-flow. Assuming a conversion efficiency of 40% from exergy to electricity, Case B should yield about 1.4 MW more electrical power output than Case A, for the conditions stipulated.

As a final note on exergy, most of the basic principles presented in this chapter were published by the author in Ref. [10] where they were applied to specific geothermal binary plants operating at low-temperature resources.

10.7 Thermal Versus Utilization Efficiency for Geothermal Plants

This concluding section is intended to point out the difference between the use of the thermal efficiency and the utilization efficiency for geothermal power plants. This has been addressed several times in other places of this book, but it may be useful to reiterate the matter here.

On the one hand, as long as a power plant functions on a closed cycle, the thermal efficiency may be used to assess its thermodynamic performance. On the other hand, if the plant functions as a series of processes starting from some initial state and ending at a different state, then the thermal efficiency cannot be applied. In this latter case, the exergetic or utilization efficiency is the only thermodynamically acceptable measure of performance. Owing to its generality, the utilization efficiency may also be used to assess the performance of cyclic power plants.

Thus, binary plants of all types, basic, dual-pressure, subcritical or supercritical, may be rated by their thermal efficiency, i.e., on how well they convert thermal input (heat) into useful electrical output (work). They may also be rated by their utilization efficiency, i.e., on how well they convert exergy input into useful electrical output (work). The exergy input may be carried into the plant with hot brine, geothermal steam, mixtures of steam and brine, etc.

Geothermal flash-steam plants, unlike binary plants, receive input in the form of geofluid at certain thermodynamic conditions, carrying exergy, and then process and use that geofluid directly in the power generating equipment, eventually discharging the geofluid in a condition far different from its inlet condition. The geofluid came to the plant from a reservoir via a well and piping system, and it normally is disposed of back to the reservoir via other wells and piping. This represents a series of thermodynamic processes, not a cycle. Humans construct cycles to operate continuously to produce power steadily without interruption. The geothermal flash plant operates only so long as the geofluid keeps flowing, in and out. Once the fluid leaves the plant and returns to the reservoir, humans no longer control it. The fluid defined as a collection of molecules may someday return to the plant after a journey through the permeable formation, or it may not.

Attempting to apply the concept of the thermal efficiency to geothermal steam plants will not only produce an erroneous thermodynamic result, but it will also confuse the issue by offering a performance measure that will inevitably be compared to thermal efficiencies for other plants such as coal- or gas-fired plants or nuclear plants which are true cycles. This unfortunate problem can simply be avoided by using the utilization efficiency in all cases of geothermal plant performance assessment and reserving the use of the thermal efficiency to only the case of binary plants.

References

- [1] Kestin J. Available work in geothermal energy. In: Kestin J, editor-in-chief, DiPippo R, Khalifa HE, Ryley DJ, editors. Sourcebook on the production of electricity from geothermal energy. U.S. Dept. of Energy, DOE/RA/4051-1, U.S. Gov. Printing Office, Washington, DC; 1980 [Chapter 3].
- [2] Bejan A. *Advanced engineering thermodynamics*. 2nd ed. New York, NY: Wiley-Interscience, John Wiley & Sons; 1997.
- [3] Reynolds WC. *Thermodynamic properties in SI: graphs, tables and computational equations for 40 substances*. Stanford, CA: Dept. of Mechanical Engineering, Stanford University; 1979.
- [4] Wepfer WJ, Gaggioli RA. Reference datums for available energy. In: Gaggioli RA, editor. *Thermodynamics: second law analysis*. ACS Symposium Series 122, American Chemical Society, Washington, DC; 1980 [Chapter 5].
- [5] Moran MJ. *Availability analysis: a guide to efficient energy use, corrected edition*. New York, NY: ASME Press, American Society of Mechanical Engineers; 1989.
- [6] Keenan JH, Keyes FG, Hill PG, Moore JG. *Steam tables: thermodynamic properties of water including vapor, liquid, and solid phases (international edition—metric units)*. New York, NY: John Wiley & Sons, Inc.; 1969.
- [7] Gallagher JS, Linsky D, Morrison G, Levelt Sengers JMH. *Thermodynamic properties of a geothermal working fluid; 90% isobutane-10% isopentane*, NBS Technical Note 1234, U.S. Dept. of Commerce; 1987.

- [8] Çengel YA, Boles MA. Thermodynamics: an engineering approach. 4th ed. New York, NY: McGraw-Hill; 2002.
- [9] Kay WC. Sc.D. Thesis, Massachusetts Institute of Technology; 1937.
- [10] DiPippo R. Second law assessment of binary plants for power generation from low-temperature geothermal fluids. *Geothermics* 2004;33:565–86.

Problems

- 10.1. Calculate and plot lines of constant exergy, $e = \text{constant}$, for pure water in the two-phase, liquid-vapor region (i.e., for quality values between 0 and 1), starting from the saturated liquid line at temperatures of 150, 200, 250, 300, 325, and 350°C. Use 20°C as the dead-state temperature. Plot the results in temperature-entropy (T - s) coordinates. Overlay the results on a scale T - s diagram (from REFPROP) showing the saturation curve and lines of constant enthalpy on the same figure. The $h = \text{constant}$ lines should begin at the saturated liquid line from the same points as the $e = \text{constant}$ lines.
- 10.2. A single-flash-steam plant operates at a reservoir having a temperature of 250°C. The condenser runs at 50°C; $T_0 = 20^\circ\text{C}$. The separator temperature is found from the “equal-temperature-split” rule. The isentropic efficiency of the turbine is 82%.
 - a. Find the specific exergy (in kJ/kg) of the geofluid at all points in the plant.
 - b. Calculate the loss of exergy (in kJ/kg) for the geofluid traveling from the reservoir to the separator (assuming saturated liquid is in the reservoir).
 - c. Calculate the loss of exergy (in kJ/kg) for the geofluid as it passes through the turbine.
 - d. If the cooling water enters the shell-and-tube condenser at 30°C and leaves at 40°C, calculate (i) the brute-force exergy efficiency of the condenser and (ii) the loss of exergy (in kJ/kg of geofluid) as it passes through the condenser.
- 10.3. A regenerator is used in a normal-pentane binary plant. N-pentane from the turbine exhaust at 88°C enters the regenerator and leaves at 60°C; the pressure is 0.13 MPa. The N-pentane from the feed pump enters the other side of the regenerator at 1.75 MPa and 40°C. The dead state temperature is 20°C and the regenerator is perfectly insulated. Calculate the following:
 - a. Outlet temperature of the N-pentane on the high-pressure side.
 - b. Second Law efficiency of the regenerator on an exergy transfer basis.
 - c. Total exergy lost in the heat exchanger, in kJ/kg.
 - d. Log mean temperature difference, in °C.

- 10.4.** In the early days of geothermal power plants, it was common to read articles that assessed their performance on the basis of the First Law of thermodynamics. The familiar thermal efficiency that was universally used to measure the efficiency of fossil-fueled plants was carried over to geothermal dry steam plants. This problem asks you to use the old method to calculate the efficiency of a hypothetical dry steam plant and to contrast the result with what comes out of the modern exergy approach. See also Problem 5.5(c).

Consider a dry steam plant receiving 110 kg/s of saturated steam at 172°C from a dry steam reservoir. The turbine may be assumed to have an isentropic efficiency of 75% and discharges to a condenser at 50°C.

Calculate:

- a. A pseudo-, gross “thermal efficiency” defined as the ratio of the turbine output to the “heat” input, where the latter is imagined as raising the condensate to the inlet steam condition.
- b. Utilization efficiency based on the exergy of the incoming geothermal steam if the dead-state temperature is 27°C.
- c. Compare the results and discuss the reasons why the pseudo-thermal efficiency is inappropriate in the case of geothermal steam or flash plants.

Part 3



GEOHERMAL POWER PLANT CASE STUDIES

- Larderello Dry-Steam Power Plants, Tuscany, Italy
- The Geysers Dry-Steam Power Plants, Sonoma and Lake Counties, California, USA
- Geothermal Power Plants of New Zealand
- Geothermal Power Plants of Indonesia
- Geothermal Power Plants in Central America and the Caribbean
- Geothermal Power Plants in Nevada, USA
- Heber Binary Plants, Imperial Valley, California, USA
- Magmax Binary Power Plant, East Mesa, Imperial Valley, California, USA
- Nesjavellir and Hellisheidi Plants, Iceland
- Raft River Plants, Idaho, USA
- Geothermal Power Plants in Turkey
- Enhanced Geothermal Systems—Projects and Plants
- Environmental Impact of Geothermal Power Plants

Geothermal electricity, unlike fossil or nuclear, cannot be ordered: it must be developed, for there is nothing more hazardous than a premature order for conversion equipment.

Joseph Kestin—July 1979

The third part of the book offers case studies of the planning, design, and performance of selected geothermal power plants, chosen to illustrate all of the traditional energy conversion systems covered in the second part. Included are plants that have played important historical roles. Some of the cases show integrated usage of geothermal energy, for heat and power, and for waste heat conversion to generate added electricity. Many more plants could have been cited but space limitations have forced us to restrict our selection. Nevertheless, this edition includes extensive coverage of plants in New Zealand, Indonesia, Central America, the Caribbean, and the county of Nevada, which if it were a country would rank eighth in the world in terms of installed geothermal power. Enhanced Geothermal Systems technology is highlighted in a separate chapter with several new European plants covered.



Las Pailas 42 MW geothermal plant, Guanacaste Province, Costa Rica.

Photo by P. Moya—From DiPippo R, Moya P. Las Pailas geothermal binary power plant, Rincón de la Vieja, Costa Rica: performance assessment of plant and alternatives. *Geothermics* 2013;48:1–15 [WWW].

Chapter 11

Larderello Dry-Steam Power Plants, Tuscany, Italy

Chapter Outline

11.1 History of Development	322
11.2 Geology and Reservoir Characteristics	324
11.3 Power Plants	328
11.3.1 Early Power Plants	329
11.3.2 Power Plants of the Modern Era	335
11.3.3 Recent Power Plant Designs	337
11.4 Mitigation of Environmental Impact	340
References	342
Nomenclature for Figures in Chapter 11	343



Valle Secolo geothermal power plant, Larderello, Italy; photo courtesy of Enel Green Power.

11.1 History of Development

The case studies section of this book begins at the birthplace of geothermal energy as a source of electricity—Larderello, Italy. It was here in this Tuscan village in 1904 that Prince Piero Ginori Conti fashioned the first electromechanical device that converted the energy of the indigenous steam, issuing from the earth for centuries, into electricity—enough to illuminate five light bulbs in his boric acid factory.

Students of ancient history are well acquainted with Julius Caesar and the Romans. The Romans knew places like Larderello very well, having built magnificent baths at many of them throughout their empire from England to Turkey, as we know them today. Certainly Larderello is a part of the ancient history of Tuscany, situated in gently rolling hills, roughly equidistant from the famous cities of Siena and Volterra.

Perhaps the best way to tell the story of ancient Larderello is with an annotated time line (Figure 11.1) [1,2]. The information contained in what follows was found in the booklet produced by ENEL, Ente Nazionale per L'Energia Elettrica (the electric authority of Italy) [1], and in Burgassi's thorough contribution to *Stories from a Heated Earth* [2].

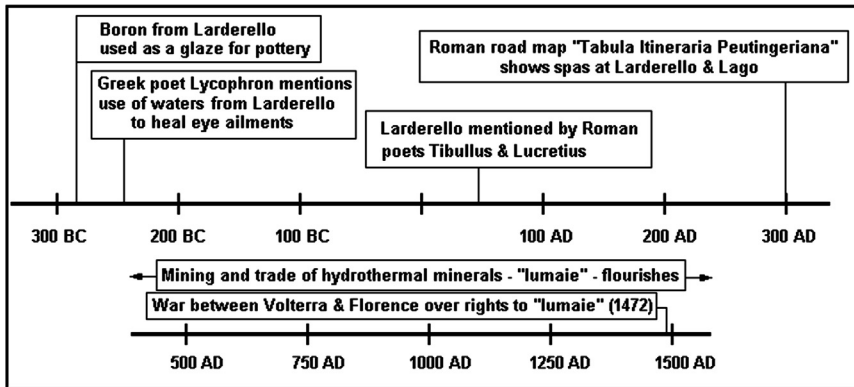


Figure 11.1 Timeline of ancient history of Larderello and the Boraciferous Region [1,2].

The main events beginning in the late eighteenth century are listed in Table 11.1 [1,2]. The destruction of practically all of the geothermal power stations at Larderello in 1944 during World War II marked the low point in production from the field [3]. The power plants were a strategic target during the Italian Campaign. Following the landing of the Allied Forces at Salerno and Anzio in late 1943 and early 1944, respectively, the battle line moved relentlessly northward toward Rome, and after its capture in June of 1944, farther north toward Florence.

TABLE 11.1 Chronology of events in the history of Larderello [1,2].

Year	Event
1777	Discovery of boric acid in “lagoni” (thermal pools) by F.U. Höfer.
1810	First try at using steam from lagoni for industrial purposes.
1812	Timber was cut and burned to supply heat to evaporate water during boron recovery.
1818	Francesco de Larderel establishes his company to recover boric acid on a commercial scale at Montecatini; eight more factories are built throughout the region over the next 17 years.
1827	Invention of the “lagone coperto” (covered pool), replaced wood with geothermal steam to provide heat for the mineral recovery process, greatly improving the efficiency of the operation.
1828	F. Larderel laid the basis for drilling for geothermal steam.
1842	Using efficient counterflow heat exchangers (Adriane boilers) devised by A. Larderello, boric acid production reached 1000 tons; in 1829 it had been 125 tons.
1865	Steam-driven pumps replaced animal- or water-wheel devices to pump the boraciferous waters.
1894	Invention of the tubular boiler using geothermal fluids by F. Raynart of the Larderel factory.
1904	On July 4, P.G. Conti ran his $\frac{3}{4}$ -horsepower reciprocating steam engine at his factory in Larderello, marking the first production of electricity from geothermal energy.
1905	A 20 kW dynamo was commissioned, driven by a 40-horsepower reciprocating steam engine to serve the Larderel factory.
1912	Construction began for the first commercial geothermal power station.
1914	On March 10, a 250 kW turbo-alternator was connected to the power distribution system of Volterra and Pomarance, marking the first commercial generation of electricity from geothermal energy.
1940	A 300 kW binary plant was installed on Ischia island.
1944	Prior to World War II, the installed capacity at Larderello had reached 136.8 MW and yearly produced more than 900 GW · h. Practically all power plants were destroyed as a result of the war; only one small generating unit survived.
1948	Reconstruction of the Larderello plants that had begun immediately after the war was completed, and the original station was retired to make way for more modern plants.
1952	A 275 kW single-flash plant was installed on Ischia island.
1959	Larderello power capacity reached 300 MW; annual generation exceeded 2000 GW · h.
1971	Successful drilling of Travale 22, the most powerful geothermal well in Italy, sparked new interest in the Travale area.
1983	Reinjection was deemed necessary to combat the decline in reservoir performance. Standardized 60 MW turbines were designed.
1988	“Program 2000” was launched to triple the electrical generation from geothermal energy from 3000 to 9000 GW · h by the year 2000.
1993	Two new 60 MW units commissioned at Valle Secolo; see chapter cover photo.
2000	Start of major renovation of power plants; over the next 5 years, 10 new plants, 254.5 MW, are installed, replacing less efficient, obsolescent plants.
2004	Deep drilling program initiated in area of Larderello—Radicondoli—Montieri. A plant at Latera, 90 km SE of Larderello, is opposed on environmental grounds causing the cancellation of the plant that had been under construction.
2008	Larderello deep drilling program was completed.
2010	22 “AMIS” H ₂ S and Hg removal systems are in operation.

Starting in February 1944, the geothermal power plants at Castelnuovo and Larderello came under attack by Allied fighter-bombers. At first the plants sustained only light damage and continued to generate electricity and to produce boric acid. From April until June, the plants were repeatedly bombed and strafed, despite being defended by six antiaircraft batteries. It was during this period that the plants were put out of commission. Remarkably, the personnel at both power plants and at the boric acid factory managed until June 28 to continue working an 8-hour shift, albeit at night. Once the plants were no longer in the line of fire, they were quickly rebuilt. Since then the geothermal facilities have continued to grow in capacity and output as older units are replaced with modern, more efficient ones.

[Note: The events during World War II related here are based on the contents of a diary kept by Mr. Geo Desi, an Italian eyewitness to the attacks at Castelnuovo and Larderello. The content of Desi's diary, in Italian, was provided to the author by Mr. Andrea Rossetto (Torreglia, Italy), through the good offices of Mr. Steve Cole (Memphis, Tennessee). Mr. Cole maintains a comprehensive web site "The Italian Campaign of World War II: September 1943–May 1945."]

11.2 Geology and Reservoir Characteristics

The anomalous geothermal activity in the southern Tuscany region arises from the collision of edges of two of the earth's tectonic plates, the European and the African. Over some 30 million years this region has been subjected to alternating periods of compressive and tensional effects. The result has been the creation of fault systems, tectonic highs, and the emplacement of magma bodies relatively close to the surface, as shallow as 7 km [4].

The geothermal areas in Italy include: Larderello and its several adjacent areas such as Lago and Travale–Radicondoli; Monte Amiata and its two foci of development at Bagnore and Piancastagnaio; and Monti Volsini and its fields at Latera and Torre Alfina near Lake Bolsena; see Figure 11.2. In this section, we will concentrate on the main area of geothermal power development, namely, the greater Larderello area.

Throughout the 400 km² Larderello–Travale–Radicondoli–Lago geothermal area, the geologic stratigraphy consists of a sequence of rock formations that can be described as follows, starting with the youngest at the surface and moving downward [4]:

- Neoautochthonous Complex, recent volcanics that cover the surface in most places.
- Flysch Facies formation, consisting mainly of shales but also of limestones and sandstones; this layer forms the cap rock above the reservoir.

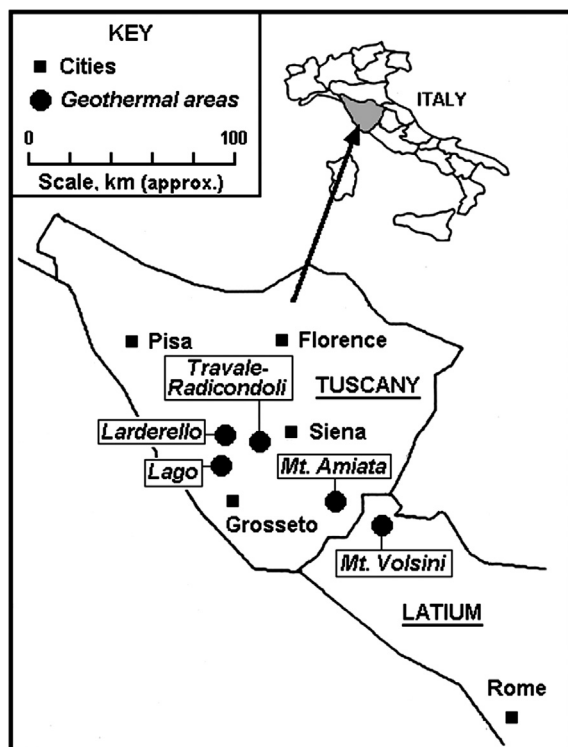


Figure 11.2 General location map of geothermal areas in Tuscany and northern Latium. Adapted and expanded from Ref. [5].

- Nonmetamorphic Tuscan unit or Tuscan Nappe, having evaporitic carbonate rocks at the bottom and a terrigenous sequence at the top; a permeable reservoir is hosted primarily in this group and the underlying Verrucano Group.
- Verrucano Group, formed as tectonic wedges consisting of metamorphic and sedimentary rocks.
- Metamorphic Tuscan units, consisting of the Amphibolitic Gneisses Group and Micaschists-Phyllites Group; this is the basement of the formation.

Underlying and embedded in the basement are the magmatic intrusions that supply the heat for the system.

The sites of the once numerous thermal manifestations correspond to structural highs of the permeable reservoir rocks, often lying no more than a few hundred meters deep. These areas are now marked by large patches of altered ground and a few active fumaroles, and include sites at Monterotondo, Sasso Pisano, Lago, Castelnovo, Serrazzano, Lustignano, and, of course, Larderello (originally Montecerboli, later renamed for Francesco de Larderel). It is reasonably certain

that the greater Larderello region was characterized by massive thermal discharge dating back at least 2300 years, and probably much longer. Recalling from Chapter 7 one of the important requirements for the creation of a dry-steam reservoir, namely, extensive, long-term release of geothermal fluids that lowers the water table, we see that this condition was certainly met at Larderello.

The areas having the thermal manifestations were obviously attractive sites for the first wells. These were drilled only to depths sufficient to win steam for either boric acid production or later to drive electric generators. Only after decades of exploitation that significantly depleted the shallow reservoir was the deep reservoir sought and explored.

The permeable reservoir rocks, the Tuscan Nappe, outcrop importantly in many places throughout the southern half of the greater Larderello region, providing an easy entry for cold recharge to the reservoir. Fortunately, the low temperatures associated with this infiltration are detected only at shallow levels owing to the vertically variable permeability within the productive reservoir that effectively isolates the deeper layers from the more shallow ones.

This can be seen very clearly in the three isotherm distribution plots in Figures 11.3–11.5, first at the top of the reservoir (which generally is less

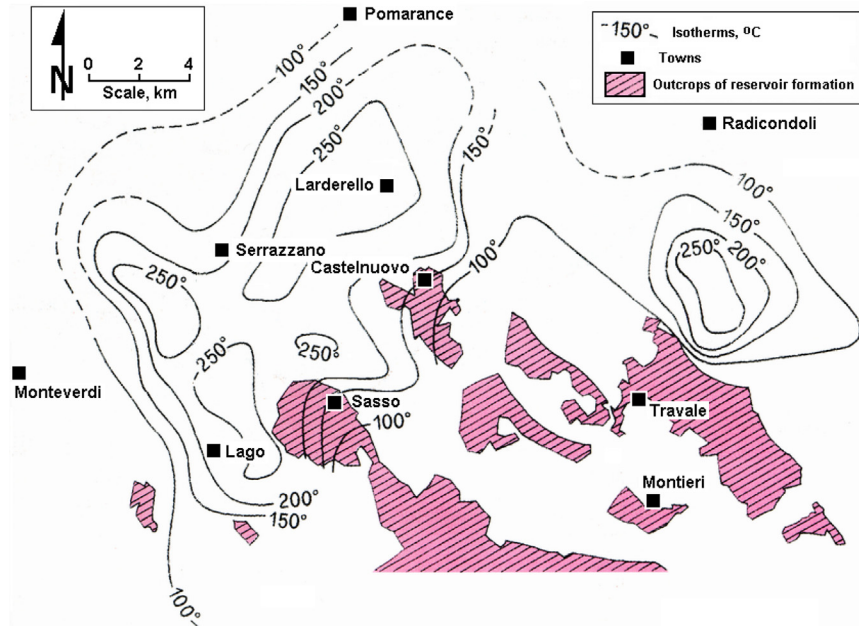


Figure 11.3 Isotherms at the top of the reservoir in greater Larderello area. After Ref. [4] [WWW].

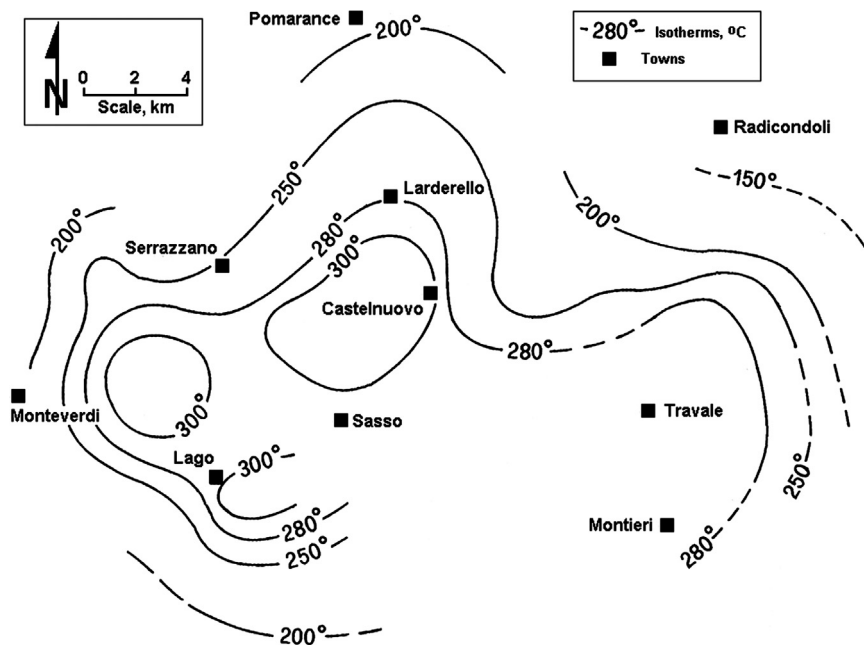


Figure 11.4 Isotherms at 2000 m b.s.l. in greater Larderello area. After Ref. [4].

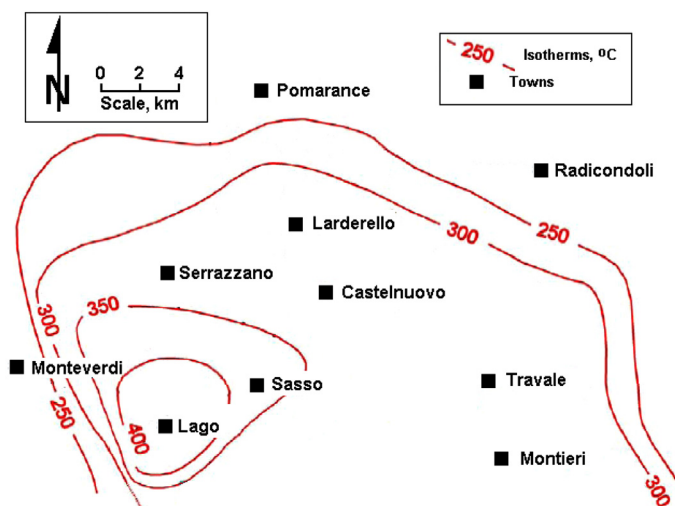


Figure 11.5 Isotherms at 3000 m b.s.l. in greater Larderello area. Highly simplified from Ref. [6] [WWW].

than 1000 m deep), next at 2000 m b.s.l., and the last one at 3000 m b.s.l. [4,6]. The influence of the cold recharge is evident in Figure 11.3 in the areas surrounding the outcrops of reservoir rocks. However, from Figure 11.4, it is clear that the high-temperature isotherms at depth form a more or less continuous pattern indicating a broad zone of reservoir having temperatures in excess of 250°C.

In Figure 11.5 we see the results of the most recent and deepest drilling. The hottest part of the reservoir lies toward the southwest in the vicinity of Lago. At 3000 m b.s.l., the 400°C isotherm approximates a 6.5 km circle centered a little north of Lago. A small, nearly circular lake lies close to Lago (from which it took its name) and is believed to be the remains of a phreatic explosion. Temperatures of 450°C are present below about 3200 m b.s.l. in the middle of the hottest area [7]. Furthermore, since the isotherms are fairly closely stacked here, heat is transferred mainly by conduction. This could indicate the proximity of a magmatic intrusion. Granitic intrusions indeed have been encountered in some of the deepest wells drilled in the region.

The most promising and so far successful exploration method for the deep reservoir is 3D reflection seismic surveys [8]. Small explosive charges, about 3 kg of TNT, are detonated in shallow holes, about 12 m deep, and the reflected waves are picked up by a large array of geophones. Rock layers that have high permeability are characterized by lower density and lower wave propagation velocity. The returns from several lines of receivers are processed into 3D plots that reveal the most promising targets for the deep wells. A portion of such a plot is shown in Figure 11.6 [8].

The most important finding of the new deep exploration program is that the greater Larderello geothermal field is unified at depth. A reservoir of enormous extent exists below 3000 m b.s.l. that feeds the entire region. There is continuity of the hottest isotherms that encompass an area of about 400 km². This will lead to more drilling in the outlying areas where no thermal manifestations are seen and below areas characterized by poor thermal gradients caused by the surface infiltration of cold meteoric water. This discovery should lead to an expansion of the geothermal power capacity of the Larderello area.

11.3 Power Plants

We will now discuss the power plants of Larderello, beginning with the early designs (1904–1968), the modern designs (1968–1995), and the recent designs (1995–present).

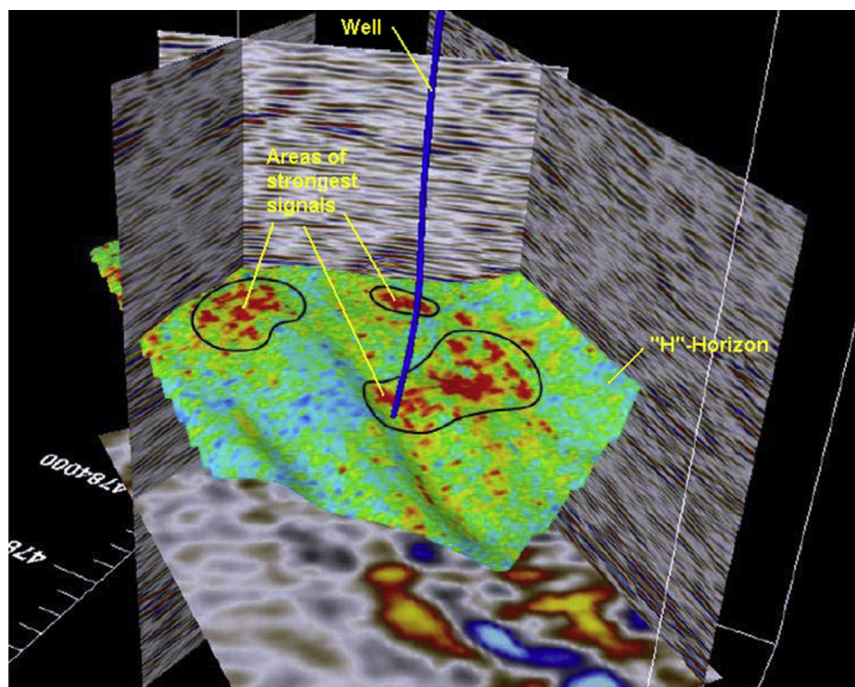


Figure 11.6 3D plot of the “H”-Horizon as determined by reflective seismic surveys. The darkest colored areas are those with the highest RMS amplitudes and could be interpreted as promising drilling targets. *Excerpted from Ref. [8] [WWW].*

11.3.1 EARLY POWER PLANTS

The design of the earliest power plants at Larderello was driven by three main considerations: (1) the steam was of low pressure; (2) it contained acidic gases and other chemical impurities that precluded its use in the prime movers of the time, either reciprocating steam engines or rotodynamic steam turbines; and (3) the geofluid had to be processed to recover the valuable minerals it contained. The latter use was the original commercial application of the fluids from the “Boraciferous Region” and would remain a lucrative venture for many decades.

Although Prince Piero Ginori Conti initially fed the geothermal steam directly from the “soffioni” into a hydraulic turbine adapted for geothermal use, and later tried to use the natural steam in his historic reciprocating engine (see Figure 7.1),

it was feared that the machines could not withstand the corrosive attack from the natural fluid. Conti even developed a method of securing somewhat higher pressure steam by boring 0.2–0.4 m diameter holes to depths of 100–180 m. This produced steam flows of 5–20 t/h at pressures from 2 to 3 bar and temperatures from 150°C to 180°C, but the steam was burdened with significant amounts of noncondensable gases (NCG). Thus, a new method would be needed for this steam to power electrical generators [9].

Thus was born the so-called “Indirect Cycle.” The geothermal steam was sent to heat exchangers where it was used to boil pure water obtained from a supply of freshwater. The drained condensed geothermal steam was then sent to the chemical recovery plant, while the clean steam powered the electrical generator; see Figure 11.7.

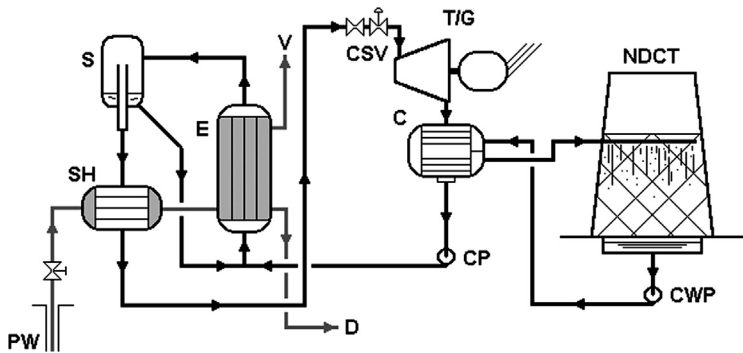


Figure 11.7 Indirect-cycle for power generation from “soffioni” at Larderello.

The evaporators were a complex set of shell-and-tube heat exchangers that were known as Kestner evaporators. An elevation view is shown in Figure 11.8 [10]. The geothermal steam from the “soffioni” entered the unit at the pure steam superheater where it flowed through aluminum tubes while the pure steam passed over the tubes. It continued into the steam manifold and was distributed to the shell side of the vertical evaporators, arranged in pairs. The spent steam drained from the bottom of the evaporators and the condensate was finally used to preheat the incoming pure water in another shell-and-tube heat exchanger. The condensate of the natural steam was then transported to the mineral recovery plant. The evaporator tubes were 7 m long, 30 mm in diameter, and also made of aluminum, which was the only metal that could withstand the corrosive attack of the sulfuric-acid-laden geothermal steam. The mechanical strength of the aluminum was less than desired and vibration problems were encountered. Also the tubes

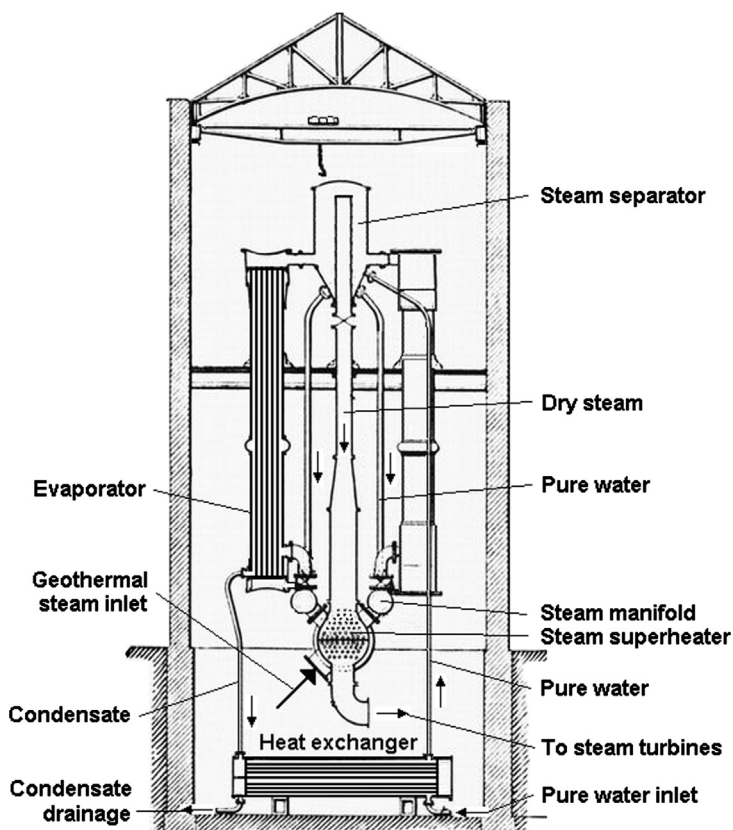


Figure 11.8 Kestner evaporators for raising pure steam from “soffioni.” After Ref. [10].

suffered somewhat from corrosion, probably at the tube sheet connections, allowing geofluid and NCG to mix with the pure water and steam. This overburdened the condenser air removal system, raising the condenser pressure, and lowering the turbine power output.

The “pure” steam was used in three 2.5 MW turbo-generator units. Photographs of the turbine hall and of one of the rotors are shown in Figures 11.9 and 11.10 [11]. The turbine was a double-flow unit with seven groups of blades; the first five groups had brass blades and the last two low-pressure groups were made of 5% nickel steel.

The pressure of the pure steam leaving the superheater was about 2 bar,a, but the turbine was designed to produce its rated power at an inlet steam pressure of only 1.2 bar,a. The steam flow rate was about 9.7 kg/s (77,000 lbm/h) per turbine [11].

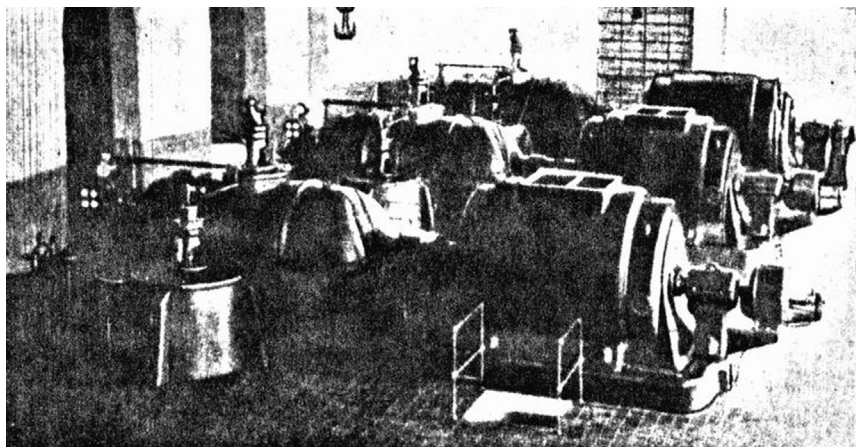


Figure 11.9 Three 2.5 MW steam turbine-generator units at Larderello, c. 1916 [11].

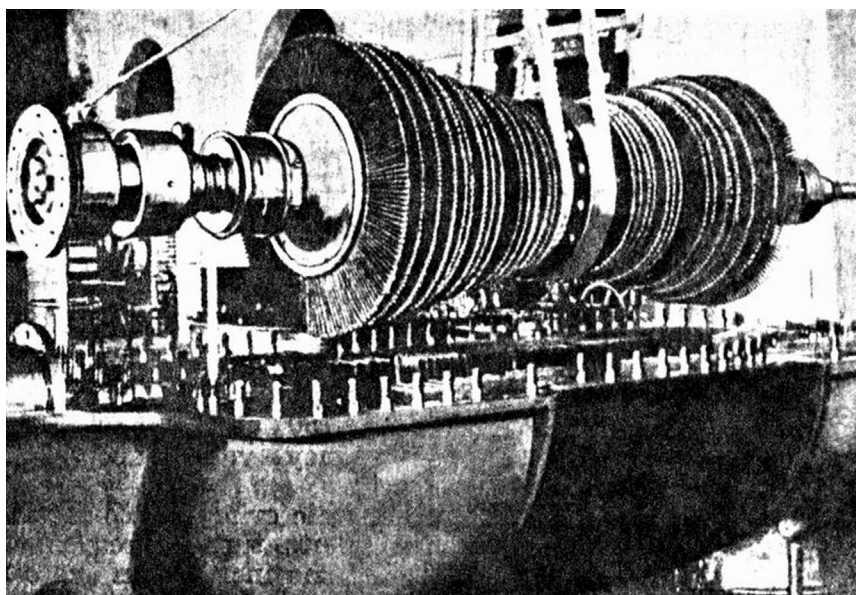


Figure 11.10 Rotor from a 2.5 MW Larderello unit, c. 1916 [11].

Integrated with the generation of electrical power was the recovery from the natural steam condensate of boric acid, H_3BO_3 , borax, $\text{Na}_2\text{B}_4\text{O}_7 \cdot 10\text{H}_2\text{O}$, and ammonium bicarbonate, NH_4HCO_3 (the main ingredient of “smelling salts”). The recovery method involved the use of the so-called Adriane boiler, a series of inclined trays through which the condensate flowed while being heated from below by the natural steam obtained from the covered pools. The natural concentration of the boric acid in the geofluid was about 2500 ppm or 0.25%; this was increased to about 8% during the process. When the solution was cooled and processed, nearly pure crystals of boric acid could be obtained.

Operating data, culled mainly from technical journals of the 1920 era, are given in Table 11.2 [9–15]. Some inconsistencies were found in the literature, so the author exercised his judgment as to which data were more likely to be correct. Although there were five sets of evaporators, each set with two evaporators, available to serve each 3 MW turbine, in fact only four sets were needed to meet the average demand of 2.5 MW. The claimed efficiency for the steam generator unit is 88% [10]. Only two of the three units actually were put into operation at Larderello, the original unit having been moved to Lago where improvements on the cycle were tested.

The remarkable thing about this data is that the utilization and thermal efficiencies are very similar to those found in many of today’s geothermal power plants. The 10% thermal efficiency is about normal for a simple binary cycle today. Nevertheless, Prince Conti and his technical staff conducted an ongoing program of research and development aimed at improving the operation. Over a period of time, the problematic Kestner boilers were replaced, eliminating the contamination of the turbine working fluid. They were replaced by what Conti called “depurators” [16] or what we would call reboilers. The system that evolved is referred to as the Cycle 2 power plant design and is shown schematically in Figure 11.11.

Finally, it is worth remembering that this early development was taking place during World War I when there were extreme shortages of conventional fuels in Italy. The price for a ton of coal sold on the wharves of Genoa was reported to be as much as \$97.33 in 1918 dollars [9]. Obviously there was enormous incentive for the Italians to develop an indigenous source of energy since the country had no supplies of coal or petroleum, relying on imports of fossil fuels and their own hydropower plants for the generation of electricity. Thus, the development of the geothermal resources in Larderello beyond the mineral recovery applications to electric power production was driven by the necessity that wartime often brings.

TABLE 11.2 Technical specifications for three original indirect-cycle units at Larderello.

Start-up year	1916	<i>Turbine:</i>	
Type	Indirect cycle	Type	Reaction, axial flow
No. of units	3	Cylinders/unit	1
Rating, MW	9 (3 × 3)	Flows/turbine	2
Net power, MW	7.5 (3 × 2.5)	Stages/flow	14
Geosteam flow rate, kg/s	29 (total, est.)	Inlet press., bar,a	1.25
Working fluid	Pure water	Mass flow/unit, kg/s	9.7
<i>Preheaters:</i>		Speed	3000
No. per unit	5 (5 × 1)	<i>Generator:</i>	
Type	Horizontal shell and tube	Type	3-phase, 50 Hz
Cond. outlet temp., °C	63	Power factor	0.7@4500 V
<i>Evaporators:</i>		<i>Condenser:</i>	
No. per unit	10 (5 × 2)	No. per unit	1
Type	Vertical shell and tube	Type	Horizontal shell and tube
No. of tubes	300	No. of tubes	3000
Tube length, m	7	Tube length, m	4.5
Tube diameter, mm	30	Tube diameter, mm	22
Tube area/unit, m ²	150	Tube area, m ²	1050
<i>Superheaters:</i>		<i>NCG removal system:</i>	
No. per unit	5 (5 × 1)	Type	Water-jet ejector
Type	Horizontal shell and tube	<i>Plant performance:</i>	
Geosteam inlet temp., °C	150–180	Net SSC, (kg/s)/MW	3.9
Geosteam inlet press., bar,a	2	Net utilization efficiency, %:	40.6
Pure steam flow rate, kg/s	15.2 (total, max)	Net thermal efficiency, %:	10.3
<i>Cooling tower:</i>			
No. per unit	1		
Type	Natural draft		
Range, °C	10		
CW flow rate, kg/s	333		

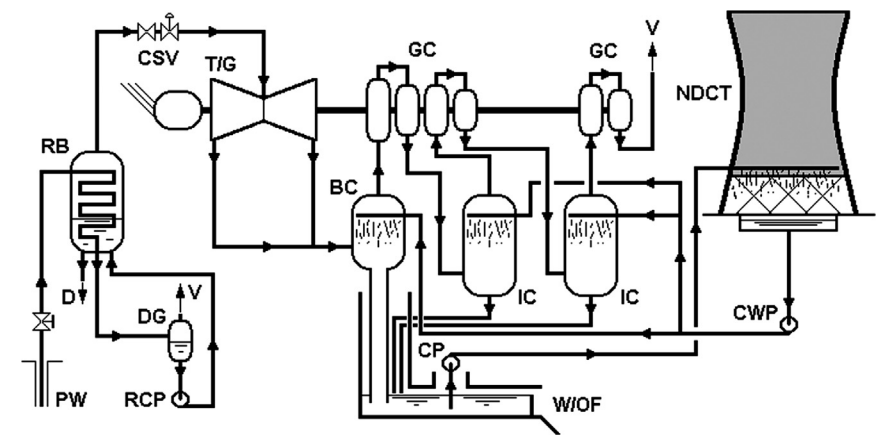


Figure 11.11 Cycle 2 plant schematic showing reboiler RB, degasser DG, recirculation pump RCP, NCG vent V, and drain for boron-rich geofluid D. An elaborate NCG compressor train was still needed because some NCG remained in the turbine steam.

11.3.2 POWER PLANTS OF THE MODERN ERA

The last of the indirect-cycle plants was taken out of service in 1968 when the plant at Castelnuovo was converted to a direct-cycle process [15]. The indirect-cycle plants had become overly expensive to operate and maintain, and the recovery of boric acid and borax was no longer economical. In fact, the mining of borax from southern California, an area that would become another important geothermal territory, essentially put the Boraciferous Region out of the boric acid and borax business. Furthermore, the materials used in the turbo-machinery had been improved through metallurgical advances and were now capable of functioning in the presence of the natural steam, eliminating the need for the intermediate heat exchangers.

Two types of plant became the standards for geothermal plants in Italy: (a) Direct-intake, exhausting-to-atmosphere units, and (b) direct-intake, condensing units. These plants are referred to as “Cycle 1” and “Cycle 3”, respectively, in the literature [15].

11.3.2.1 Direct-Intake, Exhausting-to-Atmosphere Units

Figure 11.12 shows the ultra-simple Cycle 1 flow diagram. Cycle 1 plants were used mainly where the geothermal steam contained excessive amounts of NCG such that it was uneconomical to extract them from the condenser owing to the high cost of installing and operating the gas compressors. The largest plant to operate as a Cycle 1 plant was the 15 MW unit at Piancastagnaio near Mt. Amiata, some 72 km (45 mi) southeast of Larderello. Several plants of this type were installed within the greater Larderello area, the largest there being the 7 MW Sasso 1 plant [17].

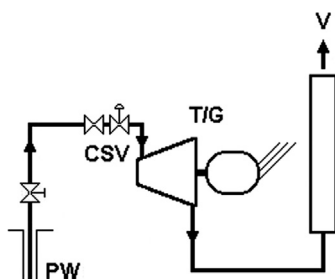


Figure 11.12 Larderello “Cycle 1” or direct-intake, exhaust-to-atmosphere plant.

When boric acid recovery was still conducted, the exhaust steam was directed to the Adriane boilers and assisted in evaporating the liquid geofluid. While these plants may have been optimal from an economic standpoint, they were

thermodynamically wasteful of the potential of the geothermal steam. Since the subatmospheric portion of the turbine expansion is absent in these units, the power output is roughly half of what a condensing turbine could produce. For example, the Piancastagnaio plant had only a 24% utilization efficiency and a specific steam consumption of 4.92 (kg/s)/MW [17].

11.3.2.2 Direct-Intake, Condensing Units

All plants operating on the shallow reservoir in the greater Larderello area used steam that was accompanied by significant amounts of NCG. When the concentration exceeded about 5% by weight of steam, Cycle 1 plants were used. Otherwise, it was feasible to install condensing units of the general arrangement shown in the schematic diagram in Figure 11.13.

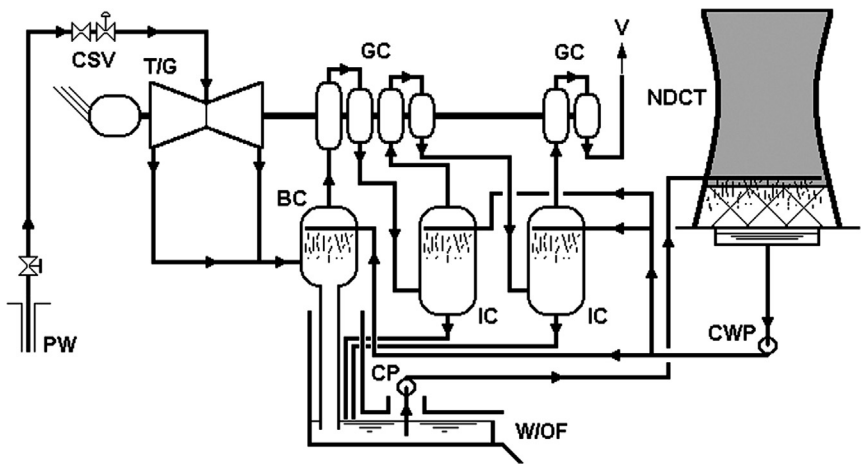


Figure 11.13 Larderello "Cycle 3" or direct-intake, condensing plant.

As can be seen, it was necessary to use several stages of gas compression to remove the NCG from the condenser to maintain the vacuum. These compressors were sometimes driven by electric motors or directly from the turbine (as shown in Figure 11.13). The compressors were fitted with intercoolers to minimize the amount of work consumed. The Cycle 3 plant that was designed to handle the highest concentration of NCG was the 26 MW Castelnuovo unit shown in Figure 11.14.

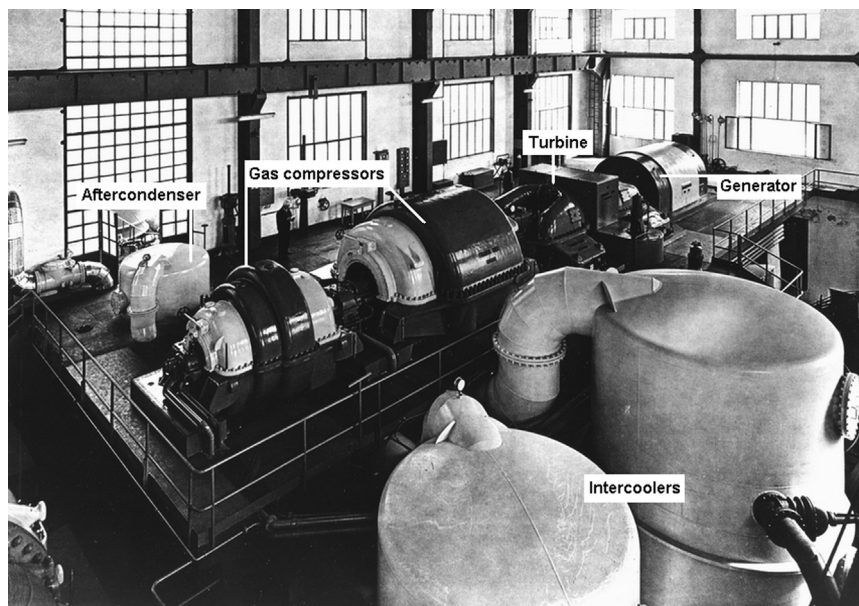


Figure 11.14 Castelnovo turbine hall showing 26 MW turbine-generator, gas compressors, intercoolers, and aftercondenser [17, 18].

This unit was one of four in the Castelnovo power station; it received the steam with the highest temperature (188°C), pressure (4.2 bar,a), and NCG (12–14%). The natural steam flow rate was 47.2 kg/s . The centrifugal turbo-compressors handled $85.9\text{ m}^3/\text{s}$ and required 2.27 MW. The net specific geosteam consumption was 2.06 (kg/s)/MW and the net utilization efficiency was 62.8%, assuming the geosteam to be pure steam. If one allows for the roughly 15% degradation of the exergy owing to the presence of the NCG in the steam [19], assuming it is all CO_2 , the utilization efficiency was even more impressive at 73.9%.

The technical details and many photographs of all the Cycle 3 plants may be found in the author's earlier book [17].

11.3.3 RECENT POWER PLANT DESIGNS

Following the discovery of the deep geothermal reservoir about 30 years ago, there has been a revolution in the way geothermal power stations are developed in Italy. Many of the older Cycle 3 plants had outlived their economic lifetimes, and Cycle 1 plants were no longer acceptable from an environmental standpoint. Instead of

designing each plant to suit the conditions of the geosteam found at each site throughout the region, it was decided to adopt standardized modular plants of a fixed nominal capacity, but with internal flexibility to allow the plants to be adjusted over their lifetimes should the steam conditions change. The modularity and flexibility also allow the plants to be moved from one site to another as conditions warrant.

The standard power ratings for the new plants are 10, 20, and 40 MW, and the steam mass flow rates are nominally 80, 130, and 250 t/h, respectively [20]. Many of the new plants are located in the old power houses, replacing the obsolete units, and as such had to conform to the dimensions of the existing structures. This has made for some interesting compromises, such as the arrangement of the condenser relative to the turbine. To save vertical space, the new turbines exhaust axially which permits direct entry into the condenser on the same level. However, owing to space restrictions, the condenser axis is perpendicular to the turbine axis and the condenser is placed outside the power house [20]. Figure 11.15 shows the arrangement.

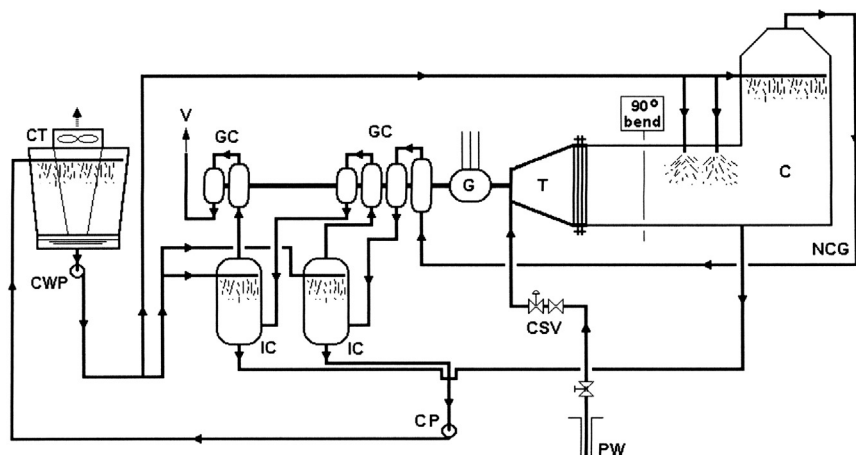


Figure 11.15 Modular plant layout for new Larderello units.

The geothermal steam remains as aggressive as ever, containing typically 5% NCG consisting of CO_2 , H_2S , and various silicates, sulfates, boric acid, and chlorides. It becomes necessary to scrub the steam prior to turbine entry when the chloride content exceeds 200–300 ppm to reduce the concentration to no more than 35 ppm. The train of gas compressors and intercoolers is essentially the same as in the Cycle 3 plants. Mechanical draft cooling towers have replaced the imposing natural draft towers that gave the Larderello landscape its distinctive appearance for many decades.

The turbines are fabricated with standard-sized rotors designed to handle the maximum expected steam flow, but can be specialized for each site by removing certain rows of nozzles and blades. To maintain a smooth steam path, the empty rows are filled with blade feet; see Figure 11.16 [20].

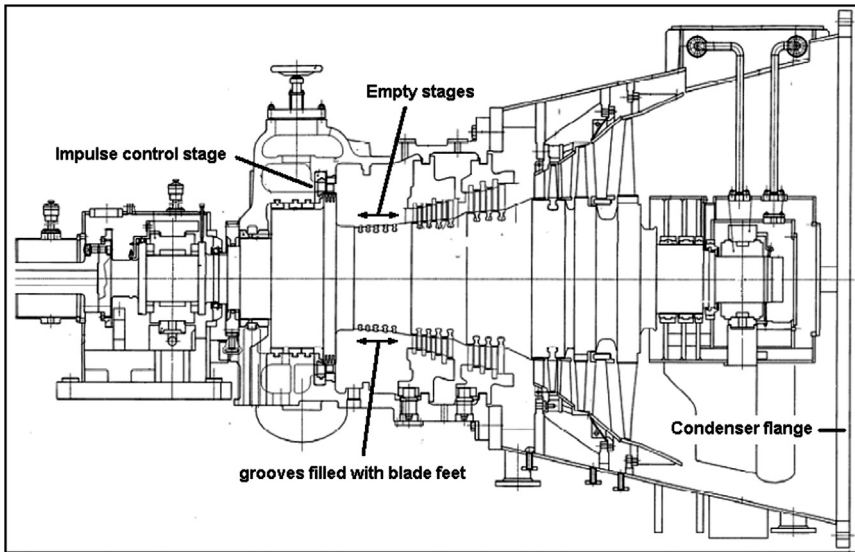


Figure 11.16 Modular turbine design. *Courtesy of General Electric Oil & Gas, Florence, Italy [20].*

Table 11.3 shows the utilization efficiencies for several of the new plants; the raw data from Santini [20] was averaged for the minimum and maximum values cited in the reference. The exergy of the inlet steam has been corrected for the gas content. The Travale plant has the benefit of the highest inlet steam pressure and temperature of the plants shown, and it is the most efficient in converting the incoming exergy into useful power output. The Lago plant is at the other end of the spectrum. The Gabbro plant, with the highest level of NCG, suffers the most in going from the gross to the net output, dropping some 13% in efficiency. Nevertheless, all the plants exhibit excellent utilization efficiencies, verifying the effectiveness of the modular design strategy.

TABLE 11.3 Utilization efficiency for selected recent plants at Larderello.

Item	Plant			
	Lago	Molinetto	Gabbro	Travale
Steam flow, kg/s	22.22	36.11	40.28	69.44
Inlet steam press., bar,a	2.5	6.5	6.5	14.0
Inlet steam temp., °C	127.4	190	162.0	195.1
NCG, % (wt)	1.7	4	12	5
Gross power, kW	8,855	19,210	19,005	43,230
Net power, kW	8,305	17,945	16,515	40,750
$\eta_{u,gr}$ %	62.1	68.3	68.7	73.1
$\eta_{u,nr}$ %	58.3	63.8	59.7	68.9

11.4 Mitigation of Environmental Impact

The extensive program to upgrade the older plants has been accompanied by more attention being paid to mitigating the environmental impact of the plants. As has been the case for many years, all excess geothermal condensate is reinjected. Furthermore, since 1994 there has been in operation a 39 km pipeline that delivers about 7600 m³/day of groundwater and geothermal fluids to the Larderello area from other geothermal sites.

A novel system for the abatement of both mercury and hydrogen sulfide from the geofluid has been designed, tested, and implemented by ENEL on several plants. The system is called AMIS (Abbattimento Mercurio e Idrogeno Solforato). Special sorbents are used to remove the Hg, and the H₂S is catalytically oxidized to sulfur dioxide which in turn is scrubbed by a side stream of cooling water. The system will be deployed at other plants as needed [21].

New plants are painted so as to blend in with the natural colors near the plants. An example of this is shown in [Figure 11.17](#) where the two 20 MW units at Carboli can be seen.



Figure 11.17 Carboli 2×20 MW power units. Photo courtesy of ENEL Green Power [WWW].

Finally, although it may not first appear to reduce the environmental impact, the use of modern, highly efficient power plants reduces the amount of geofluid that must be extracted to generate a fixed amount of electrical power. During 2002–2004, ten new plants were started up in the greater Larderello area, and of these, seven replaced obsolescent plants. From 1999 to 2003 during the renovation period, the total installed power capacity remained about constant but the electricity generated increased by 937 GW · h or by more than 20% [21]. The old plants would have had to extract and process 20% more geofluid to generate the same amount of electricity.

We can . . . give expression at this time to the expectation of conquering . . . the vast Plutonian forces which formerly manifested themselves in such spectacles as Vesuvius, Hekla, Krakatoa, and of utilizing at least a small portion of this nearly unlimited store of energy for the benefit of mankind.

George A. Orrok—November 12, 1925

References

- [1] ENEL. The history of Larderello. Public Relations and Communications Dept., Ente Nazionale per L'Energia Elettrica; May 1993.
- [2] Burgassi PD. Historical outline of geothermal technology in the Larderello region to the middle of the 20th century. In: Cataldi R, Hodgson SF, Lund JW, editors. *Stories from a Heated Earth: Our Geothermal Heritage*. Sacramento, CA: Geothermal Resources Council and International Geothermal Association; 1999. p. 194–219 [Chapter 13].
- [3] Lund JW. 100 Years of geothermal power production. *Geo-Heat Cent Q Bull* 2004;25(3):11–19.
- [4] ENEL. Geothermal energy in Tuscany and northern Latium. Generation and Transmission Dept., Relations and Communications Dept., Ente Nazionale per L'Energia Elettrica; May 1995.
- [5] ENEL. Larderello field trip: electrical power generation. Generation and Transmission Dept., Relations and Communications Dept., Ente Nazionale per L'Energia Elettrica; May 1995.
- [6] Fiordelisi A, Moffatt J, Ogliani F, Casini M, Ciuffi S, Romi A. Revised processing and interpretation of reflection seismic data in the Travale geothermal area (Italy). *Proc. world geothermal congress 2005*, Antalya, Turkey; 2005.
- [7] ENEL. Larderello field trip: geology and geothermal drilling. Generation and Transmission Dept., Relations and Communications Dept., Ente Nazionale per L'Energia Elettrica; May 1995.
- [8] Cappetti G, Fiordelisi A, Casini M, Ciuffi S, Mazzotti A. A new deep exploration program and preliminary results of a 3D seismic survey in the Larderello–Travale geothermal field (Italy). *Proc. world geothermal congress 2005*, Antalya, Turkey; 2005.
- [9] Anon. Electrical energy from the Volterra “Soffioni”. *Power* 1918;47(15):531.
- [10] Anon. Steam from the earth. *Power* June 1, 1920;51:889.
- [11] Anon. A “natural steam” turbine plant. *Power* December 24, 1918;48:935.
- [12] Hahn E. Some unusual steam plants in Tuscany. *Power* June 5, 1923;57(23):882–5.
- [13] Anon. The utilization of volcanic steam in Italy. *Sci Am* August 1924;:97.
- [14] Anon. Using volcanic steam for the production of electrical energy. *Sci Am* January 30, 1915;112:97–8.
- [15] ENEL. Larderello and monte Amiata: electric power by endogenous steam. Ente Nazionale per L'Energia Elettrica, Compartimento di Firenze, Direzione Studi e Ricerche, Roma; 1970.
- [16] Conti PG. The Larderello natural steam power plant. In: Anderson DN, Hall BA, editors. *First world power conference*, London, 1924; reprinted in *Geothermal Exploration in the First Quarter Century*, Spec. Rep. No. 3, Geothermal Resources Council; 1973.
- [17] DiPippo R. U.S. Dept. of Energy, DOE/RA/28320-1. *Geothermal energy as a source of electricity: a worldwide survey of the design and operation of geothermal power plants*. Washington, DC: U.S. Gov. Printing Office; 1980.
- [18] Villa FP. Geothermal plants in Italy: their evolution and problems. *Proc. second U.N. symposium on the development and use of geothermal resources*, San Francisco, vol. 3, 1975. p. 2055–64.
- [19] DiPippo R. Geothermal power cycle selection guidelines. Part 2 of Geothermal information series, DCN 90-213-142-02-02, Electric Power Research Institute, Palo Alto, CA; 1990.
- [20] Santini P. Modular geothermal plants in Italy: technical characteristics and operation results. *Proc. world geothermal congress 2005*, Antalya, Turkey; 2005.
- [21] Cappetti G, Cappatelli L. Geothermal power generation in Italy 2000–2004 update report. *Proc. world geothermal congress 2005*, Antalya, Turkey; 2005.

Nomenclature for Figures in Chapter 11

BC	Barometric condenser
C	Condenser
CP	Condensate pump
CSV	Control and stop valves
CW	Cooling water
CWP	Cooling water pump
D	Discharge to mineral recovery
DG	Degasser
E	Evaporator
G	Generator
GC	Gas compressor
IC	Intercooler
NCG	Noncondensable gases
NDCT	Natural draft water cooling tower
PW	Production well
RB	Reboiler
RCP	Recirculating pump
S	Separator
SH	Superheater
T	Turbine
T/G	Turbine/generator
V	Vent
W/OF	Weir/Overflow

Chapter 12

The Geysers Dry-Steam Power Plants, Sonoma and Lake Counties, California, USA

Chapter Outline

12.1 History and Early Power Plants	346
12.2 Geographic and Geologic Setting	350
12.3 Well Drilling	351
12.4 Steam Pipeline System	353
12.5 Power Plants	353
12.6 Recharging the Reservoir	360
12.7 Toward Sustainability	364
References	366



The McCabe plant, formerly Units 5 and 6, as seen from Vista Point looking across Big Sulphur Creek. This is the oldest power plant still in operation at The Geysers in the rugged Mayacamas Mountains in northern California. *Photo by author [WWW].*

12.1 History and Early Power Plants

The Geysers, the world's largest geothermal power complex, has been the subject of numerous books, articles, technical papers, theses, conferences, and workshops. As with Larderello, there is a visitor's center complete with displays and artifacts depicting the history and development of the field, and the general public can tour a part of the field and see a power plant. It is impossible, and unnecessary, to recount here all of the details of The Geysers' history; we will summarize the highlights and refer the interested reader to more complete documents.

Geothermal chronicler Susan Hodgson has divided the history of The Geysers into five distinct eras beginning with the time when it was in its natural state [1]. Native American Indians were well acquainted with the place and used its hot springs and fumaroles for many domestic and health-related activities. The White Man's history at The Geysers is reputed to have begun when a recent settler to California, William Bell Elliott, came across the impressive thermal manifestations while hunting bear in 1847. He was the person who misnamed the place "The Geysers" because there were no actual geysers at The Geysers.

Although the field covers about 30 square miles (7770 ha), thermal manifestations as observed in historic times were limited to essentially two areas: Geyser Canyon and the Little Geysers. Allen and Day of the Carnegie Institution studied these areas in the late 1920s and produced a classic reference work that describes the field in considerable technical detail and includes photos prior to major exploitation [2]. Eight shallow wells, however, had already been sunk by the time they surveyed the site. The most significant manifestations consisted of boiling pools, hot and muddy springs, fumaroles, steaming and altered ground that were confined to the very narrow Geyser Canyon that was about one-quarter mile long (400 m), and a few smaller areas not farther than 600 ft (180 m) distant.

Figure 12.1 is a map of the central thermal area as it appeared in 1927 in Allen and Day's book [2]; it has been modified from its original form for simplicity and clarity. One of the current power plants, the McCabe plant (formerly Units 5 and 6), is situated on a knoll overlooking what was once the center of thermal activity (see chapter opening photo and upper left corner of Figure 12.1). At the present time, none of the manifestations shown in Figure 12.1 remain active, the resort buildings are gone, and the canyon itself has largely been filled in. Today, small thermal pools are found only at the Little Geysers area, about five miles or so (8 km) upstream (to the southeast) along the Big Sulphur Creek.

A view of the thermal area in Geyser Canyon and the resort is shown in Figure 12.2 [3]. The abundance of steam issuing from various vents is obvious and apparently fascinating to the formally dressed visitors. The spa business thrived during the last half of the nineteenth century, achieving an international reputation. But like most thermal spas in the United States, its popularity rapidly

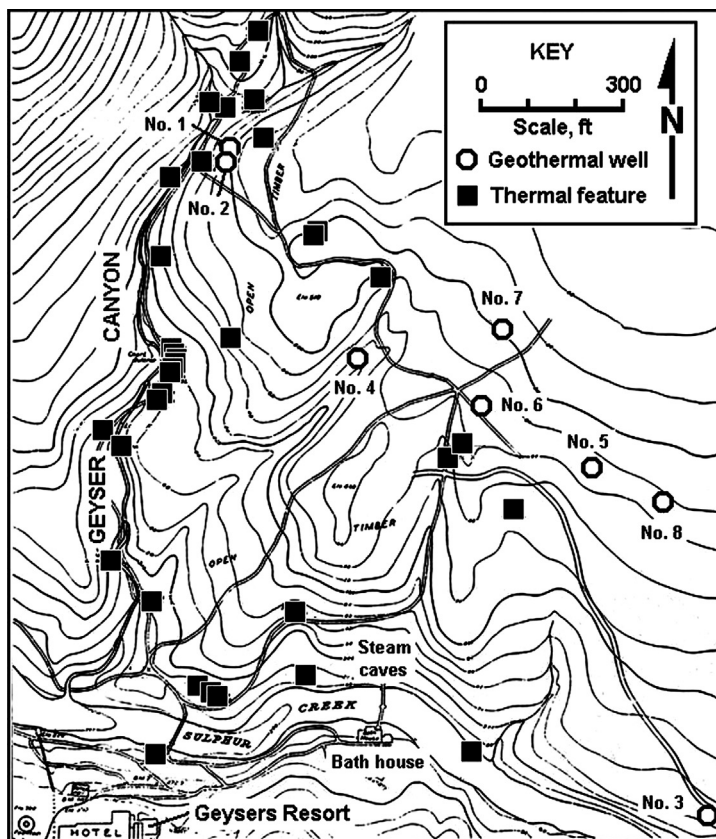


Figure 12.1 Geyser Canyon, Geysers Resort, thermal features, and original steam wells at The Geysers. *Modified from the original map from Allen and Day [2].*

declined in the early twentieth century. Remnants of the once flourishing operation remained until 1980 when the buildings were dismantled by UNOCAL, then The Geysers operator, at the request of the owner [1].

The first steam wells were completed at The Geysers in 1921 by J.D. Grant. He sited his well very close to one of the hottest thermal springs, the so-called Witches' Cauldron, at the upper end of Geyser Canyon; the well blew out at a shallow depth. Undeterred, he moved his homemade cable-tool rig across the canyon and successfully completed wells No. 1 and 2; see Figure 12.1 [1]. Both wells were able to produce abundant steam, as can be seen from Figure 12.3 in which well No. 2 is blowing across the canyon [2].

Using reciprocating steam engines built by General Electric, Grant assembled the first electrical generating plant close to his first two wells; see Figure 12.4. Of course, such a small power plant was viewed more as a curiosity than a serious source of electricity. Later, electricity was generated for the resort hotel in another tiny power house located next to the resort; see Figure 12.5.



Figure 12.2 A view looking south down the Geyser Canyon toward the Geysers Resort. From the private collection of B.C. McCabe, Magma Power Company, published in Ref. [3].

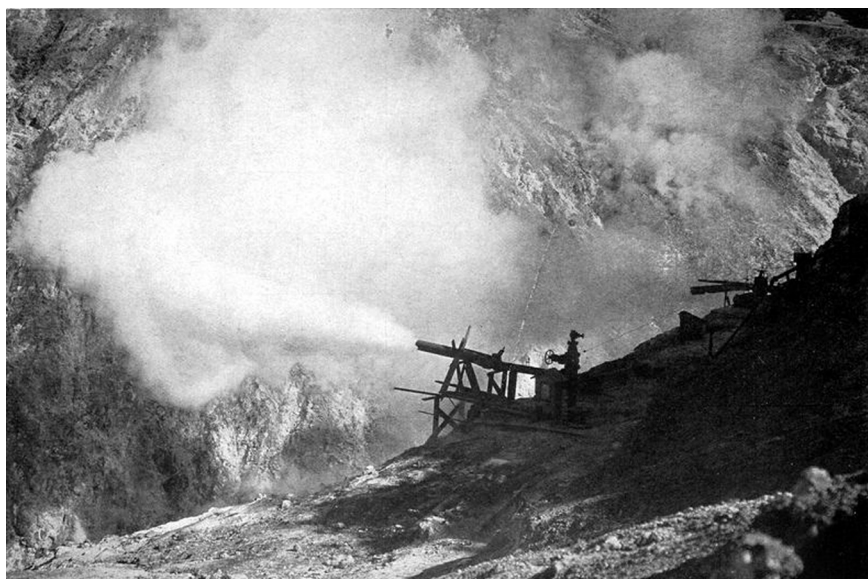


Figure 12.3 J.D. Grant's first two successful wells at The Geysers. No. 2 is blowing across Geyser Canyon; No. 1 is 12 m farther up the canyon rim. From Allen and Day [2].



Figure 12.4 The first power house at The Geysers. It was built about 24 m east of the wells No. 1 and 2, and used their steam to produce 35 kW. *Photo courtesy of Geothermal Resources Council, published in Ref. [1].*



Figure 12.5 The Geysers power plant that provided electricity to the Geysers Hotel; photographer unknown [WWW].

Given the low cost of hydropower and the difficult access to the remote and mountainous site, further development did not take place at The Geysers until the 1950s when B.C. McCabe began to drill wells using modern equipment and techniques. McCabe's company was Magma Power Company. McCabe's partner was Dan McMillan, Jr. whose company was Thermal Power Company. As a joint venture, Magma-Thermal played the pioneering role in developing the steam field that today supports 26 electrical generators with a total installed capacity of 1462 MW.

12.2 Geographic and Geologic Setting

The Geysers steam field lies some 129 km (80 mi) north of San Francisco in the Mayacamas Mountains. Productive wells have been drilled covering a surface area roughly $6.4 \text{ km} \times 11.3 \text{ km}$ ($4 \text{ mi} \times 7 \text{ mi}$), oriented NW-SE, and aligned with the regional fault system.

The reservoir is hosted in fractured graywacke, characterized by a matrix porosity associated with veins, that lies above a deep felsite intrusion [4]. The porosity is low, on the order of 1–5%, but excellent productivity is observed when a well finds an intensely fractured region of the formation. The top of the productive zone has been well documented by the more than 500 wells drilled, and Figure 12.6 depicts the results [5].

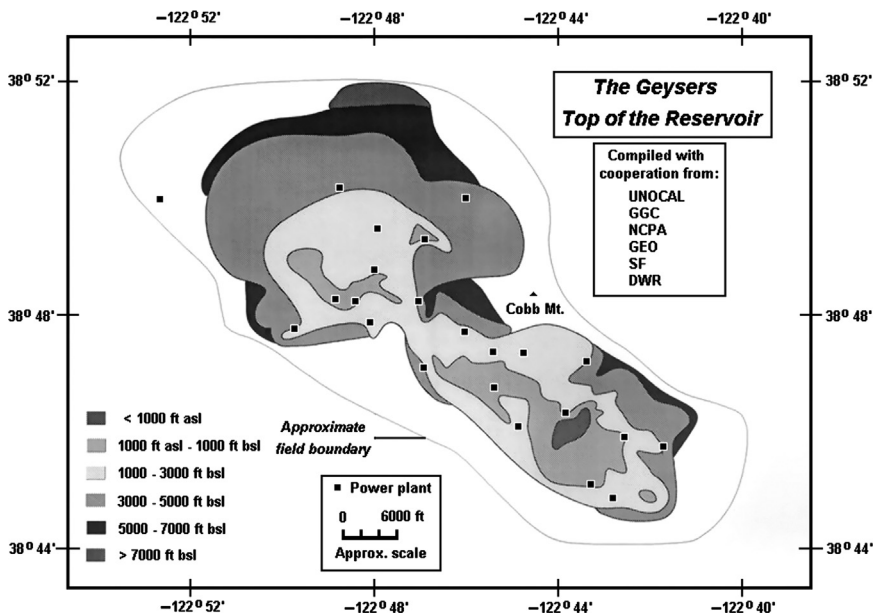


Figure 12.6 The top of The Geysers reservoir by depth interval, measured above sea level (a.s.l.) and below sea level (b.s.l.). The heat source is believed to lie beneath Cobb Mountain. Modified from Ref. [5].

The shallowest parts of the reservoir lie in the southeast area where the reservoir can be reached at levels less than 305 m above sea level (1000 ft a.s.l.) within a small area. Although the elevation of the ground surface varies considerably, it is generally between 610 and 915 m a.s.l. (2000–3000 ft a.s.l.) within the productive field.

Recalling the conditions needed to create a dry-steam reservoir (see Section 7.2), the requirement to lower the water table to extreme depths is one of the most important. It appears that there was much prehistoric thermal activity across the field, manifested today by extensive areas of altered ground. The discharge of fluids must have been prolific for long periods of time because no well so far has encountered a liquid-dominated zone beneath the steam reservoir, including wells deeper than 3000 m. Furthermore, the entire thickness of the productive formation has yet to be penetrated.

The areal extent of the reservoir is also evident from [Figure 12.6](#). It appears to be bounded along the southwest and the northeast by the Mercuryville and Collayomi fault systems, but the actual limits of production lie somewhat within those boundaries [6]. Along the southwest, there is a thin vertical plane separating productive from nonproductive wells, indicating a tight lateral boundary to the steam reservoir. This is yet another of the requirements mentioned in Section 7.2 to preserve a steam reservoir that is under-pressured from being inundated by cold water from the sides.

Drilling in the north and northwest areas has identified a very high-temperature, deep reservoir; see [Figure 12.6](#). Temperatures of 300°C (575°F) have been found but the steam is highly superheated and acidic, containing hydrogen chloride, HCl, causing it to be extremely corrosive. So far this steam has not been used in any power plant.

12.3 Well Drilling

Several problems confront the well driller at The Geysers. The terrain is rugged, making it difficult to site drilling pads. The ground can be unstable, either from landslides or thermal activity, creating a challenge for the civil engineer who must build roads, set foundations for power plants and cooling towers, and create level areas for drill sites that must support large drill rigs.

Since the formation derives its productivity from swarms of tiny fractures in otherwise hard rock, drilling in the reservoir must be conducted with air as the drilling fluid to avoid clogging the fractures. This increases the erosion on the tubular elements of the drill string, the well casing, the blowout preventer, and other surface equipment as the rock cuttings are transported to the surface from the bottom of the hole in a high-speed air jet. Mud can be used as the drilling fluid for the shallow sections of the well above the reservoir, but then another potentially serious problem can occur.

If the well passes through a permeable region at relatively shallow depth, total loss of circulation (LOC) will be encountered, necessitating the use of LOC materials or the setting of a cement plug in order to continue drilling ahead. The use of LOC materials is often a stop-gap solution that is ineffective in the long term because the formation is below hydrostatic pressure. Therefore, when the casing is cemented, the LOC material may give way under the hydrostatic pressure of the cement leaving a void behind the casing and thus endangering the life of the well.

Typical well profiles are shown in Figure 12.7 [7,8]. The well at left is a deviated well; many wells at The Geysers are drilled from a single pad to conserve space in the rugged landscape. The well at right is a forked well that allows steam to be gathered from a wider zone of the reservoir and brought to a single well-head for ease of transmission to the power plant. Notice that the wells are finished as open holes since there is little need for a liner given the competent nature of the rock in the formation.

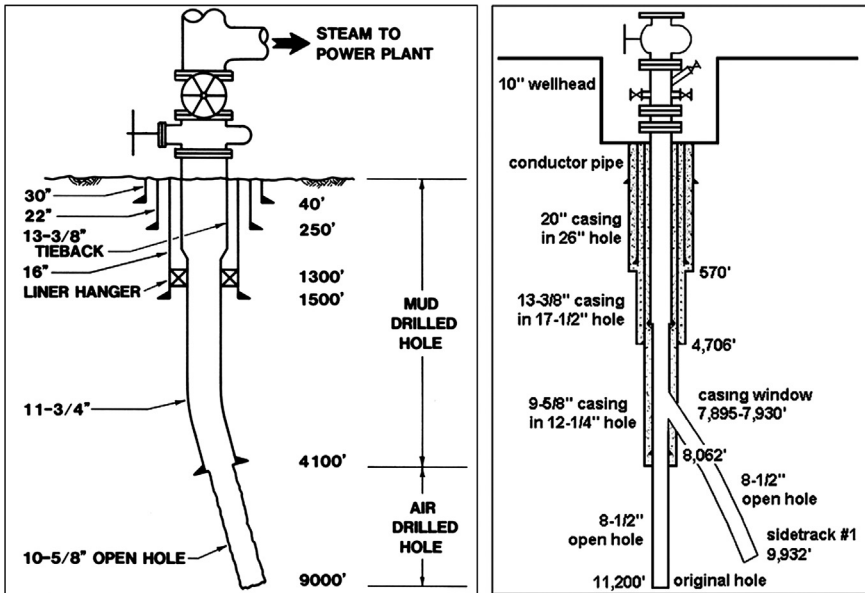


Figure 12.7 A typical deviated well (left) and forked well (right) at The Geysers [7,8].

Recent practice includes the drilling of wells with three or more forks from a single trunk. For example, the Aidlin No. 9 well has four sidetracks besides the original wellbore; the original bore and one of the sidetracks were abandoned, but the three active sidetracks produce 14.6 kg/s (116,000 lbm/h) of steam compared to 9.45 kg/s (75,000 lbm/h) for the original well, a 55% increase in productivity. Such wells are extremely difficult to complete; in the case of Aidlin No. 9, it took 97 days to finish the sidetrack redrilling operation [8].

12.4 Steam Pipeline System

In Section 7.3, we discussed in general the steam gathering system for a dry-steam plant, and the reader may wish to review that section before proceeding. Here we will show diagrams of the piping used at The Geysers between the wells and the power house. Reference [9] may be consulted for more details.

In Figure 12.8, steam from several wells at one pad is collected after passing through a wellhead particulate remover (PR) and, if the steam is wet, through a wellhead moisture remover (MR). The steam from each well is joined in a single pipeline and is connected to the main steam line, where it merges with the steam from other well pads. Along the steam lines, liquid condensate that forms from heat loss is drained (LD) to a central condensate collection basin (CCB). A vent muffler (VM) is used during emergency situations such as turbine trips to prevent damage to the wells. Before the steam enters the final steam separator (SS), it receives a spray of water (SW) that acts as a scrubber to help remove any silica that may be entrained in the steam; this prevents buildup of scale on the turbine nozzles and blades. Excess water from the cooling tower is collected in a condensate holding tank (CHT); the collected condensate drained from all sources is pumped over from the CCB to the CHT, and then is reinjected.

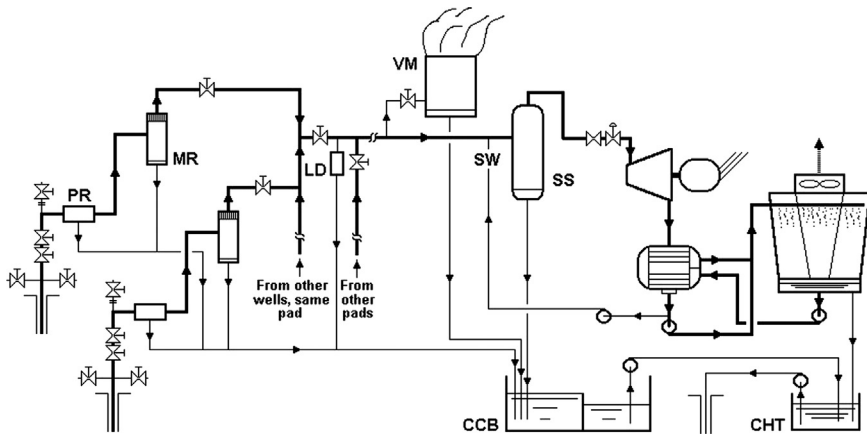


Figure 12.8 Steam and condensate piping system for a typical Geysers power plant [9].

12.5 Power Plants

There have been 23 separate power plants built at The Geysers since 1960. Figure 12.9 shows the location of each one, including those that have been retired

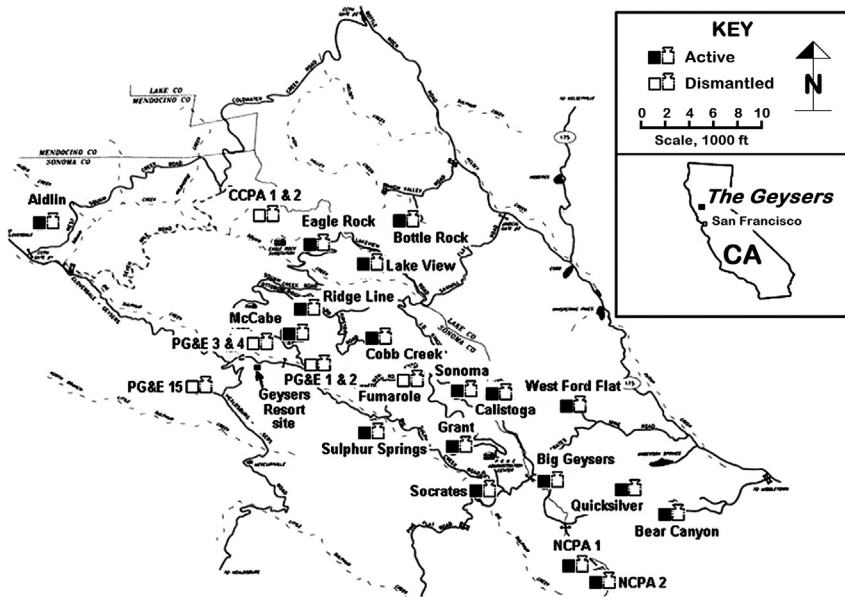


Figure 12.9 The Geysers location map showing power plants, active and dismantled since 1960. Modified from the Geysers Geothermal Association [1].

and dismantled. The two original plants that housed Units 1–2 and 3–4 were demolished along with Unit 15 and CCPA 1–2. Fumarole (originally Pacific Gas and Electric Company (PG&E) Units 9–10) is being dismantled after several years of inactivity.

The first unit, PG&E Geysers Unit 1, was a small unit, 11 MW, situated just across Big Sulphur Creek about 460 m (1500 ft) east of the site of the old Geysers Hotel. In October 1985, it was designated a National Historic Mechanical Engineering Landmark by the American Society of Mechanical Engineers [10]. Figure 12.10 shows the original power house that held both Units 1 and 2. Since the plant was so close to Big Sulphur Creek, it was able to take makeup and fire protection water from it.

In 1992, after a successful run of 32 years, the old plant was shut down in favor of the more efficient modern units, and dismantled. A view of the site in 1997 is given in Figure 12.11. In January 2004, a new well, GDC-31, was completed on the old power house site. It turned out to be the most powerful Geysers well drilled to date, capable of about 10 MW. So potent was the well that it required a separate pipeline to convey its steam to the McCabe unit [11,12].

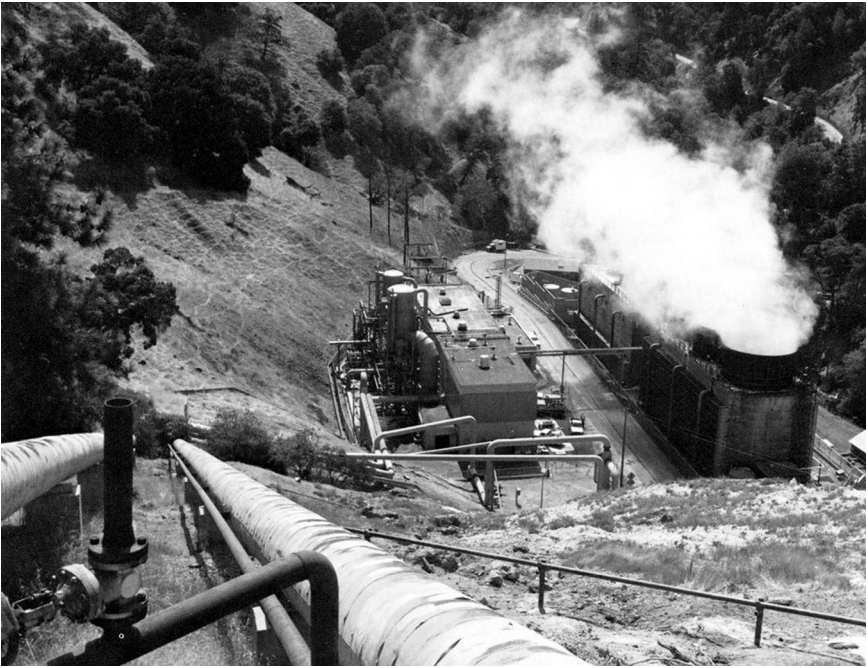


Figure 12.10 Historic photo of PG&E Geysers Units 1 and 2 looking generally east; Unit 1 is at the rear. The access road ran between the cooling tower and the power house. Big Sulphur Creek lies to the right of the plant, parallel to the main axis of the cooling tower. Note the steep terrain, approaching 45° behind the plant. *Photo from Ref. [10].*



Figure 12.11 Site of original Units 1 and 2 after demolition and prior to drilling of well GDC-31. The power house was on the left and the cooling tower was on the right. *Photo by author [WWW].*

Table 12.1 gives a summary of information on all Geysers plants that have ever been in operation. As of 2014 there are 15 power plants owned and operated by Calpine, two plants owned and operated by Northern California Power Agency (NCPA), and one (Bottle Rock) owned and operated by US Renewables Group (USRG) in partnership with Riverstone Holdings and The Carlyle Group. The last plant built was the Aidlin plant in 1989. Since then, an attempt was made to redevelop the area around the original PG&E Unit 15, but as of 2014 nothing has come of this effort.

TABLE 12.1 Summary of plant data for The Geysers: installed MW are shown.

Plant name	Original name	Start year	Rated MW	No. units	Total MW	Owner	Notes and comments
PG&E Unit 1	(same)	1960	11	1	11	PG&E	Dismantled
PG&E Unit 2	(same)	1963	13	1	13	PG&E	Dismantled
PG&E Unit 3	(same)	1967	27	1	27	PG&E	Dismantled
PG&E Unit 4	(same)	1968	27	1	27	PG&E	Dismantled
McCabe	PG&E Units 5&6	1971	2 × 53	2	106	Calpine	
Ridge Line	PG&E Units 7&8	1972	2 × 53	2	106	Calpine	
Fumarole	PG&E Units 9&10	1973	2 × 53	2	106	Calpine	Dismantled
Eagle Rock	PG&E Unit 11	1975	106	1	106	Calpine	
Cobb Creek	PG&E Unit 12	1979	106	1	106	Calpine	
Big Geysers	PG&E Unit 13	1980	78	1	78	Calpine	
Sulphur Springs	PG&E Unit 14	1980	65	1	65	Calpine	
PG&E Unit 15	(same)	1979	59	1	59	PG&E	Dismantled
WGP Unit 1	See note ^a	—	(25.5)	(1)	(25.5)	WGP	On hold
Quicksilver	PG&E Unit 16	1985	113	1	113	Calpine	
Lake View	PG&E Unit 17	1982	113	1	113	Calpine	
Socrates	PG&E Unit 18	1983	113	1	113	Calpine	
Calistoga	Santa Fe	1984	2 × 40	2	80	Calpine	
Grant	PG&E Unit 20	1985	113	1	113	Calpine	
Bottle Rock	(same)	1985	55	1	55	USRG ^b	Reactivated
Sonoma	SMUDGE#1	1983	72	1	72	Calpine	
NCPA 1	(same)	1983	2 × 55	2	110	NCPA	
NCPA 2	(same)	1985, 1986	2 × 55	2	110	NCPA	
Coldwater Creek	CCPA 1&2	1988	2 × 65	2	130	CCPA	Dismantled
Bear Canyon	(same)	1988	2 × 11	2	22	Calpine	
West Ford Flat	(same)	1988	2 × 14.5	2	29	Calpine	
J.W. Aidlin 1&2	(same)	1989	2 × 10	2	20	Calpine	
TOTALS				35	1890		
Active				26	1462		

^aUnder development on the same site as PG&E Unit 15 by Western GeoPower (WGP).

^bUS Renewables Group.

12.5.1 PLANT DESIGN UNDER PG&E

Beginning in the 1960s, PG&E owned and operated the power plants at The Geysers, and the steam was developed and delivered to the plants by a number of different companies. PG&E paid the steam suppliers according to a negotiated agreement that did not encourage the power plant owner to make the most efficient use of the steam. The formula to determine the price was based on PG&E's costs to generate electricity from its fossil-fuel and nuclear power plants. The formula used in the 1970s is given in Eq. (12.1):

$$C_S = \frac{2.11 E_F (C_F / C_F^0) (MHR / MHR^0) + E_N C_N}{E_F + E_N} \quad (12.1)$$

where C_S is the price in year n of the geothermal steam in mills/kW · h, that is, 10^{-3} \$/kW · h, and the other terms are as follows:

E_F = electricity generated from fossil fuel in year $n - 1$

E_N = electricity generated from nuclear fuel in year $n - 1$

C_F = average cost of fossil fuel in year $n - 1$

C_F^0 = average cost of fossil fuel in year 1968

C_N = average cost of nuclear fuel in year $n - 1$

MHR = minimum heat rate for fossil-fuel plants in year $n - 1$

MHR^0 = minimum heat rate for fossil-fuel plants in year 1968.

Since the amount of money paid out by PG&E was proportional to the amount of electricity generated from the geothermal steam, there was no incentive for PG&E to design their plants for high efficiency. It would cost more for them to build such plants and the extra investment could not be justified. Steam brought in “over the fence” that was not used in the plant could be “wasted” without penalty to the plant owner. It was only later when the steam purchase agreements were revised to treat the steam as a valuable commodity that more efficient plants were built.

The heat balance diagram for Unit 5, the oldest unit still in operation, is shown in Figure 12.12 [13]. It is striking in its simplicity. At the time there was no need to abate the noncondensable gases (NCG) since the amount of hydrogen sulfide being discharged to the atmosphere was within the allowable limits.

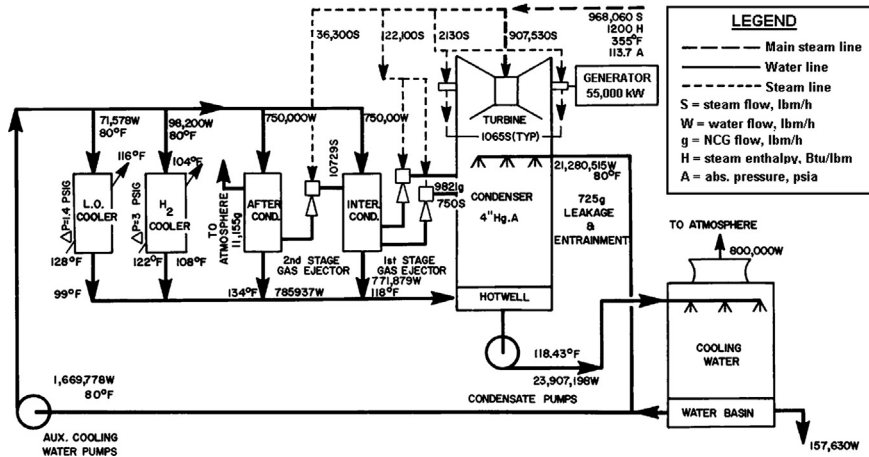


Figure 12.12 Heat balance diagram for PG&E Geysers Unit 5 [13].

The inlet steam is about 10°C (18°F) superheated. The gross output is 55,000 kW and the gross utilization efficiency based on the design wet-bulb temperature of 18.3°C (65°F) is 54.2%. There are two main parasitic power loads: water circulating pumps, 930 kW, and cooling tower fan motors, 605 kW. All other loads amount to 445 kW, leaving a net power of 53,020 kW; this gives a net utilization efficiency of 52.2%. These values indicate that the plant operated relatively efficiently, compared to flash-steam plants, owing to the availability of high-exergy steam as the primary resource.

12.5.2 SMUDGE #1 PLANT DESIGN

To illustrate the impact of the steam purchase agreement on the design of a geothermal plant, we will consider the case of the 72 MW SMUDGE #1 plant, now called Sonoma. In 1978, the Sacramento Municipal Utility District (SMUD) signed a steam purchase agreement with Aminoil USA, then a steam developer at The Geysers, to purchase 138.6 kg/s (1,100,000 lbm/h) of steam at a pressure of 793.1 kPa (115 lbf/in²) with not more than 200 ppm of H₂S. The price of the steam was \$1.00/1000 lbm, or \$1100/h at full flow rate [14]. It is clear that under this arrangement, SMUD should try to generate as much electricity as is feasible from each pound of steam. This drove the design to include many features that could not be economically justified under the PG&E-type of contract. The design that emerged is shown in the heat balance diagram of Figure 12.13 [15].

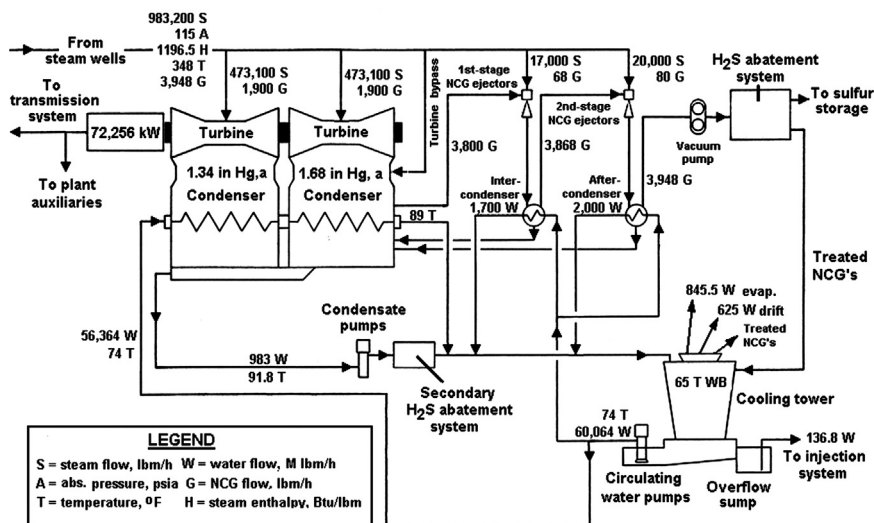


Figure 12.13 Heat balance diagram for SMUDGE #1 Geysers power plant [15].

The turbine was larger than previous machines, having 635 mm (25 in) last stage blades, four exhaust ends, with moisture removal sections after each stage, and Stellite[®] strips to protect the leading edges of the last two rows of blades [16]. The condenser was a two-zone design with dual vacuum conditions for the two turbines. The vacuum was the lowest seen at The Geysers at the time: 1.34 and 1.68 in Hg. A highly efficient means of removing the NCG was employed: a two-stage steam jet ejector followed by a liquid-ring vacuum pump. In selecting the suppliers for the other auxiliary systems, including pumps, transformers, H₂S abatement system, cooling tower, etc., a penalty was applied to any bidder for inefficient use of steam and electricity [17]. The end result was the most efficient geothermal power plant ever built: SMUDGE #1 had a gross utilization efficiency of 70.1%, and a specific steam consumption of 13.6 (lbm/h)/kW or 1.71 (kg/s)/MW.

12.5.3 POWER PLANT OPERATIONS UNDER CALPINE OWNERSHIP

With the exception of the two NCPA plants and the Bottle Rock plant, all the power plants at The Geysers and their steam resources have been owned and operated by Calpine Corporation since 1999. This unified ownership has created even more incentive for efficient use of the steam resource. The electricity generated is now sold into the power exchange where it must compete with every other source of electricity on the open market. An extensive and ongoing program of modernization and performance improvement is underway to identify areas of inefficiency and to correct them. Integrated field management has resulted in

interconnections of steam lines serving various units, allowing for balancing the supply of steam to the units and diverting steam to other units in the event of an outage or maintenance. Areas of the field, such as the northwest sector which is known to be productive but with high NCG content, may be exploited now that advanced technology is available to permit such fluids to be utilized efficiently. Finally, new wells are being drilled, such as well GDC-31 mentioned earlier, that indicate the field may be even more extensive than most believed, and may lead to the building of additional power plants after a hiatus of some 25 years. NCPA has reaped similar benefits since acquiring the rights to the steam field that supplies its two power plants in the Southeast Geysers area.

12.6 Recharging the Reservoir

One of the problems in the management of a dry-steam field is the replenishment of the fluid that is withdrawn through production. Natural recharge usually occurs at a rate far less than the rate of removal, leading to pressure reduction and a drying out of the reservoir. The contrast between a dry-steam (DS) resource and a liquid-dominated (LD) one is dramatic. Although vastly more mass is withdrawn from a LD reservoir compared to a DS one to generate the same power, 70–80% of that mass can be reinjected for the LD case, whereas only the excess steam condensate from the cooling tower, roughly 10–15%, is available in the DS case.

The trends in production and reinjection from the start of operations in 1960 through 2014 are shown in the series of graphs in [Figures 12.14–12.17 \[18\]](#). After

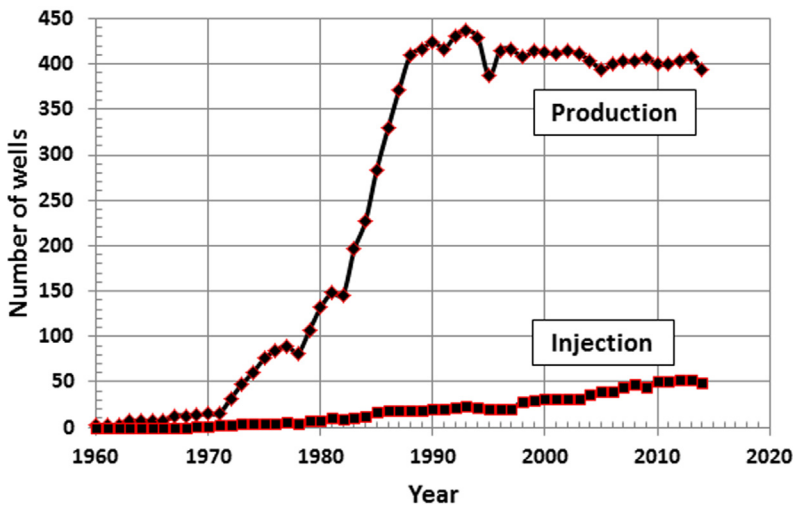


Figure 12.14 Numbers of production and injection wells at The Geysers, 2014 [18] [WWW].

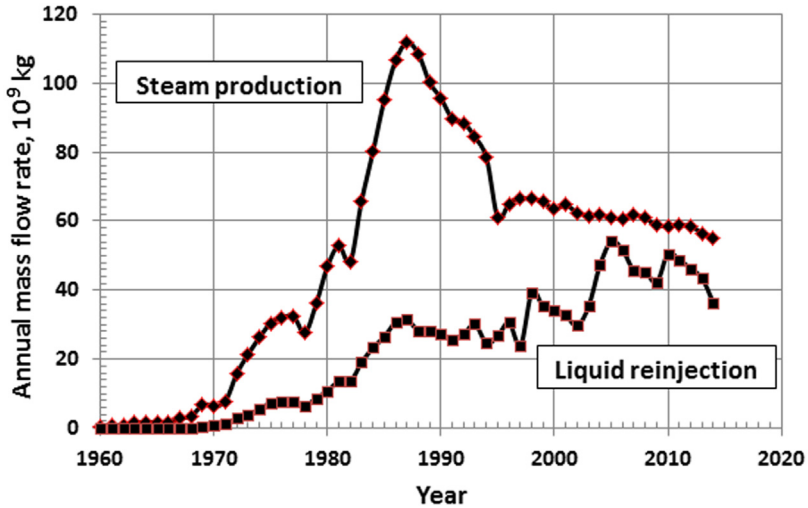


Figure 12.15 Annual steam production and liquid injection at The Geysers, 2014 [18] [WWW].

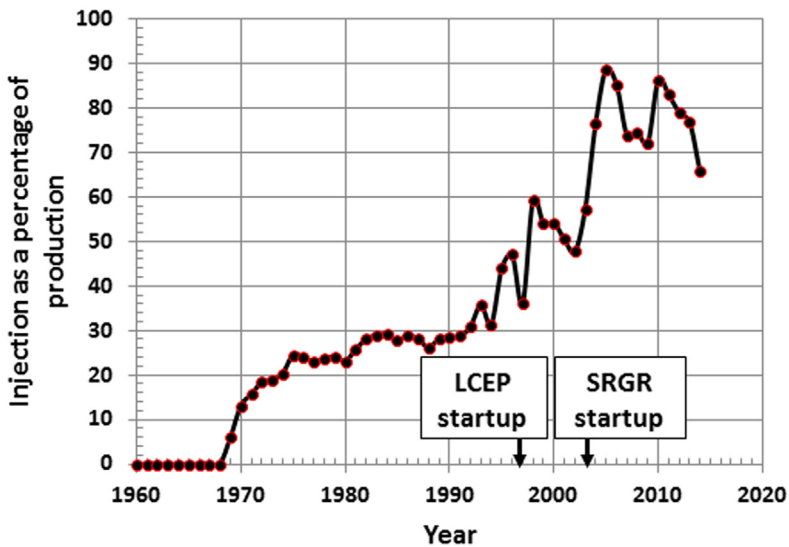


Figure 12.16 Mass of injectate as a percentage of mass removed at The Geysers, 2014 [18] [WWW].

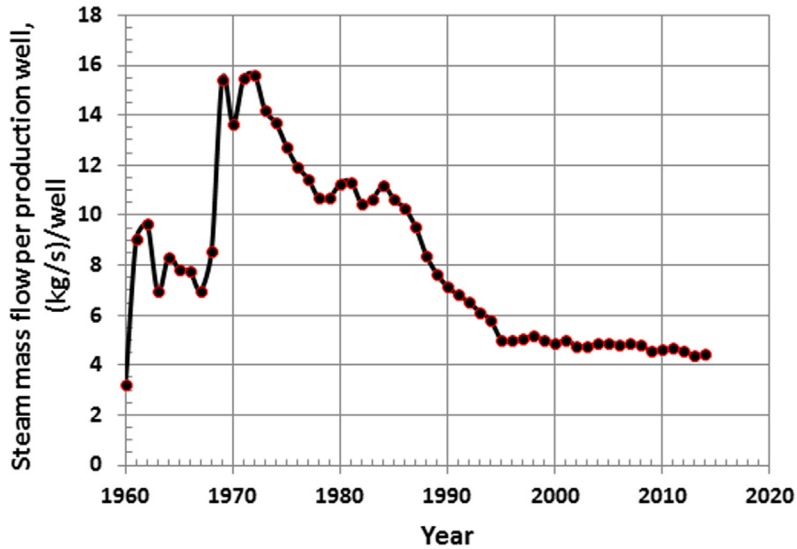


Figure 12.17 Annual steam production averaged over production wells at The Geysers, 2014 [18] [WWW].

a period of rapid growth in the 1980s, spurred by the two oil shocks of 1973 and 1979, the number of production wells drilled declined somewhat and has recently stabilized at about 400–405 (Figure 12.14). For the first nine years of operation, no reinjection was carried out at all. Thereafter, the number of injection wells has gradually grown, as has the percentage of fluid injected relative to the mass of steam removed (Figure 12.16). Besides cooling tower overflow, water has been taken from Big Sulphur Creek during the wet season, and rainwater is captured in holding ponds and then injected [19]. The field has yielded over 2.685×10^{12} kg of steam in 53 years of operation, while a little over 1.177×10^{12} kg of liquid—44% of production—has been returned to the reservoir.

The amount of steam produced per year, averaged over the number of wells, was about 8 kg/s per well in the 1960s (Figure 12.17). This jumped to 15.5 kg/s per well in the 1970s as newer parts of the field were brought into production. However, this rate was not sustainable and a general decline ensued until 1995 when this value fell to only 5 kg/s per well. Since then, it appears that the decline rate may have stabilized at roughly 0.72% per year. The most recent data for 2014 shows the average well produced 4.45 kg/s or the equivalent of about 2.63 MW. Thus 19 wells are needed to supply a 50 MW power unit.

The reason for the stabilization over the last 18 years, 1995–2013, is related to two innovative waste-water-to-electricity projects: the Lake County Effluent Pipeline (LCEP), also known as the Southeast Geysers Pipeline (SGP) project, and Santa Rosa Geysers Recharge (SRGR) project [19–23]. These were the first projects of their kind in the world.

The LCEP was put into operation on September 25, 1997 [19]. It carries secondary-treated municipal waste water from several communities along the north side of Clear Lake, south to Middletown where a second water treatment facility is located. From there, about 2.8 billion gallons of water per year (10.5×10^9 kg) is pumped through 53 miles (85 km) of 16- to 20-inch pipe into the Southeast Geysers field, gaining about 2000 ft (610 m) in elevation. Besides helping to recharge the reservoir at The Geysers, the injected water has resulted in lower NCG in the steam, reducing the parasitic power needs. Furthermore, the project has several environmental benefits, including the creation of a wetlands habitat for wildlife that also serves to polish the effluent prior to being pumped to The Geysers, and the elimination of the discharge of treated and untreated waste water into Clear Lake which is used as the source of drinking water for some communities. It is planned to extend the pipeline along the southern shore of Clear Lake to complete Project “Full Circle” [23].

The SRGR project was patterned on the successful LCEP and started up on December 5, 2003, two years later than scheduled and at a cost more than double what was expected, \$250 vs. \$102 million [21,24]. It is a 41 mile (66 km) pipeline from the City of Santa Rosa and surrounding communities to the central and northwest sectors of the field. It carries tertiary-treated waste water, essentially drinking water, to help recharge the other end of the field from the LCEP injection area [25]. The elevation gain is about 3000 ft (915 m). Since the water is so pure, some of it may be used as cooling water at those plants with high levels of H_2S in the steam condensate, eliminating the need to treat the condensate.

As of 2014, the whole field receives roughly 1003 kg/s (24 million gal/day) of municipal waste water recharge divided over three injection areas [24]:

- SRGR Project average: 490 kg/s
- Calpine Southeast Geysers Effluent Pipeline (LCEP or SGP) average: 162 kg/s
- Calpine and NCPA average: 351 kg/s.

The end result of the recharge projects has been a boost in power output due to increased steam flow amounting to over 160 MW, compared to the anticipated power without the projects. Assuming an electricity cost of $\$0.05/\text{kW} \cdot \text{h}$ and a conservative average system capacity factor of 90%, the extra power would bring in additional revenues of \$67 million per year. Future benefits may derive from

the ability to use the deep, 300°C (575°F) reservoir beneath the northwest sector of the field that produces highly superheated but extremely corrosive steam. If the pure water can dilute the native steam, then a whole new area of the field will be opened to development.

In November 2004, Calpine Corporation was honored by the US DOE and the US EPA by being selected for a “Green Power Leadership Award” for the SRGR project. The award recognizes organizations for “Innovative Use of Renewable Energy Technology” [26].

12.7 Toward Sustainability

The Geysers’ history of power generation demonstrates that geothermal energy may be used in a manner that allows it to approach sustainability, or it can be overexploited resulting in a premature demise of the resource. Lovekin [27] has described the life cycle of a geothermal field as passing through four distinct phases or periods: (1) development, (2) sustaining, (3) declining, and (4) renewable; see Figure 12.18. Only during the last phase does a geothermal resource approaches the ideal of a sustainable and renewable resource, and to attain it requires prudent management of the resource. Once a field reaches the point where the fluid extraction matches the combined natural and augmented recharge, then the plant can continue to operate essentially indefinitely, given proper maintenance and a market for its electricity at a profitable price.

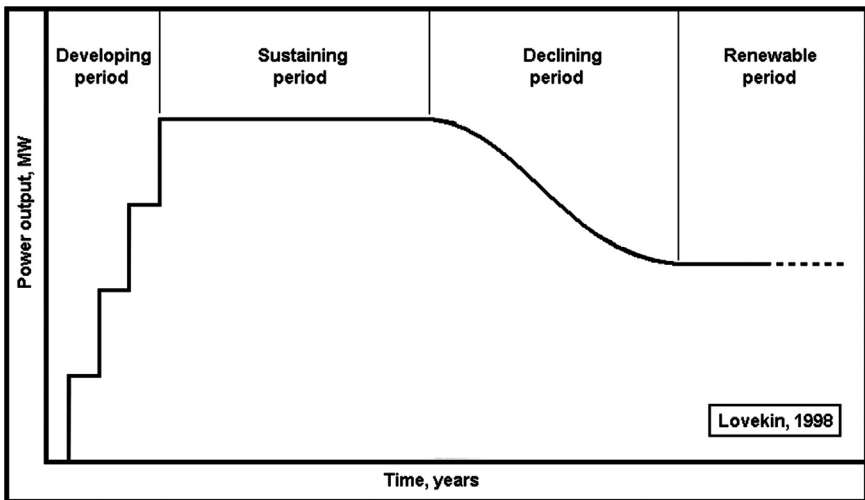


Figure 12.18 Life cycle of a geothermal field, according to Lovekin [27].

In phase 1, the field is developed incrementally, building up its power capacity in a number of plants. In phase 2, a reasonable steady state is achieved since the wells at first are operated at some fraction of their full capability. In phase 3, makeup wells are drilled to compensate for the decline in well outputs but the thermodynamic properties of the resource begin to decline under continued exploitation. By scaling back the output of the power system, a sustainable level can be achieved in phase 4, but at the sacrifice of some capital equipment that will no longer be useful. The remaining power plants can still be useful and profitable for a very long time, but at a considerably lower power capacity than what was originally installed.

The history of the two NCPA power plants illustrates this behavior; see [Figure 12.19](#). The units are identical 110 MW units that reached their rated output in 1987 but began their decline soon thereafter. By various means, the sustaining period could be stretched out for several years. In 2003, the LCEP had restored about 22 MW to the output relative to the projected decline without it, i.e., 142 MW vs. 120 MW [19]. Although the forecast does not extend into what could be the renewable period, it might be possible to achieve it, given the correct economic environment and the commitment of management to maintain the facilities even though the plant will be running at a fraction of its rated capacity.

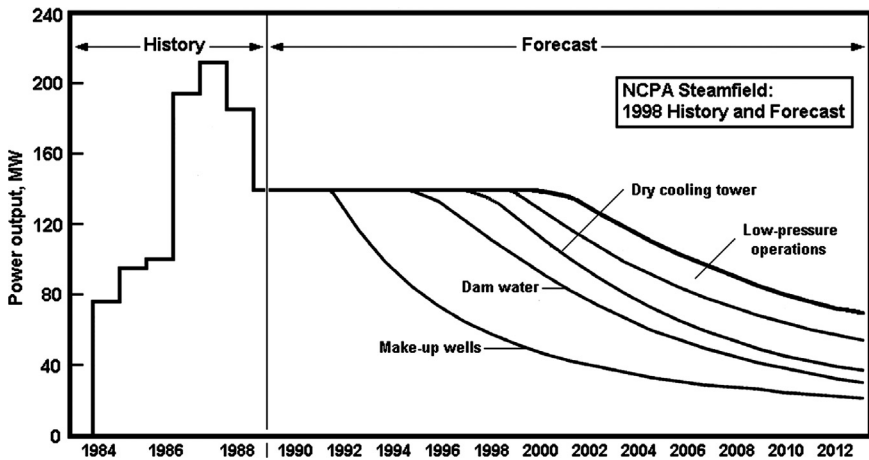


Figure 12.19 History and forecasted behavior of the NCPA steam field [19].

The problem of developing a steam plant at The Geysers has been considered ... The permanence of the steam supply may be questioned, but the origin seems to indicate a long life to the project. The marketing of the energy is not difficult and at the present time it appears as if a power plant will be installed in the near future.

J.D. Galloway—November 12, 1925

References

- [1] Hodgson SF. A geysers album: five eras of geothermal history. Pub. No. TR49, CA Dept. of Conservation, Div. of Oil, Gas, and Geothermal Resources, Sacramento; 1997.
- [2] Allen ET, Day AL. Steam wells and other thermal activity at "The Geysers" California. Washington, DC: Carnegie Institution of Washington; 1927.
- [3] Anderson DN, Hall BA, editors. Geothermal exploration in the first quarter century. Geothermal Resources Council; Spec. Rep. No. 3 1973.
- [4] Gunderson RP. Porosity of reservoir graywacke at the geysers. Monograph on the geysers geothermal field. Davis, CA: Geothermal Resources Council; 1992. p. 89–93, Spec. Rep. No. 17.
- [5] Monograph on the geysers geothermal field. Spec. Rep. No. 17, Geothermal Resources Council, Davis, CA; 1992 [appended map].
- [6] Truesdell AH, Box Jr. WT, Haizlip JR, D'Amore F. A geochemical overview of the geysers geothermal reservoir. Monograph on the geysers geothermal field. Davis, CA: Geothermal Resources Council; 1992. p. 121–32, Spec. Rep. No. 17.
- [7] Pye DS, Hamblin GM. Drilling geothermal wells at the geysers field. Monograph on the geysers geothermal field. Davis, CA: Geothermal Resources Council; 1992. p. 229–35, Spec. Rep. No. 17.
- [8] Henneberger RC, Gardner MC, Chase D. Advances in multiple-legged well completion methodology at the geysers geothermal field, California. Proc. World Geothermal Congress Florence, Italy 1995;2:1403–8.
- [9] Veizades H, Cain WJ. Design of steam gathering systems at the geysers: a state-of-the-art review. Monograph on the geysers geothermal field. Davis, CA: Geothermal Resources Council; 1992. p. 245–50, Spec. Rep. No. 17.
- [10] Anon. Pub. No. 61-8232 The Geysers unit 1: Pacific Gas and Electric Company.. American Society of Mechanical Engineers; October 1985
- [11] Box T, Stark M. Old steam field ... BIG new well. Geothermal Resour Counc Bull 2004;33(3):113–14.
- [12] Talkington K. Calpine Corporation, personal communication, December 9, 2004.
- [13] DiPippo R. U.S. Dept. of Energy, DOE/RA/28320-1. Geothermal energy as a source of electricity: a worldwide survey of the design and operation of geothermal power plants. Washington, DC: U.S. Gov. Printing Office; 1980
- [14] Anon. Sacramento Municipal Utility District SMUDGE #1, The Geysers, Sonoma County, California, undated report by Stone & Webster Engineering Corporation, Boston, MA.
- [15] Anon. SMUDGE #1 Application for Certification, Sacramento Municipal Utility District, Sacramento, CA, June 1980.
- [16] Tucker RE, Kleinhans Jr. PV, Keilman LR. SMUDGE #1 economic impacts on geothermal power plant design. Geothermal Resour Counc TRANS 1980;4:533–6.
- [17] Kleinhans Jr PV, Prideaux DL. Design, start-up and operation of SMUDGE #1. Proc. Ninth Annual Geothermal Conf. and Second IIE-EPRI Workshop Geothermal Conf. and Workshop. EPRI AP-4259-SR, Electric Power Research Institute, Palo Alto, CA; 1987. p. 13-1–7.
- [18] Anon. Production & injection. CA Dept. of Conservation, Div. of Oil, Gas, and Geothermal Resources, Sacramento, <<http://www.conservation.ca.gov/dog/geothermal/manual/Pages/production.aspx>>; 2013.
- [19] Grande M, Enedy S, Smith B, Counsil J, Jones S. NCPA at the Geysers. Geothermal Resour Counc Bull 2004;33(4):155–61.
- [20] Fraser G. NCPA gives good grade to geysers pipeline project. Geothermal Resour Counc Bull 1999;28(6):189–91.

- [21] Clutter TJ. Picking up steam. *Geothermal Resour Counc Bull* 2001;30(3):106–10.
- [22] Clutter TJ. Recharging the geysers. *Geothermal Resour Counc Bull* 2003;32(6):242.
- [23] Dellinger M, Allen E. Lake county success. *Geothermal Resour Counc Bull* 2004;33(3):115–19.
- [24] Calpine Corporation. Geysers by the numbers: the geysers geothermal field 2013 statistics. Corporate website, <<http://www.geysers.com/numbers.aspx>>.
- [25] Brauner Jr E, Carlson DC, Santa Rosa Geysers Recharge project: GEO-98-001. Final Report, Rep. No. 500-02-078V1, California Energy Commission; October 2002.
- [26] Anon. 2004 Green Power Leadership Awards. US EPA, US DOE and Center for Resource Solutions, <<http://www.epa.gov/greenpower/documents/2004awards.pdf>>.
- [27] Lovekin J. Sustainable power and the life cycle of a geothermal field. *Geothermal Resour Counc Trans* 1998;22:515–19 also, *Geothermal Resour Counc Bull*, 1999;28(3):95–9.



Chapter 13

Geothermal Power Plants of New Zealand

Chapter Outline

13.1 History of Geothermal Development in New Zealand	370
13.2 Wairakei and Related Power Stations	370
13.2.1 Geographic and Geologic Setting	370
13.2.2 Original Wairakei Power Plant	373
13.2.3 Recent Wairakei Configurations	379
13.2.4 Poihipi Road Power Plant	379
13.2.5 Wairakei Binary Plant	381
13.2.6 Te Mihi Power Plant	383
13.2.7 Capital Cost and Generation History	386
13.3 Rotokawa and NAP Power Plants	387
13.3.1 Rotokawa	387
13.3.2 Nga Awa Purua	388
13.4 Other Geothermal Plants	392
13.4.1 Kawerau	393
13.4.2 Ohaaki	395
13.4.3 Ngatamariki	397
13.5 Outlook for Development	399
References	399
Nomenclature for Figures in Chapter 13	401

We should not expect ever to utilize in practice all the motive power of combustibles. The attempts made to attain this result would be far more hurtful than useful if they caused other important considerations to be neglected. The economy of the combustible is only one of the conditions to be fulfilled in heat-engines. In many cases it is only secondary. It should often give precedence to safety, to strength, to the durability of the engine, to the small space which it must occupy, to small cost of installation, etc.

Nicholas-Leonard-Sadi Carnot—1824

Author's note: Although Carnot was writing about fossil fuel power plants, his general statements about efficiency and practicality apply equally well to geothermal power plants.

13.1 History of Geothermal Development in New Zealand

November 15, 1958, marked the first time a power plant produced electricity commercially from a liquid-dominated geothermal resource. On that day, the first unit at Wairakei on the North Island began to feed 6.5 MW of power into the New Zealand grid. From then until 1963, a dozen more units joined the plant making the total installed capacity 192.6 MW [1].

Although there had been a few very small experimental or prototype geothermal plants that used hot water as the source of energy, namely, Beppu (1925) and Hakuryu (1951) in Japan, Ischia (1941 and 1952) in Italy, and Kiabukwa (1953) in the Democratic Republic of the Congo [2], the pioneering work done in New Zealand to develop the technology and equipment that allowed the capture of geothermal energy from hot water resources and use it to generate electricity paved the way forward for many other countries to follow suit. Given the fact that dry-steam resources are extremely rare relative to hot water ones, this technological breakthrough was critical to advancing geothermal energy as a source of electricity.

Owing to its pioneering status among geothermal power plants, there exists a vast literature on all aspects of Wairakei from the geology of the site through the detailed design of all the equipment needed to convert its geothermal energy to electricity. The references cited in this chapter barely scratch the surface. Interested readers may wish to start with a special issue of the journal *Geothermics*, Ref. [3], which delves into the first 50 years of the Wairakei geothermal system.

13.2 Wairakei and Related Power Stations

13.2.1 GEOGRAPHIC AND GEOLOGIC SETTING

This section focuses on the power plants at Wairakei but a few words on the setting of the field are useful for perspective and a fuller understanding. The Wairakei field lies in the Taupo Volcanic Zone (TVZ) of the North Island, along with all but one of the developed geothermal fields; see Figure 13.1. There are nine power stations within a triangular area of roughly 450 km²: Wairakei, Te Mihi, Poihipi Road, Te Huka, Ohaaki, Nga Awa Purua (NAP) aka Taonga, Rotokawa, Mokai, and Ngatamariki. All of these lie in the south-central sector of the TVZ and have a combined power capacity of about 845 MW [5]. Figure 13.2 shows the locations of those plants in the Greater Taupo area.

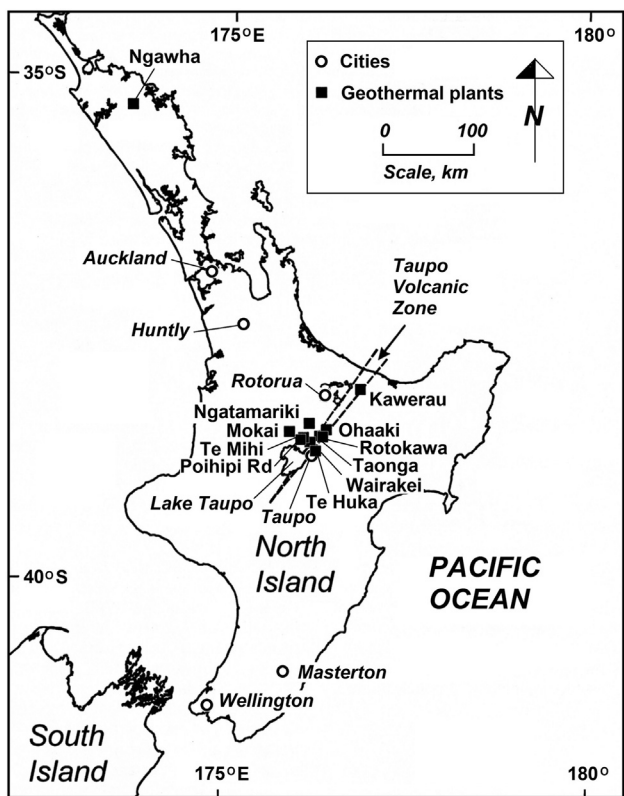


Figure 13.1 Map of New Zealand's North Island showing main cities and geothermal power plants as of 2014. Modified from Ref. [4].



Figure 13.2 Geothermal power plants in the Greater Taupo area; base map from Google Maps [WWW].

The Wairakei, Te Mihi, and Poihipi Road plants are fed with geothermal fluids obtained from different sectors of a common reservoir. Te Mihi lies roughly 5.1 km NNW and Poihipi Road lies about 5.7 km west of Wairakei. The neighboring field of Tauhara to the southeast, which hosts the Te Huka power plant, shares a common resistivity low with the Wairakei field, but is separated from it surficially by the Waikato River.

The Wairakei reservoir is extensive. Even after about 60 years of exploration, drilling, and exploitation, the field is still not well understood in many respects. The first wells drilled in the early 1950s were confined to shallow depths of less than 500 m because steam was readily available in the shallow reservoir, and the two early drill rigs did not have depth capability beyond 460 m.

Initially only the so-called Eastern Borefield (EBF) was used. Later the Western Borefield (WBF) was drilled and produced steam at a relatively shallow depth of about 600 m. More recently the Te Mihi field was discovered and is now being exploited as the EBF has been largely depleted. The WBF is composed of multiple layers and lenses with different geologic characteristics, as can be seen in Figure 13.3. This section is taken looking to the NW and is representative of the reservoir lying between the Wairakei and the Te Mihi plants.

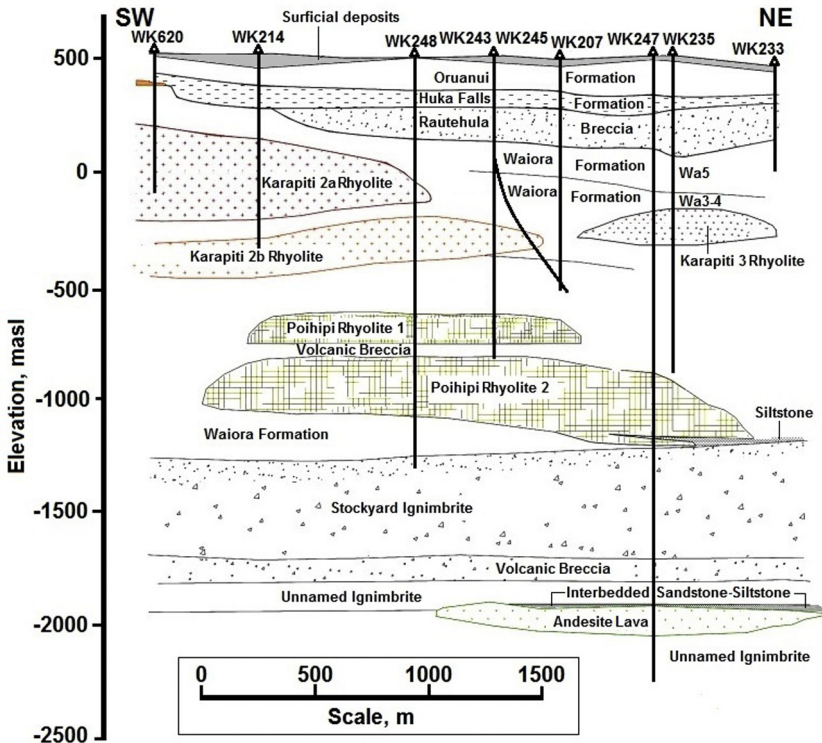


Figure 13.3 Geologic cross-section through the Wairakei reservoir [6] [WWW].

As can be seen from the drilling history in Figure 13.4, a massive amount of exploratory and development drilling took place from 1950 through 1966. This covered the period of planning, construction, and commissioning of the 13 power units. For the next 20 years drilling ceased except for two deep wells drilled in 1968 and 1984.

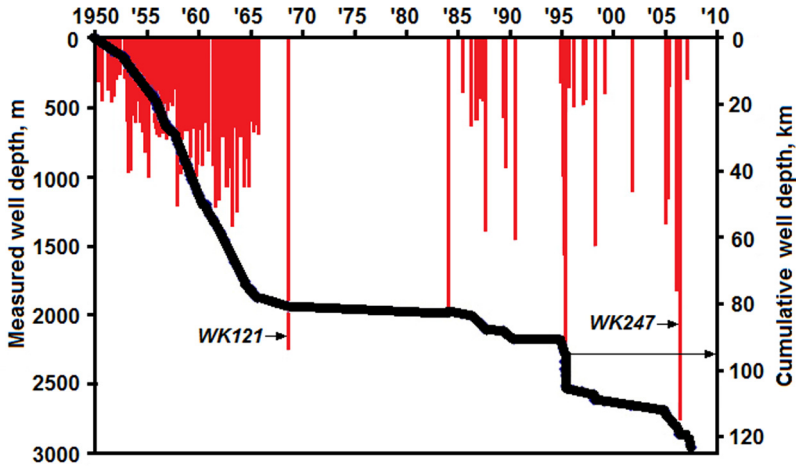


Figure 13.4 Drilling history at Wairakei from 1950 through 2007. After Ref. [7] [WWW].

Well WK121, drilled in 1968, was the deepest well at Wairakei up to that time. It was sited in the far WBF and was completed with a narrow, 4-1/2" slotted liner from 1599 to 2247 m depth. Unfortunately the well failed to produce owing to lack of permeability. No more wells were attempted until 1984. The existing wells were sufficient to supply the power plant albeit with declining pressure. That year marked the start of a renewed program of drilling that has been maintained to win sufficient steam to keep the three power plants operating, namely, Wairakei, Poihipi Road, and the new Te Mihi units.

13.2.2 ORIGINAL WAIRAKEI POWER PLANT

Among the vast number of publications on the Wairakei field and power station, the following selections, certainly nonexhaustive, include discussions of the power generating system: Refs. [1,8–12].

Since the power plant was originally designed to accommodate a heavy water facility for the United Kingdom's nuclear energy program, it was complicated in terms of the various steam pressure levels that were specified. Eventually the heavy water part of the system was canceled during the construction process, but the

power plant nevertheless had to live with the original design. Gradually over the years as the geothermal steam pressure declined, the high-pressure (HP) turbines were retired, but the overall scheme retained the peculiar form with which it had started. In a sense, having so many small units designed for various pressures provided flexibility in following the changing steam conditions. In response to those changes a simpler configuration emerged. It is certainly true, however, that had the heavy water plant never been considered, the design of Wairakei would have been less complex.

Figure 13.5 is a simplified schematic showing the original configuration of power units. There were 13 separate turbines each with a dedicated generator. These were housed in two buildings, the so-called A Station and B Station. Six units operated as back-pressure units (2×6.5 MW and 4×11.2 MW) and seven were condensing units (3×30 MW and 4×11.2 MW), each with its own condenser. Cooling water was taken from and returned to the Waikato River, greatly simplifying the cooling system compared to using cooling towers. The condensers were low-level, direct-contact, once-through type, located directly beneath each turbine.

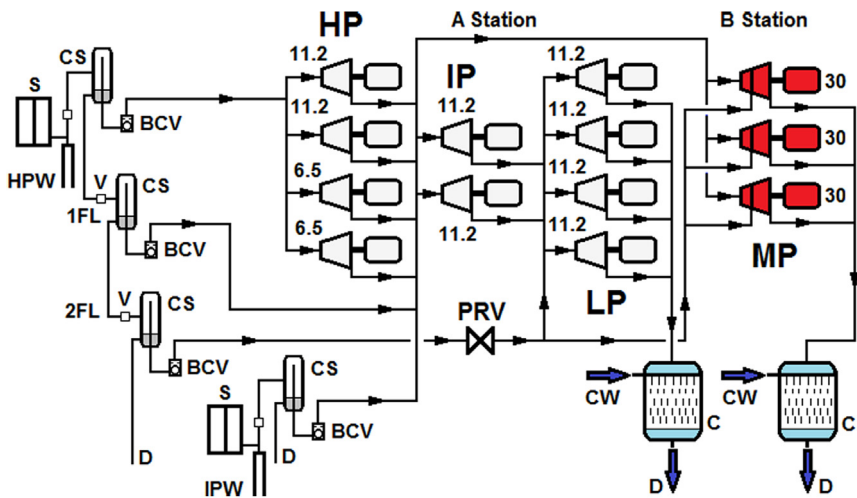


Figure 13.5 Wairakei power station original configuration; see Nomenclature. *Note:* The numbers give the MW-rating of the units [WWW].

Thus, the steam condensate was mixed with the Waikato cooling water and dumped back into the river. Since the steam condensate contained dissolved

minerals such as boron and arsenic, this practice had environmental consequences [13,14]. Because the permits for Wairakei expire in 2026, the plan is to replace the Wairakei units with the Te Mihi plant, two units of which are already online as of 2014. Once-through cooling systems were typically found in fossil-fueled plants at that time, but not at geothermal plants. To this author's knowledge, there are no other geothermal power plants that currently use once-through cooling; they use water cooling towers, air-cooled condensers, or evaporative condensers.

The tiered separators shown at the left in [Figure 13.5](#) were placed at strategic points in the field to serve clusters of wells. Three levels of steam pressure were created and dedicated transmission pipelines carried the steam from the borefield down to the power station on the bank of the Waikato River, a difference in elevation of about 85 m. Intermediate-pressure wells (IPWs) were connected to the plant and fed their steam into the manifolds at appropriate points.

The three tiers of power units in A Station were designated as high-, intermediate- and low-pressure units. The middle IP tier replaced the canceled heavy water facility. Not shown in the schematic are numerous pressure reducing valves to allow flexibility of operation. The one shown, PRV, was used to let down the pressure from the intermediate-low-pressure (ILP) steam transmission pipeline to the pressure required for the low-pressure (LP) turbines and for the last stages of the three mixed-pressure (MP) units. Presumably this was a more cost-effective method than flashing at the well field separator stations down to the turbine inlet pressure (plus pressure losses in the lines) since that would require very large diameter steam pipes. All turbines are single-flow style as would be expected for small power units. A double-flow design was considered for the 30 MW units that would have made them 60 MW units, but this was considered too aggressive a design at that time.

A great deal of planning went into the amount of moisture that could be permitted in the various stages of the turbines. Generally no more than 10% moisture was acceptable at the turbine outlet. An opportunity presented itself to dry the steam leaving the HP turbines before it mixed with IP steam from the IPW separators and from the first-stage flash separators. Vortex separators were placed in the pipelines that drained out most of the 6% moisture present in the exhaust, giving nearly dry saturated steam for the next tier of turbines. In the 30 MW turbines, moisture was removed prior to the pass-in plenum so that the inlet steam to the LP stages had a quality of about 99%. This kept the moisture at the outlet of the turbine to approximately 10% [9]; see [Figure 13.6](#).

Table 13.1 gives specifications and calculated performance values for the non-condensing units which are all located in A Station; Table 13.2 gives similar information on the condensing units. All data are for the original design condition. The efficiencies are calculated for each turbine based on either the actual output (Table 13.1) or modeled using the Baumann rule with a dry-expansion efficiency of 80% (Table 13.2). This assumed efficiency correlates very well with the capability of turbines of that era and yields power outputs in agreement with the ratings. The plant taken as a whole had a utilization efficiency of 54.9%, based on the exergy of the fluid extracted from the reservoir and a dead-state temperature of 15.8°C (289 K) [11]. Adjusting the dead state to 9.5°C (282.65 K) that is used in the present analysis, the plant's overall utilization efficiency becomes 52.8%, still a very good value for a first-generation power plant using a liquid-dominated reservoir.

TABLE 13.1 Technical details and performance for noncondensing units [9,11].

	Unit designation		
	HP	HP	IP
Start-up year	1958, 1959	1962	1959
No. of units	2	2	2
Type	1-Flash steam	1-Flash steam	1-Flash steam
Unit power rating, MW	6.5	11.2	11.2
Resource temperature, °C	250	250	250
<i>Turbine:</i>			
Cylinders	1	1	1
Flows/turbine	1	1	1
Stages/flow	5	5	3
Inlet pressure, bar,a	13.5	13.5	4.51
Inlet temperature, °C	193.4	193.4	148.0
Steam mass flow ^a , kg/s	40.19	71.69	58.0
Exhaust pressure, bar,a	4.46	4.46	1.117
Speed, rpm	3000	3000	3000
Isentropic efficiency, %	79.8	77.1	79.0
Functional efficiency ^b , %	85.5	82.6	83.3
<i>Generator:</i>			
Power rating, MW	6.5	11.15	11.15
Power factor (lagging)	0.9	0.9	0.9
Speed, rpm	3000	3000	3000

^aData are per unit.

^bBased on the change in exergy of the steam across the turbine (see Eq. 10.24); dead state is at the wet-bulb temperature, 9.5°C.

TABLE 13.2 Technical details and performance for condensing units [9,11,12].

	Unit designation	
	LP	MP
Start-up year	1959, 1960	1962, 1963
No. of units	4	3
Type	2-Flash steam	2-Flash steam
Location	A Station	B Station
Unit power rating, MW	11.2	30
Resource temperature, °C	250	250
<i>Turbine:</i>		
Cylinders	1	1
Flows/turbine	1	1
Stages/flow	10	15
Inlet pressure, bar,a	1.066	4.46/1.066
Inlet temperature, °C	100.9	147.6/100.9
Steam mass flow ^a , kg/s	36.16	50.4/63.0
Exhaust pressure, bar,a	0.0508	0.0508
Speed, rpm	3000	1500
Isentropic efficiency, %	76.4	77.8/76.4
Functional efficiency ^b , %	77.8	82.3/77.8
<i>Generator:</i>		
Power rating, MW	11.15	30
Power factor (lagging)	0.9	0.9
Speed, rpm	3000	1500
<i>Condenser:</i>		
Type	DC, low-level	DC, low-level
CW mass flow, kg/s	1398.6	2066.4
CW temperatures, °C:		
Inlet	15	15
Outlet	27.8	27.8
Wet bulb	9.5	9.5
<i>NCG system:</i>		
Steam ejector	Yes	Yes
Stages	2	2
Vacuum pump	No	No

^aData are per unit.^bBased on the change in exergy of the steam across the turbine (see Eq. 10.24); dead state is at the wet-bulb temperature, 9.5°C.

Figure 13.6 shows the processes undergone by the geofluid as it passed through the tiers of turbines. The HP turbines received steam from the separators of the HPWs. The moisture present in the exhaust was largely removed by vortex separators before the steam was sent down the line. That is, point B moved up to point C, and a small amount of condensate was subtracted from the steam path. The now-dried steam, augmented by IP steam from separators at the IPWs and by steam from the

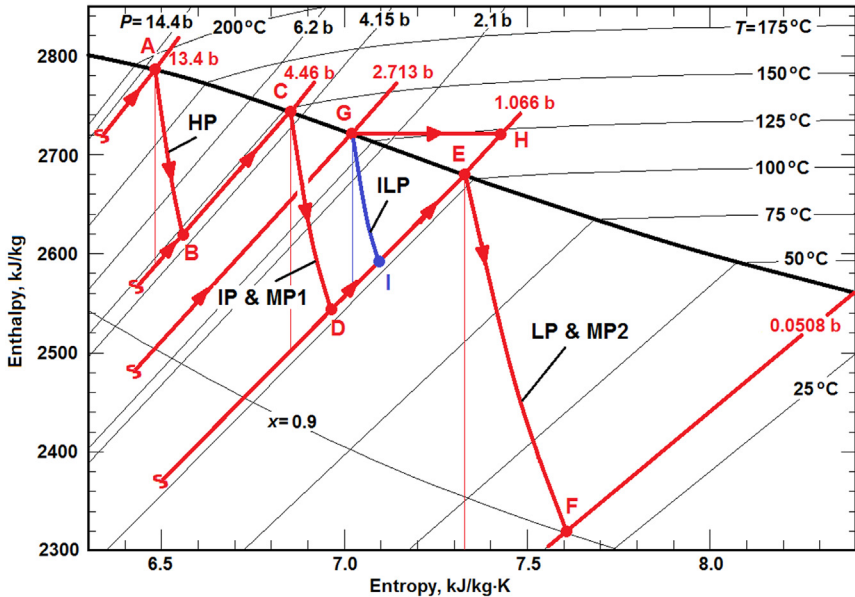


Figure 13.6 Mollier diagram for Wairakei power plant [WWW].

first-stage flash vessels, entered the IP turbines. Some of that steam went to the MP turbines in B Station and drove the first eight stages of the machines. The IP turbine exhaust moisture was centrifuged away before the steam moved to the next tier. Thus point D moved up to the saturation line at point E. ILP steam was collected from the second-stage flash and sent to the power station where it was throttled down (process $G \rightarrow H$) to the LP level needed for the four LP turbines in A Station and the last seven stages of the three MP turbines in B Station. The throttling process in the PRV created slightly superheated steam that helped dry out the steam coming from the upstream turbines. All seven of these turbines discharged to low-level, barometric, jet condensers located beneath the turbines and fed with cold water pumped directly from the Waikato River. The steam condensate and the warmed cooling water were returned to the river downstream of the plant. Later, in 1996, the PRV was replaced with a second-hand ILP turbine to generate about 3.5 MW (process $G \rightarrow I$).

Approximately 3 km downstream of the plant, the Waikato River flows through the 78 MW Aratiatia hydroelectric plant. This is essentially a run-of-the-river power station with a small dam, and so it might be said that the geothermal steam condensate and the liquid drains contribute to the output of the hydroelectric plant after powering the Wairakei geothermal plant. However, even in the early days when all of the produced geofluid, minus the steam flashed to atmospheric pressure, was ultimately discharged to the river after use in the plant, the total geofluid flow from Wairakei was less than 1% of the average water flowing through the hydropower plant.

13.2.3 RECENT WAIRAKEI CONFIGURATIONS

It took about four years from plant start-up for the reservoir drawdown to be felt in the steam supply [15]. By 1968 the pressure of the HP steam had fallen from about 13.5 bar,a to about 11 bar,a; by 1982 it reached 7.25 bar,a [12]; see Figure 13.7.

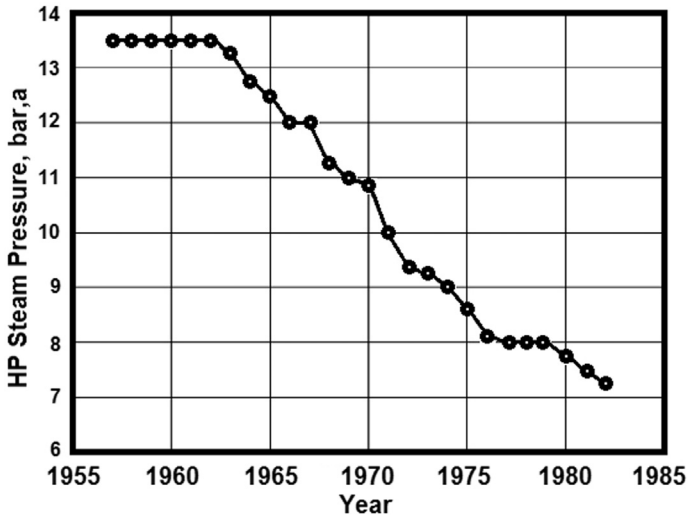


Figure 13.7 Decline in pressure from the HPWs at Wairakei [1].

This meant that the four HP turbines could no longer function. In November 1982, the HP system was decommissioned and the four HP turbines were removed. Adjustments were made to accommodate the steam that could be obtained; the HP pipelines were converted to IP pipelines and the plant functioned with only IP, LP, and MP turbines. Given the shortfall in steam, the PRV was reconsidered and replaced by a turbine to generate a few more megawatts. The plant configuration following 1996 is shown in Figure 13.8.

Thus, the plant which began its life as what might be called a triple-flash plant (one flash in the wellbore, two flashes in the flash/separation stations) now became a more conventional double-flash plant operating with two levels of pressure. By that time in the early 1980s, double-flash plants were already operating in El Salvador, Iceland, Japan, and Mexico, depriving Wairakei of its unique status in the world.

13.2.4 POIHIPI ROAD POWER PLANT

The 55 MW (gross), 52.5 MW (net) Poihipi Road plant was commissioned in May 1977. It is sometimes referred to as the McLachlan power plant. The plant is located on the west side of Poihipi Road near the western boundary of the

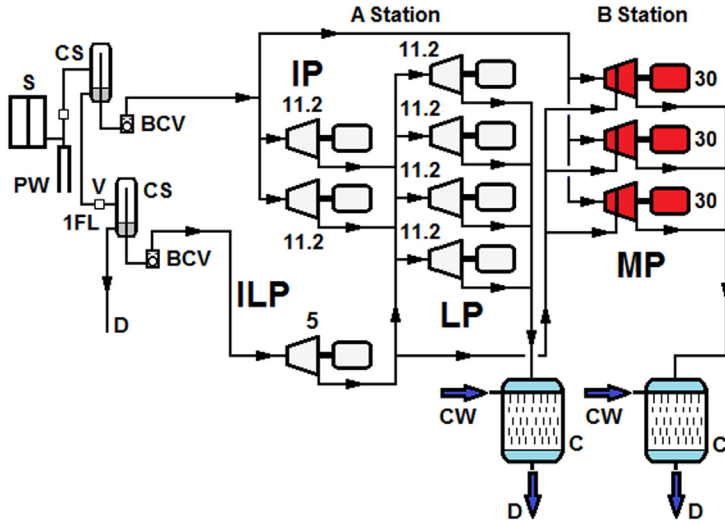


Figure 13.8 Wairakei configuration starting in 1996. Removal of HP machines took place in 1982–83. *Notes:* Each condensing turbine had its own condenser. All six 11.2 MW units were taken out of service when the Te Mihi plant came online in 2014 [WWW].

geothermal reservoir. The turbine and related auxiliary equipment were purchased as surplus from the State of California after the planned South Geysers project failed to materialize owing to a shortfall of steam, after much of the equipment had already been bought. As such the energy conversion system shown in [Figure 13.9](#) is typical of what one finds at The Geysers (see Chapter 12).

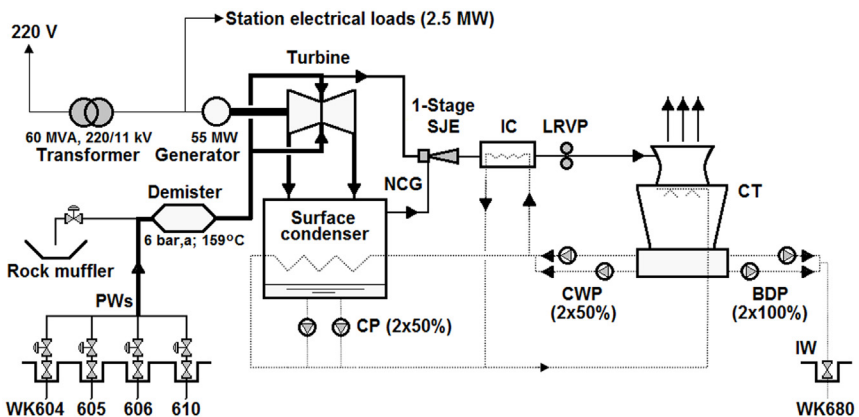


Figure 13.9 Poihipi Road power plant original flow diagram. Additional steam is provided from a pipeline from the Te Mihi field. *After Ref. [16].*

The steam comes from four dry-steam wells located on a single well pad about 1.3 km south of the power station alongside Poihipi Road, augmented with steam from wells at the nearby Te Mihi site. The turbine-generator was built by Fuji as a companion to the Bottle Rock plant at The Geysers and thus was designed for 60 Hz. The turbine was re-engineered with new blading to accommodate a new inlet steam pressure of 6 bar,_a instead of the design pressure of 7.2 bar,_a. It was also modified for 50 Hz. The full project cost of NZ \$75 million, including land and wells, translates into a specific cost of NZ \$1429/kW (net), or US \$996/kW (net), in 1996 currencies. Excluding land and well costs, the specific cost drops to NZ \$1225/kW (net) or US \$853/kW (net) [16].

Table 13.3 lists some of the technical specifications and performance measures for the Poihipi Road plant and two others that are described in the following sections. *Note:* Te Mihi data is from a combination of published sources [17–19] and an unverified computer simulation by the author.

13.2.5 WAIRAKEI BINARY PLANT

Two 8.25 MW (7 MW, net) dual-pressure binary units were installed next to the Wairakei power station in 2005. The units were supplied by Ormat Technologies, Inc. and are typical bottoming cycles that capture some of the waste exergy in the separated brine; see Figure 13.10. In this case the cycles use isopentane and require a total of 777.8 kg/s of hot brine at 127°C, divided between the two units. Each unit employs a single generator driven by two turbines connected on opposite sides. The HP turbine has an isopentane inlet pressure of 8.8 bar,_a at 109°C; the LP turbine inlet conditions are 6.9 bar,_a and 97°C. A recuperator is used after the HP turbine to improve the cycle efficiency; it is not feasible to use one after the LP turbine. The cooled brine leaves the plant at 87°C.

The 40°C drop in brine temperature means that 131.6 MW-th is delivered to the binary plant, and with a gross output of 16.5 MWe, the gross thermal efficiency comes to 12.5%. Each unit requires 600 kW to drive the 84 fans in the air-cooled condensers plus 330 kW to run the two isopentane feed pumps, for a total parasitic load of 1860 kW. Thus the plant can generate 14.64 MW (net), and the net thermal efficiency is 10.8%. The exergy utilization efficiency is 35.2% (gross), 31.2% (net), based on a 25°C dead-state temperature. After the year 2026 when the main Wairakei plant is decommissioned, it is expected that the Wairakei binary plant will continue to operate as long as brine is available.

TABLE 13.3 Technical details and performance for Poihipi, Wairakei binary, and Te Mihi power plants.

	Plant		
	Poihipi Road	Wairakei binary	Te Mihi
Start-up year	1997	2005	2014
Type	Dry steam	Dual-level cycle	Double-flash
Gross power, MW	55	16.5 (2 × 8.25)	166 (2 × 83)
Maximum power, MW	55	16.5	183.6 (2 × 91.8)
Net power, MW	52.5	14	159
Geofluid mass flow, kg/s	124.2	777.8	647 per unit
Resource temperature, °C	159	127	250
Discharge temperature, °C	—	87	—
<i>Turbine:</i>			
Working fluid	Steam	Isopentane	Steam
Cylinders	1	2	2
Flows/turbine	2	1	2/1
Stages/flow	7	3	NA
Main inlet pressure, bar,a	6.0	8.8/6.9	5.2
Main inlet temp., °C	159	109/97	153
Main mass flow, kg/s	124.2	NA	132.3 per unit
LP steam pressure, bar,a	—	—	1.14
LP steam temp., °C	—	—	103
LP steam mass flow, kg/s	—	—	45.4 per unit
Exhaust pressure, bar,a	0.105	0.886	0.065
Last-stage blade height, mm	565	NA	NA
Speed, rpm	3000	3000	3000
Isentropic efficiency, %	79.4	NA	81.7/83.7
<i>Generator:</i>			
Phases/poles	3/2	3/2	3/2
Frequency, Hz	50	50	50
Voltage, kV	11	11	11.8
Amperage, kA	NA	NA	5.319
Power factor	NA	NA	0.85
<i>Condenser:</i>			
Type	DC, low-level	Air-cooled	DC, low-level
CW flow, kg/s	2475.0	—	NA
CW temperatures, °C:			
Inlet	25.5	NA	NA
Outlet	43.8	NA	NA
Wet bulb	9.5	18.5	15.5
<i>NCG system:</i>			
Steam ejector	Yes	No	Yes
Stages	2	—	2
Steam flow, kg/s	1.383	—	NA
Capacity, m ³ /s	15.83	—	NA
Vacuum pump	Yes	No	Yes
Power, kW	350	—	NA

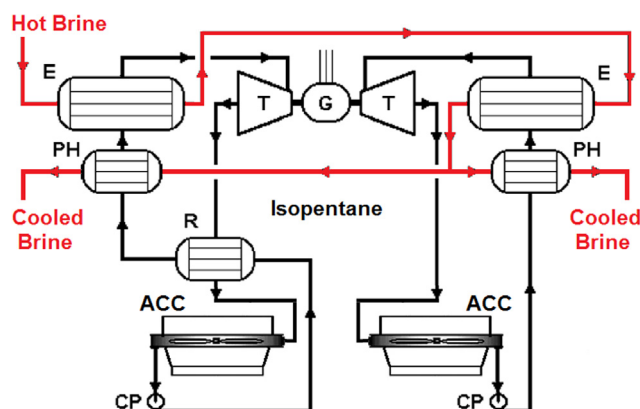
(Continued)

TABLE 13.3 (Continued)

	Plant		
	Poihipi Road	Wairakei binary	Te Mihi
<i>Plant performance:</i>			
Gross SGC, (kg/s)/MW	2.26	47.1	7.80
Net SGC, (kg/s)/MW	2.37	55.6	8.14
Utilization efficiency, %:			
Gross	52.3 ^a	26.1 ^b	47.0 ^c
Net	49.9 ^a	22.2 ^b	45.6 ^c

^aBased on the exergy of the steam into the plant.

^bBased on the brine exergy.

^cBased on the reservoir geofluid exergy; dead state is at the wet-bulb temperature.

Figure 13.10 Flow diagram for one of two units for the Wairakei binary plant [WWW].

13.2.6 TE MIHI POWER PLANT

The Te Mihi power plant came online in 2014 when the first two 83 MW units were commissioned. This power station will eventually replace the old Wairakei plant. Te Mihi is a double-flash plant receiving steam separated from each well and steam flashed at a station adjacent to the powerhouse that gathers hot water from the separators. The geofluid comes from two sources: the WBF which produces two-phase, liquid-vapor mixtures from about 600 m depth and the Te Mihi Borefield which produces dry steam from a shallow zone and two-phase, liquid-vapor mixtures from the deep reservoir.

Figure 13.11 shows an area of roughly 96 km² that encompasses the various areas of the greater Wairakei resource, including the Te Huka plant in the Tauhara area. The piping system that collects the steam and two-phase fluid is complex because the existing Wairakei plant is still being served by wells in the Te Mihi area. These wells are now being used for the first two units at Te Mihi and eventually will be disconnected from Wairakei and directed fully to Te Mihi.

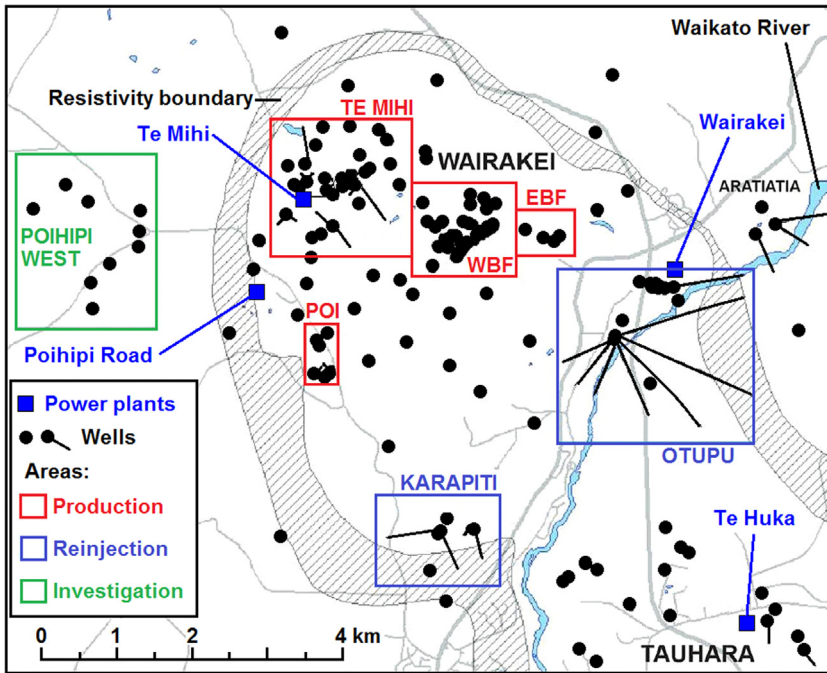


Figure 13.11 Wairakei and neighboring borefields. Modified from Ref. [17] [WWW].

Figure 13.12 is an aerial view of the Te Mihi station; the two 8-cell water cooling towers serve the two 83-MW power units. Note that there is room to accommodate another unit of the same size.



Figure 13.12 Aerial view of Te Mihi power plant and environs, looking generally north. The B Line goes to Poihipi Road power plant and the Z Line goes to reinjection wells in the Karapiti area [17]; see Nomenclature [WWW].

The turbine arrangement (see Figure 13.13) is unique among double-flash plants in that the flashed LP steam is used in a separate turbine rather than being passed into a LP stage of the main turbine. The three exhaust flows all end up in the same condenser.

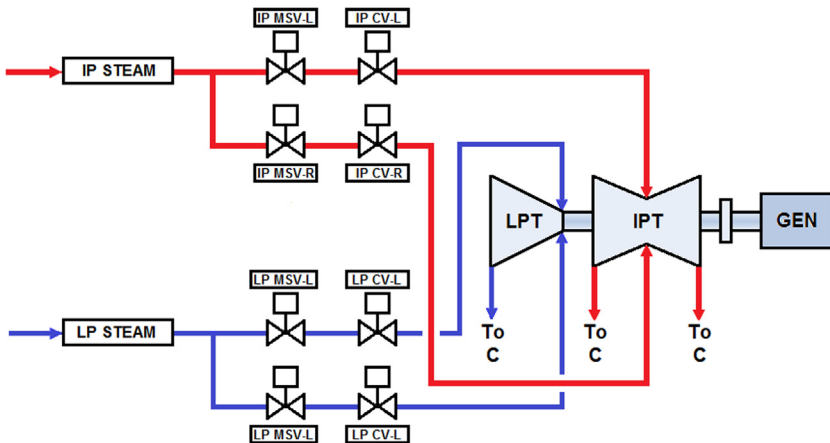


Figure 13.13 Te Mihi turbine-generator arrangement; see Nomenclature. After Ref. [20] [WWW].

13.2.7 CAPITAL COST AND GENERATION HISTORY

The cost of construction for the original Wairakei power station was reported in Ref. [9] and is given in Table 13.4. The figures in the cost column “Pounds sterling” are as reported; the other figures have been calculated and converted to US dollars, both at the time of construction in 1960 and in 2014 US dollars, adjusted for inflation. The costs per kilowatt installed were somewhat high by 1960 power plant standards, but the 2014 specific cost is fairly reasonable.

TABLE 13.4 Wairakei development and power plant costs [9].

Item	Pounds sterling	US dollars (1960)	US \$/kW (1960)	US dollars (2014)	US \$/kW (2014)
Prospecting and drilling	4,392,000	12,297,600	63.98	98,983,382	515
Geofluid gathering system	4,975,000	13,930,000	72.48	112,122,570	583
Powerhouse and plant	7,441,000	20,834,800	108.40	167,699,305	873
Cooling water system	1,262,000	3,533,600	18.39	28,441,946	148
Outdoor substation	669,000	1,873,200	9.75	15,077,387	78
Totals	18,739,000	54,469,200	283.40	438,422,591	2,281

Based on 1£ = \$2.80 from 1950 to 1967 and US inflation index of 704.9% from 1960 to 2014 [21].

The total cost of the binary plant was NZ \$44 million [1]. Thus the specific installed cost came to NZ \$2667/kW (gross) or NZ \$3005/kW (net). The corresponding figures in US dollars are: US \$27.7 million, US \$1679/kW (gross), and US \$1978/kW (net) [22]. All costs are in 2004 currencies. Since the brine is obtained from existing wells, these costs are only for the power station. The total cost for the Te Mihi project is estimated at US \$623 million (2014) [19] or \$3753/kW (gross) or US \$3918/kW (net).

In terms of generating history for the Wairakei power plant, despite experiencing a dramatic pressure decline early on, the Wairakei plant has managed to generate a steady amount of electricity all its life. Figure 13.14 presents the gigawatt-hours generated each year from 1958 through 2005. Beginning in the mid-1980s, the generation has gradually increased in spite of the loss of the HP turbines that reduced plant capacity by 35.4 MW. That trend follows the similar growth in mass extracted from the reservoir over the same period. It is interesting to view this operational behavior with an eye toward sustainability (see Section 12.7).

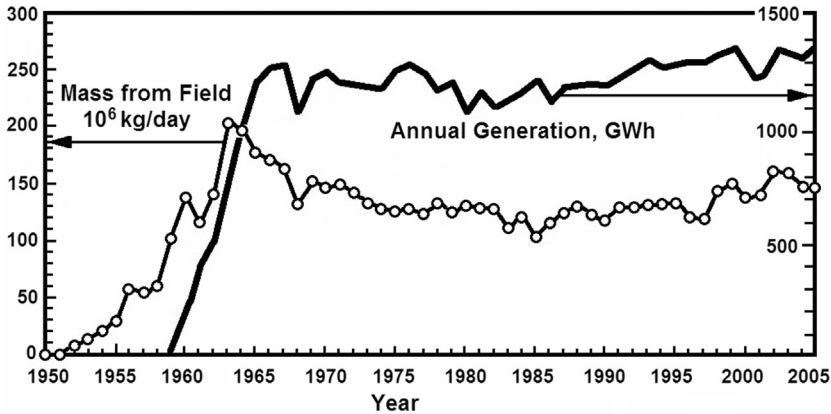


Figure 13.14 Wairakei electricity generation and mass extraction, 1950–1997 [1,15].

The peak of geofluid extraction took place in 1964 shortly after the plant was fully commissioned. In light of the ensuing production curve, that peak represented overexploitation and was not sustainable for the size of the field then being produced. There were about 20 years of gradual decay that approached an asymptotic steady state. The rise after that was related to the opening of the new Te Mihi field northwest of the original Wairakei well field.

The future of the Wairakei power system anticipates the eventual phasing out of the original Wairakei A and B Stations while retaining the Wairakei binary plant. For the near term, some of the Wairakei units will be kept online, that is, the 3.5 MW ILP turbine, one 11.2 MW LP unit in A Station and two 30 MW units in B Station. Poihipi Road will continue operating and the Te Mihi plant will eventually see a third unit of about 80 MW. That arrangement is thought to have the capability to carry Wairakei for another 50 years at least.

13.3 Rotokawa and NAP Power Plants

The Rotokawa and NAP plants feed off the same reservoir, a deep, hot, two-phase system. They are separated by a mere 850 m, some 7 km east of the Wairakei power station.

13.3.1 ROTOKAWA

The Rotokawa power plant is a hybrid cycle that is designed to take advantage of the high-temperature geofluid, $\sim 320^{\circ}\text{C}$, without facing some of the problems associated with using fluids carrying high levels of dissolved minerals [23].

It began its operating life in 1997 as a 29 MW plant with four turbo-generators: one 14 MW back-pressure steam turbine, two 5 MW binary units heated by the steam exhausted from the steam turbine, and one binary unit heated by the brine separated from the two-phase geofluid; see Figure 13.15.

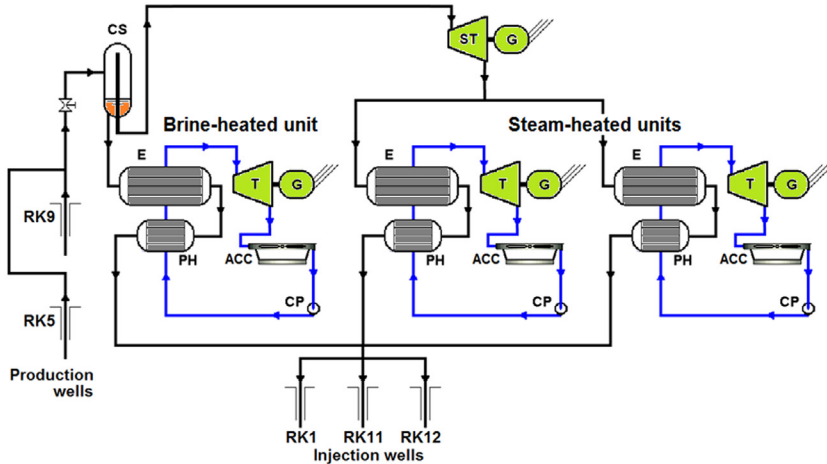


Figure 13.15 Original Rotokawa power plant in simplified schematic. After Ref. [24] [WWW].

From the process flow diagram, it can be seen that all of the geofluid produced at the wellheads ends up being returned to the reservoir at the same concentration of dissolved solids as in the original geofluid, albeit at a lower temperature. By managing the temperatures at all points in the process, scaling can be minimized, but not eliminated. Reyes et al. [23] describe the complex interactions among various elements in the brine as the geofluid undergoes boiling, cooling, dilution, separation of phases, and mixing that can lead to deposition of minerals in surface piping and other equipment. Nevertheless, the original plant had a net utilization efficiency of 43.9%. A 5 MW unit was added in 2003, raising the plant rating to 34 MW.

13.3.2 NGA AWA PURUA

This plant is a joint venture between Mighty River Power and the Tauhara North No. 2 Trust. At the time of its commissioning in 2010, NAP was the highest powered geothermal plant using a single turbine-generator—140 MW (nominal). The triple-flash system has one of the highest utilization efficiencies of any geothermal plant, 57.2% based on generator output. Another distinction of the turbine is the length of the last-stage blades, 798 mm (31.4 in). The plant was built and tested in less than 2 years and handed over to the owners some 6 weeks ahead of schedule [25].

The aerial photo in Figure 13.16 shows the power station and some major equipment items; the plant layout is shown in Figure 13.17.

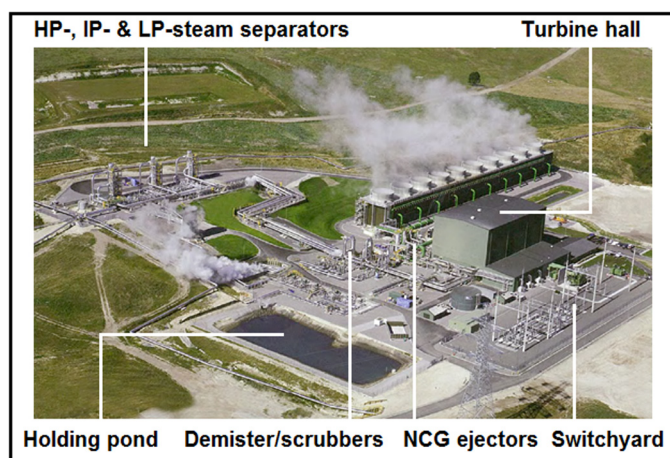


Figure 13.16 NAP power plant. Photo from Ref. [26] [WWW].

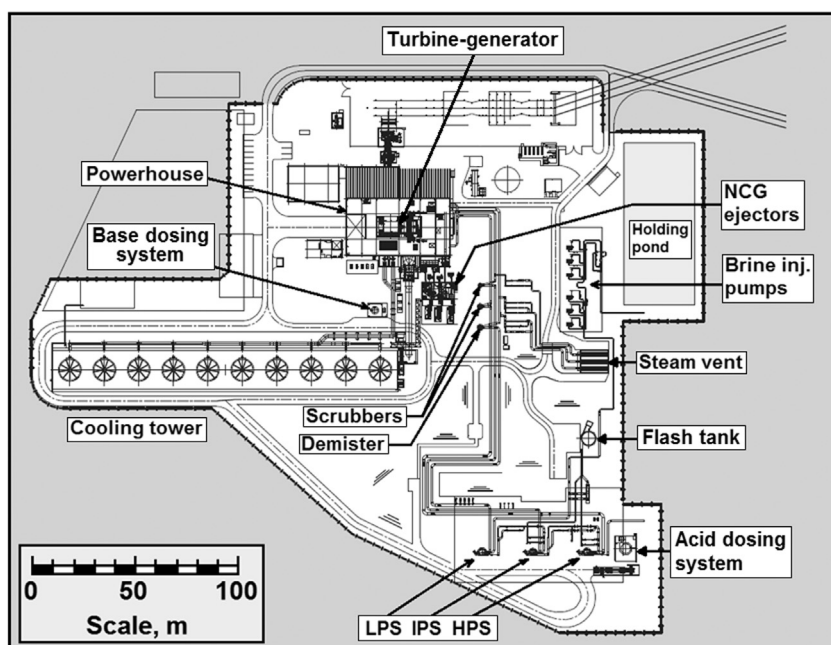


Figure 13.17 NAP plant layout; see Nomenclature. After Ref. [27].

Owing to the high pressure and temperature of the geofluid in the reservoir, the first-stage blades see an unusually high pressure for a geothermal turbine, 23.5 bar,^a. The high temperature in the reservoir, $\sim 320^{\circ}\text{C}$, means that the geofluid carries a very high concentration of silica. After only the first flash/separation, the liquid is already supersaturated with silica. The brine leaving the third-stage flash/separator is highly supersaturated with a silica supersaturation index of 2.95. The plant designers chose to employ an acid dosing system to modify and control the pH of the separated brine leaving the HP separator. This slows the kinetics of the precipitation process and creates a window of time allowing the brine to be flashed two more times to generate IP and LP steam and still pass through the discharge pipelines and into the reinjection wells without encountering silica scaling problems. A consequence of this method of avoiding operational problems with scaling is that expensive corrosion-resistant materials must be used in the brine handling system. Once the liquid returns to the reservoir and begins to heat up, the supersaturation is reduced, lowering the potential of scaling in the formation.

A plant simulation spreadsheet was written in Excel with REFPROP embedded for the properties of water to obtain performance values. The results shown in Table 13.5 are based on data reported in Ref. [26] and obtained from the simulation.

The simulation was based on the process flow diagram with state-point labels given in Figure 13.18 and the temperature-entropy process diagram is given in Figure 13.19.

TABLE 13.5 Technical details and performance for NAP plant.

Start-up date	May 15, 2010		
No. of units	1		
Type	3-Flash steam		
Unit power rating, MW	140		
Resource temperature, °C	300–320		
Total geofluid flow, kg/s	525		
<i>Turbine:</i>			
Type	Single-cylinder, double-flow, double-pass-in		
Cylinders	1		
Flows/turbine	2		
Stages/flow	11 (4–3–4)		
Stages:	HP	IP	LP
Inlet pressure, bar,a	23.5	8.4	2.3
Inlet temperature, °C	221	172	125
Steam mass flow, kg/s	171.4 ^a	31.4	28.6

(Continued)

TABLE 13.5 (Continued)

Exhaust pressure, bar,a	0.085		
Last-stage blade height, mm	797.6		
Speed, rpm	3000		
Gross power, MW	149.5		
Isentropic efficiency, % ^b	82.3	78.5	76.5
Generator:			
Type	Synchronous-totally enclosed-water-to-air cooled		
Excitation	Brushless		
Capacity, MVA	173		
Voltage, kV	11		
Phases	3		
Power factor	0.85		
Speed, rpm	3000		
Condenser:			
Type	Direct-contact, spray type		
Cooling water flow rate, kg/s	7140		
CW pump power, MW	2.74		
Plant performance:			
Rated SGC, (kg/s)/MW	3.75		
Utilization efficiency, %:			
Gross ^c	60.2		
Net ^d	57.2		

^aIncludes 2.3 wt.% NCG.

^bCalculated using Baumann rule with 85% dry expansion efficiency and no interstage moisture removal.

^cBased on generator output.

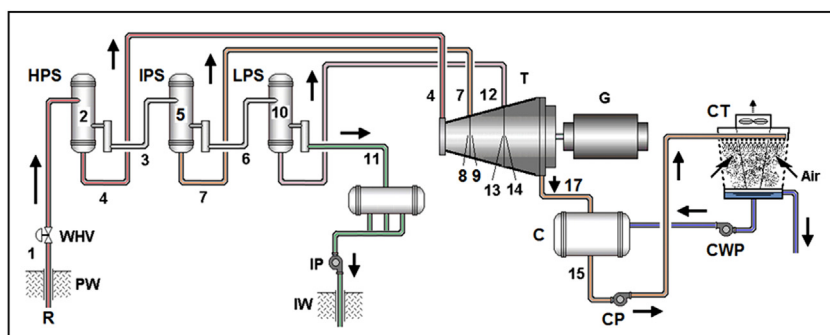
^dBased on turbine output; utilization efficiency assumes 30° C dead state.


Figure 13.18 Overall steam flow process diagram and key to Figure 13.19; see Nomenclature. *Note:* Only one half of the double-flow turbine is shown [WWW].

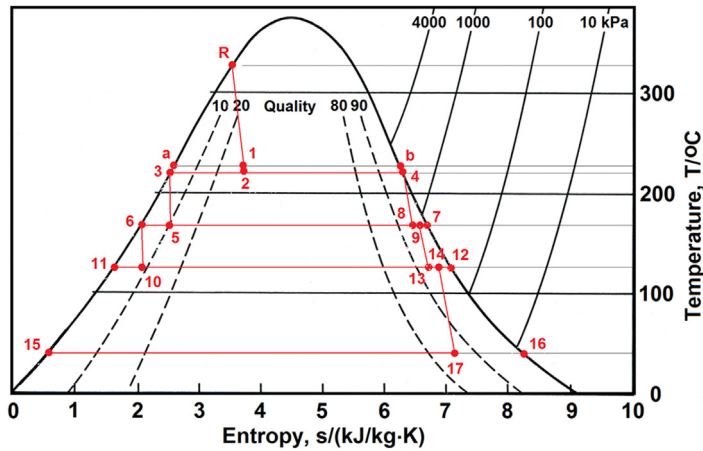


Figure 13.19 Temperature-entropy process diagram for NAP plant and basis for computer simulation of performance [WWW].

13.4 Other Geothermal Plants

There are six other locations with geothermal power plants in New Zealand, all in or close to the TVZ except one, the Ngawha plant (see Figure 13.1). Table 13.6 shows some information on these plants. This section covers three of them in some detail.

TABLE 13.6 Geothermal plants at sites other than Wairakei and Rotokawa [28].

Plant site	Plant name	Plant type	Owner	Year(s) start-up	MW _{net}
Kawerau	Tasman BP	1-Flash steam	Norske Skog Tasman	1958/2004	8
Kawerau	TG1	Binary	Nova Energy	1989	2.4
Kawerau	TG2	Binary	Nova Energy	1993	3.5
Kawerau	KA24	Binary	Eastland Generation	2008	8.3
Kawerau	Kawerau	2-Flash steam	Mighty River Power	2008	100
Kawerau	TOPP1	Binary	Norske Skog Tasman	2013	20
Ohaaki	Ohaaki	2-Flash steam	Contact Energy	1989	57
Ngawha	Ngawha	Binary	Top Energy	1998/2008	25
Mokai	Mokai	Binary	Tuaropaki Power Co.	1999/2005/2007	111
Tauhara	Te Huka	Binary	Contact Energy	2010	23
Ngatamariki	Ngatamariki	Binary	Mighty River Power	2013	82
Total					440.2

13.4.1 KAWERAU

Kawerau stands with Wairakei as one of the oldest geothermal plants to operate on a liquid-dominated resource. It began as a co-generation facility in the 1950s in conjunction with the Tasman Pulp and Paper Company that moved its operations to the site to take advantage of the geothermal energy. Initially the geofluids performed a variety of tasks besides electricity generation including clean steam production via heat exchangers, timber drying, recovery boiler shatter sprays, liquor heating, and log handling equipment [11,29]. Today there are five stand-alone power plants (one steam, the rest binary) plus one turbine integrated with the pulp and paper facility; see Figures 13.20 and 13.21.

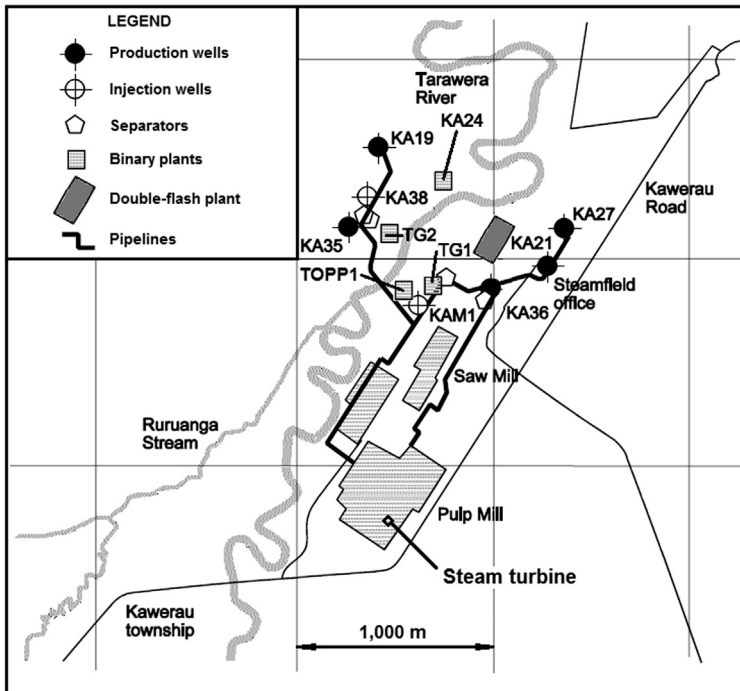


Figure 13.20 Kawerau field map showing binary plants and double-flash plant; not all wells are shown. After Ref. [29].

The 100-MW Kawerau double-flash unit that came online in 2008 is one of the largest single-cylinder geothermal turbines. It has a HP-section of six reaction stages with unidirectional flow combined with two four-stage, double-flow sections; see Figure 13.22.



Figure 13.21 Stand-alone power plants at Kawerau. *Image from Google Earth, dated 4-7-2013 [WWW].*

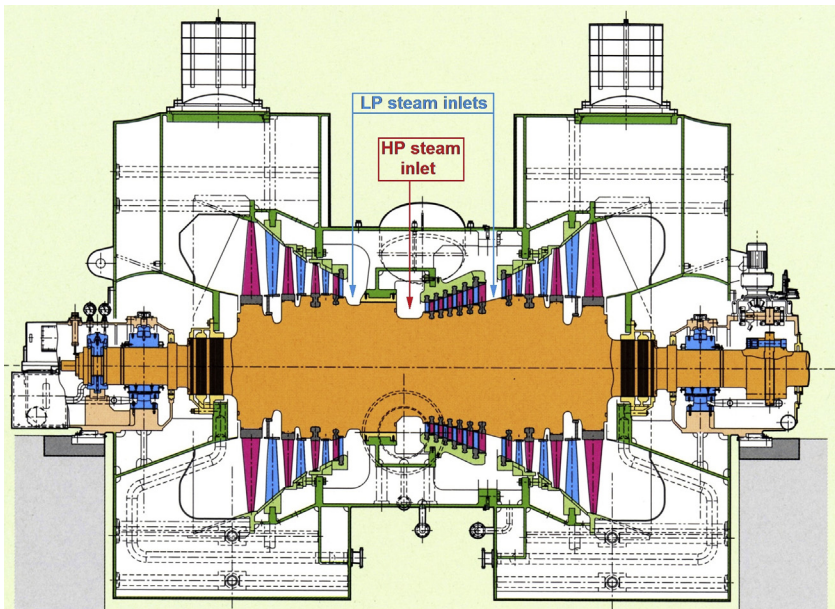


Figure 13.22 Kawerau 100-MW turbine cross-section. *After Ref. [30] [WWW].*

A computer simulation shows that the plant has a net utilization efficiency of 49.7%. Modeling the turbines with the Baumann rule using a dry efficiency of 88% yields isentropic efficiencies of 84.2% (HP) and 78.6% (LP), without accounting for any interstage moisture removal.

13.4.2 OHAAKI

Ohaaki came online in 1988 with an installed capacity of 114 MW at a cost of NZ \$320 million (US \$211 million), or NZ \$2800/kW (US \$1850/kW). Ohaaki power station, formerly known as Broadlands, has the distinction of being the only geothermal plant in New Zealand with a natural-draft cooling tower. The Waikato River divides the field into two sectors—the East and West Banks; see [Figure 13.23](#). The plant site lies about 1 km west of the river and at an elevation ~60 m above the water level and about 50 m above both well fields.

In 1988 the plant inherited the two HP 11.2 MW steam turbines from Wairakei that had been decommissioned when that station was derated. Two new 46 MW turbines were also installed to give the station a rating of 114 MW. It was expected that the HP machines would have a lifetime of about 10 years taking into account the anticipated reservoir pressure decline. This outlook was based on the observed degradation of reservoir pressure that had taken place during the long-term flow testing in the late 1980s [31].

The first well was drilled in 1965 but it took 24 years before the plant was fully online. The original plant flow diagram is shown in [Figure 13.24](#). Forty-four wells were drilled from 1966 to 1984, followed by four years of well testing and recovery. Once the plant was built and fully operational, it ran at full power from 1988 to 1993. It never again achieved that level of performance. It was able to maintain its power rating during the first 5 years by using surplus steam from the production wells [33]. However, it soon became clear that the reservoir could not sustain that level of output.

Under production drawdown, shallow wells drilled in the West Bank saw an influx of cool bicarbonate waters. This led to calcite scaling in the formation and in wells. Downhole injection of antiscaling chemicals partially solved this problem, but downhole acid treatments were often ineffective in dissolving the calcite, resulting in reduced permeability. Deep wells particularly in the East Bank do not seem to suffer from this scaling problem.

Two additional drilling campaigns were carried out, one starting in 1995 and another ten years later. These wells were deep and generally found high temperature and good permeability. However, the newly won steam quickly diminished, and after the first campaign the power dropped to 25–40 MW, necessitating the second drilling campaign. This restored the power to about 60 MW, but by 2009

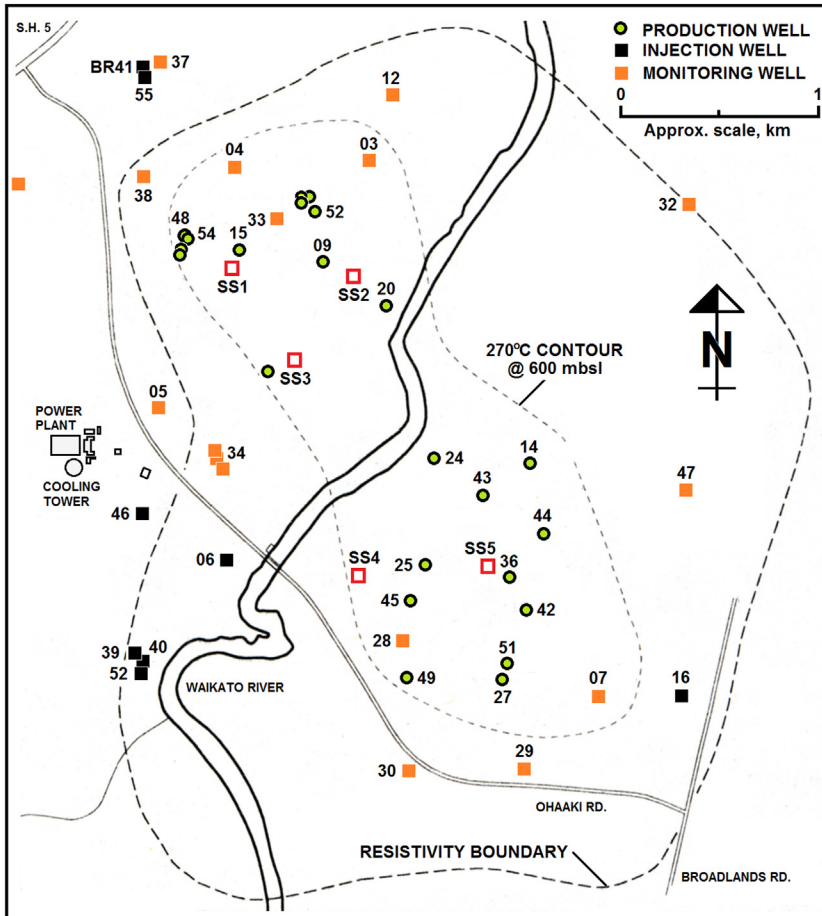


Figure 13.23 Ohaaki well field and power plant map; note all wells have a prefix BR. Note: Abandoned wells are not shown. Modified from Refs. [31,32] [WWW].

another decline had already begun. By 2011 a total of 65 wells had been drilled. Many of the original wells have been abandoned or converted to monitoring wells; see Figure 13.23.

There are five separator stations, three on the West and two on the East Bank, but one of the stations on the West Bank was decommissioned owing to lack of geofluid. As of 2014, one each of the HP and IP turbines have been decommissioned and the plant runs only when demand justifies operation. The power capacity has fallen off and now stands at about 45 MW maximum. There is some hope that the plant may reach 50 MW but not much more [28].

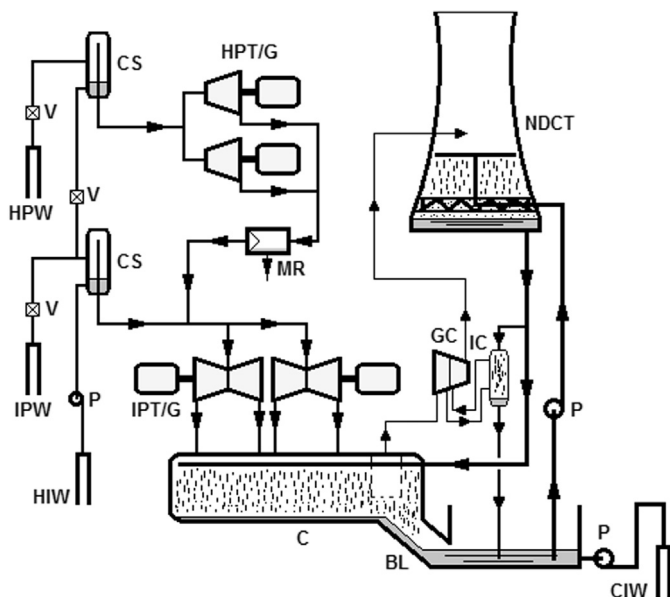


Figure 13.24 Original Ohaaki flow diagram; see Nomenclature. *After Ref. [34].*

13.4.3 NGATAMARIKI

Situated some 9 km west of Ohaaki, the Ngatamariki power plant is the quintessence of geothermal binary technology. As of 2014, it is the largest binary power station with 100 MW (gross) and 82 MW (net) produced using four identical recuperated pentane organic Rankine cycles. The air-cooled condensers are the most prominent feature of the plant, with each 25/20.5 MW unit discharging the turbine exhaust to a 3×20 array of fan cells; see [Figure 13.25](#).

The turbine-generator is the now-standard arrangement of Ormat Technologies, Inc., namely, one generator driven by two turbines, one on either side. In this case both turbines have the same inlet pressure, in contrast to Ormat's plants at Rotokawa and Mokai that have different inlet pressures (i.e., dual-pressure cycles). The geofluid reaches the surface through three wells, located to the north and south of the plant, producing from a deep, hot reservoir with temperatures from 255°C to 300°C. The wellhead temperature is 193°C. Two-phase geofluid is separated in twin vertical cyclone separators, and both the steam and the brine are used to heat and boil the pentane. In this way no geofluid leaves the plant into the surroundings and 100% of the produced fluid is condensed and reinjected. [Figure 13.26](#) identifies the main pieces of equipment for the plant.



Figure 13.25 Ngatamariki power plant. Two 25 MW (gross) units can be seen; a duplicate pair is on the other side of the air-cooled condensers. *Photo courtesy of Ormat Technologies, Inc. [WWW].*

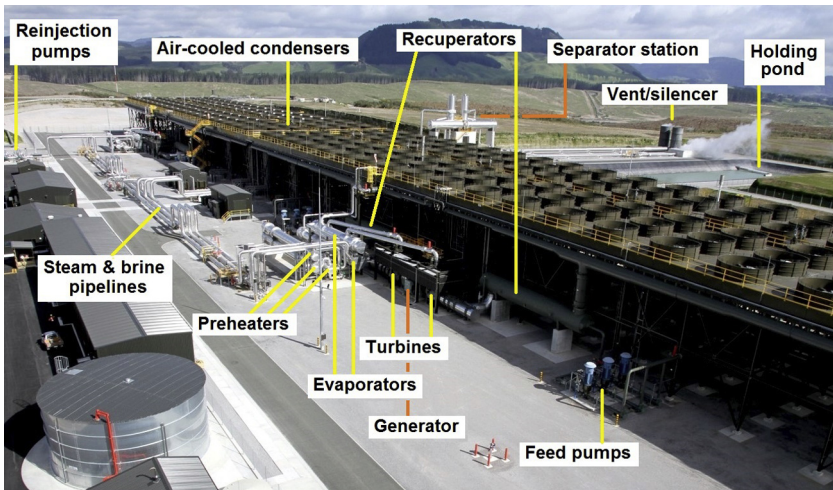


Figure 13.26 Main items at Ngatamariki power plant. *Photo courtesy of Ormat Technologies, Inc.; captions by author [WWW].*

The total specific cost of the facility including field development was NZ \$5800/kW (US \$4780/kW) on a net power basis. The power generation equipment was built and installed for US \$143 million or US \$1745/kW (net) [35].

13.5 Outlook for Development

With a population of slightly more than 4.4 million, New Zealand's ample geothermal resources together with abundant hydroelectric generation supply nearly 70% of the electricity demand of the country. In 2014, geothermal plants alone supplied about 16–17% of the country's power. As an isolated island country, New Zealand neither imports nor exports electricity. In 2010 the total installed capacity from all sources was 9679 MW and the generation was 40,760 GWh. This means that the system-wide capacity factor is only about 48%, roughly half of a typical geothermal plant but typical of a hydroelectric-dominated supply system.

Power plant construction is driven by electricity demand. At present the demand is flat placing a damper on further development of abundant geothermal resources in the country. Unless large electricity users, for example, data centers or aluminum smelters, can be attracted to New Zealand by a reliable supply of affordable and renewable electricity, it may be difficult to maintain the growth in geothermal power that has marked the most recent 10-year period.

References

- [1] Thain IA, Carey B. Fifty years of geothermal power generation at Wairakei. *Geothermics* 2009;38:48–63.
- [2] DiPippo R. Geothermal power plants: evolution and performance assessments. *Geothermics* 2015;53:291–307.
- [3] Geothermics. Special issue on the Wairakei geothermal field, New Zealand: 50 years generating electricity. March 2009;38(1).
- [4] Bolton RS. The early history of Wairakei (with brief notes on some unforeseen outcomes). *Geothermics* 2009;38(1):11–29.
- [5] Carey B, Dunstall M, et al., 2010–2015 New Zealand country update. Proc. world geothermal congress 2015. Melbourne, Australia; 19–25 April 2015.
- [6] Rosenberg MD, Bignall G, Rae AJ. The geological framework of the Wairakei-Tauhara geothermal system, New Zealand. *Geothermics* 2009;38(1):72–84.
- [7] Glynn-Morris T, King T, Winmill GEK. Drilling history and evolution at Wairakei. *Geothermics* 2009;38(1):30–9.
- [8] Armstead HCH. Geothermal power development at Wairakei, New Zealand. Proc. U.N. conference on new sources of energy. Rome, vol. 3, *Geothermal Energy: II*; 1964. p. 274–83.
- [9] Haldane TGN, Armstead HCH. The geothermal power development at Wairakei, New Zealand. *Proc Inst Mech Engrs* 1962;176(23):603–49.

- [10] Shearer AR. Power from the earth: the story of the Wairakei geothermal project. Publ. No. 50392H-74D, Gov. Printer, Wellington, New Zealand; 1974.
- [11] DiPippo R. U.S. Dept. of Energy, DOE/RA/28320-1 Geothermal energy as a source of electricity: a worldwide survey of the design and operation of geothermal power plants. Washington, DC: U.S. Gov. Printing Office; 1980
- [12] Thain IA, Stacey RE. Wairakei geothermal power station 25 years' operation. Electricity Division, Ministry of Energy, February 1984.
- [13] Axtmann RC. Environmental impact of a geothermal power plant. *Science* 1975;187:795–803.
- [14] Aggett J, Aspell A, O'Brien G. Arsenic: assessment of an environmental problem associated with operation of the Wairakei and Broadlands power plants. Proc. Pacific geothermal conference 1982, incorporating 4th New Zealand geothermal workshop, Part 1; 1982. p. 157–60.
- [15] Carey B. Forty years of successful generation at Wairakei: a successful match and marriage. Proc. 21st New Zealand geothermal workshop; 1999. p. 255–61.
- [16] Frederiksen M, Glucina M, McMahon R. Utilisation of second-hand plant to reduce capital investment and project lead times. Proc. world geothermal congress 2000, Kyushu-Tohoku, Japan, May 28–June 10, 2000.
- [17] Harwood K, Koorey K, Mann C. Te Mihi steamfield production development design. Proc. world geothermal congress 2015, Melbourne, Australia, 19–25 April 2015.
- [18] Hudson R, Morris G, Pummer B, Tearne P. Te Mihi geothermal power project—from inception to execution. Proc. New Zealand geothermal workshop 2012, 19–21 November 2012, Auckland, New Zealand.
- [19] Peltier R. Contact Energy Ltd.'s Te Mihi power station harnesses sustainable geothermal energy. *Power* 2013;157(8):38–42 <<http://www.powermag.com/contact-energy-ltd-s-te-mihi-power-station-harnesses-sustainable-geothermal-energy/>>.
- [20] Contact Energy, Ltd., Te Mihi commissioning: Te Mihi power station. Slide show; May 1, 2014.
- [21] US inflation calculator: <<http://www.usinflationcalculator.com/>>.
- [22] XE currency exchange: <<http://www.xe.com/currencytables/?from=USD&date=2004-06-01>>.
- [23] Reyes AG, Trompeter WJ, et al. Mineral deposits in the Rotokawa geothermal pipelines, New Zealand. *J Volcanol Geotherm Res* 2002;119:215–39.
- [24] Thain IA, DiPippo R. Hybrid geothermal-biomass power plants: applications, designs and performance analysis. Proc. world geothermal congress 2015, Melbourne, Australia; 19–25 April 2015.
- [25] Titchall A. Construction of Nga Awa Purua, the second power station on the Rotokawa geothermal resource north of Taupo, has just been completed. Contractor, Contrafed Publishing Co. Ltd., 34, 4 May 2010: <<http://www.contrafedpublishing.co.nz/Contractor/May+2010/Full+steam+ahead.html>>.
- [26] Fuji Electric Co., Ltd., Nga Awa Purua geothermal power station, 1 × 140 MW, Mighty River Power Ltd. & Tauhara North No. 2 Trust, New Zealand, Brochure No. 01A3-E-0027, 2012-9 (I2012/I2010)DE-K/CTP30k; September 2012.
- [27] Horie T. Kawerau and Nga Awa Purua geothermal power station projects, New Zealand. *Fuji Electr Rev* 2009;55(3):80–6.
- [28] Think GeoEnergy Magazine. Country in focus—New Zealand: geothermal plants and outlook. Issue 01, September 2013. p. 36–38: <www.thinkgeoenergy.com>.
- [29] Bloomer A. Kawerau geothermal development: a case study. *Geothermal Resour Counc Trans* 1997;21:11–15.

- [30] Fuji Electric Co., Ltd., Kawerau Geothermal Power Station, 1×100 MW, Mighty River Power Ltd., New Zealand, Brochure No. 01A3-E-0025, 2012-9(I2012/I2009)DE-K/CTP30k; September 2012.
- [31] Clotworthy A, Lovelock B, Carey B. Operational history of the Ohaaki geothermal field, New Zealand. Proc. world geothermal congress 1995, International Geothermal Association, Florence, Italy, 18–31 May 1995, vol. 3, p. 1797–1802.
- [32] Clearwater EK, Sullivan MJ, Brockbank K. An update on modelling the Ohaaki geothermal system. Proc. New Zealand geothermal workshop 2011, 21–23 November 2011, Auckland, New Zealand.
- [33] Lee S, Bacon L. Operational history of the Ohaaki geothermal field, New Zealand. Proc. world geothermal congress 2000, Kyushu-Tohoku, Japan; May 28–June 10, 2000.
- [34] Brown D. The Ohaaki geothermal development. *Geothermal Resour Counc Bull* 1989;18(10):3–7.
- [35] Ormat Technologies, Inc., Ormat successfully completed the Ngatamariki geothermal plant, <<http://www.ormat.com/news/latest-items/ormat-successfully-completed-ngatamariki-geothermal-plant>>; 2014.

Nomenclature for Figures in Chapter 13

1FL, 2FL	1st, 2nd flash
ACC	Air-cooled condenser
BCV	Ball check valve
BDP	Blowdown pump
BL	Barometric leg
C	Condenser
CIW, HIW	Cold, hot injection well
CP	Condensate pump
CS	Cyclone separator
CT	Cooling tower
CV	Control valve
CWP	Cooling water pump
CW	Cooling water
D	Drain
DC	Direct contact
E	Evaporator
EBF, WBF	Eastern, Western borefield
FP	Flash plant
G	Generator
GC	Gas compressor
HP, IP, LP	High-, intermediate-, low pressure
HPS, IPS, LPS	High-, intermediate-, low-pressure separator
HPSc, IPSc	High-, intermediate-pressure scrubber
HPW, IPW	High-, intermediate-pressure well
IC	Intercooler

IP	Injection pump
HPT, IPT, LPT	High-, intermediate-, low-pressure turbine
IW	Injection well
LPD	Low-pressure demister
LRVP	Liquid-ring vacuum pump
MP	Mixed pressure
MR	Moisture remover
MSV	Main stop valve
NCG	Noncondensable gas
NDCT	Natural draft cooling tower
P	Pump
PH	Preheater
POI	Poihipi
PRV	Pressure-reducing valve
PW	Production well
R	Recuperator
S	Silencer
SGC	Specific geofluid consumption
SJE	Steam jet ejector
SSC	Specific steam consumption
ST	Steam turbine
T	Turbine
V	Valve
WHV	Wellhead valve



Chapter 14

Geothermal Power Plants of Indonesia

Chapter Outline

14.1 Geographic and Geologic Setting	403
14.2 Early Geothermal Development	405
14.3 Kamojang and Darajat Power Stations	409
14.3.1 Geological Setting	409
14.3.2 Kamojang Power Units	410
14.3.3 Darajat Power Units	413
14.4 Wayang Windu Power Plant	418
14.5 Other Geothermal Plants	422
14.6 Outlook for Development	423
References	424
Nomenclature for Figures in Chapter 14	426

14.1 Geographic and Geologic Setting

Indonesia, having a population of 254 million, is the fifth most populous country in the world, and it is the largest country comprised solely of islands, over 17,500 of them. It is strategically located amid sea lanes between the Indian and Pacific Oceans [1]. The island arc of the Indonesian archipelago was raised by subduction of the Indian-Australian plate diving beneath the Eurasian plate. The presence of the nearby Philippine and Pacific plates creates a very active tectonic region. There are more volcanoes in Indonesia than any other country, with major volcanic activity on six islands including Sumatra, Java, and Sulawesi. The Sunda Arc, comprising a continuous chain of volcanoes stretching about 3800 km in length, forms the western edge of Sumatra, south-central areas of Java, and extends all the way eastward to the island of Alor. The northernmost end of Sulawesi, some 1000 km north of the Sunda Arc, is highly volcanic, and from its tip, a string of small island volcanoes continues 200 km northward.

Indonesia has more than 200 volcanoes, of which 129 are active [2,3]. Indonesia has been home to some of the world's most devastating volcanic eruptions including Tambora (1815) and Krakatoa (1883). Mt. Merapi, central Java, at 2968 m elevation, is currently the most active volcano in Indonesia, and is

designated a Decade Volcano [4] because of its history of eruptions and closeness to large populations; see Figure 14.1. Four islands, Sumatra (Sumatera), Java (Jawa), Sulawesi, and East Nusa Tenggara, host all of the country's geothermal power plants; see Figure 14.2.



Figure 14.1 Stratovolcano Merapi, central Java, Indonesia. Photo by J. Hoppe, 2007, Google Earth Panoramio, photo No. 2026946 [WWW].

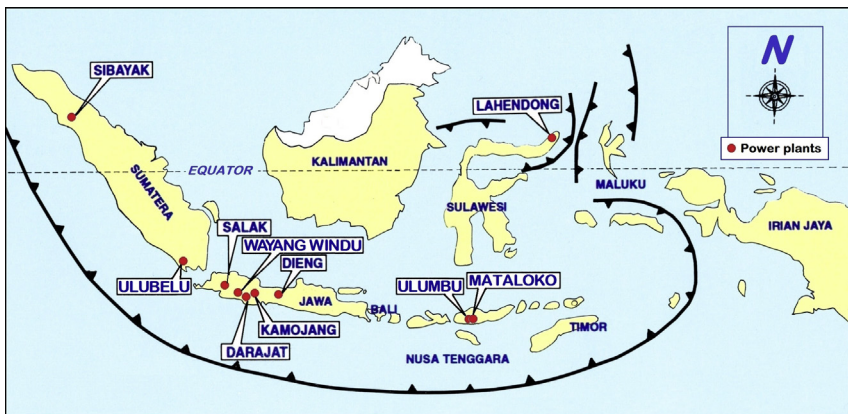


Figure 14.2 Approximate locations of Indonesian geothermal power plants as of July 2014. Updated from Ref. [5] [WWW].

The most common location of geothermal fields is on the flanks of the andesitic stratovolcanoes. Owing to highly altered andesitic tuffs, flows, and lahars, the reservoir rocks offer good permeability. Thus with abundant heat supply from

shallow magma chambers, ample rainfall to resupply the reservoirs, and sufficient permeability, these areas are excellent sources of geothermal energy to supply electric generating stations.

14.2 Early Geothermal Development

Owing to its location in an active tectonic region where three plates interact giving rise to numerous volcanoes, together with high annual rainfall, it was obvious early on that Indonesia held an enormous potential for geothermal development. In 1983 one of the early published assessments of the geothermal power potential of Indonesia placed the total at 8000–10,000 MW, accounting only for fields with presumed capacities of 100 MW or greater [6]. After years of intense exploration studies, the current estimate for all resources stands at 29,000 MW. Only about 4.6%, or 1345 MW, of this vast potential has been brought into production [2].

Serious exploration began only in 1919 with the first field survey by what is now known as the Vulcanological Survey of Indonesia (VSI). Between 1926 and 1928, five shallow wells were drilled by the Dutch government at Kamojang, which turned out to be a dry-steam resource, with a total drilled depth of only 335 m [6]. Nothing was done with those wells, but one of them, KMJ-3, is still producing dry, superheated, low-pressure steam as a tourist attraction. This well is adjacent to a large area of surface thermal manifestations probably intersected by major faults. Remarkably, through all the years of free venting of steam, there has been no sign of corrosion, no toxic gases, nor any negative effects on the environment.

There followed a long period from 1928 until 1964 during which geothermal exploration was suspended owing to lack of funds. Three agencies became involved for the next ten years: VSI, the State Electrical Company (PLN) and the Bandung Institute of Technology (ITB). At first under United Nations (UN) sponsorship, four areas were studied: Kamojang, Muria, Ijen, and Bali. But this effort was short-lived when Indonesia pulled out of the UN. The study resumed in 1969 when ITB with funding from PLN undertook a study at Dieng. Kamojang and Dieng received much attention owing to their numerous surface manifestations as well as proximity to large population centers.

In 1970 the United States got involved at Dieng through its Agency for International Development (USAID) in conjunction with the Indonesian government. Six wells with a total drilled depth of 613 m were completed. The deepest well reached only 185 m and none of them encountered steam. The project was considered a failure and Dieng was abandoned in 1972.

In 1973 the New Zealand government offered a \$24 million aid package to further explore and develop Kamojang. It was hoped that this would lead to a commercial power plant. Up to 1980, six areas were explored scientifically: Banten,

Salak, Pelabuhan Ratu, Kamojang, Bali, and Dieng. The most promising sites had exploratory wells drilled that proved up a total of 65 MW: 15 MW at Dieng, 40 MW at Kamojang, and 10 MW at Darajat, an area 10 km from Kamojang and thought to possibly be connected to its reservoir [6]. Hochstein in 1975 predicted that Kamojang had a power potential of 100–250 MW for 50 years [7]. It appears that he was right. The field began commercial generation of electricity in 1982 and as of 2014 has 200 MW installed.

Historically, however, the first power plant in Indonesia was a skid-mounted 250 kW wellhead unit (called a “Monoblok”) at Kamojang in 1978. The back-pressure unit was powered by dry steam from well KMJ-6 and later included a novel “Cycloform” steam scrubber that removed particulate matter and vented noncondensable gases (NCG) such as hydrogen sulfide. The scrubber was added after 2 years of running the turbine resulted in silica and calcium sulfate scaling on the nozzle vanes and turbine blades. The electricity was used on site until 1986 when it was retired. During its last 3 years of operation, the unit generated 2.29 GWh for a capacity factor of about 35%. Today the unit is preserved next to the Unit 4 power plant as an historical display [8]; see Figure 14.7 on page 411.

The first demonstration of power generation from an Indonesian liquid-dominated resource was from a larger Monoblok unit at Dieng; see Figure 14.3. The 2 MW unit used geofluid from well DNJ-2 and included both a wellhead separator and a Cycloform steam scrubber; see Figure 14.4. A somewhat simplified process flow diagram is shown in Figure 14.5. There was no condenser and the turbine discharged exhaust steam to the atmosphere through a diffuser. Given that the elevation at the plant site was about 2000 m a.s.l., there was naturally a



Figure 14.3 Monoblok 2 MW Dieng pilot plant discharging to atmosphere [9] /WWW/.

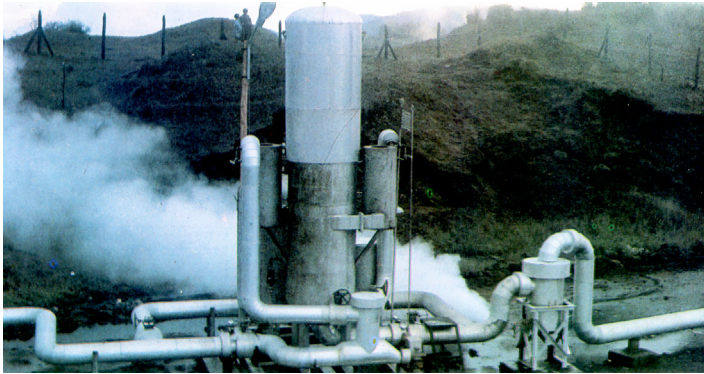


Figure 14.4 “Cycloform” scrubber. Steam from wellhead separator enters two scrubbing vessels on each side of the cyclone separator. Cleaned steam exits to turbine through the ball check valve on the right [9] [WWW].

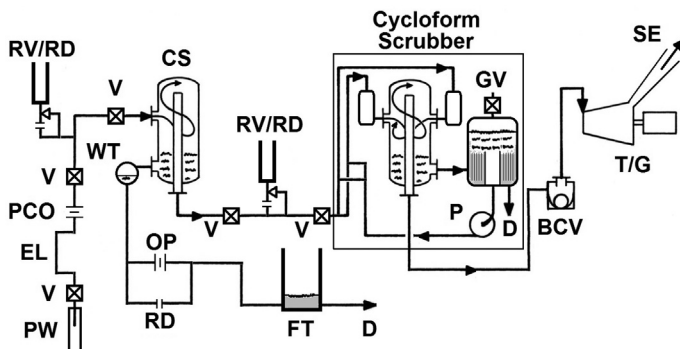


Figure 14.5 Simplified flow diagram for 2 MW Dieng wellhead unit. Not shown are five orifice condensate extraction pots between the check valve and the turbine, relief valves, rupture disks, and silencer adjacent to the Monoblok power house; see Nomenclature. After Ref. [9].

reduced ambient pressure compared to sea level: 76.5 versus 101.3 kPa. Table 14.1 lists some of the technical specifications and performance figures for the Kamojang and Dieng Monoblok units.

The performance is based on the data presented in Ref. [10] and the assumption that the reservoir fluid temperature is 230°C. Furthermore the required geofluid mass flow rate was found to be 70.7 kg/s at the wellhead. For the given steam mass flow rate and the stated power, the turbine isentropic efficiency turns out to be about 60%. This may seem low but it must be understood that the turbine was a refurbished, surplus naval propulsion unit that powered WWII-era vessels. As such it was built for rugged reliability and not for high efficiency.

TABLE 14.1 Technical specifications for Kamojang and Dieng Monoblok units [10].

	Plant	
	Kamojang	Dieng
Start-up date	November 27, 1978	May 14, 1981
Type	Dry steam, noncondensing	Single-flash, noncondensing
Rating, MW	0.25	2.0
Maximum output, MW	0.25	2.0
Resource temperature, °C	237	230
<i>Turbine:</i>		
Cylinders	1	1
Flows/turbine	1	1
Stages/flow	4	5
Inlet pressure, bar,a	4.28	7.73
Inlet temperature, °C	146	169.2 (sat.)
Steam mass flow, kg/s	1.827	7.81
Exhaust pressure, bar,a	0.83	0.765
Speed, rpm	3100	6600
<i>Generator:</i>		
Rating, MW	0.25	2.0
Speed, rpm	1500	1500
Phases	3	3
Cycles, Hz	50	50
<i>NCG system:</i>		
Stages	1	2 (parallel)
<i>Plant performance</i>		
SSC, (kg/s)/MW	7.3	3.91
Utilization efficiency, %	19.6 ^a	13.1 ^a

^aBased on a dead state at 25°C.

In 1995, the unit was dismantled and moved to Sibayak, a new geothermal field, where it began to generate power in 1996 during well drilling and field development. It continued to run for the next 13 years until 2009, producing about 43 GWh, for a capacity factor of less than 20%. Operation was hampered by numerous transmission line failures that caused the unit to trip off. Finally, having suffered severe corrosion, erosion, and general deterioration of the equipment, the unit was permanently retired in 2010. Nevertheless the pioneering unit provided 29 years of service during which time the understanding of the geothermal resources was being advanced while electricity was being made available for both site use and supplying the grid.

Both Monoblok units and Cycloform scrubbers for Kamojang and Dieng were supplied by Geothermal Power Company of Elmira, NY, USA.

14.3 Kamojang and Darajat Power Stations

The Kamojang and Darajat fields lie within 11 km of each other. Given their proximity and similar geofluid characteristics—they are both vapor-dominated fields producing only dry steam at roughly 240°C—it has been suggested that they may be connected at depth [11]. Besides Larderello and The Geysers, these are considered to be the only other known dry-steam resources in the world.

14.3.1 GEOLOGICAL SETTING

Figure 14.6 shows some of the geological features of the sites, albeit in highly simplified form. A major NE-SW fault, the Kendang fault, connects the two fields along their western margins, suggesting a possible connection at depth. Darajat lies on the eastern slope of Kendang volcano and appears to be bounded by two faults, Gagak and Cipandai, that suggest a graben structure.

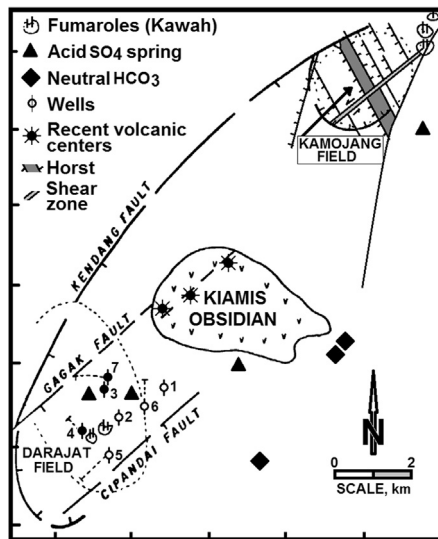


Figure 14.6 Kamojang and Darajat fields. *Based on Refs. [11,16].*

The Kamojang field lies on the western slope of the young Guntur volcano, within a graben with an orientation generally aligned with the Kendang fault. The 5 km-wide graben encompasses Kamojang and extends along the NE-SW magmatic axis in both directions toward Ciharus on the northeast and Darajat on the

southwest [11]. The structure is complex with numerous faults orthogonal to the graben leading to high fracture permeability. Nevertheless, wells within the Kamojang field show indications of a permeability barrier between the western and eastern blocks caused by a relatively impermeable horst that trends NNW-SSE. While the western wells produce from permeable zones that run horizontally along interfaces between different lithographic layers, those on the eastern side produce from structural controls such as faults and fractures [12–16]. Furthermore, production from the eastern wells does not seem to affect production from the western ones [15].

Although Kamojang currently is a dry-steam field, it evolved from a liquid-dominated system [17]. Since Darajat is known to have a deep liquid-dominated zone with a large steam reservoir contained in an upper dome, the two geothermal fields may be following similar evolutionary processes. A definitive survey of the scientific aspects of Kamojang and Darajat, and numerous other Indonesian geothermal fields may be found in Ref. [18].

14.3.2 KAMOJANG POWER UNITS

Kamojang supports four turbine-generator units that supply the Java-Bali grid. Units 1, 2, and 3 are in one powerhouse, while Unit 4 is located about 200 m to the east. The elevation at the area is about 1505 m a.s.l. Figure 14.7 is a satellite view of the power facilities. The west side of the field supplies steam for Units 1–3 while the east side supplies Unit 4. There are no provisions for sharing steam between the two operations.

Table 14.2 gives some particulars on the commercial units. All units display very high utilization efficiencies, ranging from 60–64% (gross) and 57–62% (net), owing to the fact they are fed directly by dry steam with no accompanying brine that would represent wasted exergy when disposed of. Notice the improved turbine efficiency over the years from about 80% in 1983 to 85% in 2008. The overall turbine efficiency was calculated using the data provided for the turbines and accounts for the gross power produced by the turbines to cover all parasitic power requirements. Figures 14.8 and 14.9 show the geofluid gathering system and the process flow diagram for the 60 MW (nominal) Unit 4, the newest plant.

Figure 14.10 plots the exergy in kilowatts for the geofluid starting from the reservoir through the turbine exhaust. Using this data, the exergy efficiency of the production wells and gathering system is 88.3%. That is, 11.7% of the available exergy is used up as the fluid rises to the surface and flows to the separator. The turbine utilization efficiency is 87.3% on the “brute-force” basis and 83.3% on the “functional” basis (see Section 10.6).



Figure 14.7 Satellite view of Kamojang plants. Image from Google Earth, 10-14-2013 [WWW].

TABLE 14.2 Technical details and performance for Kamojang dry-steam plants.

	Plant		
	Unit 1	Units 2 and 3	Unit 4
Start-up year	1983	1987	2008
Type	Dry steam	Dry steam	Dry steam
Power rating, MW	31.5	2×55	63.22
Net power, MW	30	2×53.5	61.0
Steam mass flow, kg/s	67.80	107.7 ^a	117.5
Resource temperature, °C	240	240	240
<i>Turbine:</i>			
Cylinders	1	1	1
Flows/turbine	2	2	2
Stages/flow	5	5	NA

(Continued)

TABLE 14.2 (Continued)

	Plant		
	Unit 1	Units 2 and 3	Unit 4
Inlet pressure, bar,a	6.5	6.5	11.0
Inlet temperature, °C	161.9	161.9	185.2
Steam mass flow, kg/s	65.5	104.8	114.0
Exhaust pressure, bar,a	0.123	0.100	0.16
Last-stage blade height, mm	420	584.2	NA
Speed, rpm	3000	3000	3000
Isentropic efficiency, %	79.8	83.7	85.1
<i>Condenser:</i>			
Type	DC, low-level	DC, low-level	DC, low-level
CW flow, kg/s	1580.6	3277.8	2011.1
<i>CW temperatures, °C:</i>			
Inlet	29.0	27.0	26.2
Outlet	49.6	45.8	51.7
Wet bulb	18.5	18.5	18.6
<i>NCG system:</i>			
Steam ejector	Yes	Yes	Yes
Stages	2	2	1
Steam mass flow, kg/s	2.297	2.906	2.25
Capacity, m ³ /s	5.09	6.64	3.13
Vacuum pump	no	no	yes
Power, kW	—	—	NA
<i>Plant performance:</i>			
Gross SSC, (kg/s)/MW	2.15	1.96	1.86
Net SSC, (kg/s)/MW	2.26	2.01	1.93
<i>Utilization efficiency, %:</i>			
Gross ^b	60.2	64.0	61.5
Net ^b	57.4	62.2	59.3

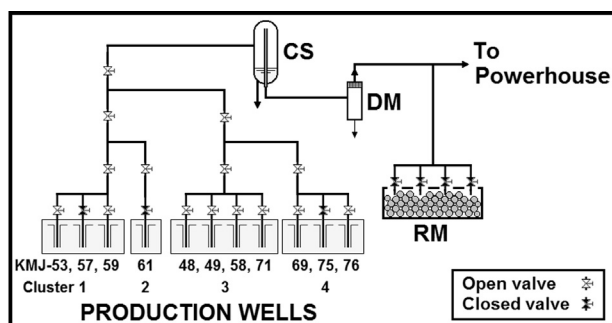
^aData is per unit.^bBased on the exergy of the steam into the plant; dead state is at the wet-bulb temperature.

Figure 14.8 Gathering system for Kamojang Unit 4; see Nomenclature.

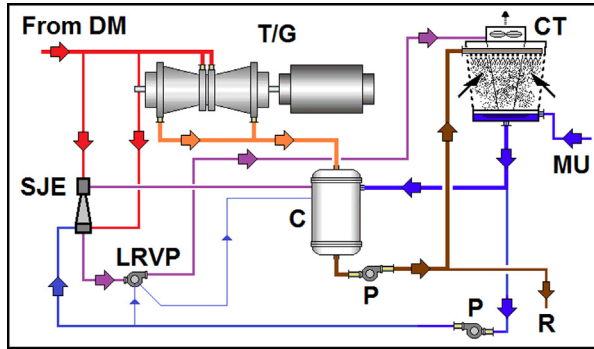


Figure 14.9 Power house process flow diagram for Kamojang Unit 4; see Nomenclature [WWW].

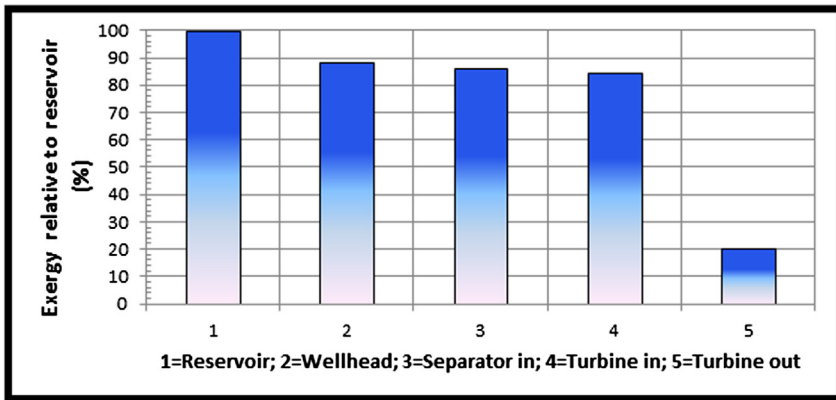


Figure 14.10 Exergy values at various states in Kamojang Unit 4 [WWW].

14.3.3 DARAJAT POWER UNITS

The Darajat power station is comprised of three units in two powerhouses that are 1.1 km apart. Unit 1 (55 MW) came online in 1994; the site elevation is 1730 m a.s.l. Unit 2 (95 MW) came online in the year 2000 in a separate powerhouse to the west and upslope at 1885 m a.s.l. Last, Unit 3 (110 MW) began commercial operation in 2007 in the same powerhouse as Unit 2. [Figure 14.11](#) is a satellite view of the power facilities.

A geologic model for the field was developed by Rejeki et al. [19]; their interpretation of the geoscientific studies is shown in [Figure 14.12](#). The best production has been found between 200 and 800 m a.s.l.



Figure 14.11 Satellite view of Darajat power plants. *Image from Google Earth, 6-27-2006 [WWW].*

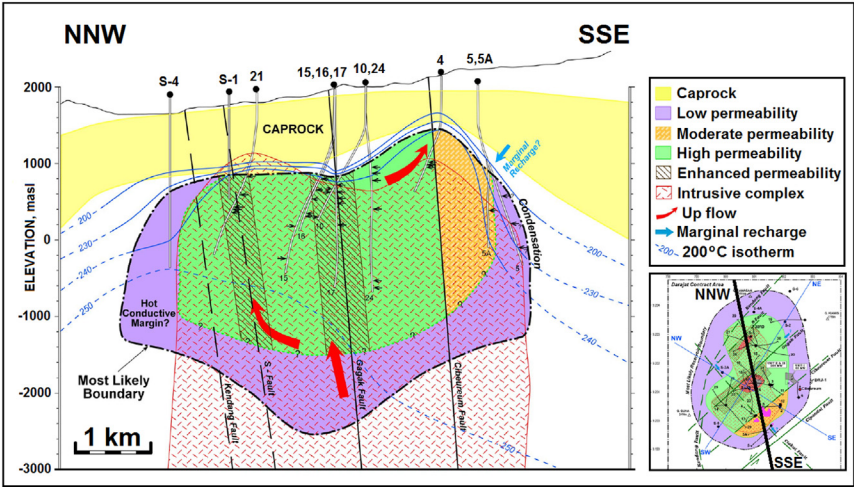


Figure 14.12 Geological cross-section of Darajat field. *After Ref. [19] [WWW].*

Figure 14.13 shows the locations of the wells at Darajat [20]. Although most wells produce dry steam from the upper vapor-dominated zone in the reservoir, several deep wells in the south sector of the field produced initially from the liquid-dominated reservoir. These wells are connected to Unit 1. The pressure drawdown caused a lowering of the liquid level, leading to a drying out of those wells. Another consequence was the superheating of the steam as it passed from the formation through the wells. By itself this might be seen as an improvement from a thermodynamic viewpoint, however, the wells began to scale and production was curtailed. A systematic cleaning of the wells by mechanical reaming was only a temporary solution. Raising the wellhead pressure was an effective means of curbing the superheat and scaling, while stabilizing the production, albeit at a lower mass flow rate [21].

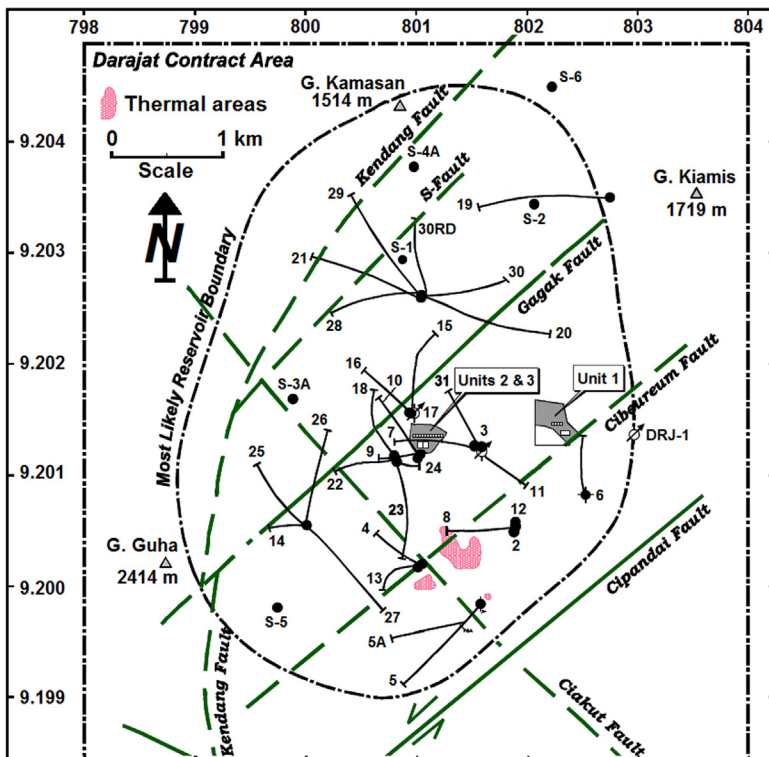


Figure 14.13 Darajat well field, major faults, and plant locations. Modified from Ref. [20] [WWW].

In May 2000, Unit 2 began as an 81.3 MW unit, but recently has been able to generate 95 MW. The Unit 2 turbine was designed to permit a maximum power generation of 100.7 MW in anticipation of more steam being made available after it was commissioned. Similarly, Unit 3 can generate up to 121 MW given

sufficient steam. The total generation at Darajat as of 2014 is 260 MW (55 + 95 + 110 MW). All three turbine-generator sets were supplied by Mitsubishi Heavy Industries, Ltd. (MHI). Figure 14.14 shows a cut-away view of the turbine for Unit 2 [22].

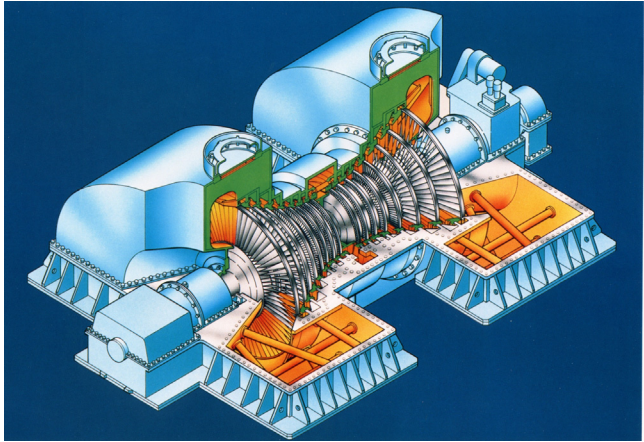


Figure 14.14 Cut-away view of Darajat Unit 2 steam turbine [22] [WWW].

Table 14.3 lists some of the technical specifications and performance measures for the three units [23]. One may notice that the newer turbines have lower isentropic efficiencies than the oldest one, with the newest having the lowest efficiency. This is not a reflection on the design of the machines but a consequence

TABLE 14.3 Technical details and performance for Darajat dry-steam plants [23].

	Plant		
	Unit 1	Unit 2	Unit 3
Start-up year	1994	2000	2007
Type	Dry steam	Dry steam	Dry steam
Gross power, MW	57.7	98	113
Net power, MW	55	95	110
Steam mass flow, kg/s	95.9	147.5	177.2
Resource temperature, °C	240	240	240
<i>Turbine:</i>			
Cylinders	1	1	1
Flows/turbine	2	2	2
Stages/flow	6	8	8
Inlet pressure, bar,a	9.926	13.07	15.14

(Continued)

TABLE 14.3 (Continued)

	Plant		
	Unit 1	Unit 2	Unit 3
Inlet temperature, °C	179.9	192.7	198.9
Steam mass flow, kg/s	94.44	144.7	174.3
Exhaust pressure, bar,a	0.105	0.0606	0.080
Last-stage blade height, mm	584.2	762.0	NA
Speed, rpm	3000	3000	3000
Isentropic efficiency, %	89.1	85.9	83.4
<i>Condenser:</i>			
Type	DC, low-level	DC, low-level	DC, low-level
CW flow, kg/s	2475.0	NA	NA
CW temperatures, °C:			
Inlet	25.5	NA	NA
Outlet	43.8	NA	NA
Wet bulb	18.5	18.5	18.5
<i>NCG system:</i>			
Steam ejector	Yes	Yes	Yes
Stages	2	2	2
Steam mass flow, kg/s	1.383	NA	NA
Capacity, m ³ /s	15.83	NA	NA
Vacuum pump	Yes	Yes	Yes
Power, kW	350	NA	NA
<i>Plant performance:</i>			
Gross SSC, (kg/s)/MW	1.66	1.51	1.57
Net SSC, (kg/s)/MW	1.74	1.55	1.61
Utilization efficiency, %:			
Gross ^a	71.2	75.5	70.8
Net ^a	67.9	73.2	68.9

^aBased on the exergy of the steam into the plant; dead state is at the wet-bulb temperature.

of the higher inlet pressures. The higher the inlet pressure the more the expansion occurs inside the liquid-vapor dome and the wetter the turbine exhaust. The presence of liquid reduces the effectiveness of the turbine. In Figure 14.15 it can be seen that the last two stages are fitted with moisture removal slits in the nozzles to reduce the liquid passing through those stages. The last two rows of blades have Stellite strips fixed to the back of the leading edges to resist the erosive attack of the liquid droplets. These means are deployed to mitigate the worst effects of the moisture at the low-pressure side of the turbine, but with such high inlet pressures, moisture will be present in some degree in each of the eight stages of the turbine.

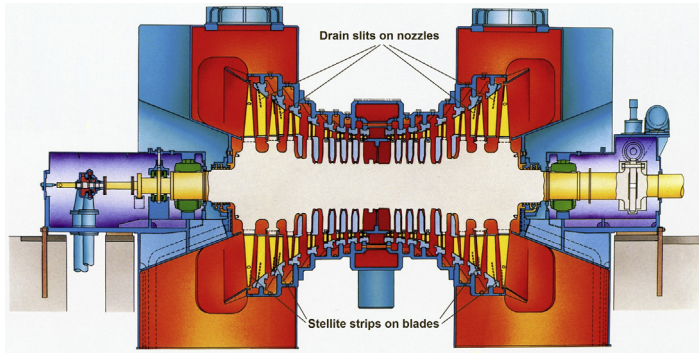


Figure 14.15 Section view of Darajat Unit 2 steam turbine. After Ref. [22] [WWW].

14.4 Wayang Windu Power Plant

Approximately 11 km west of Darajat Units 2 and 3 lies Wayang Windu, generating 227 MW with two units in a single power house. Thus within a radius of 11 km there are nine geothermal power units at three power stations contributing 687 MW to the Indonesian West Java electrical grid. Wayang Windu is a complex geological system comprised of a vapor-dominated zone several hundred meters thick overlain by a liquid-dominated formation and sitting atop a liquid-dominated or hot brine substratum [18]. Thus the wells produce a two-phase mixture of high quality at the well-heads. Two-phase pipelines convey the geofluid from each well to trunk lines that run to a bank of vertical cyclone separators, three per unit, about 600 m from the powerhouse. All the production wells are higher in elevation than the separator station. Steam is then sent to a pair of vertical scrubbers (per unit) close to the powerhouse, then to steam headers, and on to the turbines. Separated brine is sent downslope to injection wells located about 4 km south of the separators. Figure 14.16 shows a portion of the field, the separator station and the powerhouse (in the distance).

Unit 1 started up late in 1999 and commercially began delivering 110 MW to the West Java grid in June 2000, and since then has maintained an availability factor of 98% [24]. There was an 8-month delay in beginning commercial operation because the transmission line was not ready when the unit was completed [25].

The original development plan called for two identical 110 MW units to be built together and to come online at the same time. Construction commenced in 1997. However, owing to the Asian financial crisis, work on Unit 2 came to a halt after the powerhouse and the foundation for the cooling tower had been put in place. Construction on Unit 2 resumed in 2007 [26]. In the meantime, lessons had been learned from operating Unit 1 and it was decided to increase the power output of Unit 2 up to 117 MW. This had to be accomplished within tight physical constraints owing to the previous construction. The turbine-generators were identical to Unit 1. The mass flow of steam and the inlet pressure and temperature had to be the same. The areal size of the cold basin of the cooling tower was fixed.

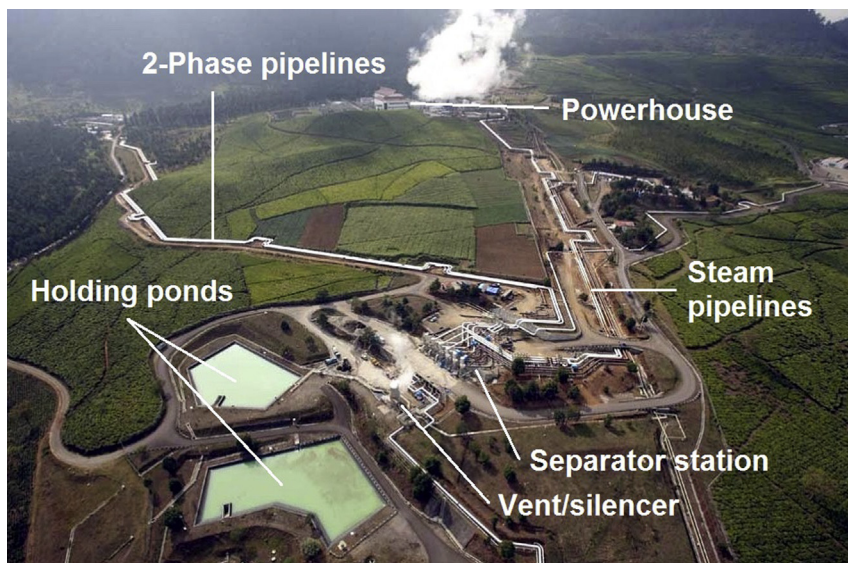


Figure 14.16 View of Wayang Windu looking east-southeast. The two-phase lines carry geofluid from the north production wells; labels by author. Base photo from: <http://www.kaskus.co.id/thread/5315f6a7bdcb17c90b8b460a/apa-itu-geothermal/> [WWW].

The only way to squeeze more power out was to lower the pressure at the turbine exhaust by increasing the cooling water flow rate and making the cooling water colder. In other words, the approach to wet-bulb temperature in the cooling tower had to be reduced. It was decided to increase the contact between the air and the falling water by raising the height of the cooling tower. This can be observed in Figure 14.17 where the right-hand tower belongs to Unit 2. The vacuum at the turbine exhaust was thereby reduced from 0.12 bar to 0.11 bar, the approach to wet bulb decreased from 8°C to 5.5°C, and the flow rate increased by about 7%. These changes resulted in 7 MW of additional power when Unit 2 began commercial operation in February 2009. Interestingly, over the period of a decade, the ambient conditions at the site changed; the wet-bulb temperature rose from 15.5°C to 17.0°C. More details on the challenges that faced the designers of Unit 2 may be found in Ref. [27].

The technical specifications for both units and some performance measures are given in Table 14.4. The turbines are designed to minimize moisture moving along the steam path. Sections where moisture is centrifuged to the outer perimeter and conveyed to the condenser are provided at the inlet, after the 5th stage, and between stages of the last three, low-pressure stages [24].

The power station including the cooling towers, turbine hall, administration building, and NCG removal systems for both units occupies about 195,000 m² (19.5 ha), as can be seen in the layout plan in Figure 14.18 [28]. With direct



Figure 14.17 Cooling towers for Wayang Windu Unit 1 (left) and Unit 2 (right). *Best available image from Ref. [28] [WWW].*

TABLE 14.4 Technical details and performance for Wayang Windu plants [26,28].

	Unit 1	Unit 2
Start-up year	2000	2009
Type	1-flash steam	1-flash steam
Gross power, MW	110	117
Net power, MW	106.5	113.5
Steam mass flow, kg/s	216.3	216.3
Resource temperature, °C	280	280
<i>Turbine:</i>		
Cylinders	1	1
Flows/turbine	2	2
Stages/flow	8	8
Inlet pressure, bar,a	10.7	10.7
Inlet temperature, °C	182.8	182.8
Steam mass flow, kg/s	213.3	213.3
Exhaust pressure, bar,a	0.12	0.11
Last-stage blade height, mm	697	697
Speed, rpm	3000	3000
Isentropic efficiency, %	78.1	81.8
<i>Condenser:</i>		
Type	DC, low-level	DC, low-level
CW flow, kg/s	4640	4970
CW temperatures, °C:		
Inlet	23.5	22.5
Outlet	44.8	44.2
Wet bulb	15.5	17.0
<i>NCG system:</i>		
Steam ejector	Yes	Yes
Stages	2	2

(Continued)

TABLE 14.4 (Continued)

	Unit 1	Unit 2
Steam mass flow, kg/s	NA	NA
Capacity, m ³ /s	NA	NA
Vacuum pump	yes	yes
Power, kW	NA	NA
<i>Plant performance</i>		
Gross SSC, (kg/s)/MW	1.66	1.51
Net SSC, (kg/s)/MW	1.74	1.55
Utilization efficiency, %:		
Gross ^a	58.1	61.8
Net ^a	56.3	60.0

^aBased on the exergy of the steam into the plant; dead state is at the wet-bulb temperature; station power assumed = 3.5 MW; auxiliary steam requirement assumed = 3 kg/s.

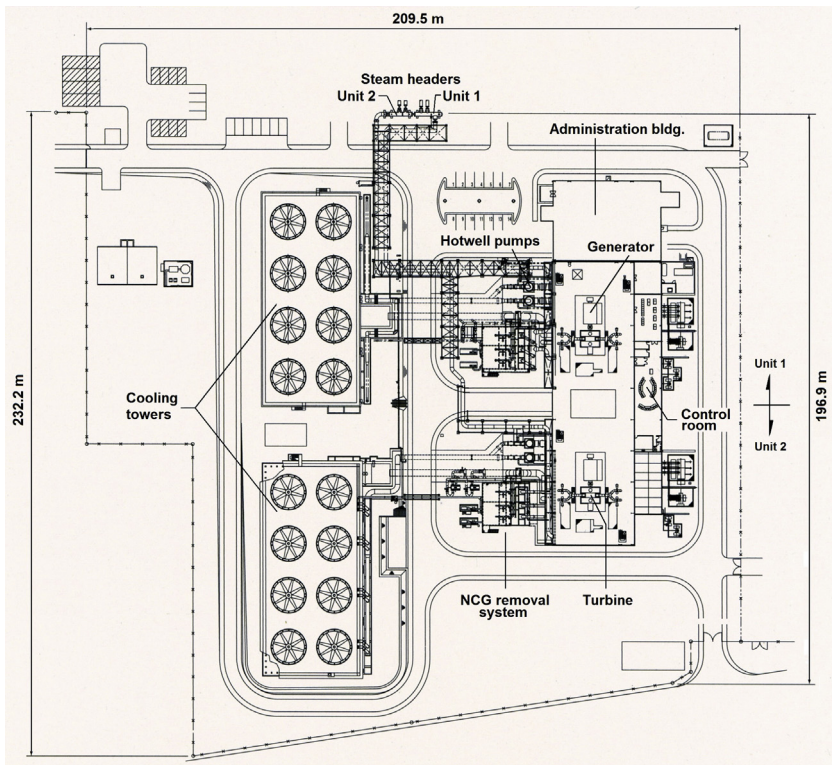


Figure 14.18 Power station layout plan for Wayang Windu Units 1 and 2. After Refs. [27,29].

pipng from each wellhead to the separator station, vapor emissions to the surroundings from steam vent structures and cooling tower plumes are confined to the area around the separators and the powerhouse. Since the plant sits amid a tea plantation, the environmental impact was reduced as much as possible. The productive reservoir may extend farther north and a third unit may be developed.

Unit 1 has an outstanding record of operations over the first 15 years of its life [30]. From June 2000 through May 2014, the 110 MW Unit 1 generated 13,281.7 GWh (gross) and 12,857.7 GWh (net). It had an availability factor greater than 96%, a gross capacity factor of 98.4% and a net capacity factor of 95.3%. The average station parasitic power was 3.46 MW. Recently, the unit has achieved gross outputs of 114–116 MW for periods of time through improvements in the efficiency of auxiliary equipment. However, the original turbine rotor had to be replaced in 2012, during a 16-day outage, because of corrosion, erosion, and general wear-and-tear after a dozen years of service [31].

14.5 Other Geothermal Plants

There are now 11 fields producing electricity in Indonesia, located on four islands: Java, Sumatra, Sulawesi, and East Nusa Tenggara. Table 14.5 offers some particulars on the other power plants in Indonesia, including the ones at Kamojang, Darajat, and Wayang Windu discussed earlier [2,32]. A mix of plant owners and field developers is evident. The state electrical company, Perusahaan Listrik Negara (PLN) either owns the plants or purchases the power through a negotiated power purchase agreement (PPA) from the operator. Pertamina, the state oil and gas company, is often the field developer, utilizing its expertise in exploration and drilling. Recently announced arrangements between PLN and Pertamina indicate that several new plants will be developed by the latter with power to be sold to the former at prices of around US \$0.091–0.097 per kWh [33].

So far, all geothermal power plants are either dry-steam or single-flash type with all waste brine and condensate being reinjected. As more experience is gained, consideration is being given to adding bottoming units to existing plants to capture some of the exergy being sent back to the reservoirs to generate additional power. For example, at the 2×55 MW Ulubelu plant, a study [34] concluded that the 772 kg/s of 175°C brine could be used in a binary plant with isobutane as the working fluid to generate 32.5 MW (net), an increase of about 30% without need for more wells. Alternatively, by deploying a low-pressure flash unit, 30.3 MW (net) could be produced. Given that the Ulubelu plant has been in operation for only about three years, more understanding of the field response to exploitation should be gained before deciding on whether to add a bottoming unit, and if so, what kind. Similar consideration might be given for

TABLE 14.5 Indonesian geothermal plants as of 2014 [2,32].

Plant	Location	Units \times MW	Start-up	Field operator	Plant owner
Kamojang	West Java	1×30 , 2×55	1983, 1987	Pertamina	PLN
Kamojang	West Java	1×60	2008	Pertamina	Pertamina
Darajat	West Java	1×55	1994	PLN	Chevron
Darajat	West Java	1×95 , 1×110	2000, 2007	Chevron	Chevron
Salak	West Java	3×55 , 3×65.6	1994, 1997, 2002	Unocal/ Chevron	Chevron
Sibayak	North Sumatra	1×12	1997	Pertamina	PLN
Dieng	Central Java	1×60	1998	Cal Energy	Cal Energy
Wayang	West Java	1×110 , 1×117	2000, 2009	Star Energy	PLN
Lahendong	North Sulawesi	1×20 1×20 1×20 1×20	2001 2007 2009 2013	Pertamina	PLN
Mataloko	E. Nusa Tenggara	1×1.8 , 1×2.5	2011, 2013	ESDM/MEMR	PLN
Ulubelu	South Sumatra	2×55	2011, 2012	Pertamina	PLN
Ulumbu	E. Nusa Tenggara	2×2.5	2011, 2012	Pertamina	PLN
Patuha	Central Java	1×55	2014	Pertamina	PLN

other power stations where significant volumes of hot brine are being reinjected, fully taking into account the impact of having to deal with lower temperature brines and the associated potential scaling and reservoir cooling problems that may be encountered.

14.6 Outlook for Development

Indonesia has the greatest potential of any country for geothermal power generation. It is highly populated with a growing demand for electricity. With appropriate incentives for investors, the goal is to have 6000 MW on line by the year 2025 [32]. However, a previous goal was to have 5000 MW in place by 2014–2015, but the actual amount is 1345 MW. Clearly, it is far easier to establish goals than to meet them, particularly in geothermal power generation, owing to numerous risk factors. Nevertheless, there are numerous prospects that are known to be excellent sites for moving toward that goal. On Sumatra, along the Sumatra Fault Zone, there are 22 attractive locations besides the two already developed. On Java, there are 20 sites besides the five already on line. Sulawesi

has two more sites besides Lahendong and Nusa Tenggara has one more besides Ulumbu and Mataloko. The resources are there and the government has committed itself to more rapid development. Once the financial conditions and risk mitigation procedures take hold, Indonesia could soon become the world's leading country for geothermal power generation.

References

- [1] Indonesia. The world factbook, U.S. Central Intelligence Agency, Washington, DC; <<https://www.cia.gov/library/publications/the-world-factbook/geos/id.html>>.
- [2] Idral A, Mansoer WR. Geothermal resources development in Indonesia: a history. Proc. world geothermal congress 2015, Melbourne, Australia, 19–25 April 2015.
- [3] List of volcanoes in Indonesia. Wikipedia, The Free Encyclopedia, <http://en.wikipedia.org/wiki/List_of_volcanoes_in_Indonesia>; July 16, 2014.
- [4] International Association of Volcanology and Chemistry of the Earth's Interior, Decade Volcano Program, <<http://www.sveurop.org/gb/articles/articles/decade.htm>>; 2009.
- [5] Alhamid I, Prijanto, et al. Indonesia geothermal reserves and resources. Jakarta, Indonesia: Pertamina; April 1994.
- [6] Soetantri B. Geothermal exploration in Indonesia. 1st meeting of standing advisory committee on geothermal training, Pisa, Italy, 11–16 November 1980.
- [7] Hochstein M. Geophysical exploration of the Kawah Kamojang geothermal field, West Java. Proc. second U.N. symposium on the development and use of geothermal resources, San Francisco, vol. 2, 1975, p. 1049–58.
- [8] Swandaru RB. The history of the earliest geothermal power plants in Indonesia. Proc. world geothermal congress 2015, Melbourne, Australia, 19–25 April 2015.
- [9] Panas Bumi dan Pengembangannya Sebagai Sumber Energi (The heat of the earth and its development as an energy source). Pertamina Public Relations Dept., Jakarta, Indonesia; 1981.
- [10] Shulman G. Geothermal power development in Indonesia. *Geothermal Resour Counc Trans* October 1981;5:37–40.
- [11] Whittome AJ, Salvesson JO. Exploration and evaluation of the Darajat geothermal field, West Java, Indonesia. *Geothermal Resour Counc TRANS* 1990;14(Part II):999–1005.
- [12] Hantono D, Mulyono A, Hasibuan A. Structural control is a strategy for exploitation well at Kamojang geothermal field, West Java, Indonesia. Proc. twenty-first workshop on geothermal reservoir engineering, SGP-TR-15. Stanford, California: Stanford University; January 22–24, 1996.
- [13] Kamah MY, et al. The productive feed zones identified based on spinner data and application in the reservoir potential review of Kamojang geothermal area, Indonesia. Proc. world geothermal congress 2005, Antalya, Turkey, 24–29 April 2005.
- [14] Zuhro AA. Numerical modelling of the Kamojang geothermal system, Indonesia. Geothermal training programme reports 2004, Number 20, Orkustofnun, Reykjavík, Iceland.
- [15] Kamojang Geothermal. Version 09, United Nations framework convention on climate change, clean development mechanism project design document form (CDM-PDD)-Version 03, March 25, 2011.

- [16] Raharso, Allagan S, Robert D. Main aspects of Kawah Kamojang geothermal field—West Java, Indonesia. *Geothermal Resour Counc Trans* 1985;9(Part I):469–72.
- [17] Utami P, Browne PRL. Subsurface hydrothermal alteration in the Kamojang geothermal field, West Java, Indonesia. Proc. twenty-fourth workshop on geothermal reservoir engineering, SGP-TR-162. Stanford, California: Stanford University; January 25–27, 1999.
- [18] Hochstein MP, Sudarman S. History of geothermal exploration in Indonesia from 1970 to 2000. *Geothermics* 2008;37(3):220–66.
- [19] Rejeki S, Rohrs D, et al. Geologic conceptual model update of the Darajat geothermal field, Indonesia. Proc. world geothermal congress 2010, Bali, Indonesia, 25–29 April 2010.
- [20] Dawud HA, Roberts J, et al. The role of boron cycling and superheat monitoring for field production and injection strategies at the Darajat geothermal field, Garut, Indonesia. Proc. world geothermal congress 2010, Bali, Indonesia, 25–29 April 2010.
- [21] Martiady K, Dawud HA, et al. Managing the decline rate at the south sector production area of Darajat geothermal field, Indonesia. *Geothermal Resour Counc Trans* 2011;35:.
- [22] Mitsubishi Heavy Industries, Ltd., Darajat geothermal power plant. Brochure SA (RF) '97-09, Tokyo, Japan.
- [23] Mitsubishi Heavy Industries, Ltd., List of geothermal power plants. August 2005, updated August 2014, Tokyo, Japan.
- [24] Wayang Windu Geothermal Energy. Star energy geothermal (Wayang Windu) Ltd., Road Town, British Virgin Islands; <<http://www.starenergy.co.id/Assets-Overview/Geothermal/Wayang-Windu.aspx>>; 2012.
- [25] Murakami H. Wayang Windu geothermal power plant. *Fuji Electr Rev* 2001;47(4):102–7 FER-47-04-000-2001.
- [26] Yamada S, Makimoto S, Shibata H. Fuji Electric's recent activities and latest technologies for geothermal power generation. *Fuji Electr Rev* 2010;56(4):118–19 FER-56-4-118-2010
- [27] Yamaguchi N. Design of Wayang Windu unit 2 geothermal power station. Proc. world geothermal congress 2010, Bali, Indonesia, 25–29 April 2010.
- [28] Participation in geothermal power business in Indonesia. Mitsubishi Corp., <<http://www.mitsubishi-corp.com/jp/en/csr/sustainability/sustainability01.html>>; 2014.
- [29] Geothermal power plant: star energy geothermal (Wayang Windu) Ltd., Indonesia Wayang Windu geothermal power plant. Fuji Electric Co. Ltd., Brochure 01A3-E-0020, 2012-9(I2012) DE-K/CTP3Ok, Tokyo, Japan; 2012.
- [30] Purnanto MH, Purwakusumah A. Fifteen years (mid-life time) of Wayang Windu geothermal power station Unit-1: an operational review. Proc. world geothermal congress 2015, Melbourne, Australia, 19–25 April 2015.
- [31] Zein A, Mulyana W, Dwi Yudha H. Unit 1 turbine rotor 110 MW replacement. Proc. world geothermal congress 2015, Melbourne, Australia, 19–25 April 2015.
- [32] Darma S, Tisnaldi, Gunawan R. Country update: geothermal energy use and development in Indonesia. Proc. world geothermal congress 2015, Melbourne, Australia, 19–25 April 2015.
- [33] Richter LX. Pertamina and PLN finalizing PPAs for geothermal plants of up to 615 MW. Think GeoEnergy; <<http://thinkgeoenergy.com/archives/18417>><http://thinkgeoenergy.com/archives/18417>>; April 25, 2014.
- [34] Agani M, Patangke S, et al. Opportunity and barriers to develop bottoming unit by utilizing separated hot brine in Ulubelu, Indonesia. Proc. world geothermal congress 2015, Melbourne, Australia, 19–25 April 2015.

Nomenclature for Figures in Chapter 14

BCV	Ball check valve
C	Condenser
CS	Cyclone separator
CT	Cooling tower
D	Drain
DM	Demister
EL	Expansion loop
FT	Flash tank
GV	Gas vent
LRVP	Liquid-ring vacuum pump
MU	Make-up water
OP	Orifice plate
P	Pump
PCO	Pressure control orifice
PW	Production well
R	Reinjection
RD	Rupture disk
RM	Rock muffler
RV	Relief valve
SE	Silencer-exhaust
SJE	Steam jet ejector
T/G	Turbine/generator
V	Valve
WT	Water tank



Chapter 15

Geothermal Power Plants in Central America and the Caribbean

Chapter Outline

15.1 Geologic Setting	428
15.2 History of Development	430
15.3 El Salvador	431
15.3.1 Ahuachapán	432
15.3.2 Berlín	437
15.3.3 Prospects	440
15.4 Nicaragua	442
15.4.1 Momotombo Station	442
15.4.2 San Jacinto Plant	444
15.4.3 Prospects	444
15.5 Costa Rica	445
15.5.1 Miravalles Station	445
15.5.2 Las Pailas Plant	446
15.5.3 Prospects	448
15.6 Guatemala	449
15.6.1 Zunil	449
15.6.2 Amatitlán	450
15.6.3 Prospects	450
15.7 Other Central American Prospects	451
15.8 Caribbean Islands	452
15.8.1 Guadeloupe: Bouillante	452
15.8.2 Other Caribbean Prospects	455
15.9 South American Prospects	455
15.9.1 Argentina	456
15.9.2 Chile	457
15.9.3 Other Prospects	458
References	458
Nomenclature for Figures in Chapter 15	460

This operating geothermal plant is a symbol of what the Salvadoran people can accomplish in the harmony of peace.

Guillermo A. Sol, CEL, speaking at the inauguration of the Berlín power plant,
El Salvador, April 10, 1999

15.1 Geologic Setting

The geothermal prospects in Central America and western South America owe their presence to subduction of the Cocos plate beneath the land masses of Central America, and the Nazca and Antarctic plates beneath South America (see Figure 1.2). Those in the Caribbean arise along the eastern boundary of the Caribbean plate where the North American and South American plates are diving beneath the Caribbean plate.

In the first case, we find a nearly unbroken string of volcanoes; see Figures 15.1–15.3. These include: in Central America, a segment 1300 km long from northern Guatemala to western Panama; in South America, one from west-central Colombia to central Ecuador, about 900 km long (called the Northern Volcanic Zone); another one from southern Peru through western Bolivia and down the northern portion of the border between Chile and Argentina, a length of about 1700 km (Central Volcanic Zone); and at the southernmost end, a string of volcanoes about 2500 km long from just east of Santiago, Chile to Tierra del Fuego at the tip of the continent. The latter string is comprised of the Southern Volcanic and the Austral Volcanic Zones. There is, however, one stretch of about 650 km from Santiago northward that lacks active volcanoes.



Figure 15.1 San Vicente volcano at sunset, El Salvador. *Photo by author, January 1998 [WWW].*

In the second case, we find a string of volcanic islands from Saba at the north end through St. Kitts and Nevis, Montserrat, Guadeloupe, Dominica, Martinique, St. Lucia, St. Vincent and the Grenadines to Grenada at the south end; see Figure 15.4. These are part of the Lesser Antilles. Many of these volcanoes have been active in recent times, and these small islands are popular tourist attractions, making it challenging to develop the geothermal projects in this region. Only one power plant exists but several other sites are being given serious consideration for exploitation.



Figure 15.2 Volcanoes in Central America. After Ref. [1] [WWW].

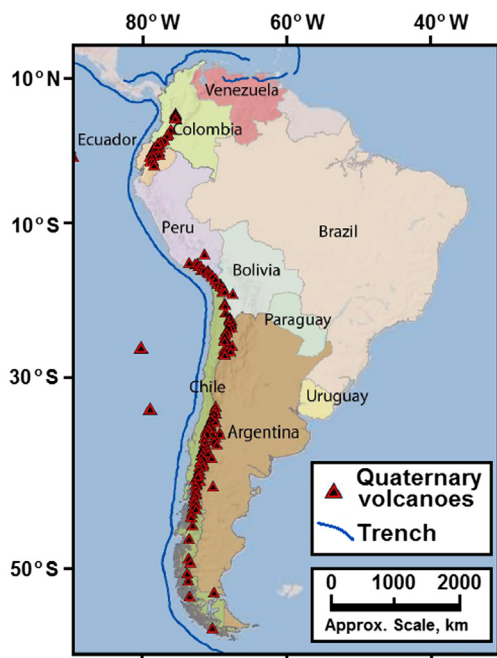


Figure 15.3 Volcanoes of South America. After Ref. [2] [WWW].

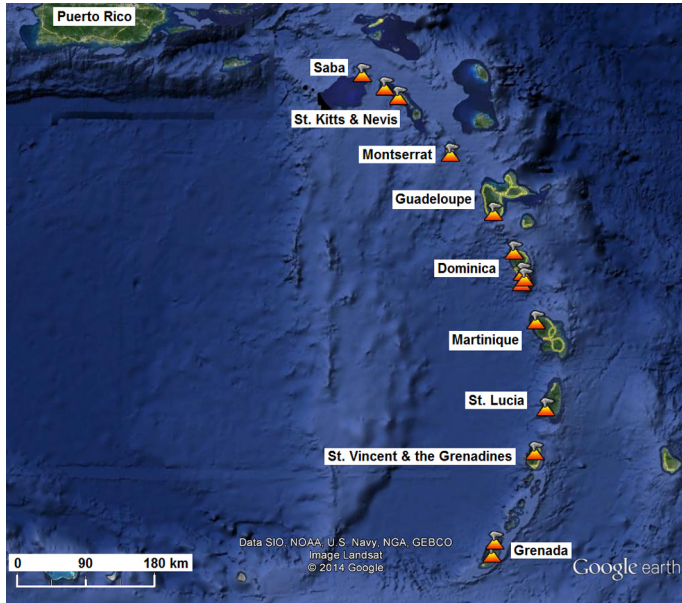


Figure 15.4 Volcanic islands along the eastern boundary of the Caribbean plate. Base map from Google Earth [WWW].

15.2 History of Development

Following the Oil Crises of 1973 and 1978, several countries in Central America began to look seriously at their indigenous energy resources to try to become more self-sufficient in the light of unstable supplies and prices for imported oil. The geothermal resources were evident but remained unexploited until these worldwide events awakened interest.

El Salvador, the smallest of the Central American nations, led the way in 1975 with the Ahuachapán power station and a drilling program at Berlín. The civil war in the 1980s interrupted development, but once peace was reestablished and the economy resumed its growth, the demand for electricity rose rapidly and provided additional impetus to geothermal developments. Furthermore, relative to a geothermal plant, the cost to generate a kilowatt hour of electricity in the mid-1970s using a conventional thermal Rankine cycle plant using Bunker C fuel oil was five times higher and using a gas turbine fired with diesel fuel was nearly 10 times higher.

Nicaragua, also beset with a civil war of its own in the 1980s, was the second country in the region to get a geothermal plant online. The first unit at Momotombo, a 35 MW single-flash unit, commenced operations in 1983,

followed by unit 2 in 1989. However, the war left the country in a devastated condition economically and the units deteriorated from lack of maintenance. Only recently has geothermal development resumed with a new plant at San Jacinto-Tezate.

Costa Rica selected the Miravalles field from among several possible sites to develop its first geothermal plant. A long period of exploration, resource characterization, drilling, and testing culminated in 1994 with the first central power unit, a 55 MW single-flash plant. Development has continued both at Miravalles and at the nearby Rincon de la Vieja field resulting in over 200 MW being online with more in the pipeline.

Guatemala also began its geothermal exploration contemporaneously with its neighbors, looking at two potential resources, Zunil and Amatitlán. A devastating and deadly landslide at Zunil in 1991 temporarily halted the drilling program. Eventually a 25 MW flash-binary plant was installed in 1999. Amatitlán followed in 2007 with a similar kind of plant rated at 20 MW.

In all these cases, the plants were initially under the auspices of the state-owned electric authorities, with financial assistance from international lending agencies. As structural reform and market liberalization took place in the region, more public–private partnerships have been established and has led to more rapid progress in getting power plants built and online.

Honduras and Panama likewise began exploring for good geothermal prospects in the same timeframe but did not pursue any of the identified sites. There is now renewed interest in both countries that have selected sites to be further developed. Belize, not normally considered a Central American country but situated in the region, has no geothermal sites suitable for geothermal power generation.

15.3 El Salvador

El Salvador is roughly the size of the state of Massachusetts in the United States and has a population of roughly 6.1 million. The population is densely packed in the capital city of San Salvador and the surrounding urban areas, whereas most of the land mass is sparsely populated. Even so, it has a very high population density. There are numerous spectacular volcanoes in the small country, many of which are visible on the horizon from almost any vantage point.

The state electric company, Comisión Ejecutiva Hidroeléctrica del Río Lempa (CEL), owns and operates the hydropower stations, while LaGeo, a private company with state participation, owns and operates the geothermal plants. In 2002, LaGeo entered into a joint-venture partnership with the Italian company ENEL Green Power (EGP). A complex dispute over the precise meaning of the language

of the contract lingered for many years, involving a series of arbitration rulings and appeals, creating uncertainty and delaying investment in geothermal projects. In September 2014, the French Supreme Court in Paris ruled in favor of EGP [3], allowing EGP to gain additional shares in LaGeo by virtue of investments in geothermal projects even if that could lead to ENEL achieving majority control of the company. The dispute was eventually settled when LaGeo bought out EGP and the Italians left the country.

El Salvador has an installed electric power capacity of about 1537 MW, of which roughly 49% comes from fossil-fuel power plants, 31% from hydroelectric plants, and 20% from renewable sources, mainly geothermal. The electricity generated, however, shows that geothermal plants produce about 24%, hydro 29%, and fossil 39% [4]; see Table 15.1. The country relies on renewable energy sources to a large degree with about 57% of its electricity coming from hydro, geothermal, and biomass. However, the country needs to import about 5% of its electricity, a situation that could be alleviated by further using more of its indigenous geothermal resources.

TABLE 15.1 Electricity situation in El Salvador for 2013 [4].

Plant type	Installed capacity		Electricity generation	
	MW	%	GWh	%
Thermal (fossil)	756.5	49.2	2355.2	38.6
Hydropower	472.0	30.7	1784.0	29.3
Geothermal	204.4	13.3	1442.5	23.7
Biomass	104.5	6.8	229.3	3.8
Imports	—	—	283.1	4.6
Totals	1537.4	100	6094.1	100

There are five geothermal areas, as shown in Figure 15.5. Ahuachapán and Chipilapa in the west are used to support one power station, with Chipilapa being the site of some reinjection wells. In the east, Berlín hosts four power units, while San Vicente and Chinameca are under exploration and development.

15.3.1 AHUACHAPÁN

The Ahuachapán power station lies 500 m north of the famous Los Ausoles hot springs that were described in 1841 by John Lloyd Stephens in H.F. Godfrey's book [6]: "... we ... came into a field smoking with hot springs. The ground was incrustated with sulphur, and dried and baked by subterranean fires. In some places were large orifices from which steam rushed out violently and with noise; in other places were pools ... of dark brown water, boiling with monstrous bubbles. ... At some distance

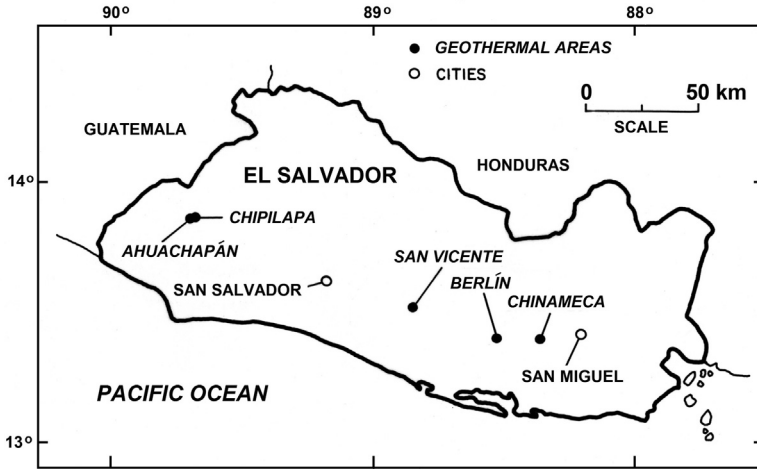


Figure 15.5 Geothermal areas of El Salvador. Power plants are operating at Ahuachapán and Berlín [5].

was a stream of sulphur water, which we followed up to a basin, where we made a dam with stones and bushes and had a most refreshing warm bath.” Nearly 175 years later, the springs still steam, hiss, and bubble, but now alongside a power plant generating 84 MW from the “subterranean fires.” See Figure 15.6.



Figure 15.6 Los Ausoles hot springs, Ahuachapán, El Salvador. *Photo by author, June 1978 [WWW].*

The production wells for the Ahuachapán project were developed on a relatively small area, roughly 1 km². After experimenting with in-field reinjection and finding unsatisfactory results, most of the waste brine was then disposed of first to the Rio Paz then later to the Pacific Ocean by means of a 71 km-long covered concrete canal having a cross-section of 1 m²; see Figure 15.7. Owing to the rugged terrain, the canal was fitted with 16 siphons [7]. Once 100% reinjection was achieved, the canal was officially decommissioned and demolished in 2004 [8].

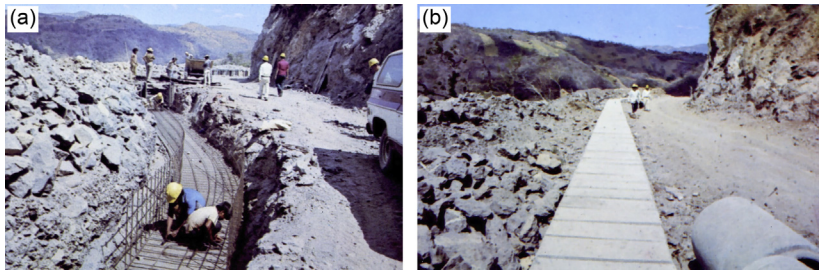


Figure 15.7 Waste brine disposal canal (a) under construction and (b) completed from Ahuachapán power plant to the Rio Paz and the Pacific Ocean [9] [WWW].

The well field has been expanded over the 40 years of plant operations to encompass more wells to the south, upslope toward the Cerro Verde volcano, and east of the plant to Chipilapa where several cold injection wells are located; see Figure 15.8. Through an extensive planting program, the wells and piping for the power station have largely been hidden from view to minimize visual impact; see Figures 23.12 and 15.9.

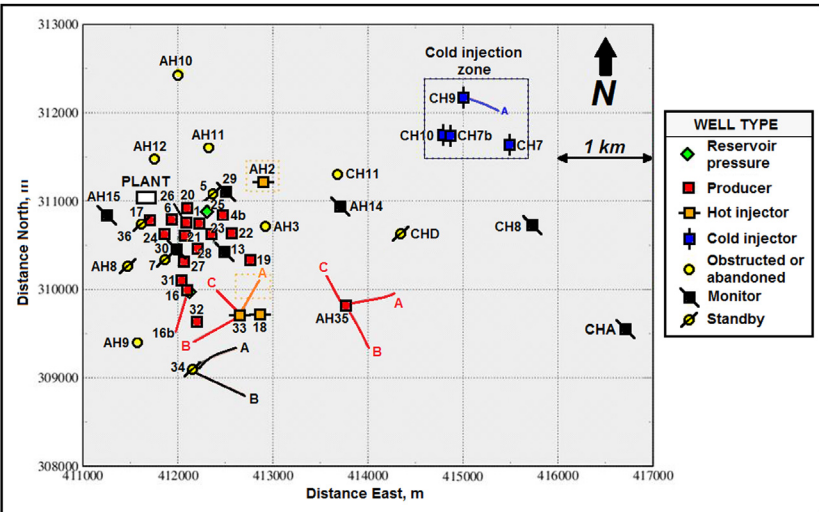


Figure 15.8 Ahuachapán well field layout as of 2012. Modified from Ref. [10] [WWW].



Figure 15.9 Well AH-6 during reforestation program. Photo by author, January 1991 [WWW].

The power plant consists of three units: two 30 MW single-flash units and one 35 MW double-flash unit that use high-pressure steam from wellhead separators and low-pressure steam flashed from the separated brine; Figure 15.10 shows a schematic of the flash equipment for Unit 3.

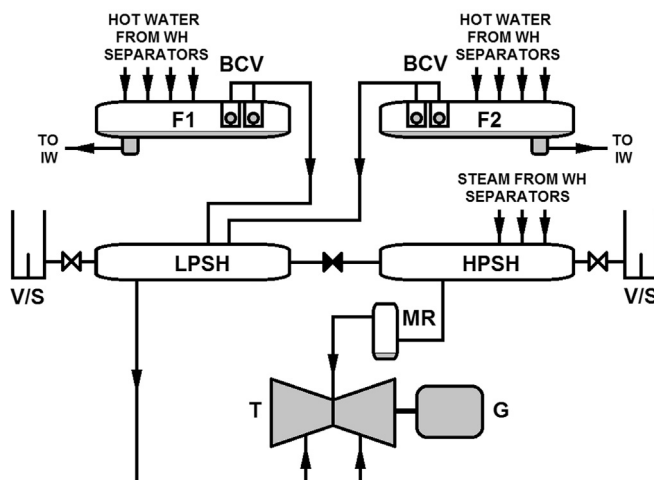


Figure 15.10 Simplified flow diagram of geofluid handling equipment for Ahuachapán Unit 3; see Nomenclature. After Refs. [7,11].

Technical particulars for all three units are given in Table 15.2. The running capacity for each of the three units as of 2014 is 28 MW, with efficiency improvements being implemented to raise the station output to its installed capacity of 95 MW [4].

TABLE 15.2 Design specifications and performance for Ahuachapán Units 1–3.

	Units 1 and 2	Unit 3
Start-up year	1975, 1976	1981
Type	Single-flash	Double-flash
Power rating, MW	2×30	35
Maximum power, MW	2×35	40
Running power, MW	2×28	28
Resource temperature, °C	230	230
<i>Turbine:</i>		
Cylinders	1	1
Flows/turbine	2	2
Stages/flow	5	3/4
Inlet pressure, bar, a	5.6	5.5/1.5
Inlet temperature, °C	156.1	155.5/111.4
Steam mass flow, kg/s	63.9 ^a	47.5, 21.3
Exhaust pressure, bar, a	0.085	0.085
Last-stage blade height, mm	520.7	563.9
Speed, rpm	3600	3600
Isentropic efficiency ^b , %	77.5	80.6/72.9
<i>Condenser:</i>		
Type	DC, spray, barometric	
CW flow, kg/s	2407	3406
CW temperatures, °C:		
Inlet	27.0	27.0
Outlet	40.5	40.5
Wet bulb	22.0	22.0
<i>Cooling tower:</i>		
Type	Mechanical induced draft, crossflow	
No. of cells	5	5
Fan power, kW/cell	80	80
<i>NCG system:</i>		
Steam ejector	Yes	Yes
Stages	2	2
Trains	2	2
Intercondensers	Yes	Yes
Aftercondensers	Yes	Yes
Steam mass flow, kg/s	1.14	NA
Capacity, m ³ /s	3.25	NA
<i>Plant performance:</i>		
Gross SSC, (kg/s)/MW	2.17	1.97
Net SSC, (kg/s)/MW	2.32	2.08
Utilization efficiency, %:		
Gross	34.0 ^c	43.7 ^d
Net	32.9 ^c	38.2 ^d

^aData is per unit.^bAssumed generator efficiency = 97%.^cBased on the exergy of the reservoir geofluid.^dBased on the exergy of HP steam and brine from which LP steam is obtained; dead state is at the wet-bulb temperature.

15.3.2 BERLÍN

The Berlín plant is located some 112 km east of San Salvador on the northern slope of the Tecapa volcano; see [Figure 15.11](#).



Figure 15.11 Berlín power plant, Units 1–3, looking south-southeast. Units 1 and 2 are in the larger building. The two cooling towers to the right supply Unit 3 [\[12\]](#) [\[WWW\]](#).

The resource is very hot, 280–300°C, with 38 total wells drilled, of which 14 are designated as producers and 20 as injectors; see [Figure 15.12](#) [\[13\]](#). These wells support four power units: two identical 28 MW single-flash units, one 44 MW single-flash unit, and a bottoming 8 MW binary cycle. Approximately 870 kg/s of geofluid is being delivered at the wellheads, with 220 kg/s being steam and the rest brine. Like Ahuachapán, Berlín reinjects 100% of the produced geofluid minus evaporative losses from the cooling towers. Initially reinjection was done via gravity feed from the higher elevation producers to the wells at lower elevations, but currently a pumping station is used at well pad TR-1 to overcome resistance in the reservoir. [Table 15.3](#) gives the technical details on these units [\[14\]](#).

Unit 4, the bottoming binary plant, is located at the well pad for TR-9, the same place where two 5 MW back-pressure units operated during the well-drilling phase for the central station from 1992 to 1999; see [Figure 15.13](#).

Two trains of heat exchangers are necessary (see [Figure 15.14](#)) because the separated brine for the plant comes from two separator stations serving wells TR-2/9 and TR-4/5, and have significantly different pressures: 19.7 and 10.6 bar,a. Mixing the fluids would cause chemical scaling problems and require throttling the high-pressure liquid that would release vapor and waste energy.

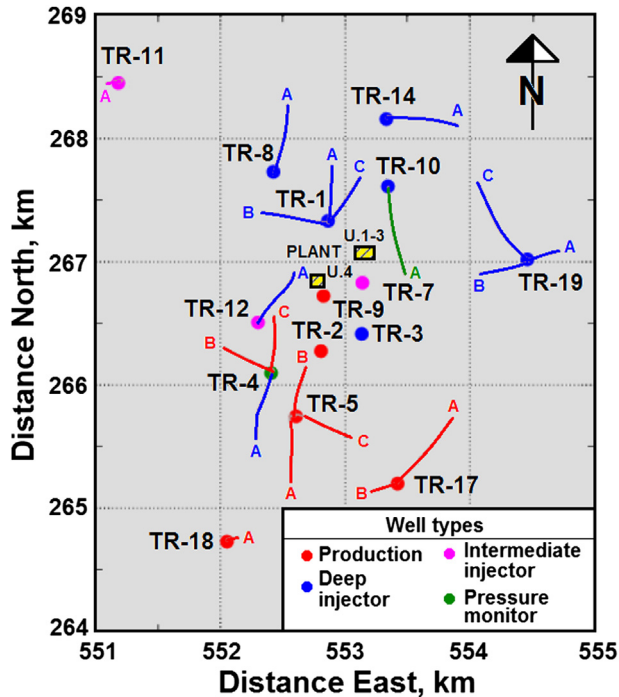


Figure 15.12 Well map at Berlín. The peak of the Tecapa volcano (elevation ~1588 m a.s.l.) lies roughly 1.5 km south of well pad TR-17 (elevation ~1085 m a.s.l.). The well designation “TR” comes from the Tronador fumarole, a prominent thermal manifestation at the field. *Modified from Ref. [13] [WWW].*

On a visit to the plant on November 4, 2010, the author observed the temperature, pressure, and mass flow rates shown in [Table 15.4](#) in ***bold, italic***. The other properties were calculated with the aid of REFPROP, assuming a 5% pressure drop in the heat exchangers. [Table 15.5](#) presents performance factors based on these data. Notice the relatively high thermal efficiencies, due mainly to the high temperature of the waste brine. The absolute utilization efficiencies (based on inlet exergy) are not very high, but the functional efficiency (based on the change in brine exergy) is impressive.

The separator pressure is kept high to mitigate the silica scaling problems owing to the very hot reservoir condition. The injection pumps are a consequence of a tight formation that produces geofluid with “excess enthalpy” wherein the mass fraction of steam at the wellhead exceeds the isenthalpic value. One final note relates to the actual brine flow to the binary plant being less than the design value, 243.6 kg/s versus 300 kg/s. This is typical of high-temperature liquid-dominated reservoirs which tend to dry out under exploitation. Bottoming binary plants should be designed to accommodate changes in brine flow as much as is feasible.

TABLE 15.3 Technical details and performance for Berlin power units.

	Units 1 & 2	Unit 3	Unit 4
Start-up year	1999	2006	2007
Type	Single-flash	Single-flash	Binary
Power rating, MW	2 × 28.12	40	8.3
Maximum power, MW	2 × 31.49	44.2	9.2
Resource temperature, °C	280–300	280–300	180
Geofluid mass flow ^a , kg/s	~200	NA	300
Working fluid	Geofluid	Geofluid	Isopentane
<i>Turbine:</i>			
Type	Axial-flow	Axial-flow	Radial-inflow
Cylinders	1	1	1
Flows/turbine	1	2	1
Stages/flow	9	7	1
Inlet pressure, bar,a	9.5	NA	See Table 15.4
Inlet temperature, °C	177.7	NA	See Table 15.4
Working fluid mass flow ^a , kg/s	50.0	NA	See Table 15.4
Exhaust pressure, bar,a	0.10	NA	See Table 15.4
Last-stage blade height, mm	581	NA	NA
Speed, rpm	3600	3600	6500
Isentropic efficiency, %	82.2	NA	80.4
<i>Generator:</i>			
Voltage, kV	13.8	13.8	13.8
Power, MVA	37.05	51.76	12.5
Power factor	0.85 (lagging)	0.85 (lagging)	0.80 (lagging)
No. of poles	2	2	4
Speed, rpm	3600	3600	1800
<i>Condenser:</i>			
Type	DC, low-level	DC, low-level	Shell-and-tube
CW flow, kg/s	1826	NA	1013
CW temperatures, °C:			
Inlet	29	NA	28.3
Outlet	42.8	NA	38.3
Wet bulb	15	15	23.9
<i>Cooling tower:</i>			
Type	Mechanical induced draft, crossflow		MID, counterflow
No. of towers ^a	1	2	1
No. of cells per tower	3	3	2
Fan power, kW, per cell	NA	NA	105
<i>NCG system:</i>			
Steam ejector	Yes	Yes	No
Trains	2	NA	
Stages	2	2	
Steam flow, kg/s	0.975	2.906	
NCG flow, kg/s	0.20	6.64	
Vacuum pump	Yes	Yes	No
power, kW	NA	NA	
<i>Plant performance:</i>			
Gross SSC, (kg/s)/MW	1.78	NA	See Table 15.5
Net SSC, (kg/s)/MW	1.92	NA	See Table 15.5
Utilization efficiency ^b , %:			
Gross	41.4	NA	See Table 15.5
Net	36.9	NA	See Table 15.5

^aData is per unit.^bBased on the exergy of the geofluid in the reservoir; dead state is at the wet-bulb temperature.

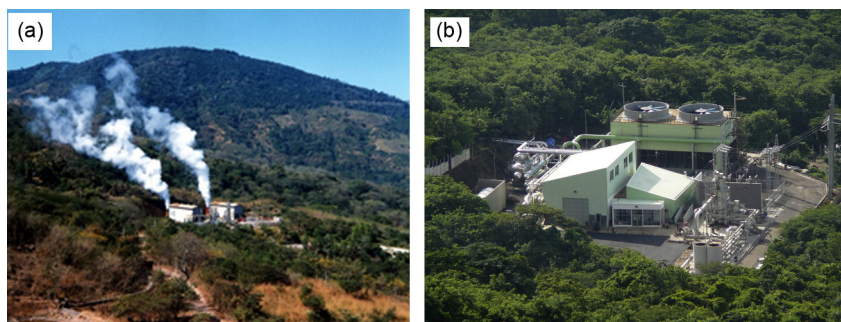


Figure 15.13 (a) Back-pressure units, 1992–1999; (b) Unit 4 bottoming binary unit. (a) Photo by author, January 1998; (b) Photo courtesy of ENEX, thanks to Alexander Richter and Friðrik Ómarsson [WWW].

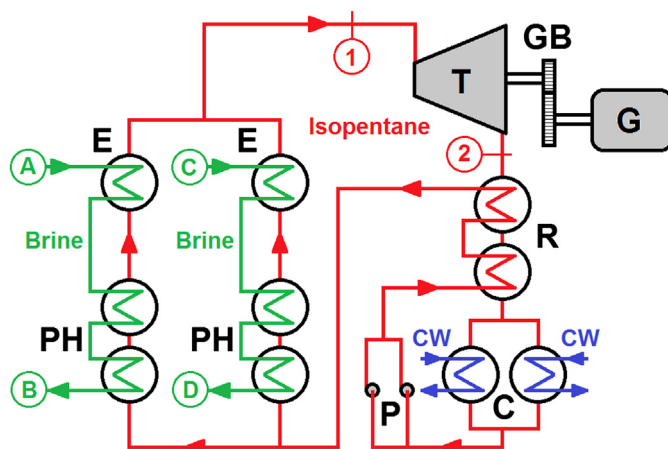


Figure 15.14 Flow diagram for Berlín binary unit; see Nomenclature [WWW].

15.3.3 PROSPECTS

The two sites deemed the best prospects for the next development are San Vicente and Chinameca; see Figure 15.5. Four exploratory wells have been completed at each site, which indicate moderate temperature resources with adequate permeability. An experiment at Berlín using solar collectors to raise the temperature of the waste brine from the bottoming binary plant is ongoing; increasing the brine temperature prior to reinjection might alleviate silica scaling in the formation [4].

TABLE 15.4 Unit 4 conditions for a generator output of 9170 kW, November 4, 2010.

State	Temperature	Pressure	Entropy	Enthalpy	Mass flow
	°C	bar,a	kJ/kg · K	kJ/kg	kg/s
<i>Brine</i>					
A	183.2	19.68	2.1689	777.64	194.39
B	135.5	18.70	1.6908	570.91	194.39
C	181.5	10.60	2.1537	769.69	49.16
D	138.4	10.07	1.7219	582.73	49.16
<i>Isopentane</i>					
1	162.3	20.8	1.4189	552.43	133.0
2	103.5	2.15	1.4655	481.35	133.0
<i>Dead state</i>					
0	25	0.9785	0.3672	104.83	—

TABLE 15.5 Thermal and utilization efficiencies for binary plant based on [Table 15.4](#).

Heat input		Exergy input	
HP brine, kWt	40,186	HP brine, kW	26,367
LP brine, kWt	9,191	LP brine, kW	6,500
Total heat, kWt	49,377	Total exergy in, kW	32,867
Power terms		Exergy discharged	
Generator, kW	9,170	HP brine, kW	13,890
Turbine, kW	9,454	LP brine, kW	3,638
Pump, kW	631.6	Total exergy out, kW	17,528
Net cycle, kW	8,538	Brine exergy change, kW	15,339
CT fans, kW	105.1		
Net plant, kW	8,328		
Thermal efficiencies		Utilization efficiencies	
Cycle thermal, gross	0.186	Cycle absolute, gross	0.279
Cycle thermal, net	0.173	Cycle absolute, net	0.260
Plant thermal, net	0.169	Plant absolute, net	0.253
		Plant functional, net	0.543

15.4 Nicaragua

By some estimates, Nicaragua holds the highest potential for geothermal power generation in Central America, with 1750 MW mentioned as the most likely value from a range of 300–4000 MW [12]. Political instability and a weak economy have hindered development, but recently private companies have been solicited by the government to participate in exploration and construction of geothermal plants. Momotombo and San Jacinto-Tizate are the sites of the two plants; see Figure 15.15.

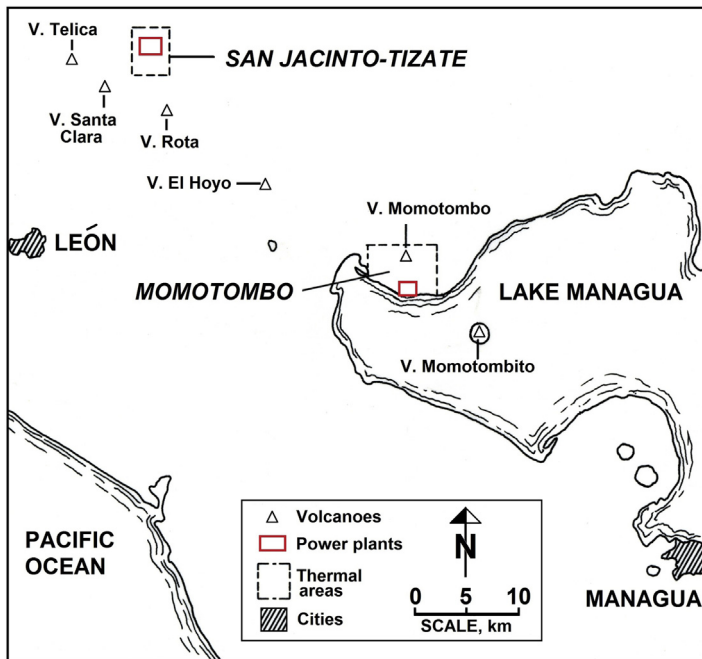


Figure 15.15 Locations of Nicaragua's two geothermal power stations [WWW].

15.4.1 MOMOTOMBO STATION

Momotombo was the first field to be brought into commercial power generation in Nicaragua. Currently the plant comprises two 35 MW single-flash units and a 7.5 MW bottoming binary unit. These are owned and operated by a locally-owned

company, Momotombo Power Company (MPC). Electricity is sold to the government electric authority, Empresa Nicaragüense de Electricidad (ENEL), through a power purchase agreement. The two flash units were installed in 1983 and 1989, but the field was overexploited during the civil war of the 1980s and the plant suffered greatly from lack of maintenance. By 1999 the running capacity had fallen to 8–10 MW. With a new operator, new deeper wells drilled, full reinjection of produced brine, the addition of the 7.5 MW binary unit, and improved reservoir management, the station now generates 30–35 MW. Continuing work is directed at restoring the full capacity of 77.5 MW [15]. Figure 15.16 shows the well locations and the power plants.

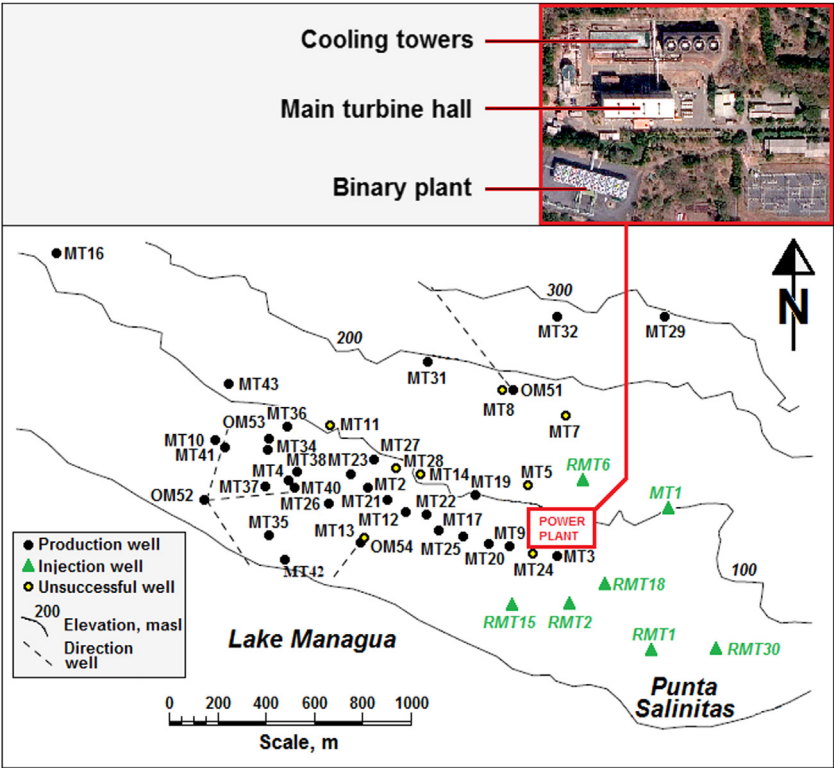


Figure 15.16 Locations of wells and power plants at Momotombo; the unsuccessful wells failed for a variety of reasons. Map after Ref. [15]; image from Google Earth, 1-15-2010 [WWW].

15.4.2 SAN JACINTO PLANT

Discovery wells were drilled at San Jacinto in the mid-1990s and confirmed a hot resource with temperatures from 260°C to 290°C. Polaris Geothermal, which became Ram Power, performed the early development work. Two 5 MW back-pressure units were first installed to provide site power and early revenues while the well-drilling program was under way. Currently two single-flash 36 MW condensing units are in operation, albeit with somewhat less steam than the design amount. The plant has a running capacity of about 50 MW. An overview of the plant is shown in [Figure 15.17](#). The current owner is Polaris Energy Nicaragua S.A. (PENSA).



Figure 15.17 San Jacinto-Tizate power plant overview; January–February 2014. Photo by F.K. Garcia Peralta, used with permission of the Geothermal Resources Council [WWW].

15.4.3 PROSPECTS

Although the El Hoyo-Monte Galán geothermal area has long been thought of as an excellent prospect having perhaps as much as 150 MW potential, exploratory drilling has revealed a moderate temperature resource, about 220°C at 2000 m depth, but with low permeability. All of the potential geothermal areas are shown in [Figure 15.18](#).

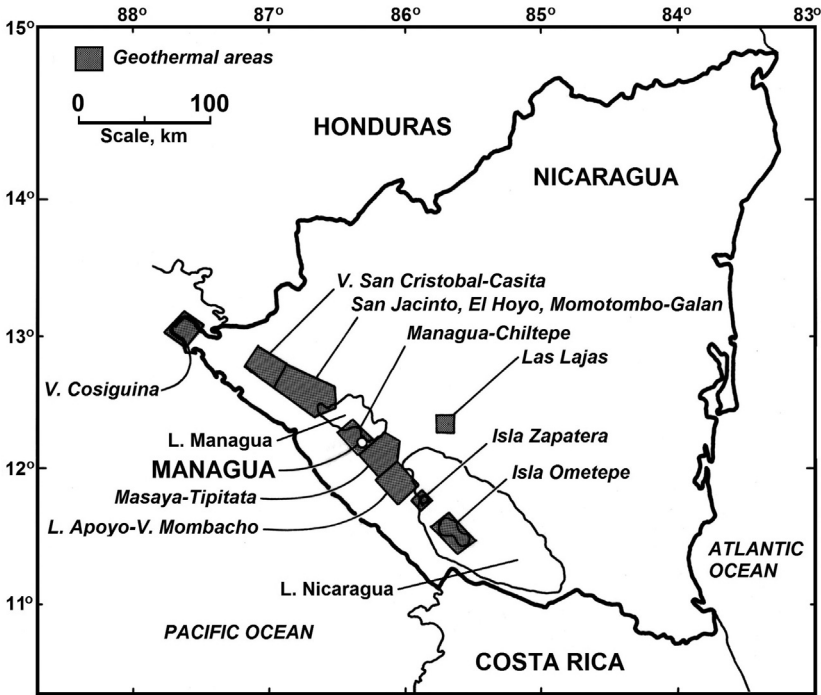


Figure 15.18 Geothermal areas of Nicaragua [5].

15.5 Costa Rica

Costa Rica has an estimated most probable geothermal power potential of 1000 MW, but many of the best areas are located in national parks and therefore off-limits for exploitation; see [Figure 15.19](#). Therefore, it will be a challenge to increase the installed capacity from the current value of 205 MW.

15.5.1 MIRAVALLS STATION

The Miravalles power station was covered extensively in Ref. [16]. The focus here will be on the new power plant at Las Pailas in the vicinity of the Rincon de la Vieja (RDLV) volcano.

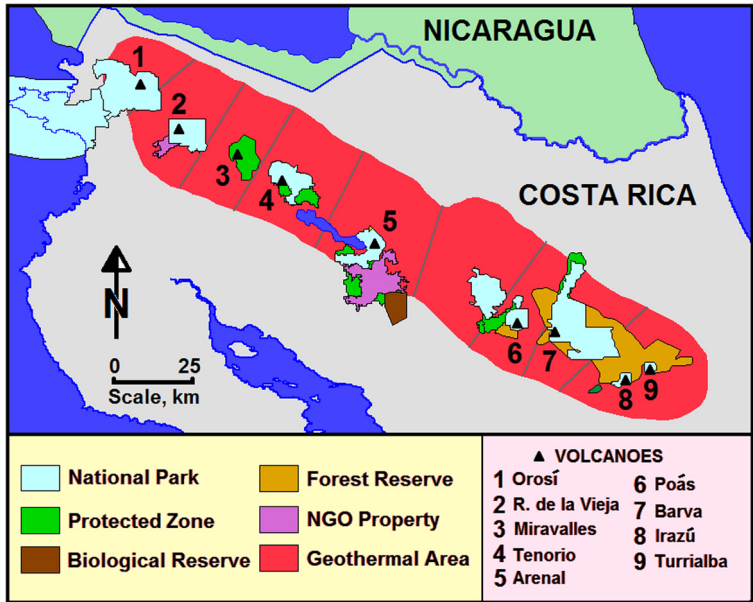


Figure 15.19 Geothermal areas vis-à-vis national parks and other protected areas [1] [WWW].

15.5.2 LAS PAILAS PLANT

Las Pailas is the name of both the hot spring/mud pot/fumarole area within the RDLV national park and the geothermal power plant that lies about 2 km from the park entrance and the thermal manifestations; see [Figure 15.20](#).

The power plant uses a binary cycle in which the two-phase geofluid from the wells is first separated, as in a flash plant, but here both the liquid and the vapor are used in heat exchangers to raise vapor for use in the turbine of the binary cycle. The working fluid is normal pentane, C_5H_{12} [17]. The cycle uses two pressure levels at the inlets to the two turbines and includes recuperators to improve the thermal efficiency, as shown in [Figure 15.21](#). Owing to the asymmetry of the recuperators, only the HP-side of the cycle benefits from the internal heating (processes 6–7–8); therefore, the process cycles are not identical for the left and right sides of the plant, as can be seen in pressure-enthalpy coordinates in [Figure 15.22](#). The performance assessment may be carried out using the equations presented in earlier sections of this book, and the results are summarized in [Table 15.6](#).

While the thermal efficiency is high but not spectacular, the utilization efficiencies are quite respectable. The functional efficiency indicates that the plant is able to convert a little over half of the exergy contributed by the geofluid into useful electrical power.



Figure 15.20 Aerial view of Las Pailas power plant, some wells, and a small part of the RDLV national park. *Image from Google Earth, 3-21-2014 [WWW].*

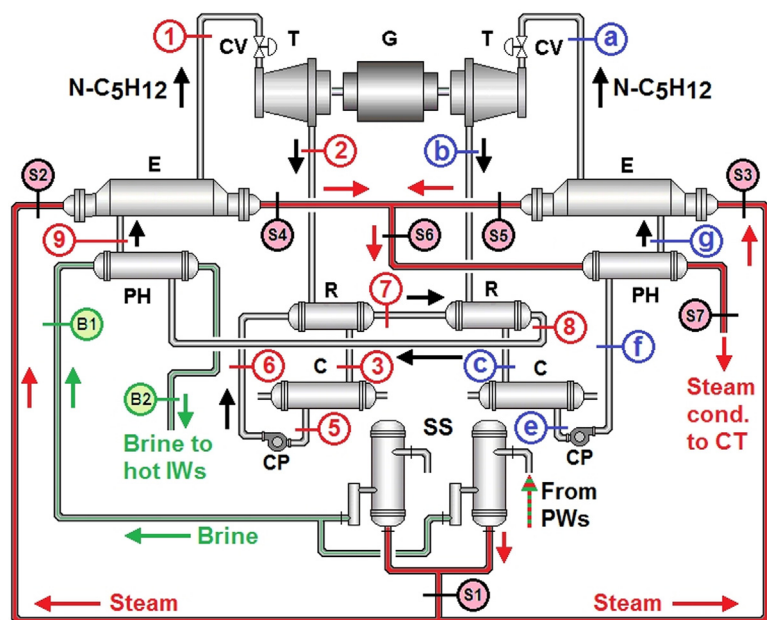


Figure 15.21 Flow diagram for one of two identical 21 MW units at Las Pailas [17]; see Nomenclature [WWW].

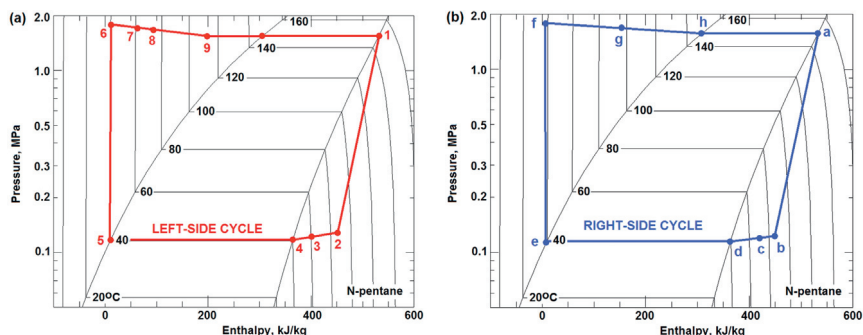


Figure 15.22 Pressure-enthalpy diagrams for the (a) left and (b) right sides of the cycle [17] [WWW].

TABLE 15.6 Summary analysis of Las Pailas power plant [17].

First Law analysis

Net Rankine cycle power, kWe	19,618
Heat into left preheater from brine, kWt	17,934
Heat into left evaporator from steam, kWt	46,707
Heat into right preheater from condensate, kWt	18,424
Heat into right evaporator from steam, kWt	46,707
Total heat rate into cycle, kWt	129,772
Thermal efficiency	0.151

Second Law analysis

Dead-state temperature, °C	25
Dead-state pressure, MPa	0.093
Exergy rate delivered by steam, kW	33,102
Exergy rate delivered by brine, kW	19,588
Total exergy input rate, kW	52,690
Exergy or utilization efficiency	0.372
Exergy rate discharged by steam condensate, kW	144.2
Exergy rate discharged by brine, kW	14,234
Total exergy rate discharged, kW	14,378
Total geofluid exergy change, kW	38,312
Functional exergy efficiency	0.512

15.5.3 PROSPECTS

Owing to the co-location of all of the good geothermal prospects with protected areas, as shown in Figure 15.19, there is little likelihood of new developments. Miravalles has essentially reached its capacity limit. It is hoped that expansion of the Las Pailas plant will occur and has received funding for further drilling. However, that field is restricted not only by the national park boundary but also by a protected NGO area, significantly limiting the possibility for additional drilling. Borinquen, an adjacent area 9 km northwest of Las Pailas, is also under investigation; exploratory

wells have shown high temperature but low permeability. Thus, unless the Costa Rican government relaxes its constraints on work within national parks and other protected areas, there will be little expansion of geothermal power.

15.6 Guatemala

Guatemala is yet another Central American country endowed with spectacular and active volcanoes that can bring benefits through geothermal power as well as destruction through devastating eruptions. The capital city of Guatemala has four dangerous volcanoes within about 35 km to the south and west: Acatanango, Fuego, Agua, and Pacaya. The last of these has been in continuous eruption for the last 50 years. The most recent major eruption of Pacaya in May 2013 partially buried one of the two geothermal power plants in the country, the 20 MW binary plant at Amatitlán that is less than 3 km from the volcano. No significant damage was sustained, but it took a coordinated and reciprocal effort by the plant operators and neighbors to remove ash from the power facilities and the nearby residences.

15.6.1 ZUNIL

The Zunil plant is located in the northwest of the country about 7 km south of the major city of Quetzaltenango. The plant is situated some 1150 m below a steep cliff within a horseshoe-shaped hollow that likely was the site of at least one ancient landslide. A deadly one occurred on January 5, 1991 that devastated a small agricultural community living within the well field; see Section 23.5.3. In such rugged terrain, it is quite a challenge to locate well pads; one has to build roads along precipitous slopes and cut-and-fill to level the land to support a drill rig. Nevertheless, several wells, mainly directionally drilled, have been completed to supply a steam–brine binary plant of 24.6 MW capacity. As of January 2014, the plant was limited to about 10–12 MW owing to a shortfall of geofluid [18].

The power plant at design conditions receives 58.3 kg/s of steam and 112.8 kg/s of brine at 182°C and 10.5 bar_a. This is used in seven identical organic Rankine cycle units to generate 24.6 MW_{net}. Air-cooled condensers are used along with seven synchronous generators turning at 1800 rpm producing three-phase power at 60 Hz and 13.8 kV [19]. For these conditions, the plant would have a design thermal efficiency of 13.9% assuming a geofluid discharge temperature of 100°C, an absolute utilization efficiency of 39.0%, and a functional utilization efficiency of 43.0%, assuming a dead-state temperature of 25°C.

Although the reservoir is hot (~300°C), the permeability is low which leads to production of steam at the expense of brine, thereby depriving the binary plant of the liquid it was designed to receive. Furthermore, the reinjected liquid does not support the reservoir pressure which exacerbates the problem of flashing in

the formation. The plant installer, Ormat, now has a contract with the Guatemalan electric authority to generate power until 2034 and will seek ways to increase geofluid flow and the power output of the plant.

15.6.2 AMATITLÁN

Lying as close as it does to the active Pacaya volcano, the Amatitlán reservoir is hot, about 285°C. Two wellhead units were installed during the field development phase as soon as sufficient steam was available. Both were 5 MW back-pressure units; the first ran from 1998 to 2001 and the second from 2002 to 2006. Then the central plant was installed and began delivering electricity in 2007. The wells produce a two-phase, liquid-vapor mixture that is separated and used in heat exchangers to drive a binary plant. The plant has a capacity of 25.2 MW but is rated at 20 MW. It has a 1.2 MW back-pressure steam turbine that discharges to two identical binary units, each with a single generator driven by two axial-flow turbines one on either side [20]. Each binary unit has a capacity of 12 MW. The turbines from each unit exhaust into a 36-cell air-cooled condenser; Figure 15.23 shows the plant. Five production wells serve the plant which is owned by the Empresa de Generacion de Energia Electrica (EGEE), a subsidiary of the Instituto Nacional de Electrificación (INDE), and operated by Ormatitlán, a subsidiary of Ormat Technologies, Inc.



Figure 15.23 Amatitlán 20 MW steam–brine binary power plant. *Photo courtesy of Ormat Technologies, Inc. [21] [WWW].*

15.6.3 PROSPECTS

The best prospects are aligned with the string of coastal volcanoes in the southern part of the country, from San Marcos in the western highlands to Moyuta, just inside the border with El Salvador and close to Ahuachapán, as shown in

Figure 15.24. Of these, the El Ceibillo field (within the Amatitlán area) and Tecuamburro appear to be the most promising. Tecuamburro is estimated to hold 50 MW potential, while El Ceibillo is on track to have a 25 MW plant installed in late 2015. A deep exploratory well EC-1 reached a temperature of 275°C, higher than anticipated. The data from EC-1 and several temperature-gradient wells are being analyzed and will result in a drilling plan.

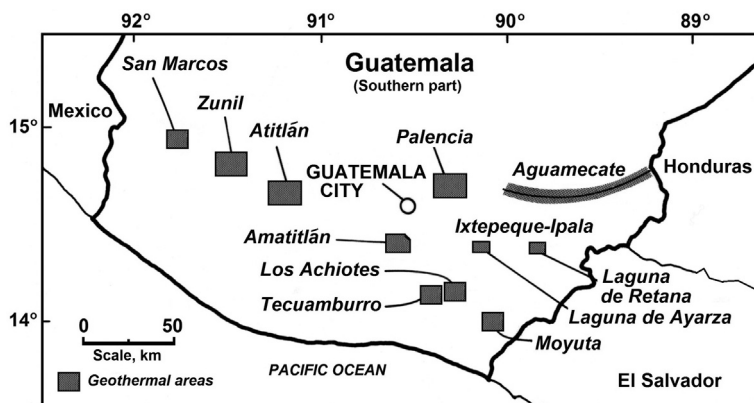


Figure 15.24 Geothermal prospects in Guatemala [5].

15.7 Other Central American Prospects

The prospects within those countries that already have operating geothermal power plants have been discussed in the preceding sections. However, Honduras and Panama may be on their way to join them. Each has a few sites that have drawn attention and may be developed to the point of commercialization.

In Honduras, there are five areas that have been extensively studied: Platanares, Azacualpa, Pavana, San Ignacio, and Sambo Creek. The first three sites are the most promising. From 1986 to 1988, three slim core holes were drilled at Platanares, two of which flowed roughly 5–10 kg/s from a reservoir at 160–165°C. The wells penetrated to only 650–680 m and thus gave information on the shallow formation. A preliminary analysis concluded that the resource could produce about 7 MW using only the shallow formation [22]. Further study has projected the existence of a deep reservoir at ~220°C and a power potential of 35 MW. Ormat Technologies, Inc. is developing Platanares and expects to have an 18 MW plant online by 2016, followed by a 17 MW plant a year later. Geopower S.A. has the concessions for Azacualpa and Pavana, both of which are at the prefeasibility stage.

In Panama, five sites have been studied: Barú-Colorado, Valle de Antón, Coiba Island, Tonosí, and Chitre de Calobre. However, results from exploratory

drilling at Barú-Colorado, close to the border with Costa Rica and thought to be the most promising site, have been disappointing. The first phase of drilling in 1976–77 involved six slim holes to roughly 1000 m and showed bottom-hole temperatures of only 100°C. Nevertheless, it has been estimated that a 24 MW plant may be possible there. The only other site for which a power estimate has been made is the Valle de Antón where a potential of 18 MW may exist. However, this area is environmentally sensitive with protected areas, and is a popular vacation area for people from Panama City [1,12].

15.8 Caribbean Islands

15.8.1 GUADELOUPE: BOUILLANTE

The only geothermal power plant in the Caribbean is the 15.7 MW flash plant at Bouillante on the French island of Guadeloupe. Small as it is, it supplies about 10% of the island's electricity. The plant is located in the heart of the coastal city, surrounded by residences and commercial establishments; see Figures 15.25 and 15.26. The geofluid is believed to be a mixture of sea water and rainwater that has percolated into the reservoir.

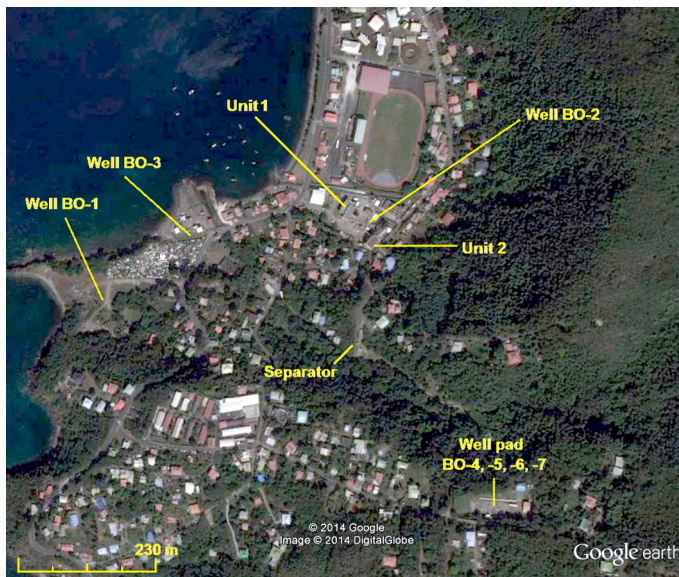


Figure 15.25 Aerial view of Bouillante, Guadeloupe, showing the power plant and well locations. *Image from Google Earth, 12-20-2012 [WWW].*

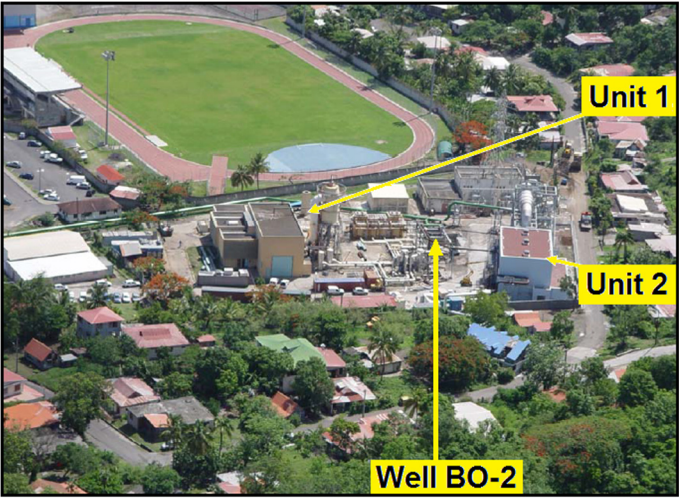


Figure 15.26 Bouillante power plant. Photo from Ref. [23]; labels by author [WWW].

The first survey of the site was done by BRGM in 1963, with the first wells sunk in 1969. Unit 1 was installed in 1986, followed by Unit 2 in 2004 after three new wells were drilled in 2001.

Unit 1 is a double-flash plant; Unit 2 is single-flash. The flow diagram and some process data for Unit 1 are shown in Figure 15.27 and Table 15.7,

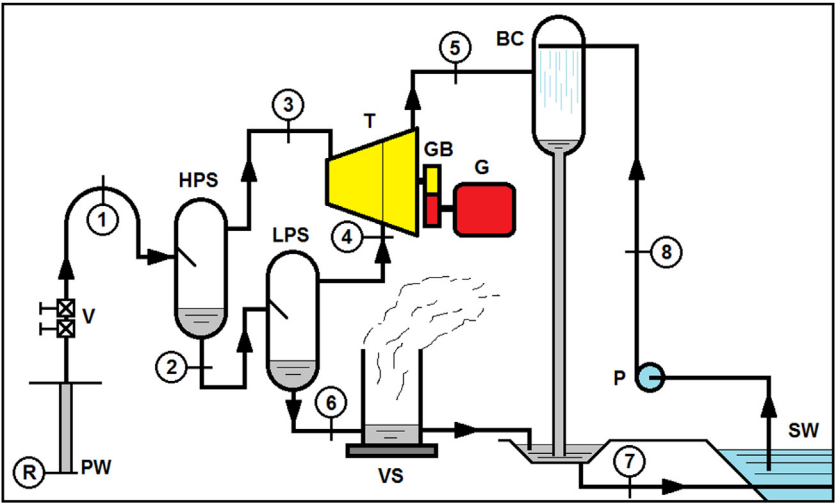


Figure 15.27 Flow diagram for Bouillante Unit 1; see Nomenclature. After Ref. [23] [WWW].

TABLE 15.7 Data for Bouillante Unit 1 [23].

State	Temperature	Pressure	Mass flow rate
	°C	bar _a	kg/s
R	250	NA	41.67
1	200	15.5	41.67
2	160	6.18	33.33
3	160	6.0	8.33
4	110	1.43	3.33
5	45	0.075	11.7
6	110	1.43	30.0
7	40	1.013	555.6
8	27.5	NA	527.8

respectively. The generator has a capability of 5300 kW and the net output is 4700 kW. The gross and net utilization efficiencies are 49.4% and 43.8%, respectively, based on the reservoir geofluid temperature of 250°C and a dead state at 27.5°C.

Unit 2 is rated at 11 MW and is supplied with geofluid from three wells. These are located upslope at an elevation of about 100 m a.s.l. The high-pressure separation occurs in an Icelandic-style horizontal separator (see Figure 5.9), with the low-pressure flash and separation taking place next to the powerhouse. Both plants use an external barometric condenser that takes cooling water directly from the Caribbean Sea. There is no reinjection to date and all excess geofluid is sent to the sea via a canal. Apparently the reservoir has not suffered because there is adequate natural recharge.

Of the seven wells drilled, only three are considered good producers: BO-2 (for Unit 1) and BO-5 and -6 (Unit 2). Wells BO-1 and -3 were drilled to 850 m depth, directly on the seashore and did not produce commercial amounts of geofluid. Well BO-4, a vertical well on the same pad as deviated wells BO-5, -6, and -7, is a poor producer but may be improved by stimulation. Well BO-7 found no permeability. Well BO-2 sits on the plant site between the two power units and lies above a very high-temperature part of the field; it is only 320 m deep but encountered 240°C fluid. The other deep wells found the same temperature between 700–800 m depth.

The challenges that were faced by the plant developers are common to all the volcanic islands in the Lesser Antilles. The terrain is steep and often rugged, placing limitations of where wells can be sited, piping installed, and the power plant located. Being close to the sea, the geofluid will likely contain a component of sea water that could result in problems of corrosion. Power equipment needs to be compatible with city life, that is, there should be minimal noise above ambient

levels, few discharges of steam, minimal visual impact, no ground water degradation, etc. The fact that Bouillante has achieved success under these tight constraints should be encouraging to others in the region.

15.8.2 OTHER CARIBBEAN PROSPECTS

There are several excellent prospects among these islands; they will be briefly described here, but a more detailed accounting may be found in Ref. [24]. These four are the most promising.

Dominica—Two sites are being studied, Wotten Waven and Soufriere/Galion. The former has already had a deep well drilled after slim holes were encouraging. The resource temperature is about 235°C at 1500 m depth. It is hoped that a plant in the power range of 10–15 MW might be possible which would be able to provide all the electricity needed by Dominica.

Montserrat—A massive volcanic eruption devastated much of the island in 1995, but that energy lies waiting to be tapped for geothermal power. Two deep exploratory wells have found temperatures of 295°C at about 2350 m depth. A 5 MW power plant is planned for operation in 2016.

St. Lucia—Detailed studies of the Soufriere area were carried out in the 1970s and 1980s. It was found that a 230°C resource was present at drillable depths, but the geofluid turned out to be highly acidic, creating materials problems for any development. There is also a shallow steam zone that may or may not be suitable for exploitation.

Nevis—Three small-diameter wells were drilled in 2008 to depths of between 782 and 1134 m in three areas: Spring Hill, Jessups, and Hamilton Estates. The wells recorded temperatures of about 225°C, but the projected resource temperature might exceed 260°C. The project is currently bogged down by a legal dispute about who has the right to develop the system. This is unfortunate since it is estimated that the resource could support 45 MW and the first phase would be a 10–15 MW unit. If the full potential can be developed, the power would be sufficient to meet the power requirements of Nevis, with enough left over to export to the nearby island of St. Kitts, thereby satisfying the electricity needs of both islands.

15.9 South American Prospects

There are no geothermal power plants anywhere in South America. Although the Andean region abounds with hot spots for geothermal development (see Figure 15.3), it is surprising that only one tiny geothermal plant has ever been installed, and it is no longer in operating condition.

15.9.1 ARGENTINA

A 670 kW geothermal unit was installed in 1988 at the Copahue field in Argentina, but was decommissioned in 1996. Located just 2.5 km east of the border between Argentina and Chile, 2 km south of the hot spring resort of Termas de Copahue, and 6.5 km east-northeast of the summit of the Copahue volcano, the power plant was a binary plant driven by steam from a single well; see [Figure 15.28](#). The plant has not been dismantled, but is in a deteriorated state; see [Figure 15.29](#).



Figure 15.28 Copahue power plant on the shore of Lake Mellizas with the Copahue volcano in the background, looking generally west. *Photo from Google Earth Panoramio No. 24447562 [WWW].*



Figure 15.29 (a) Copahue plant in disrepair with well blowing freely; (b) Abandoned binary unit heat exchangers and feed pump, c. 2012. (a) *Photo from Google Earth Panoramio No. 16514372 and (b) photo from Google Earth Panoramio No. 71686493 [WWW].*

There are four wells at Copahue, of which three are still in working condition. Table 15.8 gives some information on them. Well COP-3 was abandoned for environmental reasons [25]. The resource tapped by these wells is said to be a dry-steam reservoir, but additional, deeper wells over a wider area are needed to confirm that statement since it may be that the relatively shallow wells penetrated a steam cap.

TABLE 15.8 Data for Copahue wells [25].

Well	Depth	Bottom-hole temperature	Static pressure	Mass flow rate @WH pressure
	m	°C	MPa	kg/s@MPa
COP-1	1414	250	4.0	3.33@1.0; 4.17@1.4
COP-2	1240	235	3.5	1.67@0.6
COP-3	1067	240	4.0	13.9–16.7@1.0
COP-4	NA	235	4.0	13.9@1.0

The 670 kW plant was considered a demonstration unit and consisted of a packaged, skid-mounted, Ormat organic Rankine binary cycle with isopentane as the working fluid. It was fed by well COP-1 immediately adjacent to the powerhouse. The steam was at 166–171°C (saturated) carrying about 8% (wt.) of non-condensable gases and flowed at 1.86 kg/s. At that time the well was only 1000 m deep; it was later deepened to 1414 m.

The two-stage axial-flow turbine rotated at 3000 rpm and was coupled directly to a 400 V, 50 Hz generator. A multistage centrifugal pump circulated the isopentane working fluid from the condenser to the preheater. The shell-and-tube condenser received cooling water pumped directly from Lake Mellizas. Thus, there was no cooling tower. The warmed cooling water was discharged back into the lake. Based on the wellhead steam conditions and a dead-state temperature of 10°C at 2007 m a.s.l., the plant had a utilization efficiency of 40.9% at full power.

In order to meet the growing electrical demand in the popular tourist resort area of Copahue-Caviahue, there are plans to drill 4–5 more wells and install a 30 MW direct-steam power plant served by a water cooling tower [26]. Lake Mellizas will be a handy source of make-up water for the cooling tower, if permitted.

Two other areas in Argentina have been studied: Tuzgle in the far north and Domuyo, some 145 km north-northeast of Copahue.

15.9.2 CHILE

Chile holds an enormous potential of about 16,000 MW of geothermal power for 50 years using only resources in excess of 150°C and shallower than 3000 m.

Tolhuaca, in the central-southern volcanic region, is one of the most promising sites, having one well capable of 12 MW already in hand. A 70 MW power plant is possible there [27].

However, geothermal is the least recognized and understood renewable resource in Chile, and constitutes only a tiny fraction of perceived power potential relative to wind, solar, biomass, and small hydro [28]. The Chilean general public is wary of geothermal as a source of electricity, mainly from an accident at an old exploration well at the El Tatio geyser field, although geothermal energy is widely used for direct heat and recreational activities. A major effort is underway to explain the facts about geothermal energy so that informed decisions can be made regarding the approval of proposals for new power plants [29].

15.9.3 OTHER PROSPECTS

There are more than 70 geothermal areas in Bolivia with the most promising site being Sol de la Mañana, 25 km south of Laguna Colorada and only 15 km east of the border with Chile. The site lies about 30 km southeast of the world-famous geyser field of El Tatio in Chile. There is mining activity near Sol de la Mañana that could use the electricity generated by a geothermal plant. Six wells have been completed having a total flow rate of 100 kg/s. The resource temperature is 250–270°C and the potential is estimated to be 350 MW [2].

Colombia has one geothermal well drilled near the Nevados del Ruiz volcano but no actual development. Three areas have been studied in Ecuador but only one slim hole has been drilled. In Peru, six potential geothermal areas have been identified, but the work is in very early stages.

Altogether, it is estimated that about 30,000 MW of geothermal power might be available in the South American countries of Argentina, Bolivia, Chile, Colombia, Ecuador, and Peru, if the right technical, economic, environmental, and social conditions can be achieved.

References

- [1] Moya P. Geothermal development in central America. Geothermal resources council Trans., Vol. 38; 2014.
- [2] Lahsen A, Rojas J, Aravena D. Geothermal progress in South America. Geothermal resources council Trans., Vol. 37; 2013.
- [3] ENEL Press Release. Paris supreme court in favour of ENEL green power in El Salvador “Lageo” case, ENEL website, <http://www.enel.com/en-gb/media/press_releases/paris-supreme-court-in-favour-of-enel-green-power-in-el-salvador-147-lageo-148-case/r/1662424>; August 18, 2014.

- [4] Burgos J, Montalvo F, Gutiérrez H. El Salvador country update. Proc. world geothermal congress 2015, Melbourne, Australia, 19–25 April 2015.
- [5] DiPippo R. Geothermal developments in central America. *Geothermal Resour Counc Bull* 1986; 15:3–14.
- [6] Godfrey HF. *Your El Salvador guide*. New York, NY: Funk & Wagnalls; 1968. p. 121.
- [7] DiPippo R. DOE/RA/28320-1 Geothermal energy as a source of electricity: a worldwide survey of the design and operation of geothermal power plants, U.S. department of energy. Washington, DC: U.S. Government Printing Office; 1980.
- [8] Guidos J, Burgos J. Geothermal activity and development in El Salvador—producing and developing. Proc. short course on geothermal development and geothermal wells. UNU-GTP and LaGeo, Santa Tecla, El Salvador, March 11–17, 2012.
- [9] Comisión Ejecutiva Hidroeléctrica del Río Lempa. Informe Annual 1976, San Salvador, El Salvador, C.A., 1976, p. 13.
- [10] Mayorga H. Geothermal reinjection systems in El Salvador. Proc. short course on geothermal development and geothermal wells. UNU-GTP and LaGeo, Santa Tecla, El Salvador, March 11–17, 2012.
- [11] Ahuachapán Geothermal Power Station Unit 3, El Salvador, C.A. 40 MW, double-flash cycle. Fuji Electric Co., Ltd., GEC 81a, September 1995.
- [12] Cuellar G. Central America Region—current generation and future plans. *Geothermal resources council Trans.*, Vol. 37; 2013.
- [13] Monterossa M. Sustainability analysis of the Berlín geothermal field, El Salvador. SIMS: The 53rd Scandinavian conference on simulation and modeling, Reykjavík, Iceland, October 4–6, 2012.
- [14] Japan Consulting Institute. Consulting service report for investigation of Berlín geothermal power plant in republic of El Salvador. Fuji Electric Systems Co., Ltd.; March 2011.
- [15] Porras M, E.A. Twenty-five years of production history at the Momotombo geothermal field, Nicaragua. Proc. U.N. geothermal training programme, 30th anniversary workshop, August 26–27, 2008, Reykjavik, Iceland.
- [16] DiPippo R. *Geothermal power plants, 3rd. Ed.: principles, applications, case studies and environmental impact*. Oxford, England: Butterworth-Heinemann/Elsevier; 2012 [Chapter 16].
- [17] DiPippo R, Moya P. Las Pailas geothermal binary power plant, Rincón de la Vieja, Costa Rica: performance assessment of plant and alternatives. *Geothermics* 2013;48:1–15.
- [18] Ormat Technologies, Inc. Ormat extends PPA for its Zunil power plant in Guatemala by additional 15 years. Reno, NV, <<http://www.ormat.com/news/latest-items/ormat-extends-ppa-its-zunil-power-plant-guatemala-additional-15-years>>; January 22, 2014.
- [19] Ormat Technologies, Inc. Binary geothermal power plant, Zunil, Guatemala. Sparks, NV, undated brochure.
- [20] Global Energy Observatory. Amatitlán geothermal power plant Guatemala, <<http://globalenergyobservatory.org/geoid/43655>>; August 19, 2012.
- [21] Ormat Technologies, Inc. Amatitlán. <<http://www.ormat.com/case-studies/amatitlanguatemala>>; 2007.
- [22] DiPippo R, Goff F. Platanares geothermal field, Honduras—preliminary power assessment of the shallow reservoir. *Geothermal Sci Technol* 1994;4:19–35.
- [23] Beutin P, LaPlaigne P. Geothermal development in the Caribbean—Bouillante plant presentation. Eastern Caribbean Geothermal Energy Project, Roseau, Dominica, March 15–17, 2006.
- [24] Hutter G, LaFleur J. 2015 Country update for Eastern Caribbean nations. Proc. world geothermal congress 2015, Melbourne, Australia, 19–25 April 2015.
- [25] Mas LC. Present status of the Copahue geothermal project. Proc. world geothermal congress 2005, Antalya, Turkey, 24–29 April 2005.

- [26] Clean Development Mechanism, Document form (CDM PDD)—version 03. Copahue geothermal project. Project design ver. 01, August 22, 2010.
- [27] Lahsen A, Rojas J, et al. Geothermal exploration in Chile: country update. Proc. world geothermal congress 2015, Melbourne, Australia, 19–25 April 2015.
- [28] CORFO. Estado de Proyectos ERNC en Chile (state of non-conventional renewable energy projects in Chile). Reporte CER, Enero 2013 (in Spanish).
- [29] Otero S. Fighting the information gap and the steam monster, the Chilean experience on geothermal outreach. Proc. world geothermal congress 2015, Melbourne, Australia, 19–25 April 2015.

Nomenclature for Figures in Chapter 15

BC	Barometric condenser
BCV	Ball check valve
BRGM	Bureau de Recherches Géologiques et Minières
C	Condenser
CP	Condensate pump
CT	Cooling tower
CV	Control valve
CW	Cooling water
DC	Direct contact
E	Evaporator
F	Flasher
G	Generator
GB	Gear box
HPGH, LPSH	High-, low-pressure steam header
HPS, LPS	High-, low-pressure separator
IW	Injection well
MID	Mechanical induced draft
MR	Moisture remover
NCG	Noncondensable gases
NGO	Non-Governmental Organization
P	Pump
PH	Preheater
PW	Production well
R	Recuperator
SS	Separator station
SSC	Specific steam consumption
SW	Sea water
T	Turbine
V	Valve
V/S	Vent/silencer
WH	Wellhead



Chapter 16

Geothermal Power Plants in Nevada, USA

Chapter Outline

16.1 Geologic Setting	462
16.2 Brief History of Development	466
16.3 Steamboat Geothermal Power Complex	468
16.4 Flash Plants	471
16.4.1 Beowawe	471
16.4.2 Desert Peak 1	473
16.4.3 Dixie Valley	475
16.4.4 Brady Plant 1	477
16.5 Binary Plants	478
16.5.1 San Emidio	478
16.5.2 Soda Lake Plants 1 and 2	480
16.5.3 Desert Peak 2	480
16.5.4 Salt Wells	481
16.5.5 Blue Mountain	482
16.5.6 Beowawe Binary	484
16.5.7 Dixie Valley Bottoming Binary Plant	485
16.5.8 Jersey Valley, McGinness Hills, and Tuscarora	485
16.5.9 Patua	488
16.6 Stillwater Plants	489
16.6.1 Stillwater 1	489
16.6.2 Stillwater 2	491
16.6.3 Hybrid Geothermal–Solar Systems	491
16.7 Lessons Learned from Nevada’s Experience	495
References	496
Nomenclature for Figures in Chapter 16	498

Behold! A steamboat in the desert.

Mark Twain legendarily exclaiming about Steamboat Hot Springs when he observed steam issuing forth from the earth, reminding him of steam-chugging, paddle-wheelers on the Mississippi River, c. 1862

16.1 Geologic Setting

The state of Nevada lies within the Basin and Range geologic province. As such, across the state one encounters a succession of mountain ranges and valleys, generally oriented north-south or NNE-SSW. It has been shown that all the high-temperature systems ($>160^{\circ}\text{C}$) and many moderate-temperature ones ($100\text{--}160^{\circ}\text{C}$) reside within two structurally controlled belts that span the state along SW-NE axes: the Black Rock Desert (BRD) and the Humboldt structural zone (HSZ); see Figure 16.1 [1,2]. Two other belts exist on either side of these that encompass geothermal systems in the adjacent states of California, Oregon, Idaho and Utah.

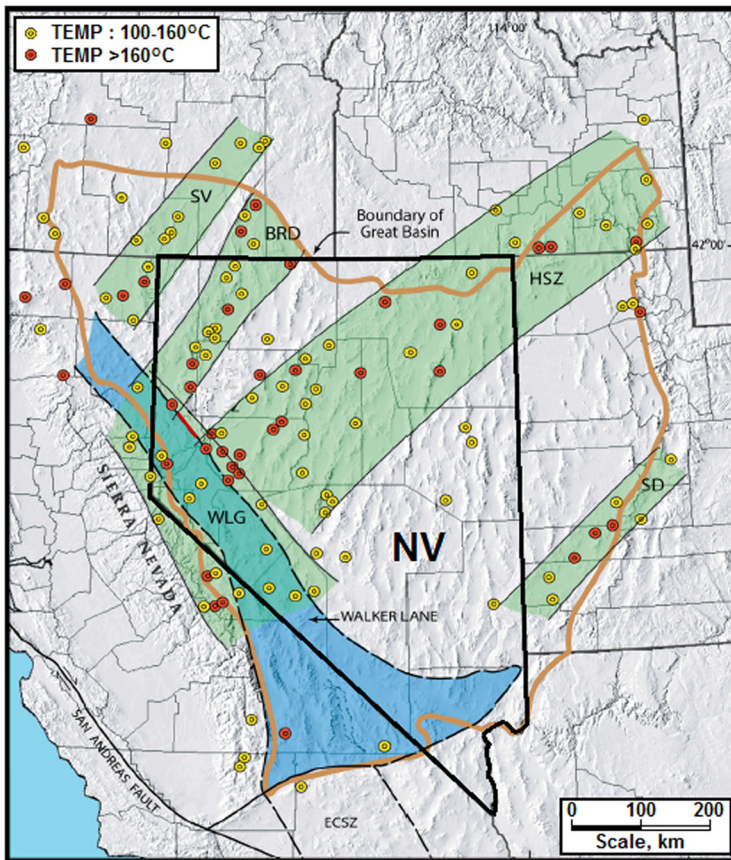


Figure 16.1 Nevada and the Basin and Range Province, showing regions of structural control that encompass high-temperature geothermal resources in Nevada and adjoining states. After Ref. [1] [WWW].

There is no active volcanism within Nevada, but traces of ancient thermal activity can be found in some places. Owing to tensional effects, thinning of the earth's crust provides higher than normal temperature gradients. Additionally, valleys tend to be bounded by normal faults associated with ranges on either side. Range faults may be identified by hot springs, of which Nevada has 312, the most of any state in the United States, or by deposits from ancient geothermal activity [3]. Geothermal prospects lie along these fault systems and draw their geofluids from deep circulation along permeable sections of those faults and secondary fractures. The systems tend to be isolated and relatively small. They are a challenge to exploit because they tend to diminish in size with depth [4].

There is one apparent exception to this general pattern—the Steamboat Springs resource that lies 16 km south of downtown Reno. Here one finds a large hydrothermal system associated with an ancient volcano, perhaps 1–2 million years old. The reservoir consists of a massively faulted and fractured formation that extends over a considerable area that includes rhyolitic domes, as contrasted with the range-fault systems that tend to be narrowly constrained along the main fault. Geofluid flow in the formation is controlled by a fault system trending generally NNE-SSW with several minor fractures; production is found within fractured volcanics and granodiorites. Hot fluid rises from beneath the Steamboat Hills area and spreads toward the NNE along the regional fault structure.

The Steamboat area hosted numerous thermal manifestations prior to geothermal power development, including geysers; see Section 5.7. All surface manifestations have largely vanished, save for a few small fumaroles near the center of the field and slight steaming in the fissures running along the sinter terrace that abuts US Highway 395A. There was also a mercury mine, now abandoned, within the area encompassed by several power plants [5].

Many homes and a few commercial establishments, including a major resort hotel, receive their heating and even cooling from a shallow warm-water aquifer, the Moana Springs Geothermal Resource Area, about 5–6 km south of Reno.

Many of Nevada's geothermal prospects are hidden (i.e., no obvious surface thermal manifestations) requiring exploration techniques that can detect normal faults and fault intersections as these may lead to high permeability. Figure 16.2 shows faults and intersections together with geothermal power plants installed as of 2014 [2]. Note that systems marked in darker shade (in red in the on-line version) have temperatures of at least 150°C, usually thought to be the minimum for commercial power plants. However, with advances in binary technology resources down to 100°C and even lower have recently been used to generate power.

A consequence of the geologic structure of a typical Nevada geothermal reservoir is often the lack of permeability as one moves away from the productive fault. There may be zones of secondary permeability close to the fault, and in some cases at intersections of faults orthogonal to the main fault, but often it is a

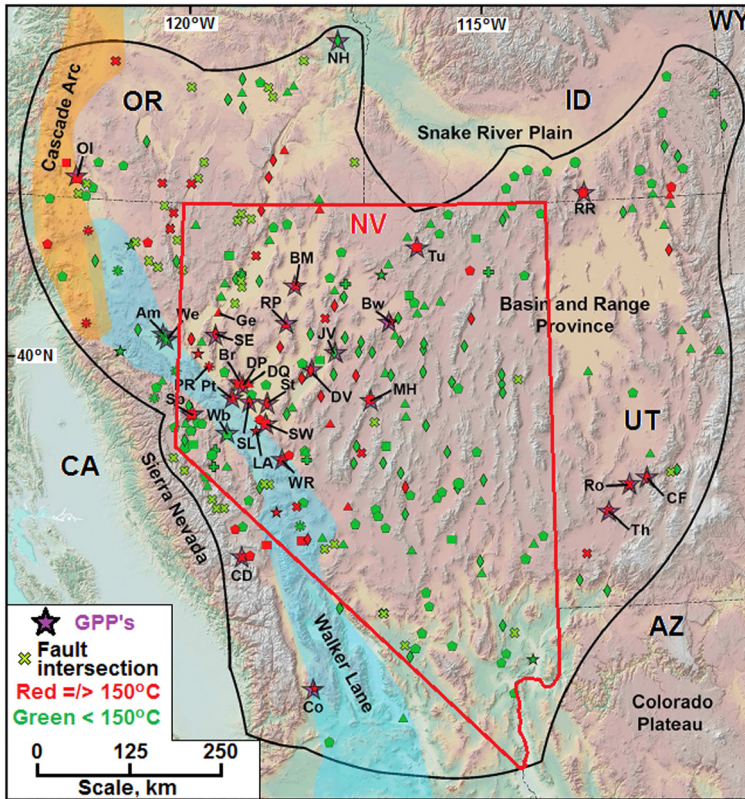


Figure 16.2 Nevada geothermal prospects and power plants; see [Figure 16.3](#) for plant names; see Ref. [2] for a description of all geologic symbols. Modified from Ref. [2] [WWW].

challenge to find areas where successful reinjection wells can be drilled. These must be in rocks of decent permeability but sufficiently distant from the production zone to avoid excessive cooling of the production zone. This factor by itself can limit the productive capacity of a power plant since all of the geofluid produced must be fully reinjected by law.

Ancient hydrothermal activity along faults carried minerals up toward the surface and deposited them in veins. Nevada is called “The Silver State” with good reason. Both gold and silver along with many other important and valuable minerals and industrial materials have been mined all over the state for over 165 years. [Figure 16.3](#) shows only the northern part of the state together with all geothermal plants and relatively nearby gold and silver mines. The hydrothermal processes that led to gold and silver deposition also created geothermal systems.

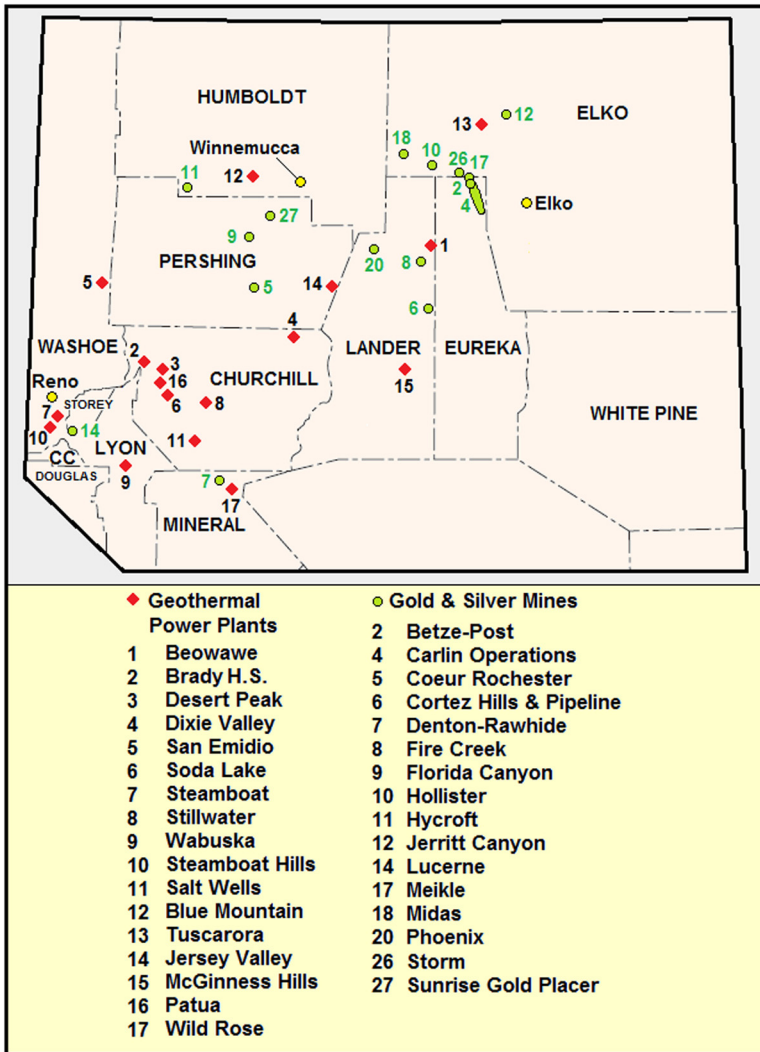


Figure 16.3 Map of northern Nevada showing geothermal power plants and mines producing gold and silver; many more mines exist but only those in the vicinity of geothermal plants are shown. Note that No. 17 Wild Rose was renamed Don A. Campbell plant. *Map modified from Ref. [6] [WWW].*

The proposition has been put forth [4] that the epithermal mineral deposition processes are still going on, and that the best geothermal productivity will be found by targeting the hottest places in the geothermal area. Such places are the “stems” of the hydrothermal system where the permeability is the greatest and the liquid is

flowing fastest toward the surface. Indeed some geothermal prospects, including Blue Mountain, Dixie Valley, and Rye Patch (Humboldt House), among others, were discovered coincidentally from drillings intended to find ore deposits.

16.2 Brief History of Development

An excellent survey of Nevada's geothermal energy history and the situation as of 2012 can be found in Ref. [7]. The first geothermal plant in Nevada was the 500 kW skid-mounted binary unit at Wabuska in 1984. The presence of hot springs at the site drew the attention of developers and led to the installation of the power plant. The plant is part of Tad's Enterprises and now consists of two small units with a rated capacity of 5.6 MW, but operates at only 1.2 MW (net) as of 2013.

By 1985 there were plants operating at Beowawe and Desert Peak. There were plans to move the US DOE 5 MW Raft River dual-boiling binary plant (see Chapter 20) and operate it at Brady Hot Springs. (*Note:* The literature is not consistent in the name of Brady Hot Springs. In various sources it is called "Brady's" or "Bradys," or "Brady." Here the latter name will be used.) The Raft River facility was sold to Hydra-Co Enterprises in a GSA disposal sale for \$750,000 in July 1984. In 1985, Munson Geothermal acquired the facility, dismantled it, and shipped it to Brady where it was to be reassembled; see [Figure 16.4](#). That plant and a number of simple binary units that had been installed at Lakeview in Oregon were intended to be part of the 9.9 MW Brady Geo Park Power Project



Figure 16.4 Raft River dual-boiling plant partially reassembled at Brady Hot Spring. Photo by author October 1991; compare with [Figures 20.11 and 20.12](#) [WWW].

that was expected to be online in 1986 [8]. But this ambitious effort was never completed. Brady saw its first power plant in 1992, a 17 MW three-unit double-flash system; see [Section 16.4.4](#).

By the end of the twentieth century, besides the plants just mentioned, there were plants operating at San Emidio (aka Empire), Steamboat (both binary and flash units), Soda Lake, Stillwater, and Dixie Valley. The sites at Desert Peak, Soda Lake, and Stillwater were blind resources, whereas the others had prominent active thermal manifestations that included hot springs, fumaroles, and even geysers (Beowawe and Steamboat). Over time, several sites were expanded with additional units as the resources became better understood.

In 1997 Nevada adopted a renewables portfolio standard (RPS) for its electric utility, NV Energy (formerly Sierra Pacific Power Company), that spurred geothermal development. The program began with a 6% requirement in 2005–2006 and gradually raised the percentage; it is 20% for 2015–2019 and is scheduled to reach 25% in 2025 and beyond [9,10]. This has provided strong incentives for more geothermal exploration and development. As of 2015, new power plants are online at Salt Wells, Blue Mountain, Tuscarora, Jersey Valley, McGinness Hills, Patua, and Don A. Campbell (formerly Wild Rose). However, the law allows credits to be earned for improved electrical system efficiency and for renewable power purchased out of state, perhaps negatively affecting in-state geothermal progress.

Through the year 2014, the state of Nevada, with a population of 2.7 million, had an installed geothermal power capacity of 524 MW, enough for it to rank in ninth place among *countries* in the world. [Figure 16.5](#) shows the growth in net electricity generation from geothermal plants starting from 1985, the first year

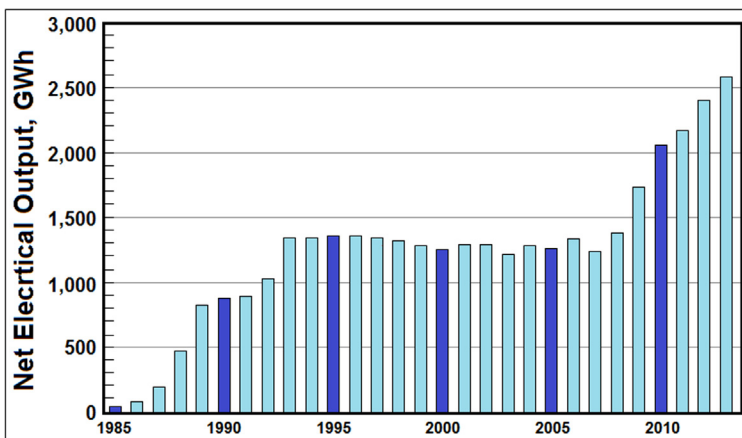


Figure 16.5 Growth of net electrical output from geothermal power plants in Nevada. Modified from Ref. [11] [WWW].

when data were published for geothermal plants. The geothermal power potential for Nevada has been estimated at between 1730 and 2179 MW [12]. In the rest of this chapter we will see how Nevada achieved this success and examine in detail some of the more interesting power plants.

16.3 Steamboat Geothermal Power Complex

The geothermal complex at Steamboat is comprised of 11 currently active power units under an integrated program of operations; see Figure 16.6. Initially, individual owners of plants competed for the resource with other plant owners and leaseholders. The competition ended in 2004 when Ormat Technologies, Inc. purchased the Steamboat Hills (originally Yankee Caithness) power plant. Since they already owned Steamboat 1 and 1A and SB-2 and -3, this gave Ormat the sole rights to the entire resource. An optimization program followed, four more plants were added, and the two oldest binary plants were put on standby.



Figure 16.6 Steamboat geothermal power complex, 16 km south of downtown Reno. Recently built US I-580 (center) cuts through the field. *Image from Google Earth April 2014, labels by author [WWW].*

As of 2014 the total installed capacity is about 111.7 MW, but the typical running capacity is 78 MW (J. Nordquist, Ormat Technologies, Inc., pers. comm., November 10, 2014). The actual output varies with the season owing to the use of air-cooled (AC) condensers for most of the binary units. One unit, Burdette (originally Galena 1), uses a hybrid wet-dry cooling system wherein freshwater from a creek is sprayed into the air stream of the AC condenser on hot summer days to enhance the net power output [13]. Table 16.1 lists some of the particulars for these plants including the average net power output for the year 2013 [14].

TABLE 16.1 Information on geothermal plants at Steamboat geothermal field.

Plant name	Type	Year	No. of units	Unit rating	Average power ^a	Type of cooling
				MW	MW	
Steamboat 1 ^b	Binary	1986	(7)	(0.86)	(6)	Air
Steamboat 1A ^b	Binary	1988	(2)	(0.55)	(2)	Air
Steamboat Hills	1-Flash	1988	1	13.2	9.4	Water
SB-2	Binary	1992	2	7	9.1	Air
SB-3	Binary	1992	2	7	9.7	Air
Burdette (Galena 1)	Binary	2006	2	13	17.4	Hybrid
Steamboat Hills expansion	Bottom binary	2007	1	5.5	NA ^c	Water
Galena 2	Binary	2007	1	13	6.4	Air
Galena 3	Binary	2008	2	13	17.3	Air
Totals			11	111.7	69.3	

^aNet, for 2013.

^bStandby.

^cIncluded in Steamboat Hills.

There are three units at the Steamboat Hills site; see Figure 16.7: the 13.2 MW single-flash plant which was the original plant at Steamboat, a bottoming binary cycle using separated hot brine, and Galena 2, a binary unit that derives its thermal input from steam and brine. The flow diagram for Galena 2 is shown in Figure 16.8.

Since the bulk of the power is generated from binary plants using air cooling, and essentially all of the geofluid drawn from the reservoir must be reinjected, the amount of spent geofluid being continuously returned to the formation is very large. Data from 2007 indicate the following average mass flow rates of injected fluid: 240 kg/s from SB-1 and -1A, 1085 kg/s from SB-2 and -3, and 210 kg/s from Steamboat Hills. The average concentration of dissolved solids is about



Figure 16.7 Steamboat Hills plants: single-flash, adjacent bottom binary and Galena 2 binary units. There is a change in elevation of 120 m between the separator station and the well pad at the upper left. *Image from Google Earth April 2014, labels by author [WWW].*

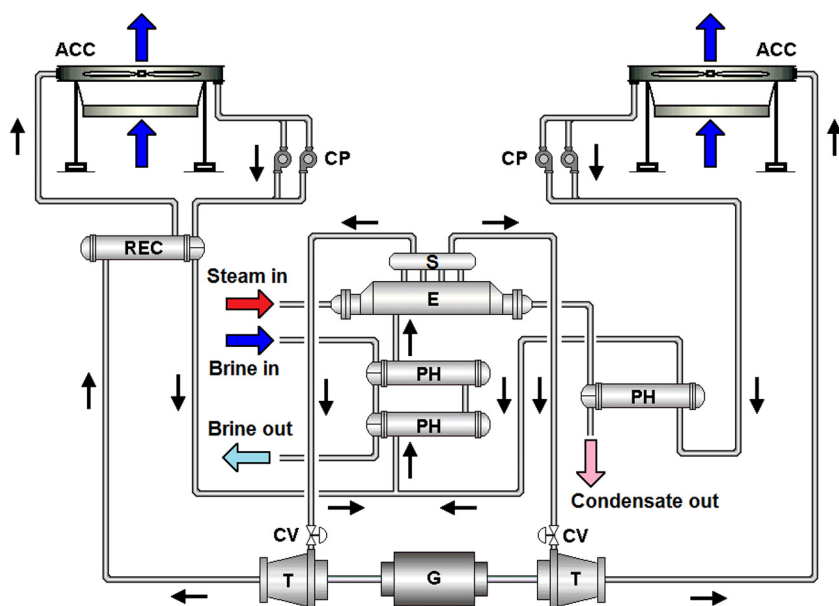


Figure 16.8 Flow diagram for Galena 2. Note the use of the recuperator on only one side of the system associated with the HP turbine; see Nomenclature [WWW].

2300 ppm, with the major constituents being chloride (800–900 ppm), boron (36.1–42.5 ppm), fluoride (2.48 ppm), and arsenic (1.5–3.2 ppm). The temperature of the injectate ranges from about 79°C to 104°C. Injecting over 1500 kg/s continuously in an area of roughly 3.25 km² requires injection wells to have excellent permeability and no direct connection to producing wells where the fluid temperature is between 166°C and 215°C [15]. To accomplish this requires a detailed understanding of the reservoir, plus the ability to site and drill wells directionally to appropriate depths to create a sustainable energy production system.

16.4 Flash Plants

Four flash plants have been built in Nevada besides the one at Steamboat Hills. All of them began as stand-alone double-flash plants, but now each has an associated binary unit. In the case of Desert Peak, the binary plant replaced the original flash plant. Some information on each flash plant is presented in Table 16.2 and in the sections that follow. The total mass flow rate of the geofluid generally is not reported in the literature, making it impossible to calculate the utilization efficiency without making assumptions.

16.4.1 BEOWAWE

The Beowawe plant was developed at one of the sites in Nevada that hosted natural geysers. Once drilling began and flow testing was conducted, there were changes in the thermal manifestations that resulted in cessation of geysering on the high sinter terrace, but seemed to enhance the geysers on the valley floor. However, sometime prior to 1972, four wellheads were destroyed by vandals that allowed the geothermal fluid from one of the wells to flow unabated to the surroundings. None of the geysers survived [16].

The double-flash plant operates from a reservoir at about 200°C. At the start of plant operation in 1985, the resource was as hot as 215°C. The unit has a four-cell cooling tower to supply cold water to the direct-contact condenser. Plant construction was simplified by using a side-by-side arrangement for the turbine and condenser with a cross-over pipe carrying the turbine exhaust to the condenser. In 2013, the plant generated 131,732 MWh (gross) and 110,307 MWh (net) or on average 15.0 MW (gross) and 12.6 MW (net). The average parasitic power was 2.45 MW or 16.3% of the gross. The capacity factors for the year were 90.6% (gross) and 75.9% (net) [14]. A 1.5 MW bottoming binary unit was added in 2011; see Section 16.5.6. Additional particulars on Beowawe may be found in Ref. [17]. A map of the area and an aerial view of the plant are shown in Figure 16.9.

TABLE 16.2 Design specifications for Nevada's flash plants other than Steamboat.

	Beowawe	Desert Peak 1	Dixie Valley	Brady 1
Start-up year	1985	1985 ^a	1988	1992
Type		Double-flash		
Power rating, MW	16.6	9	60.5	26
Resource temperature, °C	215	209	218	177
<i>Turbine:</i>				
Type	Dual pressure	Two-pressure + RST	Dual pressure	Single pressure
Blading		Impulse-reaction		
Cylinders	1	1	1	3 ^b
Flows/turbine	1	NA	2	2
Stages/flow	NA	NA	4/3-3	6
Inlet pressure, bar,a	4.22/0.932	6.14/1.38	6.2/1.43	4.31/2.24
Inlet temperature, °C	146/99	160/109	162/113	146/125
Steam mass flow, kg/s	NA	11.0	NA	~77/27.5
Exhaust pressure, bar,a	0.041	0.076	0.055/0.090	~0.045
Last-stage blade height, mm	635	NA	658	NA
Speed, rpm	3600	3600	3600	4353 ^c
<i>Condenser:</i>				
Type		DC, spray		
CW flow, kg/s	1470	423	4085	NA
CW temperatures, °C:				
Inlet	16	11.7	22.2	21.7
Outlet	28	40.6	NA	NA
Wet bulb	12.2	NA	NA	NA
<i>Cooling tower:</i>				
Type		Mechanical induced draft, crossflow		
No. of cells	4	2	7	3
Fan power, kW/cell	NA	~100	NA	NA
<i>NCG system:</i>				
Steam ejector	Yes	Yes	Yes	Yes
Stages	1	NA	NA	2
Trains	—	NA	NA	1
Intercondensers	Yes	NA	NA	Yes
Aftercondensers	Yes	NA	NA	NA
Steam flow, kg/s	0.214	NA	NA	NA
Gas capacity, kg/s	0.158	NA	NA	NA
Vacuum pump	Yes	NA	NA	NA

^aDecommissioned in 2006.^bTwo HP turbines and one LP turbine.^cGenerators turn at 1800 rpm through a gear box.

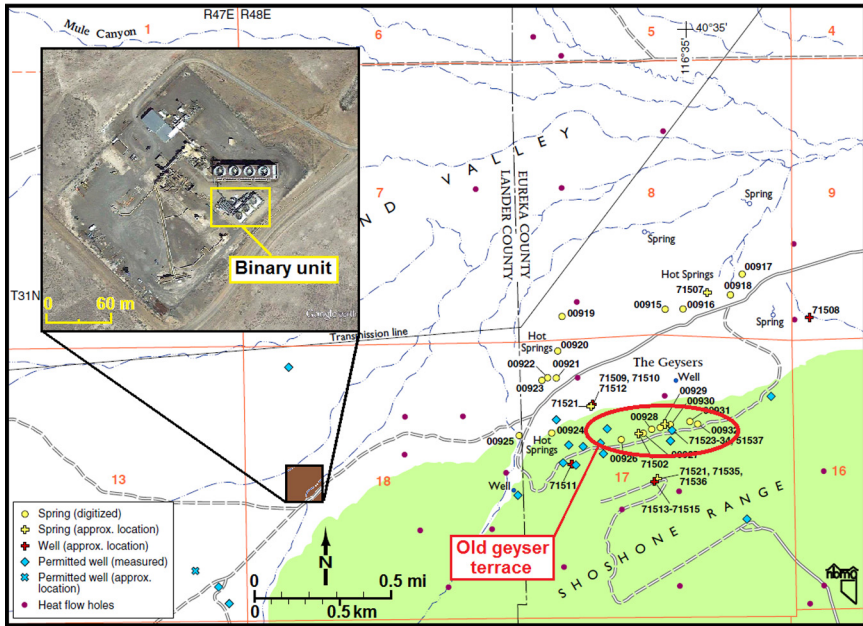


Figure 16.9 Beowawe site map with power plants insert. Map modified from Ref. [18]; image modified from Google Earth August 3, 2013 [WWW].

16.4.2 DESERT PEAK 1

Installed in 1985, the original Desert Peak power plant incorporated a Biphasic Rotary Separator Turbine (RST) with a dual-admission steam turbine. The RST is described in Section 9.5.2. In effect, the RST provided separation of the two-phase fluid while generating power. At the same time, it repressurized the separated liquid which was here used to yield some low-pressure (LP) steam in addition to what was produced in the LP flasher. The flow diagram for this unique system is shown in Figure 16.10. The reservoir temperature ranged from about 205°C to 212°C [20].

A spreadsheet simulator was written using the specifications shown in the literature [21] and yielded the performance figures given in Table 16.3. Both steam turbines were assumed 80% efficient. The Second Law utilization efficiencies were based on a reservoir temperature of 209°C and an average dead state of 10°C. It will be noted that the RST generated almost enough power to take care of the plant parasitic power requirements.

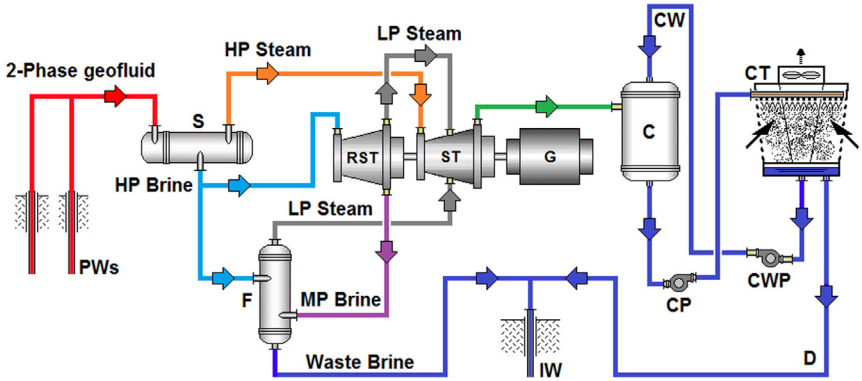


Figure 16.10 Flow diagram for Desert Peak 1 showing the RST incorporated with a dual-admission steam turbine. After Ref. [19] [WWW].

TABLE 16.3 Performance of Desert Peak 1.

Item	Value	Units
RST power	650.4	kW
HP turbine power	2009.8	kW
LP turbine power	7569.0	kW
Total turbine (gross) power	10,229.2	kW
Total pump and fan power	715	kW
Net plant power	9514.2	kW
Power plant η_u (Gross)	38.5	%
Power plant η_u (Net)	35.8	%
RST isentropic efficiency	35.5	%
RST functional utilization efficiency	42.7	%
HPT functional utilization efficiency	79.2	%
LPT functional utilization efficiency	82.3	%

A horizontal separator and a vertical flash vessel were used to process the two-phase geofluid coming from two production wells, DPU 67-21 and DPU 86-21, both at an elevation greater than the power plant site; see Figure 16.11 [22]. The waste brine was reinjected into one well DPU B21-2. The original flash plant was shut down in 2006, one year after construction of a new 23 MW binary unit which continues to operate as of 2014 [7]; see Section 16.5.3.



Figure 16.11 Separator (center) and flasher (right) at Desert Peak power plant. *Photo from Ref. [22]; photographer unknown.*

16.4.3 DIXIE VALLEY

The double-flash plant at Dixie Valley is the largest flash plant in Nevada and will probably hold that distinction for the rest of its life. The field lies on the east side of the Stillwater Range at the northern end of the Dixie Valley. The production wells are clustered in two separate areas along a NS axis with the injection wells located between the areas. The resource temperature is about 250°C. The geology is dominated by two fault zones as shown in [Figure 16.12](#), one associated with the Stillwater Range (left) and the other with a buried fault about 1.5 km offset to the east of the range fault. However, the productive portions of the reservoir at a depth of 2400–3050 m arise from complex interactions among smaller fractures associated with the Dixie Valley range fault, leading to good permeability [\[23,24\]](#).

The turbine was supplied by Fuji Electric and features an asymmetric design; see [Figure 16.13](#). High-pressure (HP) steam is admitted to a four-stage section at the center of the rotor; one of the two LP steam flows enters and mixes with the HP flow leaving the fourth stage, while the other enters a three-stage section on the opposite side of the rotor. The unbalanced axial forces are counteracted by thrust bearings on the rotor shaft. Although the turbine is rated at 60.5 MW, the generator is capable of being pushed beyond the rating. A bottoming binary unit was installed in 2011; see [Section 16.5.7](#).

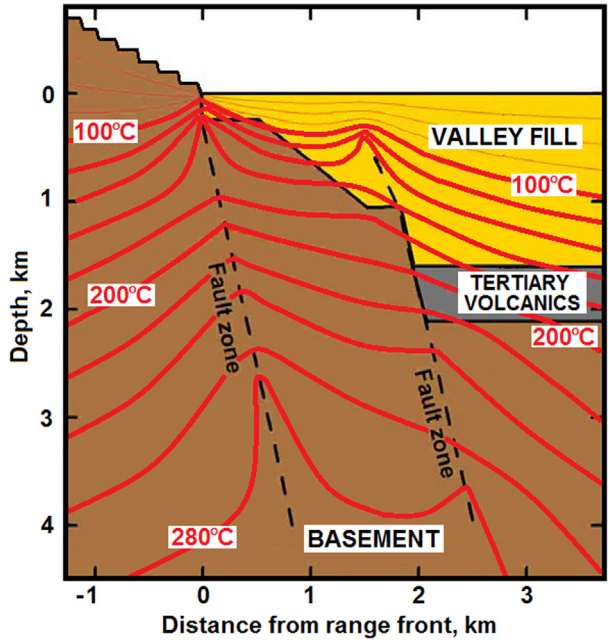


Figure 16.12 Highly simplified geologic cross-section of Dixie Valley reservoir, looking generally north. Modified from Ref. [23] [WWW].

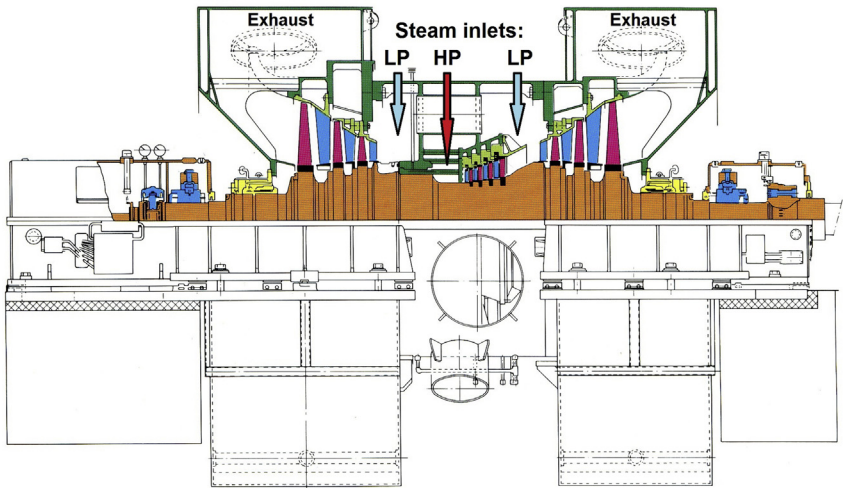


Figure 16.13 Cross-section of the Dixie Valley steam turbine. Modified from Ref. [25] [WWW].

16.4.4 BRADY PLANT 1

The Brady double-flash plant was distinctively designed to make use of surplus US Navy steam turbines. A large number of these machines were owned by Geothermal Power Company and three of them were arranged as shown in Figure 16.14 to produce a power station with a rating of 26 MW (gross) and 20 MW (net). The temperature-entropy process diagram is given in Figure 16.15.

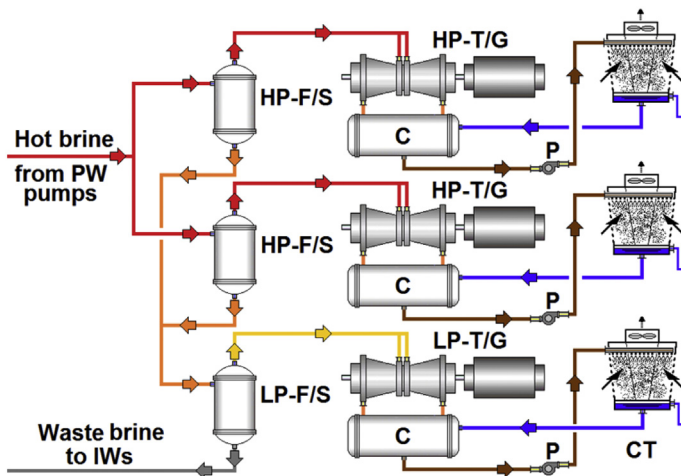


Figure 16.14 Simplified flow diagram for Brady H.S. double-flash plant; see Nomenclature. After Ref. [26] [WWW].

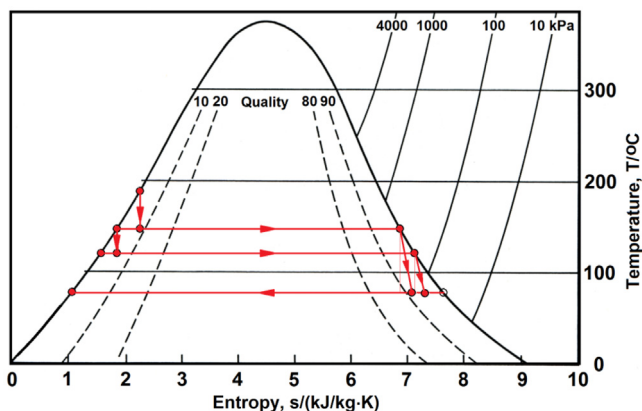


Figure 16.15 Temperature-entropy process diagram for Brady plant 1 [WWW].

There were eight production wells, all of them pumped, and four reinjection wells. The design mass flow rate of hot brine was 730.8 kg/s, of which roughly 7.1% or 51.6 kg/s was flashed into HP steam that was divided between two 9 MW turbine-generator sets. The separated brine from the two HP separators yielded another 29.8 kg/s of LP steam upon flashing in the LP separator that was used in a 7.5 MW turbine-generator.

Assuming the reservoir temperature is 177°C, the dead state is at 20°C, and the turbine-generators actually delivered full rated power, the plant would have a utilization efficiency of 28.3% (gross) and 21.8% (net). However, a check of the turbine isentropic efficiencies for this condition yielded unrealistically high values (>95%) which implies that the actual power was less than the rated values. Assuming a turbine efficiency of 75%, perhaps a bit generous for these refurbished machines, one obtains a total output of 20.0 MW, with 14.2 MW coming from the two HP turbines and 5.8 MW from the LP turbine. Thus, the utilization efficiencies probably should be closer to 21.8% (gross) and 15.3% (net), assuming 6 MW for auxiliary power requirements including well pumping.

In 2002 a bottoming binary unit was added. It has two turbines driving a single generator and is rated at 5 MW (nominal). Heat comes from the waste brine leaving the flash plants and results in a lowering of the reinjection temperature from about 107°C to 81°C. Production data for the entire plant in 2013 show that the average output was 11.5 MW (gross), 6.44 MW (net); the parasitic power was 5.06 MW or 44% of the gross power [14]. In 2013 a US DOE cost-shared project attempted to stimulate one well lying south of the production area with the goal of increasing the power output by 2–3 MW; the project is expected to conclude in 2015.

16.5 Binary Plants

This section will cover the binary plants in Nevada other than the ones at Steamboat that were described in [Section 16.1](#), at Brady ([Section 16.4.4](#)), and Stillwater which will be covered in [Section 16.6](#).

16.5.1 SAN EMIDIO

In the 1960s the hydrothermal resource at San Emidio was discovered during drilling for sulfur. Thus, mining exploration led to a blind geothermal prospect coming to light. The productive area is related to a steeply dipping fault, offset from the range fault to the east of the site. A cross-section and plan view ([Figure 16.16](#)) shows that the hot geofluid rises along the fault and is confined to a relatively narrow zone.

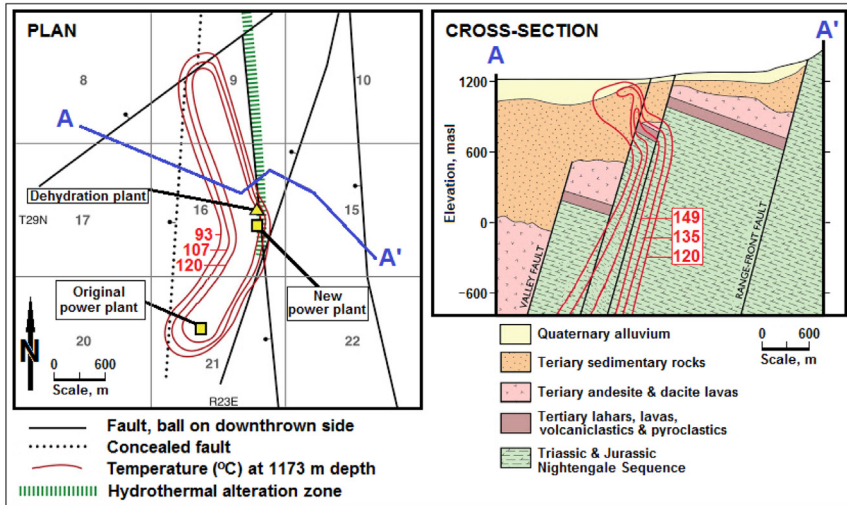


Figure 16.16 Plan and cross-section views of geologic structure of San Emidio. Modified from Ref. [27] [WWW].

In 1987 four skid-mounted binary units were installed at the Empire power plant. Each unit was only 0.9 MW in capacity so the plant was rated at 3.6 MW. In 2008 the plant was sold to US Geothermal, Inc. (USGeo), the same company that had already redeveloped the Raft River project; see Chapter 20. The new owners decided to renovate the existing plant which was able to generate no more than about 2.5 MW.

An ambitious program got underway to replace the four isopentane units with one unit using the same production and injection wells and designed for the same flow rates. However, the new unit would be far more efficient and generate about three times the power. A first-of-its-kind, water-cooled, supercritical cycle with R134a as the working fluid was selected. The new plant came online in May 2012, and after some early problems it was operating with high reliability by 2013. The total net generation for the year 2013 was 76,697 MWh which comes to an average of 8.75 MW (net). The average brine temperature to the plant was 140°C at an average flow rate of 247.7 kg/s. The availability factor for the year 2013 was 94.9%. For the year 2014, the corresponding values were: 76,894 MWh net generation, 8.78 MW (net) average generation, 139.2°C brine temperature, and 262.3 kg/s brine flow. Other data for 2014 include the following: average brine return temperature was 52.0°C;

utilization efficiency was 44.5% (gross) or 32.7% (net); thermal efficiency was 12.4% (gross) and 9.1% (net); and total parasitic power, including well pumps, was about 26% of the gross power. Since the plant uses a water cooling (WC) tower, the wet-bulb temperature is an important site parameter; the average value was 6.7°C for the year 2014. In early 2014 a turbine design defect that had been recognized in 2012 was corrected, so that for the last 8 months of 2014, the plant operated at 98.4% availability. Currently, the plant is running at 110% capacity factor, producing more than design power but at an efficiency somewhat lower than the design value [28].

16.5.2 SODA LAKE PLANTS 1 AND 2

Soda Lake Plants 1 and 2 were installed in 1987 and 1991, respectively. The site lies about 4 km northeast of Soda Lake and about 10 km northwest of Fallon at an elevation of about 1215 m a.s.l. The reservoir temperature is 182°C and consists of permeable pumice tuff. Geofluids migrate up from the central Carson Basin, then move horizontally through permeable sedimentary strata. A northeast-striking fault provides vertical movement of the geofluid within the reservoir formation.

Soda Lake 1 is comprised of three organic Rankine cycles (ORCs) with water-cooled condensers fed from a cooling tower and has an installed gross nameplate rating of 5.1 MW. Soda Lake 2 has six, AC ORCs for a total installed gross rating of 18 MW. Neither plant is performing close to its rated capacity. For 2012, Plant 1 produced on average only 1.67 MW (gross) and 1.02 MW (net), Plant 2 produced only 10.22 MW (gross) and 6.31 MW (net), and the parasitic power for the plants averaged about 38% of the gross power [7].

16.5.3 DESERT PEAK 2

In 2005, Ormat Nevada, Inc. (now Ormat Technologies, Inc.) constructed a new binary power plant at Desert Peak adjacent to the existing double-flash geothermal power plant; see Figure 16.17. A year later the flash plant was decommissioned. The new project, Desert Peak 2, consists of two binary power plants of 15 and 11 MW, the former using air-cooled (AC) condensers and the latter water cooling (WC). The net rated power is 23 MW. In 2012, the plants generated 127,681 MWh (gross) and 98,681 MWh (net), yielding capacity factors of 63.2% and 48.6%, respectively; the parasite power averaged 23% of the gross power.

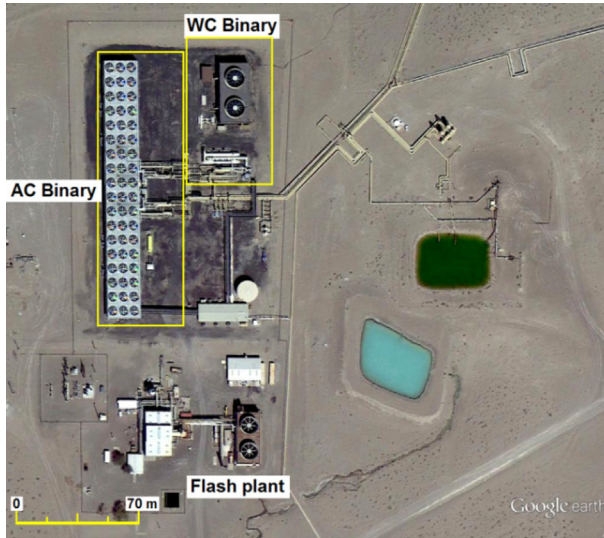


Figure 16.17 Desert Peak power plants. Image from Google Earth 2013-08-02 [WWW].

16.5.4 SALT WELLS

The 24 MW (nominal) Salt Wells plant is effectively one-half of the 47.2 MW Stillwater plant described below in [Section 16.6](#). The site is 25 km southeast of Fallon and 8.5 km south of the Salt Wells junction on US Rt. 50, in a desolate area also known as Eight Mile Flat; see [Figure 16.18](#). There are numerous springs lying between the plant and Rt. 50.



Figure 16.18 Salt Wells plant under construction in December 2008. Photo by author [WWW].

Development of the prospect has passed through several hands. In 1980 and 1985 Anadarko Production Company drilled the first commercial-sized wells, followed by Nevada Geothermal Specialists LLC who planned to drill more wells and to build a 20 MW power plant. In 2004 AMP Resources LLC purchased the project, and in 2007 the project assets were acquired by the current owner, Enel Green Power, who constructed the two-unit, 24 MW plant and a 9.6 km-long, 230 kV transmission line to deliver power to the Sierra Pacific Power Company (now NV Energy). The plant was commissioned in 2009. Geofluid is pumped from a shallow reservoir at a temperature of about 140°C, but there are indications of a deeper, hotter zone perhaps as hot as 220°C [29].

The plant is comprised of two isobutane ORC turbine-generator units each with a capability of 12 MW. In 2012, the plant generated 144,886 MWh (gross) and 105,676 MWh (net), with the average gross power output being 16.5 MW, the average net output being 12.0 MW; the gross and net capacity factors were 69.9% and 51.0%, respectively; the parasitic power averaged 27.1% of the gross power. As of 2014, the plant was limited to 13.4 MW [7].

16.5.5 BLUE MOUNTAIN

Blue Mountain lies about 33 km west of Winnemucca. There are no active geothermal manifestations at the site which was discovered as a result of exploration drilling for minerals. There are, however, several indications of ancient hydrothermal processes, such as fossil hot spring deposits.

The production wells deliver liquid from a reservoir where fluids are at temperatures of 188–197°C, and reside at a relatively shallow depth of 610 m [30,31]. Two deep injection wells (>1700 m) were found with higher temperatures, about 210–219°C, while one shallow injector (474 m) shows only 74°C; see Figure 16.19.

The Blue Mountain plant, named Faulkner 1, was developed by Nevada Geothermal Power, Inc. (NGP) and includes three dual-level ORC units, each having a capability of 16.5 MW, giving the plant a nameplate rating of 49.5 MW (gross) and 38.8 MW (net); parasitic power is about 22% of the design gross power. The plant started up in 2009 using five production and six injection wells. In 2012 it averaged 39.0 MW (gross) and 29.3 MW (net), about 10 MW below expectations [7]. Notice that under these operating conditions the parasitic power remains about the same, ~10 MW, but makes up nearly 25% of the actual gross power. This typically happens when a binary plant falls short of its design output since the pumps and fans still need to operate.

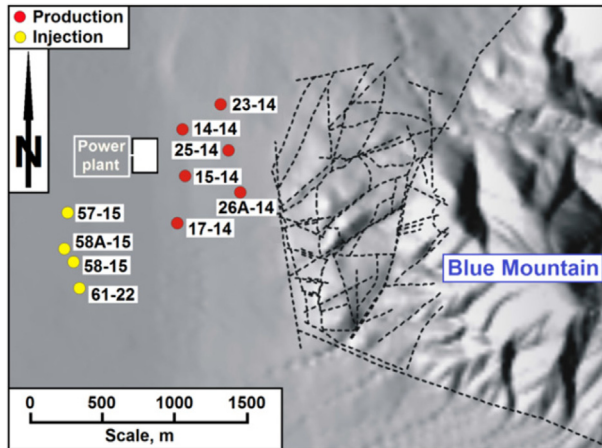


Figure 16.19 Blue Mountain well field and power plant location; dashed lines represent inferred faults. *Modified from Ref. [30] [WWW].*

Owing to high silica content in the reservoir geofluid, about 400–430 ppm, a chemical inhibitor is injected to prevent precipitation after cooling in the heat exchangers and piping where the supersaturation index is 1.5–1.7 at a temperature of 70°C.

The total cost for the plant came to \$180 million, with \$76 million going for the engineering, procurement, and construction contract (EPC) with Ormat Technologies, Inc. who supplied the energy conversion system. Shortly after the plant officially came online in October 2009, an optimization program had to be undertaken at a cost of \$8.4 million to drill one more production and two more injection wells owing to a shortfall of production [32].

Project financing came through a variety of sources including: a grant of \$58 million in 2009 from the US Department of Treasury (USDOT) under the American Recovery and Reinvestment Act of 2009 (ARRA) in lieu of a tax credit; an \$88.4 million mezzanine loan from the investment firm EIG Global Energy Partners (EIG); and a loan guarantee of \$78.8 million from the USDOT issued in September 2010 through John Hancock Financial Services (JHFS). The shortfall in output and consequently in revenues forced NGP into default on its loans. By the end of year 2012, NGP owed \$84.2 million to JHFS and \$97.4 million to EIG. After negotiations, in March 2013 NGP transferred its holdings in the Blue Mountain plant to Blue Mountain Power LLC, a subsidiary of EIG, in exchange for full release from its debt. And in April 2013, the principals involved in NGP reorganized themselves into a new company, Alternative Earth Resources, Inc. (AER). The power plant continued to operate under the supervision of an NGP subsidiary until January 31, 2014, at which time the operations were transferred to a new entity designated by EIG [33].

16.5.6 BEOWAVE BINARY

A 2 MW (nominal) subcritical binary bottoming cycle was added to the Beowawe station in 2011, raising the plant output to about 18 MW. Unlike most binary plants in arid Nevada, this one is water cooled since it takes advantage of the condensate from the main Beowawe flash plant. The process cycle diagram is shown in temperature-entropy coordinates in Figure 16.20, and selected performance values are given in Table 16.4.

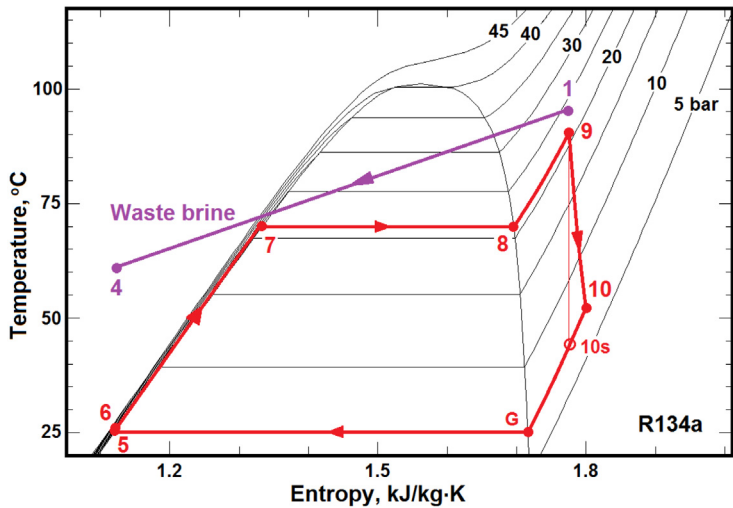


Figure 16.20 Temperature-entropy process diagram from Beowawe bottoming binary cycle [WWW].

TABLE 16.4 Performance values for Beowawe bottoming binary plant.

Item	Value	Units
R134a turbine power	2739.1	kW
R134a pump power	371.7	kW
Cycle net power	2367.4	kW
Total CW pump and CT fan power	354.0	kW
Net plant power	2013.4	kW
Plant net thermal efficiency	6.5	%
Plant net utilization efficiency	18.0	%
Plant net functional utilization efficiency	32.5	%
R134a turbine isentropic efficiency	79.9	%
R134a pump isentropic efficiency	77.7	%

16.5.7 DIXIE VALLEY BOTTOMING BINARY PLANT

A bottoming binary unit using R134a as the working fluid and having a power rating of 5 MW (gross), 4.2 MW (net) was installed in 2011, raising the total plant capacity to 64.7 MW. This plant received a \$2 million grant from the US Dept. of Energy under the ARRA-2009 program that partially offset the plant cost of \$15.5 million [34]. The plant feeds off the waste brine from the double-flash plant at a temperature of 106°C; the reinjection temperature is 77°C [35]. The binary plant data for March 2014 show that the plant can produce about 3.5 MW (net) at a net thermal efficiency of 8.5% and a net utilization efficiency of 22.9% based on the incoming brine exergy, and a net Second Law functional efficiency of 32.7% based on the change in exergy of the brine as it passes through the bottoming unit [36]. For the first 4 months of 2014, the unit averaged 3.62 MW (net), the average parasitic load was 1.14 MW, and had an availability of 98.9% [37].

16.5.8 JERSEY VALLEY, MCGINNESS HILLS, AND TUSCARORA

These three plants were installed and are owned and operated by Ormat Technologies, Inc. They came online in 2011–12 and are of similar design, albeit with different power ratings. All use dual-level ORC systems with two turbines driving a common generator. As usual, the wells are pumped.

Jersey Valley is about 40 km NE of the Dixie Valley plant, just on the west flank of Mount Moses. It uses one standard ORC power unit plus a “half unit” that yields a plant rating of 22.5 MW; see Figure 16.21. AC condensers are used.

McGinness Hills is roughly 17 km NE of the community of Austin in relatively smooth terrain. There are three AC, dual-level units each with a rating of 17.3 MW. Success with this plant has led to plans to expand the plant, and site preparations for a companion plant were underway as of spring 2014, as may be seen in Figure 16.22.

Tuscarora is about 110 km NNE of Beowawe and about 58 km south of the Nevada-Idaho state border, making it the northernmost geothermal power plant in Nevada. The site used to be known as Hot Sulphur Springs; thermal manifestations lie close to the power plant and include six hot springs, a fumarole, and a geyser. The terrain is fairly rugged as the plant sits in a narrow valley among mountains.

Several companies attempted to develop this site but each failed for a variety of reasons [7]. Ormat originally planned to build a 16 MW, AC unit, but as drilling progressed, the plant was enlarged to 32 MW and the cooling was switched to water instead of air as there turned out to be sufficient freshwater available to supply makeup to the WC tower. Two dual-level units give the plant a rated



Figure 16.21 Jersey Valley power plant. Google Earth image, May 25, 2014 [WWW].

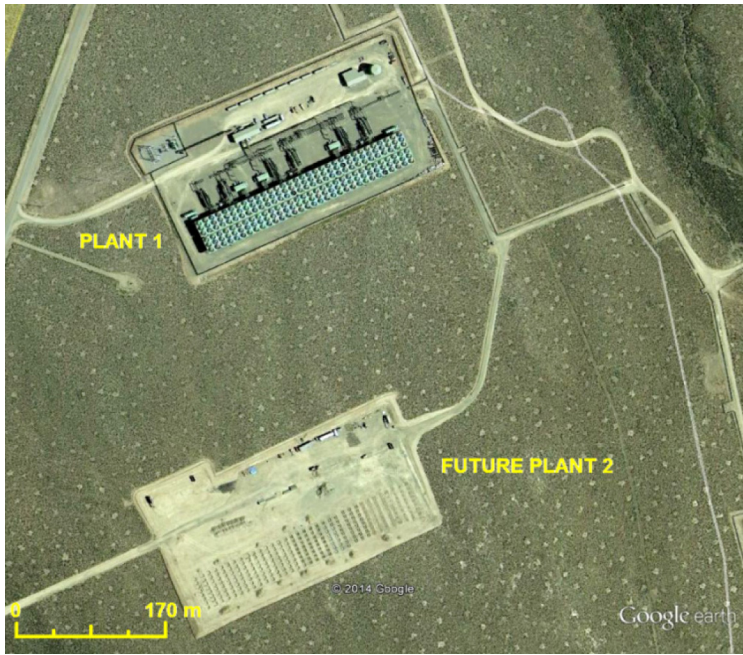


Figure 16.22 McGinness Hills power station. Google Earth image, May 25, 2014 [WWW].

power of 32 MW and are shown in Figure 16.23. The production wells were drilled directionally from pads adjacent to the power house, while the injection wells are located north of the plant site. The plant came online officially in the first quarter of 2012 but began generating power in 2011.

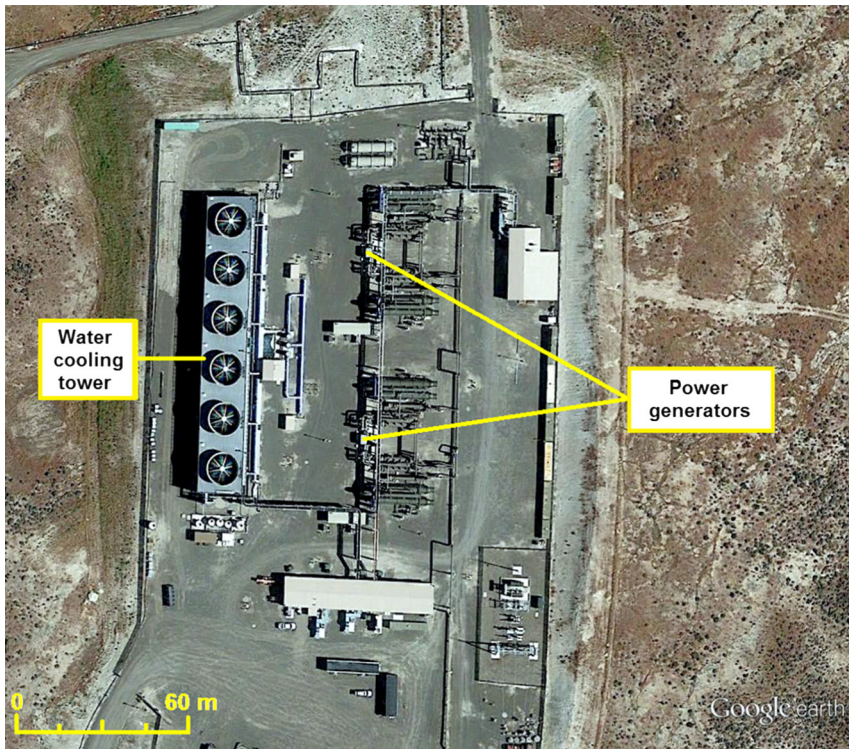


Figure 16.23 Tuscarora power plant. Google Earth image, July 4, 2014 [WWW].

Table 16.5 gives the performance of these three power plants based on the most recent data of 2013 [14].

TABLE 16.5 Performance for three power plants in 2013 [14].

Plant	Rating	Generation		Average power		Capacity factor	
	MW	MWh-G	MWh-N	MW-G	MW-N	%, gross	%, net
Jersey Valley	23.5	107,857	76,248	12.31	8.70	52.4	37.0
McGinness Hills	52	391,928	328,814	44.74	37.54	86.0	72.2
Tuscarora	32	205,360	149,313	23.44	17.04	73.3	53.3

The Jersey Valley plant, which started up in 2011, as of 2013 had yet to achieve its design power output with its net power falling 14.8 MW below the 23.5 MW rating. The parasitic power is about 29% of the gross power. McGinness Hills officially went commercial on July 26, 2012, but had been producing power before that. Output for 2013 exceeded the nominal plant rating and the units were uprated from 2012. This plant is the most successful of these three plants. Its parasitic power is about 16% of its gross, the lowest of the three plants. Tuscarora, like Jersey Valley, is still short of reaching its rated power and operated at a gross capacity factor of 73.3%, a net capacity factor of 53.3%, and had a parasitic load that was 27.3% of gross power.

In 2011 the developer of these three plants, Ormat Technologies, Inc., benefited from a loan guarantee from the US DOE for up to \$350 million that facilitated the financing of these projects [38].

16.5.9 PATUA

The Patua geothermal resource area is marked by numerous thermal manifestations, including over a dozen hot springs with temperatures ranging from 28°C to 96°C. Early exploratory wells drilled by Magma Power Company showed that high temperatures were present at very shallow depths: 132°C between 91 and 228 m [39]. Figure 16.24 shows the project site which is just north of US Rt. 50A near Hazen. The project developer is Gradient Resources, Inc. (GRI), formerly Vulcan Power Company. GRI believes the resource extends well to the south of the highway and plans to develop a second project in that area.

A power purchase agreement with the Sacramento Municipal Utility District (SMUD) was signed in April 2010 that covers a 21-year period for purchase of up to 132 MW. At that time, it was anticipated that the plant would be online in the first quarter of 2012. A loan of \$108 million from Denham Capital in February 2010 [41] enabled work to begin in earnest on the site in 2011 with the drilling of several wells. Financing for construction of the plant was obtained in December 2012 through a \$155 million loan from Union Bank, N.A., including Canadian Imperial Bank, ING Capital LLC, and Siemens Financial Services.

The current project started its life as a proposed 120 MW power plant that has been reduced in size over time as the drilling progressed. In 2012 it was being seen as a 60 MW plant, yet at that time GRI stated that it expected to ultimately raise the output to 300 MW [42]. In December 2013 the first unit began operating with a power rating of 15 MW. The power system is a supercritical binary cycle with R134a as the working fluid. It was supplied by TAS Energy, Inc. and it is that company's third such plant, the others being at Neal Hot Springs in Oregon and San Emidio in Nevada (see Sect. 16.5.1).

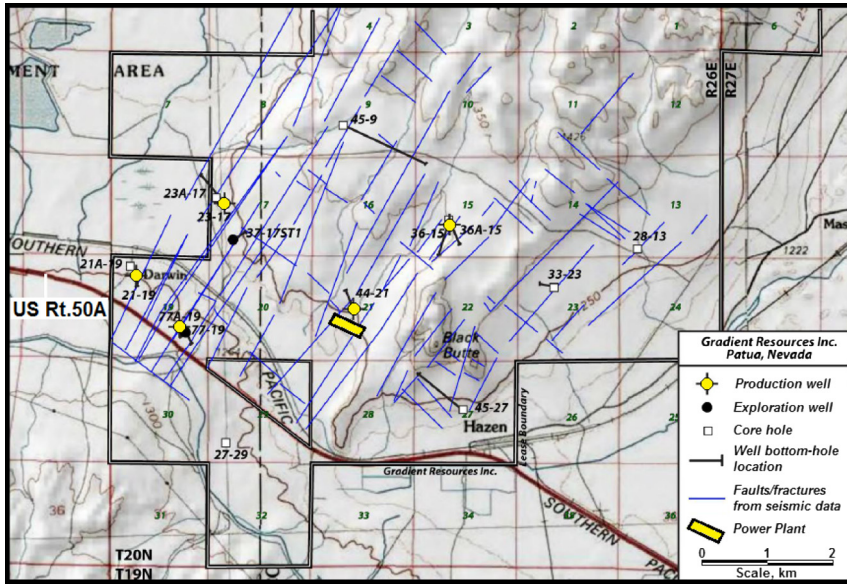


Figure 16.24 Patua well field and plant location. Modified from Ref. [40] [WWW].

Data for the month of December 2013 show a gross generation of 2880 MWh and a net generation of 1709 MWh [14]. The exact date of startup is not known so the average power cannot be determined. However, the parasitic load for this initial operation was 40.7% of the gross, a very high value, perhaps understandable under startup conditions.

16.6 Stillwater Plants

16.6.1 STILLWATER 1

The first Stillwater power plant went online in 1989 and was comprised of seven dual-level ORCs. Since each level of this early dual-level ORC had its own generator, the plant was counted as having 14 units. Level 1 received the hottest brine that entered the evaporator and then traveled to the evaporator of Level 2. The brine then was divided and passed through the Level 1 and 2 preheaters in parallel, as shown in Figure 16.25. AC condensers were deployed.

Each power cycle used n-pentane as the working fluid. Each generator was rated at 1.5 MW, with a plant rating of 13 MW gross. The original rating was 17 MW [43] but the rating was lowered soon after the plant went into operation. A site photo is presented in Figure 16.26 and a detailed view of one level is shown in Figure 16.27.

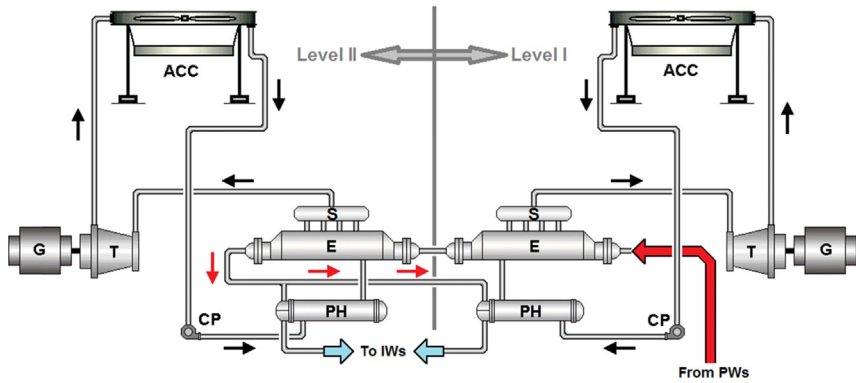


Figure 16.25 Stillwater 1 flow diagram, one of seven identical modules [WWW].

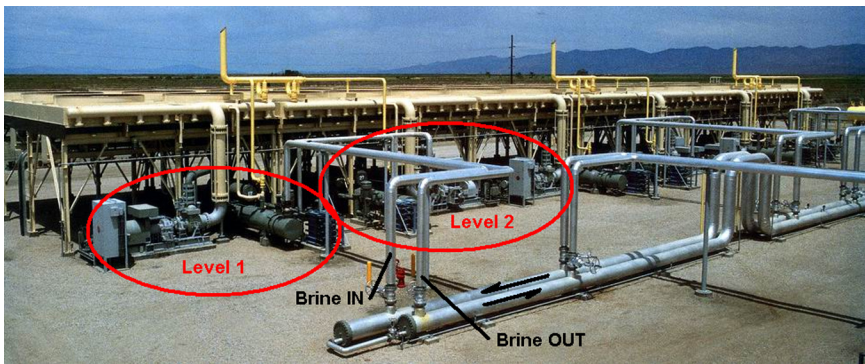


Figure 16.26 Stillwater 1 showing the three north modules; four more were on the south side. Photo courtesy of Ormat Technologies, Inc., labels by author [WWW].

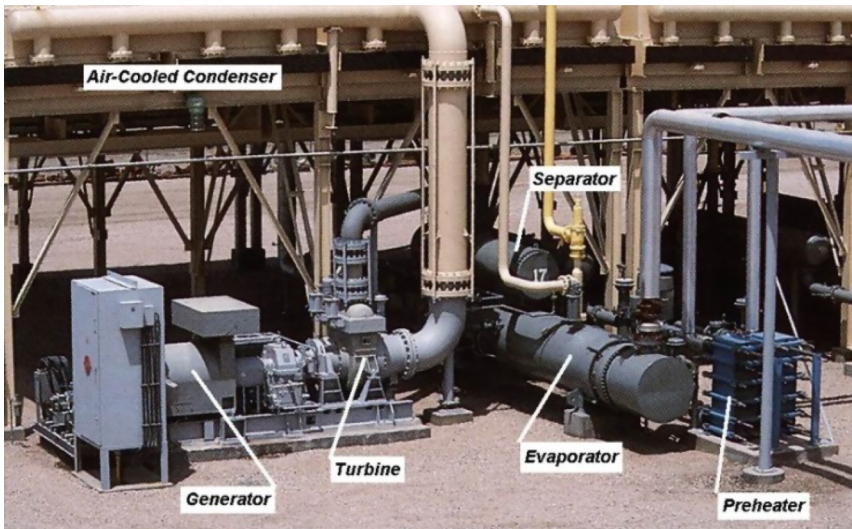


Figure 16.27 Components of a typical Level 1 at Stillwater 1 power plant. Photo courtesy of Ormat Technologies, Inc., labels by author [WWW].

The plant suffered from a low capacity factor, as shown in the graphs of [Figure 16.28A and B](#). Also the parasitic load was excessive; beginning in 1996 parasitic power was greater than 30% of the gross power and steadily grew to 45% just before the plant was decommissioned in 2008 [7].

16.6.2 STILLWATER 2

The new plant, the 47.2 MW Stillwater 2, comprised of four identical 12 MW (nominal) units, started up in 2009. So far, it too shows relatively low capacity factors and high parasitic loads; see [Figure 16.28C and D](#). In fact the new plant began its operation with lower capacity factors than the original plant owing to insufficient geofluid production and reinjection capacity. In 2012 it reached the same performance level as the old plant when that one was shut down.

It may be concluded that the Stillwater 2 plant was designed and built for a power rating that was greater than the resource could support. Since the capacity factor is roughly 50%, the plant could have better utilized the available geofluid by having only two instead of four units. It is not feasible to operate half the plant since the parasitic loads need to be met regardless of the gross power being generated. From [Figure 16.28D](#), it can be seen that the parasitic loads are running higher than 35% of the gross power. The likely cause of the low geofluid throughput lies in inadequate injection capacity owing to poor permeability outside of the production zone.

16.6.3 HYBRID GEOTHERMAL–SOLAR SYSTEMS

One way to generate additional power at Stillwater is by deploying solar photovoltaic (PV) panels. In 2011–12, a large array of 89,000 polycrystalline PV panels covering 47 hectares was installed; see [Figure 16.29](#). The PV system can generate 26 MW peak power that is delivered to the grid via the same transmission lines and infrastructure that serve the geothermal plant. However, the power is not used to assist the geothermal plant, such as by running pumps and fans or meeting other station electrical needs. It is estimated that 40,000 MWh will be generated by the PV units, which means a capacity factor of 17.6%.

The contrast between the required surface area for the binary and the PV plants is striking. Using the binary plant's rated capability (actual output is less owing to a deficiency of geofluid) and the PV plant's peak capacity, the specific area usage for the binary plant is 953 m²/MW and for the PV plant it is 18,077 m²/MW. Using the binary plant's actual average net power for 2013, 17.6 MW, and the effective average power for the PV plant, the specific area usage comes to 2555 m²/MW (binary) and 102,900 m²/MW (PV). Thus, on an actual output basis, the Stillwater PV system requires about 40 times more surface

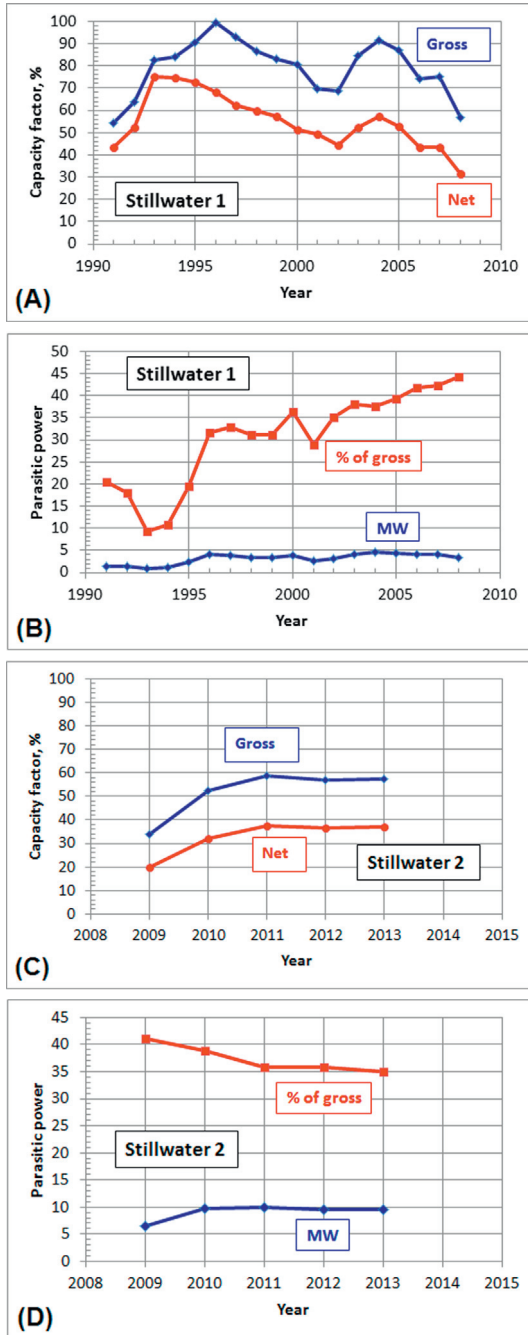


Figure 16.28 Performance data for Stillwater 1 and 2: capacity factors and parasitic power [WW/W].

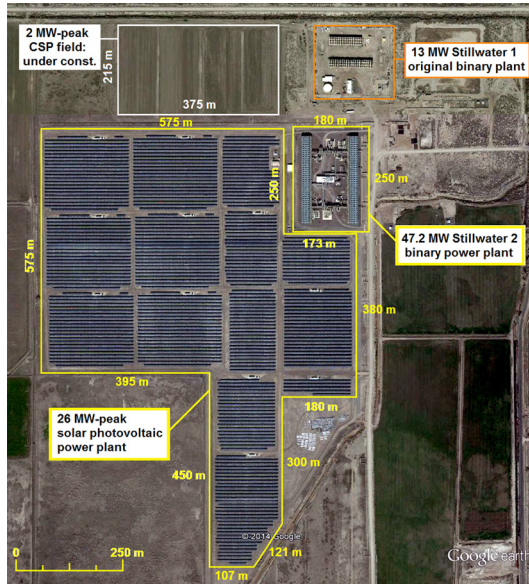


Figure 16.29 Aerial view of Stillwater 1 and 2, PV array, and CSP field. Note the CSP collectors were installed after this image was taken and the collectors are aligned N-S with single-axis tracking. Google Earth image, March 22, 2014 [WWW].

area per effective MW than the binary plant. If the binary plant had been better sized to the resource, the factor would be about twice as large. Figure 16.30 shows the plant and only a tiny portion of the PV array.

A new concentrating solar power (CSP) system was installed in 2014 that consists of 22 rows of north-south, single-axis tracking, parabolic trough solar collectors, covering a ground surface area of $80,625 \text{ m}^2$ with a collector area of $26,000 \text{ m}^2$ (see Figure 16.29). The height of the aperture of the collectors is 6 m. The function of the CSP system is to boost the temperature of the pumped geofluid from the wells before it enters the Stillwater 2 binary plant heat exchangers [44,45]. This is a variation on the design shown in Figure 9.26; see Figure 16.31.

The added solar portion is aimed at overcoming one of the problems facing the Stillwater 2 plant, namely, that over the years the temperature of the resource has declined. The new CSP system should restore the brine inlet temperature to its design value. The temperature of the heat transfer fluid, a pressurized mixture of demineralized water and a corrosion inhibitor, is about 199°C entering the heat exchanger. The temperature of the brine leaving the heat exchanger depends on the inlet temperature and the flow rate, but is limited to 167°C . This should be sufficient to raise the binary plant output by roughly 2 MW [44,45] while the hybrid system is in operation. However, there is no thermal storage so that the hybrid plant only operates when the sun is shining; otherwise, it reverts to pure geothermal. Figure 16.32 shows an aerial view of the Stillwater power complex.



Figure 16.30 Stillwater 2 with a tiny portion of the PV array. Photo by author July 29, 2012 [WWW].

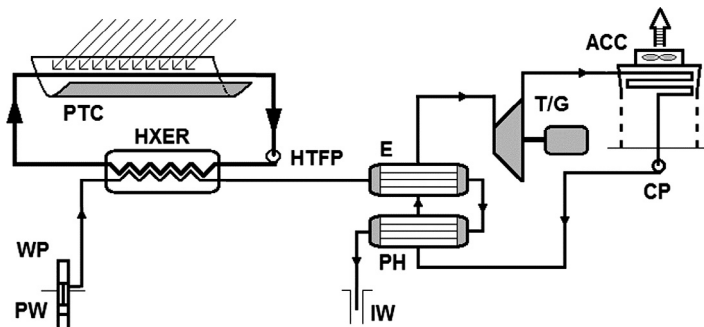


Figure 16.31 Simplified flow diagram for Stillwater CSP-geothermal binary hybrid plant; see Nomenclature.

About 3500 MWh of electricity per year is expected from the CSP system, which means about 0.4 MW increase in Stillwater power output, on average over a year. Thus, the incremental capacity factor for the CSP system is 20% [46]. The CSP facility costs \$14.5 million (F. Bizzarri, ENEL Green Power SpA, pers. comm., November 14, 2014).



Figure 16.32 Stillwater hybrid geothermal-PV-CSP plant; viewed to the SW. A portion of the PV array is at top left; the CSP collectors are at right [45]. *Photo courtesy of Enel Green Power North America [WWW].*

16.7 Lessons Learned from Nevada's Experience

Geothermal plants can be developed in the Basin and Range Province at the most remote locations, provided sufficient financial incentives exist, i.e., loan guarantees, outright grants, and power purchase agreements driven by RPS. Project costs usually involve installation of a transmission line to connect the plant to the grid.

Although many of the sites are hidden resources, a review of drilling and exploration for irrigation water and minerals often leads to exploitable geothermal resources.

Most of Nevada's geothermal resources are associated with fault/fracture systems related to range faults, and tend to be relatively small and linear in surface expression. Production may be relatively easy to obtain, but injection capacity for full reinjection can be a limiting factor owing to lack of good permeability away from the production zones. The potential for cooling the production wells can prevent plants from achieving their full-rated capacity, particularly if plants are designed and built before a full understanding of the reservoir is achieved.

A microcosm of the worldwide evolution of geothermal binary plant technology took place in Nevada over the 30-year period from 1984 to 2014. The power plants grew from tiny, water-cooled, skid-mounted, 500 kW units to modular, AC, dual-level, 15,000 kW units that can be installed in multiples at given sites. Economies of scale have kicked in as experience was acquired and confidence gained at 17 different resource sites.

Unitizing a resource under the control of a single entity usually leads to more efficient operation and more sustainable reservoir management than having several developers competing for geofluid at the expense of others. In California this was demonstrated at The Geysers. In Nevada the resources are usually small so this is not a widespread problem, but the Steamboat system is a case in point where under a single owner the resource appears to have achieved a sustainable level of performance.

In a few cases, power plants have been designed and built for a power level that exceeded the capacity of the resource. This is the classic problem facing geothermal developers. This was enunciated back in 1980 by Dr. Joseph Kestin and is repeated in the Preface of this book for emphasis. By oversizing the plant and ordering equipment before the resource is sufficiently understood, one can turn a potentially successful project, if it had been properly matched to the resource, into one that will struggle to maintain economic viability. The developer is thus placed in jeopardy of defaulting on debt obligations and of losing the plant.

References

- [1] Rhodes GT, Faulds JE, Teplow W. Structural controls of the San Emidio desert geothermal field, Northwestern Nevada. *Geothermal Resour Counc Trans* 2010;34:819–22.
- [2] Faulds JE, Hinz NH, et al. The hybrid model—the most accommodating structural setting for geothermal power generation in the Great Basin, Western USA. *Geothermal Resour Counc Trans* 2013;37.
- [3] National Geophysical Data Center Listings. Nevada Hot Springs, <<http://www.hot springsenthusiast.com/Nevada.asp>> [accessed 18.10.14].
- [4] Blackwell DD, Waibel AF, Richards M. Why Basin and Range systems are hard to find: the moral of the story is they get smaller with depth!. *Geothermal Resour Counc Trans* 2012;36.
- [5] Bailey EH, Phoenix DA. Quicksilver deposits in Nevada,”. *U. Nevada Bulletin, Nevada State Bureau of Mines* 1944;38(5):190–2.
- [6] Perry R, Visher M. Major mines of Nevada 2013. Mineral industries in Nevada’s economy: Nevada Bureau of Mines and Geology. Special Pub. P-25, Nevada Division of Minerals; 2014.
- [7] Shevenell L, McDonald B. Geothermal energy. Special Publication MI-2012, The Nevada Mineral Industry 2012. Nevada Bureau of Mines and Geology; 2014. p. 126–48.
- [8] Garside LJ. Geothermal energy. Special Publication MI-1985, The Nevada Mineral Industry-1985. Nevada Bureau of Mines and Geology; 1986. p. 25–30.
- [9] Public Utilities Commission, State of Nevada. Renewable portfolio standard, <http://puc.nv.gov/Renewable_Energy/Portfolio_Standard/>; 2014.

- [10] US Dept. of Energy, DSIRE. Nevada Incentives/Policies for Renewables & Efficiency, Energy portfolio standard, <http://www.dsireusa.org/incentives/incentive.cfm?Incentive_Code = NV01R>; 2014.
- [11] State of Nevada, Division of Minerals. NV geothermal power production, <<http://minerals.nv.gov/Programs/Geothermal/>>; 2014.
- [12] Shevenell L, Morris C, Blackwell D. Update on near-term geothermal potential in Nevada. *Geothermal Resour Counc Bull* 2008;37(3):29–32.
- [13] Kaplan U, Reiss Z, Sullivan B. Evaporative cooling enhancement at the steamboat complex and condenser performance research and development efforts. *Geothermal Resour Counc Trans* 2011;35.
- [14] State of Nevada, Division of Minerals. Geothermal production summary—2013, <<http://minerals.nv.gov/Programs/Geothermal/>>; 2014.
- [15] Nevada Division of Environmental Protection, Underground Injection Control Program. UIC permit fact sheet, Pursuant to NAC 445A.874. Permittee name: Ormat Nevada Inc., permit number: UNEV2007204; July 2007.
- [16] Univ. Nevada Reno and Nevada Bureau Mines and Geology, “Beowawe,” <<http://www.nbmng.unr.edu/geothermal/SiteDescriptions/Beowawe.pdf?sid = Beowawe>>; 2010.
- [17] OpenEI, Geothermal energy. Beowawe hot springs geothermal area, <http://en.openei.org/wiki/Beowawe_Hot_Springs_Geothermal_Area>; 2014.
- [18] Nevada Bureau of Mines and Geology. Detailed maps of geothermal areas—Beowawe geysers, <<http://www.nbmng.unr.edu/geothermal/DetailedMaps.html>>; 2014.
- [19] Blockley WE, Gonser WC. Northern Nevada geothermal developments and the 9 MWe power plant at Desert Peak. *Proc. ninth annual geothermal and second IIE-EPRI geothermal conference and workshop*, vol. 2: English vers., EPRI AP-4259-SR, Palo Alto, CA, August 1987, p. 30-1–30-9.
- [20] Faulder DD, Johnson SD. Desert Peak geothermal field performance. *Geothermal Resour Counc Trans* 1987;11:527–33.
- [21] Cerini DJ, Diddle CP, Gonser WC. Project development Desert Peak 9 MW power plant. *Geothermal Resour Counc Trans* 1984;8:33–9.
- [22] Geothermal Hot Line. Phillips Desert Peak project on line. California Div. of Oil and Gas, Pub. No. TR02, vol. 15, No. 2, December 1985, p. 88–9.
- [23] Blackwell DD, Smith RP, et al. Why Basin and Range systems are hard to find II: structural model of the producing geothermal system in Dixie Valley, Nevada. *Geothermal Resour Counc Trans* 2009;33.
- [24] Online Nevada Encyclopedia. Dixie Valley geothermal field. Nevada Bureau of Mines and Geology, <<http://www.onlinenevada.org/articles/dixie-valley-geothermal-field>>; January 21, 2009.
- [25] Fuji Electric. Brochure 01A3-E-0013 Terra-Gen Power, LLC, USA. Dixie Valley Geothermal Power Plant. Tokyo, Japan: Fuji Electric Co. Ltd; September 2012.
- [26] Ettinger T, Brugman J. Brady hot springs geothermal power plant. *Geothermal Resour Counc Bull* 1992;21(8):258–60.
- [27] Nevada Bureau of Mines and Geology, NBMG geothermal gallery, “San Emidio Desert”: <<https://picasaweb.google.com/GreatBasinGeothermalEnergy/SanEmidioDesert#>>.
- [28] Kitz K. Daily data for San Emidio. US Geothermal, Inc., January 15–23, 2015.
- [29] OpenEI. Salt wells geothermal area, <http://en.openei.org/wiki/Salt_Wells_Geothermal_Area>; 2011.

- [30] Casteel J, Trazona R, et al. A Preliminary conceptual model for the Blue Mountain geothermal system, Humboldt County, Nevada. Proc. world geothermal congress 2010, Bali, Indonesia, 25–29 April 2010.
- [31] OpenEI. Blue Mountain geothermal area, <http://en.openei.org/wiki/Blue_Mountain_Geothermal_Area>; 2012.
- [32] Power-Technology. Blue Mountain geothermal power plant, United States of America, <<http://www.power-technology.com/projects/bluemountaingeotherm/>>; 2011.
- [33] Alternative Earth Resources Inc. Management’s discussion and analysis for the three and nine months ended March 31, 2014, <http://www.nevadageothermal.com/i/pdf/MDA_2014Q3_FINAL.pdf>; 2014.
- [34] Open EI. Dixie Valley Bottoming Binary Project Geothermal Project, <http://en.openei.org/wiki/Dixie_Valley_Bottoming_Binary_Project_Geothermal_Project>; July 22, 2011.
- [35] McDonald D. Dixie Valley Bottoming Binary Cycle. Geothermal technologies program 2010 peer review, US Dept. of Energy, <http://energy.gov/sites/prod/files/2014/02/t7/low_mcdonald_dixie_valley.pdf>; May 19, 2010.
- [36] National Geothermal Data System (NGDS). Dixie Valley Binary Cycle Production Data Dixie DOE Data—January–December, <<http://geothermaldata.org/dataset/dixie-valley-binary-cycle-production-data-dixie-doe-data-january-december-2014-xlsx>>; 2014.
- [37] Brown D. DOE monthly report—April 2014. Terra-Gen Dixie Valley LLC, May 8, 2014.
- [38] Electric Light & Power. Ormat wins commitment for \$350 million DOE loan guarantee, <<http://www.elp.com/articles/2011/06/ormat-wins-commitment-for-350-million-doe-loan-guarantee.html>>; June 10, 2011.
- [39] Gradient Resources, Inc. Patua, Nevada, <<http://www.gradient.com/portfolio/patua-nv/>>; 2014.
- [40] Combs J, Peterson N, et al. Reservoir testing and analysis at the Patua geothermal federal unit, Northwestern Nevada. Geothermal Resour Counc Trans 2012;36:31–6.
- [41] Power-Technology. Patua geothermal power plant, United States of America, <<http://www.power-technology.com/projects/patua-plant/>>; 2011.
- [42] Cichon M. Geothermal heating up in Nevada despite frigid industry climate. Renewable energy world, <<http://www.renewableenergyworld.com/rea/news/article/2012/01/geothermal-heating-up-in-nevada-despite-frigid-industry-climate>>; January 18, 2012.
- [43] Herrick AD. Stillwater Geothermal I Project. Geothermal Resour Counc Bull 1989;18(6):2–4.
- [44] Fehrenbacher K. A first-of-its-kind project makes energy from a triple whammy: Hot rocks, solar panels and mirrors. Gigaom, <<https://gigaom.com/2014/08/05/a-first-of-its-kind-project-makes-energy-from-a-triple-whammy-hot-rocks-solar-panels-and-mirrors/>>; August 5, 2014.
- [45] Hashem H. World’s first commercial CSP-geothermal hybrid underway. CSP Today, May 16, 2014.
- [46] Bizzarri F. Materials and technologies for renewable energy. ENEL Green Power S.p.A., Slide Presentation, April 13, 2011.

Nomenclature for Figures in Chapter 16

AC	Air cooled
ACC	Air-cooled condenser
C	Condenser
CP	Condensate pump
CT	Cooling tower
CV	Control valve

CW	Cooling water
CWP	Cooling water pump
D	Drain
E	Evaporator
F/S	Flasher/separator
G	Generator
HP, LP	High-, low-pressure
HXER	Heat exchanger
IW	Injection well
P	Pump
PH	Preheater
PTC	Parabolic trough collector
PW	Production well
REC	Recuperator
RST	Rotary separator turbine
S	Separator
ST	Steam turbine
T	Turbine
T/G	Turbine/generator
WC	Water cooled
WP	Well pump



Chapter 17

Heber Binary Plants, Imperial Valley, California, USA

Chapter Outline

17.1 Introduction	501
17.2 Exploration and Discovery	502
17.3 The First Heber Binary Plant	503
17.4 The Second Heber Binary Plant	506
References	512
Nomenclature for Figures in Chapter 17	512

Hitch your engine to a volcano, not a live, active volcano, but one that has simmered down after a few hundred or a few thousand centuries and now contents itself with spouting up steam.

Warren Bishop—October 1921

17.1 Introduction

Heber is a town in Imperial County, California, located some 6 miles (10 km) north of the United States–Mexico border. Situated in the fertile Imperial Valley, it is the home to 3000 people who are mainly engaged in agriculture and raising livestock. The Imperial Valley is flat for miles in all directions, being bounded on the west by the Santa Rosa and Coyote Mountains and on the east by the Chocolate Mountains.

Heber is also home to two geothermal power stations, one a 47 MW double-flash plant and one a 33 MW binary plant; see [Figure 17.1](#). It is this latter plant that will be the focus of this chapter. Both plants in recent years have been augmented by small binary units to optimize the use of the resource. In addition, there used to be a 45 MW binary plant, just south of the current binary plant, and that will be an important part of the story.

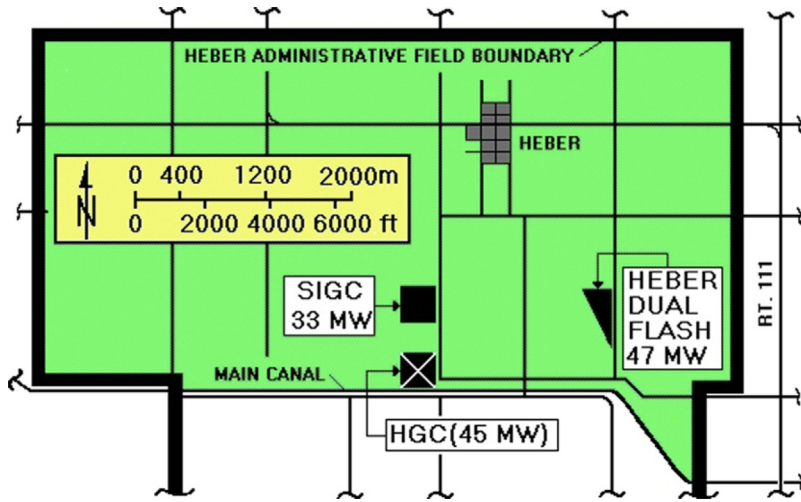


Figure 17.1 Map of a portion of the Heber KGRA showing the town and its geothermal power stations; filled symbols represent operating plants. SIGC is now called Heber 2; Heber Dual Flash is now Heber 1 [WWW]. After Ref. [1].

17.2 Exploration and Discovery

There are no surface thermal manifestations at Heber, but the Salton Trough is marked by thermal anomalies from the Salton Sea at its northern extremity, through the Imperial Valley, into Mexico, and all the way into the Gulf of California. The entire region is an active spreading zone characterized by higher than normal heat flow and recent volcanism.

In fact Heber was first explored as an oil and gas prospect by Chevron in the 1960s, based on a positive gravity anomaly just south of the town of Heber [2]. In the 1970s, spurred by the recent geothermal discovery at Cerro Prieto to the south, several shallow temperature gradient wells were drilled. It became clear that there coincided a thermal and a gravity anomaly that extended over an area of at least 6 mi^2 (15.5 km^2).

Two wells drilled in 1972 confirmed the existence of a liquid-dominated, moderate-temperature, low-salinity reservoir: the No. 1 Holtz well drilled by Magma Energy with financial support from Chevron, and the No. 1 Nowlin Partnership well by Chevron. The reservoir was seen to consist mainly of sandstones with porosities of 15–30% lying below a caprock of shale at about 2000 ft (600 m). The shales and sandstones are interbedded between 8000 and 10,000 ft (2400–3000 m), with the shales being thinner at the deeper depths [3]. The geofluid emanated from a source at about 380°F (195°C) some 2 mi to the SSE of the town, and spread toward the

NNW as it rose through the formation, yielding fluids in the range of 350–370°F (175–188°C) at depths of about 4000 ft (1200 m) [2].

The early development planning was very optimistic. It was envisioned that seven power plants with a combined capacity of 500 MW would be built— 3×100 MW and 4×50 MW, all within an area of approximately 1.5 mi^2 (4 km^2). This plan failed to anticipate that the production wells to support such a large-scale development would most likely be drawing from the same geofluid source and therefore would interfere with each other. Indeed, interference was observed soon after the first two nominal 50 MW plants were put online at about the same time in 1985, and further power development beyond the 80–90 MW level has not taken place.

17.3 The First Heber Binary Plant

The US Department of Energy (DOE) had as one of its missions in the early 1980s the development of geothermal resources, particularly moderate-temperature ones, for the generation of electricity. The Heber field was chosen to host a joint government–industry–utility partnership to demonstrate the viability of this concept. In 1980, the DOE signed an agreement with the San Diego Gas & Electric Company (SDG&E) to build a commercial-scale binary plant at Heber. SDG&E, which owned 82.5% of the plant, provided 48.9% of the funding, DOE put in 34.8%, and eight other partners contributed the remaining 16.3%; the Electric Power Research Institute (EPRI) and the Imperial Irrigation District (IID) were the next largest at about 6% each [4].

At the same time, another binary power plant—the Magmamax plant—was going through its startup operations at East Mesa, some 17 mi (27 km) to the east of Heber; see Chapter 18. That plant was rated at 12.5 MW, so the new demonstration plant would have to be larger in accordance with the principle of economy of scale. Since the early Heber plans had envisioned plants of either 50 or 100 MW, it was decided to make the demonstration plant a nominal 50 MW plant.

It had already become clear that the initial design of the Magmamax plant was overly complex and had led to many operational problems. By the end of 1982, the Magmamax plant had been rebuilt to correct the original design problems. The new Heber plant would be relatively simple and consist of a basic Rankine cycle with a single power loop and one working fluid for the cycle. Nevertheless, the state-of-the-art demonstration plant would showcase a mixed hydrocarbon working fluid, the properties of which would need to be determined by a separately funded research program with the National Bureau of Standards [5]. Furthermore, it would feature the largest hydrocarbon turbine ever built, one with a rated power capacity of 70 MW.

The flow diagram for the Heber Binary Demonstration plant (also known as the Heber Geothermal Corporation plant) is shown in Figure 17.2. The plant required an estimated 15 production wells to provide the plant with 7,450,000 lbm/h (940 kg/s) of 360°F (182°C) brine, assuming each well produces 500,000 lbm/h (63 kg/s), along with 9 injection wells. The working fluid in the cycle was a mixture of 90% isobutane and 10% isopentane. The turbine inlet pressure was set at 580 lbf/in² (40 bar), supercritical. Eight massive heat exchangers were arranged in two trains; each exchanger was 80 ft long by 80 in in diameter (24 × 2 m) and weighed 319,000 lbm (145,000 kg). The turbine-generator assembly was 61 ft (18 m) long and weighed 460,000 lbm (209,000 kg). There were two condensers that received cooling water from a nine-cell, induced-draft, counterflow cooling tower. The total parasitic power requirements for the cooling water pumps, cooling tower fans, working fluid circulating pumps, etc. came to 18.5 MW. The brine production and injection pumps added another 4.9 MW to the station load. Thus the net power at full design conditions would be 46.6 MW [6].

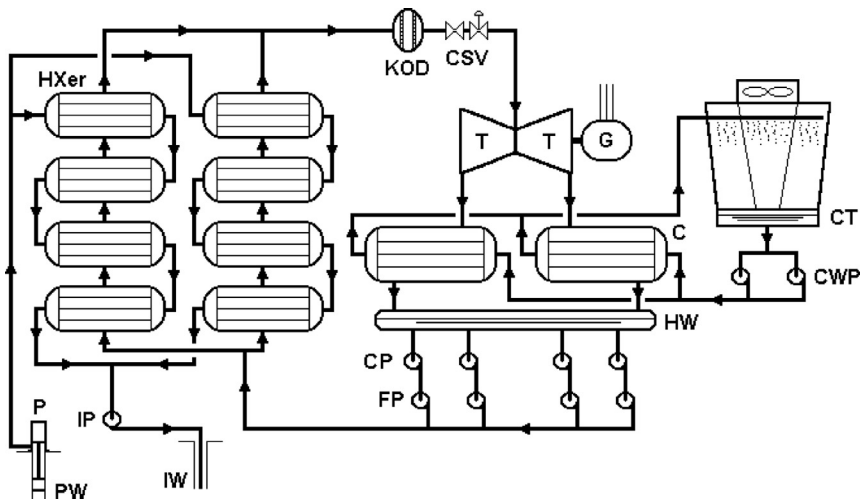


Figure 17.2 Flow diagram for the first Heber binary plant. *After Ref. [6].*

Owing to the availability of only six production wells when the plant was ready for operation, it was decided to run just one train of heat exchangers and operate the plant at about half-load until all the production wells became available. However, the plant was plagued by numerous equipment failures during its first 2 years of operation [4], including excessive vibrations in many components, cracked valve seats, valves that did not close, and working fluid pump breakdowns, all of which resulted in very sporadic operation. The downwell pumps did perform reliably but with so many plant equipment failures, this was small consolation.

The highest plant output occurred after a prolonged shutdown when eight wells returned to production and for a short time yielded about 20% more flow than under steady conditions. The plant generated 36 MW (gross) and 21 MW (net) from a brine flow of 4,870,000 lbm/h (614 kg/s) for that short period [4]. On another occasion in 1986, the flow rate to the binary plant increased by 30% over the previous steady value when the neighboring flash plant was taken out of service for maintenance [7], clear evidence of interference between the production wells for the two plants. An aerial view of the plant is shown in Figure 17.3.

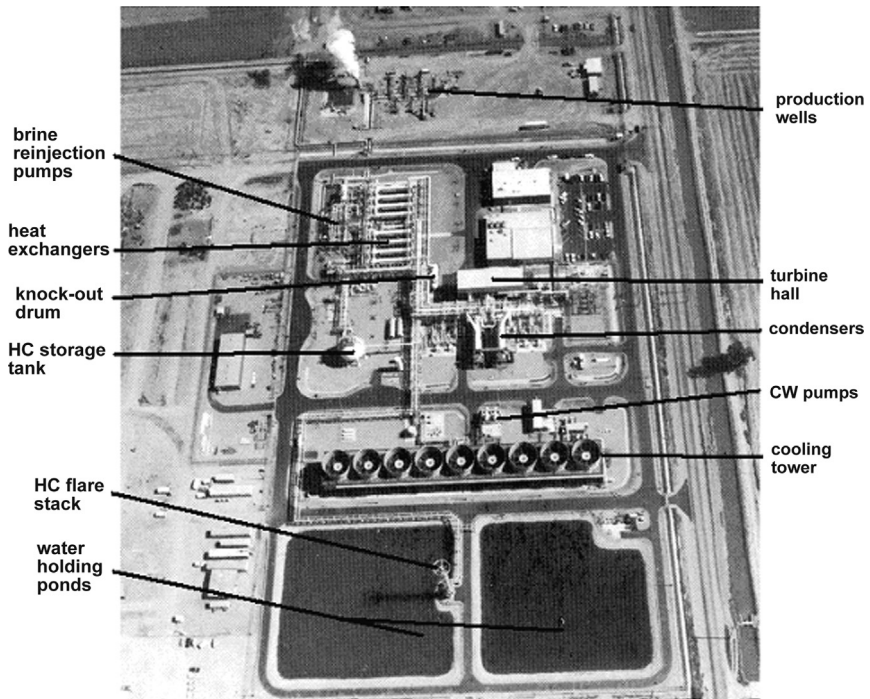


Figure 17.3 Overview of the first Heber binary plant, looking north. *After Ref. [4].*

One of the weaknesses of the design was that the parasitic power requirements were not proportional to the load, and remained high even when the turbine was running at 40–50% of its rated capacity. The cooling tower, for example, had to run at full capacity even under 50% power load. Another problem was related to the use of a supercritical pressure for the working fluid that raised the cycle internal pumping power without raising the net power relative to a subcritical pressure cycle [8]. Finally, toward the end of the plant's operation, the pressure needed to force the waste brine into the injection wells began to increase, possibly

owing to scaling in the reinjection wells. This in turn increased the power to drive the reinjection pumps and further exacerbated the already high parasitic power demands.

A Second Law analysis of the results of the part-load operation [9] based on an EPRI report [7] showed that the plant should have been able to meet its design objectives if it had been supplied with the design brine flow rate. Unfortunately, the needed production wells were not completed as the schedule called for and the owner of the plant, SDG&E, decided to halt operations in June 1987 [4]. The plant was decommissioned, placed on a long-term storage status, and eventually dismantled.

17.4 The Second Heber Binary Plant

The second attempt to develop the Heber resource with binary technology began in 1992 when the Second Imperial Geothermal Company (SIGC) undertook to construct and operate a 48 MW(nameplate), 33 MW (net) modular-type binary plant [8]. The brine temperature had fallen to about 330°F (165°C) owing to the continued operation of the double-flash plant since July of 1985.

The development of binary plants for geothermal power generation saw two competing concepts: (1) the use of a large turbine-generator in a Rankine cycle, relying on the principle of economy of scale that applied in conventional fossil and nuclear power plants, versus (2) the use of modular Rankine cycles wherein a number of small turbine-generator units would be connected to the brine in parallel to generate a reasonable amount of power. The failure of the Heber Geothermal Corporation binary plant and several successful applications of the latter option led to the modular approach as the more effective one. By 1990, the Ormat companies had installed 68 small binary units in four power plants at the nearby East Mesa field that were generating about 55 MW. Furthermore, the technology of binary plants had advanced on a practical level to achieve higher efficiencies through more effective matching of brine cooling curves with working fluid heating curves. This experience was then applied to the Heber resource with the installation of the SIGC plant that was designed with six clusters of two-level power units.

The flow diagram for Ormat's Integrated Two-Level Unit (ITLU) is shown in Figure 17.4. The Rankine cycle is designed with a subcritical boiler pressure using isopentane as the cycle working fluid. Two sets of turbine-generators are used for each modular cluster, the upper one, Level 1, being rated at 4.5 MW (gross) and the lower one, Level 2, at 3.5 MW (gross); the net power for the entire cluster is about 6.8 MW.

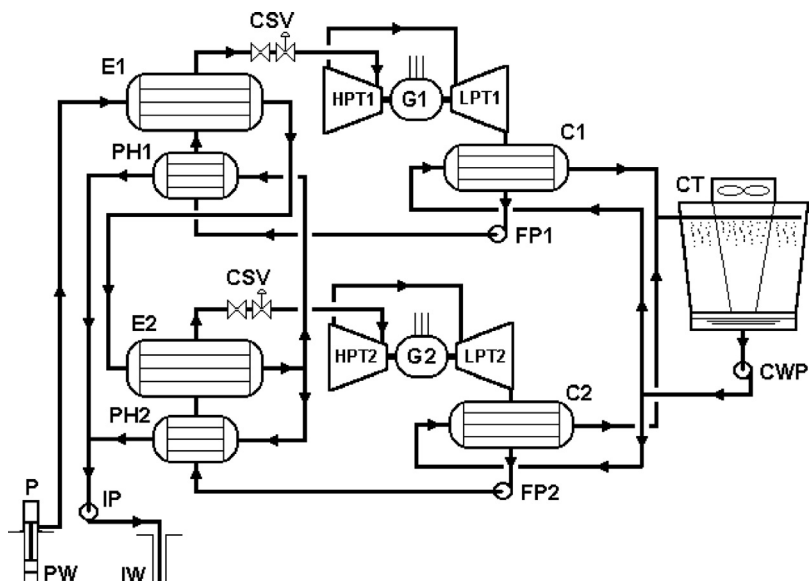


Figure 17.4 Flow diagram for Ormat's Integrated Two-Level Unit.

The SIGC Heber plant (now Heber 2) consists of six ITLUs and can deliver 33 MW of electricity (net). [Figure 17.5](#) shows one of the six modular clusters [\[10\]](#).

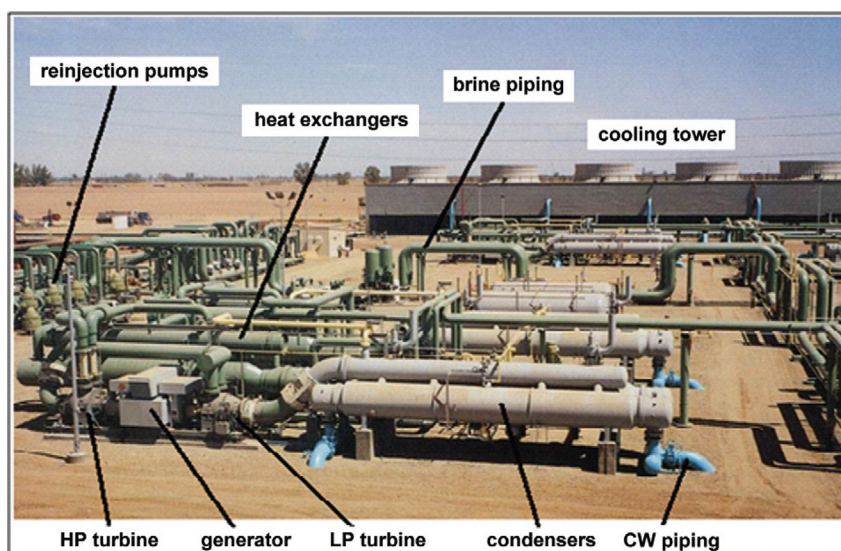


Figure 17.5 A view of the SIGC binary plant at Heber. *Photo courtesy of Ormat, Inc. [10] [WWW].*

Figure 17.6 is an aerial view of the configuration of the ITLUs, cooling towers, brine piping, and reinjection pumps.



Figure 17.6 SIGC Heber binary plant showing six clusters of ITLUs. Brine reinjection pumps are located in the upper center of the photograph. The photograph in Figure 17.5 was taken from the top of the left (southern) cooling tower. *Photo courtesy of Ormat, Inc. [WWW].*

The technical specifications and performance figures for the SIGC plant are given in Table 17.1. Note that the Second Law cycle utilization efficiency is roughly the same as for a single-flash plant, and that the First Law cycle thermal efficiency is the typical value for a simple binary plant. If this is compared to the cycle efficiency for Miravalles Unit 5 (see Chapter 16), it will be seen that the presence of the recuperator and the lack of reinjection pumps at Miravalles resulted in an increase in the net efficiency of about 3.5 percentage points, or a gain of over 30%.

The SIGC plant is served by 11 production wells having an average depth of 4000 ft (1219 m); each well is pumped by a motor-driven, line-shaft, centrifugal pump set at 1400 ft (427 m). The average flow rate from the wells is 1600 gpm or 722,650 lbm/h (91 kg/s). Only seven wells were needed to meet, and actually exceed by 13%, the design power output on startup in 1993 [8]. There are 13 reinjection wells, averaging 4500 ft (1370 m) in depth.

In the year 2000, after six years of continuous operation it was reported that the plant was online 99% of the time and averaged over 90% annual capacity factor [8]. This high reliability comes about partly through redundancy. If a component of some unit needs replacing, only that unit needs to be removed from service. The other units can receive some of the brine from the down unit, and can be over-driven for a short period of time to compensate for the lost power. Say 4 MW is lost from one Level 1 unit; each of the other 11 units needs to boost its output by only 365 kW to keep the whole plant at its rated output. In addition, the units are

TABLE 17.1 Technical specifications for SIGC Heber binary plant.

Start-up year	1993
Type	ITLU, dual-pressure cycle
No. of units ^a	12 (6 × 2)
Rating, MW	44
Net power, MW	33
Brine flow rate, lbm/h	1,000,000/ITLU
Working fluid	isopentane, i-C ₅ H ₁₂
<i>Preheaters:</i>	
No. per ITLU	2
Type	Shell and tube
Brine outlet temperature, °F	154
Heat duty, MW-th/ITLU	8.94 (L. 1), 9.44 (L. 2)
<i>Evaporators:</i>	
No. per ITLU	2
Type	Shell and tube
Brine inlet temperature, °F	330
Heat duty, MW-th/ITLU	18.0 (L. 1), 15.7 (L. 2)
<i>Condensers:</i>	
No. per ITLU	4
Type	Shell and tube
Heat duty, MW-th	22.7 (L. 1), 22.1 (L. 2)
CW temperatures, °F:	
Inlet	68.0
Outlet	82.4
<i>Turbine:</i>	
Type	Axial inflow
Cylinders/ITLU	2
Flows/turbine	1
Stages/turbine	2
Inlet temperature, °C	NA
Inlet pressure, psia	225
Speed, rpm	1800
<i>Feed pumps:</i>	
No. per ITLU	2
Power input, kW	225 (L. 1), 120 (L. 2)
<i>Plant performance:</i>	
Net SGC, lbm/kW · h	181.8
Utilization efficiency, %:	
Gross	42.4
Net	35.0
Thermal efficiency, %:	
Gross	12.7
Net	10.5

^aThroughout this book, a "unit" refers to a generator, whether it is driven by one or two turbines.

manufactured and largely assembled and tested in the factory, leaving only bolting and welding to be done on site. This means a high level of quality control can be maintained.

The current SIGC Heber binary plant (Heber 2) has achieved the success that was hoped for but not realized when the original Heber demonstration plant was built. The technical reasons for this outcome have been described in this chapter. One other important reason is that the power plants at both Heber sites and the Heber reservoir are now under the ownership of a single company, which has led to a better understanding of the reservoir. The conceptual model and reservoir simulation have been improved, allowing for better placement of new production and injection wells that has greatly reduced the interference between the production wells for the binary plant and the double-flash plant.

This knowledge has also led to the construction of two 10 MW binary units, Gould II and Heber South, immediately to the west of the main plant; see Figure 17.7.

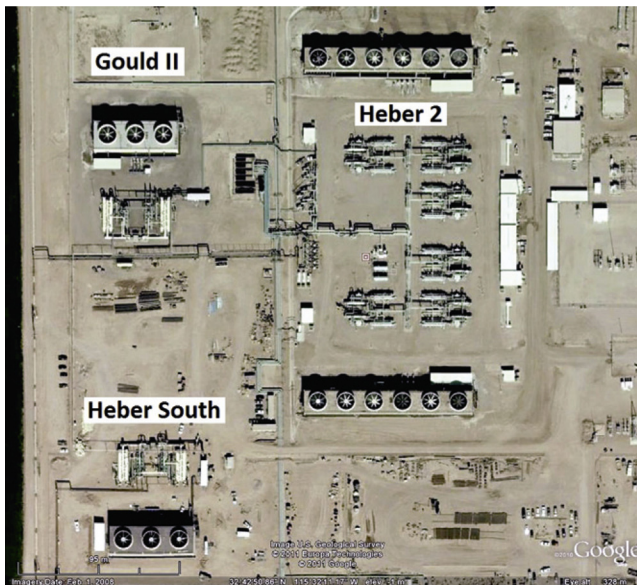


Figure 17.7 Heber 2 complex. Google Earth image, February 1, 2008; labels by author [WWW].

To further optimize the performance of the entire Heber power complex, in 2006 a bottoming binary facility, Gould I, was added to the Heber 1 double-flash plant; see Figure 17.8. The “full OEC” has two turbines driving a 5 MW generator; the “ $\frac{1}{2}$ OEC” is a 2.5 MW unit; and the “TP unit” is a unique turbine-driven

brine injection pump system; see Figure 17.9. All four turbines operate in parallel using waste brine from the flash vessels at Heber 1. As with the new OECs at Heber 2, all units employ water-cooled condensers in conjunction with cooling towers.



Figure 17.8 Gould 1 bottoming binary units installed just south of the Heber 1 double-flash plant. Google Earth image, February 1, 2008; labels by author [WWW].



Figure 17.9 Turbine (center left)—injection pump (center right) unit at Gould 1 bottoming plant south of Heber 1 double-flash plant. Photo courtesy of Ormat.

As of this writing (November 2014) the entire Heber complex has 110 MW installed using 19 units, separated by about one mile (1.6 km). The two plant sites occupy slightly over 0.4 km² with several outlying well pads each approximately 0.01 km² in area. The areal power density is roughly 275 MW/km² of surface area usage.

References

- [1] DiPippo R. Geothermal electric power production in the United States: a survey and update for 1990–1994. *Proc. 1995 world geothermal congress, international geothermal association*, vol. 1; 1995, p. 353–62.
- [2] Salveson JO, Cooper AM. Exploration and development of the Heber geothermal field, Imperial Valley, California. *Geothermal Resour Counc Trans* 1979;3:605–8.
- [3] Tansev EO, Wasserman ML. Modeling the Heber geothermal reservoir. *Geothermal Resour Counc Trans* 1978;2:645–8.
- [4] Berning J, Bigger JE, Fishbaugher J. Special Report EPRI AP-5787-SR Heber binary-cycle geothermal demonstration power plant: half-load testing, performance, and thermodynamics. Palo Alto, CA: Electric Power Research Institute; 1988.
- [5] Gallagher JS, Linsky D, Morrison G, Levelt Sengers JMH. Note 1234 Thermodynamic properties of a geothermal working fluid; 90% isobutane–10% isopentane, NBS Tech. Washington, DC: National Bureau of Standards, US Gov. Printing Office; 1987.
- [6] Nelson TT. Heber binary project. *Geothermal Resour Counc Trans* 1987;11:459–63.
- [7] Berning J, Bigger JE, Fishbaugher J. Special Report EPRI AP-5240-SR Heber binary-cycle geothermal demonstration power plant: startup and low-power testing. Palo Alto, CA: Electric Power Research Institute; 1987.
- [8] Sones R, Krieger Z. Case history of the binary power plant development at the Heber, California geothermal resource. *Proc. world geothermal congress 2000, international geothermal association*; 2000, p. 2217–9.
- [9] DiPippo R. Heber binary demonstration plant: a second law assessment of low-power tests. *Geothermal Hot Line* 1988;18:67–8.
- [10] Anon. Heber Second Imperial Geothermal, Imperial County, California, USA. Data sheet, Ormat, Inc., Sparks, NV, undated.

Nomenclature for Figures in Chapter 17

C	Condenser
CP	Condensate pump
CSV	Control and stop valves
CT	Cooling tower
CWP	Cooling water pump
E	Evaporator
FP	Feed pump

G	Generator
HPT	High-pressure turbine
HW	Hotwell
HXer	Heat exchanger
IP	Injection pump
IW	Injection well
KOD	Knock-out drum
LPT	Low-pressure turbine
P	Pump
PH	Preheater
PW	Production well
T	Turbine



Chapter 18

Magmamax Binary Power Plant, East Mesa, Imperial Valley, California, USA

Chapter Outline

18.1 Setting and Exploration	515
18.2 Magmamax Binary Power Plant	516
18.3 Modified Magmamax Binary Power Plant	524
18.4 Conclusion	527
References	528

... the greatest dividend I ever had in my life came the day I went into the geothermal steam business, not from the standpoint of money, but from the standpoint of mental interest.

Barkman C. "B.C." McCabe—1969

18.1 Setting and Exploration

The East Mesa geothermal field lies roughly 17 miles (27 km) east of Heber in California's Imperial Valley, across the flat, irrigated fields of alfalfa. The East Mesa resource is about five miles (8 km) east of the city of Holtville and one mile (1.6 km) east of the East Highline Canal, on the unirrigated side in flat desert land. It stretches for four miles (6.4 km) north-south, just north of Interstate 8, and covers an area of 6–8 mi² (15.5–20.7 km²).

Like the Heber field, East Mesa is a "hidden" geothermal resource, lacking any surface thermal manifestations; see Chapter 17. Interest in this area began in 1968 with the passage by the US Congress of the Colorado River Basin Project Act (Public Law 90–537). The intent was to augment the water supply from the Colorado River that was under heavy pressure from agricultural interests for irrigation usage. The idea was to desalinate the geothermal brines that were known to exist in aquifers beneath sections of the Imperial Valley. The energy contained in the hot brines could be used to generate electricity that in turn could be used to pump water from the Salton Sea for reinjection into the geothermal reservoir and thereby provide replenishment of the extracted fluids and lower the level of the Salton Sea.

The US Bureau of Reclamation (USBR) was given the task of making this a reality. It contracted for an exploration program with the University of California at Riverside that produced geophysical studies showing a well-defined thermal anomaly with temperature gradients exceeding $20^{\circ}\text{C}/100\text{ m}$, coinciding with a residual Bouguer gravity high of more than 5 mgal and a seismic ground-noise anomaly of 42 dB [1–3].

In the summer of 1972, the discovery well, Mesa 6–1, was drilled to 8030 ft (2450 m) into the center of the anomaly. The reservoir temperature was 399°F (204°C); the well could produce 222,000 lb/h (28 kg/s) at a wellhead pressure of 65 lbf/in² (4.5 bar), and the reservoir pressure was 3175 lbf/in² (219 bar). Four more wells were completed soon thereafter, and the USBR constructed a test facility at the site. In keeping with the aim of the law, the initial focus was on producing as much fluid as possible from the reservoir and desalinating it using two proposed processes: a multistage flash process and a vertical tube evaporation process [4]. Since the geofluid after desalination would be delivered off-site, the resource would become depleted unless make-up water could be found and reinjected. This led to tests of reinjection using the one of the five wells, Mesa 5–1, as the designated receiving well.

Concurrent with the desalination research, other tests were conducted on corrosion of materials exposed to the brines, on heat exchangers, and on a tiny mobile power plant—a helical rotor expander built by the Hydrothermal Power Company (see Section 9.5.3). The latter test produced 18 kW of electric power using part of the flow from well Mesa 6–1 [4]. All of this work was carried out in the late 1970s and would pave the way for the power plants that would be built in the coming years.

18.2 Magmamax Binary Power Plant

The only geothermal binary power plant in existence in the 1970s was the 670 kW unit at Paratunka on the Kamchatka peninsula in Russia that was put into operation in 1967 [5]. At that time, research into developing a practical binary plant that could use low-to-moderate-temperature resources was being carried out in the United States, England, Poland, and Russia [6]. However, up to 1970 there was little reported in the technical literature except for a few Russian articles cited in Ref. [6].

In March 1970, B.C. McCabe, Chairman and CEO of Magma Energy, Inc., a subsidiary of Magma Power Company, informed his stockholders of the company's intention to develop a new process for the utilization of liquid geothermal resources. He named it the “Magmamax” process and received US Patent No. 3,757,516. Magma acquired Federal leases at East Mesa in 1974, conducted drilling and well testing, and in 1976 announced their intention to construct the Magmamax plant at a location about one mile (1.6 km) SSW of the USBR Test

Site. Two years later, construction got underway and the plant came online in September 1979 [7]. The flow diagram for the 12.5 MW (gross), 11 MW (net) power plant is shown in Figure 18.1.

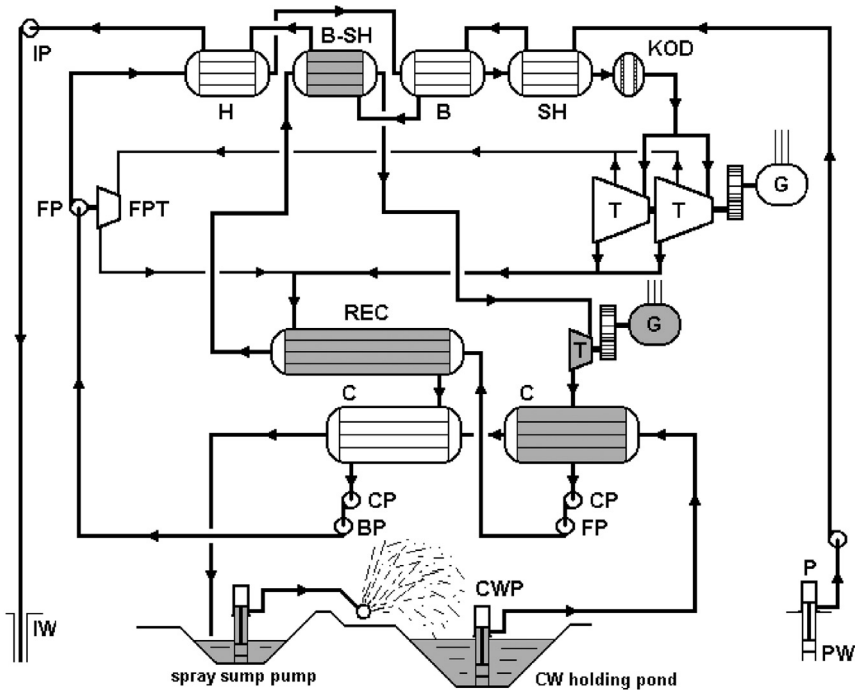


Figure 18.1 Flow diagram for the original MagmaMax binary plant.

The unique features of the MagmaMax design are as follows:

- Downwell pumps are used to prevent flashing.
- True counterflow heat exchangers are used to maximize heat transfer.
- Two Rankine cycles with different working fluids are used, one with isobutane and one with propane (shaded components in Figure 18.1).
- A heat recuperator couples the two cycles.
- 100% of the brine is reinjected.
- Cooling is achieved by spray evaporation.
- Ponds hold the cooling water for use at optimum times.

As a first-of-a-kind power plant, there was a great deal of engineering that needed to be done. The consulting firm of J. Hilbert Anderson was hired to perform the engineering for the plant [8]. Particular attention was paid to the heat exchangers that would transfer the thermal energy of the geothermal brine to the

cycle working fluid, and to the recuperator that coupled the two cycle working fluids. Since there were no commercial hydrocarbon turbines for this type of service, they also had to be designed from scratch. Furthermore, the novel cooling system was intended to take maximum advantage of the desert climate to enhance the plant power output during times of peak electrical demand [9,10].

The heat exchanger configuration was driven by the need to have easy access to the internals for purposes of cleaning the surfaces that might become fouled from scale deposition. The brine was placed on the shell side, with the hydrocarbons on the tube side. This somewhat unusual design was chosen because the pressure of the hydrocarbon working fluids was greater than that of the brine, allowing for lighter materials and lower cost. However, this meant that the tube bundles would have to be removed for cleaning the outside surfaces of scale deposited by the brine. Also since the isobutane was at a supercritical pressure, the heating and vaporization processes could best be achieved with the fluid confined within the tubes, as was common in fossil-fired supercritical steam power plants.

To achieve pure counterflow, the heat exchanger shells would be long, 80 ft (24 m) and slender, and there would be no baffles in the brine path. To enhance heat transfer, the tubes would have very thin walls, 35 mils or 0.035 in (0.0014 mm). To allow for thermal expansion, there would be a floating head at one end to allow the tube bundle to grow and shrink as the unit was subjected to varying temperatures. A floating balance piston, lubricated by oil, would prevent mixing of the brine and the hydrocarbon working fluids [11]. The units were specially engineered and constructed to specification, rather than “off-the-shelf.” The heat exchangers are shown in [Figures 18.2 and 18.3](#).



Figure 18.2 Overview of heat exchangers, original Magmamax design. Brine-hydrocarbon heat exchangers are in center; recuperator is at upper left. *June 1981, photo by author.*



Figure 18.3 Isobutane liquid heaters. Note vertical brine crossover pipes (shell side) and horizontal end-connectors carrying isobutane (tube side) from one heater to the next. June 1981, photo by author.

The recuperator was a one-of-a-kind component that provided heating and boiling of the propane within a single tube pass. It supplied 75% of the total heat into the propane bottoming loop, the remaining 25% coming from a relatively small brine heat exchanger; see the shaded elements, B-SH and REC, in Figure 18.1. The recuperator is shown in Figure 18.4, along with the condensers.

The York Division of Borg-Warner Corporation designed and built the 10 MW isobutane turbine, a two-cylinder, tandem-compound, three-stage, radial-flow, single-extraction machine. This was essentially a compressor that had been modified for expansion duty. It was compact and had several advantages relative to steam turbines of the same rating. The extraction point was used to bleed off sufficient isobutane to drive an auxiliary turbine that was connected to the final boiler feed pump through a reduction gear box. This was seen as another efficiency measure whereby internal power from the cycle would be used for this parasitic load, rather than using a motor-driven pump and purchasing electricity from the grid. In Figure 18.5 it is seen awaiting installation at the East Mesa site; in Figure 18.6 it is in operation.

As for the cooling system, the designers decided against a simple cooling tower and instead opted for a phased or batch cooling system with daytime storage and nighttime cooling via spray ponds. Daytime temperatures at East Mesa during the summer can reach 125°F (50°C), but clear nights can result in low temperatures due to radiational cooling. To capitalize on this, two daytime



Figure 18.4 Condensers and recuperator (upper vessel) at original plant. The two condensers on the near side are for the main isobutane cycle; the third one behind them served the propane cycle. June 1981, photo by author.

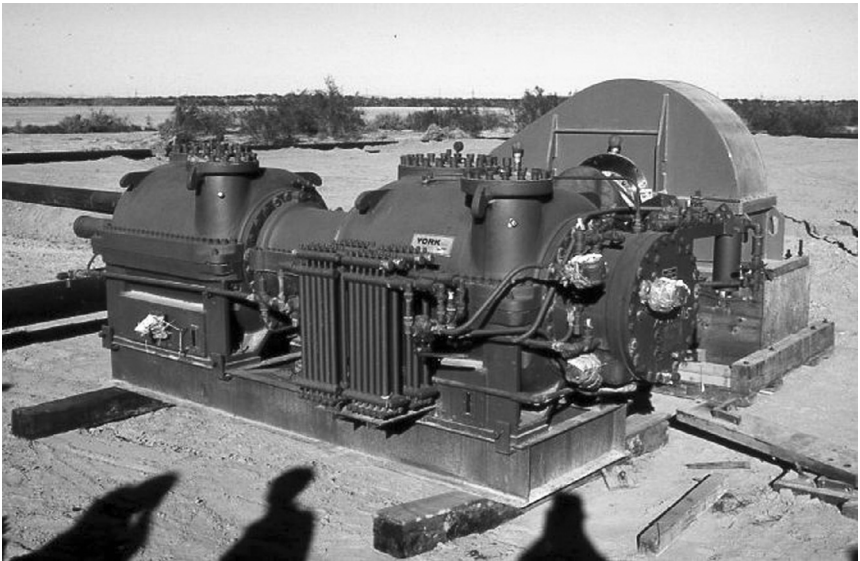


Figure 18.5 Original turbine awaiting installation at East Mesa. The reduction gear is behind the turbine. March 1978, photo by author.



Figure 18.6 Isobutane turbine in operation. *June 1981, photo by author.*

holding ponds were excavated into the desert soil to receive the spent cooling water from the condensers, and one deep stratified holding pond for the water that had been cooled overnight. The deepest layers in this pond held the coldest water, and the circulating pump was designed to draw water from different levels depending on where the coldest water happened to be. This approach was designed to reduce the parasitic power requirements associated with cooling water pumps and cooling tower fans.

Make-up water to account for the water lost to evaporation in the spray process was obtained from the nearby East Highline Canal. The use of the heat recuperator had the added benefit of lowering the heat load on the condensers and therefore reduced the amount of heat that had to be rejected to the cooling water. The ponds are shown in [Figures 18.7 and 18.8](#).

[Table 18.1](#) displays the design technical specifications for the MagmaMax plant in its original configuration. [Table 18.2](#) shows the cost of the plant by major category [10].



Figure 18.7 Cooling water spray pond. *October 1980, photo by author.*



Figure 18.8 Deep holding pond for cooling water with pump island. Note spray facility at right; cooled water drains by gravity to the holding pond. *October 1980, photo by author.*

TABLE 18.1 Design specifications – original Magmamax dual-fluid binary plant.

Start-up year	1979	<i>Recuperator:</i>	
Type	Dual-fluid, recuperative	No. per unit	1
No. of units	2	Type	Shell/tube, counterflow
Rating, MW	12.5 (10 + 2.5)	Hot-side temperatures, °F:	
Net power, MW	11.2 (9 + 2.2)	<i>i</i> -C ₄ H ₁₀ inlet	225
Brine flow rate, lbm/h	1,426,400	C ₃ H ₈ outlet	177
Working fluid 1	Isobutane, <i>i</i> -C ₄ H ₁₀	Cold-side temperatures, °F:	
Working fluid 2	Propane, C ₃ H ₈	C ₃ H ₈ inlet	72.5
<i>i</i> -C ₄ H ₁₀ preheaters:		<i>i</i> -C ₄ H ₁₀ outlet	150
No. per unit	6	<i>i</i> -C ₄ H ₁₀ condensers:	
Type	Shell/tube, counterflow	No. per unit	2
Inlet pressure, psi,a	605	Type	1-pass shell, 2-pass tube
Temperatures, °F:		Inlet temperature, °F	150
Inlet	93	Outlet temperature, °F	87
Outlet	275	<i>C</i> ₃ H ₈ condensers:	
Brine outlet temperature, °F	180	No. per unit	1
<i>C</i> ₄ H ₁₀ evaporators:		Type	1-pass shell, 1-pass tube
No. per unit	2	Inlet temperature, °F	115
Type	Shell/tube, counterflow	Outlet temperature, °F	72.5
<i>C</i> ₄ H ₁₀ superheaters:		<i>Cooling water:</i>	
No. per unit	2	Temperatures, °F:	
Type	Shell/tube, counterflow	Inlet to C ₃ cond.	62.0
<i>i</i> -C ₄ H ₁₀ outlet temperature, °F	345	Outlet from C ₃ cond.	65.5
Brine inlet temperature, °F	360	Inlet to <i>i</i> -C ₄ cond.	65.5
<i>C</i> ₃ H ₈ superheater:		Outlet from <i>i</i> -C ₄ cond.	79.5
No. per unit	1	Flow rate, gal/min	25,000
Inlet temperature, °F	177	<i>i</i> -C ₄ H ₁₀ feed pumps:	
Outlet temperature, °F	205	No. per unit	3
<i>i</i> -C ₄ H ₁₀ turbine:		Temperatures, °F:	
Type	Radial inflow, extraction	Inlet	87
Cylinders/unit	2	Outlet	93
Flows/turbine	1	<i>Plant performance:</i>	
Stages/flow	3	Net SGC, (lbm/h)/kW	127.4
Inlet temperature, °F	345	Utilization efficiency, %:	
Outlet temperature, °F	225	Gross	46.1
Inlet pressure, psi,a	500	Net	41.3
Outlet pressure, psi,a	60	Thermal efficiency, %:	
Speed, rpm	6391	Gross	16.2
<i>C</i> ₃ H ₈ turbine:		Net	14.5
Type	Radial inflow		
Cylinders/unit	1		
Flows/turbine	1		
Stages/flow	3		
Inlet temperature, °F	205		
Inlet pressure, psi,a	460		
Outlet pressure, psi,a	129		

TABLE 18.2 Cost of the plant by major category [10].

Category	Total cost, 1980 \$	Cost, \$/net kW
Land improvements	531,700	47.50
Building	319,500	28.50
Cooling system	3,472,700	310.00
Power equipment	1,017,400	90.80
Isobutane system	2,382,800	212.75
Propane system	1,050,000	93.75
Brine system	2,026,100	180.90
General support system	1,565,100	139.75
Engineering	948,000	84.65
Overhead and A&G	1,413,900	126.25
Total	14,727,200	1314.90

18.3 Modified Magmamax Binary Power Plant

After about two years of sporadic operation during which the propane bottoming cycle never was put into use, the plant was shut down for an extensive modification. The troubles had begun even before the plant went into full operation. Just around the time when the plant had been undergoing its original startup procedure, there was a severe earthquake centered in the Imperial Valley (October 19, 1979). Although there was no obvious external damage to the plant, the brine heat exchangers sustained internal damage to the joints between the tubes and the tube sheets. This only became clear after it was noticed that leaks were present that allowed brine to mix with the isobutane [10]. Upon inspection, it was seen that corrosion was present in the brine system and that the 35 mil-thick carbon steel tubes were undergoing corrosion at rates of between 5 and 25 mils/year [12]. The balance piston at the floating end of the heat exchangers had been damaged and also was leaking. There were also numerous problems related to excessive vibrations of various components, including the main turbine.

Following various attempts to patch the problems, it was decided to conduct a major overhaul. Magma hired Dow Engineering Company to carry out the modifications. What emerged in the fall of 1982 was a drastically different plant. Gone were the main turbine, the true counterflow heat exchangers, and the interconnected Rankine cycles. In their place, one found a simple, non-extraction, isobutane turbine from Mafi Trench, and nine larger brine heat exchangers (60 ft × 29 in) with the brine on the tube side and the hydrocarbons on the shell side. The isobutane needed to drive the boiler feed pump turbine (BFPT) came from a separate side-stream off the superheater. A pressure-letdown (throttle)

valve was inserted to lower the isobutane pressure to match the BFPT inlet pressure. The recuperator was still there but it now served only as a preheater for the isobutane cycle; the propane cycle was now independent of the isobutane cycle. Figure 18.9 is a flow diagram for the new MagmaMax design; Figures 18.10 and 18.11 show the reconfigured heat exchangers.

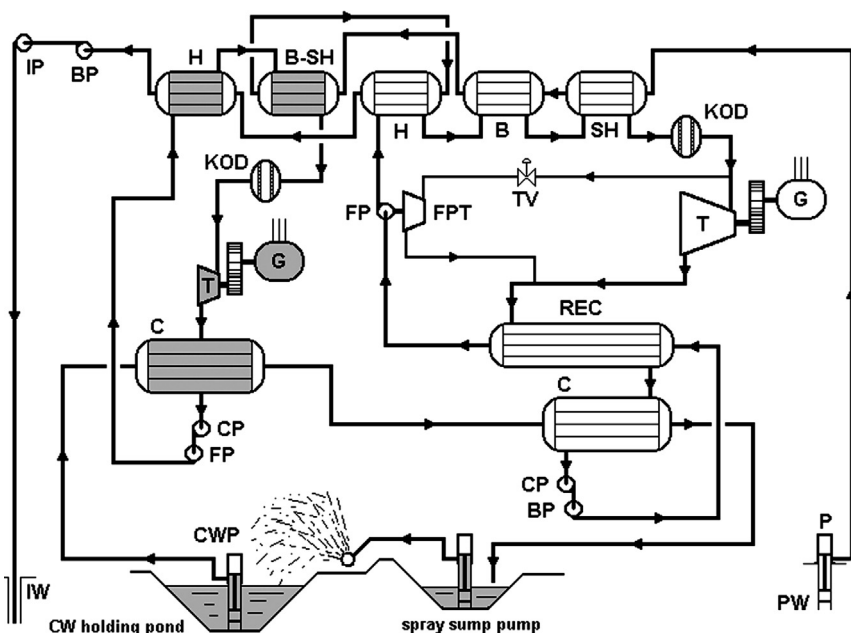


Figure 18.9 Flow diagram for redesigned MagmaMax binary plant.

A summary of the technical specifications for the redesigned plant is given in Table 18.3 [7]. Note that the brine inlet temperature is 10°F lower than the original plant. Also the brine is cooled to 167°F , 13°F lower than the original design. Together with the increased brine flow rate, the new plant receives 21% more heat from the brine. The new utilization efficiencies are: 41.1% gross, 36.8% net; the new thermal efficiencies are: 13.4% gross, 12.0% net. All of these values are significantly lower than the original design.

The new plant began its operating life in October 1982 and went through a 2-month period of adjustment and repair for relatively minor problems. Then the plant entered into a period of essentially continuous operation except for scheduled outages for maintenance and inspection. For the next 15 months, excluding scheduled outages, the plant averaged 96.8% online availability [7].



Figure 18.10 Overview of redesigned MagmaMax plant. Note new heat exchangers and the Y-connecting pipe (center) between the single exhaust of the new turbine and the recuperator. *October 1984, photo by author.*



Figure 18.11 Isobutane boiler-superheaters at redesigned plant. Note brine vertical connectors on the tube side; isobutane connectors (shell side) are seen between alternating sets of heat exchangers. *October 1984, photo by author.*

TABLE 18.3 Specifications for redesigned MagmaMax plant [7].

Item	Value
<i>Mass flow rates:</i>	
Brine	1,700,000 lbm/h
Isobutane	1,300,000 lbm/h
Propane	342,500 lbm/h
<i>Brine temperatures:</i>	
Inlet	350°F
Outlet	167°F
<i>i-C₄H₁₀ turbine:</i>	
Mass flow rate	1,150,000 lbm/h
<i>Temperatures:</i>	
Inlet	335°F
Outlet	209°F
<i>Pressures:</i>	
Inlet	565 psi,a
Outlet	70 psi,a
Generator output	10,500 kW
<i>i-C₄H₁₀ boiler feed pump turbine:</i>	
Mass flow rate	150,000 lbm/h
<i>Temperatures:</i>	
Inlet	285°F
Outlet	209°F
<i>Pressures:</i>	
Inlet	300 psi,a
Outlet	70 psi,a
Pumping power	1120 kW
<i>C₃H₈ turbine:</i>	
<i>Temperatures:</i>	
Inlet	205°F
Outlet	120°F
<i>Pressures:</i>	
Inlet	480 psi,a
Outlet	155 psi,a
Generator output	2000 kW
<i>Cooling water:</i>	
Volumetric flow rate	25,000 gal/min

18.4 Conclusion

In 1983, Magma signed a 30-year power purchase agreement with Southern California Edison (SCE), whereby SCE would buy all the power that the MagmaMax plant could generate. In honor of Magma's founder and geothermal pioneer, the plant was renamed the "B.C. McCabe Power Plant." In the early

1990s the plant was sold to GEO East Mesa L.P. and was renamed yet again to “GEM-1.” Eventually the plant was taken over by Ormat as part of their other holdings in the East Mesa area and decommissioned and dismantled.

The downwell pumps that had been so problematic in the early years became very reliable and operated routinely for up to two years without trouble. This improvement in brine production was the key to further development of the moderate-temperature geothermal resources in East Mesa. Today, there are five geothermal power plants at East Mesa, all operated by Ormat; see [Figure 18.12](#). With the exception of the two double-flash units at GEM-2 and -3, the plants are modular binary units.

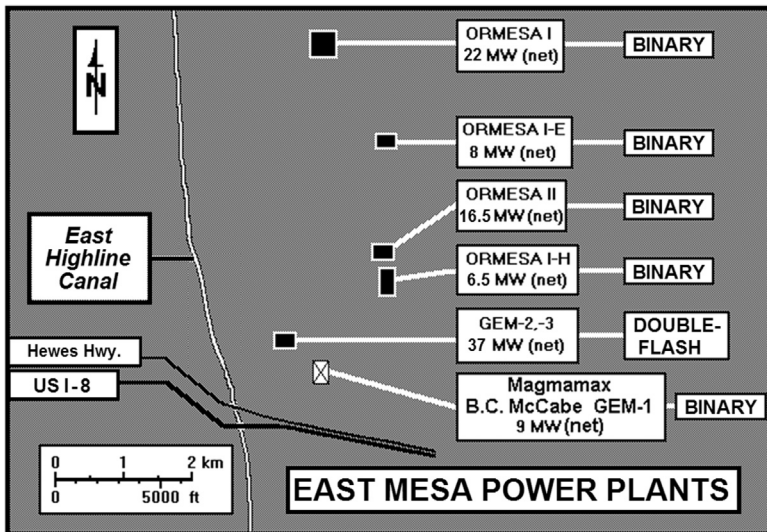


Figure 18.12 East Mesa geothermal power plants as of 2014; filled rectangles denote operating plants.

The technology that was brought to life by Magma in 1979 is now flourishing in the desert of East Mesa, generating about 90 MW in a reliable and environmentally friendly fashion.

References

- [1] Combs J. Heat flow and geological resource estimates for the Imperial Valley. Cooperative geological-geophysical-geochemical investigations of geothermal resources in the Imperial Valley of California. Educational Research Services, University of California at Riverside; 1971. p. 5–27
- [2] Bielher S. Gravity studies in the Imperial Valley. Cooperative geological-geophysical-geochemical investigations of geothermal resources in the imperial Valley of California. Educational Research Serv., University of California at Riverside; 1971. pp. 29–41

- [3] Douze EJ. Seismic ground-noise survey at the Mesa Anomaly. Dallas, TX: Teledyne-Geotech; 1971.
- [4] Anon. Geothermal resource investigations: East Mesa test site, Imperial Valley, California, status report, US Bureau of Reclamation; April 1977.
- [5] DiPippo R. US Dept. of Energy, DOE/RA/28320-1 Geothermal energy as a source of electricity: a worldwide survey of the design and operation of geothermal power plants. Washington, DC: US Gov. Printing Office; 1980
- [6] Moskvicheva VN, Popov AE. Geothermal power plant on the Paratunka river. Geothermics—special issue 2, U.N. symposium on the development and utilization of geothermal resources, Pisa, 1970;2(Pt. 2):1567–71.
- [7] Hinrichs TC. MagmaMax power plant—success at East Mesa. EPRI AP-3686. Proc. eighth annual geothermal conference and workshop, Electric Power Research Institute, Palo Alto, CA; 1984. p. 6-21–6-30.
- [8] Anderson JH. The vapor-turbine cycle for geothermal power generation. In: Kruger P, Otte C, editors. Geothermal energy: resources, production, stimulation. Stanford, CA: Stanford University Press; 1973 [chapter 8].
- [9] Dambly BW. Heat exchanger design for geothermal power plants. Proc. 13th intersociety energy conversion engineering conference, V. 2, Society of Automotive Engineers; 1978. p. 1102–8.
- [10] Hinrichs TC, Dambly BW. East Mesa MagmaMax power process geothermal generating plant: a preliminary analysis. EPRI TC-80-907. Proc. fourth annual geothermal conference and workshop, Electric Power Research Institute, Palo Alto, CA; 1980. p. 5-1–5-13.
- [11] Pundyk JM. Performance evaluation of Magma 11.2 MWe binary plant. Proc. third annual geothermal conference and workshop, Electric Power Research Institute, Palo Alto, CA; 1979. p. 2-24–2-30.
- [12] Shannon DW. Monitoring the chemistry and materials of the Magma geothermal binary cycle generating plant. Geothermal Mater Rev 1982;4(4): US DOE/SF/11503-03



Chapter 19

Nesjavellir and Hellisheidi Plants, Iceland

Chapter Outline

19.1 Introduction	531
19.2 Geology and Geosciences	532
19.3 Nesjavellir Power Plant	535
19.4 Hellisheidi Power Plant	541
References	544

What angered the gods, when the lava flowed, on which we are standing now?

Snorri Godi, Kristni Saga

19.1 Introduction

Iceland, sitting astride the Mid-Atlantic Ridge with abundant active volcanism and a population of around 332,000, has the highest per capita concentration of geothermal energy of any country in the world. Furthermore, most of the residents are clustered in the Reykjavik metropolitan area making it feasible to use geothermal energy to provide electricity and heat to nearly everyone living in Iceland.

Between geothermal and hydro, about 86% of Iceland's primary energy needs are being met with renewable sources. Geothermal contributes 68% of the total need. Space heating from geothermal hot water takes care of 90% of all the homes. In addition, the hot water is used in greenhouses, fish farming, snow melting, swimming pools, and various industries. The most recent estimate of direct heating (2015) is 8030 GWh-th. The total installed geothermal electric power capacity stands at 663 MW with an annual generation of 5245 GWh. The system has an overall capacity factor of 90%. Geothermally produced electricity accounts for 29% of the total in the country [1].

The full listing of the geothermal power plants in Iceland can be found in Appendix A.6.2. This chapter focuses on two power stations that lie close to Reykjavik and on opposite sides of the Hengill volcano: Nesjavellir and Hellisheidi.

19.2 Geology and Geosciences

Iceland is being pulled apart at an average rate of 2 cm per year as the American and European plates separate from each other. This places enormous tensile stress on the Earth's crust that underlies the island. The effects are manifest on the surface along wide bands of intense faulting that run continuously from the north to the south and then to the southwest. From [Figure 19.1](#) it may be seen that the major high-temperature geothermal fields lie within the youngest formations, but that low-temperature fields are abundant everywhere except along the eastern and southeastern coasts.

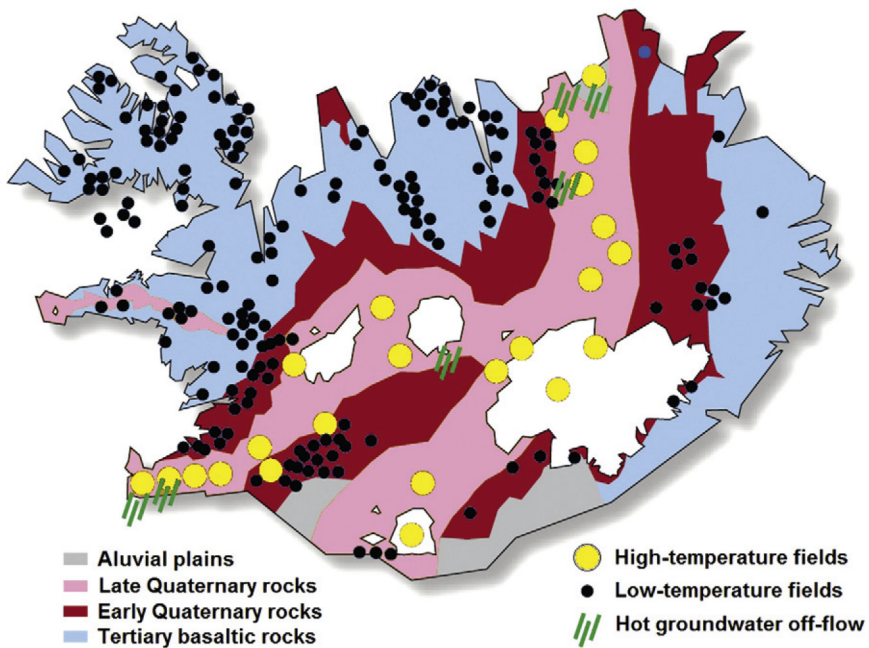


Figure 19.1 Highly simplified geologic map of Iceland [2] [WWW].

The Hengill volcano is about 30 km east of Reykjavik in the north branch of the Rift Zone. Three volcanic systems comprise the Hengill region; these have been active within the last 11,000 years, including the most recent eruption some 2000 years ago. The volcanic region covers an area of 112 km², one of the largest in all of Iceland.

The Nesjavellir and Hellisheidi power plants lie along the north-northeast trending fault zone, about 10.5 km apart; the Hengill volcano sits between them about 3.5 km from Nesjavellir. The surface expressions of many of the faults are clearly visible in the aerial image in [Figure 19.2](#).

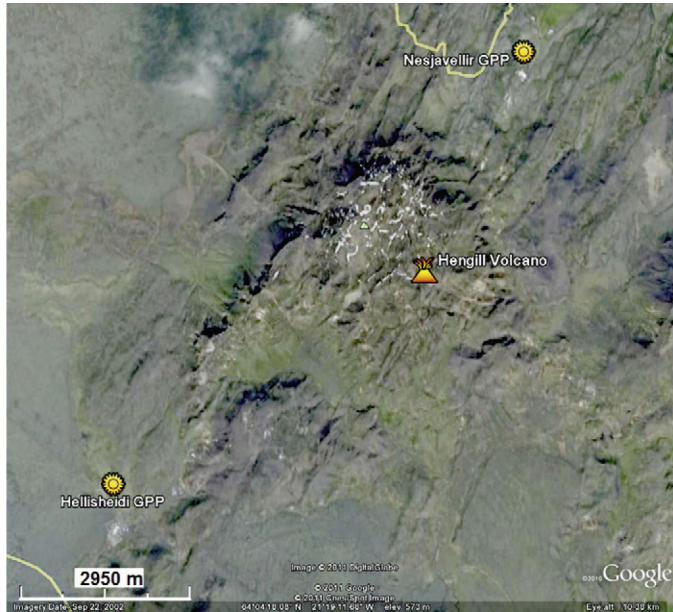


Figure 19.2 Aerial view of Hengill geothermal area. Google Earth image, September 22, 2002 [WWW].

A conceptual model of the Hengill geothermal field, Figure 19.3, has been developed [3]. It shows that there are two apparent heat sources for the two power plants although both are related to the Hengill volcano. The model indicates a central upflow zone beneath the volcano and outflows to the southwest and north-east. On the Nesjavellir side, in some areas the 300°C isotherm rises to about 1000 m of the surface.

Figure 19.4 depicts a cross-section along the direction of the fault zone at Nesjavellir [3] showing a multilayered formation with alternating hyaloclastites and lavas consisting of basaltic dykes. The Hengill system has an estimated age of 300,000–400,000 years. The basaltic intrusions and shallow-dipping diorite intrusions contribute to the permeability of the reservoir. There is a similar pattern in the Hellisheidi area but the volcanics are found at a somewhat deeper depth.

The faults are nearly vertical throughout the area, necessitating directionally drilled wells to intercept as many faults as possible. The wellhead locations at the Hellisheidi and Nesjavellir fields are shown in Figure 19.5, along with wells in two other nearby areas. There is no power plant at Hveragerdi but there are numerous wells that are used for other purposes in the town. This area is no longer volcanically active but thermal manifestations are present, and there could be sufficient stored thermal energy to support a new power plant.

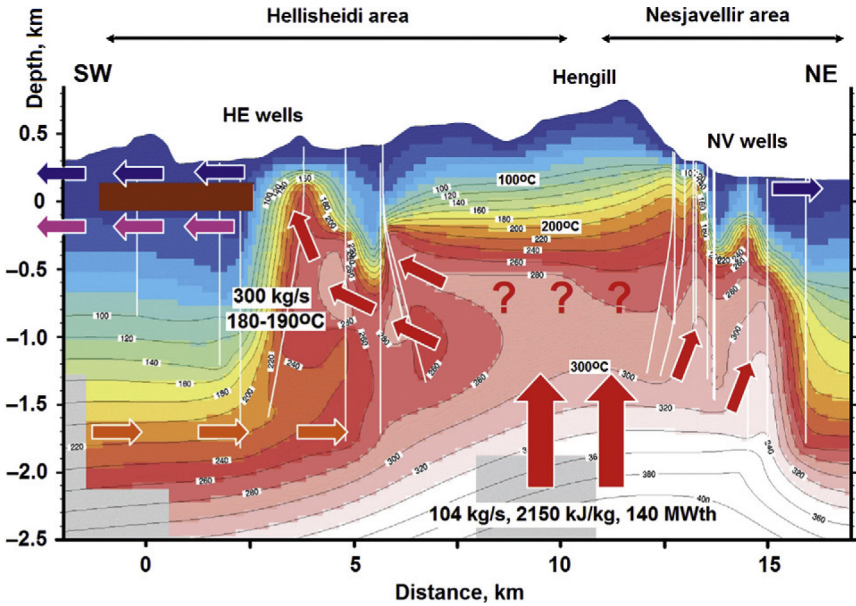


Figure 19.3 Conceptual model of Hengill geothermal formation. After Ref. [3] [WWW].

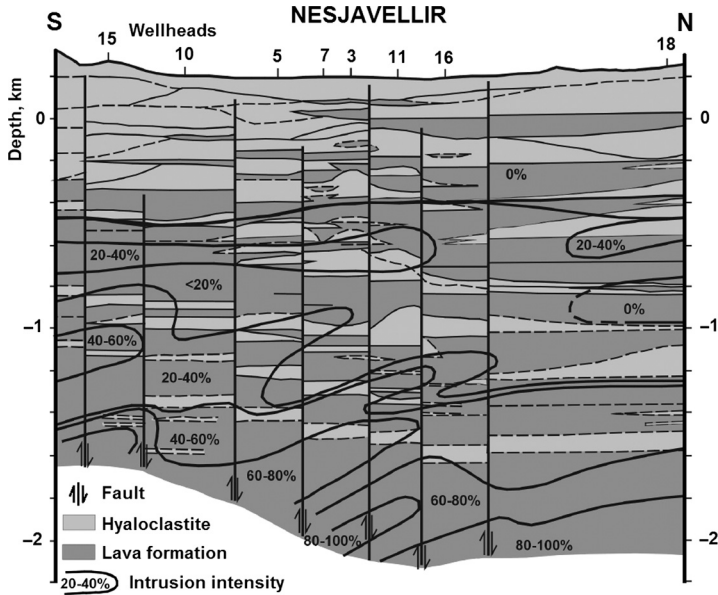


Figure 19.4 Lithology of the Nesjavellir reservoir. After Ref. [3].

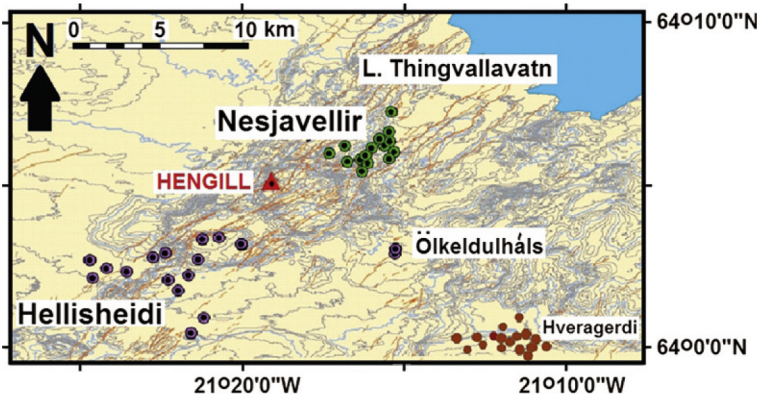


Figure 19.5 Wellhead locations in Hengill area. After Ref. [4] [WWW].

19.3 Nesjavellir Power Plant

Originally, the Nesjavellir power plant was built to supply hot water to Reykjavik. Several stages of development followed that included incremental installations of power turbines and an increase in the hot water flow to Reykjavik. Studies began in 1947 but drilling started at Nesjavellir in 1965 along with a series of geologic, geochemical, and geophysical surveys of the wide area surrounding Hengill. The plant began supplying 100 MW-th of hot water to Reykjavik in 1990 [5]. The route of the pipeline from Nesjavellir to Reykjavik is shown in Figure 19.6.

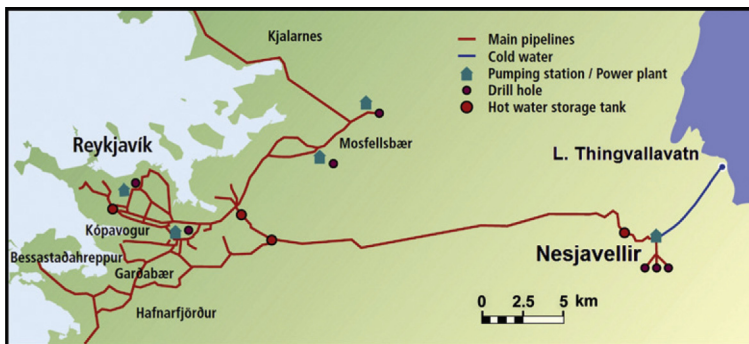


Figure 19.6 Pipeline route from Nesjavellir to Reykjavik. After Ref. [2] [WWW].

The first generation of electricity began in 1998 with the installation of two 30 MW turbines. The plant's power capacity was raised to 90 MW in 2001 and to 120 MW in 2005 by adding 30 MW turbines to reach the current state of the plant. The hot water rate also increased in increments over this period, as shown in [Table 19.1](#).

TABLE 19.1 History of development at Nesjavellir [6].

Year	Hot water		Electric power
	L/s	MW-th	MW
1990	560	100	—
1991	840	150	—
1998	1120	200	60 (2 × 30)
2001	1120	200	90 (3 × 30)
2003	1640	290	90 (3 × 30)
2005	1640	290	120 (4 × 30)

Since the heating demand varies by season, the plant is designed to be flexible to accommodate these seasonal swings in demand. When excess steam is available, the plant can generate more electricity, and if the heating demand exceeds the normal value, steam can be diverted from the turbines to the heating plant.

[Figure 19.7](#) shows the locations of the wells in the Nesjavellir area. The combined heat-power plant operates as follows; see [Figure 19.8](#). Geothermal fluid is produced from wells and fresh, cold water is pumped from wells near Lake Thingvallavatn. The geofluid is sent to the plant via two-phase, liquid–vapor pipelines. A geofluid header receives the fluid and passes it to a set of horizontal separators, the inlet ends being outside and the outlet ends being inside the separator building. The steam is sent to the turbine hall, passing through a set of horizontal moisture removers before entering the powerhouse. The steam drives the turbine-generators and discharges axially into the steam condenser. The latter is an element in the heating plant to raise the freshwater temperature to a sufficient level to make the trip to Reykjavik and to serve the heating needs of the city. There is another heat exchanger downstream of the condenser to subcool the condensate and preheat the freshwater. Then the steam condensate is either reinjected or sent to a drainage channel.

The cold water is pumped into a storage tank from whence it is divided into two flow paths; one goes to the aforementioned steam heat exchangers and one goes to a set of brine heat exchangers. The brine that is separated from the steam in the separators is sent to a set of heat exchangers that raise the cold water temperature to the desired level, with the help of the steam condenser from the turbine of

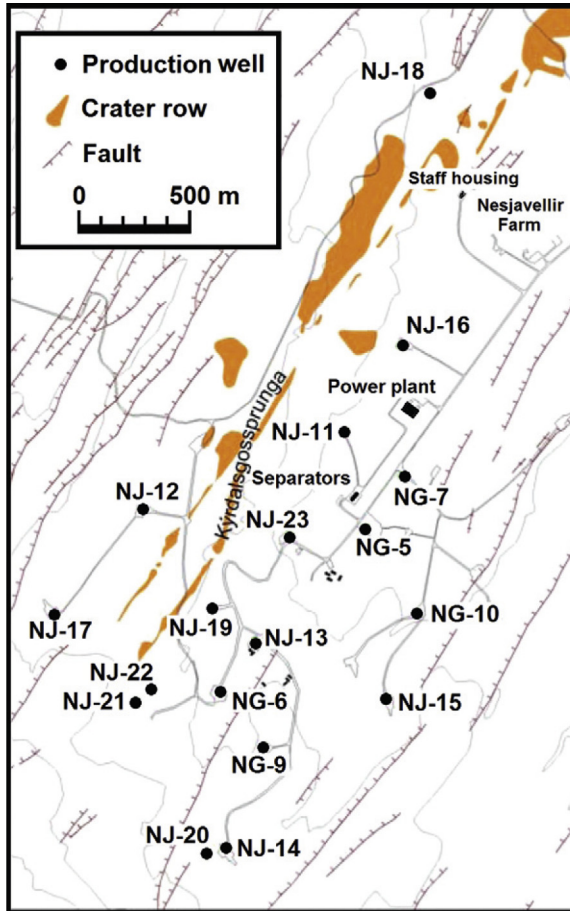


Figure 19.7 Location map of wellheads at Nesjavellir. After Ref. [7] [WWW].

the second unit. Since the geofluid characteristics differ from well to well, the two units are not identical in term of flow rates and temperatures, as can be seen from Figure 19.8, and thus must be carefully controlled to maintain proper and stable conditions. The pressure regulation steam stacks are essential to keeping the plant running smoothly, even though it may appear to be wasteful of steam.

Once the cold water is heated to the required 88°C, it must be processed to remove all dissolved oxygen which is highly corrosive in hot water. This is accomplished in deaerators by means of a vacuum flash process that produces a small amount of steam and releases the oxygen and other noncondensable gases (NCGs). These are vented (not shown in Figure 19.8) to the atmosphere while the steam is condensed by a very small flow rate of cold water that is sprayed into

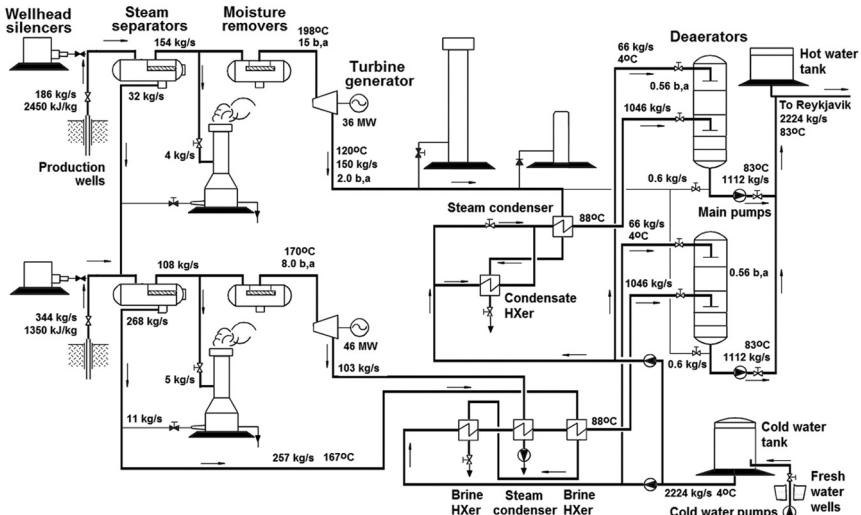


Figure 19.8 Simplified process flow diagram for Nesjavellir cogeneration Units 1 and 2. After Ref. [6].

the top of the deaerator. The last step occurs at the bottom of the deaerator where a tiny flow of steam bled from the turbine exhaust is fed into the hot water just before it leaves the plant for the hot water storage tank. This removes any residual oxygen that might have survived the deaeration process by reacting it with the hydrogen sulfide (H_2S) in the steam, adjusts the pH of the hot water to about 8.5, and imparts a “hot spring” smell to the water, which is evident to anyone who takes a shower in Reykjavik or any other place that receives geothermally heated water for domestic uses.

It may be noted from Figure 19.8 that the turbines are shown with power ratings higher than their nominal 30 MW ratings. By oversizing the turbine-generators, the plant can take advantage of those times when the heating demand is low and produce excess electricity which is always in demand. Also there are no cooling towers shown because the cold water drawn from freshwater wells serves the purpose of cooling water in the steam condensers. The plant does include a four-cell cooling tower as a backup system; this is much smaller than a 120 MW geothermal plant normally would require.

The technical specifications for the turbine, condenser, NCG extractor, and cooling tower may be found in Tables 19.2–19.5, respectively [8]. A site photograph with captions identifying the major items is given in Figure 19.9; a scale layout of the plant is shown in Figure 19.10 [9]; and the layout of one turbine-generator in the powerhouse is shown in Figure 19.11 [9].

TABLE 19.2 Turbine specifications for Nesjavellir Units 1–4 [8].

Type	Single-cylinder, single-flow, reaction blading, axial exhaust
Manufacturer	Mitsubishi Heavy Industries (MHI)
Rated capacity	30.0 MW
Maximum capacity	31.5 MW
No. of stages	8
Speed	3000 rev/min
Steam inlet pressure	1197.5 kPa (173.6 lbf/in ² ,a)
Steam inlet temperature	188°C (370°F)
Exhaust pressure	21.5 kPa (3.12 lbf/in ² ,a)
Steam mass flow rate	57.25 kg/s (454,390 lbm/h)
Last-stage blade height	609.6 mm (24 in)

TABLE 19.3 Condenser specifications for Nesjavellir Units 1–4 [8].

	Units 1–3	Unit 4
Type	Surface, shell-and-tube	Surface, shell-and-tube
Manufacturer	MHI	MHI
Shell pressure	20.0 kPa (2.90 lbf/in ² ,a)	10.0 kPa (1.45 lbf/in ² ,a)
Cooling water inlet temperature	4°C (39.2°F)	20°C (68°F) + 10°C (50°F)
Cooling water outlet temperature	57°C (134.6°F)	39°C (102.2°F)
Cooling water flow rate	574.4 kg/s	1268 kg/s + 99.26 kg/s

TABLE 19.4 Gas extractor specifications for Nesjavellir Units 1–4 [8].

	Units 1–3	Unit 4
Type	Vacuum pumps	Vacuum pumps
Manufacturer	MHI	MHI
No. of sets	1 set (each 50%)	1 set (each 33%)
Suction pressure	19.0 kPa (2.76 lbf/in ² ,a)	9.32 kPa (1.35 lbf/in ² ,a)
Discharge pressure	99.14 kPa (14.4 lbf/in ² ,a)	99.14 kPa (14.4 lbf/in ² ,a)
NCG capacity	18,530 m ³ /h (10,902 ft ³ /min)	27,795 m ³ /h (16,353 ft ³ /min)
Power consumption	300 kW (150 kW × 2)	450 kW (150 kW × 3)

TABLE 19.5 Cooling tower specifications for Nesjavellir plant [8].

Type	Mechanical draft, counterflow
Manufacturer	MHI
No. of cells	4
Warm water temperature	46°C (114.8°F)
Cold water temperature	20°C (68°F)
Design wet-bulb temperature	12°C (53.6°F)
Fan type	Vertical axial

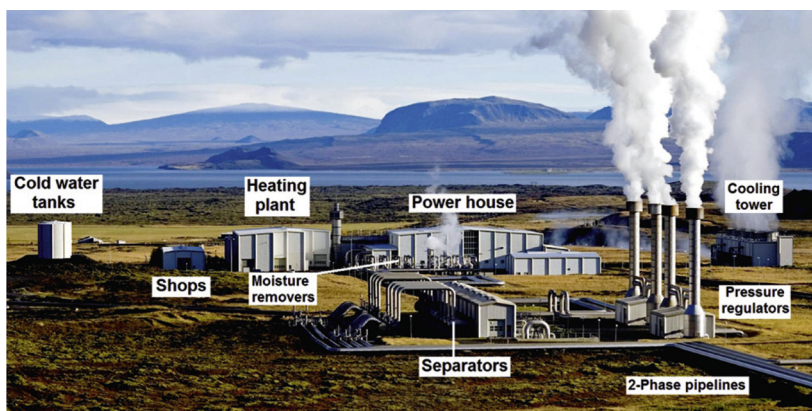


Figure 19.9 Nesjavellir plant with captions. Modified from: http://en.wikipedia.org/wiki/File:NesjavellirPowerPlant_edit2.jpg [WWW].

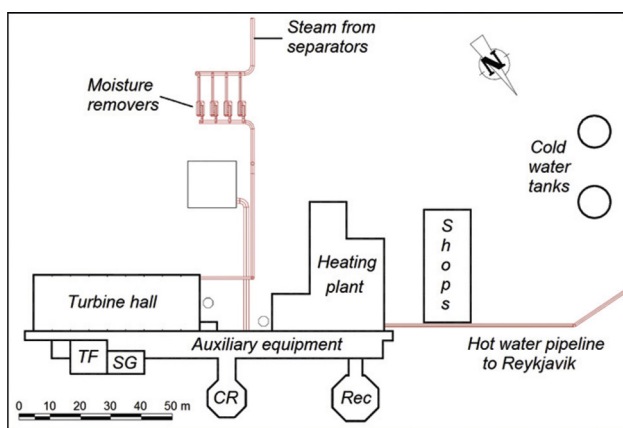


Figure 19.10 Nesjavellir power station layout. Simplified from Ref. [9] [WWW].

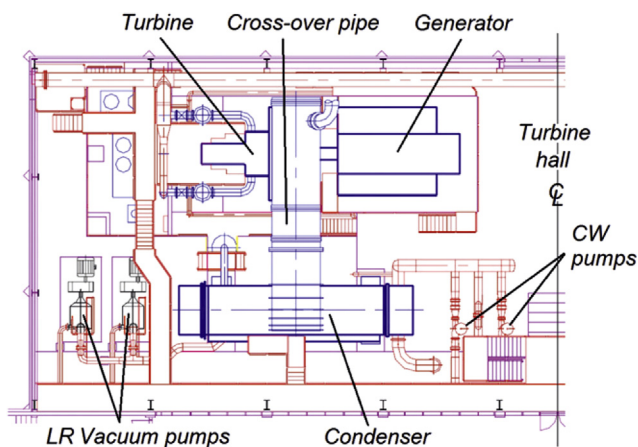


Figure 19.11 Nesjavellir turbine hall arrangement (one unit). Simplified from Ref. [9] [WWW].

19.4 Hellisheidi Power Plant

Once the Nesjavellir plant was brought to its full level of exploitation in 2005, attention turned to the other side of the Hengill volcano, the Hellisheidi field. As it happened, this field proved to be even larger in capacity than Nesjavellir.

As can be seen from Figure 19.3, the two reservoirs share similar characteristics. The wells at Hellisheidi produce geofluids that are somewhat lower in temperature but still high enough to support several moderate-sized power plants. Unlike Nesjavellir, Hellisheidi was first developed as an electricity-generating station and then later became a cogeneration, heat and power plant. Table 19.6 shows the timeline of development.

TABLE 19.6 History of development at Hellisheidi [10].

Phase	Year	Hot water MW-th (total)	Electric power MW (total)
1	2006	—	90 (2×45)
2	2007	—	123 ($2 \times 45 + 1 \times 33$)
3	2008	—	213 ($4 \times 45 + 1 \times 33$)
4	2010	133	213 ($4 \times 45 + 1 \times 33$)
5	2011	400	303 ($6 \times 45 + 1 \times 33$)

A total of 57 wells have been drilled to depths of 2000–3000 m in support of the fully developed plant [11]. All the units are owned and operated by Orkuveita Reykjavíkur (Reykjavik Energy). Whereas the hot water is sent to Reykjavik, the electricity is mainly sent to nearby aluminum refineries.

The first two power plants are single-flash type; see Table 19.7 for details on the turbine. Given the large volume of hot water that is available from the separators, a bottoming flash plant was built to capitalize on this source of energy or exergy. The process flow diagram and some state-point properties for this unit are given in Figure 19.12.

TABLE 19.7 Turbine specifications for Hellisheidi Units 1–2 [8].

Type	Single-cylinder, single-flow, impulse blading, axial exhaust
Manufacturer	Mitsubishi Heavy Industries (MHI)
Rated capacity	40.0 MW
Maximum capacity	47.0 MW
No. of stages	6
Speed	3000 rev/min
Steam inlet pressure	750.3 kPa (108.8 lbf/in ² , a)
Steam inlet temperature	167.8°C (334°F)
Exhaust pressure	9.8–21.6 kPa (1.42–3.13 lbf/in ² , a)
Steam mass flow rate	75.0 kg/s (595,242 lbm/h)
Last-stage blade height	762 mm (30 in)

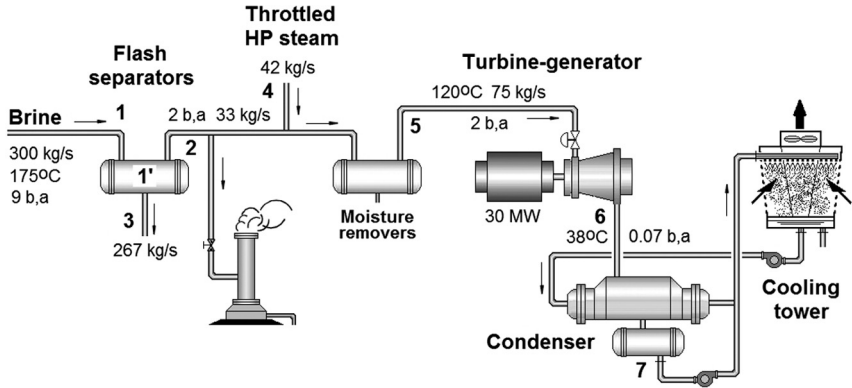


Figure 19.12 Process flow diagram for Hellisheidi LP-flash plant. After Ref. [12].

The processes for this plant are shown in Figure 19.13; the state points are identified in the plant flow diagram. State A represents the high-pressure steam from the inlet to the turbines for Units 1 and 2 that is throttled down to the LP turbine inlet pressure of 2 bar,a. This slightly superheated steam (state 4) is mixed with the steam from the flash separator (state 2) to form the inlet steam condition for the LP turbine (state 5). State 6s is the ideal isentropic turbine outlet point and state g represents the saturated vapor at the condenser pressure.

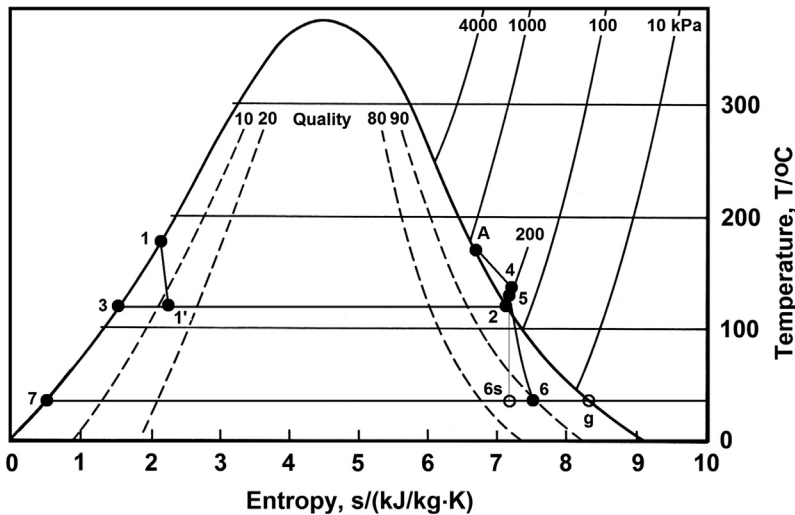


Figure 19.13 Temperature-entropy process diagram for the Hellisheidi LP-flash plant.

The results are shown in Table 19.8 where the calculated values were obtained using REFPROP and the specifications cited in Ref. [12]. Note the slight differences between some of the quantities. The Baumann rule was used to find the actual turbine outlet state assuming a dry expansion efficiency of 85%. The actual turbine efficiency is about 81%, the outlet quality is 90%, and the calculated turbine power is 30,082 kW.

TABLE 19.8 State-point analysis for the Hellisheidi LP-flash plant.

State	Pressure kPa	Temperature °C	Entropy kJ/kg · K	Enthalpy kJ/kg	Quality —	Mass flow kg/s
1	900	175	2.0940	742.56	0	300
1'	200	120	2.1349	742.56	0.1080	300
2	200	120	7.1269	2706.2	1	32.4
3	200	120	1.5302	504.70	0	267.6
A	750	168	6.6836	2765.6	1	42
4	200	148	7.2727	2765.6	SH	42
5	200	136	7.2104	2739.7	SH	74.4
6s	7		7.2104	2239.6	0.8621	
6	7	39	7.5177	2335.5	0.9019	74.4
7	7	39	0.5590	163.35	0	74.4
g	7	39	8.2745	2571.7	1	

The Second Law utilization efficiency of the LP unit is simply the ratio of the power output to the input exergy of the brine and steam. The steam condition should be taken as the high-pressure state before throttling since that steam could have been used in a HP turbine. The dead state was taken at the design wet-bulb temperature of the neighboring Nesjavellir plant, namely, 12°C or 285.15 K and the local atmosphere pressure was taken as 98.2 kPa, corresponding to the plant elevation of 260 m a.s.l. The inlet brine exergy rate is 43,934 kW, the inlet steam exergy rate is 36,152 kW, with a total inlet exergy of 80,086 kW; thus the utilization efficiency comes to 37.6%.

Lastly, in an experiment to demonstrate carbon sequestration by means of mineral carbonation, the Hellisheidi reservoir received aqueous CO₂ (a kind of seltzer water) via injection wells to learn whether the CO₂ can be reacted with the basalt to form solid limestone as a permanent means of disposing of unwanted CO₂ [13]. Early results of Project CarbFix are encouraging [14]. A similar effect was observed at the EGS test site at Ogachi in Japan when CO₂ was used as the heat transfer fluid in the reservoir; see Section 22.3.2.

References

- [1] Ragnarsson Á. Geothermal development in Iceland 2010–2014. Proc. world geothermal congress 2015, paper 01077, Melbourne, Australia; April 19–25, 2015.
- [2] Nesjavellir power plant. Orkuveita Reykjavíkur (Reykjavik Energy); 2006.
- [3] Franzson HE, Gunnlaugsson KÁ, Rnason K, Sæmundsson B, Steingrímsson, Harðarson BS. The Hengill geothermal system, conceptual model and thermal evolution. Proc. world geothermal congress 2010, paper 1177, Bali, Indonesia; April 25–29, 2010.
- [4] Mutonga MW, Sveinbjörnsdóttir A, Gíslason G, Amannsson H. The isotopic and chemical characteristics of geothermal fluids in Hengill area, SW-Iceland (Hellisheidi, Hveragerdi and Nesjavellir fields). Proc. world geothermal congress 2010, paper 1434, Bali, Indonesia; April 25–29, 2010.
- [5] Zarandi SSMM, Ivarsson G. A review on waste water disposal at the Nesjavellir geothermal power plant. Proc. world geothermal congress 2010, paper 0242, Bali, Indonesia; April 25–29, 2010.
- [6] Gunnarsson A, Steingrímsson BS, Gunnlaugsson E, Magnússon J, Maack R. Nesjavellir geothermal co-generation power plant. *Geothermics* 1992;21:559–83.
- [7] Gíslason G, Ívarsson G, Gunnlaugsson E, Hjartarson A, Björnsson G, Steingrímsson B. Production monitoring as a tool for field development: a case history from the Nesjavellir field, Iceland. Proc. world geothermal congress 2005, paper 2415, Antalya, Turkey; April 24–29, 2005.
- [8] Mitsubishi Heavy Industries, Ltd. List of geothermal power plants; August 2005.
- [9] Ballzus C, Frimannson H, Gunnarsson GI, Hrólfsson I. The geothermal power plant at Nesjavellir, Iceland. Proc. world geothermal congress 2000, Kyushu-Tohoku, Japan; May 28–June 10, 2000. p. 3109–14.
- [10] Bertani R. Geothermal power generation in the world 2005–2010 update report. Proc. world geothermal congress 2010, paper 0008, Bali, Indonesia; April 25–29, 2010.
- [11] Blog at WordPress. Iceland: Hellisheidarvirkjun: Hellisheidi geothermal power plant, <<http://systemsthatseep.wordpress.com/2010/02/15/iceland-hellisheidarvirkjun-hellisheidigeothermal-power-plant/>>; February 15, 2010.
- [12] Kjartansson G. Low pressure flash-steam cycle at Hellisheidi—selection based on comparison study of power cycles, utilizing geothermal brine. Proc. world geothermal congress 2010, paper 2643, Bali, Indonesia, April 25–29, 2010.
- [13] Matter JM, Broecker WS, et al. The CarbFix pilot project – Storing carbon dioxide in basalt; *Energy Procedia* 4 (2011) 5579–5585.
- [14] Fountain H. Turning Carbon Dioxide Into Rock, and Burying It, <http://www.nytimes.com/2015/02/10/science/burying-a-mountain-of-co2.html?_r=0>; 9 February 2015.



Chapter 20

Raft River Plants, Idaho, USA

Chapter Outline

20.1 Introduction	545
20.2 Geology and Geosciences	546
20.3 Original Development—DOE Pilot Plant	550
20.3.1 Original Wells and Power Plant	550
20.3.2 Design Performance Assessment	554
20.3.3 Actual Performance Assessment	557
20.3.4 Cooling Tower Make-Up Water Treatment	558
20.3.5 Plant Photographs	558
20.3.6 Lessons Learned	561
20.3.7 Concluding Remarks	561
20.4 New Development—USGeo Plant	562
20.4.1 Site Renewal Process and Well Modifications	562
20.4.2 Power Plant Design	565
20.4.3 Design Performance Assessment	567
20.4.4 Actual Performance Assessment	567
20.4.5 Conclusion	571
References	573

A pessimist sees the difficulty in every opportunity; an optimist sees the opportunity in every difficulty.

Sir Winston Churchill

20.1 Introduction

The Raft River geothermal field in southeastern Idaho has been the site of two power plant developments. The original nominal 5 MW project was supported by the United States Department of Energy (USDOE), and the other, a nominal 10 MW plant, is a private project of U.S. Geothermal, Inc. (USGeo). The contrast between these two efforts is illuminating. They represent two approaches to exploitation of the same geothermal resource.

The chapter begins with a description of the geologic setting that is common to the two projects, and includes descriptions of the means of geofluid production, energy conversion systems, cooling systems, power plant performance, environmental impact, and economics for both plants.

20.2 Geology and Geosciences

The Raft River of southern Idaho flows directly through the Raft River geothermal field in a generally northeast direction. [Figure 20.1](#) shows the location of the field and includes an aerial view of the site from *Google Earth* as of April 27, 2015. The reservoir lies in a basin bounded on the west by low-angle faults and on the east by secondary faulting associated with the Black Pine Mountains; see [Figure 20.2](#). The basement rocks lie about 1600 m (5250 ft) deep and are traversed at depth by a northeast-trending lineament known as the Narrows Structure, thought to be caused by basement shear.

[Figures 20.3 and 20.4](#) illustrate the reservoir concept; the former was presented in 1982 and the latter in 2011. Geofluid production occurs at the intersection of the Bridge Fault zone and the Narrows Structure. The hot fluid was originally thought to rise along the Narrows Structure and then spread through the sedimentary formations along other faults and fractures. More recent thinking posits two feed zones [\[6\]](#), one from the northwest along the Horse Well Fault zone and one from the southeast, perhaps associated with the deep Narrows Structure.

[Figures 20.5 and 20.6](#) show, respectively, the well field layout and the main fault zones that control the geothermal and groundwater flows, and the presumed flows of these fluids within the formation [\[7\]](#). Numerous shallow water and monitoring wells exist across the field, denoted by small circles and thin lines in [Figures 20.5 and 20.6](#), respectively.

The Group 1 groundwater appears to be of recent meteoric origins, whereas the other three fluids share a common parent believed to be of glacial origins [\[7\]](#). The difference in their chemical characteristics is attributable to the different paths they have taken to arrive at the Raft River field. The SE geofluid has taken a deeper path, is hotter, and has been in contact with evaporites, accounting for its higher dissolved solids relative to the NW geofluid.

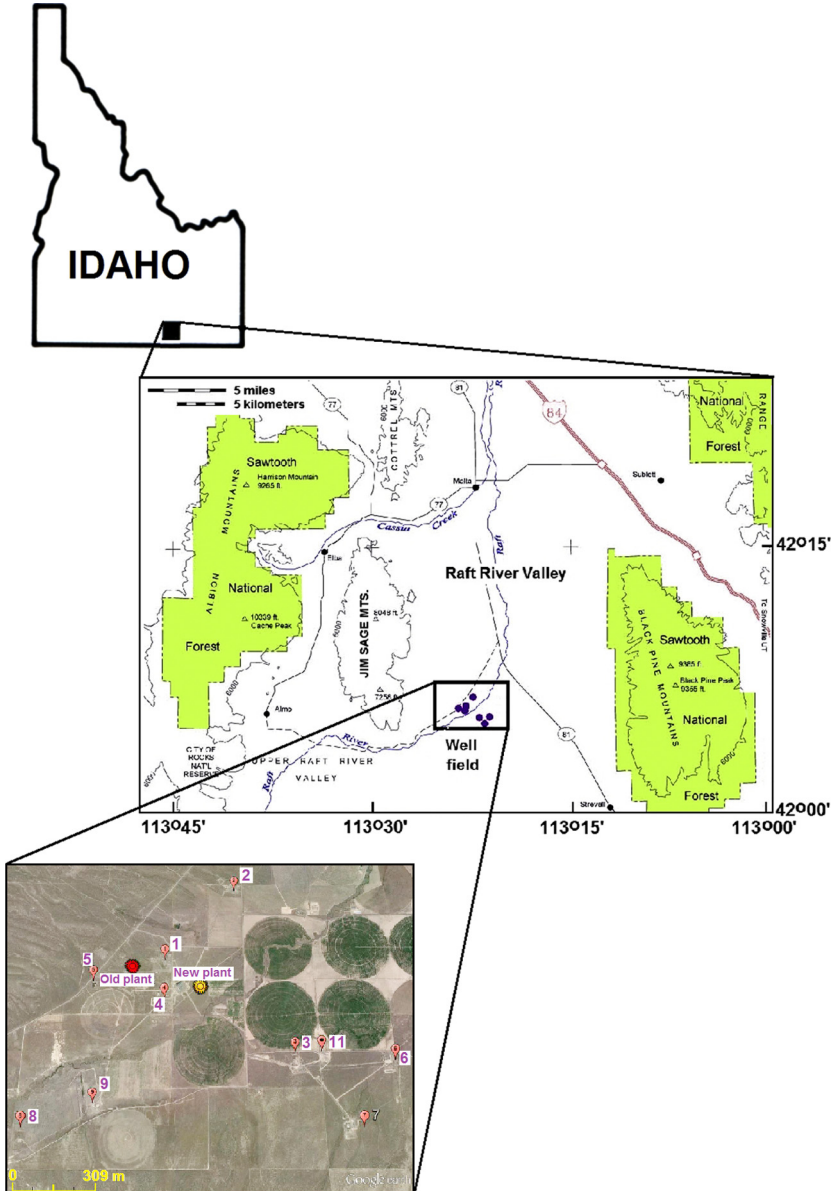


Figure 20.1 Location of the Raft River geothermal field [1–3] [WWW].

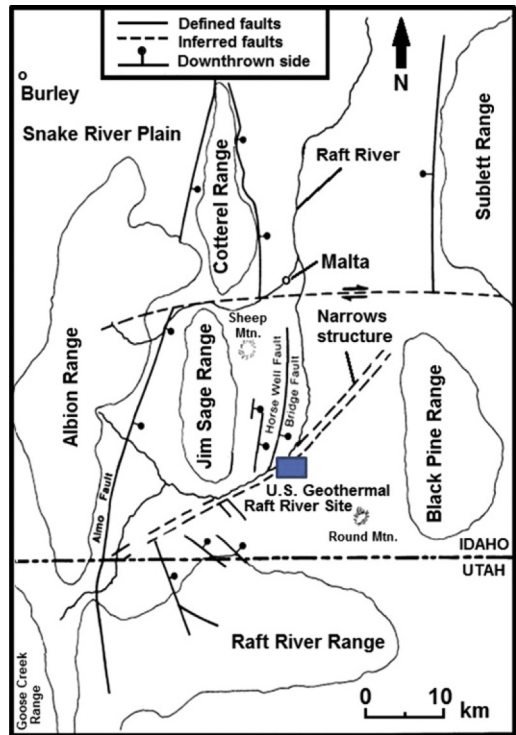


Figure 20.2 Mountain ranges and fault mapping surrounding the Raft River area. After Ref. [4] [WWW].

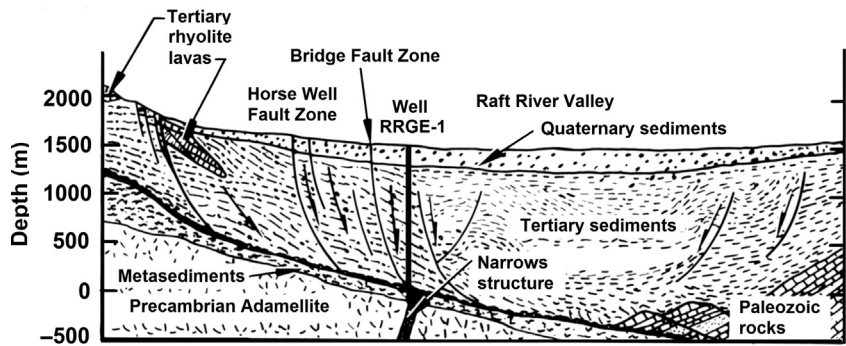


Figure 20.3 East-west cross-section through the formation, from 1982. After Ref. [5].

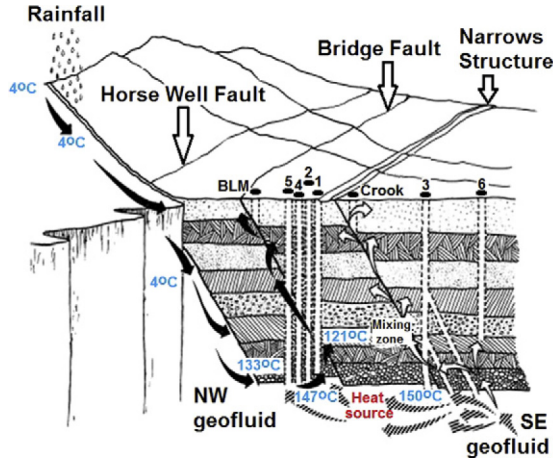


Figure 20.4 Conceptual model of the reservoir in 2011. Wells 1–6 are geothermal wells; BLM and Crook are shallow wells. After Ref. [4] [WWW].

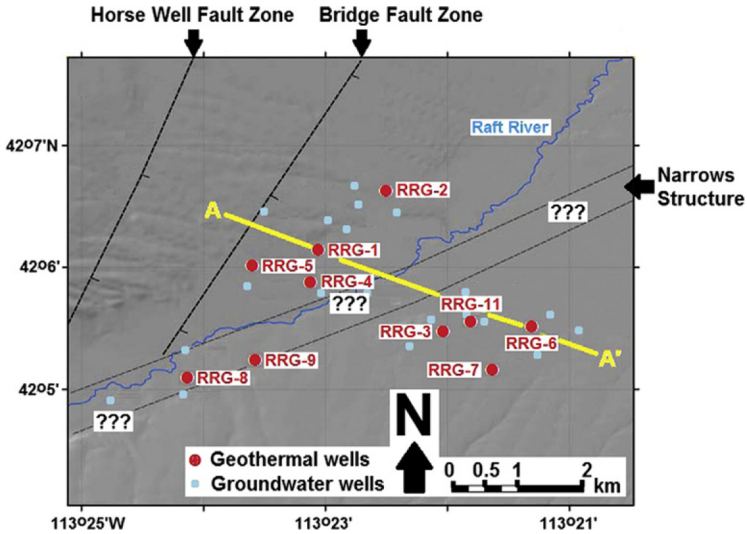


Figure 20.5 Well field layout including major controlling features. After Ref. [7] [WWW].

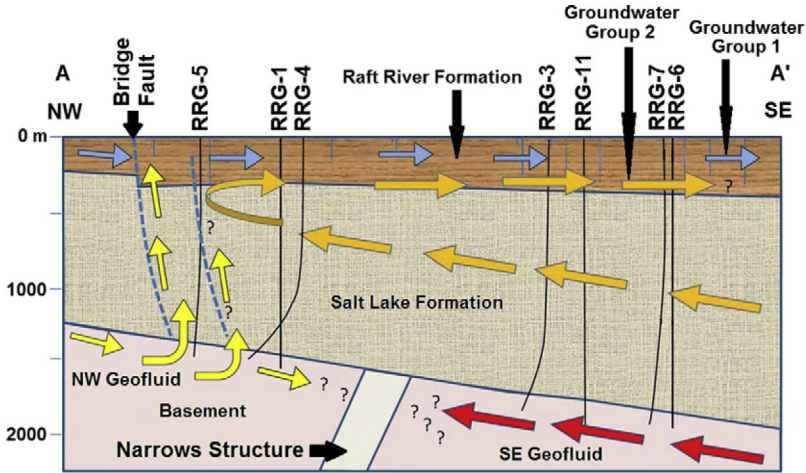


Figure 20.6 Speculative model of fluid flow in the Raft River system. Section taken across A-A' shown in [Figure 20.5](#). After Ref. [7] [WWW].

20.3 Original Development—DOE Pilot Plant

20.3.1 ORIGINAL WELLS AND POWER PLANT

The early development from 1974 to 1978 involved drilling seven deep wells, RRGE-1 to RRGE-7; see [Figure 20.7](#). The discovery well RRGE-1 was targeted to intercept the Bridge Fault toward the bottom of its planned total depth. It was completed in April 1975 at a total depth of 1521 m (4989 ft). It penetrated 35 m (116 ft) of the metasedimentary formation and bottomed in the basement rock. The primary production horizon was near the bottom of the Tertiary sediments from 1128 to 1372 m (3700–4500 ft). The well was capable of artesian flow. Although the development strategy called for production wells to be sited to the northwest and injection wells to the southeast, well RRGE-3 was used for production since RRGE-4 was incapable of sufficient flow. Thus only two wells, RRGE-6 and -7, served as injectors. [Table 20.1](#) lists some properties of the seven wells [8].

All wells were fitted with pumps to increase the flow rates. For example, RRGE-1 was able to flow only 300 GPM under artesian conditions but 1120 GPM when pumped. Originally electric submersible pumps were planned to be installed but were abandoned after problems with cable and motor failures. Peerless line-shaft multistage centrifugal pumps were more successful at each production well. [Table 20.2](#) gives some information on the production well

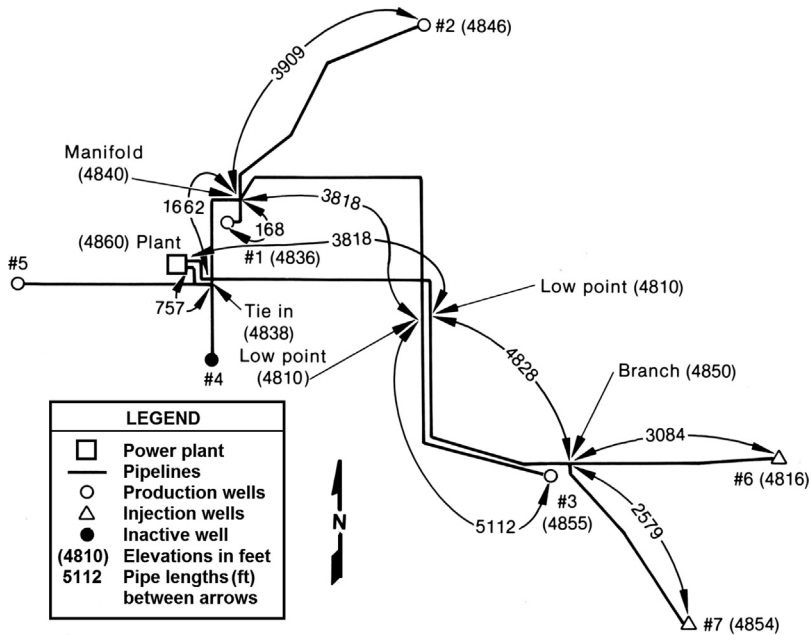


Figure 20.7 Original Raft River deep wells; all wells are designated RRGE. *After Ref. [8].*

pumps. The two injection wells received spent brine into holding ponds at each well that served as a fluid capacitor to allow smooth operation of the entire flow system. The brine was pumped out of the ponds by means of vertical-turbine pumps and delivered to each injection well.

The geofluid was delivered from the well pumps to the plant via buried concrete-asbestos pipes. Owing to thermal expansion and contraction during plant operations, these pipes suffered cracks and led to loss of hot brine. The location of the cracks was evident from surface pools of hot brine. The operators were forced to adopt a practice of making gradual changes in all operating procedures to reduce the effect of temperature changes on the buried pipes.

Given the low temperature of the geofluid, a binary plant was designed for the Raft River site. In the late 1970s a binary plant was a novelty with only one plant installed in the world, in Russia at Paratunka [9]. Thus, the USDOE was breaking new ground with the Raft River demonstration of binary plant. Approximately \$13 million was spent on the project.

The cycle chosen was a dual-pressure (dual-boiling) Rankine cycle, similar, but not identical, to the cycle discussed in Section 8.4.2. Figure 20.8 is a simplified flow diagram. The cycle working fluid was isobutane, $i\text{-C}_4\text{H}_{10}$.

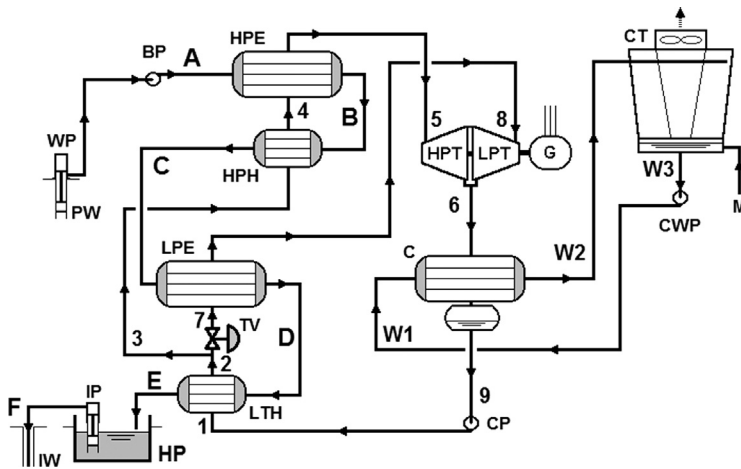
TABLE 20.1 Well characteristics—original wells [8].

Well	Type	Total depth, ft	Casing size		Bottom-hole temperature, °F	Flowing temperature, °F	Wellhead pressure, psig	Max. artesian flow, GPM
			Diameter, in	Depth, ft				
RRGE-1	Production	4989	30	40	294	279	134	300
			20	901				
			13-5/8	3623				
RRGE-2	Production	6543	30	40	296	280	121	250
			20	901				
			13-5/8	4227				
RRGE-3	Production	^a	20	120	298	296	102	200
			13-5/8	1383				
			9-5/8	3565				
RRGE-4	Unusable	^b	20	150	273	248	126	55
			13-5/8	1915				
			9-5/8	3408				
RRGE-5	Production	^c	20	150	168	257	110	200
			13-5/8	1510				
			9-5/8	3408				
RRGE-6	Injection	3888	13-5/8	1698	253	NA	38	NA
RRGE-7	Injection	3444	13-5/8	2044	162	NA	4	NA

^aForked well with three legs: A-5853, B-5532, and C-5917.^bForked well with two legs: A-4911 and B-5115.^cForked well with two legs: A-4911 and B-4925.

TABLE 20.2 Characteristics of production well pumps [2].

Well	Set depth, ft	Flow rate, GPM	TDH ^a , ft	Motor horsepower
RRGE-1	1000	1120	1340	500
RRGE-2	1000	680	1340	350
RRGE-3	998	375	1425	250

^aTotal Developed Head.**Figure 20.8** Simplified flow diagram for the original power plant. After Ref. [8].

The pressurized geofluid passed sequentially through the high-pressure evaporator (HPE), the high-pressure preheater (HPH), the low-pressure evaporator (LPE), and finally the low-temperature preheater (LTH). Notice that there is only one isobutane circulating pump (CP); it produces the high-pressure (HP) fluid for all the HP elements. The LTH operates with the maximum isobutane flow and at the high pressure. The fluid is divided as it leaves the LTH into two streams; one continues on to the HPH and the rest is throttled down to the low-pressure (LP) portion of the cycle by a control valve (TV) and enters the LPE. The turbine was a radial-inflow machine within a single cylinder but containing both the HP and LP wheels. The turbine drove a generator through a gear box. There was a common exhaust (state 6) that discharged into the water-cooled condenser (C). Figure 20.9 shows the processes followed by the isobutane as it passes through the plant components. The reader may wish to compare this to Figure 8.11.

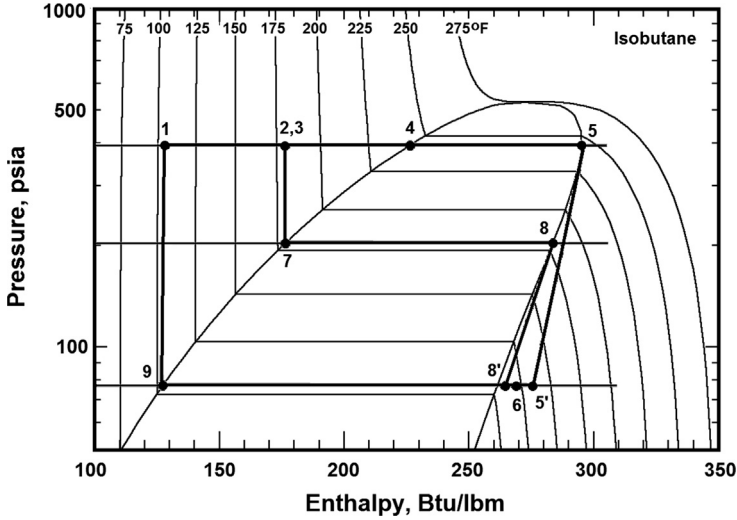


Figure 20.9 Pressure-enthalpy process diagram for the original plant.

20.3.2 DESIGN PERFORMANCE ASSESSMENT

The performance of the plant can be determined for the design conditions, which did not actually materialize, as well as for the few test runs that were carried out. Table 20.3 lists the cycle properties for the nominal design case [10]; the state-point labels correspond to those shown in Figure 20.8. Table 20.4 includes the enthalpy and entropy values, in US Customary units, taken from the NIST REFPROP Database, and serves as the basis for the cycle and plant analysis.

The property values shown in Table 20.4 were used to calculate the design performance of the cycle. Pressure losses in piping and heat exchangers were neglected and therefore the results will be somewhat optimistic.

The cycle power terms may be calculated from the following equations, with reference to Figures 20.8 and 20.9:

$$\dot{Q}_{LTH} = \dot{m}_1(h_2 - h_1) \quad (20.1)$$

$$\dot{Q}_{LPE} = \dot{m}_7(h_8 - h_7) \quad (20.2)$$

$$\dot{Q}_{HPH} = \dot{m}_4(h_4 - h_3) \quad (20.3)$$

$$\dot{Q}_{HPE} = \dot{m}_4(h_5 - h_4) \quad (20.4)$$

$$\dot{Q}_C = \dot{m}_1(h_6 - h_9) \quad (20.5)$$

$$\dot{W}_{HPT} = \dot{m}_4(h_5 - h_{5'}) \quad (20.6)$$

TABLE 20.3 Nominal design specifications for original plant.

State	Temperature		Pressure		Mass flow rate	
	°C	°F	MPa	psia	kg/s	10 ⁶ lbm/h
<i>Geothermal fluid</i>						
A	143	290	91.1	628	131.0	1.04
B	121	250	NA	NA	131.0	1.04
C	106	222	NA	NA	131.0	1.04
D	88	190	NA	NA	131.0	1.04
E	62	144	NA	NA	131.0	1.04
F	62	144	NA	NA	131.0	1.04
<i>Isobutane</i>						
1	41	105	2.63	381.6	117.7	0.934
2	82	180	2.63	381.6	117.7	0.934
3	82	180	2.63	381.6	77.24	0.613
4	116	240	2.63	381.6	77.24	0.613
5	116	240	2.63	381.6	77.24	0.613
6	53	128	0.534	77.5	117.7	0.934
7	82	180	1.40	203.0	40.45	0.321
8	82	180	1.40	203.0	40.45	0.321
9	38	101	0.534	77.5	117.7	0.934
<i>Cooling water</i>						
W1	24	75	1.99	289	948.8	7.53
W2	35	95	NA	NA	948.8	7.53
W3	35	75	0.087	12.6	948.8	7.53

Data from Ref. [8].

$$\dot{W}_{LPT} = \dot{m}_7(h_8 - h_{8'}) \quad (20.7)$$

$$\dot{W}_{CP} = \dot{m}_1(h_1 - h_9) \quad (20.8)$$

The equations for the turbine power contain the terms $h_{5'}$ and $h_{8'}$ which represent the actual exhaust states for the HP and LP turbines, respectively, prior to merging in the single pipe to the condenser. These were found from the isentropic efficiency equations with an assumed value of 85% for each machine:

$$h_{5'} = h_5 - 0.85(h_5 - h_{5s}) \quad (20.9)$$

$$h_{8'} = h_8 - 0.85(h_8 - h_{8s}) \quad (20.10)$$

The terms h_{5s} and h_{8s} represent the ideal isentropic turbine exhaust states. These may be calculated in the manner shown in Eq. (5.14). Table 20.5 presents the findings. The efficiency values were found from:

$$\eta_{CYC} = \dot{W}_{NET} / \dot{Q}_{IN} \quad (20.11)$$

$$\eta_{PLANT} = \dot{W}_{PLANT} / \dot{Q}_{IN} \quad (20.12)$$

TABLE 20.4 Nominal design properties for original plant.

State	Temperature, °F	Pressure, psia	Entropy, Btu/lbm · °F	Enthalpy, Btu/lbm	Mass flow rate, 10 ⁶ lbm/h
<i>Geothermal fluid</i>					
A	290	628	0.42391	259.6	1.04
B	250	NA	0.36804	218.8	1.04
C	222	NA	0.32733	190.4	1.04
D	190	NA	0.27893	158.2	1.04
E	144	NA	0.20533	112.1	1.04
F	144	NA	0.20533	112.1	1.04
<i>Isobutane</i>					
1	105	381.6	0.31569	128.42	0.934
2	180	381.6	0.39539	176.43	0.934
3	180	381.6	0.39539	176.43	0.613
4	240	381.6	0.46563	223.55	0.613
5	240	381.6	0.56790	295.12	0.613
6	128	77.5	0.56773	269.01	0.934
7	180	203.0	0.39746	176.63	0.321
8	180	203.0	0.56500	283.72	0.321
9	101	77.5	0.31376	125.65	0.934
<i>Cooling water</i>					
W1	75	289	0.08404	43.1	7.53
W2	95	NA	0.12073	63.1	7.53
W3	75	12.6	0.08404	43.1	7.53

Note: All geothermal fluid and cooling water properties are for saturated liquid. Isobutane properties at states 4, 5, 7, 8, and 9 are for saturated conditions.

TABLE 20.5 Results of power analysis for original Raft River plant.

Quantity	Value	Units
\dot{Q}_{LTH}	13.1	MW-th
\dot{Q}_{LPE}	10.1	MW-th
\dot{Q}_{HPH}	8.47	MW-th
\dot{Q}_{HPE}	12.9	MW-th
\dot{Q}_C	39.2	MW-th
\dot{Q}_{IN}	44.5	MW-th
\dot{Q}_{NET}	5.30	MW-th
\dot{W}_{HPT}	3.97	MW
\dot{W}_{LPT}	2.10	MW
\dot{W}_{T-TOT}	6.08	MW
\dot{W}_{CP}	0.758	MW
\dot{W}_{NET}	5.32	MW
η_{CYC}	11.9	%
\dot{W}_{AUX}	0.7	MW
\dot{W}_{PLANT}	4.62	MW
η_{PLANT}	10.4	%

The plant design auxiliary power requirements were taken from Ref. [8]; these account for the cooling tower fans, cooling water circulating pump, and the geofluid boost pump, but not the production well pumps or the injection pumps.

Utilization efficiencies based on the Second Law can also be calculated using as the dead-state conditions the design wet-bulb temperature of 65°F and the local ambient pressure of 12.1 psia at 4800 ft elevation. The reference enthalpy h_0 is 33.13 Btu/lbm and reference entropy s_0 is 0.06516 Btu/lbm · °F. Thus the exergy of the geofluid at reservoir conditions relative to the dead state may be found from:

$$\dot{E}_{GEO} = \dot{m}_A [h_R - h_0 - T_0(s_R - s_0)] \quad (20.13)$$

where $h_R = 259.62$ Btu/lbm and $s_R = 0.4239$ Btu/lbm · °F. This comes to 11.63 MW. Thus, the design cycle utilization efficiency is 45.7% ($5.32 \times 100/11.63$) and the overall design plant utilization efficiency is 39.7% ($4.62 \times 100/11.63$).

The resulting thermal and utilization efficiencies are typical of binary plants operating on lower temperature geothermal resources. However, several simplifying and optimistic assumptions went into these calculations.

20.3.3 ACTUAL PERFORMANCE ASSESSMENT

It is very difficult to obtain actual plant operating data from the final report for the Raft River project [8]. The turbine failed to perform for about half of the small number of tests that were conducted, and the inconsistencies in the data from various instruments made it nearly impossible to obtain a clear assessment of the performance. Nevertheless, the final report does list the results from one test that may shed some light even though the test parameters were not identical with the design values. The observed power terms and calculated thermal efficiencies are shown in Table 20.6. Adopting the dead-state conditions for the test, the geofluid exergy at plant inlet is 13.69 MW; this means the cycle utilization efficiency was 24.7% and the plant efficiency was 10.7%.

Based on this single test result, the Raft River plant performed well below the design expectations for many reasons, including lower geofluid temperatures, malfunctions of various components, poor design of the geofluid gathering system, and inconsistencies among measurements.

TABLE 20.6 Performance results from test 1A as reported in Ref. [8].

Quantity	Value	Units
\dot{Q}_{LTH}	11.7	MW-th
\dot{Q}_{LPE}	8.81	MW-th
\dot{Q}_{HPH}	9.78	MW-th
\dot{Q}_{HPE}	9.96	MW-th
\dot{Q}_C	35.6	MW-th
\dot{Q}_{IN}	40.25	MW-th
\dot{Q}_{NET}	4.62	MW-th
\dot{W}_{HPT}	NA	
\dot{W}_{LPT}	NA	
\dot{W}_{GEN}	4.010	MW
\dot{W}_{CP}	0.633	MW
\dot{W}_{NET}	3.377	MW
η_{CYC}	8.39	%
\dot{W}_{BP}	0.115	MW
$\dot{W}_{CT-FANS}$	0.134	MW
$\dot{W}_{CT-PUMPS}$	0.388	MW
$\dot{W}_{PW-PUMPS}$	0.821	MW
$\dot{W}_{IW-PUMPS}$	0.448	MW
\dot{W}_{AUX}	1.906	MW
\dot{W}_{PLANT}	1.471	MW
η_{PLANT}	3.65	%

20.3.4 COOLING TOWER MAKE-UP WATER TREATMENT

The plant used a water cooling tower that requires a continuous flow of make-up water to compensate for the water that evaporates to create the cooling effect plus blowdown and drift. The available surface waters in the area are neither plentiful nor of very high quality, which led to an innovative means of providing for the make-up. Approximately 18% of the total spent brine was side-streamed to a chemical treatment facility where it was made suitable for use as make-up. Figure 20.10 is a flow diagram of the processes. The system was plagued by numerous mechanical failures mainly involving chemical feed pumps [2].

20.3.5 PLANT PHOTOGRAPHS

The photographs shown in Figures 20.11–20.14 were taken by the author in March 1981.

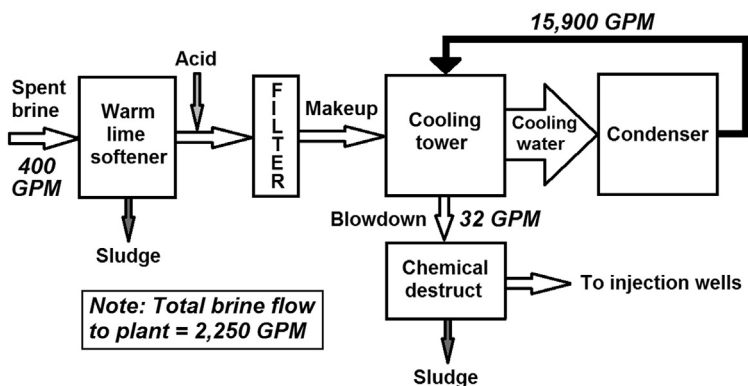


Figure 20.10 Make-up water treatment system.



Figure 20.11 Heat exchangers. LTH is at lower right, LPE is at upper right, HPH is at lower center, and HPE is above the HPH. The condenser is the large horizontal vessel at the upper left rear [WWW].



Figure 20.12 Preheaters and evaporators: lower row (L–R)—HPH and LTH; upper row (L–R)—HPE and LPE [WWW].



Figure 20.13 Turbine-generator on elevated pedestal [WWW].



Figure 20.14 Turbine showing dual inlet pipes, control valves, and position indicators; large horizontal pipe at left center is the exhaust pipe [WWW].

20.3.6 LESSONS LEARNED

Although the pilot plant never completed the full five years of operation and testing that was anticipated at the outset, several important conclusions could be drawn from the limited test program. These include:

- It is technically viable to operate an organic Rankine cycle (ORC) at a moderate-temperature geothermal resource.
- In spite of the complex nature of the dual-pressure (dual-boiling) Rankine cycle, there were no plant operational problems and the performance was predictable.
- The gathering system pipes should not be made of concrete-asbestos since this places severe restrictions on plant operations owing to thermal expansion problems.
- Line-shaft mechanical well pumps were preferred over electric submersible pumps, at the time of the project.
- The use of waste brine for cooling tower make-up, while technically feasible, was chemically complex and problems were encountered owing to the use of carbon steel condenser tubes. Appropriate coatings on the tubes would alleviate these problems.
- Feed pumps should be oversized to allow sufficient working fluid flow rate to overcome pressure losses in the flow circuit.
- Kettle-type evaporators should be operated with relatively low liquid levels and fitted with moisture separators to eliminate liquid carryover to the turbine.
- To fully exploit a demonstration project, adequate funding should be allocated at the outset to ensure the project will complete its full series of tests.

20.3.7 CONCLUDING REMARKS

After nine years of research and development and the expenditure of \$13 million dollars, the Raft River power plant project fell victim to budget cuts and a philosophical change in direction for the USDOE from demonstration to research-oriented projects. As a result it operated only briefly during the fall of 1981 and spring of 1982; it was permanently shut down on June 15, 1982. Eventually, the equipment was bought by a private company, dismantled, and partially reassembled at the Brady Hot Spring geothermal field, but it never operated again (see Figure 16.4).

20.4 New Development—USGeo Plant

20.4.1 SITE RENEWAL PROCESS AND WELL MODIFICATIONS

Following the termination of the Raft River demonstration project by the USDOE, although the equipment was dismantled and removed, the wells remained in a closed condition, perhaps in anticipation of another attempt to develop the field. That opportunity came 20 years later when in 2002 USGeo set about renewing the Raft River prospect. USGeo is a Canadian company headquartered in Vancouver, BC, with an office in Boise, Idaho.

Some important events in the chronology of the project are summarized below [11].

June 2002	USGeo acquires old DOE Raft River parcel, including five production wells, two injection wells, and seven monitoring wells; see Figure 20.7 .
April 2004	Flow tests conducted on the production wells with a grant from DOE.
January 5, 2005	USGeo signs a Power Purchase Agreement (PPA) with Idaho Power Company (Idaho Power) for 10 MW from Phase 1 Raft River plant.
December 7, 2005	USGeo enters into a \$20.3M Engineering, Procurement, and Construction (EPC) contract with Ormat Nevada for Phase 1; contract duration is 21 months.
January 10, 2006	Raft River Energy 1 (RRE1), a subsidiary of USGeo, seeks \$35M to construct a 13.8 MW (gross), 10 MW (net) power plant; expects to be online early in 2007. Phase 2 envisioned to cost \$70M for two 10 MW plants.
January 31, 2006	Air quality application for Permit To Construct submitted to Idaho Department of Environmental Quality (IDEQ).
February 8, 2006	Request for authorization for non-contact cooling water reuse filed with the IDEQ.
March 9, 2006	Interconnection agreement signed with Raft River Rural Electric Co-Op (RRREC) to wheel power from Phase 1 power plant to Bridge, Idaho, substation on a new 3.2 mile, 34.5 kV transmission line to be constructed by RRREC, paid for by RRE1, and owned by RRREC.
April 4, 2006	Sale completed of \$Cn25M in shares in USGeo.
April 27, 2006	USGeo issues Notice to Proceed to Ormat Nevada to start work on the EPC contract that calls for 10 MW average monthly power for 20 years delivered to Idaho Power Company in accord with USGeo's PPA.
May 26, 2006	IDEQ issues the Permit to Construct.
August 10, 2006	Project financing completed: \$34M for Phase 1.
August 15, 2006	Union Drilling mobilizes its rig, under a May 25, 2006 contract, to begin the well improvement program by deepening the two existing injection wells, RRG-6 and -7. Then it will drill an additional production leg in each of two existing production wells. Total time to complete job expected to be 90 days.
August 17, 2006	Geofluid gathering and distribution system 30% complete under a \$2.6M contract with Industrial Builders of Ontario, Oregon; production piping is 10" and 12" diameter; injection piping is 16" and 24" diameter.

October 19, 2006	Upon completion of deepening RRG-6 and -7 and progress reports from major contractors, project on schedule to be online in September 2007. RRG-6 and -7 turn out to be excellent producers, with flowing wellhead temperatures of 240°F and 270°F, respectively. RRG-7 has a 300°F feed zone at the bottom, indicating cool water inflow somewhere along the open hole. Both wells flow more than 1000 gallons per minute (GPM).
October 19, 2006	Redrilling of RRG-4 is 20% complete; deviated sidetrack being drilled through the casing at 2800 ft toward the Bridge Fault zone and planned to reach a depth of 5400 ft (see Figure 20.4).
December 14, 2006	RRG-4 completed; several permeable zones encountered, indicative of passing through the Bridge Fault zone. The existing leg in RRG-3 is deepened from 5937 to 6185 ft and a new second leg is drilled to 5735 ft. Several highly permeable sand layers, fractures, and lost circulation zones are encountered in the new leg. Piping gathering system 95% complete.
February 2007	Mechanical construction work is awarded to Industrial Builders of Ontario, Oregon, by Ormat Nevada.
March 21, 2007	PPA with Idaho Power amended to 45.5 MW annual average for 25 years, including 13 MW from Phase 1.
April 23, 2007	RRREC completes construction of 3.2-mi power transmission line. Well improvement program nearly done: four wells enhanced by deepening or adding extra legs; two new wells drilled for Phase 2; well RRG-7 to become a producer and RRG-3 an injector.
May 2007	Electrical construction work awarded to Merit Electric.
June 22, 2007	USGeo leases 1685 acres (2.6 mi ²) from US Bureau of Land Management (BLM), increasing its Raft River holdings area by 31.7% to 6933 acres (10.8 mi ²).
July 25, 2007	A 29-stage, 900 hp production pump installed in producer RRG-2; a 33-stage, 1000 hp pump to be installed in RRG-1. Both pumps are from Goulds Pumps/ITT. Two more production well pumps scheduled for delivery to site within 60 days. Seven technicians being trained to operate the plant. Plant expected online in 4th quarter 2007.
September 26, 2007	25-year 13 MW PPA for Phase 1 officially signed with Idaho Power.
October 2007	Test runs of power plant conducted from October 18 to 23; plant ran for 108 hours and total gross generation was 1022 MWh, that is, 9.5 MW average power; a few mechanical problems were found and repaired. Commercial operation set for the end of the 4th quarter, 2007.
November 22, 2007	Test runs resume after repairs to two injection pumps and the HP turbine; testing and training will continue for 60–90 days.
December 3, 2007	Plant capacity test begins at 6:15 P.M.
December 4, 2007	Plant capacity test ends at 6:15 A.M. Plant meets contractual net output.
December 28, 2007	Construction is substantially complete; four production wells in operation; net output is 8–9 MW; 14.4 and 9.5 MW, max. and min. gross outputs; 9.4 and 7.1 MW, max. and min. net outputs.
January 3, 2008	Raft River 1 officially achieves commercial power generation status.
June 19, 2008	With four production and four injection wells in operation, net power output is between 10.5–11.5 MW; the maximum net output achieved during March, April, and May were 11.2, 12.0, and 11.7 MW, respectively; plant had a 99% availability during that period. Reservoir studies continue with the aim of determining how best to use the existing wells.

August 27, 2008	For the past 3 months, plant had net output of 9.5–10.5 MW and 99.9% operating availability. New reservoir model completed and being used to plan new well drilling to increase geofluid flow to raise annual average power up to the PPA rating of 13 MW. Options include: adding more legs to existing production wells, drilling a new production well, and perhaps a new injection well to support increased production.
October 14, 2008	DOE announces grant of \$9M to USGeo to demonstrate the viability of Enhanced Geothermal Systems (EGS) at Raft River. DOE will provide up to \$6M while USGeo will contribute the rest in “in kind” contributions. Program to perform a monitored thermal stimulation of an existing injection well to improve permeability.
October 14, 2008	Raft River 1 operated at 99.9% availability for the past 6 months. Power generation is increasing, currently producing 11.0–11.5 MW (net). Reverse osmosis filtering unit being installed to significantly reduce chemical treatment costs for cooling tower and reduce high levels of dissolved chloride from the cooling tower feed water. Discussions underway with several parties to examine the viability of cascaded use of the geothermal energy, including year-round heating of greenhouses, etc.
September 15, 2009	DOE officially awards \$10.21M to USGeo, wherein DOE to provide up to \$7.39M with rest coming from USGeo in “in kind” contributions. This is the same award that was announced 11 months earlier.
February 23, 2010	Raft River EGS project gets underway. Program teams consist of the Energy & Geoscience Institute (EGI), The University of Utah (program lead), USGeo, APEX Petroleum Engineering Services, and HiPoint Reservoir Imaging. USGeo contributed an existing production well (for Phase 2) for testing thermal fracturing of reservoir rock some 6000 ft below the surface. Halliburton Energy Services placed bridge plug in well RRG-9 at 2235 ft. Work in this portion of the program includes: borehole imaging, fracture analysis, development of a geologic-structural reservoir model, interference testing, construction of injection pipelines, and installation of a liner in the wellbore to the stimulation target horizon.
June 2010	Production well RRG-2 shut down after a pump failure.
May 16, 2011	Pump rig mobilized to the site and begins work on well RRG-2.
May 17, 2011	USGeo signs \$1.65M Repair Services Agreement (RSA) between its wholly owned subsidiary US Geothermal Services and RRE1 for the repair of two production wells, RRG-2 and RRG-7. Production well RRG-7 has a leak in a cement seal that failed where two steel casing sections overlap, allowing cooler geothermal fluid to enter the well bore. Thus, over the last 2 years, wellhead temperature declined from 299°F to 240°F. Successful work-overs to these wells should raise net power from 8 to 10 MW, annual average. Flow stimulation technique called deflagration (controlled, rapid combustion that produces jets of high-temperature, high-pressure gas that impact the wellbore in selected areas) will also be applied to wells RRG-2 and RRG-7 to increase fluid flow.
July 2, 2011	RRG-7 successfully repaired and put back into service after a cement squeeze job to fix the casing leak; the production pump was refurbished and the well is now flowing 1300 GPM of geofluid at 297°F. RRG-2 is now under repair.

20.4.2 POWER PLANT DESIGN

The new USGeo Raft River power plant is located about 600 m SSE of the site of the original plant; see [Figure 20.15](#).



Figure 20.15 USGeo Raft River, aerial view from *Google Earth* image, April 27, 2015 [WWW].

The energy conversion system is a partially recuperated, dual-level, double-pressure binary cycle. There is one unit with two axial-flow turbines driving a common central generator [12]. A four-cell water cooling tower provides chilled water for the shell-and-tube condensers. Make-up water is obtained from water wells and requires treatment to maintain water quality in the towers. About 3,150,000 lbm/h (397 kg/s) of 280°F (138°C) brine is pumped to evaporators and preheaters where the heat is absorbed by the cycle working fluid, isopentane, $i\text{-C}_5\text{H}_{12}$ [13]. The recuperator is used only in the high-pressure (HP) cycle. The process flow diagram is shown in [Figure 20.16](#) [12]; a site photograph is given in [Figure 20.17](#) [14].

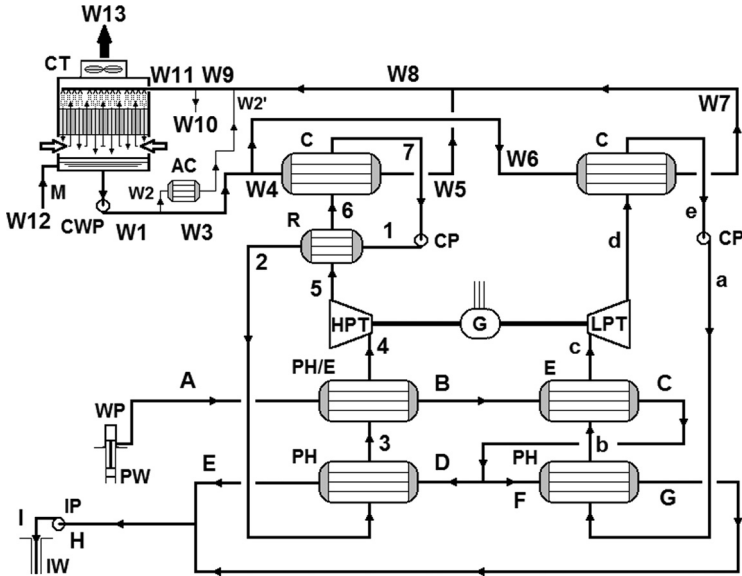


Figure 20.16 Simplified process flow diagram for USGeo Raft River power plant. After Ref. [12].

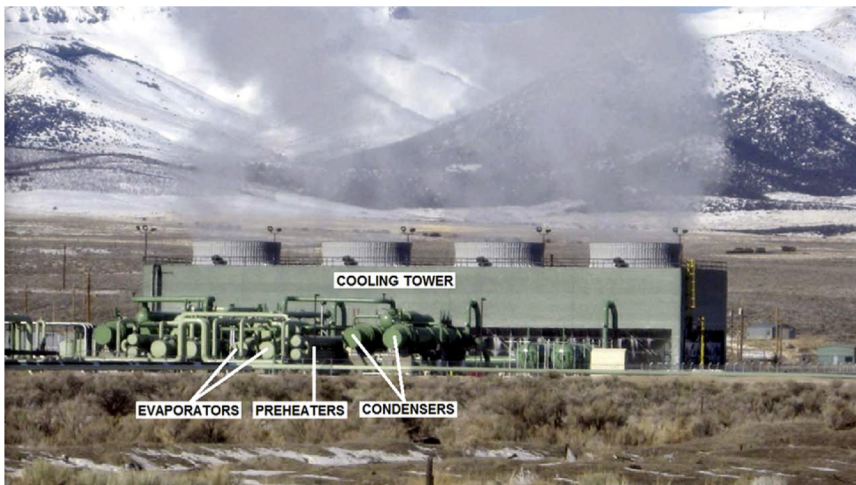


Figure 20.17 USGeo Raft River plant: Equipment is arrayed symmetrically on the left and right of generator except for the recuperator, which is above the condensers on the HP side of the plant only. *After Ref. [14] [WWW].*

20.4.3 DESIGN PERFORMANCE ASSESSMENT

With the arrangement of the components shown in the flow diagram, [Figure 20.16](#), together with key parameters obtained from the manufacturer's (Ormat) heat balance diagram (HBD) and the governing equations from thermodynamics, all the state-point properties can be found, and the heat and work terms computed. [Table 20.7](#) shows temperatures, pressures, and mass flow rates from the HBD, keyed to the state labels used in [Figure 20.16](#). The design wet-bulb temperature (assumed as the dead-state temperature) is 39.8°F.

Next, these data were analyzed and the values of temperature, pressure, entropy, and enthalpy were found with the aid of REFPROP; the results are given in [Table 20.8](#).

The working fluid processes are shown in the pressure-enthalpy diagram, [Figure 20.18](#). Note that state d, the exhaust from the LP turbine, contains some superheat, 44.1°F, but the designers chose not to employ a recuperator in the LP cycle, whereas they did so in the HP cycle where the exhaust superheat (state 5) was significantly greater, 68.5°F. Given the extra cost for the recuperator and the limited value it could contribute with only 44°F of superheat, it was not cost-effective for the LP cycle. To make a fair comparison with the original plant (see [Figure 20.9](#)), the pressure losses in piping and heat exchangers were ignored.

Using the thermodynamic governing equations (similar to Eqs. 20.1–20.13), all the heat and work transfer terms were calculated for the design case. These results appear in [Table 20.9](#) for each of the two cycle loops; [Table 20.10](#) shows the results for the plant as a whole. The heat transfer in the recuperator, \dot{Q}_R , is the average of the values obtained from using the heat released by the vapor (state 5 to 6) and the heat picked up by the liquid (state 1 to 2); the difference is very small, about 1.5%.

The HP cycle is more thermally efficient, 14.1% versus 10.1%. The plant as a whole has a thermal efficiency of 12.2% and converts 37.3% of the incoming brine exergy to useful power. This accounting includes all cycle parasitic loads but does not account for the power to run the production well pumps and injection pumps. And it should be emphasized that these results are for the design case.

20.4.4 ACTUAL PERFORMANCE ASSESSMENT

The actual plant performance has been limited by the available flow rate from the production wells. Instead of the design flow rate of 3,150,000 lbm/h, the actual mass flow rate during the capacity tests for performance validation averaged only 2,510,234 lbm/h or about 80% of the design value. The brine temperature was slightly higher than design, 282.7°F versus 280°F. The tests were conducted on

TABLE 20.7 Nominal design specifications for USGeo plant.

State	Temperature		Pressure		Mass flow rate	
	°C	°F	MPa	psia	kg/s	10 ⁶ lbm/h
<i>Geothermal fluid</i>						
A	137.8	280	0.772	112	396.9	3.15
B	110.0	230	NA	NA	396.9	3.15
C	87.4	189.4	NA	NA	396.9	3.15
D	87.4	189.4	NA	NA	198.4	1.575
E	68.2	154.8	0.634	92	198.4	1.575
F	87.4	189.4	NA	NA	198.4	1.575
G	63.0	145.4	0.634	92	198.4	1.575
H	65.6	150.1	0.634	92	396.9	3.15
I	65.8	150.5	NA	NA	396.9	3.15
<i>Isopentane—HP cycle</i>						
1	NA	NA	0.9566	138.7	139.3	1.1057
2	38.1	100.6	0.9566	138.7	139.3	1.1057
3	113.1	235.6	0.9566	138.7	139.3	1.1057
4	113.1	235.6	0.9566	138.7	139.3	1.1057
5	62.4	144.3	0.0897	13.0	139.3	1.1057
6	40.3	104.5	0.0897	13.0	139.3	1.1057
7	19.9	67.8	0.0897	13.0	139.3	1.1057
<i>Isopentane—LP cycle</i>						
a	NA	NA	0.5124	74.3	128.8	1.0226
b	84.3	183.7	0.5124	74.3	128.8	1.0226
c	84.3	183.7	0.5124	74.3	128.8	1.0226
d	48.2	118.7	0.0876	12.7	128.8	1.0226
e	19.4	66.9	0.0876	12.7	128.8	1.0226
<i>Cooling water</i>						
W1	11.9	53.5	0.2828	41	3010.9	23.896
W2	11.9	53.5	0.2828	41	78.8	0.6256
W2'	14.4	58.0	0.1655	24	78.8	0.6256
W3	11.9	53.5	0.2828	41	2932.1	23.270
W4	11.9	53.5	0.2828	41	1466.0	11.635
W5	20.7	69.2	0.1655	24	1466.0	11.635
W6	11.9	53.5	0.2828	41	1466.0	11.635
W7	20.3	68.6	0.1655	24	1466.0	11.635
W8	20.5	68.9	0.1655	24	2932.1	23.270
W9	20.3	68.6	0.1655	24	3010.9	23.896
W10	20.3	68.6	0.1655	24	17.63	0.1399
W11	20.3	68.6	0.1655	24	2993.3	23.756
W12	11.9	53.5	NA	NA	52.97	0.4204
W13	NA	NA	NA	NA	35.31	0.2802

Data from Ref. [12].

TABLE 20.8 Nominal design state-point properties for USGeo plant.

State	Temperature, °F	Pressure, psia	Entropy, Btu/lbm · °F	Enthalpy, Btu/lbm	Mass flow rate, 10 ⁶ lbm/h
<i>Geothermal fluid</i>					
A	280	112	0.4101	249.49	3.15
B	230	105	0.3390	198.69	3.15
C	189.4	99	0.2779	157.79	3.15
D	189.4	99	0.2779	157.79	1.575
E	154.8	92	0.2230	123.09	1.575
F	189.4	99	0.2779	157.79	1.575
G	145.4	92	0.2076	113.68	1.575
H	150.1	92	0.2153	118.38	3.15
I	150.5	NA	NA	NA	3.15
<i>Isopentane—HP cycle</i>					
1	68.8	137.55	−0.0140	−6.8982	1.1057
2	100.6	137.55	0.0180	10.524	1.1057
3	235.6	137.55	0.1504	93.613	1.1057
4	235.6	137.55	0.3101	204.65	1.1057
5	144.3	13.00	0.3225	174.40	1.1057
6	104.5	13.00	0.2931	157.24	1.1057
7	67.8	13.00	−0.0145	−7.7488	1.1057
<i>Isopentane—LP cycle</i>					
a	67.4	73.49	−0.0152	−7.8181	1.0226
b	183.7	73.49	0.1002	59.620	1.0226
c	183.7	73.49	0.2958	185.48	1.0226
d	118.7	12.70	0.3044	163.30	1.0226
e	66.9	12.70	−0.0154	−8.2327	1.0226
<i>Cooling water</i>					
W1	53.5	41	0.04296	21.704	23.896
W2	53.5	41	0.04296	21.704	0.6256
W2'	58.0	24	0.05171	26.162	0.6256
W3	53.5	41	0.04296	21.704	23.270
W4	53.5	41	0.04296	21.704	11.635
W5	69.2	24	0.07313	37.367	11.635
W6	53.5	41	0.04296	21.704	11.635
W7	68.6	24	0.07199	36.767	11.635
W8	68.9	24	0.07256	37.067	23.270
W9	68.6	24	0.07199	36.767	23.896
W10	68.6	24	0.07199	36.767	0.1399
W11	68.6	24	0.07199	36.767	23.756
W12	53.5	NA	NA	NA	0.4204
W13	NA	NA	NA	NA	0.2802

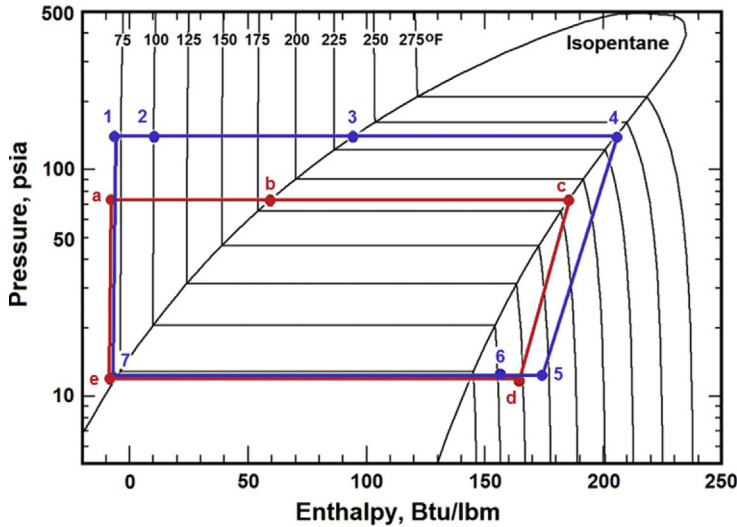


Figure 20.18 Pressure-enthalpy process diagram for USGeo Raft River plant [WWW].

TABLE 20.9 USGeo Raft River cycle analysis: LP and HP cycles.

LP cycle			HP cycle		
\dot{Q}_{LPH}	20.21	MW-th	\dot{Q}_{HPH}	26.93	MW-th
\dot{Q}_{LPE}	37.72	MW-th	\dot{Q}_{HPE}	35.98	MW-th
\dot{W}_{LPT}	6.65	MW	\dot{W}_{HPT}	9.80	MW
\dot{Q}_R		(none)	\dot{Q}_R	17.29	MW-th
\dot{Q}_{LPC}	51.41	MW-th	\dot{Q}_{HPC}	53.47	MW-th
\dot{W}_{LPP}	0.134	MW	\dot{W}_{HPP}	0.276	MW
$\dot{Q}_{IN, LP}$	57.93	MW-th	$\dot{Q}_{IN, HP}$	62.91	MW-th
$\dot{W}_{CT, FANS}$	0.2875	MW	$\dot{W}_{CT, FANS}$	0.2875	MW
\dot{W}_{CWP}	0.375	MW	\dot{W}_{CWP}	0.375	MW
$\dot{W}_{NET, LP}$	5.86	MW	$\dot{W}_{NEF, HP}$	8.86	MW
$\eta_{TH, LP}$	10.1%		$\eta_{TH, HP}$	14.1%	

Note: CT fan and CW pump power for each cycle are assumed half the total for the plant.

December 3–4, 2007, from 6:15 P.M. to midnight on the 3rd and continuing from midnight to 6:15 A.M on the 4th. Besides the geofluid flow rate and temperature, there were several other off-design conditions that needed to be corrected for using appropriate factors. Under the off-design conditions, the average plant performance is shown in Table 20.11; these were calculated using the actual data recorded during the test and provided by Ormat [12].

TABLE 20.10 Design performance for new Raft River plant, excluding field pumps.

$\dot{W}_{T, TOT}$	16.45 MW
$\dot{W}_{P, TOT}$	0.410 MW
$\dot{W}_{CT, FANS}$	0.575 MW
\dot{W}_{CWP}	0.750 MW
$\dot{W}_{NET, OEC}$	14.72 MW
$\dot{Q}_{IN, TOT}$	120.84 MW-th
$\eta_{TH, OEC}$	12.2%
$\dot{E}_{IN, BRINE}$	39.42 MW
$\eta_{U, OEC}$	37.3%

TABLE 20.11 Performance for plant during capacity test conditions.

$\dot{W}_{OEC, GROSS}$	14.602 MW
$\dot{W}_{PLANT, NET}$	9.609 MW
$\dot{E}_{IN, BRINE}$	35.452 MW
$\eta_{U, GROSS}$	41.2%
$\eta_{U, NET}$	27.1%

From these data, since the brine return temperature is not given, the heat input to the isopentane could not be determined and so the thermal efficiency could not be calculated. However, using a dead-state temperature of 33°F (the actual wet-bulb temperature during the test was below freezing), the incoming brine exergy can be found and the utilization efficiency calculated. The utilization efficiency for the actual conditions fell 10% points or 27% below the design value.

When the actual performance results were corrected using factors derived from the variation between the design and actual site conditions, the corrected net power was 13.906 MW which exceeded the guaranteed net power at the design point of 13.735 MW. Thus the plant passed its acceptance test.

20.4.5 CONCLUSION

The original (DOE) and the new (USGeo) Raft River plants have very similar design performance, despite using quite different energy conversion systems. The

DOE plant was based on a geofluid temperature of 290°F and a 65°F wet-bulb temperature (assumed dead-state temperature); the USGeo plant uses 280°F brine temperature and a quite low 39.8°F wet-bulb temperature. Table 20.12 compares some important results for the plants. Note that the design performance for the USGeo plant has been calculated at its own wet-bulb temperature and at that for the DOE plant (values in parentheses) to put them on a common footing for utilization efficiency. The design thermal efficiency is roughly the same, with the USGeo plant holding a 2.5% advantage. The DOE plant has a 9.6% advantage in specific output, Wh/lbm, mainly due to the higher geofluid temperature. When the plants are designed for the same wet-bulb (dead-state) temperature of 65°F, they are essentially identical in terms of utilization efficiency, each plant converting about 45.5% of the geofluid exergy into useful output.

TABLE 20.12 DOE and USGeo Raft River power plants compared.

	DOE	USGeo
T_{GEO} , °F	290	280
\dot{m}_{GEO} , 10 ⁶ lbm/h	1.04	3.15
$\dot{W}_{NET, OEC}$, MW	5.32	14.72
$\eta_{TH, OEC}$, %	11.9	12.2
T_0 , °F	65	39.8 (65)
$\eta_{U, OEC}$, %	45.7	37.3 (45.4)
$\dot{W}_{NET, OEC} / \dot{m}_{GEO}$, Wh/lbm	5.12	4.67

The DOE plant suffered from some serious design flaws and from a lack of reliable geothermal well pumps. The USGeo plant is well designed, constructed, and uses very reliable downhole pumps, but is lacking sufficient geofluid flow to meet the design output, a fundamental problem that is shared by some other recent geothermal plants. The only solution is to drill more wells, both producers and injectors, to raise the flow rate. However, the reservoir itself is capable of yielding and accepting only so much fluid within the leasehold. Since 100% of the produced fluid must eventually be returned to the formation, the lack of injection capacity is often the real limitation on plant output. For example, the newly refurbished well, RRG-7, which was switched from being an injector to a producer, will increase the hot brine flow, but unless all of that fluid can be effectively reinjected, the gain may not be fully realized.

References

- [1] Google Earth, 5.2.1.1588, Build date: September 1, 2010, imagery date June 24, 2009.
- [2] Toth WJ. Raft River Colloquy: a series of papers on geothermal development at Raft River, Idaho. *Geothermal Resour Counc Bull* 1982;11(2):4–5.
- [3] U.S. Geothermal Inc., <<http://www.usgeothermal.com/RaftRiverProject.aspx>>; [accessed 06.05.11].
- [4] Mattson E, Plummer M, Palmer C, Hull L, Miller S, Nye R. Comparison of three tracer tests at the Raft River geothermal site. Proc. thirty-sixth workshop on geothermal reservoir engineering, Stanford University, Stanford, California; January 31–February 2, 2011, Rep. No. SGP-TR-191.
- [5] Tullis JA, Dolenc MR. Geoscience interpretations of the Raft River resource. *Geothermal Resour Counc Bull* 1982;11(2):6–9.
- [6] Holt RJ. Numerical model development and results: Raft River geothermal field, cassia, county, Idaho. Geothermal Science, Inc., Technical report, prepared for U.S. Geothermal, Inc.; 2008.
- [7] Ayling B, Molling P, Nye R, Moore J. Fluid geochemistry at the Raft River geothermal field, Idaho: new data and hydrogeological implications. Proc. thirty-sixth workshop on geothermal reservoir engineering, Stanford University, Stanford, California; January 31–February 2, 2011, Rep. No. SGP-TR-191.
- [8] Bliem CJ, Walrath LF. Rep. EGG-2208 Raft River binary-cycle geothermal pilot power plant final report. Idaho Falls, ID: Idaho National Engineering Laboratory, EG&G Idaho, Inc.; April 1983.
- [9] Moskvicheva VN, Popov AE. Geothermal power plant on the Paratunka River. *Geothermics—special issue 2*, U.N. symposium on the development and utilization of geothermal resources, Pisa, 1970;2(Pt. 2):1567–71.
- [10] Ingvarsson IJ, Madsen WW. Determination of the 5 MW gross nominal design case binary cycle for power generation at Raft River, Idaho Rep. TREE-1039 Idaho Falls, ID: Idaho National Engineering Laboratory, EG&G Idaho; December 1976.
- [11] U.S. Geothermal, Inc., Boise, Idaho, news releases, various dates <<http://www.usgeothermal.com/>>; News releases.
- [12] Bronicki L. Ormat, Inc.; July 14, 2011.
- [13] Peltier R. Raft River Geothermal Project, Malta, Idaho. POWER, <http://www.powermag.com/issues/cover_stories/Raft-River-Geothermal-Project-Malta-Idaho_231.html>; December 15, 2007.
- [14] Richter LX. Geothermal could be significant source of power in Idaho, ThinkGeoEnergy, <<http://thinkgeoenergy.com/archives/8161>>; July 24, 2011.



Chapter 21

Geothermal Power Plants in Turkey

Chapter Outline

21.1 Geologic Setting	575
21.2 Kızıldere Single-Flash Plant	577
21.2.1 Early History and Pilot Plant	577
21.2.2 Wells	579
21.2.3 Kızıldere Unit 1	581
21.2.4 Kızıldere Unit 2 and Future Plans	584
21.3 Salavatlı Binary Plants	586
21.3.1 Dora 1	586
21.3.2 Dora 2	591
21.3.3 Dora 3A, 3B, 4, and 5	593
21.4 Germencik Double-Flash Plant	593
21.4.1 Overview	593
21.4.2 Geologic Setting	594
21.4.3 Germencik Double-Flash Power Plant	595
21.5 Pamukören Binary Plant	600
21.6 Environmental Impact	602
21.7 Current State and Future Prospects of Geothermal Power	603
References	605
Nomenclature for Figures in Chapter 21	607

Everything we see in the world is the creative work of women.

Mustafa Kemal Atatürk

21.1 Geologic Setting

Turkey lies in a highly active tectonic region, the Alpine-Himalayan orogenic belt. There are almost 200 geothermal prospects, but nearly all of them are suitable only for low-temperature applications. The one area that has high-temperature resources is associated with the Büyük Menderes Graben in western Anatolia.

All of Turkey's operating power plants lie in this region. In fact they are roughly aligned in an east-west direction approximately along the 38°North parallel, together with the famous Pamukkale UNESCO World Heritage Site. The latter is a popular tourist attraction consisting of numerous travertine terraces formed from hot springs that issue from the northeast side of the graben. Because the geofluid is supersaturated with calcium carbonate, when it reaches the surface and the dissolved carbon dioxide is released to the atmosphere, calcium carbonate precipitates and eventually hardens into spectacular white terraces. Unfortunately, the geothermal fluids produced at the fields supporting power plants also suffer from calcium carbonate scaling in the production wells, forcing the operators to resort to various means to remedy the situation.

Starting from Pamukkale, Turkey's oldest geothermal power plant, Kızıldere, is about 25 km west, followed by Salavatlı which is about 66 km west of Kızıldere, and ending at Germencik, about 40 km west of Salavatlı. Figure 21.1 shows the geologic setting for Turkey's geothermal power plants. The prominent graben lies between two parallel horsts in an alternating pattern of subsidence and uplift. To date high-temperature geofluids have been found only in wells drilled into the slip-step faults that form the northern boundary of the graben. These faults appear to be the main fluid controlling structures all across the east-west extent of the graben from Germencik to Kızıldere.

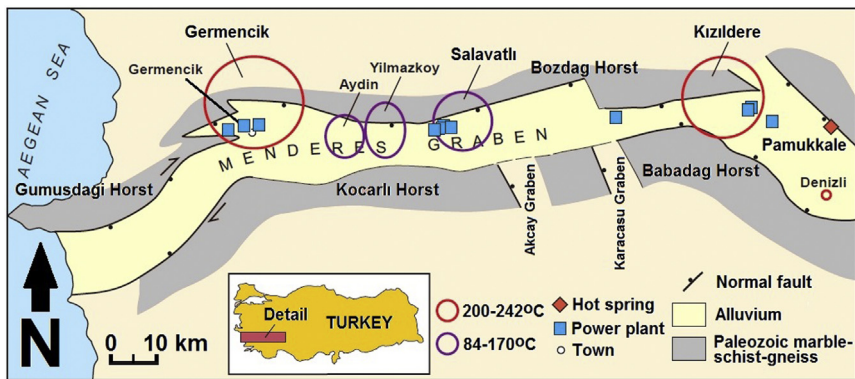


Figure 21.1 Menderes Graben and locations of Turkey's geothermal power plants; note Tuzla-Çanakkale power plant is off the map to the top left. After Refs. [1] and [2] [WWW].

Figure 21.2 presents a cross-section of the region with the location of the Kızıldere power plant and the hot spring Tekke Hamam thermal spa, a few kilometers apart on opposite sides of the Menderes River. Hot springs are found on both the north and south sides of the graben. The basement rock is gneiss and numerous layers of various formations constitute the lithology of the reservoir.

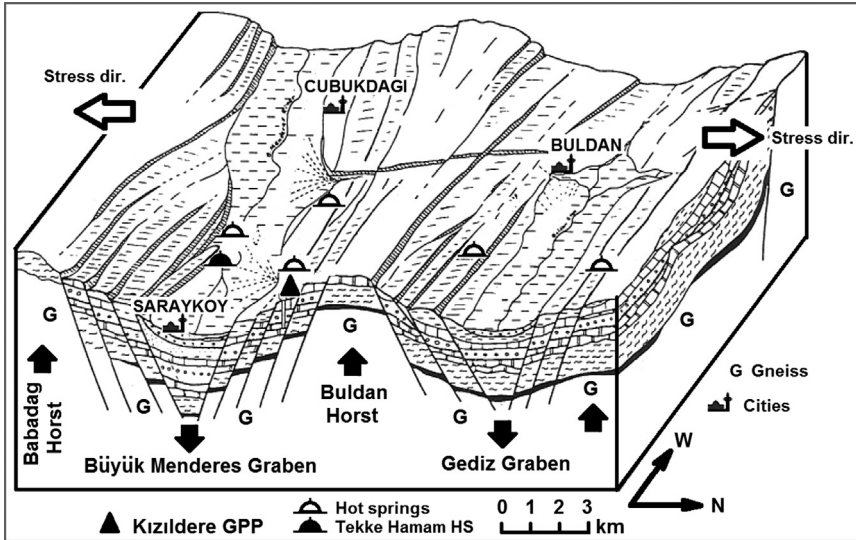


Figure 21.2 Geologic cross-section showing Büyük Menderes Graben and associated horsts. Modified from Ref. [3] as shown in Ref. [4].

At the eastern end of the Büyük Menderes Graben, in the vicinity of Kızıldere, three distinct production zones have been identified by well drilling. The first and shallowest is the Sazak Formation between Pliocene units; it extends to 706 m and has a temperature of 190–200°C. The next one in depth is the Igdecik Formation of Menderes metamorphics which reaches to 1261 m and has a temperature of 200–212°C. The deepest one consists of gneiss and quartzite under the mica schists. There may even be a fourth, very deep (~3000 m), reservoir with a possible temperature in the 250–260°C range [5]. The upper layer, the cap rock, is comprised of Pliocene-aged clay, marl and altered sandstones.

21.2 Kızıldere Single-Flash Plant

21.2.1 EARLY HISTORY AND PILOT PLANT

Discovered in the 1960s, the Kızıldere resource is a liquid-dominated reservoir at a temperature of between 200°C and 242°C, with low total dissolved solids (TDS ~2500–3200 ppm), but very high noncondensable gases (NCG ~2.5% by weight of brine in the reservoir, 5% by volume of steam, 10–21% by weight of steam, and an average 13% by weight of steam at the turbine inlet). The NCG also contain 96–99% (by weight) carbon dioxide (CO₂) and 100–200 ppm of hydrogen sulfide (H₂S). The steam fraction (by weight) at the wellhead is 10–12% [6].

The field was first exploited by a small pilot plant under the direction of the General Directorate of Mineral Research and Exploration (MTA). The 0.5 MW noncondensing turbine went into operation in 1974 and ran for six years while providing free electricity to three neighboring communities. The turbine and associated piping and equipment were fabricated by MTA and served to demonstrate that the resource could be used for practical power generation. Figures 21.3 and 21.4, provided to the author by Mr. Orhan Mertoğlu in 1981, show the pilot plant attached to well KD-13 and the turbine-generator hall, respectively.

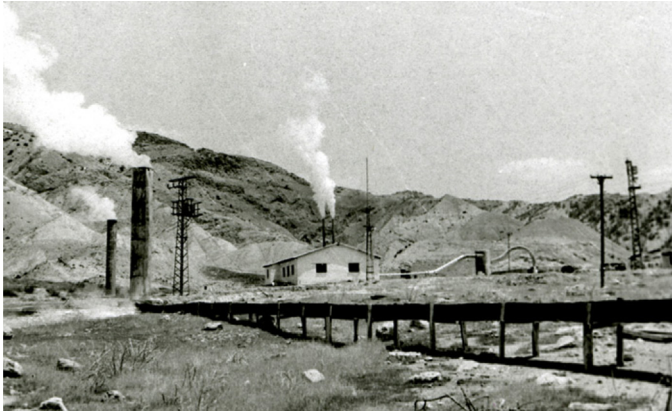


Figure 21.3 Kızıldere 0.5 MW pilot plant [7]. *Photo courtesy of O. Mertoğlu.*

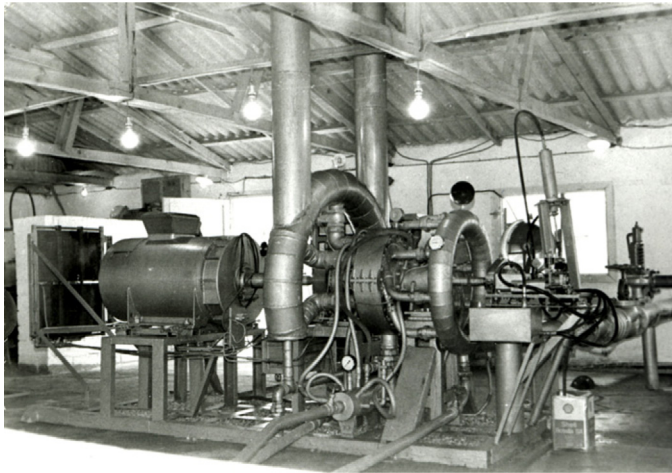


Figure 21.4 Steam turbine and generator for Kızıldere 0.5 MW pilot plant [7]. *Photo courtesy of O. Mertoğlu.*

The wellhead unit was designed to the following specifications as given in Table 21.1.

TABLE 21.1 Technical specifications for Kızıldere pilot wellhead unit [7].

Item	Value
Turbine type	Single-cylinder, Curtis stage, back-pressure, geared
Rated capacity	500 kW
Speed, turbine/generator	4500/1500 rev/min
Maximum pressure	786 kPa (114 lbf/in ² ,a)
Steam pressure	486 kPa (70.5 lbf/in ² ,a)
Steam temperature	150°C (302°F)
Exhaust pressure	115 kPa (16.7 lbf/in ² ,a)
Steam mass flow rate	3.61 kg/s (28,660 lbm/h)
NCG	17% by wt. of steam
Blade height	76 mm (3 in)

21.2.2 WELLS

The wells supplying the plant were drilled starting in the 1970s, as shown in Table 21.2. The location of the wells is presented in Figure 21.5. For more than 25 years the plant operated with no reinjection, disposing of the waste liquid via runoff channels to the Büyük Menderes River. In 1997 R-1 was drilled specifically as an injection well, being some 1.8 km southwest of the center of the production area. However, it was found that R-1, the deepest well, was also the hottest and very productive, having a power capability of about 6 MW. Thus, in 2001 it was incorporated into the plant as a producer and the output of the plant increased by 6.5%. The wells TH-1 and TH-2 (Figure 21.5) were sited on the south side of the river not far from the Tekke Hamam hot spring spa as potential injection wells. These wells showed little permeability and were abandoned. Reinjection is complicated by the high reservoir pressure, at least when the plant first began operating, that requires high-pressure (HP) pumping to overcome the reservoir pressure. After some 20 years of operation, the reservoir pressure has declined by about 10 bar alleviating the reinjection problem [8].

Given the present understanding of a three-layered reservoir, a methodology has been proposed [9] to produce from the deepest layer and reinject the hot separated water into the shallow layer within the productive area. Since the separated water is at about 147°C and the limit temperature to avoid silica scale is 115°C, there should be no plugging of the injection wells. The cooler waste water would then be sent to injection wells outside the production area to the south and west of the field.

TABLE 21.2 Well information [4–6].

Well	Date	Depth m	T_{res} °C	T_{sep} °C	P_{sep} kPa	\dot{m}_{tot} kg/s	\dot{m}_{st} kg/s	\dot{m}_{liq} kg/s	% CO ₂ wt. of steam
KD-1	1968	540	198			NA			
KD-2	1968	769	174			18.6(*)			
TH-1	1968	615.5	116			NA			
KD-1A	1969	573.1	195			37.5(*)			
KD-3	1969	370	172			NA			
KD-4	1969	486	178			NA			
KD-III	1969	505.9	152			NA			
KD-6 (P)	1970	851	194	147	367	23.32	2.80	20.52	20.0
KD-7	1970	667.5	208			70.0(*)			
KD-8	1970	576.5	190			NA			
KD-9	1970	1241	172			42.8(*)			
KD-12	1970	404.7	148			NA			
KD-14 (P)	1970	597	210	148	387	29.13	3.50	25.63	10.0
KD-13 (P)	1971	760	198	145	377	26.31	3.16	23.15	17.4
KD-15 (P)	1971	510	208	147	377	31.59	3.79	27.80	17.5
KD-16 (P)	1975	666.5	212	148	387	45.45	5.45	40.00	12.0
KD-17	1975	365.2	144			NA			
KD-21 (P)	1985	898	204	147	387	32.03	3.84	28.19	10.6
KD-22 (P)	1985	888	205	147	367	28.24	3.39	24.85	14.0
KD-20 (P)	1986	810	205	147	377	30.48	3.66	26.82	13.7
TH-2 (A)	1996	2001	168			11.67			
R-1 (P)	1997	2261	242	148	369	44.44	5.33	39.10	21.0
R-2 (I)	2002	1371	197			55.55			

(*) = Maximum flow, (P) = production, (I) = injection, and (A) = abandoned.

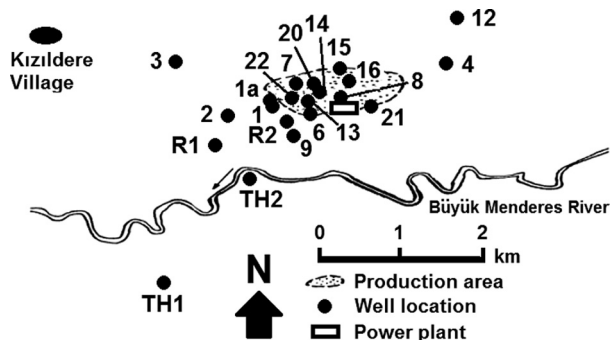


Figure 21.5 Well field and power plant location. After Ref. [6].

The calcite scaling in the production wells required frequent work-overs to remove the deposits, reducing plant output and increasing the operating and maintenance costs. Recently, following the 2008 sale of the plants to a private company, the Zorlu Group, a system of downhole injection of scale inhibitor was initiated to prevent the formation of calcite. Such a system is used in several fields that are subject to this problem; see Section 16.5 for a discussion of the system as used at Miravalles in Costa Rica.

21.2.3 KIZILDERE UNIT 1

The main challenge for the exploitation of the resource is the very high percentage of NCG in the steam [10]. The central station that was constructed at Kızıldere followed the practice developed at Larderello, Italy, to cope with the high levels of NCG, namely, the use of turbo-compressors connected to the turbine shaft. Kızıldere Unit 1 (see Figures 21.6 and 21.7) came online in 1984 and had a rated power of 20.4 MW but recently operated at 12–15 MW [11]. Figure 21.8 shows the plant flow diagram in highly simplified form. The flow diagram shows the NCG being vented, but since 1985 an adjacent CO₂ plant has been in operation taking all of the NCG from the plant and producing 120×10^6 kg of liquefied CO₂ and dry ice per year [2].

The high parasitic power needed to operate the turbo-compressors—they take 17% of the gross power—motivated a study to remove the NCG from the steam



Figure 21.6 Kızıldere Unit 1. *Photo by author April 2005 [WWW].*



Figure 21.7 Turbo-compressors at Kızıldere Unit 1. Photo by author April 2005 [WWW].

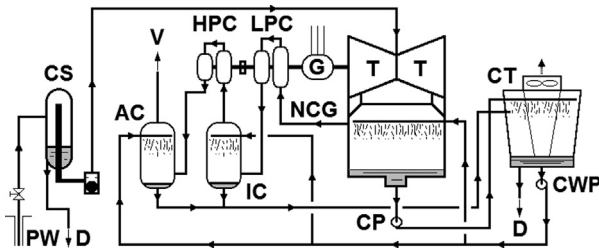


Figure 21.8 Simplified flow diagram for Kızıldere Unit 1.

upstream of the turbine. The compressors alone consume 2.38 MW and the total plant parasitic load is 3.0 MW. A reboiler system was studied, and a pilot-scale unit was built and tested on a side-stream from one well [12,13] but has not been implemented in full scale.

Tables 21.3 and 21.4 show the technical particulars for the turbine-generator and the NCG compressors. Based on these data and neglecting the power generated by the expanding NCG, the turbine has an isentropic efficiency of 71.5%; modern geothermal steam turbines have efficiencies about 15 percentage points higher.

Table 21.5 lists the plant parasitic load. The total, 2851.6 kW, amounts to 16% of the rated capacity of the plant. Cooling water is produced by a four-cell, mechanical-draft, counterflow cooling tower. Make-up water is taken from the Büyük Menderes River.

TABLE 21.3 Turbine-generator specifications for Kızıldere Unit 1 [7].

Turbine type	Single-cylinder, double-flow, reaction blading
Manufacturer	Ansaldo
Rated capacity	17.8 MW
No. of stages	7 per flow
Speed	3000 rev/min
Steam inlet pressure	378 kPa (54.8 lbf/in ² ,a)
Steam inlet temperature	147°C (297°F)
Exhaust pressure	10.19 kPa (1.467 lbf/in ² ,a)
Steam mass flow rate ^a	42.42 kg/s (336,670 lbm/h)
Generator rating	20.6 MVA@10.5 V
Manufacturer	Ansaldo

^aAt maximum power output.

TABLE 21.4 Turbo-compressor specifications for Kızıldere Unit 1 [7].

Compressor type	Centrifugal
No. of stages	2 with intercondenser and aftercondenser
Speed	3000 rev/min, LP; 3900 rev/min, HP
Rated power input	2.38 MW
Inlet gas mass flow rate ^a	8.91 kg/s (70,715 lbm/h)
LP inlet pressure	80 kPa (11.6 lbf/in ² ,a)
LP inlet temperature	53°C (127°F)
LP outlet pressure	101.3 kPa (14.7 lbf/in ² ,a)
LP outlet temperature	51°C (124°F)
HP inlet pressure	93 kPa (13.5 lbf/in ² ,a)
HP inlet temperature	51°C (124°F)
HP outlet pressure	340 kPa (49.3 lbf/in ² ,a)
HP outlet temperature	37.5°C (99.5°F)
Manufacturer	Franco-Tosi

^aIncludes 6.44 kg/s NCG and 2.47 kg/s steam at LP inlet.

TABLE 21.5 Auxiliary power requirements for Kızıldere Unit 1 [7].

Item	No. of units	Total power (kW)
Compressor	1	2380.0
Cooling tower fan motor	4	149.14
Chlorinated water pump	2	74.0
Service air compressor	2	74.0
Water pump	2	74.0
Main lube oil pump	1	37.3
Emergency bearing lube pump	1	37.3
Sand filters water pump	2	15.0
Sand filters back-wash pump	2	6.0
Miscellaneous	7	4.86
Total	24	2851.6

21.2.4 KIZILDERE UNIT 2 AND FUTURE PLANS

The Zorlu Energy Group, owners of Kızıldere since September 2008, has constructed a second unit, Kızıldere Unit 2, with a power rating of 80 MW. The plant was commissioned in October 2013 and has been operating very successfully; see Figure 21.9.



Figure 21.9 Kızıldere Unit 2, 80 MW hybrid three-flash-steam and binary power plant. Google Earth Panoramio No. 101346359; photo by A. Layz, June 11, 2013 [WWW].

The new plant uses 20 new wells or deepened existing wells that tap a hotter reservoir at temperatures of at least 225°C and at depths of up to 3000 m [14–16]. The new plant is a unique design comprised of a triple-flash steam system with two embedded binary units; see Figure 21.10. The steam turbines contribute 60 MW and the two binary units add 10 MW each.

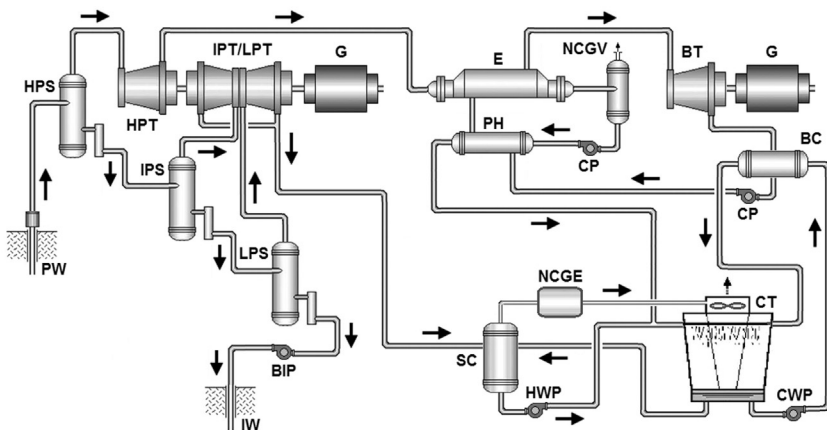


Figure 21.10 Simplified flow diagram for Kızıldere Unit 2 power plant. Note: There are two binary units (only one shown for clarity); see Nomenclature. After Ref. [16].

Since the geofluid carries high NCG content, 16–20% (wt.), the HPS is set at a high pressure and captures nearly all of the NCG in the steam flow, which passes through the HPT and the binary evaporators. The NCG are then vented before the steam condensate is pumped to the binary cycle preheaters [17]. The amount of NCG that passes through the IPT and LPT turbine sections is not excessive and is typical of normal geothermal plants (see Table 21.6); the NCG ejectors remove these gases from the steam condenser to maintain a good vacuum. Since the steam condensate is relatively free of dissolved solids, it can be used for cooling tower make-up. This avoids having to use air-cooled condensers for the binary cycles. The binary unit condensers are of course shell-and-tube type, but the one for the steam turbines is an advanced direct-contact condenser (ADCC). This energy conversion system arrangement is patented [16].

The unique tandem-compound, triple-admission steam turbine was supplied by Fuji Electric and is shown in cross-section in Figure 21.11; Table 21.6 gives some particulars on the steam turbine.

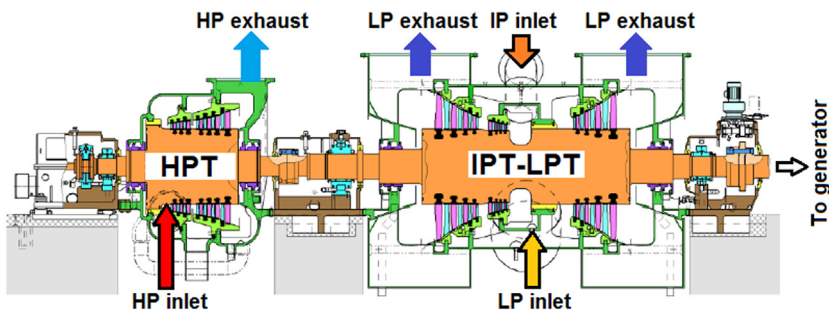


Figure 21.11 Cross-section of Fuji steam turbine assembly for Kızıldere Unit 2 power plant. After Ref. [17] [WWW].

TABLE 21.6 Kızıldere Unit 2 steam turbine specifications [17].

Turbine section	HPT	IPT	LPT
Inlet pressure, bar,a	8.45	3.5	1.1
Inlet temperature, °C	169 (sat.)	139 (sat.)	102 (sat.)
NCG, wt. %	16.7	0.40	0.06
Exhaust pressure, bar,a	1.1	—	0.105
Condensing temperature, °C	102.3	—	46.8
Mass flow rate, kg/s	103.3	35.8	58.3
Rotational speed, rpm	3000	3000	3000

The gross utilization efficiency is 27.5% based on a reservoir temperature of 230°C and a dead state of 25°C. For this calculation, the exergy of the incoming geofluid has been lowered by 16.7% from the pure water value, according to the rule of thumb that 1% NCG (assumed all CO₂) causes a 1% reduction in the specific exergy of water.

Zorlu also plans to rehabilitate Unit 1 and has already restored the output to 17.4 MW by cleaning out the calcite from the production wells, thereby increasing the flow rate to the plant. They anticipate an expenditure of \$250 million for the entire project which includes about \$60 million for the new wells.

21.3 Salavatlı Binary Plants

There are two binary power plants in operation near the village of Salavatlı about 66 km west of Kızıldere. The geologic setting is similar to that found at Kızıldere since they lie in the same Büyük Menderes Graben. Reservoir temperatures reached so far are somewhat lower than those in the deep reservoir at Kızıldere, but the NGC contents are about the same.

21.3.1 DORA 1

The first geothermal power plant to be built by a private company came online in April 2006 on the outskirts of the Salavatlı village and has been producing power continuously since May 2006. It is a 6.5 MW (net) integrated-two-level binary power station that was developed by the Menderes Geothermal Elektrik Üretim A.Ş. (MEGE). MEGE also drilled the wells, constructed the power plant, and has maintained it since it commenced operation. The power block equipment was supplied by Ormat [18].

There are two production wells, AS-1 and ASR-2, and one reinjection well, AS-2. Another reinjection well was drilled, ASR-1, but it proved to be such a good producer, capable of 97.2 kg/s total flow, that it was reserved for the second power unit. The reservoir temperature is about 170°C and the combined flow from the two producers is 157.9 kg/s [19]. The geofluid is separated at the well-heads by means of vertical cyclone separators, and steam and brine are conveyed to the plant. Well AS-2 is immediately adjacent to the plant whereas AS-1 requires 900 m of steam and water pipelines and ASR-2 100 m of pipelines. The plant is at an elevation 13 m lower than the more distant producer, AS-1. At the plant there is a moisture remover to dry the steam and an accumulator to collect the brine. Figure 21.12 shows the locations of all wells to date that will serve both Dora units at Salavatlı. Figure 21.13 is an aerial view of the field. Note the close proximity of the Linde Gaz CO₂ facility to the power plant.

The geofluid at the wellhead consists of mainly liquid with a small weight percentage of steam and NCG, about 2.2%, however the NCG make-up more than 50% of the vapor phase. The vapor fraction passes to the Level 2 vaporizer where it gives up its latent heat and condenses. The condensate is used no further and is pumped to the reinjection line. The liquid fraction (brine) passes first to the Level 1 vaporizer, then to the Level 2 vaporizer where it travels through a set of tubes separate from those used by the steam, and then is split into two

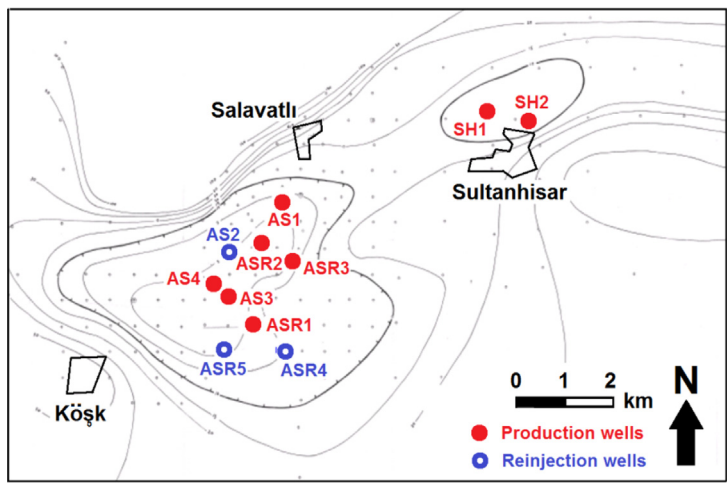


Figure 21.12 Salavatlı wells drilled for Dora 1 and Dora 2 power plants. *After Ref. [8] [WWW].*



Figure 21.13 Salavatlı Dora 1 plant and wells. Google Earth, April 10, 2010 [WWW].

streams for use in the preheaters of each level. The cooled brine is then at a temperature of about 78–80°C.

The process flow diagram is given in Figure 21.14. Components labeled with “1” and “2” are for Levels 1 and 2, respectively. Notice that half of the air-cooled condenser cells serve each level separately. Furthermore, after the steam fraction passes through the Level 1 vaporizer, no further use is made of it and its condensate is reinjected. The wells are designated in accordance with June 2011 operation. Figures 21.15 and 21.16 are site photographs [18].

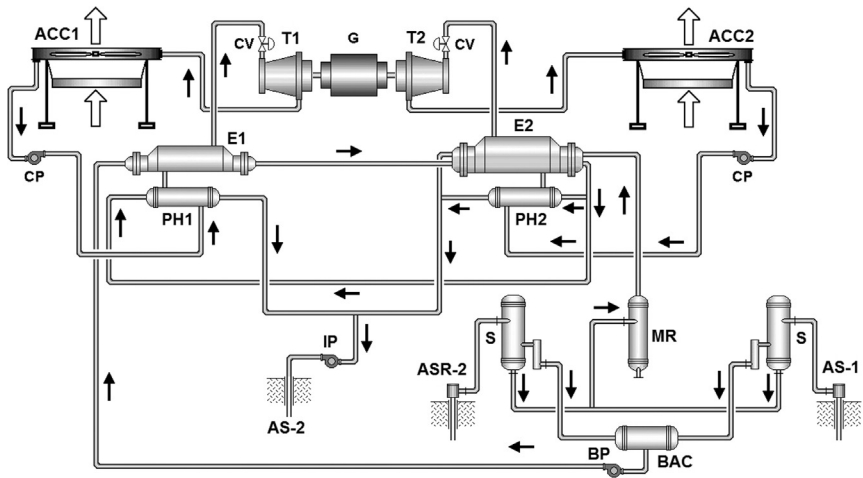


Figure 21.14 Salavatlı Dora 1 flow diagram. The organic Rankine cycle (ORC) working fluid is n-pentane.



Figure 21.15 Salavatlı Dora 1 power plant [18], before construction of Linde Gaz plant. Reinjection well AS-2 is in the front [WWW].

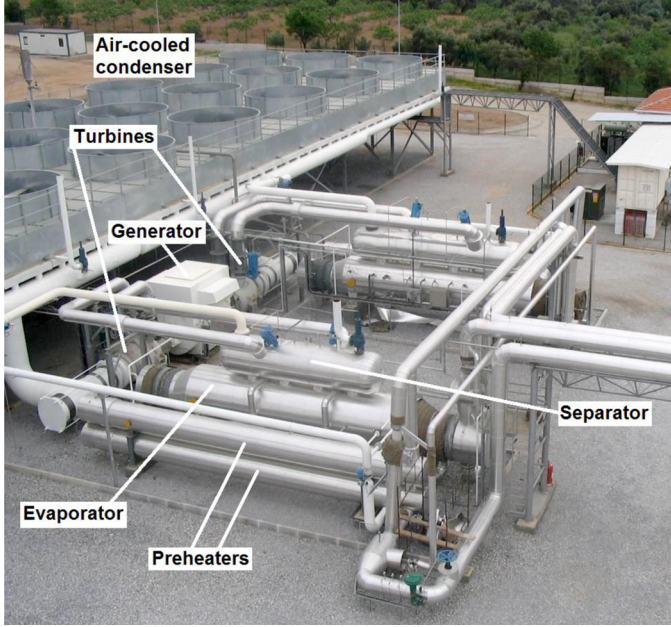


Figure 21.16 Turbines, generator, and heat exchangers at Salavatlı Dora 1 plant; Level 1 is in the foreground, Level 2 is at the rear [18] [WWW].

The mass flows and geofluid conditions into and out of the power plant are shown in Figure 21.17. Additionally, but not shown, there is a vent stream that discharges the NCG and a small amount of steam: NCG flow rate is 2.10 kg/s and steam flow is 0.49 kg/s. Both of these are sent via pipeline to a CO₂ facility operated by Linde Gaz which is adjacent to and just north of the power plant.

Leaving aside the internal details of the ORC, the overall plant performance can be calculated from the external flows and the power generation. Table 21.7 lists the flows, their enthalpies and exergies for the fluids as they enter the ORC.

From these values the thermal and exergetic (utilization) efficiencies can be found.

Thermal efficiency:

$$\eta_{th} = \frac{\dot{W}}{\dot{Q}_{in}} \quad (21.1)$$

$$\dot{Q}_{in} = \dot{Q}_{in,brine} + \dot{Q}_{in,steam} + \dot{Q}_{in,NCG} \quad (21.2)$$

$$\dot{Q}_{in,i} = \dot{m}_i(\Delta h_i) \quad (21.3)$$

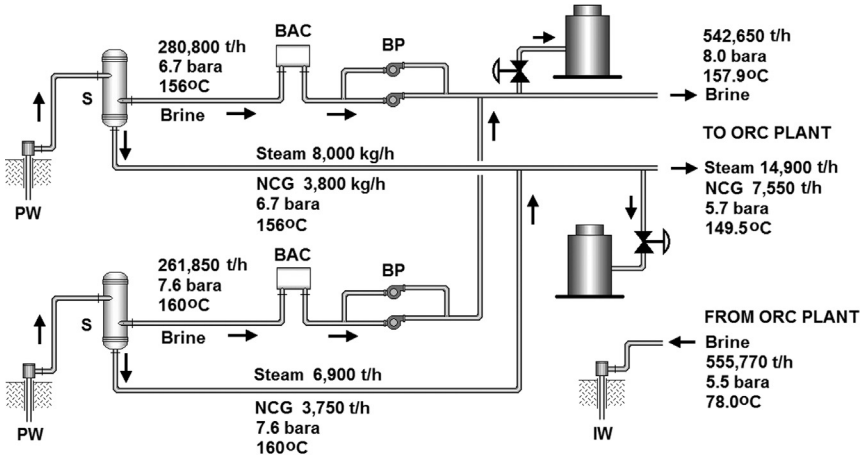


Figure 21.17 Production steam and brine flows at Salavatlı Dora 1 plant, original design; NCG vent not shown.

TABLE 21.7 Properties of flows into and out of ORC.

Item	Mass flow rate kg/s	Enthalpy kJ/kg	Exergy ^a kJ/kg	Exergy rate kW
Brine in	150.7	666.36	110.75	16,693.8
Steam in	4.139	2745.3	761.63	3152.3
NCG in	2.097	618.81	20.30	42.57
Brine out	154.4	327.0	23.96	3699.4
Steam out	0.494	2625.8	491.4	242.7
NCG out	2.097	572.3	8.917	18.70

^aRelative to a dead state at 17.1°C and 1 bar,*a*.

Utilization efficiency:

$$\eta_u = \frac{\dot{W}}{\dot{E}_{in}} \quad (21.4)$$

$$\dot{E}_{in} = \dot{E}_{in,brine} + \dot{E}_{in,steam} + \dot{E}_{in,NCG} \quad (21.5)$$

$$\dot{E}_{in,i} = \dot{m}_i[h_{i,in} - h_{i,0} - T_0(s_{i,in} - s_{i,0})] \quad (21.6)$$

The gross power for Dora 1 is 7350 kW and the net power is 6500 kW. Thus, the thermal efficiency comes to 12.2% (gross) and 10.8% (net); the exergetic efficiency is 37.0% (gross) and 32.7% (net).

Owing to the displacement of fossil-fuel-generated electricity, the Dora 1 plant meets the requirements as a greenhouse gas reduction facility under the Voluntary

Carbon Standard 2007.1 (VCS 2007.1). Over the period of inspection to verify compliance, that is, July 1, 2008, to July 31, 2009, Dora 1 generated 54,560 MWh, net of electricity. Each MWh in Turkey offsets 0.591 tCO_{2,e} and thus the plant constituted a reduction of 32,245 tCO_{2,e} [20]. Including any planned or forced shutdowns over that period, the average net power output was 5.74 MW and its capacity factor was 88.3% based on the design net power.

21.3.2 DORA 2

The second power plant is located about 2 km south of Dora 1. It was dedicated on March 25, 2010. The geofluid conditions are very nearly the same and they share essentially the same design of the power conversion equipment. The geofluid mass flow rate is higher allowing a higher power output, namely, 11.5 MW (gross), 9.5 MW (net). The capital cost was \$45 million [21].

The photograph in Figure 21.18 shows the heat exchangers; notice that there is only one shell for the preheater per level (left side) whereas Dora 1 has two (cf. Figure 21.16). Figure 21.19 shows the turbines and generator at the plant dedication.



Figure 21.18 Heat exchangers at Salavatlı Dora 2 plant; Level 1 is at left, Level 2 is at right [22] [WWW].

The layout of the Dora 2 site is shown in Figure 21.20. The northern wells are producers and the two wells at the south are injectors.



Figure 21.19 Dedication of Salavatlı Dora 2 plant on March 25, 2010; background: Level 1 (L) and Level 2 (R) turbines and generator (C) [22] [WWW].

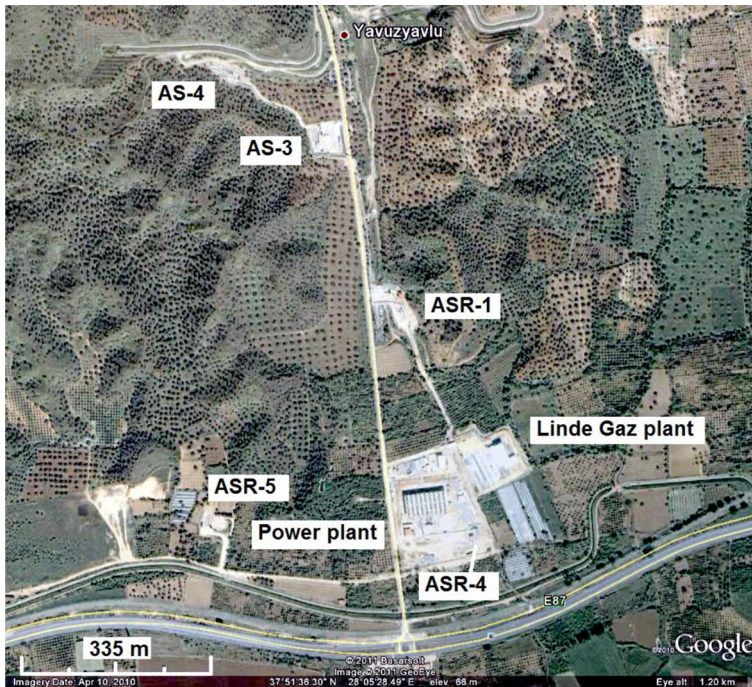


Figure 21.20 Salavatlı Dora 2 plant and wells. Google Earth, April 10, 2010 [WWW].

21.3.3 DORA 3A, 3B, 4, AND 5

The third and fourth power plants in the Salavatlı area are designated Dora 3A and 3B. They are rated at 17 MW each, and came online in 2013 and 2014, respectively. They are located close to the first two plants: Dora 3A is about 700 m southeast of Dora 1, and Dora 3B is about 1.6 km west of Dora 2. Two more plants, Dora 4 and Dora 5, are being planned. Groundbreaking for Dora 4 took place in June 2014 and it is expected to be online in 2015. The well field serving the first four Dora power plants is shown in Figure 21.21.

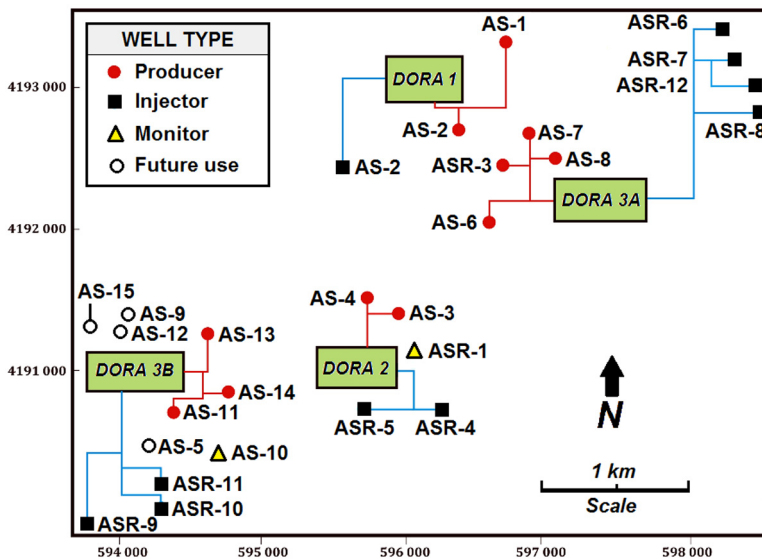


Figure 21.21 Well field for the first four Dora binary plants. After Ref. [23] [WWW].

21.4 Germencik Double-Flash Plant

21.4.1 OVERVIEW

The first double-flash plant in Turkey came online on February 28, 2009, and began feeding electricity into the grid in March. It has a rated capacity of 47.4 MW and uses geofluid from eight wells drilled to depths between 965 and 2432 m. The maximum reservoir temperature so far observed is 232°C. The total produced fluid is about 2500 t/h with a temperature of 228°C at the wellhead. The plant owner is Gürmat, a subsidiary of the Gürış Group, making the plant the

first of its type in Turkey to be privately financed. The new renewable energy law that provides \$0.105/kWh has motivated this and other geothermal projects that may have been previously marginal financially [24,25].

21.4.2 GEOLOGIC SETTING

Germencik is the last of the important, high-temperature geothermal resources along the Büyük Menderes Graben, moving from east to west. The field lies just south of the northern fault boundary of the graben and is host to hot springs and fumaroles. The boundary fault appears to be fractionated into several parallel faults at depth, creating what has been called a “horse-tail fault zone”; see Figure 21.22 [26].

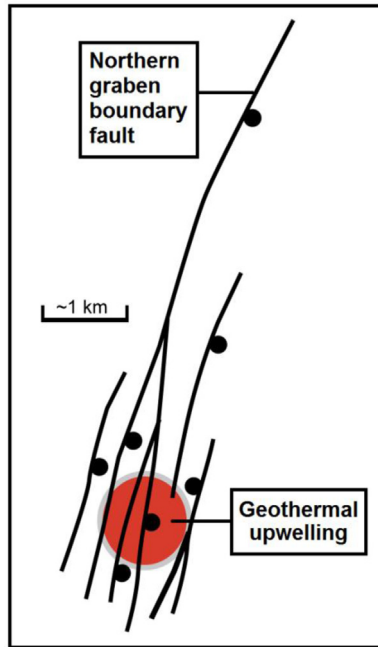


Figure 21.22 Possible “horse-tail” faulting effect at Germencik. After Ref. [26] [WWW].

Also, the Germencik area is subject to much earthquake activity with numerous quakes in the 3–5 magnitude range and a few in the range 5–6 [27]. This activity keeps the fault zones alive and ever-changing and promotes permeability in the reservoir. It is noteworthy that the highest levels of earthquake activity are focused at the west and east ends of the graben where Germencik and Kızıldere, the most productive Turkish fields, happen to be located.

21.4.3 GERMENCİK DOUBLE-FLASH POWER PLANT

The design of the power plant was settled upon after a study of a wide range of possible types of energy conversion systems and specific equipment. Capital and operating costs as well as practicality played crucial roles in the process. The plant engineering was performed by Power Engineers (Boise, Idaho); steam and brine piping design was done by Veizades & Associates (San Francisco); reservoir engineering was performed by Geologica (Berkeley, California); and the construction was done by the Turkish company Gürış Group that owns the plant owner Gürmat. In selecting equipment for the plant, priority was given to materials and equipment that could be sourced locally as an in-country benefit of the project [28].

Among the designs considered were single-flash (rejected due to less efficient utilization of the resource), simple binary (rejected for the same reason, owing to the high temperature of the geofluid); and hybrid flash-binary (rejected due to complexity with only a small improvement in efficiency). Double-flash plants have been installed successfully at resources of similar temperature, e.g., Ahuachapán, El Salvador, exhibit good efficiency, and are relatively straightforward to operate—all advantages in a situation where the plant will be locally owned and operated.

The main challenges to be overcome were the high potential for wellbore scaling from calcium carbonate and the high percentage of NCG in the geofluid, both common problems for all Turkish geothermal power plants. After a study of various calcite inhibitors, one was selected for injection downhole below the flash point. The antiscalant used is called Geosperse (PowerChem Technology, Minden, Nevada). The NCG are handled by a hybrid extraction system with first stage steam-jet ejectors followed by liquid-ring vacuum pumps. The steam-jet ejectors are comprised of three ejectors in parallel, having capacities of 25%, 40%, and 60%, to allow flexibility in dealing with variations in NCG over time. Turbo-compressors were considered but were not cost-effective either in capital or operating costs for this set of geofluid conditions.

A simplified process flow diagram is given in Figure 21.23. There are seven production wells located generally to the north and southeast of the plant, seven hot injection wells located to the west, southwest, and south of the plant, and one cold injection well for the cooling tower overflow to the east of the plant [Pers. Comm. R. Kaderli, Gürış, June 23, 2011]; see Figure 21.24. Table 21.8 gives some data for the first nine wells. For the Germencik geofluid conditions, a wellhead mass flow of 100 kg/s corresponds roughly to 7 MW of power. The plant incorporates two high-pressure (HP) vertical cyclone separators, two low-pressure (LP) flash vessels, a demister for each steam flow (not shown in Figure 21.23), a dual-pressure, pass-in steam turbine with vertical exhaust to a compact ADCC that is located outside the turbine building, vertical hot-well pumps, a hybrid NCG extraction system, and a seven-cell, counterflow, low-clog film-fill water cooling tower.

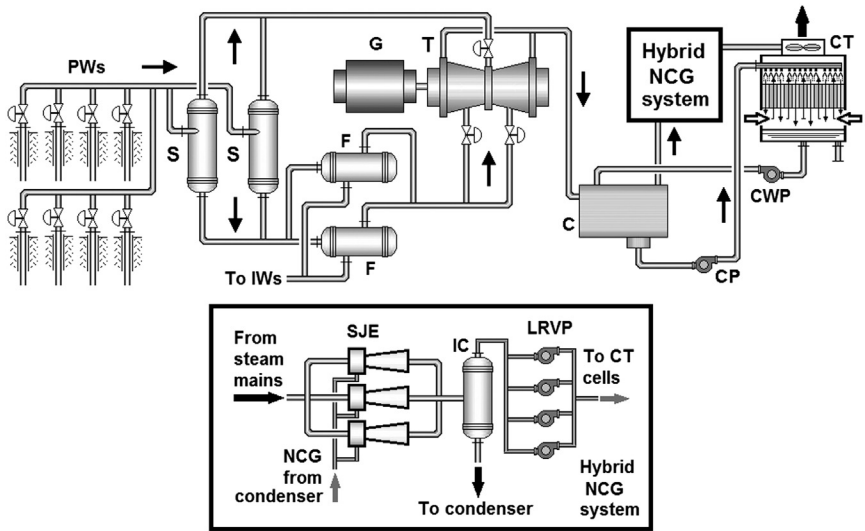


Figure 21.23 Simplified process flow diagram for 47.4 MW Germencik double-flash plant. *Note:* There is a back-up SJE in parallel with the LRVP to allow maintenance without interruption of operations.

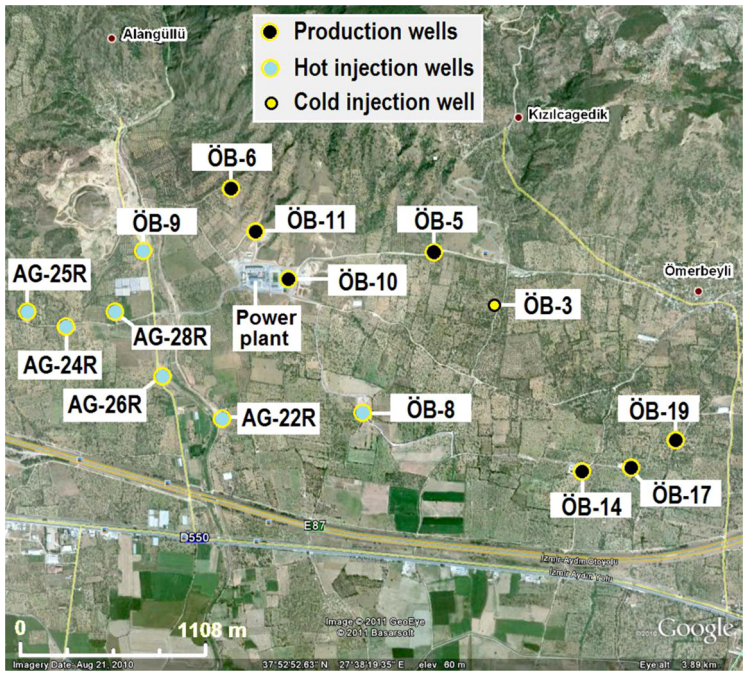


Figure 21.24 Aerial view of the Germencik field showing wells and power plant locations. Google Earth, August 21, 2010 [WWW].

TABLE 21.8 Properties of the first nine deep wells drilled at Germencik [29].

Well no.	Date	Depth, m	Temperature, °C	Mass flow rate, kg/s
OB-1	1982	1000	203	NA ^a
OB-2	1982	975.5	231	25
OB-3	1983	1196.7	230	65
OB-4	1984	285	213	180–100
OB-5	1984	1302	221	65
OB-6	1984	1100	221	140
OB-7	1985	2398	203	65
OB-8	1986	200	219.87	120
OB-9	1986	1464.7	223.8	145
Average			218.4	

^aGeysering flow.

A close-up aerial view of the power house and its associated equipment is given in Figure 21.25 and a site photograph is presented in Figure 21.26. The powerhouse is the large blue building, the geofluid processing equipment is to the right of the powerhouse adjacent to the holding pond. The NCG extraction system and the external condenser lie to the north of the powerhouse between it and the



Figure 21.25 Aerial view of Germencik plant layout. The pipeline at the bottom foreground is the brine reinjection line carrying the fluid to the left. Google Earth, August 21, 2010 [WWW].



Figure 21.26 Germencik double-flash power plant. Google Earth Image 21329604, by E. Atilir [WWW].

cooling tower. In [Figure 21.26](#), the insulated pipelines in the background carry the waste brine to the reinjection wells.

Early trial deployments of the innovative ADCC were done as retrofits at The Geysers in California, but this was the first use in a new power plant as large as Germencik. The technology was developed at the US National Renewable Energy Laboratory (NREL) and commercialized by Ecolaire (Bethlehem, Pennsylvania), specifically for renewable energy applications such as ocean thermal and geothermal power plants; see [Figure 21.27](#).

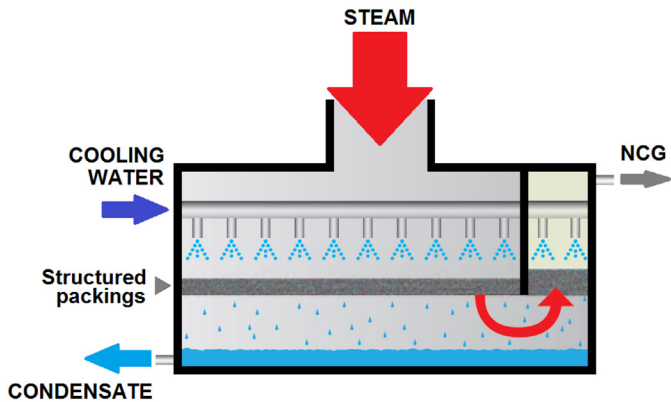


Figure 21.27 Advanced direct-contact condenser (ADCC) [WWW].

The internal surfaces are made of stainless steel to resist corrosion. There is a large area of packing (fill) that enhances heat and mass transfer by means of a very large surface area of contact between the steam and cooling water. In this way the unit mimics the behavior of a wetfilm fill cooling tower. It also results in less subcooling of the condensate and lower NCG exit temperatures leaving the gas cooler section (upper right corner in Figure 21.27). The benefits of using this innovative condenser design include [28]:

- Lower cooling water flow, lower cooling water system capital cost and parasitic loads;
- Lower NCG cooler outlet temperature and vapor flow rate, lower NCG system capital costs, and lower ejector steam and vacuum pump electrical consumption.

An estimate of the performance of the plant can be made from the reported mass flow rate of geofluid, $2500 \text{ t/h} = 694.4 \text{ kg/s}$ [24], and the assumed reservoir temperature (at saturated liquid) of 218°C , obtained as the average temperature of the first nine deep wells drilled at Germencik (see Table 21.8). The specific exergy of the geofluid in the reservoir is 205.4 kJ/kg ; the rate of exergy produced is 142.6 MW . Thus the utilization efficiency is 33.2% (gross) and 31.6% (net).

The performance record from startup through May 2011 shows that the plant has operated highly successfully [Pers. Comm., R. Kadirli, Güriş, June 20, 2011]. The data are summarized in Table 21.9. Since June 2009 through May 2011, the plant has been in operation a total of $17,345.2 \text{ h}$ out of a possible total of $17,520 \text{ h}$, for a remarkable availability of 99.0% . The parasitic power consumption is 16.9% of the gross power, essentially the same as for the Kızıldere plant.

TABLE 21.9 Performance of the 47.4 MW Germencik double-flash plant

	2009 ^a	2010	2011 ^b
Avg. monthly maximum load, MW	48.97	48.31	48.52
Avg. monthly gross generation, MWh	33,382	33,481	33,115
Total gross generation, MWh	233,675	401,770	165,574
Avg. monthly net generation, MWh	27,530	27,963	27,620
Total net generation, MWh	192,707	335,559	138,099
Avg. monthly hours of operation	722.6	722.9	722.4
Avg. monthly capacity factor, %	95.98	96.54	96.41
Avg. monthly load factor, %	93.42	93.78	93.26
Avg. monthly availability factor, %	98.44	99.01	99.68

^aSeven months from June.

^bFive months through May.

Table 21.10 lists the cumulative production and reinjection since February 2009. About 76% of the produced geofluid is being reinjected back into the formation.

TABLE 21.10 Cumulative geofluid production and reinjection in 10^6 kg.

From February 2009 through	Production	Reinjection	Net extraction
December 2010	36,800	28,212	8588
January 2011	38,933	29,483	9450
February 2011	40,565	30,766	9799
March 2011	42,377	32,196	10,181
April 2011	44,124	33,568	10,557
May 2011	45,931	34,947	10,984

A more refined calculation can be made of the plant utilization efficiency from one month for which data are available, May 2011: the plant operated full time for 744 h, received 1807×10^6 kg of geofluid from the reservoir (674.7 kg/s), and generated an average of 44.38 MW (gross) and 36.91 MW (net). Assuming a reservoir at 218°C , the specific exergy of the geofluid is 205.4 kJ/kg or a rate of 138.6 MW. Thus the plant has a utilization efficiency of 32.0% (gross) and 26.6% (net).

21.5 Pamukören Binary Plant

One of the newer plants in Turkey is the Pamukören plant in Aydın province, about 28 km west of Kızıldere and just 2 km north of the main highway, E87. In fact, nearly all of the geothermal power plants in Anatolia lie very closely on a straight, 128 km-long, east-west line from Denizli-Gerali on the east to Aydın-Gümüşköy on the west. Alasehir (under construction) and Tuzla-Çanakkale are the exceptions, lying well north of this axis; see Figure 21.1.

The plant is owned by Celikler Jeotermal and was built by a consortium of three companies headed by Atlas Copco Gas and Process. The design follows the emerging standard for geothermal binary plants, that is, two turbines jointly driving a common generator through an integral gear box. In this case the turbines are radial inflow machines; see Figure 21.28. The working fluid is commercial-grade n-butane. Each unit has an electrical output of 22.5 MW and uses air-cooled condensers. The plant uses wellhead separators and individual steam and brine pipelines to convey the geofluid to the plant. Steam, together with the NCG, provides heating for one of the evaporators, while the brine is used in the other evaporator and in the preheating of the n-butane. A recuperator

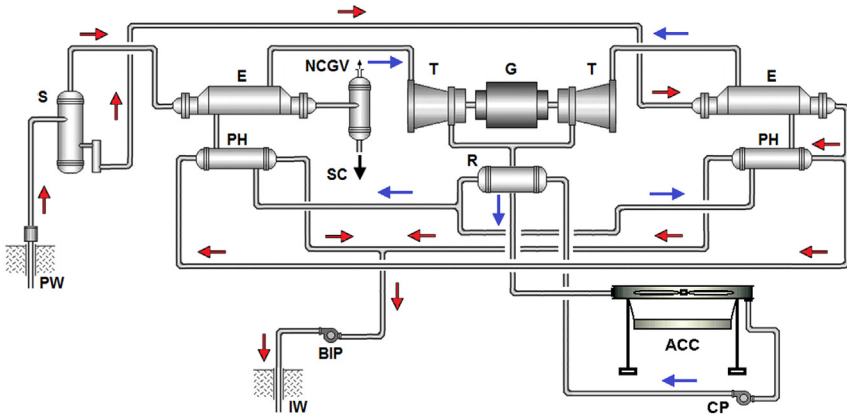


Figure 21.28 Simplified flow diagram for one 25 MW unit of the Pamukören power plant. After Ref. [25] [WWW].

makes use of the superheat in the turbine exhaust to help preheat the n-butane. The NCG are vented and the steam condensate may be reinjected or used for other purposes.

The two n-butane turbines and the generator have the following design conditions [25]:

- Inlet pressure: 25.0 bar,a
- Inlet temperature: 125°C
- Outlet pressure: 2.90 bar,a
- Outlet temperature: 54.7°C
- n-butane mass flow rate: 165 kg/s
- Turbine power output: 12.12 MW, each
- Generator output: 22.5 MW.

The geofluid design conditions are:

- Geofluid inlet temperature: 161°C
- Brine inlet mass flow rate: 388.9 kg/s
- Steam inlet mass flow rate: 15.28 kg/s
- NCG inlet mass flow rate: 6.111 kg/s
- Reinjection temperature: 80°C.

Based on these design values, the plant would have a gross utilization efficiency of 46.5% and a net utilization efficiency of 43.2%, using 25°C as the dead-state temperature. The thermal efficiency of the plant would be 17.8% (gross) and 16.5% (net). These are all impressive figures and are due in some measure to the use of the recuperator.

21.6 Environmental Impact

The only plant that has been in operation long enough to assess the environmental impact is the Kızıldere Unit 1. The two units at Salavatlı are closed-loop binary plants that practice full reinjection which renders their impact on the environment negligible. As a flash plant, Germencik does have some impact on the environment owing to releases of steam and NCG to the atmosphere, but it is too early to assess its full impact. Furthermore, if a carbon dioxide capture plant is built, as has been done at the other three power plants, the impact will be minimal.

The impact of the Kızıldere plant centers on the disposal of the waste brine. Since in its early days, the plant did not reinject any brine, all of it was sent to the Menderes River via drainage channels. As of 2005, roughly 278 kg/s was being discharged with no treatment [4]. The brine temperature is about 140°C and the main problem constituent is boron with a concentration of 25 ppm. Since this amount of boron is excessive relative to its use in agricultural irrigation, three possible solutions have been considered: (1) reinjection, (2) removal of boron, and (3) disposal of brine into the Aegean Sea.

The latter, although theoretically feasible, was ruled out on the basis of cost, practicality and effectiveness. The second option is promising but as yet unproven on the scale needed for Kızıldere. Thus the only realistic solution is reinjection.

Given the three-layer nature of the Kızıldere reservoir, it has been suggested that one way to carry out this program would be to produce from the deepest, high-temperature but low-permeability reservoir and reinject into the middle-depth formation that has a moderate temperature but high permeability [9]. There are clear advantages to a properly planned and executed reinjection program but its success hinges on a reliable reservoir model.

One potential major environmental impact is avoided by the CO₂ capture facility adjacent to the Kızıldere plant. About 120,000 t/year (33,333 kg/s) of CO₂ is recovered from the plant, purified, and sold as liquefied CO₂. In fact this one plant supplies over 90% of the demand of the carbonated beverage industry in Turkey.

The last of the impacts to be discussed is the impact on naturally occurring hot springs. The nearby Kızıldere spa lost its natural source of hot water as a result of the lowering of the water table by the producing wells. However, the plant sends cooled waste brine to the spa to make-up for this loss. After some 27 years of operation, no impact from Kızıldere has been observed at the famous Pamukkale hot springs and terraces that lie about 25 km to the east.

21.7 Current State and Future Prospects of Geothermal Power

Turkey operates 18 geothermal power units at nine different locations; see Table 21.11. Note: The literature is confusing and inconsistent in the naming of plants; plants are identified by the field, locale, developer and/or owner, etc.

TABLE 21.11 Installed geothermal plants in Turkey as of December 2014 [19,30,31]

Plant name	Year of start-up	Type	No. of units	Installed capacity, MW(g)/MW(n)
Kızıldere Unit 1	1984	Single-flash	1	20.4/17.4
Salavatlı: Dora 1	2006	Binary	1	7.95/6.5
Bereket: Sarayköy ^a	2007	Binary	(1)	(6.35/5.5)
Germencik Unit 1	2009	Double-flash	1	47.4/45
Tuzla-Çanakkale	2009	Binary	1	7.5/6
Salavatlı: Dora 2	2010	Binary	1	11.5/9.5
Denizli: Jeoden	2011	Binary	3	0.78/0.75
IREM: Aydın-Hıdırbeyli	2011	Binary	1	20/17
Kızıldere Unit 2	2013	Triple-flash/binary	3	80/72
Aydın-Pamukören I	2013	Binary	1	25/22.5
Salavatlı: Dora 3A	2013	Binary	1	18.5/17
Salavatlı: Dora 3B	2014	Binary	1	20/17
Aydın-Pamukören II	2014	Binary	1	25/22.5
Aydın-Gümüşköy I	2014	Binary	1	6.6/5.1
Aydın-Gümüşköy II	2015	Binary	1	6.6/5.1
Totals			18	296.73/263.35

^aNot operating since 2008.

The Bereket binary unit was designed to receive the 145°C waste brine from the Kızıldere power plant some 2 km to the west. Besides generating electricity the plant was also supposed to provide district heating to the town of Sarayköy, about 8 km away from the plant, but several problems arose that rendered the plant of no use [19]. The make-up water for the wet cooling tower was not available for most of the time, being sourced from an irrigation canal. The water quality was also deficient and led to scaling problems. Eventually an air-cooled condenser was installed. There was a temperature mismatch between the brine leaving the binary unit and the requirements of the district heating system that led to a failure to meet the heating needs in the winter of 2008. Finally, once the Kızıldere was privatized, the new owners decided that the waste brine would be better reinjected and the source of fluid for the Bereket plant was no longer available [Pers. comm., U. Serpen, June 6, 2011].

Three small PureCycle binary units were delivered to Jeoden Geothermal, a private company, in 2011 and are installed close to the towns of Sarayköy and Gerali, north of Denizli, to operate on geofluids at temperature of 120°C.

The Tuzla-Çanakkale binary plant is located in northwest Turkey about 50 km south of the western entrance to the Dardanelles strait. The flow rates and temperatures (max. 174°C) observed in the first two deep wells were very encouraging, but later wells drilled to support the 7.5 MW plant have been disappointing.

The 13.2 MW Aydın-Gümüşköy plant consists of two air-cooled units of 6.6 MW(g), 5.1 MW(n). The reservoir fluid is at 182°C and each unit requires 120 kg/s of brine flow. This plant lies at the west end of the line of geothermal plants that lie along the Büyük Menderes Graben. The owner, BM Holdings, is planning to add a solar collector field to augment the geothermal power. This will be of particular use on hot days when the geoplant is limited by its air-cooled condensers [32].

In light of the favorable support for geothermally generated electricity under the new Turkish law for renewable energy, many new projects have come online in the last several years and many are now in the planning stage; see [Tables 21.11 and 21.12](#). However, the new 2007 Geothermal Code is not without its drawbacks [19]. First, all geothermal activities were frozen for one year at the

TABLE 21.12 Planned geothermal plants in Turkey as of December 2014, various sources

Plant location	Capacity, MW	Geofluid estimated temperature, °C
Manisa-Alaşehir	40 (30 ^a + 10 ^b)	200
Germencik Unit 2	47	218
Salavatlı: Dora 4	17	171
Salavatlı: Dora 5	17	171
Aydın-Hıdırbeyli (SINEM)	24	146
Aydın-Hıdırbeyli (DENİZ)	24	146
Manisa	15	200
Manisa-Sarıköz	10	200
Manisa-Alaşehir: Turkerler	24	200
Manisa-Alaşehir: Zorlu	30	200
Manisa-Merkez	24	200
Aydın-Nazilli	20	127
Aydın-Germencik	163	239
Salavatlı-Sultanhisar	34	171
Salihli-Caferbeyli-1	15	168
Salihli-Manisa: Caferbeyli-2	15	168
Total	519	

^aFlash plant.

^bBinary plant.

beginning. Second, there is still a formidable bureaucratic structure to navigate before a project can be approved. And last, it was decided to divide the geothermal land leases into smallish parcels that could lead to overexploitation of resources by neighboring developers. This last difficulty was instrumental in the rapid decline of The Geysers in California when competing developers tried to extract as much fluid as they could without regard to the overall benefit of the resource. Nevertheless, there are currently in planning enough megawatts to increase the installed geothermal capacity by 270%.

References

- [1] [Faulds JE, Bouchot V, Moeck I, Oğuz K. Structural controls on geothermal systems in Western Turkey: a preliminary report. *Geothermal Resour Counc Trans* 2009;33:375–81.](#)
- [2] [Şimşek Ş. Present status and future development possibilities of Aydın-Denizli geothermal province. International geothermal conference, Reykjavik, session 5, paper 034; September 2003.](#)
- [3] [Şimşek S. Geothermal model of Denizli-Buldan area. *Geothermics* 1985;14\(2–3\):155–69.](#)
- [4] [Şimşek Ş, Yıldırım N, Gülgör A. Developmental and environmental effects of the Kızıldere geothermal power project, Turkey. *Geothermics* 2005;34:234–51.](#)
- [5] [Kaya T, Kindap A. Kızıldere—new geothermal power plant in Turkey. In: Popovski K, Vranovska A, Vasilevska SP \(Eds.\), Proc. international conference on national development of geothermal energy use and international course/EGEC business seminar on organization of successful development of a geothermal project, Slovakia; 2009.](#)
- [6] [Koyun A. Energy efficiency and renewable energy: Turkey—national study. Mediterranean and national strategies for sustainable development, priority field of action 2: energy and climate change, plan bleu, Regional Activity Centre, Sophia Antipolis; March 2007.](#)
- [7] [DiPippo R. Progress in geothermal power development in the Azores, the People's Republic of China, Costa Rica, El Salvador, Indonesia, Kenya, Turkey, and the U.S.S.R. Proc. fifth annual geothermal conference and workshop, EPRI rep. no. AP-2098; November 1981, p. 7-66–7-71.](#)
- [8] [Serpen U, Aksoy N. Reassessment of reinjection in Salavatli-Sultanhisar field of Turkey. Proc. world geothermal congress 2010, paper 2302, Bali, Indonesia; April 25–29, 2010.](#)
- [9] [Serpen U, Satman A. Reassessment of the Kızıldere geothermal reservoir. Proc. world geothermal congress 2000, Kyushu-Tohoku, Japan, May 28–June 10; 2000, p. 2869–74.](#)
- [10] [Gökğöz A. Geochemistry of the Kızıldere-Tekkehamam-Buldan-Pamukkale geothermal fields, Turkey. U.N. university, geothermal training programme, Reykjavik, Iceland, Rep. No. 5; 1998.](#)
- [11] [Mertoğlu O, Şimşek Ş, Dagistan H, Bakir N, Dogdu N. Geothermal country update report for Turkey \(2005–2010\). Proc. world geothermal congress 2010, paper 0119, Bali, Indonesia; April 25–29, 2010.](#)
- [12] [Gökçen G, Coury GE. Upstream reboiler design and testing for removal of noncondensable gases from geothermal steam at Kızıldere geothermal power plant, Turkey. Proc. world geothermal congress 2000, Kyushu-Tohoku, Japan, May 28–June 10; 2000, p. 3173–8.](#)
- [13] [Gökçen G, Özcan NY. Performance analysis of single-flash geothermal power plants: gas removal systems point of view. Proc. world geothermal congress 2010, paper 2613, Bali, Indonesia; April 25–29, 2010.](#)

- [14] Tayman E. Zorlu discovers new geothermal field. *Hürriyet Daily News & Economic Review*, <<http://www.hurriyetdailynews.com/n.php?n=zorlu-finds-new-geothermal-field-2009-10-05>>; October 5, 2009.
- [15] Kindap A, Kaya T, Hakhdır FST, Bükülmez AA. Privatization of Kizildere geothermal power plant and new approaches for field and plant. *Proc. world geothermal congress 2010*, paper 0708, Bali, Indonesia; April 25–29, 2010.
- [16] Lewis W, Wallace K, et al. Kızıldere II multiple-flash combined cycle: a novel approach for a Turkish resource. *Proc. world geothermal congress 2015*, Melbourne, Australia; April 19–25, 2015.
- [17] Tamaya Y, Muto T. Unique steam turbine for Kizildere geothermal power plant in Turkey. *Proc. world geothermal congress 2015*, Melbourne, Australia; April 19–25, 2015.
- [18] Shoshan G, Serpen U. Turkey—the first private geothermal power plant. *Geothermal Resour Couns Trans* 2009;33:69–72.
- [19] Serpen U, Aksoy N, Öngür T, Korkmaz ED. Geothermal energy in Turkey: 2008 update. *Geothermics* 2009;38:227–37.
- [20] Verification report of the Dora 1 geothermal power plant project in Turkey, voluntary carbon standard 2007.1. Report No. V001, rev. 03, Germanischer Lloyd Certification GmbH, Hamburg, Germany; September 30, 2009.
- [21] European Bank for Reconstruction and Development (EBRD), Renewable Development Initiative, <<http://ws2-23.mylloadspring.com/sites/renew/geothermal.aspx>>; 2011 [accessed 09.06.11].
- [22] Richter LX. Dora-2 geothermal plant goes online in Turkey. *Think Geoenergy*, <<http://thinkgeoenergy.com/archives/4245>>; Original source (in Turkish), <<http://www.mucadele.com.tr/haber/aydin/dora-2-jeotermal-enerji-santrali-elektrik-uretimine-basladi/19592>>; March 27, 2010.
- [23] Serpen U, Aksoy N, Öngür T. 2015 Reinjection update of Salavatlı geothermal field in Turkey. *Proc. world geothermal congress 2015*, Melbourne, Australia; April 19–25, 2015.
- [24] Richter LX. Geothermal plant goes online in Turkey. *ThinkGeoEnergy*, <<http://thinkgeoenergy.com/archives/1069>>. Original source (in German), <http://www.tiefengeothermie.de/index.php?id=49&tx_ttnews%5bpointer%5d=1&tx_ttnews%5btt_news%5d=200&tx_ttnews%5bbackPid%5d=48&cHash=073bf4e0e0>; March 3, 2009.
- [25] Agahi R, Valdimarsson P. Field performance evaluation of the largest geothermal organic Rankine cycle plant. *Proc. world geothermal congress 2015*, Melbourne, Australia; April 19–25, 2015.
- [26] Faulds J, Coolbaugh M, Bouchot V, Moeck I, Oğuz K. Characterizing structural controls of geothermal reservoirs in the Great Basin, USA, and Western Turkey: developing successful exploration strategies in extended terranes. *Proc. world geothermal congress 2010*, paper 1163, Bali, Indonesia; April 25–29, 2010.
- [27] Kumsar H, Aydan Ö, Tano H, Ulusay R, Celik SB, Kaya M, et al. An on-line monitoring system of multi-parameter changes of geothermal systems related to earthquake activity in Western Anatolia in Turkey. *Proc. world geothermal congress 2010*, paper 1389, Bali, Indonesia; April 25–29, 2010.
- [28] Wallace K, Dunford T, Ralph M, Harvey W. Aegean steam: the Germencik dual flash plant. *GeoFund-IGA geothermal workshop “Turkey 2009,” Geothermal energy in ECA region countries*, Istanbul, <http://pangea.stanford.edu/ERE/pdf/IGAstandard/GeoFund/Turkey2009/6._wallace.pdf>; February 16–19, 2009.
- [29] Filiz S, Tarcan G, Gemici U. Geochemistry of the Germencik geothermal fields, Turkey. *Proc. world geothermal congress 2000*, Kyushu-Tohoku, Japan, May 28–June 10, 2000, p. 1115–20.
- [30] Özcan NY. Modeling, simulation and optimization of flashed-steam geothermal power plants from the point of view of noncondensable gas removal systems. PhD Thesis in Mechanical Engineering, The Graduate School of Engineering and Sciences, Izmir Institute of Technology, Izmir, Turkey; June 2010.

- [31] Mertoğlu O, Şimşek S, Başarı N. Geothermal country update report of Turkey (2010–2015). Proc. world geothermal congress 2015, Melbourne, Australia, April 19–25, 2015.
- [32] Kuyumcu ÖÇ, Solaroğlu UZD, et al. Hybrid geothermal and solar thermal power plant case study: Gümüşköy GEPP. Geothermal Resour Counc Trans 2012;36.

Nomenclature for Figures in Chapter 21

AC	Aftercondenser
ACC	Air-cooled condenser
BAC	Brine accumulator
BC	Binary condenser
BIP	Brine injection pump
BP	Brine pump
BT	Binary turbine
C	Condenser
CP	Condensate pump
CS	Cyclone separator
CT	Cooling tower
CV	Control valve
CWP	Cooling water pump
D	Drain
E	Evaporator
F	Flash vessel
G	Generator
HPC, LPC	High- and low-pressure compressor
HPT, IPT, LPT	High-, intermediate-, and low-pressure turbine
HPS, IPS, LPS	High-, intermediate-, and low-pressure separator
HWP	Hot water pump
IC	Intercondenser
IP	Injection pump
IW	Injection well
LRVP	Liquid-ring vacuum pump
MR	Moisture remover
NCG	Noncondensable gases
NCGE	NCG ejector
NCGV	NCG vent
PH	Preheater
PW	Production well
R	Recuperator
S	Separator
SC	Steam condenser
SJE	Steam-jet ejector
T	Turbine
V	Vent



Chapter 22

Enhanced Geothermal Systems—Projects and Plants

Chapter Outline

22.1 Definitions	610
22.1.1 Hot Dry Rock	610
22.1.2 Enhanced Geothermal Systems	610
22.1.3 Deep Hydrothermal Systems	610
22.2 Early Projects	612
22.2.1 Fenton Hill HDR Project	612
22.2.2 Rosemanowes, England	614
22.3 Later Projects	617
22.3.1 Hijiori, Japan	617
22.3.2 Ogachi, Japan	624
22.3.3 Basel, Switzerland	627
22.4 EGS Power Plants	632
22.4.1 Soultz-Sous-Forêts, France	632
22.4.2 Neustadt-Glewe, Germany	638
22.4.3 Landau, Germany	640
22.4.4 Unterhaching, Germany	642
22.4.5 Bruchsal, Germany	644
22.4.6 Other Geothermal Plants in Germany	644
22.4.7 Habanero, Innamincka, Australia	645
22.5 Proposed Projects	651
22.5.1 Germany	651
22.5.2 United States	652
References	653

Any time you try to do something innovative, you should expect that there's always going to be people who doubt it, who suggest that perhaps you'd be better off doing something else.

Irwin Jacobs, Qualcomm founder—2011.

22.1 Definitions

In Section 1.5.1 we introduced the concept of hot dry rock (HDR) as a potential system for exploiting certain types of geothermal resources. The basic premise is to create a commercial grade geothermal system that mimics a natural hydrothermal reservoir. Originally geothermal regions having high temperature but lacking sufficient permeability or fluid in the formation were seen as candidates for this approach. However, as drilling technology has advanced and as the urgency for finding alternative sources of energy has intensified, other potential sites have become targets for this type of development. New language has come into use and definitions are appropriate.

22.1.1 HOT DRY ROCK

Formations consisting primarily of granites that have high temperature but very low permeability and lack of stored fluid are the candidates for HDR development. The first site for this work was the Valles Caldera in New Mexico at the Fenton Hill project. In some cases where the permeability was somewhat higher, the term hot fractured rock has been used. Fracture creation and stimulation by means of hydraulic fracturing (“hydrofracking”) or hydraulic shearing (“hydro-shearing”) techniques are essential to produce a commercial grade resource.

22.1.2 ENHANCED GEOTHERMAL SYSTEMS

Originally called engineered geothermal systems, enhanced geothermal systems (EGS) are formations that may possess some desirable characteristics of commercial hydrothermal reservoirs but are lacking in others. This is similar to HDR in that a heat source is inferred but fluid in-place or adequate permeability is lacking. Portions of known hydrothermal reservoirs that lie on the periphery of the developed area are good candidates for EGS. Other locations believed to lack sufficient permeability but which might yield attractive temperatures at deeper depths are also seen as appropriate for EGS development. As with HDR, hydrofracking or hydroshearing is needed to create a productive reservoir.

22.1.3 DEEP HYDROTHERMAL SYSTEMS

This new category of geothermal resource came into existence upon the discovery at several recent EGS projects where permeable and fluid-saturated formations were encountered at depths of 2500–5000 m. In deep hydrothermal systems (DHS), the fluids were under sufficient pressure to allow them to flow to the

surface without the need for pumps. Since these regions are not associated with elevated geothermal temperature gradients, the fluid temperature was low to moderate, say 120–140°C, but high enough to be used in a suitable binary power plant. Downwell pumps could be deployed in some cases to enhance flow rates and guarantee that the geofluids remain in the liquid state. Also while some stimulation of the formation may be performed to enhance permeability, it is typically nothing more than is routinely done at normal hydrothermal systems. DHS should be distinguished from very deep wells drilled at existing hydrothermal plants that aim to reach parent fluids that feed the shallower layers of the formation. For example, at Larderello in Italy, wells are now being drilled to 4000 m and beyond to reach steam both beneath the existing reservoir and in areas surrounding the known steam fields.

A useful way to view the EGS/HDR/DHS spectrum is by examining the relationship between the geothermal temperature gradient and the natural formation permeability; see Figure 22.1 [1]. Bear in mind that the average geothermal gradient is about 33°C/km. Thus even at that gradient, if the formation is highly permeable (upper right corner), one has the potential for a low-grade hydrothermal system, but this will require very deep wells to achieve temperatures suitable for power generation. This would be a DHS. In the diagonally opposite corner, one finds very little permeability (lack of natural fractures) but a very high-temperature gradient. Thus it might be possible with relatively shallow wells to achieve commercial grade production by means of hydrofracking. This is the classic EGS system.

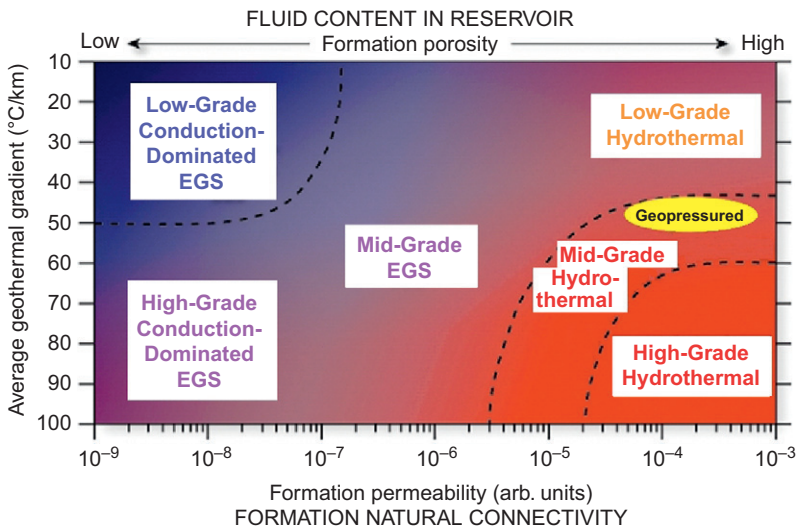


Figure 22.1 The EGS spectrum: temperature gradient versus formation permeability. After Ref. [1] [WWW].

22.2 Early Projects

We will describe two programs that began in the 1970s and 1980s which aimed to develop the HDR concept to the commercial stage: the Fenton Hill and the Rosemanowes projects.

22.2.1 FENTON HILL HDR PROJECT

The US Department of Energy sponsored a major HDR effort at the Fenton Hill site within the Valles Caldera in New Mexico from 1973 to 1996 [2]. In the first phase of the project, from 1973 to 1979, two wells were successfully drilled to a depth of about 2600 m (8500 ft) in hot, fractured crystalline basement rock [3]. The wells communicated through a fracture field in the 185°C (365°F) artificially created reservoir and were capable of producing pressurized liquid at 135–140°C (275–285°F) at flow rates ranging from 7 to 16 kg/s (55,500–127,000 lbm/h). A 60 kW binary plant was installed as a means of generating power from the hot water as it circulated through the loop.

During the second phase, starting in 1979, two new wells were drilled about 50 m apart on the surface with the intention of achieving the reservoir conditions as shown in Figure 22.2a. The deeper one extended to 4390 m (14,400 ft) into 327°C (620°F) rock. Unfortunately the two new wells did not communicate; the fracture patterns did not conform to the expected ones based on the results of the first phase. After several periods of massive hydraulic fracturing and redrilling, the final configuration shown in Figure 22.2b was achieved.

A simplified schematic of the flow test facility is shown in Figure 22.3 and some of the results of flow tests are summarized in Table 22.1. The reader is referred to Refs. [2–4] for more details.

All of the thermal power developed by the circulating water during the Phase II experiments was dissipated by an air-cooled heat exchanger; no attempt was made to generate any power as had been accomplished in Phase I. The apparent water “loss” needs some explanation. The term “loss” may be a misnomer because the fractures widen under increasing pressure, retract with decreasing pressure, and the rock may contract while being cooled by the circulating water. Thus some injected water could be viewed as stored within the reservoir or outlying fractures. In fact, some tests showed a higher production rate than injection rate depending on the history of injection pressures. In any case, under steady operating conditions, a fairly large percentage of makeup water would be required to keep a power plant running steadily.

Although the Fenton Hill experiments have ended and the facility dismantled, the basic idea of HDR is being applied to some hydrothermal systems that have

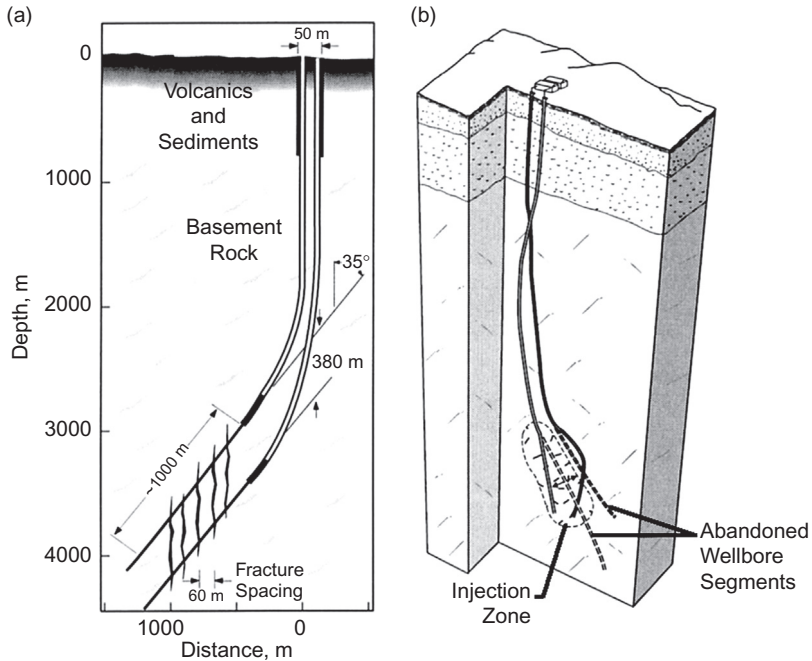


Figure 22.2 Fenton Hill HDR well configuration: (a) conceptual design and (b) actual [2].

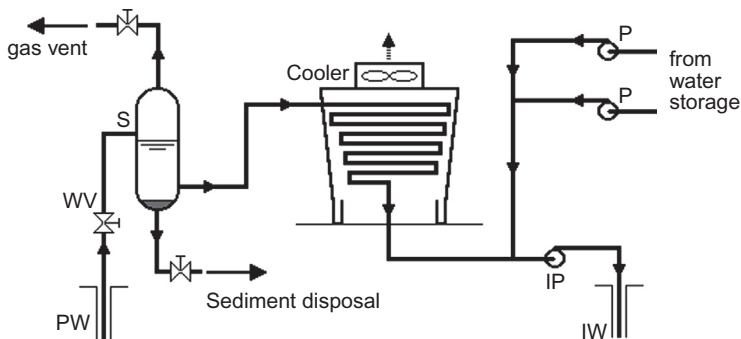


Figure 22.3 Fenton Hill HDR surface testing facility. After Ref. [2].

been partially depleted owing to exploitation. Since roughly 80% of the thermal energy of a hydrothermal reservoir resides in the hot rocks, the life of a reservoir can be extended by external fluid injection. The case of The Geysers mentioned earlier is such an example.

TABLE 22.1 Fenton Hill HDR flow test results [2–4].

Item	Phase I 1977	Phase II 1986	Phase II 5/1993	Phase II 5/1995	Phase II 6/1995
Reservoir depth (m)	2700	3550	4204	4204	4204
Reservoir temperature, (°C) ^a	185	232	228	227	227
Injection flow rate (kg/s)	NA	NA	8.14	7.98	7.82
Injection pressure (MPa)	NA	NA	26.54	27.3	27.3
Injection temperature (°C)	NA	NA	22.3	22 (est.)	22 (est.)
Production flow rate (kg/s)	7–16	12–14	6.85	5.82	5.52
Production pressure (MPa)	NA	NA	9.74	9.65	15.2
Production temperature, (°C)	NA	NA	190.3	185	183
Thermal power (MW)	3	10	5.50	4.7	5.5
Water “loss” (kg/s)	NA	NA	1.29	2.16	2.3
Water “loss” (%)	7–1	35–19	16	27	29

^aAll Phase II temperatures were taken at 3280 m depth.

22.2.2 ROSEMANOWES, ENGLAND

The Rosemanowes quarry was the site of England’s first experimental HDR project. It is located in the far southwest corner of the country about 4.5 km from Falmouth; see [Figure 22.4](#). Because of extensive mining in the area, records were available on the type of rocks that would be encountered down to 1 km. The temperature gradient was reasonably favorable at 30–40°C/km. The purpose of this experiment was to study the mechanisms appropriate to create artificial fractures in granite, and not to generate power. The maximum temperatures in the reservoir were purposely kept below 100°C [5]. The project was undertaken in 1977 by the Camborne School of Mines [6].

Initially several shallow, 300 m, wells were drilled but the granite at that depth was not representative of the deep formation. Then in 1980, two deep wells were drilled, RH11 and RH12; see [Figure 22.5](#). The bottom-hole temperature in the injection well RH12 was 79°C. Stimulation was carried out by injecting up to 100 kg/s of cold water into RH12 using a wellhead pressure of 14 MPa. It was expected that the fracturing of the near-vertically jointed granite would progress upward from RH12 to RH11, but the opposite happened, which led to poor connection between the two wells.

Since a highly fractured formation had thus been created below RH12, in 1983 a third well, RH15, was drilled into the lower formation; see [Figure 22.5](#). RH15 went to a total vertical depth (TVD) of 2652 m and encountered granite at about 100°C. Following stimulation, RH15 was connected to the original injection well RH12 and a series of circulation flow tests were conducted from 1985 through 1990 under various flow rates and wellhead pressures. The long-term tests were run over the last four years and showed a cooling of the formation from 80.5°C to 70.5°C. Flow rates varied from 5 to 24 kg/s: when 5 kg/s was

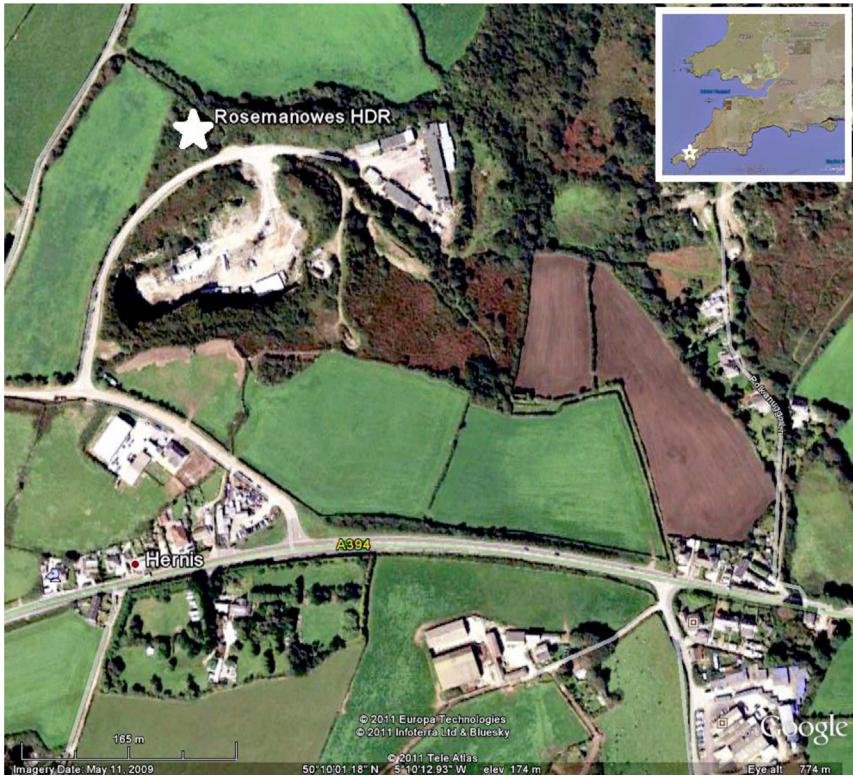


Figure 22.4 Location of the Rosemanowes HDR project, *Google Earth*, May 11, 2009 image [WWW].

injected in RH12, 4 kg/s was returned in RH15 at a wellhead pressure of 40 bar,a; however, when 24 kg/s was injected, only 15 kg/s was returned at 10.5 MPa. At the higher flow rate, a short circuit was created (low flow resistance, short residence time) that allowed cold water to travel rapidly through the formation without heating sufficiently. Since flow rates of at least 25 kg/s are essential for a commercial power plant, this result was discouraging.

Although the Rosemanowes project did not achieve all of its goals, it demonstrated that hydrofracking alone could be used to create a fracture network in hot, naturally fractured granitic rocks. The main findings included:

1. Regardless of the details of the hydrofracking method, the natural fractures in the granite will control the creation of the fracture network [7].
2. Natural fractures are widely found in crystalline rocks at all depths and all locations that were studied. Thus, an artificial fracture will quickly intersect the natural system within meters of the well, and the natural system will dominate the spread of the fracture system from there.

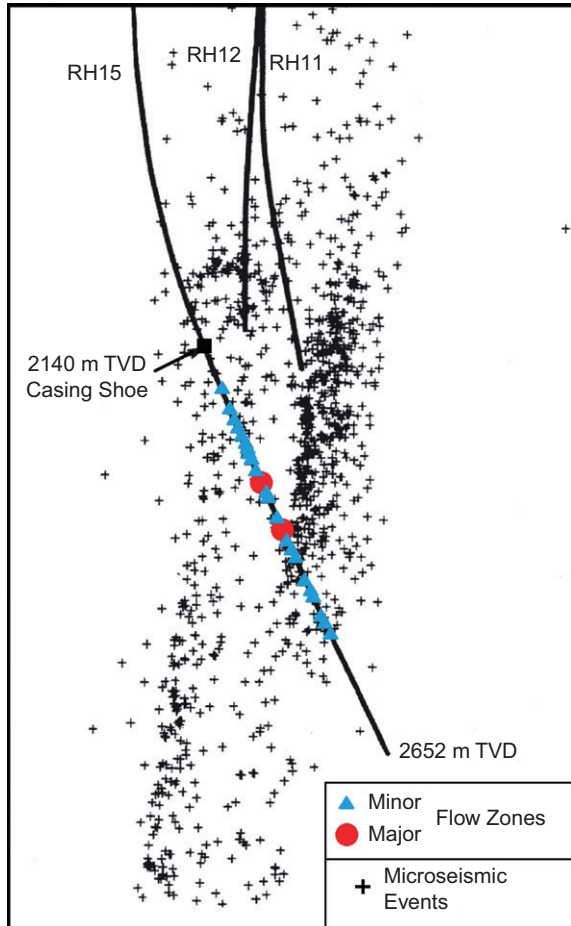


Figure 22.5 Flow zones and induced microseismicity in well RH15 [6] [WWW].

3. The use of excessive wellhead pressure at the injection well can result in overstimulation of the fracture system and create too direct a connection from the injector to the producer, resulting in lower production temperatures.
4. Finally, it must be recognized that everything one does to a reservoir during hydrofracking is irreversible and can be detrimental to establishing a productive flow loop through the formation. High pressures can move rocks creating permanent short circuits or open pathways to the far field resulting in excessive water loss to the formation [6].

The expertise and knowledge obtained there was put to use later in France at the Soultz-sous-Forêts project (see [Section 22.4.1](#)). The research facilities and the project staff were transferred to the Camborne School of Mines Associates Ltd. (CSMA) in 1992. Asea Brown-Boveri in 1997 acquired from CSMA the Rosemanowes quarry and all the assets of the project including its intellectual property. In 2004 Schlumberger bought the intellectual property and hired members of the technical staff with expertise in microseismic monitoring. They then sold the quarry. Most recently, in 2006, the site was acquired by 3K Facilities, a company that offers deep borehole test facilities in one of the most well-logged sites in the world. Researchers can gain access to the three deep boreholes for a range of down-hole testing. Additionally there are four uncased 300 m holes and one 150 m 30°-deviated hole, as well as a microseismic test station and a wind turbine test facility on the 81,000 m² site [\[8\]](#).

22.3 Later Projects

22.3.1 HIJIORI, JAPAN

Japan has invested in fundamental and applied HDR research at two sites in the northern part of Honshu: at Hijiori [\[9\]](#), Yamagata Prefecture ([Figures 22.6–22.8](#)), and at Ogachi [\[10\]](#), Akita Prefecture. Hijiori will be covered in this section; Ogachi in the next one.



Figure 22.6 HDR research facility at Hijiori, Japan. Shown are silencers at the production well during a 2-year circulation test, 2000–2002. The reservoir lies at a depth of 2300 m, with a temperature of 270°C [\[11\]](#) [\[WWW\]](#).



Figure 22.7 Hijiori HDR test facility showing the makeup water holding pond, production well HDR-2a (rear left), production well HDR-3 (center), and separator-silencer station (right); best available photo [11] [WWW].



Figure 22.8 Experimental binary-type power plant at Hijiori HDR test facility; best available photo [12] [WWW].

The Hijiori HDR project (1985–2002) was sponsored by Japan's New Energy and Industrial Technology Development Organization (NEDO). NEDO was a partner, along with West Germany, in the Fenton Hill project from 1981 to 1986.

As can be seen from [Figure 22.9](#), the NEDO approach differed in several ways from the Fenton Hill experiment. First, the reservoir is considerably shallower, reaching only to 1800–2200 m. Next, the induced fractures lie in a generally horizontal orientation, separated by some 400 m, and follow the natural fractures in the formation. There are two injection wells and two production wells, with each injection well dedicated to one of the fracture zones: SKG-2 to the shallow zone and HDR-1 to the deep zone. Also there is a river adjacent to the site, the Nigamizu River, that supplied water for the injection. Even with a river at hand, there was a backup holding pond with a capacity of 450,000 kg. And lastly, a 130 kW binary power plant was installed in the last stage to convert some of the thermal power into electrical power.

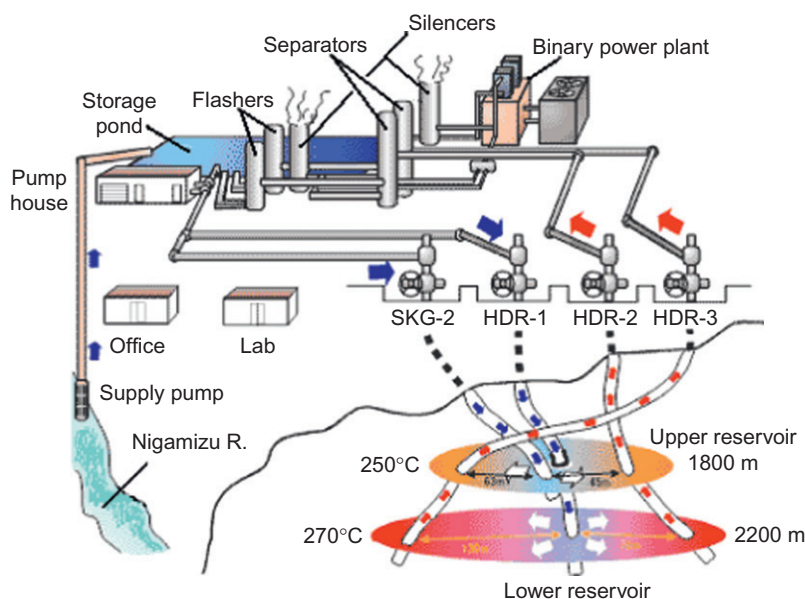


Figure 22.9 Schematic of Hijiori HDR reservoirs, test facility, and power plant. *After Ref. [9] [WWW].*

Hijiori is located about 1 km southwest of the Hijiori Hot Springs at the southern boundary of a small, 2 km diameter caldera, in northern Honshu; see [Figure 22.10](#). The site is about 50 km west-southwest of the Onikobe power plant.

Work began at the site in 1985 under the auspices of NEDO. There were two phases of the project. In the first stage from 1985 to 1991, only the shallow reservoir was explored using SKG-2 as the injector and HDR-1, -2, and -3 as producers. All the wells were drilled to about 1800–1900 m for this phase. The distances from the injector to the producers were intentionally short, i.e., 38 m to

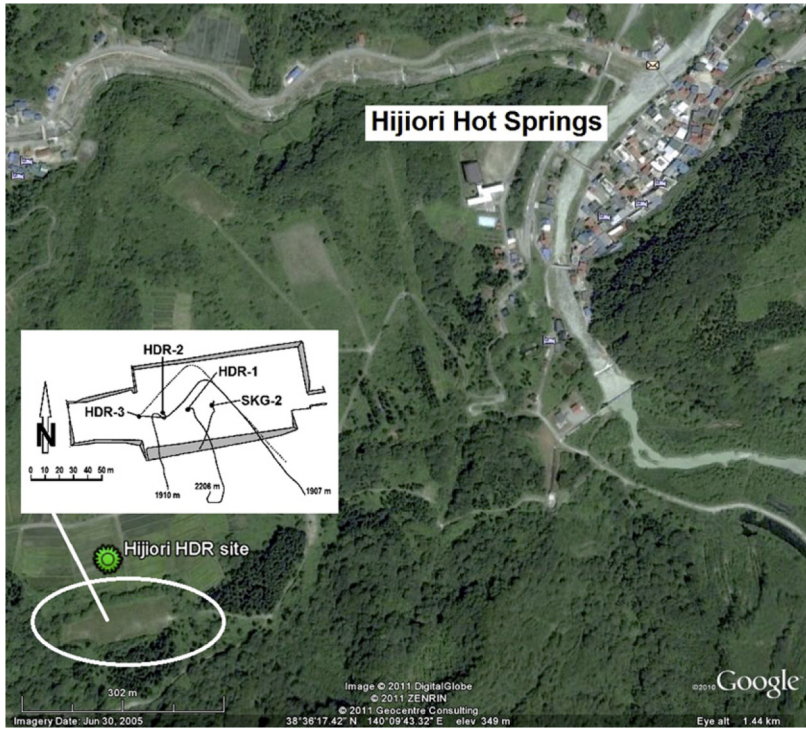


Figure 22.10 Former site of Hijiori HDR project, *Google Earth*, June 30, 2005 [13] [WWW].

HDR-1, 33 m to HDR-2, and 63 m to HDR-3. The wells were drilled successively and the formation was stimulated by circulation among the wells as they were completed. Table 22.2 provides the steps involved.

TABLE 22.2 Stages in well drilling and stimulation for Phase 1 at Hijiori [13].

Year	Events
1986	Hydrofracking at 1800 m via well SKG-2; 1000 m ³
1987	Well HDR-1 drilled
1988	2-week circulation from SKG-2 to HDR-1
1989	Well HDR-2 drilled; 1-month circulation from SKG-2 to HDR-1 and -2
1990	Well HDR-3 drilled
1991	90-day circulation from SKG-2 to HDR-1, -2, and -3

The 90-day flow test conducted in 1991 had the injection point in SKG-2 at a vertical depth of 1801 m; fluid entered all three producers at the following main depths: HDR-1 at 1784 m; HDR-2 at 1753 and 1761 m; and HDR-3 at 1754 m; there were several other secondary fluid entry points in the wells. The flow rates

for each of the production wells are shown in Figure 22.11. Under stable conditions achieved after about 50 days, the flow rates from HDR-2 and -3 were both about double that from HDR-1. The retaining pond was used to hold cold water pumped from the river prior to injection along with the fluids produced from the wells.

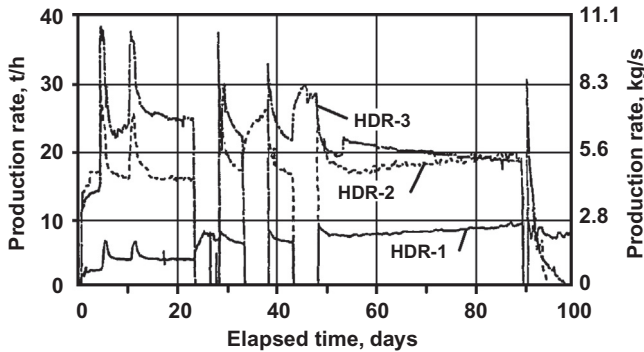


Figure 22.11 Flow rate results of 90-day circulation flow test in the shallow reservoir at Hijiori in 1991 [13].

Fluid temperatures issuing from each producer are shown in Figure 22.12. The temperature of the injectate was roughly 50°C , having been obtained from the retention pond. Well HDR-1 was the hottest well at about 190°C and was continuing to heat up as the test came to an end; HDR-3 was the next hottest at 165°C , and HDR-2 appeared to be stabilizing at about 150°C at the end. Note that the natural reservoir temperature at the shallow zone is about 250°C . At the conclusion of the test, the total mass flow rate was slightly less than 50 t/h (13.9 kg/s) and the thermal power extracted from the reservoir was about 8 MW-th . Had a binary plant been installed, this would have supported about $0.8\text{--}1\text{ MW}$ of electrical generation.

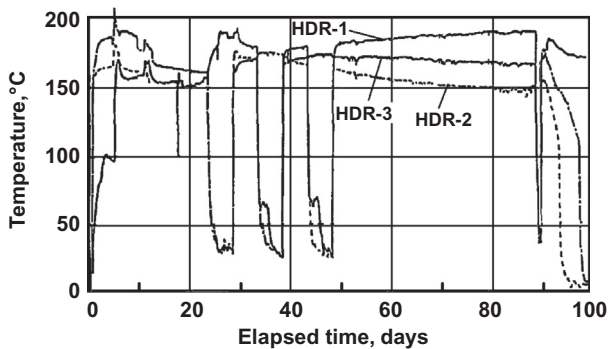


Figure 22.12 Temperature results of 90-day circulation flow test in the shallow reservoir at Hijiori in 1991 [13].

The second phase began in 1992 and involved the deepening of the three HDR wells into the deeper fracture zone. Prior to deepening, well HDR-2 was plugged back to about 1600 m and side-tracked; to avoid confusion, it was then renumbered as HDR-2a; see Figure 22.13 [14].

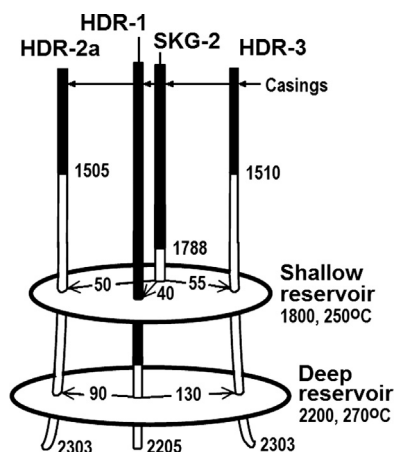


Figure 22.13 Configuration of Hijiori wells after deepening [14].

The deeper reservoir was stimulated in 1992, followed by flow tests in 1994, 1995, and 1996; an analysis of these tests can be found in Ref. [15]. From December 2000 to August 2002, a 19-month long-term circulation test (LTCT) experiment was carried out. The first year was dedicated to evaluating just the deep reservoir with HDR-1 serving as the injector and HDR-2 and -3 as the producers. The last seven months involved injection into both reservoirs with the addition of SKG-2 as an injector. The binary plant was in operation for the last three months of the testing program [9].

The mass flow rates achieved for the first year of tests are shown in Figure 22.14; the temperatures recorded for the last three months are shown in Figure 22.15.

One of the most serious, and unexpected, problems encountered during the LTCT was the precipitation of anhydrous calcium sulfate (anhydrite), CaSO_4 , in the two production wells, HDR-2a and -3 [16]. It was explained by the dissolution of anhydrite by the cold injectate as the water from the holding pond was delivered to the deep reservoir since calcium exhibits retrograde solubility, i.e., it is more soluble in water at low temperature and becomes supersaturated at high temperatures (opposite of silica). Then as the water makes its way through the hot formation at some point, it reaches supersaturation and precipitation becomes possible; see Figure 22.16.

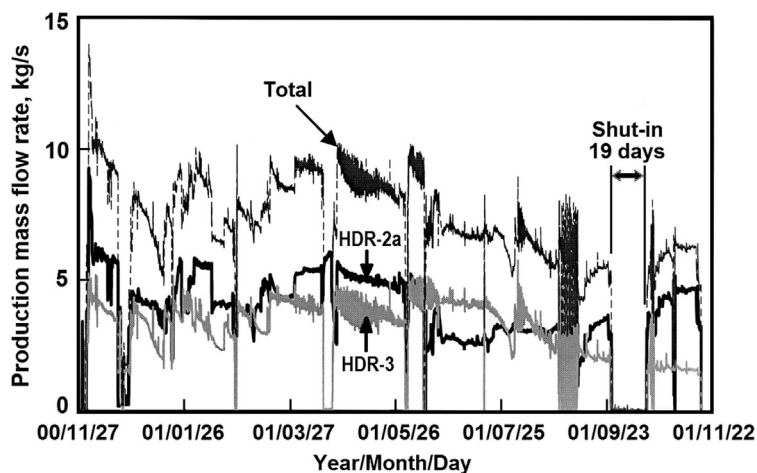


Figure 22.14 Long-term flow tests mass flow rates for Hijiori [16].

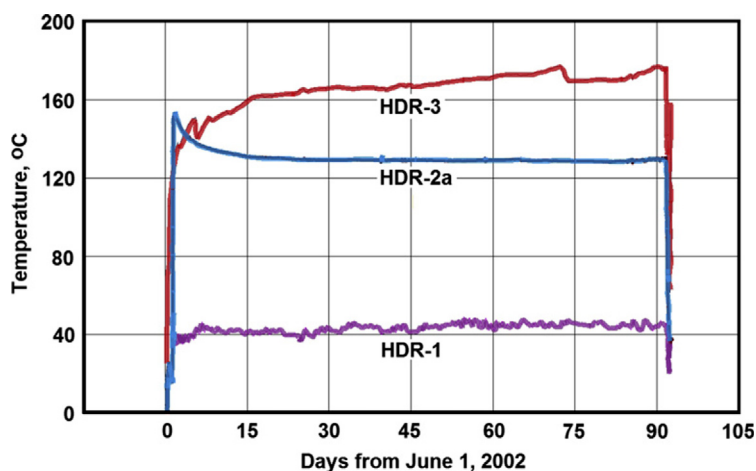


Figure 22.15 Temperature of production wells (HDR-2a and -3) and injection well (HDR-1) [17] [WWW].

However, the problem was further complicated by calcite and amorphous silica scale in both wells and surface pipelines, depending on the temperature of the fluids. Since the fluid was collected in the pond and recirculated during the LTCT, the dissolved minerals became concentrated and exacerbated the situation. This problem had not appeared for the previous 1-month flow tests presumably because insufficient time had elapsed to reach supersaturation conditions. The problem first appeared after 4–5 months of the LTCT [16].

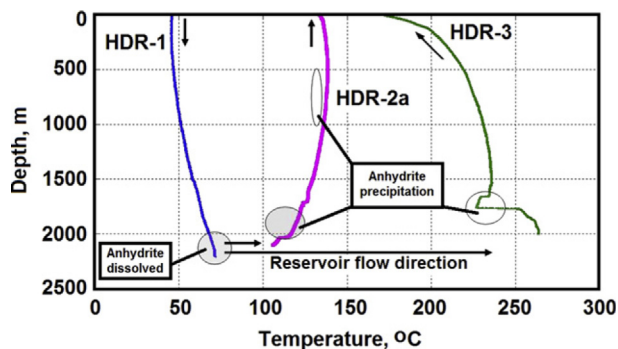


Figure 22.16 Anhydrite precipitation model for Hijiori project [17] [WWW].

At the end of the project, a committee reviewed the results focusing on five aspects: (i) overall system design, (ii) field characterization, (iii) reservoir creation, (iv) circulation/heat extraction, and (v) monitoring [9]. A search of the literature turned up no mention of the fate of the project, but an aerial view of the site from *Google Earth* dated June 30, 2005 (see Figure 22.10), clearly shows the site restored to its undisturbed condition. The insert plot map is from Ref. [13].

22.3.2 OGACHI, JAPAN

The Ogachi HDR project was conducted during the same time period as the one at Hijiori. Its success as an HDR project was limited owing to lack of support for a multi-well/multi-reservoir system, such as the Hijiori project. In 1990 the original well OGC-1 was drilled to 1000 m depth into a 228°C uplifted mylonitized granodiorite basement characterized by two major faults; see Figure 22.17. This well was used to stimulate both fault zones. In 1992 a production well OGC-2 was drilled directionally to intercept both reservoirs; its true length was 1100 m [Kaieda-Sasaki GRC v26 2002]. A circulation test resulted in only 3% recovery of injected water in OGC-2. After further hydrofracs, first to OGC-2 and then to both wells simultaneously, the rate of recovery improved in steps to 10–25%.

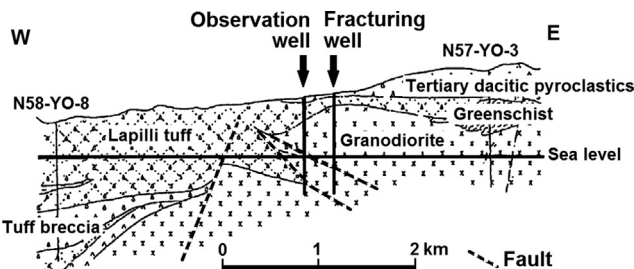


Figure 22.17 Geologic cross-section at Ogachi [18].

The acoustic emissions (AE) from the stimulations were analyzed to determine the extent of the newly fractured region as well as the local stress field. Then in 1999 a new well OGC-3 was drilled to about 1300 m into the new fractures. A flow test from OGC-1 to OGC-3 indicated connections at three locations at 770, 950, and 970 m depths, as predicted by the AE analysis [19].

In the course of this program, a great deal of geoscience was performed that increased the understanding of how the local stress field and natural fractures affect the creation of fluid flow paths between wells. A planned long-term flow test using the three Ogachi wells was never carried out. However, the wells were later used to study the concept of carbon dioxide sequestration in geothermal formations [10]. The basic concept is illustrated in Figure 22.18 where a mixture of water saturated with dissolved CO_2 is forced down a well into a porous formation. Under the reservoir pressures and temperatures, the CO_2 exists in a supercritical state with enhanced ability to dissolve minerals from the formation. As the fluid migrates through the reservoir, chemical processes including degassing and precipitation occur in various parts of the formation.

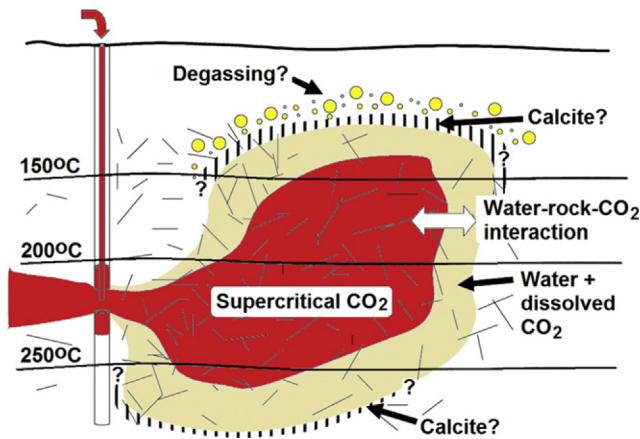


Figure 22.18 Conceptual model of CO_2 sequestration in geothermal reservoirs [20] [WWW].

At Ogachi, experiments were carried out using the existing wells. The first test was run in 2006 with 6.3 kg/s of neutralized river water being injected at a pressure of 15 MPa into OGC-1 and 0.67 kg/s produced via OGC-2; the produced fluid was at 127.5°C. For these experiments, OGC-3 was an observation well. Upon reaching steady conditions, CO_2 was introduced at the injection well as centimeter-size cubes of dry ice. Since the produced fluids were a mixture of the injectate and natural geofluids, no determination could be made about the fixation of carbon in the formation. In 2007 the next test involved injecting the dry ice/water mixture into OGC-2; see Figure 22.19. The results indicated that the injected CO_2 precipitated as carbonates within a few days [20].

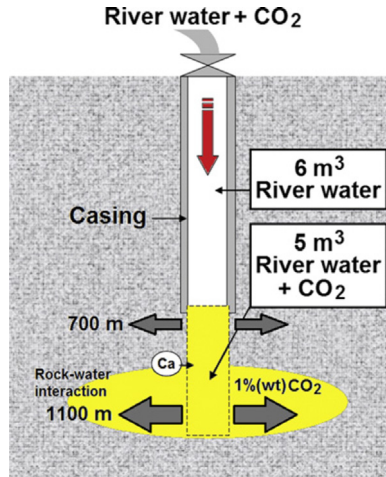


Figure 22.19 Carbon dioxide sequestration experiment at Ogachi HDR project [20] [WWW].

The importance of the Ogachi experiments lies in improving the understanding of CO₂–rock interactions in a non-aqueous, hot formation. It has been proposed that CO₂ may be a useful working fluid in an EGS system, instead of water [21]. Figure 22.20 is a schematic of how a CO₂-EGS reservoir might behave. The three zones will have different modes of interaction with the formation. Zone 1 is devoid of any natural water since it is assumed to be both displaced by and dissolved into the CO₂ stream. As such, the CO₂ would not be a super-solvent as it would be in a

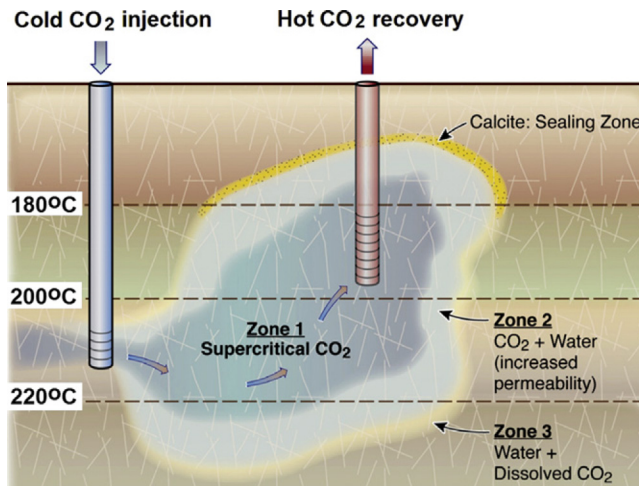


Figure 22.20 Conceptual model of CO₂ injection/production in an EGS reservoir [9] [WWW].

supercritical ionic aqueous mixture. This would eliminate the removal of minerals from the rock that would later precipitate and cause trouble in the flow paths. Moreover, loosely bound water molecules in some minerals could be removed and lead to improved permeability [9]. All of these hypotheses must await further experiments for verification.

22.3.3 BASEL, SWITZERLAND

The city of Basel was selected for an HDR combined heat and power (CHP) project partly because there was a demand for electric power and a district heating system was already in place. The geology was also favorable since Basel lies at the southernmost end of the Rhine Graben [22] and has a higher than normal heat flux. The fact that the wells would be sited within Switzerland's second largest metropolitan center with 830,000 area residents that include communities in France and Germany attested to the confidence that the developers had in the safety of their technology. The project was known as the Deep Heat Mining Basel (DHMB) project and was conducted by Geopower-Basel, a consortium of 11 public and private entities.

In a 2002 report to the International Energy Agency, the subject of environmental impact was discussed briefly. The issues to be studied are given in Table 22.3.

TABLE 22.3 Environmental issues of concern to the DHMB project [23].

Impact area	Possible relevant aspects
Water—ground and surface	Contamination, change of groundwater level and/or flow direction
Soil	Contamination, deposition, and treatment
Air	Emission of pollutants, smoke, and odor
Noise	Emissions generated during construction, operation, and related transports
Vibrations	Ground vibrations caused by construction, operation, and related transports
Traffic	Change of traffic volume
Induced seismicity	Change of seismicity through activities in deep rock formations

It is obvious that these are generic issues for any large construction project except for the last item. Apparently no serious risk assessment was carried out beforehand on the important matter for any EGS project.

The project officially got started in 1996 with support from the Swiss Federal Office of Energy, although theoretical research had been going on for 20 years prior. For the next 10 years, feasibility studies were performed and sites examined as possible locations for the first deep heat mining project in Switzerland. As a

private project, the federal government would not be an owner of the facility. The city of Basel expressed an interest and being situated favorably as mentioned above, it was selected as the project site.

The plant was designed to produce 3 MW electric and 20 MW thermal using one injection well and two production wells drilled to about 5000 m depth into 200°C rock. The produced fluid was to be 170°C and the reinjection temperature would be 70°C. The power would be generated in a binary plant with the cooled discharged fluid being used in a heat exchanger array to heat water for the district heating system before being returned to the reservoir. The original design mass flow rate was an ambitious 70 kg/s, nearly three times greater than had ever been achieved in any EGS experiments [22], but was later scaled back to 50 kg/s [24].

The first well (OT-1) was spudded in June 1999 in the Otterbach area. After reaching a depth of 1537 m, drilling problems forced the abandonment of the well in January 2001. The measured shallow temperature gradient, down to 537 m, was extrapolated to 42°C/km. The well was converted into a seismic monitoring station by the Swiss Seismological Service.

The second well (OT-2) was started in March 2001 using the same site for OT-1 but with a higher capacity drill rig. It was completed to a total depth of 2755 m in June 2001. The well was left as an open hole from 2030 to 2755 m with a diameter of 5–7/8". The measured temperature gradient was 38°C/km. The deep formation was tight, fractured granite. This well provided data to allow for planning of the 5000 m wells and was converted to another seismic monitoring station, one of six to monitor the deep system. By early 2006, all monitoring wells were ready at depths of around 2700 m, just into the top of the granitic basement.

Prior to the start of drilling of the first deep well, the developers, R.J. Hopkirk and M.O. Häring, wrote these prescient words:

Nature does not obey laws set by mankind and surprises are to be expected. Only if project planning and management . . . can meet and deal with such surprises can any serious projections for hot fractured rock EGS be made. [25]

Basel-1, the first deep well in the DHMB program, was drilled from May to October of 2006 in the industrial section called Kleinhüningen; see Figure 22.21. It reached a depth of 5000 m, the lower 2.6 km being in the granitic basement; see Figure 22.22 for the detailed casing and temperature profiles [L&H GRC 2009]. The thermal perturbations at about 2700 m and just below the final casing shoe are noteworthy in they indicate interceptions with fractures or faults. The zone at 2700 m was a source of hot water at 120–125°C and possibly might be able to support a small binary plant depending on the flow rate. The obstruction

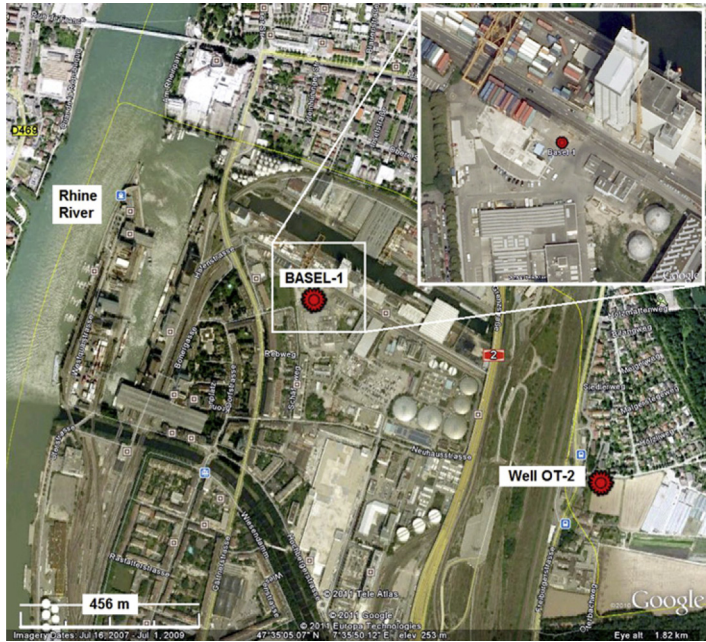


Figure 22.21 Location map for wells Basel-1 and OT-2, *Google Earth*, July 1, 2009 [WWW].

shown near the bottom of the well could not be removed as the cutting tool itself got stuck. The locations for Basel-1 and one of the monitoring wells, OT-2, are shown in [Figure 22.23](#) against the background of the geologic formation.

Prior to the main stimulation procedure, a brief injection test was carried out in November 2006 under low-pressure and low-flow conditions. The entry to the formation was at the major, highly altered fractures identified at 4700 and 4835 m depths. It became clear that although the formation contained fluids, the well would not flow under artesian conditions.

The massive stimulation began on December 2 using water pumped from the Rhine River basin adjacent to the well. The flow rate was raised in steps up to 1.67 kg/s over the next 16 hours, at which time the wellhead pressure reached 110 bar. Further injection over the next several days eventually reached 55 kg/s with the wellhead pressure at 296 bar. There was a continuing high frequency of microseismic events observed during this period, and when a seismic reading of magnitude 2.7 was noted, the injection rate was lowered in the morning of December 8. But the seismic activity continued, so 5 hours later, the injection was stopped. While plans were being made to bleed off the well, a magnitude 3.4 event occurred. This was felt in the community and caused great fear among the

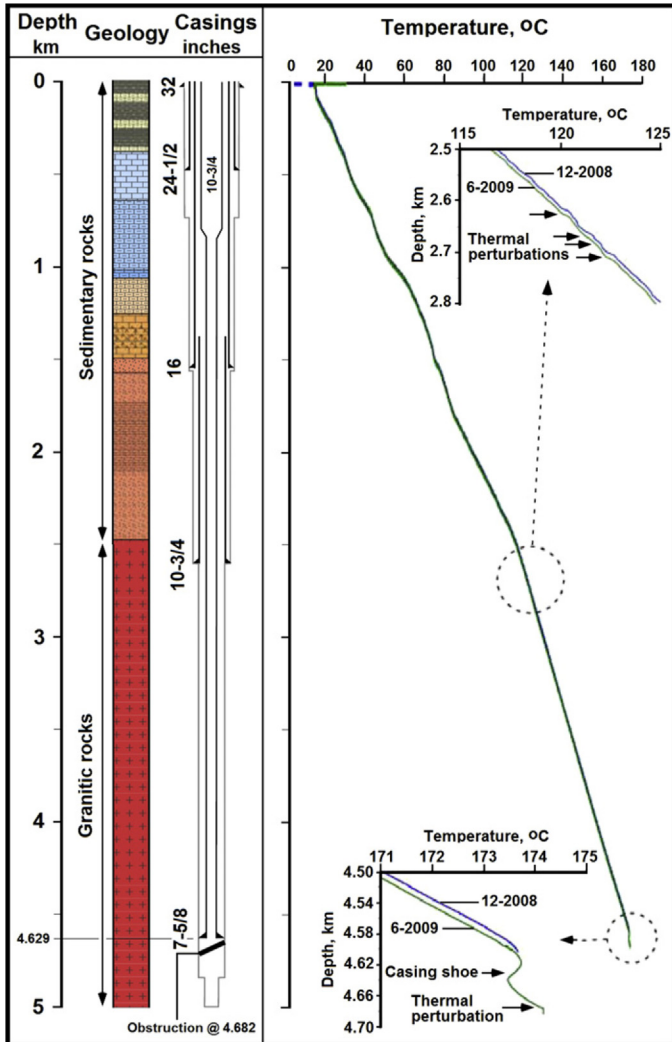


Figure 22.22 Well profile for Basel-1 including temperature measurements [26] [WWW].

citizens who were well aware of the historic magnitude 6.5–6.9 earthquake that destroyed Basel in 1356. While a 3.4 event is not expected to cause damage, apparently some homes suffered cracked plaster walls and similar problems.

The stimulation procedure was highly instrumented with six borehole seismic observation sites arrayed around the Basel-1 well; see Figure 22.24. The area was fitted with predefined triggers for several color-alerts, a so-called traffic light arrangement, set to deploy when seismic events of various magnitudes were recorded, starting with magnitude 2.9 and ground motion of 5 mm/s.

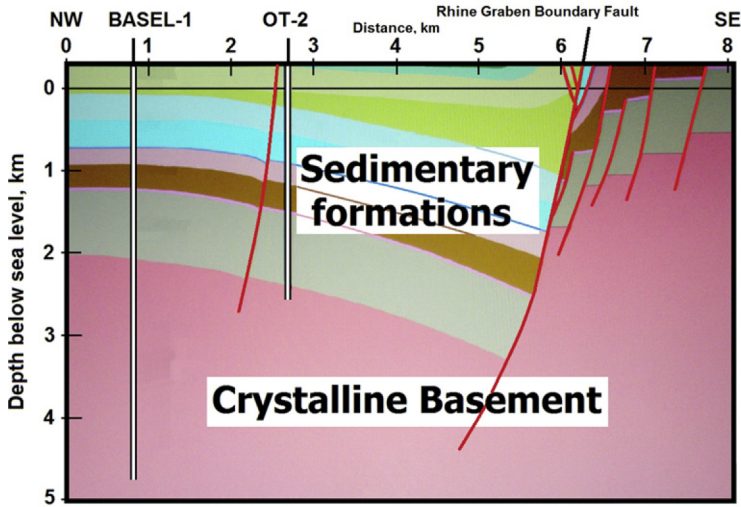


Figure 22.23 Geologic cross-section through the eastern end of the Rhine Graben showing wells Basel-1 and OT-2. Modified from Ref. [27] [WWW].

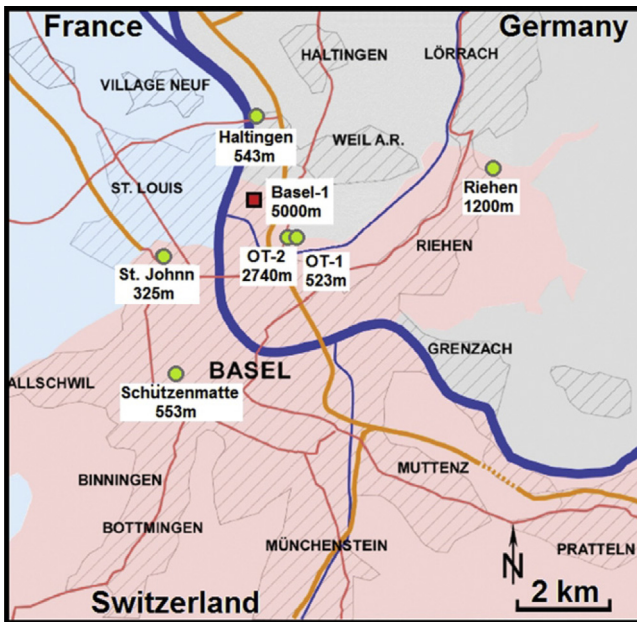


Figure 22.24 Well field at Basel: circles are monitoring well showing depth of sondes [24] [WWW].

In the 4-month aftermath of the stimulation, the seismic monitoring network recorded over 13,500 potential events, of which the strongest 200 were between 0.7 and 3.4 magnitude with nine being 2.5 or greater [28]. A post-event risk analysis was ordered by the government and the results of that study effectively put an end to the DHMB project. The study showed that the risk of a major earthquake from reservoir stimulation was low, the risk of similar low-magnitude, but damage-causing events was very high. The estimated cost to repair damage to homes was put at around \$7–9 million per year. The study also did not rule out the possibility that other EGS projects might be acceptable in other locations in Switzerland and elsewhere, provided a careful technical plan was worked out ahead of time including a thorough risk assessment [29].

A detailed technical analysis of the fluid–rock mechanics involved in the stimulation can be found in Ref. [30]. The main conclusions are: (i) the natural fracture system dictated the growth plane induced by the stimulation; (2) the created reservoir was essentially planar in the vertical direction; (3) the displacement achieved was irreversible, and (4) the hypothesis that a highly fractured, interconnected reservoir network could be formed by a massive stimulation was false, at least at Basel. The project developers speculated that by using a more gradual stepwise stimulation process using lower flow rates and wellhead pressures together with a waiting period between pulses (“nudge and let it grow”), it might be possible to avoid the type of seismic events that led to the project’s demise in December 2009.

22.4 EGS Power Plants

22.4.1 SOULTZ-SOUS-FORÊTS, FRANCE

The EGS effort at Soultz-sous-Forêts, France, got started in 1987 with a research program aimed at developing a fractured reservoir using three deep wells, roughly 5000 m in depth, and ultimately producing both heat for the local district heating system and electric power. In mid-June 2008, the first electricity flowed from the 1.5 MW organic Rankine cycle pilot plant. A timetable of major events is given in Table 22.4.

An enormous amount of scientific and engineering work has been carried out over the last 28 years and the reader may wish to consult a Special Issue of the journal *Geothermics* [33] and a detailed survey article [33a] as good starting points for further study. The Soultz plant is situated on the French side of the Rhine Graben near the border with Germany, about 25 km west of Karlsruhe; see Figure 22.25.

TABLE 22.4 Summary of Soultz project [31,32].

Year	Event
1987	GPK-1 drilled to 2002 m
1989	Three existing oil wells deepened as monitoring wells for microseismicity
1990	Existing oil well EPS-1 deepened to 2227 m
1991	GPK-1 stimulated from 1420 to 2002 m
1992	GPK-1 deepened to 3590 m
1993	GPK-1 stimulated from 2850 to 3590 m
1994	GPK-1 goes into production
1995	GPK-2 drilled to 3876 m GPK-2 stimulated from 3211 to 3876 m 2-week circulation test between GPK-1 and GPK-2
1996	GPK-2 restimulated from 3211 to 3876 m
1997	Highly successful 4-month circulation test between GPK-1 and GPK-2
1999	GPK-2 deepened to 5084 m
2000	Seismic monitoring well OPS-4 drilled to 1537 m GPK-2 stimulated from 4431 to 5084 m
2002	GPK-3 drilled to 5031 m
2003	Injection test of GPK-2 while observing GPK-3 shows strong connection 2-week test: injection in GPK-2, production from GPK-3 (as yet unstimulated) GPK-3 stimulated 16-day circulation test between GPK-3 (I) and GPK-2 (P) GPK-4 (P) drilling started
2004	GPK-4 completed to 5105 m and stimulated
2005	6-month circulation test among GPK-2 (P), GPK-3 (I), and GPK-4 (P)
2008	1.5 MW pilot power plant installed and two circulation tests
2008–09	Tests of line-shaft and electric submersible pumps in GPK-2 and GPK-4
2010–	Continuing tests of reservoir, pumps, and power plant

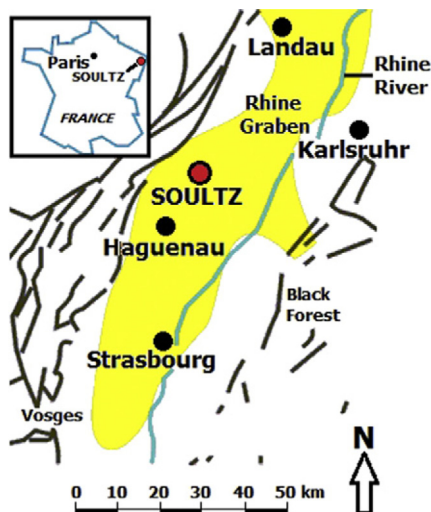


Figure 22.25 Soultz location map; colored area has high potential for EGS [WWW].

There are three 5000 m wells that serve as one injector and two producers for the plant: GPK-2, -3, and -4. Several other wells have been either drilled from scratch or deepened (see Table 22.4 and Figure 22.26) and an extensive array seismic monitoring stations are in place.

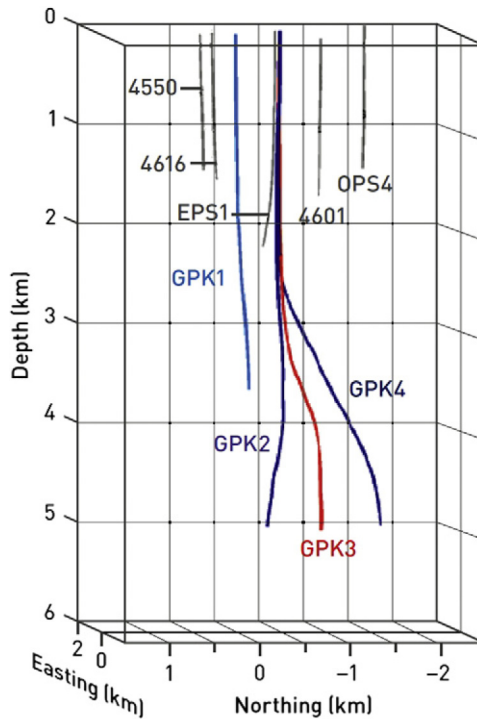


Figure 22.26 Well profiles at Soultz [6] [WWW].

Soultz is characterized by an exceptionally high near-surface gradient, about $110^{\circ}\text{C}/\text{km}$, about three times higher than normal. Each of the three deep wells revealed an interesting temperature profile, as shown in Figure 22.27 in which the high near-surface gradient lies above 2.5 km of nearly isothermal rock where the gradient is only $5^{\circ}\text{C}/\text{km}$, while the lowest 1.5 km is marked by the expected gradient of about $30^{\circ}\text{C}/\text{km}$. Evidently there is a large section of the formation in which convection plays an important role, lifting high-temperature fluids close to the surface and influencing the near-surface gradient. The perturbations seen in the temperature curve in Figure 22.27 indicate fluid entry or exit points.

The geofluid is a sodium-chloride brine with about 100,000 ppm total dissolved solids (TDS), a pH of 4.9, and a reservoir temperature of 200°C , in equilibrium with the rock. By the time it reaches the plant, the temperature falls to 175°C .

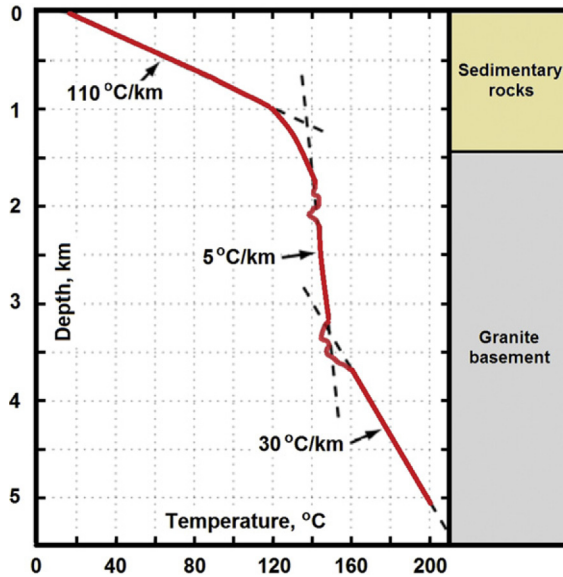


Figure 22.27 Temperature profile in Soultz reservoir. After Ref. [34] [WWW].

The power plant was designed and built in 2007–8 and has functioned as a test station while producing power from time to time. A site photograph (Figure 22.28) shows a compact arrangement made possible because the three wells lie in a line with 6 m separation between them. A 3D schematic diagram (Figure 22.29) shows the locations of the major pieces of equipment in the power plant.



Figure 22.28 Soultz 1.5 MW pilot power plant [35]. Geofluid is passed through a series of filters (foreground) before entering the heat exchangers [WWW].

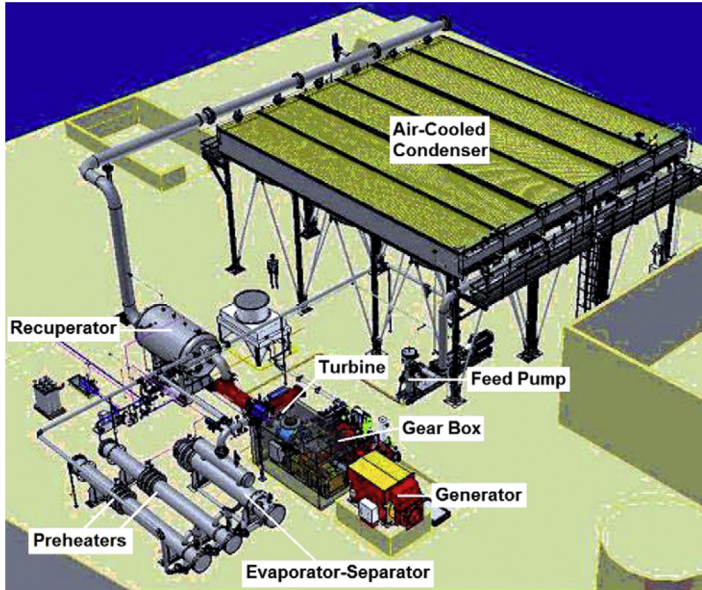


Figure 22.29 Schematic 3D visualization of Soudz power plant. After Ref. [35] [WWW].

Figure 22.30 is the simplified flow diagram with labeled state points for ease of analysis. The geofluid is produced from GPK-2 with a line-shaft pump and from GPK-4 with an electric submersible pump. After it passes through the heat exchangers of the power cycle, it is filtered and pumped back into the reservoir via GPK-3. The turbine is a 1.5 MW radial-flow machine supplied by Cryostar-Turboden turning at 13,000 rpm and driving a 1500 rpm, 11 kV asynchronous

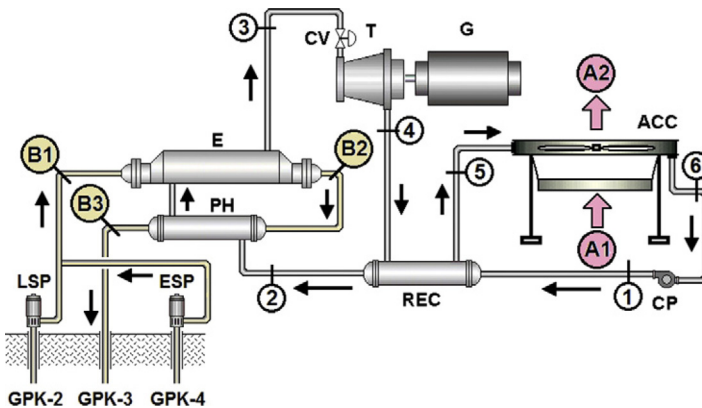


Figure 22.30 Soudz simplified flow diagram; filters omitted for clarity [WWW].

generator through a gearbox. The power is stepped up and fed into the local 20 kV electrical grid. The plant operates with an air-cooled condenser (ACC) due to the lack of available freshwater at the site.

The thermodynamic cycle properties are given in Table 22.5 in which the pressures, temperatures, and mass flow rates were taken from Ref. [36], but all the other properties were calculated using REFPROP. The pressure-enthalpy diagram for the cycle is shown in Figure 22.31; the colored band represents the heat transfer in the recuperator.

TABLE 22.5 Soultz state-point information [36].

State	Temperature °C	Pressure bar,a	Entropy kJ/kg · K	Enthalpy kJ/kg	Mass flow kg/s
<i>Isobutane</i>					
1	32.3	30.97	1.2528	278.32	34.76
2	50.5	30.57	1.3980	323.91	34.76
3	127.7	30.50	2.4064	702.58	34.76
4s	50.004	4.65	2.4064	629.59	
4	57.3	4.65	2.4493	643.60	34.76
5	32.4	4.25	2.3177	598.10	34.76
6	30.9	4.15	1.2530	273.45	34.76
<i>Geofluid</i>					
B1	175		2.0906	741.02	31.23
B2					31.23
B3	70		0.9551	293.07	31.23
<i>Air</i>					
A1	20.0	3.00	3.5513	419.03	
A2	29.6	2.90	3.5937	428.75	

It is obvious that the original specifications were taken for an assumed ideal, isentropic feed pump since the entropy at states 1 and 6 are essentially identical. In determining the performance, it was here assumed that the feed pump is 75% efficiency; the turbine specifications from Ref. [36] indicate that an 80.8% efficiency was used, a reasonable value.

The cycle analysis reveals that under these conditions, the power cycle would have a thermal efficiency of 13.9% and a brine utilization efficiency of 40.0% based on a dead-state temperature of 20°C. The presence of the recuperator adds about 1.5 percentage points to the thermal efficiency of a non-recuperated cycle or a gain of about 11.6%. These values do not account for the external power requirements such as the fan motors in the ACC, geofluid production pumps, and other system pumps. Taking all parasitic power into account is expected to lower the thermal efficiency to about 11.4%.

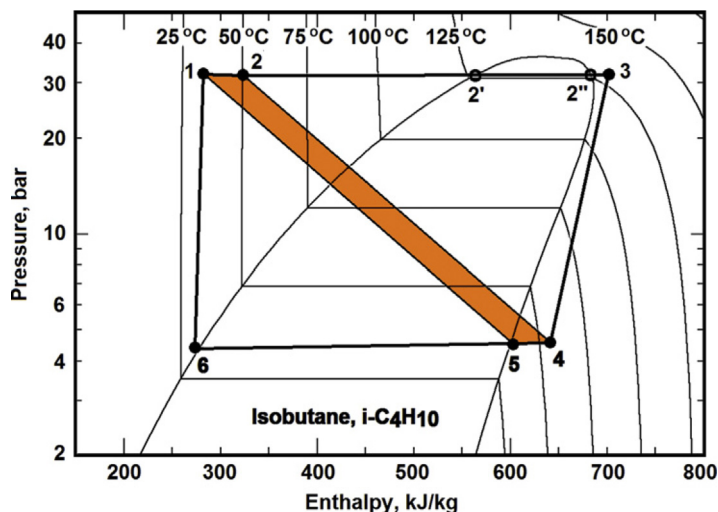


Figure 22.31 Pressure-enthalpy process diagram for design conditions at Soultz [WWW].

22.4.2 NEUSTADT-GLEWE, GERMANY

Neustadt-Glewe, a town of about 8000 residents, is in northern Germany about 70 km south of the Baltic Sea. It is the site of a CHP plant that uses both geothermal and fossil energy to provide district heating and electricity. The heating plant went into operation in 1995 to be followed by the electric power plant some eight years later. It is served by two wells, one producer and one injector, located 1350 m apart. Depending on demand, the flow rate can vary between 12.8 and 38.2 kg/s. The geofluid is a sodium-chloride brine containing roughly 220,000 ppm TDS and has a density of 1147 kg/m³ [37]. The production zone lies at 2216–2248 m within a 67 m thick sandstone formation.

The EGS power plant at Neustadt-Glewe, the first one in Germany, went into commercial production in November 2003, five years before Soultz [38]. However, this plant belongs more in the category of DHS than EGS. It tapped into the water-saturated sedimentary formations that are prevalent in some parts of Germany and other European countries. The sole production well is 2250 m deep and yields highly mineralized water at 98°C. This fluid is used primarily in a district heating system with excess hot water feeding a binary power plant (ORC). In summer when heating demand is very low, essentially all of the hot water goes to the power plant. The thermal power is 11 MW-th of which about 6 MW-th is supplied by hot geofluid (the rest is provided in a peak mode by natural gas) whereas the small binary power unit is rated at 230 kW; see Figure 22.32 [39]. The annual electricity generation has been about 1.2 million kWh for the last few years [40].

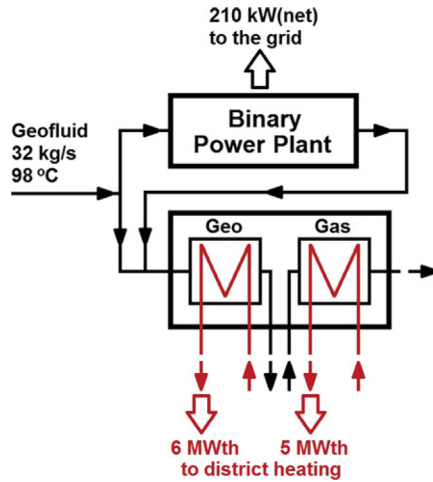


Figure 22.32 Simplified schematic of Neustadt-Glewe CHP plant.

The power plant is operated by Erdwärme-Kraft GbR. The unit receives 32 kg/s of geofluid at 98°C which transfers heat to perfluoropentane (C_5F_{12}), the cycle working fluid, and is discharged at 72°C. C_5F_{12} has a normal boiling point of about 30°C and a critical point at 147°C and 2 MPa, making it well suited to this geofluid. The turbine is a single-stage axial-flow machine with three inlet nozzles. Owing to the corrosive nature of the brine, the heat exchangers are made of titanium [41,42]. It uses a wet cooling tower with a dedicated fresh water well to provide makeup.

Although the plant was commissioned in November 2003, it underwent several modification as problems became apparent. In 2004, the condenser was replaced; see Figure 22.33. In August 2004 it began continuous operation only to be shut down for the winter from November 2004 to March 2005. From April to May 2005, a burned generator bearing caused an outage, immediately followed by another outage from June to August 2005 because of a leaky valve in the ORC. Then a brine pump failed causing another outage from October to November 2005. The total investment cost as of 2006 was €950,000 (about \$1.2 million) [42].

The cycle has a thermal efficiency of 6.6%, allowing for a 5% pressure loss in the preheater and assuming a 70% isentropic turbine efficiency and a 65% isentropic pump efficiency. The utilization efficiency based on the exergy of the incoming brine and a dead-state temperature of 20°C is 17.7%. Since the turbine exhaust is superheated, it is possible to incorporate a recuperator into the cycle (at additional cost) and the thermal efficiency would then rise to 8.3%. This analysis is based on the technical specifications for the plant; for an analysis of some early performance data, see Ref. [43]. In 2012, the power generating system was dismantled due to poor economic conditions; the heat portion of the plant continues to operate [43a].



Figure 22.33 Neustadt-Glewe skid-mounted power unit with new condenser installed in 2004 [41] [WWW].

22.4.3 LANDAU, GERMANY

Located about 34 km northeast of Soultz-sous-Forêts in the Upper Rhine Graben (URG), the Landau power plant is the first geothermal CHP to be connected to the grid; see [Figure 22.34](#). The electric power part was the first to go online; the district heating was added later.

A timeline of progress is given in [Table 22.6](#). The Landau project was supported by the German Federal Ministry for the Environment, Nature Conservation, and Nuclear Safety (BMU). In addition, the German state of Rhineland-Palatinate assisted with the geological exploration mitigated the financial risk by providing an exploration subsidy and a state loan guarantee [45].

A pair of wells, a doublet, constitutes the geothermal connection to the reservoir. One well, Landau 1 having a deviation of 33° , produces fluids at a temperature of about 155°C with the aid of a pump from a highly permeable formation in the Malm limestone. This well is so productive that no stimulation was needed. The other, Landau 2 with a deviation of 25° , is the reinjection well. This well was not so productive and required both massive hydraulic stimulation and acidizing to improve the injectivity [46]. They are separated by about 1200 m in the reservoir. After these efforts circulation tests proved that the doublet could support the 3 MW binary power plant.

From the temperature profiles in [Figure 22.35](#), it can be seen that there is a convective part of the formation beginning just below 2200 m depth; cf. [Figure 22.27](#) for the Soultz wells. In this case, the drilling was stopped just below 3000 m depth and production was taken from this permeable layer.

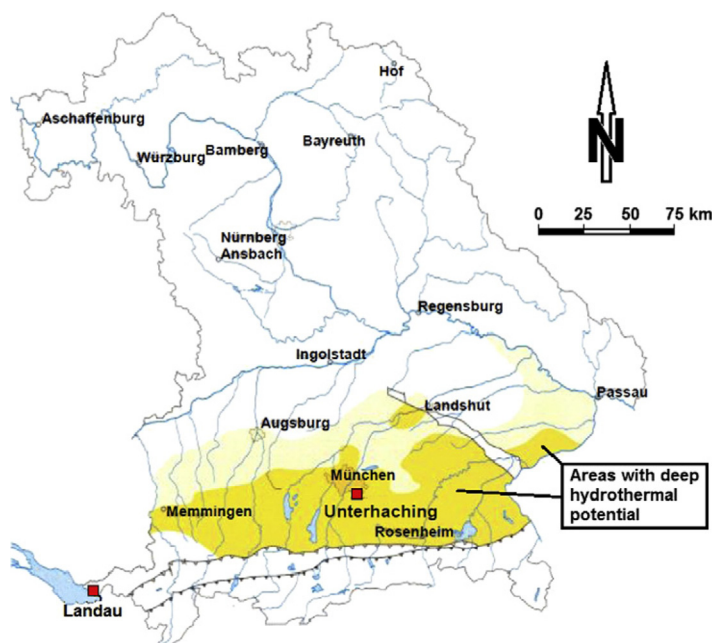


Figure 22.34 Southern Germany and the Molasse Basin (MB) showing locations of Landau and Unterhaching geothermal power plants [44] [WWW].

TABLE 22.6 Chronology of milestones for Landau power plant [45,47].

Date	Event
May 2003	Beginning of project
August–November 2005	Drilling of production well Landau 1
January–April 2006	Drilling of injection well Landau 2
February 2006	Begin power plant design
March–April 2006	Stimulation and acidizing of Landau 2
March–May 2006	Run circulation flow tests
December 2006	Begin power plant construction
April–May 2007	Circulation test of Landau 2
May 2007	Install power plant cooling system
August 2007	Install power plant turbine-generator
November 21, 2007	Power plant commissioned
January 2008	Start of continuous operation
August 15, 2009	Microearthquake ML = 2.7; continuous operation curtailed, but research operation allowed
September 2009	Plant required to reduce output and reinjection pressure
November 2009	40 residents report cracks in walls of homes
December 2010	Official report: Landau operations very likely the cause for microearthquakes; requires monitoring wells be emplaced around the plant and €50 million in liability insurance be purchased by the plant owners

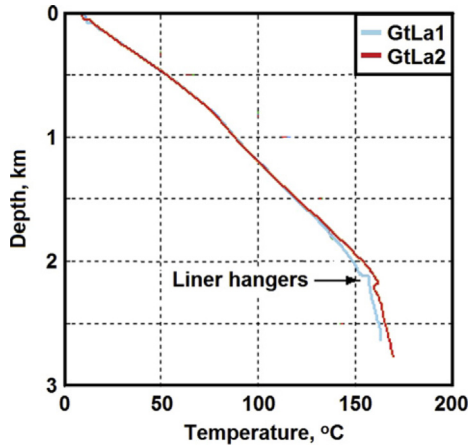


Figure 22.35 Temperature profiles in Landau wells. After Ref. [46] [WWW].

The power plant is a conventional, air-cooled, basic binary cycle that uses isopentane as the working fluid most appropriate for a geofluid temperature of 160°C. The brine discharge temperature from the unit is 72°C. This fluid then passes to the district heating plant and, after providing heat to the town's hot water system, is returned to the reservoir under pressure at 50°C via the 3170 m Landau 2 well. The average net power generated over a typical year is about 2.9 MW.

On August 15, 2009, the residents of Landau were jolted by a loud noise that many likened to a sonic boom. A magnitude 2.9 microearthquake had occurred. It was determined that the epicenter lay 500 m from the well at the plant and at a depth that corresponded to the reservoir. A special investigation was conducted and in 2010 concluded that the plant operation was very likely the cause of the event. Immediately after the microquake, the plant was forced to curtail power and reduce the reinjection pressure. After the final report, the plant was allowed to continue operating but with added seismic monitoring around the plant, which is located on the southern limit of the town. The plant was also forced to buy a €50 million per annum liability insurance policy to cover any future damage to property caused by its operations [47].

22.4.4 UNTERHACHING, GERMANY

With reference to Figure 22.34, Unterhaching lies in southern Germany's Molasse Basin, roughly 290 km southeast of Soultz or Landau. In this area it is possible to reach reservoir temperatures of 120–140°C at depths of 3000–3500 m. Figure 22.36 shows a north–south schematic cross-section of the geology in the area.

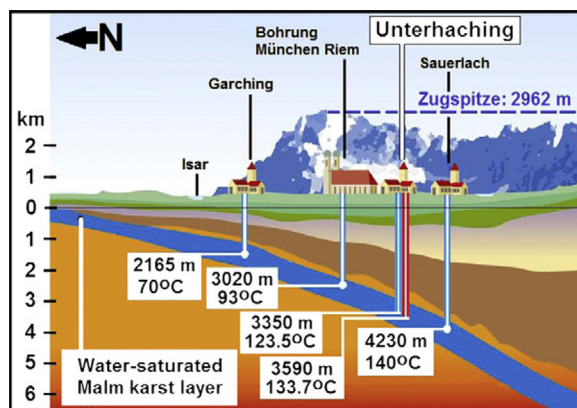


Figure 22.36 North-south schematic section through Molasse Basin [48] [WWW].

Like Landau, Unterhaching operates with a doublet of wells: the injector reaches a depth of 3350 m and a temperature of 123.5°C; the producer goes to a depth of 3590 m and yields fluid at 133.7°C. Both wells are capable of flowing at least 150 kg/s. Both wells experience good inflows from about 3100 to 3340 m in Gt Uha1a and from 3350 to 3700 m in Gt Uha2. Several faults or fault zones are responsible for the good flow conditions. The wellheads are about 3 km apart. The geofluid is a bicarbonate water with low TDS of 600–1000 ppm, of which 300–400 ppm is bicarbonate; the pH is 8.8 [49].

The plant receives 150 kg/s of geofluid, but 25 kg/s is sent to the district heating plant directly. After the 125 kg/s is used to drive the 3.38 MW Kalina cycle, it rejoins the discharge brine from the heating plant and is reinjected at 60°C. The Kalina cycle uses a water–ammonia mixture as its working fluid: 11% H₂O + 89% NH₃. The thermal efficiency is reported to be 12%. The electricity generated is compensated at a rate of €0.15/kWh according to the feed-in tariff of Germany's Renewable Energy Act. This allows the plant to be profitable. As of 2007 the total investment cost for the town of Unterhaching in the CHP plant was €60 million (about \$75 million) [50].

The history of the project is summarized in Table 22.7.

TABLE 22.7 Short history of events for Unterhaching project [49].

Date	Event
January–September 2004	Drilling of production well Gt Uha1a to 3350 m depth
September 2004	Successful acidizing of Gt Uhaa
June–November 2006	Drilling of injection well Gt Uha2 to 3331 m depth
January 2007	Deepening of Gt Uha2 to 3590 m and successful acidizing of Gt Uha2
January 2007	Completion of plant building
October 2007	Commissioning of 27 MW-th heating plant
June 2009	Commissioning of 3.38 MW Kalina cycle power plant

The Unterhaching project achieved several “firsts” for Germany:

- It marked the first time that the MB in southern Germany was exploited for geothermal electricity generation.
- It was the first time that a Kalina cycle was used to produce power on an industrial scale.
- It was the first time in the MB that a geothermal well was fitted with a submersible pump and produced a mass flow rate of up to 150 kg/s at a temperature of 123.5°C.
- Lastly, Gt Uha2 was the deepest geothermal well ever drilled in the MB, reaching a TVD of approximately 3590 m.

22.4.5 BRUCHSAL, GERMANY

Located about 35 km east of Landau on the eastern border of the URG, Bruchsal hosts a small, 0.55 MW pilot power plant that uses a Kalina cycle fitted with a novel radial outflow turbine (Euler turbine) with a titanium rotor. The turbine operates at 28,000 rpm and drives an induction generator through a single speed-reducing gearbox. The turbine has a reported efficiency of 82.4% [51]. The geo-fluid temperature is 118°C. The unit came online late in 2009. It underwent extensive reconstruction starting in 2012 and a pump test in early 2013 that meant the plant was not in continuous operation. The plant was able to generate 1.2 GWh of electricity in 2013, i.e., it ran at an average load of only 0.137 MW or an average capacity factor of 25% [43a].

22.4.6 OTHER GEOTHERMAL PLANTS IN GERMANY

- Dürrenhaar—Electric generation started at the 5.5 MW Dürrenhaar plant in December 2012.
- Insheim—Electric generation started at the 5.0 MW Insheim plant in November 2012.
- Kirchstockach—Electric generation started at the 5.5 MW Kirchstockach plant in March 2013; see [Figure 22.36a](#).
- Sauerlach—Electric generation started at the 5.0 MW Sauerlach plant in March 2013. Instead of the usual doublet of wells, this plant uses one production and two injection wells.
- Simbach-Braunau—This 200 kWe CHP plant shut down the power generating unit in 2012 owing to poor economic conditions; the heat side of the plant continues to operate.



Figure 22.36 (a) 5.5 MW Kirchstockach geothermal power plant, Germany [43a] /WWW].

22.4.7 HABANERO, INNAMINCKA, AUSTRALIA

Australia's southeastern sector could become a resource for EGS development. It is an area currently devoid of any overt manifestations of natural geothermal activity, but has deep hot rocks that have been shown by drilling to be water-saturated. The reservoirs also are highly overpressured by about a factor of two relative to hydrostatic conditions at the depths of 4000–5000 m.

The region evolved over the last 350 million years beginning with an uplift of molten magma that solidified into a granite mass roughly $20 \text{ km} \times 50 \text{ km}$ in areal extent. The stages in the evolution are depicted schematically in Figure 22.37.

Weathering, glaciation, and sedimentary deposition left a high-temperature, partially fractured, water-saturated body of granite isolated from the surface by impermeable, highly altered sedimentary layers. Radiogenic decay of uranium, thorium, and potassium in the granite has maintained the rock at an elevated temperature. Owing to the 250°C nominal rock temperature, the thermal gradient is about $60^\circ\text{C}/\text{km}$, roughly double the average normal value. The last important aspect relates to the regional stress field that switched from extensional to compressive, helping to create fractures in the granite.

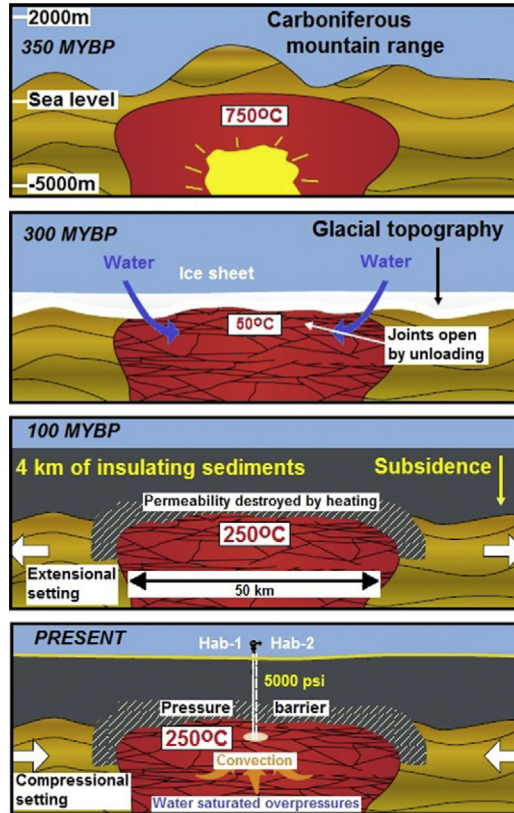


Figure 22.37 Geological evolution of Cooper Basin, Australia [52] [WWW].

This resource has been studied and researched through drilling by Geodynamics Ltd. (GDY), a company formed in 2000 specifically to exploit this resource. Early business plans from 2003 were aggressive and envisioned the building of a commercial demonstration EGS power plant in 2006 and a large-scale base-load plant by the end of 2007. However, numerous drilling problems have disrupted the development despite much excellent work in understanding the unique characteristics of the potentially valuable but exceedingly challenging resource.

The first well, intended as an injection well, Habenero-1 (Hab-1), was drilled and completed to a depth of 4421 m in October 2003 at a site 8 km south of the small community of Innamincka in the state of South Australia, just west of the border with Queensland. The well confirmed the high temperatures that were expected, about 250°C , but this well also discovered the overpressured nature of the formation, along with the surprising presence of water in the fractures of the granite. The geofluid was at 750 bar in the formation. The developers had anticipated a true HDR project but found that the well flowed on its own. In 2004, Hab-1 was massively stimulated to create a very large fracture zone, actually seven

times greater than anticipated. [52]. Further stimulation in 2005 extended the fracture volume to cover an area of about 4 km^2 , based on acoustic emissions. The total fractured volume, in the shape of an elliptical pancake, was estimated at 1 km^3 .

The second well, Hab-2, a production well, was drilled and completed in December 2004 to a depth of 4359 m. In May 2005, high temperature geofluid flowed to the surface in the first such demonstration in Australia. However, Hab-2 would be plagued by problems caused by well obstructions in the deep fracture zone that could not be retrieved, and which led, after several failed attempts at side-tracking, to its abandonment. The difficulty in drilling was caused by the combination of high temperature and high pressure in the fracture zones.

A new production well, Hab-3, was drilled in 2007 with a new, more robust rig to a depth of 4221 m into the stimulated fracture zone created by Hab-1. The two wells were in immediate communication as evidenced by pressure readings on Hab-1. Hab-3 had an open hole with a diameter of 8–1/2" to promote a higher flow rate. A circulation flow test between Hab-1 and -3 showed a mass flow of 27 kg/s, essentially the minimum required for a demonstration plant.

A distinctive 1 MW binary plant was built to operate with the Hab-1/Hab-3 doublet and to supply free electricity to Innamincka; see Figures 22.38–22.40.

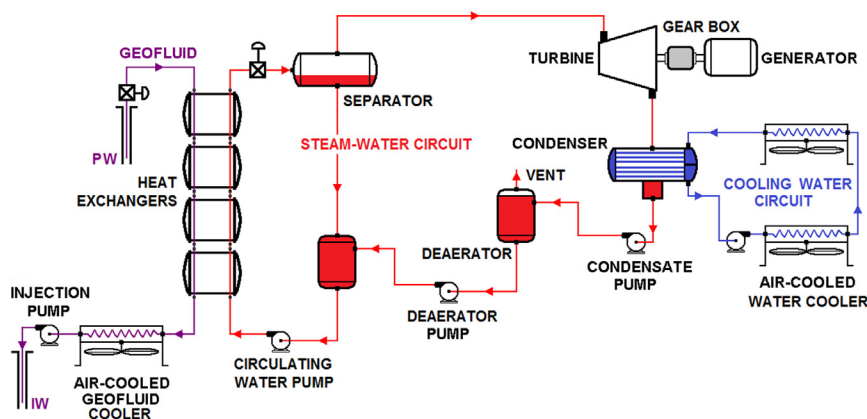


Figure 22.38 Flow diagram for 1 MW Habanero EGS power plant. After Ref. [52a] [WWW].

This plant is not a typical EGS-type of plant. All others are binary plants that use moderate-temperature geofluids as heating media for low-boiling-point working fluids. Here pure water is used in a Rankine cycle that has elements usually found in conventional fossil-fueled power plants. The reasons for this design stem from the characteristics of the geofluid and from the financial situation of the company developing the project. The geofluid pressure is extraordinarily high for a geothermal resource, namely, 350 bar which is much higher than the steam inlet pressures at advanced fossil-fueled power plants.



Figure 22.39 Turbine and associated equipment at the 1 MW Habanero power plant, Innamincka, Australia. *Photo courtesy of Geodynamics Ltd [WWW].*

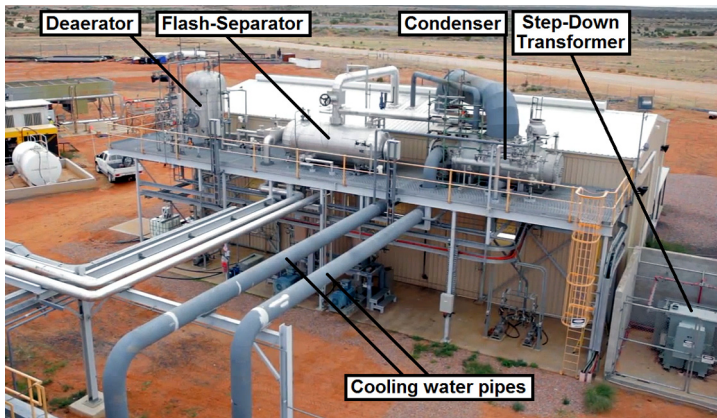


Figure 22.40 Exterior view of Habanero power plant. Step-up transformer is just to the right. *Photo courtesy of Geodynamics Ltd.; labels by author [WWW].*

Another difficulty in implementing the power plant at Innamincka is that the extremely high reservoir pressure of 750 bar dictated a very high pressure for the reinjection process. Since the surface pressure of the brine is 350 bar, the reinjection pumps must raise the pressure to about 450 bar to force it back into the formation. The seals on commercially available pumps could not withstand these pressures and no supplier could initially be found for the reinjection pumps. A development program resulted in serviceable pumps for the operational tests.

The developers found that a new plant would be prohibitively expensive and opted for used surplus equipment from a steam power plant. The geofluid was

passed through a train of four heat exchangers in which pure water was heated and boiled while the geofluid was cooled. It was further cooled prior to being reinjected into the formation. Since water is a scarce commodity in the dry region of Innamincka, a closed cooling water circuit was used to supply the steam condenser. Air coolers that had been used during flow tests were repurposed for the cooling tasks in the new plant.

Finally after surmounting these difficulties, the plant was completed and tested, and was ready to be commissioned when disaster struck. The new production well, Hab-3, experienced a “well control incident,” that is, it suffered a blowout. This occurred on April 24, 2009, late in the evening, only days before the hot commissioning of the 1 MW demonstration plant [53]. A loud noise was heard followed by the discharge of steam and water from the area around the wellhead; see Figure 22.41. It took 28 days to bring the well under control with cement plugs, during which time the well discharged geofluid to the surface unabated.



Figure 22.41 Habanero-3 discharging water and steam after blowout on April, 24, 2009. *Courtesy of Geodynamics Ltd., best available photo [53] [WWW].*

Analysis pointed to failed steel casings under corrosive attack by the geofluid in the form of hydrogen embrittlement from the dissolved gases in the brine, exacerbated by the high temperature and pressure. Since Hab-1 and -2 were cased with the same materials, both of them were plugged as a precaution, leaving the Innamincka site with no wells to serve the power plant. Further analysis showed that the geofluid would cause corrosion in the surface equipment and stibnite (or antimonite) deposition was also observed. This crystalline substance would cause severe problems in heat exchanger tubes and would need to be periodically cleaned during the test runs of the power plant.

Despite these serious issues, a new deep well, Hab-4, was drilled in 2012 near the original three wells. It has a depth of 4204 m and a bottom-hole temperature of 242°C [53a]. Hab-4 was flow tested and found capable of flowing 40 kg/s in open flow (not reinjected to the formation) at wellhead temperatures as high as 213°C. This allowed the well to provide fluid to the power plant. The original exploration well, Hab-1, was rehabilitated as an injection well, albeit a poor one that could only accept 15–19 kg/s owing to an obstruction in the well. The plant underwent shakedown runs from February to April 2013, and was commissioned on April 30, 2013, and on May 2 it officially produced the first EGS electricity in Australia. In June it operated in stand-alone mode without the need for auxiliary diesel power. After a generally successful test run, the plant was shut down on October 7, 2013 [52a], thus ending a 10-year effort to develop this resource. As of 2014, the project has been put on indefinite hold while Geodynamics refocuses its attention on conventional hydrothermal prospects in the islands of the South Pacific.

Throughout the operating period, the power generated was dissipated in a load bank at the plant, rather than being delivered to Innamincka. The power output was limited by the rate at which spent fluid could be reinjected. The plant could run in a self-sustaining manner (no net power) while receiving and reinjecting 17 kg/s, i.e., the generator could just meet the parasitic load of roughly 650 kW. When 2.5 kg/s of spent brine were diverted to a holding pond, while 16.5 kg/s were reinjected, then the plant generated a net power output of 150 kW. Geodynamics Ltd. calculated that if the circulating brine loop could handle 40 kg/s, about 2.5 MW (net) could be produced with an appropriately sized power plant [52a]. As of 2014, the Habanero pilot plant appears more likely to be used for heat supply than electricity generation, in conjunction with natural gas developments in the area [54].

One of the important lessons learned from this project is that the permeability of the formation is associated with a preexisting, near-horizontal fault through which all four wells had passed, but that the hydrofracking had failed to produce the desired extension of the permeable zone.

Meanwhile, Geodynamics Ltd. explored other sites in the vicinity and drilled two other wells: Jolokia 1 in 2008 to 4911 m and 279°C, and Savina 1 in 2009 to 3700 m before suspending operations [55]. While it was still pursuing the deep EGS program, Geodynamics Ltd. decided to embark on a “shallows” program aimed at exploiting the hot sedimentary aquifers that are only 2000–3000 m deep. These formations do not require massive stimulation and fracture creation, but contain fluids at lower temperatures than the deep formation, about 135–150°C. However, in 2013, it was announced that the “shallows” program had been discontinued.

Finally, by the close of 2014, Geodynamics Ltd. shifted its focus from EGS to conventional hydrothermal resources, focusing on exploration projects on islands in the South Pacific, the first two of which are Savo Island (Solomon Islands) and at Takara on Efate Island (Vanuatu), while broadening its scope of interest to

clean energy and energy services. At the same time, the political climate changed in Australia, leading Geodynamics Ltd. to conclude that renewable energy projects in the country now face “an environment hostile to investment” [55a].

22.5 Proposed Projects

22.5.1 GERMANY

The geothermal industry in Germany is currently being stimulated by the generous feed-in tariff provided by the federal government of €0.15/kWh (\$0.19/kWh) for electricity generated by geothermal energy. There are three areas that are suitable for low-temperature binary cycle applications including the North German Basin, NGB (e.g., Neustadt-Glewe), the URG (e.g., Landau), and the MB, in the south (e.g., Unterhaching). Not including the 24 large hydrothermal district heating plants now in operation, there are several electric power projects in progress or under consideration. These include, but are not limited to the following: Taufkirchen (MB), Kirchweidach (MB), and Brühl (NGB).

As was mentioned earlier, geofluids from the URG and NGB tend to be highly mineralized having TDS concentrations two to seven times greater than seawater, whereas geofluids from the MB are very clean. A research facility has been installed at Groß Schönebeck to study means of coping with the high-TDS, high-NCG geofluids in the NGB; see Figure 22.42. It includes three small, water-cooled binary units (140, 330, and 550 kW) that can operate in various combinations [56]. The state of Germany’s geothermal power plants at the end of 2014 may be found in Appendix A.7.



Figure 22.42 Three power modules at Groß Schönebeck, Helmholtz Centre Potsdam of the GFZ German Research Centre for Geosciences. *Photo from GFZ web site [56] [WWW].*

22.5.2 UNITED STATES

There was an aborted attempt to stimulate an old, unproductive well at The Geysers field in California by AltaRock Energy, Inc. (AltaRock). The project was canceled because the formation was so porous and “mushy” that it could not be drilled, let alone stimulated. A few other efforts were made on the fringes of commercial geothermal fields, such as Coso in California and Desert Peak in Nevada, but these have not been particularly successful.

Currently the main area for an EGS project is the Newberry Volcano in Oregon, about 32 km (20 mi) south of Bend. AltaRock is also the developer for Newberry, but as a partner with Davenport Newberry [57,58]. This is a basic research project aimed at demonstrating that stimulation techniques used elsewhere can be adopted and adapted to US fields. The developers plan to use a method called “hydraulic shearing” or “hydroshearing” instead of hydrofracking to minimize the risk of induced seismicity. There are five goals for the project:

1. Demonstrate current technology and advances in EGS by:
 - a. Stimulating at least three fracture zones in a single well
 - b. Demonstrating diverter technology for multiple zone stimulation
 - c. Demonstrate single-well test methods to assess productivity after stimulation
2. Drill two production wells into a newly created EGS reservoir
3. Produce economic quantities of fluid per production well
4. Establish circulation through a three-well system (a triplet)
5. Develop a conceptual model of the complete EGS system.

Newberry Volcano is classified as a shield volcano, being made up of hundreds of small vents clustered on a raised mound landform. It is one of the largest and youngest volcanoes in the United States. The area is a well-known geothermal anomaly, having been estimated to potentially yield 740 MW for 30 years by the US Geological Survey. In fact in 1995, CalEnergy drilled four wells, two of them deep, very near the site currently being investigated. The two deep wells encountered high temperatures, approximately 315°C, and flowed for about four hours each after being stimulated by nitrogen injection. But the permeability was extremely low and the site was deemed noncommercial [59].

Funding for the project includes a grant of \$21.45 million from the US American Reinvestment and Recovery Act and \$22.36 million from the AltaRock–Davenport Partnership. The project is being subjected to intense scrutiny by the environmental community in light of the European experiences with induced seismicity. Extraordinary precautions are in place whenever any stimulation of the formation is under way. The test site lies about 15 km (9 mi)

east of the small community of Pinecrest and about 20 km (12 mi) from the town of La Pine. The Paulina Lake Lodge lies 3 km (1.9 mi) southeast of the injection well site. The future of EGS projects in the United States is probably riding on the success or failure of the Newberry Volcano project.

The unique feature of AltaRock's approach (which is patented) is to use a thermal- and biodegradable filler material that allows a length of the well to be temporarily sealed off while a deeper length of well is stimulated. This process can be repeated as many times as the geometry of the well allows. The chemical nature of the filler will be matched to the reservoir rock conditions, and the particulate material will be ground to a size appropriate for the preexisting fractures in the rock.

At the end of the hydroshearing process, the well is shut in and allowed to reheat. The filler material dissolves in the hot water within the fractures, and once the well is allowed to flow, the dissolved material comes to the surface where it can be controlled and disposed of. Thus the plan is to create a long, high permeability section of the well, as contrasted with only one or two thin layers with high permeability typical of normal stimulation techniques. If the hydroshearing stimulation process can create fractures of significant length into the formation away from the well, it may be possible to engineer a large volume of fractured rock that could be penetrated by other wells and used to form a connected network of injection and production wells. This has always been the goal of EGS but has yet to be achieved in any way approaching commercial status. Whether or not this can be accomplished by AltaRock's method, this novel approach still may be useful to enhance the permeability of existing wells now serving conventional geothermal power plants.

References

- [1] Thorsteinsson H, Augustine C, Anderson BJ, Moore MC, Tester JM. The impacts of drilling and reservoir technology advances on EGS exploitation. Proceedings of the 33rd workshop on geothermal reservoir engineering. Stanford University, Stanford, CA; 2008, SGP-TR-18.
- [2] Duchane DV. Hot dry rock development program: progress report, fiscal year 1993. LA-12903-PR, Los Alamos National Laboratory, Los Alamos, NM; 1995.
- [3] Tester JW, Brown DW, Potter RM. Hot dry rock geothermal energy—a new energy agenda for the 21st century. LA-11514-MS, Los Alamos National Laboratory, Los Alamos, NM; 1989.
- [4] Brown DW. 1995 Reservoir flow testing at Fenton Hill, New Mexico. Proceedings of the 3rd international HDR forum, Santa Fe, NM; 1996. p. 34–7.
- [5] Batchelor AS. The stimulation of a hot dry rock geothermal reservoir in the Cornubian granite, England. Proceedings of the 8th workshop on geothermal reservoir engineering, Stanford, CA; 1982. p. 237–48.
- [6] Tester JW, Anderson BJ, Batchelor AS, Blackwell DD, DiPippo R, Drake EM, et al. ISBN 0-615-13438-6, <<http://geothermal.inel.gov>> The future of geothermal energy: impact of enhanced geothermal systems (EGS) on the United States in the 21st century. Cambridge, MA: Massachusetts Institute of Technology; 2006

- [7] Batchelor AS. Hot dry rock and its relationship to existing geothermal systems. Proceedings of the Camborne School of Mines international hot dry rock conference, Robertson Scientific Publications, ISBN 1-85365-217-2; 1989. p. 13–29.
- [8] Rosemanowes quarry. Wikipedia, <http://en.wikipedia.org/wiki/Rosemanowes_Quarry>.
- [9] Matsunaga I, Niitsuma H, Oikawa Y. Review of the HDR development at Hijiori site, Japan. Proceedings of the world geothermal congress 2005, paper 1635, Antalya, Turkey; 2005.
- [10] Xu T, Kaieda H, Ueda A, Sugiyama K, Ozawa A, Wan Y, et al. Fluid–rock interactions in enhanced geothermal systems with CO₂ as working fluid: modeling of geochemical changes induced by CO₂ injection into the Ogachi (Japan) EGS site. *Geothermal Resour Counc Trans* 2010;34:497–502.
- [11] Vuataz F-D. Hijiori hot dry rock project, northern Japan. Steinmaur, Switzerland: Swiss Deep Heat Mining Project; 2004.
- [12] NEDO. Development of a hot dry rock power generation system. Kanagawa, Japan: New Energy and Industrial Technology Development Organization; 2004.
- [13] Yamaguchi T, Hiwaki N, Abe T, Oikawa Y. 90-Day circulation test at Hijiori HDR test site. *Geothermal Resour Counc Trans* 1992;16:417–22.
- [14] Tenma N, Yamaguchi T, Tezuka K, Oikawa Y, Zyvoloski G. Comparison of heat extraction from production wells in the shallow and the deep reservoirs at the Hijiori HDR test site using Fehm code. Proceedings of the 26th workshop on geothermal reservoir engineering, Stanford, CA; 2001, SGP-TR-168.
- [15] Kruger P, Karasawa H, Tenma N, Kitano K. Analysis of heat extraction from the Hijiori and Ogachi HDR geothermal resources in Japan. Proceedings of the world geothermal congress 2000, International Geothermal Association, 2000, p. 2677–82.
- [16] Kawasaki K, Oikawa Y, Sato Y, Tenma N, Tosha T. Heat extraction experiment at Hijiori test site (first year). Proceedings of the 27th workshop on geothermal reservoir engineering, Stanford, CA; 2002, SGP-TR-171.
- [17] Yanagisawa N. Ca and CO₂ transport and scaling in the Hijiori HDR system, Japan. Proceedings of the world geothermal congress 2010, paper 3123, Bali, Indonesia; 2010.
- [18] Hori Y, Kitano K, Kaieda H. Outline of Ogachi project for HDR geothermal power in Japan. *Geothermal Resour Counc Trans* 1994;18:439–43.
- [19] Kaieda H, Ito H, Suenaga H, Kusunoki K, Suzuki K, Kiho K, et al. Review of the Ogachi HDR project: search for water flow paths in HDR reservoir. *Geothermal Resour Counc Trans* 2002;26:225–8.
- [20] Ueda A, Kuroda Y, Sugiyama K, Ozawa A, Kaieda H, Kaji Y, et al. CO₂ sequestration into hydrothermal system at Ogachi HDR site. Proceedings of the world geothermal congress 2010, paper 3703, Bali, Indonesia; 2010.
- [21] Pruess K. Enhanced geothermal systems (EGS) using CO₂ as working fluid—a novel approach for generating renewable energy with simultaneous sequestration of carbon. *Geothermics* 2006;35:351–67.
- [22] Häring MO, Hopkirk RJ. The Swiss deep heat mining project—the Basel exploration drilling. *GeoHeat Center Bulletin*, Oregon Institute of Technology, Klamath Falls, OR; 2002. p. 31–3.
- [23] Hopkirk RJ. Annual report for 2002 on the Swiss participation in the GIA—the IEA geothermal implementing agreement; includes the tasks undertaken by the chairman of the executive committee and progress in annex III (Hot Dry Rock). IEA; 2002.
- [24] Häring MO, Ladner F, Schanz U, Spillmann T. Deep Heat Mining Basel, preliminary results. Geothermal Explorers Ltd, Schlossstrasse 3, CH-4133 Pratteln, Switzerland; 2007.
- [25] Hopkirk RJ, Häring MO. The Swiss deep heat mining programme: activities & perspectives. Engine launching conference, BRGM, Orléans, France; 2006.

- [26] Ladner F, Häring MO. Hydraulic characteristics of the Basel 1 enhanced geothermal system. *Geothermal Resour Counc Trans* 2009;33:.
- [27] Hopkirk RJ, Häring MO. The Swiss deep heat mining programme: activities & perspectives. Presentation slides, engine launching conference, BRGM, Orléans, France; 2006.
- [28] Wikipedia. Induced Seismicity in Basel, <http://en.wikipedia.org/wiki/Induced_seismicity_in_Basel>; 2010.
- [29] Brutschin C, Hofer J. Geothermal project “Deep Heat Mining Basel” cannot be resumed. Dept. of Economics, Society and Environment for Basel-Stadt, Basel, Switzerland, 2009 (in German), <<http://www.bs.ch/mm/showmm.htm?url52009-12-10-wsd-001.htm>>.
- [30] Häring MO, Schanz U, Ladner F, Dyer BC. Characterisation of the Basel 1 enhanced geothermal system. *Geothermics* 2008;37:469–95.
- [31] Hettkamp T, Baumgärtner J, Baria R, Gérard A, Gandy T, Michelet S, et al. Electricity production from hot rocks. Proceedings of the 29th workshop on geothermal reservoir engineering, Stanford University, Stanford, CA; 2004, SGP-TR-175.
- [32] Cuenot N, Frogneux M, Dorbath C, Calo M. Induced microseismic activity during recent circulation tests at the EGS site of Soultz-Sous-Forêts (France). Proceedings of the 36th workshop on geothermal reservoir engineering, Stanford University, Stanford, CA; 2011, SGP-TR-191.
- [33] Special Issue: The deep EGS (enhanced geothermal system) project at Soultz-Sous-Forêts (Alsace, France). *Geothermics* 2006;35:473–710.
- [33a] Ledéserf BA, Hébert RL. The Soultz-sous-Forêts’ enhanced geothermal system: a granitic basement used as a heat exchanger to produce electricity, Chapter 18. In: Mitrovic J, editor. Heat exchangers—basics design applications. InTech; 2012, <<http://cdn.intechopen.com/pdfs/30777.pdf>>.
- [34] Genter A, Evans KF, Cuenot N, Fritsch D, Sanjuan B. Contribution of the exploration of deep crystalline fractured reservoir of Soultz to the knowledge of enhanced geothermal systems (EGS). *C R Geosci* 2010;342:502–16.
- [35] Genter A, Fritsch D, Cuenot N, Baumgärtner J, Graff J-J. Overview of the current activities of the European EGS Soultz Project: from exploration to electricity production. Proceedings of the 34th workshop on geothermal reservoir engineering, Stanford University, Stanford, CA; 2009, SGP-TR-187.
- [36] Cuenot N, Faucher J-P, Fritsch D, Genter A, Szablinski D. The European EGS project at Soultz-sous-Forêts: from extensive exploration to power production. Engine report; 2008.
- [37] Schneider H, Seibt P, Menzel H. Hydrogeothermal energy use—the example of the Neustadt-Glewe geothermal plant, Germany. Proceedings of the European geothermal conference Basel ’99, vol. 2, Basel, Switzerland; 1999.
- [38] Schellschmidt R, Sanner B, Jung R, Schulz R. Geothermal energy use in Germany. Proceedings of the European geothermal congress 2007, Unterhaching, Germany; 2007.
- [39] BINE Information Service. Geothermal electricity generation in Neustadt-Glewe. Bonn, Germany; 2009.
- [40] EGEC—European Geothermal Energy Council, K4RES-H, key issue 5: innovative applications. Combined Geothermal Heat and Power Plants (CHP); 2005.
- [41] Broßmann E, Koch M. First experiences with the geothermal power plant in Neustadt-Glewe (Germany). Proceedings of the world geothermal congress 2005, paper 1316, Antalya, Turkey; 2005.
- [42] Funke T. ORC power plant Neustadt-Glewe: operational experience since 2004. Presentation at electricity generation, combined heat and power, Strasbourg; 2006.
- [43] Köhler S. Analysis of the combined heat and power plant Neustadt-Glewe. Proceedings of the world geothermal congress 2005, paper 1309, Antalya, Turkey; 2005.

- [43a] Weber J, Ganz B, et al. Geothermal energy use in Germany. Proceedings of the world geothermal congress 2015, Melbourne, Australia; 2015.
- [44] Schönwiesner-Bozkurt C. Geothermal energy pilot project Unterhaching, Germany. Presentation, Strasbourg; 2006.
- [45] BINE Information Service. Geothermal electricity generation in Landau, <<http://www.bine.info/en/hauptnavigation/topics/renewable-energy-sources/geothermal-energy/publikation/geothermischestromerzeugung-in-landau/?artikel5221>>; 2007.
- [46] Schindler M, Baumgärtner J, Gandy T, Hauffe P, Hettkamp T, Menze H, et al. Successful hydraulic stimulation techniques for electric power production in the Upper Rhine Graben, Central Europe. Proceedings of the world geothermal congress 2010, paper 3163, Bali, Indonesia; 2010.
- [47] The Local: Germany's New in English. Geothermal plant likely cause of earthquakes, <<http://www.thelocal.de/sci-tech/20101208-31671.html>>; 2010.
- [48] Imolauer K. Geothermal project Unterhaching & risk management. Presentation, Asian-Pacific Berlin Week; 2009.
- [49] Wolfgramm M, Bartels J, Hoffmann F, Kittl G, Lenz G, Seibt P, et al. Unterhaching geothermal well doublet: structural and hydrodynamic reservoir characteristic, Bavaria (Germany). Proceedings of the European geothermal congress 2007, Unterhaching, Germany; 2007.
- [50] Rubner J. Test facilities—solar and geothermal power plants: power from heaven and earth. Siemens, Research & Development, <http://www.siemens.com/innovation/en/publikationen/publications_pof/pof_fall_2007/solar_and_geothermal_power_plants.htm>; 2007.
- [51] Bruchsal Germany 600 kW Kalina Cycle Euler Turbine. Emergent Corporation, Santa Ana, CA, <<http://www.emergent.net/documents/bruchsal.pdf>>; 2011.
- [52] Annual Report 2006. ABN 55 095 006 090, Geodynamics Ltd., Milton, Queensland, Australia, 2006, p. 18–9.
- [52a] Mills T, Humphreys B. Habanero pilot project—Australia's first EGS power plant. Proceedings of the Australian geothermal energy conferences 2013, Brisbane, Australia; 2013.
- [53] Annual Report 2009. ABN 55 095 006 090, Geodynamics Ltd., Milton, Queensland, Australia, 2009, p. 8.
- [53a] 1 MW Habanero pilot plant virtual tour. Geodynamics Ltd., Milton, Queensland, Australia, <<http://www.geodynamics.com.au/Resource-Centre/Our-Videos.aspx>>.
- [54] 2013 Annual general meeting shareholder presentation. Geodynamics Ltd., Milton, Queensland, Australia; November 28, 2013.
- [55] Quarterly report, period ending 31 March 2011. Geodynamics Ltd., Milton, Queensland, Australia, p. 4–5.
- [55a] Spence K. Chairman's address to shareholders. Geodynamics Ltd. 2014 Annual General Meeting, Brisbane, Australia; 2014.
- [56] Huenges E. Geothermal research platform Groß Schönebeck. Helmholtz Centre Potsdam, GFZ German Research Centre for Geosciences, <<http://www.gfz-potsdam.de/en/scientific-services/laboratories/gross-schoenebeck/picture-gallery/>>.
- [57] Newberry EGS enhanced geothermal systems demonstration. Poster, Alta Rock Energy, Inc., Seattle, WA, <<http://www.altarockenergy.com/>>.
- [58] AltaRock Energy and Davenport Newberry to demonstrate innovative geothermal technology, Press Release, AltaRock Energy, Inc., <<http://www.newberrygeothermal.com/index.htm>>; 2010.
- [59] Spielman PB, Finger JT. Well test results of exploration drilling at Newberry Crater, Oregon in 1995. Proceedings of the twenty-second workshop on geothermal reservoir engineering, SGP-TR-158, Stanford University, Stanford, CA; 1998.



Chapter 23

Environmental Impact of Geothermal Power Plants

Chapter Outline

23.1 Overview	658
23.2 Regulations	658
23.3 General Impacts of Electricity Generation	659
23.4 Environmental Advantages of Geothermal Plants	660
23.4.1 Gaseous Emissions	660
23.4.2 Land Usage	663
23.4.3 Solids Discharge	667
23.4.4 Water Usage	668
23.4.5 Water Pollution	669
23.5 Environmental Challenges of Geothermal Plants	670
23.5.1 Land Subsidence	670
23.5.2 Induced Seismicity	673
23.5.3 Induced Landslides	674
23.5.4 Noise Pollution	676
23.5.5 Disturbance of Natural Hydrothermal Manifestations	677
23.5.6 Disturbance of Wildlife Habitat, Vegetation, and Scenic Vistas	678
23.5.7 Catastrophic Events	680
23.5.8 Thermal Pollution	680
23.6 Summary	681
References	682

While offering no detailed challenge to the proposition that beauty is in the eye of the beholder, I do insist that the Wairakei borefield ranks high in New Zealand's superb hierarchy of visual delights. If a tramper on Highway 1 were to pause at dusk 8 km north of Taupo on a moist day with a stiff breeze, he would see an eerie scene of haunting beauty. Scores of fleecy plumes are skyward only to be seized and devoured by green demons that haunt the boughs of imperial conifers;

bundles of silvery bullwhips, cracked by an invisible giant who lurks behind the western hill, are caught in stop-action as they rise and fall in unison. It is an odd amalgam of technology and nature, of the Tin Woodsman of Oz and the Sorcerer's Apprentice, gently underscored by the whispering, slightly syncopated "whuff-whuff . . . whuff . . . whuff" of the wellhead silencers.

Robert C. Axtmann—1975

23.1 Overview

At various points throughout this book (e.g., in Sections 5.7, 6.7, 7.6, and 8.6), and in the case studies, some of the environmental effects of geothermal power plant operations have been discussed in the context of the subject at hand. This concluding chapter aims to present a comprehensive picture of the environmental advantages offered by geothermal power plants as well as their possible detrimental effects.

Certain environmental impacts associated with the development of geothermal sites and the operation of plants are inevitable. However, under normal conditions they are generally confined to the immediate vicinity of the plant and are of lesser impact than those of other electric power generation technologies, particularly those using carbon-based fossil fuels and nuclear fuels.

There have now been more than one hundred years of experience in developing geothermal fields, and in building, operating, upgrading, and even decommissioning geothermal plants of various types. In the earliest days, drilling of wells could be a hazardous undertaking and the behavior of geothermal reservoirs was mysterious. Early developers and operators learned by doing, and eventually a scientific understanding of the nature of the resource evolved. Along with this came the technology of how best to exploit geothermal energy and how to deal with the potential environmental impacts.

This chapter is loosely based on Chapter 8 of Tester et al. [1], much of which was written by the author. Besides this source, the reader may wish to consult Refs. [2–11] for further information.

23.2 Regulations

Most countries have laws that regulate the construction and operation of power plants with the intent of preserving the natural environment and safeguarding the health and well-being of people as well as the flora and fauna of the region. The United States has federal, state, and local regulations that cover a broad range of possible environmental impacts. Being subject to these regulations means that geothermal power plants must be built and designed so as to minimize, if not

eliminate, all possible adverse environmental impacts. The following laws and regulations must be adequately addressed before any geothermal project can be completed [1,8]:

- Clean Air Act
- National Environmental Policy Act
- National Pollutant Discharge Elimination System Permitting Program
- Safe Drinking Water Act
- Resource Conservation and Recovery Act
- Toxic Substance Control Act
- Noise Control Act
- Endangered Species Act
- Archeological Resources Protection Act
- Hazardous Waste and Materials Regulations
- Occupational Health and Safety Act, and
- Indian Religious Freedom Act.

The comprehensive spectrum of impacts covered in this list practically ensures that no geothermal power plant will be a threat to the environment anywhere in the United States. Although there are no uniform international standards regarding the environmental impact of geothermal plants, it is common for most countries to require that plants meet appropriate environmental regulations; see, e.g., Refs. [12–15].

23.3 General Impacts of Electricity Generation

The list of possible environmental impacts from any kind of electricity-generating power plant is long. Most of the items shown below apply to all power plants, but all of them apply to geothermal plants in varying degrees:

- Gaseous emissions to the atmosphere
- Water pollution
- Solids emissions to the surface and the atmosphere
- Noise pollution
- Land usage
- Land subsidence
- Induced seismicity
- Induced landslides
- Water usage
- Disturbance of natural hydrothermal manifestations
- Disturbance of wildlife habitat and vegetation
- Alteration of natural vistas, and
- Catastrophic events.

Of these some are of serious concern for geothermal plants. Abatement technology is available and usually deployed to mitigate the most potentially harmful impacts. Compared with other types of power plants, geothermal plants hold significant advantages for many of these impacts. In the sections that follow, it will be seen that geothermal plants are relatively benign in the areas of atmospheric emissions, particularly with regard to “greenhouse gases,” land usage, solids emissions, water usage, and water pollution. Although they are rarely encountered, land subsidence and induced seismicity can have serious consequences. Matters relating to noise abatement, assuring personnel safety, avoiding catastrophic events, and preserving natural thermal features and vistas all deserve the power plant developer’s attention.

23.4 Environmental Advantages of Geothermal Plants

There is great concern worldwide about atmospheric emissions of carbon dioxide, CO_2 , owing to its heat-trapping properties and the fear of its effect on the global climate. Geothermal power plants have very low gaseous emissions, albeit most of which is CO_2 , on a per MWh-generated basis, when compared with all other power generation technologies that emit CO_2 as a normal part of operation. Geothermal binary plants normally emit no gases at all. Using the same basis of comparison, geothermal plants use much less land than any other type of power plant. With one notable exception, geothermal fluids used in power plants are fairly innocuous chemically and pose little hazard in terms of solids pollution. Reinjection of waste brines from geothermal plants avoids contamination of surface and groundwater aquifers. Thus, taken in broad scope, geothermal power plants are one of the most, if not the most, environmentally benign sources of electrical power.

23.4.1 GASEOUS EMISSIONS

Gaseous emissions from dry- and flash-steam geothermal plants stem from the noncondensable gases (NCG) that are carried in the geofluid in dissolved form. Unless the NCG are removed upstream of the turbine (which is currently not done in commercial plants), the NCG will accumulate in the condenser, thereby raising the backpressure on the turbine. This will cause a significant reduction in turbine power output. With reference to Figure 5.9, as the condenser pressure rises, so does the condensing temperature, thereby elevating the line 6–7. This causes the enthalpy of state 5 to increase and reduces both the enthalpy drop across the turbine and the power output. For this reason, the NCG are removed from the condenser by some means (e.g., steam-jet ejectors, vacuum pumps,

turbo-compressors; see Figures 5.6, 6.6, 7.10, 11.14, and 11.15). This comes at the expense of some steam or power, but always results in a higher net power than if the NCG were left to accumulate.

Carbon dioxide and hydrogen sulfide, H_2S , are the most common and prominent NCG in geothermal steam, but gases such as methane, hydrogen, sulfur dioxide, or ammonia can also be found, usually in very low concentrations. Currently it is not required to capture or treat CO_2 , but H_2S is strictly regulated in the United States owing to its offensive odor at very low concentrations, 30 parts per billion, and to its toxicity at higher levels [7]. If necessary, the NCG can be chemically treated or scrubbed after removal from the condenser to remove the H_2S . It is also possible to compress the NCG, redissolve them into the waste brine, and inject them back into the reservoir. This latter approach, however, may lead to an increase in the NCG concentration in the geofluids coming from the production wells. In the case of binary plants, where the brine is produced in the liquid phase with the NCG still in solution, the NCG remain in solution throughout the heat transfer processes and return to the reservoir with the waste brine during reinjection.

In an attempt to control global warming, rules and regulations are being discussed around the world that would penalize plants that emit carbon into the atmosphere. One approach would place a “cap” on carbon emissions for power plants; another would institute a “carbon tax” on emissions. However, currently there are no restrictions on the discharge of CO_2 from power plants. Geothermal binary plants emit no CO_2 whereas steam and flash plants emit much less CO_2 per MWh generated than do fossil-fueled plants. Having no, or relatively low, CO_2 emissions, geothermal plants should be in a favorable position if and when some type of restriction is placed on the emissions of carbon. If a “carbon tax” were to be implemented, the cost to generate a kilowatt-hour of electricity from fossil-fueled plants would be affected far more than less polluting technologies, such as geothermal. Under a program of “carbon emission credits,” geothermal power plants could gain an additional revenue stream by selling carbon credits in a trading market.

With regard to the US-regulated pollutants, nitrogen oxides, NO_x , and sulfur dioxide, SO_2 , geothermal steam and flash plants emit negligible amounts. Table 23.1 shows a comparison of gaseous emissions from typical geothermal plants with other types of power plants [8]. It is worth noting that the NO_x and SO_2 emissions at The Geysers only result from the method used to treat H_2S in the NCG, namely, a combustion process that oxidizes the H_2S in a few of the units. Most geothermal steam plants do not rely on combustion for H_2S abatement and therefore emit no NO_x at all.

The amounts of CO_2 and H_2S that could theoretically be emitted are shown in Figures 23.1 and 23.2 as functions of their concentrations in the NCG and of the

TABLE 23.1 Gaseous emissions from various power plants [8].

Plant type	CO ₂ , kg/MWh	SO ₂ , kg/MWh	NO _x , kg/MWh	Particulates, kg/MWh
Coal-fired steam plant	994	4.71	1.955	1.012
Oil-fired steam plant	758	5.44	1.814	NA
Gas turbine	550	0.0998	1.343	0.0635
Hydrothermal—flash-steam	27.2	0.1588	0	0
Hydrothermal—The Geysers dry-steam	40.3	0.000098	0.000458	Negligible
Hydrothermal—closed loop binary	0	0	0	Negligible
EPA average, all US plants	631.6	2.734	1.343	NA

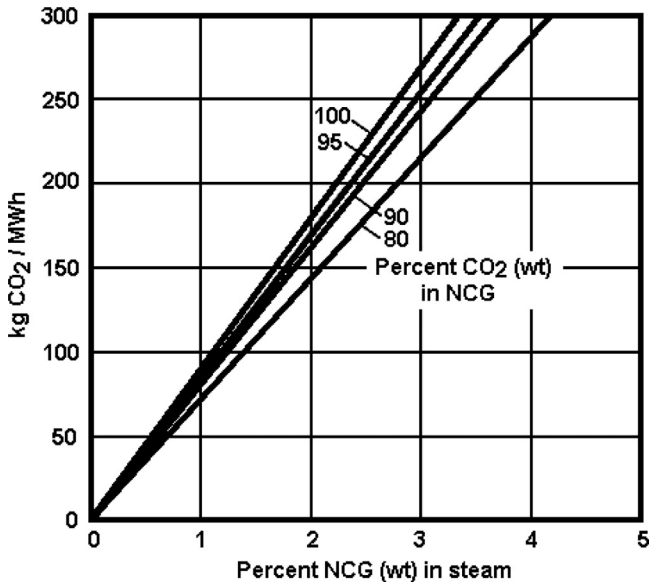


Figure 23.1 Potential unabated carbon dioxide emissions (kg/MWh) for various concentrations of CO₂ in the NCG as a function of the concentration of NCG in the steam [6].

concentration of the NCG in the steam [6]. Since typical NCG concentrations range from 0.5% to 1.0% (wt) of steam, with CO₂ constituting about 95% of the NCG and H₂S generally no more than 1–2% of the NCG, the typical *unabated* emissions of these two gases range from 50 to 80 kg/MWh for CO₂ and 0.5 to

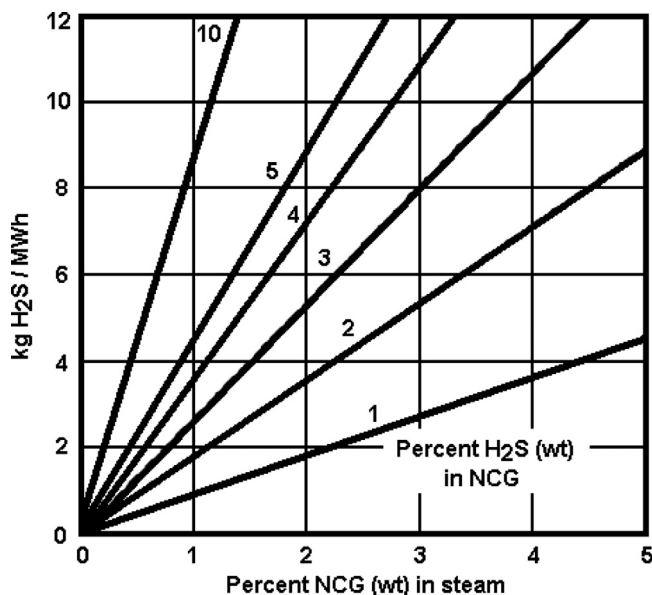


Figure 23.2 Potential unabated hydrogen sulfide emissions (kg/MWh) for various concentrations of H_2S in the NCG as a function of the concentration of NCG in the steam [6].

1.8 kg/MWh for H_2S . Abatement systems are commercially available that drastically lower the H_2S emissions. For example, one manufacturer claims that a redox chemical treatment system can be designed to achieve over 99.9% H_2S removal [16].

23.4.2 LAND USAGE

The area required to support a geothermal power plant, including the well field, substation, access roads, and auxiliary buildings, depends on the power plant rating, the type of energy conversion system, the properties of the geothermal reservoir fluid, and the piping system chosen for collecting the geofluid from the production wells and disposing of the waste brine to the injection wells. The power plant must be built close to the production wells to avoid thermodynamic losses caused by long geofluid pipelines. Although a well field for a 20–50 MW power plant can cover a considerable area, 5–10 km² or more, the well pads themselves typically cover only about 2% of the total area. Directional drilling allows multiple wells to be drilled from a single pad and minimizes the area needed for the well pads.

The pipelines used to convey the geofluids are usually mounted on stanchions, run along service roads, and incorporate vertical and horizontal expansion loops. Well fields are thus compatible with other uses such as agriculture, aquaculture,

and the raising of livestock. [Figure 23.3](#) illustrates this, showing a wellhead, two-phase pipeline, and some cattle grazing at the Miravalles plant in Costa Rica. Another example of multiple use is the prawn farm that is adjacent to the Wairakei power station in New Zealand (see [Figure 23.6](#)). The prawns are raised in freshwater ponds that are heated to about 24–28°C using residual brine from the plant, creating a product that cannot otherwise be grown in New Zealand.



Figure 23.3 Typical pipeline at Miravalles geothermal power plant, Costa Rica. *Photo by author.*

[Table 23.2](#), using data from Ref. [6] and elsewhere, presents a comparison of land usages for typical geothermal flash and binary plants with those of coal, nuclear, hydroelectric, solar thermal, photovoltaic, and wind plants [1]. Realistic capacity factors have been used in the calculations for each technology; furthermore, average power outputs, not rated values, were used for the solar plants.

A geothermal flash or binary plant requires (per MW) 5% of the area needed for a solar thermal plant, and 2% for a solar photovoltaic plant located in the best insolation area in the United States. The ratios are similar on a per MWh basis. The coal plant, including 30 years of strip mining, requires between 30 and 35 times the surface area for a flash or binary plant, on either a per MW or MWh basis. The nuclear plant occupies about seven times the area of a flash or binary plant. The highest land usage among geothermal plants occurs in the case of those using hypersaline brines; they require about 75% more land than either simple flash or binary, owing to the size of the chemical treatment facilities that render the brines manageable. The advantage that geothermal plants hold over the alternatives is striking.

TABLE 23.2 Comparison of land requirements for typical power generation options [1,6].

Power plant technology	Land usage, m ² /MW	Land usage, m ² /GWh
110 MW geothermal flash plant (including wells)	1260	160
20 MW geothermal binary plant (excluding wells)	1415	170
49 MW geothermal FCRC plant (excluding wells) ^a	2290	290
2258 MW coal plant (including strip mining)	40,000	5700
670 MW nuclear plant (plant site only)	10,000	1200
95 MW hydroelectric plant (reservoir only) ^b	1,200,000	250,000
47 MW solar thermal plant (Mojave Desert, CA)	28,000	3200
10 MW solar PV plant (Southwestern US) ^c	66,000	7500
25 MW wind farm (10 × 2.5 MW) ^d	16,000	7300

^aTypical flash-crystallizer/reactor-clarifier plant at Salton Sea, CA; see Section 9.9.

^bAverage of 10 plants at the Cumberland River Basin, Tennessee Valley Authority system.

^cBy deploying PV panels on rooftops of existing buildings, no additional land would be needed.

^dAssumes a clear area with a radius equal to the hub height.

We have chosen as one example to illustrate the land usage for a binary plant the water-cooled 53 MW Heber 2 plant complex (formerly designated and referred to elsewhere in this book as SIGC); see Section 17.4. The 33 MW SIGC plant was augmented by a 2 × 10 MW two-unit binary plant, part of the Gould Project [17]. Figure 23.4, an aerial view courtesy of *Google Earth* [18], shows how a power plant can operate compatibly within an agricultural setting; see Figure 17.6. The developed area sits among irrigated crop fields and covers a total of 0.29 km² (385 m × 765 m); however, only about 60% of this (the northern part) is used for the power station, that is, Heber 2, Gould II, Heber South, and the main production well pad. The unused land to the south was the location of the original Heber Binary Demonstration plant that was decommissioned and dismantled; see Section 17.3 and Figure 17.3. The specific area usage for the current 53 MW Heber 2 complex is about 3340 m²/MW. The plant equipment by itself (14 individual units, cooling towers, and on-site wells, excluding the outlying wells) covers approximately 0.081 km² or about 1530 m²/MW.

The next example is for a relatively new air-cooled binary power plant. Figure 23.5, courtesy of *Google Earth* [18a], is an aerial view of the 2008 Steamboat Galena 3 binary plant located about 10 miles (16 km) south of Reno, Nevada. The plant has an installed power capacity of 26 MW using two 13 MW units. The area occupied by the power station, excluding wells and pipelines, but including the switchyard, is 19,750 m² or about 760 m²/MW. This may be compared to the water-cooled Heber 2 plant with 1780 m²/MW (33 MW, 58,800 m²).



Figure 23.4 Aerial view of the Heber 2 binary plant near Heber, CA [18]. The 10 MW Gould II unit (with a three-cell cooling tower) lies just west of the original SIGC plant. Heber South is just south of Gould II; see Figure 17.6. Google Earth image from 1-31-2008 [WWW].

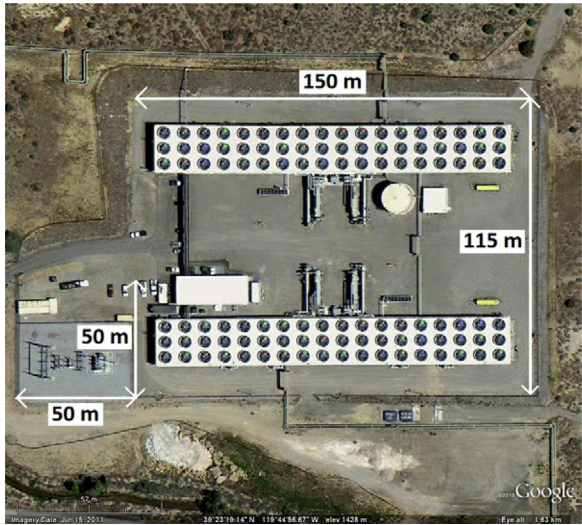


Figure 23.5 Steamboat Galena 3 binary plant, with air-cooled condensers, Nevada, [18a] [WWW].

The smaller specific area needed for the air-cooled plant versus the water-cooled plant is surprising. In general, the use of air-cooled condensers for heat rejection significantly increases the specific footprint of the plant compared to a plant of the same power rating using a wet cooling tower. For instance, the water cooling towers at Heber 2 occupy only 5% of the land area proper for the Heber 2 plant and require roughly $91 \text{ m}^2/\text{MW}$, whereas the air-cooled condensers at Galena occupy about 31.5% of the power station area (excluding the switchyard) and require $209 \text{ m}^2/\text{MW}$. In these cases, the more than 2:1 disadvantage in cooling area per MW is more than offset by improvements in binary turbine technology, both in terms of increased capacity and improved efficiency, which allows for a more compact site arrangement per installed power.

23.4.3 SOLIDS DISCHARGE

The solids that could potentially be discharged into the environment from geothermal plants are confined to materials that are initially dissolved in the geofluid and which precipitate during the processes undergone within the power plant. Of all the plants now in operation around the world, only those at the Salton Sea field in Southern California (see Section 9.8) pose a threat in this regard. The concentration of dissolved solids in a sample brine is given earlier in Table 9.2. Clever engineering, evolved over years of research and development sponsored by government and private industry, has tamed these very aggressive brines to the extent that over 300 MW of generating capacity are installed and operating with negligible impact from solids pollution.

The two methods for coping with these high-salinity brines, namely, flash-crystallizer/reactor-clarifier (FCRC) and pH-modification (pH-mod) systems, were discussed in Sections 9.8.1 and 9.8.2. By controlling the precipitation of the solids, these methods allow either for the solids to remain in solution long enough to pass through the plant and be reinjected back into the reservoir (pH-mod) or for the solids to precipitate in a manner and place where they can be removed from the geofluid and collected for proper disposal (FCRC). The latter approach cleans the brine and permits it to be reinjected without the possibility of solids precipitation within the reservoir where it could adversely affect the permeability of the formation. Thus, with proper design of the treatment system, the solids naturally occurring in the brine are not allowed to escape uncontrolled into the environment.

Other common dissolved minerals such as silica and calcium occur in modest concentrations that can be managed relatively easily, either by chemical pretreatment of the brines while they are still in the production wells or by post-utilization settling ponds [19].

In the case of highly mineralized geofluids, the levels of valuable elements might be sufficient to economically justify a mineral recovery system. A pilot zinc recovery facility was designed and built to accompany the Salton Sea Unit 5, but it did not perform well and was eventually dismantled. Since the recovery plant was one part of an integrated brine processing and power generation complex, any problems with the pilot plant had adverse effects on the brine handling and power generation sides of the operation.

23.4.4 WATER USAGE

Water is needed at every stage of development of a geothermal project. This is no different from any other large power development project. However, the needs for geothermal projects are relatively easy to satisfy. Furthermore, water use can be managed in most cases to minimize environmental impacts. The two main areas of water usage are the drilling of wells and the discharge of waste heat if a water cooling tower is used.

Well drilling. Chapter 3 describes the drilling operations for geothermal wells. The water required during this phase of development cools the drill bit, removes rock chips, and provides structural integrity of the hole until casing can be set. This water, or “mud,” is actually a mixture of water and chemicals. It is recirculated after being cooled in a small cooling tower and strained to remove the rock fragments at the surface. Thus a very small amount of freshwater is needed to compensate for evaporation losses during cooling. Usually this can be provided by local surface water from ponds, streams, or shallow wells.

Cooling water for heat rejection. Whenever power is generated on a continuing basis, the rejection of heat into the environment is an inevitable consequence of the Second Law of thermodynamics. The customary method of discharging waste heat in geothermal steam or flash plants is the use of water cooling towers. Furthermore, such plants provide their own make-up water requirements for the cooling towers since the steam condensate is sufficient to cover the evaporative loss of water from the tower. There is nevertheless a need for relatively small quantities of freshwater for blowdown to avoid a buildup of solids in the cooling tower cold well. This water, like that for drilling fluid make-up, can usually be taken from streams or other water sources.

It is not necessary to use any water for cooling purposes if a dry cooling system is adopted. Air-cooled condensers are widely used with binary plants where water may be in short supply since binary plants do not supply their own make-up water as do flash-steam and dry-steam plants (see Chapter 7). While air-cooled condensers eliminate the need for fresh make-up water, they

occupy large tracts of land, as mentioned earlier, owing to the poor heat transfer properties of air versus water. Additionally, there is a larger parasitic power requirement compared to water cooling towers owing to the large number of electric motor-driven fans. For example, in the case of the 15.5 MW Unit 5 bottoming binary plant at the Miravalles field in Costa Rica, a design comparison between a water cooling tower and an air-cooled condenser showed that the air-cooled condenser would cost more than three times as much, weigh more than two and a half times as much, cover about three times as much surface area, and consume about three times more fan power than a water cooling tower [20].

23.4.5 WATER POLLUTION

There are several places where geofluids may get into the environment during field development or normal operations. Since these fluids may contain minerals and elements harmful to humans, flora, or fauna, the onus is on the plant designers to provide barriers to prevent these fluids from entering the biosphere. The amount of dissolved solids increases significantly with temperature, making high-temperature geofluids more risky than moderate- or low-temperature ones. Some of these dissolved minerals (e.g., boron and arsenic) could poison surface water or groundwater and also harm vegetation or animals.

The well casing is the first barrier against pollution of groundwater. Damaged casings may allow brines to mingle with freshwater aquifers. Therefore, particular care is taken to install and cement multiple casings at shallow depths to provide extra barriers (see Figure 3.7). Cement-bond logs (integrity tests) are performed to assure the driller that there are no blind spots behind the casing that could rupture under thermal stress caused by repeated opening and closing of the well.

Liquid streams might endanger surface waters through runoff during well testing. Thus, fluids discharging during tests are directed to impermeable holding ponds. Also, steam pipelines are fitted with traps to remove condensate (see Figure 7.7) and that liquid is sent by pipelines to holding ponds. Later the collected fluids are reinjected deep underground.

Despite all these design precautions, it is nevertheless prudent to have monitoring wells strategically located in the well field to rapidly detect any problems with subsurface leakage and permit prompt remediation. For those few developments where 100% reinjection of residual brines is still not practiced, it is essential to monitor all discharge streams to avoid exceeding allowable limits of contaminants.

23.5 Environmental Challenges of Geothermal Plants

23.5.1 LAND SUBSIDENCE

It is difficult to draw generalizations about subsidence because of a wide range of experiences among geothermal fields. Larderello, the large dry-steam field in Italy, has been in operation for over 100 years with negligible subsidence. In New Zealand, both the Wairakei and Ohaaki fields have experienced subsidence: at Wairakei the depression or “bowl” is very large but located some 1.5 km from the center of the production field, whereas at Ohaaki the subsidence is relatively small but, being centered on the production field, has caused serious problems with wells and pipelines. The large geothermal area in the Imperial Valley of the United States supports nearly 500 MW of power generation, and Cerro Prieto in Mexico, in an extension of the same geological formation, supports over 700 MW, and neither area has experienced significant subsidence [21]. Subsidence would be extremely disruptive here since the land in the Imperial Valley is generally flat and arid, with irrigation canals in place to distribute water to vast farms (e.g., see Figure 23.4).

Geothermal reservoir production at rates much greater than recharge can lead to surface subsidence. This was observed, for example, beginning with the first few years of operation of the power plant at Wairakei when all the residual brine was allowed to flow to the adjacent Waikato River. The production wells at Wairakei were drilled through a relatively shallow cap rock (Huka Falls Formation) containing pumice breccias and mudstones. The thickness of the cap rock varies from 150–200 m in the northern part of the field to only 30–90 m in the western part. Tests have shown that the pumice breccias and mudstones exhibit compressibilities sufficiently high to account for the subsidence [22]. It is important to note that the greatest subsidence correlates with the thickest part of the cap rock (R. Glover, pers. comm., May 16, 2007).

During nearly 50 years of operation, much of it without reinjection, subsidence rates in one area of Wairakei reached nearly 500 mm/year; the maximum depression now exceeds 15 m. Although recently the rate of subsidence has decreased substantially to about 70 mm/year within the deepest depression, a projection indicates that the total subsidence should increase by an additional 20 m by the year 2050 [23,24]. Furthermore, the subsidence has now spread across the field, covering an area extending to about 5 km to the southwest and 4 km to the northwest of the current bowl [25]. Figure 23.6 is a map showing the rates of subsidence and other important features and structures in the most affected part of the field [26].

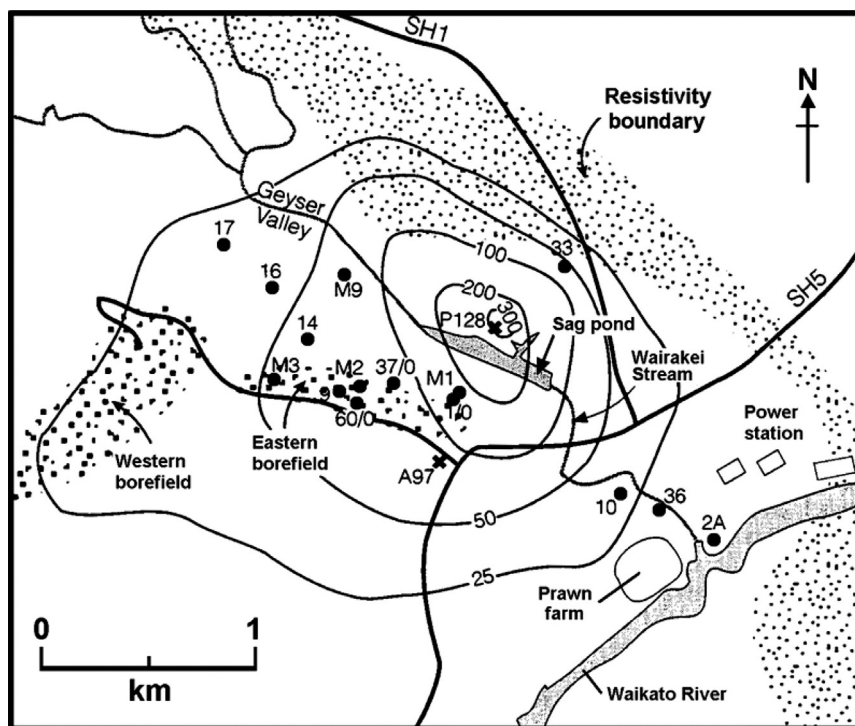


Figure 23.6 Subsidence in the northern sector of the Wairakei field: numbered contours show average rates of subsidence in mm/year from 1986 to 1994; filled circles are selected wells; crosses are leveling benchmarks. Redrawn from Ref. [26].

Figure 23.7 shows the Wairakei drop structure (drainage channel to the Wairakei Stream) that was impacted by the subsidence. The area of maximum subsidence lies just to the north of the Wairakei Stream some 150–200 m upstream of the drop structure. About 20 years after the first power units came online, subsidence caused a flume that fed the waste brine into the canal to fail. All plant operations were halted and it took 3 days to repair the broken connection. The canal is still in operation but carries only about 40% of the waste brine flow since over 50% is now being reinjected (I. Thain, pers. comm., May 1, 2007).

Subsidence is more likely to occur in formations where the fluid in place is under lithostatic, rather than hydrostatic pressure. For example, this condition is present in the geopressed resources along the Gulf Coast of the United States; see Section 9.6.3. Here the pressure of the fluid contributes to the support of the overburden and its removal leaves the overburden partially unsupported. Subsidence is less likely in competent formations with fracture-dominated



Figure 23.7 Wairakei drop structure (hot-water drainage channel) to the Wairakei Stream not far from the area of maximum subsidence. *Photo courtesy of S. Tamanyu, Geological Survey of Japan; photo first published on the cover of Chishitsu News, No. 531, 1998 [WWW].*

permeability. For example, at The Geysers field in California, which consists of fractured greywacke, a maximum subsidence rate of 47 mm/year was observed from 1977 to 1996, an order of magnitude lower than the maximum seen at Wairakei [27].

Although reinjection does not guarantee the avoidance of subsidence, it can reduce the risk, provided it is carried out so as to maintain reservoir fluid pressure. Nowadays, geothermal developers normally incorporate reinjection into reservoir management programs right from the start both to minimize this risk and to prolong the life of the reservoir.

23.5.2 INDUCED SEISMICITY

Induced seismicity is a phenomenon in which a change in fluid pressure within a stressed rock formation leads to movement of the fractured rocks. The energy released is transmitted through the rock and may reach the surface with enough intensity to be heard or felt by persons in the area. This may happen, for example, when the reservoir for a hydroelectric station is first filled, when fossil fuels are extracted from oil and gas fields, or when fluids are injected underground at high pressure. The likelihood and the severity of the event depend on the local state of stress within the formation.

Nearly every geothermal field under exploitation has experienced induced seismicity to some degree [28]. In a normal hydrothermal setting this has not been a problem since high pressures are not needed for the reinjection of residual brines. This may be a more important problem for the emerging technology of Enhanced (or Engineered) Geothermal Systems or EGS [1]. Whereas injection of waste fluids is an ancillary, albeit important, activity at a hydrothermal power plant, injection of high-pressure fluids is one of the critical features associated with the creation and maintenance of an EGS reservoir; see Chapter 22. A 2007 incident at an EGS site in Basel, Switzerland, resulted in a magnitude 3.3 earthquake and caused considerable alarm among residents [29]. The problem is deemed significant enough to warrant annual workshops on the subject; see, for example, Ref. [30].

Granted the obvious problems that can be created by strong induced seismic events, there are several positive aspects of induced microseismicity, the type more commonly associated with hydrothermal operations. The acoustic noise generated may be monitored with sensitive, high-precision instruments to provide real-time information regarding the behavior of the reservoir. For example, the 3D acoustic noise pattern can shed light on the movement of the injected water front as it moves through the fractures in the formation. It can help delineate the permeable portions of the formation, i.e., the locations of the fractures and faults.

In EGS applications, it is being used to map the growth and extent of the fractures as they are being created. Figure 23.8 shows one such application for the Soultz field in France [31]. During the six days while the well was shut in after stimulation, the 3D swarm of acoustic noise grew to the extent shown in the figure, indicating the growth of the fracture pattern in the formation.

Since it is often difficult to discern natural from induced seismic events, it is wise to collect baseline data prior to field development and drilling at a selected site. Also, a thorough scientific study should be carried out before drilling to determine the geologic and tectonic conditions existing at the site. This should

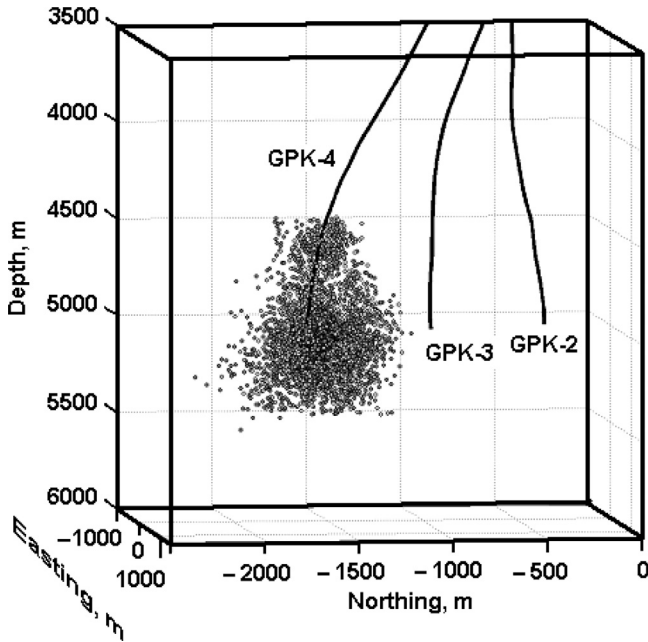


Figure 23.8 Stimulation of well GPK-4 during a 2004 test: seismic event swarm shown after the well was shut in for 6 days [31].

provide the data needed to avoid the inadvertent lubrication of a major fault that could cause a significant seismic event. It is useful also to monitor the site for any unexpected natural or induced microseismic events after field work commences. Finally, if there are residents in the neighborhood of the site, an educational program should be put in place to inform people of the possibility, unlikely though it may be, of felt seismic events, and to set up a hotline where they can report such occurrences [1].

23.5.3 INDUCED LANDSLIDES

Many geothermal fields lie in rugged volcanic terrain prone to natural landslides. Indeed, some fields have been developed atop ancient landslides. Landslides can be triggered by earthquakes, and, as we have discussed, while it is possible that geothermal production or injection could lead to induced seismicity, it is highly improbable that such activities could lead to an event large enough to cause a major earthquake.

Landslides have occurred at geothermal fields, but the cause is often unclear. The worst disaster happened at the Zunil field in Guatemala in January 1991 in which at least 23 people were killed [32]. Figure 23.9 shows the devastation



Figure 23.9 January 5, 1991, landslide at Zunil geothermal field, Guatemala. At least six houses were destroyed and the main highway was buried [33]. *Photo courtesy of Geothermal Resources Council.*

when a large portion of a steep slope above the field collapsed, spreading rock and moisture-laden debris a distance of 800–1200 m onto a relatively flat plateau [33]. Approximately 10^6 m^3 of earth was released. The slide also buried one of the wells, ZCQ-4, that stood at the base of the scarp, close to the Zunil fault; see Figure 23.10. A thorough examination of the site done soon after the event (before the excavation of the buried well) concluded that the scarp had been in a state of unstable equilibrium owing to the steepness of the slope, the abundance of hydrothermally altered rock, and the proximity to the Zunil fault. Seasonally high groundwater levels also played a role in priming the slope for failure. A later analysis [34] identified several precursor events—a minor landslide at the foot of the scarp about one week earlier, the increase in flow of spring water issuing from the toe of the scarp, followed by a change in the color of the water, and finally its abrupt cessation just before the large slide. Construction and road building activities that began in 1981 probably also set the stage for the 1991 catastrophe.

While it is difficult to pin down the precise trigger for the disaster, it seems that the slope was gradually weakening and the imperceptible movement of the slope had at first increased the permeability around the Zunil fault allowing the spring flow to increase, but eventually the movement sealed off the flow paths.

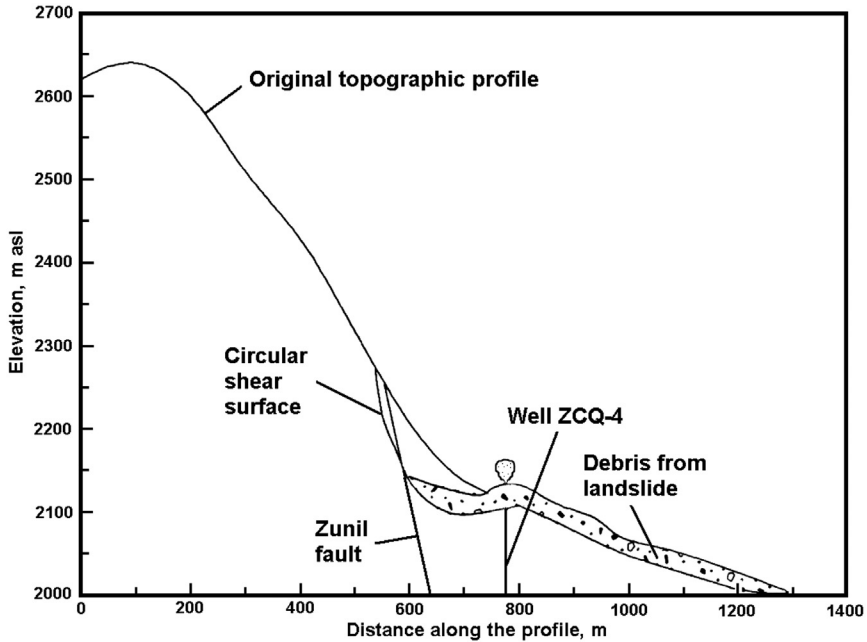


Figure 23.10 Cross-section through the Zunil landslide [33].

The subsequent buildup of piezometric pressure behind the scarp then became high enough to cause the slope first to slump near the toe and then for the weakened scarp wall to completely collapse [34].

Both studies, Refs. [33] and [34], offered general recommendations for the prevention of similar catastrophes. These include: (1) development of a hazard map identifying all potential landslide areas, (2) slope monitoring instrumentation, (3) monitoring of springs for changes in flow rate, temperature, chemistry, and clarity, (4) installation of drains in slopes to remove moisture, and (5) avoidance of obvious unstable areas for wells, roads, and other construction activity.

23.5.4 NOISE POLLUTION

In the development stage of a geothermal power project, noise is generated during road construction, excavation for drilling sites, well drilling, and well testing. While these may be disturbing to nearby residents (if any), they are of limited duration. Furthermore, the most objectionable sounds can be significantly reduced with appropriate mufflers and other sound-deadening materials. During normal plant operations, various components are sources of noise; these include transformers, generators, water cooling towers, motors, pumps and fans for circulating

water and air associated with the heat rejection system, brine and steam flowing through pipes, etc. These are generally confined to the area within the plant fence boundary. However, cooling towers or air-cooled condensers are relatively tall structures having fans on top. Thus these may be the dominant source of noise during normal operation. Since air-cooled condensers use numerous cells each fitted with a fan (e.g., see Figure 9.12), they generate more noise than water cooling towers, which are smaller and use far fewer cells for a given plant power rating.

If the turbine should trip for any reason, such as a problem in the electrical transmission system, it is usually necessary to direct the full steam flow away from the turbine for a short time using the emergency steam venting system. This allows the wells to continue to flow avoiding a sudden closure that could damage the casings or wellhead equipment. During the outage, steam is typically sent to relief valves and rock mufflers where the steam velocity is reduced drastically to lower the noise associated with the venting process; see Figures 7.8 and 7.9. Since the noise generated by a moving gas stream is proportional to the velocity raised to the 8th power, reducing the steam velocity by a mere factor of 2 will cut the sound emitted by a factor of 256, or more than two and a half orders of magnitude.

The highest noise levels occur during the drilling and testing of wells. Noise levels can reach 114 decibels A-weighted (dB-A) near the drill site when drilling with air, as would be the case if the reservoir were characterized by tiny fractures in the production zone. Since the intensity of sound drops rapidly as one moves away from the source, geofluids issuing vertically from a wide open well would register only 71–83 dB-A at a distance of 900 m. Thus, under normal operating conditions, the noise emanating from a plant situated within the boundaries of a large geothermal field should not be objectionable to anyone living nearby.

To give some perspective to these numbers, [Table 23.3](#) gives the noise levels for several everyday activities and various geothermal processes.

23.5.5 DISTURBANCE OF NATURAL HYDROTHERMAL MANIFESTATIONS

As described in Section 5.7, there have been numerous cases where hydrothermal developments have compromised or totally destroyed natural hydrothermal manifestations such as geysers, hot springs, mud pots, etc. [35,36]. The drawdown, or lowering of the hydrostatic water level, from production wells disturbs the natural thermohydraulic balance that gives rise to the manifestations. In particular, geysers are delicate phenomena that are subject to nature's whims, even without humankind's interference. A study of the geysers at Yellowstone National Park in the United States will show that geysers are ephemeral, coming and going with the seismic events associated with the region. Commercial developments at Beowawe and Steamboat in Nevada extinguished the geysers that used to be seen in both places, thus depriving future generations from enjoying their beauty.

TABLE 23.3 Geothermal noise relative to other sources.

Noise source	Level (dB-A)
Jet aircraft @ 30 m	120–130
Geothermal air drilling rig @ 8 m (25 kg/s steam entry, no muffler)	114
Automobile freeway or a subway train @ 6 m	90
Geothermal air drilling rig @ 8 m (25 kg/s steam entry, with muffler)	84
Pneumatic drill @ 15 m	80
Geothermal steam well, wide-open vertical discharge @ 900 m	71–83
Vacuum cleaner @ 3 m	70
Geothermal air drilling rig @ 75 m (25 kg/s steam entry, with muffler)	65
Normal speech @ 0.3 m	65
Business office	50
Residential area in evening	40

The Wairakei Geyser Valley, a famous tourist attraction in the late nineteenth and early twentieth centuries, straddled the upper Wairakei Stream for a distance of some 750 m, and was home to 22 active geysers along with other thermal features until field development began (see [Figure 23.6](#)). By the mid-1970s, the geysers were extinguished [37]. Instead tracts of steaming and hot ground intensified, particularly in an area to the northeast of the Geyser Valley. The center of the subsidence bowl, discussed earlier in Section 23.5.1, is about 1 km to the southeast of the old Geyser Valley. A sag pond has since formed in the Wairakei Stream near the bottom of the subsidence bowl (R. Glover, pers. comm., May 14, 2007).

Apart from these generally negative consequences of development, there is another viewpoint on this subject. It has been argued that there can be beneficial effects on thermal manifestations as a result of geothermal development [38]. For example, in New Zealand, besides the loss of many thermal features, several have been created or enhanced, such as the enlarged areas of steaming ground at Wairakei, and increased boiling of hot springs at other sites.

23.5.6 DISTURBANCE OF WILDLIFE HABITAT, VEGETATION, AND SCENIC VISTAS

Considering the relatively small area needed for geothermal development and operations, the potential impact on wildlife, vegetation, and vistas can be minimized with proper planning and engineering. Furthermore, in the United States and most countries, an Environmental Impact Statement must be filed before any permits are granted for a geothermal project.

Certainly, any power generation facility constructed where none existed will alter the view of the landscape. Conventional power plants in developed, commercial, or industrial settings, while objectionable to many for other reasons, do not stand out as sharply as a geothermal plant in a flat agricultural region or on the

flank of a volcano. Even so, with care and creativity geothermal plants can be designed to blend into the surroundings.

In areas having natural foliage, it is necessary to clear some of it to make room for roads, well pads, pipe routes, separator stations, holding ponds, and the powerhouse and its associated facilities. Once the construction phase is over and operations begin, the disturbed area can be replanted to regain a semblance of its original natural appearance.

The Ahuachapán plant in El Salvador is an interesting case in point. Figures 23.11 and 23.12 show the facility soon after commissioning around 1977 [39] and then after the planting of trees and vegetation in 2005.



Figure 23.11 Ahuachapán geothermal facility after commissioning around 1977 [39]. Owing to areas of acidic soils and hot ground, initially there was little natural vegetation around the plant [WWW].



Figure 23.12 Ahuachapán geothermal facility showing growth of eucalyptus trees circa 2005 [40]. Eucalyptus trees are resistant to the hostile soil conditions found there. Other areas that were formerly crop lands have been planted with various native species. Thus the plant site is now more foliated than before the plant was built and the area has been partially restored to what it might have resembled hundreds of years ago (J.A. Rodriguez, pers. comm., May 2, 2007). Photo courtesy of LaGeo S.A. de C.V., El Salvador [WWW].

Compared to wind turbines, solar thermal “power towers,” or fossil-fueled or nuclear plants, geothermal plants generally have a low profile and are less conspicuous. The exceptions are the geothermal plants that use natural-draft cooling towers: several older plants at Larderello (Italy), and those at Matsukawa (Japan) and Ohaaki (New Zealand). Buildings and pipelines can be painted with appropriate colors to help mask them from a distance (e.g., see Figure 11.17). While it is impossible to conceal steam rising from silencers or cooling towers at geothermal plants, most people find the sight of white steam clouds unobjectionable.

It should be obvious that sites of rare natural beauty such as national parks ought to be off-limits to geothermal or any other type of industrial or commercial development.

23.5.7 CATASTROPHIC EVENTS

Besides landslides, some other serious events that might occur at a geothermal plant include well blowouts, phreatic explosions, ruptured steam pipes, turbine failures, fires, etc. Most of these accidents are similar to what can happen at any power generation facility and have been known to cause casualties. The ones that are unique to geothermal power plants involve well drilling and testing. In the early days of geothermal energy exploitation, well blowouts during drilling were a fairly common occurrence, but nowadays the use of fast-acting blowout preventers have practically eliminated this potentially life-threatening problem. Better understanding of the geology of the site obtained using modern geoscientific methods further reduces the danger of surprises during drilling. The monitoring of reservoir pressures, commonly done at most fields, will give an early indication of a potentially dangerous situation that might result in a phreatic explosion. Lastly, proper engineering and adherence to design and building codes should also minimize, if not completely eliminate, the chance of a mechanical or electrical failure that could cause serious injury to plant personnel or local inhabitants. Since many geothermal plants are located in earthquake-prone regions, it is worth noting that geothermal plants have many times withstood strong earthquakes, including the massive 9.0 magnitude earthquake off the coast of Japan on March 11, 2011, without suffering major damage or failures leading to environmental contamination. Of the ten Japanese geothermal units close to the epicenter, one was out of service for maintenance, six automatically tripped off-line instantly, while three continued to operate. The plants that shut down were all back on line within four days [41].

23.5.8 THERMAL POLLUTION

Although thermal pollution is currently not a specifically regulated quantity, it does represent an environmental impact for all power plants that rely on a heat

source for their motive force. As was discussed in Section 5.4.6, heat rejection from geothermal plants is higher per unit of electricity production than for fossil-fueled or nuclear plants. Figure 23.13 shows a comparison between a geothermal single-flash plant and several alternative cycles. For example, using a reservoir fluid temperature of 220°C , the flash plant rejects about three times as much heat per unit of useful electrical generation as an ideal Carnot cycle operating between the reservoir temperature and the assumed condensing temperature of 52°C . The other practical cycles all reject far less heat per unit of generation than the flash plant.

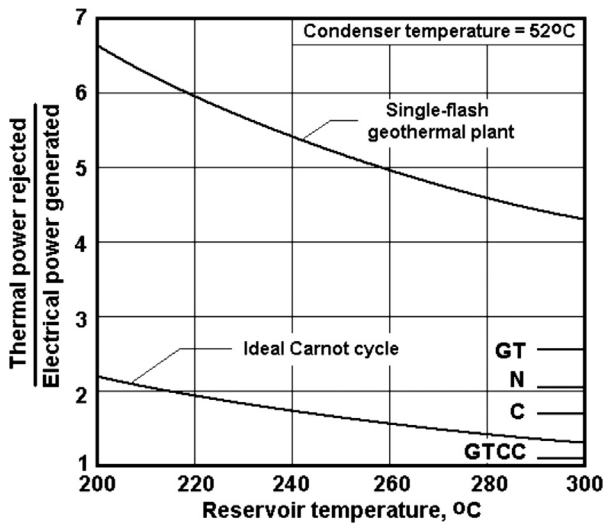


Figure 23.13 Heat rejection per unit of electrical generation for various plants: GT = simple gas turbine; N = nuclear; C = coal; GTCC = gas turbine combined cycle [5].

23.6 Summary

From the long list of potential environmental impacts from geothermal power plants, we have seen that some of them warrant serious attention of scientists and engineers. These include subsidence, induced seismicity, and landslides, all of which can have serious and possibly disastrous consequences. Several of the others are fairly easily controlled with current technology—air and water pollution, and noise abatement. Failure of equipment can be avoided through proper design, engineering, and construction. Geothermal plants are far less environmentally intrusive than alternative plants in several respects—very low carbon dioxide emissions, essentially no NO_x and SO_2 emissions, extremely low H_2S emissions

using appropriate NCG cleanup equipment, low land usage per installed megawatt, and very low water usage for steam plants. Geothermal binary plants are environmentally benign, essentially zero-emission plants, especially when fitted with air-cooled condensers.

References

- [1] Tester JW, Anderson BJ, Batchelor AS, Blackwell DD, DiPippo R, Drake EM, et al. The future of geothermal energy: impact of enhanced geothermal systems (EGS) on the United States in the 21st century. Cambridge, MA: Massachusetts Institute of Technology; 2006<<http://geothermal.inel.gov>>.
- [2] Armstead HCH. Geothermal energy. 2nd ed., London: E. and F. N. Spon; 1983.
- [3] Armstead HCH, Tester JW. Heat mining. London: E. and F. N. Spon; 1987.
- [4] Burnham L, Johansson TB, Kelly H, Reddy AKN, Williams RH. In: Burnham L, editor. Renewable energy: sources for fuels and electricity. Washington DC: Island Press; 1993.
- [5] DiPippo R. Geothermal energy: electricity production and environmental impact, a worldwide perspective. Energy and environment in the 21st century. Cambridge, MA: MIT Press; 1991. p. 741–54.
- [6] DiPippo R. Geothermal energy: electricity generation and environmental impact. Energy Policy 1991;19:798–807.
- [7] Hartley RP. Environmental considerations. In: Kestin J, editor-in-chief, DiPippo R, Khalifa HE, Ryley DJ, editors. Sourcebook on the production of electricity from geothermal energy, US Dept. of Energy, DOE/RA/4051-1, US Gov. Printing Office, Washington, DC; 1980 [chapter 9].
- [8] Kagel A, Bates D, Gawell K. A guide to geothermal energy and the environment. Washington, DC: Geothermal Energy Association; 2007<<http://www.geo-energy.org/reports/Environmental%20Guide.pdf>>.
- [9] Mock JE, Tester JW, Wright PM. Geothermal energy from the earth: its potential impact as an environmentally sustainable resource. Ann Rev Energy Environ 1997;22:305–56.
- [10] Pasqualetti MJ. Geothermal energy and the environment—the global experience. Energy (UK) 1980;5:111–65.
- [11] Tester JW, Drake EM, Golay MW, Driscoll MJ, Peters WA. Sustainable energy: choosing among options. Cambridge, MA: The MIT Press; 2005.
- [12] Pascual RVJ. Impacts of Philippine environmental regulatory policies on PNOC-EDC's corporate environmental management initiatives. Proc. world geothermal congress 2005, paper no. 0305, International Geothermal Association, Antalya, Turkey; 2005.
- [13] Dickie BN, Luketina KM. Sustainable management of geothermal resources in the Waikato region, New Zealand. Proc. world geothermal congress 2005, paper no. 0303, International Geothermal Association, Antalya, Turkey; 2005.
- [14] Mwawughanga FM. Regulatory framework for geothermal in Kenya. Proc. world geothermal congress 2005, paper no. 0312, International Geothermal Association, Antalya, Turkey; 2005.
- [15] Guido H., S., O. Vallejos R, E. Sánchez R. Environmental management at the Miravalles geothermal field. Proc. world geothermal congress 2005, paper no. 0248, International Geothermal Association, Antalya, Turkey; 2005.
- [16] Merichem Chemicals & Refinery Services LLC, Gas Technology Products, <<http://www.merichem.com/gas>>; 2015.

- [17] Ormat Technologies, Inc. 10K Report; March 12, 2007. p. 32.
- [18] Google Earth, 6.1.0.5001, Build date: 10/17/2011, Image date: 1/31/2008.
- [18a] Google Earth, 5.2.1.1588, Build date: 9/1/2010, Image date: 6/14/2011.
- [19] DiPippo R. US Department of Energy, DOE/RA/28320-1 Geothermal energy as a source of electricity: a worldwide survey of the design and operation of geothermal power plants. Washington, DC: US Government Printing Office; 1980.
- [20] Moya RP, DiPippo R. Miravalles unit 5 bottoming binary plant: planning, design, performance and impact. *Geothermics* 2007;36:63–96.
- [21] Narasimhan TN, Goyal KP. Subsidence due to geothermal fluid withdrawal. Earth Sciences Div., Lawrence Berkeley Laboratory, Rep. No. LBL-10967, GSRMP-14; October 1982.
- [22] Allis RG, Barker P. Update on subsidence at Wairakei. Proc. Pacific geothermal conference and 4th New Zealand geothermal workshop, Part 2; 1982, p. 365–70.
- [23] Allis RG, Zhan X. Predicting subsidence at Wairakei and Ohaaki geothermal fields, New Zealand. *Geothermics* 2000;29:479–97.
- [24] White PJ, Lawless JV, Terzaghi S, Okada W. Advances in subsidence modelling of exploited geothermal fields. Proc. world geothermal congress 2005, paper no. 0222, International Geothermal Association, Antalya, Turkey; 2005.
- [25] White PJ. Latest developments in subsidence at Wairakei-Tauhara. Proc. 27th New Zealand geothermal workshop; 2005.
- [26] Allis RG, Zhan X, Carey B. Modelling of subsidence at Wairakei and Ohaaki fields. Proc. 19th New Zealand geothermal workshop; 1997.
- [27] Mossop A, Segall P. Subsidence at The Geysers geothermal field, N. California from a comparison of GPS and leveling surveys. *Geophysical Res Lett* 1997;24:1839–42.
- [28] Kugaenko Y, Saltykov V, Chebrov V. Seismic situation and necessity of local seismic monitoring in exploited Mutnovsky steam-hydrothermal field (Southern Kamchatka, Russia). Proc. world geothermal congress 2005, paper no. 0260, International Geothermal Association, Antalya, Turkey; 2005.
- [29] Pancevski, B., “Green energy” project gives Swiss the shakes, London Sunday Telegraph, <<http://www.telegraph.co.uk/news/worldnews/1543048/Green-energy-project-gives-Swiss-theshakes.html>>; February 19, 2007.
- [30] Majer E, Baria R. Induced seismicity associated with enhanced geothermal systems: state of knowledge and recommendations for successful mitigation. Working paper presented at the Stanford Geothermal Workshop, Stanford University, CA; 2006.
- [31] Baria R, Baumgaertner J, Teza D, Michelet S. Reservoir stimulation and testing techniques for EGS systems (Soultz). Presented at EGS workshop, Massachusetts Institute of Technology, Cambridge, MA; November 10, 2005.
- [32] Global Volcanism Program, Smithsonian National Museum of Natural History, Landslide in geothermal field; 23 people reported dead, <<http://www.volcano.si.edu/world/volcano.cfm?vn=342040>>; 1991.
- [33] Flynn T, Goff F, Van Eeckhout E, Goff S, Ballinger J, Suyama J. Catastrophic landslide at Zunil I geothermal field, Guatemala, January 5, 1991. *Geothermal Resour Counc Trans* 1991;15:425–33.
- [34] Voight B. Causes of landslides: conventional factors and special considerations for geothermal sites and volcanic regions. *Geothermal Resour Counc Trans* 1992;16:529–33.
- [35] Jones GL. Geysers/Hot Springs damaged or destroyed by man, <<http://www.wyojones.com/destroye.htm>>; 2006.
- [36] Keam RF, Luketina KM, Pipe LZ. Definition and listing of significant geothermal feature types in the Waikato region, New Zealand. Proc. world geothermal congress 2005, paper no. 0209, International Geothermal Association, Antalya, Turkey; 2005.

- [37] White PJ, Hunt T. Cessation of spring flow and spring feed depths, Geyser Valley, Wairakei. Proc. 23th New Zealand geothermal workshop; 2001, p. 173–8.
- [38] Bromley CJ. Advances in environmental management of geothermal developments. Proc. world geothermal congress 2005, paper no. 0236, International Geothermal Association, Antalya, Turkey; 2005.
- [39] DiPippo R. The geothermal power station at Ahuachapán, El Salvador. *Geotherm Energy Mag* 1978;6:11–22.
- [40] LaGeo, Brochure. Energía limpia para un planeta mejor. Santa Tecla, El Salvador.
- [41] Yasukawa K. All geothermal power plants in northeastern Japan survived the M9.0 earthquake. IGA News, No. 84, April–June 2011, p.8–10.

Appendix A

Worldwide State of Geothermal Power Plant Development as of December 2014

If you cannot measure it, you cannot improve it.

Lord Kelvin

As of the writing of this book (December 2014), there are 28 countries that either currently produce electricity from geothermal energy or used to do so. Four countries (Argentina, Democratic Republic of the Congo, Greece, and Zambia) have shut down very small power plants.

The growth of geothermal power worldwide is shown in a semilog plot in [Figure A.1](#). It can be seen that the geothermal industry has experienced several different periods of development. Until World War II, Italy was the only country

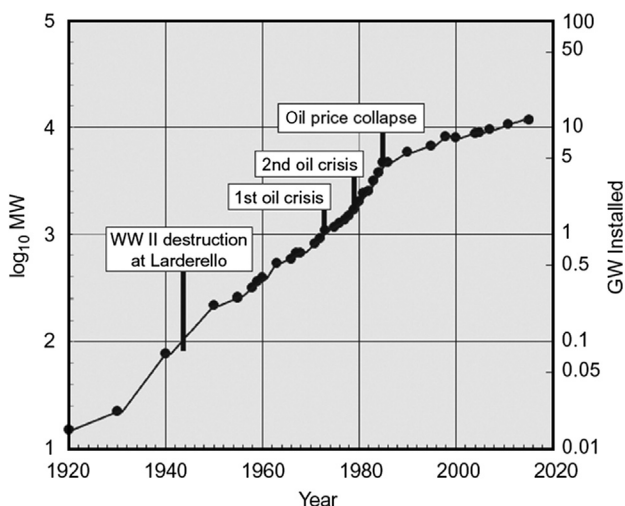


Figure A.1 Growth of worldwide geothermal power installation.

with commercial geothermal power plants. From 1930 to 1944, the average annual growth was about 14%. New Zealand (1959) and the United States (1960) were next to place geothermal plants into commercial operation, followed by Japan (1967), Iceland (1969), Mexico (1973), and the Philippines (1979). From 1920 to 1977, the annual average growth rate was 8.2%.

The first great oil crisis (1973) and the second one (1979) spurred many countries to develop their geothermal resources, but it took a few years before the momentum built. From 1977 to 1985 the annual growth rate accelerated to 17.1%. Since then until 2014, the growth rate has slowed to about 3.2%. Geothermal development is influenced by the worldwide price of oil (relatively low, ~\$60/barrel, as of December 2014) and governmental financial incentives that are subject to political and ideological persuasions of those in power and tend to vary in unpredictable ways.

The rest of this appendix consists of a series of tables showing the details of the installed geothermal power around the world by country, by capacity (Table A.1), by number of units (Table A.2), and by type of energy conversion system (Tables A.3–A.5). Detailed compilations for each country that has or had operating geothermal power plants are also included (Tables A.6–A.20). It must be borne in mind that the power capacities listed are the *installed values*, but that the actual running capacities may be different, sometimes higher, but usually lower, and depend on local conditions, such as field and reservoir behavior and demand for electricity.

TABLE A.1 Status of geothermal power plant development ranked by MW.

Rank	Country	No. of units	MW
1	United States	197	3134.48
2	Philippines	50	1881.96
3	Indonesia	30	1385.1
4	New Zealand	43	948.4
5	Italy	34	855.5
6	Mexico	28	839.4
7	Iceland	29	663.4
8	Kenya	29	563.5
9	Japan	34	517.843
10	Turkey	18	296.73
11	Costa Rica	8	205
12	El Salvador	7	204.3
13	Nicaragua	5	149.5
14	Russia	12	79
15	Papua-New Guinea	6	56
16	Guatemala	9	44.6
17	China	14	27.78
18	Germany	7	27.2
19	Portugal—Azores	5	23
20	France—Guadeloupe	2	15.7
21	Ethiopia	1	8.5
22	Austria	3	1.45
23	Thailand	1	0.3
24	Australia	1	0.15
25	Argentina	0	0
26	Democratic Republic of the Congo	0	0
27	Greece	0	0
28	Zambia	0	0
Totals		573	11,928.79

TABLE A.2 Status of geothermal power plant development ranked by number of units.

Rank	Country	No. of units	MW	MW/unit
1	United States	197	3134.48	15.91
2	Philippines	50	1881.96	37.64
3	New Zealand	43	948.4	22.06
4	Italy	34	855.5	25.16
5	Japan	34	517.843	15.23
6	Indonesia	30	1385.1	46.17
7	Iceland	29	663.4	22.88
8	Kenya	29	563.5	19.43
9	Mexico	28	839.4	29.98
10	Turkey	18	296.73	16.49
11	China	14	27.78	1.98
12	Russia	12	79	6.58
13	Guatemala	9	44.6	4.96
14	Costa Rica	8	205	25.63
15	El Salvador	7	204.3	29.19
16	Germany	7	27.2	3.89
17	Papua-New Guinea	6	56	9.33
18	Nicaragua	5	149.5	29.90
19	Portugal—Azores	5	23	4.60
20	Austria	3	1.45	0.48
21	France—Guadeloupe	2	15.7	7.85
22	Ethiopia	1	8.5	8.50
23	Thailand	1	0.3	0.30
24	Australia	1	0.15	0.15
25	Argentina	0	0	0.00
26	Democratic Republic of the Congo	0	0	0.00
27	Greece	0	0	0.00
28	Zambia	0	0	0.00
Totals		573	11,928.793	20.82

TABLE A.3 Geothermal power plants: installed MW for each type of plant.

Country	Dry steam	1-Flash	2-Flash	3-Flash	Binary	Flash- binary	Hybrid; total flow	Total
United States	1477	49	732.5	98.9	739.08	30	8	3134.48
Philippines	0	1685.74	54.24	0	0	141.98	0	1881.96
Indonesia	445	940.1	0	0	0	0	0	1385.1
New Zealand	55	68.2	356	140	191.2	138	0	948.4
Italy	834.5	20	0	0	1	0	0	855.5
Mexico	0	399.4	440	0	0	0	0	839.4
Iceland	30	564.7	60	0	8.7	0	0	663.4
Kenya	0	451.7	0	0	1.8	110	0	563.5
Japan	23.5	354.64	135	0	4.703	0	0	517.843
Turkey	0	20.4	47.4	60	168.93	0	0	296.73
Costa Rica	0	144	0	0	61	0	0	205
El Salvador	0	160	35	0	9.3	0	0	204.3
Nicaragua	0	142	0	0	7.5	0	0	149.5
Russia	0	79	0	0	0	0	0	79
Papua-New Guinea	0	56	0	0	0	0	0	56
Guatemala	0	0	0	0	0	44.6	0	44.6
China	0	0.3	24.18	0	0	0	3.3	27.78
Germany	0	0	0	0	27.2	0	0	27.2
Portugal—San Miguel	0	0	0	0	23	0	0	23
France—Guadeloupe	0	11	4.7	0	0	0	0	15.7
Ethiopia	0	0	0	0	0	8.5	0	8.5
Austria	0	0	0	0	1.45	0	0	1.45
Thailand	0	0	0	0	0.3	0	0	0.3
Australia	0	0	0	0	0.15	0	0	0.15
Totals	2865	5146.18	1889.02	298.9	1245.313	473.08	11.3	11,928.79
% of total	24.02	43.14	15.84	2.51	10.44	3.97	0.09	100

TABLE A.4 Geothermal power plants: number of units for each type of plant.

Country	Dry steam	1-Flash	2-Flash	3-Flash	Binary	Flash- binary	Hybrid; total flow	Total
United States	26	3	27	2	127	10	2	197
Philippines	0	44	1	0	0	5	0	50
New Zealand	1	4	6	1	15	16	0	43
Italy	32	1	0	0	1	0	0	34
Japan	1	16	3	0	14	0	0	34
Indonesia	7	23	0	0	0	0	0	30
Iceland	1	19	2	0	7	0	0	29
Kenya	0	17	0	0	1	11	0	29
Mexico	0	24	4	0	0	0	0	28
Turkey	0	1	1	1	15	0	0	18
China	0	1	8	0	0	0	5	14
Russia	0	12	0	0	0	0	0	12
Guatemala	0	0	0	0	0	9	0	9
Costa Rica	0	4	0	0	4	0	0	8
El Salvador	0	5	1	0	1	0	0	7
Germany	0	0	0	0	7	0	0	7
Papua-New Guinea	0	6	0	0	0	0	0	6
Portugal—San Miguel	0	0	0	0	5	0	0	5
Nicaragua	0	4	0	0	1	0	0	5
Austria	0	0	0	0	3	0	0	3
France—Guadeloupe	0	1	1	0	0	0	0	2
Ethiopia	0	0	0	0	0	1	0	1
Thailand	0	0	0	0	1	0	0	1
Australia	0	0	0	0	1	0	0	1
Totals	68	185	54	4	203	52	7	573
% of total	11.87	32.29	9.42	0.70	35.43	9.08	1.22	100

TABLE A.5 Summary: geothermal power plants by number of units and installed capacity.

Type:	Dry steam	1-Flash	2-Flash	3-Flash	Binary	Flash-binary	Hybrid; total flow	Total
No. of units:								
Totals	68	185	54	4	203	52	7	573
% of total	11.87	32.29	9.42	0.70	35.43	9.08	1.22	100
MW:								
Totals	2865	5146.18	1889.02	298.9	1245.313	473.08	11.3	11,928.79
% of total	24.02	43.14	15.84	2.51	10.44	3.97	0.09	100
MW/unit	42.13	27.82	34.98	74.73	6.13	9.10	1.61	20.82

TABLE A.6 China.

Plant	Year	Type	MW-rated	No. of units	MW-total	Comments
Dengwu:						
Unit 1	1970	1-Flash	(0.086)	(1)	(0.086)	Retired
Unit 2	1977	Binary	(0.2)	(1)	(0.2)	Retired
Unit 3	1984	1-Flash	0.3	1	0.3	aka Fengshun
Huailai:	1971	Binary	(0.285)	(1)	(0.285)	Retired
Wentang:	1971	Binary	(0.05)	(1)	(0.05)	Retired
Huitang:	1975	1-Flash	(0.3)	(1)	(0.3)	Retired
Chingshui:	1981	1-Flash	(3)	(1)	(3)	Inactive
Xiongyue:	1978	Binary	(0.1)	(1)	(0.1)	Retired
Tuchang:	1985	Binary	(0.3)	(1)	(0.3)	Inactive
Langjiu:						
Unit 1	1987	2-Flash	(1)	(1)	(1)	Retired
Unit 2	1988	2-Flash	(1)	(1)	(1)	Retired
Yangbajing:						
Unit 1	1977	1-Flash	(1)	(1)	(1)	Retired
Unit 2	1984	2-Flash	3	1	3	
Unit 3	1981	2-Flash	3	1	3	
Units 4–9	1982–92	2-Flash	3	6	18.18	
Unit 10	2009	Total flow	1	1	1	
Unit 11	2010	Total flow	1	1	1	
Nagqu:						
Unit 1	1993	Binary	(1)	(1)	(1)	Retired, 1999
Yangyi:						
Unit 1	2011	Total flow	0.40	1	0.40	
Unit 2	2012	Total flow	0.50	1	0.50	
Liubei:	2011	Total flow	0.40	1	0.40	
Totals				14	27.78	

TABLE A.7 Iceland.

Plant	Year	Type	MW-rated	No. of units	MW-total	Comments
Namafjall:	1969	1-Flash	3.2	1	3.2	Back-pressure
Bjarnarflag						
Krafla:						
Unit 1	1978	2-Flash	30	1	30	
Unit 2	1997	2-Flash	30	1	30	
Svartsengi:						
Unit 1	1978	1-Flash	1	1	1	
Unit 2	1979	1-Flash	1	1	1	
Unit 3	1981	1-Flash	6	1	6	
Unit 4	1989	Binary	1.3	3	3.9	
Unit 4 Extension	1993	Binary	1.2	4	4.8	
Unit 5	1999	1-Flash	30	1	30	
Unit 6	2007	Dry steam	30	1	30	
Nesjavellir:						
Units 1–2	1998	1-Flash	30	2	60	
Unit 3	2001	1-Flash	30	1	30	
Unit 4	2005	1-Flash	30	1	30	
Husavik	2000	Binary	(2)	(1)	(2)	Kalina, inactive
Reykjanes:						
Salt Plant	1983	1-Flash	0.5	1	0.5	
Units 1–2	2006	1-Flash	50	2	100	
Hellisheidi:						
Units 1–2	2006	1-Flash	45	2	90	
Unit 3	2007	1-Flash	33	1	33	
Units 4–5	2008	1-Flash	45	2	90	
Units 6–7	2011	1-Flash	45	2	90	
Totals				29	663.4	

TABLE A.8 Indonesia.

Plant	Year	Type	MW-rated	No. of units	MW-total	Comments	
Java:							
Kamojang:							
Wellhead Unit	1978	Dry steam	(0.25)	(1)	(0.25)	Retired	
Unit 1	1983	Dry steam	30	1	30		
Unit 2	1987	Dry steam	55	1	55		
Unit 3	1987	Dry steam	55	1	55		
Unit 4	2008	Dry steam	60	1	60		
Dieng:							
Wellhead Unit	1980	1-Flash	(2)	(1)	(2)	Moved	
Unit 1	1998	1-Flash	60	1	60		
Darajat:							
Unit 1	1994	Dry steam	55	1	55	aka Awibengkok	
Unit 2	2000	Dry steam	95	1	80		
Unit 3	2007	Dry steam	110	1	110		
Gunung Salak:							
Units 1–2	1994	1-Flash	55	2	110		
Units 3–6	1997	1-Flash	55	4	220		
Wayang Windu:							
Unit 1	1999	1-Flash	110	1	110		
Unit 2	2009	1-Flash	117	1	117		
Patuha:							
Unit 1	2014	1-Flash	55	1	55		
North Sulawesi:							
Lahendong:							
Pilot Unit	1992	1-Flash	(2.5)	(1)	(2.5)	Inactive	
Unit 1	2002	1-Flash	20	1	20		
Unit 2	2008	1-Flash	20	1	20		
Unit 3	2009	1-Flash	20	1	20		
Unit 4	2012	1-Flash	20	1	20		
Sumatra:							
Sibayak:							
Unit 1	1996	1-Flash	(2)	(1)	(2)	Retired	
Units 2–3	2007	1-Flash	5.65	2	11.3		
Ulubelu:							
Unit 1	2011	1-Flash	55	1	55		
Unit 2	2012	1-Flash	55	1	55		
East Nusa Tenggara:							
Ulumbu:							
Plant 1	2011–12	1-Flash	2.5	2	5		
Plant 2	2014	1-Flash	2.5	1	2.5		
Mataloko:							
Unit 1	2010	1-Flash	1.8	1	1.8	From Dieng	
Unit 2	2013	1-Flash	2.5	1	2.5		
Totals				30	1385.1		

TABLE A.9 Italy.

Plant	Year	Type	MW-rated	No. of units	MW-total	Comments
Larderello:						
Larderello 2:						
Units 1–4	1938	Dry steam	(14.5)	(4)	(58)	Retired
Unit 5	1938	Dry steam	(11)	(1)	(11)	Retired
Larderello 3:						
Unit 1	1965	Dry steam	(24)	(1)	(24)	Retired
Unit 2	1983	Dry steam	(26)	(1)	(26)	Retired
Unit 3	1964	Dry steam	(24)	(1)	(24)	Retired
Unit 4	1965	Dry steam	(24)	(1)	(24)	Retired
Nuova Larderello	2005	Dry steam	20	1	20	
Castelnuovo:						
Unit 1	1946	Dry steam	NA	NA	NA	Retired
Unit 2	1948	Dry steam	(11)	(1)	(11)	Retired
Unit 5	1967	Dry steam	(11)	(1)	(11)	Retired
Nuova Castelnuovo	2000	Dry steam	14.5	1	14.5	
Gabbro	1969	Dry steam	(15)	(1)	(15)	Retired
Nuova Gabbro	2002	Dry steam	20	1	20	
Valle Secolo:						
Unit 1	1991	Dry steam	60	1	60	
Unit 2	1992	Dry steam	60	1	60	
Farinello	1995	Dry steam	60	1	60	
Le Prata	1996	Dry steam	20	1	20	
Monteverdi 1–2	1997	Dry steam	20	2	40	
Selva	1997	Dry steam	20	1	20	
Lago:						
Unit 1	1960	Dry steam	(6.5)	(1)	(6.5)	Retired
Unit 2	1960	Dry steam	(12.5)	(1)	(12.5)	Retired
Unit 3	1964	Dry steam	(14.5)	(1)	(14.5)	Retired
Nuova Lago	2002	Dry steam	10	1	10	
Cornia:						
Unit 1	1987	Dry steam	(20)	(1)	(20)	Retired
Unit 2	1994	Dry steam	20	1	20	
San Martino:						
Unit 2	1985	Dry steam	(20)	(1)	(20)	Retired
Unit 3	1985	Dry steam	(20)	(1)	(20)	Retired
Nuova San Martino	2005	Dry steam	40	1	40	
Molinetto	1982	Dry steam	(8)	(1)	(8)	Retired
Nuova Molinetto	2002	Dry steam	20	1	20	
La Leccia	1983	Dry steam	(8)	(1)	(8)	Inactive
Lagoni Rossi:						
Unit 1	1960	Dry steam	(3.5)	(1)	(3.5)	Retired
Unit 2	1969	Dry steam	(3)	(1)	(3)	Retired
Unit 3	1981	Dry steam	(8)	(1)	(8)	Retired
Nuova Lagoni Rossi	2009	Dry steam	20	1	20	
Monterotondo	1968	Dry steam	(12.5)	(1)	(12.5)	Retired
Nuova Monterotondo	2002	Dry steam	10	1	10	

(Continued)

TABLE A.9 (Continued)

Plant	Year	Type	MW-rated	No. of units	MW-total	Comments
Sasso Pisano 1:						
Units 1–2	1969	Dry steam	(3.5)	(1)	(3.5)	Retired
Sasso Pisano 2:						
Unit 1	1968	Dry steam	(12.5)	(1)	(12.5)	Retired
Unit 2	1968	Dry steam	(3.2)	(1)	(3.2)	Retired
Serrazzano:						
Units 1–2	1967	Dry steam	(12.5)	(2)	(25)	Retired
Unit 5	1975	Dry steam	(15)	(1)	(15)	Retired
Nuova Serrazzano	2002	Dry steam	60	1	60	
Carboli:						
Unit 1	1998	Dry steam	20	1	20	
Unit 2	1997	Dry steam	20	1	20	
Nuova Sasso	1996	Dry steam	20	1	20	
Sasso 2	2009	Dry steam	20	1	20	
Sesta	2002	Dry steam	20	1	20	
Subtotals				22	594.5	
Mt. Amiata:						
Bagnore:						
Bagnore 1–2	1945	Dry steam	(3.5)	(2)	(7)	Retired
Unit 1	1959	Dry steam	(0.9)	(1)	(0.9)	Retired
Unit 2	1962	Dry steam	(3.5)	(1)	(3.5)	Retired
Unit 3	1998	1-Flash	20	1	20	
Binary Unit 3	2013	Binary	1	1	1	
Bellavista	1987	Dry steam	(20)	(1)	(20)	Retired
Piancastagnaio:						
Unit 1	1969	Dry steam	(15)	(1)	(15)	Retired
Unit 2	1969	Dry steam	(8)	(1)	(8)	Retired
Unit 3	1990	Dry steam	20	1	20	
Unit 4	1991	Dry steam	20	1	20	
Unit 5	1994	Dry steam	20	1	20	
Subtotals				5	81	
Travale-Radicondoli:						
Radicondoli:						
Units 1–2	1979	Dry steam	(15)	(2)	(30)	Retired
Rancia	1986	Dry steam	20	1	20	
Pianacce	1987	Dry steam	(20)	(1)	(20)	Inactive
Rancia 2	1988	Dry steam	20	1	20	
Travale 21	1991	Binary	(0.7)	(1)	(0.7)	Retired
Travale 3	2000	Dry steam	20	1	20	
Travale 4	2002	Dry steam	40	1	40	
Nuova Radicondoli	2002	Dry steam	40	1	40	
Nuova Radicondoli 2	2010	Dry steam	20	1	20	
Chiusdino 1	2010	Dry steam	20	1	20	
Subtotals				7	180	
Totals				34	855.5	

TABLE A.10 Japan.

Plant	Year	Type	MW-rated	No. of units	MW-total	Comments
Kyushu:						
Tsurumi	1925	Dry steam	(0.00112)	(1)	(0.00112)	Experimental
Hakuryu	1951	Dry steam	(0.3)	(1)	(0.3)	Experimental
Otake	1967	1-Flash	12.5	1	12.5	
Otake Pilot	1978	Binary	(1)	(1)	(1)	Retired
Hatchobaru 1	1977	2-Flash	55	1	55	
Hatchobaru 2	1990	2-Flash	55	1	55	
Hatchobaru 3	2006	Binary	2	1	2	
Suginoi	1981	1-Flash	1.9	1	1.9	
Kirishima Kokusai	1996	1-Flash	0.1	1	0.1	
Takenoyu	1991	1-Flash	0.05	1	0.05	
Kujukannko	1998	1-Flash	0.99	1	0.99	
Takigami	1996	1-Flash	27.5	1	27.5	
Takigami Binary	1997	Binary	(0.49)	(1)	(0.49)	Retired
Ogiri	1996	1-Flash	30	1	30	
Yamakawa	1995	1-Flash	30	1	30	
Beppu Spring	2014	Binary	0.125	4	0.5	
Goto-en	2014	Binary	0.045	2	0.09	
Hagenoyu	2014	Binary	0.667	3	2.0	
Oguni Matsuya	2014	Binary	0.06	1	0.06	
Honshu:						
Matsukawa	1966	Dry steam	23.5	1	23.5	
Onuma	1974	1-Flash	9.5	1	9.5	
Onikobe	1975	1-Flash	15	1	15	
Kakkonda 1	1978	1-Flash	50	1	50	
Kakkonda 2	1996	1-Flash	30	1	30	
Sumikawa	1995	1-Flash	50	1	50	
Uenotai	1994	1-Flash	28.8	1	28.8	
Yanaizu-Nishiyama	1995	1-Flash	65	1	65	
Hachijo-Jima	1999	1-Flash	3.3	1	3.3	
Abo Tunnel	2013	Binary	0.003	1	0.003	
Sachimi Spring	2014	Binary	0.02	1	0.02	
Yumura Spring	2014	Binary	0.03	1	0.03	
Hokkaido:						
Mori	1982	2-Flash	25	1	25	
Nigorikawa Pilot	1978	Binary	(1)	(1)	(1)	Retired
Totals				34	517.843	

TABLE A.11 Kenya.

Plant	Year	Type	MW-rated	No. of units	MW-total	Comments
Olkaria:						
Olkaria I:						aka East Olkaria
Unit 1	1981	1-Flash	15	1	15	
Unit 2	1982	1-Flash	15	1	15	
Unit 3	1985	1-Flash	15	1	15	
Units 4–5	2014	1-Flash	70	2	140	
Olkaria II:						aka NE Olkaria
Units 1–2	2003	1-Flash	35	2	70	
Unit 3	2010	1-Flash	35	1	35	
Olkaria III—OrPower 4:						aka West Olkaria
Units 1–2	2000	Flash-binary	4.6	2	9.2	Plant 1, Phase 1
Unit 3	2000	Flash-binary	2.8	1	2.8	Plant 1, Phase 1
Units 4–6	2009	Flash-binary	13.6	3	40.8	Plant 1, Phase 2
Plant 2	2013	Flash-binary	13.2	3	39.6	
Plant 3	2014	Flash-binary	8.8	2	17.6	
Olkaria Central:						Oserian Co.
Unit 1	2004	Binary	1.8	1	1.8	
Unit 2	2007	1-Flash	1.4	1	1.4	Back-pressure
Olkaria IV:						
Units 1–2	2014	1-Flash	70	2	140	
Olkaria WHU:						
OW-37	2013	1-Flash	5	1	5	
OW-43	2014	1-Flash	3.2	4	12.8	
Eburru:						
Unit 1	2012	1-Flash	2.5	1	2.5	
Totals				29	563.5	

TABLE A.12 Mexico.

Plant	Year	Type	MW-rated	No. of units	MW-total	Comments
Pathé: Pilot plant	1959	1-Flash	(3.5)	(1)	(3.5)	Dismantled
Cerro Prieto:						
Cerro Prieto I:						
Units 1–2	1973	1-Flash	(37.5)	(2)	(75)	Inactive
Units 3–4	1979	1-Flash	(37.5)	(2)	(75)	Inactive
Unit 5	1981	1-Flash	30	1	30	
Cerro Prieto II:						
Units 1–2	1984	2-Flash	110	2	220	
Cerro Prieto III:						
Units 1–2	1985	2-Flash	110	2	220	
Cerro Prieto IV:						
Units 1–4	2000	1-Flash	25	4	100	
Los Azufres:						
Unit 1	1982	1-Flash	(5)	(1)	(5)	Dismantled
Units 2–5	1982	1-Flash	5	4	20	Noncondensing
Unit 6	1986	1-Flash	5	1	5	Noncondensing
Unit 7	1988	1-Flash	50	1	50	
Units 9–10	1990–92	1-Flash	5	2	10	Noncondensing
Units 11–12	1993	Binary	(1.5)	(2)	(3)	Inactive
Units 13–16	2003	1-Flash	26.5	4	106	
Los Humeros:						
Units 1–2	1990	1-Flash	(5)	(2)	(10)	Standby
Unit 3	1991	1-Flash	5	1	5	Noncondensing
Unit 5	1991	1-Flash	(5)	(1)	(5)	Standby
Unit 6	1992	1-Flash	5	1	5	Noncondensing
Unit 7	1994	1-Flash	(5)	(1)	(5)	Standby
Unit 4	2003	1-Flash	(5)	(1)	(5)	Standby
Unit 8	2008	1-Flash	5	1	5	Noncondensing
Los Humeros IIA	2012	1-Flash	26.7	1	26.7	
Los Humeros IIB	2013	1-Flash	26.7	1	26.7	
Tres Virgines:						
Units 1–2	2002	1-Flash	5	2	10	
Maguarichic:						
Piedras de Lumbre	2001	Binary	(0.3)	(1)	(0.3)	Inactive
Totals				28	839.4	

TABLE A.13 New Zealand.

Plant	Year	Type	MW-rated	No. of units	MW-total	Comments
Wairakei:						
Unit 1	1959	2-Flash	(11.2)	(1)	(11.2)	Retired
Unit 2	1958	1-Flash	(6.5)	(1)	(6.5)	Retired
Unit 3	1959	1-Flash	(6.5)	(1)	(6.5)	Retired
Unit 4	1959	2-Flash	(11.2)	(1)	(11.2)	Retired
Units 5–6	1962	1-Flash	(11.2)	(2)	(22.4)	Moved
Units 7–8	1959	3-Flash	(11.2)	(2)	(22.4)	Retired
Units 9–10	1960	3-Flash	(11.2)	(2)	(22.4)	Retired
Unit 11	1962	2-Flash	30	1	30	
Units 12–13	1963	2-Flash	30	2	60	
Unit 14	NA	1-Flash	5	1	5	
Poihipi	1996	Dry Steam	55	1	55	
Bottoming unit	2005	Binary	7	2	14	
Te Mihi	2014	2-Flash	83	2	166	
Kawerau:						
Unit 1	1961	1-Flash	(10)	(1)	(10)	Retired
TG1	1989	Binary	1.2	2	2.4	
TG2	1993	Binary	3.5	1	3.5	
Tasman	2004	1-Flash	5	1	5	Back-pressure
KA24	2008	Binary	8.3	1	8.3	
Mighty River Power	2008	2-Flash	100	1	100	
TOPP1	2013	Binary	23	1	23	
TAUHARA:	2010	Binary	13	2	26	aka Te Huka
Ohaaki:						
Unit 1	1988	1-Flash	(11.2)	(1)	(11.2)	Retired
Unit 2	1988	1-Flash	11.2	1	11.2	From Wairakei
Unit 3	1988	1-Flash	(46)	(1)	(46)	Retired
Unit 4	1988	1-Flash	47	1	47	
Mokai:						
Mokai I	1999	Flash-binary	25, 5	1, 6	55	
Mokai II	2005	Flash-binary	33, 6	1, 1	39	
Mokai IA	2007	Binary	17	1	17	
Ngawha:						
Unit 1	1998	Flash-binary	5	2	10	
Unit 2	2008	Binary	15	1	15	
Rotokawa:						
Combined cycle	1997	Flash-binary	14, 5	1, 3	29	
Extension	2003	Flash-binary	5	1	5	
Nga Awa Purua	2010	3-Flash	140	1	140	
Ngatamariki:	2013	Binary	20.5	4	82	
Totals				43	948.4	

TABLE A.14 Philippines.

Plant	Year	Type	MW-rated	No. of units	MW-total	Comments
Luzon:						
Makiling-Banahaw:						aka Mak-Ban
Plant A: Units 1–2	1979	1-Flash	63.2	2	126.4	
Plant B: Units 3–4	1980	1-Flash	63.2	2	126.4	
Plant C: Units 5–6	1984	1-Flash	55	2	110	
Binary I	1994	Binary	(3)	(2)	(6)	Inactive
Binary II	1994	Binary	(3)	(2)	(6)	Inactive
Binary III	1994	Binary	(3)	(1)	(3)	Inactive
Binary IV	1994	Binary	(0.73)	(1)	(0.73)	Inactive
Plant D: Unit 9	1996	1-Flash	20	2	40	
Plant E: Unit 10	1996	1-Flash	20	2	40	
Maibarara:	2014	1-Flash	20	1	20	
Tiwi:						
Plant A: Units 1–2	1979	1-Flash	60	2	120	
Plant B: Units 3–4	1980	1-Flash	(55)	(2)	(110)	Retired
Plant C: Units 5–6	1982	1-Flash	57	2	114	
Bacon-Manito:						
Palayan: Units 1–2	1993	1-Flash	55	2	110	aka Bac-Man
Cawayan: Unit 3	1994	1-Flash	20	1	20	Reactivated
Botong: Unit 4	1998	1-Flash	(20)	(1)	(20)	Retired
Manito Lowland	1998	1-Flash	1.5	1	1.5	
Leyte:						
WH Unit	1977	1-Flash	(3)	(1)	(3)	Retired, 1994
Units 1–3 Tongonan I	1983	1-Flash	37.5	3	112.5	
Units 13–15 Mahanagdong	1997	1-Flash	60	3	180	
Unit 16 Tongonan	1997	1-Flash	6.5	3	19.5	Topping
Units 18–20 Mahanagdong	1997	1-Flash	6.5	3	19.5	Topping
Unit 8 Malitbog	1996	1-Flash	77.5	1	77.5	
Units 21–22 Malitbog	1997	1-Flash	77.5	2	155	
Unit 17 Malitbog	1997	1-Flash	16.7	1	16.7	Bottoming
Units 4–7 Upper Mahiao	1996	Flash-binary	34.12, 5.5	4, 1	141.98	
Southern Negros:						
Palinpinon I:						
WH Units 1–2	1980	1-Flash	(1.5)	(2)	(3)	Retired, 1994
WH Units 3–4	1982	1-Flash	(1.5)	(2)	(3)	Retired
Units 1–3	1983	1-Flash	37.5	3	112.5	
Palinpinon II:						
Balas-balas Unit 5	1993	1-Flash	20	1	20	aka Okoy 5
Nasuji Unit 4	1994	1-Flash	20	1	20	
Sogongon Units 6–7	1995	1-Flash	20	2	40	
Nasulo	2012	1-Flash	30	1	30	From N. Negros
Mindanao:						
Unit 1 Matingao	1996	1-Flash	54.24	1	54.24	
Unit 2 Sandawa	1999	2-Flash	54.24	1	54.24	
Northern Negros:						
Unit 1	2007	1-Flash	(49)	(1)	(49)	Moved
Totals				50	1881.96	

TABLE A.15 Russia.

Plant	Year	Type	MW-rated	No. of units	MW-total	Comments
Paratunka:						
Unit 1	1967	Binary	(0.68)	(1)	(0.68)	Retired
Pauzhetka:						
Units 1–2	1967	1-Flash	2.5	2	5	
Unit 3	1981	1-Flash	6	1	6	
Verkhne-Mutnovsky:						
Unit 1	1998	1-Flash	4	1	4	
Units 2–3	1999	1-Flash	4	2	8	
Mutnovsky:						
Unit 1	2002	1-Flash	25	1	25	
Unit 2	2004	1-Flash	25	1	25	
Okeansky:						
Unit 1	2000	1-Flash	1.7	1	1.7	
Unit 2	2001	1-Flash	1.7	1	1.7	
Goryachii Plyazh:	2004	1-Flash	1.3	2	2.6	
Totals				12	79	

TABLE A.16 Turkey.

Plant	Year	Type	MW-rated	No. of units	MW-total	Comments
Kızıldere:						
Wellhead Unit	1974	1-Flash	(0.5)	(1)	(0.5)	Dismantled
Unit 1	1984	1-Flash	20.4	1	20.4	
Unit 2	2013	3-Flash, binary	60, 10	1, 2	80	
Salavatlı:						
Dora 1	2006	Binary	7.95	1	7.95	
Dora 2	2010	Binary	11.5	1	11.5	
Dora 3A	2013	Binary	18	1	18	
Dora 3B	2014	Binary	20	1	20	
Germencik	2009	2-Flash	47.4	1	47.4	
Tuzla-Çanakale	2009	Binary	7.5	1	7.5	
Saraköy: Bereket	2007	Binary	(6.35)	(1)	(6.35)	Inactive
Denizli: Jeoden	2011	Binary	0.26	3	0.78	
Aydın-Hıdırbeyli: IREM	2011	Binary	20	1	20	
Aydın-Pamukören:						
Unit I	2013	Binary	25	1	25	
Unit II	2014	Binary	25	1	25	
Aydın-Gümüşköy:						
Unit I	2014	Binary	6.6	1	6.6	
Unit II	2015	Binary	6.6	1	6.6	
Totals				18	296.73	

TABLE A.17 United States: California.

Plant	Year	Type	MW-rated	No. of units	MW-total	Comments
The Geysers:						
Unit 1	1960	Dry steam	(11)	(1)	(11)	Dismantled
Unit 2	1963	Dry steam	(13)	(1)	(13)	Dismantled
Unit 3	1967	Dry steam	(27)	(1)	(27)	Dismantled
Unit 4	1968	Dry steam	(27)	(1)	(27)	Dismantled
McCabe	1971	Dry steam	53	2	106	
Ridge Line	1972	Dry steam	53	2	106	
Fumarole	1973	Dry steam	(53)	(2)	(106)	Dismantled
Eagle Rock	1975	Dry steam	106	1	106	
Cobb Creek	1979	Dry steam	106	1	106	
Big Geysers	1980	Dry steam	78	1	78	
Sulphur Springs	1980	Dry steam	65	1	65	
Unit 15	1979	Dry steam	(59)	(1)	(59)	Dismantled
Quicksilver	1985	Dry steam	113	1	113	
Lake View	1982	Dry steam	113	1	113	
Socrates	1983	Dry steam	113	1	113	
Calistoga	1984	Dry steam	40	2	80	
Grant	1985	Dry steam	113	1	113	
Bottle Rock	1985	Dry steam	15	1	15	Reactivated
Sonoma	1983	Dry steam	72	1	72	
NCPA 1	1983	Dry steam	55	2	110	
NCPA 2	1985–86	Dry steam	55	2	110	
Coldwater Creek	1988	Dry steam	(65)	(2)	(130)	Dismantled
Bear Canyon	1988	Dry steam	11	2	22	
West Ford Flat	1988	Dry steam	14.5	2	29	
J.W. Aidlin	1989	Dry steam	10	2	20	
Subtotals — The Geysers				26	1477	
Imperial Valley:						
Brawley: Pilot plant	1980	1-Flash	(10)	(1)	(10)	Dismantled 1985
North Brawley:	2010	Binary	10	5	50	
East Mesa:						
GEM 1	1979	Binary	(13.4)	(1)	(13.4)	Dismantled
GEM 2	1989	2-Flash	18.5	1	18.5	
GEM 3	1989	2-Flash	18.5	1	18.5	
GEM Bottoming Unit	2007	Binary	9	1	9	
ORMESA I	1987	Binary	(0.923)	(26)	(24)	Original plant
ORMESA I	2003	Binary	10, 1	2, 2	22	
ORMESA II	1988	Binary	(0.825)	(20)	(16.5)	Original plant
ORMESA II	2008	Binary	11.75	2	23.5	
ORMESA IE	1988	Binary	0.83	12	10	
ORMESA IH	1989	Binary	1.1	12	13.2	
Subtotals — East Mesa				33	114.7	
Heber:						
Binary Demo	1985	Binary	(45)	(1)	(45)	Dismantled
Heber 1	1985	2-Flash	47	1	47	
Heber 2	1993	Binary	2.75	12	33	Orig. SIGC
Gould I	2006	Binary	2.5	4	10	
Gould II	2006	Binary	10	1	10	
Heber South	2008	Binary	10	1	10	
Subtotals — Heber				19	110	

(Continued)

TABLE A.17 (Continued)

Plant	Year	Type	MW-rated	No. of units	MW-total	Comments
Salton Sea:						
Unit 1	1982	1-Flash	10	1	10	1st FC/RC plant
Unit 2	1990	2-Flash	10, 5, 4	3	19	
Unit 3	1989	2-Flash	49.8	1	49.8	
Unit 4	1989	2-Flash	39.6	1	39.6	
Unit 5	2000	3-Flash	49	1	49	
Vulcan	1985	2-Flash	29, 8	2	37	Orig. Del Ranch
A.W. Hoch	1989	2-Flash	35.8	1	35.8	
J.J. Elmore	1989	2-Flash	35.8	1	35.8	
J.M. Leathers	1989	2-Flash	35.8	1	35.8	aka Hudson Ranch 1
John L. Featherstone	2012	3-Flash	49.9	1	49.9	
Subtotals – Salton Sea				13	361.7	
Casa Diablo:						
						aka Mammoth
MP-I	1984	Binary	3.5	2	7	
MP-II	1990	Binary	5	3	15	
PLES-I	1990	Binary	3.3	3	10	
Subtotals – Casa Diablo				8	32	
Honey Lake:						
Wineagle	1985	Binary	0.35	2	0.7	
Amedee	1988	Binary	0.8	2	1.6	
Honey Lake:	1989	Hybrid	30	1	6	
Subtotals – Honey Lake				5	8.3	
Coso:						
Navy I Unit 1	1987	2-Flash	34.1	1	34.1	
Navy I Unit 2	1988	2-Flash	34.1	1	34.1	
Navy I Unit 3	1988	2-Flash	34.1	1	34.1	
Navy II Unit 4	1989	2-Flash	33.3	1	33.3	
Navy II Unit 5	1989	2-Flash	33.3	1	33.3	
Navy II Unit 6	1989	2-Flash	33.4	1	33.4	
BLM East Unit 7	1988	2-Flash	33.3	1	33.3	
BLM East Unit 8	1988	2-Flash	33.3	1	33.3	
BLM West Unit 9	1989	2-Flash	33.3	1	33.3	
Subtotals – Coso				9	302.2	
Totals				118	2455.9	

TABLE A.18 United States: Nevada, Utah, Hawaii, Idaho, Alaska, New Mexico, Oregon, and Wyoming.

Plant	Year	Type	MW-rated	No. of units	MW-total	Comments
Nevada:						
Wabuska 1	1984	Binary	0.75	1	0.75	
Wabuska 2	1987	Binary	1.0	1	1.0	
Beowawe	1985	2-Flash	16	1	16	
Beowawe Bottoming	2011	Binary	2	1	2	
Desert Peak 1	1985	2-Flash	(7)	(1)	(7)	Retired
Desert Peak 2	2005	Binary	15, 11	2	26	
San Emidio	1987	Binary	(0.9)	(4)	(3.6)	Inactive
San Emidio	2012	Binary	11.5	1	11.5	
Steamboat 1	1986	Binary	(0.86)	(7)	(6)	Inactive
Steamboat 1A	1988	Binary	(0.55)	(2)	(1.1)	Inactive
Steamboat 2	1992	Binary	7	2	14	
Steamboat 3	1992	Binary	7	2	14	
Steamboat Hills	1988	1-Flash	13	1	13	
Steamboat Hills 2	2007	Binary	6	1	6	
Burdette	2006	Binary	13	2	26	Orig. Galena 1
Galena 2	2007	Binary	13	1	13	
Galena 3	2008	Binary	13	2	26	
Soda Lake 1	1987	Binary	1.2	3	3.6	
Soda Lake 2	1991	Binary	2	6	12	
Stillwater 1	1989	Binary	(0.93)	(14)	(13)	Retired
Stillwater 2	2009	Binary	12	4	48	
Stillwater CSP	2014	Solar	2	1	2	Hybrid
Dixie Valley	1988	2-Flash	60.5	1	60.5	
Dixie Valley Bottoming	2011	Binary	5	1	5	
Brady I	1992	2-Flash	6	3	17	
Brady II	2002	Binary	3	1	3	
Rye Patch	2001	Binary	(2.5)	(5)	(12.5)	Inactive
Faulkner	2009	Binary	16.5	3	49.5	aka Blue Mountain
Salt Wells	2009	Binary	9	2	18	
Jersey Valley	2011	Binary	15	1	15	
McGinness Hills	2012	Binary	17.3	3	52	
Tuscarora	2012	Binary	16	2	32	
Patua	2013	Binary	15	1	15	
Don A. Campbell	2013	Binary	22.5	1	22.5	aka Wild Rose
Subtotals – Nevada				51	524.35	

(Continued)

TABLE A.18 (Continued)

Plant	Year	Type	MW-rated	No. of units	MW-total	Comments
Utah:						
Blundell Unit 1	1984	1-Flash	26	1	26	
Cove Fort 1	1985	Binary	(0.5)	(4)	(2)	Inactive
Cove Fort 2	1988	Dry steam	(2)	(1)	(2)	Inactive
Cove Fort 3	2013	Binary	25	2	25	
Bonnett	1990	Dry steam	(7)	(1)	(7)	Inactive
Blundell Unit 2	2007	Binary	11	1	11	
Thermo HS: Hatch	2008	Binary	(0.2)	(50)	(10)	Inactive
Thermo HS 2	2013	Binary	10	1	10	
Subtotals – Utah				5	72	
Hawaii:						
Puna PGV-1	1992	Flash-binary	3	10	30	
Puna Extension	2011	Binary	8	1	8	
Subtotals – Hawaii				11	38	
Idaho:						
Raft River	1981	Binary	(5)	(1)	(5)	Dismantled 1982
USGeo Phase 1	2008	Binary	13	1	13	
Subtotals – Idaho				1	13	
Alaska:						
Chena H. S. Units 1–2	2006	Binary	0.2	2	0.4	
Chena H. S. Unit 3	2010	Binary	(0.2)	(1)	(0.2)	Inactive
Subtotals – Alaska				2	0.4	
New Mexico:						
Burgett Greenhouse	1995	Binary	(0.35)	(1)	(0.35)	Inactive
Burgett Greenhouse	1995	Binary	(0.4)	(2)	(0.8)	Inactive
Burgett Greenhouse	2008	Binary	0.2	2	0.4	
Lightning Dock 1	2013	Binary	4	1	4	
Subtotals – New Mexico				3	4.4	
Oregon:						
Oregon Inst. of Tech.	2010	Binary	0.28	1	0.28	
Oregon Inst. of Tech.	2014	Binary	1.75	1	1.75	
Neal Hot Springs	2012	Binary	7.3	3	21.9	
Paisley	2014	Binary	2.5	1	2.5	
Subtotals – Oregon				6	26.43	
Wyoming:						
RMOTC	2008	Binary	(0.25)	(1)	(0.25)	Inactive
Totals				79	678.58	

TABLE A.19 Countries with fewer than 10 units.

Plant	Year	Type	MW-rated	No. of units	MW-total	Comments
Australia						
Mulka: Unit 1	1986	Binary	(0.02)	(1)	(0.02)	Inactive
Birdsville: Unit 1	1992	Binary	0.15	1	0.15	
Innamincka	2013	Binary	(1.0)	(1)	(1.0)	Inactive
Totals					0.15	
Austria						
Bad Blumau	2001	Binary	0.25	1	0.25	
Altheim: Unit 1	2002	Binary	1	1	1	
Simbach/Braunau	2009	Binary	0.2	1	0.2	
Totals				3	1.45	
Costa Rica						
Miravalles:						
Wellhead Unit 1	1995	1-Flash	5	1	5	
Wellhead Unit 2	1996	1-Flash	(5)	(1)	(5)	Dismantled 1998
Wellhead Unit 3	1997	1-Flash	(5)	(1)	(5)	Dismantled 1998
Unit 1	1994	1-Flash	55	1	55	
Unit 2	1998	1-Flash	55	1	55	
Unit 3	2000	1-Flash	29	1	29	
Unit 5	2004	Binary	9.5	2	19	
Las Pailas Plant 1:						
Unit 1	2011	Binary	21	1	21	
Unit 2	2011	Binary	21	1	21	
Totals				8	205	
El Salvador						
Ahuachapán:						
Unit 1	1975	1-Flash	30	1	30	
Unit 2	1976	1-Flash	30	1	30	
Unit 3	1981	2-Flash	35	1	35	
Berlín:						
Wellhead Unit 1	1992	1-Flash	(5)	(1)	(5)	Retired
Wellhead Unit 2	1992	1-Flash	(5)	(1)	(5)	Retired
Units 1–2	1999	1-Flash	28	2	56	
Unit 3	2007	1-Flash	44	1	44	
Bottoming Unit	2007	Binary	9.3	1	9.3	
Totals				7	204.3	
Ethiopia						
Langano: Unit 1	1998	Flash-binary	3.9, 4.6	1	8.5	Reactivated 2007
Totals				1	8.5	

(Continued)

TABLE A.19 (Continued)

Plant	Year	Type	MW-rated	No. of units	MW-total	Comments
France						
Guadeloupe:						
Bouillante: Unit 1	1986	2-Flash	4.7	1	4.7	
Bouillante: Unit 2	2004	1-Flash	11	1	11	
Totals				2	15.7	
Germany						
Neustadt-Glewe	2003	Binary	(0.2)	(1)	(0.2)	Retired
Landau	2007	Binary	3.0	1	3.0	
Unterhaching	2009	Binary	3.36	1	3.36	Kalina cycle
Bruchsal	2009	Binary	0.55	1	0.55	Kalina cycle
Simbach-Braunau	2010	Binary	(0.2)	(1)	(0.2)	Retired
Durrnhaar	2012	Binary	5.5	1	5.5	
Insheim	2012	Binary	4.3	1	4.3	
Kirchstockach	2013	Binary	5.5	1	5.5	
Sauerlach	2013	Binary	5.0	1	5.0	
Totals			27.2	7	27.2	
Guatemala						
Zunil: Orzunil Unit 1	1999	Flash-binary	3.5	7	24.6	
Amatitlán:						
Wellhead Unit 1	1997	1-Flash	(5)	(1)	(5)	Dismantled 2001
Geotermica	2003	1-Flash	(5)	(1)	(5)	Dismantled
Calderas Unit 1	2007	Flash-binary	10	2	20	
Totals				9	44.6	
Nicaragua						
Momotombo:						
Unit 1	1983	1-Flash	35	1	35	
Unit 2	1989	1-Flash	35	1	35	
Unit 3	2002	Binary	7.5	1	7.5	
San Jacinto-Tizate:						
Unit 1	2006	1-Flash	(5)	(2)	(10)	Inactive
Unit 2	2012	1-Flash	36	1	36	
Unit 3	2012	1-Flash	36	1	36	
Totals				5	149.5	

(Continued)

TABLE A.19 (Continued)

Plant	Year	Type	MW-rated	No. of units	MW-total	Comments
Papua-New Guinea						
Lihir:						
Unit 1	2003	1-Flash	6	1	6	Back-pressure
Unit 2	2005	1-Flash	10	3	30	Condensing
Unit 3	2006	1-Flash	10	2	20	Condensing
Totals				6	56	
Portugal (Azores)						
Sao Miguel:						
Pico Vermelho:						
Wellhead Unit 1	1980	1-Flash	(3)	(1)	(3)	Dismantled 2005
Unit 2	2006	Binary	10	1	10	
Ribeira Grande:						
Phase A	1994	Binary	2.5	2	5	
Phase B	1998	Binary	4	2	8	
Totals				5	23	
Thailand						
Fang: Unit 1	1989	Binary	0.3	1	0.3	
Totals				1	0.3	

TABLE A.20 Countries with only retired/inactive plants.

Country: plant	Year	Type	MW-rated	No. of units	MW-total	Comments
Argentina:						
Copahue: Unit 1	1988	Binary	(0.67)	(1)	(0.67)	Retired 1996
Democratic Republic of Congo:						
Kiabukwa	1952	Vacuum flash	(0.2)	(1)	(0.2)	Dismantled c. 1956
Greece:						
Milos: Unit 1	1985	1-Flash	(2)	(1)	(2)	Retired 1989
Zambia:						
Kapisya	1986	Binary	(0.1)	(2)	(0.2)	Inactive
Totals				(5)	(3.07)	

Appendix B

Units Conversions

Regarding units, there is no uniformity of usage across the world. The United States uses their own version of the old British system of units, the US Customary System of Units, while the rest of the world has adopted the *Système International des Unites* (International System of Units) or the SI System. Thus there is a need for the table given here.

Multiply to obtain	→	by or by	→	to obtain Divide
ft		0.3048		m
m		3.281		ft
in		25.4		mm
km		0.6214		mi
cm/s ²		0.0328		ft/s ²
gal		0.1337		ft ³
gal/min or GPM		0.2272		m ³ /h
g/cm ³		0.06242		lbm/ft ³
kg		2.2046		lbm
kg/s		7936.56		lbm/h
t/h		0.2778		kg/s
g/cm ³		1000		kg/m ³
lbm/ft ³		16.02		kg/m ³
lbf/in ² or psia		0.06895		bar
lbf/in ² or psia		6.895		kPa
MPa		145		lbf/in ² or psia
bar		14.5		lbf/in ² or psia
kg/cm ² or ata		0.9807		bar
in Hg		3.386		kPa
°C/m		0.549		°F/ft
K		1.8		°R
J/g or kJ/kg		0.430		Btu/lbm
cal/cm ² · s		4.184		J/cm ² · s
cal/cm ² · s		41.84		kJ/m ² · s
W/m · °C		0.5779		Btu/h · ft · °F
kJ/kg · K		0.2388		Btu/lbm · °R
kW or kJ/s		3412		Btu/h
°C	→	1.8 and add 32	→	°F
°F	→	0.5556 after subtracting 32	→	°C

Appendix C

Energy Equivalents

These tables give the *approximate* equivalent electrical energy, in kW · h, for various primary sources of energy. We state the type of power plant in use; typical utilization efficiencies were assumed to arrive at the equivalent electricity. Actual plants may differ from these approximate values by $\pm 15\%$. For geothermal binary plants, the brine outlet temperature is very important and will strongly affect the output.

TABLE C.1 US customary units.

Primary “fuel” source	Electricity kW · h	Conversion system
1000 ft ³ natural gas	100	Simple cycle gas turbine
1000 ft ³ natural gas	160	Combined steam and gas turbine
1 barrel fuel oil	720	Double-reheat, regenerative Rankine cycle
1 ton (2000 lbm) lignite	1260	Single-reheat Rankine cycle
1 ton (2000 lbm) bituminous coal	2820	Double-reheat, regenerative Rankine cycle
1 ton (2000 lbm) garbage and trash	1025	Single-reheat Rankine cycle
1 lbm natural uranium	310	Pressurized water reactor
Sun on 10 ft ² of earth, 1 day	0.75	Photovoltaic cell @ 10% efficiency
1000 lbm geoliquid, 300°F	3.3	Binary plant
1000 lbm geoliquid, 350°F	5.6	Single-flash plant
1000 lbm geoliquid, 400°F	10.4	Double-flash plant
1000 lbm geoliquid, 450°F	14.5	Double-flash plant
1000 lbm geosteam, 350°F	53.5	Typical dry-steam plant

TABLE C.2 SI units.

Primary “fuel” source	Electricity kW · h	Conversion system
100 m ³ natural gas	353	Simple cycle gas turbine
100 m ³ natural gas	565	Combined steam and gas turbine
100 liter fuel oil	450	Double-reheat, regenerative Rankine cycle
1 tonne (1000 kg) lignite	1390	Single-reheat Rankine cycle
1 tonne (1000 kg) bituminous coal	3110	Double-reheat, regenerative Rankine cycle
1 tonne (1000 kg) garbage and trash	1130	Single-reheat Rankine cycle
1 kg natural uranium	140	Pressurized water reactor
Sun on 1 m ² of earth, 1 day	0.75	Photovoltaic cell @ 10% efficiency
1000 kg geoliquid, 150°C	7.3	Binary plant
1000 kg geoliquid, 175°C	12.3	Single-flash plant
1000 kg geoliquid, 200°C	22.9	Double-flash plant
1000 kg geoliquid, 235°C	32.0	Double-flash plant
1000 kg geosteam, 175°C	118	Typical dry-steam plant



Appendix D

Elements of Thermodynamics

Die Energie der Welt ist constant. Die Entropie der Welt strebt einem Maximum zu.

Rudolf J. Clausius, on the First and Second Laws of thermodynamics—1865

D.1 Purpose

This appendix is intended to give the reader a thumbnail sketch of the elements of thermodynamics, sufficient to allow an understanding of the concepts used in Parts 2 and 3 of the book. It cannot replace a proper exposition of the subject, which normally takes several semesters of study in an engineering curriculum.

D.2 Systems and Properties

A thermodynamic *system* is a well-defined region of space, within which resides the focus of one's attention, e.g., a turbine, heat exchanger, flash vessel, etc. A system can be: (1) *closed* (no mass crosses the system boundary), (2) *open* (mass crosses the boundary), or (3) *isolated* (the system does not interact with its surroundings in any way).

A system that is *perfectly insulated* from its surroundings is said to have *adiabatic walls* or to be *adiabatic*; one that is *perfectly coupled thermally* to its surroundings is said to have *diathermal walls* or to be *diathermal*.

The system is described by its *properties*, physical characteristics that can be measured or calculated. Properties can be: (1) *extensive* (dependent on the size or extent of the system, such as mass, volume, energy), (2) *intensive* (independent of the size or extent of the system, such as temperature, pressure), or (3) *specific* (an extensive property per unit mass, such as specific volume). When the array of properties has a fixed set of values, the system exists in a certain *state*.

The *Gibbs Phase Rule* says that the number of *independent intensive thermodynamic properties*, f , is given by:

$$f = C - P + 2 \quad (\text{D.1})$$

where C is the number of pure substances present and P is the number of distinct phases present. Thus, for a single pure substance existing in a single phase (vapor, liquid, or solid), there are two independent intensive properties. Any other property can therefore be expressed in terms of the two independent ones, giving a surface in the space defined by the three properties. Special cases occur when more than one phase is present, reducing the generality of the surface. For example, a ruled surface results when two phases are present (say, liquid and vapor).

The properties are related through the *equation of state*. Gases and some vapors can be approximately described by the simple *perfect gas equation of state*,

$$PV = mRT \quad (\text{D.2})$$

where P is the absolute pressure, V is the volume, m is the mass, T is the absolute temperature (kelvins or degrees Rankine), and R is the individual gas constant given by:

$$R = \mathbf{R}/M \quad (\text{D.3})$$

where M is the molar mass and \mathbf{R} is the Universal Gas Constant, 8.314 kJ/kmol · K or 1.986 Btu/lbmol · R. More complex equations of state, such as the van der Waals, the Beattie-Bridgeman, or the Benedict-Webb-Rubin, can more accurately describe other real substances. Computer programs are available for the properties of a large number of substances and their mixtures, e.g., the National Institute of Standards and Technology (NIST) *Standard Reference Database 23*, known as REFPROP.

A system undergoes a *process* when at least some of its properties change their values. Processes may be: (1) *irreversible* (real, with a definite direction, finite rate, accompanied by losses), (2) *reversible* (ideal, in equilibrium throughout, equidirectional, infinitely slow, no losses), or (3) *quasistatic* (sufficiently close to equilibrium internally to allow reversible equations to be used as a good approximation). Once a system has undergone an irreversible process, it is impossible to restore the system to its original state without causing the surroundings to change from their initial state. Thus, every irreversible process leaves a lasting effect.

When an *open system* undergoes a process, it can be either (1) *steady* (the values of system properties may vary spatially but are constant with time) or (2) *unsteady* (values of system properties at any fixed point in space vary with time). The thermodynamic equations used to describe a system depend on whether it is open or closed, and whether it operates steady or unsteady.

D.3 First Law of Thermodynamics for Closed Systems

The most general form of the First Law for a closed system is:

$$Q_{1,2} - W_{1,2} = E_2 - E_1 \quad (\text{D.4})$$

where $Q_{1,2}$ is the heat transfer, $W_{1,2}$ is the work transfer, and $E_2 - E_1$ is the change in the system energy during the process. This form applies to all closed thermodynamic systems, no matter the type of process.

If the process is assumed to be *ideally reversible* or *quasistatic*, then the following differential form may be used:

$$\delta Q - \delta W = dE \quad (\text{D.5})$$

where the terms are defined as follows:

δQ = heat exchanged during an infinitesimal step in the process; mathematically, this is an *imperfect differential* that integrates to $Q_{1,2}$;

δW = work exchanged during an infinitesimal step in the process; another *imperfect differential* that integrates to $W_{1,2}$;

dE = change in total system energy during an infinitesimal step in the process; this is a *perfect differential* that integrates to $E_2 - E_1$.

D.4 First Law of Thermodynamics for Open Systems

The First Law for open systems undergoing a *steady process* was given in Section 10.2, and is repeated here:

$$\dot{Q} - \dot{W}_s = - \sum_{i=1}^n \dot{m}_i (h_i + 0.5 \mathcal{V}_i^2 + gz_i) \quad (\text{D.6})$$

Each term is defined as follows:

\dot{Q} = rate of heat transfer (thermal power) between the system and its surroundings (+ when heat enters the system)

\dot{W}_s = rate of work transfer (mechanical power) between the system and the surroundings (+ when work is delivered to the surroundings by the system)

i = an index that accounts for all inlets and outlets of the system

n = total number of inlets and outlets

\dot{m}_i = mass flow rate crossing each inlet or outlet

h_i = specific enthalpy of the fluid at each inlet or outlet

\mathcal{V}_i = velocity of the fluid at each inlet or outlet

z_i = elevation of each inlet or outlet relative to an arbitrary datum

g = local gravitational acceleration, 9.81 m/s² or 32.2 ft/s².

To analyze a system fully, it is necessary also to use the *principle of conservation of mass*, which in steady state requires that

$$\sum_{i=1}^n \dot{m}_i = 0 \quad (\text{D.7})$$

It is important to note that when using Eqs. (D.6) and (D.7) mass flows are taken as positive when entering the system and negative when leaving.

The First Law for open systems undergoing an *unsteady process* is mathematically more complex than for steady operation. Rather than an algebraic working equation, a differential equation must first be integrated before numerical values can be substituted. Since the electro-mechanical systems covered in this book have all been assumed to be operating steadily, this form of the First Law is not needed for our current purposes, but is included here for the sake of completeness. The most general form is:

$$\delta Q - \delta W - P dV = d(mu) - \sum_{i=1}^n dm_{\xi i} (h_{\xi} + \frac{1}{2}V_{\xi}^2 + gz_{\xi})_i \quad (\text{D.8})$$

The new terms in the equation are defined as follows:

PdV = expansion or compression work exchanged during an infinitesimal step in the process via a reversible deformation of system boundary; generally negligible for rigid systems;

$d(mu)$ = change in system internal energy during an infinitesimal step in the process; mathematically this is a *perfect differential* that integrates to $m_2u_2 - m_1u_1$;

ξ = subscript referring to properties of streams entering or leaving the system; dm = increment of mass entering (positive) or leaving (negative) the system during infinitesimal step in process; another *perfect differential*.

This time the *principle of conservation of mass* requires that

$$\sum_{i=1}^n \dot{m}_i = \frac{dm}{dt} \quad (\text{D.9})$$

or that the net influx of mass across the boundary equals the time rate of increase of mass within the system.

D.5 Second Law of Thermodynamics for Closed Systems

The Second Law appears in many forms, some verbal and some mathematical. Often it is expressed as a negative statement or a mathematical inequality because

the nature of the Second Law is to place restrictions on what can be accomplished during energy conversion processes. Here we summarize some of the common expressions of the Second Law.

D.5.1 CLAUSIUS STATEMENT

It is impossible for heat to flow *spontaneously* from a body of lower temperature to one of higher temperature. If this were not true, it would be possible for refrigerators to operate without any motive energy being supplied.

D.5.2 KELVIN-PLANCK STATEMENT

It is impossible to operate a cycle such that the only effects are the transfer of heat from a *single heat source* and the delivery of an equal amount of work from the cycle to the surroundings. If this were not true, it would be possible to operate power plants without rejecting any heat to the surroundings, and the plants would have a thermal conversion efficiency of 100%.

D.5.3 CLAUSIUS INEQUALITY

Clausius also gave us a mathematical expression of the Second Law, namely:

$$\oint \frac{\delta Q}{T} \leq 0 \quad (\text{D.10})$$

where \oint means a *closed line integral* or a sum taken completely around the cycle of operations. The equality sign is used when all the heat transfer takes place *reversibly*, i.e., when there is no temperature difference across the heat transfer surface, whereas the inequality applies to *irreversible* heat transfer.

The Clausius Inequality may also be expressed in the following manner: It is impossible for any system to operate on a *cycle* such that

$$\oint \frac{\delta Q}{T} > 0 \quad (\text{D.11})$$

D.5.4 EXISTENCE OF ENTROPY

The Second Law implies the existence of a property called entropy, S , which is found from the equation:

$$dS = \frac{\delta Q^{rev}}{T} \quad (\text{D.12})$$

The term dS is a mathematical *perfect differential*, and Eq. (D.12) may be integrated to obtain:

$$S_2 - S_1 = \int_1^2 \frac{\delta Q^{\text{rev}}}{T} \quad (\text{D.13})$$

This is quite significant in light of the fact that δQ^{rev} by itself is an *imperfect differential*. The quantity $1/T$ is an *integrating factor* for heat, creating a quantity that is a perfect differential. To carry out the integration of Eq. (D.13), it is necessary to substitute for the reversible heat transfer using Eq. (D.5).

Since entropy is a *thermodynamic property* and a *mathematical potential*, we are only interested in *differences* in entropy, not the actual value of entropy. Furthermore, once the entropy difference has been found between a given pair of states by using Eq. (D.13), *the result will be the same no matter what type of process connects the two states*. This latter point is often not understood by beginners to the subject who mistakenly believe that the entropy change will differ if one process is irreversible and one is ideally reversible. Only the initial and final states determine the entropy change, not the process between them.

That having been said, the *calculation* of the entropy change must be done using a *reversible process*, as shown explicitly in Eq. (D.13).

D.5.5 PRINCIPLE OF ENTROPY INCREASE

This statement of the Second Law is intrinsically tied to the concept of an irreversible process. The Principle of Entropy Increase (PEI) may be stated as follows:

When an *adiabatic* system undergoes an *irreversible* process from an initial state 1 to a final state 2, the entropy of the system can only *increase*, i.e.,

$$S_2 - S_1 > 0 \quad (\text{D.14})$$

Since all real processes are irreversible and since the selection of the system boundary is arbitrary, some people have extended the boundary to include the entire Universe, and have concluded that the entropy of the Universe is constantly increasing. This would be true provided that the Universe is bounded by an adiabatic wall, which has yet to be verified.

The PEI may be put into an alternative, negative form in keeping with the general theme of the Second Law, namely:

When an *adiabatic* system undergoes an *irreversible* process from an initial state 1 to a final state 2, it is impossible for the entropy of the system to *decrease*.

If an *adiabatic* system were to undergo an ideally *reversible* process, then the entropy of the system would remain *constant*, i.e., $S_2 = S_1$.

D.6 Second Law of Thermodynamics for Open Systems

We presented the general form of the Second Law in Section 10.3 while introducing the concept of exergy, and repeat it here for completeness. The most general form that applies to open systems is:

$$\dot{\theta}_p = \frac{dS}{d\tau} - \sum_{i=1}^n \dot{m}_i s_i - \int_{\tau_1}^{\tau_2} \frac{1}{T} \frac{dQ}{d\tau} \quad (\text{D.15})$$

Each new term is defined as follows:

$\dot{\theta}_p$ = rate of entropy production for the system caused by irreversibilities

τ = time

s_i = specific entropy of the fluid at each inlet or outlet, S_i/m_i

T = absolute temperature (in K or °R) associated with the heat transfer.

The first term on the right-hand side vanishes for steady operation, the term on the left-hand side vanishes for reversible processes, and the last term on the right vanishes for adiabatic systems.

D.7 Thermodynamic State Diagrams

We will conclude this brief review of basic thermodynamics with some examples of thermodynamic diagrams. It is helpful to view processes in thermodynamic state diagrams. Such diagrams provide a “road map” for visualizing, understanding, and analyzing the changes that occur when systems undergo various changes of state. Processes are usually characterized by whatever property remains constant during the process. Thus, a process at constant temperature is called “isothermal,” one at constant pressure is called “isobaric,” etc.

The framework for the diagram is an appropriate projection of the working fluid surface of equilibrium states. The fluid can be represented by a three-dimensional surface as long as it is a pure substance, in accordance with the Gibbs Phase Rule.

Some of the more useful choices for the independent properties, i.e., the coordinates of the two independent axes of the diagram, are: (1) pressure-volume, P - v ;

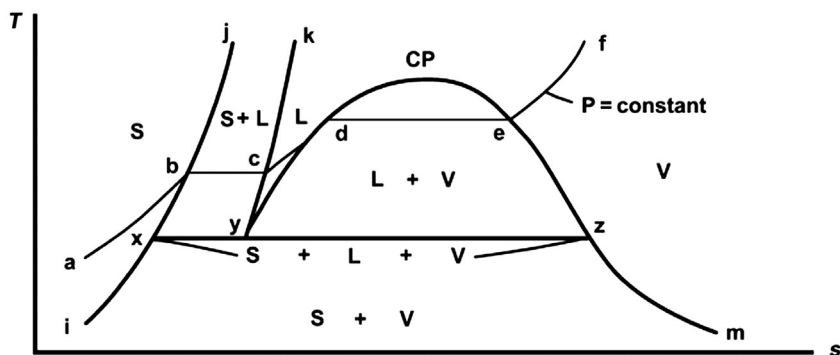


Figure D.1 Temperature-entropy diagram for a typical pure substance. Key: S = solid, L = liquid, V = vapor, CP = critical point, x-y-z = triple line, a-b-c-d-e-f = typical isobar, i-x = saturated solid in equilibrium with vapor, x-j = saturated solid in equilibrium with liquid, y-k = saturated liquid in equilibrium with solid, y-CP = saturated liquid in equilibrium with vapor, z-CP = saturated vapor in equilibrium with liquid, and m-z = saturated vapor in equilibrium with solid.

(2) temperature-entropy, T - s ; (3) enthalpy-entropy, h - s ; and (4) pressure-enthalpy, P - h . The latter three are particularly helpful for the cases studied in this book.

Figure D.1 shows a skeleton T - s diagram for the full spectrum of possible phases, followed by Figure D.2, which gives the liquid-vapor and superheated portions of the phase space for water.

Figure D.3 gives the high-quality liquid-vapor and superheated regions for water, followed by Figure D.4, which shows a skeleton h - s diagram for all possible phases.

Figure D.5 shows a skeleton $\log P$ - h diagram for all possible phases, followed by Figure D.6, which gives the liquid, liquid-vapor, and superheated vapor regions for propane.

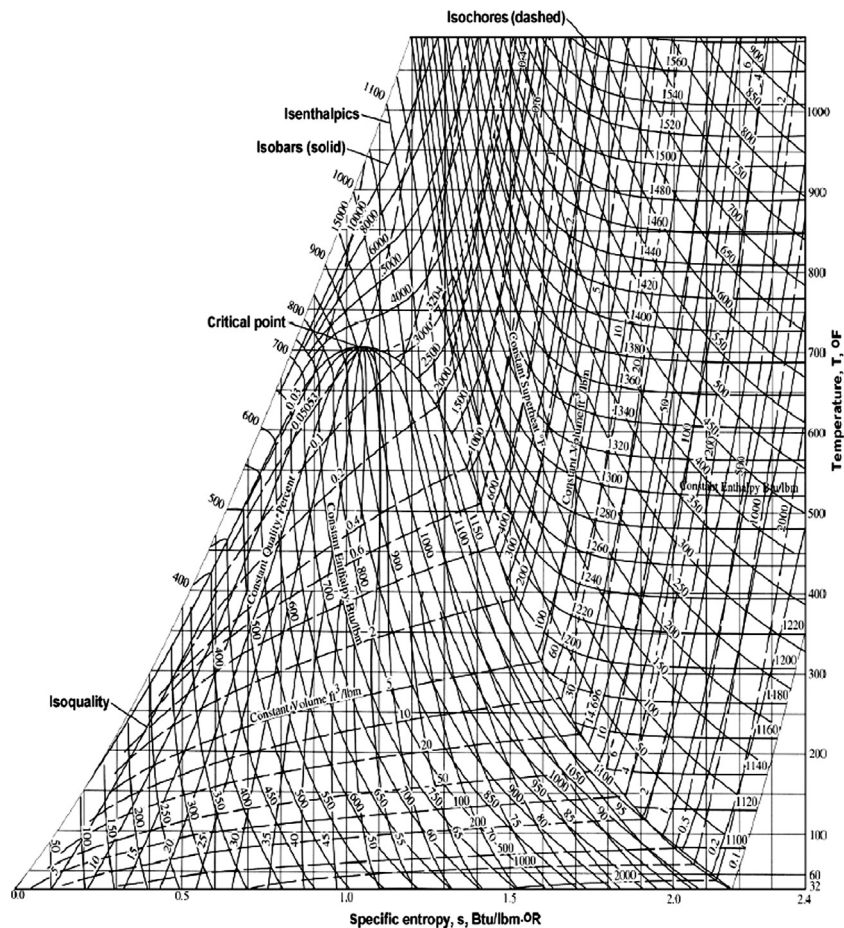


Figure D.2 Temperature-entropy diagram for water in US customary units, showing the liquid-vapor and superheated regions.

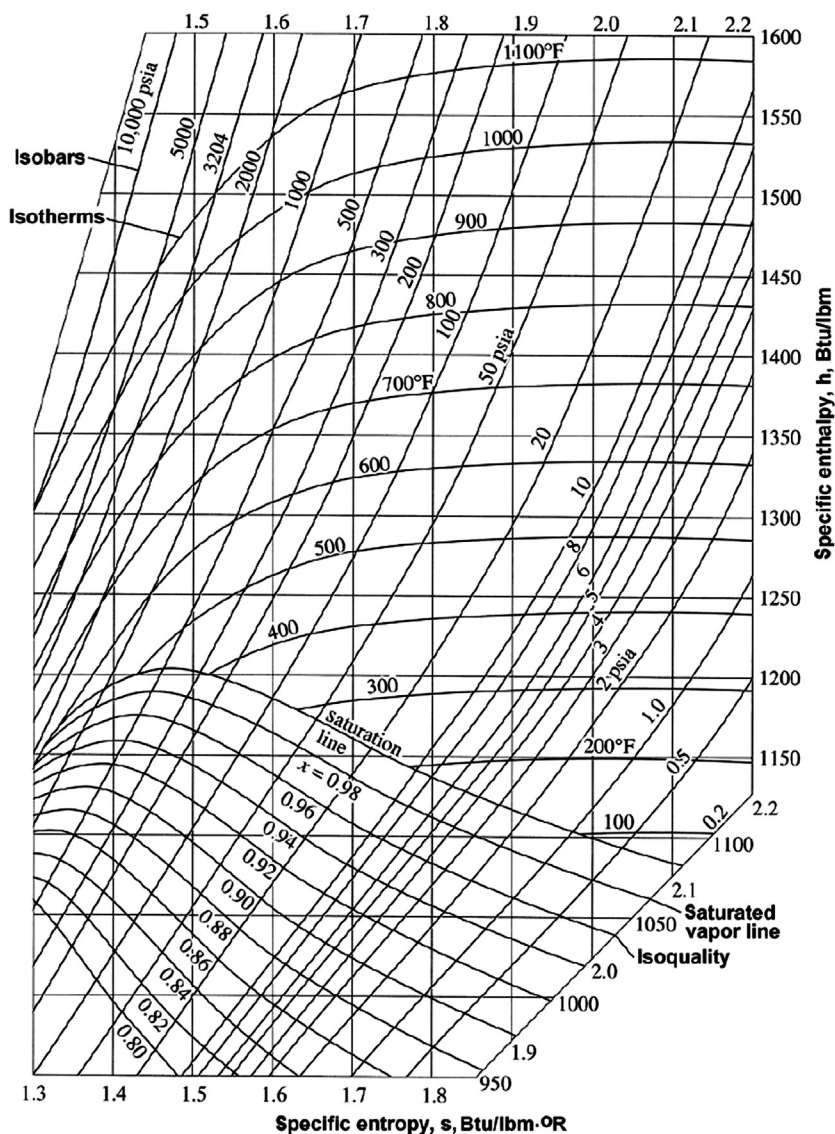


Figure D.3 Enthalpy-entropy (Mollier) diagram for water in US customary units, showing the superheated region and the high-quality liquid-vapor region.

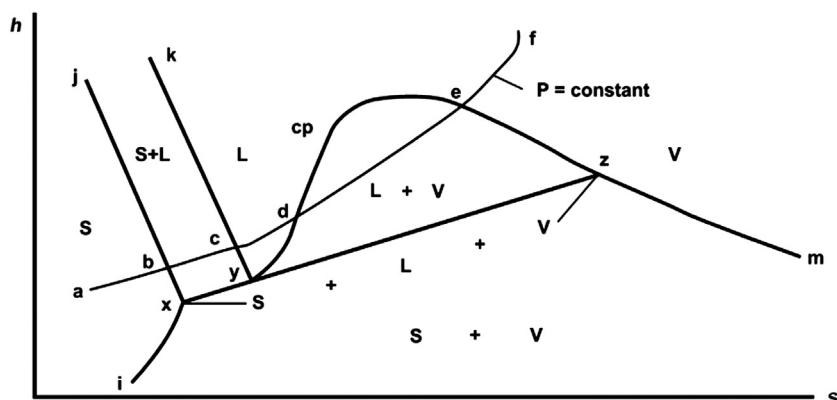


Figure D.4 Enthalpy-entropy (Mollier) diagram for a typical pure substance. Key: S = solid, L = liquid, V = vapor, CP = critical point, x-y-z = triple line, a-b-c-d-e-f = typical isobar, i-x = saturated solid in equilibrium with liquid, x-j = saturated solid in equilibrium with vapor, y-k = saturated liquid in equilibrium with solid, y-CP = saturated liquid in equilibrium with vapor, z-CP = saturated vapor in equilibrium with liquid, and m-z = saturated vapor in equilibrium with solid.

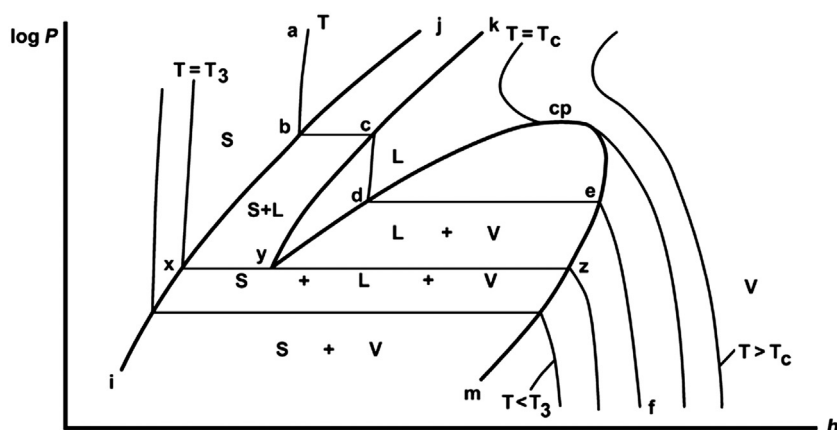


Figure D.5 Log (pressure)-enthalpy diagram for a typical pure substance. Key: S = solid, L = liquid, V = vapor, CP = critical point, x-y-z = triple line, a-b-c-d-e-f = typical isotherm ($T_3 < T < T_c$), i-x = saturated solid in equilibrium with liquid, x-j = saturated solid in equilibrium with vapor, y-k = saturated liquid in equilibrium with solid, y-CP = saturated liquid in equilibrium with vapor, z-CP = saturated vapor in equilibrium with liquid, and m-z = saturated vapor in equilibrium with solid.

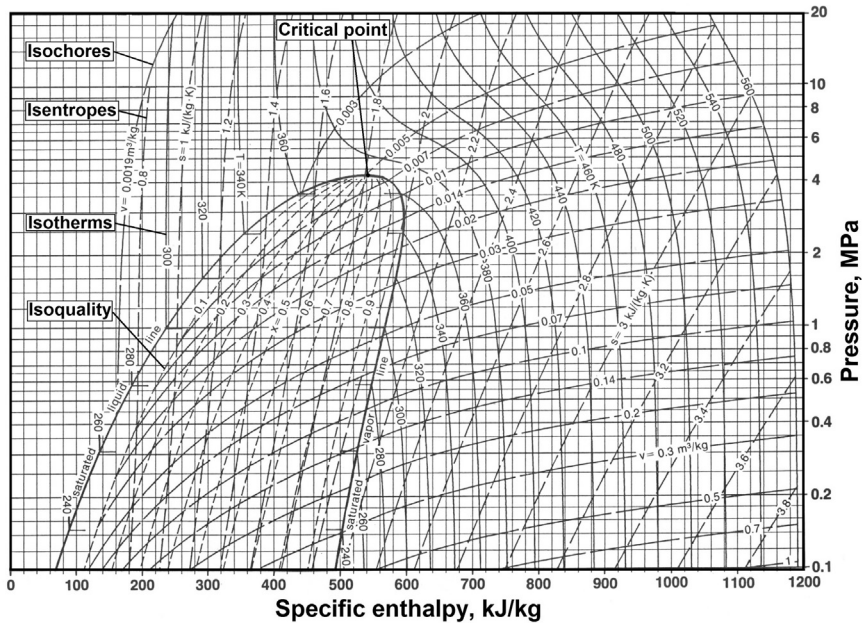


Figure D.6 Pressure-enthalpy, semilog diagram for propane in SI units, showing the liquid, liquid-vapor, and superheated regions.



Appendix E

Answers to Selected Practice Problems

For every complex question, there is an easy answer—neat, simple and wrong.

H.L. Menchen

Chapter 1

- 1.1 Thickness = 19.6 km = 12.25 mi.
- 1.2 Temperature = 1075°C, for 25°C surface temperature.
- 1.3 Temperature difference = 630°C.
- 1.4 Depth = 6.9 km.
- 1.5 Depth = 3790 m = 12,500 ft.
- 1.10 (a) Depth = 4761 m.

Chapter 2

- 2.1 (a) 14°F/100 ft; 25.5°C/100 m.
- 2.2 (a) SiO₂ (msl): (1) AH-1, 240°C; AH-5, 224°C; AH-26, 229°C. (2) H-4, 257°C; H-6, 246°C. (3) CP-avg., 263°C.
(c) Na/K: (1) AH-1, 269°C; AH-5, 245°C; AH-26, 261°C. (2) H-4, 226°C; H-6, 221°C. (3) CP-avg., 292°C.
- 2.3 (a) Temperature = 230°C; (b) 251°C.
- 2.9 (A) 125°C; fairly reliable. (B) 425°C; unreliable, too large an extrapolation.
- 2.12 (A) (a) 265.3°C; (b) 254.2°C. (B) 690.0 ppm. (C) The value in the data set, 537 ppm, is somewhat higher than the calculated reservoir value, i.e., 480 ppm, and lower than the separated brine value of 690 ppm. The actual reservoir temperature is lower than predicted by Na/K/Ca method. The actual temperature in the reservoir was about 235°C.

Chapter 3

- 3.1 47.8 yd³.
- 3.2 (A) 9426 lbf.

Chapter 4

- 4.1 Critical point: 374.2°C (705.5°F) is reached at 2343 m (7688 ft) (const. density); 3770 m (12,370 ft) (var. density); 3196 m (10,485 ft) (James).
- 4.2 185.5 m.
- 4.3 (a) At 100 m radius, $\Delta P = 106.7$ atm; (b) At 100 l/s, $\Delta P = 117.8$ atm.
- 4.4 (a) At 100 kg/s, flash depth = 373 m; at 150 kg/s, flash depth = 616 m.
- 4.6 632 m.
- 4.7 (a) 72.1 kg/s. (b) (i) Flashing will occur inside the well; (ii) flashing will occur in the formation leading to “excess” steam and enthalpy at the wellhead.
- 4.9 (a) 92.2 m. (b) 0.044 (4.4% vapor). (c) 3 kPa/m.
- 4.10 (b) 256.6 kPa/(kg/s). (c) 795.8 m below the surface, in the deeper casing.
- 4.11 (a) 213.9 m. (b) 0.0723 (7.23% vapor).

Chapter 5

- 5.2 Turbine A: 77,933 kW; Turbine B: 67,746 kW.
- 5.3 (a) 77.86 kJ/kg.
- 5.4 (a) 8922 kW; (b) 4.39; (c) (i) 38.3%, (ii) 44.6%.
- 5.5 (a) 9.50 MW; (b) (i) 48.3%; (c) 11.3%.
- 5.6 (a) 460.6 kPa owing to a 72.6 kPa pressure drop.

Chapter 6

- 6.1 (a) 189.3 kJ/kg.
- 6.2 (e) 120.8 kJ/kg; (f) 45.7%.
- 6.3 (d) 176 MW.
- 6.4 (a) Undersaturated. (b) Supersaturated, expect silica precipitation.
- 6.5 (A) 174.7 kJ/kg.
- 6.6 Pass-in turbine: (A) 85.5 kJ/kg; Separate turbines: (A) 73.9 kJ/kg.
- 6.7 (C) 146.9 MW.

Chapter 7

- 7.1 (a) 654 kPa.
- 7.2 (b) (i) 53.3%.
- 7.3 (a) 78.9%; (b) 526.9 kJ/kg; (c) 58.9%.
- 7.4 (a) 184.4°C; (b) 531.5 kJ/kg.
- 7.5 (a) (i) 7500 kW, (ii) 12,476 kW.
- 7.6 (B) 0.852. (C) 49.1%.
- 7.7 (A) 49.0%; 47.5%. (B) 73.0%. (C) 88.8%.
- 7.8 (B) (a) 76.4 MW; (b) 119.3 MW.

Chapter 8

- 8.1 (a) 56.0 kg/s; (b) 830 m²; (c) 63.5%.
- 8.2 (a) 89.2 kJ/kg.
- 8.3 (a) 8.46%; (b) 80.2 kg/s; (d) 14.4%.
- 8.4 (a) (i) 18.06°C; (ii) 10.19°C; (c) 82.6%.
- 8.5 (a) 27.44 kJ/kg; (c) 206.9 kJ/kg; (e) 12.07%.
- 8.6 (a) 0.5236; (b) 72.75°C; (c) 75.2%; (d) 209.6 kg/s; (g) 7446 kW, 28.5%.
- 8.7 (c) 18.0%; (d) (2) 24.98 kg/s; (e) 49.0%.
- 8.8 (c) ≈ 329 K; (d) (i) 22.46 kg/s, (ii) 25.24 kg/s; (e) 13.1%.
- 8.10 (A) 146.4 kg/s; (C) 390.3 K; (D) 22.2%.
- 8.11 (C) 17.19 kJ/kg or 15.45%.
- 8.12 (C) 77.84 kJ/kg. (D) 14.97%. (E) 1.3484. (F) 35.6%. (G) 7. (H) Need to check the pinch-points to make sure they are feasible. The pinch is about 20°C and occurs at the hottest end of the superheater. It could be tightened up a bit. That would improve the efficiency.

Chapter 9

- 9.1 (a) 1118 kJ/kg; (b) 34.4%; (c) 1117 kJ/kg; (d) 39.4%; (e) 1.098.
- 9.2 (a) 42.49%; (b) 54.10%.
- 9.3 (a) 52.7%.
- 9.4 (a) 32.28 kg/s; (b) (i) 5627 kW, (ii) 1753 kW; (d) 44.6%.
- 9.5 (a) 75.6 kg/s; (c) 1.089; (d) 0.9914; (e) 2.313.
- 9.6 (a) 1068 kJ/kg; (b) 706.5 kJ/kg; (c) 4.00.
- 9.7 $t\text{-SiO}_2$ (nsl) = 194.5°C; $t\text{-SiO}_2$ (msl) = 186.6°C; $t\text{-(Na/Cl)}$ = 320.5°C; $t\text{-(Na/K/Ca)}$ = 244.9°C.
- 9.9 (C) (a) 40.38 kW/(kg/s); (b) 0.161 kW/(kg/s); (c) 40.22 kW/(kg/s). (E) 17.4%.
- 9.10 (A) 63.64 kJ/kg. (D) 13.55%. (G) 183.9 kg/s. (H) 36.2%. (I) 79.3%.
- 9.11 (C) 49°C. (D) 3.631. (H) (a) 23.48 kJ/kg; (b) 14.29 kJ/kg. (I) 5.12 MW. (J) 48.5%.
- 9.12 (A) (a) 106.5 kW/(kg/s); (d) 150.1 kW/(kg/s). (B) (a) 38.8%; (d) 54.7%.
- 9.13 (A) 85.38 kW/(kg/s). (B) (a) 13.9%; (b) 14.2%.

Chapter 10

- 10.2 (b) 35.24 kJ/kg; (c) 19.43 kJ/kg; (d) (i) 60.7%.
- 10.3 (a) 62.1°C; (b) 77.4%; (d) 22.83°C.
- 10.4 (a) 18.7%; (b) 61.5%.

I wish I had an answer to that because I'm tired of answering that question.

Yogi Berra



Appendix F

REFPROP Tutorial with Application to Geothermal Binary Cycles

If the automobile had followed the same development cycle as the computer, a Rolls-Royce would today cost \$100, get a million miles per gallon, and explode once a year, killing everyone inside.

Robert X. Cringely, *InfoWorld* magazine

F.1 Introduction

REFPROP—Reference Fluid Thermodynamic and Transport Properties—is a product of the United States National Institute of Standards and Technology (NIST) [1]. It is a very accurate and comprehensive software program that yields all thermophysical properties of interest to scientists and engineers and covers a very large number of pure substances and predefined mixtures. Users can also define mixtures of particular interest to them. Version 8.0 was released in April 2007; Version 9.0 was released in November 2010. A free student version is also available, albeit with a limited number of substances.

This appendix will show how REFPROP can be used to analyze geothermal power plants. As such, it will presume a basic familiarity with the program. A User's Guide is available from NIST and should be consulted for the basic principles used and the general capabilities of the program.

F.2 Typical Geothermal Binary Power Cycle

To illustrate REFPROP we will examine a simple Rankine cycle with superheat. Such a cycle may be used in a binary geothermal power plant.

Figure F.1A shows the plant. The following nomenclature describes each component: T = turbine, G = generator, C = condenser, P = pump, PH = preheater, EV = evaporator, SH = superheater, CW = cooling water, AIR = cooling air, B = geothermal brine. We will assume that the cycle working fluid is *n*-pentane.

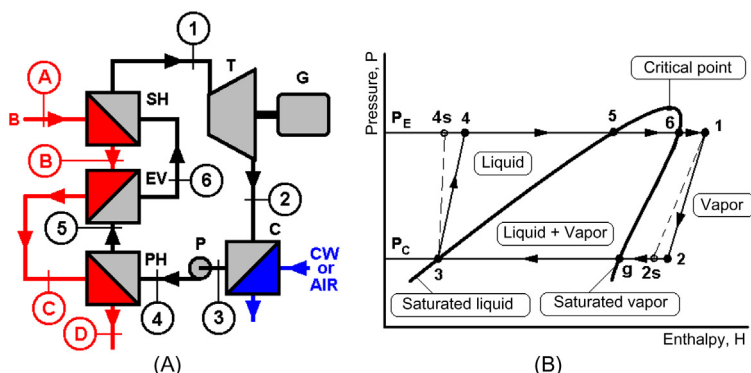


Figure F.1 (A) Plant flow diagram; (B) Pressure-enthalpy process diagram [WWW].

Figure F.1B shows the processes undergone by *n*-pentane in pressure-enthalpy coordinates. State 2s is the ideal turbine exhaust state ($s_{2s} = s_1$) and state 4s is the ideal pump outlet state ($s_{4s} = s_3$).

The high pressure in the cycle is P_E and the condensing pressure is P_C . We will assume that both pressures are given along with the turbine inlet temperature, T_1 . Furthermore we will assume that the turbine has an isentropic efficiency of 85% while the pump efficiency is 75%. These data are sufficient to allow the determination of all heat transfer and work transfer terms, as well as cycle efficiencies.

The overall plant performance depends on the properties of the geothermal brine, B, which will be taken as pure water. We will assume that the inlet brine pressure, temperature, and mass flow rate are all given.

The analysis of the cycle and plant requires us to find the enthalpy, h , at all state points and entropy, s , at selected points. This is where REFPROP comes in. REFPROP can be used in either of two ways to solve the problem: (1) it can find specific properties for a given set of independent properties, or (2) it can be used as an Excel function, similar to trigonometric or statistical functions, allowing the cycle to be analyzed parametrically with Excel. We will illustrate both approaches.

F.3 REFPROP State-Point Properties

Let us establish the given data set first. We will present the data in the following table.

State	Pressure kPa	Temperature °C	Quality —	Entropy kJ/kg · K	Enthalpy kJ/kg
1	1300	145	n.d.		
2 _s	250				
2	250				
g	250		1		
3	250		0		
4 _s	1300		n.d.		
4	1300		n.d.		
5	1300		0		
6	1300		1		
A	1500	165	n.d.		

Notice that states 2_s and 4_s are not actual states but are needed to find states 2 and 4, respectively. Similarly, state g (saturated vapor) occurs somewhere in the condenser between states 2 and 3. Note also that the quality is not defined (n.d.) outside the two-phase liquid-vapor region. For this tutorial, we will ignore pressure losses in all piping and heat exchangers.

Now REFPROP will be used to find the enthalpy values at the required state points. First, select “pentane” from the Substance menu. Then under Options, go to Units, and select “SI with Celsius”; also select “kPa” as the pressure units since the problem uses kPa, not MPa. Under the Calculate tab, check “Specified state points.” This will allow us to find state 1; enter 145 and 1300, and get 35.846 kg/m³ for the density, 534.80 kJ/kg for the enthalpy, and 1.3878 kJ/kg · K for the entropy. We do not need the density and could have de-selected it from the Options/Properties menu. Copy the h and s values into our table.

The table below will be filled in according to our use of REFPROP, so follow the text below for the sequence of operations.

State	Pressure kPa	Temperature °C	Quality —	Entropy kJ/kg · K	Enthalpy kJ/kg
1	1300	145	n.d.	1.3878	534.80
2s	250	98.419		1.3878	469.89
2	250				479.627
g	250	65.409	1	1.2024	404.06
3	250	65.409	0	0.22095	71.799
4s	1300	65.876	n.d.	0.22095	73.610
4	1300		n.d.		74.214
5	1300	138.73	0	0.75865	275.54
6	1300	138.73	1	1.3483	518.40
A	1500	165	n.d.	1.9913	697.69

Next we realize that state 2s has the same entropy as state 2, so copy that value into 2s. Next we have the pressure and entropy at state 2s and can go to REFPROP with those to get the enthalpy at 2s. The obtained values have been pasted into the table.

Now to find the state 2 we need the definition of the turbine efficiency, namely,

$$\eta_t = \frac{w_{t,act}}{w_{t,s=const}} = \frac{h_1 - h_2}{h_1 - h_{2s}} \quad (F.1)$$

Thus we can calculate the enthalpy at state 2 from

$$h_2 = h_1 - \eta_t(h_1 - h_{2s}) \quad (F.2)$$

and add the answer to the table.

Continuing through the cycle in order, we see that state g is next. Since it is a saturation state, we need to select Calculate/Saturation points (at equilibrium). This will open a new window in REFPROP which can be dragged on the screen to allow it to be viewed together with our first window. Enter the pressure of 250, and get the results. The vapor values belong to state g, and the liquid values to state 3.

Next we deal with the pump. The entropy at state 4s is the same as at state 3, so we can use the first REFPROP window to get the enthalpy there. Enter an entropy of 0.22095, and a pressure of 1300, and see the results.

Note: You can easily copy and paste between REFPROP windows by highlighting and using Ctrl-C and then Ctrl-V. This conveniently eliminates possible typing and round-off errors.

Now to find the state 4 we need the definition of the pump efficiency, namely,

$$\eta_p = \frac{w_{t,s=const}}{w_{t,act}} = \frac{h_{4s} - h_3}{h_4 - h_3} \quad (\text{F.3})$$

Thus we can calculate the enthalpy at state 4 from

$$h_4 = h_3 + (h_{4s} - h_3)/\eta_p \quad (\text{F.4})$$

and add the answer to the table.

Only states 5 and 6 remain, and they are both saturation states. So we revert to the second REFPROP window using a pressure of 1300 and get the results, placing the vapor values in the table for state 6 and the liquid values for state 5. Thus the table is now complete for the *n*-pentane enthalpy values. If needed, property values for the still blank entries could be found from REFPROP.

To find the brine properties, we need to change the Substance in REFPROP to “water.” This opens a third window. Then enter the brine pressure, 1500, and the temperature, 165, and get the results.

The rest of the analysis of the cycle and plant can now be carried out using the standard thermodynamic equations. The results are summarized in the table below. The reader should verify the results for himself/herself.

Item	Value
Total heat added	460.586 kJ/kg of <i>n</i> -pentane
Heat rejected	407.828 kJ/kg of <i>n</i> -pentane
Work of turbine	55.173 kJ/kg of <i>n</i> -pentane
Work of pump	2.415 kJ/kg of <i>n</i> -pentane
Net cycle work	52.758 kJ/kg of <i>n</i> -pentane
Cycle thermal efficiency	0.1145 (11.45%)

In the case of compressed liquid states, a word of caution is in order. Owing to the non-unique relationship between the enthalpy *h* and temperature *T*, for certain values of these independent variables, two different physical states are possible. This is illustrated in [Figure F.2](#), a Mollier diagram (enthalpy plotted against entropy) for water substance, when *T* and *h* are used as independent variables. All substances behave similarly. Namely, isotherms exhibit a minimum in enthalpy for intermediate values of entropy, whereas they rise steeply at low values, and rise and taper off asymptotically at high values. Thus, for a given temperature, say 575.02°C, and a given enthalpy, say 3000 kJ/kg, there are two possible values of entropy, namely, point A, 3.72 kJ/kg · K, and point B, 5.45 kJ/kg · K. Under these and similar conditions, REFPROP might return a message of non-convergence. Point A corresponds to an extremely high pressure, ~1200 MPa, and is unrealistic for geothermal

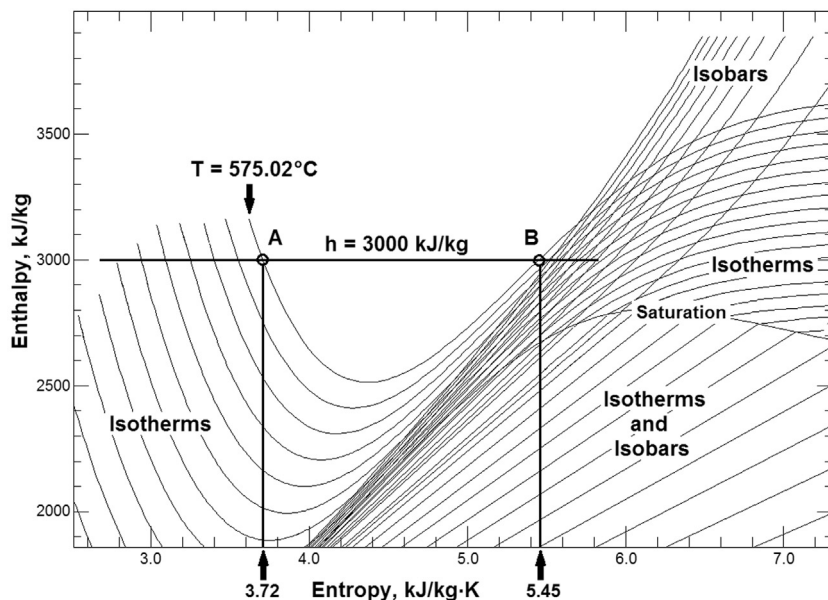


Figure F.2 Mollier diagram for water.

applications. If this convergence problem should arise, there is a way around it. From Figure F.2, it is clear that the enthalpy h is monotonic in pressure P . Thus, switching the independent variables to P and h should eliminate any problem.

F.4 REFPROP as an Excel Function

As explained in the REFPROP 8.0 User's Guide (p. 86ff), REFPROP can be linked to Excel using a .dll statement. Once this is properly set up, it allows Excel to call up thermophysical properties in the same way as any other library function, such as "average," "sum," etc. The properties of most interest to us include the enthalpy, entropy, pressure, and temperature, both for saturated states and single-phase liquid and vapor states. There are many other properties available and can be found in the User's Guide (pp. 87–88).

For single-phase liquid or vapor states for a pure substance, we need two independent properties to nail the value of any other property. Thus if we need the enthalpy, we must supply to the calling function the values of, say, the pressure and temperature. REFPROP allows the use of many combinations of

independent properties (User's Guide, p. 89). The most useful to us in our work are the following: TP, PH, and PS, where T = temperature, P = pressure, H = enthalpy, and S = entropy.

The general format of the calling function for the enthalpy as a function of temperature and pressure is as follows:

= enthalpy(*substance name*, "TP", *units*, *T-value*, *P-value*)

For *substance name*, you can either type in the name, such as water, or enter an Excel cell in which the name of the substance has been typed. The latter way is very handy especially when the problem involves two fluids, as in the example being studied. For *units*, the same options apply; it is convenient to just type the preferred units into a cell and insert that cell into the function calling statement. Also SI with C can be abbreviated as C. English units are also available in REFPROP. The pair of independent variables (in this case "TP") must be enclosed within quotes.

The entropy can be found from a similar function:

= entropy(*substance name*, "TP", *units*, *T-value*, *P-value*)

Another useful function is:

= enthalpy(*substance name*, "PS", *units*, *P-value*, *S-value*)

This one comes in handy when we seek the ideal outlet states from turbines or pumps where we know the pressure and entropy.

If we need to know the temperature that corresponds to a given pressure and enthalpy, we can use:

= temperature(*substance name*, "PH", *units*, *P-value*, *H-value*)

For saturated liquid states, the general calling function for the enthalpy as a function of saturation temperature is:

= enthalpy(*substance name*, "Tliq", *units*, *T-value*)

For saturated vapor states, the general calling function for the enthalpy as a function of saturation temperature is:

= enthalpy(*substance name*, "Tvap", *units*, *T-value*)

For saturated liquid states, the general calling function for the enthalpy as a function of saturation pressure is:

= enthalpy(*substance name*, "Pliq", *units*, *P-value*)

For saturated vapor states, the general calling function for the enthalpy as a function of saturation pressure is:

= enthalpy(*substance name*, “Pvap”, *units*, *P-value*)

The saturation pressure for a pure substance that corresponds to a given temperature can be found from:

= pressure(*substance name*, “Tliq”, *units*, *T-value*)

The saturation temperature for a pure substance that corresponds to a given pressure can be found from:

= temperature(*substance name*, “Pliq”, *units*, *P-value*)

In the case of azeotropic mixtures, the last two expressions suffice. For non-azeotropic mixtures, the last two expressions will give the values on the saturated liquid line, but to find the values on the saturated vapor line, one must insert “Tvap” and “Pvap” for “Tliq” and “Pliq”, respectively.

Let us now revisit the Rankine cycle and use Excel to analyze the system. Using the appropriate functions, the following spreadsheet can be obtained.

WF = <i>n</i> -pentane: work and heat per kg/s of <i>n</i> -pentane flowing in the cycle							
PE	PC	t_c	t_E	h_3	s_3	h_{4s}	eta-P
MPa	MPa	C	C	kJ/kg	kJ/kgK	kJ/kg	
1.3	0.25	65.41	138.73	71.80	0.220954	73.61	0.75
						pentane	C
h4	h5	h6	T1	h1	s1	s2s	sg
kJ/kg	kJ/kg	kJ/kg	C	kJ/kg	kJ/kgK	kJ/kgK	kJ/kgK
74.22	275.54	518.40	145.00	534.80	1.3878	1.3878	1.2024
h2s	eta-T	h2	w-T	w-P	w-NET	q-IN	eta-TH
kJ/kg		kJ/kg	kW/(kg/s)	kW/(kg/s)	kW/(kg/s)	kW/(kg/s)	%
469.89	0.85	479.63	55.17	2.42	52.75	460.58	11.45

In the actual Excel spreadsheet, these numbers would be arrayed across the page; they have been repackaged here to fit the width of the page.

The results are of course identical with the first approach. This method facilitates parametric studies. For example, the high pressure PE can be varied over a range to see its effect on net work and efficiency. For example, the results shown in [Figure F.3](#) were obtained rapidly by sweeping the spreadsheet over pressure values from 1.10 to 1.45.

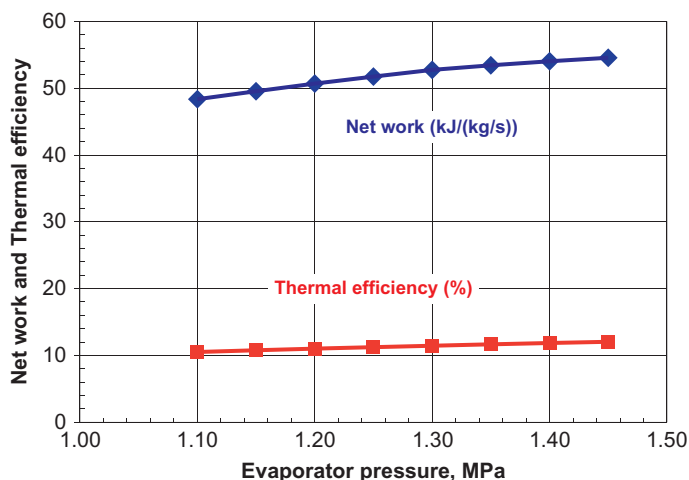


Figure F.3 Variation in specific net work and thermal efficiency with evaporator pressure [WWW].

To complete the analysis of the plant, one must apply the First Law of thermodynamics to the heat exchanger train, knowing the brine inlet pressure, temperature, and mass flow rate. One additional parameter is needed, namely, the pinch-point temperature difference between the brine and the *n*-pentane as they interact thermally in the heat exchangers. REFPROP will yield all the enthalpies and temperatures needed to complete the solution, using the same methodology illustrated in these notes, together with the governing equations developed in Chapter 8.

Reference

- [1] National Institute of Standards and Technology (NIST), US Department of Commerce, <<http://www.nist.gov/srd/nist23.cfm>>.

Index

Note: Page numbers followed by “*f*” and “*t*” refer to figures and tables, respectively.

A

- Abbattimento Mercurio e Idrogeno Solforato (AMIS), 340
- Accelerational pressure drop, 113
- Accumulators, 224
- Acoustic noise, 673
- Active geothermal regions, 7–10
- Adiabatic systems/walls, 715, 721
- Adriane boiler, 333, 335–336
- Advanced binary cycles, 208–218
- Advanced direct-contact condenser (ADCC), 585, 598*f*
- Advanced geothermal energy conversion systems, 241
 - combined heat and power plants, 267–269
 - enhanced geothermal systems, 610
 - hot dry rock, 12–14, 610
 - hybrid flash-binary systems, 247–252
 - hybrid fossil-geothermal systems, 263–267
 - hybrid single- and double-flash systems, 243–246
 - hybrid solar-geothermal plants, 274–277
 - plants for saline brines, 269–274
 - practice problems, 281–289
 - total flow systems, 256–263
- AER. *See* Alternative Earth Resources, Inc. (AER)
- Aerial photography, 26
- Aeromagnetic measurements, 27
- Ahuachapán power station, 432–436
 - design specifications and performance for, 436*t*
 - geofluid handling equipment for, 435*f*
 - Los Ausoles hot springs, 433*f*
 - pipelines, 109, 111*f*
 - waste brine disposal canal, 434*f*
 - well AH-6 during reforestation program, 435*f*
 - well discharge, 50*f*
 - well field, 91–92
 - wellhead separator system, 110*f*
 - vegetation restoration, 679, 679*f*
 - well field layout as of 2012, 434*f*
- Air
 - emissions, 660–663, 662*f*, 663*f*
 - mass conservation of, 124–125
- Airborne surveys, 26–27
- Air-cooled condensers, 667–669
- Air-cooled plant *versus* the water-cooled plant, 667
- Alaska, 706*t*
- AltaRock, 646–647, 650
- Alternative Earth Resources, Inc. (AER), 483
- Amagat’s law of additive partial volumes, 311
- Amatitlán power plant, 450, 450*f*
- American Recovery and Reinvestment Act of 2009 (ARRA), 483
- AMIS. *See* Abbattimento Mercurio e Idrogeno Solforato
- Ammonia, 204*t*, 206*t*, 207*t*, 217, 217*f*
- Amorphous silica, 157, 157*f*. *See also* Silica
- Anadarko Production Company, 482
- Anchor casing, 56
- Anhydrite precipitation model, for Hijiori project, 624*f*
- Anhydrous calcium sulfate, 622
- Annual growth rate of world plants, 687*f*
- Answers to problems, 727
- Approach, cooling tower, 125
- AQUA 3D, 89*t*
- Archie’s Law, 38
- Architecture of reservoir models, 85–86
- Argentina, 456–457, 710*t*
- ARRA. *See* American Recovery and Reinvestment Act of 2009 (ARRA)
- Asthenosphere, 9–10
- Atmosphere, 4–7
- Australia, 645–651, 708*t*
 - EGS development in, 644
 - geological evolution of Cooper Basin, 646*f*
- Austria, 708*t*
- Available work, 296
- Axial separators, 177*f*
- Axial-flow impulse turbines, 256–263

B

- Back-pressure turbines, 251–252
- Back-up systems
 - basic binary plants, 224
 - double-flash steam power plants, 162
 - dry-steam power plants, 188
- Bandung Institute of Technology (ITB), 405
- Basel, Switzerland, 627–632
- Basic binary systems, 196–203
- Batch cooling systems, 519–521
- Baumann rule, 121–122, 151, 181
- B.C. McCabe Power Plant, 527–528
- Benedict-Webb-Rubin equation, 311
- Beowawe, Nevada, geyser disappearance, 135, 677
- Beowawe bottoming binary cycle, 484
 - performance values for, 484*t*
 - temperature-entropy process diagram from, 484, 484*f*
- Beowawe double-flash plant, Nevada, 147*f*, 471–472
- Berlin plant, 437–439, 437*f*
 - binary unit, 440*f*
 - technical details and performance for, 439*t*
 - well map at, 438*f*
- Binary cycle power plants, 193. *See also* Hybrid systems
 - advanced binary cycles, 208–218
 - basic binary systems, 196–203
 - binary cycle analysis example, 218–222
 - downhole pumps, 225–229
 - environmental aspects, 223
 - equipment lists, 223–225
 - installed MW per country, 691*t*
 - installed MW worldwide, 692*t*
 - practice problems, 234–239
 - pumps, 225–231
 - silica precipitation, 160
 - surface pumps, 229–231
 - thermal efficiency, 125
 - total units worldwide, 693*t*
 - units per plant type per country, 692*t*
 - working fluid selection, 203–208
 - world distribution, 195
- Binary cycles
 - advanced, 208–218
 - analysis example, 218–222
 - basic, 196–203
 - dual pressure, 209–212
 - dual-fluid, 212–216
 - environmental impacts, 223
 - ideal, 208–209
 - Kalina, 216–218
 - Binary plants, 478–489
 - with air cooling, 231
 - Beowawe binary, 484
 - Blue Mountain, 482–483
 - Desert Peak 2, 480
 - Dixie Valley bottoming binary plant, 485
 - Jersey Valley plant, 485, 488
 - McGinness Hills, 485, 488
 - Patua geothermal resource area, 488–489
 - Salt Wells, 481–482
 - San Emidio, 478–480
 - Soda Lake Plants 1 and 2, 480
 - Tuscarora, 485, 488
 - with water cooling towers, 231
 - Biphase Rotary Separator Turbine (RST), 473
 - Biphase Turbine, 260
 - Bituminous coal, 713*t*, 714*t*
 - Black Rock Desert (BRD), 462
 - Blowout preventers, 56–58, 57*f*
 - Blue Mountain, 482–483
 - well field, 482, 483*f*
 - Boraciferous Region, 322*f*, 329, 335
 - Boric acid, 322, 333, 335
 - Bouguer gravity anomaly, 39
 - Bouillante plant, Guadeloupe, 452–455, 452*f*, 453*f*
 - Boundary conditions in reservoir models, 85
 - Brady Plant 1, 477–478, 477*f*
 - temperature-entropy process diagram for, 477*f*
 - BRD. *See* Black Rock Desert (BRD)
 - Brine transfer and reinjection pumps, 229, 231
 - Brines
 - disposal systems, 225
 - environmental aspects of solids
 - discharge, 667
 - hypersaline, 269–274
 - scale potential, 156–160
 - supply systems, 161, 223
 - Brine/working fluid heat exchangers, 224
 - Broadlands. *See* Ohaaki power station
 - Bruchsal, Germany, 644
 - Brute force exergy efficiency, 299–315
 - Bubble point, 305
 - Burbank, California, 265
 - Butane, 204*t*
 - Büyük Menderes Graben, 576*f*, 577*f*
- C**
 - Calcite, 622
 - basic binary systems, 196–197
 - scaling, 196–197

- Calcium
 - environmental aspects, 667
 - ion concentration, 82
 - Na/K/Ca geothermometers, 34
- Calcium carbonate. *See* Calcite
- Calcium-rich geofluids, 34
- Calderas, 16, 27–29, 612, 619
- Calibration of reservoir models, 86–87
- California *See also individual plants*
 - geothermal power plants, 704*t*
- California Energy Commission, 264–265
- Calorimeter method for wellhead flow, 78, 79*f*
- Calpine Corporation, 359–360
- Camborne School of Mines Associates Ltd. (CSMA), 617
- Camouflaging plants, 340, 678–679
- Capacity (installed MW)
 - per country, 689*t*
 - per plant type per country, 691*t*
 - worldwide geothermal power, 687*f*
- Carboli, Larderello, Tuscany, Italy, 341*f*
- Carbon dioxide, 660–661
 - calcite solubility, 82
 - environmental aspects, 660–663, 662*f*, 662*t*
 - geothermometers, 34
 - safety precautions, 56–58
- Carbon emission credits, 661
- Carbon tax, 661
- Caribbean islands, 452–455
 - Bouillante, 452–455
 - volcanic islands, 430*f*
- Carnot cycle, 208, 297, 680–681
- Carnot efficiency, 208, 297
- Case studies, 586–591
 - EGS plants, 612–651
 - Germencik, 593–600
 - The Geysers dry-steam power plants, 345
 - Heber binary plants, 501
 - Kizildere, 577–586
 - Larderello, 321
 - Magmamax binary power plant, 515
 - Nesjavellir and Hellisheidi plants, 531
 - Pamukören binary plant, 600–601, 601*f*
 - Raft River Plants, Idaho, USA, 545
- Casings (well), 54, 82, 669
- Castelnuovo, Italy, 322–324, 335–337, 337*f*
- Catastrophic events, 680
- Caufourier's 4-stage flash steam plant, 263–264, 264*f*
- Cement-bond logs, 669
- Cementing casings, 54
- Central America, geothermal power plants in, 451–452
- Costa Rica, 445–449
 - Las Pailas plant, 446–447
 - Miravalles station, 445
 - prospects, 448–449
- El Salvador, 431–441
 - Ahuachapán, 432–436
 - Berlín, 437–439
 - prospects, 440–441
- geologic setting, 428–429
- Guatemala, 449–451
 - Amatitlán, 450
 - prospects, 450–451
 - Zunil plant, 449–450
- history of development, 430–431
- Nicaragua, 442–444
 - Momotombo station, 442–443
 - prospects, 444
 - San Jacinto plant, 444
- Cerro Prieto Power Station, Baja California Norte, Mexico, 93–95
 - aerial view of, 94*f*
 - geography and geology, 350–351
 - image from Google Earth, 95*f*
 - production and injection wells, and evaporation pond, 96*f*
- Chemical tracers, 82
- Chile, 457–458
- China, 693*t*
- Choked well flow, 127–129
- Clausius inequality, 719
- Clausius statement, 719
- Clear Lake, 363
- Closed line integral, 719
- Closed systems, 715, 717–721
- Coal, 713*t*, 714*t*
- Cocos plate, 9
- Collayomi fault system, 351
- Colombia, 458
- Color of plants, 680
- Colorado River, 270, 515
- Combined flash-binary systems, 247–249
- Combined geothermal power generating plants, 267–269
- Combined heat and power plants, 267–269
- Combined heat-power (CHP) plant, 637
- Combined single- and double-flash systems, 246
- Commercial requirements, 10, 15
- Composite maps, 40
- Compressors, 308–311
- Concentrating solar power (CSP) system, 493–494
- Conceptual models, 29, 29*f*, 49, 85
- Condensate disposal system, 188

- Condensate pumps, 229, 231
- Condensers
- basic binary plants, 224
 - basic binary systems analysis, 198
 - double- and triple-flash steam power plants, 162
 - dry-steam power plants, 179, 187
 - dual-pressure binary plants, 211
 - Magmamax binary plant, 519, 520*f*
 - mixed working fluid condensers exergy efficiencies, 305–306
 - single-flash steam power plants, 118–119
- Condensing process
- double- and triple-flash steam power plants, 152
 - dry-steam power plants, 183
 - single-flash steam power plants, 123
- Conductivity, 36
- Conservation of mass, 124–125, 718
- Conti, Prince Piero Ginori, 170, 170*f*, 322, 329–330
- Continental drift, 4
- Continuity equation, 68
- Continuity of mass, 63–64
- Convection, 37
- Conversion of units, 711
- Conversion process thermodynamics, 119–127, 148–153
- Cooling towers
- double- and triple-flash steam power plants, 152
 - dry-steam power plants, 183
 - single-flash steam power plants, 119, 123–126
- Cooling water
- environmental aspects, 668–669
 - heat rejection, 668
 - spray ponds at Magmamax binary plant, 519–521, 522*f*
- Cooling water circulating pumps, 230–231
- Copahue power plant, 456, 456*f*, 457*t*
- Copenhagen Amendment, 207
- Corrosion, 118
- Costa Rica, 431, 445–449, 708*t*
- Las Pailas plant, 446–447
 - Miravalles station, 445
 - prospects, 448–449
- Costs of Magmamax binary plant, 525*f*
- Crust thickness and composition, 4–7
- CSP system. *See* Concentrating solar power (CSP) system
- Cycle 1 plants, Larderello, 335, 335*f*
- Cycle 2 plants, Larderello, 333, 334*f*
- Cycle 3 plants, Larderello, 335, 337–338
- Cycle performance, 202–203
- Cycle thermal efficiency, 254–255
- Cyclic power plants, 125
- “Cycloform” steam scrubber, 406–407, 407*f*
- Cyclone moisture removers, 117*f*, 117*t*
- Cyclone separators, 108, 109*f*, 114, 117*f*, 147*f*
- D**
- Dakhnov’s Law, 38
- Dalton’s law of additive partial pressures, 311
- Darajat dry-steam plants, technical details and performance for, 416*t*
- Darajat field, geological cross-section of, 414*f*
- Darajat power units, 409, 409*f*, 413–417
- geological cross-section of, 414*f*
 - geological setting, 409–410
 - satellite view of, 414*f*
 - technical details and performance for, 416*t*
- Unit 2 steam turbine
- cut-away view of, 416*f*
 - section view of, 418*f*
 - well field, 415*f*
- Darcy’s Law, 63
- Databases, 25
- Dead state, 294–297
- Deep Heat Mining Basel project (DHMB), 626–627
- Deep hydrothermal resources, 17–18
- Deep hydrothermal systems (DHS), definition of, 610–611
- Democratic Republic of Congo, 710*t*
- Depurators, 333
- Desert Peak 1, 473–474
- flow diagram for, 474*f*
 - performance of, 474*t*
 - separator and flasher at, 475*f*
- Desert Peak 2, 480, 481*f*
- Development history. *See* History
- Deviated wells, 352, 352*f*
- Dew point, 305
- Diathermal walls, 715
- Dieng geothermal field, Indonesia, 51*f*
- Direct-contact condensers, 118–119, 123, 123*f*, 179
- Direct-intake
- condensing units, 336–337, 336*f*
 - exhausting to atmosphere units, 335–336, 335*f*
- Directional drilling, 50–51, 177*f*, 663
- Discovery of Heber field, 502–503
- Discovery wells, 50–51
- Disposal systems, 188, 225
- Disposal wells, 90

- Dixie Valley, 475–476
 bottoming binary unit, 485
 steam turbine, 475, 476*f*
- DOE Raft River pilot plant, 550–553
 actual performance assessment, 557
 cooling tower makeup water treatment, 558
 design performance assessment, 554–557
 make-up water treatment system, 559*f*
 nominal design properties for, 555*t*
 nominal design specifications for, 555*t*
 original wells and power plant, 550–553
 performance results, 558*t*
 plant photographs, 558–560
 power analysis results, 556*t*
- Dominica, 455
- Dora 1 power plant, 586–591
- Dora 2 power plant, 591–592
- Dora 3A, 593
- Dora 3B, 593
- Dora 4, 593
- Dora 5, 593
- Double- and triple-flash steam power plants, 143
 conversion process thermodynamics, 148–153
 energy conversion system, 147
 environmental aspects, 161
 equipment lists, 161–163
 gathering systems design, 144–146
 practice problems, 163–168
 scale potential in waste brine, 156–160
 silica scaling potential, 158–160
- Double-flash steam power plants. *See also*
 Hybrid systems
 Germencik, 595–600
 installed MW per country, 691*t*
 installed MW worldwide, 692*t*
 total units worldwide, 693*t*
 units per plant type per country, 692*t*
- Downhole pressure, 66, 80
- Downhole pumps, 225–229
- Downwell pumps and motors, 223
- Drawdown pressure and coefficient, 63–64, 67, 69–70, 72
- Drilling, 49
 bits, 51
 catastrophic events, 680
 directional, 50–51, 177*f*, 663
 drill pads, 51, 52*f*
 environmental aspects, 663, 668, 680
 equipment, 50–51
 exploratory wells, 41, 49
 fluids, 53
 The Geysers dry-steam power plants, 351–352
 hot dry rock concept, 12–14
 International Continental Scientific Drilling Program, 5
 mud, 53
 operations, 51–56
 rig setup, 51, 52*f*
 safety precautions, 56–58
 Salton Sea Deep Drilling Program, 5
 site preparation, 50–51
 water usage, 668
- Dryness fraction, 72, 82–83, 113
- Dry-steam power plants, 169
 energy conversion system, 179–183
 environmental aspects, 185–186
 equipment lists, 187–188
 fields and plants, 170
 The Geysers case study, 345
 installed MW per country, 691*t*
 installed MW worldwide, 692*t*
 Larderello case study, 321
 nature of resources, 171–176
 optimum wellhead pressure, 183–185
 origins of resources, 171–176
 practice problems, 190–192
 steam gathering system, 177–178
 total units worldwide, 693*t*
 units per plant type per country, 692*t*
- Dry-steam reservoirs
 fluid behavior mechanism, 171
 general characteristics, 171
 origins and nature, 171–176
 pressure deficiency, 175
 typical well completion, 56*f*
 world distribution, 170
- Dry-turbine expansion process, 182, 182*f*
- Dual-admission turbines, 147, 150–151, 150*f*, 211
- Dual-fluid binary cycles, 212–216
- Dual-pressure binary cycles, 209–212
- Dunes field, Imperial Valley, California, 37
- ## E
- Earthquakes, 5, 7, 8*f*, 9–10, 39, 524
- Earth's atmosphere, 4–7
- Earth's crust, 4–7
- Earth's inner structure, 5
- East African Rift zone, 9
- East Highline canal, 521
- East Mesa. *See also* Magmamax binary power plant
 geothermal field, 515
 geothermal power plants, 528*f*

- Eastern Borefield (EBF), 372
 EBF. *See* Eastern Borefield (EBF)
 Efficiency. *See also* Thermal efficiency;
 Utilization efficiencies
 Carnot efficiency, 208, 297
 exergy, 299–315
 feed pumps, 199
 turbines, 121–122, 181–183, 299–302
 EGEE. *See* Empresa de Generacion de Energia
 Electrica (EGEE)
 EGS power plants, 632–651
 Bruchsal, Germany, 644
 Landau, Germany, 640–642
 Neustadt-Glewe, Germany, 638–639
 Simplified schematic of, 639*f*
 Soultz-sous-Forêts, France, 632–637
 Unterhaching, Germany, 642–644
 EIG Global Energy Partners, 483
 Eight Mile Flat, 481
 El Salvador, 430–441, 708*t*. *See also*
 Ahuachapán Power Station
 Berlín plant, 437–439, 437*f*
 electricity situation in 2014, 432*t*
 ENEL Green Power, 431–432
 geothermal areas of, 433*f*
 prospects, 440–441
 Electric Power Research Institute, 153, 271
 Electric submersible downhole pumps, 226, 226*f*,
 227*t*
 Electric submersible pump (ESP), 635
 Electricity
 environmental aspects of generation, 659–660
 gross electrical power equation, 121, 152, 181
 resistivity, 38
 Electricity generation, general impacts of,
 659–660
 Elements of thermodynamics, 715
 Emergency pressure relief stations, 177, 178*f*
 Emergency steam stacking, 179*f*
 Emissions
 carbon emission credits, 661
 environmental aspects for gases, 660–663,
 662*f*, 663*f*
 radon, 35
 Empresa de Generacion de Energia Electronica
 (EGEE), 450
 ENEL Green Power, 431–432, 482
 Energy conversion systems
 advanced systems, 241
 binary cycle power plants, 193
 double- and triple-flash steam power plants, 147
 dry-steam power plants, 179–183
 single-flash steam power plants, 114–119
 Energy equivalents, 713
 Enhanced Geothermal Systems (EGS), 12, 609
 definitions, 610–611
 deep hydrothermal systems, 610–611
 enhanced geothermal systems, 610
 hot dry rock, 610
 early projects, 612–617
 Fenton hill HDR project, 612–613
 Rosemanowes, England, 614–617
 EGS power plants, 632–651
 Bruchsal, Germany, 644
 Landau, Germany, 640–642
 Neustadt-Glewe, Germany, 638–639
 Soultz-sous-Forêts, France, 632–637
 Unterhaching, Germany, 642–644
 later projects, 617–632
 Basel, Switzerland, 627–632
 Hijiori, Japan, 617–624
 Ogachi, Japan, 624–627
 proposed projects, 644
 Australia, 645–651
 Germany, 651–653
 United States, 651–652
 Enthalpy, 68, 79, 122. *See also* Pressure-enthalpy
 diagrams
 Enthalpy-entropy (Mollier) diagrams
 pure substance, 725*f*
 steam, 180*f*, 184*f*
 water, 173, 724*f*, 735–736, 736*f*
 Entropy, 719–720. *See also* Enthalpy-entropy
 (Mollier) diagrams; Temperature-entropy
 diagrams
 Environmental aspects, 657
 advantages of plants, 660–669
 binary cycle power plants, 207–208, 223
 catastrophic events, 680
 challenges for plants, 670–681
 cooling water, 668
 double- and triple-flash steam power plants,
 161
 dry-steam power plants, 185–186
 electricity generation, impacts of, 660–669
 gaseous emissions, 660–663, 662*f*, 663*f*
 induced landslides, 674–676
 induced seismicity, 673–674
 integrated flash-binary plants, 249, 251–256
 Lake County Effluent Pipeline (LCEP), 363
 land subsidence, 670–672
 land usage, 663–667, 665*t*
 Larderello, 340–342
 natural hydrothermal manifestations, 677–678
 noise pollution, 676–677
 overview, 658

- regulations, 658–659
 - scenic vistas, 678–680
 - subsidence, 670–672
 - thermal pollution, 680–681
 - vegetation, 678–680
 - visual pollution, 678–680
 - water pollution, 669
 - water usage, 668–669
 - well drilling, 668
 - wetland habitats, 363
 - wildlife habitats, 678–680
 - working fluids in binary plants, 207–208, 207*t*
 - Environmental impact, of geothermal power plants, 657
 - advantages, 660–669
 - gaseous emissions, 660–663
 - land usage, 663–667
 - solids discharge, 667–668
 - water pollution, 669
 - water usage, 668–669
 - challenges, 670–681
 - catastrophic events, 680
 - induced landslides, 674–676
 - induced seismicity, 673–674
 - land subsidence, 670–672
 - natural hydrothermal manifestations, disturbance of, 677–678
 - noise pollution, 676–677
 - thermal pollution, 680–681
 - wildlife habitat, vegetation and scenic vistas, disturbance of, 678–680
 - electricity generation, general impacts of, 659–660
 - regulations, 658–659
 - Environmental Impact Statement, 678
 - Equal-temperature-split rule, 132, 153, 159–160
 - Equations of state, 716
 - Equipment
 - basic binary plants, 223–225
 - double- and triple-flash steam power plants, 161–163
 - drilling, 50–51
 - dry-steam power plants, 187–188
 - Ethiopia, 708*t*
 - Ethyl chloride, 194
 - Evaporators
 - basic binary systems analysis, 199–202
 - indirect-cycle, Larderello, 330, 331*f*, 334*t*
 - Kestner, 330–331, 331*f*
 - preheater-evaporator exergy efficiencies, 303
 - Exergy
 - analysis, 291
 - applications to geothermal plants, 299–315
 - efficiency, 299–315
 - first law for open, steady systems, 292–293
 - fluid streams, 294–297
 - general concept, 294
 - heat transfer, 297
 - open, steady systems, 292–293, 298–299
 - second law for open, steady systems, 293
 - work transfer, 297–298
 - Exploration programs
 - drilling, 41
 - Heber binary plant, 502–503
 - MagmaMax binary power plant, 516
 - objectives, 24
 - phases, 25–39
 - practice problems, 43–47
 - strategies and techniques, 23
 - synthesis and interpretation, 40–41
 - Exploratory wells, 17*f*, 41, 49
 - Explosions, phreatic, 680
 - Extensive properties, 715
- F**
- Far-field reservoir pressure, 63–64
 - FCRC. *See* Flash-crystallizer/reactor-clarifier
 - FDM. *See* Finite difference method
 - Feed pumps, 199, 224
 - FEHMN, 89*t*
 - FEM. *See* Finite element method
 - Fenton Hill Hot Dry Rock Project, Valles Caldera, New Mexico, 612–613
 - Finite difference method (FDM), 88
 - Finite element method (FEM), 88
 - Fire protection systems, 225
 - First law of thermodynamics, 65, 79, 119, 123, 125, 292–293, 717
 - Fish Lake Valley Well FPL-1, 26*t*
 - Flash, wellbore, 71–74
 - Flash horizon, 67–70
 - Flash plants, 229–231, 471–478. *See also*
 - Double-flash steam power plants;
 - Hybrid systems; Single-flash steam power plants
 - Beowawe plant, 471–472
 - Brady Plant 1, 477–478
 - Desert Peak 1, 473–474
 - Dixie Valley, 475–476
 - flash-binary plants, 247–252, 691*t*, 692*t*
 - Flash point, 67–68, 114
 - Flash pressure, 114, 152
 - Flash process, 114, 149–150
 - Flash temperature, 154, 244–245
 - Flash vessels, 306–308

Flash-crystallizer/reactor-clarifier (FCRC)
systems, 271–274, 667

Flashers

double- and triple-flash steam power plants,
144–146
satellite, 145, 145*f*, 146*f*

Flow patterns, 113

Flow testing, 612

Fluid

behavior in dry-steam reservoirs, 171
restoration. *See* Reinjection
selection, 203–208

Forecasting, 87–88, 365–366, 365*f*

Forked wells, 352, 352*f*

Fossil systems, 263–267

Fossil-superheat systems, 263–265

4-stage flash steam plants, 263–264, 264*f*

Fourier's Law, 35–36

France, 708*t*

Friction, 66, 68–71, 73, 110–112

Fuel oil, 713*t*, 714*t*

Fuji Electric, 475

Fumaroles, 10–11

Functional exergy efficiency, 299–315

G

Gabbro plant, Larderello, Tuscany, Italy, 339

Galena 2, flow diagram for, 469, 470*f*

Garbage energy equivalents, 713*t*, 714*t*

Gas

compressors, 308–311
ejection equipment, 162, 187
emissions, 660–663
environmental aspects of emissions, 660–663,
662*f*, 663*f*
geochemistry, 34–35
natural, 264–265, 713*t*, 714*t*
noncondensable, 329–330, 335, 660–663,
662*f*, 663*f*
perfect gas equation of state, 716
radon emissions, 35
sensors, 56–58
toxic gas safety precautions, 56–58

Gathering systems

double- and triple-flash steam power plants,
144–146
dry-steam power plants, 177–178
single-flash steam power plants, 108–114

GDC-31, The Geysers well, 354, 359–360

GEM plant, East Mesa, Imperial Valley,
California, 196, 527–528

Geochemical surveys, 30–35

Geofluids, 482

calcium-rich, 34

disposal systems, 156, 162–163

flow, 463

reservoir temperatures, 33–34

Geography

The Geysers dry-steam power plants, 345

Magmamax binary power plant, 516–523

Geoliquids, energy equivalents, 713*t*, 714*t*

Geology

Büyük Menderes Graben, 575–577, 577*f*

Cooper Basin, 646*f*

geothermal regions, 7–10

Hengill geothermal field, 532–534

Larderello, Tuscany, Italy, 324–328

Ogachi, 624

practice problems, 21–22

Raft River, 546–549

Rhine Graben, Basel, 631*f*

surveys, 27–29

Geophysical surveys, 35–39

Geopressure energy source, 265–267

Geopressure reservoirs, 14–15

Geopressure-geothermal hybrid systems,
265–267

Geosteam energy equivalents, 713

Geothermal power generating systems. *See also*

Binary cycle power plants; Double-flash
steam power plants; Dry-steam power
plants; Single-flash steam power plants;
individual plants and plant types

advanced, 241

annual growth rate, 687–688, 687*f*

combined flash-binary systems, 247–249

combined heat and power plants, 267–269

combined single- and double-flash systems,
246

countries ranked by installed MW, 689*t*

countries with fewer than 10 units, 708*t*

countries with more than 10 units, 694*t*, 695*t*,
696*t*, 698*t*, 702*t*, 703*t*, 704*t*, 706*t*

countries with retired/inactive plants, 708*t*

exergy analysis, 291

hot dry rock, 12–14, 610

hybrid single-flash and double-flash systems,
243–246

hybrid-fossil geothermal systems, 263–267

hypersaline brines, 269–274

installed MW per plant type per country, 691*t*

installed MW worldwide, 692*t*

integrated flash-binary plants, 249–252

integrated single- and double-flash systems,
244–245

- thermal *versus* utilization efficiency, 315–316
- total units per country, 690*t*
- total units per plant type per country, 693*t*
- total units worldwide, 693*t*
- total-flow systems, 256–263
- worldwide status (December 2014), 687–688, 689*t*, 690*t*, 691*t*, 692*t*, 693*t*, 694*t*, 695*t*, 696*t*, 698*t*, 699*t*, 700*t*, 701*t*, 702*t*, 703*t*
- Geothermal well drilling. *See* Drilling
- Geothermal-preheat systems, 265
- Geothermometers, 32–34, 33*f*
- Geovolcanology, 27
- Germany, 651–653, 708*t*
- Germencik double-flash plant, 593–600
- Geyser Canyon, 346–350
- The Geysers dry-steam power plants, California
- Beowawe, Nevada, 677
- blowout preventers, 56–58
- Calpine Corporation plant designs, 359–360
- case study, 345
- development history, 346–350
- disappearance, 677
- fluid restoration by injection, 175–176
- environmental impacts, 677–678
- geography, 350–351
- geology, 350–351
- historical development, 346–350
- hybrid fossil-geothermal plants, 264–265
- PG&E plant designs, 357–358
- power plants, 353–360
- reservoir recharging, 360–364
- SMUDGE #1 plant design, 358–359
- steam gathering system, 177–178, 177*f*, 178*f*, 179*f*, 353
- sustainability, 364–365
- well drilling, 351–352
- Geysers dry steam field, 88–89
- Geysers Resort, 347*f*, 348*f*
- Gibbs Phase Rule, 715–716, 721
- Global warming, 207, 661
- Gradient Resources, Inc. (GRI), 488
- Grant, J.D., 347, 348*f*
- Gravitational pressure drop, 113
- Greece, 710*t*
- GRI. *See* Gradient Resources, Inc. (GRI)
- Groundwater pollution, 669
- Growth rate of world plants, 687–688, 687*f*
- Guadeloupe, 452–455
- Guatemala, 431, 449–451, 674–676, 675*f*, 708*t*
- Amatitlán, 450
- prospects, 450–451, 451*f*
- Zunil plant, 449–450
- Gulf of Mexico, 14, 265–266
- ## H
- Habanero-3, 646*f*
- Habenero-1 (Hab-1), 646–647
- Habitats, 363, 678–680
- Hawaii, 16, 706*t*
- HDR. *See* Hot dry rock
- Health, 207–208
- Heat balance diagram (HBD), 358*f*, 359*f*, 567
- Heat exchangers, 559*f*
- basic binary systems, 199–202, 224
- brine/working fluid heat exchangers, 224
- exergy efficiencies, 302–306
- original Magmamax binary plant, 518–519, 518*f*
- redesigned Magmamax binary plant, 524–525, 525*f*, 526*f*
- shell-and-tube, 302, 330–331, 331*f*
- Heat flow/flux, 35–37
- Heat recuperators, 212
- Heat rejection, cooling water for, 668
- Heat rejection ratio, 203
- Heat rejection systems
- basic binary plants, 224
- cooling water, 668
- double- and triple-flash steam power plants, 162
- dry-steam power plants, 187
- environmental aspects, 668, 680–681, 681*f*
- thermal pollution, 680–681, 681*f*
- Heat transfer, exergy, 297
- Heat transfer coefficient, 201–202
- Heber binary plant, Imperial Valley, California
- exploration and discovery, 502–503
- first binary plant, 503–506
- Heber 2 binary plant land usage, 665*t*, 666*f*
- second binary plant, 506–512
- working fluids, 204
- Helical screw expanders, 261–263
- Hellisheidi plants, Iceland, 541–543
- case study, 531
- conceptual model of, 533, 534*f*
- development history, 541*t*
- geothermal view of, 533*f*
- process flow diagram for, 542*f*
- state-point analysis for, 543*t*
- temperature-entropy process, 542*f*
- turbine specifications for, 541*t*
- wellhead locations in, 535*f*
- Hengill volcano, 532
- High-pressure (HP) cycle, 565
- High-pressure (HP) steam, 475
- High-pressure (HP) turbines
- expansion process, 150–152

High-pressure (HP) turbines (*Continued*)
 Nga Awa Purua (NAP) power plant, 390
 Wairakei geothermal system, 373–374, 377–379
 Hijiori, Japan, 617–624
 anhydrite precipitation model for, 624f
 experimental binary-type power plant, 618f
 former site of, 620f
 HDR research facility, 617f
 schematic of HDR reservoirs, 619f
 Hijiori Hot Dry Rock Project, Honshu, Japan, 617–624
 History
 The Geysers dry-steam power plants, 346–350
 Larderello, 322–324, 323t
 matching in reservoir models, 87
 NCPA power plants, 365–366
 Holding ponds, 519–521, 522f
 Honduras, 431
 Horizontal pipe flow patterns, 113
 Horner plot, 80, 81f
 “Horse-tail fault zone,” 594
 Hot dry rock (HDR) concept, 12–14, 610
 Hot Fractured Rock (HFR), 610
 Hot water geothermal resource model, 10
 HP steam. *See* High-pressure (HP) steam
 HP turbines. *See* High-pressure (HP) turbines
 HSZ. *See* Humboldt structural zone (HSZ)
 Humboldt structural zone (HSZ), 462
 Hybrid geothermal–solar systems, 491–494
 Hybrid systems
 geopressure-geothermal hybrid systems, 265–267
 hybrid flash-binary plants, 247–252, 691t, 692t
 hybrid fossil-geothermal systems, 263–267
 hybrid single- and double-flash systems, 243–246
 installed MW (capacity) per country, 691t
 installed MW worldwide, 692t
 solar-geothermal plants, 274–277
 total units worldwide, 693t
 units per plant type per country, 692t
 Hydraulic fracturing, 12
 Hydraulic shearing, 647
 Hydrochloric acid, 273
 Hydrofracking, 12, 610
 Hydrogen, geothermometers, 34
 Hydrogen sulfide, 661
 AMIS, 340
 environmental aspects, 661–663, 663f
 geothermometers, 34
 safety precautions, 56–58

Hydrologic surveys, 30
 Hydrostatic forces/pressure, 14, 66, 72, 265–266
 HYDRO-THERM, 89t
 Hydrothermal geothermal resource model, 10–12
 Hydrothermal manifestations, environmental aspects, 677–678
 Hydrothermal Power Company, 262
 Hypersaline brines, 269–274, 271t

I

Iceland, 532f, 694t
 Idaho, 545, 547f, 706t
 Ideal binary cycles, 208–209
 IFDM. *See* Integral finite difference method
 Imperfect differential, 717, 720
 Imperial Valley, California, 37. *See also* Heber binary plant; Magmax binary power plant; Salton Sea
 Impulse turbine, 256–259, 259f
 Impulse-reaction blading, 179
 Inactive plants, 710t
 INDE. *See* Instituto Nacional de Electrificación (INDE)
 Indirect cycles, 330, 330f, 334t
 Indonesia, geothermal power plants of, 403, 695t
 Darajat power units, 409f, 413–417
 geological setting, 409–410
 development, outlook for, 423–424
 early geothermal development, 405–408
 geographic and geologic setting, 403–405
 geothermal plants as of 2014, 423t
 Kamojang power units, 409f, 410–412
 geological setting, 409–410
 Wayang Windu power plant, 418–422
 West Java electrical grid, 418
 Induced landslides, 674–676
 Induced microseismicity, 673
 Induced seismicity, 673–674
 Infrared imaging, 26
 Injection. *See* Reinjection
 Installed MW, 689t, 691t, 692t
 Instituto Nacional de Electrificación (INDE), 450
 Instruments for pressure and temperature, 75–76
 Integral finite difference method (IFDM), 88, 89t
 Integrated flash-binary plants, 249–256
 Integrated single- and double-flash plants, 244–245
 Integrated Two-Level Units (ITLU), 506, 507f
 Intensive properties, 715
 Intermediate-pressure wells (IPWs), 375
 Internal roughness of pipes, 111–112

International Continental Scientific Drilling Program (ICDP), 5
 International Energy Agency (IEA), 627
 International System of Units, 711, 714*t*
 Internet literature surveys, 25
 Inverse modeling, 87
 IPWs. *See* Intermediate-pressure wells (IPWs)
 Irreversible processes, 716, 719–720
 Isenthalpic process/flow, 65, 68, 72, 120
 Isentropic feed pump efficiency, 199
 Isentropic turbine efficiency, 121, 181, 300
 Isobaric process, 721
 Isobutane liquid heaters, 519*f*
 Isobutane turbines, 519, 521*f*, 524–525
 Isobutane-boiler superheaters, 526*f*
 Isolated systems, 715
 Isopentane, 204*t*, 206*t*, 207*t*, 218–222
 Isotherm distribution, 326–328, 326*f*, 327*f*
 Isothermal process, 721
 Italy
 geothermal power plants, 696*t*
 ITB. *See* Bandung Institute of Technology (ITB)
 ITLU. *See* Integrated Two-Level Units (ITLU)
 iTOUGH2, 89*t*

J

James' lip pressure method, 79–80
 Japan, 617–627, 698*t*
 Jersey Valley plant, 485, 488
 Jersey Valley power plant, 485, 486*f*
 JHFS. *See* John Hancock Financial Services (JHFS)
 John Hancock Financial Services (JHFS), 483

K

Kalina binary cycles, 216–218, 643
 Kamojang power units, 409*f*, 410–412
 geological setting, 409–410
 satellite view of, 411*f*
 technical details and performance for, 411*t*
 Units 1–3, 410
 Unit 4
 exergy values at various states in, 413*f*
 gathering system for, 412*f*
 power house process flow diagram for, 413*f*
 Kawerau geothermal plant, 392*t*, 393–395
 field map, 393*f*
 100-MW turbine cross-section, 394*f*
 stand-alone power plants at, 394*f*
 Kay's rule, 311
 Kelvin-Planck statement, 719
 Kenya, 699*t*

Kestner evaporators, 330–331, 331*f*
 Kiabukwa binary plant, DRC, 194–195
 Kilauea Iki, Hawaii, 16
 Kizildere single-flash plant, 577–586
 auxiliary power requirements for, 583*t*
 early history and pilot plant, 577–579
 Kizildere Unit 1, 581–583
 Kizildere Unit 2, 584*f*, 585*t*
 and future plans, 584–586
 Fuji steam turbine assembly for, 585*f*
 turbine-generator specifications for, 583*t*
 turbo-compressor specifications for, 583*t*
 wells, 579–581
 KMJ-3, 405
 Kuster K10 geothermal tool, 76*f*

L

Lago plant, Larderello, Tuscany, Italy, 339
 Lake County Effluent Pipeline (LCEP), 363, 365–366
 Land subsidence. *See* Subsidence
 Land usage
 environmental aspects, 663–667
 power plants comparative data, 664, 665*t*
 Landau, Germany, 640–642
 milestones for, 641*t*
 temperature profiles in, 642*f*
 Landslides, 674–676
 Larderello, Tuscany, Italy
 case study, 321
 direct-intake, condensing units, 336–337
 direct-intake, exhausting to atmosphere units, 335–336
 early plants, 329–334
 environmental impact mitigation, 340–342
 geology, 324–328
 history of development, 322–324
 indirect cycle, 195
 major dry-steam fields, 170
 modern era plants, 335–337
 power plants, 328–339
 recent plants designs, 337–339
 reservoir characteristics, 324–328
 Larderello–Travale–Radicondoli–Lago
 geothermal area geology, 324–325
 Las Pailas plant, Costa Rica, 446–447, 447*f*, 448*f*, 448*t*
 piping layout, 108–109, 110*f*
 Lava lakes, 16
 Lawrence Livermore Laboratory impulse total-flow turbine, 259*f*
 Laws for environmental aspects, 658–659

Layouts. *See* Schematic diagrams
 LCEP. *See* Lake County Effluent Pipeline
 Lessons learned from Nevada's experience, 495–496
 Lever rule, 121, 306
 Life cycle of geothermal fields, 364
 Lignite energy equivalents, 713*t*, 714*t*
 Lineshaft mechanical downhole pumps, 226, 226*f*, 227*t*
 Line-shaft pump (LSP), 635
 Liquid pipe pressure losses, 112
 Liquid pressure behavior
 through centrifugal pump, 228*f*
 Liquid pump, 311*f*
 Liquid-ring vacuum pumps (LRVP), 230, 230*f*
 Liquid-vapor regions, 723*f*, 724*f*
 Literature surveys, 25
 Lithologic logs, 41
 Lithosphere, 9–10
 Lithostatic pressure, 671–672
 Little Geysers, 346
 Log data for wells, 25
 Log pressure-enthalpy diagrams, 725*f*
 Long Valley caldera, California, 16, 17*f*, 27, 28*f*, 29, 29*f*
 Loss of circulation, 54, 352
 Low pressure turbines, 147, 148*f*
 expansion process, 150–152
 Low-temperature systems, 18–19
 Lumped-parameter approach, 62–63, 70
 Lysholm expander, 262

M

Magma energy, 15–17
 Magma Energy Inc., 516–517
 Magma Energy Program, 16
 Magma Power Company, 348*f*, 488, 516–517
 Magmamax binary power plant, East Mesa, Imperial Valley, California, 515
 dual-fluid binary cycle, 212, 215–216
 geothermal fluid composition, 271*t*
 modified Magmamax binary power plant, 524–526
 original Magmamax binary power plant, 516–523
 setting and exploration, 515–516
 unique design features, 517
 Magmamax process, 516–517
 Magmatic zones, 9–10
 Mass
 balance, 30
 conservation of, 124–125, 718
 Mass flow rates
 direct measurements, 76–78
 indirect measurements, 78–80
 Maximum power output, 294
 Maximum steam loss silica geothermometers, 33
 Maximum work output, 294
 Mayacamas Mountains, California, 350
 McCabe, Barkman C., 348*f*, 516–517, 527–528
 McCabe plant, 346
 McGinness Hills, 485, 486*f*, 488
 McLachlan power plant. *See* Poihipi Road plant
 Mechanical, induced-draft cooling towers, 124*f*
 Mechanical lineshaft downhole pumps, 226, 226*f*, 227*t*
 Mercury, 340
 Mercuryville fault system, 351
 Meteoric waters, 171
 Methane, 15, 34, 266–267
 Mexico, 700*t*. *See also* Cerro Prieto Power Station, Baja California Norte
 MHI. *See* Mitsubishi Heavy Industries, Ltd. (MHI)
 Microearthquakes, 39
 Microseismicity, 673
 Mid-Atlantic Ridge, 9
 Minerals, 667, 669
 Miravalles station, 445
 Mitsubishi Heavy Industries, Ltd. (MHI), 415–416
 Mixed working fluid condensers, 305–306
 Moana Springs Geothermal Resource Area, 463
 Models and modeling
 hydrothermal geothermal resource, 10–12
 reservoir engineering, 62, 83–88
 reservoir-well model, 62–74
 Modular plants, 337–338, 338*f*
 Moisture removers, 117*f*, 117*t*
 Mokai, 392*t*
 Molinetto plant, Larderello, Tuscany, Italy, 340*t*
 Mollier diagram. *See* Enthalpy-entropy (Mollier) diagrams
 Momentum equation, 66
 Momotombo station, 442–443, 442*f*
 locations of wells at, 443*f*
 Monoblok, 406–407, 406*f*
 Montreal Protocol, 207
 Montserrat, 455
 Mufflers, 676–677
 MULKOM, 89*t*
 Munson Geothermal, 466–467
 MW
 capacity ranking by country, 689*t*
 plant types per countries, 691*t*
 total worldwide, 693*t*

N

- NAP power plant. *See* Nga Awa Purua (NAP) power plant
- National Institute of Standards and Technology (NIST), 716
- National Oceanic and Atmospheric Administration (NOAA) map, 7
- Natural gas, 264–265, 713*t*, 714*t*
- Natural hydrothermal manifestations, disturbance of, 677–678
- Natural recharge, 172
- Natural thermal manifestations destruction, 677–678
- Nazca plate, 9
- NCG. *See* Noncondensable gases (NCG)
- NCPA. *See* Northern California Power Agency
- NEDO. *See* New Energy and Industrial Technology Development Organization
- Nesjavellir geothermal plant, Iceland, 535–540
case study, 531
condenser specifications for, 539*t*
cooling tower specifications for, 539*t*
development history, 536*t*
gas extractor specifications for, 539*t*
geology and geosciences, 532–534
lithology of, 534*f*
pipeline route in, 535*f*
process flow diagram for, 538*f*
turbine specifications for, 539*t*
- Net positive suction head (NPSH), 228–229
- Net power
basic binary systems, 203
dry-steam power plants, 181
integrated flash-binary plants, 254
- Net salable power, 121
- Neustadt-Glewe, Germany, 638–639
- Nevada (USA), geothermal power plants in, 461, 706*t*
binary plants, 478–489
Beowawe binary, 484
Blue Mountain, 482–483
Desert Peak 2, 480
Dixie Valley bottoming binary plant, 485
Jersey Valley plant, 485, 488
McGinness Hills, 485, 488
Patua geothermal resource area, 488–489
Salt Wells, 481–482
San Emidio, 478–480
Soda Lake Plants 1 and 2, 480
Tuscarora, 485, 488
development, brief history of, 466–468
flash plants, 471–478
Beowawe plant, 471–472
Brady Plant 1, 477–478
Desert Peak 1, 473–474
Dixie Valley, 475–476
geologic setting, 462–466
lessons learned from Nevada's experience, 495–496
Steamboat geothermal power complex, 468–471, 677, 706*t*
Stillwater plants, 489–494
hybrid geothermal–solar systems, 491–494
Stillwater 1, 489–491, 490*f*
Stillwater 2, 491, 494*f*
- Nevada Geothermal Power, Inc. (NGP), 482
- Nevis, 455
- New Energy and Industrial Technology Development Organization (NEDO), 617
- New Zealand, geothermal power plants of, 370, 371*f*, 701*t*. *See also* Wairakei
Kawerau, 393–395
Nga Awa Purua (NAP) power plant, 146, 388–391, 389*f*
layout, 391*f*
process flow diagram, 391*f*
Technical details and performance for, 390*t*
temperature-entropy process diagram for, 392*f*
- Ngatamariki, 397–399
- Ohaaki land subsidence, 670
- Ohaaki power station, 395–396
- outlook for development, 399
- Rotokawa power plant, 387–388
- Wairakei and related power stations, 134–135, 370–387
capital cost and generation history, 386–387
geographic and geologic setting, 370–373
original Wairakei power plant, 373–378
Poihipi Road plant, 379–381
recent configurations, 379
Te Mihi power plant, 383–385
Wairakei binary plant, 381–382
- Newton's Second Law of Motion, 66
- Nga Awa Purua (NAP) power plant, 146, 388–391, 389*f*
layout, 391*f*
process flow diagram, 391*f*
Technical details and performance for, 390*t*
temperature-entropy process diagram for, 392*f*
- Ngatamariki power plant, 392*t*, 397–399, 398*f*
- Ngawha, 392*t*
- NGP. *See* Nevada Geothermal Power, Inc. (NGP)

Nicaragua, 430–431, 442–444, 708*t*
 geothermal areas of, 445*f*
 Momotombo station, 442–443
 prospects, 444
 San Jacinto plant, 444
 Nigamizu River, 618
 NIGHTS, 89*t*
 NIST. *See* National Institute of Standards and Technology
 Nitrogen oxide, 661
 No steam loss silica geothermometers, 32
 Noise
 abatement systems, 162, 188
 everyday activity levels, 677, 678*t*
 geothermal activity levels, 676–677, 678*t*
 pollution, 676–677
 3-dimensional acoustic noise patterns, 673, 674*f*
 Non-choked well flow, 129–130
 Noncondensable gases (NCG), 329–330, 335, 406, 581, 585, 600–601, 660–663, 662*f*, 663*f*
 Northern California Power Agency (NCPA)
 power plants, 359–360, 365–366, 365*f*

O

Ogachi, Japan, 617, 624–627
 carbon dioxide sequestration experiment, 626*f*
 conceptual model of CO₂ injection/production, 626*f*
 geologic cross-section, 624*f*
 Ohaaki, New Zealand land subsidence, 670
 Ohaaki power station, 392*t*, 395–396, 397*f*
 well field and power plant map, 396*f*
 Oil crisis, 687*f*, 688
 Oil energy equivalents, 713*t*, 714*t*
 Oil price collapse, 687*f*, 688
 Once-through steam generators, 215–216
 Onikobe power plant, 619
 Open, steady systems, 292–293, 298–299
 Open systems, 292–293, 298–299, 715–718, 721
 Optimization
 double- and triple-flash steam power plants, 152–153
 example, 153–155
 single-flash choked well, 127–129
 single-flash non-choked well, 129–130
 single-flash steam power plants, 127–130
 Optimum separator temperature approximate
 formulation, 130–132
 Optimum wellhead pressure, 183–185

ORCs. *See* Organic Rankine cycles (ORCs)
 Organic Rankine cycles (ORCs), 480
 Ormat Integrated Two-Level Units, 506
 Ormat integrated two-level units, 507*f*
 Ormat Nevada, Inc., 480
 Ormat Technologies, Inc., 468, 483, 488
 Overall heat transfer coefficient, 201–202, 202*t*
 Ozone depletion potential, 207

P

Pacific Gas and Electric Company (PG&E), 353–354, 355*f*, 357–358
 Pacific Ring of Fire, 9
 Painting plants for camouflage, 340, 680
 Pamukkale UNESCO World Heritage Site, 575–577
 Pamukören binary plant, 600–601, 601*f*
 Panama, 431
 Pangaea, 4
 Papua New Guinea, 708*t*
 Parasitic loads/power requirements, 121, 505–506
 Paratunka binary plant, Kamchatka Peninsula, Russia, 194, 223
 Partial pressure of carbon dioxide, 82
 Particulate removers, 179
 Patua geothermal resource area, 488–489
 Patua well field and plant location, 488, 489*f*
 PDEs. *See* Positive displacement expanders
 PEI. *See* Principle of entropy increase
 Pentane, 204*t*, 206*t*, 207*t*
 Perfect differential, 717–718, 720
 Perfect gas equation of state, 716
 Perfluoropentane, 638
 Permeability, 63, 85–86
 Pertamina, 422
 Peru, 458
 Perusahaan Listrik Negara (PLN), 422
 PG&E. *See* Pacific Gas and Electric Company
 pH, 82, 157
 Phased cooling systems, 519–521
 Philippine plate, 9
 Philippines, 255–256, 702*t*
 pH-modification (pH-mod) system, 272–274, 667
 Photography, aerial, 26
 Photovoltaic (PV) plants, 491–493
 Phreatic explosions, 680
 Piancastagnaio, Larderello, Tuscany, Italy, 335
 Piezoelectric pressure transducers, 76
 Pinch point temperature difference, 201
 Pipelines

- diameter and pressure drop, 110–111
 - environmental aspects, 663–664, 664*f*
 - The Geysers dry-steam power plants, 353
 - single-flash steam power plants, 108
 - Plant equipment, 115
 - Plant flow diagram, 732*f*
 - Plant schematics. *See* Schematic diagrams
 - Plate tectonics, 3–4, 324
 - Pleasant Bayou, Texas, 266–267
 - PLN. *See* Perusahaan Listrik Negara (PLN); State Electrical Company (PLN)
 - Poihipi Road plant, 379–381
 - technical details and performance for, 382*t*
 - Pollution
 - control, 162, 187
 - double- and triple-flash steam power plants, 162
 - dry-steam power plants, 187
 - noise, 676–677
 - thermal, 680–681
 - visual, 678–680
 - water, 669
 - Portugal, 708*t*
 - Positive displacement expanders (PDEs), 262
 - Potassium, 31, 34
 - Power. *See also* Net power; Specific power
 - basic binary systems, 198–199
 - developed by turbines, 121
 - double-flash optimization, 153–155
 - dry-steam power plants, 181
 - exergy, 294
 - output per maximum steam flow rate, 185, 186*f*
 - output *versus* separator temperature, 128
 - single-flash steam power plants, 108
 - total generated equation, 152
 - Power purchase agreement (PPA), 422
 - Power rating
 - binary cycle power plants, 195
 - double- and triple-flash steam power plants, 147
 - Prawn farms, 663–664
 - single-flash steam power plants, 108
 - PPA. *See* Power purchase agreement (PPA)
 - Precipitation of silica, 156–158, 246, 249
 - Preheater-evaporators exergy efficiencies, 303
 - Preheaters, 199–202
 - and evaporators, 559*f*
 - Pressure
 - buildup test, 80, 81*f*
 - deficiency, 175
 - dry-steam reservoirs, 175
 - gauges, 75
 - instruments, 75–76
 - losses, 110–114
 - productivity curves, 73, 73*f*
 - reservoir and well, 63–64
 - single-flash steam power plants, 110–114
 - Pressure-enthalpy diagrams
 - basic binary plants, 197, 197*f*
 - for DOE Raft River plant, 554*f*
 - dual-pressure binary plants, 210*f*
 - propane, 726*f*
 - pure substance, 725*f*
 - Pressure-enthalpy process diagram, 732*f*
 - Principle of entropy increase (PEI), 720–721
 - Production casing, 56
 - Production wells
 - exergy analysis, 313–315
 - Productivity curves
 - choked well flow, 128
 - double-flash optimization, 153
 - dry-steam power plants, 184*f*
 - non-choked well flow, 129
 - Project Moho, 5
 - Propane, 204*t*, 206*t*, 207*t*, 726*f*
 - Province, Costa Rica
 - land usage environmental aspects, 663–664
 - Psychrometric charts, 125
 - Pumice breccias, 670
 - Pumps, 225–231
 - downhole pumps, 225–229
 - exergy efficiencies, 311–313, 311*f*
 - surface pumps, 229–231
 - PV plants. *See* Photovoltaic (PV) plants
- ## Q
- Quartz, 31–32, 157
 - Quasistatic processes, 716
- ## R
- Radioactive elements, 7*t*
 - Radon emissions, 35
 - Raft River dual-boiling binary plant, 466–467, 466*f*
 - Raft River Dual-Boiling plant, Idaho, 212
 - Raft River Plants, Idaho, USA, 545
 - DOE pilot plant, 550–561
 - actual performance assessment, 557
 - cooling tower makeup water treatment, 558
 - design performance assessment, 554–557
 - make-up water treatment system, 559*f*
 - nominal design properties for, 555*t*
 - nominal design specifications for, 555*t*

- Raft River Plants, Idaho, USA (*Continued*)
 original wells and power plant, 550–553
 performance results, 558*t*
 plant photographs, 558–560
 power analysis results, 556*t*
 well characteristics, 552*t*
 geology and geosciences, 546–549
 USGeo plant, 562–572
 actual performance assessment, 567–571
 cycle analysis, 570*t*
 design performance assessment, 567
 design performance for, 571*t*
 nominal design specifications for, 568*t*
 nominal design state-point properties for, 569*t*
 performance for, 571*t*
 power plant design, 565–566
 site renewal process and well modifications, 562–564
- Range, cooling tower, 125
- Rankine cycle, 204–205, 212, 506, 713*t*, 714*t*
- Rankine-type power plant, 15
- Reboilers, 333
- Recharging reservoirs. *See* Reinjection
- Recuperators, 217, 517, 520*f*, 521, 524–525
- REFPROP (Reference Fluid Thermodynamic and Transport Properties), 716, 731
 as an Excel function, 736–739
 state-point properties, 733–736
 typical geothermal binary power cycle, 732–733
- Refrigerants, 207
- Reinjection
 dry-steam fields, 175–176
 examples, 91–95
 The Geysers dry-steam power plants, 360–364
 motivation, 88–90
 pumps, 229, 231
 reservoir engineering, 88–95
 strategies, 90–91
 subsidence, 671–672
- Renewables portfolio standard (RPS), 467
- Reservoir engineering, 61
 calcite scaling in well casings, 82–83
 modeling and simulation, 83–88
 reinjection, 88–95
 reservoir flow, 62–74
 well flow, 62–74
 well testing, 75–82
- Reservoir replenishment, 90
- Reservoirs
 The Geysers dry-steam power plants, 350–351
 Larderello, 324–328
 pressures, 63–64
 reinjection, 175–176, 360–364, 672
 simulators, 83–88
 working model, 62
- Reservoir-well model, 63–64
- Resistivity, 38–39
- Restricted dead state, 296–297
- Retired plants, 710*t*
- Retrograde fluids, 205
- Reversible Carnot cycle, 297
- Reversible processes, 716, 720
- Reynolds number, 66–67, 69, 111–112
- Rifting and rift zones, 7, 9
- Rock mufflers, 179*f*
- Rocky Mountain Oilfield Testing Center (RMOTC), 19
- Roosevelt Hot Springs, Utah, 261, 265
- Rosemanowes, England, 614–617
- Rotary drilling, 51–53
- Rotary separator turbine, 260–261
- Rotary Separator Turbine (RST), 473
- Rotokawa power plant, 387–388, 388*f*
- RPS. *See* Renewables portfolio standard (RPS)
- RST. *See* Rotary Separator Turbine (RST)
- Russia
 geothermal power plants, 703*t*
 Paratunka binary plant Russia, 194, 223
- ## S
- Sacramento Municipal Utility District (SMUD), 358–359, 488
- Safety issues, 56–58, 207–208, 680
- Salable power, 121
- Salavatli binary plants, 586–593
 Dora 2, 591–592
 Dora 3A, 3B, 4, and 5, 593
- Salavatli power unit, Turkey
 well field, 92, 93*f*
- Salinity, 38, 82, 157
- Salt Wells plant, 481–482, 481*f*
- Salton Sea, Imperial Valley, California
 East Mesa geothermal field, 515
 flash-crystallizer/reactor-clarifier system, 272–274
 hypersaline brines, 269–274
 pH-Mod plants, 272–273
 solids discharge, 667–668
- Salton Sea Deep Drilling Program, 5
- Salton Trough, 502
- San Andreas Fault, 7
- San Diego Gas & Electric Company (SDG&E), 503
- San Emidio, 478–480

- San Jacinto plant, 442*f*, 444, 444*f*
 San Vicente volcano, 428*f*
 Sand removers, 196–197
 Sandia National Laboratory, 16
 Santa Rosa Geysers Recharge (SRGR) project, 363
 Satellite separators
 double- and triple-flash steam power plants, 145*f*
 single-flash steam power plants, 108
 Saturated steam maximum enthalpy, 173
 Saturation pressure, 74
 Scale
 basic binary systems, 196
 calcite, 82, 196–197
 combined single- and double-flash systems, 247–249
 double- and triple-flash steam power plants, 156–160
 pH-Mod plants, 272–274
 potential in brine, 156–160
 Scenic vistas, 678–680
 Schematic diagrams
 basic binary cycle power plants, 196*f*
 binary cycle power plants, 196*f*, 210*f*, 211*f*, 216*f*, 217*f*, 242*f*
 Caufourier's 4-stage flash steam plant, 264*f*
 combined geothermal heat and power plants, 268*f*
 combined single- and double-flash systems, 246*f*
 combined single-flash-binary systems, 249–252
 Cycle 2 plants, 334*f*
 Cycle 3 plants, 336*f*
 direct-intake, condensing plant, 336*f*
 double-flash power plants, 148*f*, 242*f*
 dry-steam power plants, 180*f*, 242*f*
 dual-fluid binary plants, 213*f*
 dual-pressure binary plants, 210*f*, 211*f*
 enhanced geothermal systems, 613*f*, 619*f*
 Fenton Hill Hot Dry Rock Project, 613*f*
 flash vessels, 306*f*
 flash-crystallizer/reactor-clarifier, 272*f*
 fossil-superheat systems, 264*f*
 gas compressors, 294–297
 geopressure-geothermal hybrid systems, 266*f*
 Germencik, 596*f*
 The Geysers power plants, 353*f*
 Heber Binary Demonstration Plant, 504*f*
 Hellisheidi, 542*f*
 Hijiori Hot Dry Rock Project, 619*f*, 620*f*
 hot dry rock schemes, 613*f*, 619*f*, 620*f*
 hybrid fossil-geothermal systems, 264*f*, 266*f*
 hypersaline brines, 272*f*, 273*f*
 indirect-cycle, 330*f*
 integrated flash-binary plants, 250*f*
 integrated single- and double-flash systems, 244*f*
 Kalina cycle, 216*f*, 217*f*
 Kızıldere Unit 1, 582*f*
 Kızıldere Unit 2, 584*f*
 Larderello, 330*f*, 334*f*, 335*f*, 338*f*
 Maggmax binary plant, 517*f*, 525*f*
 modular layout, 338*f*
 Nesjavellir, 538*f*
 Neustadt-Glewe, 639*f*
 original Magmax binary plant, 517*f*
 Ormat integrated two-level units, 507*f*
 pH-Mod system, 273*f*
 Raft River DOE plant, 554*f*
 Raft River USGeo plant, 566*f*
 redesigned Magmax binary plant, 525*f*
 Salavatli Dora 1, 588*f*
 single-flash power plants, 115*f*, 242*f*
 Soultz-sous-Forêts, 636*f*
 SDG&E. *See* San Diego Gas & Electric Company
 Sea-floor spreading, 4
 Second Imperial Geothermal Company (SIGC), 506, 665, 666*f*
 Second Law efficiencies, 312
 Second Law of Thermodynamics, 35–36, 126, 293, 718–721
 Second-law efficiency, 299–315
 Seismic activity monitoring, 39
 Seismicity, 673–674
 Sensors for gases, 56–58
 Separation process, 159
 double- and triple-flash steam power plants, 149–150
 single-flash steam power plants, 121
 Separator temperatures
 double-flash optimization, 154
 versus flash temperature, 152
 optimum approximate formulation, 130–132
 single-flash optimization, 127–130
 Separators
 cyclone, 108, 114–115, 147*f*
 double- and triple-flash steam power plants, 144–146, 154
 single-flash steam power plants, 115, 117*f*
 stations location, 108
 SHAFT, 89*t*
 Sharp-edged orifice flow meter, 77
 Shell-and-tube heat exchangers, 302, 330–331, 331*f*

- Shut in, downhole pressure, 80
- SI system (Système International des Unites), 711, 714*t*
- Sierra Pacific Power Company, 482
- SIGC. *See* Second Imperial Geothermal Company
- Silencers, 617*f*
- Silica. *See also* Scale
 amorphous, 156–158
 binary cycle power plants, 160, 196–197
 chemistry, 156–158
 combined flash-binary systems, 249
 combined single- and double-flash systems, 246
 double-flash steam plants, 158–160
 environmental aspects, 667
 geofluid temperature correlation, 31
 geothermometers, 33–34, 33*f*
 pH-Mod plants, 272–273
 precipitation, 156–158, 246, 249
 scaling potential, 158–160
 solubility, 156–158
- Simulators, 83–88
- Single-flash steam power plants, 107. *See also* Hybrid systems
 combined heat and power plants, 267–269
 considerations pertaining to, 133–135
 conversion process thermodynamics, 119–127
 energy conversion system, 114–119
 environmental aspects for, 132–135, 133*t*
 equipment list for, 136–138
 backup systems, 138
 condenser, gas ejection, and pollution control, 137–138
 geofluid disposal system, 138
 heat rejection system, 138
 noise abatement system, 138
 turbine-generator and controls, 137
 wellhead, brine, and steam supply system, 136–137
 gathering system design, 108–114
 installed MW per country, 691*t*
 installed MW worldwide, 692*t*
 optimization example, 127–130
 separator temperature optimization, 130–132
 total units worldwide, 693*t*
 units per plant type per country, 692*t*
- Siphon effect, 65
- Site preparation for drilling, 50–51
- Skin factor, 82
- SMUD. *See* Sacramento Municipal Utility District (SMUD)
- SMUDGE #1 plant design, 358–359
- Soda Lake Plants 1 and 2, 480
- Sodium/potassium (Na/K) ratio, 34
- Sodium/potassium/calcium (Na/K/Ca) geothermometers, 34
- Soffioni, 329–331, 330*f*
- Solar energy, 275–276
- Solar plants, 664
- Solar-geothermal hybrid plants, 274–277
- Solids discharge environmental aspects, 667–668
- Solubility, 82, 156–158, 267
- Sonic velocity, 205–207
- Soultz field, France, 673
- Soultz-sous-Forêts, France, 632–637
 location map, 633*f*
 power plant, 635*f*
 pressure-enthalpy process diagram, 638*f*
 schematic 3D visualization of, 636*f*
 simplified flow diagram, 636*f*
 state-point information, 637*t*
 temperature profile, 635*f*
 well profiles, 634*f*
- South American prospects, 455–458
 Argentina, 456–457
 Chile, 457–458
- Southeast Geysers Pipeline Project, 363
- Southern California Edison, 527–528
- Specific power, 128, 130, 154, 182–183
- Specific properties, 715
- Spray ponds, 519–521, 522*f*
- “Squeeze job,” 55
- SRGR project. *See* Santa Rosa Geysers Recharge (SRGR) project
- St. Lucia, 455
- STAR, 89*t*
- State diagrams. *See also* Enthalpy-entropy (Mollier) diagrams; Pressure-enthalpy diagrams; Temperature-entropy diagrams
 thermodynamic, 721–722
- State Electrical Company (PLN), 405
- Static reservoir pressure, 80
- Steady processes, 716–717
- Steam gathering systems
 dry-steam power plants, 177–178
 The Geysers dry-steam power plants, 353
 single-flash steam power plants, 108
- Steam pipelines
 dry-steam power plants, 177, 178*f*
 The Geysers dry-steam power plants, 353
 pressure losses, 110–114
- Steam supply systems
 double- and triple-flash steam power plants, 161
 dry-steam power plants, 187

Steam tables, 32–33, 69, 72
 Steam traps, 177, 178*f*
 Steamboat geothermal power complex, 468–471, 468*f*
 Steamboat Hills plants, 469, 470*f*
 Steamboat Springs, Nevada, natural geyser disappearance, 135, 677
 Steamboat Springs resource, 463
 Steam-heated pools, 10–11
 Stellite, 118
 Stereographic images, 26
 Stillwater 1, 489–491, 490*f*
 aerial view of, 493*f*
 performance data for, 492*f*
 Stillwater 2, 491
 aerial view of, 493*f*
 performance data for, 492*f*
 Stillwater CSP collector, 493, 495*f*
 Stillwater plants, 489–494
 hybrid geothermal–solar systems, 491–494
 Stillwater 1, 489–491, 490*f*
 Stillwater 2, 491
 Stillwater Range, 475
 Stratovolcano Merapi, 404–405, 404*f*
 Subcritical cycle, 215
 Subduction and subduction zones, 7, 9–10, 9*f*
 Subsidence
 environmental aspects, 670–672
 geopressure reservoirs, 14–15
 Sulfur dioxide, 661
 Sunda Arc, 403
 Supercritical cycles, 204, 215
 Superheaters, 526*f*
 Surface casing, 56
 Surface pumps, 225, 229–231
 Surface-type condensers, 118–119, 123, 179
 Sustainability, 364–365
 Swamee-Jain equation, 66–67
 Synthesis maps, 40
 Système International des Unites, 711, 714*t*

T

Tauhara, 392*t*
 Te Mihi power plant, 372, 383–385
 technical details and performance for, 382*t*
 Technical specifications
 Heber binary plant, 509*t*
 Larderello indirect-cycle units, 334*t*
 original Magmamax dual-fluid binary plant, 523*t*
 redesigned Magmamax binary plant, 527*t*
 Tectonics, 3–4, 324
 Temperature. *See also* Separator temperatures
 amorphous silica solubility, 156–158
 equal-temperature-split rule, 132, 153, 159–160
 flash temperature, 154, 244–245
 geothermometers, 32–34, 33*f*
 gradients, 35–36, 37*f*, 40*f*
 optimum separator approximate formulation, 130–132
 pinch point, 201
 quartz solubility, 156–158
 Temperature-entropy diagrams
 binary cycle power plants, 205*f*, 209*f*, 213*f*, 243*f*
 binary plant working fluids, 205*f*
 combined single- and double-flash systems, 247*f*
 combined single-flash-binary systems, 248*f*
 double- and triple-flash steam power plants, 148–149
 double-flash steam power plants, 243*f*
 dry and wet turbine expansion process, 182*f*
 dry-steam power plants, 174*f*, 180*f*, 243*f*
 dual-fluid binary cycle plants, 213*f*
 dual-fluid binary plants, 214*f*
 exergy efficiencies for turbines, 300*f*, 301*f*
 flash vessels, 306*f*
 gas compressors, 310*f*
 ideal binary cycles, 209*f*
 integrated single- and double-flash systems, 245*f*
 integrated single-flash-binary systems, 250*f*, 251*f*
 normal and retrograde saturated vapor curves
 comparison, 205*f*
 single-flash steam power plants, 120, 120*f*, 243*f*
 total flow expander concept, 257*f*
 total-flow and single-flash turbines
 comparison, 258*f*
 typical pure substance, 722*f*
 water, 723*f*
 Temperature-entropy process diagram from
 Beowawe bottoming binary cycle, 484, 484*f*
 Temperature-heat transfer diagrams
 basic binary systems, 200*f*
 dual-fluid binary plants, 215*f*
 Testing methods for wells, 75–82
 TETRAD, 89*t*
 Thailand, 708*t*
 Thermal conductivity, 35–36
 Thermal efficiency, 125, 479–480, 485
 basic binary systems, 212*t*

- Thermal efficiency (*Continued*)
 dual-fluid binary plants, 215
 dual-pressure binary plants, 212
 integrated flash-binary systems, 255
versus utilization efficiency, 315–316
- Thermal gradients, 35–36
- Thermal pollution, 223, 680–681
- Thermal Power Company, 350
- Thermodynamic state diagrams, 721–722.
See also Enthalpy-entropy (Mollier)
 diagrams; Pressure-enthalpy diagrams;
 Temperature-entropy diagrams
- Thermodynamics
 basic binary systems, 197
 binary plant working fluids, 204–205
 conversion process, 148–153
 double- and triple-flash steam power plants,
 148–153
 dual-fluid binary cycles, 212–216
 elements of, 715
 first law, 119, 123, 125, 292–293, 717
 properties, 715–716
 Second Law of Thermodynamics, 35–36, 126,
 293, 718–721
 single-flash steam power plants conversion
 process, 119–127
 systems, 715–716
- Thief zones, 54
- Thinning, 7
- 3-dimensional acoustic noise pattern, 673
- 3-dimensional reflection seismic surveys, 328, 329*f*
- Thrusting, 7
- Time-dependent pressure measurements, 80
- Total-flow systems, 256–263
- TOUGH, 89*t*
- TOUGH2, 89*t*
- Toxic gas safety precautions, 56–58
- Tracers, 82
- Transform faults, 7
- Transient pressure measurements, 80–82
- Trash energy equivalents, 713*t*, 714*t*
- Travale plant, Italy, 339
- Trenching, 7, 9–10
- Triangular cycles, 208–209
- Tri-cone roller bit, 51–53, 53*f*
- Triple-flash plants, 144, 691*t*, 692*t*
- Turbine expansion process
 double- and triple-flash steam power plants,
 150–152
 dry-steam power plants, 180–183
 single-flash steam power plants, 121–122
- Turbine-generators, 381, 397
 basic binary plants, 224
 binary cycle, 197*f*
 double- and triple-flash steam power plants,
 161
 dry-steam power plants, 187
 on elevated pedestal, 560*f*
- Turbines
 analysis, 197–198
 axial-flow impulse, 256–259
 basic binary systems, 197–198
 binary plant working fluids, 206*t*
 construction materials, 118, 119*t*
 corrosion, 118
 double- and triple-flash steam power plants,
 147
 dry-steam power plants, 179, 181–183
 dual-admission, 211
 dual-pressure binary plants, 209–212, 212*t*
 efficiency, 121, 181–183, 299–302
 exergy efficiencies, 299–302
 isobutane, 517, 519*f*, 521*f*
 Magmamax binary plant, 517–518, 520*f*, 521*f*,
 524–525
 modular design, 339, 339*f*
 outlet state, 122
 recent plants at Larderello, Tuscany, Italy,
 338*f*, 340*t*
 rotary separator, 260–261
 single-flash steam power plants, 121–122
 size, 206–207
 total-flow and single-flash comparison,
 256–259
- Turkey, geothermal power plants in, 575, 703*t*
 current state and future prospects of, 603–605
 environmental impact, 602
 geologic setting, 575–577
 Germencik double-flash plant, 593–600
 design of, 595–600
 geologic setting, 594
 Kizildere single-flash plant, 577–586
 early history and pilot plant, 577–579
 Kizildere Unit 1, 581–583
 Kizildere Unit 2 and future plans, 584–586,
 584*f*, 585*t*
 wells, 579–581
 Pamukören binary plant, 600–601, 601*f*
 Salavatli binary plants, 586–593
 Dora 2, 591–592
 Dora 3A, 3B, 4, and 5, 593
- Tuscan Nappe, 325
- Tuscarora, 485, 488
- Tuscarora power plant, 485–487, 487*f*
- Tuzla-Çanakkale binary plant, 604
- Twain, Mark, 231

Two-phase flow in wells, 70–71
 Two-phase friction factor, 71–72
 Two-phase gathering systems, 109*f*
 Two-phase pipelines, 145
 Two-phase steam-liquid pipeline pressure drops, 112
 Typical geothermal binary power cycle, 732–733

U

Ulubelu plant, 422–423
 United States Bureau of Reclamation (USBR), 516–517
 United States Customary System of Units, 711, 713*t*
 United States Geological Survey (USGS), 25
 Units
 numbers per country, 690*t*
 numbers per plant type per country, 692*t*
 total number worldwide, 693*t*
 Units conversion (measures), 711
 UNOCAL, 346–347
 Unsteady processes, 716, 718
 Unterhaching, Germany, 642–644
 history of events for, 643*t*
 Upper Mahiao integrated flash-binary power plant, Leyte, Philippines, 256*f*
 Uranium energy equivalents, 713*t*, 714*t*
 US Agency for International Development (USAID), 405
 US American Reinvestment and Recovery Act (ARRA), 650
 US Department of Treasury (USDOT), 483
 US geothermal plants, 704*t*. *See also individual plants*
 Alaska, New Mexico, Oregon, Wyoming, 706*t*
 California, 704*t*
 Nevada, Utah, Hawaii, Idaho, 706*t*
 USAID. *See* US Agency for International Development (USAID)
 USBR. *See* United States Bureau of Reclamation (USBR)
 USDOT. *See* US Department of Treasury (USDOT)
 USGS. *See* United States Geological Survey (USGS)
 Utah, 706*t*
 Utilization efficiencies, 126–127, 410, 471, 478
 basic binary systems, 203, 211, 212*t*
 basic systems comparison, 243*t*
 binary cycle analysis example, 222

combined heat and power plants, 267–268
 double- and triple-flash steam power plants, 152
 double-flash optimization, 154
 dry-steam power plants, 183
 dual-pressure binary plants, 211, 212*t*
 integrated flash-binary plants, 255
 optimum, 130
 single-flash steam power plants, 126–127
versus thermal efficiency, 315–316

V

Validation of reservoir models, 86–87
 Valle Secolo geothermal power plant, Larderello, Tuscany, Italy, 322*f*
 Valles Caldera, New Mexico, 612–613
 Vapor compressors, 308–311
 Vapor-dominated reservoirs, 171–172, 172*f*
 Vegetation, 678–680
 Venturi meters, 77
 Vertical pipes, 112–113
 Viscous effects, 113
 Vistas, 678–680
 Visual pollution, 678–680
 Void fraction, 113
 Volcanism, 27
 Volcanoes
 in Central America, 429*f*
 of South America, 429*f*
 Volume ratio, 262–263
 Volumetric flow rate, 63–64, 67, 76–77
 VSI, 405

W

Wabuska, 466
 Wairakei binary plant, 381–382
 flow diagram for, 383*f*
 technical details and performance for, 382*t*
 Wairakei field land subsidence, 670–672
 Wairakei geothermal system, 134–135, 370, 373–378
 capital cost and generation history, 386–387
 condensing units, technical details and performance for, 377*t*
 Decline in pressure from the HPWs at, 379*f*
 drilling history at, 373*f*
 electricity generation and mass extraction, 387*f*
 geographic and geologic setting, 370–373
 high-pressure (HP) turbines, 373–374, 377–379
 Mollier diagram for, 378*f*
 and neighboring borefields, 384*f*
 noncondensing units, technical details and performance for, 376*t*

- Wairakei geothermal system (*Continued*)
 power plant costs, 386*t*
 recent configurations, 379, 380*f*
 Western Borefield (WBF), 372, 372*f*
- Wairakei Geyser Valley extinguished geysers, 678
- Wairakei Power Station prawn farm, 663–664
- Waste heat beneficial use, 223
- Waste-water-to-electricity projects, 363
- Water
 mass conservation of, 124–125
 pollution, 669
 thermodynamic properties, 204*t*
 usage concerns, 668–669
- Water-ammonia mixtures, 217
- Water-cooled plant *versus* air-cooled plant, 667
- Wayang Windu plants
 technical details and performance for, 418–422, 420*t*
 view of, 419*f*
- Wayang Windu Unit 1 and 2
 cooling towers for, 420*f*
 power station layout plan for, 421*f*
- WBF. *See* Western Borefield (WBF)
- Webre-type separator, 115–116
- Weir factor, 79–80
- Well casings, 82
- Well drilling, 668
- Wellbore flashing, 71–74
- Wellhead dryness fraction, 72
- Wellhead equipment, 677
 double- and triple-flash steam power plants, 161
 single-flash steam power plants, 115
- Wellhead pressures, 66, 72, 127, 183–185
- Wellhead separators, 109, 110*f*, 145*f*, 146
- Wells. *See also* Drilling
 blowouts, 680
 casings, 54–55, 82, 669
 exploratory, 17*f*, 41, 49, 50*f*
 flow, 62–74
 Internet resources, 25
 log data, 25
 pads, 50–51, 663
 pressures, 63–64
 profiles, 352
 testing, 75–82
- Western Borefield (WBF), 372
- Wet turbine expansion process, 182
- Wet-bulb temperature, 479–480, 567
- Wetland habitats, 363
- Wildlife habitats, 678–680
- Wilson line, 205
- Witches' Cauldron, 347
- Work transfer and exergy, 297–298
- Working fluid selection, 203–208
- World War II, 322–324
- Worldwide status (December 2014), 687–688, 689*t*, 690*t*, 691*t*, 692*t*, 693*t*, 694*t*, 695*t*, 696*t*, 698*t*, 699*t*, 700*t*, 701*t*, 702*t*, 703*t*
- Y**
- Yamagata Prefecture, Honshu, Japan, 617
- Yellowstone National Park, 677
- Z**
- Zambia, 690*t*
- Zinc recovery, 668
- Zorlu Energy Group, 584, 586
- Zunil fault, Guatemala, 674–676
- Zunil geothermal field, Guatemala, landslides, 674–676, 676*f*
- Zunil plant, 449–450